86-5

AGARD-CP-97

AGARD

ADVISORY GROUP FOR AEROSPACE RESEARCH & DEVELOPMENT

7 RUE ANCELLE 92 NEUILLY SUR SEINE FRANCE

AGARD CONFERENCE PROCEEDINGS NO. 97

on

Radar Propagation in the Arctic

NORTH ATLANTIC TREATY ORGANIZATION

DISTRIBUTION AND AVAILABILITY
ON BACK COVER

AGARD-CP-97

NORTH ATLANTIC TREATY ORGANIZATION

ADVISORY GROUP FOR AEROSPACE RESEARCH AND DEVELOPMENT

(ORGANISATION DU TRAITE DE L'ATLANTIQUE NORD)

RADAR PROPAGATION IN THE ARCTIC

Papers presented at the Specialists Meeting of the Electromagnetic Wave Propagation Panel of AGARD, held at the Max-Planck-Institut für Aeronomie, Lindau/Harz, Federal Republic of Germany, 13-17 September 1971.

THE MISSION OF AGARD

The mission of AGARD is to bring together the leading personalities of the NATO nations in the fields of science and technology relating to aerospace for the following purposes:

- Exchanging of scientific and technical information;
- Continuously stimulating advances in the aerospace sciences relevant to strengthening the common defence posture;
- Improving the co-operation among member nations in aerospace research and development;
- Providing scientific and technical advice and assistance to the North Atlantic Military Committee in the field of aerospace research and development;
- Rendering scientific and technical assistance, as requested, to other NATO bodies and to member nations in connection with research and development problems in the aerospace field.
- Providing assistance to member nations for the purpose of increasing their scientific and technical potential;
- Recommending effective ways for the member nations to use their research and development capabilities for the common benefit of the NATO community.

The highest authority within AGARD is the National Delegates Board consisting of officially appointed senior representatives from each Member Nation. The mission of AGARD is carried out through the Panels which are composed for experts appointed by the National Delegates, the Consultant and Exchange Program and the Aerospace Applications Studies Program. The results of AGARD work are reported to the Member Nations and the NATO Authorities through the AGARD series of publications of which this is one.

Participation in AGARD activities is by invitation only and is normally limited to citizens of the NATO nations.

Published January 1972

621.396(98)

Printed by Technical Editing and Reproduction Ltd
Harford House, 7-9 Charlotte St. London W1P 1HD

THEME

Studies of the characteristics and the effects of the arctic ionosphere on radio and radar propagation have been conducted for many years. The experimental and theoretical efforts recently expended necessitated a meeting of active workers in this field. The objectives were to summarize the current state of knowledge of radar-arctic propagation and to determine and recommend where additional investigations are required.

The characteristics of radar propagation in the arctic ionosphere, such as amplitude, phase and angle scintillation, auroral clutter and auroral noise affecting VHF-UHF transmissions are of concern. For HF transmissions, the additional ionospheric phenomena of interest are, spread F, sporadic E, auroral absorption, polar cap absorption, and traveling ionospheric disturbances. The current status of experimental and theoretical data on the propagation limitations of these effects in the frequency range from approximately 1 MHz to 10 GHz and the correlation of these effects with such phenomena as magnetic activity, optical aurora and particle precipitation were considered at the meeting.

CW and pulse transmissions were treated for propagation paths traversing the arctic regions. Investigations of the arctic-ionospheric propagation characteristics utilizing radio astronomical and satellite transmissions were particularly applicable to this meeting.

George H.Millmann

Program Chairman

Dr George H.Millmann
General Electric Company
Building 9, Room 8
Court Street Plant
Syracuse, New York 13201
United States of America

Program Committee

Mr O.Bratteng
The Auroral Observatory
P.O.Box 387, Norway

Dr G.Lange-Hesse
Max-Planck-Institut für Aeronomie
3411, Lindau/Harz
Germany

Mr R.L.Leadabrand
Stanford Research Institute
Menlo Park, California, 94022
United States of America

Dr A.McNamara
National Research Council
Ottawa, Ontario,
Canada

Prof. E.Shearman
Department of Electrical Engineering
University of Birmingham
P.O.Box 363
Birmingham
United Kingdom

Editor

Dr Jon Trithagen
The Norwegian Defence Research Establishment
P.O.Box 25
2007 Kjeller
Norway

Electromagnetic Wave Propagation Panel Chairman

Dr Olav Holt
The Auroral Observatory
9001, Tromsø
Norway

Host Nation Meeting Coordinator

Dr Gunther Lange-Hesse
Max-Planck-Institut fur Aeronomie
3411, Lindau Harz
Germany

CONTENTS

EDITOR'S FOREWORD

This book contains papers and discussions of the Electromagnetic Wave Propagation Panel Specialists Meeting on "Radar Propagation in the Arctic" held at Lindau/Harz, Federal Republic of Germany in September 1971.

This type of book is of little value if it is not made quickly available to the scientific and technical community. For this reason the Program Chairman selected the papers to be presented and included in the Proceedings, on the basis of abstracts that were submitted 6 months before the meeting. The authors were asked to complete their papers and prepare them for photocopying before the meeting. The papers have not been edited or changed in any fashion in the interest of rapid publication.

The discussions were recorded by having the participants write down their own questions, answers or comments during or after the sessions.

The Editor has made some changes in the discussion comments in view of the contents of the written versions of the papers.

The discussion of Session VII was recorded on tape, transcribed, condensed and rephrased by the Editor.

J.Frihagen

RESEARCH TASKS CONCERNING NATO SURVEILLANCE IN THE ARCTIC REGION

by

H.J. ALBRECHT

Chairman, NATO-TACSATCOM Committee

Without going too much into the historic development of the North Atlantic Treaty Organization, we should remember that this great international community was born in 1949 as the answer of the West to the threat presented by the steadily increasing strength of the Soviet Bloc. In subsequent years, more and more nations joined this collective defence system and now cooperate in the protection of the whole of the Atlantic Area.

During the last twenty years, the NATO-created balance of military forces between East and West has prevented further communist gains. More and more examples of Soviet expansion tendencies have confirmed the need of strong Western forces which help to maintain this balance of power.

The Eastern Nations have combined their forces in accordance with the Warsaw Pact. Their strength has increased more rapidly than that of NATO. On the other hand, the higher quality of the military power available on the Western side has to be emphasized. An additional, perhaps more political aspect is presented by the fact that Soviet troops in Central Europe have to be considered as part of an occupational force.

The threat to which Western Nations are exposed is generally analyzed in accordance with geographic regions. Recent reports have frequently referred to the increase of Soviet naval power in the Mediterranean Area. On the other hand, there are the Central European and the northern regions. Since one of the main tasks of NATO is the maintenance of forces and a steady surveillance in all geographic areas of strategic importance, the northern and the central zones must not be neglected, even if major attention is directed at the balance of power in another area.

With regard to the northern flank of NATO, the appropriate military command is represented by AFNORTH, the Northern European Command located at Kolsaas in Norway and the Allied Command Atlantic, called ACLANT with its headquarters at Norfolk, Virginia, United States of America. Analyzing in detail the military threat in the Arctic Region, the effective frontier between NATO and Warsaw Pact Nations leads from Northern Norway via Spitzbergen at 650 km from the extreme North of Norway to Greenland, and extends towards the islands of Northern Canada and Alaska. Beside national troops and units integrated in NATO, a mobile force under direct NATO command is of extreme importance for the defence of the northern NATO region. It has been established to be available at short notice and comprises army units from Canada, Italy, and the United Kingdom and paratroops from Belgium, the Netherlands, United Kingdom, and United States of America.

With particular regard to naval activities, the Soviet navy is considerably active in the Northern Atlantic Region. In principle, Soviet fleets may be capable of challenging the West wherever accessible waters exist. An important factor is presented by the submarine force and by naval units capable of missile launching. This leads to another important type of threat: short-range and long-range missiles. Their warheads may be of conventional or nuclear type. Flight paths in the Arctic Region display relatively short distances between launching bases and some NATO countries.

Summarizing, the northern part of the geographic area covered by the North Atlantic Treaty Organization is particularly exposed to enemy attack. The degree of threat has to be recognized and monitored constantly. This is one of the essential tasks of NATO surveillance.

Depending upon the actual objective, surveillance can best be achieved by optical, electronic, or even acoustic means. Optical and acoustic methods of detecting enemy movements on land, on sea, in air or in space require relatively short distances between the object and the monitor.

One of the most important methods of surveillance is represented by electronic means. In principle, both, passive and active methods, exist. The former include all monitoring systems directed at the enemy's transmissions for the purpose of communications, navigation, as well as his radar surveillance. On the other hand, the last-mentioned method represents the active type if used in the conventional way of analyzing one's own signal reflected by an enemy object, i.e. by RADAR. The more elaborate the systems, the more conclusive can be the results.

With particular reference to the methods of surveillance used on the northern flank of the NATO strategic environment, electronic warning systems play a decisive role. The northern frontier between NATO- and Warsaw Pact Nations is completely covered by radar warning systems. Radar may be used on suitable frequencies which extend from HF to VHF and UHF ranges. In principle, the utilization of radar and radio links is limited by several factors, one of them being the be-

haviour of the propagation medium. Such limitations are particularly pronounced in certain geographical zones. Predominant are the effects on "Radar Propagation in the Arctic".

Your specialists' meeting on this topic will deal in particular with all the relevant results of research work achieved up to now. It will thus present a summary of the current state of understanding the problems connected with radar propagation in this geographic region of so vital importance to NATO. The different Arctic propagation effects to be dealt with by this meeting cover more than those relevant to radar use, because the effectiveness of propagation limitations on communication and navigation links is very similar.

The aurora zone is frequently taken as an indication of particularly intense changes in propagation conditions.

Following the fundamental research work by Sir Edward Appleton and his collaborators in the early twenties, the analysis of the ionosphere was carried out on a world-wide basis. Particular attention has been paid to the polar region on account of the higher variability and larger number of unknowns in that geographic area. In combination with optical observations of aurora activities and, later on, the aurora backscatter for VHF and UHF transmissions, more and more information was gathered on the effects of Arctic propagation media. Yet, even at this stage, quite a number of unknown factors exists and presents themselves as research objectives.

To some degree, the progressive change in communication systems emphasizes the importance of gaining complete understanding on the behaviour of propagation media. A typical example is represented by the use of satellites for communication and navigation purposes. With terrestrial terminals in higher latitudes, elevation angles appropriate for NATO satellite communication links are small with satellite orbits around the equatorial plane. Thus paths affected are longer and detrimental effects are enhanced. Typical visibility ranges for a satellite in geostationary orbit show a NATO-wide coverage. A complete session in your meeting will deal with polar scintillations which have a decisive bearing on amplitude and phase stability of signals passing through the atmosphere to spacecraft or satellites.

In principle, there is no technical system which cannot be improved if time and appropriate means are available. Although the surveillance systems presently used by NATO may already be regarded optimum, their effectiveness can still be improved if new progress in research and development is taken into account.

With regard to the subject under discussion in this lead paper, three main areas of possible progress are indicated:

technology
recognition and extension of system limitations
definition and accurate prediction of propagation-medium behaviour.

As an example, technological progress may establish the usefulness of new portions of the electromagnetic frequency spectrum and thereby extend the system limitations beyond the range 1 MHz to 10 GHz. Appropriate work is being undertaken on a NATO-wide basis and particular attention has to be paid to the applications of those frequencies in the polar region. Obviously, one of the important limitations with regard to such high frequencies is presented by the propagation medium itself. Thus the third point mentioned is of equal if not more importance.

As another possible example of improving the surveillance, the general field of combining several surveillance subsystems may offer new aspects. Such hybrid systems have come into being with the development of computers and their general employment in the strategic and tactical field. Progress being constantly made in the field generally defined as Command and Control will open up new roads to better surveillance.

Ever since the commencement of the North Atlantic Treaty Organization in 1949 and the associated programmes of research, development and production, new results have been obtained on a NATO-wide basis. The multinational cooperation has been mutually profitable for all participating nations. This is continuously being verified by programmes which have already been concluded and other projects still being undertaken by NATO or a number of nations belonging to NATO. It has also been proved that efficient management on a multinational basis is extremely important and represents one of the secrets of success. As an example, complete duplication of research work may be considered a useless expenditure, but permitting two or more groups to investigate simultaneously the same project on somewhat different lines certainly results in a stimulation of activities.

Nowadays, as never before, the safety of a nation or a union of nations is so much connected to and so much depends on results gained in the development of new defence means. Historically, even Roman troops more than 2000 years ago used technical aids which had to be developed and tested. Even then, some kind of defence research work had to be carried out to keep equipment modern.

Especially with engineering progress during the last few centuries, the utilization of technical means advanced more and more and increased its share as well as its right of priority in planning for efficient defence. NATO as the great block of Western Nations uses surveillance and alertness as methods of modern defence.

And within NATO, the Advisory Group for Aerospace Research and Development or "AGARD" fulfills the tasks of managing and coordinating many essential R&D projects. The founder and first chairman of AGARD, Dr. von Karman, once said:

> "Scientific results cannot be used efficiently by soldiers who have no understanding of them, and scientists cannot produce results useful for warfare without an understanding of the operations".

One of AGARD's major achievements has been the establishment of such mutual cooperation.

Twenty years ago, competent representatives of NATO nations recommended the formation of AGARD. It might perhaps be advisable to quote here Dr. von Karman again, from his reply to Professor Henri Laugier, Assistant Secretary General for Social Affairs in the 1947 newly created United Nations, who had asked Dr. von Karman for ideas on the contribution scientists could make to maintaining world peace:

> "I urged as a first step toward permanent peace the establishment of key international research centres, designed to attract learned men of all countries who would come to exchange ideas. I envisioned a return of the vagantes, or wandering scholars of the Middle Ages, who would, I felt, act as ambassadors to lay the foundations of international good will."

In this way, and by its publication of scientific results obtained by multinational cooperation, and by providing NATO with the advisory capacity necessary to fulfill the military tasks, AGARD contributes to maintaining and safeguarding world peace.

AGARD's Symposia, Specialists' Meetings and Lecture Series enjoy a high reputation among scientists and military users. Your meeting will be of direct concern to one of NATO's essential surveillance tasks. I would like to conclude by wishing you the utmost of success.

MORPHOLOGY OF RADIO-RADAR POLAR PROPAGATION EFFECTS

T.R. Hartz
Communications Research Centre
P.O. Box 490, Station 'A', Ottawa, K1N 8T5, Canada

ABSTRACT

Radio-wave propagation through the upper atmosphere at high latitudes is conditioned by effects arising from the influx of energetic charged particles. Some of these effects are associated with the auroral phenomena and have been studied for many years in that context, mainly from ground stations. More recently such observations have been supplemented by rocket and satellite measurements, and also have been extended to include particle-induced phenomena not directly linked to the aurora. This paper will review a variety of observational data on the polar upper atmosphere, and particularly on the morphological patterns deduced for the particle precipitation associated with auroral phenomena and with polar-cap disturbances. The significance of different portions of such patterns will be discussed with reference to particle energies, sources, and ionospheric changes during particular disturbed intervals. Statistical data on the diurnal, seasonal, and spatial variation of such associated propagation effects as absorption, scintillation, dispersion, etc., will be examined, along with their correlation with magnetic activity, spread F, sporadic E, visual aurora, and radio noise observations. In addition, the storm-time variation of some of these phenomena will be discussed from the point of view of their short-term effects on radio-wave propagation.

1. INTRODUCTION

This paper will attempt to provide a general-background description of some of the high-latitude phenomena that occur in the upper atmosphere. All too frequently one tends to think of such phenomena as disturbances or anomalous features in what might otherwise be a regular, easily-describable situation, but this attitude has been conditioned largely by low-latitude experience. The low- and middle-latitude ionosphere can generally be described in terms of solar illumination and processes that depend principally on the ultra-violet, optical, and infra-red radiations. At high latitudes the additional influences of energetic charged particles have to be considered and the extrapolation from the better-known low-latitude situation has introduced considerable confusion in terminology. The literature is full of abnormalities and disturbances of various kinds, and all too frequently the disturbances are meaningful only in terms of the particular observing equipment used so that their manifestation in another type of observation cannot readily be predicted.

The essential point is that at high latitudes there is an additional energy source for upper-atmospheric phenomena in the form of energetic charged particles and that this is a normal rather than abnormal situation. Accordingly, the polar propagation effects of concern here are those resulting from particle precipitation, and the latitudes of interest are those where particle effects are observed. Historically, the most obvious effects are the auroral phenomena, though for purposes of this symposium the interest is more in the ionization features and the direct influence of these on radio-wave propagation. From a practical point of view there are two main particle populations to consider; these can be identified in terms of their atmospheric effects as polar-cap-absorption (PCA) particles and auroral particles. The basic distinction between the two classes hinges on the energy and number density of the particles. The PCA events are associated primarily with incoming protons having energies of the order of 10 MeV, but whose number density is sufficiently low that particle interactions are not significant above a height of about 1000 Km; as a consequence their motions in the geomagnetic field can be fairly well approximated by Størmer's theory for individual particles in a dipole field. The auroral phenomena, on the other hand, are associated with a substantially greater flux of lesser-energy electrons and protons and their behaviour in the geomagnetic field is more complicated because of particle interaction effects. As a result these particles precipitate in a characteristic pattern which is related to the geometry of the magnetosphere and which, when described statistically, is known generally as the Auroral Zone.

The paper will describe the average precipitation pattern for the auroral particles; it will also indicate very briefly the effects of PCA particle influx. It will review some of the gross observational evidence on the auroral phenomena and on the associated ionization features in different regions of the ionosphere. This general morphological picture is intended to serve as a background for some of the subsequent discussions in the symposium. In addition some of the short-term effects observable in various phenomena during magnetospheric storms and sub-storms will be discussed briefly in relation to the general precipitation pattern.

2. AURORAL PARTICLE PRECIPITATION

In considering the effects of the influx of auroral particles into the upper atmosphere one can outline a number of possible processes whose relative probability will depend somewhat on such factors as energy, number flux, and the nature of the atmospheric constituents. These processes, along with their respective manifestations, are summarized in Figure 1-1. In general most of the effects can be attributed to electrons, though the consequences of incoming protons are rather similar but not always as marked. These processes are expected in addition to those arising from sunlight or ultra-violet radiation; consequently, all these effects, plus perhaps several others, are to be considered in the category of auroral phenomena.

It is important to note that a one-to-one correspondence between the different observable phenomena shown in Figure 1-1 is not necessarily anticipated, nor is it found in practice. The radio-wave propagation effects are mainly associated with the ionization, the transport of ionization, and the associated small scale features, structures, and gradients that arise in the ionosphere. The statistical patterns for these effects can differ in some details from the auroral statistical picture, which depends on atomic and molecular excitation through several processes most of which are indirect. Additional complications may arise from observability factors such as aspect angle or daylight. Nevertheless, to the extent that the

statistics of each phenomenon are somehow indicative of the precipitating particle flux, one would expect the precipitation pattern resulting from each process to show gross similarities. This has indeed been demonstrated, and as such provides most of the basis for the morphological summary that follows.

It will be obvious that this method of arriving at a particle precipitation pattern or a gross morphological picture is hazardous. It involves the averaging or generalizing of detailed observations; in rocket or satellite data ambiguities of time and space need to be overcome, while in ground-based observations interpolations and extrapolations are required to off-set any deficiencies in station locations. Such procedures tend to smooth out the fine details in the data at the expense of the overall picture. There is thus a constant danger that the real physical situation might be obscured and replaced by a pattern forced by the processing used. One must also be cautious in treating the various observable features identified in Figure I-1 as equivalent; certainly they are not, even though various workers have been zealous in associating the adjective 'auroral' with many of them. Thus one finds auroral hiss, auroral absorption, auroral sporadic E, radio aurora, auroral X-rays, etc., where the association with aurora may be questionable. In the analysis undertaken here different data have been examined for general characteristics; these generalizations are not intended primarily to provide a faithful description of one or other of the phenomena in question, but rather to reveal a gross pattern or patterns for the particle precipitation which can be taken as meaningful in terms of the ionospheric or magnetospheric processes.

At various times in the past statistics on the occurrence of aurora in the night sky have been compiled. Until very recently these were based on visual or photographic observations from the ground and suffered from problems of cloud cover, twilight or daylight, limitations in station locations, etc. In spite of these difficulties a meaningful geographical distribution has resulted. Figure I-2 shows the Northern Auroral Zone, or the region in which nighttime aurora is seen overhead most frequently (1), (2). Most people are familiar enough with the geographic location of the zone maximum, but they do not always remember that this zone has some substantial width and that it represents the statistical rather than an instantaneous situation. In Figure I-2 the edges of the shaded region mark the half-maximum contours, while the maximum or most intense shading represents the regions over which auroras are observed on more than 90% of the nights.

This distribution indicates where the nighttime visual phenomena are observed, but give no information at other times of day. Because the centre of this annular ring corresponds with the north geomagnetic pole, it is convenient to use a coordinate system involving latitude and longitude, or local time, based on the geomagnetic poles, and Figure I-3 shows auroral statistical data for the northern hemisphere as a function of geomagnetic latitude and geomagnetic local time (3). The pattern is that of an eccentric ring, which has become known generally as the 'auroral oval' and which shows a fairly constant probability of occurrence throughout the day, with slightly higher values in the night hours.

3. PRECIPITATION PATTERNS

Because of some uncertainties in the daytime data, and bearing in mind the distinction between aurora and other observables that has already been noted in regard to Figure I-1, a number of workers have undertaken statistical studies of various observations to derive particle precipitation patterns. One such study was that of Hartz and Brice, who examined mainly data from ground-based instrumentation (4). They found a two-zoned pattern for the particle influx, one zone corresponding more or less with the auroral oval and the other consisting of an annular ring at a constant latitude of about 65° geomagnetic. Their study was based on auroral absorption data, all-sky camera data, magnetometer data, micro-pulsations, mantle aurora, various types of radio aurora, VLF radio noise and auroral hiss data, observations of spread F and sporadic E ionosonde echoes, balloon X-ray data, and satellite observations of the 10 keV and 40 keV electron flux. In almost every case they found indications of two general classes of characteristics which could be sorted into the two different diurnal patterns.

It should be noted that the Hartz-Brice pattern was an idealized diagram; it represented the latitude and time regions in which a number of presumed auroral parameters were found to occur most frequently and in which they showed similar general characteristics. The analysis leading to that diagram set out to identify common properties in the various data and in the process tended to force a set of observations into one of only two categories. As a consequence, a lot of detailed features and fine structure were smoothed out, the degree of overlap of the two regions was de-emphasized, and the particular observational parameters were generalized. The two zones were portrayed as rather narrower than warranted by the data in order to accentuate the distinction between the two; probably a more realistic representation would have shown some overlapping at all hours of the day.

In spite of such short-comings that pattern has served a very useful purpose in distinguishing two quite dissimilar types of particle precipitation. Since it was produced there have been many additional data from rocket-, satellite-, and aircraft-borne instrumentation, as well as from ground stations. It now appears that some modifications to that diagram are called for, mainly in connection with the inner or 'splash' zone, or auroral oval, as it is better known. This oval can be associated with the boundary between the open and closed field lines in the magnetosphere and there are philosophical arguments which lead one to expect that phenomena on the day and night sides should differ. In the one case the boundary lies deep in the magnetospheric tail in association with the plasma sheet, and in the other case it is linked to the neutral point or cusp on the surface of the magnetosphere and thus probably to the magneto-sheath plasma. Observationally, there are substantial data that indicate that the auroral phenomena near noon have quite different properties from those at night. Whereas the nighttime aurora is primarily substorm related, of limited duration, localized, rather sporadic, and at a height near 105 Km, the daytime phenomenon apparently occurs virtually 100% of the time at heights in excess of about 140 Km (5), (6), (7). Recently Akasofu (8) and Romick (9) have reported midday auroras with intense red (6300 Å) color, characteristic of the greater heights and low-energy particle precipitation, and similar findings have been reported by Eather (10), by Eather and Mende (11), and by Buchau et al (12). These auroras tend to be of the glow type with some arcs and ray structure that exhibit a green (5577 Å) lower border, but with a relatively high red-to-green intensity ratio. They occur in the higher-latitude portion of the oval, above about 75° geomagnetic, whereas the lower-latitude side of the oval seems to show auroras with more structure that appear typical of a more-energetic particle influx.

Various other data have been obtained on the day side of the oval that indicate different properties from those at night. The direct particle observations of Burch (13), Hoffman and Berko (14), Johnson and Sharp (15), Heikkila and Winningham (16), Frank (17), and Frank and Ackerson (18) show intense fluxes of soft electrons near noon, with energies characteristically less than 1 keV, and with indications of a somewhat harder flux at slightly lower latitudes. The VLF and LF emission observations of Gurnett (19), Hughes and Kaiser (20), Laaspere et al (21), Dunkel and Helliwell (22), Hartz (23), Barrington et al (24), and Gurnett and Frank (25), insofar as they can be taken to portray the electron influx, show very intense levels in the day and afternoon sectors. The magnetometer data also show very significant day-to-night differences in the oval, as described by Mishin, et al (26), and somewhat similar conclusions have been expressed in regard to a number of other parameters (cf. Nishida (27), Andrews and Thomas (28), and Lebeau (29)). As a consequence several revisions of or alternatives to the Hartz-Brice precipitation pattern have been advanced, of which the one described by Hartz (23) will be outlined here.

Consideration of the various observational data mentioned above has led to the revised precipitation pattern shown in Figure I-4. Here the phenomena on the day side of the oval have been distinguished from those at night on the basis of general characteristics rather than simply on an energy basis. The distinctive midday influx is represented by the stars, while the rest of the diagram essentially corresponds to the earlier version. Again this is to be taken as an idealized diagram depicting the average situation; the observations of particular phenomena suggest rather more overlapping of the three principal zones with a more gradual transition from one to the other than is shown here. For instance the results presented by Burch (13), and Hoffman and Berko (14) and by Eather and Mende (11) would suggest that a hard (~5 keV) electron precipitation in the noon sector occurs in the latitude region 70 - 75°, which may not have been adequately represented by the symbols shown in that time sector in Figure I-4. Those authors have described the hard zone as being generally featureless, which would imply that it should probably be identified with the drizzle zone. If so, the drizzle precipitation, in this time sector at least, has a significant lower-energy component that appears at higher latitudes than depicted in the figure, which would then overlap with the edges of the splash zone and also with the soft zone. Similarly, the nighttime splash zone has been depicted on the basis of the more energetic flux and probably does not adequately represent the low-energy precipitation events which tend to lie at slightly higher latitudes (cf. Eather and Mende (11)) and which are likely the low-energy tail of the splash events. However, Figure I-4 is intended to emphasize the different characteristics for the precipitation, not merely energy differences, and each population includes a spectrum of energies. Accordingly, some latitude spreading and overlapping of the regions should be read into the diagram, particularly since it represents an average over all degrees of disturbance.

4. PRECIPITATION CHARACTERISTICS

In each of the three principal regions identified in Figure I-4 one finds, in general, a rather distinctive type of precipitation. The distinguishing characteristics are summarized in Table 1. Insofar as possible, these are generalized characteristics and are not limited to only one observable parameter. Two of the categories have already been described by Hartz and Brice (4), while some aspects of the third must still be considered as rather tentative at this stage and are designated as such with parentheses. Obviously, these characteristics of the precipitation must be taken in a relative rather than an absolute sense.

Generally speaking the foregoing pattern depicts the electron precipitation; the proton precipitation is not as well defined, though the existing data would indicate a general similarity except that in the afternoon and evening portion of the oval they appear at slightly lower latitudes (see Figures I-5 and I-6).

Table 1 Precipitation Zone Characteristics

Noon Peak ★	Night Peak Λ	Morning Peak ●
Continuous or quasi continuous	Sporadic, abrupt onset	Long duration, gradual onset
Widespread, some fine structure	Localized	Widespread, little structure
Stable, fine structure changes	Rapidly changing, impulsive	Quasi stable, slow changes plus quasi-periodic modulation
(Not substorm associated)	Substorm associated	Substorm associated
Flux not K_p dependent	Flux K_p dependent	Flux K_p dependent
Latitude shift with K_p	Latitude shift with K_p	No latitude shift with K_p
(No time shift with K_p)	No time shift with K_p	Time shift with K_p
Peaked spectrum, principal flux ~ few tenths keV	Steep spectrum, principal flux ~ few keV	Fairly flat spectrum, principal flux ~ few tens keV
Main ionization in F region	Main ionization in E region	Main ionization in D region
(Maximum in summer)	Maximum at equinoxes	(Minimum in summer)

It would be overstating the case to claim that all portions of Figure I-4 are equally well determined. The sections of the auroral oval between about 6 and 9 hours and between about 15 and 18 hours are still rather uncertain. Some data show gaps here, others seem to show some confusion of phenomena which probably depends on the degree of disturbance. Eather and Mende (11) show these portions with question marks, as indicated here in Figure I-5 for electrons and Figure I-6 for protons. Lassen (30) and Mishin et al (26) have suggested that the oval is not continuous through these time intervals. They suggest that the auroral data are better represented by two horse-shoe-shaped zones that do not overlap -- a high-latitude zone for the dayside and a lower-latitude one at night. The more recent data from aircraft flights and the preliminary auroral survey data from the ISIS-II satellite (31) would seem to support the oval configuration, but possibly with some discontinuities. In any case more observations should resolve this problem, as well as clarify the dependence of the aurora and E-region phenomena on the low-energy tail of the drizzle precipitation on the dayside.

5. PRECIPITATION AND IONIZATION EFFECTS

In the light of the foregoing gross statistical pattern with the indicated characteristics for the precipitation, one may ask the question, what significance does this have as far as radio propagation is concerned? Some of the answers may be found by looking at the interrelation between various phenomena in the different portions of Figure I-4, by trying to relate these to magnetospheric processes, by looking at the sequence of events for particular intervals such as sub-storms and storms, and by looking at some of the distributional details in certain of the ionization data.

In Figure I-4 the inner zone follows the auroral oval of Feldstein, and while his data did not show these same diurnal maxima, it is well known that the most active auroral features appear near midnight. This particular region occurs at the feet of the field lines that are located at or very near the boundary between the 'open' and 'closed' field lines in the magnetospheric tail and is associated with the plasma sheet and with the substorm processes that originate there. It is also apparent that the outer zone in the figure is not represented in the conventional or all-sky camera auroral statistics, though there is good reason to believe that the mantle aurora identified by Sandford (32) is meaningful here. This 'drizzle' precipitation is at about a constant geomagnetic latitude and undoubtedly is of more energetic ($\lesssim$ 40 keV) electrons that can lead to D-region phenomena such as auroral absorption. The diurnal maximum falls in the forenoon hours at a latitude that is associated with magnetic field lines which lie deep in the trapped particle zones. Accordingly, it seems clear that this morning peak must constitute the principal sink for the outer Van Allen radiation belt.

The noon maximum can be associated directly with magnetosheath particles that have entered the magnetosphere through the polar cusp region or neutral field point. The particle energies correspond with those of the magnetosheath and the influx appears to be more or less continuous. In Figure I-7 are shown data from the soft particle spectrometer on ISIS-I obtained on a trans-polar pass going from the dayside to the nightside of the magnetosphere. The electron energy and number flux are displayed as a function of latitude, and in the lower frame are shown the radio noise data obtained at the same time at a frequency of 200 kHz (23). The intense electron flux at an energy of about 200 eV and the corresponding high noise levels can be seen in the region of the polar cusp. In the polar cap the influx is quite low, with the occasional sporadic burst. On the night side the flux is more intense and again sporadic, with a trend toward higher energies. This diagram exemplifies some of the general characteristics already described for the high-latitude precipitation.

Figure I-8 shows data from another trans-polar pass of the ISIS-I satellite, obtained under high K_p conditions. Again the electron flux and the noise emissions are shown; also shown is the electron density near the satellite, normalized to remove the variation with satellite height, and a measure of the electron-density fine structure or 'spread'. Note that the maximum electron density and maximum fine structure do not correspond with the particle influx but seem to be shifted several degrees toward higher latitude. It appears that the electron influx penetrates to the ionospheric F region where ionization is produced, and then is redistributed. The ionization transport is mainly upward along the field lines, though some movement to higher latitudes may also take place as suggested in Figure I-9. At the satellite height (in this case $\sim$1500 km) this upward flux of thermal ionization appears very structured.

Unfortunately, detailed studies of this nature have not yet been carried out at all times of the day and for all disturbance conditions. The preliminary observations of Gurnett and Frank (25) in the evening hours would seem to indicate that the upward flow of ionospheric electrons is on the low-latitude side of the energetic electron influx in that time sector. Further studies are obviously required, and much more study is required of the associated transport and ionization-redistribution processes in the F region. These requirements are not easily met; the top-side ionosonde data are difficult to interpret in terms of ionization transport since they give electron density profiles or the gross distribution of ionization during the satellite transit, as exemplified by Figure I-10 for the afternoon hours (33). Statistical treatments of such results tend to show several outstanding features; the polar peak near midday and the mid-latitude trough at night, as illustrated in Figure I-11 (27). Such gross features, to the extent that they represent abnormal ionization levels and gradients, will affect radio wave propagation in those regions; the former apparently is associated with the midday precipitation, while the latter represents depletion of ionization, presumably by transport into the magnetosphere.

On a smaller scale, electron density irregularities or 'spread' have been studied by various people. Petrie's work on the top-side ionosphere for low K_p conditions showed that the maximum occurrence region at a height of 1000 Km corresponded fairly well with the auroral oval, as illustrated in Figure I-12 (34). His findings have been extended by other workers (35), (36), (37), and the results would indicate that the high-latitude ionosphere, i.e., above about 55° geomagnetic, is very irregular a high percentage of the time, and shows scale sizes that range from $\sim$1 Km to $>$100 Km. The irregularities appear to be field aligned and can be described in terms of sheets or cylindrical ducts that are quite elongated, often extending from the F region up to satellite heights of several thousand kilometers. During the daytime the irregularities generally occur more frequently above the F-region peak than below it. At 1000 Km the distribution of the most intense spread is more restricted in latitude than near the F-region peak and appears to agree fairly well with the electron precipitation region, though some preliminary results would suggest a displacement of

several degrees, toward higher latitude in the day sector, and toward lower latitudes in the evening. Unfortunately the detailed studies of ionization transport associated with such irregularities are still very inadequate at all heights in the ionosphere. The scintillation results are, of course, relevant in this context, though there are problems in sorting out effects occurring over an extended height range in those data. The polar wind studies of Banks and Holzer (38), and others, are also very pertinent, as are the observations of Timleck and Nelms (39) of very low electron densities at times in the polar topside ionosphere.

As far as E-region effects are concerned the statistical data are less satisfactory. The sporadic-E phenomena in ionosonde data are not sufficiently homogeneous or extensive to provide a good synoptic pattern, though the average diurnal distribution at auroral latitudes has been determined for some types as shown in Figure I-13. Here the auroral sporadic E is shown in the upper frame, and in the lower frame, the low-altitude, diffuse sporadic E (40). The latter data are probably more dependent on the drizzle particle influx, with perhaps some influence from direct solar radiation, while the former apparently depend on the splash particle precipitation. Somewhat similar results have been obtained in the case of VHF radio aurora; here in Figure I-14 are shown the distribution of type A_2 data obtained by Vogan (41) as representative of the ionization irregularities in the E region associated with the sporadic particle influx or splashes. The more diffuse A_3 type of radio aurora have an occurrence pattern that seems to follow the drizzle precipitation, as shown in Figure I-15.

A serious impediment to the compilation of extensive statistics on E- and F-region ionization effects on radio propagation has been the lack of suitable criteria for intercomparing data taken at different locations under conditions of different observability factors, such as aspect angle, observing frequency, and equipment sensitivity. The height distribution for the irregularities has not been too well established as a consequence. The auroral sporadic E and many of the radio auroral results have been associated with ionization irregularities at a height of about 110 km, though in the latter data this may not represent a reliable observation in every case. There seems little doubt, however, that the splash precipitation produces irregularities principally in the E region, i.e., between 90 and 150 Km. The ionization irregularities observed below this height tend to be more continuous in character and can be used for ionospheric scatter communications in consequence (42). They apparently are associated with turbulence in the D and lower E regions and with the more energetic particle influx at the high latitudes.

Radio wave absorption effects occur mainly in the D-region, and are principally associated with the drizzle zone, as shown in Figure I-16 (43). However, the very intense nighttime splashes also show increased absorption effects; these tend to be much more short-lived, though the peak absorption in such events may exceed that in the forenoon hours. The other main absorption type is the polar-cap absorption (PCA) which follows certain large solar flares (44). The particles responsible are mainly protons with energies of the order of about 10 MeV; these precipitate more or less uniformly over the polar cap and penetrate down to the D region, producing only very minor effects at greater height. The resulting ionization is dependent on ion-chemical processes so that the free electron population, and hence the observed absorption, is controlled by direct solar illumination that can dissociate negative ions. Accordingly the sunlit D region produces much more absorption during a PCA event than does the nighttime D region. The typical PCA event has a duration of several days, during which the absorption rises rapidly to a maximum then slowly decays, with a diurnal or sunlight modulation superimposed. The lower-latitude limit for PCA is approximately that of the auroral zone, but this limit may move equatorward when a strong geomagnetic storm starts during the course of a PCA.

Ionization irregularities are not a very prominent feature of the D region, though short-term structure is observed on the energetic particle influx, and in the associated X-ray data. The A_3 radio aurora apparently indicates D-region structures, and some irregularities observed with ionosondes and designated as sporadic E may also extend into the D region, but for most propagation applications absorption is the main effect introduced by the ionization in this height region.

Regarding the interrelation between events in the different zones shown in Figure I-4, the sequential pattern is by no means completely determined. It appears that the noon precipitation is a fairly constant phenomenon with some modulation in number flux or energy flux, depending on solar-wind conditions. Apparently the magnetosphere is fed by magnetosheath material through the polar cusp region a high percentage of the time, so that this would seem to be the source of much of the F-region ionization and the ionization irregularities at this time of day.

The nighttime splash precipitation is a direct result of substorm generation in the magnetospheric tail and in the so-called plasma sheet in the tail. The particles precipitate directly into the nighttime ionosphere producing the various sporadic or short-lived effects. At the same time it appears that some portion of the precipitation goes into the trapped radiation belts and the drizzle zone shows a build up and decay of activity on a time scale rather longer than that of the substorm; these effects apparently occur at all longitudes to some extent but are most prominent in the late morning sector. Figure I-17 shows the average absorption in the morning drizzle zone relative to the substorm commencement time, and also a control curve showing the average morning absorption in the absence of substorms (45). These results show that the events in the drizzle zone are sequentially related to the substorms and the splash events.

6. CONCLUDING REMARKS

This paper has outlined the general precipitation pattern for auroral particles at high latitudes. The earlier pattern identified by Hartz and Brice has been revised somewhat using more extensive and more recent observations on a variety of aurorally-related phenomena. These additional data indicate that the midday portion of the auroral oval has properties distinctly different from the night portion, so that a three-zoned pattern would seem required to describe the auroral particles. The splash zone is mainly associated with the nighttime hours; it involves short term processes that are generally described as substorms, is located in or near the boundary between the open and closed field lines in the magnetospheric tail, and presumably is fed from the so-called plasma sheet and/or the immediately adjacent tail regions. The drizzle zone is mainly a morning or forenoon feature, though it may extend to other hours of the day; it appears to involve a later stage in the substorm, is associated with the trapped zone of particles in the

magnetosphere, and apparently constitutes the sink for such particles. The third zone is a daytime feature; it appears to be continuous or quasi-continuous in time rather than substorm related, and apparently represents the direct entry of solar wind (i.e. magnetosheath) plasma through the magnetospheric cusp regions.

It must be emphasized that the process of identifying these distinctive regions has smoothed out a lot of detail that was inherent in the original data. The emphasis has been placed on the dominant or most outstanding characteristics in each instance, so that the regions where the different zones overlap, or where two different phenomena occur simultaneously, are not represented too reliably and the final pattern is therefore somewhat idealized. Nevertheless, it should serve as a useful guide in sorting out the various effects of the high-latitude particle influx.

As already indicated, the three different zones have been identified with different probable source regions in the magnetosphere, though there is not yet agreement as to all the magnetospheric features. They also tend to be identified with ionization effects in three different height regions in the ionosphere, the D, E, and F regions, though the demarcation is not always clear cut.

The response of the F region to the soft particle influx is rather involved. There is a general increase in the ionization density, so that in a statistical sense this is a significant source of ionization for the high-latitude ionosphere. However, the increased ionization is accompanied by ionization redistribution, which depends on additional factors such as electron temperature, electric fields, and magnetospheric convection. As a consequence, the F region and most of the top-side ionosphere, extending to great heights, is characterized by ionization irregularities that are aligned with the geomagnetic field. Statistically the zone of maximum irregularity in the topside ionosphere seems to coincide with, or to be only slightly separated from the zone of particle influx.

The E-region effects seem to follow the substorm-induced nighttime splashes fairly well, though the continuity to the day side is not firmly established. This height region can support significant electric currents, or auroral electrojets, leading to distinctive magnetic effects. However, ionization redistribution is not a major factor, as it is in the F region, rather the ionization irregularities appear to be related to the scale of the particle splashes and to such in-situ processes as turbulence, plasma instabilities, and winds.

The D-region effects are associated with the most energetic components of the auroral particle influx; at night this is in short-lived sporadic events while in the late morning this is a much longer-lived influx or drizzle. This height region is also the only one that appears to be appreciably affected by PCA particles, though for that phenomenon the whole of the polar cap seems to show absorption effects that depend quantitatively on solar illumination and on ion-chemical processes. Ion chemistry probably also plays some role in auroral absorption, but the effects are much less obvious. Ionization irregularities also seem to be less important at these heights.

The radio propagation effects that are most relevant in the F region are refraction and scattering, in the E region, scattering and in the D region, absorption.

Finally, it is instructive to relate the foregoing to geographic coordinates. The general precipitation pattern for auroral particles illustrated in Figure I-4 is to be thought of as fixed in space with the earth rotating beneath it. An observer in the polar regions will then see different effects according to his location and local time. Figure I-18 shows this situation for the northern hemisphere for one time of day, namely for midnight over central Europe. The geographic regions where the various precipitation effects are expected have been indicated; the situation for any other time of day can be obtained by a relative rotation of the overlay on the map. It must be re-emphasized that this is an average picture, representative of all degrees of disturbance, and that the pattern for any particular time may depart significantly from it.

REFERENCES

1. Feldstein, Y.I., "Investigations of the Aurorae", Bulletin of the International Geophysical Year, 4, 61, 1960.

2. Feldstein, Y.I. and Solomatina, F.K., "Geographical Distribution of Aurorae in the Southern Hemisphere", J. Phys. Soc. Japan, 17, Supp. A-I, 223, 1962.

3. Feldstein, Y.I., "Peculiarities in the Auroral Distribution and Magnetic Disturbance Distribution in High Latitudes caused by the Asymmetrical Form of the Magnetosphere", Plan. Space Sci., 14, 121, 1966.

4. Hartz, T.R. and Brice, N.M., "The General Pattern of Auroral Particle Precipitation", Plan. Space Sci., 15, 301, 1967.

5. Lassen, K. "Polar Cap Emissions", Atmospheric Emissions, B.M. McCormac and A. Omholt, Van Nostrand Reinhold Co., New York, p. 63, 1969.

6. Starkov, G.V., "Auroral Heights in the Polar Cap", Geomag. Aeron. 8, 28, 1968.

7. Starkov, G.V. and Feldstein, Y.I., "Scheme of an Elementary Disturbance in Auroras on the Day Side of the Earth", Geomag. Aeron. 7, 294, 1967.

8. Akasofu, S.-I., "A Photographic Study of the Midday Aurora", Trans. Am. Geophys. Union, 51, 370, 1970.

9. Romick, G.J., "Photometric Measurements Across the Noon Sector of the Auroral Oval", Trans. Am. Geophys. Union, 51, 370, 1970.

10. Eather, R.H., "Latitudinal Distribution of Auroral and Airglow Emissions: The 'Soft' Auroral Zone", J. Geophys. Res., 74, 153, 1969.

11. Eather, R.H. and Mende, S.B., "High Latitude Particle Precipitation, and Source Regions in the Magnetosphere". Proceedings of Advanced Study Institute on Magnetosphere-Ionosphere Interactions, Dalseter, Norway, April 1971.

12. Buchan, J., Whalen, J.A. and Akasofu, S.-I., "On the Continuity of the Auroral Oval", J. Geophys. Res., 75, 7147, 1970.

13. Burch,J.L., "Low-Energy Electron Fluxes at Latitudes above the Auroral Zone", J. Geophys. Res., 73, 3585, 1968.

14. Hoffman, R.A. and Berko, F.W., "Primary Electron Influx to Dayside Auroral Oval", J. Geophys. Res., 76, 2967, 1971.

15. Johnson, R.G. and Sharp, R.D., "Satellite Measurements on Auroral Particle Fluxes", Atmospheric Emissions, B.M. McCormac and A. Omholt, Van Nostrand Reinhold Co., New York, p. 219, 1969.

16. Heikkila, W.J. and Winningham, J.D., "Penetration of Magnetosheath Plasma to Low Altitudes through the Dayside Magnetospheric Cusps", J. Geophys. Res., 76, 883, 1971.

17. Frank, L.A., "Plasma in the Earth's Polar Magnetosphere", J. Geophys. Res., 76, 5202, 1971.

18. Frank, L.A. and Ackerson, K.L., "Observations of Charged Particle Precipitation into the Auroral Zone", J. Geophys. Res., 76, 3612, 1971.

19. Gurnett, D.A., "A Satellite Study of VLF Hiss", J. Geophys. Res., 71, 5599, 1966.

20. Hughes, A.R.W. and Kaiser, T.R., "VLF Radio Emissions and the Aurora", The Radiating Atmosphere, B.M. McCormac, D. Reidel Publ. Co., Dordrecht-Holland, 1971.

21. Laaspere, T., Johnson, W.C., and Semprebon, L.C., "Observations of Auroral Hiss, LHR Noise, and Other Phenomena in the Frequency Range 20 Hz - 540 kHz on Ogo 6", J. Geophys. Res., 76, 4477, 1971.

22. Dunckel, N. and Helliwell, R A., "Whistler-Mode Emissions on the OGO 1 Satellite", J. Geophys. Res., 74, 6371, 1969.

23. Hartz, T.R., "Particle Precipitation Patterns", The Radiating Atmosphere, B.M. McCormac, D. Reidel Publ. Co., Dordrecht-Holland, 1971.

24. Barrington, R.E., Hartz, T.R. and Harvey, R.W., "Diurnal Distribution of ELF, VLF and LF Noise at High Latitudes as Observed by Alouette 2", J. Geophys. Res., 76, 5278, 1971.

25. Gurnett, D.A. and Frank, L.A., "VLF Hiss and Related Plasma Observations in the Polar Magnetosphere", J. Geophys. Res. (in press).

26. Mishin, V.M., Saifudinova, T.I. and Zhulin, I.A., "A Magnetosphere Model Based on Two Zones of Precipitating Energetic Particles", J. Geophys. Res., 75, 797, 1970.

27. Nishida, A., "Average Structure and Storm-Time Change of the Polar Topside Ionosphere at Sunspot Minimum", J. Geophys. Res., 72, 6051, 1967.

28. Andrews, M.K. and Thomas, J.O., "Electron Density Distribution above the Winter Pole", Nature, 221, 223, 1969.

29. Lebeau, A., "Sur L'Activité Magnétique Diurne Dans LesCalottes Polaires", Ann. Geophys. 21, 167, 1965.

30. Lassen, K. "Morning Discontinuity of the Auroral Precipitation Zone", Symposium on Aurora and Airglow, I.A.G.A., Moscow, August 1971.

31. Shepherd, G.G., Private Communication.

32. Sandford, B.P., "Aurora and Airglow Intensity Variations with Time and Magnetic Activity at Southern High Latitudes", J. Atmos. Terrest. Phys., 26, 749, 1964.

33. Nelms, G.L. and Lockwood, G.E.K., "Early Results from the Topside Sounder in the Alouette II Satellite", Space Research VII, Amsterdam, North Holland, 1967.

34. Petrie, L.E., "Preliminary Results on Mid and High Latitude Topside Spread F", Spread F and Its Effects on Radiowave Propagation and Communication, P. Newman, Technivision, Maidenhead, Engl., 1966.

35. Dyson, P.L., "Comparison of Irregular Features Appearing on Ionograms Recorded by Topside and Ground-Based Sounders", J. Atmos. Terrest. Phys., 29, 881, 1967.

36. Calvert, W. and Warnock, J.M., "Ionospheric Irregularities Observed by Topside Sounders", Proc. I.E.E.E., 57, 1019, 1969.

37. Dyson, P.L. and Zmuda, A.J., "Some Ionospheric Properties at 1000 Kilometers Altitude within and Near the Auroral Zone", J. Geophys. Res., 75, 1893, 1970.

38. Banks, P.M. and Holzer, T.E., "The Polar Wind", J. Geophys. Res., 73, 6846, 1968.

39. Timleck, P.L. and Nelms, G.L., "Electron Densities less than 100 Electron Cm^{-3} in the Topside Ionosphere", Proc. I.E.E.E., 57, 1164, 1969.

40. Olesen, J.K. and Wright, J.W., "The Relationship of Low-Height Ionosonde Echoes to Auroral-Zone Absorption and VHF D Scatter", J. Geophys. Res., 66, 1127, 1961.

41. Vogan, E.L., Private Communication.

42. Bailey, D.K., "Some Quantitative Aspects of Electron Precipitation in and Near the Auroral Zone", Reviews of Geophysics, 6, 289, 1968.

43. Hartz, T.R., Montbriand, L.E., and Vogan, E.L., "A Study of Auroral Absorption at 30 Mc/s", Can. Jour. Phys., 41, 581, 1963.

44. Reid, G.C., "Solar Cosmic Rays and the Ionosphere", Physics of the Earth's Upper Atmosphere, C.O. Hines, I. Paghis, T.R. Hartz, and J.A. Fejer, Prentice-Hall Inc., New Jersey, 1965.

45. Jelly, D.H. and Brice, N.M., "Changes in Van Allen Radiation Associated with Polar Substorms", J. Geophys. Res., 72, 5919, 1967.

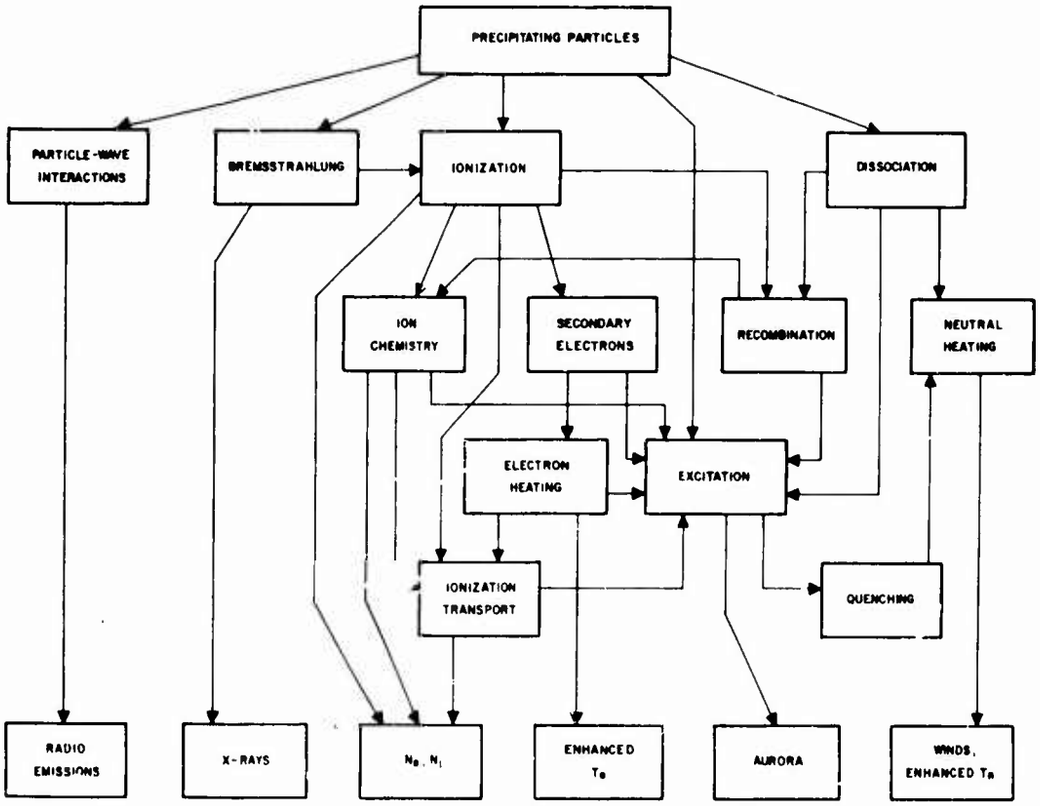

Fig.1-1 Schematic representation of upper-atmospheric processes resulting from the influx of energetic charged particles.

Fig.1-2 The location of the Auroral Zone in the northern hemisphere. The zone maximum, marked by the most intense shading, corresponds to regions where auroras are observed on more than 90% of the nights, the edges of the shaded region mark the half-maximum contour. (After Feldstein (1))

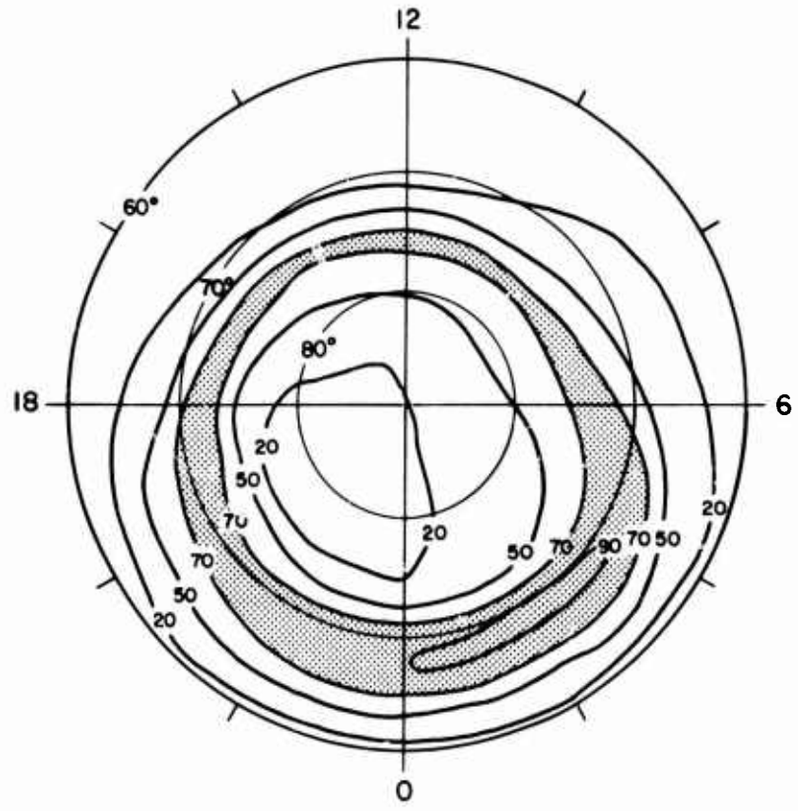

Fig. I-3 The percentage occurrence of zenithal aurora in all-sky-camera records, plotted as a function of geomagnetic latitude and geomagnetic local time. (After Feldstein (3))

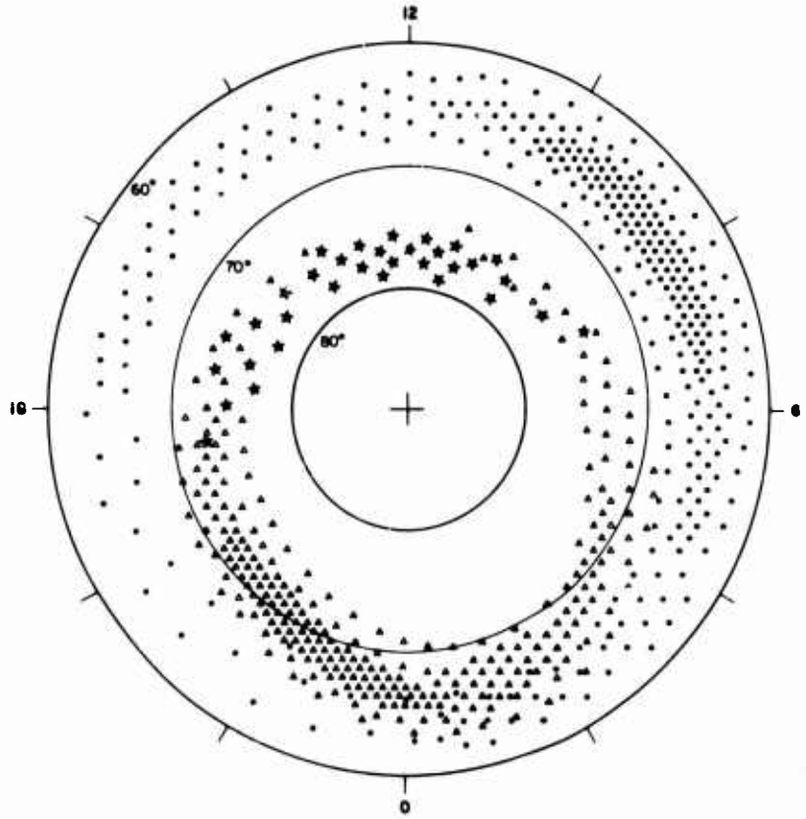

Fig. I-4 An idealized representation of the three-zoned auroral-particle precipitation pattern, plotted as a function of geomagnetic latitude and geomagnetic local time. The average flux is indicated very approximately by the density of symbols. The splash type of precipitation is represented by the triangles, the drizzle type by the dots, and the quasi-continuous inflow at midday by the stars.

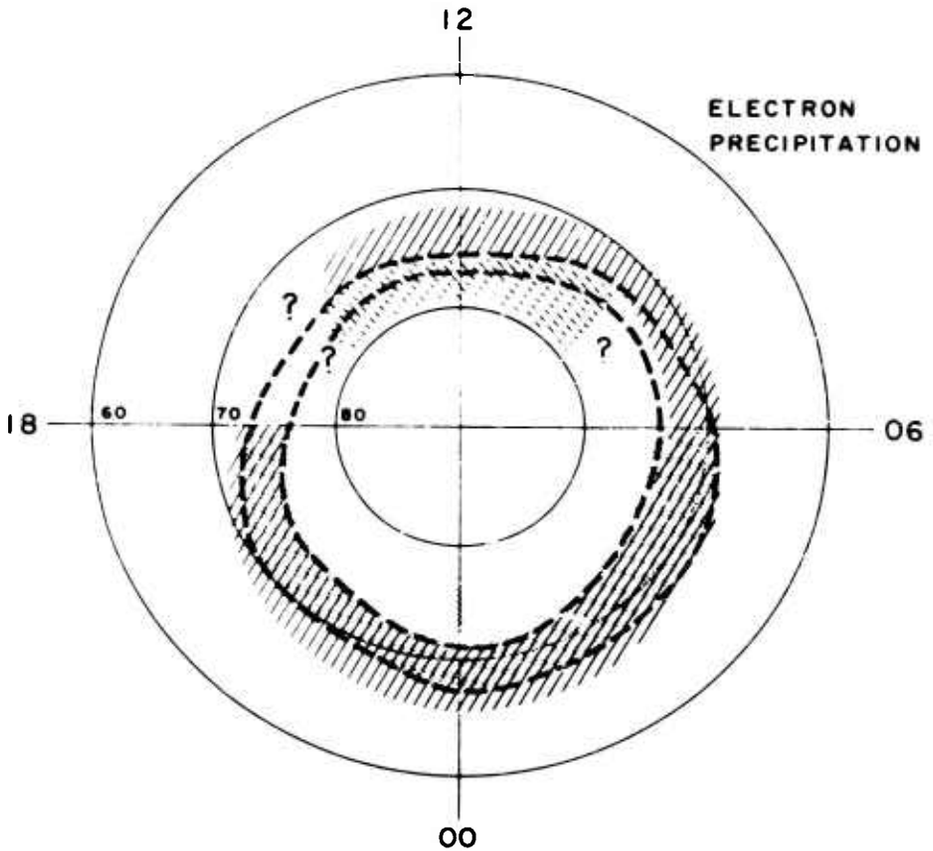

--- AURORAL OVAL, Q = 1

"AURORAL" (1 – 10 KEV) AND "HARD" DAYTIME PRECIPITATION

DAYSIDE SOFT (0.1 – 0.5 KEV) ZONE

NIGHTSIDE SOFT (0.5 – 2 KEV) ZONE

Fig. I-5 Precipitation pattern for electrons. (After Eather and Mende (11))

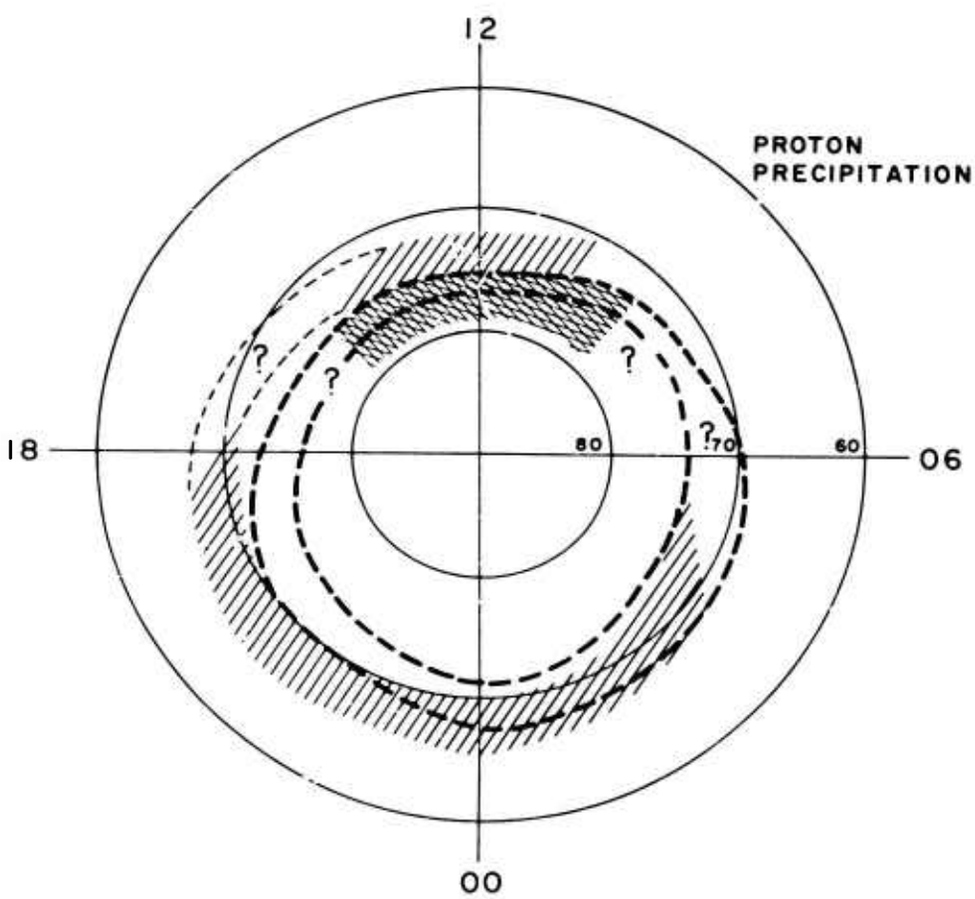

--- AURORAL OVAL, Q = 1

"AURORAL" (1 – 20 KEV) AND "HARD" DAYTIME PRECIPITATION

DAYSIDE SOFT (≤ 1 KEV) ZONE

Fig. I-6 Precipitation pattern for protons. (After Eather and Mende (11))

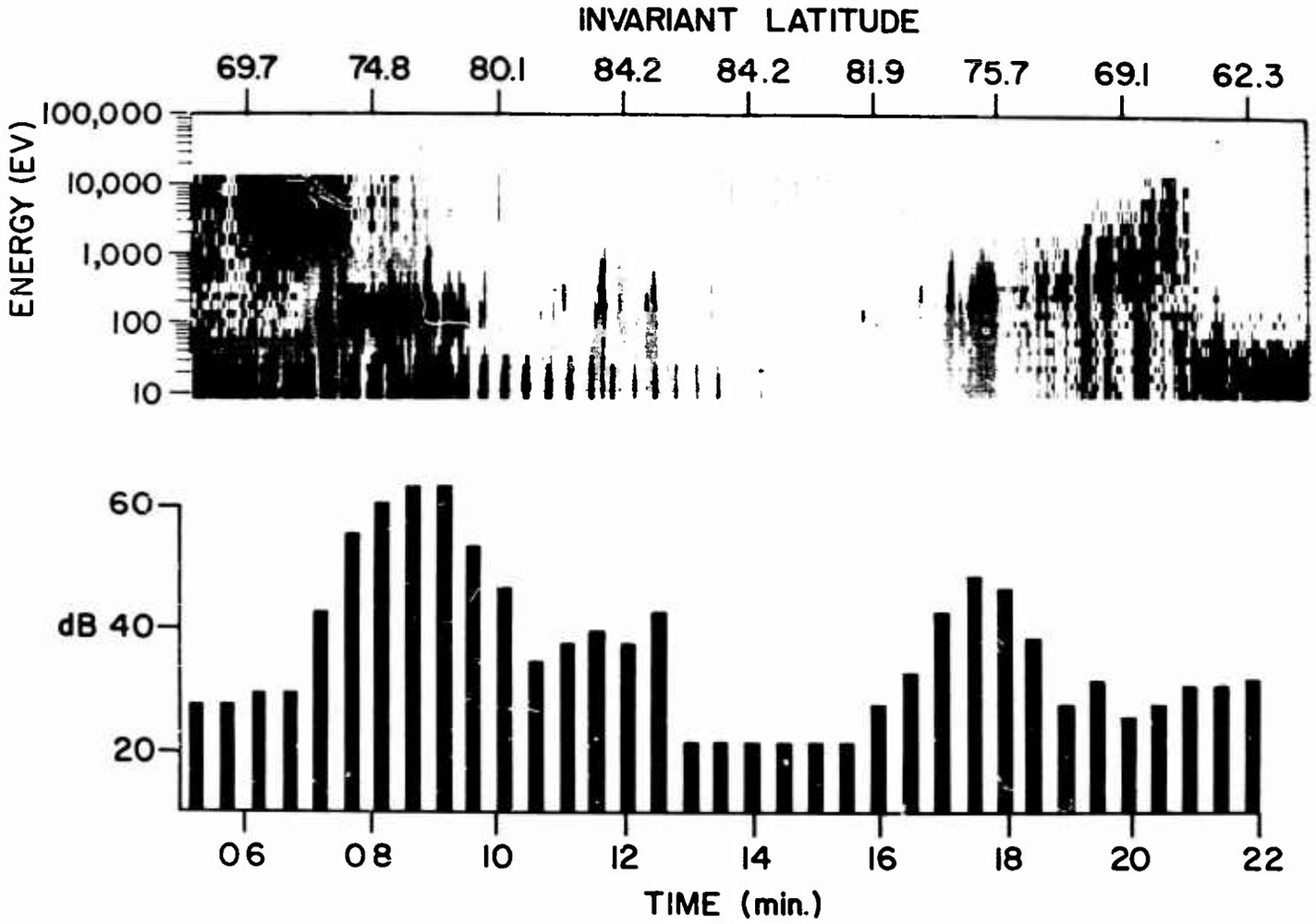

Fig I-7 (a) Electron data from the Soft Particle Spectrometer on ISIS-I obtained on Feb. 4, 1969, between 0203 and 0223 U.T. on a trans-polar pass from day to night, with the density of the trace for each spectral sweep modulated by the counting rate. (Courtesy of W.J. Heikkila and J.D. Winningham)

(b) The corresponding radio noise intensity at 0.2 MHz in decibels relative to the receiver threshold. (After Hartz (23))

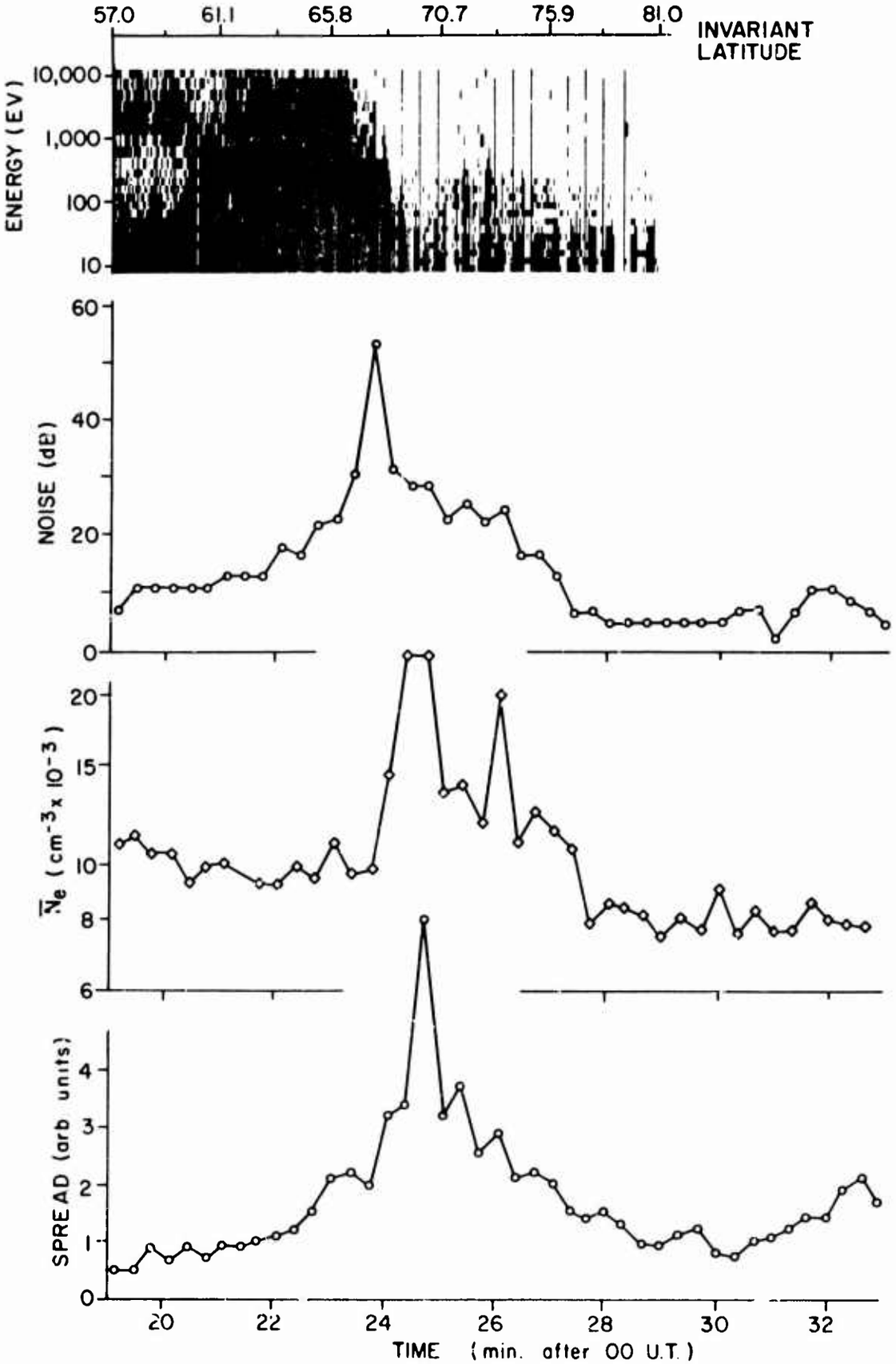

Fig 1-8 Intercomparison of data from the ISIS-I satellite taken on February 3, 1969; electron data from the Soft Particle Spectrometer (courtesy of W.I. Heikkila and J.D. Winningham), radio noise intensity at 200 kHz, the relative electron density at the satellite normalized to remove variations due to changes in height, and a measure of the irregularity of the local ionization or 'spread'.

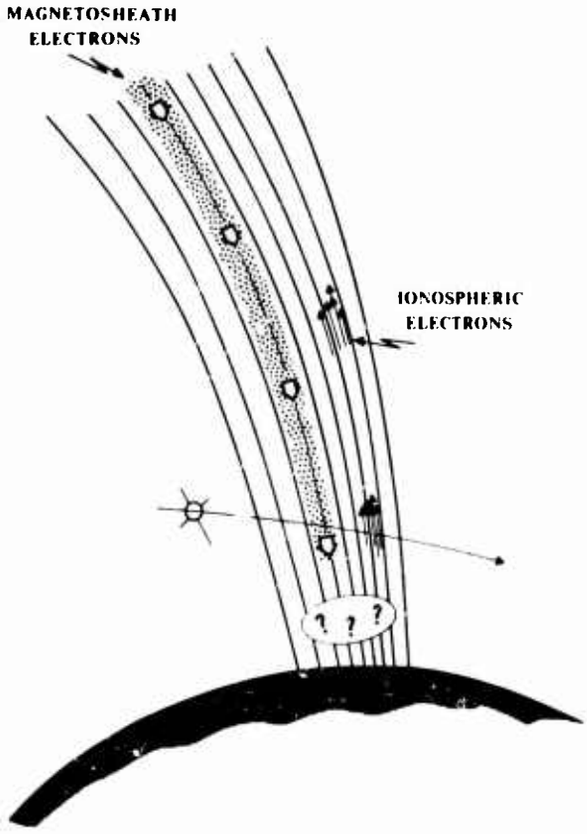

Fig. I-9 Illustrative model showing the midday precipitation region for soft electrons and their relationship to up-going ionospheric electrons and ionization irregularities.

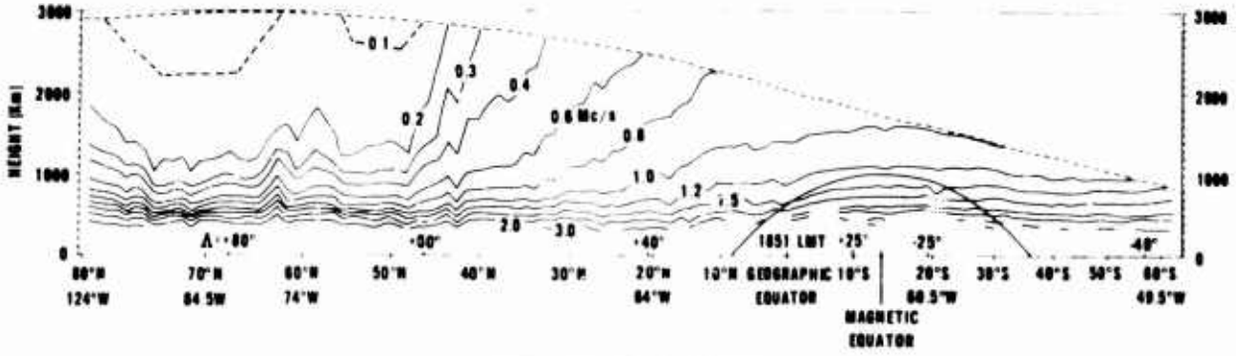

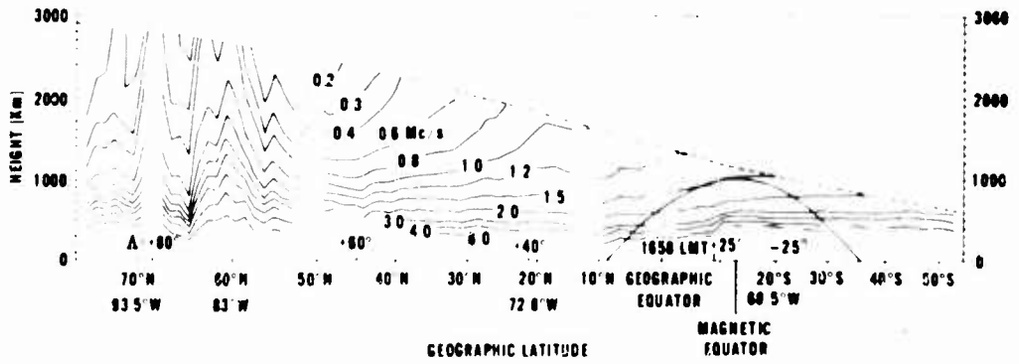

Fig I-10 Contours of constant plasma frequency as a function of height and geographic latitude determined from Alouette II sounder data. (After Nelms and Lockwood (33))

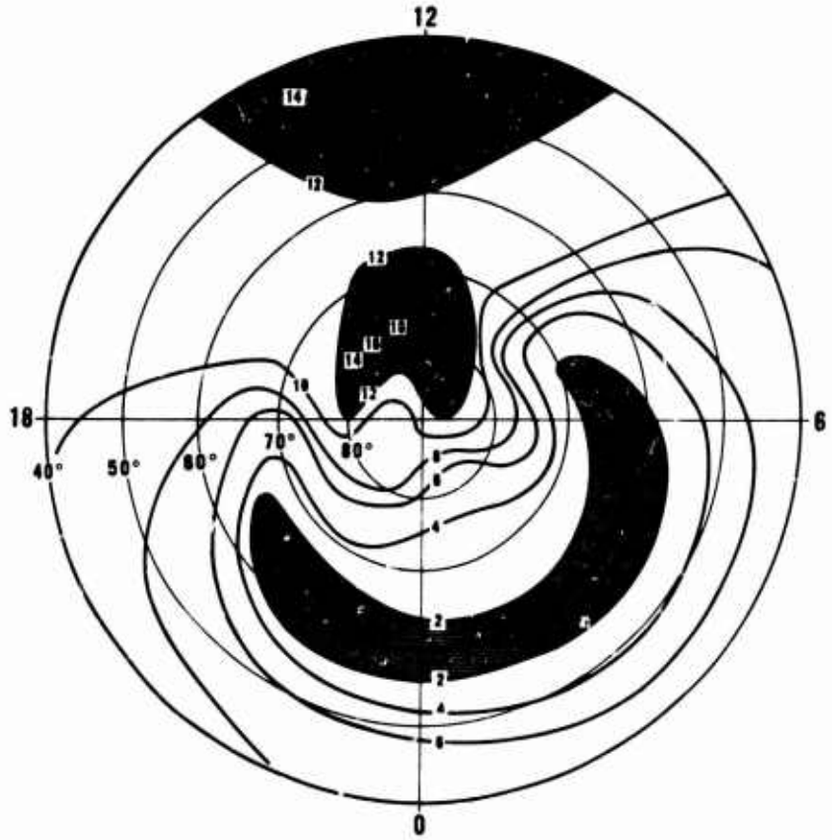

Fig.I-11 Distribution, in geomagnetic latitude and geomagnetic local time, of the average electron density in autumn for geomagnetically quiet intervals at a height of 950 Km. (After Nishida (27))

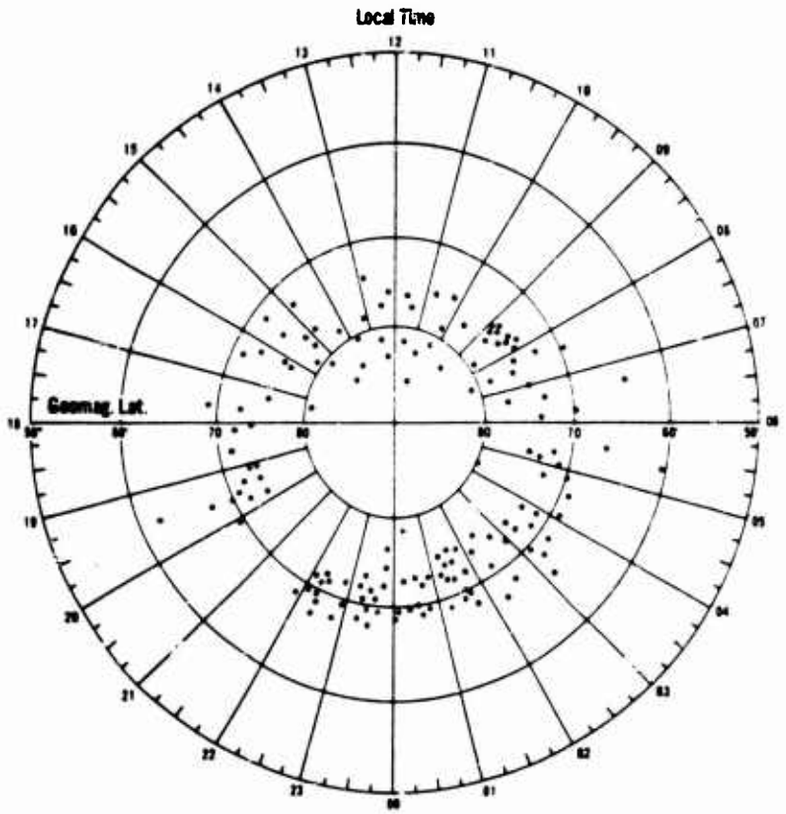

Fig.I-12 Distribution, in geomagnetic latitude and local time, of the maximum frequency range for the spread echoes observed with Alouette I at 1000 Km height, for Kp $\leq$ 2. (After Petrie (34))

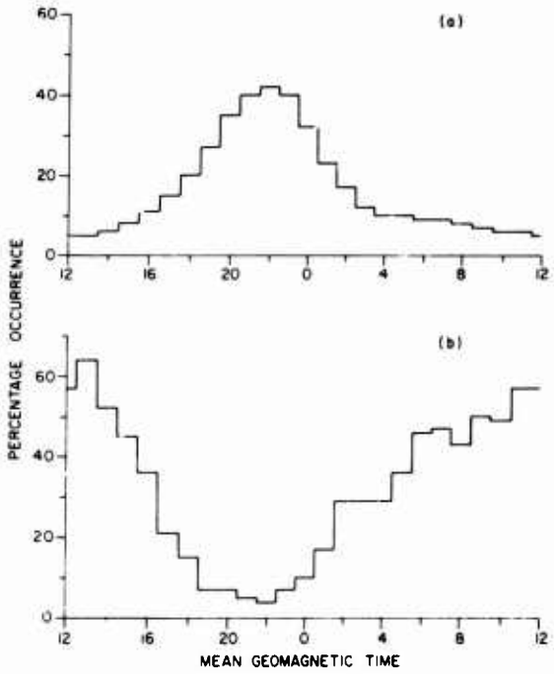

Fig. 1-13 The diurnal variation in the percentage occurrence of

(a) auroral sporadic-E echoes extending beyond 7 MHz on ionosonde records, averaged for the Pt. Barrow, Churchill and Ft. Chimo stations. (Courtesy of E.L. Hagg and D. Muldrew)

(b) low-altitude, diffuse sporadic E at Narssarssuak. (From Oleson and Wright (40))

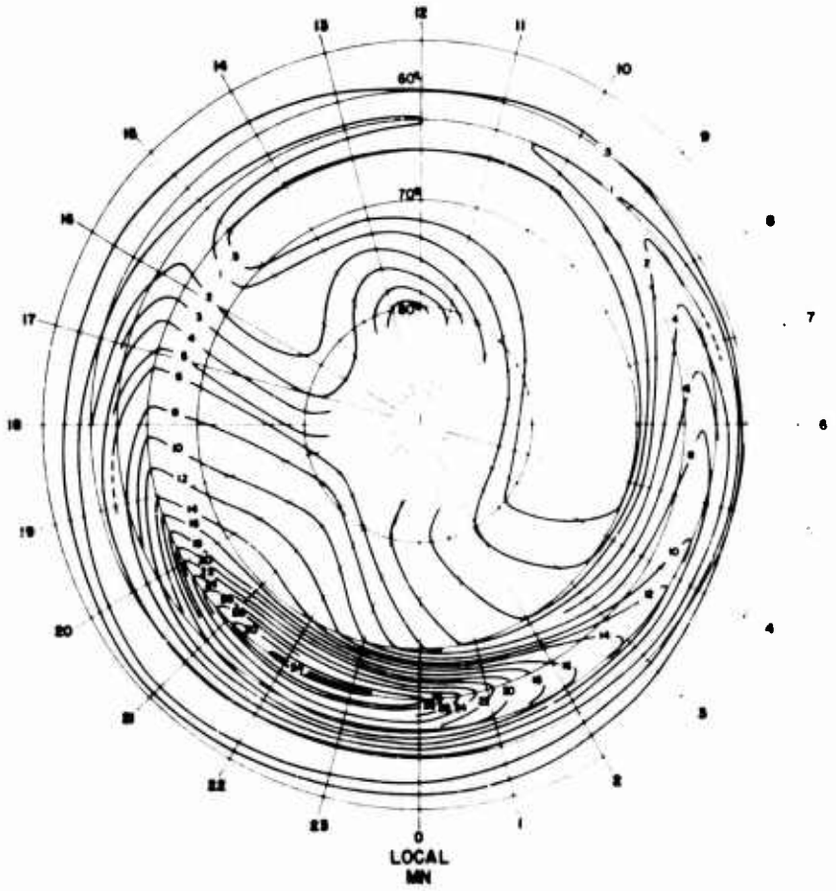

Fig 1-14 Percentage occurrence of A_2 radio aurora, plotted as a function of geomagnetic latitude and geomagnetic local time at the mid point of the propagation circuit. (Courtesy of E.L. Vogan)

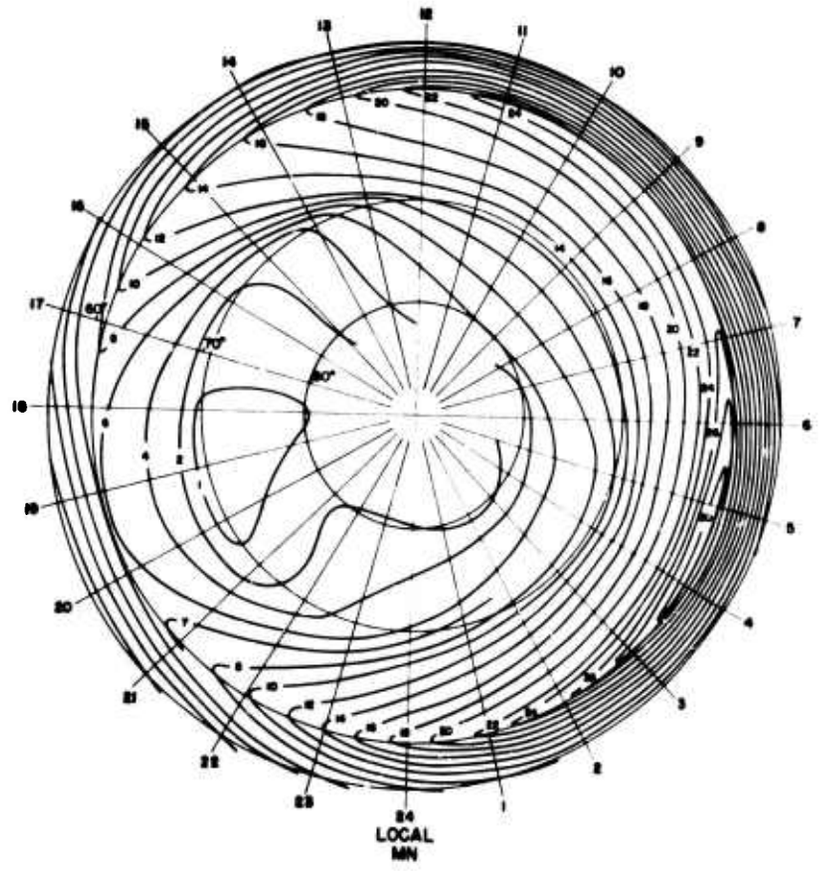

Fig.I-15 Percentage occurrence of A_4 radio aurora, plotted as a function of geomagnetic latitude and geomagnetic local time at the mid point of the propagation path. (Courtesy of E.L. Vogan)

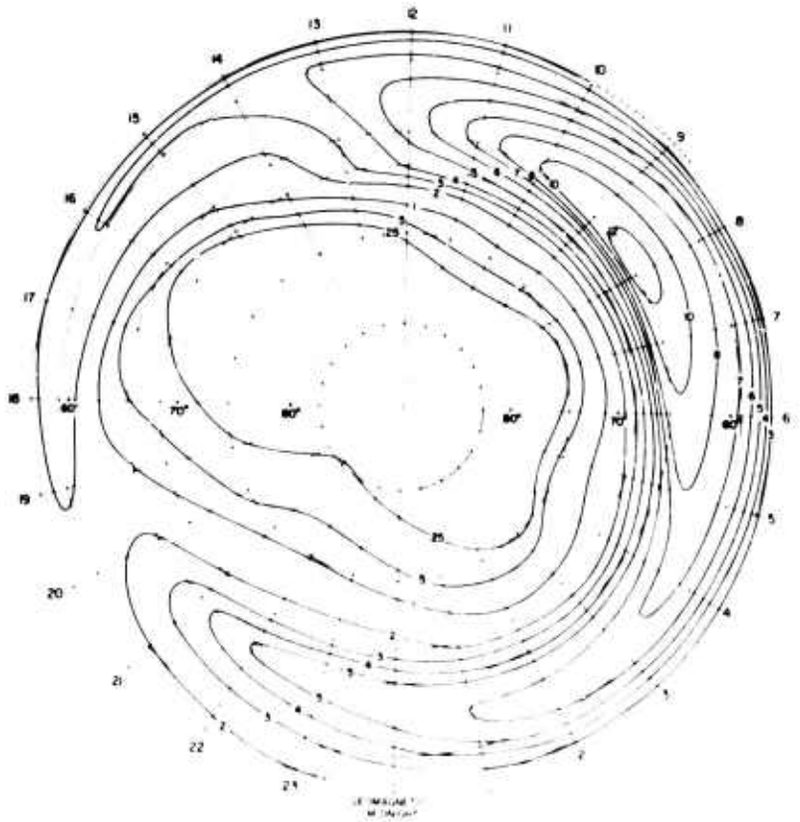

Fig I-16 Percentage of the time that auroral absorption of 1.0 db or more occurred at 30 MHz, plotted as a function of geomagnetic latitude and geomagnetic local time. (After Hartz et al (43))

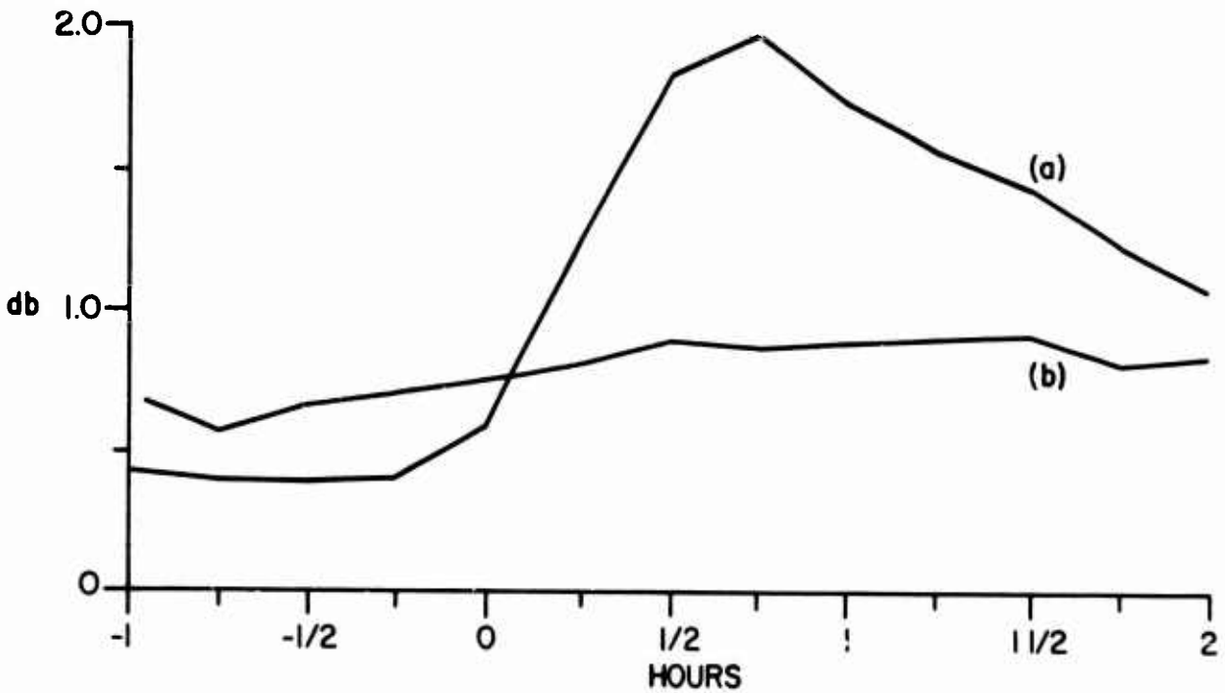

Fig. I-17 Comparison of average riometer absorption in the forenoon hours (at Kiruna) (a) associated with substorms identified in the night hours (at Churchill), and (b) for control times that were taken to be the same zero time on the day preceding each of the substorms included in (a). (after Jelly and Brice (45))

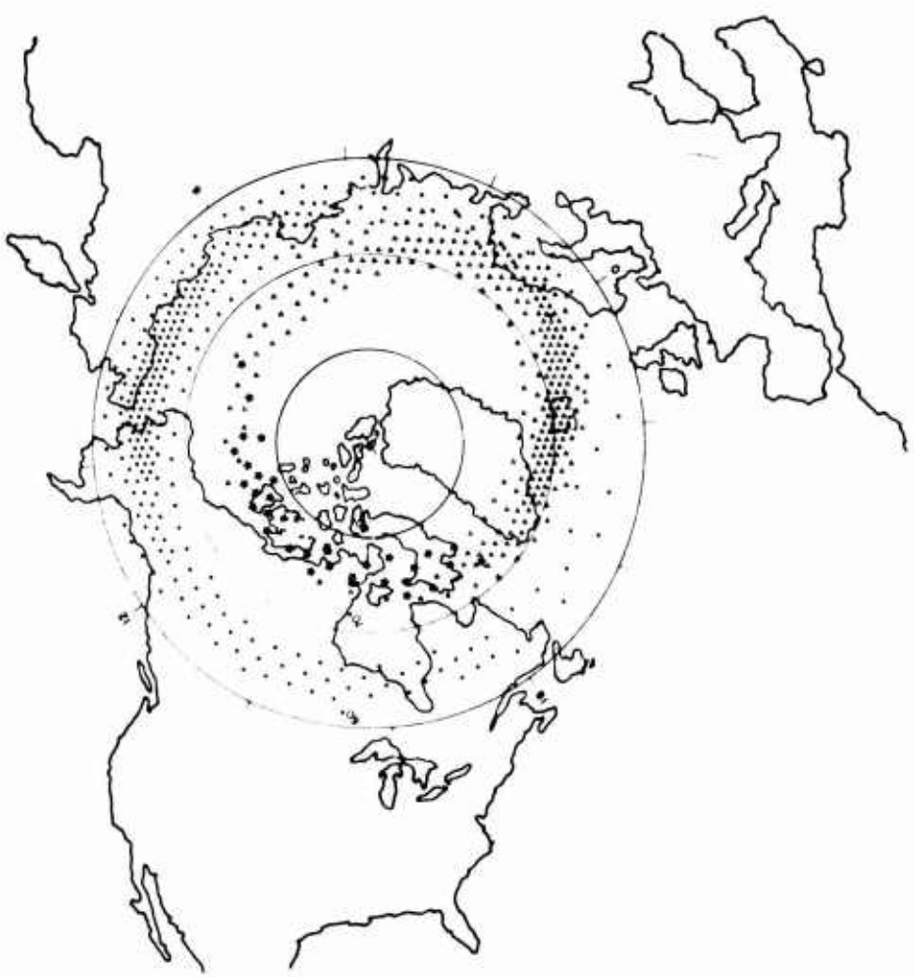

Fig. I-18 Relative location of particle precipitation pattern in geographic coordinates for one time of day, namely local midnight for Central Europe.

ON MODELLING THE ARCTIC IONOSPHERE

G.J. Gassmann
USAF Cambridge Research Laboratories
Bedford, Mass., 01730, USA

SUMMARY

The discovery of the auroral oval and the subsequently developed concepts of particle precipitation have provided new ordering schemes for arctic ionospheric data. The re-ordering of tabulated past data, mostly from the IGY, has already brought to light a number of arctic features which in former statistical treatments were barely apparent or completely smeared out. Those features are: the absorption zone, the belts of E_s, the F-layer polar ring and the main trough. The dependences of these features on the parameters UT, Season, Sunspot number and Kp are now to a varying degree established.

Besides these more or less statistical data recent airborne and satellite measurements have provided a number of cross-sections from which parts of the arctic ionosphere can be described in individual quasi-instantaneous pictures. Those three-dimensional electron density profiles show the true shapes of those features mentioned and others, in particular the frequent occurrence of steep tilts against the horizontal. Comparison of equivalent data from different times shows large variations which explain why data averaging may completely obscur many ionospheric features which are important to HF and VHF propagation. This fact also demonstrates that average propagation conditions cannot be derived from average ionospheric conditions. One important new parameter which appears to control many features is the substorm-time and some pertinent correlations have already been established.

It appears that the prediction of the arctic ionosphere in the manner and with the accuracy as it is being accomplished for moderate latitudes is not yet possible. However, from the already established general patterns it seems feasible to provide an hourly updated and fairly accurate description by real-time processing of data from a few observing stations. A number of suitable observing techniques have emerged.

1. INTRODUCTION

The special nature of the arctic ionosphere had been suspected since the early days of radio when transmissions across the North Pole were accomplished even during the arctic winter. Within the last 22 years vertical soundings from ice-islands and airborne soundings have shown that even during long lasting absence of solar illumination an ionospheric F-layer exists, often accompanied by an E- and a D-layer. One feature was always recognized, the very high variability of the arctic ionosphere, its seemingly complex nature and its sporadic behavior defying prediction. Systematic investigations although conducted at times intensely by various groups, were always hampered by the scarcity of observing stations. The efforts to establish the morphology of the arctic ionosphere, to understand it or to predict it were in general unsuccessful. Even with the advent of satellites this situation started to improve only very slowly. In retrospect, this was due to the satellites main handicap, namely its orbit's confinement to particular local times. The real breakthrough came from systematic ground observations of the visible aurora during the IGY and the subsequent development of the concept of the "auroral oval" by Russian scientists. This concept inspired a whole series of re-examinations of old data and of new observations. Suddenly a new ordering scheme for arctic data was available and has since proven its high usefulness in interpreting both satellite and ground based observations. New aircraft flights carrying ionospheric sounding and optical equipment and operating in the arctic under the guiding concept of the auroral oval produced a number of new insights of fundamental importance. The time has now arrived that one can start to arrange all known information on the arctic ionosphere, although still fragmentary, into a cohesive and consistent picture. This can serve as a realistic model for assessing HF and radar propagation conditions in the Arctic. At the same time such a model could serve as a working concept for further research.

2. THE CONCEPTS USED IN DATA ANALYSIS

The most useful concept for ordering arctic observations has been that of the "Auroral Oval" (Feldstein and Starkov, 1967). Although its present definition might be modified and improved during the coming years this concept has brought a high degree of order into past optical and ionospheric data and has inspired systematic new observations. Gone is now the "auroral zone" and gone are now the "spirals" along which the aurora, sporadic E and other phenomena supposedly occurred. Instead, those phenomena can now be described as fixed patterns in a map-like display using the horizontal coordinates CGL/CGT (Corrected geomagnetic latitude/corrected geomagnetic time) after Hultquist (1958) and Hakura (1965). The coordinate systems orientation is fixed with the sun, while the earth rotates relatively to it. At present this coordinate system, in which the original Feldstein oval concept is defined, appears satisfactory and sufficiently precise. There exists improvements and adjustments on the corrected geomagnetic coordinate system by Gustafsson (1970); and there is also the "invariant latitude". Those above differ from the original CGL/CGT system by not more than one degree in some locations and therefore may also be used for describing arctic phenomena, in view of the limited accuracy presently achievable. The problem which geomagnetic coordinate is most appropriate for describing arctic atmospheric phenomena will arise when the observations become more sophisticated with respect to absolute location. At present, we continue to use the original CGL/CGT coordinate system as tabulated by Hakura (1965), especially since the various auroral ovals in dependence of the parameter Q have been defined in this coordinate system. Details of these facts have been reviewed in connection with the auroral oval plotter and nomograph by Whalen (1970 a).

The shape of the auroral oval is related to the geomagnetic activity and has been defined by Feldstein and Starkov (1967) as a function of the parameter Q. Their definition of Q although following that of Bartels is specially tailored. The value of Q for a particular (15 minute) time interval had been derived

from those magnetograms taken at locations which happened to be situated (at a particular UT) in the night sector of the auroral oval, that is near magnetic midnight ±3 hours and at corrected geomagnetic latitudes from 63° to 72°. Since the value of Q, so defined, is not readily available we have tentatively substituted the value of Kp and found this a useful procedure to relate experimental data to one of Feldstein's ovals. It is likely that eventually the parameters Q or Kp for the purpose of defining arctic atmospheric phenomena will be abandoned in favor of parameters such as the solar wind vector and the tilt angle of the earth's magnetic axis.

One other important phenomenon for ordering arctic observations is now the "substorm" and this requires the introduction of "substorm time". This implies a determination of the time zero when a substorm starts and involves the subsequent accounting of time in minutes for a period of about two hours. Although a wealth of information as to the visual phenomena and their correlation to processes in the magnetosphere is known (Akasofu, 1968), the morphology of ionospheric features during substorms has only recently begun to emerge.

A certain amount of data ordering has been and will be achieved from the assumption that some arctic and antarctic effects are magnetically conjugate. However, care is required in the meaning of conjugacy. Although cases of simultaneous conjugacy of auroral arcs have been confirmed, most other conjugacies do not occur simultaneously; that means the phenomena are symmetrical in magnetic coordinates but unsymmetrical in time. It is for example known (and indeed not surprising) that in the Arctic and Antarctic similar patterns occur at UT - hours $\frac{1}{2}$ day apart and in months $\frac{1}{2}$ year apart (Pike, 1971 a).

3. THE PLAN FOR AN ARCTIC IONOSPHERE MODEL

a. The meaning of the word model in this context is to serve the purposes of operational long range radio and radar circuits. The model in this definition does not include minute details of high spatial resolution, which are beyond potential predictability.

The model should be a dynamic model in that it should specify all variations in time and space which hopefully may be identifyable and potentially predictable. These aims for a dynamic model and the particular conditions in the Arctic lead to the term "quasi-instantaneous model" as a building block. In view of the great variability of the arctic ionosphere it is clear from the beginning that any averaging which smoothes out large-scale irregularities (associated with large tilts against the horizontal) must be avoided. This is so even for the case that only average propagation conditions shall be derived from the model, say for example for the design of a communication or HF radar system. This follows from the nature of ionospheric radio propagation in which the statistics of the propagation conditions have a complex and very non-linear relation to the statistics of the ionosphere. Consequently, an averaged ionosphere does not allow to compute the average propagation conditions. For this and all other cases, where an assessment or a computation of the propagation conditions is required an instantaneous picture of the arctic ionosphere is desirable.

Modelling of the arctic ionosphere must therefore strive to provide snapshots as close to reality as to avoid a damaging smear effect. In practice, this requirement for a "quasi-instantaneous model" implies that its variations and statistics must be built-in. Such model can describe one instant ±10 minutes (shorter periods might have to be considered) and should contain the essentials for long-range propagation. Its spatial resolution in the horizontal plane aims for an absolute accuracy of ±100 km in CGL/CGT coordinates. Higher relative accuracy to a particular reference point (see anchor points below) can be achieved if desired. Thus the modelling of the arctic ionosphere will consist of a variety of individual "quasi-instantaneous models" specified below. The said variety will contain the statistical behavior.

b. Characteristics to be specified:

(1) Plasma frequency in MHz,
(2) Absorption in dB, MHz^2,
(3) Sporadic E in fE_s (MHz),
(4) Small scale irregularities, non-deterministic, causing scatter, units to be decided on.

Most of the above will be specified in two separate parts. One part which originates from the presence of solar radiation, if any, will be specified in geographical coordinates versus UT (see d. (1) below). The other part originating from the specific processes in the Arctic will be specified in CGL/CGT coordinates. Transformation from one coordinate system to the other and vice versa is being prepared as a computer program. The two parts above are defined in such a way that their combined effect can be computed in a simple manner. In case of the E-layer (in which the recombination rate goes linear with the square of the electron densities) the resulting total equilibrium electron density will be the square root of the sum of the two electron densities squared. In case of the F-layer above 250 km where the recombination rate goes linear with the electron density the two electron densities will be simply added.

c. Coordinates (and desirable incremental ranges):

(1) CGL (Corrected geomagnetic latitude) from 60° to 90° continuous
(2) Height from 0 to 1000 km continuous
(3) CGT (Corrected geomagnetic time) from 00 to 24 in 2 hour increments

Number of Increments: 12

d. Controlling parameters (and desirable incremental ranges):

(1) UT for specifying solar controlled part:
from 00 to 24 in 1 hour increments (24)
(2) UT for specifying arctic part:
(00-12) and (12-24), Number of Increments: 2

(3) Kp:
(0-2^+) (3^--4^+) (5^--7^+) (8^--9^+), Number of Increments: 2

(4) Sunspot Number:
(0-80) (80-150) (150-200), Number of Increments: 3

(5) Season:
(Nov Dec Jan Feb) (Mar Apr Sep Oct) (May Jun Jul Aug) Number of Increments: 3

(6) Substorm Time:
(0-20) (20-40) (40-60) (60-80) Minutes Number of Increments: 4

(7) Others, effect not yet identified (siderial time, solar wind speed, interplanetary magnetic field vector, etc.) Number of Increments: ?

e. Model Diversification:

Omitting the last item d. (7) above the number of desirable two-dimensional vertical profiles (presenting one or more characteristics (see 1.) versus CGL and height) will be 3,460 or larger, assuming that the variation due to parameter d. (1) will be defined separately as a routine modification (24 fold) to the 3,460 profiles. With this 24 fold modification the end product of this model will consist of 82,800 individual meridional cross-sections across the magnetic pole.

In contrast to this desirable variety, the material presently evaluated for the model is less diversified. In the presently existing fragments of the model a number of parameter ranges are lumped together.

f. Error Marks:

(1) Uncertainty (limits of confidence) of each part of the model due to insufficient statistics, bias, etc. should be expressed by $\pm$ marks, MHz values for example by $\pm$%, magnetic latitude values by $\pm$ degrees. Although at present wide limits of confidence must be attached to some model features it it important to state that the actual deviations show a high spatial correlation along constant CGL for all CGTs. This becomes important for real-time specification using anchor points (see below).

(2) Fluctuations, usually occurring within 20 minutes about the model due to unidentifiable and random causes should be expressed as RMS value. Those fluctuations occur in cells of all sizes, most notorious are those of medium scale having linear dimensions of up to 1000 km.

If numerical error marks for either (1) or (2) or both cannot be given, an estimate of the accuracy and the statistical significance of each statement defining part of the model should be added as verbal addendum.

(3) Anchor points. The possibility to reduce the uncertainty under (1) by defining one or more anchor points within the synoptic maps at which the uncertainty would be zero will be considered. This could be achieved by real-time measurements from monitor stations. In this case the uncertainty at points removed from the anchor points will be greatly reduced. The feasibility of monitoring certain features of the arctic ionosphere has been demonstrated in a variety of cases.

4. METHODOLOGY

The basic situation in producing an arctic ionosphere model is that the information available is of a large variety; each item being fragmentary in itself is however interrelated to others. Besides ionospheric vertical soundings there are oblique and backscatter soundings, topside soundings, riometer and scintillation records, optical emission recordings in the visible and IR range, spectrum-, flux- and pitch angle - measurements of precipitating or trapped particles, rocket observations, magnetometer recordings on ground and in rockets and satellites, etc.

In this situation a word on statistical data evaluation is in order. The essential characteristic of the model we aim for is to use terms of description which are as deterministic as possible. If a statistical description of some parameter dependencies must be substituted because of lack of better information then it will be most useful if the quasi-instantaneous cross-sections (acc. to 3. e. totaling 3460) be grouped into a number of types. This procedure allows a description of the statistical distribution of those types and prevents a smear out of the physical features. The data evaluation must therefore proceed by identifying the correlations of the various dependencies and by trying to arrive at information from which quasi-instantaneous pictures or models can be assembled. Without establishing the various cross-correlations the statistics of single characteristic values, such as foF2 at one location, are not useful. The completed model, of course, will show certain statistics of its own; but those will be statistics of more complex features such as the location and steepness of the "plasma ring" (see under 5.). Accordingly, any trend analysis of data from a single station or satellite is often meaningless in the Arctic; instead, trend analysis must be applied to features of higher complexity and must therefore be preceeded by a data analysis designed to derive the behavior of the said feature.

The necessity to assemble single quasi-instantaneous models (being the building blocks of the whole model) from fragments of information makes it mandatory to utilize inference as much as possible, even up to the point of speculation. Information on electron density, the basic characteristic of the model, can indeed be inferred from satellite data, optical data and from other types of data with a varying level of confidence. Almost none of the inferences is completely safe since part of the necessary information is usually missing. For example, for precipitation flux data either the spectrum or the pitch angle distribution may be poorly known; in case of air glow data the height distribution of the emission is often known only with a wide margin of uncertainty. Thus, the assembly of the model is a trial and error method in which progress is measured in terms of internal consistency.

5. NARRATIVE OF MODEL INGREDIENTS

a. Sporadic E

The presence of a certain type of E_s, often classified as E_{ss}, in close correlation with the occurrence of discrete auroral arcs had been noticed for many years. Airborne investigations have shown that E_{ss} occurs in the form of a narrow band stretching approximately east-west; its latitude of occurrence is indeed close to the location of a discrete arc; however, in the case of a moving arc the spatial correlation is best, almost one, with a latitude where the auroral arc spent most of its time during the preceeding 20 minutes. The height of occurrence is from 110 to 140 km. Oblique E_{ss}-traces occur on arctic ionograms up to virtual heights of several hundred km. This indicates a backscatter mechanism from irregularities and excludes a wind-shear-produced horizontal discontinuity which would not allow backscattering other than in the vertical direction.

The statistics of occurrence have been extracted from IGY data and were correlated with those of the visible aurora as documented in Feldstein's ovals (Pittenger et al., 1971). For this purpose the published E_s - data were replotted in CGL/CGT coordinates, whenever possible, and resulted in a variety of patterns depending on magnetic activity. An example is shown in Figure 1 which shows the occurrence of E_s for moderate magnetic activity and for two threshold values of fE_s. The patterns, besides following closely the shape of the Feldstein oval (for Q=3) shows, in addition, a large enhancement of occurrence in the sector from 19 to 01 CGT. It is known that most auroral sub-storms commence in that sector.

b. Night E

This type of E-layer, classified as E_a and also observed as such for many years, has now been shown to have a distinct correlation to the auroral oval. This statement resulted solely from airborne measurements and was first obtained in the noon sector (Whalen et al., 1971). The measurements now have been extended to other sectors (see Wagner and Pike in this Volume). Figure 2 shows the extent of occurrence of E_a for moderate magnetic activity and the spatial relation to the auroral oval. The statement on its probability of occurrence is still of a statistical nature as in that of the oval (75% of time). This layer has a regular critical frequency which during the arctic winter ranges between 2 and 3 MHz. During sunlit periods it shows up as a small enhancement (0.3 MHz) of the regular solar produced E-layer. Its height $h'E_a$ is between 120 and 140 km. At its northern edge the night E-layer terminates at a latitude where the airglow at 6300Å has maximum intensity and where visible discrete aurora and E_s appears most of the time. The night E-layer produces in ionograms most of the time a trace spread in frequency indicating that it is interspersed by irregularities.

c. HF-Absorption

The general pattern of HF absorption is shown in Figure 2 as marked by D_d (>200 dB.MHz^2). The value is for night conditions; it is normalized for 1 MHz by assuming a frequency dependence $1/f^2$. This assumption, although known to be only of approximate validity, is good enough at the presently achievable accuracy. A number of details are known how this pattern may change with season and in that part of the Arctic which is illuminated by the sun. The main sources for this information are: Hook (1968), Zhulina (1969), Berkey et al. (1971) and Berkey priv. comm. (1971). The results of Gorbushina (1970) although of considerable interest are not yet included. It is also known that in the sector 19 to 01 CG very strong but short living bursts of absorption occur when substorms are in progress, (marked D_s). The information of substorm absorption morphology is contained in the results by Fritz (1968), Hartz and Brice (1967), Berkey et al. (1971), Hargreaves (1969) and Jelly (1969).

d. The F-layer

The arctic F-layer undergoes the largest known day to day variations of any layer, but the controlling parameters are poorly known so far. Nevertheless, the following important features have now been firmly established. The data sources are from our own observations mostly by aircraft, and the results from Sato and Colin (1969), Heikkila and Winningham (1971), Frank and Ackerson (1971), Thomas and Andrews (1968), Petrie (1966) and Burch (1968). North of about 60° CGL is a sometimes drastic decrease of ionization, the "trough", stretching east-west and noticeable most of the time. This southern edge of the trough is assumed, for the purpose of the model, as being identical with the northern edge of the plasmasphere (P in Figure 2). The position of the plasmapause is assumed to follow that described by Carpenter (1966). For the position and morphology of the trough our observations have been combined with the results by Muldrew (1965) and by Nishida (1967). The northern edge of the trough is located at a latitude within the auroral oval. The electron density contour lines have steep slopes at both edges of the trough and are such that they give rise to oblique radio sounding reflections up to 60° off the vertical. In northerly direction the trough is terminated by the presence of a ring of enhanced ionization ("plasma ring" or "irregularity zone", F in Figure 2) which surrounds the magnetic pole and leaves a circular area of lower ionization ("polar cavity") (Pike, 1971b). The ring of enhanced ionization is heavily interspersed with irregularities. These produce a peculiar and long known type of "spread" on ionograms which allows to infer that the spread is produced by backscatter of non-vertical rays from field aligned columns embedded in the F-layer (Gassmann, 1957). Figure 3 shows the F-layer features for two different UT's 12 hours apart. There is a UT dependence of the arctic (and antarctic) F-layer which had already been noticed from IGY data of the Antarctic (Pike, 1970) and which shows in the Arctic at 18:00 UT a fully developed "plasma ring". In the example shown it has been attempted to arrive at some statement on both the uncertainty of the model and the fluctuations about the model. This assessment, indicated in the figure caption, appears poor in content and meager in extent. Improvement however is possible only after collection and analysis of a larger data base.

Figure 4 shows a snapshot of the arctic ionosphere in the form of a vertical cross-section. Although the same uncertainties and fluctuations apply as indicated above the general character of the picture is genuine and typical. It shows the occurrence of large tilts of the refracting layers against the horizontal. This fact together with the map of figure 3 makes it obvious that any detailed assessment of HF and VHF wave propagation in the arctic cannot be accomplished without a versatile three-dimensional ray tracing computer program.

6. REAL-TIME SPECIFICATION AND PREDICTIONS

Since not all controlling parameters have been identified which are associated with large observable variations the arctic ionosphere cannot yet be predicted. Neither the particular size of the auroral oval follows clearly from magnetic variations nor can other fluctuations be correlated clearly with precursors observable somewhere else. An easier task is the specification in real-time. The model under development is to a great deal based on and tied to the nine sizes of auroral ovals for Q from 0 to 8 as listed and plotted by Whalen, 1970. The ionosphere defined by the model is fixed as soon as the particular reference auroral oval is known. This seems possible. It has been possible to identify by HF-backscatter soundings the edges of the trough from large distances. In addition the latitude of Es could be determined by oblique soundings from a distance up to 800 km. Several existing and new observatories including one to be established by us at Goose Bay are available for this purpose. The latter station will include Loran A recordings which have proven to be useful to determine the latitude of absorption. This station will also facilitate the determination of another F-layer feature not yet mentioned, the scintillation boundary (see J. Aarons, this Volume). At this time it is not resolved why this boundary does not coincide with the southern edge of the irregularity zone (see 5.d.). The location of the auroral electrojet, which in the present model is assumed being identical to the location of discrete auroral arcs can be inferred from magnetometer stations arranged in a chain, of which two exist in North America. Certain satellite flux data and topside soundings are available from which the instantaneous latitude of the "plasma ring" and of the "trough" along a particular orbit can be obtained. That it is hoped and assumed that the entire arctic picture can be inferred from those few real-time observations, appears justified in view of the high consistency of the model developed so far. The model does not yet deal with very disturbed conditions. It also has not yet been refined to include detailed behavior during substorms.

ACKNOWLEDGEMENTS

The development of an arctic ionosphere model which as outlined here is a continuing effort to which my colleagues J. Buchau, C.P. Pike, R.A. Wagner and J.A. Whalen have significantly contributed and continue to do so. Highly competent technical help in airborne data collection was due to R. Gowell, J. Waaramaa, G. MacNeil, J. Smith and J. Doody. The operations were skillfully controlled by T. Sizoo and E. Pittenger.

LIST OF REFERENCES

1. Feldstein, Y.I. and Starkov, G.V., "Dynamics of Auroral Belt and Polar Geomagnetic Disturbances", Planet. Space Sci. 15, 209-230, 1967.

2. Hultqvist, B., "The Geomagnetic Field Lines in Higher Approximation", Ark. Geofys. 3, 63-77, 1958.

3. Hakura, Y., "Tables and Maps of Geomagnetic Coordinates Corrected by the Higher Order Spherical Harmonic Terms", Rep. Ionosph. Space Res., Japan 19, 121-157, 1965.

4. Gustafsson, G., "A Revised Geomagnetic Coordinate System", Arkiv för Geofysik 5(40), 595-617, 1970.

5. Whalen, J.A., "Auroral Oval Plotter and Nomograph", Environmental Research Paper No. 327, AFCRL-71-0422, Bedford, Mass. 01730, 1970.

6. Akasofu, S.-I., "Polar and Magnetospheric Substorms", Springer, New York, 1968.

7. Pike, C.P., "A Comparison of the North and South Polar F-layers", Journ. Geophys. Res., 76, in print 1971a.

8. Pittenger, E.W. and G.J. Gassmann, "High Latitude Sporadic E", AFCRL-71-0082, Bedford, Mass. 01730, 1971.

9. Whalen, J.A., J. Buchau and R.A. Wagner, "Airborne Ionospheric and Optical Measurements of Noontime Aurora", Journ. Atm. Terr. Phys. 33(4), 661-678, 1971.

10. Wagner, R.A. and C.P. Pike, "A Discussion of Arctic Ionograms", this AGARDOGRAPH.

11. Hook, J.L., "Morphology of Auroral Zone Radiowave Absorptions in the Alaska Sector", JATP 30, 1341-1351, 1968.

12. Zhulina, Ye.M., "Seasonal Variations in the Position of the Auroral Absorption Zone", Geomagn. and Aeronomy (Translation AGU) 8(3), 376-380, 1968.

13. Berkey, F.T., V.M. Driatskiy, K. Henriksen, D.H. Jelly, T.I. Shchuka, A. Theander, J. Yliniemi, "Temporal Development of the Geographical Distribution of Auroral Absorption for 30 Substorm Events in Each of IQSY (1964-65) and IASY (1969), Kiruna Geoph. Observatory, Preprint 71:301, May 1971.

14. Berkey, T., University of Alaska, private communication, 1971.

15. Gorbushina, G.N., "The latitude distribution of auroral absorption and the Es-layer", STP Symposium, May 1970, Leningrad.

16. Fritz, Th.A., "High-latitude outer zone boundary region for >40 keV electrons during geomagnetically quiet periods", JGR 73(23), 7245-7256, 1968.

17. Hartz, T.R. and N.M. Brice, "The general pattern of auroral particle precipitation", Plan. Space Sci. 15, 301-329, 1967.

18. Hargreaves, J.K., "Auroral absorption of HF radio waves in the ionosphere: A Review of Results from the First Decade of Riometry", Proc. IEEE 57(2), 1348-1373, 1969.

19. Jelly, D.H., "On the morphology of auroral absorption during substorms", Can. Jour. Phys. 48, 335-345, 1969.

20. Sato, T. and L. Colin, "Morphology of Electron Density Concentration Enhancement at a Height of 1000 km at Polar Latitudes", JGR 74(9), 2193-2207, 1969.

21. Heikkila, W.J. and J.D. Winningham, "Penetration of magnetosheath plasma to low altitudes through the dayside magnetospheric cusp", JGR 76(4), 883-391, 1971.

22. Frank, L.A. and K.L. Ackerson, "Observations of changed particle precipitation into the auroral zone", JGR 76(16), 3612-3643, 1971.

23. Thomas, J.O. and M.K. Andrews, "Transpolar exospheric plasma", JGR 73(23), 7407-7418, 1968.

24. Petrie, L.E., "Preliminary results on mid and high latitude spread F", in Spread F (P. Newman, editor), Technivision Press, Maidenhead, England, 1966.

25. Burch, J.L., "Low energy electron fluxes at latitudes above the auroral zone", JGR 73(11), 3585-3591, 1968.

26. Carpenter, D.L., "Whistler studies of the plasmapause in the magnetosphere", JGR 71( ), 693- , 1966.

27. Muldrew, D.B., "F-layer ionization troughs deduced from Alouette data", JGR 70(11), 2635-2650, 1965.

28. Nishida, A., "Average structure and stormtime change of the polar topside ionosphere at sunspot minimum", JGR 72(23), 6051-6062, 1967.

29. Pike, C.P., "A latitudinal survey of the daytime polar F-layers", Journ. Geophys. Res., 76( ), in print, 1971b.

30. Gassmann, G.J., "Measurements of Irregularities and Drifts in the Arctic Ionosphere Using Airborne Techniques", Polar Atmosphere Symposium, pp. 44-51, Pergamon Press, New York, 1957.

31. Pike, C.P., "Universal time control of the south polar F-layer during the I.G.Y.", Journ. Geophy. Res. 75(25), 4871-4876, 1970.

32. Aarons, J., "Satellite scintillations in the high latitude F-layer irregularity zone", this AGARDOGRAPH.

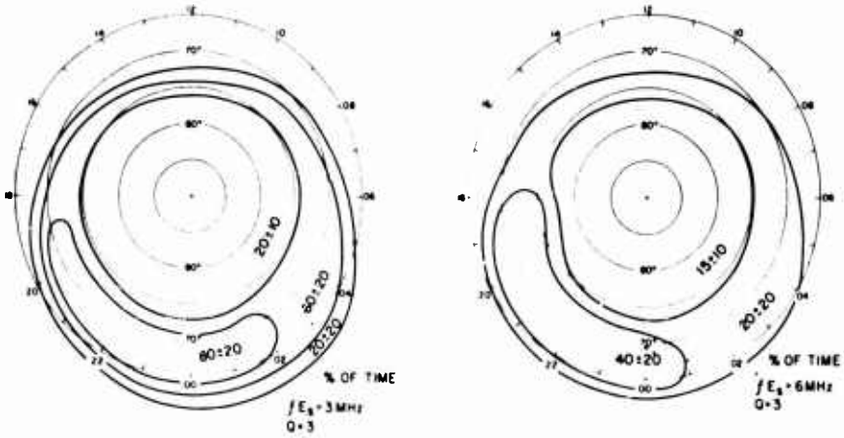

Figure 1. Occurrence of sporadic E in the Arctic during moderate magnetic activity (after Pittenger et. al. 1971), in CGL/CGT coordinates.

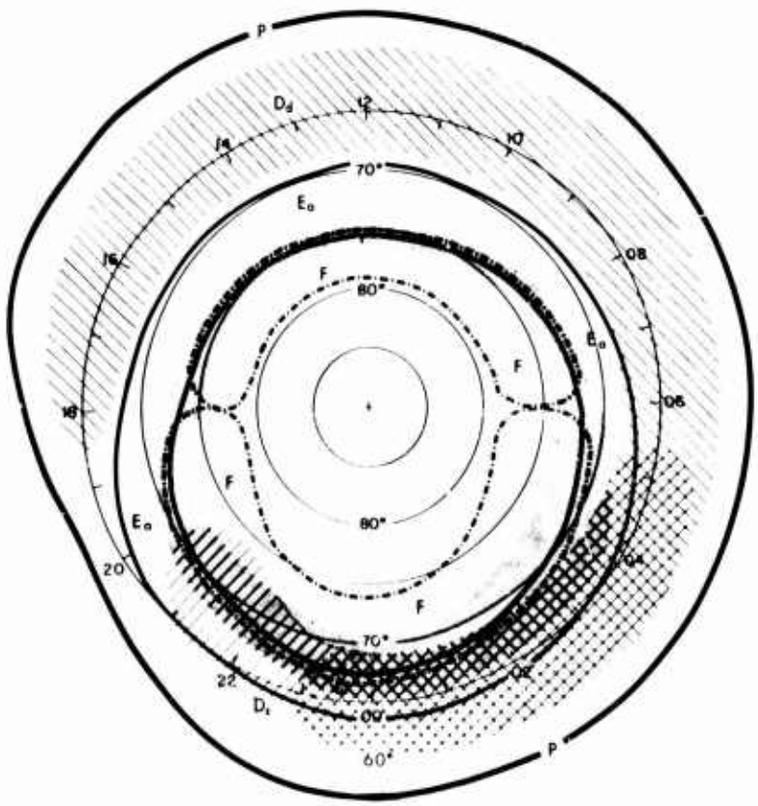

Figure 2. Schematic of arctic ionosphere in relation to auroral oval in CGL/CGT coordinates. Example for Feldstein Oval Q=2 (dotted area), winter night 1970.

Dd (cross hatched +45°). "drizzle", HF absorption >200 dB.MHz^2, steady for 1-2 hours after each substorm.

Ds (cross hatched -45°). "splash", HF absorption >>200 dB.MHz^2, short (<10 minutes) duration (at start of substorm).

Ea (area between solid lines). Auroral or night E-layer.

F (area between dotted lines). Enhanced F-layer density at 18 UT (the area is UT dependent), irregular, observed as "irregularity zone", "plasma ring", "polar cusp", "auroral cliff", "polar ring", "polar peak", etc. The break at the 18-06 CGT line indicates a tentative distinction presently pending.

P Plasmapause, average position projected onto map. The F-layer "trough" occurs north of P.

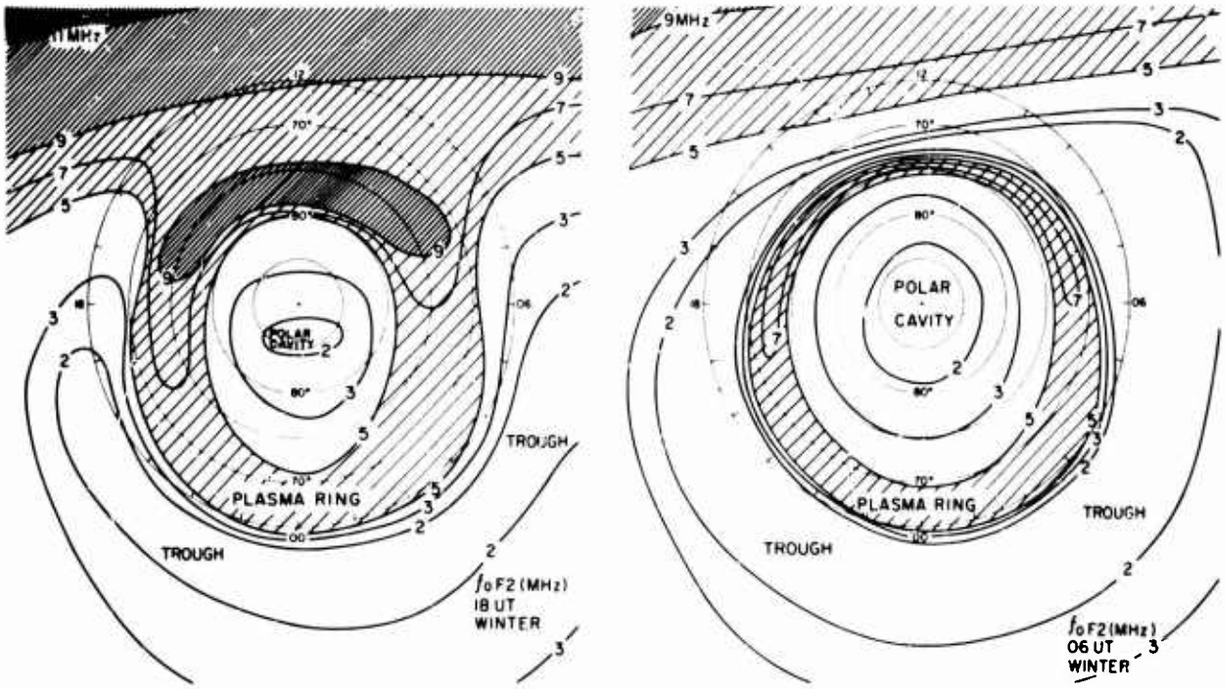

Figure 3. Example of the arctic F-layer; for two UTs 12 hours apart; for winter, moderate magnetic activity. Contour lines of median critical frequencies (MHz) are plotted in CGL/CGT coordinates.

Present Uncertainty: MHz - value ±30%, latitude ±3° CGL however spatially correlated in whole Arctic.

Non-deterministic Fluctuations: RMS 50% in large cells <1000 km.

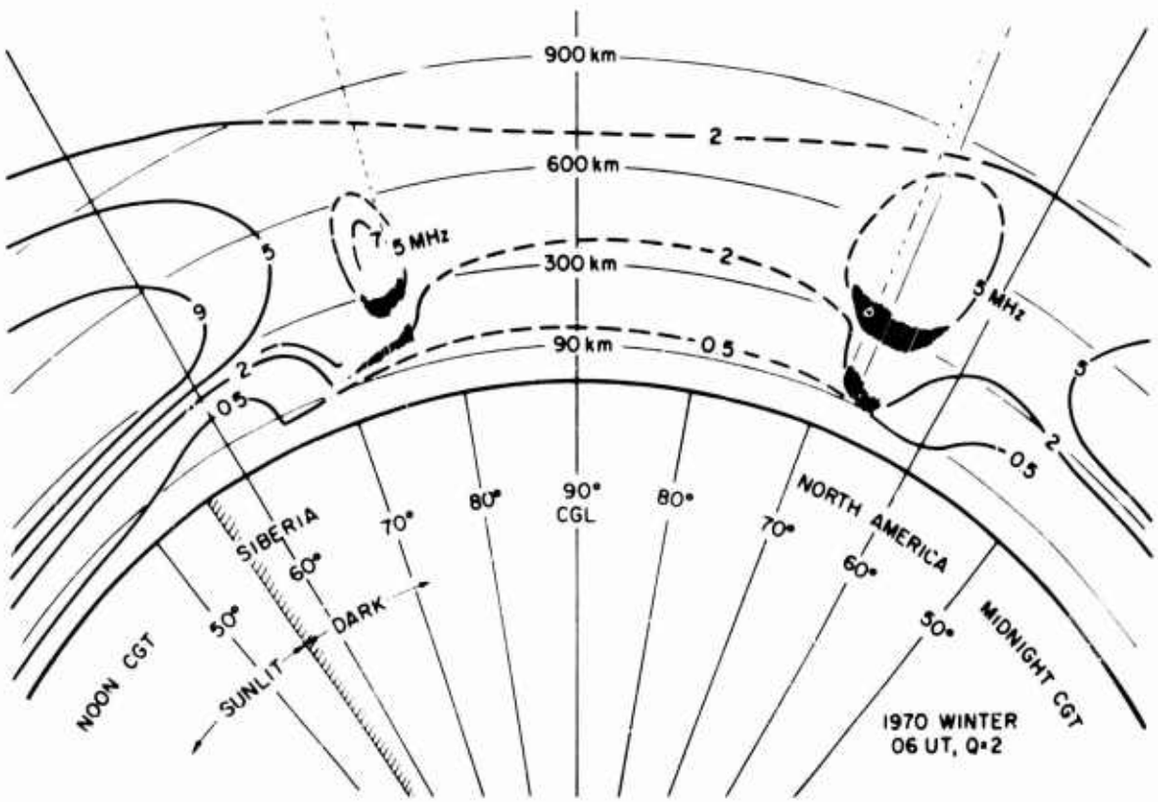

Figure 4. Example of a quasi-instantaneous vertical profile of the arctic ionosphere from magnetic noon to midnight; for winter, 06 UT, moderate magnetic activity. Contour lines of median plasma frequencies are plotted (MHz). Vertical height scale is 3 times horizontal scale.

THE POLAR EXOSPHERIC PLASMA

J.O. Thomas and A.D.R. Phelps
Physics Dept., Imperial College, London

SUMMARY

The main features of the spatial distribution of plasma in the earth's polar exosphere deduced from satellite observations are described and related to recent measurements of incoming particles of magnetospheric origin, particularly in the low energy range (∿1000 eV). The topics covered briefly include: (1), the termination of the terrestrial plasmasphere; (2), the identification and location of a ring or torus of enhanced plasma density surrounding each pole, stationary with respect to the sun and under which the earth rotates; (3), the geomagnetic control of the ionization with the recognition of paramount effects occuring at certain universal times associated with the geometry of the geomagnetic axis - Earth-Sun line system, and (4) the polar wind. Some of the main physical processes contributing to both the relatively static as well as the dynamic features of the overall structure of the polar plasma distribution are introduced.

1. INTRODUCTION

A large amount of data on the nature of the ionosphere at high latitudes has been collected from ground-based stations in past decades. The great variability in the different parameters deduced, both hourly and diurnally, has usually resulted in the presentation of the results in the form of averages, often for individual stations [1,2,3]. Sato and Rourke [4] have attempted to construct approximately instantaneous contours of electron density at a particular time over the polar cap. The poor spatial resolution resulting from the limited number of stations in their network and the limited time resolution (usually not better than 10 or 15 minutes) does not reveal the fine spatial and temporal structure of these regions.

In the last decade, however, satellite-borne instruments of both the probe and sounder type have enabled a much more detailed study to be made of the polar exospheric plasma by providing a virtually continuous record of the electron density variation along the track of the satellite. The topside sounder satellites Alouette I and II and more recently Isis I and II have contributed a vast amount of useful information, from which some of the main features of the polar exospheric plasma have been deduced.

2. MORPHOLOGY OF THE EARTH'S POLAR EXOSPHERIC PLASMA

The distribution of electrons along individual satellite tracks, derived at different times have been shown to be particularly important and suggest that there is a characteristic polar electron density distribution along a satellite track at a particular angle to the earth-sun line [5], and this distribution is essentially independent of longitude i.e. of universal time. Therefore, there exists a polar plasma distribution stationary with respect to the sun and under which the earth rotates.

Another important observation is of the presence of very large systematic spatial gradients of electron density and of marked enhancements of ionization confined within fairly narrow and well-defined latitude and altitude limits. The most consistently observed feature at high latitudes is an abrupt decrease in the electron density as measured at a particular altitude, by up to an order-of-magnitude or more, in a horizontal north-south distance, sometimes, of less than 100 km. This is followed by a recovery (sometimes very rapid) to larger values at higher latitudes. This effect has been noted independently in a number of experiments and the feature has been termed the mid-latitude trough [6].

Thomas and Dufour [7] suggested that the trough was a demarcation between the solar and aurorally produced ionization and commented upon the possible association between the trough and the plasmapause, or knee in the equatorial electron density profile at a geocentric distance of about 4 earth radii (R_e). In view of the success of theories predicting protonospheric electron densities from the assumption that diffusive equilibrium prevails along geomagnetic tubes of force [8], it appears reasonable that any association would be via field lines.

Whistler measurements combined with topside sounding data were used by Rycroft and Thomas [9] to examine the link between the centre of the trough and the plasmapause. They used measurements on the nightside of the earth and showed that for quiet magnetic conditions, the centre of the trough appeared to lie on the same L-shell as the mid-point of the plasmapause. This work was extended by Thomas and Andrews [5] and it was suggested that it might be more meaningful in any attempt to correlate the plasmapause and trough positions to associate the mid-point of the low latitude "wall" of the trough with the centre of the plasmapause as observed in whistler data.

Although an exact quantitative description of the overall polar morphology is not possible for the reasons given earlier, it is possible to state that there is in general a monotonic decrease in the plasma density at 1000 km altitude with increasing latitude, values ranging from a few times 10^4 electrons/cc at mid-latitudes to $\sim 10^3$/cc near the magnetic poles, with daytime values higher than night-time densities. The decrease is however not regular: there usually occurs a rather sudden fall-off especially during the evening hours. Often an order-of-magnitude decrease occurs in a horizontal distance of ∿100 km. Even during the day-time the density often falls to low values at latitudes rather lower than would be expected on simple theory. Fig. 1 shows the densities encountered on a traversal of the northern polar region in December 1962, together with F-peak densities expected from a Chapman layer with a 10 MHz overhead-sun critical frequency. While such theory is obviously inadequate, it does illustrate that the densities did not begin to rise for some twelve degrees of latitude after solar photo-ionization might be expected to have been noticeable, and not for sometime after the whole ionosphere was sunlit. When it did occur, the rise was very sudden as shown to the north of the frequently observed shoulder of ionization in the noon sector labelled (1) in Fig. 1. The sudden rise is much steeper in slope than that of the Chapman curve

and the whole picture is suggestive of a 'compression' or removal of the plasma at the highest latitudes. Beyond the shoulder labelled (1) the density increases (arrow 2, Fig. 1) towards the equator though irregularities exist. The plasmasphere 'termination' is readily identifiable at night and is often detectable as a 'ledge' or 'shoulder' in the ionization distribution during the day.

3. THE TERMINATION OF THE TERRESTIAL PLASMASPHERE

The plasmasphere termination introduced in Section 2 is here discussed in more detail. In particular the position of the low latitude boundary of the main trough is described. From a real height-density analysis of a sequence of topside ionograms, Thomas et al. [10] were able to show the presence of the trough simultaneously at all altitudes from the F layer peak up to the vehicle. Using ion traps Sharp [11] detected the presence of the trough at various heights in the F region from variations in the positive ion concentration. Using differential Faraday rotation measurements from the Beacon Satellite S-66, Liszka [12] has shown the trough is present in total electron content measurements, confirming that the phenomenon is not simply a redistribution of ionization.

It has been pointed out [10] that the spread nature of echoes on topside ionograms polewards of the mid-latitude trough indicates that the ionosphere here is more disturbed than at low latitudes. Results from the Alouette II topside sounder have shown that at altitudes of 2000 - 3000 km, there is a fall in electron density at a latitude approximately equalling that of the F region main trough, but that polewards of this, there is not the enhancement mentioned in Section 2 and described in more detail in Section 4.

As noted in Section 2, the positions of the plasmapause (projected back along a field line, specified by a diurnally averaged geomagnetic field model, from its equatorial plane position to an altitude of 300 km in the northern polar region) do not quite coincide with the observed positions of the plasmasphere termination as measured in the ionosphere using Alouette I data. In fact on the dayside, the plasmapause lies at a lower latitude than the low latitude wall of the trough whereas on the night-side the trough lies below the plasmapause. This can be attributed, at least in part, to the compression of field lines by the solar wind on the dayside bringing the plasmapause or 'knee' to a smaller geocentric radius in the equatorial plane while the compressed field line reaches the earth at a higher latitude than the diurnally-averaged field maps indicate [5]. The reverse applies on the night-side. However, it is unlikely that the compression near 3.5 Re is large enough on the dayside to explain this effect. With increasing magnetic activity, the plasmasphere termination occurs at a progressively lower latitude. The local time sector involved determines the precise position. A typical linear regression equation giving the position, Λ' in invariant latitude of the foot of the low latitude side of the trough (i.e. plasmasphere termination $\Lambda'_{P.T.}$) for the 10.00 local time sector reads [5],

$$\Lambda'_{P.T.} = 62.09 - 1.01\ K_p$$

For $K_p = 0$, Table 1 gives the position of the plasmasphere termination near 1000 km. Its position for $K_p = 3$ in relation to the auroral zone is discussed in the next section.

The trough is narrower on the evening side than during the morning hours, the plasma termination being particularly sharp during the afternoon hours. During the noon hours the trough is usually absent but a 'shoulder' of ionization (Fig. 1) is often seen. This is to be expected since the noon ionization is sufficiently extended towards the north in latitude to overlap the normal enhancement (described in Section 4).

4. POLAR PLASMA ENHANCEMENTS

By examining the exospheric plasma distribution on successive satellite transits across the winter pole Thomas and Andrews [13,14] have been able to establish that a ring of enhanced plasma density occurs at higher latitudes than the plasmapause termination. The ratio of peak to trough values of plasma density at 1000 km may exceed 25 to 1. In fact the lower latitude edge of this halo or ring of enhanced density forms one of the sides of the main trough. A schematic diagram illustrating this is shown in Fig. 2. Over the polar cap itself there is a plasma depletion or cavity, elongated and displaced in the midnight direction. The 'gap' between the plasmasphere termination and the stationary plasma ring is somewhat crescent shaped, being widest during the morning hours, narrow on the evening side. Inside the gap, very low plasma densities prevail especially at night. Near noon the gap is obscured due to the encroachment to higher latitudes of the solar produced ionization, overlapping the plasma ring.

The statistical positions of the density enhancements have been presented by Andrews and Thomas [13,14]. The distribution shown in Fig. 2 is of course highly idealized, individual passes depart from this distribution in detail but are similar in character.

In Fig. 3 the auroral oral of Feldstein [15] is superimposed on the boundaries of the density enhancements for a K_p index of 3. The plasmasphere termination in the F region as given by Thomas and Andrews [5] is also shown together with the 40 kev electron trapping boundary. Attention is drawn to a number of important features of Fig. 3 in which the boundaries of the density enhancements are defined. It should be noted that the boundaries are the statistical position of the mid-points of the sloping 'sides' of the density enhancements. Perhaps a more geophysically meaningful quantity would be the base width (in degrees) of the enhancements. In practice it might be expected that on average the density would in fact be enhanced approximately 1° on each side of the zone shown in Fig. 3. The invariant latitude Λ'_D (noon) and Λ'_N (midnight) of the upper boundary are 76° and 74° respectively.

It is interesting to examine the movement of the ring of enhanced plasma density in the same way as the main trough movement has been examined. The lower boundary of the plasma ring moves equatorwards with increasing magnetic activity. During December 1962 for the 0000 - 0200 local time sector the equation for the position Λ' in invariant latitude of the lower boundary was

$$\Lambda' = 65.3 - 2.3\ K_p$$

The position of the upper boundary of the ring is rather variable, but it too moves to lower latitudes with increasing K_p.

One important consequence of the identification and location of a stationary plasma ring is the recognition by Andrews and Thomas [13], that high latitude ionospheric observatories on the ground will rotate under the stationary ionization pattern - and may or may not intersect it depending on their precise geographic locations. The effects of the stationary plasma ring should therefore be detectable for example as anomalously dense layers giving rise to high critical frequencies and 'oblique' traces on ionograms. These effects were in fact found in the f-plot data examined for a number of high latitude stations [13]. It is predicted that similar effects are likely to be found in absorption measurements since it is likely that the ring pattern extends from the lower ionosphere up to altitudes of a few thousand kilometres. Observed MUFs are also likely to be affected at high latitudes.

The observations discussed by Thomas and Andrews[5] related to a period of low solar activity and to the northern hemisphere. It is clear that the same basic density configuration is present in both hemispheres [16], despite the different relationship between magnetic and geographic co-ordinates, and also at times of higher solar activity [17].

5. GEOMAGNETIC CONTROL AND U.T. EFFECTS

It was noted by Thomas et al. [10], that the trough positions on successive transits follow L shells rather than geographic latitude. Geomagnetic control constrains the trough at a fixed local time to move along a contour of constant L or Λ' as the earth rotates beneath it. Their data showed that the largest values of electron density recorded in the enhancements tended to occur in a period centred around 1800 - 1900 U.T. which corresponds to magnetic noon (Fig. 4) with very few occuring after magnetic sunset or before magnetic sunrise. Clearly the histogram shows that the large peaks are predominantly a magnetic daytime effect. It is clear that the enhancements respond to geomagnetic control the largest enhancements being observed near magnetic noon when the angle between the geomagnetic dipole axis and the solar direction is a minimum at ~1800 U.T. Thomas and Andrews [5] showed that the trough is moved towards and away from the equator in synchronization with the rotating L pole, the trough being closest to the equator at the universal time when the eccentrically rotating L pole enters the local time sector concerned. The trough however follows a more constant value of invariant latitude indicating geomagnetic control.

Universal time effects observed in the polar ionosphere by a number of workers have been summarized by King et al. [18]. It is clear from a great number of independent observations that the maximum electron densities in the F region are observed near 0600 U.T. in southern hemisphere and near 1800 U.T. in the northern hemisphere. There is also evidence that the height of maximum electron density in the southern polar regions is a maximum near 0600 U.T. and minimum 12 hours later, and at many southern observatories the maximum electron density in the F2 region has its lowest value near 1800 U.T., the form of the height and density curves being approximately sinusoidal and in phase.

6. PARTICLE PRECIPITATION AND THE POLAR WIND

It has been pointed out that the disturbed nature of the polar ionosphere, including such features as thin, magnetically aligned sheets of ionization strongly suggests collision ionization. To produce significant amounts of F region ionization, it is known that fluxes of electrons with initial energies of about 1 kev are required. Recently, such particles have been measured directly [19,20,21,22]. Significantly, these fluxes also show a cavity over the pole, where their intensity drops by at least two orders of magnetude. The high latitude boundaries, Λ'_D and Λ'_N in invariant latitudes, of the soft electron fluxes in the noon-midnight meridian are compared in Table 2 with the equivalent day and night boundaries of the plasma density ring. The positional agreement between the precipitation and the enhanced densities strongly suggests cause and effect.

Calculations [19], which include the effects of plasma diffusion above 200 km altitude, indicate that the fluxes reported by Burch [21] are sufficient to produce collision ionization densities equal to those observed. The average soft zone spectra found by Burch [21] were,

$$J = 2.7 \times 10^{7} E^{-1.48} / cm^2/ster/kev/sec \quad \text{(nightside)}$$

$$J = 3.0 \times 10^{7} E^{-2.26} / cm^2/ster/kev/sec \quad \text{(dayside)}$$

for 0.1 kev $\leq$ E $\leq$ 1.3 kev.

The calculation of the ionizing effects of such a flux is complex but may be simplified by the technique introduced by Rees [20] based on the measured absorbtion of a mono-energetic beam of electrons as it traverses a gas. In his calculation Andrews [19] neglected the effect of the magnetic field, which is permissible for an extended precipitation source in a uniform field. This is required by the lack of pitch angle information in any case. He used a mid-latitude atmospheric model with parameters selected to approximate to low solar activity, but higher temperatures corresponding to polar latitudes. The model used was CIRA 1965, 1400 hrs, for a solar 10.7 cm flux of $150 \times 10^{-22} w/m^2/Hz$.

After making the assumption that 35 eV is required for production of one ion-electron pair the production rate was calculated as a function of height. It was estimated that the maximum production rate of O^+ in the soft zone due to electron precipitation was 255 cm^{-3} sec^{-1} at 235 km on the dayside and 270 cm^{-3} sec^{-1} at 180 km on the nightside.

In order to convert the profiles of production rate into electron density profiles the steady state continuity equation with no horizontal movements was used. For ease of solution diffusive equilibrium was assumed to exist at 1000 km altitude. In calculating the ambipolar diffusion in the altitude range 200 km to 1000 km the scale height was matched to experimentally derived polar values. Losses due to recombination were calculated using laboratory measurements of the reaction rates and also inferred ionospheric values of these rates. Andrews [19] calculated the density at the maximum of the F2 layer to be 2.7×10^5

to 5.3 x 10^5 cm^{-3} on the dayside and 1.6 x 10^5 to 3.6 x 10^5 cm^{-3} on the nightside. From Alouette data for the period of 1962/63, densities at the F layer peak were found to be ∿0.5 x 10^5/cc in the trough and the polar depletion. In the nightside peaks, typical densities were in the range 1.5 - 2.5 x 10^5/cc, rising to 3.5 - 4.5 x 10^5/cc on the dayside. Hence the day-night asymmetry in the density observations agreed with the asymmetry predicted by the precipitation measurements. The quantitative agreement is good considering the assumptions made in the calculations.

The excess ionization near local noon peaked near L = 25, [10] so that the Alouette I observations of polar enhancements agree well with those of Maehlum [22] and Burch [21]. It is difficult not to interpret their results as confirming our general model of the plasma ring essentially resulting from particle precipitation. The movement of the plasma ring hypothesized and detected by Andrews and Thomas [5] has been placed on a quantitative basis by Maehlum [22] who has determined both the daytime and night-time movement with universal time of the poleward boundary of low energy electrons. He finds during the summer of 1967 that Λ'_D follows an approximately sinusoidal curve with a maximum near 1800 U.T. and a minimum near 0800 U.T. (Λ' = 84° and 74° respectively). The size of the polar cavity (180° - (Λ'_D + Λ'_N)) is least (∿20°) at 1800 - 2000 U.T. i.e. near magnetic noon, and a maximum (∿35°) at 0600 - 0800 U.T., i.e. near magnetic midnight. The plasma ring under which the earth rotates thus responds in universal time to the changing geometry of the geomagnetic axis in relation to the sun-earth line. Maehlum [22] points out that since the universal time variations in electron fluxes are related to geomagnetic field distortions associated with the varying tilt of the geomagnetic axis with respect to the solar wind, significant seasonal variations should be detectable in the electron fluxes in polar regions. It is of importance therefore to derive the seasonal variation in the plasma distribution along the track of the Alouette I satellite over the polar region. It is interesting that Maehlum finds Λ'_D winter to be less than Λ'_D summer by ∿5° for the few winter passes studied by him.

The importance of the polar wind theory [25] in determining this morphology was first recognized as a result of latitudinal surveys of the topside ionosphere scale height. Real height-density analyses of ionograms in the region were performed [26] to provide information on the changes taking place across the pole. Fig. 5 gives graphically the results of such an analysis of a sequence of ionograms, during which the satellite crossed the morning trough from mid-latitudes, and entered a polar peak of ionization. The scale height H of the topside plasma, defined by

$$H = -N \frac{dh}{dN}$$

may be shown to carry information basically on the ratio $(T_i + T_e)/m_i$, where T_i, T_e refer to ion and electron temperatures, and m_i is the mean ionic mass. The sudden fall in scale height at great heights on entering the trough is consistent with a rise in mean ionic mass, so that the ionosphere at high latitudes is composed mainly of oxygen ions. This abrupt change from mid-latitudes is illustrated in the profiles A and B. The former alone shows the curvature near 600 km caused by a change in composition to ions lighter than O^+ at greater heights. At the same time, the steeper slope of profile B below 500 km, where the dominant ion must be O^+, implies the temperature of the polar ionosphere is greater than at mid-latitudes. Profile C, taken inside a polar peak, is interesting as it indicates the composition of the ionization peak is remarkably similar to the trough, i.e. predominantly hot O^+, even though the densities differ by an order-of-magnitude.

At magnetic latitudes above about 80°, profiles corresponding to the night hours frequently show a fall of scale height, below 500 km, compared with values at latitudes a few degrees south, to values difficult to explain on the assumption that diffusive equilibrium applies. Such a depression of H below 500 km, however, is what might be expected as a consequence of the polar wind, where O^+ ions flow upwards through the neutral atmosphere to replenish the outflowing protons by charge exchange with neutral hydrogen atoms. In doing so, the scale height of the flowing O^+ plasma becomes depressed below that expected in diffusive equilibrium, and is nearer that of the neutral atmosphere.

7. CONCLUSIONS

The answers to the overall questions of the winter source of polar ionization, and the morphology of that ionization are becoming known. There are several factors responsible for this increased knowledge including the data collected by satellite-borne experiments and aircraft-borne experiments and the realization of the most useful schemes for data ordering.

The polar wind is a mechanism of plasma removal which has been shown to be operative in parts of the polar exosphere. The exact extent to which the polar depletion is a result of plasma removal or simply the absence of the ionizing source of precipitation is not completely decided.

ACKNOWLEDGEMENTS

This paper summarizes recent work by the authors and their colleaques on the polar exospheric plasma distribution. It draws heavily on material already published in the scientific literature, in a number of papers referred to above.

LIST OF REFERENCES

1. Patton, D. E., V. L. Peterson, G. H. Stonehocker and J. W. Wright, Characteristic variations in the Antarctic ionosphere, Geomag. and Aronomy, AGU Antarctic Research Series, vol. 4, 47-75, 1965.

2. Hill, G. E., Anomalous f_oF_2 variations in the Antarctic, J.G.R., 65, 2011-2023, 1960.

3. Bellchambers, W. H., L. W. Barclay and W. R. Piggott, The Royal Society IGY Expedition Halley Bay 1955-59, 179-221, published by Roy. Soc. London, 1962.

4. Sato, T. and G. F. Rourke, F-region enhancements in the Antarctic, J.G.R., 71, 1345-1356, 1964.

5. Thomas, J. O. and M. K. Andrews, Transpolar exospheric plasma 1. Plasmasphere termination, J.G.R. 73, 7407, 1968.

6. Muldrew, D. B., F-layer ionization troughs deduced from Alouette data, J.G.R. 70, 2635, 1965.

7. Thomas, J. O. and S. W. Dufour, Electron density in the whistler medium, Nature, 206, 567-571, 1965.

8. Angerami, J. J. and J. O. Thomas, Studies of Planetary atmospheres, 1, The distribution of electrons and ions in the earth's exosphere, J.G.R. 69, 4537-4560, 1964.

9. Rycroft, M. J., and J. O. Thomas, The magnetospheric plasmapause and the electron density trough at the Alouette I orbit, Planet. Space Sci., 18, 65-80, 1970.

10. Thomas, J. O., M. J. Rycroft, L. Colin and K. L. Chan, The topside ionosphere II. Experimental results from the Alouette I satellite, Proc. NATO-ASI Finse, Norway, p. 322-357, ed. J. Frihagen, North-Holland Publishing Co., Amsterdam, 1966.

11. Sharp, G. W., A mid-latitude trough in the night-time ionosphere, J.G.R. 71, 1345-1356, 1966.

12. Liszka, L., The high latitude trough in the ionospheric electron content, J. Atmos. Terr. Phys., 29, 10, 1243-1259, 1967.

13. Andrews, M. K. and J. O. Thomas, Electron density distribution above the winter pole, Nature, 221, 5177, 223-227, 1969.

14. Thomas, J. O. and M. K. Andrews, The trans-polar exospheric plasma, 3: a unified picture, Planet. Space Sci., 17, 433, 1969.

15. Feldstein, Y. I., Some problems concerning the morphology of auroras and magnetic disturbances at high latitudes, Geomag. Aeronomy, 3, 183-191, 1963.

16. Pike, C. P., A comparison of the North and South polar F-layers, J.G.R., 76, in the press, 1971.

17. Pike, C. P., Universal time control of the south polar F-layer during the I.G.Y., J.G.R., 75, 4871-4876, 1970.

18. King, J. W., H. Kohl, D. M. Preece and C. Seabrook, An explanation of phenoma occuring in the high latitude ionosphere at certain universal times, J.A.T.P., 30, 11-23, 1968.

19. Andrews, M. K., "Plasma studies related to observations made by ionospheric "topside sounder" satellites", Ph.D. Thesis, London University, 1969.

20. Rees, M. H., Auroral ionization and excitation by incident energetic electrons, Planet. Space Sci., 11, 1209, 1963.

21. Burch, J. L., Low energy electron fluxes at latitudes above the auroral zone, J.G.R., 73, 3585, 1968.

22. Maelhum, B. N., Universal time control of the low energy electron fluxes in the polar regions, J.G.R., 73, 3459, 1968.

23. Evans, J. E., R. G. Johnson, R. D. Sharp and J. B. Reagan, Recent results from satellite measurements of low-energy particles precipitated at high latitudes, Space Sci. Rev., 7, 263, 1967.

24. Hoffman, R. A., Low-energy electron precipitation at high latitudes, J.G.R., 74, 2425, 1969.

25. Banks, P. M. and T. E. Holzer, The polar wind, J.G.R., 73, 6846, 1968.

26. Thomas, J. O. and M. K. Andrews, The polar exospheric plasma, in The Polar Ionosphere and Magnetospheric Processes, ed. G. Skovli, Gordon and Breach, New York, 1969.

TABLE 1

Local Time Sector	$\Lambda'_{P.T.}$
0600	57.3
1000	62.1
1200	68.0
1800	66.6

The invariant latitude, $\Lambda'_{P.T.}$, of the plasmasphere termination near 1000 km as measured by the foot of the low-latitude side of the 'trough'.

TABLE 2

Observation	Λ'_D	Λ'_N	$\Lambda'_D - \Lambda'_N$	Cavity size
Electrons, .08 - 21 kev, winter 1963	78	72	6	30°
Electrons, .05 - 1 kev, summer 1967	83	72	11	25°
Plasma Density, K_p = 3, winter 1962	76	73	3	31°

Comparison between plasma cavity position and the precipitating particle boundary.

F-PEAK DENSITIES IN THE NOON SECTOR

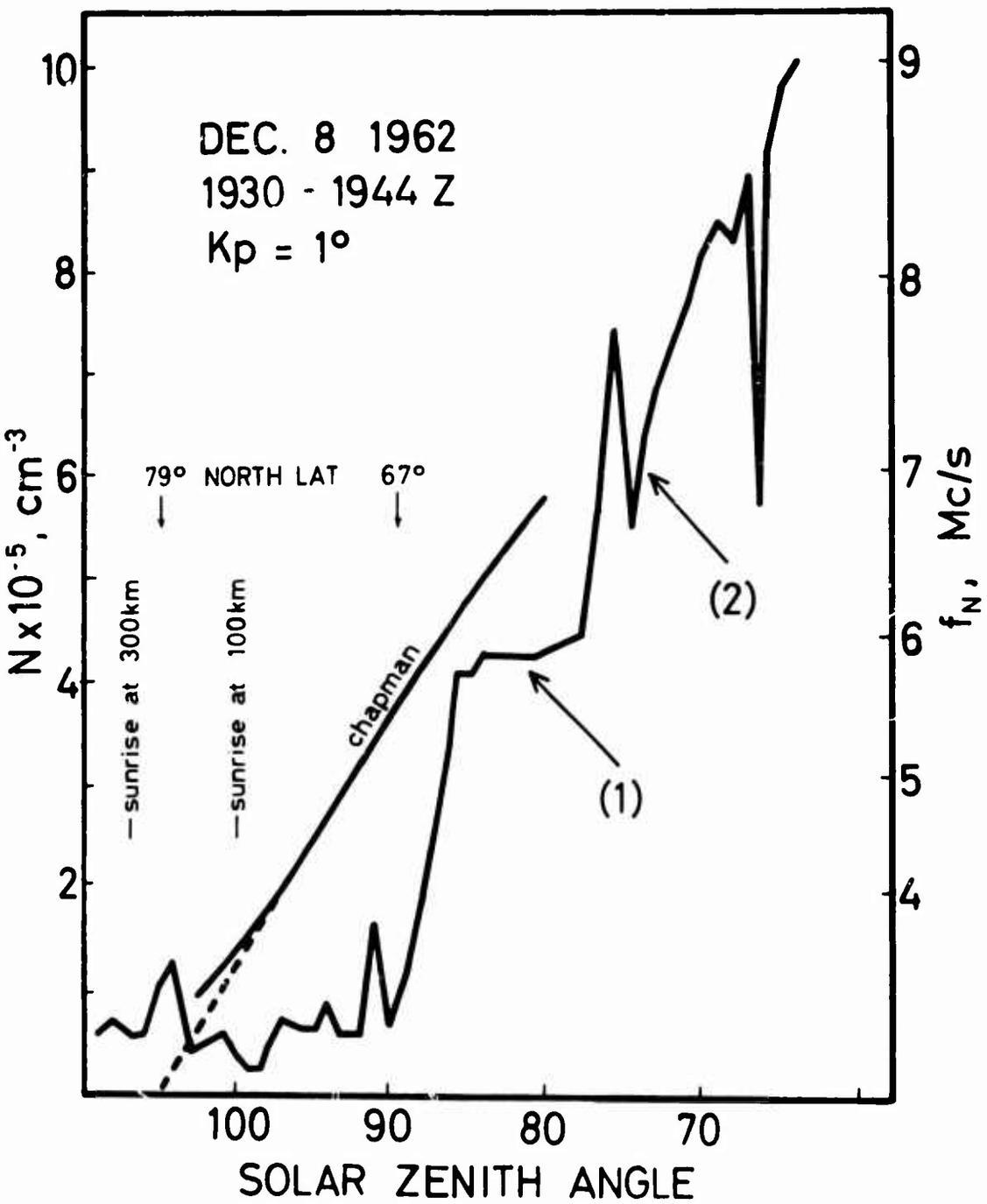

Fig. 1 The experimentally observed electron density, N_mF2, as a function of solar zenith angle (or of latitude) for a dayside pass on which the vehicle was travelling towards the sun in the noon sector. The shoulder of ionization frequently seen in this region is marked (1), and the steep gradients (arrow 2) encountered between the shoulder region and the mid-latitude wall of the trough seen at other local times. The upper curve labelled 'Chapman' illustrates the approximate variation of N_mF2 expected from simple theory. It is clear that on the occasion illustrated the ionosphere terminates at a lower latitude than is suggested by simple theory. The sudden fall-off in ionization just north of the arrow (1) represents the plasmasphere termination (from ref. 14).

IDEALISED DISTRIBUTION OF POLAR ELECTRON DENSITY

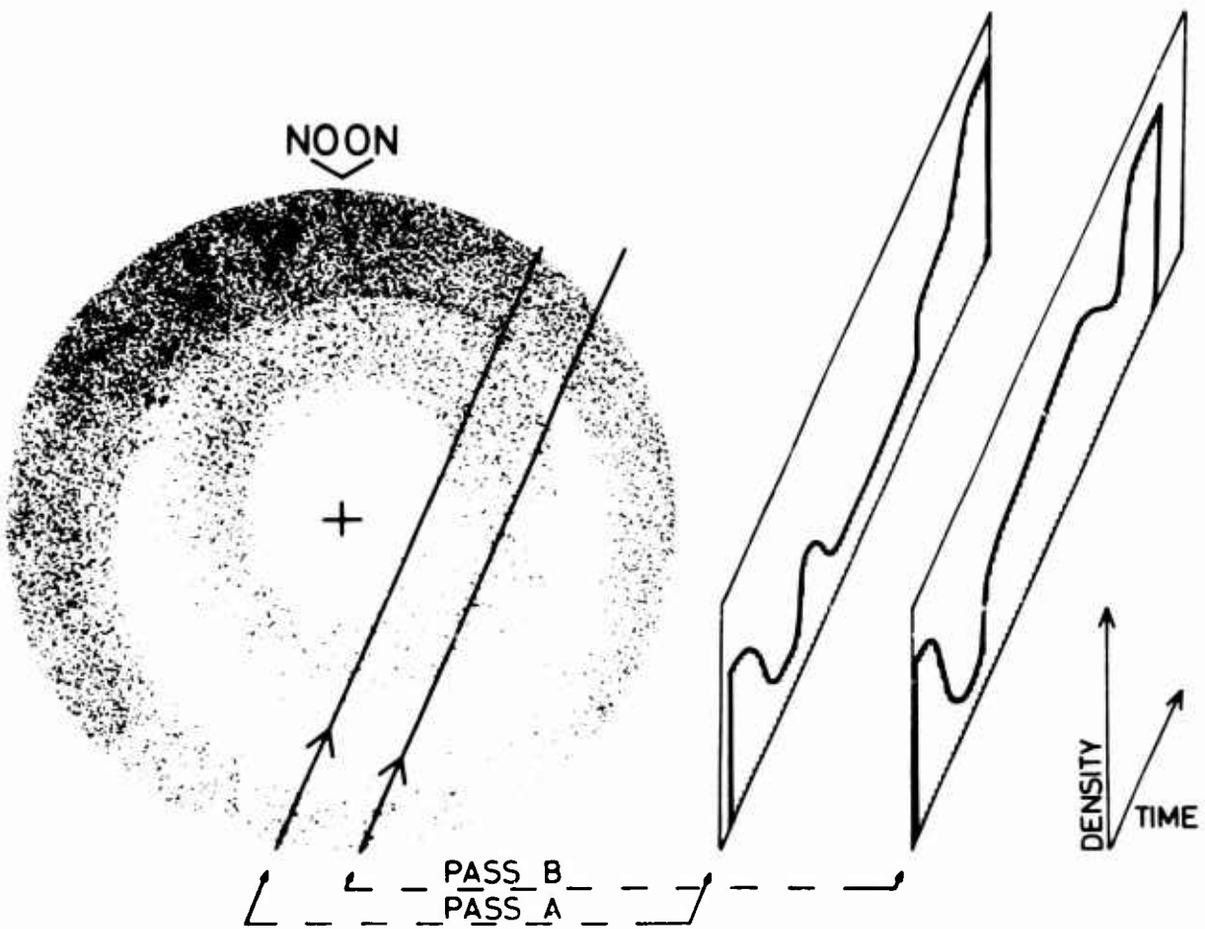

Fig. 2 Schematic diagram showing the distribution of electrons in the altitude range 300 - 1000 km above the winter polar region. The particle density is greater where the density of dots is greater. The polar cap depletion, the trough and plasmasphere termintaion and the plasma ring are shown. The sketch on the right shows two possible distributions that might be observed along the satellite track from the same basic pattern if the whole distribution moved with respect to geographic co-ordinates, as it might, for example, if it followed magnetic control as the earth rotates. Compared with the density pattern, i.e. magnetic co-ordinates, the satellite tracks A and B would appear displaced as indicated (from ref. 13).

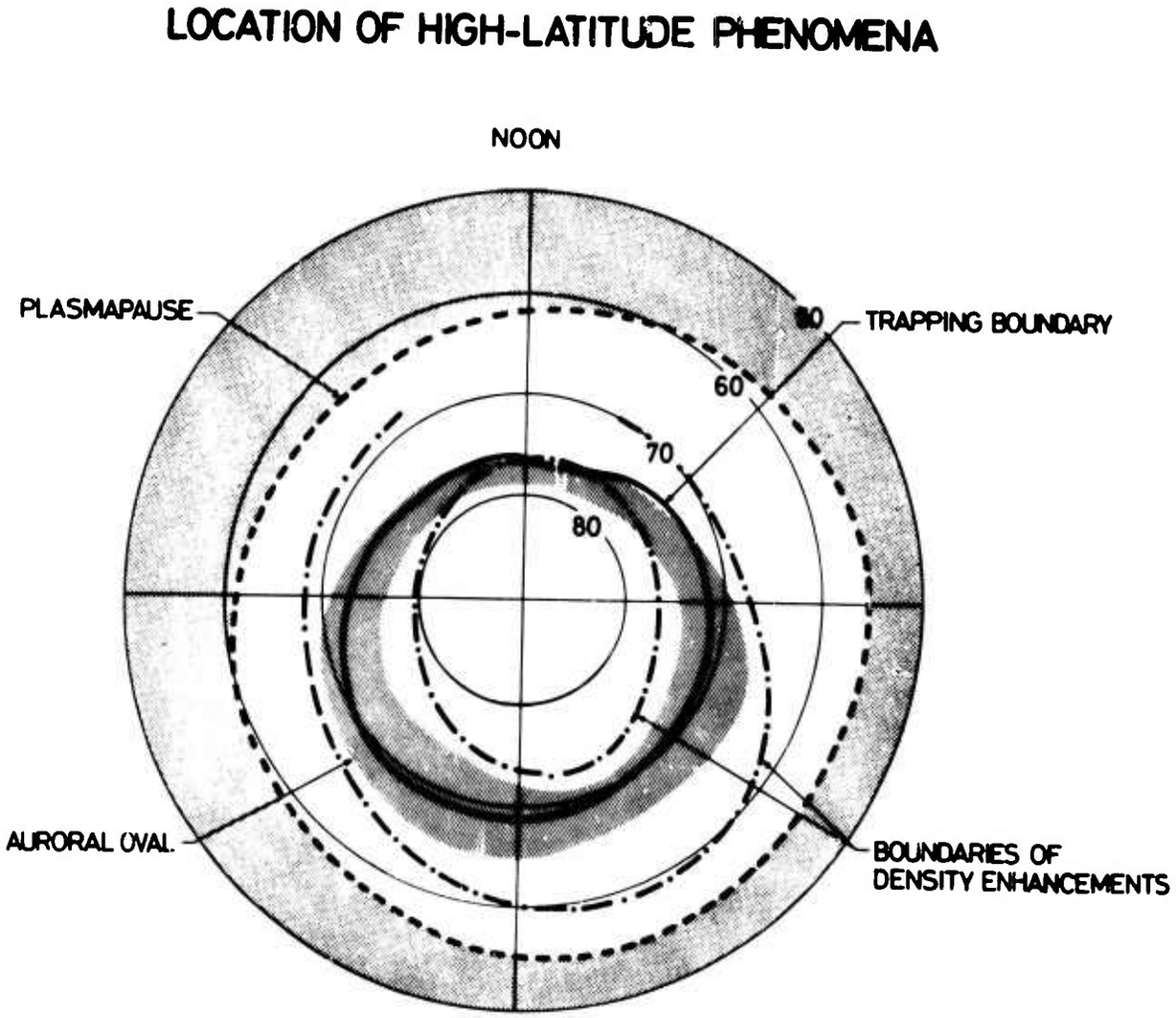

Fig. 3 The relative locations of various high latitude phenomena discussed in the text in terms of invariant latitude and local time for a K_p of 3. The plasmasphere termination is clearly seen. The smoothed upper and lower boundaries of the high latitude ring of enhanced plasma density are also plotted. The trapping boundary shown is that for 40 kev electrons and the positions of the other features correspond to the winter of 1962/63 (from ref. 13).

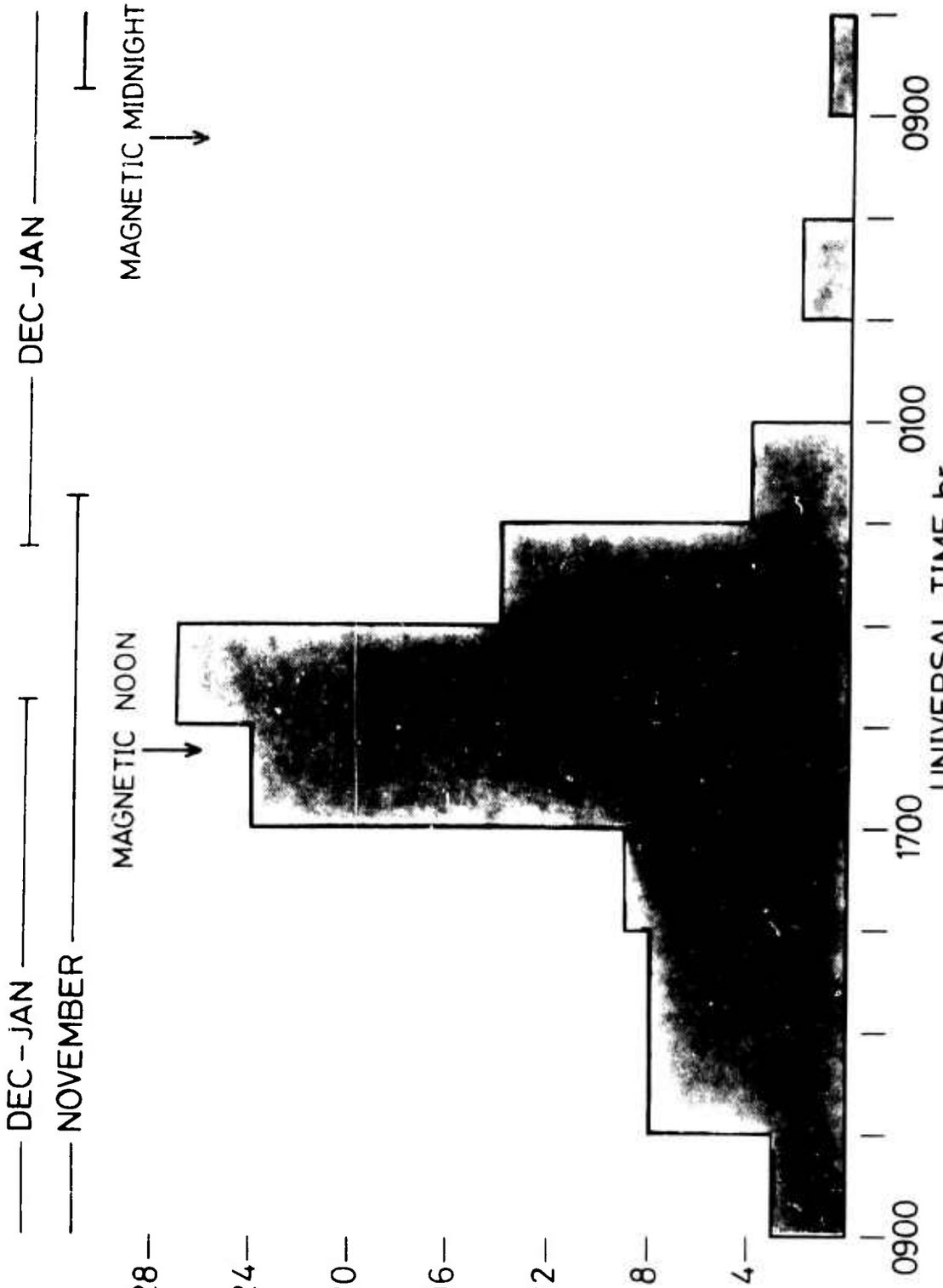

Fig. 4 Histogram showing the universal time of occurrence of passes with winter high latitude enhancements in excess of 15,000 electrons cm^{-3} (after ref. 14).

ALOUETTE I N(h) ANALYSIS

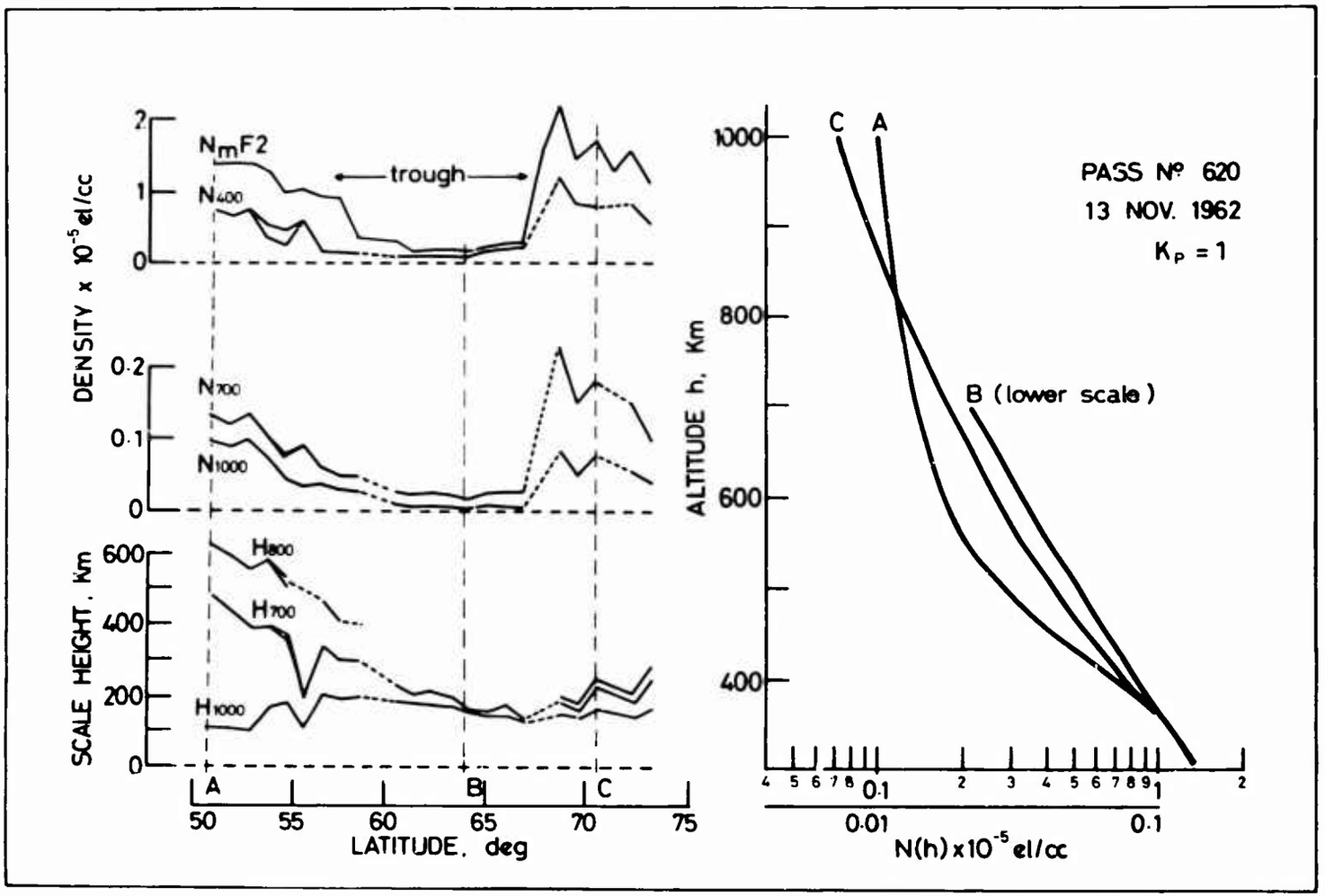

Fig. 5 The results of real height-density analyses of a sequence of ionograms during which the satellite crossed the mid-latitude trough and entered a polar peak of ionization. From the data, it appears that the ionosphere in and above the trough consists of a hotter, predominantly oxygen plasma, at all altitudes up to the vehicle (from ref. 26).

A Discussion of Arctic Ionograms

R.A. Wagner and C.P. Pike
USAF Cambridge Research Laboratories
Bedford, Mass., 01730, USA

SUMMARY

Examples of arctic ionogram sequences, recorded on the AFCRL Flying Ionospheric Laboratory, are presented. The purpose of this paper is to show that: a) ionogram sequences, recorded on arctic flights, facilitate the interpretation of oblique incidence echoes from E- and F-layer heights. b) parameters of the arctic ionosphere can be mapped by using the "auroral oval" as an ordering system, c) vertical and oblique incidence echoes, appearing on ground station ionograms, can be interpreted in terms of the station's position relative to the auroral oval.

The analysis of a three hour flight with 6 latitudinal scans underneath an auroral band shows the close relationship between auroral type sporadic E echoes (E_{sa}) and discrete aurora. The investigation of 49 latitudinal scans through the auroral oval during times of low magnetic activity revealed the existence of a particle produced E layer which is oval aligned, is 2° to 6° wide in corrected geomagnetic latitude and occurs at all corrected geomagnetic times. This layer produces the night E echoes.

A new ionogram analysis procedure, which uses oblique incidence F-layer echoes, is demonstrated, and the feasibility of monitoring the latitude of the southern edge of the polar F-layer irregularity zone by using this new analysis procedure is demonstrated.

1. INTRODUCTION

Vertical incidence ionograms, recorded in high latitude regions, are often highly complex. Spread echoes and a variety of oblique echoes, which originate in E- and F-layer heights of the ionosphere, complicate ionograms. In E-layer heights different types of echoes are often simultaneously observed, and their appearance may change rapidly. These complications are the well-known cause of the difficulties which are encountered in scaling and interpreting of arctic ionograms.

It is often difficult to interpret echoes on complex ionograms when only individual sweeps, recorded at long time intervals, are considered. Ionogram analysis and interpretation can be aided by using ionogram sequences. This technique was used for instance, by Hanson et al(1) to show movements of the night E-layer, and is presently being used in recording vertical incidence swept frequency ionograms on the AFCRL Flying Ionospheric Laboratory. An ionospheric sounder, carried on a high-speed aircraft, is a valuable tool for investigating the arctic ionosphere.

For planning arctic flights the "auroral oval" (Feldstein and Starkov, (2)) has been used as a frame of reference, since it has proved to be an ordering system for many arctic geophysical phenomena. The auroral oval, defined as the region of maximum occurrence of visible aurora at a given instant, is an oval shaped belt surrounding the geomagnetic pole. The oval's position is fixed with respect to the sun and the earth rotates underneath it. A high-speed aircraft, flying at high latitudes against the earth's rotation, can stay at constant CG local time for many hours while, at the same time, making latitudinal scans. By flying in the direction of the earth's rotation the aircraft's movement relative to the oval can be accelerated, and the entire oval can be investigated in one 10 hour flight. The corrected geomagnetic (CG) coordinate system (Hultquist, (3), (4), Hakura, (5)) is used throughout this paper.

Examples are discussed in this paper which demonstrate the usefulness of ionogram sequences, recorded on flights and on the ground, in interpretation of oblique incidence echoes from E- and F-layer heights. Analysis of ionogram sequences, accumulated in cross-section flights through the auroral oval at all CG local times, has permitted the mapping of the occurrence of auroral E and auroral E_s relative to the location of the auroral oval. A special analysis procedure, which uses oblique incidence F-layer echoes for monitoring the latitude of the southern edge of the polar F-layer irregularity zone, is presented.

2. E REGION

Many statistical investigations and single case studies have been made of the relationship between ionospheric E-region echoes and the visual aurora.

Results, obtained from simultaneous ionogram recordings and observations of aurora, show that good correlation exists between: a) sporadic E (E_s) range and elevation of aurora (Knecht (6), Buchau et al. (7), Whalen et al. (8)), b) auroral brightness and the top frequency of E_s echoes (Knecht (6), Hunsucker and Owren (9)), c) auroral brightness and the inverse of the virtual height of E_s echoes for the case of overhead aurora (Harang (10), Knecht (6)). The results of the work of many researchers are reconsidered in relation to the auroral oval, in a study of the distribution of occurrence of Es in high latitudes, by Pittenger and Gassmann (11). E_s echoes with top frequencies >5 MHz were found to occur in an oval pattern and to have a pronounced maximum in the oval's night sector, indicating a close relationship to the location of maximum occurrence of visual aurora.

Simultaneous occurrence at a station of night E (or "auroral E", a term proposed by Penndorf (12) for this particle produced layer) and aurora has been reported by King (13) and Bullen (14). On the other hand Hanson et al. (1) found no hour-to-hour correlation of night E with aurora. Night E has also been observed equatorward of visual aurora (King (15)). With increasing magnetic activity auroral E (night E) is observed at lower latitudes than in quiet conditions, which suggests a relationship between auroral E and the auroral oval. Whalen et al. (8) found close relation between non-discrete, continuous aurora and auroral E (night E) on cross-section flights through the noon sector of the auroral oval.

Observations of the relationship between E_{sa} echoes and aurora and between night E and the location of the auroral oval, reported here, were made during cross-section flights through the auroral oval.

2.1. RELATIONSHIP BETWEEN AURORAL E_s AND VISUAL AURORA

A section of a flight is discussed where the aircraft crossed several times underneath a stable auroral band. Vertical incidence ionograms and all-sky photographs used for this analysis were simultaneously recorded at one minute intervals on 14 December 1968 during a flight from Labrador to Alaska. The flight track was planned so that the midnight sector of the auroral oval could be monitored for more than 9 hours while 18 latitudinal cross-sections, extending over 3° to 3-1/2° CG latitude, were made within the auroral belt. Recording of ionograms and all-sky photographs started on scan 4 and continued through the end of the flight. The flight track is shown in Figure 1 in geographic coordinates on the left side and in CG latitude and CG local time on the right side.

Quiet magnetic conditions prevailed during the flight, $K_p = 0_+, 1, 1$. In the first part of the flight no discrete aurora was observed, and only occasional brightening of the sky and very faint unstructured forms in the north were observed. No E_s was recorded during this time; however, a band of auroral E was observed which will be discussed later. At 6 UT (at the start of latitudinal scan 7) an oval-aligned arc developed which extended from the west to the east horizon. During the following 6 hours this aurora was seen constantly while the aircraft moved to the west, crossing underneath the aurora from south to north respectively north to south 12 times. In the last three hours of the flight (9 to 12 UT) the aurora was at times very active often filling the entire field of view of the all-sky camera (1000 km diameter); quiet conditions returned in between. During the 6 hours when discrete aurora was observed auroral E_s was recorded continuously; auroral type E_s, as described in the IGY Manual (16), page 94—95. Figure 2, lower part, shows an E_{sa} echo recorded during this flight. When the aircraft approached an arc or band, passed underneath it, and then moved away from it, the virtual height of the E_{sa} echo regularly decreased from high ranges, levelled off at a minimum value and increased again. When overhead aurora was observed over the entire width of the latitudinal scans, the time history of any of the individual bands or other forms could not be followed, the $h'E_{sa}$ stayed at minimum values, no oblique traces were seen. As soon as a band or arc could again be defined and it's zenith angle determined, the time variation of $h'E_{sa}$ and of the slant ranges to the aurora coincided again.

In the upper part of Figure 3, the virtual height of E_{sa} (open circles) and the slant ranges to the visible aurora (full circles connected by dotted line) are plotted versus UT. They were recorded during the 3 hours when a stable auroral arc or band was crossed 6 times. Encircled numbers indicate the scan number in the sequence of latitudinal crossings. The slant ranges to the aurora were determined from the all-sky photographs assuming that the lower edge of the aurora was 120 km above ground. The slant ranges to the aurora and h'E coincide very well. Approach to and movement away from the aurora can be followed in passes 9 through 12 since the location of the bands (extending east-west) was in the center latitude of the scans. In scan 7 the aircraft turned before reaching the northern edge of the aurora, and on the return scan the southern edge had moved to the north. The fact that the virtual height of the E_{sa} and the slant range to the aurora change simultaneously during the 6 crossings underneath the auroral band indicates that the region of ionization, causing the E_{sa} echoes, must be limited in latitudinal extent to the vicinity of the discrete aurora.

The auroral brightness increased during the period investigated. During passes 7 and 8 the aurora was very faint, $h'E_{sa}$ was 130-135 km when the aurora was overhead. Increased auroral brightness was observed in passes 9 and 10, the recorded minimum virtual height of E_{sa} was 120 km when the aurora was overhead. Finally, (passes 11 and 12) $h'E_{sa}$ had decreased to 105 km, and the brightness of the overhead aurora had again increased. From 0610 to 0730 UT (i.e. pass 7 through most of pass 9) simultaneous photometer measurements of the 5577Å emission were made (Whalen, private communication). When visible aurora was overhead during this time, the correlation between the spectral line intensity and the inverse virtual height of E_{sa} is good, even for short-time fluctuations.

Assuming that the height above ground of the lower edge of the auroral form, is identical with the virtual height of the E_{sa} when the aurora is in the aircraft zenith, the slant ranges were replotted for passes 7, 8, 11 and 12; The improved fit of the resulting slant ranges to the aurora and $h'E_{sa}$ curves is shown in the lower part of Figure 3. (Arrows below the time scale in pass 12 indicate the times for which ionograms and all-sky photographs are shown later, in Figure 5).

The correlation between auroral brightness and top frequency (fE_{sa}) of the E_{sa} echoes, found by other investigators, is confirmed by the measurements of this flight: faint aurora from (6-7 UT) is accompanied by fE_{sa} only occasionally over 4 MHz; increased auroral brightness (from 7-8 UT) by $fE_{sa} = 5$ MHz; rather bright aurora (from 8-9 UT), by fE_{sa} between 8 and 9 MHz. Therefore, it follows that the $h'E_{sa}$ is inversely related to fE_{sa}. In Figure 4 the virtual height of E_{sa}, recorded in passes 7 through 12 when aurora was observed in the zenith, are plotted versus the top frequency of the E_{sa} echo.

Figure 5 gives examples of ionograms and all-sky photographs recorded on pass 12. Simultaneously recorded ionograms and all-sky frames are labelled a. through d. and show that the range of the E_{sa} echo decreases when the auroral band is approached. Arrows below the time scale (pass 12) of Figure 3, lower part, indicate the times when the frames were recorded.

2.2 OCCURRENCE OF AURORAL E (NIGHT E) IN RELATION TO THE AURORAL OVAL

The close association between E_{sa} echoes and discrete aurora has been demonstrated. A few examples follow of the occurrence of auroral E (night E) echoes in relation to the auroral oval. The auroral E (night E) echoes were identified according to the description on page 106 of the IGY Manual (16). This definition, originally given by Hanson et al. (1), was found to be clear and comprehensive. Figure 2, upper part, shows two examples of auroral E (night E) echoes, recorded during arctic flights. A band of auroral E (night E) was regularly found in the three flights of December 1968 with a total of 16 cross-sections of the auroral oval at CG noon in darkness, reported by Whalen et al. (8). Characteristics of this particle

produced continuous E layer that are of interest here, are as follows: In the noon sector it extends about 5° southward from the instantaneous location of the discrete aurora; at the northern edge, at the location of overhead aurora, the typical E-echoes transform to E_{sa} at the same virtual height; from north to south the critical frequency of the auroral E layer increases, while the virtual height decreases.

Subsequent investigations of ionogram sequences from cross-section flights through other sectors of the auroral oval confirmed the existence of an oval aligned E- layer of particle origin.

AURORAL E OBSERVED IN THE NIGHT SECTOR OF THE AURORAL OVAL

In Figure 6 the tracks of cross-section flights through the night sector of the auroral oval are shown. The flights were made during the time from February 1968 through February 1971, and they were selected for this survey because of quiet magnetic conditions during the flights. K_p indices were 0 to 2 during most of the time; exceptions are K_p = 3 for part of flights d and e, and K_p = 4- at the start of flight b. A total of 33 latitudinal scans through, or within the night sector of the oval were made along the flight tracks; flights d, e, and f are "oval stationary" flights with several scans in the same CG time sector; 2 flights were made along flight route c. The heavy dotted lines indicate the flight tracks where auroral E (night E) with critical frequencies >2 MHz was observed; 2 MHz being the low frequency limit of the airborne sounder. Auroral E occurs in a continuous band that extends over several degrees of latitude. A black bar across the flight track indicates the location of the maximum critical frequency recorded on that scan. In the oval stationary flight d auroral E was present continuously in all 6 scans; in 3 or 4 scans for flight e; and in 5 out of 15 scans for flight f. The f_oE maximum was found at identical latitudes in every scan of a particular oval stationary flight. This is true also for the second maximum at 69° CG latitude in flight e. In the last of the 4 scans of flight e nondeviative absorption had increased, auroral E with $f_oE < fmin$ may have been present.

Flight f is the flight of 14 December 1968 where, as mentioned before, no auroral bands or arcs were observed in the first part of the flight, only some barely visible forms and areas of brightness were noticed. Auroral E was observed continuously until E_{sa} appeared simultaneously with the auroral arc that had formed. (Occasionally oblique E echoes could be seen in the presence of E_{sa}.) This observation confirms the relation of auroral E and a non-discrete form of aurora, found in the noon sector of the auroral oval (Whalen et al. (8)). For all other flights the location of the band of night E relative to the position of discrete aurora is not investigated here.

In the latitudinal distribution of f_oE a second maximum, as seen in flight e, is sometimes observed during more disturbed conditions. Concluding from the results of Whalen et al. (8), electron precipitation with a spectrum, hardening equatorward, is likely responsible for the auroral E-layer. Proton precipitation was found to be the cause for a second maximum in the north, recorded in a previous flight and not included here. Conditions in flight e are still under investigation. No second maximum of f_oE was observed in the other flights shown in Figure 6. In flights b and d, and perhaps in some scans of f, the auroral E (night E) region may have extended farther to the north of the flight tracks, and a second maximum may, therefore, have excaped observation. However, no increase in the E critical frequency was indicated near the northern end of the scans. Figure 6 summarizes the observations of cross-section flights through the night sector of the auroral oval in quiet magnetic conditions: a) Auroral E occurs in bands several degrees wide in latitudinal extent; and b) the pattern of f_oE increase with decreasing latitude that was established for the noon sector in darkness, is found to exist in the night sector also.

ENHANCED f_oE IN THE DAY SECTOR OF THE AURORAL OVAL, IN SUNLIGHT

Particle produced ionization in E-layer height has also been observed in the sector 08 through 21 CG time for times of low magnetic activity under sunlit conditions. In daylight the normal E-layer is produced by photoionization; where particle precipitation causes additional ionization, an enhanced critical frequency of the E layer is measured, with an f_oE that is higher than that corresponding to the zenith angle of the sun at that given time and location. Figure 7 shows (plotted in CG latitude and CG time) the routes of 9 flights performed in the summer of 1970 and 1971 which yielded a total of 16 cross-sections through the auroral oval. All flights were made in daylight and during magnetic conditions characterized by K_p 0 to 3- (except for one crossing with K_p 4-). Heavy black lines along the flight tracks indicate the latitudes where enhanced f_oE was recorded. Dotted lines indicate those areas where the enhancement was very little. In every crossing of the oval a single belt of enhanced f_oE was observed, the latitudinal extent of which varied from 2° to 6°. Considerable variation in the location of the enhanced f_oE region is observed mainly in the 6 crossings in the 10 to 14 CG time sector. The center latitude of the region is located between 67° and 73° CG latitude compared with 71° and 78° for 16 crossings through the noon sector in darkness on the 3 flights of December 1968. In the evening, 18 through 21 CG time, the center latitude of the region of enhanced E ionization is found at 70° to 71° CG latitude in 5 out of 8 cases. This coincides with the results from cross-section flights during the same time interval, presented in Figure 6.

SPREAD E

Characteristic of the auroral E (night E) echo trace observed during dark hours is the spread near the critical frequency. Spread near the critical frequency of the E layer is also observed in ionograms recorded in the region of f_oE enhancement, in daylight. The spread E is observed so regularly with enhanced f_oE that Bullen (14) uses occurrence of spread E in daytime ionograms as one criterion to determine from ionograms the existence of particle produced ionization. In Figure 8 an example is given to illustrate the change in appearance of the E echo traces from normal to spread and back to normal. The ionograms were recorded during a flight in daylight across the oval belt. Within the latitude band where foE was enhanced, spread E was observed continuously. However, on the return (N to S), when the aircraft crossed the region of enhanced E again, the spread near the critical frequency of E was rather weak and not seen in every ionogram (one ionogram per minute being recorded).

AURORAL E OBSERVED CONTINUOUSLY AROUND THE AURORAL OVAL

The cross-section flights through the auroral oval belt at nearly all times accumulated statistical evidence for the validity of the E layer pattern which was first established for the noon sector in darkness. The question arises whether this pattern is also valid as an instantaneous picture around the auroral oval.

In the 10 hour circumoval flight of 5 January 1970 nearly the entire oval belt was investigated. In Figure 9 the thin continuous line is the flight track plotted in CG latitude and CG local time. The decrease of f_0E with increasing CG latitude was found in all sections of the flight where the flight track deviated from its primarily eastward course and crossed through several degrees of latitude toward the N or the S. This latitudinal dependence is particularly evident from 7 to 9 CG local time, 14 to 16 CG local time, and at the end of the flight near midnight. Using the f_0E values from analysis of the ionograms recorded during the flight, contour lines of f_0E were drawn, shown as heavy lines in Figure 9; the dotted lines connect extrapolated values. At 02 and 04 CG local time (in Figure 9) E echoes were seen obliquely; they originated from a layer S of the flight track, as could be determined by photometric measurements. The figure presents a quasi-instantaneous picture of the occurrence of auroral E (night E) as derived from data taken on this flight. The 5th of January 1970 was a day of low magnetic activity.

GROUND STATION DATA REVIEWED IN RELATION TO OVAL-ALIGNED E LAYER PATTERN

The E layer pattern for quiet days, derived from the aircraft data, can be tested by ground station data. As an example in Figure 10, in the center, a graph is shown from Hanson, et al. (1) of the time variation of the critical frequency of a night E echo observed during a 5 hour period at Fort Chimo on 26 January 1952, a magnetically quiet day. The ionograms, from which the critical frequencies are derived, are reproduced in their paper and show typical examples of night E (auroral E) echoes. The hour by hour positions of the station relative to the Q=1 auroral oval are marked by triangles, the first corresponding to 16 LT (local time at Fort Chimo). If on this day an approximately oval-aligned E region was present as indicated, the station would be south of the E region through about 1745 LT. Rotating further toward the auroral oval it would move under the 3.0 MHz f_0E contour at 18 LT. Due to the steep gradient versus latitude in f_0E at the southern edge of the E region, the narrow band of maximum f_0E is overhead before 19 LT. From 19 to 20 LT the station moves through the northern part of the night E region.

2.3. SUMMARY AND RESULTS

1) Analysis of ionogram sequences and simultaneous all-sky photographs from a flight making six latitudinal scans in the midnight sector of the auroral oval under quiet magnetic conditions shows that: a) The recorded auroral type Es echo (E_{sa}) is returned from a spatially limited area confined to the latitudinal extent of the visible aurora, b) Good correlation exists between the brightness of aurora in the zenith, the inverse of the virtual height of the E_{sa}, and the top frequency of the E_{sa}. Consequently, in case of overhead aurora, the top frequency increases with decreasing virtual height of the E_{sa}. The results of the analysis also appears to support the assumption that the E_{sa} echoes originate from a height identical with that of the lower edge of the aurora.

2) Ionogram sequences from cross-section flights through the oval belt during times of low magnetic activity show the existence of an oval-aligned region of auroral E (night E) which has a width of 2°-6° latitude. It extends equatorward from the location of the auroral oval in the day sector of the auroral oval and is located within the oval belt in the night sector. Of a total of 49 latitudinal scans through the oval belt, at times from 07 through noon to 04 Corrected Geomagnetic Time, 38 show the presence of auroral E. 16 of the 22 scans through the auroral oval's night sector exhibit the same latitudinal pattern found (by Whalen et al. (8)) in the noon sector in darkness; namely, decrease of virtual height of the E layer from north to south corresponding to precipitating particles with a hardening of the spectrum from northern to southern latitudes; and an increase of the E layer critical frequency from north to south. The analysis of day flights through the auroral oval resulted in the mapping of the regions where enhanced foE was recorded, i.e. where foE was higher than to be expected from photoionization. Although the latitudinal distribution of the amount of f_0E enhancement was not established here, the pattern is consistent with that derived from the measurements in darkness, as are the results of a 10 hour circumoval flight in which auroral E (night E) was continuously observed.

3. POLAR F-LAYER

The high-latitude F layer has been investigated by many workers, and several basic features are now known. Muldrew (18), using Alouette topside ionograms, first showed the existence of the main F-layer trough. Petrie (19) established that the occurrence of spread F on Alouette ionograms maximized in an oval-shaped region which encircled the geomagnetic pole. Akasofu (20) later identified Petrie's spread-F region as being coincident with the quiet time auroral oval, hence a "spread-F oval". Thomas and Andrews (21) showed that the distribution of topside F-layer electron density enhancements, scaled from Alouette ionograms, maximized in an elongated ring, the "plasma ring", which, similar to the spread-F oval, encircled the geomagnetic pole. Ionograms recorded on the Flying Ionospheric Laboratory during cross-section flights through the day sector of the auroral oval were compared with Alouette electron density data and showed that the topside polar F-layer plasma ring existed in the bottomside as an F-layer irregularity zone (22). On these flights the latitudinal extent of the F-layer irregularity zone was determined from ionogram movies recorded on the aircraft sounder. An example which illustrates how the aircraft's motion is used to interpret F-layer features on ionograms is shown in this next section.

3.1. AIRBORNE F-LAYER MEASUREMENTS

In the top half of Figure 11 the aircraft's flight route on August 22, 1970 is indicated by the dashed line drawn on a CG latitude and CG local time grid. The night sector of the auroral oval for Q=2 magnetic conditions is indicated by heavy solid lines. A sequence of aircraft ionograms is shown in the bottom-half of Figure 11. The letters next to the ionograms refer to the aircraft's positions, marked by the same

letters on the flight route map, when the ionograms were recorded. In ionogram A there is a vertical incidence F-layer echo at 280 km, the first and second F-layer multiple echoes, and an extra echo at about 425 km. In ionogram B the extra echo is at a range of about 490 km; while in ionogram C, recorded just before the aircraft turned, the extra echo is at a range of about 530 km. The change in range of the extra echo corresponds to about the distance that the aircraft flew away from the southern edge of the oval between the times ionograms A and C were recorded. The extra echo is then an oblique incidence echo which, most likely, is produced by a reflecting surface located north of the aircraft near the oval. Ionograms D and E show the oblique incidence echo moving down in slant range as the aircraft flies back towards the oval. In ionogram F the oblique incidence echo is now closer in slant range than the vertical incidence F-layer echo. Thus, the original vertical incidence F-layer echo is an oblique incidence echo, and a new F layer, the original oblique incidence echo, is moving down in range and will become a vertical incidence F-layer echo. The slant range to the extra echo is plotted versus universal time in Figure 12. The letters on the abscissa refer to the aircraft's positions which are noted in Figure 11 by corresponding letters. All of the ionograms, recorded at the rate of one per minute, contain a strong oblique incidence echo, therefore, the slant range to the oblique incidence echo could be plotted with an accuracy of ±10 km. One sees a uniform increase in slant range as the aircraft flies south, away from the oval. The inflection point of the curve corresponds to the time during which the aircraft turned, and the decrease in slant range is due to the aircraft flying north, towards the oval. This example demonstrates how F-layer echoes, which occur in a sequence of ionograms, can be uniquely identified and followed when the aircraft is flying relative to a stable reflector.

3.2. F-LAYER MEASUREMENT AT GOOSE BAY

From October 27-29, 1970 the Flying Ionospheric Laboratory was located on the ground at Goose Bay, Labrador. Goose Bay is located at geographic coordinates 54°N, 60°W or at CG coordinates 65.5°N, 22°W. The location of Goose Bay, indicated by triangles, and the Q=3 auroral oval have been plotted in Figure 13 on a CG latitude and time grid. From Figure 13 one can see that Goose Bay moves towards the oval during the afternoon and evening, that Goose Bay is underneath the oval near midnight, and that Goose Bay moves away from the oval in the morning. During this three day period at Goose Bay the aircraft sounder was operated continuously; the photometer and auroral all-sky camera were used at night for auroral measurements. Vertical and oblique incidence F-layer echoes, seen on the Goose Bay ionograms, are discussed here; schematic drawings, showing the main F-layer trough and the F-layer irregularity zone, are presented.

A sequence of Goose Bay ionograms, recorded on October 27, 1970, is shown in Figure 14. These ionograms were recorded during the late afternoon and evening from 1720 to 2110 local time, and F-layer sunset occurred at about 1830 local time. Analysis of these ionograms, recorded on 35 mm film, was facilitated by viewing a 16 mm movie of the ionograms a number of times and by following F-layer features frame by frame in the movie. Later, these features were identified and numbered on these single 35 mm frames. Ionogram A shows well defined ordinary and extraordinary wave components of an echo, labelled I, from an F layer produced by the sun and an extra echo, labelled III, at 725 ± 20 km between the first and second solar F-layer multiple echo. Ionogram B shows that echo III has moved down in range to 625 ± 20 km and has become better defined than before. The movie presentation of the ionograms, recorded between these two selected frames, shows echo III moving down in range. Ionogram C shows the solar F-layer echo, echo I, the first solar F-layer multiple echo, labelled I', echo III, and a new extra echo, labelled II, at 475 ± 10 km. Echoes, similar to those labelled II and III, have been identified by Stanley (23) and Bowman (24) as echoes which are produced by oblique incidence reflections from the poleward wall of the main F-layer trough. Echoes II and III are also similar to the oblique incidence echo that was reflected from the region of the oval in the airborne ionogram sequence in Figure 11. Thus, echoes II and III are probably oblique incidence echoes which are produced by reflecting surfaces located north of Goose Bay in the vicinity of the main F-layer trough and the F-layer irregularity zone. Ionogram D shows the solar F-layer echo, echo I, with no multiple echoes and the oblique incidence echo, echo II. The absence of a solar F-layer multiple echo would suggest that at this time a curvature in the structure of the plasma frequency contours is passing over Goose Bay and is causing ionospheric defocussing. Further suggestion for the presence of a curvature is the 30 km increase in virtual height of the solar F-layer echo which occurs between ionograms B and D. In ionogram E one sees echo I from the solar F layer, oblique incidence echo II, and what may be the reappearance of oblique incidence echo III. Bates (25) has pointed out that since aspect sensitivity of the reflecting surface is a problem encountered in the analysis of oblique incidence echoes, the appearance and disappearance of oblique incidence echoes can often be impossible to follow. Ionogram F contains a complex overlapping of echoes I, II, and III between 275 and 400 km which cannot be interpreted with certainty. However, a multiple reflection of echo II may now be seen; thus, echo II must be nearly overhead at this time.

A sequence of schematic drawings of F-layer structure, which could produce echoes I, II, and III, can provide some understanding of the ray path geometry involved in producing these echoes. The schematics, seen in Figure 15, were drawn by assuming that during the late afternoon and evening the main F-layer trough and the F-layer irregularity zone would move from the north towards Goose Bay. The schematics are composed of constant plasma frequency contours which extend north and south from Goose Bay. One schematic cross-section has been drawn for each ionogram in Figure 14. Virtual heights and plasma frequencies, taken from ionograms A through F, were used as the quantitative basis for the respective schematics. The earth's curvature was taken into account when the grid for the schematics was drawn. The ionosonde in the aircraft has a frequency threshold of 2 MHz. The trough, which has an foF2 equal to or less than 2 MHz (18) (23), was not seen directly on the ionograms, and its presence has been inferred by ionogram interpretation. Schematic A shows the plasma frequency contours which could produce the echoes in ionogram A. The solar F-layer echo, echo I in ionogram A, can be produced by ray path I in schematic A. Echo III can be produced by ray path III which has been constructed by assuming that a reflecting surface is located north of Goose Bay at about the 250 km level. Accordingly, the 725 km slant range to echo III in ionogram A corresponds to a northward horizontal distance of about 650 km as is shown in schematic A. The reflecting surface has been assumed to be the F-layer irregularity zone and has been represented in the schematics by a kink in the plasma frequency contours. In schematic B the irregularity zone is closer to Goose Bay than in schematic A, while in schematic C the distance between Goose Bay and the irregularity zone has not changed. These distances are consistent with the slant ranges to echo III which are seen in ionograms B and C. The appearance of echo II in ionogram C is interpreted as indicative of the onset of the trough. The formation of the trough would be expected

at this time because solar production, which fills in and smooths over the trough during daytime (26), has almost ceased by now. The shape of the trough has been drawn by using Bowman's (24) trough contours as a model with the exceptions that the troughs, which he saw during the IGY, were wider by a factor of 4 or 5 and deeper than the trough shown here. In ionogram D the absence of multiple echoes suggests that the trough is passing near Goose Bay at this time and is causing defocussing. For this reason, the trough is shown nearly overhead of Goose Bay in schematic D. Echo III is missing in ionogram D. One reason for this may be aspect sensitivity of the reflecting surface or, as indicated in the schematic, E_s or absorption may be blocking radio waves from reaching the irregularity zone. In schematic E ray path III is drawn because ionogram E may contain echo III. The trough has been drawn with about the same shape in schematic E as it had been drawn in schematic D. Because ionogram F contains a very complex overlapping of echoes, the interpretation given to these echoes in schematic F should be treated with caution. The appearance of a multiple echo of echo II, which up to now had been oblique and did not display a multiple echo, suggests that the trough has passed over Goose Bay and that Goose Bay is now located on the poleward side of the trough. Echoes I and III are barely discernable in ionogram F but, after examining other ionograms which were recorded at about the same time as this ionogram, the complex overlapping of these echoes has been interpreted as seen in schematic F. That is, it appears that echo I has moved out in range since the time that ionogram E was recorded; while echo III appears to have moved down in range since then.

3.3 MONITORING THE F-LAYER IRREGULARITY ZONE

In this section a new ionogram analysis procedure is presented, and examples are shown which demonstrate how this procedure can be used to monitor the CG latitude of the southern edge of the F-layer irregularity zone. A slant range plotter has been constructed so that the virtual heights of oblique incidence echoes, similar to those labelled III in Figure 14, could be utilized in ionogram analysis and not omitted as they generally are. This plotter (shown in Figure 16) permits the virtual height of an oblique incidence echo to be plotted versus the left ordinate; the CG latitude, which corresponds to an echo at this slant range, has been labelled on the right ordinate. Thus, the CG latitude of the F-layer irregularity zone can be monitored during the late afternoon and evening, when the irregularity zone is far to the north of Goose Bay, by plotting the virtual heights of Echo III onto the slant range plotter. A 250 km F-layer reflection height has been assumed for reflections which come from the F-layer irregularity zone. Some error in determining the latitude of the southern edge of the irregularity zone may be introduced by this assumption but it should not be greater than $\pm 0.5°$. The slant ranges to echo III in the October 27 ionograms have been plotted on the slant range plotter in Figure 16. The squares indicate that reflections from the irregularity zone were clearly seen at that particular time; while a series of squares, connected by a line, indicates that the irregularity zone echo was seen on each ionogram recorded during this period. The irregularity zone echo closely follows the southern edge of the oval, and the CG latitude of the southern edge of the irregularity zone can be followed as a function of local time. The aircraft contains a photometer and an auroral all-sky camera which were also operated but, because of partial cloud cover on this night, the all-sky camera data cannot be used. The 5577Å spectral line of the photometer operated very well through the cloud cover and responded to the presence of aurora in the zenith at 2140 LT (indicated in Figure 16 by an arrow). The onset of the F-layer irregularity zone overhead is then closely related to the presence of aurora in the zenith in the late evening sector. Bates (27) and Bates et al. (28), studying the correlation between radio and optical aurora in the night sector, noted close but not exact spatial coincidence between optical aurora and HF auroral backscatter. A study of the correlation between radio and optical aurora was not intended here, but it appears that the F-layer irregularity zone is closely related to the F region which Bates has identified as the source of HF backscatter.

The slant range plotter for October 28, 1970 is seen in Figure 17. The letter b indicates the presence of overhead blanketing Esa which did not permit the detection of oblique incidence F-layer echoes. The presence of aurora in the zenith, noted by the arrow at 2000 LT, was again determined from the intensity of the 5577Å spectral line and it occurred about 1 3/4 hours earlier than on the previous night. Similarly, the irregularity zone, indicated by squares, was detected earlier than on the previous night. The daily sum of the geomagnetic activity indices, Kp, on Oct. 27 was $\Sigma Kp=9$ and on Oct. 28 was $\Sigma Kp=22+$. The difference in onset times of the irregularity zone on these two days can readily be explained by the difference in magnetic activity on the two days. If one puts the slant range data for these days onto auroral ovals of different Q value, then the reason for the difference in the onset times between the two days can be seen clearly. A Q=1 and a Q=3 oval were selected for the data of October 27 and 28 respectively, and they are seen in Figures 18 and 19. The data points are plotted on a CG local time and CG latitude grid. In general the data points fit the two different ovals quite well but, in Figure 19, there is a sudden departure of the data points from the southern edge of the oval at about 17 to 18 CG time. This appears to be a real effect because it was possible to follow an echo, similar to echo III in Figure 14, on each ionogram recorded during this period. If the reflecting surface underwent an latitudinal oscillation at this time, it could produce this effect. It appears then that the latitude of the southern edge of the F-layer irregularity zone can be monitored by plotting the slant ranges to certain oblique incidence echoes onto the slant range plotter.

3.4 CONCLUSIONS

A special analysis of vertical and oblique incidence F-layer echoes, seen on vertical incidence ionograms, was presented. Results from the analysis suggest that the latitude of the southern edge of the polar F-layer irregularity zone can be monitored, therefore, on the spot analysis of ground station ionograms from Goose Bay, Labrador, can probably lead to a real-time or near real-time monitoring of the polar F-layer irregularity zone for 6 to 8 hours of each day. Furthermore, the time when the main F-layer trough passes over Goose Bay can be specified on each day. The close coincidence which was shown to exist between the location of aurora and the F-layer irregularity zone suggests that the CG latitude of the southern edge of the auroral oval, in the afternoon and evening sectors, can similarly be monitored.

ACKNOWLEDGEMENTS

The authors wish to thank the following: D. Kimball, for the detailed evaluation of the all-sky photographs recorded on the flight of 14 December 1968, J.A. Whalen for comparison with his photometer data and helpful discussions, G.J. Gassmann, J. Buchau, R. Penndorf for valuable comments and discussions. The successful operation of all instruments was under the direction of R.W. Gowell, Major A.H. Sizoo coordinated the flight schedules, and the aircraft was operated by the aircrew members of Test Operations of the 3245th Air Base Group.

REFERENCES

1. Hanson, G.H., Hagg, E.L., and Fowle, D., "The Interpretation of Ionospheric Records". Canadian Defense Research Telecommunications Estab. Rep. No. R-2, 1953.

2. Feldstein, Y.I. and Starkov, G.V., "Dynamics of Auroral Belt and Polar Geomagnetic Disturbances". Planet. Space Sci., 15, 209, 1967.

3. Hultqvist, B., "The Spnerical Harmonic Development of the Geomagnetic Field, Epoch 1945, Transformed into Rectangular Geomagnetic Coordinate Systems". Arch. Geophys., 3, 53, 1958a.

4. Hultqvist, B., "The Geomagnetic Field Lines in Higher Approximation". Arch. Geophys., 3, 63, 1958b.

5. Hakura, Y., "Tables and Maps of Geomagnetic Coordinates Corrected by the Higher Order Spherical Harmonic Terms" Rep. Ionosphere Space Res. Japan, 19, 121, 1965.

6. Knecht, R.W., "Relationships between Aurora and Sporadic E Echoes at Barrow, Alaska". J. Geophys. Res., 61, 1, 59, 1956.

7. Buchau, J., Whalen, J.A., and Akasofu, S.-I., "Airborne Observation of the Midday Aurora". J. Atmos. Terr. Phys., 31, 1021, 1969.

8. Whalen, J.A., Buchau, J., and Wagner, R.A., "Airborne Ionospheric and Optical Measurements of Noontime Aurora". J. Atmos. Terr. Phys., 33, 661, 1971.

9. Hunsucker, R.A. and Owren, L., "Auroral Sporadic E Ionization". J. Res. Nat. Bureau of Standards, 66D, 581, 1962.

10. Harang, L., "The Aurorae". John Wiley and Sons, Inc., New York, 1951.

11. Pittenger, E.W. and Gassmann, G.J., "High Latitude Sporadic E". AFCRL Environmental Research Paper, No. 347, 1971.

12. Penndorf, R., "High-Latitude Propagation Study". RADC-TR-70-240, Vol. 1, Final Technical Report, 1971.

13. King, G.A.M., "The Aurora and the Night E layer". J. Atmos. Terr. Phys., 27, 426, 1965.

14. Bullen, J.M., "Enhanced Activity in the Ionosphere E Region at Cape Hallet and Campbell Island". J. Atmos. Terr. Phys., 28, 879, 1966.

15. King, G.A.M., "The Night E Layer", in "Ionospheric Sporadic E". E.K. Smith and S. Matsushita, Ed., Pergamon Press, New York, 219, 1962.

16. IGY Instruction Manual, The Ionosphere, Annals of the International Geophysical Year, Vol. III, Pergamon Press, 1957.

17. Whalen, J.A., Private Communication, AFCRL.

18. Muldrew, D.B., "F-Layer Ionization Troughs Deduced from Alouette Data". J. Geophys. Res., 70, 11, 2635, 1965.

19. Petrie, L.E., "Preliminary Results on Mid and High Latitude Spread F", in "Spread F and Its Effect on Radio Wave Propagation and Communication". AGARDograph 95, edited by Philip Newman, Technivision Press, 67, 1966.

20. Akasofu, S.-I., "Polar and Magnetospheric Substorms". D. Reidel Publishing Company, Dordrecht, 1968.

21. Thomas, J.O. and Andrews, M.K., "The Trans-polar Exospheric Plasma, 3: A Unified Picture". Planet. Space Sci., 17, 439, 1969.

22. Pike, C.P., "A Latitudinal Survey of the Daytime Polar F Layer". J. Geophys. Res., to appear 1971.

23. Stanley, G.M., "Ground-Based Studies of the F Region in the Vicinity of the Mid-Latitude Trough". J. Geophys. Res., 71, 21, 5067, 1966.

24. Bowman, G.G., "Ionization Troughs Below the F2-Layer Maximum". Planet. Space Sci., 17, 777, 1969.

25. Bates, H.F., "The Aspect Sensitivity of Spread-F Irregularities". J. Atmos. Terr. Phys., 33, 111, 1971.

26. Thomas, J.O. and Rycroft, M.J., "The Exospheric Plasma During the International Years of the Quiet Sun". Planet. Space Sci., 18, 41, 1970.

27. Bates, H.F., Belon, A.E., Romick, G.J., and Stringer, W.J., "On the Correlation of Optical and Radio Auroras". J. Atmos. Terr. Phys., 28, 439, 1966.

28. Bates, H.F., Sharp, R.D., Belon, A.E., and Boyd, J.S., "Spatial Relationships Between HF Radar Aurora, Optical Aurora and Electron Precipitation". Planet. Space Sci., 17, 83, 1969.

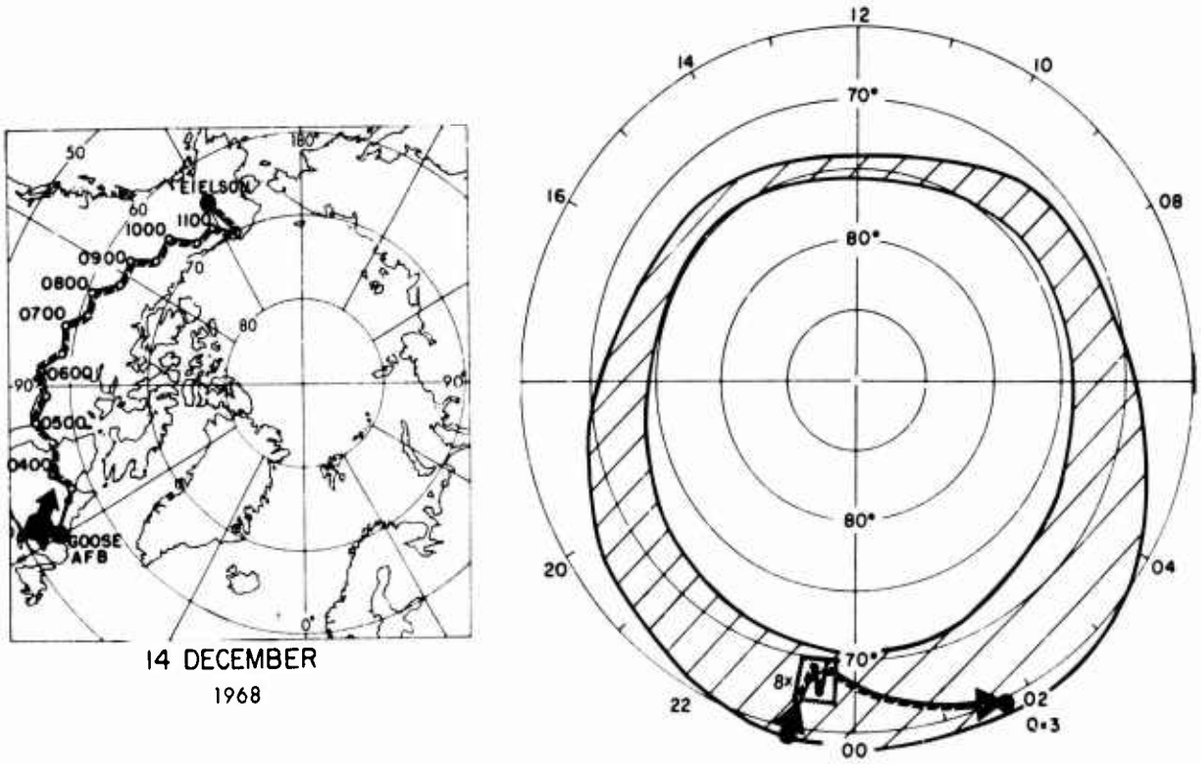

Figure 1. Flight track of the flight of 14 December 1968 in geographic (left) and CG coordinates (right). The Q=3 oval is indicated by heavy solid lines.

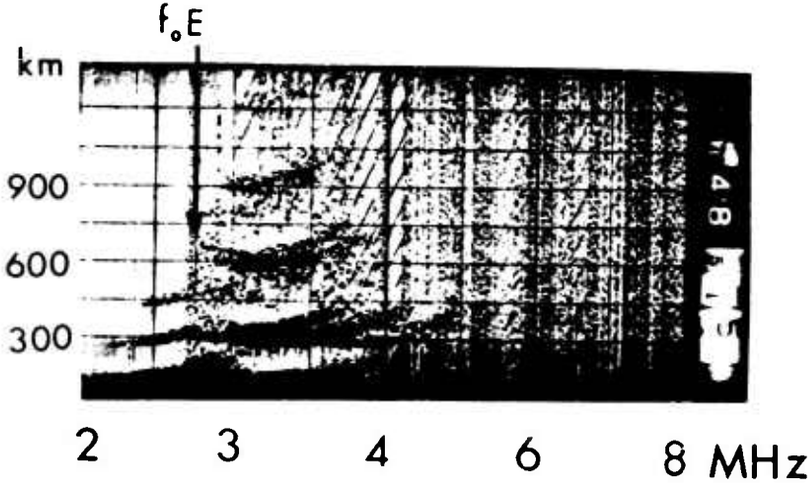

AURORAL E (NIGHT E)
5 JAN. 1970, 0848 UT, 70°N - 150°W (GEOGR.)

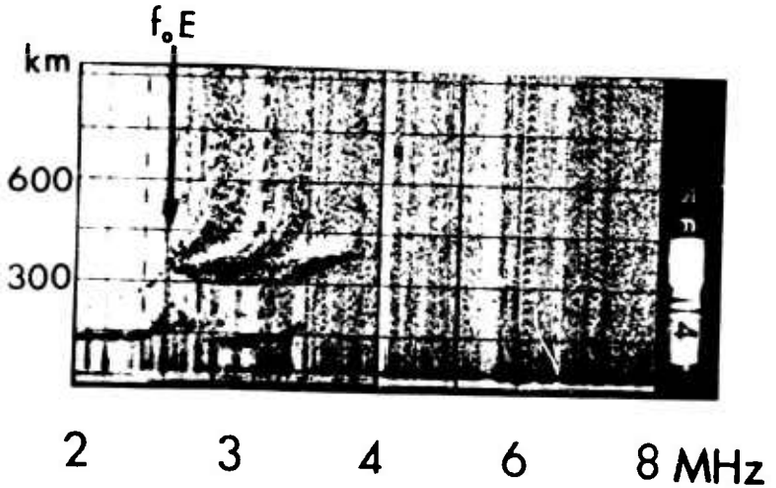

AURORAL E (NIGHT E)
14 DEC. 1968, 0556 UT, 56°N - 93°W (GEOGR.)

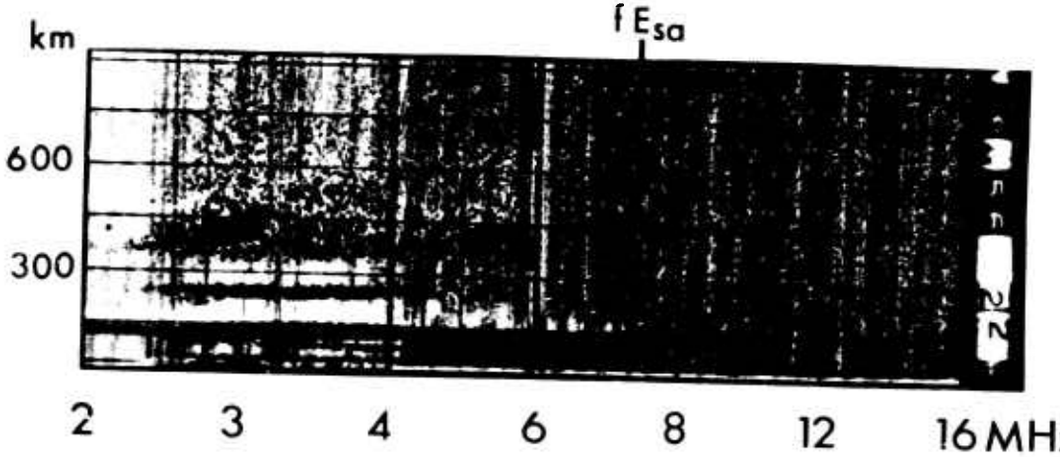

E_{sa}
14 DEC. 1968, 0856 UT
53°N - 122°W (GEOGR.)

Figure 2. Examples of ionograms which show night E (auroral E) and E_{sa} echoes.

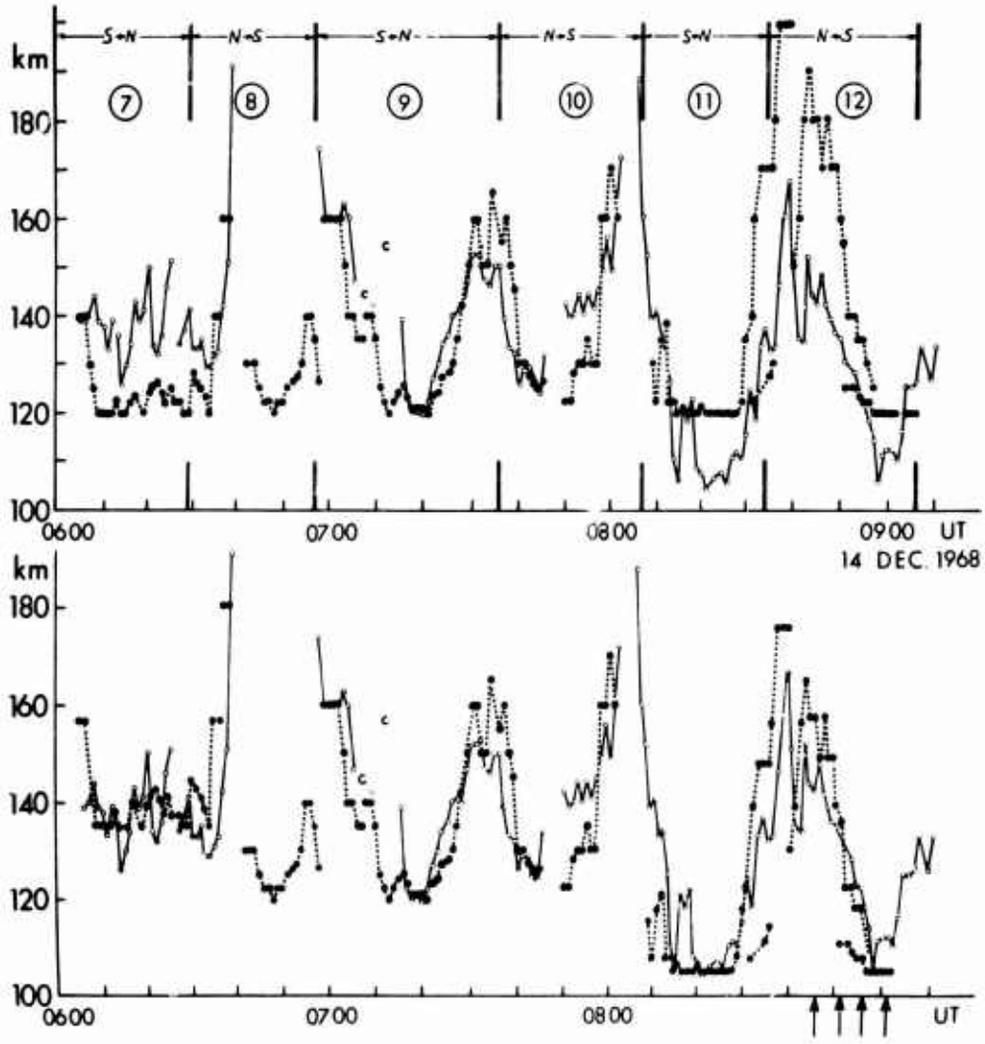

Figure 3. Virtual heights of E_{sa} versus UT, open circles; and slant ranges to the aurora versus UT, full circles, connected by dotted lines. The encircled numbers are the numbers in the sequence of 18 latitudinal scans. The vertical double lines indicate the aircraft turns at the northern or southern end of the scans. Upper part: slant ranges to the aurora, when actual height of aurora is assumed to be 120 km above ground; lower part: slant ranges to the aurora when actual height of aurora is assumed to be identical to the virtual height of E_{sa}, measured when aurora is overhead. The arrows on the abscissa mark the times when the ionograms and all-sky photographs, shown in Figure 5, were recorded.

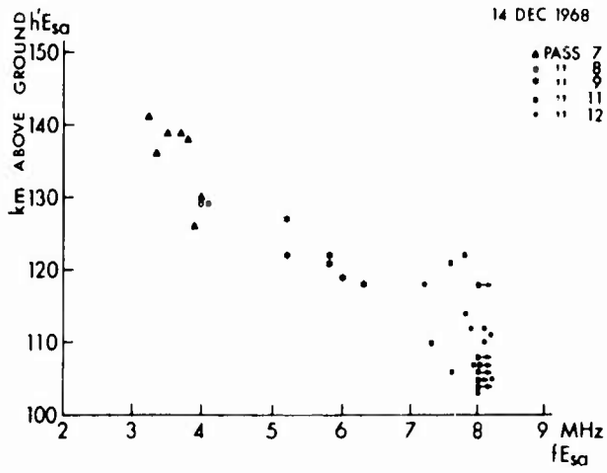

Figure 4. Virtual height of E_{sa} echo versus top frequency of E_{sa} for 14 December 1968. The values were recorded when aurora was overhead. The arrows at some of the 8 MHz values indicate that the top frequencies were higher than the high frequency limit of the sweep.

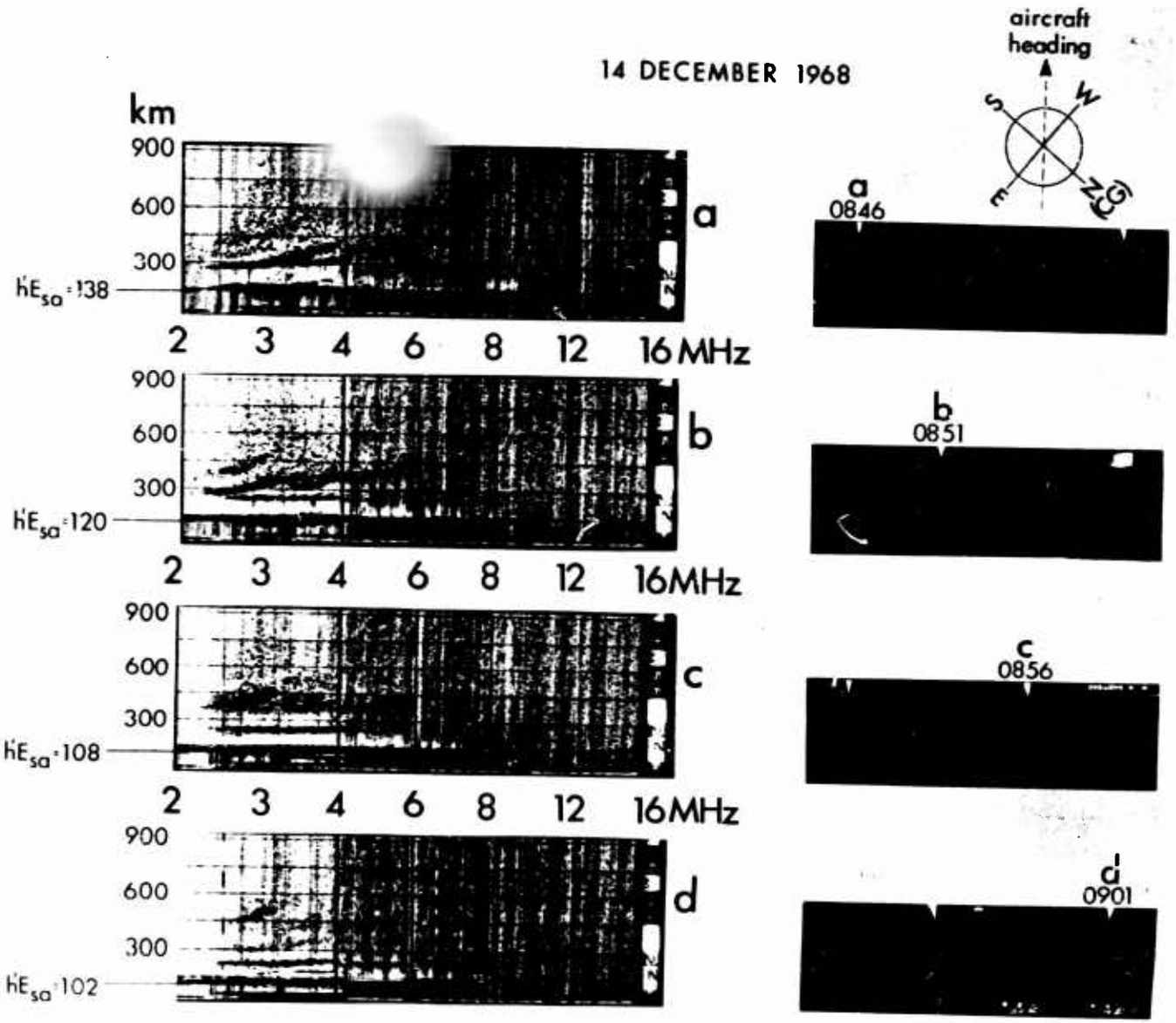

Figure 5. Ionograms and all-sky photographs simultaneously recorded on 14 December 1968, pass 12.

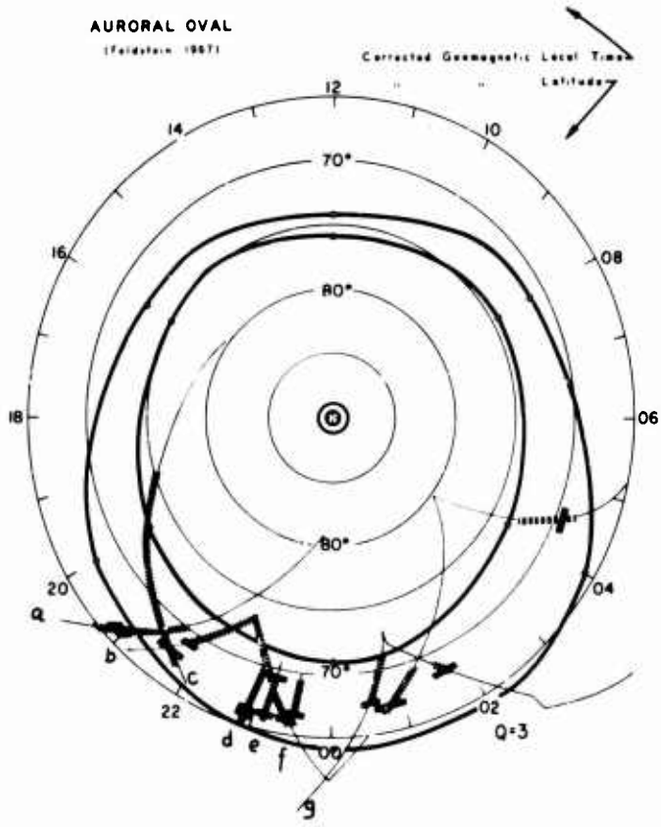

Figure 6. Flight tracks of flights through the night sector of the auroral oval; thick dotted lines mark the latitudes where night E (auroral E) was observed; black bars indicate the location of maximum f_0E for each latitudinal scan: a) 10/11 October 1969, b) 21 April 1969, c)12 and 14 Dec. 1969, d) 24 November 1970, e) 1/2 February 1971, f) 14 December 1968, and g) 5/6 February 1968.

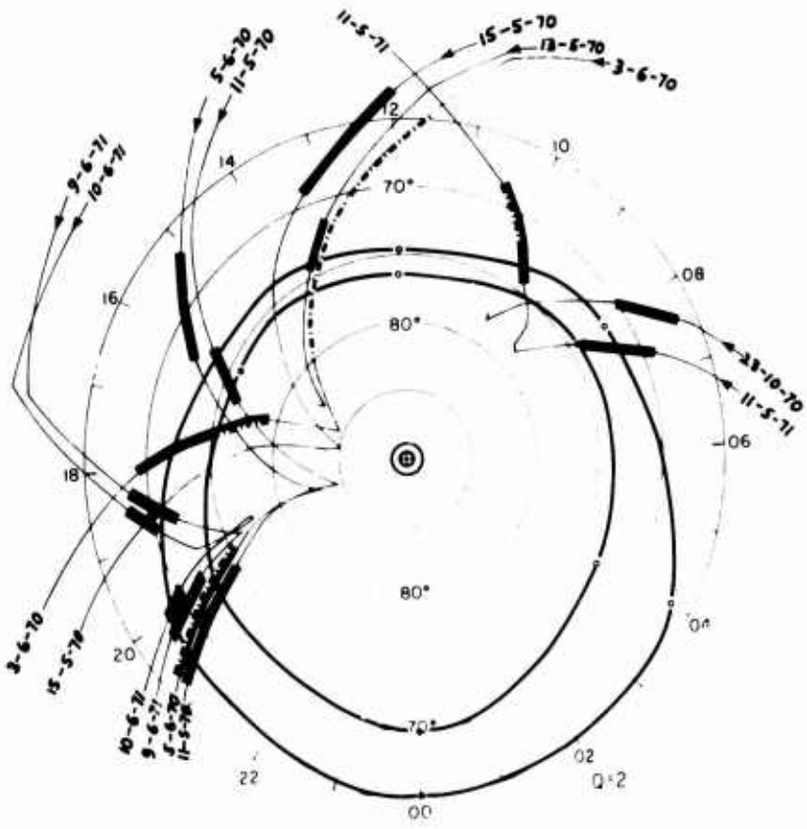

Figure 7. Flight tracks of cross-sections through the oval in daylight conditions. Latitudes where enhanced f_0E was observed are marked by thick black lines; dotted sections are less certain.

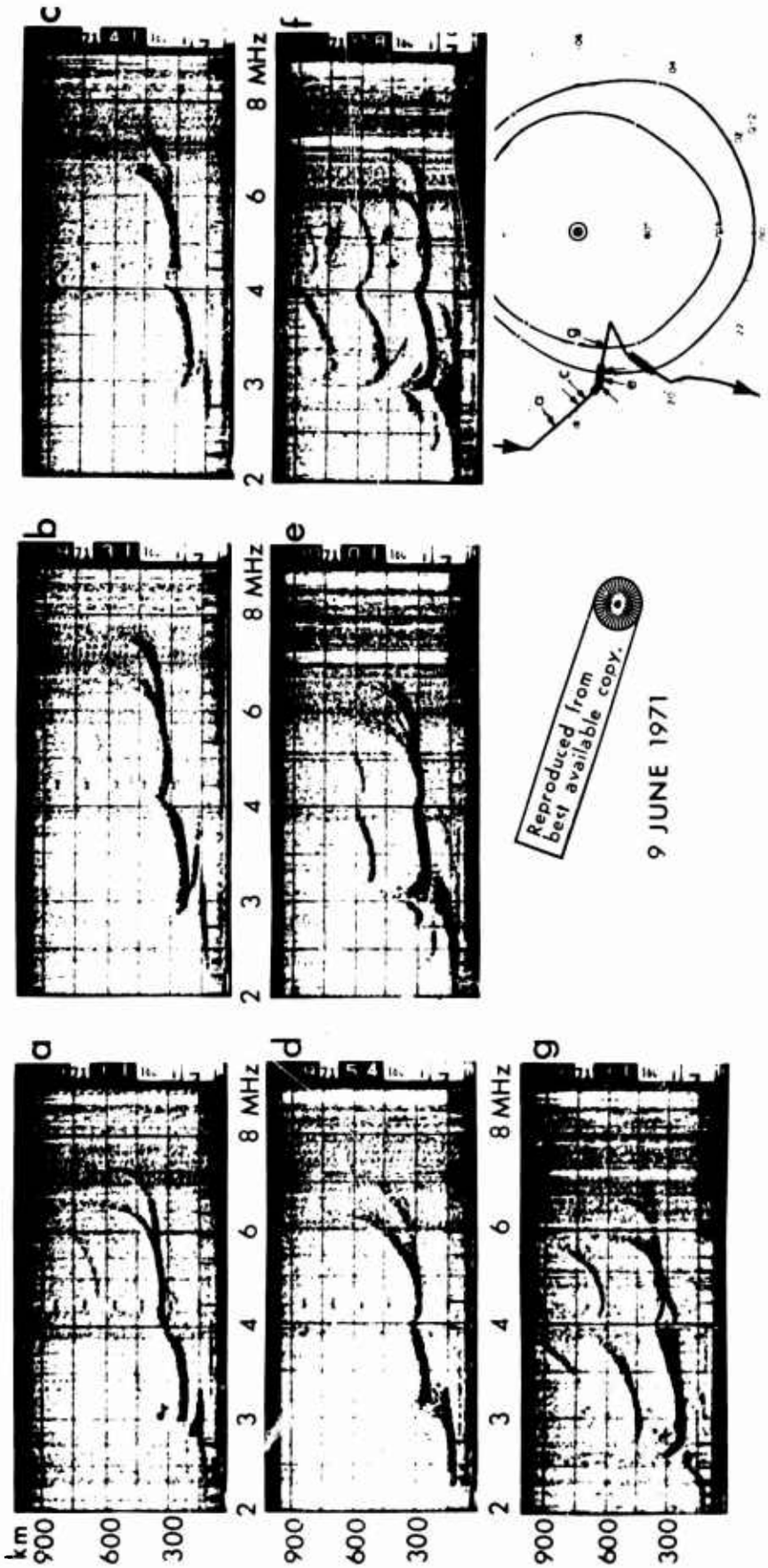

Figure 8. Ionograms recorded on a flight traversing a region where enhanced foE was observed on 9 June 1971. On the flight track, plotted in CG coordinates, heavy lines indicate the latitudes of enhanced foE. The arrows mark the locations where ionograms a. through g. were recorded.

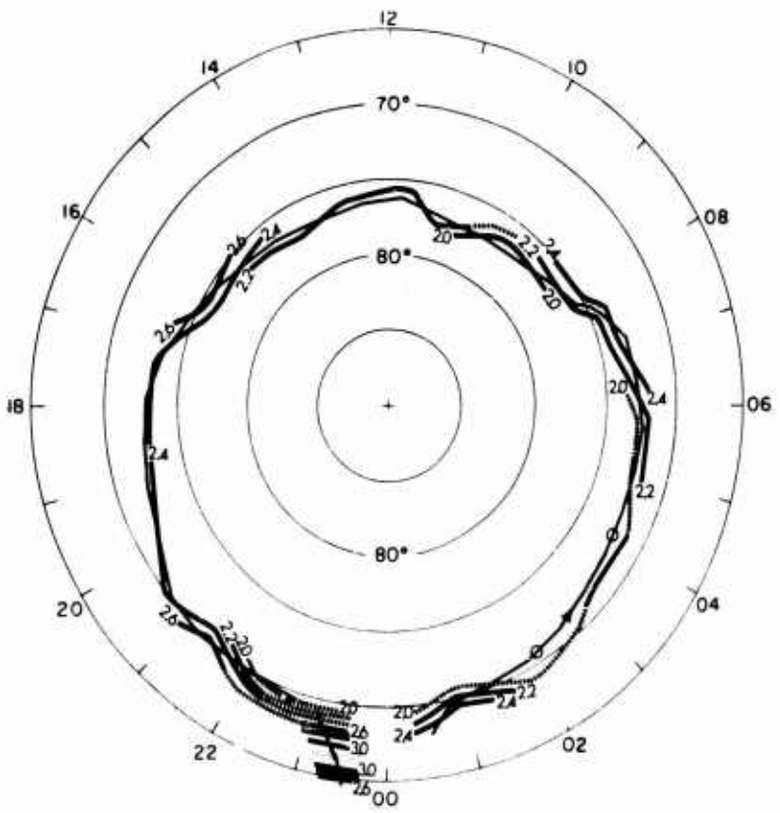

Figure 9. Contours of f_0E for the flight of 5 January 1970.

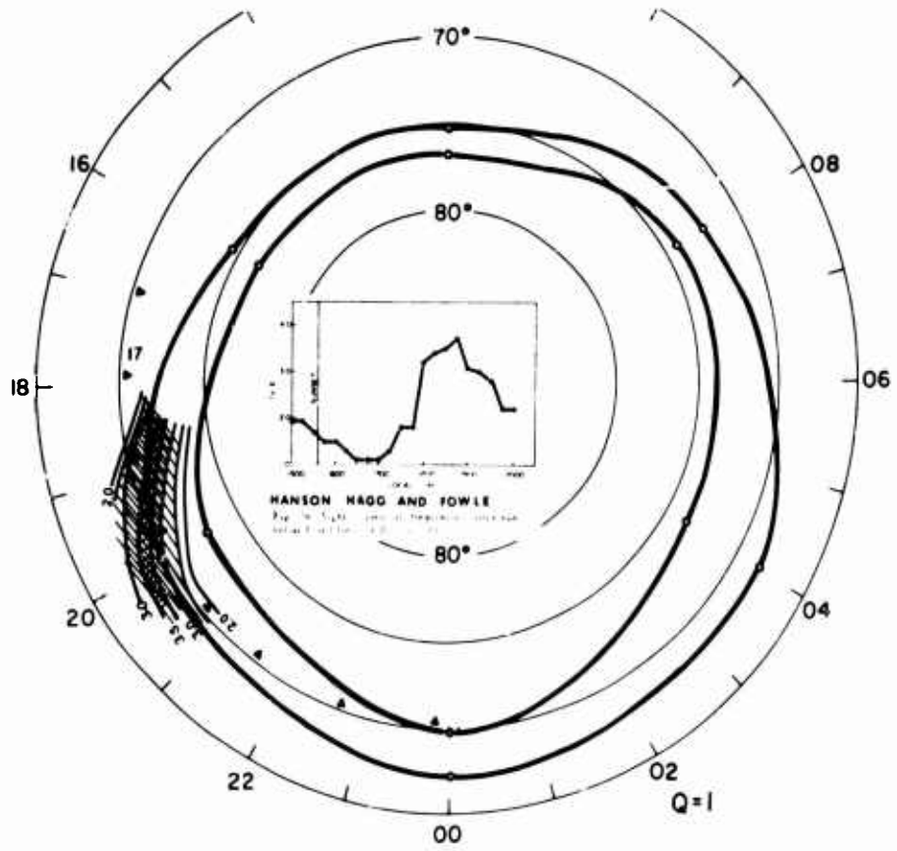

Figure 10. Time variation of f_0E as experienced by a ground station moving, relative to the oval, through a belt of E ionization.

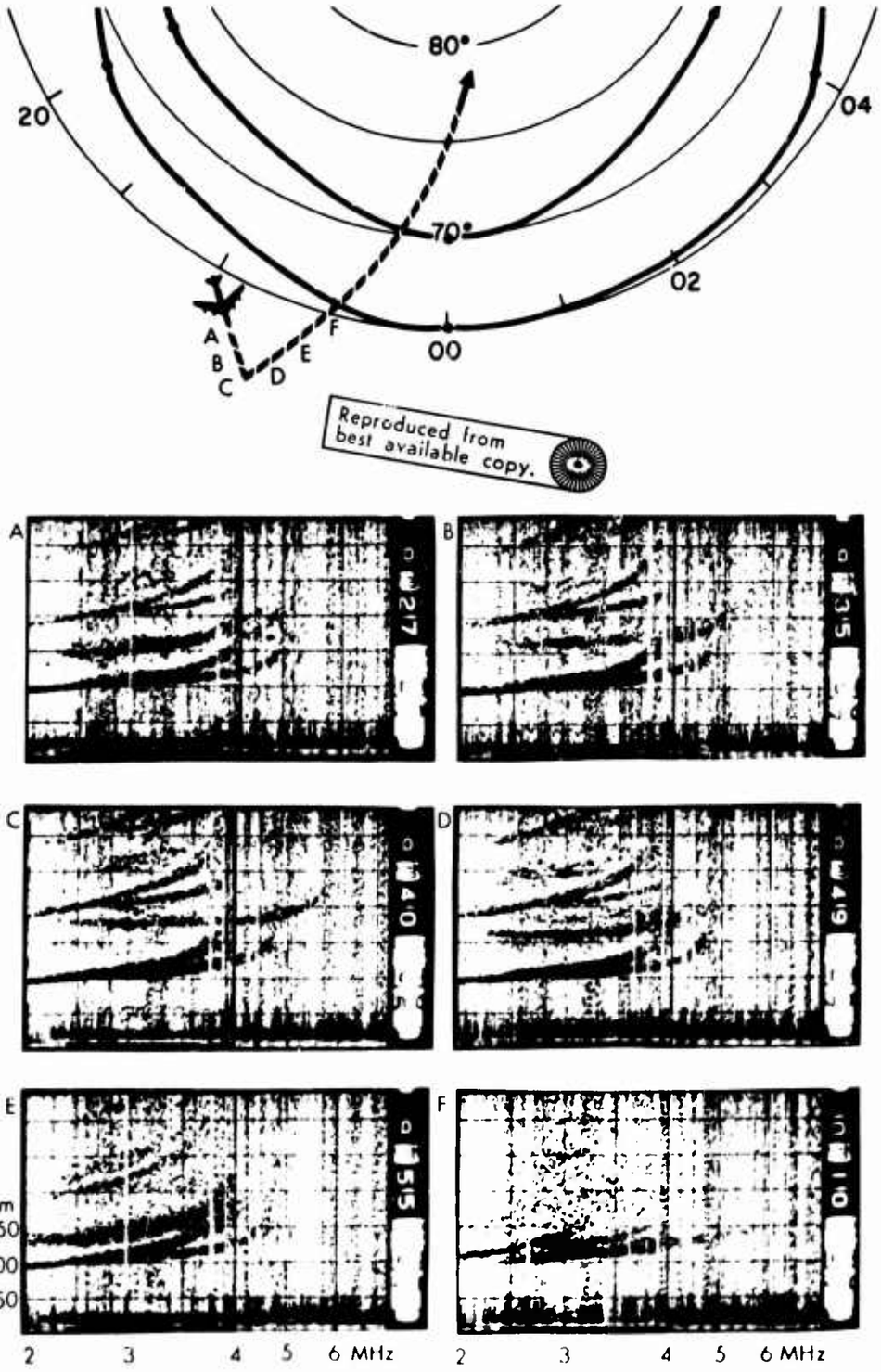

Figure 11. Aircraft flight route on August 22, 1970 is drawn on a CG latitude and CG local time grid. The night sector of the Q=2 auroral oval is indicated by heavy solid lines. A sequence of airborne ionograms, recorded at the positions marked by letters next to the flight route, is shown.

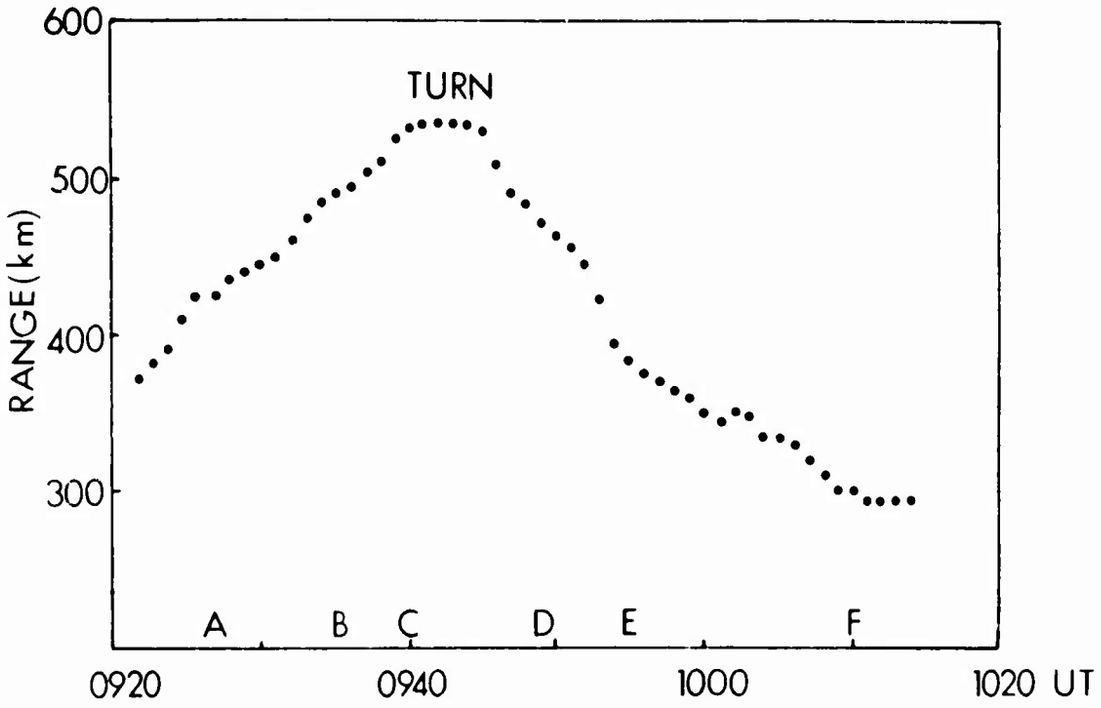

Figure 12. The slant range to the extra echo seen in the airborne ionogram sequence is plotted versus universal time. The letters refer to the aircraft's position.

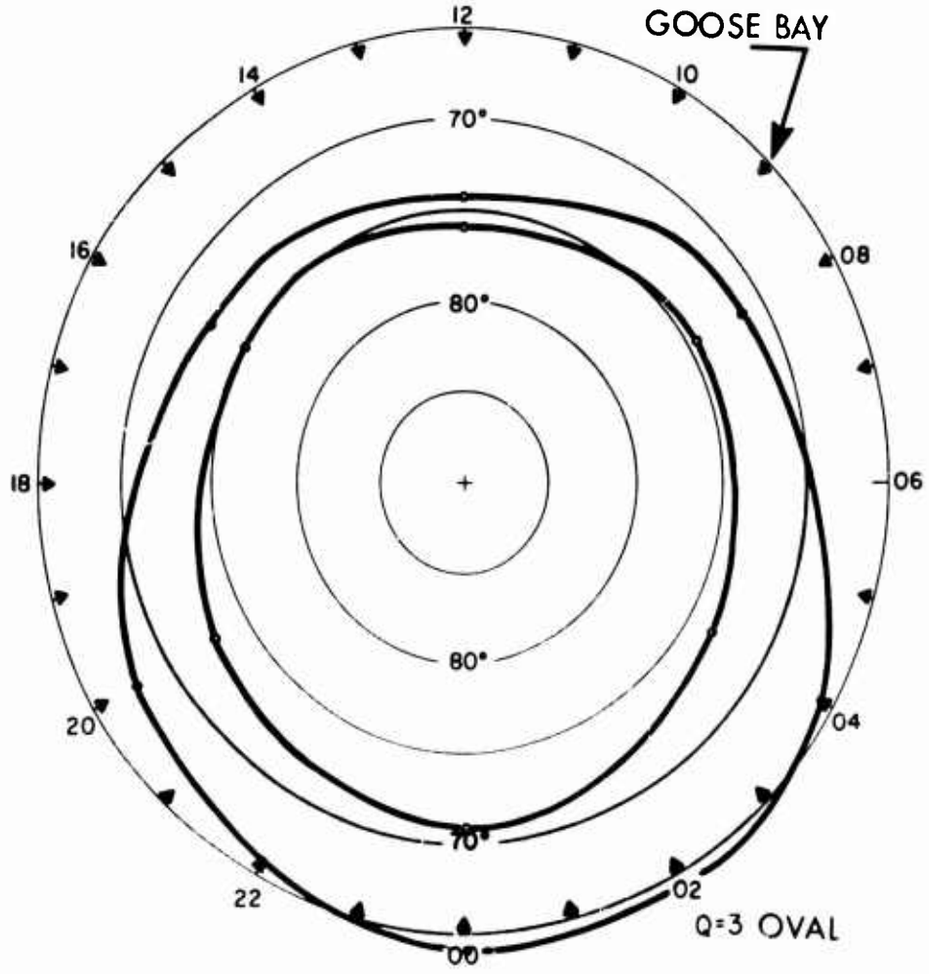

Figure 13. The Q=3 auroral oval is plotted on a grid of CG latitude and CG local time, and the location of Goose Bay is indicated by triangles.

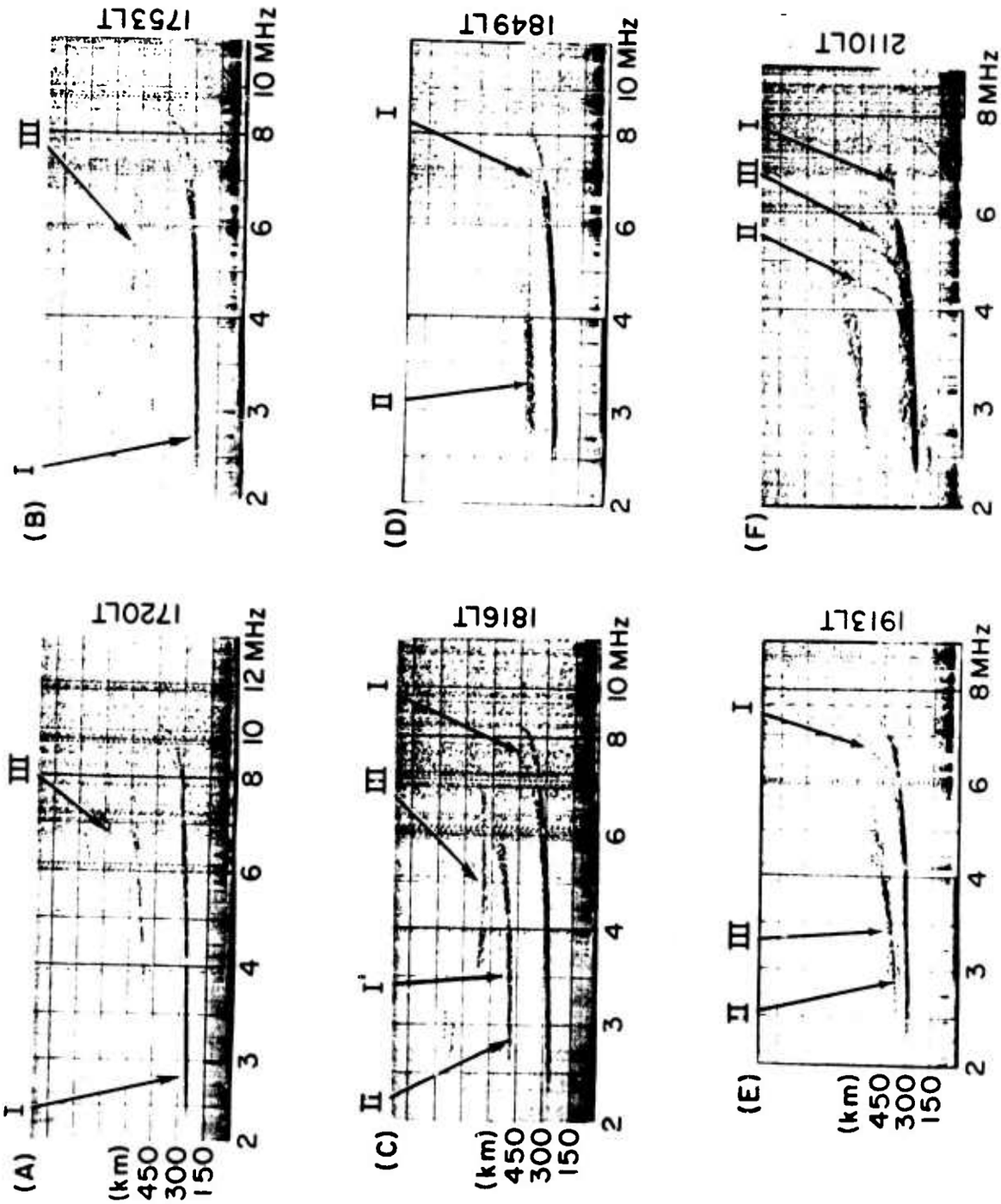

Figure 14. Goose Bay ionograms recorded on October 27, 1970.

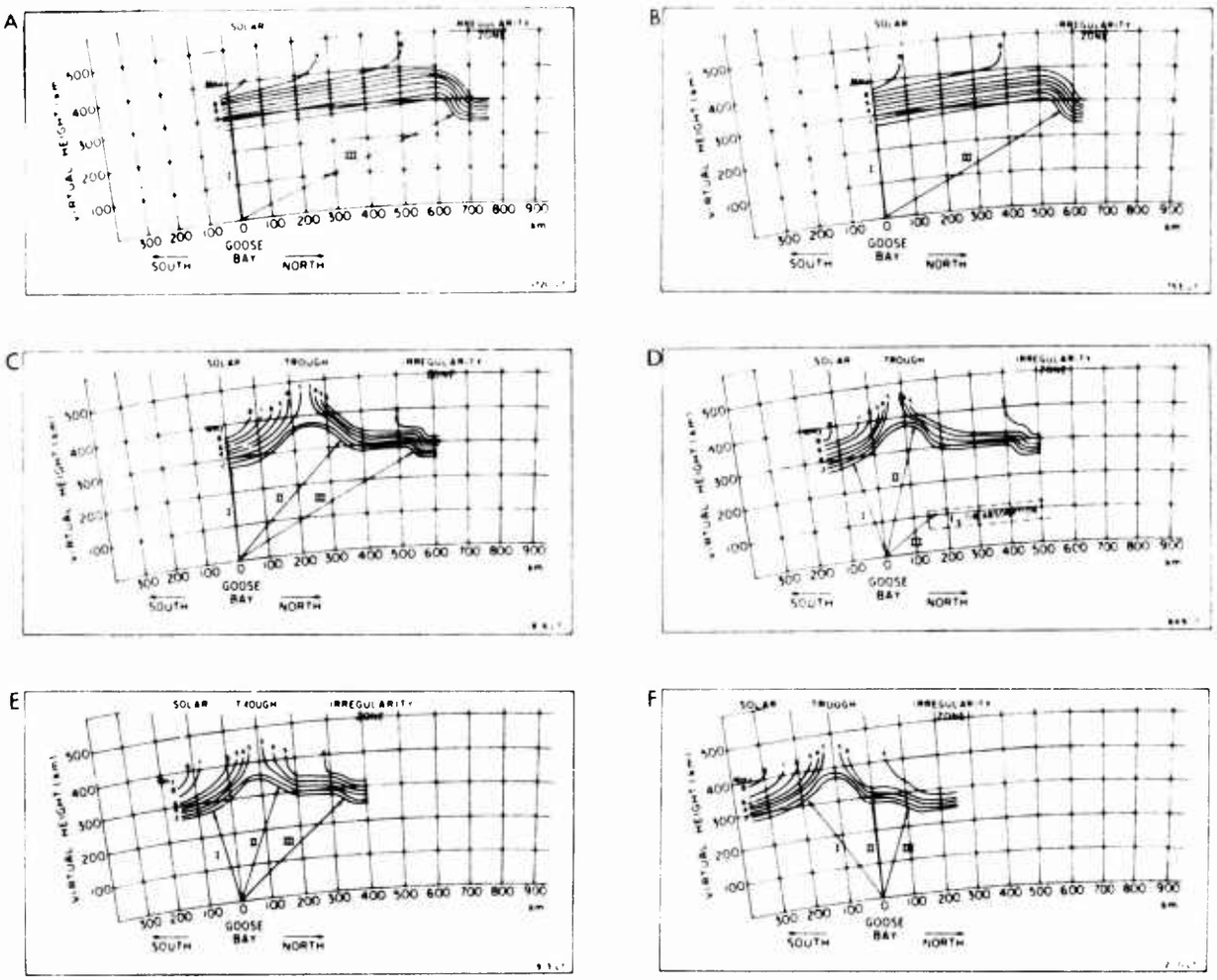

Figure 15. Schematic drawings of plasma frequency contours over Goose Bay are shown.

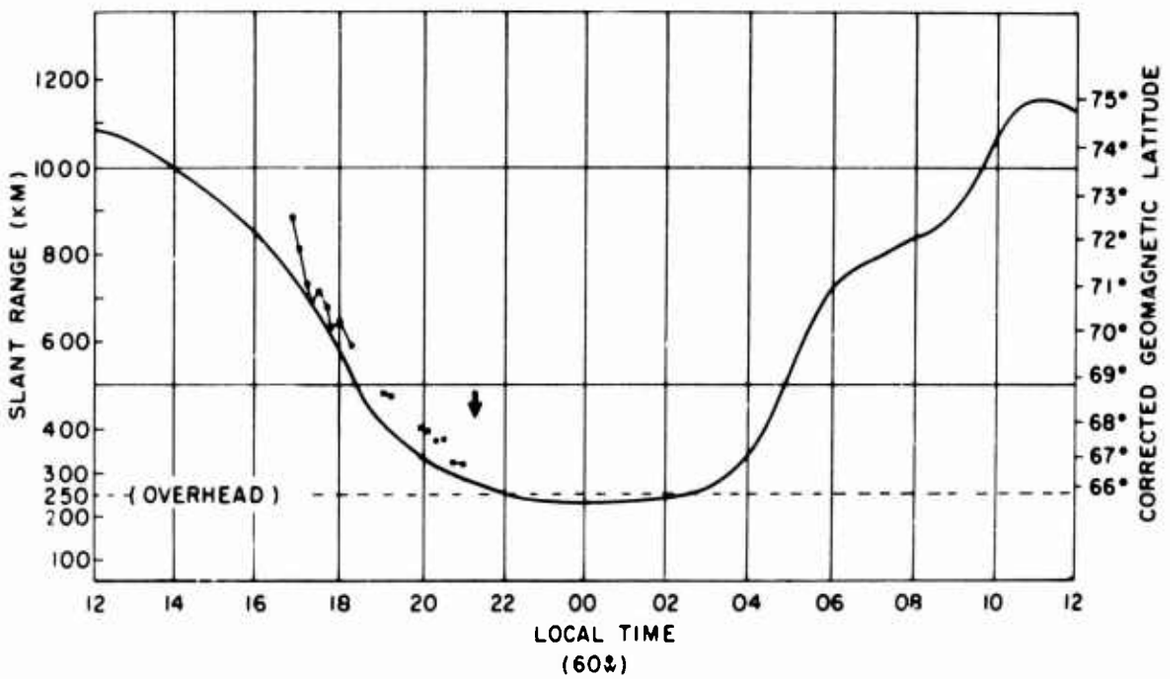

Figure 16. The slant range to the southern edge of the auroral oval from Goose Bay is plotted as a heavy solid line versus 60°W local time. The slant range to the F-layer irregularity zone from Goose Bay on October 27, 1970 is indicated by squares. An arrow indicates the onset of aurora in the zenith at Goose Bay.

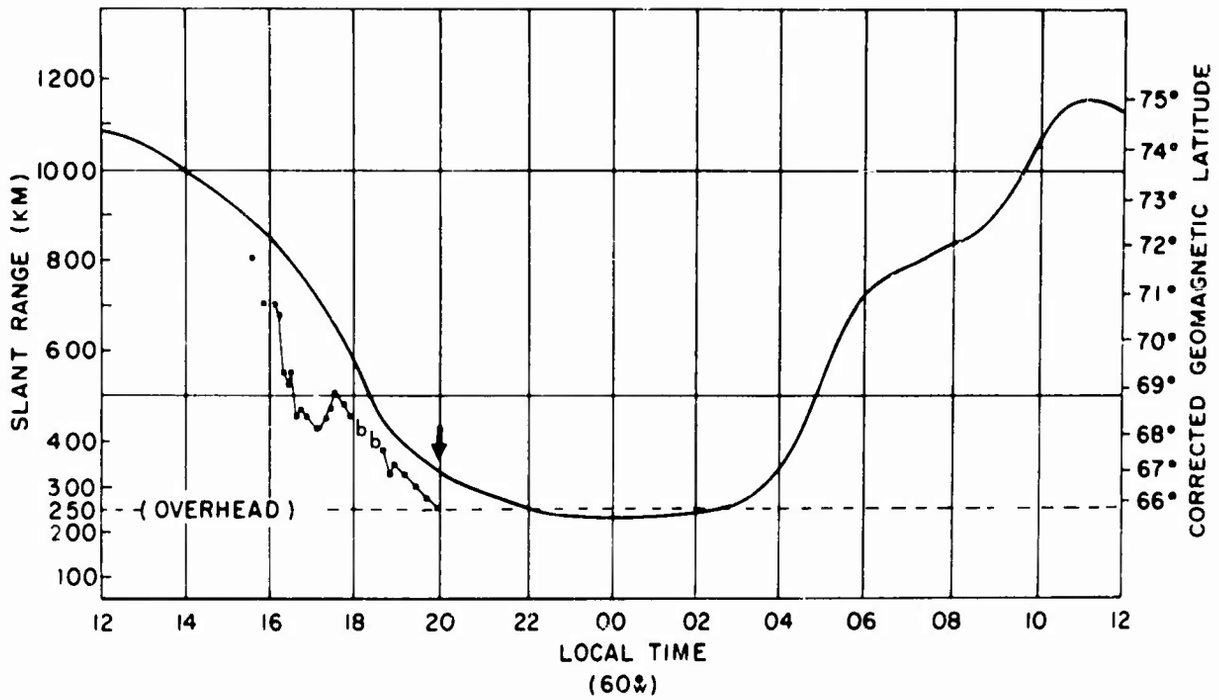

Figure 17. The slant range to the southern edge of the auroral oval from Goose Bay is plotted as a heavy solid line versus 60°W local time. The slant range to the F-layer irregularity zone from Goose Bay on October 28, 1970 is indicated by squares. An arrow indicates the onset of aurora in the zenith at Goose Bay.

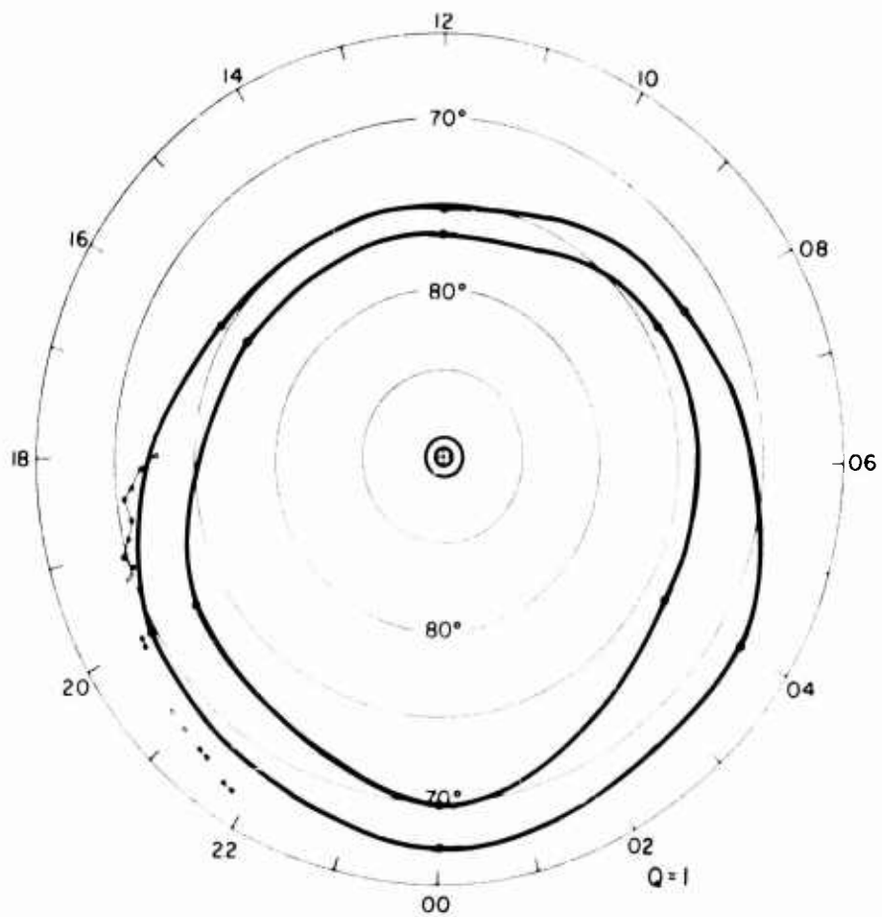

Figure 18. The latitude of the southern edge of the F-layer irregularity zone on October 27, 1970, indicated by squares, is plotted on a CG latitude and CG local time grid. The Q=1 oval is indicated by heavy solid lines.

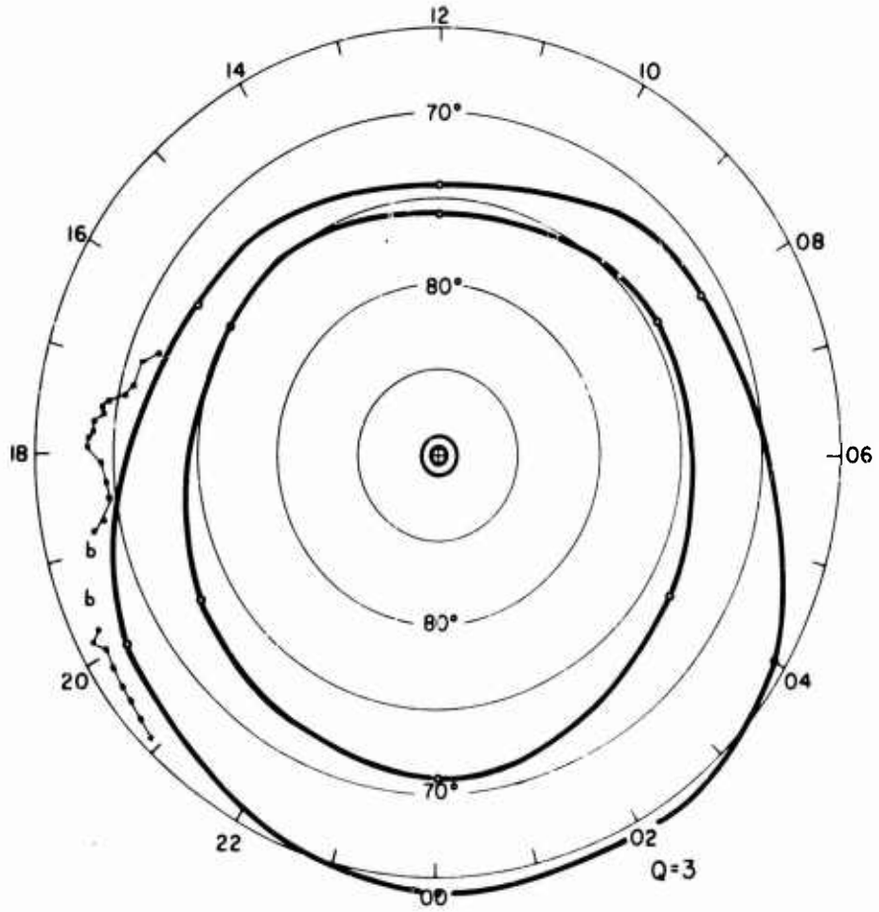

Figure 19. The latitude of the southern edge of the F-layer irregularity zone on October 28, 1970, indicated by squares, is plotted on a CG latitude and CG local time grid. The Q=3 oval is indicated by heavy solid lines. The letter b indicates the presence of blanketing Esa.

SESSION I

POLAR MORPHOLOGY

CHAIRMAN'S REPORT

by T.Hagfors

The review paper given by T Hartz was concerned with the pattern of particle precipitation in the polar regions. It was pointed out that it is still somewhat uncertain whether the precipitation pattern really is in the form of an oval or in the form of two horshoes with a break in between. Three characteristic regions were described, One region occurring during the daytime has a maximum at noon a widespread pattern and rather continous precipitation. This daytime precipitation was thought to be caused by influx from the magnetosheath or from injected solar wind particles. The night zone also falling along the auroral oval shows a different behavior in that the precipitation is local and rather impulsive. In addition to these zones a third was identified, equatorward of the auroral oval, having a maximum in the early morning. This zone was thought to be associated with trapped radiation.

Manifestations of auroral activity, such as luminosity, hiss, enhanced ionization, absorption etc. were then related to the various types of precipitation. A missing ingredient in this excellent paper, in the reviewer's opinion, was the association of the particle precipitation picture with the generation of electric fields which plays such a dominent role in the excitation of E-region irregularities giving rise to radar aurora.

G.Gassmann presented two papers describing the investigations of the auroral ionosphere using both ground-based and air-borne ionosondes. It was shown how well the data obtained fall into a consistent pattern when they are ordered according to the various Feldstein ovals selected according to magnetic activity as measured by Q. It was also shown how the position of the trough can be monitored by analyses of ionosond data. Finally a discussion was given at the seemingly impossible task of modelling the polar ionosphere for ray-tracing purposes.

J. O. Thomas presented a very interesting paper on the studies at ionization processes over the polar cap based on topside sounder data. It was pointed out that the dependence of ionization on solar zenith angle found at middle latitudes break down over the trough and that the layer profile becomes distorted. A discussion was also given of the production mechanisms for ionization well within the polar cap in terms of photo-ionization and particle precipitation.

DISCUSSION

E Shearman

Would Dr Gassman define the parameter "Q" made use of in Feldstein's auroral oval concept?

G J Gassmann

Feldstein adopted and modified the definition of "Q" for characterising fast variations of magnetic activity in arctic regions. "Q" was originally proposed by Bartels and defined from the horizontal components of magnetograms of all auroral zone stations. Feldstein's intuitive decision was to utilise only those stations within the auroral zone which at a particular UT happened to be located near local magnetic midnight.

The editor

A question was raised on how the L parameter and invariant latitude is defined. The following is a synthesis of the answers given. Further reference is given to CE McIlwain JGR 66, 3681, November 1961 and CE McIlwain in the book Radiation trapped in the earths magnetic field, edited by BM McCormack, D Reidel publishing Co, Holland 1966.

The L parameter is a very useful coordinate for ordering particle data. Many features of the polar ionosphere are closely related to particle precipitation and should be described relative to the same coordinate.

A charged particle that is trapped in the geomagnetic field will bounce along field lines, between mirroring points, as it drifts in longitude. The trajectory of the particle will form a closed"magnetic shell". Other particles observed on a field line in this shell, will to a good approximation be trapped in the same shell.

L is a parameter by which we can label all points in space by a number that is unique for each shell, it is constant along a field line. For a dipole field this can be done exactly. L then gives the distance from the centre of the dipole to the equatorial crossing of the field line. For a more realistic field model the parameter is approximate. Near the magnetopause or the tail region the parameter is practically meaningless.

Invariant latitude is defined by the relation $\cos^2\Lambda = \frac{1}{L}$

T Hagfors

The propagation of radio waves in the E and possibly the F-region is often greatly affected by the presence of small scale irregularities which are thought to be closely related to the presence of DC electric fields. What if any is the relationship between the particle precipitation and the origin of these electric fields?

T R Hartz

Data on electron density, density gradients and irregularities are much more numerous than data on electric fields. Electric field data do exist but not in sufficient quantity to get a statistical picture yet. Ionization movement depend on electric field among other parameters but the full nature of this dependence is not yet well established.

K Toman

I noted a difference between the crescent shape ionization trough shown by Thomas and the distribution of an ionization minimum shown by Hartz in paper 1 for a height of 900 km. Is Hartz's contour to be considered a portion only of the crescent shape trough?

J O Thomas

I have not compared the data of Hartz with mine in great detail but from the slide shown, and previously published work I do not believe there is any difference. Of course the precipitation shown by Hartz on the night side will extend into the trough region. In other words even in the trough there may be an ionization source from particles.

A Egeland

The 6 keV particle data (cf paper 10) show marked discontinuities with morning and evening during low to medium magnetic activity, indicating that the auroral luminosity can not easily be fitted into a Feldstein oval. However, the 40 keV trapping boundary is homogeneous around the pole. Based on these facts I would like to ask two questions:

1) Are E_s-layers mainly caused by 6 or 40 keV electrons?

2) Would it not be better to refer the E_s data to the 40 keV trapping boundary instead of the Feldstein oval?

G J Gassmann

The auroral sporadic E (E_{sa}) is probably not directly caused by any precipitation but is due to irregularities induced by the electrojet.

It must be emphasized that there are, without doubt, several superimposed precipitation patterns in the Arctic. One of basec importance occurs definitely in form of an oval and is likely produced by the fact that the magnetic field lines in the auroral zone are diurnally opened and closed. Related to both the oval and to the 40 keV boundary are precipitation patterns of semi-circular shape (along constant magnetic latitudes) which are very likely produced from temporarily trapped particles. These precipitations cause absorption and night-E. Inside the oval occurs a highly diversified precipitation from open field lines. The 6 keV precipitation reported in Egelands paper appears to be singular part of the latter.

J O Thomas

1 keV electrons will penetrate to about 150 km in the ionosphere. Roughly 6 keV electrons are associated with the optical aurora observed near 100 km. Thus the Feldstein oval may well correspond with enhancements of the ionization in the E and polar sporadic E layers. However, in the F region enhanced ionization in the polar ring extends considerably North and South of the Feldstein oval and is associated with soft electron precipitation (about 1 keV).

POLAR PROPAGATION EFFECTS ON VHF-UHF RADARS

Walter G. Chesnut
STANFORD RESEARCH INSTITUTE
Menlo Park, California, U.S.A.

ABSTRACT

The effects upon VHF-UHF radar of concern in this paper will be wave distortion caused by wave interaction with E- and F-region auroral ionization. The two primary effects are auroral backscatter--called auroral clutter--and forward scatter that leads to amplitude and angle scintillation. Almost all such effects are caused by small-scale size fluctuations in electron density--sizes on the order of tens of centimeters to meters where backscatter is of concern--hundreds of meters to several kilometers where amplitude and angle scintillation are of concern.

The most important development in recent years has been the emergence of a variety of instability concepts that seem capable of explaining the production of ionization irregularities or structure that is needed to interpret disturbed polar radar propagation. Most promising is the fact that these concepts aid in understanding morphological relations that have been empirically derived over many years.

The paper reviews recent results of pulse-radar-backscatter studies from aurora and describes how these data seem to fit in with new theories of irregularity production. Aurorally produced radar tracking and amplitude scintillation are discussed. Some results from aurorally disturbed monopulse tracking of satellites will be presented.

1. INTRODUCTION

For more than 20 years it has been known that radar propagation in polar regions is affected by aurorally produced ionization. The earliest effect discovered--and the most thoroughly investigated--is auroral radar clutter, sometimes called radio aurora, radar aurora, auroral-radar reflections, auroral echoes, etc. Perhaps the first investigation of the phenomenon was by Harang and Stoffegren (1940), though Stormer (1955) does mention unexplained long-delayed radio echoes reported in the late 1920s.

Studies of radio star scintillations since the early 1950s have indicated that radar signals can be affected by transmission through auroral ionization. The earliest systematic radar transmission measurements were performed by reflecting radar signals from the moon (James et al., 1960). Radars that have sufficient power and sensitivity to make measurements of auroral effects on tracking of satellites and space vehicles are extremely expensive and have until very recently been unavailable to the propagation research community. Much of what we currently know about radar transmission through the auroral ionosphere has been learned from studies of one-way radio star and satellite beacon transmissions. Most of this work has been carried out at frequencies below 150 MHz, which makes extrapolation to the higher frequencies of primary concern in this study somewhat uncertain.

This paper is organized as follows: In Section 2 we very briefly discuss aurorally produced radar noise. Such noise can, in principle, degrade the detection sensitivity of radar receivers if the noise indeed exists. In Section 3 we discuss auroral radar reflection phenomena. The first part of Section 3 will describe what we believe to be the current state of experimental data. Most of the work of recent years has been concerned with relating experimental observations to various theoretical models; the latter half of Section 3 will be devoted to a summary and analysis of such relationships. Section 4 will be devoted to radar transmission effects. These can be characterized as amplitude scintillation, angular scintillation, spatial coherence at the receiver antenna, angular spectra, etc. Our concern is primarily with the ways in which tracking radars will operate in the auroral environment.

2. AURORALLY PRODUCED VHF/UHF NOISE

Aurorally produced radar noise was the subject of several papers in the early 1950s. Forsyth et al. (1949) and Forsyth et al. (1950) present discussions of experiments they thought had detected auroral radiation at 3000 MHz. Hartz et al. (1956) report detection of auroral noise at VHF. Later, Hartz (1958) seems to have detected auroral radiation at 500 MHz. Egan and Peterson (1960) claim to have detected auroral radiation at 30 MHz and ascribe this to synchrotron noise produced by trapped electrons. VLF frequency noise emissions also have been observed and studied--but they are not of immediate concern here.

To the best of our knowledge there do not seem to be other more recent detections of aurorally-produced radar noise. The early observations, except those at 30 MHz, do not seem to have been confirmed by others. It is our belief that these early detections may be attributable to other causes than simple auroral emissions. We do not intend to review this subject; however, we present the following, abbreviated status report on possible noise-source mechanisms.

There are three mechanisms known to this writer that could produce noise. The first is thermal emission from the auroral ionization. By Kirchoff's law (of thermodynamics), if a region absorbs energy it also emits black-body radiation, with its emissivity at each frequency equal to the absorbtivity at the same frequency.* If one is concerned with frequencies above 150 MHz, it is very difficult to produce auroral absorption of sufficient magnitude that the resulting black-body thermal emission can be significant compared with cosmic noise background. For example, to obtain significant absorption at a frequency of 100 MHz at an altitude of 80 km, electron densities in excess of 10^6 per cubic centimeter are required. More than 4×10^7 el/cm^3 are needed at an altitude of 100 km to produce significant absorption. These densities are excessively high--by nearly one order of magnitude.

A second noise source is synchrotron radiation produced by aurorally-trapped radiation. The most significant source ever of near-earth synchrotron radiation was produced by the Star Fish high-altitude nuclear detonation in 1962 (Dyce and Horowitz, 1963). High-energy beta rays with energies as high as several MeV (Peterson and Hower, 1963) were produced by beta decay of the fission products of the nuclear device. These high-energy electrons were trapped in the earth's magnetic field. Their gyration around magnetic field lines produced synchrotron radiation at HF and VHF. Though the Star Fish synchrotron noise at frequencies from 30 MHz to 120 MHz was readily detected by equipment located at the equator, when the synchrotron noise spectrum was extrapolated to higher radar frequencies, it became less than the natural cosmic sources. Therefore, from a practical radar-system point of view the Star Fish synchrotron radiation would not seem to be a significant noise source, yet the trapped Star Fish electron-energy spectrum and intensity were many times more favorable to producing synchrotron noise than is the trapped auroral spectrum and intensity. It is concluded (Peterson and Hower, 1963) that synchrotron radiation is not a significant radar problem in polar regions.

---

*Strictly speaking, Kirchoff's law applies only to systems that are in thermodynamic equilibrium. Auroral ionization may not satisfy this requirement well enough to validate our arguments--but no one seems to have pursued this question.

A third source of radar noise could be electromagnetic radiation from excited plasma instabilities in the auroral ionosphere. We know of no theories that suggest radiation at frequencies much above the ionospheric plasma frequency, which we doubt ever exceeds several tens of megahertz. We suspect that auroral emissions due to cooperative phenomena (plasma oscillations) in the auroral ionosphere do not exist at VHF and UHF.

With the exception of synchrotron noise at 30 MHz (Egan and Peterson, 1960), we are not convinced that the noise detected at higher frequencies and reported in the references listed above was indeed produced by auroral phenomena. It seems more likely to this reviewer that the experiments detected radar interference propagated by way of auroral reflections; a phenomenon not known to exist for UHF frequencies in the early 1950s.

3. AURORAL RADAR REFLECTION

Reflection of radar and radio signals from the aurora have been observed for many years. Measurements have been made using pulse-backscatter radar, bistatic CW radar, and bistatic reception of signals of opportunity. Each technique has its own particular features that commend it. Much experimental work has shown that radar reflections are far more intense at lower frequencies in the HF band than at the higher VHF/UHF frequencies. Dr. H. B. Möller will be reviewing polar propagation effects on HF radars. Therefore we shall confine our attention generally to frequencies above 50 MHz except where lower-frequency data are pertinent. Dr. T. R. Hartz will be reviewing the morphology of radio-radar polar propagation effects. Therefore we shall not be concerned with this general subject. Our principal concern will be with the detailed characteristics of the observed radar reflections. The relationships between regions where radar waves reflect and regions where other auroral phenomena occur will be studied. Finally, we review information about the reflection environment that provides us with a better understanding of the underlying physics.

3.1 Current State of Experimental Observations

For radar frequencies above 100 MHz and possibly above 40 MHz, it is believed that reflections result from scattering of radar waves from fluctuations in electron density generally in the E region and lower F region. In the early period of study of auroral reflections, it was suggested that reflections could be due to regions overdense to the radar frequencies that were used at that time. This explanation is untenable at frequencies above 100 MHz. Current opinion seems to be that electron densities in the auroral scattering regions seldom exceed 10^7 electrons per cubic centimeter--which is overdense to frequencies up to 28 MHz.

When it is important for presenting experimental results, we shall assume that observed scattering is due to underdense reflections from spatial fluctuations in electron density as originally proposed by Booker (1956). We have likened this to Bragg scattering--which means that if there are density fluctuations present with spatial wavelengths that are equal to one-half the radar wavelength, then backscattering takes place. The conditions for bistatic scattering, we assume, also require that the Bragg condition be met for the particular geometry.

3.1.1 Aspect Sensitivity

Basing his hypothesis on the shape of visual auroral forms, Chapman (1952) suggested that radar reflections from aurora should be strongest when the propagation path into and out of the refracting region satisfied the specular condition with respect to the earth's magnetic field. For backscatter radars this condition means that the radar beam-line makes a 90° angle with respect to the earth's magnetic field in the scattering volume. We speak of the angular variation with respect to the magnetic specular angle (90° in backscatter) as the magnetic aspect angle. Subsequent work has shown that Chapman's hypothesis was indeed borne out by experiments. The extreme variation of reflected power with variations in aspect angle that we now find was not dreamed of in the early 1950s.

The experimenter has at least three different ways that he can organize his data to demonstrate the magnetic aspect sensitivity of auroral-radar scattering. The first of these is to measure radar signal strengths at a variety of aspect angles over a long period of time and hope that every region that he samples experiences, on the average, the same auroral excitation conditions as every other region. He can then plot the average received power as a function of aspect angle to provide a measure of aspect sensitivity. Figure 3.1 shows some data obtained by Chesnut et al. (1968) organized in this way. The curves of average power versus aspect angle presented in Figure 3.1 are flattopped, or even dip slightly at zero magnetic aspect. This result would seem to argue that strongest echoes do not come from regions of exact magnetic perpendicularity. We believe that signals should be strongest when exact perpendicularity is achieved. To preserve this concept of aspect dependence, it is hypothesized that aurora distorts the magnetic field sufficiently to move the perpendicular regions around.

When aurora is weak, the magnetic field is undistorted, so echoes are obtained from regions of zero aspect angle (exactly perpendicular to the undisturbed field). As the intensity of the magnetic disturbance increases, the magnetic field becomes distorted, so new regions, formerly somewhat off perpendicular, now become regions of microscopic perpendicularity. Because the magnetic disturbance is stronger,

echo amplitudes are stronger. Thus, we believe that the data in Figure 3.1 represent some sort of convolution of a steep aspect dependence with distortions of the earth's magnetic field in the scattering region during periods of magnetic disturbance.

The radar that obtained the data presented in Figure 3.1 was located such that undisturbed magnetic perpendicularity of the radar beam line at 110 km altitude--where most echoing takes place--occurs on magnetic azimuths restricted to within $\pm 10^{\circ}$ of magnetic north. If Farley's (1963) two-stream-instability hypothesis is correct (see Section 3.2), and if auroral Hall currents flow mostly east-west in the most intense scattering regions, then scattering from fluctuations induced by the two-stream instability is discriminated against in regions of exact perpendicularity by the geometry of the experiment that produced the data of Figure 3.1. On the other hand, the same equipment also produced data that contradict this latter hypothesis.

A second way to organize aspect-sensitivity data is to observe auroras over a long period of time and plot the data on the basis of frequency of occurrence versus aspect angle. Figure 3.2 from Chesnut et al. (1968) shows data organized in this way. These data show that echoes are most likely in regions of near perfect orthogonality. It is suspected that the offsets of the center of symmetry of the data of Figures 3.1 and 3.2 with respect to 0° result from a less than perfect magnetic field model. With the data plotted in this way, Figure 3.2 does not show the flattopped behavior evident in Figure 3.1.

A third way of studying magnetic-aspect sensitivity is to observe the scattering intensity of a single aurora whose environmental properties seem the same over many aspect angles. Data obtained in this way probably are indicative of the microscopic aspect-angle dependence of auroral scattering. These data tell us the scattering angular dependence with respect to the local magnetic field, whether or not the field is distorted. These data are, then, the best to use for comparison with theories that purport to predict the nature of ionization irregularities responsible for scattering.

Data of this kind were obtained by Barber et al. (1962). Their data are presented in Figure 3.3.* These data suggest that at 500 MHz, the aspect-angle dependence is about 10 dB per degree to off-specular angles as large as 2°. Note that the data were obtained from various magnetic azimuths. The aspect sensitivity does not show an obvious dependence on beam direction with respect to direction of auroral electrojet current flow.

Leadabrand et al. (1965a) have studied aspect sensitivity in this way at 401 and 800 MHz. Their measurements include 0° aspect angle. These measurements did <u>not</u> show a zero slope behavior when they were made very close to exact perpendicularity. The angular dependence of aspect sensitivity of their measurements is very similar to that obtained by Barber et al. (1962).

Measurements of the frequency dependence of aspect sensitivity are very difficult to accomplish. Leadabrand et al. (1965a) find only a small difference between 401 and 800 MHz. Chesnut et al. (1968) claim that the microscopic aspect dependence is only very weakly dependent on radar frequencies from a frequency as low as 50 MHz, to 3000 MHz. Bates and Albee (1969b) have found that in order to explain oblique-backscatter data, the aspect sensitivity at frequencies between 4 MHz and 40 MHz must be nearly as steep as that measured by Chesnut et al. at frequencies of 50 MHz and higher. Combining these results would imply that the reflected radar power decreases from 5 to 10 dB per degree off of microscopic perpendicularity at almost all radar frequencies.

In order to explain their results, Bates and Albee invoke ionospheric refraction as do Chesnut et al., to obtain their 50-MHz aspect data. Statistical data obtained by Leadabrand et al. (1965a) at 30 MHz initially implied very weak aspect sensitivity. Unwin (1968) has shown how that data imply very steep aspect sensitivity when ionospheric refraction effects are included. If Unwin's conclusions are accepted, then the Leadabrand data at 30 MHz would be consistent with the extreme aspect dependence that Bates and Albee, and Chesnut et al. claim.

McDiarmid and McNamara (1967) have studied statistical occurrence of auroral reflections at 50 MHz and have concluded from their data that reflection strengths decrease by 10 dB for aspect-angle changes of 20°, rather than 10 dB for 1° as do the other observers. Data by Dyce (1955) at 51.9 MHz imply a steeper dependence than do the data of McDiarmid and McNamara but neither of these experiments has been evaluated in light of ionospheric refraction and D-region absorption. This reviewer is of the opinion that the very steep aspect dependence of 5 to 10 dB per degree applies to nearly all frequencies, but he cannot absolutely prove it. The data of McDiarmid and McNamara could be responding in fact to a phenomenon not detected by the other experiments.

---

*Note: The authors state that the data labeled in the figure as cross-polarized scattering are in fact not due to cross polarization. Rather they state that their cross-polarized feed was imperfect, and responded to the parallel polarization with 9 dB attenuation and therefore acted as a second, parallel-polarization-measurement channel with reduced sensitivity. Measurements by Leadabrand (1965a) of the cross-polarized scattering at 400 MHz shows that this cross-polarized component is typically 20 dB weaker than the direct polarized component.

The magnetic-aspect sensitivity has been measured at 400 MHz out to angles as large as 8° (Jaye et al., 1969). These data, presented in Figure 3.4, were organized by computing average signal strength as a function of quiescent-magnetic angle, as were the data presented in Figure 3.1. For comparison, Figure 3.4 also presents 398-MHz measurements obtained near zero-magnetic aspect that have been organized in two ways by Chesnut et al. The broad curve with a dip at zero degrees was obtained simultaneously with the 139- and 850-MHz data of Figure 3.1--but not plotted there, to avoid cluttering that figure. The line sloping downward from 0° to +1.7° was obtained by dissection of a single auroral arc in a manner that is similar to that used by Barber et al. and presented in Figure 3.3.

The two-stream instability of Farley (1963) suggests that the scattering strength of radar aurora depends not only on the microscopic magnetic-aspect angle, but also on the direction of the radar beam line with respect to the auroral electrojet in the scattering region. The auroral electrojet is an extremely complex phenomenon; it is not clear how experimental data can be organized in a manner to evaluate this potential dependence. Under the assumption that the auroral electrojet flows generally east-west at the altitude of maximum auroral clutter, one might expect that the intensity of auroral echoes would show a dependence on the magnetic azimuth of the radar beam. Jaye et al. (1969) have plotted average signal amplitude for various aspect angles as a function of azimuth. These data are shown in Figure 3.5.

At the larger off-perpendicular angles, those greater than 5.5°, the data of Figure 3.5 do suggest an azimuthal dependence that seems consistent with the Farley hypothesis, though the weakness of the variation leaves us not completely convinced that the data prove the Farley hypothesis.

3.1.2 Frequency Dependence

Many authors have published results of experiments that were designed to determine frequency dependence of auroral-radar backscatter. Generally the scattering strength of radar aurora is very much greater at low radar frequencies than at higher frequencies. Auroral-radar returns have been observed as high as 3000 MHz (Leadabrand et al., 1967b).

Early radar measurements of aurora were generally confined to frequencies below about 100 MHz. Early frequency-dependence experiments were attempts, in the main, to determine the peak electron density in the scattering regions. It was believed that electron densities in the auroral E region could be as great or greater than 10^7 per cubic centimeter. A rather sophisticated analysis was performed by Lyon and Forsyth (1962) utilizing bistatic radar measurements obtained simultaneously at frequencies of 42, 60, 82, and 104 MHz. Their analysis led them to conclude that the auroral scattering environment was sometimes overdense at 42 MHz (which requires 2.25×10^7 el/cm^3) and very occasionally was overdense even at 104 MHz (which requires more than 10^8 el/cm^3). Extreme heating of the ionosphere would result from the excitation necessary to produce these very high electron densities. Chesnut et al. (1968) compute heating rates of 200° K per second to maintain a density of 10^8. The temperatures of aurorally-excited ionosphere, as deduced from optical-rotational-spectral measurements, would be much greater than are actually observed. Other kinds of measurements, both ground-based optical and in-situ rocket measurements never seem to find electron densities this high.

Moorcroft (1966) has reviewed the data of Lyon and Forsyth (1962) using various plausible models of "blobs" of overdense plasma. His reexamination leads him to deduce that the data cannot be reasonably interpreted as indicating the presence of electron densities that are overdense at 40 MHz or higher.

Flood (1965) has made pulse-backscatter measurements using scaled antenna beams at frequencies at 49.7, 143.5, and 226 MHz. He related his signal strengths at pairs of frequencies by a power of the wavelength ratio. In this way, then, the ratio of signal strength at 143.5 MHz to that at 49.7 MHz was usually about $\lambda^{3.5}$ to $\lambda^{3.7}$. Likewise when he observed echoes at 226 MHz, implying a strong aurora, he found a wavelength dependence of $\lambda^{6.5 \pm 1.3}$. During times of extremely strong aurora, he found instances of the ratio of 226 to 143 MHz as steep as $\lambda^{12.9 \pm 1.2}$.

It has recently been recognized (Unwin, 1968; Chesnut et al., 1968; and Bates and Albee, 1969b) that refraction can play a significant role in measurements of magnetic-aspect angle. Refraction changes the radar-beam angle in the scattering regions so that the actual magnetic-aspect angle at HF and VHF is not the angle that is computed in the absence of refraction. As a result, the interpretation of signal strengths at these lower frequencies can become somewhat uncertain. The role that D-region absorption plays is also quite uncertain, although it is known that the one-way vertical absorption at 30 MHz can at times exceed 10 dB as measured by a riometer. For a round-trip, oblique path this absorption might be significantly increased by increased path length and might affect frequencies as high as 100 MHz. As a result, it is difficult to know how to interpret HF and low VHF radar echo intensities in terms of the scattering environment.

The hypothesis that regions of the ionosphere are overdense to 50-MHz frequencies would have profound effects on the HF measurements of Bates et al. (1966). For densities greater than this, their oblique, HF measurements would give detectable echoes to their highest frequency, which is 64 MHz. Bates (private communication) has indicated that he virtually never sees auroral E echoes to frequencies this high.

The first attempt to measure the frequency dependence at higher, UHF radar frequencies was carried out by Presnell et al. (1959). A later study by Leadabrand et al. (1965) employed frequencies of 401 and 800 MHz, and scaled antenna beams. More recent work (Chesnut et al., 1968) has extended the frequency coverage to frequencies of 50, 139, 398, 850, 1210, and 3000 MHz. For practical engineering reasons, scaled antenna-beam patterns could not be used in this latter experiment. In order to deduce frequency dependence of auroral scatter, Chesnut et al. assumed that the scattering layer was on the order of 8 km thick in the vertical direction. It was found that the scattering intensity as a function of frequency can be well fitted by the following analytical form:

$$P(f) = P_0 \, e^{-f/f_0} \quad . \tag{3.1}$$

The quantity f_0 is called the "scale frequency."

Figure 3.6 presents volume-scattering coefficients versus radar frequencies for the five lower frequencies as measured by Chesnut et al. This particular data set was obtained during very special aurora (long, stable-radar arc) that they claim enabled them to correct for refraction at 50 MHz. That refraction definitely plays a role at 50 MHz was demonstrated by the fact that 50-MHz echoes were absent or very weak in the region of the radar arc where the magnetic-aspect angle was 0. The higher, unrefracted frequencies gave the greater signal return.

On some occasions auroral echoes were obtained at 3000 MHz, but they were so very weak that the measurement of signal power necessitated 1 minute of integration. Figure 3.7 presents results of the frequency dependence measured when 3000-MHz echoes were observed. Also shown in Figure 3.7 as a dashed line are the data of Figure 3.6. We note that the general slope of the plot is more gradual for the data set containing 3000-MHz echoes. These data indicate that the frequency dependence of auroral-radar scattering is not constant in time.

A set of 36 separate measurements of the frequency dependence of auroral backscattering, using the four intermediate frequencies (139, 398, 850, and 1210 MHz) were fitted by Eq. (3.1). A histogram of the scale frequency for values is presented in Figure 3.8. The data of Figure 3.7 gave a scale frequency of 220 MHz, which value is not shown in Figure 3.7, since the determination was obtained in a different manner than were the data for Figure 3.7. More recently, study suggests that the data set from which the histogram of Figure 3.7 was obtained were prebiased by the way data were selected.

We suggest that the scale-frequency concept, which always seems to fit the data of Chesnut et al., has utility as an analytical fit to the frequency dependence of auroral-radar reflections. But the origin of variations in scale frequency, and its correlation with other geophysical phenomena, are unknown at this time.

The work at lower frequencies by Lyon and Forsyth (1962) and by Flood (1965) suggest very much steeper frequency dependence than was found at higher frequency by Chesnut et al. In fact the data quoted by Flood produce "scale frequencies" of between 12 and 30 MHz, rather than the value of 126 MHz found at higher radar frequencies. This frequency-dependence work may imply that there are at least two separate mechanisms that operate to produce the structured ionization from which radars scatter. This result may also imply that there is curvature to a proper fit to the frequency dependence that is not well detected by Chesnut et al. (1968). If there are two mechanisms, then one mechanism could produce a very steep behavior at HF and VHF--and another produces less steep behavior in the higher UHF band. This latter deduction is reinforced by the fact that the data of Chesnut et al. (1968) do extend into the VHF region--and show, for their particular observation, a shallow frequency dependence in contradiction to Flood's results over the same frequency interval.

There has been no explicit correlation of the frequency-dependence measurements with the nature of the radar aurora; using the nomenclature of Unwin (1959), these are diffuse, diffuse with structure, short discrete, and long discrete. Unwin and Knox (1968) also suggest that different mechanisms may be involved in producing these different kinds of radar aurora.

3.1.3 Relationship to Other Auroral Phenomena

A variety of auroral phenomena have been correlated with radar aurora. An excellent summary of gross correlations between radar and other auroral phenomena is given by Leadabrand (1964). We do not intend to review all such relationships. Some relationships are of particular interest because they may reveal the basic nature of the scattering environment. Generally, when geomagnetic activity is high, all auroral phenomena are active. So there is a statistical relationship between all auroral phenomena, including radar aurora.

Our concern here is with the detailed relationships of collocation in space and time, in particular we are interested in the correlation of radar echoes with visual aurora, with satellite-measured particle precipitation, and with surface-measured magnetic-field fluctuation, since all of these may (or may not) be related to the immediate scattering environment. The satellite data are just beginning to become available. It is expected that soon there will be extensive results of these programs.

The first apparent attempt to compare radar and visual aurora was performed by Bowles (1955). In this study he tried to relate the shape of radar aurora at 106 MHz to the shape recorded in photographs taken from his radar site. Briefly, he found no reliable correlation between the shapes and locations of visible and radar aurora. Also, there was no correlation between the presence and absence of either phenomenon anywhere in the sky.

A rather significant statement in his report (Bowles, 1955) is that whenever radar aurora was present, he could see the shadows of trees in his photographs. When radar aurora was not present, the trees could not be seen. The deduction was that when radar aurora is present, there exists (in the nighttime anyway) some diffuse visual glow--perhaps without well defined features.

Bates et al. (1966) have also attempted to correlate the location of visual and radar aurora. Bates claims that he very often finds near-collocation of optical and HF radar echoes on the night side of the auroral oval, but that more often than not the radar echoes seem to be adjacent to, rather than superposed upon, the visual forms. However, he does have one case of collocation within his range resolution. This work was performed using measurements from all-sky cameras (Bates et al., 1966) assuming a height of visual aurora of 100 km. A separate study (Bates, 1969a) used photometric triangulation.

Chesnut et al. (1968) have attempted to relate visual and radar aurora. In their technique they triangulated between two all-sky cameras to find the location of visual auroral features. A great variety of cases existed with radar but no visual aurora present, and vice versa. On a few occasions, radar and visual aurora were simultaneously detected and produced patterns as in Figure 3.9. The data were obtained with sufficient care that the nonoverlap of the two phenomena is considered real.

We conclude that there is no obvious relation between bright, visual auroral features such as one detects on all-sky photographs. On the other hand, it does not appear that a careful correlation study has been made to determine if any detectable luminosity is present in regions that do scatter radar waves but in which there is no obvious, bright visual aurora. Bowles (1955) does claim that nighttime radar aurora was seen only when his photographs revealed some sky glow, though he does not appear to have performed a systematic study.

The geometry of radar and visual arcs being observed simultaneously adjacent to one another--but not superposed--as shown in Figure 3.9 and as reported by Bates et al. (1966) and Chesnut et al. (1968) may have implications regarding the two-stream instability hypothesis of Farley (1963). It is known (Wescott et al., 1970; Aggson, private communication) that electric fields tend to be larger adjacent to, but outside of, visual auroral arcs. Since the Farley two-stream instability is produced by electric fields--not ionospheric currents that are known to flow in visual arcs--these data help support the two-stream-instability concept.

It has been proposed (Chesnut et al., 1968) that when auroral activity becomes very intense, electric fields inside visual arcs may exceed the Farley threshold. In this case, since electron densities are higher inside of arcs, it is likely that the strongest radar aurora would coincide with visual phenomena. During these dynamic, auroral periods it is exceedingly difficult to obtain meaningful radar visual correlations, so that no data are currently available.

The correlation of radar echoes with the location and intensity of precipitating particles has been studied by Leadabrand and Hodges (1967a), Chesnut, Hodges, and Leadabrand (1971--in preparation), Hagfors (1970), and Bates et al. (1969a). Leadabrand and Hodges (1967) found no radar echoes on several satellite passes during which no precipitation was measured above the satellite's particle-detection threshold. On one satellite pass, auroral radar echoes were observed at 139 and 398 MHz. The location of the radar echoes seemed to correlate best with the location of precipitation of electrons with energies greater than 2 keV. A region where 1-keV electrons were precipitating and a broad region of proton precipitation did not correlate well with the UHF radar echoes.

Chesnut, Hodges, and Leadabrand (1971) have compared locations of auroral radar echoes with peaks in energy deposition by electrons and protons for 14 satellite passes. The energy deposition was computed by multiplying particle flux by average particle energy. During three passes, auroral activity was very high and radar aurora was present almost everywhere in the surveillance region. During the 11 other passes, radar echoes and precipitation-energy peaks were sufficiently confined that meaningful relationships could be sought.

Chesnut et al. (1971) have found that peaks in proton precipitation were never collocated with peaks in radar returns. Peaks in electron energy deposition tended not to be collocated with radar returns, though there were some examples of superposition. Significantly, though, wherever there were radar returns, it was inferred from the satellite measurements that there was enough particle precipitation to produce E-region electron densities on the order of 10^5 per cubic centimeter. This density is probably sufficient to explain observed radar echo strengths in terms of Bragg scattering from fluctuations in electron density (Booker, 1956).

Bates et al. (1969a) have sought correlations between HF aurora and electron precipitation. Their results were based on 16 satellite passes. They found that on the night side of the earth, gross position and occurrence of precipitating electrons were in good agreement, however, exact correspondence--

or a unique spatial relationship--was not clearly apparent. On the day side of the earth, part of the electron precipitation was not generally accompanied by radar aurora, though they suggest that D-region absorption might have prevented echo observations.

Recently, Hagfors (1970) reported simultaneous observation of proton precipitation nearly collocated with radar echoes obtained at a frequency of 1288 MHz. No electron precipitation was observed in the same region. Hagfors finds that the region of peak proton flux was about 1 degree north of radar auroral-echo horizon. The radar echo intensity was increasing toward the more northerly regions--over the horizon--but the data presented do not resolve whether radar-auroral returns could have been obtained from the region of peak proton-flux deposition.

Hagfors states that the proton flux was insufficient to explain the ionization needed for radar reflection. On the other hand, this was an afternoon observation, so that solar ionization of the E region was present; it is believed that daytime E-region electron densities are great enough to produce radar clutter provided it is structured by plasma instability processes to produce fluctuation scale sizes on the order of tens of centimeters.

We note that Bates finds different correspondences between particle-precipitation type and location relative to HF radar echoes for day-side and night-side measurements. Hagfors' inference of peak radar echo collocated with proton precipitation might then not contradict the nighttime data obtained by Chesnut, Hodges, and Leadabrand (1971).

We conclude that data currently on hand show that nighttime radar aurora occurs in regions where some auroral precipitation is occurring. Thus we have an explanation for the presence of the ionization to explain nighttime auroral echoes. The correlation of radar aurora in detail with peaks in electron-precipitation number or energy density appears nearly random at this point in time with a preference for nonoverlap. The relationship between radar aurora and proton precipitation on the night-side, according to the limited data base currently on hand, shows no clear examples of collocation of radar aurora with peaks in proton precipitations, though some weaker proton precipitation does sometimes take place into the radar scattering region. One day-side measurement may have been revealed collocation of radar aurora and a peak in the proton precipitation flux.

The correlation of radar aurora with magnetic disturbance indices is of obvious interest. There have been several studies showing, for example, that radar aurora generally move southward with increased planetary magnetic activity (Leonard, 1962; Egeland, 1962; Unwin, 1966b). Egeland computed the correlation coefficient between the percent occurrence of radar aurora during each 24-hour period and the local geomagnetic Q indices as measured at Kiruna and Trömso. The Trömso magnetic observatory is closer to the region of scatter; its correlation coefficient was greater, but both were fairly large (0.59 and 0.65, respectively).

Unwin (1966b) has shown that local magnetic activity as measured by the local K index near the scattering region correlates well with radar echoes. The planetary K_p index correlated somewhat better with late-afternoon diffuse echoes than did the local magnetic index; the local index correlated best with the other radar forms.

Leadabrand et al. (1965a) displayed auroral echo intensity at 401 MHz for various elevation angles (therefore various ranges) obtained from Fraserburg, Scotland, along with the H trace from the Lerwick, Scotland magnetic observatory. That observatory is beneath the auroral reflecting region, 300 km to the north of the radar. Detailed H-component fluctuations often seem to be accompanied by radar-intensity fluctuations. The trace correlation seems best with the echoes that occur nearly directly over the magnetic observatory.

Leadabrand et al. (1965a) also display a detailed "trajectory" of signal strength versus H component. The H component is seen to increase while no radar aurora is present. Then very abruptly the auroral echoes start to occur with a 20-to-45-dB signal-to-noise ratio. Leadabrand suggests that the detailed comparison that shows an abrupt turning-on of the radar aurora indicates an activity threshold as predicted by Farley (1963).

It must be borne in mind that surface-measured magnetic activity is responding to currents in the ionosphere; scattering intensity depends on irregularity-density variations, generation of ion-acoustic waves depends on ionospheric electric fields. Thus, surface-measured magnetic activity cannot be expected to correlate perfectly with radar-reflection activity if the Farley ion-acoustic-wave hypothesis is correct.

3.1.4 Amplitude Distribution of Radar Echoes

Auroral radar returns are characterized by rapid fluctuating amplitude--called rapid fading. The statistical characteristics of the amplitude distribution of radar returns are of interest to those concerned with auroral-clutter rejection and also to those concerned with the physics of the scattering environment. The fact that the clutter echo amplitude seems to decorrelate in very short times indicates a rather broad Doppler spread of the return signals. The fading characteristics have also been used to

support the argument that the scattering takes place from a large assembly of essentially independent random scatterers.

The most detailed study of the amplitude statistics seems to be that performed by Egeland (1962). In this experiment he measured the statistics of the signal amplitude of a 92.8-MHz FM broadcast station. The signal was received by bistatic scattering via radio aurora. He was interested in determining whether a coherent signal component existed--or whether the signal-amplitude distribution was totally consistent with having been propagated by scattering from a random assembly of scatters. The presence of a coherent component would lead to the Rice amplitude distribution--which, for a large coherent component, is approximated by a Gaussian distribution. If the signal was propagated by an assembly of independent scatters, then the signal-amplitude distribution would be Rayleigh distributed--provided, of course, that the average scattering intensity remained, in expectation, constant over the time of the measurement. Figure 3.10 presents some of Egeland's results. Egeland states that these data support the conclusion that the aurorally propagated wave is the aggregate of a large number of scattered wavelets that are uncorrelated in phase. We note that should a coherent component exist, but the average scattered power vary over the period in which measurements are made, then a Rice distribution--or its Gaussian approximation--might be smeared in a way that could simulate the Rayleigh distribution. In this reviewer's opinion, that seems unlikely. At 90 MHz and higher frequencies few investigators doubt the conclusions about the scattering environment deduced by Egeland.

Flood (1965) has also studied the amplitude statistics of returns at frequencies of 49.7, 143.5, and 226 MHz using pulsed-radar techniques. As with Egeland, Flood found that the amplitude distribution for all three frequencies was well approximated by a Rayleigh distribution. His data sets were each averaged over a 30-second time interval.

3.1.5 Height of Radar Aurora

The height and vertical thickness of the auroral radar-reflection region has been of considerable interest. The height distribution seems to depend on the type of radar aurora that is being observed. Unwin (1959), defines four types of radar aurora as observed by his equipment at 55 MHz. These are diffuse, diffuse with structure, short discrete, and long discrete. Other measurements at higher frequency (Presnell et al., 1959), using pencil-beam radars, find two types, labeled discrete and diffuse. Generally, the diffuse echoing region is a thin (vertically) region that extends over large geographical areas. Discrete echoes are limited in range extent (north-south) but may extend to high altitudes--consistent, apparently, with the magnetic-aspect requirements.

Unwin (1959) presents data on the height of diffuse aurora as a function of range (generally north-south), and finds that the height is remarkably independent of range over distances of 700 km. Figure 3.11 presents two histograms of Unwin's measurements. The first is a histogram of all height measurements. The second is a histogram of daily averages.

Unwin (1959) and Presnell et al. (1959) find a tendency for the height of diffuse aurora to increase at ranges closer to the radar. This effect is not well confirmed. Leadabrand et al. (1958) also found a consistent height variation of diffuse aurora as a function of azimuth angle. Abel and Newell (1969) also appear to find a dependence of height of return on viewing azimuth, but their distribution is opposite to that found by Leadabrand. These results are compared in Figure 3.12.

Many attempts have been made to measure the vertical thickness of radar aurora. To measure the vertical thickness accurately, one requires high angular resolution and a short pulse length. Furthermore, one needs to carefully define what is meant by vertical thickness, in that the echo intensity, though dropping off rapidly with height change away from the region of maximum reflectivity, continues to be detectable at quite different heights.

Abel and Newell (1969) estimate a vertical thickness at 1295 MHz that varies from 5 to 20 km--centered around 106 km. Despite this assertion, Newell and Abel (1968) show Doppler data obtained from altitudes as much as 20 km above the center of the aurora. These measurements serve to remind us that "thickness" may mean full width at half power--or rms thickness, or something of that sort. Leadabrand et al. (1965a) estimate that the vertical thickness is no greater than 10 to 20 km. Unwin (1959) estimates that the layer he observes is less than 5 km in vertical thickness, and thinks it is probably less than 2.5 km. This conclusion is based on the visibility of the fringes in the lobing pattern of his Lloyd's mirror experiment.

Measurements of the vertical extent of discrete aurora are probably limited by the fact that if the radar beam-line fulfills the magnetic-aspect requirement at an altitude of 110 km or so, then at higher altitude the aspect condition becomes less favorable. At northern latitudes, an increase in altitude from 110 to 125 km produces about a 1° change in aspect angle. Meeting the aspect condition at higher altitudes usually means locating radars farther from the geomagnetic pole, in which case aurora becomes less frequent. Furthermore, there is no way of knowing whether the high-altitude aurora observed by this technique is connected to usual E-region aurora of the discrete or diffuse type.

Unwin (1959) gives values of height of center for short discrete and long discrete auroras as 120 km and 100 km or less, respectively. He estimates thicknesses of 10 to 26 km for short discrete and

15 or more for long discrete auroras. Leadabrand et al. (1959) do not estimate vertical extent of discrete aurora. However, Schlobohm et al. (1959) report observing auroral radar echoes at an altitude as high as 300 km at a frequency of 106.1 MHz. The radar was far south of the normal region for probing aurora; it was located at Stanford, California, at a geomagnetic latitude of 43°. Whether the high-altitude echoes were accompanied by the usual 110-km radar aurora is not known, for the magnetic perpendicularity condition is very poorly met from Stanford in the appropriate region.

High-altitude radar auroras as high as 180 km have also been seen by Barber, Sutcliffe, and Watkins (1962) at frequencies of 300 and 500 MHz. Leadabrand et al. (1965a) report high-altitude echoes up to 200 km, as seen from Frazerburg, Scotland. Bates (1966) reports HF auroral echoes from F-region heights often where HF-propagated communication signal would normally reflect from the polar-F layer. There is no doubt that these high-altitude reflection phenomena are real. It also appears that the reflectivity of the higher altitude radar aurora is considerably less than that observed at the more conventional E-region heights.

3.1.6 Doppler

The earliest radar studies of aurora noted that motions of radar auroral forms are to the west before midnight and to the east after midnight. Generally, the Doppler shift of auroral radar returns, which shows the drift direction of the individual scattering irregularities, is in the same direction as the motion of the radar auroral forms. It is now believed that Doppler shift and spread measurements hold the key to understanding the underlying mechanisms that produce the electron-density irregularities from which radar energy scatters. This belief springs from the indisputable value of the Doppler measurements made in the equatorial electrojet by Bowles, Cohen, Balsley, and others. Unfortunately attempts to unravel polar-ionosphere plasma-instability theories are severely hampered because the auroral electrojet is complicated in its direction of flow; it is also unpredictable, unreliable, sporadic, and even capricious in its behavior, which makes the performance of geometrically unambiguous experiments nearly impossible. Nevertheless, Doppler measurements do seem to be the best currently available observational technique for relating theories of irregularity formation with the nature of the environmental properties.

Bowles (1955) displayed some of the earliest Doppler measurements. His measurements were made by bistatic CW at frequencies of 25 and 50 MHz in New York and in Alaska. His data showed various kinds of Doppler spectra at various times. Based on spectra that he displays, quite often, apparently, he obtains line spectra that we now associate with two-stream instability-produced ion-acoustic waves. The earliest systematic study of Doppler shifts at UHF frequencies was performed by Leadabrand et al. (1959). These data do not show unambiguous Doppler-shifted line spectra. Later, Leadabrand (1965b) presented auroral Doppler frequency measurements at 401 MHz as a function of azimuth angle from Frazerburg, Scotland. He pointed out that according to the two-stream instability concept, one would observe a line component that showed either a positive or negative shift as a function of observing azimuth. Some features of the spectra that Leadabrand obtained were consistent with ion-acoustic waves, but there clearly were other mechanisms that had to be contributed to the scattering. For example, scattering was obtained from due north, where the radar beam-line was nearly perpendicular to the direction of assumed electron drift. According to the Farley concept alone, no energy should be obtained from this region. Furthermore, when observing at this azimuth the Doppler spectrum was very broad and centered on zero frequency shift.

Chesnut, Hodges, and Leadabrand (1968) have made simultaneous Doppler measurements at frequencies of 139, 398, 850, and 1210 MHz. Doppler spectral forms varied considerably; only a few examples were obtained showing unambiguous line components. The measurements showed that when line elements could be identified, the Doppler shifts tended to be proportional to frequency within the measurement resolution, as one would expect. Chesnut et al. (1968) recorded Doppler shifts at 398 MHz corresponding to irregularity velocities as high as 1200 m/s.

They also show some records where two radar aurora located several hundred kilometers apart showed oppositely directed Doppler shifts. Chesnut et al. interpret these results as meaning that they were observing residual premidnight aurora at one range and the postmidnight aurora at a greater range. The geometry of these echoes was consistent with the model of the auroral electrojet current proposed by Akasofu et al. (1965).

Farley's theory predicts slight phase-velocity variations with wavelength of ion-acoustic waves. Careful measurements by Cohen and Bowles (1967) of Doppler shifts in scattering from the equatorial electrojet show this variation. No sufficiently accurate measurements have been performed in the auroral scattering regions to show this predicted shift.

Camnitz, Tsunoda, and Barczys (1969) have reported results of bistatic CW measurements of Doppler-shifted auroral scatter at 143.5 MHz. Measurements were made from Buffalo, New York. A few Doppler spectra were also obtained at 226 MHz. Receiving bandwidths of 5° in azimuth were used, receiving beams were scanned from 17° west to 12° east of magnetic north. A total of 163 spectra were categorized according to their general characteristics. Only 63 of their 163 spectra did they categorize as being broad--meaning that energy was returned over a wide spread of frequencies. They could not identify a line component in only six of these 63 cases. Of the 163 individual spectra, there are 67 in which Camnitz et al. identify two simultaneous line components. Often these line components are in the same direction, implying possible existence of aurora at two different distances with differing characteristics.

Spectral peaks were observed with shifts corresponding to velocities from 0 to 1800 m/s. Only 12 percent of the peaks, though, had velocities greater than 800 m/s. They state that their data provide strong support for the thesis that Doppler velocities with magnitudes from 325 to 800 m/s were due to scattering from irregularities produced by two-stream instability. They attribute their anomalously high velocities (of up to 1800 m/s) to high ion velocities at higher altitudes where the Pedersen conductivity predominates, as discussed by Unwin and Knox (1968).

Hofstee and Forsyth (1969) have reported bistatic CW Doppler measurements over two paths from sites located in Ottawa, London, and St. Catharines, Canada. The experiment was laid out so that a common volume of scattering region was sampled at two effective angles with respect to the average direction of the electrojet. These effective angles were separated by about 20° and were oriented near magnetic north (i.e., as with the experiment of Camnitz et al., this experiment would be sampling waves that would grow at nearly right angles to the average direction of the electrojet).

The results of this study are that only a few occasions did Hofstee and Forsyth observe line spectra associated with Farley's ion-acoustic waves. During late-afternoon diffuse aurora, they never observed line components.

Newell and Abel (1968, 1969) have mapped Doppler profile versus range, azimuth, and height using the very high angular-resolution capability of the 1295-MHz Millstone radar. They measure the shift of the peak of the Doppler spectrum and show that this behaves, in azimuth and in elevation, in a manner that is consistent with the Farley two-stream instability hypothesis convolved with a height-varying vector conductivity (Hall conductivity dominated near 110 km, and Pedersen conductivity dominated at altitudes above 120 km). The Doppler shifts correspond to irregularity velocities of from 350 to 460 m/s. They also present data on Doppler shift versus azimuth for fixed-antenna elevation angles. These data are shown in Figure 3.13. Doppler shifts of 4 kHz at 1295 MHz correspond to radial velocities of 460 m/s.

More recently, the Millstone radar has obtained considerably improved Doppler spectra at 1295 MHz. Details of measurements are not yet available in print. Generally, though, the spectra that are obtained are reported to be very complex.

Doppler-shift measurements show generally westward drifts before midnight, and eastward drifts after midnight. A number of investigators regularly obtain line spectra corresponding to ion-acoustic waves at radar frequencies from 139 through 1300 MHz. The spectra contain other Doppler information that is not consistent with ion-acoustic waves. As measuring capability improves, detailed spectra are beginning to look more and more complicated. One experiment at 40 MHz (Hofstee and Forsyth) has observed line spectra corresponding to ion-acoustic waves, but the Doppler spectrum that is usually obtained shows spreading about the transmitter frequency. It is suggested here that the geometry of the Hofstee-Forsyth experiment, which probes approximately on azimuths of 5° magnetic east and 16° magnetic west, may not measure sufficiently parallel to the direction of average electron drift to observe very often the primary ion-acoustic waves that are seen so regularly by others.

3.2 Description of Scattering Environment

In this section we review what appears to be the current understanding of the region of the ionosphere from which auroral radar echoes are obtained.

3.2.1 Nature of Scattering Process

There appears to be nearly unanimous agreement that radar energy at frequencies above 100 MHz--and probably above 50 MHz--scatters from fluctuations in electron density generally at E-region heights. The mathematical treatment that describes scattering of this kind in the auroral ionosphere is an application of the Born approximation that was developed by Booker (1956).

Booker's expression for the scattering intensity per unit volume is

$$\eta_v = \eta_T \overline{\Delta n_e^2}\, \Phi(k_r, k_\theta, k_z) \quad . \tag{3.2}$$

The quantity η_v is the volume scattering coefficient for radar scattering.

In this expression η_T is the Thomson radar scattering cross section for a free electron,* $\overline{\Delta n_e^2}$ is the variance in electron-density fluctuation; and $\Phi(k_r, k_\theta, k_z)$ is the three-dimensional spectral function.

---

*Radar cross section is defined as the differential scattering cross section for scattering at 180° (backscatter). Unlike cross sections used in other disciplines, the differential scattering cross section is defined as that per 4π steradian rather than per steradian. Thus, the value of η_T that one uses in Eq. (3.2) is 4π times the value for backscatter obtained from books on atomic physics. This important point has often been overlooked.

Radar scattering of this sort is called underdense scattering from electron density irregularities. The radar frequency is higher than the plasma frequency in the scattering region. There are four primary ingredients necessary in order that reflections may be observed. First, there must be electrons present; second, there must be fluctuations in this electron density; third, the spatial wave lengths of these fluctuations must satisfy the so-called Bragg condition, and fourth, the radar must have adequate sensitivity. In practice, it seems that n_e ought to be about $10^5/cm^3$ or larger; $\Delta n/n$ seems to be between 1 and 10 percent. The measured scattering intensity is many orders of magnitude greater than can be attributed to the so-called Thomson incoherent backscatter process.

The various components of the scattering wave number in Eq. (3.2) are given here in cylindrical coordinates. This is the wave number for electron-density fluctuations that satisfy the Bragg scattering condition for the radar frequency of concern. Booker assumed azimuthal symmetry so that k_θ would not be used.

To provide a quantitative evaluation of his scattering concept, Booker hypothesized a Gaussian form for the spatial-frequency spectral-density function. By use of the Wiener-Kinchine theorem this function is transformed into the spatial autocorrelation function of density fluctuations that researchers have, in the past, attempted to relate to their measurements. Booker chose the autocorrelation function to be Gaussian, to be cylindrically symmetric about magnetic field lines, and to vary more slowly along field lines than it did across field lines. In fact, nature determines the form of this autocorrelation function; having no guide, Booker used the analytical convenience of the Gaussian function.

Booker's real contribution to the whole art of auroral-radar scattering was the introduction of a scattering concept that would relate the nature of observed radar echoes to the scattering medium. This is very important in that experimentalists could begin to talk about the nature of the medium rather than just about voltages, etc., in their radar receivers. At the time Booker introduced Born-approximation scattering to radar physicists, he did not have a good explanation for the origin of the fluctuations, which he found were necessary to explain the auroral radar measurements. It is the origin of these fluctuations that determines the precise form one should use for the 3-dimensional spectral function Φ. Section 3.1 was designed to summarize those measurements that validate the scattering concept proposed by Booker. The summary was also intended to provide an experimental base to support our later discussion on mechanisms that cause the auroral-E region to structure itself into the density fluctuation described by Φ.

The frequency-dependence work by many authors provides the main support for the conclusion that the scattering takes place from fluctuations in electron density in the ionospheric plasma. Also supporting this conclusion is the fact that the frequency dependence is fairly continuous, though monotonically decreasing with increasing frequency, for frequencies above 50 MHz. Most data about the E-region scattering environment indicate that the plasma does not become overdense at radar frequencies above 50 MHz. Furthermore, quantitative comparison of estimates from Booker's theory show that the magnitude of underdense scattering from fluctuations in electron density is sufficiently large to explain the observed auroral-radar scattering.

The amplitude statistical studies performed by Egeland (1962) and Flood (1965) are consistent with scattering resulting from an assemblage of independent scattering centers. The frequent observation that radar echoes come from regions of the sky in which there are no bright auroral forms, such as shown by Bowles (1955), and Chesnut et al. (1968), in essence proves that for the higher frequencies an underdense scattering mechanism is required. If the auroral radar reflections were due to overdense scattering, then the scattering would be strongest from regions where ionization production is greatest--i.e., in the brightest regions. Finally, some of the very-high-range-rate observations by Leonard (1971), Hardin (1969), and Fremouw (1971) corresponding to velocities of 8 to 10 kilometers per second and higher are totally inconsistent with the concept of an overdense plasma traveling at that velocity. We conclude that there is no useful alternative to the underdense scattering concept given us by Booker.

3.2.2 Generation of the Scattering Irregularities by Farley's Two-Stream Instability

The structuring of the scattering region by nature determines the form of the function Φ in Booker's scattering formula. Booker, Gartlein, and Nichols (1955) had suggested coherent scattering from underdense, long luminous auroral features. When Booker (1956) developed his Born-approximation theory, he found that in order to explain observational data he had to postulate scale sizes of density fluctuations of several meters and smaller, not the kilometers and larger dimensions of the visible aurora rays. He suggested that turbulence might be responsible, though he had several reservations about this hypothesis.

In 1960 Bowles et al. (1960) suggested that the field-aligned radar scattering observed to originate within the equatorial electrojet, demonstrated properties similar to those observed by Leadabrand et al. (1969) in auroral scattering. The equatorial-electrojet scattering produced by fluctuations in electron density behaved, not like blobs of differing electron densities drifting in some direction, but like scattering from density fluctuations associated with plane waves traveling through the E-region ionization. The plane waves always seemed to travel radially with respect to the radar location, with a velocity near sonic.

Another important result of the radar measurements of the equatorial-electrojet scattering was the revelation that the presence, or absence, of scattering was dependent on the strength of the

equatorial electrojet--scattering being present very strongly (at least 20-dB signal to noise), or wholly absent--with the system sensitivity employed at that time. This suggested that a threshold phenomenon was operative; fluctuations would grow to large intensity, or they would not grow at all.

In 1963 Farley (1963) proposed and then developed a theory of production of plane waves in the E-region ionosphere due to the development of longitudinal, electrostatic plasma waves. The introduction of this concept and the subsequent success of his proposal opened the flood gates to the introduction of plasma-instability theory into ionospheric physics to explain many kinds of irregularities in the earth's ionosphere.

Farley's paper is a rather complete, usable description of the theory. The theory is complex and does not easily allow the average reader to understand how the instability mechanism works. If the reader is familiar with the observation that traveling-wave tubes actually amplify signals, then he can relate that familiarity to the Farley instability mechanism.

It may also be well known to the reader that a current flowing through a plasma can produce growing waves of various kinds. For the wave growth to be most efficient, the streaming-particle velocities should be slightly in excess of the velocity of the growing waves. Landau (1946) showed, however, that if the streaming-particle velocities were widely distributed as, for example, by thermal-velocity spread within the streaming-particle beam, existing waves would be damped, and no waves would grow. This phenomenon is called Landau damping.

Figure 3.14 shows schematically several sets of particle-velocity distributions along the direction in which one would look for growing waves. The vertical axis is the particle number density per velocity interval; velocity is plotted horizontally. In Figure 3.14(a) we show the ion and the electron-velocity distributions schematically in the presence of a small electric field. This electric field gives rise to a mean drift velocity of v_D between the two species. The electrons and ions are assumed to be in thermal equilibrium. A vertical, dotted line indicates the velocity v_w of the wave that we expect to grow. In the Farley wave case the wave velocity is nearly equal to the ion-acoustic velocity. Because the electrons are so very light relative to the ions, their mean thermal velocity is extremely large compared with the ion's thermal velocity. Figure 3.14(a) illustrates this extreme velocity spread. The figure is conceptually valid, (1) if there is no magnetic field, (2) if we are considering the velocity distribution along an axis nearly parallel to a magnetic field, or (3) if the electron collision frequency (with ions or neutral particles) is so high that magnetic constraints upon electron motion are destroyed.

For purposes of explanation, we shall assume that the electron-velocity distribution of Figure 3.14(a) represents the electron-velocity distribution parallel to the earth's magnetic field. In the altitude regions where auroral-radar echoes are observed, it is believed that the electron-collision frequency is small compared with its gyrofrequency. In this case, the electron velocity normal to the magnetic field is its E X B drift velocity--sometimes called its "guiding-center velocity." For wave motions with frequencies that are small compared with this electron gyrofrequency, and for wavelengths that are large compared with the electron gyroradii (both conditions apply for the waves of concern here), it is the electron "guiding-center" rather than the electron-linear velocity that really matters. Under these conditions the effective velocity distribution along the earth's magnetic field is spread as if there were no magnetic field; parallel to the field, the field has no effect. However, across the magnetic field, there is virtually no velocity spread in the "guiding-center" approximation, except for the spread produced by residual electron-neutral collisions whose collision frequency is small compared with the electron gyrofrequency. Therefore, the effective electron-velocity distribution can be very narrow, as we have depicted in Figure 3.14(c), when measured exactly perpendicular to the earth's magnetic field.

In Figure 3.14(c) we have illustrated this effect; in this figure there is also superposed a drift velocity due to the presence of an electric field normal to the earth's magnetic field. In Figure 3.14(c), the conditions are proper for the growth of longitudinal plasma waves; Landau damping due to velocity spread of the electrons is not operative, since the effective velocity spread of the electrons is extremely narrow compared with the normal thermal spread. At some angle slightly off the exact perpendicular, the electron-velocity distribution will appear as in Figure 3.14(b). A situation as depicted in Figure 3.14(b) will be on the threshold of producing growing waves, but Landau damping due to the velocity spread in the electron-velocity distribution is just sufficient to prevent wave growth. The velocity distribution of Figure 3.14(b) also depicts a possible electron-velocity distribution exactly perpendicular to the earth's magnetic field lower in the ionosphere where collisions destroy the monochromaticity of the "guiding-center" approximation.

3.2.3 Attempts to Relate Two-Stream Instability to Auroral Radar Observations

There have been a number of attempts to relate auroral radar backscattering to the predictions of Farley two-stream theory. The Farley theory predicts that scattering should be magnetic-aspect-sensitive. The theory also predicts weaker scattering at the higher UHF frequencies. The most unique prediction is the unique velocity of the scattering features irrespective of the angle that the radar beam-line makes with the direction of the electron E X B drift.

The first attempt to relate Farley's concepts to radar measurements of aurora was performed by Leadabrand (1965a). Leadabrand presented Doppler-shift-vs.-azimuth data obtained at 400 MHz for auroral

reflections obtained from northern Scotland. These data showed that when the radar beam-line was generally parallel to the assumed direction of Farley waves (which travel generally parallel to the Hall current at 110 km altitude), a peak in the Doppler return was observed that was consistent with Farley's two-stream theory. When the radar beam was perpendicular to the assumed direction of the Hall current, in which direction no Farley waves are expected, there were no peaks in Doppler shifts, but radar scattering was observed and showed a wide spread in return frequencies corresponding to many velocities between the limits that one might predict from Farley's theory.

At all azimuths some energy was scattered with Doppler shifts that were less than those predicted by Farley and that could even be in the wrong direction. Leadabrand concluded that there were some aspects of his data that were consistent with Farley's two-stream instability theory, but he concluded that some other processes were also necessarily operative.

Gadsden (1967) attempted to relate the data obtained by Leadabrand et al. (1959) and that of Unwin, showing a thin layer, to the two-stream instability theory. He pointed out that for a uniform applied electric field, the direction of electron-ion relative drift changes with altitude. Thus, a north-south electric field produces at 110 kilometers an east-west Hall current. At the higher altitudes, 120 to 130 km, the Pedersen conductivity becomes greater than the Hall conductivity so that the direction of electron drift relative to the ion drift is rotated to a more north-south direction. On the basis of this model, auroral-radar layers would appear to be at a higher altitude when the radar is observing due north than when observing at azimuths on either side of north. This conclusion seemed to be consistent with the height-vs.-azimuth data obtained by Abel and Newell (1969) and shown in Figure 3.12 for a north-south electric field. Explaining the results by Leadabrand et al. (1959) on the layered, daylit afternoon diffuse auroral echoes requires an east-west electric field. Gadsden also pointed out that the observation of a thin layer at nearly uniform height was also consistent with the two-stream hypothesis.

Newell and Abel (1968) capitalized on Gadsden's realization of the effects of Hall and Pedersen conductivities in order to analyze the Doppler shift of radar echoes obtained at 1288 MHz. If they mapped mean Doppler shift of auroral echoes as a function of azimuth from the radar, and as a function of height of the echo volume, they found that the Doppler behavior was consistent with the Farley two-stream hypothesis.

The data of Jaye et al. presented in Figure 3.5 are perhaps consistent with the Farley hypothesis but do not necessarily prove that the two-stream instability is totally responsible for structuring the E-region ionization.

Unwin and Knox (1968) have attempted to relate the characteristics of their 50-MHz data with the two-stream-instability hypothesis. They have taken estimates of the ionospheric electric fields to compute the altitude, diurnal, and latitudinal behavior of the diffuse echoes. They find a level of agreement between their calculations and the 50-MHz morphological observations; their work shows that late-afternoon diffuse aurora could be produced by the Farley instability. Their equipment does not permit measurement of the Doppler shift.

Under the assumption that there is an intimate relation between Farley two-stream velocity and the group motion, Unwin and Knox (1968) compare their group radial velocities with the predictions of the Farley theory. There appears to be some level of agreement between these data, though some will doubt that the group velocity and the Doppler velocity should be related in the manner employed.

Unwin and Knox (1968) also computed the layer height and thickness as a function of time of day, latitude, and direction of their radar beams. In this comparison they find much to support the Farley hypothesis. They also find that auroral forms that they label long discrete do not fit Farley's hypothesis at all well. They therefore assume that these are created by some other mechanism.

Hofstee and Forsyth (1969) have used a coherent bistatic radio system to look for the displaced-line-spectrum characteristic of scattering from the Farley ion-acoustic waves. Their work was performed at 40 MHz. On occasion they observed line components, but the ratio of the energy of the line component to the nonwave-scattered signal varied considerably, with the line component not even observable at times. They conclude that the ion-acoustic waves predicted by the Farley theory do occur in auroral plasma phenomena, but that the waves cannot be the only source of radio-wave scattering. They do not find line components from afternoon diffuse aurora and therefore assume that the Farley mechanism is not responsible for it. They reject the contention of Unwin and Knox (1968) that discrete nighttime and morning echoes are due to scattering from concentrations of electrons formed by particle precipitation.

Unwin and Knox (1971) have provided a rebuttal to Hofstee and Forsyth. The only observation of line spectra obtained by Hofstee and Forsyth occurred at night. This observation weakened the Unwin and Knox thesis that afternoon diffuse aurora would have resulted from the two-stream hypothesis. Unwin and Knox contend that too many features of afternoon diffuse aurora are consistent with the ion-acoustic-wave mechanism. Unwin and Knox suggested that during the afternoon aurora the waves grow almost only along the direction of current flow. Therefore what is observed with Doppler instruments that do not probe nearly along the direction of current flow will be secondary waves produced perhaps by the conceptual mechanism suggested by Dougherty and Farley (1967).

Hagsfors (1970) has also obtained spectra from afternoon diffuse aurora. His spectra do not show a line spectrum characteristic of the Farley mechanism, but again the growth angle of Farley waves in the afternoon ionosphere may be so narrow that not only must perpendicularity to the magnetic field be met, but the radar beam-line may have to be almost exactly parallel to the velocity vector of streaming electrons. The data of Camnitz, Tsunoda, and Barczys (1969) show very complicated Doppler spectra with many features attributable to ion-acoustic waves. In fact most of their Doppler spectra contain line elements.

3.2.4 Theoretical Attempts to Explain Other Features of Observed Irregularity Structure

Dougherty and Farley (1967) hypothesized that the nontwo-stream echoes observed by Cohen and Bowles (1967) in the equatorial electrojet could be explained in terms of a nonlinear interaction of Farley waves. They did not concern themselves with the detailed origin of the nonlinear interaction. Their suggestion was a heuristic approach that showed that a nonlinear interaction leads to cross-modulation products and harmonics of the waves. The waves, of course, have a vector characteristic and therefore the cross-modulation analysis occurs in a vector space. This interaction can lead to waves of many velocities traveling in a variety of directions. As is well known, Farley waves grow generally in the direction of electron-drift velocity. Growth of waves in directions away from parallel require higher intrinsic electron-drift velocity. The observation of scattering from the equatorial electrojet when the radar beam-line was actually perpendicular to the electron drift cannot be produced, in principle, by Farley waves. The observed scattering at that geometry was taken as evidence that nonlinear interactions take place.

There is little doubt that nonlinear effects must be important in the growth of Farley waves. Clearly, some mechanism must cause the waves to cease growing. It is therefore not difficult to believe that these nonlinear effects can produce cross-modulation waves that display all the effects predicted by Dougherty and Farley.

Subsequent to the publication of the paper by Dougherty and Farley (1967), Balsley (1969) showed that scattering is observed when the electron-drift velocity in the electrojet is less than that required for the Farley instability. This has led some to believe that the Dougherty-Farley work is no longer relevant. This is not the case; cross modulation of some sort is inevitable in nature. Unwin (1970)--(unpublished) has utilized pulsating radar aurora associated with Pc5 events to show how he can coherently organize some observations utilizing the heuristic arguments of Dougherty and Farley. If Unwin's work is correct, it can provide a logical explanation for the auroral scattering of the layered afternoon diffuse aurora that does not show the line spectra of the Farley instability.

Skadron and Weinstock (1969) have performed nonlinear analysis in which they permit wave-particle trapping that leads to wave-wave interaction. It is perhaps too soon to evaluate the validity of their theory. The theory is extremely complex and difficult to follow. However, they do produce a proposed turbulent spectrum. Like all turbulent spectra, their spectrum peaks at some wavelength and decays on either side. Unfortunately their analysis as given in their Figure 1 does not show turbulent energy with wavelengths shorter than about 3/4 meters that can scatter radar energy at 200 MHz. Thus, they do not predict the structuring necessary for UHF and higher frequency observed scattering.

Scattering work by Balsley (1969) has shown that there is another instability operative in the equatorial-E region that scatters VHF radar waves. This instability he calls his Type II instability. The Doppler response of the radar returns are consistent with the scattering centers moving in the direction of the electron drift with the radar measuring the projection of that velocity along the radar beam-line of sight. The Doppler spectrum is broad but does peak as described above.

Recently Rogister and D'Angelo (1970) have proposed a theory of equatorial Type II instabilities. The characteristics of this instability as determined by experiments suggest requirement of an electron drift velocity gradient in possibly a gradient of ionization. Balsley (1969) sees a bifurcation of echoes occurring at an altitude of 100 kilometers and 115 kilometers (approximate). As the electric field excitation increases, the two layers expand toward one another and essentially coalesce when the Farley two-stream instability onsets. They indicate that their theory predicts that vertical, as well as horizontal echoes should be observed at the equator. They predict drift velocities that are consistent with Balsley's observations. They also claim that the theory predicts bifurcation of echoing regions. Rogister and D'Angelo do not suggest experimental tests of the theory that can be applied in the auroral zone.

Whitehead (1971) also puts forward a theory based upon the gradient instability of Simon (1963) and Hoh (1963). The theory is too new for this writer to have digested.

The relevance of the Type II instability to the auroral ionosphere has not been proven. Until we better understand the details of the theories by Whitehead (1971) and by Rogister and D'Angelo (1970) we shall not be able to assess their significances, nor possibly the significance of Type II instabilities to the aurora.

To explain discrete echoes that are observed at nighttime at lower frequencies, Unwin and Knox (1970, unpublished) have proposed that ray structured visible aurora produces sufficiently strong horizontal ionization gradients that a form of the Simon gradient-drift instability may be initiated. They believe that at lower altitudes (100 to 150 kilometers) in the highly excited auroral ionosphere, short wave-length structure that will scatter HF and VHF radars will be created.

3.3 Summary of Auroral Radar Scattering

It appears that much recent experimental work has been oriented toward validating the contribution to the scattering irregularity structure by ion-acoustic waves theoretically predicted by Farley (1963). Many of the general features of radar aurora are consistent with predictions of this theory. The principal technique that is currently being employed to certify the contributions of the ion-acoustic wave is Doppler analysis of returning echoes.

Radar studies at the equator reveal Doppler returns that are consistent with the two-stream instability concept. However, other irregularity-generating mechanisms must also be present. Balsley (1969) has studied, by Doppler analysis, the equatorial-electrojet scattering and has deduced the presence of another instability that he labels the Type II instability. Apparently--at times--he also observes a line spectrum that is not Doppler-shifted at all (see Camnitz et al., 1969).

One's intuition indicates that these other mechanisms must play a role in the polar ionosphere. At this writing, not enough is known about these alternative mechanisms and the details of the environment needed for their growth, to plan useful experiments to seek their existence in polar aurora.

The nonlinear coupling concept of Dougherty and Farley (1967) must play a role in producing irregularities. A detailed nonlinear coupling mechanism was not proposed by them, but that does not matter. The concept has been useful for organizing data (Unwin, 1970--prepublication). A quantitative nonlinear theory has been developed (Skadron and Weinstock, 1969), though it is not yet clear how experiments can test the validity of the proposal.

Two theoretical explanations for the equatorial Type II instabilities have been proposed (Rogister and D'Angelo, 1970; Whitehead, 1971). More study is required of the environmental conditions necessary to produce these instabilities before we can intelligently apply the concepts to auroral-scattering data.

Recently, Unwin and Knox (1970--unpublished preprint) have proposed that a form of the gradient-drift instability first theoretically analyzed by Simon (1963) and Hoh (1963) is capable of explaining the characteristics of discrete aurora. They base their study on the work of Whitehead (1968). They show that, based on the gradient-drift instability, discrete aurora will form adjacent to visual forms. The discrete forms will be observed predominantly at the lower radar frequencies. Furthermore, though not stated by them, the Doppler shifts can be as low as zero and as high as the E x B drift.

4. RADAR TRANSMISSION THROUGH AURORAL IONIZATION

In this section we shall discuss propagation of radar signals through high-altitude auroral ionization. Our primary concern will be with radar frequencies in excess of 100 MHz. Running through our commentary will be our explicit concern with the effects of propagation on the acquisition of data obtained by radars that are performing accurate target tracking and are obtaining target-signature information. This means that the antenna system has a fairly high angular resolution--usually on the order of 1° or so in both horizontal and vertical directions.

It is known that structured ionization refracts--and defracts--radar energy so that the angle of apparent arrival of a signal from a source on the other side of the structured ionization changes with time and location of the target. This phenomenon is called angle scintillation. Some radar measurements of space vehicles use the variation of satellite signal intensity as a function of time to determine the nature, the size, the rotation, and the nutation characteristics of the target. Structured auroral ionization will modulate target-echo amplitude leading to obscuration of the target's normal signature information.

In addition to effects caused by structured auroral ionization, very accurate tracking radars will experience angular deviations produced by smooth refraction in the normal E- and F-layer ionization. These angular deviations can also change with time due to the passage of aurorally-induced gravity waves. Our detailed concern will be directed to those effects that are produced by structured and aurorally-induced ionization. Simple refraction due to the natural ionosphere will not be discussed.

It is believed that the structured ionization that affects radars with frequencies above 100 MHz to several thousand megahertz is the same ionization structure that is responsible for the effects reviewed by Liszka in "Polar Propagation Effects on Radio Astronomical and Satellite Transmissions." We presume that the morphological behavior of the structured ionization will be discussed there, and it will therefore not be pursued here.

Radars that track space objects require very-high-power transmitters, very large antenna systems, and usually very complex computer and display equipment. As a result, the instrumentation is extremely expensive; it is usually built for operational space-data-acquisition purposes, and is therefore usually not

available for propagation studies. There is, therefore, a very meager base of directly applicable measurements. Very recently the Millstone radar operated by MIT Lincoln Laboratory has been configured to perform comparative tracking studies simultaneously at 400 to 1200 MHz. Data are just beginning to become available with this instrument. Stanford Research Institute is currently locating its 1300-MHz Thomson-scatter radar at Fairbanks, Alaska; this instrument has monopulse tracking capability and has been used in the past for satellite tracking purposes. It is expected that this radar may provide some propagation information in the future. In conjunction with its Homer auroral-radar installation, SRI is also installing a 400-MHz phased-array radar that will have tracking capability. A polar satellite carrying phase-coherent signals from 138 MHz through 3000 MHz is also being designed, to be used in studies of bandwidth and other characteristics of auroral-radar propagation. All of these experimental programs are in early phases and have not yet produced data. At this writing the radar-propagation data base is very small.

4.1 Propagation Concepts

A radar wave passing through structured ionization suffers wavefront distortion. This means that the phase fronts of the wave are no longer spherical (with centers located at the source); rather, the wavefront surfaces become bumpy. Radar energy will then leave the distorting region in wavelets that travel in a variety of directions that are no longer radial with respect to the signal source. A familiar optical analog of this situation is the bumpy glass that is often placed in bathroom showers or in windows that are intended to admit light while maintaining privacy. A single light source behind such a bumpy glass screen may appear as many light sources--or as a larger light area--as a result of refraction of the light in passing through this screen.

Some of the earliest quantitative theory that has been applied to radio/radar propagation was performed by Bramley (1951, 1955). Bramley's concern was with the relationship between the refracting screen and the signal characteristics as received by ground-based point receivers and interferometers. A very readable, tutorial introduction to these concepts was prepared by Ratcliffe (1956). Another important paper with regard to receiver power and interferometric studies was that of Briggs and Parkin (1963), in which they suggest means of comparing data obtained by propagation at various oblique angles through striated ionization and also define various ways of expressing scintillation indices. In the main, these papers utilize a technique that is called the thin-phase-screen approximation to determine the "bumpiness" of the surfaces of constant phase of the wave at the output of the diffracting medium. There have been some studies on ways of extending the calculation of the perturbed wavefronts into the regime in which the thin-phased-screen approximation does not work. (Chernov, 1960; Uscinski, 1968.)

Before the radar-propagation problem is fully understood, the properties of the structured ionization that cause radar-wave distortion must be empirically determined. Though there are many analytical ways of computing wavefront distortion, there are at present no physical theories capable of describing the environment necessary for understanding propagation perturbations.

Morphological studies (Aarons and Allen, 1971; Liszka, 1967) using satellite beacon transmissions indicate that the F region of the polar ionosphere is often perturbed near the region called the mid-latitude trough. An example obtained by Evans et al. (1970) found the perturbations on the northern side of the trough. The northern edge of the trough is found to be rather abrupt; the peak F-region electron density changes by a factor of 25 over a relatively small horizontal distance.

This environment seems very likely to contain conditions that will cause instabilities to develop. It has also been suggested that the structure is due to structured particle precipitation. In view of the very long ionic lifetimes at 350-km altitudes, this suggestion does not seem, at the outset, very plausible for high-altitude structured ionization. Fremouw (1968) does find a strong relationship between line-of-sight auroral luminosity and radio star visibility fades. It is suggested that these fades may result from E- and lower F-region auroral ionization where ionic lifetimes are measured in seconds.

The crinkled wavefront that emerges from the structured ionization usually must propagate long distances to the radar receiver. Ratcliffe (1956) describes how to analytically determine the Fresnel pattern at the receiver site. The actual evaluation of the analytics displayed by Ratcliffe is extremely difficult and tedious. Therefore, a number of approximate analytical techniques have been developed to perform the propagation described by Ratcliffe. The best known of these is the Fresnel-Kirckhoff technique. Ratcliffe's techniques are readily adaptable to take advantage of the fast-Fourier-transform capabilities of modern digital computers (Cooley and Tukey, 1965). As a result, this calculational technique is becoming very popular for propagation work. The propagation of a wave from a disturbed region to a radar can produce a number of effects. We give here an intuitive description of various phenomena that can be important. If there is a very large blob or field aligned striation of ionization, then radar rays will be refracted by it as if the blob is a large lens. Since blobs of ionization appear as a negative lens, there can be defocusing (signal reduction). Such an environment can be analyzed by purely refractive techniques and propagation performed by ray tracing.

If the electron density on the axis of the blob becomes sufficiently large and the receiver is far enough away, then the refracted ray may cross at some point between the receiver and the ionized blob. In this situation the target can be observed also as refracted by way of the ionized blob. In fact the radar will, for this example, observe three images. Figure 4.1 is a pictorial display showing how refraction produces these multiple images as a target passes behind a long, magnetic field aligned striation

or blob of ionization. Actually, finite-aperture antennas with finite beamwidths would probably "observe" more than one of these images at a time--which leads to interference and therefore amplitude and angle scintillation. The sizes of the "dots" representing the target are indicative of the target signal strength. Note the "defocusing" as the target passes behind the ionization blob.

At the small end of the size spectrum of ionospheric blobs, one finds that ray theory is not a valid way to compute the propagation. Physically, what happens is that blobs are smaller than a Fresnel zone and therefore energy can be scattered by a single blob to angles that are very great compared to what one would have computed based on refraction alone. Clearly, if the blob were comparable in size to the radar wavelength, then the energy could even be backscattered, which means refracted or diffracted through 180°. This is, of course, what the entire preceding section was all about. It is therefore necessary in computing the propagation of signals between the output of the perturbed region to the radar to take account of the phase path to the receiver from all small-scale blobs even if they are quite far off the propagation path.

As an example, let us hypothesize small-amplitude phase perturbations on the wave phase-front. Let us suppose that the phase perturbation is of a single, spatial wavelength with wavelength that is smaller than a Fresnel zone. Under these circumstances the medium will begin to behave as a diffraction grating that diffracts energy at preferred angles--called first order, second order, etc., grating lobes. An optical analogy is, of course, the optical grating that is used, for example, for spectroscopic measurements of auroral emissions. If one should attempt to compute the angular deviation of a wave through such a screen, by refraction theory, he would find that the wave is virtually unaffected, which result, of course, is not valid.

The whole point of this discussion is to indicate that a variety of propagation effects can occur between the perturbing region and receiver. There will be lensing effects of all kinds due to large scale-size ionization structures. These effects will lead to focusing, defocusing, and ray-path crossing, which we sometimes refer to as multipath, and there can be caustics. If the perturbed structure size is comparable to or smaller than the first Fresnel zone, then there will be a variety of effects that we characterize as diffraction effects; all of these lead to signal-amplitude fluctuation and apparent angle-of-arrival changes at the receiver antenna. One must use care when calculating, to be sure that the technique used will be properly applicable.

The final link in the chain of events leading to the radar response is the interaction of the distorted wave with the radar antenna system. This relationship is not always simple. The work by Bramley, Briggs, and Parkin, and others, was concerned with point receivers and spaced-point receivers used as interferometers. Most radars that we are concerned with have a distributed antenna system that accepts energy from a limited span in angle. Furthermore, the kinds of radars that one would actually use for space-vehicle tracking must have means for moving the radar beam direction in order to track space objects. This latter requirement can be satisfied, from an engineering point of view, by several tracking techniques; examples are spiral-scan, amplitude monopulse, and phase monopulse.

The ultimate response of the radar system in its tracking mode will depend not only on the interaction of the radar wave with the tracking antenna system, but also on how that information is used to direct the antenna system to follow the target. The complexity of these potential problems is so great that it is probably outside the purview of this review to dwell on them at length. However, we believe it would be useful to demonstrate how the antenna system interaction with the waveform may not be simple and straightforward.

In order to better understand some of these problems we have been performing tracking simulation studies using a one-dimensional model of a phased-array antenna.* We present an example of this work here; this example was used as a program check to demonstrate certain kinds of behavior that we had expected in advance.

In the results of the study to be shown below in Figure 4.2, a phase-perturbing screen has been placed at a range of 300 kilometers from the radar. At this range the first Fresnel zone is about 450 meters. We have assumed that the phase perturbations are created by cylindrical columns of enhanced electron density with on-axis densities of 10^7 el/cm^3. This value of electron density was thought to be representative of extreme auroral conditions. This density gives an on-axis critical frequency of 28 MHz. The computations have been carried out for one-way propagation at 450 MHz. The radial density profile of these striations were taken to be Gaussian in form.

We have chosen for the work to be displayed here, a phase screen that contains two sizes of striations. The phase-screen aperture contains an isolated striation with 1/e radius of 500 meters. Nearby, not quite far enough away to prevent interaction with the isolated striations, is a pair of striations of the same size. This pair is so located that their effects will strongly interact. We have also placed a similar arrangement of a single striation and a pair of striations farther across the phase-screen aperture. These striations have 1/e radii of 1500 meters. They also have the same on-axis electron density as the small striations.

---

*This work is being carried out jointly by Mr. Gary Price and the author.

The simulated antenna total beamwidth was about 1.2°. The antenna simulation was that of amplitude monopulse, which means that two beams, squinted off by one-half beamwidth to the right and left, are compared. The propagation from the phase-perturbing screen to the radar plane was carried out by the technique described by Ratcliffe (1956) utilizing fast-Fourier-transform techniques. For this particular arrangement of striations, the smaller striations were made to be larger than a fresnel zone, but the radar was located at a distance beyond the point where caustics form. We chose the large-size striations so that the onset of caustics occurs behind the position of the radar.

Figure 4.2 shows the results of this work. Across the top, the phase perturbations caused by the thin diffraction screen are shown. This indicates the sizes of the striations. Arrows in each of the three subfigures show the axial positions of the striations. The relative voltage of the received radar signal is shown in the center panel of Figure 4.2 as the signal source (target) passes behind the columns of ionization. We note that ray crossing leads to rapid amplitude scintillation for the isolated, small striation and also for striation pairs due to phase mixing. The isolated, large striation, which does not produce ray crossing, demonstrates a simple focusing-defocusing pattern as the target travels behind the screen.

At the bottom of the figure is the angular error of the radar's monopulse responses as a function of target position. It is easily shown from refraction theory that the maximum angular deviation to be expected from these striations is 0.174°. In fact the large, isolated striation does produce a peak angular error of this value since no ray mixing occurs. We note that as a result of ray mixing--or, if you wish, diffraction--larger angular errors are measured as the target moves behind the small striation.

Another concern of radar designers will be the maximum antenna size that can be built without decorrelation of the wavefront occurring over the aperture size. This information can be determined by interferometer experiments that have been performed over many years. Conceptually, when the "angular spectrum" of waves leaving the diffraction screen is comparable to the angular resolution of the radar antenna system, then the span of the antenna aperture is so great that the wavefront is decorrelated over this aperture.

4.2 Experimental Data

As we stated earlier, relevant radar tracking experiments are just beginning to be performed. Therefore the directly applicable data base for presentation here is quite small. Some data we shall present were obtained by one-way transmission from radio stars or satellites. Radar signals must traverse both directions. It can be shown by reciprocity that this two-way transmission leads to a squaring of the one-way received amplitude. We have not found that angular effects will be changed, though.

As early as 1957, Jaye et al. (1961) observed extreme amplitude fluctuations due to signal transmission through an auroral-type disturbance. At the time, Jaye et al. were observing passage of Soviet satellites by radar backscatter at a frequency of 106.1 MHz. On at least one occasion, backscatter from an aurora at an altitude of 300 km over Seattle, Washington, was observed to be present during the satellite pass. As the satellite passed through the radar beam, amplitude fluctuations were observed.

Later a joint effort between the Lincoln Laboratories, the Defense Telecommunication Research Establishment, and SRI was undertaken (James et al. 1960). This experiment studied amplitude scintillation of 440-MHz signals that had been propagated from Alaska to the moon, reflected off the moon, and received near Boston, Massachusetts, and also at James Bay, Ontario. One of the concerns was polarization rotation, which we shall not pursue in this work. On occasion, signals passed through aurora. The signal fading rate and the depths of the fades were increased significantly. (Normal moon radar echoes fade slowly due to moon libration.) No quantitative scintillation indices were presented. However, it was noted that there was no decrease in average signal power.

Flood (1963), using the radio star Cassiopeia A and multiple-base-line interferometers at frequencies of 52 and 147 MHz investigated the phenomenon of "radio star fadeout." As a radio star slowly traverses the field of view, the interferometer output from the star will vary in nearly sinusoidal fashion as the star passes through the interferometer lobes. A radio star fadeout--or visibility fade--means that the sinusoidal, lobing pattern disappears, or fades. The destruction of this lobing pattern is caused by phase-path fluctuations that destroy the wave's phase coherence over distances corresponding to the interferometer base-line.

In his work Flood defines a "cone angle of arrival θ" and shows that it is proportioned to λ^2/L. The quantity L is the correlation length for visibility fades under the assumption that the spatial autocorrelation function for phase fluctuation is Gaussian with 1/e value L. This relation seems to be often used to scale angular scintillation--or angular flicker--data measured at one frequency for use at other frequencies. In his paper Flood scales his data to provide "pessimistic" estimates of angular resolution of radar systems operating through the auroral ionosphere. Table 1 presents his conclusions.

This work has been more recently extended by Anderson and Tsunoda (1969) using the same techniques at frequencies of 52, 147, and 294 MHz. They have presented their estimates of Flood's cone angle of arrival θ for their three frequencies in the form of histograms. We show these for their 147-MHz data in Figure 4.3. The reader should note that these data are slightly prejudiced, since the measurements were made only

Table 1

LIMITATION TO ANGULAR RESOLUTION DUE TO IONOSPHERIC PHASE-PATH FLUCTUATIONS

Frequency (MHz)	50	150	300	1200
Angular Resolution				
In milliradians	360	40	10	0.6
In degrees	20.6	2.3	0.57	0.0342

when a radio-star fade was taking place. We note that cone-of-arrival angles as large as 30 mrad (1.7°) in an east-west direction were observed. The maximum north-south cone angle was 10 mrad (0.57°), which is consistent with ionized blobs that are aligned with their thin, long axis aligned along magnetic field lines.

As a test of the λ^2 dependence for Flood's cone angle, Anderson and Tsunoda present a histogram of occurrences of the wavelength dependence that they had measured. Figure 4.4 presents these data. We note that the median value is about 2, in agreement with Flood's (1963) derivation, but individual measurements scatter considerably.

Anderson and Tsunoda (1969) also present histograms of measured axial ratios for the ionized blobs. Figure 4.5 shows these data. The peak of their distribution, a value of 2.2, is very much smaller than is generally quoted elsewhere. Liszka (1963) quotes axial ratios of 8 through 21. Jones (1960) gives a median value slightly greater than 5. The origin of these variations from experiment to experiment is unknown; it is possible that the more southerly experiments (Flood, Anderson, and Tsunoda) respond more to E- and lower F-region aurorally-produced ionization. Also, measurement technique may play an important role.

A few of the angular errors obtained by a monopulse tracking system have been presented by Fremouw (1967). The equipment used was the NASA Gilmore Creek data-acquisition facility near Fairbanks, Alaska. The system consisted of an 85-foot dish with mechanical drives servoed to monopulse error sensors. Figure 4.6 presents an example of a pass of the Nimbus satellite. The upper record is signal intensity; the lower is the error on one of the two antenna mount axes. The first angular deviation of nearly 2° is not accompanied by a signal fade. The second angular excursion of about 1° is accompanied by about a 20-dB signal reduction--presumably due to defocusing. Both of the two refraction effects were closely associated with auroral luminosity as recorded on an all-sky camera.

The angular excursions indicated in Figure 4.6 are consistent with the estimates made by Flood (1963) suggesting that radio-star data obtained by radio inferometers can be applied to radar-like tracking systems.

It can be shown that mechanical dish-type monopulse tracking systems such as the Gilmore Creek facility can be driven so as to lose track if the propagation conditions lead to severe multipath. Fremouw reports (private communication) that at times propagation conditions deteriorate sufficiently that operators at the Gilmore Creek facility have changed from auto track to program track at 136 MHz. The system would be turned over to program track in order to be certain that data would be successfully recorded. (Program track means a Newtonian orbit--fitted to the early tracking data--would be used to guide the antenna to keep track of the target.)

Lansinger and Fremouw (1967) have performed calculations of the expected amplitude scintillation of signals that have traversed structured ionization. Their work, based on prior developments by Ratcliffe (1956), and Briggs and Parkin (1963), demonstrates that the frequency dependence of the scintillation index is not simple but lies between λ^1 and λ^2. The scintillation index is defined as

$$S = \frac{\overline{P_i - \bar{P}_i}}{\bar{P}_i} \quad . \tag{4.1}$$

They have obtained radio-star data at 68 and 223 MHz. Figure 4.7 from Lansinger and Fremouw (1967) presents a scatter plot of simultaneous scintillation index measurements versus that for their higher frequency of 223 MHz. This scatter plot gives the scintillation-index ratio between 68 and 223 MHz versus the index measured at 223 MHz. The plot dramatizes the lack of uniqueness for frequency scaling. Theoretically, the λ^2 frequency scaling is the limit to weak scattering conditions, and λ^1 is a limit they obtain for a more perturbing environment. The scatter plot tends only very weakly toward these relations.

Lansinger and Fremouw (1967) also present data on the fading rate of radio-star signals. They find that the power spectral density function of the scintillation frequencies is about the same for both 68 and 223 MHz. These spectra change from time to time, probably reflecting change in speed and size of ionized blobs that traverse their propagation path. The examples they present show energy as high as 0.5 Hz. The scintillation rate experienced by a radar tracking a space object behind an auroral phase-perturbing

screen will be determined more by the scale size of the ionized irregularities and the vehicle's velocity than by irregularity-drift velocity.

Pope and Fritz (URSI-1971) have reported measuring amplitude scintillation in the aurora using 137 MHz and 1695 MHz simultaneously. They used the Gilmore Creek data acquisition facility that was also used by Fremouw. They state that 1695-MHz scintillations were observed when the VHF scintillation was near saturation. They state that the wavelength power law between λ^1 and λ^2 broke down; when observed, scintillations at 1695 MHz were about one-tenth the VHF amplitudes.

Craft (1971) has reported amplitude scintillation through equatorial irregularities at frequencies of 4 and 6 GHz. Rapid fluctuations as large as ±4 dB were seen. It is possible, then, that the polar ionosphere could also affect frequencies this high in a similar fashion.

Recently, Lincoln Laboratories (Evans et al., 1970) have begun a series of tracking experiments using a monopulse radar that measures angle of arrival at 1295 MHz and 400 MHz simultaneously. The equipment consist of an 84-foot dish antenna with 1295-MHz monopulse radar. There is also a 400-MHz, monopulse telemetry reception feed that uses the 84-foot dish. Angles of arrival at the two frequencies are then compared.

At this writing only very preliminary results of tracking radio stars have been reported. These data show angular effects at 400 MHz.

Elkins (1971) has recently scaled data obtained by Little et al. (1962) to provide an estimate of probability of angular scintillation exceeding various cone angles. These data are presented in Figure 4.8 for radar frequencies of 400 and 1300 MHz. According to these data, expected angular errors are usually quite small; only 1 percent of the time will a 400-MHz radar operating in Alaska experience angular jitter in excess of 0.3 mrad, which is about 0.017°. At 1300 MHz the corresponding figure is 0.0016°.

These angular-error data imply very much smaller angular errors than estimated by Flood (1963). Flood reports that during 375 days of continuous observation, auroral disturbances caused radio-star fadeouts at lower culmination 32 percent of the time. Cassiopeia A traverses lower culmination at an elevation angle of 10°. The interferometer operated at 52 MHz with a 900-foot base-line. This fade, when scaled to 400 MHz using Flood's scaling procedure, gives cone angles of 0.06 to 0.13°--which values are also consistent with those reported by Anderson and Tsunoda (1969). These values are nearly a factor-of-ten larger than Elkins (1971) estimates.

One is forced to conclude that, accepting the validity of all work quoted, angular (and therefore amplitude) scintillation is much greater for radars looking north from locations south of the auroral zone (Flood, Anderson, and Tsunoda) than it is for radars located in the auroral zone (Little et al., 1962). Furthermore, the frequency of occurrence of significant angular jitter is greater at the location south of the northern auroral zone.

The data of Little et al. were obtained during the 1957-1958 period of high geomagnetic activity when auroral effects are expected to be observed farther from the poles than at other times. The data processed by Flood was obtaining in 1960-1961 during a period of weaker activity. We do not know quite how to relate these facts except to hypothesize that the region in which the propagation problems were occurring was to the south of the region probed by Little et al., during their data-taking period, and in the field of view of Flood (1963) and Anderson and Tsunoda (1969) during their data-taking period.

We summarize our state of understanding of the radar transmission data. At present there are available to the propagation community no recent round-trip radar studies of the problems introduced by irregularities in the polar ionosphere. Early data obtained by Jaye et al. (1961) and James et al. (1960) only studied amplitude scintillation--and then only as an adjunct to their primary experiments. There exist several interferometric studies of radio-star fadeouts using the Cassiopeia A and the Cygnus source. These data can be related to real radar tracking--with some reservations. Inferences concerning radar operation made by using radio-star data have led to an apparent conflict of estimates of frequency of occurrence and magnitude of angular scintillation to be expected by UHF and higher-frequency radars. The conflict may be resolvable through study of the morphological behavior of the location of the midlatitude trough, scintillation boundary, and aurorally-produced ionization (the auroral oval).

Polar tracking experiments using one-way satellite transmission and a monopulse tracking system show that effects can be severe to accurate tracking systems at frequencies of 136 MHz. Extrapolated to higher-frequency radars where angular tracking accuracies of 0.1 mrad are sought indicates that this level of accuracy may not be achievable at will at frequencies of 400 MHz, but probably can be achieved at 1300 MHz. However, the recent scintillation data obtained by Pope and Fritz (1971) at a frequency of 1695 MHz in the auroral zone--and the equatorial scintillations of ±4 dB observed at 4 GHz and 6 GHz (if confirmed)--indicate that we probably do not yet have a good understanding of the problems faced by accurate space-tracking radars operating through the polar-disturbed ionosphere.

4.3 Theory of Ionization Structuring Process

HF and VHF satellite transmission measurements (Liszka, 1968; Aarons and Allen, 1971) have shown that many regions of the earth's ionosphere exhibit magnetic field aligned ionization density perturbations. They are observed regularly in equatorial regions as well as in polar regions. In equatorial regions, solar-heating-induced vertical motion of the ionosphere produces conditions that are thought to produce interchange instabilities that are the density perturbations. As we also know, structured ionization is regularly observed in the polar ionosphere.

It is tempting to hypothesize that all ionospheric structuring is due to plasma instability processes. However, data correlations made by Fremouw (1968) suggest an intimate association between radio-star visibility fades and auroral luminosity. As we suggest later this observation and the low axial ratios measured by Flood (1963) and Anderson and Tsunoda (1969) may mean that auroral precipitation produced E- and lower F-region ionization is also important in producing structured ionization that can affect radar. We shall discuss, briefly, both processes here. We investigate particle precipitation first.

4.3.1 E-Region Ionization Produced by Particle Precipitation

Auroral particle precipitation regions move fairly rapidly. Therefore the ionization produced by the particle precipitation can only build up to large values that can affect radar in regions where ionospheric chemistry is fast. Ionic equilibration times are on the order of seconds at altitudes between 100 and 120 km. Between 250 and 450 km, ionic equilibration times are tens of minutes. To produce high electron densities by particle precipitation at these higher altitudes would require a very stable, long duration auroral form lasting tens of minutes that did not move its own width.

The work by Fremouw (1968) demonstrates a near one-to-one correspondence between radio-star visibility fades and auroral optical excitation along the line of sight to the star. Height distributions presented by Liszka (1968) do indicate amplitude scintillation production at E-region heights. The height distributions presented by Liszka are based upon satellite amplitude scintillation measurements. The most likely heights for the scintillation causing irregularities is between 250 and 450 km. However, amplitude scintillation is not necessarily accompanied by angular effects as measured by interferometers. Moorecroft and Forsyth (1963) first pointed out some of the apparent contradictions that seemed to result when only amplitude scintillations are considered. Severe phase-dominated scintillation--that leads to radar angular errors--is only unambiguously diagnosed by use of interferometers. Therefore we hypothesize below that the radio-star visibility fades that were the concern of Flood (1963), Fremouw (1968), and Anderson and Tsunoda (1969) are produced by aurorally produced ionization at E- and lower F-region heights.

For illustration purposes, we describe two types of visible auroral forms and show how they can lead to axial ratios (Anderson and Tsunoda, 1969) of less than and greater than one. For the first case we choose a long, east-west, homogeneous arc. We assume that the arc moves slowly towards the north or south. At an altitude of 110 km, the fast ionic chemistry allows electron densities to build up to their large, steady-state values during the passage of the arc. The particles do not penetrate below some altitude, say 90 km, thereby providing a lower border to the ionization region. At altitudes above 150 km, the ionic chemistry is so slow that as the arc moves past a parcel of gas, the ionization level does not build up to an appreciable value. Therefore the slowly moving, homogeneous arc will produce a nearly horizontal rod of ionization. The rod of ionization might be tens of kilometers in the vertical direction and hundreds of kilometers in east-west extent. This rod of ionization would lead to radar elevation angle errors. Interferometers of the type used by Anderson and Tsunoda (1969) would interpret this ionization rod as having an axial ratio much less than one. Their instrument would characterize it as pancake-shaped blobs of ionization.

For our second example, we assume that rayed structure develops in the arc. Since visible rays seem to be on the order of a kilometer or so in size, we now see that the rayed-arc would produce a horizontal rod of ionization with strong magnetic field aligned columns imbedded inside. For this situation, the interferometers would determine an axial ratio that would be greater than one.

Thus, we see that particle precipitation can produce ionization structures at E- and lower F-region heights that will have axial ratios that may be less than or greater than one. The data of Anderson and Tsunoda (1969) presented in Figure 4.5 show such a variation. Fremouw (1968) indicates auroral luminosity whenever radio-star fadeouts were observed, such fadeouts imply severe angular scintillation. Plasma instabilities of some sort may also play a role in structuring the E-region ionization--but particle precipitation inhomogeneities as we describe above also seem capable of producing the needed ionization structure.

Based upon all data scanned by this reviewer, it is his opinion that angular scintillation in radar propagation is produced mainly by intense ionization irregularities generated in the F and lower F region by auroral particle precipitation. The data seem, without question, to show that severe angular jitter that produces interferometer radio-star visibility fades occurs on propagation paths that traverse regions where particle precipitation is occurring. Though it may be premature, this reviewer assumes that the scintillation-producing irregularities that exist at high altitudes and described by Liszka (1968) develop angular spectra (cone angles of arrival) that are too narrow for current interferometer experiments to detect as visibility fades. This reviewer also suggests that the high axial ratios inferred by Liszka

(1968), Aarons (1971), and many others utilizing satellite amplitude scintillation measurements are applicable to the high altitude density fluctuations--namely between 250 and 450 km.

4.3.2 F-Region Irregularities and Interchange-Plasma Instabilities

As indicated earlier, it is tempting to ascribe density fluctuations to plasma instabilities of some kind. Morphological studies (Liszka, 1967; Aarons and Allen, 1971) show that the high altitude structured ionization is often associated with the northern boundary of the midlatitude trough in polar regions. It has been suggested that the trough is produced by a Westward E X B drift before midnight and an Eastward E X B drift after midnight. This mechanism will deplete the regions around magnetic midnight that are subject to these electric fields, but the mechanism does not allow the trough's continuity through the day side. These electric fields, if they do occur in the north-south gradient of ionization, may cause that gradient to become unstable by a plasma-instability mechanism that may be related to the Kelvin-Helmholtz instability of classic fluid dynamics. For the reader who is not well versed in instability theory, the Kelvin-Helmholtz instability is responsible for the production of surface waves when the wind blows across the surface of a body of water. The plasma analogy would require collocation of a gradient in electric field and a parallel (or antiparallel) gradient in plasma density. In this way there is velocity shear across a density gradient--low-density plasma (the wind) sliding by high-density plasma (the water surface).

An alternative hypothesis is that there is an eastward-directed electric field, with appropriate north-south gradient, that causes E X B drift of F-region ionization northward out of the trough into the northern border. In this situation, conditions seem right for the onset of the gradient-drift instability of Simon (1963) and Hoh (1963).

The difficulty with these hypotheses is that, though Liszka (1967) has shown that the northern side of the trough is characterized by large scintillation indices, he claims that the scintillation is not connected with the gradient of electron content nor is it caused by the increased electron content to the north of the gradient.

Nevertheless it has been proposed by Cunnold (1969) that the very-high-altitude F-region density fluctuations are in fact propagated upward along the earth's magnetic field from lower-altitude operating plasma instabilities. The instability that he had in mind was a generic form of the Simon-Hoh, gradient-drift instability (Simon, 1963; Hoh, 1963). This instability requires the presence of a magnetic field, that there be a gradient in ionization density, and that there be a collisional interaction between the neutral and the ionized portions of the ionosphere. The instability is most effective when the coupling between the electrons and the neutral gas is sufficiently weak that the electrons are almost free to move independently of the neutral particles.

Plasma instabilities seem to be very important in producing the structures that affect high altitude radar propagation. This is true both for transmission effects, of concern in this section, and for clutter, of concern in Section 3. The Simon-Hoh, gradient-drift instability probably is an important process in producing E-region clutter, Sporadic-E and, most interesting here, possibly in structuring very high altitude F-region ionization. Because of its importance we shall attempt here to provide some physical insight into the instability mechanism.*

We hypothesize a plasma cloud as in Figure 4.9. We suppose that neutral particles (the neutral wind) are flowing through a plasma cloud as indicated. (Because of the very low density at high altitudes, the neutral and ionized particles can slide by one another.) It is the relative motion of the ions and neutral particles that matters. If our frame of reference is chosen to be stationary with respect to the ions, we then speak of the neutral wind flowing through the ions. If we chose our frame of reference to be stationary with respect to the neutral particles, then we state that the ionized cloud is moving under the action of an E X B drift. This description is not completely rigorous, but it does enable us to discuss generic behavior of the phenomena more readily. For our discussion we shall stay with the ions and let a neutral wind flow through the plasma as shown in Figure 4.9.

A neutral wind flowing through the plasma will impart momentum to the plasma particles by collisions. In the presence of a magnetic field, the charged particles will then have a tendency to flow across the cloud, generating a current as shown. If the cloud was a piece of copper, we'd call this an eddy current. If there is a closed current path outside the cloud--say, down to the E region--then a j X B, Lorentz force is generated by the eddy current. This Lorentz force acts upon the plasma, which then resists the neutral wind force that is attempting to drag the plasma with it.

We now investigate the gradient of the cloud out of which the neutral particles flow. Figure 4.10(a) is an illustration of this side of the plasma cloud. In this figure the magnetic field is assumed to be out of the sheet. Higher density plasma is on the left, low density plasma on the right; between is the gradient region. As indicated above, there exists a neutral-wind, collision-caused current that flows through the plasma with the current return elsewhere as, for instance, in the E region. This current flows downward in this figure.

---

*Figures 4.9 and 4.10 to be shown and the basic arguments to be presented are a product of discussions with Drs. Joseph Workman, Lewis Linson, and Albert Simon though the author accepts responsibility for errors.

In Figure 4.10(a) we have schematically illustrated the collision produced trajectories of the electrons and ions. Since these collision produced drifts are in opposite directions, these drifts lead to the current that we described macroscopically by means of Figure 4.8.

Let us introduce into the gradient a region of slightly increased plasma density as indicated in Figure 4.10(a). The neutral wind collision induced motion of the ions and electrons in the higher density region is the same as elsewhere. Therefore the collision-induced trajectories cause the ions and electrons to separate as we have illustrated by the solid and dashed circles indicating the higher density region. The charge separation produces the surface charges that are shown. These surface charges produce a local electric field inside of the higher density plasma blob which field acts to prevent continued charge separation. This electric field is oriented vertically upwards in the figure.

In Figure 4.10(b), at the inset to the right, we have illustrated the trajectories of electrons and positive ions in the presence of an upward directed electric field and an outward directed magnetic field. Both the electrons and the ions E × B drift to the right--with the same velocity. Thus, they move together. This, then, is the ultimate motion of the plasma blob that we placed in the density gradient.

We have illustrated this motion by the change in the position of the slight density increase in the gradient region. The blob moves from the region of high density to the region of low density. The blob is now surrounded by lower density plasma than before. Therefore the fractional variation in plasma density from outside to inside the blob has increased.

If instead of an isolated, slight density increase, we had introduced a "bump" of higher density plasma on the left protruding into the gradient region, the same effects would apply and the bump would move off to the right. Moving into a region of lower ion density would make it appear as though the bump was growing, and again the fractional variation in local plasma density would increase.

In fact such bumps will grow from naturally occurring statistical density fluctuations. They will produce magnetic field aligned blobs or striations of ionization. Again the requirements are that there be a magnetic field and a plasma with a gradient. There must also be relative motion between ions and neutral particles (a neutral wind if you stay with the ions, an E × B drift if you stay with the neutrals). If the reader has followed our arguments above, then he also can show for himself that in order for the instability to grow--to mix blobs of high density plasma into regions of low density plasma--the neutral wind must blow from high density plasma into low density plasma. If the wind blows the other way--from the low density plasma into the high density region--bumps will move back and the gradient region will become smooth.

Cunnold (1969) has proposed that this gradient drift instability takes place in the lower F region and its effects are amplified up the earth's magnetic field lines. At this writing there is insufficient additional work, analysis, and rebuttal to evaluate the validity of this concept. As with all other instability concepts, it is the large-amplitude, nonlinear regime that is actually observed by radar-propagation measurements. These currently are not handled by theory.

The F-region irregularities in the polar ionosphere that cause radar-perturbation problems are often modeled as elongated blobs of ionization that are characteristically a kilometer in diameter and 5 to 20 kilometers or so long. In actuality, measurements usually determine an aspect ratio (length to diameter) of a spatial autocorrelation function that is used as a statistical description of the phase-perturbing screen. An actual visualization of a structured polar F-region ionization is afforded by photographs of structured-barium clouds. The deployment of barium vapor in the ionosphere in the presence of sunlight leads to the generation of a plasma cloud containing gradients in ionization that take place over a few kilometers. Relative motion of barium and neutral particles is created by wind or electric fields. The structure of a barium cloud is revealed optically by the resonance reradiation of sunlight.

Figure 4.11 presents a pair of photographs of a fairly large barium-vapor release after the cloud has gone unstable. One photograph is nearly exactly along magnetic field lines, the other views the cloud from the side. It is thought that the cloud becomes structured by a generic form of Simon-Hoh instability (Linson and Workman, 1970; Simon, 1970). This is the instability that Cunnold has suggested initiates the structuring of the polar F region. If this is the case, then the two photographs of Figure 4.11 that show a view of the barium cloud from the side and directly up the magnetic field lines give us a visualization of what the structured polar ionization may be like.

4.4 Summary of Radar Transmission Through Polar Ionization

Radio star and satellite transmission studies show that radar propagation in the polar ionosphere will suffer amplitude and angular scintillation. The polar ionospheric regions that cause scintillation are thought to be associated with the northern side of the midlatitude, F-region trough. Scintillation seems to be produced mainly by structured ionization at altitudes between 250 and 450 km. Fremouw (1968) states that the most severe angle scintillation (visibility fades) occur when intense auroral optical emissions are observed along the line of sight to the radio source. It is also observed (Anderson and Tsunoda, 1969) that severe angular jitter leading to radio-star fades is produced by structured ionization that is magnetic field aligned with axial ratios between 1/2 and 7. The axial ratios measured in conjunction with amplitude scintillation of satellite signals (Liszka, 1963) seem much greater (8 to 21).

We are led to hypothesize the following: Radar refraction errors (angular jitter, angular flicker or angular scintillation) probably are caused by E- and lower F-region ionization produced by precipitating auroral particles. The structure of the ionization may be produced in part by structure in the precipitating particle flux and partly (for small axial ratio cases) by the dynamics of the E-region ionic chemistry. Plasma instabilities in the E-region ionization could also play a role though our experience with magnetic instabilities suggests that if these were important, larger axial ratios than Anderson and Tsunoda (1969) measure would be found. Certainly the more severe radar effects are associated with regions of optical emission.

Radar amplitude scintillation will be produced by E- and F-region ionized structure. Measurements to date using interferometers suggest to us that the angular spread produced by regularly observed F-region irregularities is too narrow to have been detected as visibility-fades even though they produce amplitude scintillation. On this basis we suspect that the F-region irregularities may not produce significant angular errors to radars operating at frequencies above several hundred megahertz.

If our hypotheses above are correct, the significant radar angular effects are probably associated with the auroral oval which generally lies to the north of the midlatitude trough. Amplitude scintillation can be expected to be experienced for radar signals that traverse the F region north of the scintillation boundary--which boundary is situated on the northern side of the midlatitude trough. It is well known that higher-frequency radar systems are less subject to propagation problems that result from traversal of structured ionization. From an engineering and an economics point of view it is not always possible to design adequate radars to perform the needed missions at, say, L band and higher frequencies. Therefore it is necessary to determine the ultimate accuracy that polar propagation will permit for VHF and UHF radars.

Actual propagation tests with real, high-performance radars are just beginning. Usable results are expected within the next year.

Extrapolation from radio-star studies have been made. These extrapolations suggest that UHF radars may not always be able to achieve angular tracking accuracies that are needed. Angular scintillation conditions at L band, as extrapolated from VHF radio-star measurements, seem sufficiently benign to allow achievement of tracking accuracies in the 0.1-mrad (0.006°) region.

Recent measurements at 1675 MHz and even at 4 GHz and 6 GHz indicate occasional large-amplitude scintillations that could compromise acquisition of signature data even for L-band and S-band radar frequencies.

There have been several mechanisms proposed to explain the generation of high-altitude irregularities. As far as we know, the authors of these ideas have not yet provided unique experimental concepts that can be used to validate their proposals.

REFERENCES

Aarons, J., and R. S. Allen, 1971, "Scintillation Boundary During Quiet and Disturbed Magnetic Conditions," J. Geophys. Res., Vol. 76, pp. 170-177.

Abel, W. G., and R. E. Newell, 1969, "Measurements of the Afternoon Radio Aurora at 1295 MHz," J. Geophys. Res., Sp. Phy., Vol. 74, pp. 231-245.

Akasofu, S. I., S. Chapman, and C. I. Meng, 1965, "The Polar Electrojet," J. Atm. Terr. Phys., Vol. 27, pp. 1275-1305.

Anderson, L. J., and R. T. Tsunoda, 1969, "Angular Scintillation of VHF Radars in an Auroral Environment," Tech. Report, Cal. No. UB-2448-P-2.

Balsley, B. B., 1969, "Some Characteristics of Non-Two-Stream Irregularities in the Equatorial Electrojet," J. Geophys. Res. Sp. Phy., Vol. 74, pp. 2333-2347.

Barber, D., H. K. Sutcliffe, and C. D. Watkins, 1962, "Some Radar Observations of Meteors and Aurorae at 300 and 500 Mc/s Using a Large Radio Telescope--II," J. Atm. Terr. Phy., Vol. 24, pp. 599-607.

Bates, H. F., A. E. Belon, G. J. Romick, and W. J. Stringer, 1966, "On the Correlation of Optical and Radio Auroras," J. Atm. Terr. Phys., Vol. 28, pp. 439-446.

Bates, H. F., R. D. Sharp, A. E. Belon, and J. S. Boyd, 1969a, "Spatial Relationships Between HF Radar Aurora, Optical Aurora, and Electron Precipitation," Planet Space Sci., Vol. 17, pp. 83-95.

Bates, H. F., and P. R. Albee, 1969b, "Aspect Sensitivity of HF Auroral Echoes," J. Geophy. Res. Sp. Phy., Vol. 74, pp. 1164-1168.

Booker, H. G., C. W. Gartlein, and B. Nichols, 1955, "An Interpretation of Radio Reflections from the Aurora," J. Geophy. Res., Vol. 60, pp. 1-22.

Booker, H. G., 1956, "A Theory of Scattering By Nonisotropic Irregularities With Application to Radar Reflections from the Aurora," J. Atm. Terr. Phys., Vol. 8, pp. 204-221.

Bowles, K. L., 1954, "Doppler Shifted Radio Echoes From Aurora," J. Geophy. Res., Vol. 59, pp. 553-555.

Bowles, K. L., 1955, "Some Recent Experiments with VHF Radio Echoes from Aurora and Their Possible Significance in the Theory of Magnetic Storms and Auroras," Tech. Report 22, Cornell University, Contract DA 36-039-sc-56748.

Bowles, K. L., R. Cohen, G. R. Ochs, and B. B. Balsley, 1960, "Radio Echoes from Field-Aligned Ionization Above the Magnetic Equator and Their Resemblance to Auroral Echoes," J. Geophy. Res., Vol. 65, pp. 1853-1855.

Bramley, E. N., 1951, "Diversity Effects in Spaced-Aerial Reception of Ionospheric Waves," Proc. Instr. Elect. Engrs., Pt. 3, Vol. 98, pp. 19-25.

Bramley, E. N., 1955, "Some Aspects of the Rapid Directional Fluctuations of Short Radio Waves Reflected at the Ionosphere," Proc. Instr. Elect. Engrs., Vol. B102, pp. 533-539.

Briggs, B. H., and I. A. Parkin, 1963, "On the Variation of Radio Star and Satellite Scintillations With Zenith Angle," J. Atm. Terr. Phys., Vol. 25, pp. 339-355.

Camnitz, H. G., R. T. Tsunoda, and D. A. Barczys, 1969, "Project Aurechoes--Auroral Echoes and the Two-Stream Instability," Tech. Report/Cal 2469-P-1, Cornell Aerospace Lab.

Chapman, S., 1952, "The Geometry of Radio Echoes from Aurorae," J. Atm. Terr. Phys., Vol. 3, pp. 1-20.

Chesnut, W., J. C. Hodges, and R. L. Leadabrand, 1968, "Auroral Backscatter Wavelength Dependence Studies," RADC-TR-68-286, Stanford Research Institute, Contract No. AF 30(602)-3734.

Chesnut, W. G., J. C. Hodges, and R. L. Leadabrand, 1971 (Private Communication).

Chernov, L. A., 1960, Wave Propagation in a Random Medium (McGraw-Hill Book Co., Inc., New York, New York, 1960).

Cohen, R., and K. L. Bowles, 1967, "Secondary Irregularities in the Equatorial Electrojet," J. Geophys. Res., Vol. 7, pp. 885-894.

Cooley, J. W., and J. W. Tukey, 1965, "An Algorithm For The Machine Calculation of Complex Fourier Series," Math. of Computation, Vol. 19, pp. 297-301.

Craft, H. D., 1971, "Some Measurements of Ionospheric Scintillations at 4 GHz and 6 GHz," Paper III, 1-4; Spring 1971 Meeting, URSI.

Cunnold, D. M., 1969, "Drift-Dissipative Plasma Instability and Equatorial Spread F," J. Geophys. Res. Sp. Phy., Vol. 74, pp. 5709-5720.

Dougherty, J. P., and D. T. Farley, 1967, "Ionospheric E-Region Irregularities Produced by Nonlinear Coupling of Unstable Plasma Waves," J. Geophys. Res., Vol. 72, pp. 895-901.

Dyce, R. B., 1955, "Auroral Echoes Observed North of the Auroral Zone on 51.9 Mc/sec.," J. Geophys. Res., Vol. 60, pp. 317-323.

Dyce, R. B., and S. Horowitz, 1963, "Measurements of Synchrotron Radiation at Central Pacific Sites," J. Geophys. Res., Vol. 68, pp. 713-722.

Egan, R. D., and A. M. Peterson, 1960, "Auroral Noise at HF," J. Geophys. Res., Vol. 65, pp. 3830-3832.

Egeland, A., 1962, "Study of Auroral Reflections in the VHF Band," Arkiv. för Geofysik, Vol. 4, pp. 103-169.

Elkins, T. J., 1971, "Ionospheric and Tropospheric Limitations to Radar Accuracy," D. L. Evans, Compiler, AFCRL-71-0169, Air Force Cambridge Research Center.

Evans, J. V., 1970, "The Millstone Hill Propagation Study: Progress in FY 1970," ESD-TR-70-357, Lincoln Lab., MIT, Massachusetts.

Farley, D. T., Jr., 1963, "A Plasma Instability Resulting in Field-Aligned Irregularities in the Ionosphere," J. Geophys. Res., Vol. 68, pp. 6083-6097.

Flood, W. A., 1963, "A Study of Radio Star Fadeouts and Their Application to Radar Resolution," J. Geophys. Res., Vol. 68, pp. 4129-4140.

Flood, W. A., 1965, "Part 1: Some Evidence for the Occurrence of High Electron Densities in the Auroral D and E Region, Part II: An Analysis of the Statistics of Simultaneous Auroral Echoes," AFCRL-65-451, Cal. Report No. CN-1677-p-1.

Forsyth, P. A., W. Petrie, and B. W. Currie, 1949, "Auroral Radiation in the 3,000 Mc Region," Nature, Vol. 164, p.453.

Forsyth, P. A., W. Petrie, and B. W. Currie, 1950, "On the Origin of Ten Centimeter Radiation From the Polar Aurora," Can J. Res., Vol. 28, pp. 324-335.

Fremouw, E. J., 1967, Effects of Ionospheric Irregularities, in Propagation Factors in Space Communication, Chap. 3, Blackband, Ed. (Mackay and Co., London).

Fremouw, E. J., 1968, "On Radio-Star Visibility Fades and the Aurora," Planet. Space Sci., pp. 1155-1159.

Fremouw, E. J., 1971 (Private Communication).

Gadsden, M., 1967, "The Origin of Afternoon "Auroral" Radar Echoes," Planet. Space Sci., pp. 893-898.

Hagfors, T., 1970, see Evans, J. V., 1970.

Harang, L., and W. Stoffegren, 1940, "Echoversuche Auf Ultrakurz-Wellen," Hochfreq. u. Elektrock, Vol. 55, pp. 105-108.

Hardin, R., 1970 (Private Communication).

Hartz, T. R., T. R. Reid, and E. L. Vogan, 1956, "VHF Auroral Noise," Can J. Phys., Vol. 34, pp. 728-729.

Hartz, T. R., 1958, "Auroral Radiation at 500 Mc," Can J. Phys., Vol. 36, pp. 677-682.

Hofstee, J., and P. A. Forsyth, 1969, "Ion-Acoustic Waves in the Auroral Plasma," Can J. Phys., Vol. 47, p. 2797.

James, J. C., L. E. Bird, R. P. Ingalls, M. L. Stone, J. W. B. Day, G. E. K. Lockwood, and R. I. Presnell, 1960, "Observed Characteristics of an Ultra-High-Frequency Signal Traversing an Auroral Disturbance," Nature, Vol. 185, pp. 510-512.

Jaye, W. E., R. B. Dyce, and R. L. Leadabrand, 1961, "Radar Echoes Obtained from Earth Satellites 1957 Alpha and 1957 Beta," Planet. Space Sci., Vol. 5, pp. 50-58.

Jaye, W. E., W. G. Chesnut, and B. Craig, 1969, "Analysis of Auroral Data From the Prince Albert Radar Laboratory," Contract 601932, Bell Telephone Lab., New Jersey.

Jones, I. L., 1960, "Further Observations of Radio Stellar Scintillation," J. Atmos. Terr. Phys., Vol. 19, p. 26.

Landau, L. D., 1946, J. Phys., USSR Vol. 10, p. 25.

Lansinger, J. M., and E. J. Fremouw, 1967, "The Scale Size of Scintillation-Producing Irregularities in the Auroral Ionosphere," J. Atmos. Terr. Phys., Vol. 29, pp. 1220-1242.

Leadabrand, R. L., and A. M. Peterson, 1958, "Radio Echoes from Auroral Ionization Detected at Relatively Low Geomagnetic Latitudes," Proc. IRE, AP-6, pp. 65-79.

Leadabrand, R. L., R. I. Presnell, M. R. Berg, and R. B. Dyce, 1959, "Doppler Investigations of the Radar Aurora at 400 Mc," J. Geophys. Res., Vol. 64, pp. 1197-1204.

Leadabrand, R. L., 1964, in Walt, M., Auroral Phenomena (Stanford University Press, Stanford, California, 1965).

Leadabrand, R. L., J. C. Schlobohm, and M. J. Baron, 1965a, "Simultaneous Very High Frequency and Ultra High Frequency Observations of the Aurora at Fraserburgh, Scotland," J. Geophys. Res., Vol. 70, pp. 4235-4285.

Leadabrand, R. L., 1965b, "A Comparison of Radar Auroral Reflection Data With Acoustic Wave Theory," Rad. Sci., Vol. 69D, pp. 959-964.

Leadabrand, R. L., and J. C. Hodges, 1967a, "Correlation of Radar Echoes From the Aurora With Satellite-Measured Auroral Particle Precipitation," J. Geophys. Res., Vol. 72, pp. 5311-5317.

Leadabrand, R. L., A. G. Larson, and J. C. Hodges, 1967b, "Preliminary Results on the Wavelength Dependence and Aspect Sensitivity of Radar Auroral Echoes Between 50 and 3000 MHz," J. Geophys. Res., Vol. 72, pp. 3877-3887.

Leonard, R. S., 1962, "Distribution of Radar Auroras over Alaska," J. Geophys. Res., Vol. 67, pp. 939-952.

Leonard, R. S., 1971 (Private Communication).

Linson, L. M., and J. B. Workman, 1970, "Formation of Striations in Ionospheric Plasma Clouds," J. Geophys. Res. Sp. Phy., Vol. 75, pp. 3211-3219.

Liszka, L., 1967, "The High-Latitude Trough in Ionospheric Electron Content," J. Atmos. Terr. Phys., Vol. 29, pp. 1243-1250.

Liszka, L., 1968, Scintillations of Satellite Signals, in Low Frequency Waves and Irregularities, D'Angelo (Ed.) (D'Reidel Pub., Dordrecht-Holland).

Little, C. G., G. C. Reid, E. Stiltner, and R. P. Merritt, 1962, "An Experimental Investigation of the Scintillation of Radio Stars Observed at Frequencies of 223 and 456 Megacycles per Second from a Location Close to the Auroral Zone," J. Geophys. Res., Vol. 67, pp. 1763-1784.

Lyon, G. I., and P. A. Forsyth, 1962, "Radio-Auroral Reflection Mechanisms," Can J. Phys., Vol. 40, pp. 749-757.

McDiarmid, D. R., and A. G. McNamara, 1967, "VHF Radio Aurora: Simultaneous Observation of Auroral Ionization By Two Separated Radars," Can J. Phys., Vol. 45, pp. 3009-3027.

McDiarmid, D. R., and A. G. McNamara, 1969, "A Physical Model of a Radio Aurora Event," Can J. Phys., Vol. 47, pp. 1271-1281.

Moorcroft, D. R., 1961, "Models of Auroral Ionization, Part I. Auroral Ionization Models and Their Radio-Reflection Characteristics," Can J. Phys., Vol. 39, pp. 677-694.

Moorcroft, D. R., and P. A. Forsyth, 1963, "On the Relation between Radio-Star Scintillations and Auroral and Magnetic Activity," J. Geophys. Res., Vol. 68, pp. 117-124.

Moorcroft, D. R., 1966, "The Interpretation of the Frequency Dependence of Radio Aurora," Planet. Space Sci., Vol. 14, pp. 269-275.

Newell, R. E., and W. G. Abel, 1968, "Indirect Experimental Evidence For the Existence of Hall and Pedersen Currents in the Auroral E Region," Nature, Vol. 218, pp. 454-456.

Peterson, A. M., and G. L. Hower, 1963, "Synchrotron Radiation From High-Energy Electrons," J. Geophys. Res., Vol. 68, pp. 723-734.

Pope, J. H., and R. B. Fritz, 1971, "High-Latitude Scintillation Effects on VHF and S-Band Satellite Transmission," Paper III, 2-7; Spring Meeting, URSI.

Presnell, R. I., R. L. Leadabrand, A. M. Peterson, R. B. Dyce, J. C. Schlobohm, and M. R. Berg, 1959, "VHF and UHF Radar Observations of the Aurora at College, Alaska," J. Geophys. Res., Vol. 64, pp. 1179-1190.

Ratcliffe, J. A., 1956, "Some Aspects of Diffraction Theory and Their Application to the Ionosphere," Reports on Progress in Physics Vol. XIX (1956) (The Physical Society), pp. 188-267.

Rogister, A., and N. D'Angelo, 1970, "Type II Irregularities in the Equatorial Electrojet," J. Geophys. Res. Sp. Phys., Vol. 75, pp. 3879-3887.

Schlobohm, J. C., R. L. Leadabrand, R. B. Dyce, L. T. Dolphin, and M. R. Berg, 1959, "High-Altitude 106.1-Mc Radio Echoes from Auroral Ionization Detected at a Geomagnetic Latitude of 43°," J. Geophys. Res., Vol. 64, pp. 1191-1196.

Simon, A., 1963, "Instability of a Partially Ionized Plasma in Crossed Electric and Magnetic Fields," Phys. Fluids, Vol. 6, pp. 382-388.

Simon, A., 1970, "Growth and Stability of Artificial Ion Clouds in the Ionosphere," J. Geophys. Res., Vol. 75, pp. 6287-6294.

Skadron, G., and J. Weinstock, 1969, "Nonlinear Stabilization of a Two-Stream Plasma Instability in the Ionosphere," J. Geophys. Res. Sp. Phy., Vol. 74, pp. 5113-5126.

Störmer, C., 1955, The Polar Aurora (Oxford: At the Clarendon Press).

Unwin, R. S., 1959, "Studies of the Upper Atmosphere From Invercargill, New Zealand, Part I--Characteristics of Auroral Radar Echoes at 55 Mc/sec.," Ann. de Geophys., pp. 377-394.

Unwin, R. S., 1966a, "The Morphology of the VHF Radio Aurora at Sunspot Maximum--I," J. Atmos. Terr. Phys., Vol. 28, pp. 1167-1181.

Unwin, R. S., 1966b, "The Morphology of the VHF Radio Aurora at Sunspot Maximum--II," J. Atmos. Terr. Phys., Vol. 28, pp. 1183-1194.

Unwin, R. S., 1966c, "The Importance of Refraction in the Troposphere and Ionosphere in Determining the Aspect Sensitivity and Height of the Radio Aurora," J. Geophys. Res., Vol. 71, pp. 3677-3686.

Unwin, R. S., and F. B. Knox, 1968, "The Morphology of the VHF Radio Aurora at Sunspot Maximum--IV," J. Atmos. Terr. Phys., Vol. 30, pp. 25-46.

Uscinski, B. K., 1968, "The Multiple Scattering of Waves in Irregular Media," Phil. Trans., Royal Soc. of London, Vol. A. 262, pp. 609-643.

Wescott, E. M., J. D. Stolarik, and J. P. Heppner, 1969, "Electric Fields in the Vicinity of Auroral Forms from Motions of Barium Vapor Releases," J. Geophys. Res. Sp. Phy., Vol. 74, pp. 3469-3487.

Whitehead, J. D., 1968, "Low Frequency Plasma Instabilities in the Ionosphere," J. Atmos. Terr Phys., Vol. 30, pp. 1563-1570.

Whitehead, J. D., 1971, "The Equatorial Electrojet and the Gradient Instability," J. Geophys. Res., Vol. 76, pp. 3116-3126.

ACKNOWLEDGMENTS

The author wishes to thank the Stanford Research Institute for the support provided him during the preparation of this review. While he was assembling the materials for this review the author had the benefit of discussion with a number of individuals. Mr. Ray Leadabrand, Dr. Charles Rino, Dr. Walter Flood, Dr. Lewis Linson, and Dr. Albert Simon have graciously scanned the manuscript and made numerous suggestions. The author wishes to especially thank Dr. Edward Fremouw who particularly aided the author in assembling the material in Section 4. Conversations regarding specific data have been held with Mr. James Hodges, Dr. Robert Leonard, Mr. Roland Tsunoda, and Dr. Joseph Workman. The author's interpretation and understanding of auroral radar data and theory may have been considerably colored by numerous discussions over the years with Dr. Howard Bates, Dr. Ben Balsley, Dr. George Millman, and Mr. Robert Unwin.

During the preparation of this review the author has rapidly become aware of the enormous quantity of literature in the field of polar radar propagation that had previously passed unnoticed by him. Much excellent work has not been included because of time limitations. We fervently hope that aggrieved researchers will forgive the author--and, at the same time, enter his name on their reprint distribution list. Thank you.

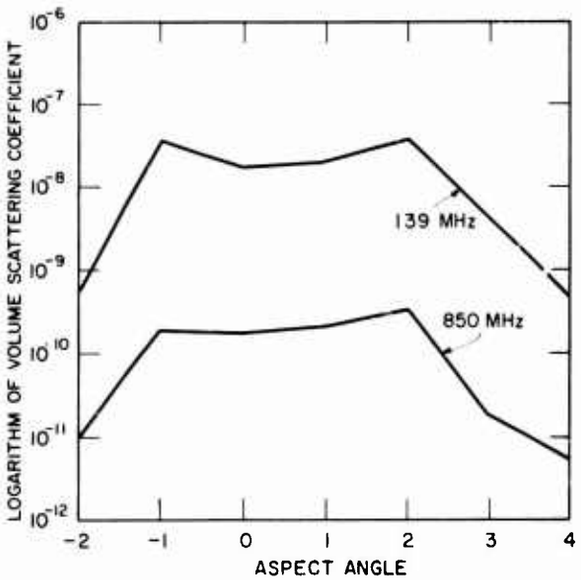

Figure 3.1 Logarithm of Volume Scattering Coefficient vs. Quiescent Magnetic Aspect Angle in Echoing Region

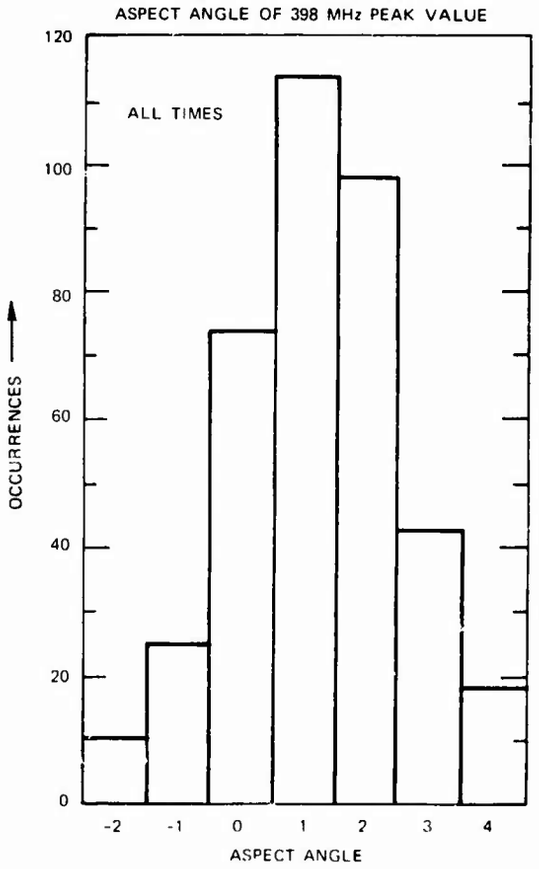

Figure 3.2 Histogram of Occurrence of Peak Returns at 398 MHz vs. Aspect Angle

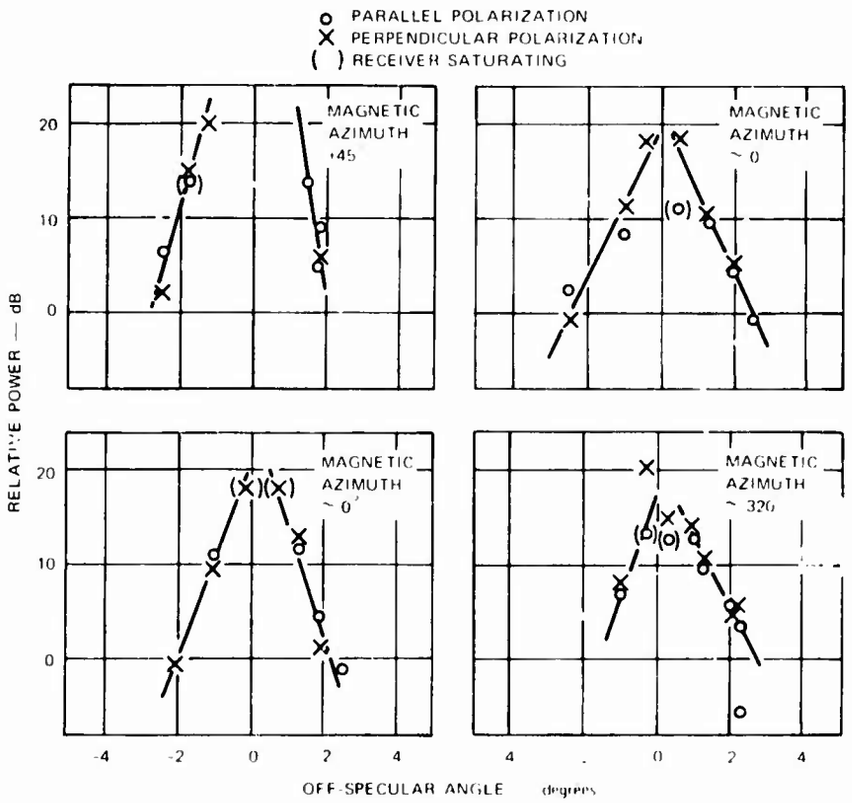

Figure 3.3 The Variation of Echo Power with Off-Specular Angle During Four Elevation Scans

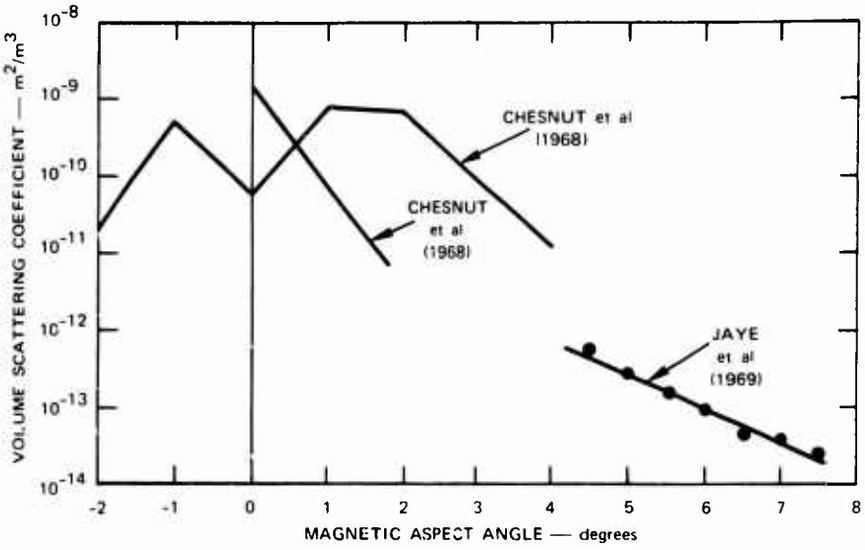

Figure 3.4 Composite Plot of Volume Scattering Coefficient vs. Magnetic Aspect Angle as Obtained by Several Experiments at Frequencies Near 400 MHz

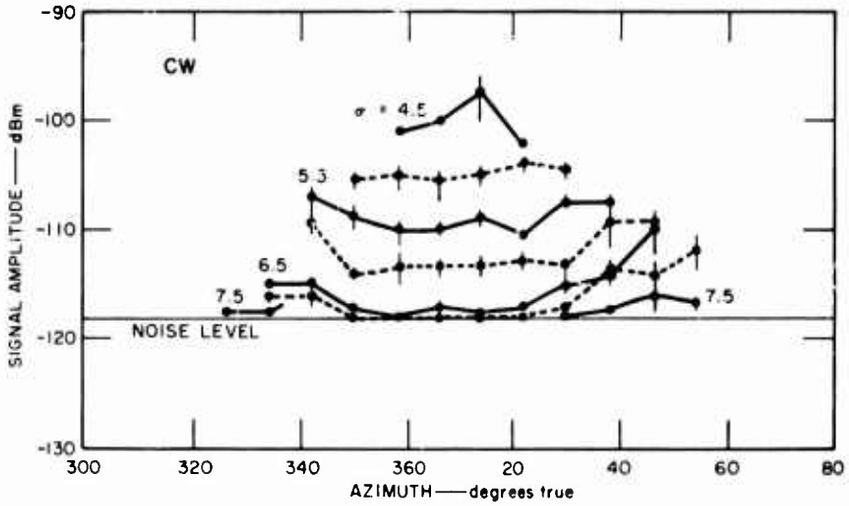

Figure 3.5 Average Echo Power as a Function of Azimuth for Data Obtained at the Indicated Magnetic Aspect Angles

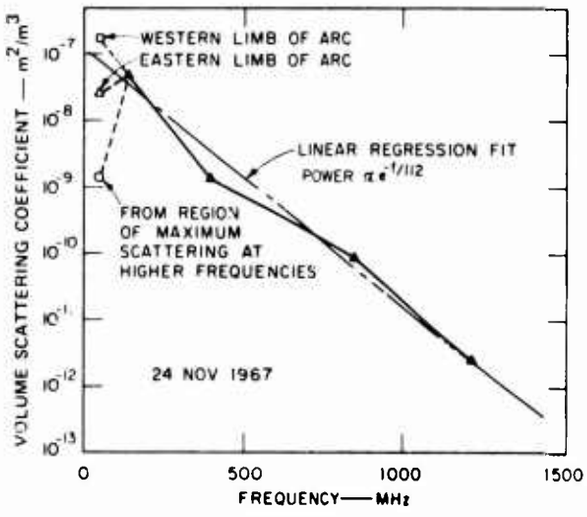

Figure 3.6 Logarithm of Volume Scattering Coefficient vs. Frequency

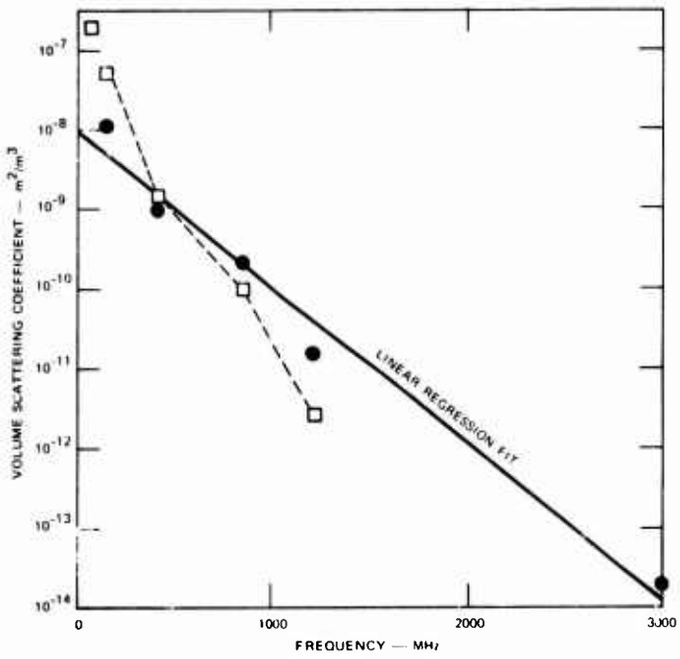

Figure 3.7 Logarithm of Volume Scattering Coefficient vs. Frequency for Data Obtained when 3000-MHz Echoes were Observable

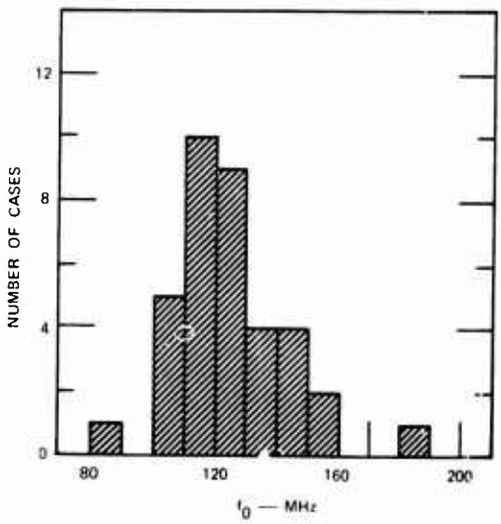

Figure 3.8 Histogram of Occurrence of Scale Frequency, f_0

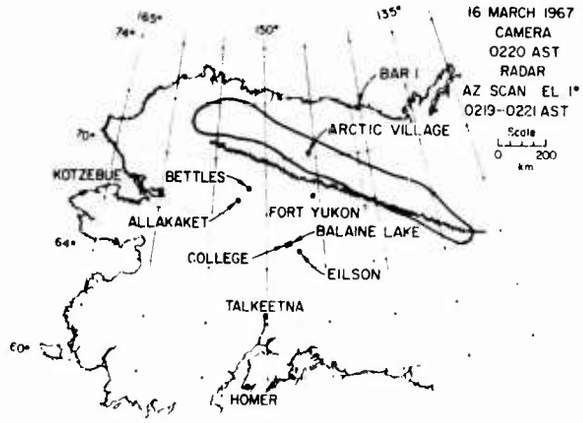

Figure 3.9 Radar-Optical Correlation Map--16 March 1967, 0220, Alaska Standard Time

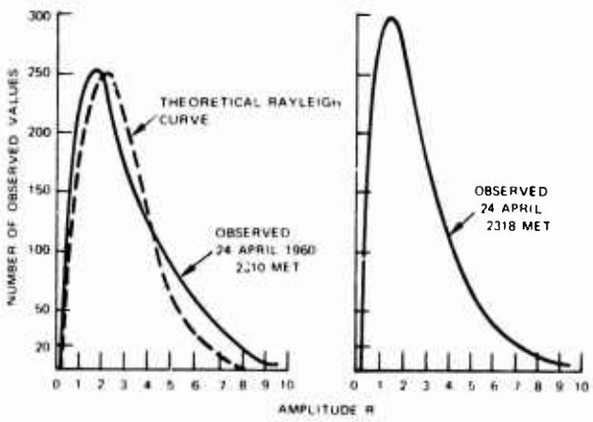

Figure 3.10 Observed Amplitude Distribution of Auroral Echoes

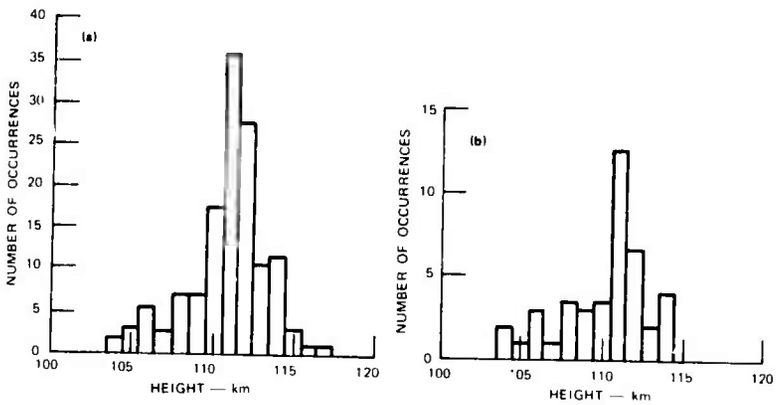

Figure 3.11 Histograms of Average Heights of Regions Producing Diffuse Echoes

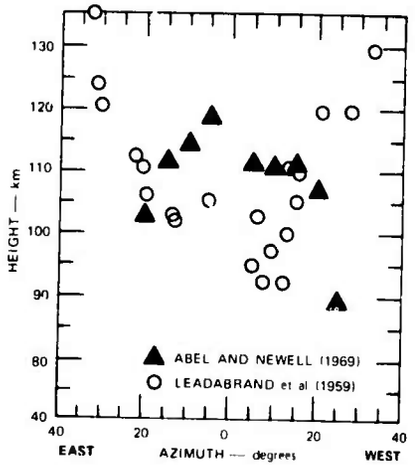

Figure 3.12 Height of Reflection as a Function of Magnetic Azimuth Angle

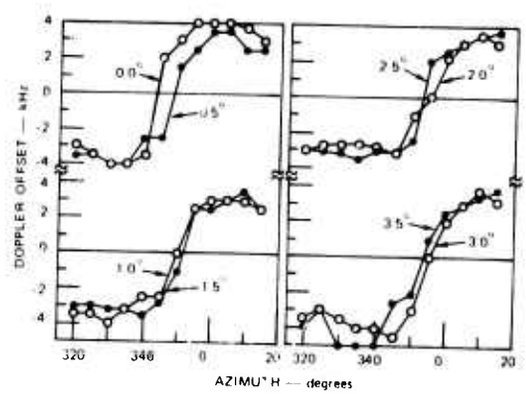

Figure 3.13 Doppler Shift of Auroral Echo as a Function of Elevation and Azimuth--5 November 1965, 1713-1740 EST

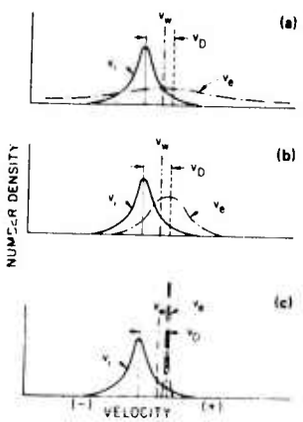

Figure 3.14 Conceptual Number Density vs. Velocity Distributions for Electrons and Ions in a Magnetic Field

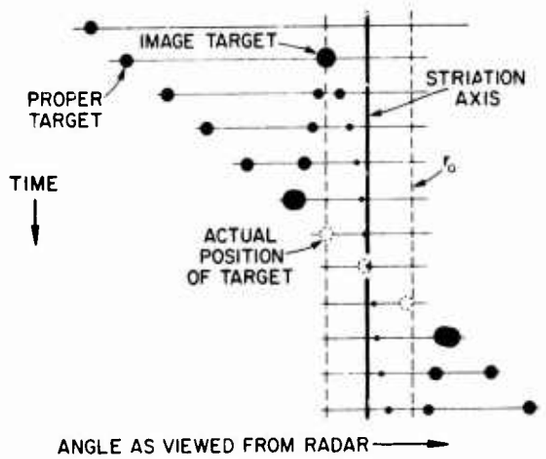

Figure 4.1 Target Image Structure as the Target Passes Behind a Highly Refracting Ionized Blob

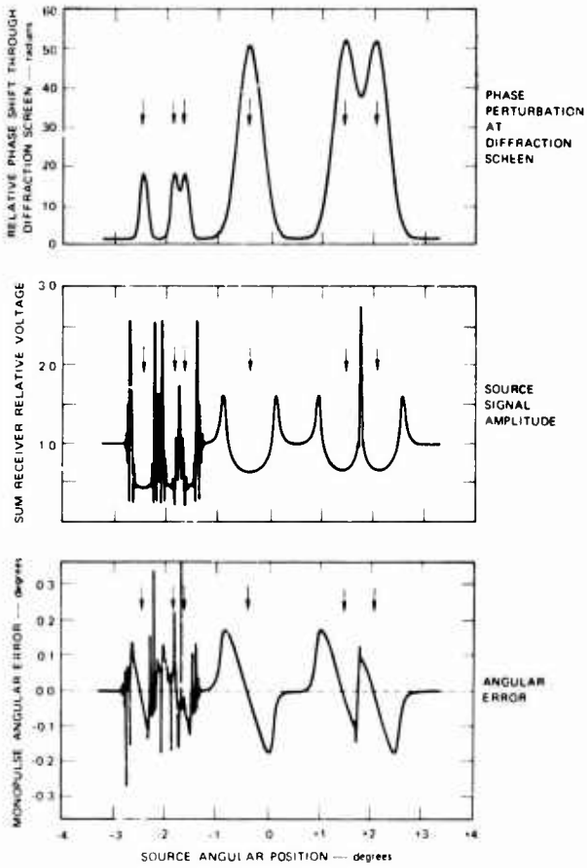

Figure 4.2 Amplitude Monopulse Response to a Set of Gaussian Profile Ionized Cylinders

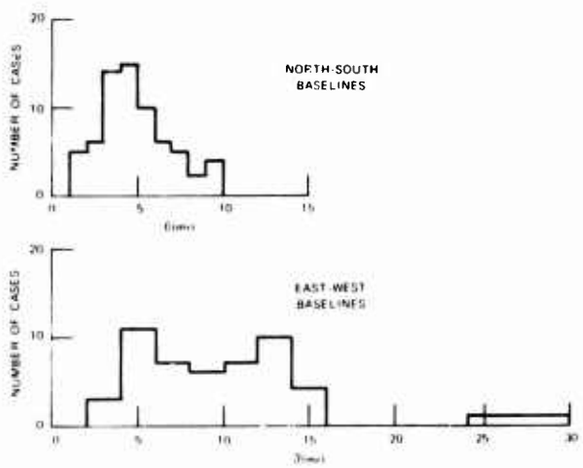

Figure 4.3 Distribution of Core Angles of Arrival During Visibility Fades at 47 MHz

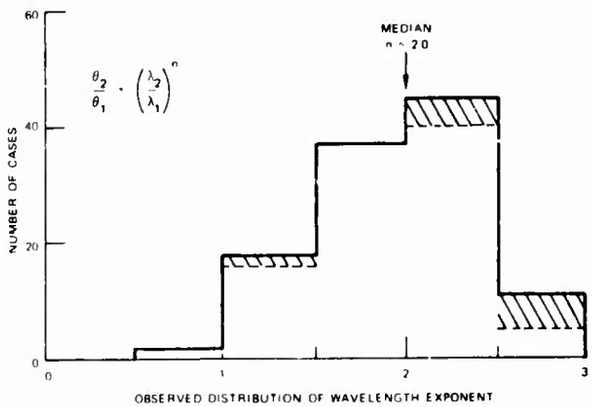

Figure 4.4 Observed Distribution of Wavelength Exponent for Frequency Scaling of Cone Angle of Arrival. Cross-hatched areas compare 147 and 294 MHz

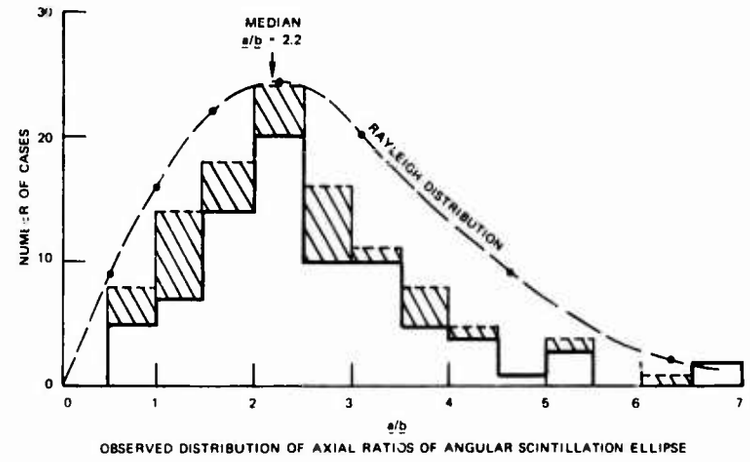

Figure 4.5 Observed Distribution of Axial Ratios of Angular Scintillation Ellipse

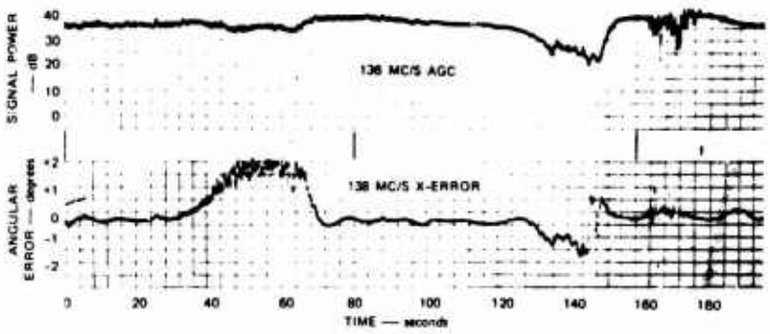

Figure 4.6 Nimbus Satellite Telemetry Signal as Recorded at Gilmore Creek NASA Data-Acquisition Station

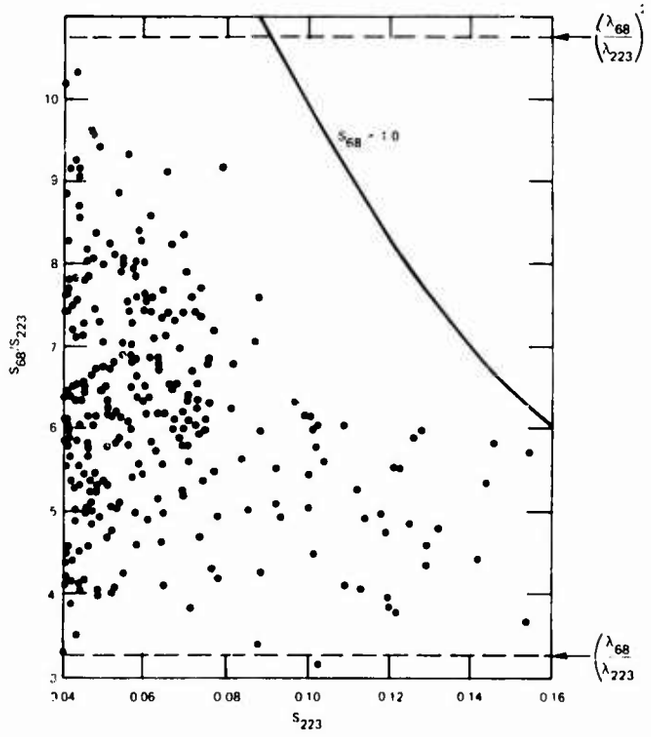

Figure 4.7 Observed Values of the Ratio S_{68}/S_{223} as a Function of the Value of S_{223}

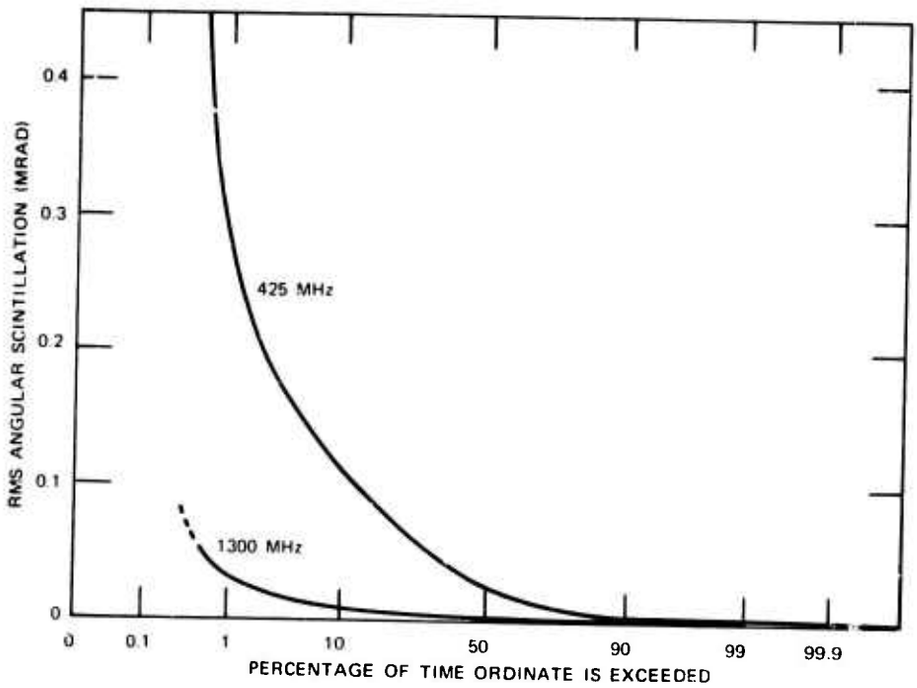

Figure 4.8 Probability Density of Angular Flicker at Fairbanks, Alaska for 425 MHz and 1300 MHz

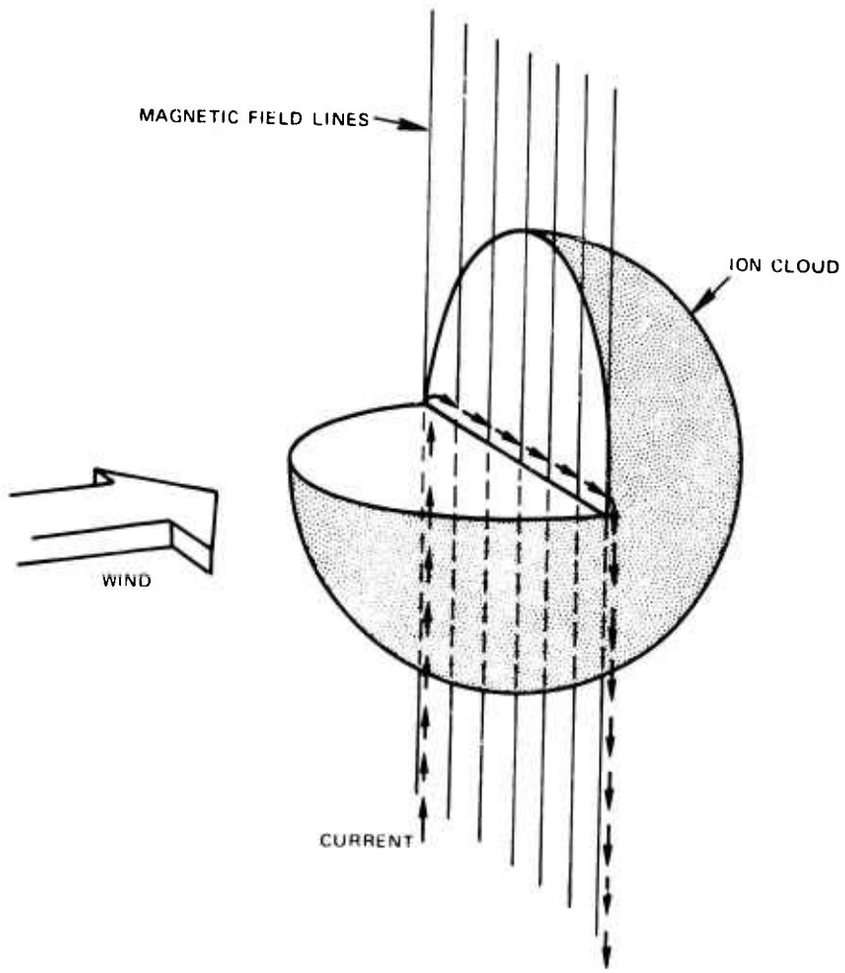

Figure 4.9 Ion-Cloud Model

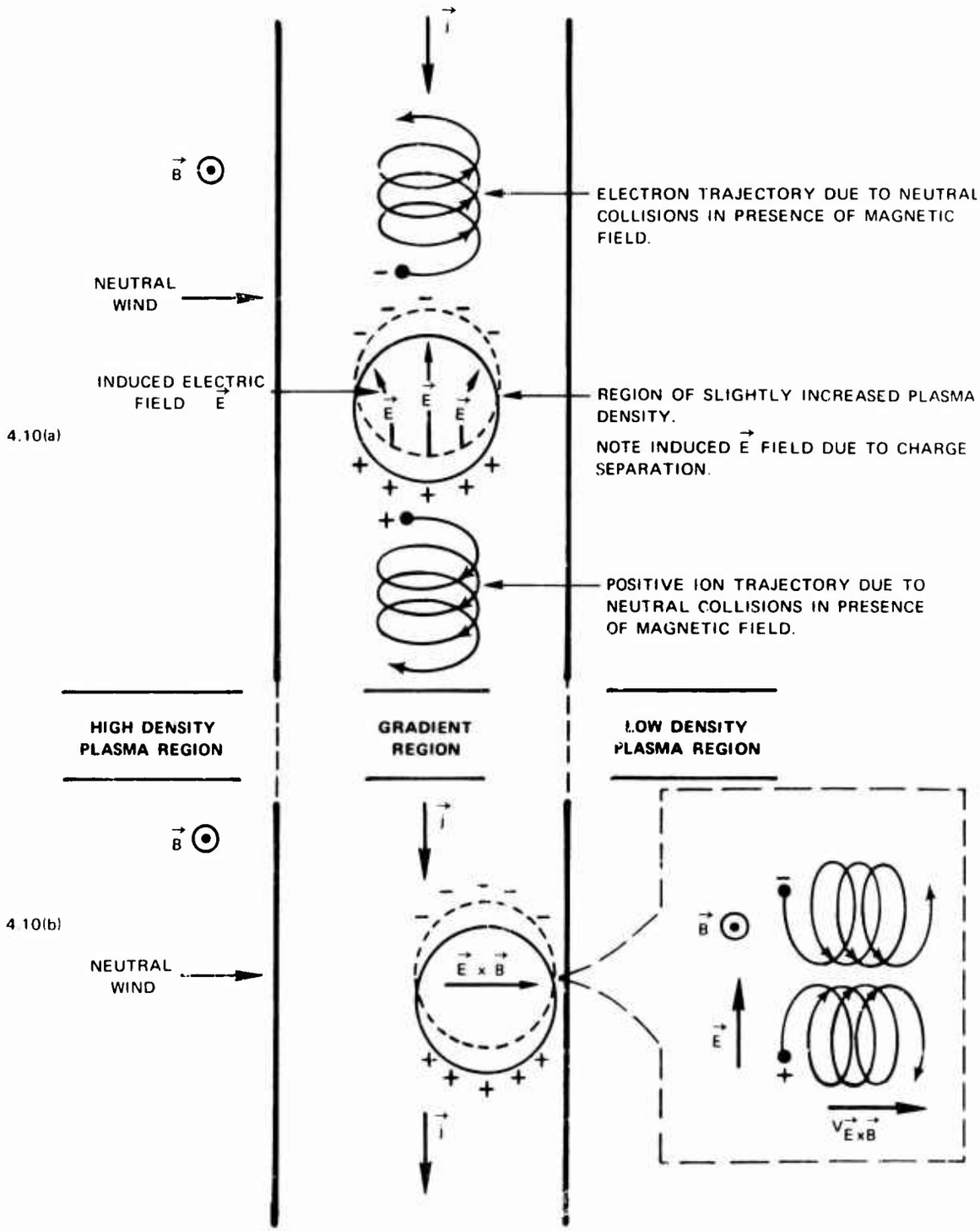

Figure 4.10 Region of Plasma Gradient Illustrating Gradient-Drift Instability Process

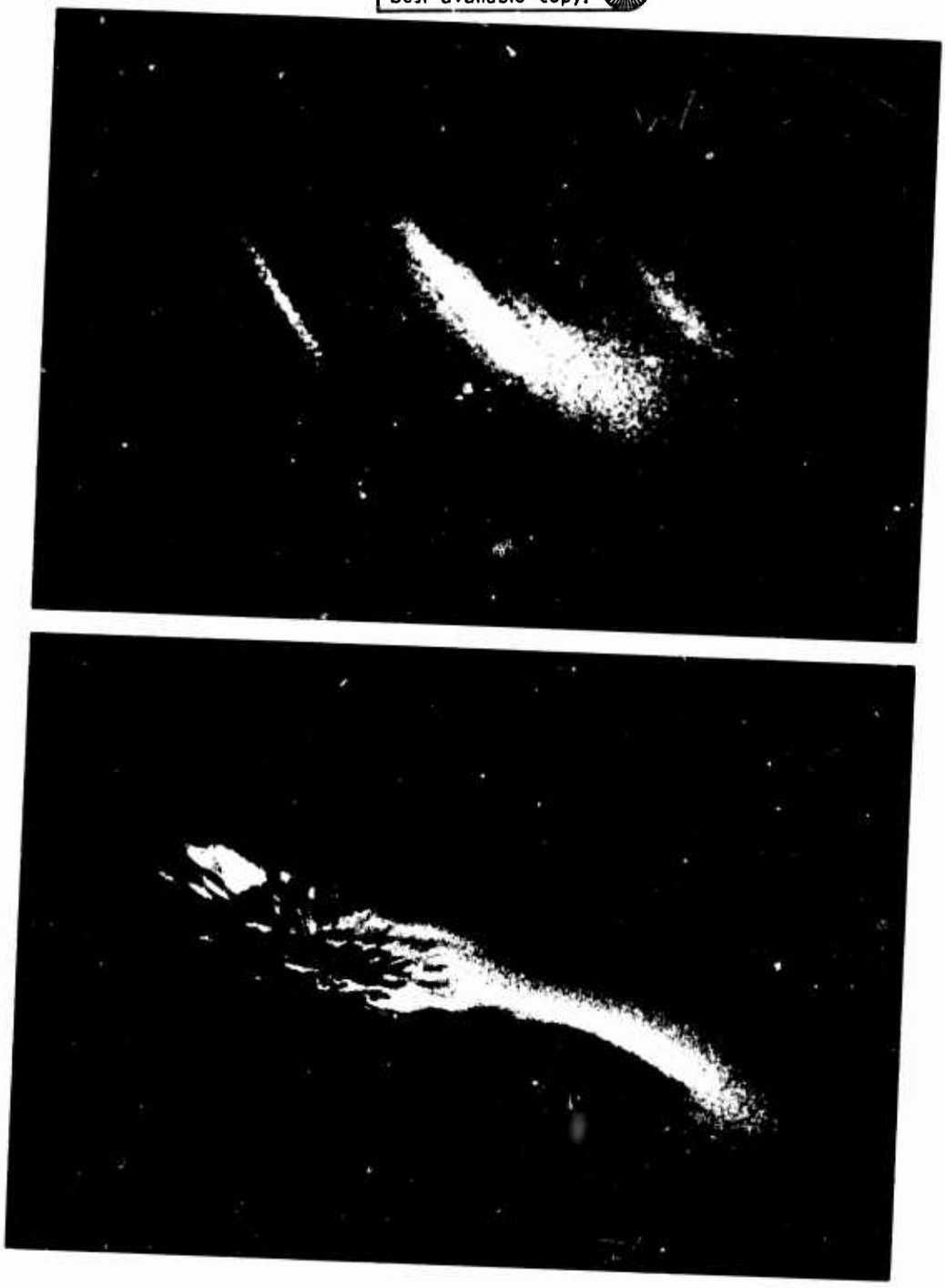

Figure 4.11 Photographs of Striated Barium Cloud

OBSERVATIONS OF 48 MHZ AURORAL RADAR PROPAGATION ON A NETWORK IN THE AURORAL ZONE

A.G. McNamara
Astrophysics Branch
National Research Council
Ottawa, Canada

SUMMARY

Four auroral radars are operated on a continuous basis at Ottawa, Thompson, Churchill, and Great Whale. The Ottawa radar is at 45° latitude and the other three are at approximately 57°, in the auroral zone. The high incidence of auroral activity at these locations permits both statistical and detailed single event studies of radio aurora morphology and scattering mechanisms. In spite of magnetic aspect control, strong auroral backscatter signals are detected at all azimuths with aspect angles of up to 25° from the magnetic perpendicular. These observations create difficulties in explaining radar aurora in terms of ion acoustic waves developed from linear models such as the two-stream instability theory. As well as direct auroral backscatter, the radars sometimes detect sporadic-E propagated ground scatter, usually in association with auroral disturbance. The simultaneous observations of these various auroral phenomena by the multiple stations permit more definitive measurements of the processes involved.

1. INTRODUCTION

Since 1955, various combinations of auroral radar stations have been in operation in Canada to study the morphology and mechanisms of radio aurora. The VHF auroral radars have been operated at Ottawa, Saskatoon, Thompson, Churchill, Baker Lake, Resolute, and Great Whale. This paper presents data obtained mainly from the presently operating network at Ottawa, Thompson, Churchill, and Great Whale. These stations are identified in the text by the mnemonics OT, CH, TH, GW, respectively. The latter three stations are in the auroral zone and the Ottawa station is well south of the zone. The network was selected for optimum overlap of their beam coverage to permit simultaneous viewing of a common volume of the auroral ionosphere from widely varying aspect angles, with the object of detailed study of aspect dependence and plasma instability scattering mechanisms. Figure 1 shows the location of the radars and their 1000 km range circles. The data presented here are a preliminary study of the characteristics of the auroral backscatter as seen by this network.

2. EQUIPMENT PARAMETERS

The radar frequencies are closely spaced about a nominal value of 48.5 MHz. A 300 μs pulse of 1 kw peak power is transmitted at a repetition rate of 70 per second. A common antenna is used for transmitting and receiving, and consists of stacked array of driven and reflecting elements with a one-way gain of 9 db, and a half-power beam width of 74°. In the transmit/receive mode, the antenna gives a gain of 18 db and a beam width of 52°. The antenna rotates 360° continuously with a period of one minute. These radars operate and record data continuously and unattended[1].

3. ASPECT ANGLES

Measured survey values of the earth's average magnetic field have been used to compute the aspect angles of the radars. The computations were done for two heights of reflection, 100 km and 110 km, based upon previous measurements of the scattering height[2,8]. The computer output was printed as an array of values in latitude and longitude, and contours of constant aspect angle drawn through them. A sample aspect contour map is shown in Fig. 2, for the Churchill radar and an assumed reflection height of 100 km. The locations of the four radar stations are also indicated. By appropriate selections of the geographic coordinate increments and the computer print format, the printout grid can be made to represent approximately a map projection. Table I gives the station coordinates, the best aspect angles for 100 km and 110 km reflection heights, and the Universal Time equivalents of local midnight at the best aspect region.

TABLE I

Characteristic parameters of the Radar Network Geometry

STATION / PARAMETER	OT	CH	TH	GW
Station lat. and long.	45.3°N,75.6°W	58.8°N,94.0°W	55.8°N,97.8°W	55.4°N,77.8°W
Best aspect lat. and long.	51.5°N,78°W	66°N,97°W	62.5°N,98°W	62°N,84°W
Best aspect angle for 100 km height	0.8°	7.9°	6.5°	5.5°
Best aspect angle for 110 km height	1.3°	8.6°	7.2°	6.2°
Time of local midnight at best aspect point	05:12 UT	06:28 UT	06:32 UT	05:36 UT

A previous paper[4] has presented an analysis of aspect angle dependence using data from part of the IGY network of similar radars. Simultaneous echoes seen southward from Baker Lake and northward from Saskatoon, encompassing off-perpendicular aspect angles from 5° to 20°, yielded an average attenuation rate of 1.2 db/degree. The present radar network comprising OT, CH, TH, and GW views a much larger common volume with aspect angles in the range 5° to 20° off-perpendicular, and a much greater range of azimuth angles.

4. EXAMPLES OF DIREC" AURORAL BACKSCATTER AND E_s GROUND SCATTER

Figure 3 shows examples of radar returns on the range-azimuth display of the Churchill radar. The time is approximately 06:00 U.T. (00:00 C.S.T.). Direct backscatter from radio aurora is occurring over ranges from 200 to 800 km, and at all azimuths. In fact, during part of the time there is a gap in the echo in the north and northwest sectors — the region where the aspect angle is most favorable.

At ranges from 1000 to 1500 km are seen sporadic-E propagated ground backscatter, occurring principally on a southerly azimuth. This phenomena occurs relatively infrequently but in association with auroral disturbance. However, at any given time it may or may not be occurring in association with a direct backscatter echo at one-half the apparent range. Hence it probably does not originate with the same mechanism which creates the direct backscatter condition. Direct measurements of auroral electron densities by rocket probes[3], have shown thick bands of ionization to be present with densities of typically 10^{12} electrons/m^3. At a ground scatter range of 1000 km, the sec ϕ factor is between 4 and 5, and oblique specular reflection to frequencies of 50 MHz is possible. This appears to be a reasonable mechanism for this echo component. In a c.w. forward scatter link, this E_s mode will be very strongly enhanced relative to the true auroral scattering mode, and may even dominate the signals received at times.

Figure 4 is a composite plot of 7 hours of a radio aurora event recorded at Churchill. The direct backscatter signal (the radio aurora) occurred over ranges from 200 to 800 km in azimuths centred on 330° and 90°. The E_s-propagated ground scatter occurred relatively independently in time and at ranges from 500 to 1500 km in azimuths centred on 330° and 90°. At times, one type would be present while the other was not.

At the present time, insufficient azimuth data have been scaled from this network to build up reliable azimuth distributions for all stations. However, some azimuth distributions from the high-latitude IGY stations are shown in Figure 5. It should be noted that aspect angle is not the dominating factor at Baker Lake and Resolute, where the best aspect angle is again to the north.

5. DIURNAL AND GEOGRAPHICAL OCCURRENCES

Data from the year 1969 have been scaled for the four stations OT, CH, TH, GW, are plotted in Figure 6. The principal peak occurs at 05:30, 06:00, and 04:00 U.T. for CH, TH, and GW respectively. Reference to Table I shows coincidence with local midnight for CH and TH, but the maximum occurs about 1 hour earlier for GW. The OT distribution shows a double-humped distribution with a minor minimum just prior to midnight. During the daylight hours, TH and GW show similar activity, but at a greater level of activity than CH.

At the diurnal maximum, the three auroral zone stations recorded an occurrence frequency of 70%. Over the year 1969, the average total occurrence for these three stations was 23-32% of the time, and 11% for Ottawa.

6. SIMULTANEOUS OCCURRENCE

Initial statistical analysis of the 1969 data has yielded a rough measure of the approximate time correlation of the radio aurora at these stations. The analysis is based on time of occurrence only, with half-hour time resolution. The percentage of echo occurrences which were simultaneously observed at different pairs of stations are summarized by matrix of Table II. The correlation of the auroral zone stations is fairly high. To obtain a measure of the multiple station correlation, the simultaneous occurrence values were computed for the CH, TH, GW combination, and for the OT, CH, TH, GW combination. These values were 25% and 7% respectively.

TABLE 2

Percentage coincidence of occurrence on radars, calculated on half-hour time intervals.

	OT	CH	TH	GW
OT	100			
CH	20	100		
TH	19	46	100	
GW	17	42	39	100

7. SCATTERING MECHANISMS

Previous papers[4,5] have employed part of the IGY radar network data to explore the applicability of the ion acoustic wave model[6,7,8,9] to the observed radio aurora characteristics. These papers have shown that the model is reasonable in some respects, but does not entirely explain the observed aspect effects. It appears that other mechanisms contribute or that non-linear processes introduce significant departures from the linear theory. A major objective the radar network described here is to attempt to resolve some of these problems.

For 48.5 MHz backscatter, the ordered structure required to produce an enhanced reflection from a

plasma instability is approximately 3 meters. A spectrum of scale sizes, including both larger and smaller scales, has been observed directly with rockets flown in a complementary program at Churchill[3,8] The measured spatial spectrum of the density fluctuations fits an expression of the form

$$S(f) \sim e^{-f/f_o}$$

Depending upon certain assumptions about the shape and motion of such microstructures, the value of f_o was found to be in the range 60 to 400 MHz.

REFERENCES

1. McNamara, A.G. "A Continuously Recording Automatic Auroral Radar" Can. J. Phys. Vol. 36, p. 1, 1958.
2. McNamara, A.G. and Currie, B.W. "Radio Echoes during Aurora" J. Geophys. Res., Vol. 59, p. 279, 1954.
3. McNamara, A.G. "Rocket Measurements of Plasma Densities and Temperatures in Visual Aurora" Can. J. Phys., Vol. 47, p. 1913, 1969.
4. McDiarmid, D.R. and McNamara, A.G. "VHF Radio Aurora : Simultaneous Observation of Auroral Ionization by Two Separated Radars" Can. J. Phys., Vol. 45, p. 3009, 1967.
5. McDiarmid, D.R. and McNamara, A.G. "A Physical Model of a Radio Aurora Event" Can. J. Phys., Vol. 47, p. 1271, 1969.
6. Farley, D.T. "A Plasma Instability Resulting in Field-Aligned Irregularities in the Ionosphere" J. Geophys. Res., Vol. 68, p. 6083, 1963.
7. Hofstee, J. and Forsyth, P.A. "Ion Acoustic Waves in the Auroral Plasma" Can. J. Phys., Vol. 47, p. 2797, 1969.
8. McNamara, A.G., in "The Radiating Atmosphere", p. 301, Reidel Publishing Company, 1971.
9. McDiarmid, D.R. "Ion Acoustic Waves and Radio Aurora" Can. J. Phys., Vol. 48, p. 1863, 1970.

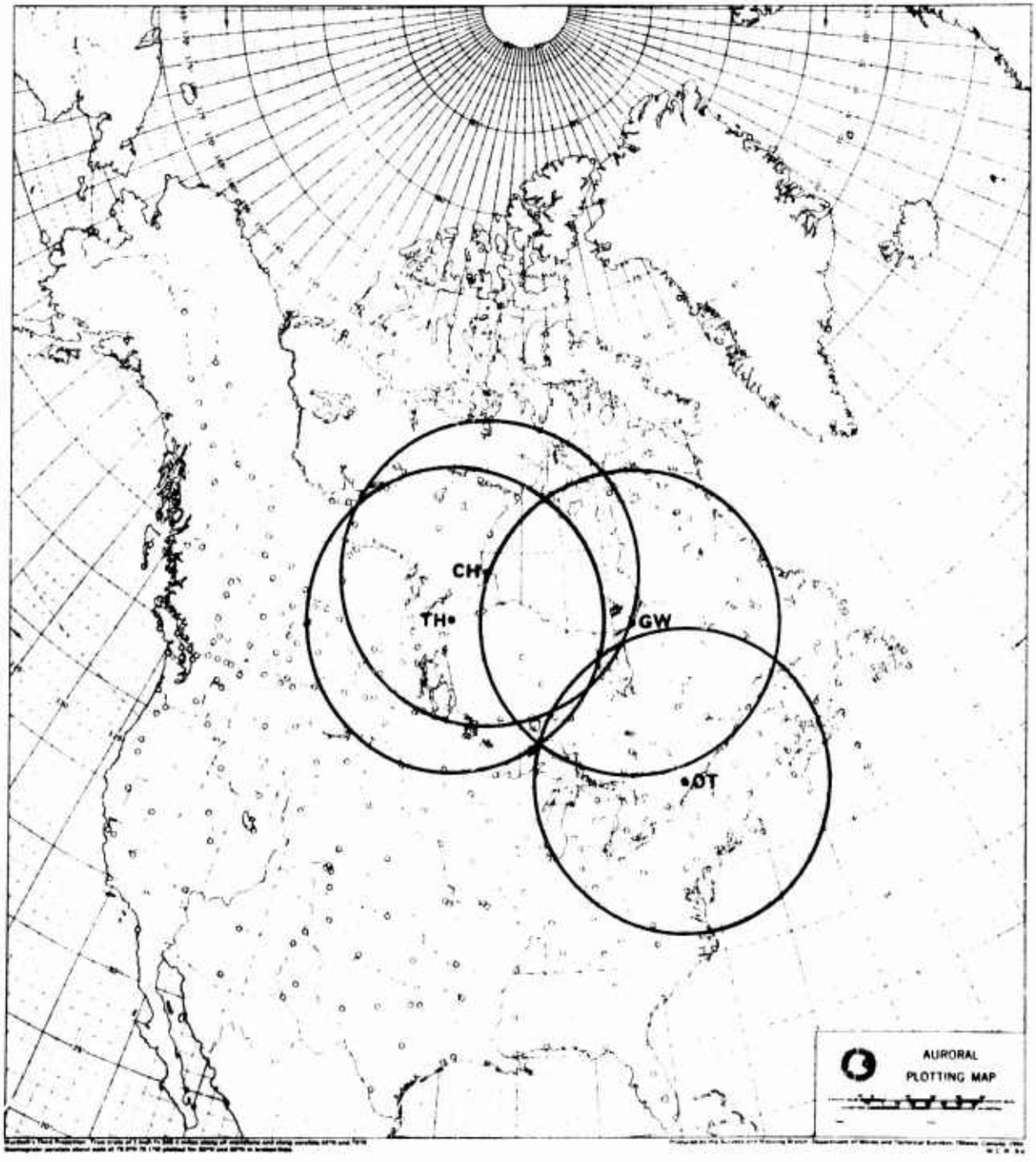

Fig. 1 Locations and coverage of the auroral radars at Ottawa, Thompson, Churchill, and Great Whale. The range circles are 1000 km radius.

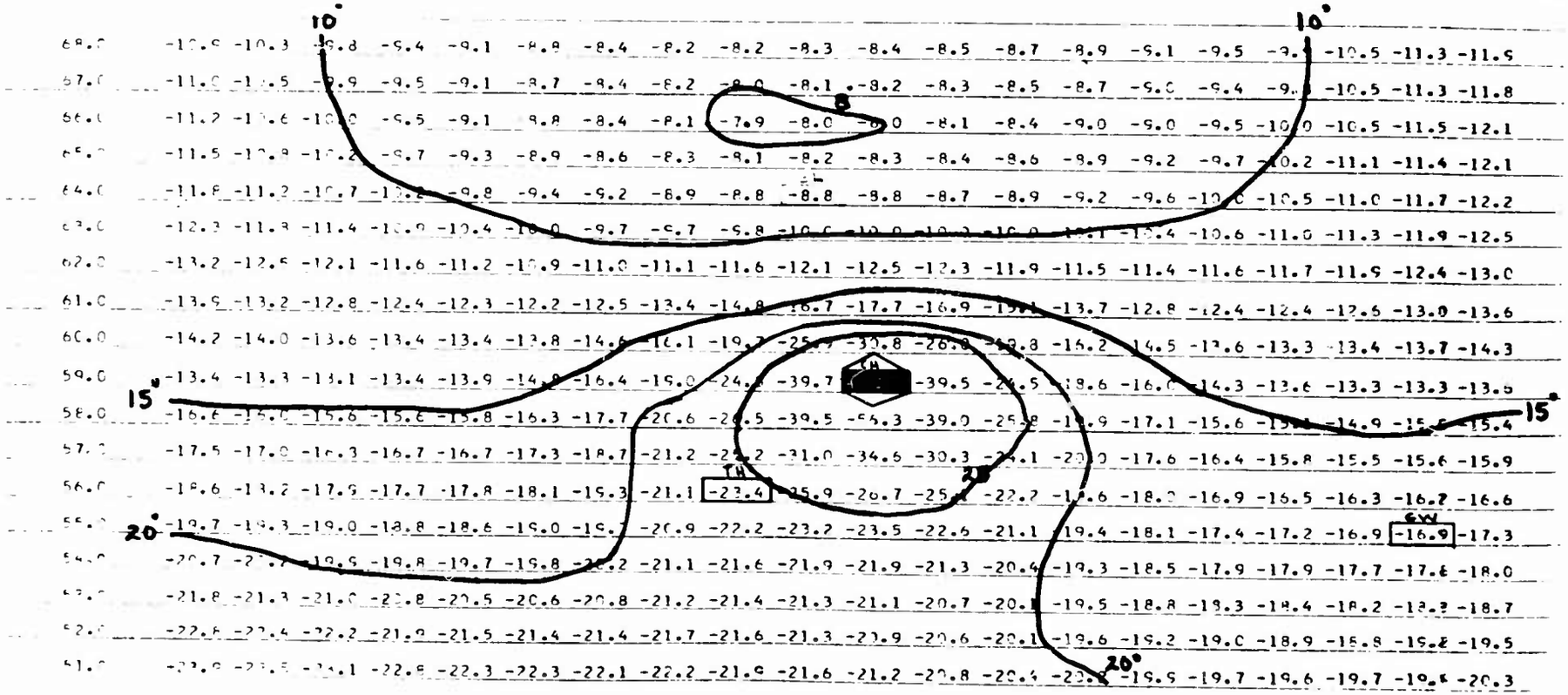

Fig. 2 Magnetic field aspect contours for the Churchill radar.

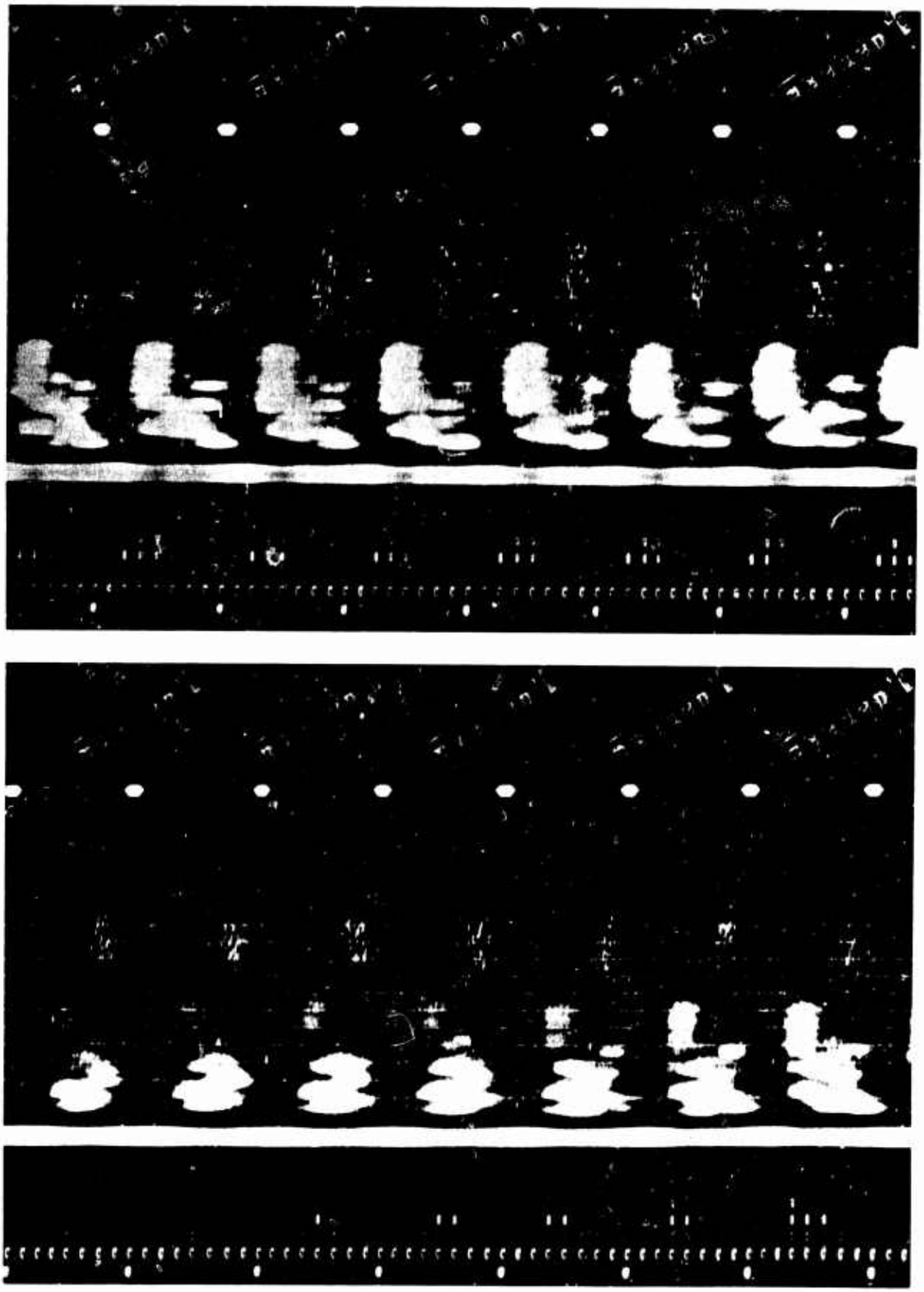

Fig. 3 Photographic recording of the cathode ray tube range-vs-time display of the Churchill radar. The antenna rotates with a period of one minute. Direct auroral backscatter and E_s-propagated ground scatter are present.

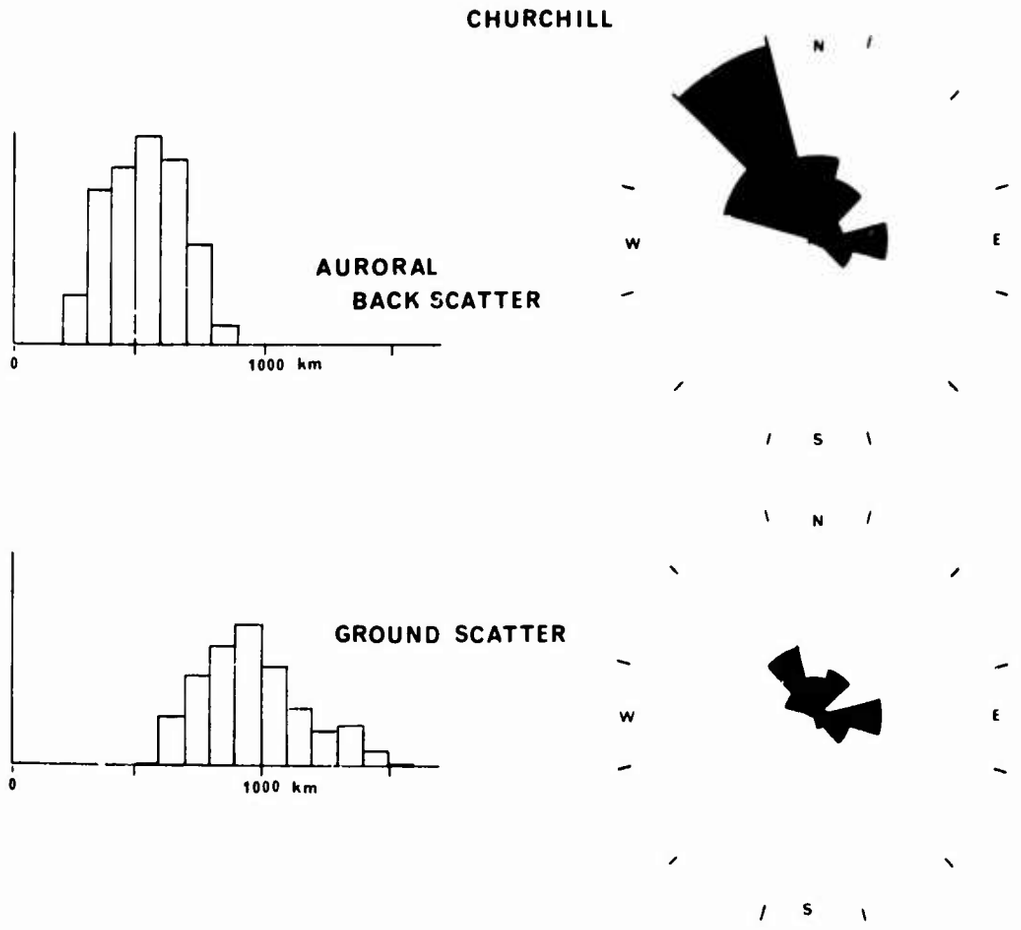

Fig. 4 Range and azimuth distributions for seven hours of echoes on the Churchill radar.

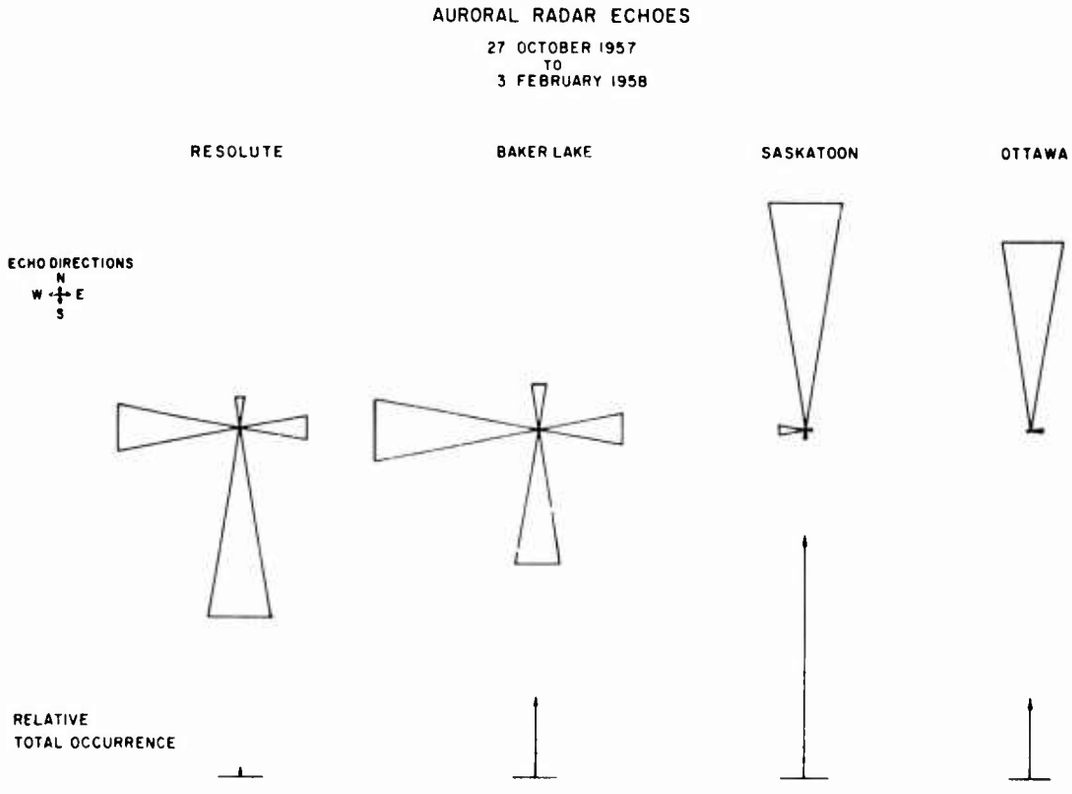

Fig. 5 Azimuthal distribution of radio aurora on the IGY radar network.

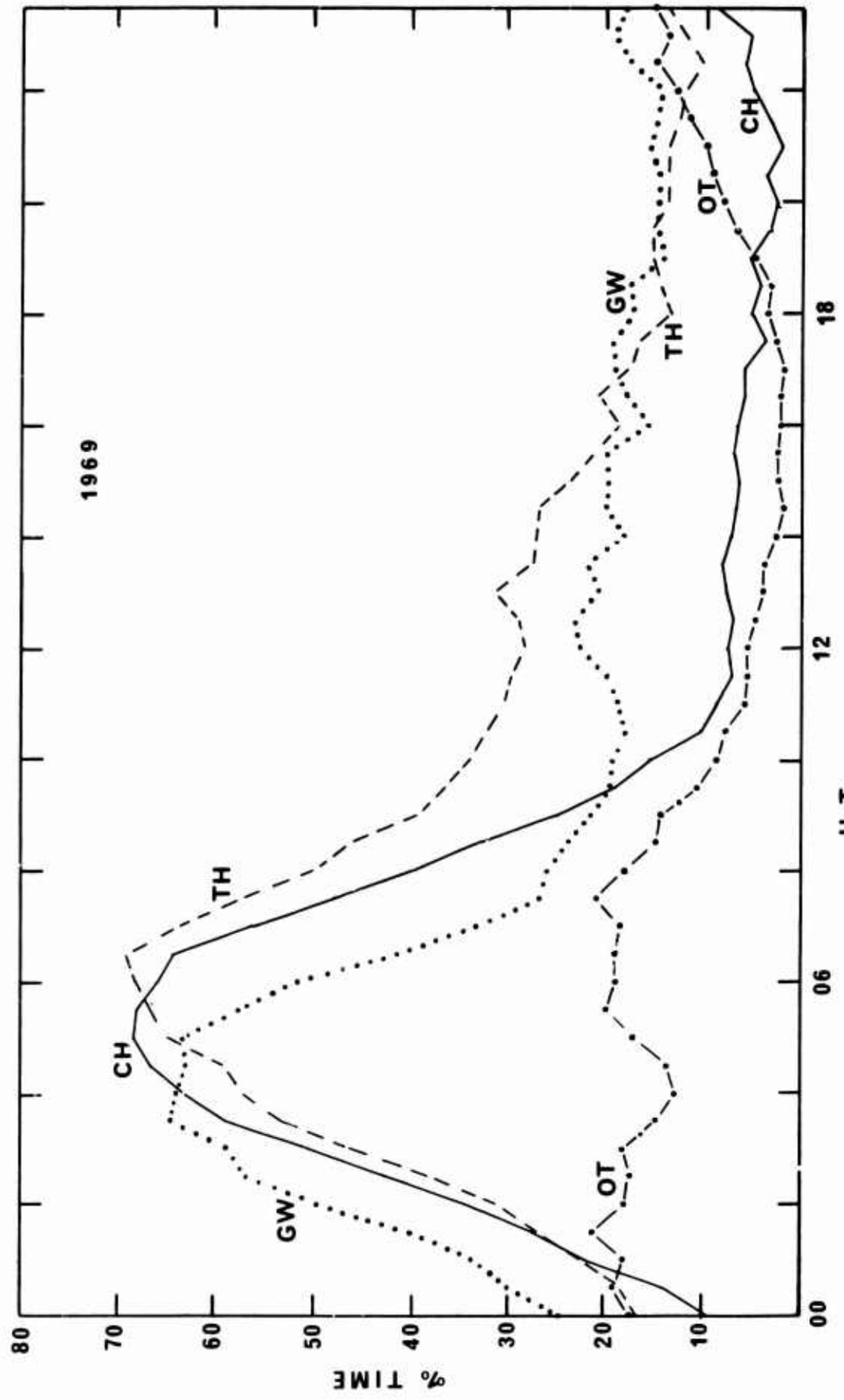

Fig. 6 Diurnal variations of radio aurora in 1969 for OT, TH, CH, and GW.

CURRENT EXPERIMENTAL RESULTS FROM A VHF-CW AURORAL BACKSCATTER NETWORK IN SCANDINAVIA

G. Lange-Hesse

Max-Planck-Institut für Aeronomie
P.O. Box 20
3411 Lindau/Harz, W.Germany

SUMMARY

VHF bistatic continuous waves auroral backscatter communications (radio aurora) carried out since autumn 1967 on a network in Scandinavia and northern Germany are analyzed with respect to the influence of daytime, season and geomagnetic latitude on the frequency of occurrence of this phenomenon. Furthermore exemples are presented which show the close control of the VHF auroral backscatter by the polar electrojet. Finally some exemples are shown about the correlation between optical and radio aurora.

1. INTRODUCTION

Observations of VHF continuous waves bistatic auroral backscatter communications are carried out by the Max-Planck-Institute for Aeronomy at Lindau/Harz,West Germany since autumn 1967 by using a network of VHF continuous waves beacon transmitters and receiving stations in Scandinavia and northern Germany. These observations are carried out in cooperation with several Norwegean and Swedish institutes, boards and observatories. Since September 1969 simultaneous optical observations of the aurora are carried out by all-sky cameras and meridian scaning photometers in northern Scandinavia in cooperation with the Auroral Observatory Tromsö in northern Norway and the Geophysical Observatory Sodankylä in northern Finland to study the correlation between optical and radio observations of the aurora. The whole network is shown in Fig. 1.

The reduction of the observations with the network shown in Fig. 1 has shown that the backscattering of VHF radio waves by aurora is controlled not only by the visual aurora but obviously on a larger scale by the polar electrojet (PEJ). About eight years ago Buneman [4] and Farley [13] independently pointed out that in an ionospheric current system, e.g. the equatorial electrojet (EEJ), plasma instabilities of a "two-stream" type can occur so that acoustic plasma waves are generated. The plasma instability appears when the relative drift velocity between the ions and electrons in the electrojet (EJ) exceeds a certain critical speed which is close to the thermal velocity of the ions. It is said that the electrojet at this phase has exceeded the threshold. Acoustic plasma waves then are generated in the shape of longitudinal density waves, which propagate along the electrojet transverse to the geomagnetic lines of force.The periodical density oscillations caused by the plasma waves (which represents a special fine structure of the EJ) are the field aligned centers (field aligned to the geomagnetic lines of force) which give rise to the backscattering of VHF radio waves. Bowles et al. [3] and Cohen and Bowles [5] have shown that the VHF waves backscattering centers in the EEJ are caused by acoustic plasma waves. In the same publication the authors pointed out that the VHF waves backscattering centers in the PEJ obviously are caused by the same mechanism. There is no doubt that the acoustic plasma waves irregularities in the PEJ after Farley [13] and Buneman [4] give rise to at least some radio aurora (Abel and Newell [1]; Hofstee and Forsyth [15]. However, there is also good qualitative evidence that irregularities caused by the so called cross-field or drift-gradient instability give rise to special types of radio aurora (Unwin and Knox [21]; Knox [16]). Finally I should like to mention that obviously irregularities can occur in the PEJ which give rise to special type of radio aurora produced by a mechanism which is not known at the present time.

The maximum of the current density of the PEJ fits together in a first approximation with the visual aurora. Previously, therefore, it was assumed that the normal ionization in the region of

the visual aurora directly causes the backscattering of VHF radio waves. The reduction of the observations carried out with the network shown in Fig. 1 and the reduction of similar observations carried out at other places, however, indicate that the fine structure of the PEJ is the more controlling element of the VHF auroral backscatter phenomenon. If the PEJ (in a fine structure that backscattering centers are produced in it by any mechanism) intersects a backscatter curve in Fig. 1 then VHF auroral backscatter communications ought to occur between the pairs of stations belonging to the backscatter curve. For a pair of stations the appertaining backscatter curve represents the center of a region where the most favorable geometrical conditions (also called "ideal backscatter conditions") are fulfilled for VHF auroral backscatter communications. These curves are calculated in Fig. 1 for a height of 110 km. Ideal backscatter conditions mean that at the backscattering center the angle of incidence is equal to the angle of reflection referred to a plane vertical to the geomagnetic line of force (Fig.2). The geometry of the propagation paths referred to the geomagnetic lines of force is much more complicated for bistatic auroral backscatter communications between stations close to the auroral zone (Fig. 1 and 2) compared to radar backscatter measurements at the EJJ as described by Bowles et al. [3] and Cohen and Bowles [5]. This is why the reduction of all bistatic backscatter observations with respect to other geophysical phenomena is difficult. For more details about VHF auroral backscatter see Czechowsky [6], [7], Czechowsky and Lange-Hesse [11], [12], Lange-Hesse [17], [18], [19], Lange-Hesse and Czechowsky [20].

2. THE CONTROL OF RADIO AURORA BY THE POLAR ELECTROJET

On February 27, 1969, a geomagnetic storm started at about 1400 UT (Fig. 4) and reached its peak disturbance of Kp = 6+ from about 1600 to 2000 UT. During this time VHF auroral backscatter echoes were recorded with the network in Fig. 1. These observations are now compared with simultaneous geomagnetic records i.e., with the location, direction and intensity variations of the PEJ. In the magnetograms of Fig. 4 bays occurred in the afternoon and early evening of February 27. From the sign of the bays in Z and from the positive sign in H (not shown here) it can be derived that from about 1400 to 1900 UT the center of the current is located north of Lerwick and south of Leirvogur and flows from west to east. If one takes the PEJ model after Heppner [14] the observed current must be the eastward flowing current of the PEJ system (Fig. 8). This part of the PEJ between Lerwick and Leirvogur intersects the region of the Borlänge-Kjeller backscatter curve (solid curve in Fig. 1). At about 1420 UT the first backscatter signal is recorded. At this moment the amplitude of the bay in the H magnetogram from Lerwick (Fig. 4) is of the order of 100 γ. If one takes the model of Farley [13] and Buneman [4] for the producing of the backscattering centers in the PEJ the threshold must be reached at this time and the generation of ion acoustic waves starts. The peak of the first smaller bay in the H magnetogram in Fig. 5 occurs at about 1440 UT simultaneously with the first peak in the Borlänge-Kjeller backscatter signal. Exactly during this peak a short backscatter signal with small amplitude appears on the more southern Borlänge-Norddeich line indicating that the PEJ extends to the south so that it could just intersect the region of the Borlänge-Norddeich backscatter curve. No backscatter signal, however, occurs during this time on the southernmost line in Fig. 5 (Borlänge-Lindau).

The strongest bay with about 400 γ amplitude appears in the magnetogram in Fig. 5 at about 1630 UT. Simultaneous peaks in the backscatter signal now occur on all three lines of Fig. 5. The amplitude of the peaks on the two northern lines now are of the same order, however, the amplitude on the southernmost Borlänge-Lindau line is much smaller. This indicates that compared to 1440 UT the current has extended further to the south which now enables it to intersect the region of all three appertaining backscatter curves simultaneously.

A second stronger bay with an amplitude of about the same order as the first appears from about 1720 to 1815 UT. This bay is bifurcated and shows two peaks. Simultaneously with the magnetic peaks, peaks in the backscatter signals occur on the lines from Borlänge to Norddeich and Lindau. The magnetic bifurcation is best reproduced in the Borlänge-Lindau backscatter signal trace. Strong backscatter signals are also recorded during the bifurcated bay on the northernmost line (Borlänge-Kjeller). If one assumes that the VHF waves backscattering centers are produced in the PEJ by

acoustic plasma waves, according to the theory of Farley and Buneman a broad eastward flowing current beyond the threshold must have intersected the region of the three appertaining backscatter curves simultaneously from about 1700 to 1815 UT.

The last bay which is smaller in amplitude occurs in the H magnetogram from Lerwick at about 1840 UT. Simultaneously, a peak in the backscatter signal appears on the Borlänge-Kjeller and Norddeich lines but barely a signal appears on the southernmost Borlänge-Lindau line. This indicates that the PEJ and the backscattering centers show a contraction to the north with declining substorm. The results shown in Fig. 5 exhibit that the centers backscattering the VHF waves show a similar behavior during a substorm as the visual aurora: extension to the south just after the start of the substorm and a contraction to the north towards the end. There are fairly good evidences that obviously there is also an extension to the north of the backscattering centers like the visual aurora just after the start of a substorm (Czechowsky and Lange-Hesse [12]). A more detailed study of the magnetograms from a chain of stations in the N-S direction indicates that during a substorm the PEJ also extends to the north and south and reaches its peak extension during the peak of the substorm (Boström [2]).

In the following section the close relation between VHF auroral backscatter echoes and the geomagnetic disturbance is investigated in detail. In this special case the H magnetogram from Lerwick and the VHF backscatter recordings from Borlänge-Kjeller both for February 27, 1969 from Fig. 5 are used in Fig. 6. The variation of the backscattered echo signals (in scale units = Skalenteile) as a function of the horizontal perturbation vector H_d (in γ) from Lerwick is shown in Fig. 6 in the lower diagram. The H_d vector is computed from the values ΔH, ΔD and the base line value H_o. In can be seen from the lower diagram in Fig. 6 that a threshold value of the order of 100 γ must be exceeded before the VHF auroral backscatter process starts at about 1420 UT. If one assumes that the VHF waves backscattering centers are produced in the PEJ by acoustic plasma waves (according to the theory of Farley and Buneman) the threshold indicates the start of the generation of ion acoustic waves. A hysteresis like behavior can also be seen in the lower diagram of Fig. 6 which means that a stronger PEJ current (higher H_d value) is necessary for the generation of plasma waves than for the maintenance of the waves which give rise to the backscattering process. A hysteresis like behavior was already observed at the EEJ by Bowles et al. [3]. Hysteresis like behavior of the PEJ also was observed e.g. by Czechowsky [7] and Lange-Hesse [18].

The results shown in Fig. 5 indicate, that in order to interpret VHF aurora backscatter communications, it is necessary to get informations about the location, the extend, the movement, and the strength of the polar electrojet. The method used before to interpret the backscatter recordings in Fig. 5 and locate the PEJ only by using the sign of the bays in the H and Z magnetograms is a relatively rough methode. A much more precise method to get the wanted informations about the PEJ was developed by Czechowsky [8], [9]. In this paper a method is presented to calculate an equivalent current system by determining the unknown parameters (e.g. height, direction, width of the current, etcetera) from the measured disturbance vectors of the earth's magnetic field, ΔH, ΔD, and ΔZ. With a model of a simple current density distribution it is possible to solve the Biot-Savart formula. In Fig. 7 results are shown for a current system calculated after this methode with the values of ΔH, ΔD, and ΔZ from the magnetograms of Leirvogur, Lerwick, Eskdalemuir, and Hartland during a period of about five hours during the strong geomagnetic storm (Kp up to 8o) on March 23/24, 1969 compared with simultaneous VHF aurora backscatter recordings on the network in Fig. 1. From the upper diagram in Fig. 7 it can be seen, that the PEJ has a large north-south extension of the order from 10 to 18 latitudes degrees which enables it to intersect the region of all backscatter curves in Fig. 1. During the peaks of the storm the most southern extension of the PEJ goes down to 55°-56° geomagnetic latitudes about from 2200 to 2300 UT and from 0200 to 0300 UT. During this time backscatter signals occur on the southernmost lines Garding-Lindau and Bielstein-Lindau. It can be seen from Fig. 1 that the backscatter curves of these two lines have a most southern extension down to 56° and 55° geomagnetic latitude respectively. In many cases the large north-south extension of the PEJ (especially during stronger geomagnetic storms as in Fig. 7) makes it diffucult to interpret in details VHF auroral backscatter communications. During lower geomagnetic activity, however, the north-south extension of the PEJ is smaller.

3. DAILY AND SEASONAL VARIATIONS OF VHF AURORAL BACKSCATTER

Fig. 8 shows on the right side the average daily variation of the frequency of occurrence of VHF auroral backscatter for the years from 1967 (upper diagram) to 1969 (lower diagram). The 1967 diagram represents only the observations from September to December. The 1968 and 1969 diagrams, however, have been computed from all 12 months of the year. In each diagram the maximum number of backscatter echoes (written in each diagram) is made equal to 100%. This does not mean, that backscatter echoes occur during the whole observation time but only the maximum number of observed echoes. This procedure makes it easier to compare the three diagrams eachother. A pronounced minimum occurs in the diagrams of Fig. 8 at about 2200 hours MEZ (MEZ = Central European Time = Time 15° East, this is about the local time). This minimum is called the evening minimum. A second broader minimum occurs in the forenoon from about 0800 to 1400 local time and is called the forenoon minimum. Two maxima occur, the first, the early evening maximum, at about 1800 to 1900 hours local time and the second, the night time maximum, at about 0000 to 0200 hour local time. On a first look it is surprising that a minimum occurs in the evening around 2200 local time since the auroral oval after Feldstein (Fig. 9) has its southernmost extension during this time, that means that the frequency of visual auroras has a maximum in the region of the backscatter curve for the Borlänge-Kjeller line mentioned in Fig. 8 (see also the location of the apertaining backscatter curve in Fig. 1). One reason for this minimum could be given if on assumes that the backscattering centers in the PEJ are generated by ion acoustic waves after Farley and Buneman. The model of the PEJ after Heppner [14] in Fig. 8 left shows a strong main east current in the afternoon and early evening hours between about 62° to 72° geomagnetic latitude. At about 2200 local time (the time of the evening backscatter minimum) the main current reverses the direction from east to west and at the reversal time the current strength is very low or zero. At this time no ion acoustic waves can be generated since the current strength is far below the threshold that means that no backscattering centers are produced. The time of the reversal of the main current of the PEJ around 2200 local time can change from day to day in an interval from the order of one hour. That obviously is the reason that the evening minimum of the frequency of occurrence of VHF auroral backscatter is smoothed in the average daily variations in Fig. 8 right and does not dip to zero which often can be observed on single days.

The forenoon minimum in Fig. 8 is broader than the evening minimum. The center of the minimum is around 1000 local time. At this time again a reversal of the PEJ main current occurs in the same manner as during the evening backscatter minimum. The current reversal seems to give only a small contribution to the morning minimum. The main reason seems to be that at this daytime the auroral oval and also the PEJ is located at higher latitudes (Fig. 9) well north of the regions of the backscatter curves of Fig. 1 so that an intersection between backscatter curves and PEJ is impossible under normal conditions.

The average daily variation of the frequency of occurrence of VHF auroral backscatter divided into summer and winter time observations on the two lines Borlänge-Lycksely and Borlänge-Oslo (Kjeller) (see also Fig. 1) is shown in Fig. 10. There is a striking difference between the summer and winter time average daily variations. In summer time the evening minimum is well pronounced and very low on both lines. In winter time, however, this minimum is less pronounced. No difference occurs in the maximum frequency of occurrence between summer and winter on the Borlänge-Lycksele line (right side of Fig. 10). On the Borlänge-Oslo (Kjeller) line, however, this maximum frequency is lower in summer, about 2/3 of the winter time value.

4. INFLUENCE OF LATITUDE

The influence of latitude on the average daily variation of the frequency of occurrence of VHF auroral backscatter shows Fig. 11 for the 12months interval from April 1970 to March 1971. The maximum number of VHF auroral backscatter observations on the northernmost line Borlänge-Lycksele is 169 in 12months that means in average about every second day a backscatter occurrence. On the next southern line Borlänge-Oslo (Kjeller) this maximum number is 91 or in average about every forth day a backscatter occurrence. On the southernmost line Borlänge-Norddeich, however, every 23rd day in average a backscatter occurs.

5. CORRELATION BETWEEN RADIO AURORA AND OPTICAL AURORA

A comparison between the occurrence of optical aurora and radio aurora is shown in Fig. 12. The diagrams at the top show the brightness of the 5577 Å emission at different times observed at Tromsö with a meridian scaning photometer. The brightness is given in kR (kilo Rayleigh). The first optical observation on that day is made at about 1520 UT. From the sign of the bays in the Z and H magnetograms from Abisko it can be derived that the center of the PEJ is south from Abisko from about 1430 to 1700 UT and over Abisko from about 1700 to 2000 UT. From the Tromsö magnetograms (not shown in Fig. 12 due to lack of space) it can be derived that the PEJ has an extension to the north at least up to Tromsö which enables it to intersect the backscatter curves of the Borlänge-Lycksele and the Borlänge-Kjeller line. The backscattering of VHF radio waves starts on the northernmost Borlänge-Lycksele line at about 1415 UT when the amplitude of the H magnetogram is of the order of about 100 γ, which again indicates a threshold. The backscatter signals disappear on this line at about 2000 UT. At this time the amplitude of the H magnetogram is of the order of 30 γ, which indicates the hysteresis like behavior as shown in Fig. 6. The variations of the Abisko H magnetogram and of the fieldstrength of the backscattered signal at Lycksele show a close correlation which again indicates the control of VHF auroral backscatter by the PEJ. A comparison between the amplitude of the backscattered signal and the brightness of the 5577 Å emission shows that the brightness maxima occur during the peaks of the backscattered signal and also during the peaks of the magnetic bays. When the signal amplitude decreases the brightness of the aurora also uses to decrease, see e.g. on the Borlänge-Lycksele line at about 1520 UT (the first optical observation at Tromsö on that day) and at about 1730 UT and 2000 UT. The backscatter on on the more southern line Borlänge-Kjeller starts about 30 minutes later as on the northernmost line, at this time the center of the PEJ starts to move to the south from Abisko and during the peak of the substorm at about 1545 UT the backscatter signals on both lines (especially on the Borlänge-Kjeller line) show a pronounced maximum.

The Doppler shift of the backscattered signal at Kjeller (Fig. 12) shows a positive sign during increasing fieldstrengt at Kjeller (from about 1445 to 1515 UT, and from about 1820 to 1835 UT) and a negativ sign during decreasing fieldstrength. The interpetration of the Doppler shift recordings is difficult. One reason for it is the fact that the half power width of the receiving antenna is very broad ($\pm$ 30°) that means that one gets contributions to the Doppler shift from different directions. Plasma acoustic waves propagate with the sound velocity in the region of the PEJ at about 110 km height. On the frequency of 145,900 MHz this sound velocity gives a Doppler shift of $>$400 Hz. The observed Doppler shifts in Fig. 12 show peak values up to 150 Hz. This is not in accordance with the plasma acoustic wave theory. Doppler shifts of the order of 400 Hz have been observed on the network, but not very often.

Another comparison between the occurrence of optical aurora and radio aurora is shown in Fig. 13. The H magnetogram from Tromsö shows three bigger positive bays between about 2040 and 2300 UT. The variations of the H magnetogram during these bays show a good correlation with the amplitude variations of the backscattered signal at Lycksele (the northernmost line). The peaks of the magnetic bays fit together with the peaks of the backscattered signa which again indicates the controll of the backscatter by the PEJ. At about 1900 UT a very weak backscatter signal occurs at lycksele of the order of 1 to 2 db above noise leve which lasts about until 2040 UT. During this time the H magnetogram shown an amplitude of about 50 to 70 γ and has a relatively smoothed shape with no bays. The optical observations of the all-sky camera at Tromsö show no aurora at about 1830 UT when no backscatter signal occurs. The bright light on the right and bottom side of the all-sky pictures is artifical light from the town of Tromsö. During the occurrence of the low backscatter signa at lycksele the all-sky pictures show a homogeneous stable are at the zenith of Tromsö. During the bays in the H magnetogram after about 2100 UT especially during the amplitude peaks of the backscattered signal the all-sky pictures show the break up phase of the auroral substorm. When the backscattered signal shows a pronounced decrease e.g. at about 2220 UT the auroral activity on the all-sky picture also shows a decrease. The backscattered signal disappear at Lycksele at about a few minutes after 2300 UT. The amplitude of the H magnetogram at this time is of the order of about 20 γ (hysteresis) and the all-sky picture shows a faint homogeneous stable arc

low in the north outside the backscatter region of the Borlänge-Lycksele line (Fig. 1).

The Doppler shift of the backscattered signal at Lycksele shows a positive sign during the time when the signal increases (from about 2050 to 2105, from 2125 - 2155, and from 2230-2245 UT). When the backscattered signal decreases (from about 2110 to 2125 and from 2200 to 2230 UT) the Doppler shift is around zero. During the weak backscatter signal at the time of the homogeneous stable arc no Doppler shift occurs.

On the southernmost line Borlänge-Kjeller backscatter signals occur, when the Z magnetogram from Tromsö shows a strong negative bay from about 2100 to 2220 UT. The sign of the amplitude in the H and Z magnetogram indicate that at this time the center of the PEJ is south of Tromsö which enables it to intersect the backscatter curve of the Borlänge-Kjeller line (Fig. 1). The peak of the backscattered signal on the Borlänge-Kjeller line occurs exactly during the peak of the bay in the Z magnetogram. At the same time the brightness of the 5577 Å emission at Tromsö (lower diagrams in Fig. 13) shows its absolute maximum during the observation time shown in Fig. 13. About 15 minutes later (at about 2205 UT), when the bay in Z has nearly disappeared and the backscattered signal on both lines also has considerably decreased, the brightness of the 5577 Å emission shows a decrease down to about one third of the maximum value. When the backscattered signal increases again at about 2235 UT (in this case only on the northernmost line Borlänge-Lycksele) the brightness of the 5577 Å emission also shows a pronounced increase and a decrease about 10 minutes later when the backscattered signal decreases again.

A last comparison between the occurrence of optical aurora and radio aurora is shown in Fig. 14 in the same manner of representation as in Fig. 12. Fig. 14, however, shows in addition to Fig. 12 the H and Z magnetogram from Abisko. The optical observations in Fig. 14 have been restricted (due to meteorological reasons at Tromsö) from about 1905 to 2100 UT. The amplitude of the H magnetogram from Tromsö predominantly has a positive sign during the whole observation time in Fig. 14. At about 1800 UT the first backscatter signal occurs on the northernmost Borlänge-Lycksele line when H has an amplitude of about 50 γ (threshold). The signals disappear on this line at about 2100 UT when H has an amplitude of about 20 γ (hysteresis). On the southernmost Borlänge-Kjeller line backscatter signals only occur during the time when a negative bay occurs in Z magnetogram from Tromsö. The sign of the bays in H and Z at Tromsö indicate that at this time the center of the PEJ is south of Tromsö which enables it to intersect the backscatter curve for the Borlänge-Kjeller line (Fig. 1). During the peak of the magnetic substorm from about 1950 to 2020 UT the backscatter signal on both lines shows its peak amplitude. At the same time the brightness of the 5577 Å Emission at Tromsö also shows its peak value of the whole observation time shown in Fig. 14. When the backscatter signal on both lines shows a pronounced decrease from about 2015 to 2100 UT the 5577 Å brightness also shows a pronounced decrease. The Doppler shift of the backscattered signal at Lycksele shows a positive value up to about 150 Hz nearly during the whole time when backscatter signals occur at this station. When the backscatter signal shows a pronounced decrease on both lines around 2030 UT the Doppler shift is zero.

6. CONCLUSIONS

In summary it can be said that there is a good correlation between optical aurora and VHF continuous wave radio aurora under the assumption that the optical aurora is observed in the region where the backscattering centers for the VHF radio waves are located (in the case of the line Borlänge-Lycksele the backscattering centers are located in the region of Tromsö). In this case there is a good correlation between the peak amplitudes of the backscatted VHF radio waves and the peak brightness of the 5577 Å emissions. One also observes strong backscatter amplitudes during the break up phase of the auroral substorms. There is always a close control of the VHF backscatter phenomenon by the polar electrojet. The shape of the geomagnetic variations in the H magnetogram below the center of the PEJ (especially the substorm bays) show a close correlation with the shape of the amplitude variations of the backscattered signal. In addition to this VHF aurora backscatter measurements (especially the threshold) give informations about a special fine structure of the PEJ which obviously can not be got by geomagnetic measurements, perhaps by a special kind of pulsations, but

this, so far as I know, has to be investigated.

REFERENCES

[1] Abel, W.G. and Newell, R.E.: 1969 "Measurements of the Afternoon Radio Aurora at 1295 MHz", J. Geophys. Res. 74, 231-245.

[2] Boström, R.: 1971 "Polar Magnetic Substorms" in the Radiating Atmosphere, pp. 357-365, edited by B.M. McCormac, D.Reidel Publishing Company, Dordrecht-Holland.

[3] Bowles, K.L., Balsley, B.B., and Cohen, R.: 1963 "Field-aligned E-Region Irregularities Identified with Acoustic Plasma Waves", J. Geophys. Res. 68, 2485-2501.

[4] Buneman, O.: 1963 "Excitation of Field-Aligned Sound Waves by Electron Streams", Phys. Rev. Letters 10, 285-287.

[5] Cohen, R. and Bowles, K.L.: 1963 "The Association of Plane-Waves Electron-Density Irregularities with the Equatorial Electrojet", J.Geophys. Res. 68, 2503-2525.

[6] Czechowsky, P.: 1966 "Analyse von Rückstreubeobachtungen ultrakurzer Wellen an Polarlichtern", Diplom-Arbeit (Master's Thesis) University of Göttingen, Germany.

[7] Czechowsky, P.: 1969 "Statistische Auswertung von Polarlicht-Rückstreubeobachtungen und Vergleich mit der Theorie der Plasma-Instabilität", Kleinheubacher Berichte, Band 13, 97-103. Published by Fermeldetechnisches Zentralamt, D 33, Darmstadt.

[8] Czechowsky, P.: 1971a "Calculation of an equivalent current system in the polar E region", Radio Science, 6, 247-253.

[9] Czechowsky, P.: 1971b "Berechnung eines äquivalenten Stromsystems aus erdmagnetischen Registrierungen", Kleinheubacher Berichte, Bd. 14, under the press, published by Fernmeldetechnisches Zentralamt, D 33, Darmstadt.

[10] Czechowsky, P., Kochan, H. Lange-Hesse, G., Lauche, H., and Möller, H.G.: 1970 "Simultaneous observations of various ionospheric phenomena during the geomagnetic storm of Oct. 31 to Nov. 2, 1968", Z. Geophys. 36, 77-103, and Report UAG 8, Part 1, Data on Solar-Geophysical Activity, Oct. 24-Nov.6, 1968 (compiled by J.V. Lincoln), World Data Center A, Upper Atmosphere Geophysics, Boulder, Color., p. 296.

[11] Czechowsky, P. and Lange-Hesse, G.: 1970 "Substorm Influences on VHF Continuous Wave Auroral Backscatter", in Intercorrelated Satellite Observations Related to Solar Events pp. 405-412, edited by V.Manno and D.E. Page, D. Reidel Publishing Company, Dordrecht-Holland.

[12] Czechowsky, P. and Lange-Hesse, G.: 1971 "Optical and Radio Observations of the Aurora", in The Radiating Atmosphere pp. 306-318, edited by B.M. McCormac, D.Reidel Publishing Company, Dordrecht-Holland.

[13] Farley, D.T., Jr.: 1963 "A Plasma Instability Resulting in Field-Aligned Irregularities in the Ionosphere", J. Geophys. Res. 68 (1963), 6083-6097.

[14] Heppner, J.P.: 1967 "High Latitude Magnetic Disturbances", in Aurora and Airglow pp. 75-92, edited by B.M. McCormac, Reinhold Publishing Corporation, New York.

[15] Hofstee, J. and Forsyth, P.A.: 1969, Can. J. Phys. 47, 2797.

[16] Knox, F.B.: 1971, to be submitted to J. Atmosph. Terr. Phys.

[17] Lange-Hesse, G.: 1967 "Radio Aurora, I. Observations, II. Comparison of the Observations with a Theoretical Modell", in AURORA and AIRGLOW, pp. 519-562, edited by B.M. McCormac, Reinhold Publishing Corp. New York.

[18] Lange-Hesse, G.: 1968 "VHF Bistatic Auroral Backscatter Communications", in IONOSPHERIC RADIO COMMUNICATION IN THE ARCTIC, pp. 174-205, Publisher: Plenum Press, New York.

[19] Lange-Hesse, G.: 1969 "Radio Observations of the Aurora by Continuous Wave Transmissions", in ATMOSPHERIC EMISSIONS, pp. 201-212, edited by B.M. McCormac and A. Omholt, Van Nostrand Reinhold Company, New York 1969.

[20] Lange-Hesse, G. and Czechowsky, P.: 1966 "VHF Bistatic Auroral Backscatter Communications — Comparison of the Observations with the Theory", ARCHIV ELEKTR. ÜBERTRAGUNG (AEÜ). 20, 365-373.

[21] Unwin, R.S. and Knox, F.B.: 1970 "Radio Aurora and Electric Fields", Paper presented at Upper Atmosphere Currents and Electric Fields Symposium, Boulder, Colorado, Sept. 1970. To be published in Radio Science, April 1972.

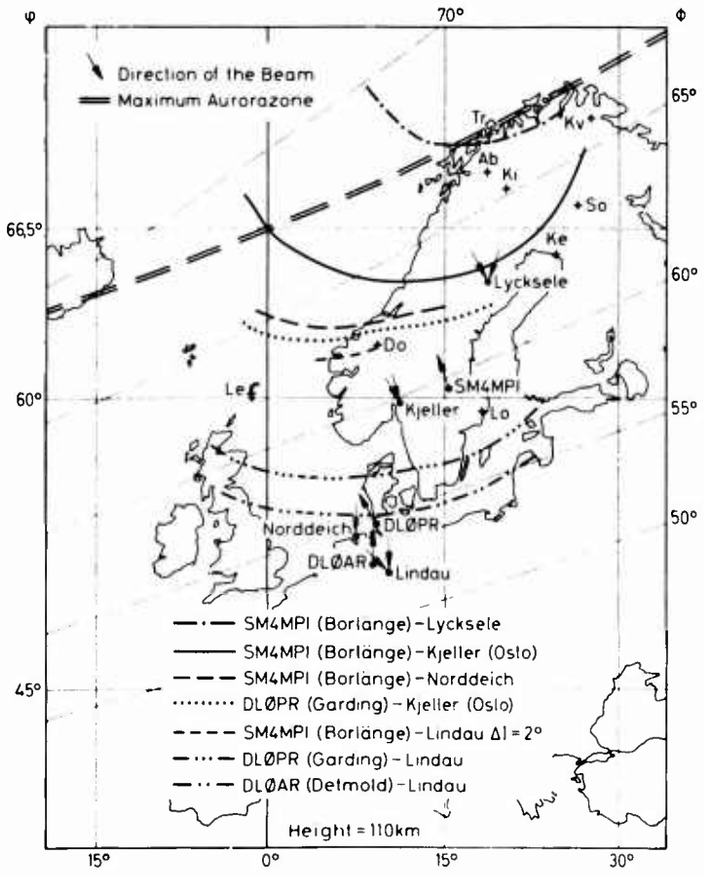

Fig. 1 Position of the VHF beacon transmitters (SM4MPI, recently changed in SK 4 MPI, near Borlänge, 145.960 MHz; DL ∅ PR, Garding, 145,971 MHz; DL ∅ AR, Detmold, 29.0 MHz) and of the receiving stations (Lycksele, Kjeller, Norddeich, and Lindau) with the appertaining backscatter curves for the pairs of stations mentioned in the figure. The arrow at the stations indicates the direction of the antenna beam (half-power width $\pm 30^{\circ}$). The backscatter curves represent the location at the 110 km height level (frequency maximum of the auroras) where the ideal backscatter conditions are fulfilled (Lange-Hesse and Czechowsky [20] ; Lange-Hesse 17) meaning where the backscattering centers (which obviously are spatially and temporally correlated with the PEJ beyond the threshold) must be located in case of the occurrence of auroral backscatter communications between the pairs of stations specified in the Figure. Tr = Auroral Observatory Tromsö; Ki = Geophysical Observatory, Kiruna; So = Geophysical Observatory Sodankylä; Ab, Lo, Do, Le = Geomagnetic Observatories Abisko, Lovö, Dombås and Lerwick, respectively. Φ = geomagnetic latitude, φ = geographic latitude.

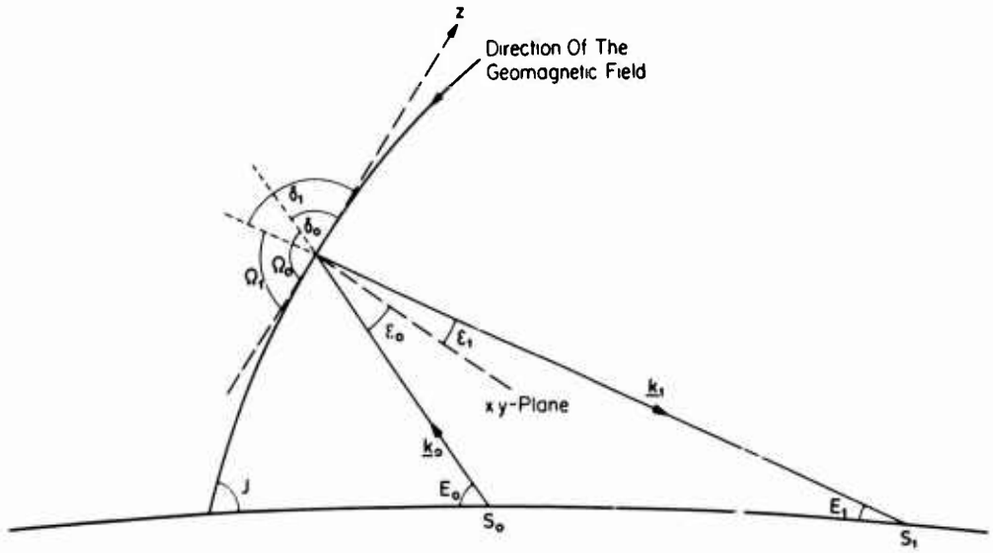

Fig. 2 Cross-sectional view of the earth with the geometry of the propagation path in the vertical direction for VHF bistatic auroral backscatter propagation between the two points S_0 and S_1

k_0, k_1 vector of the wave normal of the incident and backscattered wave, resp.

ε_0, ε_1 angle between k_0 and k_1, resp. and the xy-plane.

J magnetic dip angle

Ω_0, Ω_1, propagation angle = angle between the direction of radio wave propagation and the magnetic lines of force

E_0, E_1, elevation angle above the horizontal

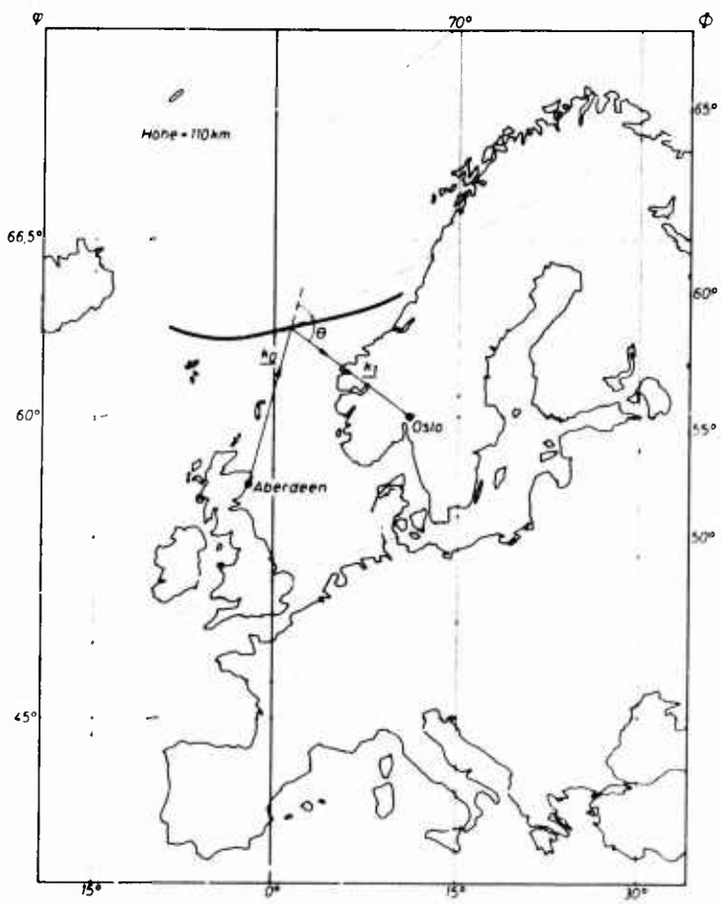

Fig. 3 Geometry in the horizontal direction for VHF bistatic auroral backscatter communications between the two points Aberdeen and Oslo. The solid curve is the backscatter curve for the pairs of stations mentioned above.

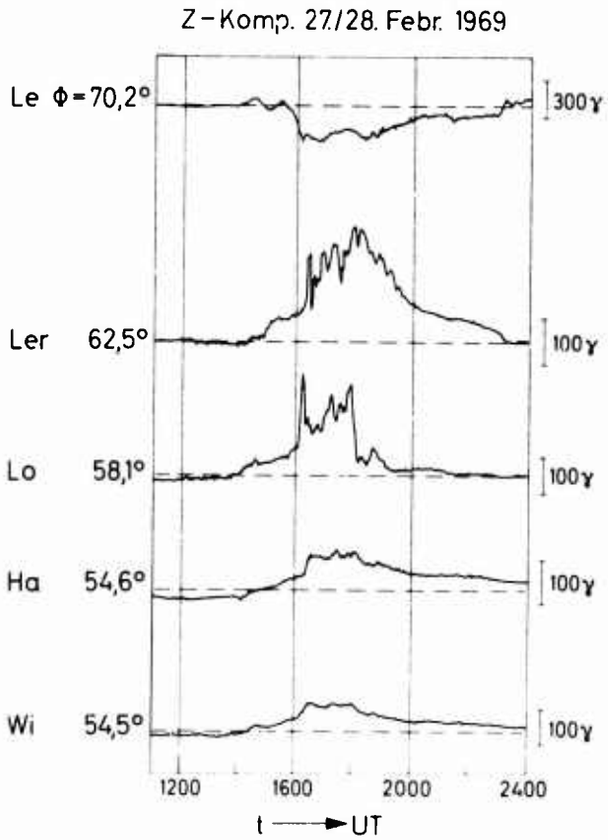

Fig. 4 Z magnetograms, February 27, 1969, from different European Observatories: Le = Leirvogur (Iceland); Ler = Lerwick; Lo = Lovö/Stockholm; Hartland/southern England; Wi = Witteveen/ Netherlands. Φ = geomagnetic latitude.

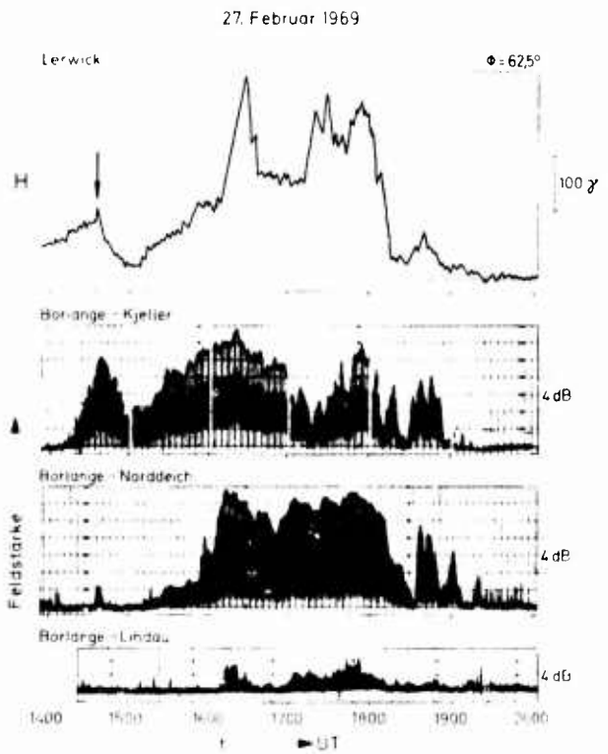

Fig. 5 VHF auroral backscatter recordings from the beacon station Borlänge, SK 4 MPI, 145.960 MHz at three different stations compared with the simultaneous H magnetogram from Lerwick (see Fig. 1). The northern most receiving station (Lycksele) did not yet work at this time. After Czechowsky [7].

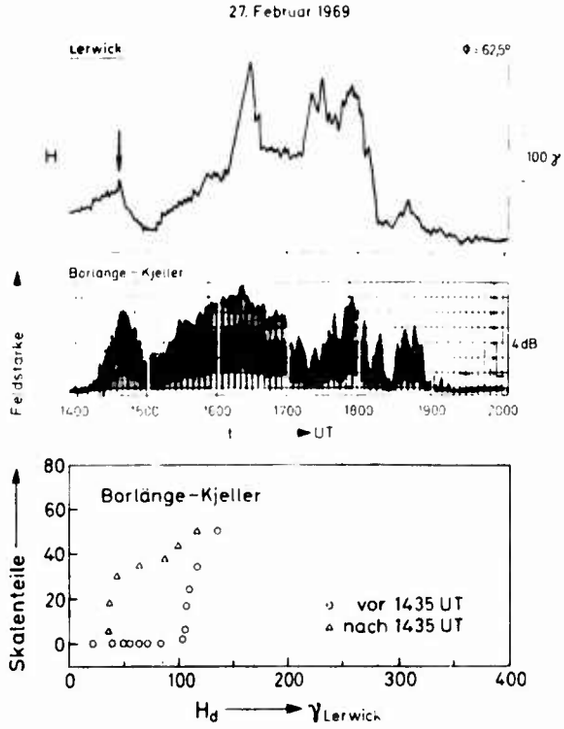

Fig. 6 Relation between the amplitude of auroral backscatter echoes on the Borlänge-Kjeller line and the variation of the horizontal disturbance vector H_d at Lerwick (see Fig. 1 and Fig. 5) The circle values ○ are before (vor) and the triangle values △ after (nach) 1435 UT in the lower diagram. The time 1435 UT is marked by an arrow in the Lerwick magnetogram.

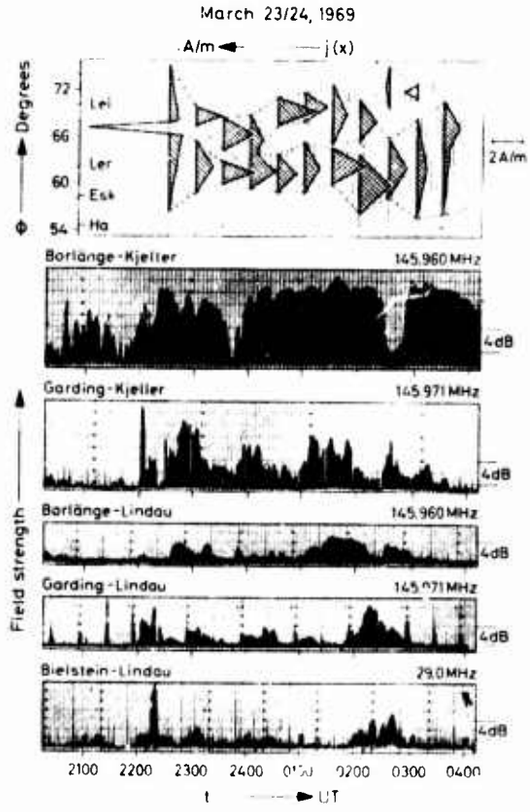

Fig. 7 The location, width and current strengs of the polar electrojet during the strong geomagnetic storm on March 23/24, 1969 compared with the simultaneous VHF aurora backscatter recordings on the network in Fig. 1. After Czechowsky [8], [9].

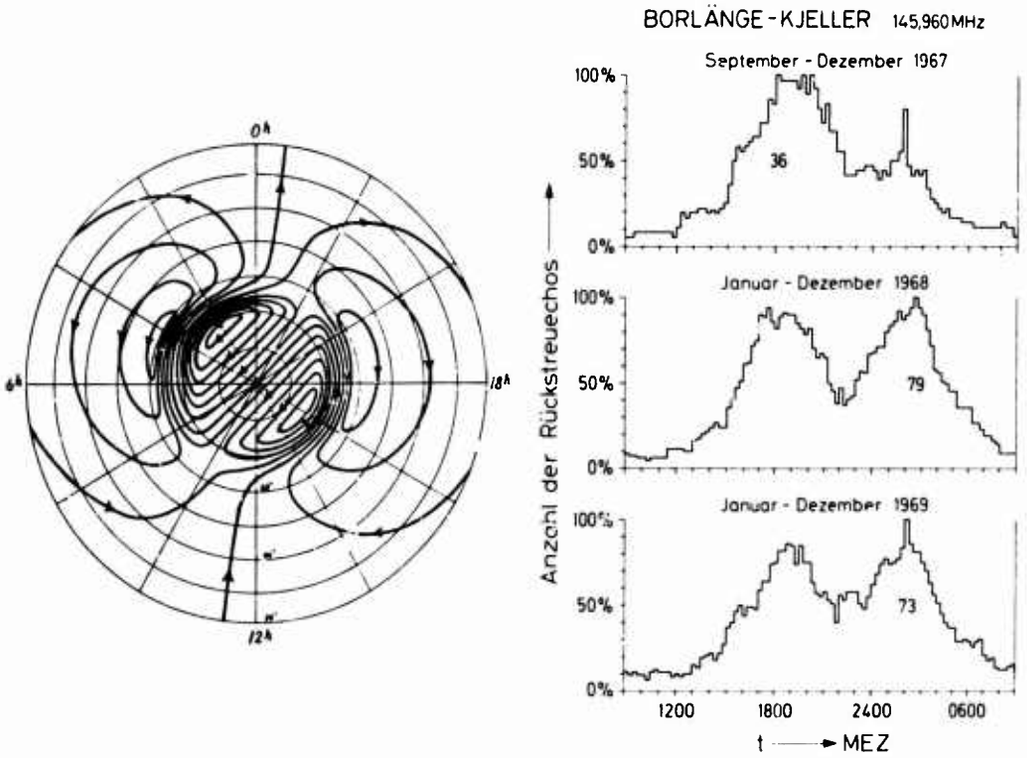

Fig. 8 Average daily variation of the frequency of occurrence of VHF auroral backscatter on the Borlänge-Lindau line for the years from 1967 to 1969 (right side) and a polar cap map (left side) with geomagnetic parallels of latitude and a picture of the polar electrojet (PEJ) after Heppner [14]. MEZ = Central European Time = Time 15° East. Anzahl der Rückstreuechos = Number of backscatter echoes. In each diagram on the right side the maximum number of backscatter echoes (written in the diagram) is made equal to 100%. This does not mean that backscatter echoes occur during the whole observation time but only the maximum number of observed echoes.

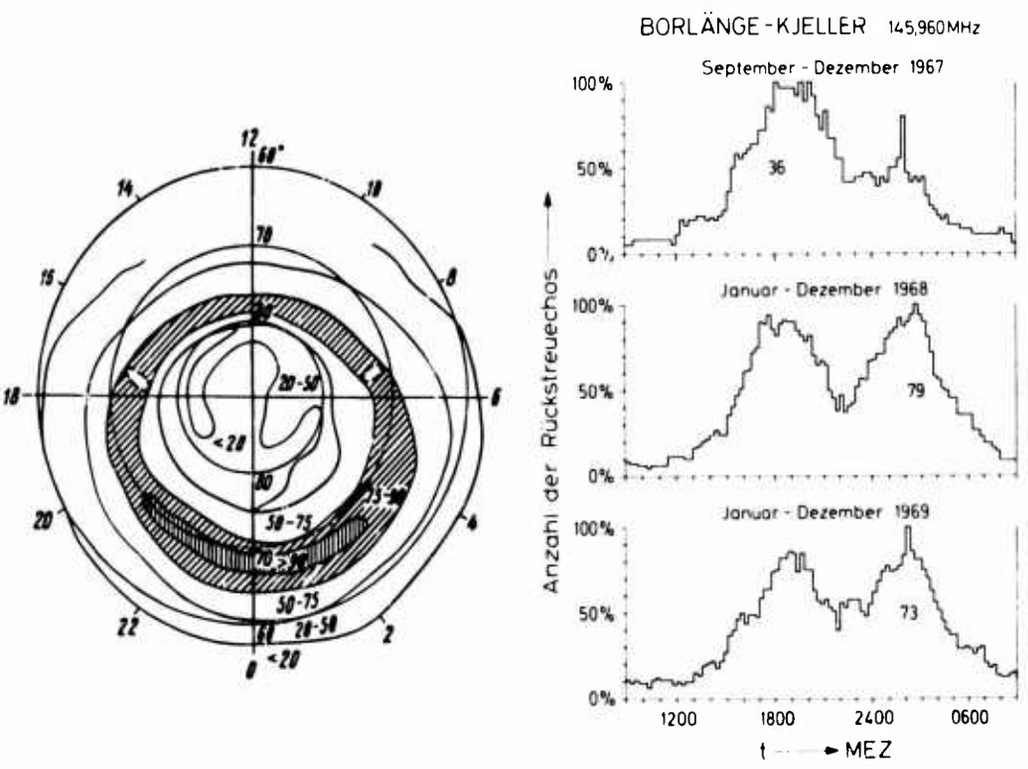

Fig. 9 On the right side same representation as in Fig. 8 right side. On the left side a polar cap map with geomagnetic parallels of latitude and a picture of the auroral oval (after Feldstein).

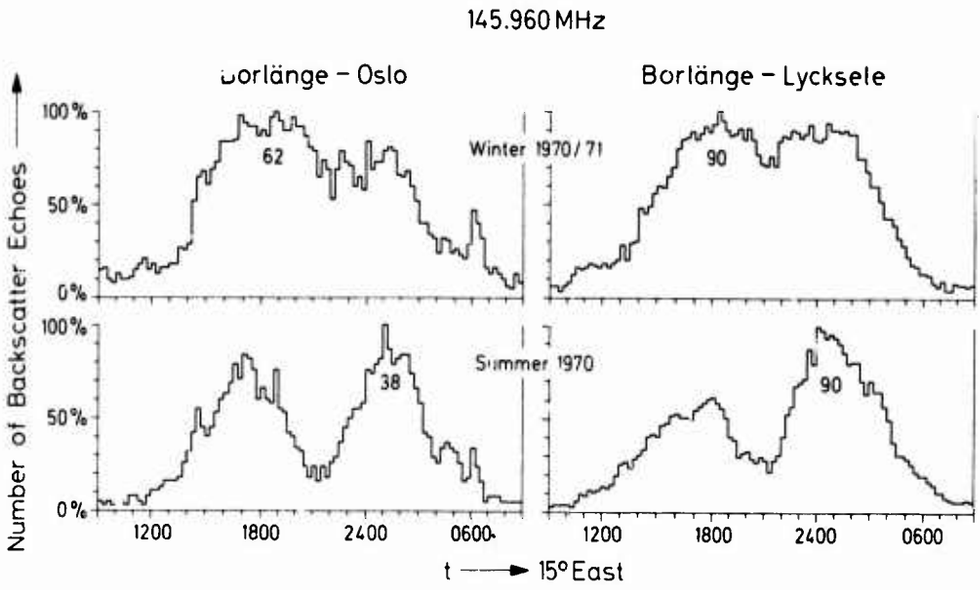

Fig. 10 Average daily variation of the frequency of occurrence of VHF auroral backscatter on the Borlänge-Oslo (Kjeller) and Borlänge-Lycksele line in Winter 1970/71 (upper diagrams) and in Summer 1970 (lower diagrams). See also Fig. 1. Same kind of representation as in Fig. 8 right side.

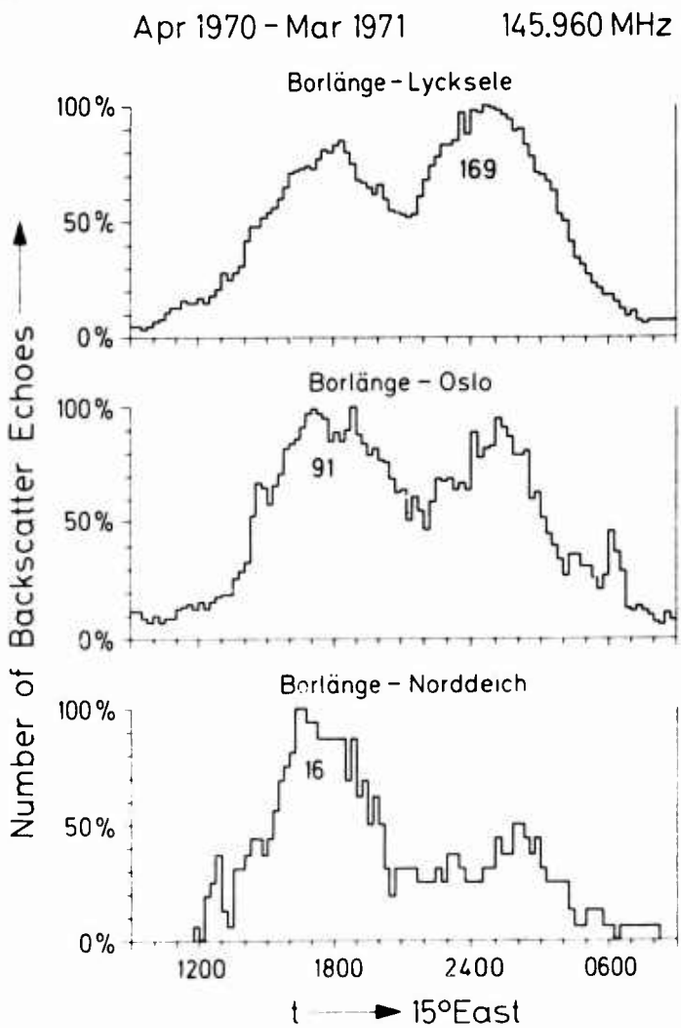

Fig. 11 Average daily variation of the frequency of occurrence of VHF auroral backscatter in different latitudes. The upper diagram represents the northernmost line Borlänge-Lycksele and the lower diagram the southernmost line Borlänge-Norddeich. Same kind of representation as in Fig. 8 right-side. See also Fig 1.

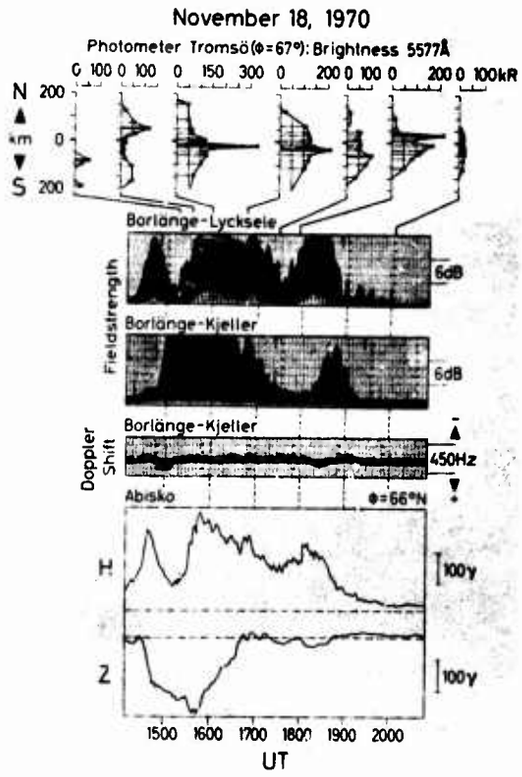

Fig. 12 Comparison of optical auroral observations at Tromsö (upper diagrams) with VHF auroral backscatter (radio aurora) recordings on the lines Borlänge-Lycksele and Borlänge-Kjeller (145,960 MHz), and with Doppler shift recordings of the backscattered signal on the Borlänge-Lycksele line, and with geomagnetic recordings from Abisko (see Fig. 1).

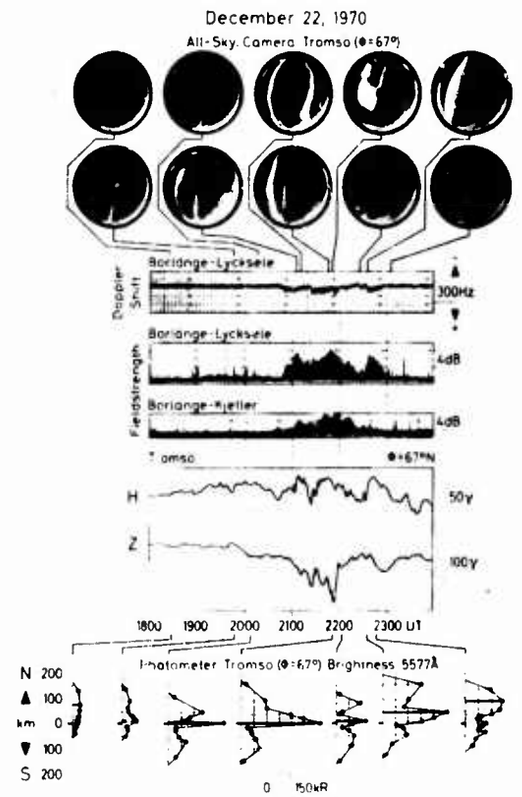

Fig. 13 Comparison of optical auroral observations at Tromsö (all-sky camera pictures in the upper part of the Figure and photometer observations in the lower part of the Figure) with VHF auroral backscatter (radio aurora) recordings on the lines Borlänge-Lycksele and Borlänge-Kjeller (145,960 MHz) and with Doppler shift recordings of the backscattered signal on the Borlänge-Lycksele line, and with geomagnetic recordings from Tromsö (see Fig. 1). On all all-sky camera pictures is north to the left.

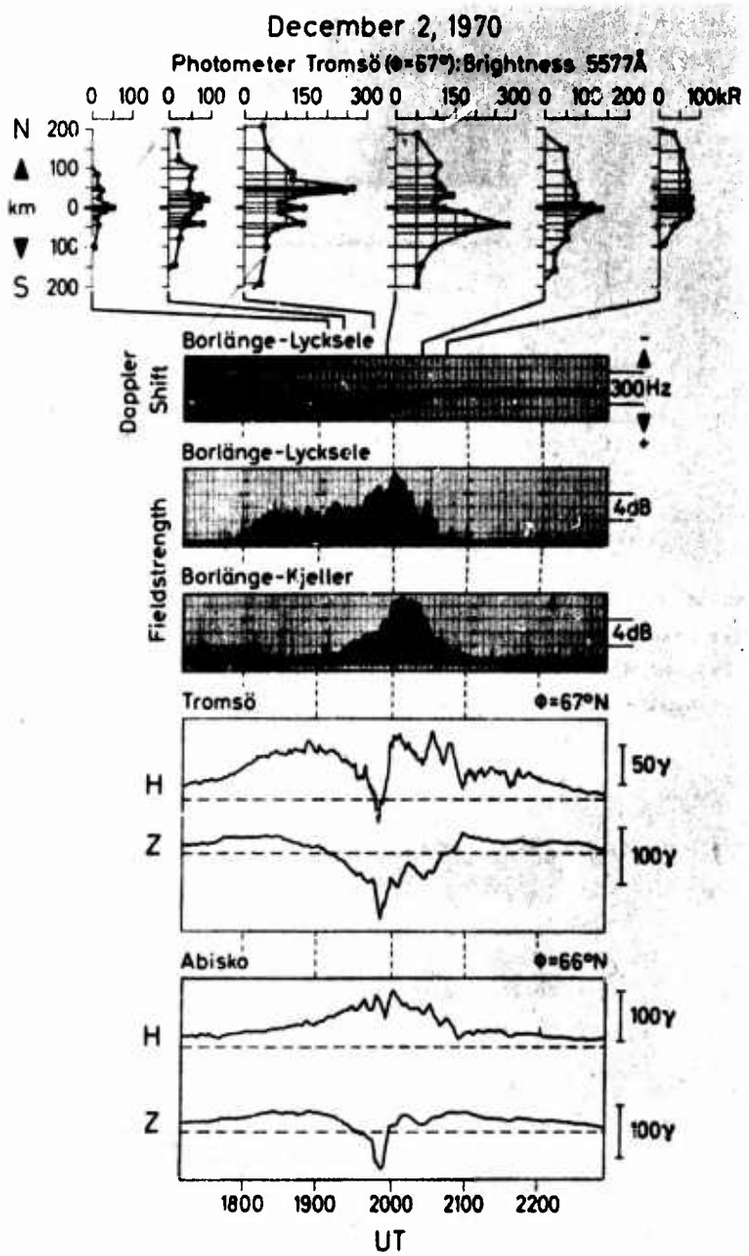

Fig. 14 Comparison of optical auroral observations at Tromsö (upper diagrams) and VHF auroral backscatter (radio aurora) recordings on the lines Borlänge-Lycksele and Borlänge-Kjeller (145,960 MHz), and with Doppler shift recordings of the backscattered signal on the Borlänge-Lycksele line, and with geomagnetic recordings from Tromsö and Abisko (see Fig. 1).

AURORAL RADAR BACKSCATTER STUDIES FROM HOMER, ALASKA

W. G. Chesnut, J. C. Hodges, R. L. Leadabrand
STANFORD RESEARCH INSTITUTE
Menlo Park, California, U.S.A.

ABSTRACT

Radar aurora have been studied using a backscatter radar at six frequencies from 50 MHz to 3,000 MHz. It has been found that the frequency dependence of the volume scattering cross section of the auroral echoes is nearly exponential with frequency. The slope of this frequency dependence was found to vary with time but averaged 33 dB per 1,000 MHz. The magnetic aspect sensitivity was found to be nearly independent of frequency; the scattering cross section decreased by about 10 dB per degree of aspect angle.

Auroral radar echoes at a frequency of 139 MHz have been compared with the location of particle precipitation as measured during fourteen passes of the OV1-18 satellite. It is found that, except for periods of very active aurora, nighttime radar aurora was never collocated with peaks in proton energy flux. The positions of nighttime radar aurora show a tendency not to be collocated with peaks in electron energy flux but there were some instances of spatial superposition. With only a few exceptions, wherever radar aurora was located, measured particle precipitation fluxes were adequate to produce equilibrium E-region electron densities greater than 7×10^4 el/cm^3. Thus, E-region electron densities necessary for radar aurora seem to be produced by precipitating particles.

1. INTRODUCTION

For a number of years Stanford Research Institute has been operating a radar complex at Homer, Alaska. The radar is operated only during specific data-taking periods. Usually these periods correspond to times when other experimenters are making special efforts to acquire auroral data that can be correlated with response of the radar. A specific example of this coordinated effort has been the operation of the Homer radar during times when the OV1-18 particle precipitation satellite, flown by the Lockheed Space Science Laboratory, was acquiring data. In this paper we shall discuss some of the frequency-dependence measurements that have been made with the radar. We shall also present some results of studies that have been made of the relation between radar echoes at 139 MHz, and proton and electron precipitation as recorded by the OV1-18 satellite.

2. INSTRUMENTATION

The radar equipment used for this work is located at Homer, Alaska. The radar utilizes simultaneously six radar frequencies. All frequencies are fed into a 60-foot, fully steerable parabolic antenna. The frequencies presently being used are 50, 139, 398, 850, 1,210, and 3,000 MHz. All frequencies except for 50 MHz are phase coherent.* The radar can be operated using a variety of pulse lengths. The transmitters operate with peak powers of 30 to 200 kW, depending on frequency. Auroral radar returns are recorded for later analysis. Table 1 gives a brief description of the radar parameters.

Table 1

CHARACTERISTICS OF HOMER AURORAL RADAR

Frequency (MHz)	50	139	398	850	1,210	3,000
Peak power (kW)	30	50	50	40	40	200
Pulse length (μs)	Variable from 10 to 1,000					
PRF (p/s)	15 to 150					
Phase Coherent	No*	Yes	Yes	Yes	Yes	Yes
Antenna	Steerable 60-ft diameter paraboloid					
Antenna half-power beamwidth (deg)	25	9	3	1.5	1	0.4
Receiver dynamic range	Approximately 80 dB					

* The 50-MHz radar is also phase coherent but is presently operated like phase path sounders used in RF ionospheric work.

3. FREQUENCY-DEPENDENCE MEASUREMENTS

Two aspects of the frequency dependence of radar aurora have been investigated. The first dependence is the radar-reflection coefficient versus radar frequency. The second is the frequency dependence of the magnetic aspect sensitivity. In these studies we have made an effort to measure the magnetic aspect dependence at frequencies as low as 50 MHz and as high as 3,000 MHz.

We have shown that refraction effects in E-region ionization are very important at 50 MHz, so that corrections must be made during measurement of magnetic aspect dependence. The 3,000-MHz estimates of aspect dependence can be based only on statistical inferences.

3.1 Analyzing Data Containing 50-MHz Reflections

The 50-MHz radar of the Homer installation has a very large beamwidth compared with the other frequencies. As a result, interpretation of radar echoes must be performed in a very special manner. Meaningful analysis of these data requires the existence of a very stable radar auroral arc.

Figure 1 presents a map of Alaska; Homer is located at the bottom of the map. Contours of constant magnetic aspect angle at an altitude of 110 km are shown. Across the top of Alaska we have drawn a line corresponding to a radar auroral arc obtained on 24 November 1967. We have also indicated signal strength at 398 MHz as a function of position along the arc. The position and intensity of this arc was remarkably stable over a 20-minute period. The arc was well defined by frequencies of 139 MHz through 1,210 MHz and was very thin in north-south extent. The 50-MHz echoes that were obtained also arose from scattering from within the same arc.

Figure 2 shows the 398-MHz signal strength plotted against magnetic aspect angle along the arc. In fact, we have plotted signal strength versus aspect angle in several ways. Clearly, the data of Figure 2(b) are most self-consistent. In these data we assume that magnetic field lines are depressed by one-half degree relative to our model of the quiescent magnetic field orientation. The data fitted to these curves give a signal change of about 12 dB per degree change in magnetic aspect angle. This deduction assumes, of course, that the scattering properties in the arc are the same at all positions. We cannot prove that this is so.

Figure 3 presents a signal strength as a function of azimuth for the four middle radar frequencies. We have indicated by the arrow-T in the figure the minimum detectable signal for each frequency. We note that the intensity behavior versus azimuth (which means a unique aspect angle at each azimuth) is very similar for all frequencies and suggests at most a weak frequency dependence on the aspect sensitivity over this frequency range.

If we assume that this radar arc, well defined at higher frequencies, was also the source of scattering at 50 MHz, then we find that the thin arc gives us a very high angular resolution at 50 MHz despite the very broad antenna beam at this frequency. The reason for this is that the 50-MHz radar's 200-microsecond pulse converts high range resolution into high angular resolution, as shown in Figure 4. As a result the 50-MHz signal strength can be plotted as a function of magnetic aspect angle in the western and eastern limits of the auroral radar arc.

The results of this measurement technique are shown in Figure 5. This figure shows that the 50-MHz echo strength is a maximum for signals reflected from the extreme eastern and western extremities of the arc. These regions are very far from zero magnetic aspect. We have also found, but do not show here, that the signal strength at 50 MHz is weakest from regions at which other radar frequencies are observing their strongest scatter.

If we assume that the refraction in E-region ionization bends the 50-MHz beam line to magnetic orthogonality in the eastern and western limbs, then we deduce that the electron density in the western limb will correspond to a plasma frequency of 7.2 MHz. The plasma frequency in the eastern limb would be between 7.0 and 9.1 MHz. From these data we deduce that the 50-MHz signal strength changes by as little as 7 dB per degree to as much as 12 dB per degree on either side of the maximum.

This result is in disagreement with the magnetic aspect sensitivity measured by McDiarmid and McNamara.[1] Our steep aspect dependence at 50 MHz is consistent with that inferred by Bates and Albee.[2]

3.2 Analyzing Data Containing 3,000-MHz Reflections

Because of their intrinsic weakness, it is only very occasionally that 3,000-MHz echoes can be observed with the Homer radar. When these are observable, the radar pulses must be integrated for a period of up to one minute in order to obtain a statistically meaningful measurement.

Figure 6 presents a scatter plot of signal strength at each frequency shown, versus the signal power simultaneously obtained at 398 MHz. These data were obtained from regions of the sky corresponding to quiescent magnetic aspect of $+0.5^{\circ}$ to $+2.5^{\circ}$. There are 57 separate 55-second integrations shown in this plot. The boxes containing numbers show the number of data points on either side of the lines drawn at 45°. A number count shows that the 45° lines are adequate fits for the four sets of data.

From the general nature of the scatter diagram of Figure 6, we conclude that the frequency dependence of auroral scattering, when 3,000-MHz echoes are obtained, does not vary very much from measurement to measurement as it does with data sets not containing the 3,000-MHz echoes. If this dependence did vary, the scatter of data points would be very much greater for the 3,000-MHz data than it is for those frequencies that are very close to 400 MHz. Inasmuch as these data were taken at a variety of aspect angles, we also infer that the aspect dependence at 3,000 MHz must be similar to that at the other frequencies; otherwise the 3,000-MHz data points would either scatter much more than they do, or display a pattern that should be curved.

3.3 Frequency Dependence from 50 MHz to 3,000 MHz

We have found that the frequency dependence of auroral radar returns can usually be adequately fitted by an equation of the form

$$P = P_o \exp(-f/f_o) \quad .$$

We call the quantity f_o the scale frequency. The data obtained from the radar auroral arc give a value of f_o of 112 MHz. When we fit our data that contain 3,000 MHz echoes, we find a value of 222 MHz for f_o. It is quite clear that the frequency dependence of auroral radar echoes it not time-invariant.

In order to better understand the frequency dependence we have measured the scale frequency of 36 independent measurements of the frequency dependence between 139 and 1,210 MHz. We have also determined the quantity P_o for these 36 cases. Figure 7 presents a scatter plot of these data versus magnetic aspect angle, time of day of observation, azimuth of measurement, and a cross correlation between scale frequency (expressed as dB per 1,000 MHz)* and zero frequency interception. For this data set there seems to be no obvious correlation between these various quantities. Based on more recent studies, we are now gaining the impression that the scale frequency becomes larger (weaker frequency dependence) as the intensity of aurora increases. This impression is not well documented yet.

3.4 Summary of Frequency-Dependence Measurements

Based upon the data that we have presented here we conclude the following:

(1) E-region refraction affects magnetic aspect measurements at 50 MHz.

(2) If E-region refraction is taken into account, we infer that the magnetic aspect dependence of 50-MHz radar echoes is similar to that measured at higher frequencies up to at least 1,210 MHz.

(3) Based on dissection of the radar auroral arc of Figure 1, we find that all frequencies from 50 to 1,210 MHz demonstrate nearly the same magnetic aspect dependence.

(4) We find that the frequency dependence of radar echoes from 139 to 1,210 MHz changes with time. We have not yet found a correlation with other geophysical quantities.

(5) When 3,000-MHz echoes are obtainable we find a larger scale frequency (weaker frequency dependence), which result may simply reflect our system sensitivity.

(6) When 3,000-MHz echoes are present, based on the scatter diagram of Figure 6, the frequency dependence does not seem to be a function of signal intensity.

(7) Inasmuch as the 3,000-MHz data have been obtained from a variety of magnetic aspect angles, the data of Figure 6 suggest that the magnetic aspect dependence is the same at 3,000 MHz as it is at the lower frequencies.

4. CORRELATION OF RADAR ECHOES WITH SATELLITE-BORNE PARTICLE PRECIPITATION MEASUREMENTS

In this section we compare some results of the simultaneous measurement of radar aurora and particle precipitation. In anticipation of satellite passes, satellite ephemerae were obtained and the radar scan mode was chosen in an attempt to probe the E regions down the magnetic field lines from the satellite position. Data have been provided to us by the Lockheed Space Science Laboratory for 14 satellite passes during which the Homer radar detected auroral echoes.

The satellite instrumentation details are given elsewhere.[3] Basically, the satellite measures precipitating electron intensity and spectrum using five energy-selecting electron counters in an energy range from 0.8 to 37 keV. Data were made available to us from two proton counters. One measures proton fluxes for proton energies greater than 10 keV; the other measures proton fluxes for protons with energies greater than 38 keV.

---

* It is easily shown that $f_o = 4340/\text{slope}$ where "slope" is expressed in dB per 1,000 MHz.

4.1 Examples of Data

In this section we review very briefly the form of the data that have been obtained. The particle flux data provided by the Lockheed Corporation gives proton flux in each of the two counters, electron average energy, and total electron energy flux (product of energy times particle number) as a function of satellite time. From these data we compute the average proton energy under the assumption that the proton spectrum is exponential with energy. Proton energy flux (particle number times energy) is then computed as a function of satellite time.

The Homer radar enables us to map out location of radar aurora and provides us with a measure of radar auroral scattering intensity. A series of maps have been made from these data. Figure 8 presents one example for illustration purposes. Figure 8 is a map of Alaska with the satellite orbit indicated by a line. Alaska Standard Time is shown by tick marks. Radar aurora was observed along the satellite trajectory in the regions between heavy dashed lines that are lightly speckled. In this particular figure the heavy speckled profile that is symmetric on either side of the satellite trajectory gives the electron energy precipitation flux (particle number flux times particle energy). The data correlations that we shall show are based on visual inspections of 14 figures of this sort for electron precipitation and 14 for proton precipitation.

4.2 Correlation of Regions of Peak Energy Flux with Locations of Radar Aurora

The data from 14 satellite passes have been studied to seek a variety of correlations. Table 2 presents one set of correlations of these data. The first column of Table 2 identifies satellite pass number.

Table 2

COINCIDENCES AND ANTI-COINCIDENCES BETWEEN RADAR AURORA AND PEAKS IN ENERGY PRECIPITATION FROM SATELLITE MEASUREMENTS

Pass Number	Type of Auroral Event*	Electron Precipitation			Proton Precipitation			Simultaneity in Time of Radar Measurements and Satellite Pass
		Coincidence	Anti-Coincidence		Coincidence	Anti-Coincidence		
			Radar	Electron Peaks		Radar	Proton Peaks	
A157	--	1	1	5	0	2	1	Good
A232	E, wp	1	1	1	0	2	1	Good
A369	E, wp	3	1	Widespread	0	4	1	Radar 1 minute late--radar aurora moving south
A388	E	0	1	Widespread outside radar's view	0	1	1	Good
A431	E, P	0 to 1(?)	4 → 3(?)	Many peaks	0	4	1	Satellite data 3 minutes earlier than radar data
A518	--	2	0	0	0	2	1	--
A624	--	1	1	2	0	2	1	Good
A641	--	0	3	2	No protons	No protons	No protons	Poor--radar map is 13 minutes later than satellite pass
A657	E, wp	0	1	Many peaks	0	1	1	Good
A676	E	0	1	2 → 3	0	1	1	Good
A751	E	?	?	Several	0	2	1	Good
A2964	E	1 → 2(?)	2 → 1(?)	0 → 1	0	2	0	Good
A2979	E, P	Widespread	Widespread	Widespread	Widespread	Widespread	Widespread	Good
A2995	E, P	Widespread	Widespread	Widespread	Widespread	Widespread	Widespread	Good

* E--fairly large total electron energy flux; P--fairly large total proton flux; wp--moderate to weak total proton energy.

We have categorized the type of auroral event that was occurring in Column 2. If there is no symbol, the event was a weak precipitation event, meaning that the particle fluxes were quite low but were measurable in some parts of the trajectory. If, in our judgment, the energy flux of electrons (not the number flux) was large, then we have placed an E in this column. If proton precipitation was weakly observable over a reasonable portion of the orbit, we have placed wp, meaning moderate to weak total proton energy. Three events have been labeled with a P because the proton energy flux was very large. For our own work we have named these "proton events."

In the electron precipitation columns we have defined collocation of electron energy peaks and radar aurora as coincidences. This means that radar aurora seemed to be located in the same regions in which there is a local maximum in the energy flux of precipitating electrons. We have also counted the number of isolated radar aurora and peaks in electron energy flux that were not associated with each other, and have called these anti-coincidences. We have done the same for proton precipitation. The last column gives a measure of the simultaneity of the radar and satellite measurements (during the earlier experiments the ephemeris data available at Homer was less accurate than we would have desired).

The determination of these correlations can be quite subjective. In some areas there will be many, closely spaced, intense precipitation peaks. In some cases the radar auroral boundary may be located at the particle precipitation peak. We have tried to be consistent in calling these coincidences. The subjectivity of the interpretation should be evident by the way we have filled out our columns.

Examination of the table reveals the following:

(1) In the auroras that we have not categorized as proton events, there are no coincidences between radar returns and peaks in proton precipitation.

(2) There are some coincidences between peaks in electron energy fluxes but there are many more anti-coincidences.

(3) For two of the proton events, since radar aurora is nearly everywhere, there are many peaks in energy deposition, so that coincidences are everywhere and may therefore not be meaningful.

(4) The electron coincidence enumeration suggests to us that coincidences between peaks of electron precipitation with radar aurora are almost a random phenomenon. There appears to be no clear-cut trend.

In summary, we believe the data in Table 2 indicate that except for intense proton events, radar aurora is not coincident with peaks in proton energy flux. Peaks in electron precipitation may or may not be coincident with radar aurora; we have not discerned a meaningful trend although there seems to be a tendency toward anti-correlation.

4.3 Production of Nighttime E-Region Ionization by Particle Precipitation

The previous section showed that regions of <u>peak</u> energy deposition did not seem to be located, necessarily, in regions where radar echoes were obtained. In this section we study whether any precipitation at all was occurring in the radar-reflecting regions, to determine whether particle precipitation can explain the existence of nighttime E-region ionization necessary for these reflections.

All 14 satellite passes occurred during E-region darkness. Radar aurora requires the presence of E-region ionization. Studies of radar/visual aurora correlation show that the visual forms do not necessarily correlate well, in position, with radar returns. One is therefore led to wonder what produces the ionization that is necessary for radar scattering. We shall be concerned with the presence or absence of any particle precipitation in regions from which auroral echoes are obtained.

We have investigated the particle flux precipitation in regions from which radar echoes were being obtained even if these were not regions of peak energy flux. Table 3 presents these results. On four of the passes listed in the table there were radar echoes from regions in which particle precipitation levels were below the detection threshold of the satellite. For two of these passes the simultaneity of the measurements was poor due to poor pre-pass ephemeris data, so that comparisons probably are not too meaningful. The two passes labeled A2964 and A2995 had regions of no detectable electron or proton precipitation where radar echoes were being obtained. However, in these cases the particle flux nearby was decaying very slowly as the satellite approached the scattering regions. We are led to believe, but cannot prove, that the particle fluxes were below but very near the threshold detection level.

We estimate that, provided particle energy is great enough to penetrate to 110 km altitude, the threshold detection flux of the satellite counters produce at this altitude an electron density of about 7×10^4 if the particles are electrons, and 2×10^4 if the particles are protons. The spatial variation of these particle flux intensities on the two passes A2964 and A2995 leads us to believe that electron densities were of the order of 5×10^4 el/cm^3 in regions from which radar backscatter was obtained but in which precipitation intensity was below satellite detection threshold. These data suggest that there

was some particle precipitation flux wherever radar aurora was found. The data of Table 3 and our other inferences imply that the nighttime, widespread particle precipitation as measured by the OV1-18 during our 14 passes is adequate to produce the ionospheric electron densities needed to explain observed radar aurora.

Table 3

COINCIDENCES AND ANTI-COINCIDENCES BETWEEN RADAR AURORA AND MEASURABLE PARTICLE PRECIPITATION

Pass Number	Number of Radar Clutter Regions	Measurable Electron Precipitation in Region of Radar Aurora	Measurable Proton Precipitation in Region of Radar Aurora	Simultaneity in Time of Radar Measurements and Satellite Pass
A157	2	Yes	No	Good
A232	2	Yes	Yes	Good
A369	4	3 Yes 1 No	2 Yes 2 No	Radar 1 minute late--radar aurora moving south
A388	1	No	No	Good
A431	3	3 Yes	2 No 1 Yes	Satellite 3 minutes early
A518	2	Yes	No	--
A624	2	Yes	No	Good
A641	3	No	No	Poor--radar map is 13 minutes later than satellite pass
A657	1	Yes	No	Good
A676	1	Yes	No	Good
A751	2	Yes	No	Good
A2964	2	1 Yes 1 Part yes, part no	No	Good
A2979	1	Yes	Yes	Good
A2995	6	4 Yes 2 No	4 Yes 2 No	Good

5 CONCLUSIONS AND SUMMARY

Our measurements reported above demonstrate that the magnetic aspect dependence of radar aurora is only very weakly dependent upon frequency. Our measurements down to a frequency of 50 MHz were made during a quiescent auroral period in which a stable, radar-auroral arc was present. These data seem to be in conflict with those of McDiarmid and McNamara.[1] Our technique for analysis of the 50-MHz aspect sensitivity cannot be applied at times of intense radar aurora. It could be that another scattering mechanism whose magnetic aspect properties are very much weaker is present during intense aurora.

We infer from our measurements that the magnetic aspect dependence at 3,000 MHz is like the dependence we measure at lower radar frequencies. Over a very broad frequency range we find that the echo power versus frequency is reasonably well fitted by an exponential form. The scale-frequency that categorizes the slope of the frequency dependence is found to vary from time to time in a manner that is not yet understood.

Cross-correlation of radar echoes with particle precipitation on the night side of the auroral oval indicates that there is poor correlation between the location of radar aurora and peaks in electron energy flux. Except for two periods of very widespread proton precipitation and radar aurora, during which a meaningful measurement cannot be made, we find that radar aurora and peaks in proton energy flux are never collocated. We also infer from the precipitation measurements and from estimates of E-region ionic chemistry that the ionization needed for radar reflections during nighttime periods is produced by particle precipitation.

ACKNOWLEDGMENTS

The authors gratefully acknowledge the support provided for various facets of this work by the Defense Atomic Support Agency, the National Science Foundation, and the Rome Air Development Center.

REFERENCES

1. D. R. McDiarmid and A. G. McNamara, "VHF Radio Aurora: Simultaneous Observation of Auroral Ionization by Two Separated Radars," Can. J. Phys., Vol. 45, p. 3009 (1967).

2. H. F. Bates and P. R. Albee, "Aspect Sensitivity of HF Auroral Echoes," J. Geophys. Res., Vol. 74, p. 1164 (1969).

3. J. E. Evans and R. G. Johnson, "Auroral Input-Output Measurements," Contract Nonr-3398(00), Task No. NR 087-135, Lockheed Missiles and Space Company, Palo Alto, California (10 March 1966).

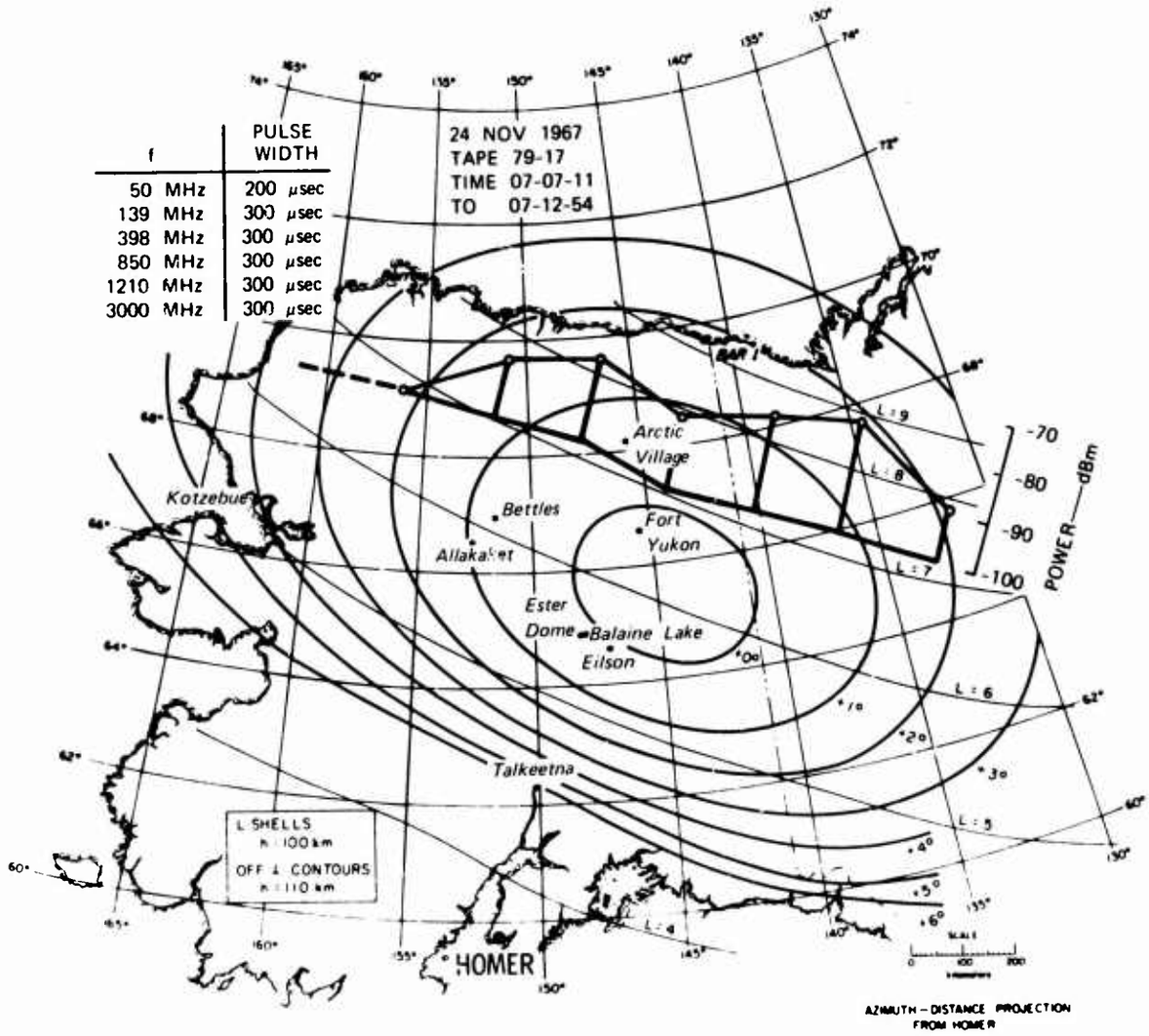

Figure 1 Map of Position of Radar Auroral Arc at 07:07 AST--24 November 1967

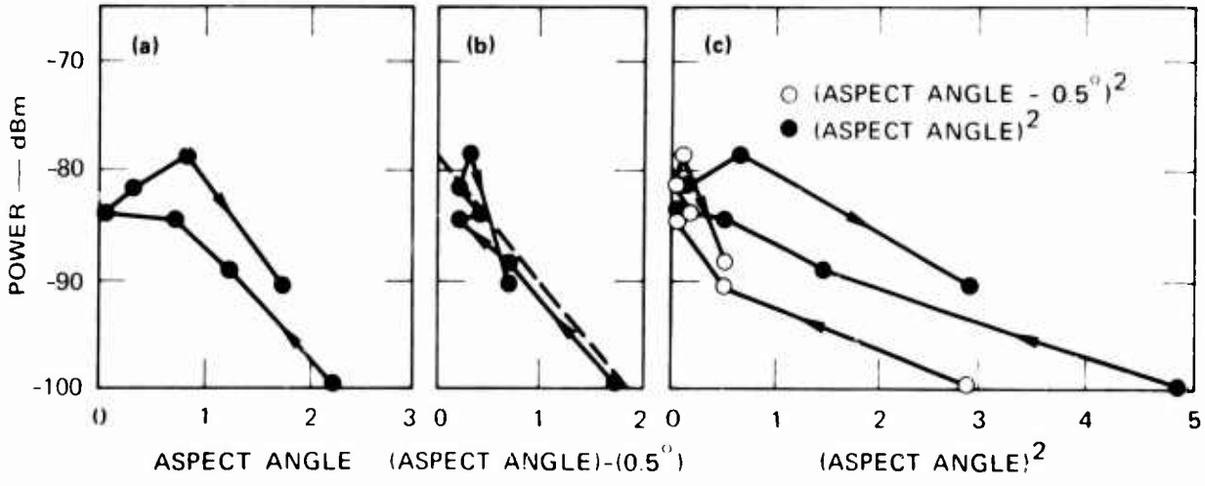

Figure 2 Scattered Power in Decibels at 398 MHz for Radar Auroral Arc of Figure 1 Plotted vs. Several Functions of Aspect Angle

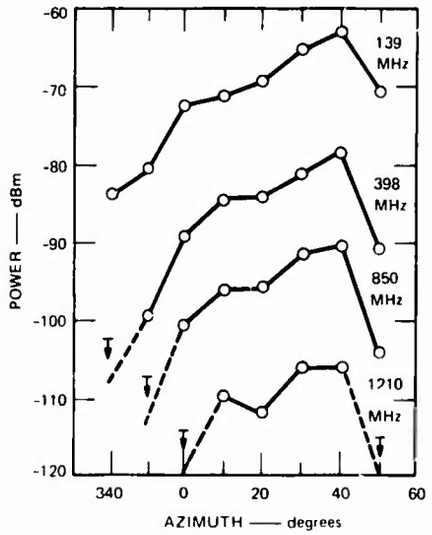

Figure 3 Scattered Power in dBm vs. Azimuth for Four Frequencies--Data from Radar Auroral Arc of Figure 1

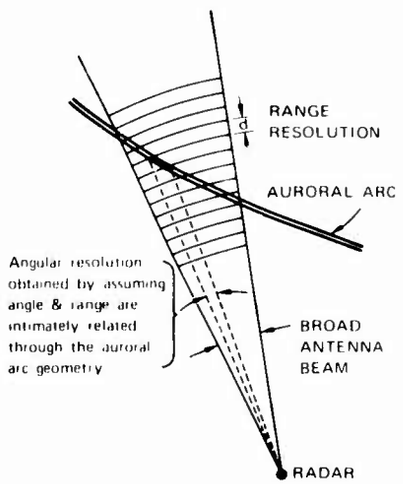

Figure 4 Diagram Illustrating Geometry of Auroral Arc That Allows for High Angular Resolution at 50 MHz Through Equivalence of Range and Angle

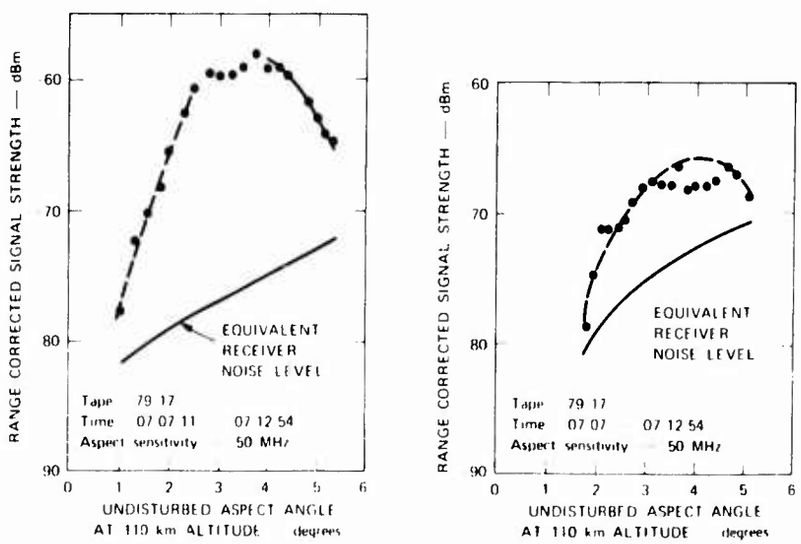

Figure 5 50-MHz Signal Strength vs. Calculated Magnetic Aspect Angle Along the Western and Eastern Limbs of the Auroral Arc of Figure 1

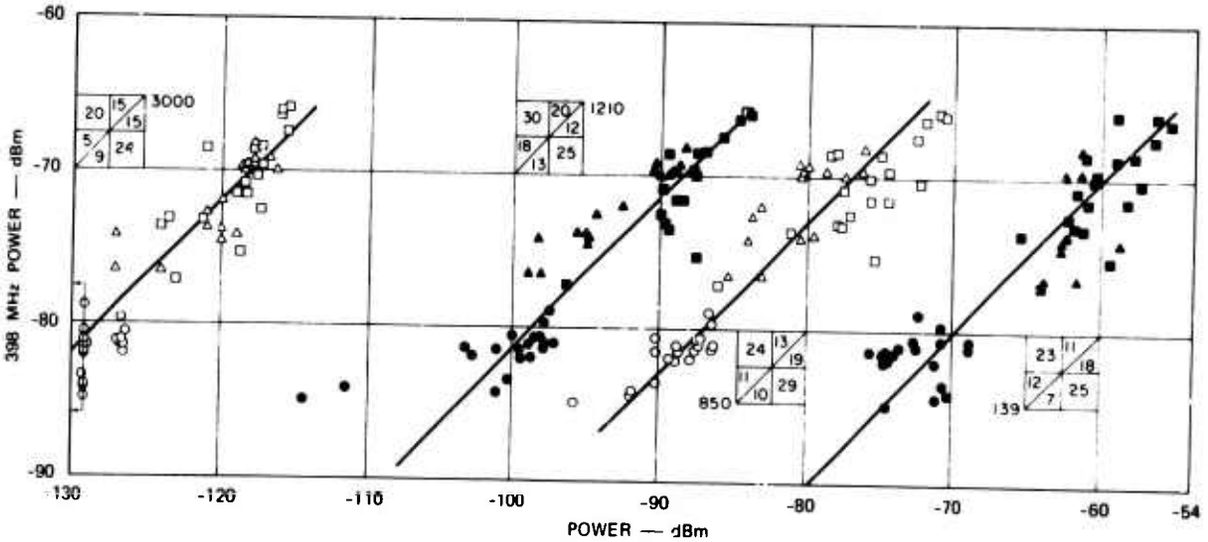

Figure 6 Scatter Diagrams of Signal Intensity vs. Simultaneous 398-MHz Signal Intensity for All 55-Second Integration Periods. (Numbers in boxes show distribution of data points about straight-line fits by eye.)

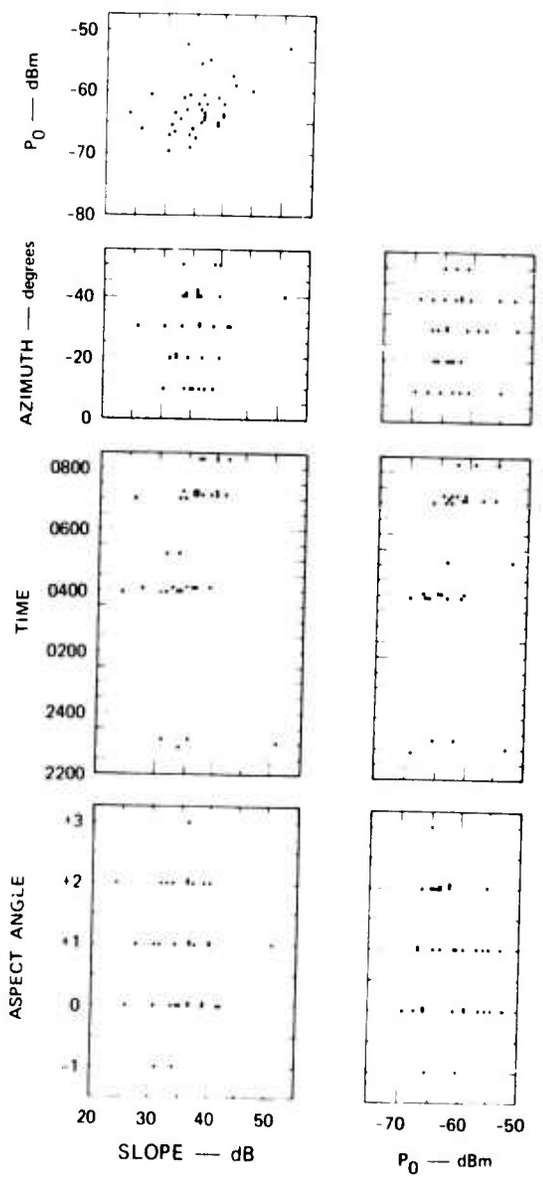

Figure 7 Scatter Diagrams for Slope and P_o vs. Various Quantities

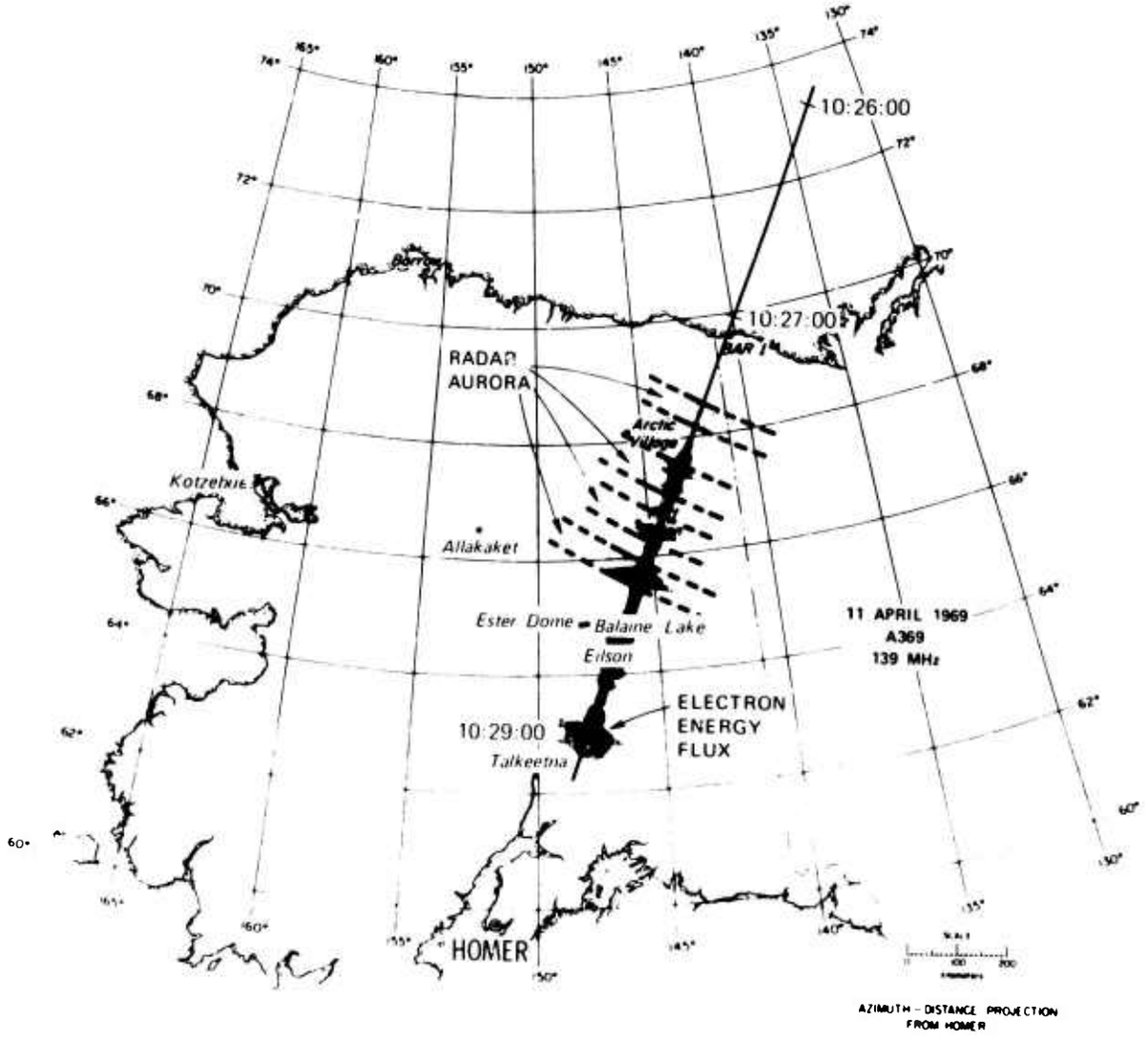

Figure 8 Electron Energy Flux and Radar Aurora Along OV1-18 Track--11 April 1969, 10:26-10:29 AST

SOME PROPERTIES OF RADAR AURORAL ECHOES AS OBSERVED AT A FREQUENCY OF 1295 MHz

T. Hagfors
M.I.T. LINCOLN LABORATORY
Lexington, Massachusetts
U.S.A.

SUMMARY

Some recent observations of radar aurora made at a frequency of 1295 MHz from Millstone Hill (42° 38' N, 71° 30' W) are described. From maps of power returned versus azimuth, elevation angle and range of specific events of diffuse aurora it is found that a mean height of auroral echoes is close to 110 km, that the half power thickness is 7 km and that the power scattered drops 3 db when the aspect angle with respect to the magnetic field is increased from zero to 0.4°. Spectral analysis of echoes returned from a volume of 10 x 10 x 10 km^3 with a resolution of 600 Hz reveals a great variety of spectra, many of which are narrow and displaced as if from an ion-acoustic density instability. Other spectra are wide and contain contributions from approaching and receding waves simultaneously. The wide spectra apparently are associated with regions where the radar beam is normal to the electrojet current. Simultaneous observations of scintillation of satellite signals and radio aurora has failed to uncover any detailed relationship between the two phenomena. Simultaneous observations of auroral echoes and particle precipitation show that radio aurora may be observed without any measurable electron precipitation.

1. INTRODUCTION

Much work has been carried out over the last fifteen years to study so-called auroral radar echoes. Auroral radar echoes may be a misnomer since attempts to correlate the occurrence of radar echoes with visual auroral activity has proven mostly negative[1]. An association of radio aurora and particle precipitation has been sought, but no one-to-one relationship has been found[2]. There appears to exist only a general statistical relationship between the radar aurora and other geophysical phenomena it might reasonably be expected to correlate with.

At the moment the general consensus is that the occurrence of radar aurorae is closely related to the presence of large scale electric fields and that the direct cause of the wavelike density irregularities seen by the radar system is a plasma instability. There is sufficient confidence in this explanation to cause Unwin and Knox[3] to suggest the study of radio aurora as a means of obtaining information of electric fields in the auroral ionosphere. This technique has in the past been used successfully for some time to study electric fields in the equatorial ionosphere[4] where plasma instabilities similar to the ones occurring in the auroral ionosphere regularly are found.

The theory of the origin of the irregularities which has received the widest acceptance is the one due to Farley[5] and Buneman[6]. The condition for spontaneous growth of the density waves is found by equating to zero the longitudinal dielectric constant of the medium allowing for a relative drift of electrons and ions. A critical relative velocity is found, depending on scale size, angle of the wave normal with respect to both the magnetic field and drift direction and on the collision frequency of ions with neutrals. Conditions for growth are thus found, but precious little can be said about the final state of the plasma after non-linear effects have stopped the growth (see, however Skadron and Weinstock[7]). One suspects that the frequencies with the most rapid growth will dominate in the spectral distribution. Some of the spectra observed, e.g., see Balsley[4], seem to bear this out, at least in the equatorial electrojet. However, often the spectra are considerably widened so that both positive and negative frequencies are represented. This could either be caused by the local fluctuation spectrum itself or by a smearing effect due to large resolution cells so that the observed volume may encompass a region of varying electric field, conductivity, neutral drift, precipitation etc. To provide further insight into the scattering mechanism it is, therefore, desirable to analyze the signal with the greatest time space and frequency resolution possible. For several excellent reviews of work on radio auroras the reader is referred to Booker[8], Chamberlain[9], Hultquist and Egeland[10] and Lange-Hesse[11].

In earlier work at Millstone, reported by Newell and Abel[12] and Abel and Newell[13] radio auroral echoes observed during the afternoon period 1700-2100 were collected on 26 days during the period May 1965 to January 1966. It was found that the echoes were returned from a layer-like region having a thickness of 5-20 km and located at an average height near 110 km. The echoes were strongly aspect sensitive, and none were obtained from regions where the aspect angle was greater than about 3°. Both the occurrence of auroral echoes and the southernmost limit of the echo region were found to correlate with the magnetic index Kp. The Doppler spectra of the echo region show approaching velocities to the east of the magnetic meridian and receding velocities to the west with a rapid changeover at the meridian. The magnitude of the Doppler offset and the variation of offset with azimuth thus favored the two-stream plasma instability theory of Farley as an explanation of auroral echoes. It was also suggested that the direction of plasma wave motion together with the variations of electrojet current with altitude may explain the presence of echoes at the magnetic meridian (not expected from the Farley theory for an east-west current).

Further measurements were made during the period January-March 1968 and included samples on 8 days. Pulse lengths of 500, 100, 50 and 10 μsec were used. For various practical reasons the Doppler data could not be retrieved. The signal-to-noise ratios were considerably higher than those measured in 1965 and absolute volume reflectivity values were up to 20 db above previous values; calibration difficulties brought about essentially by the much stronger signal do not allow an exact comparison to be made. The strong signal also made the side-lobe effects much more in evidence in synthesized range-height cross-sections. Beam-width pul -length smearing was also evident as absolute reflectivity measurements made at 500 and 100 μsec in the same echo differed by up to 6 db. A complete stepped-scan was made with each

Paper presented at AGARD Technical Meeting in Lindau/Harz in September 1971.

pulse length in turn and the procedure repeated for eight hours so that this difference is not simply a consequence of time changes in the scattering volume.

The present paper describes some selected observations made at the Lincoln Laboratory Millstone Radar at a frequency of 1295 MHz during 1970-1971. It is not the purpose of the observations to provide additional morphological or temporal data on the phenomenon. Rather, the observations were designed primarily to provide more detailed information on the frequency spectra of the scatter signals with higher spatial and frequency resolution than before and also to obtain some further information on height variation of the scattering and aspect sensitivity at this frequency. No very definite conclusion about the nature of the auroral irregularities is deduced in this paper. The data to be presented will provide details which may prove useful when the complete picture of the origin and nature of the irregularities emerges.

In the next section, we describe the observational techniques, the data processing, the geometry of the site with respect to the geomagnetic field and the auroral oval. In section 3, we present data from a few selected observational periods and extract some of the properties of the observed returns. In section 4, we discuss the results in the light of existing ideas about the nature of the echoes.

2. OBSERVATIONAL PROCEDURES

Two different procedures have been developed for the observation of radio aurora at 1295 MHz at Millstone. In one, the so-called STARE (short time analysis of radar echoes) program, major emphasis is on the extraction of some of the echo properties rapidly, albeit coarsely in order to catch temporal and spatial variations. In the other, the two-pulse program, the emphasis is on the detailed spectral analysis of the returns from a small volume cell, but at the expense of good time resolution.

Before giving any further details about the observational procedures we summarize the parameters of the Millstone radar in Table 1. The pointing is corrected by means of a standard tropospheric correction table corresponding closely to an exponential refractivity profile with a surface refractivity N of 310 units (Bean and Dutton[14]). This should give a pointing accuracy better than 0.1° under practically all conditions. The magnetic field model used to calculate aspect angles uses the Hendricks and Cain multiple field coefficients. The subroutine was supplied by L. Coury of IBM[15]. The field model, which

Table 1. The Millstone Radar Parameters

Frequency	1295 MHz
Transmitter power	150 KW average
	5 MW peak
Pulse lengths	10-4000 μsec
PRF	≤ 50 Hz
Duty cycle	< 3%
System temperature	200°K
Collecting area	210 m^2
Gain	46.7 db
Beamwidth	0.6°
Polarization	Circular
Feed configuration	Cassegrain
Scan rate	< 2°/sec
Antenna mount	Az-El
Latitude	42° 37' 47"N
Longitude	71° 29' 47"W

has evolutionary terms, is repudiated to have an overall accuracy of 1.5° in magnetic field orientation. Figure 1 shows the loci of zero aspect angle to the magnetic field for rays originating at the Millstone radar. The parameter is the altitude above ground. We have also plotted some constant range contours on the plot for convenient reference in the subsequent parts of the paper.

2.1 The Stare Observations

The Stare program performs several tasks. It directs the antenna in either of two modes, continuous or stepped scanning. In the former a specification is made of the scan rates and the extremes of the scan and the data integration time must be chosen with regard to scan rate and the width of the polar diagram. In the latter of the two modes, the stepped scan mode, one can select either an azimuth or an elevation scan and the step size and scan extremes must be specified. During the data integration the antenna sits in a fixed position and only moves between integration times. This is the mode most often used.

The program also sorts and to some extent analyzes the data during the data integration. The system transmits alternately 50 μsec and 500 μsec pulses, the time between consecutive pulses being 20 msec. After the 50 μsec pulse a 4 msec data window is started at a time delay corresponding to an altitude of 85 km - appropriately rounded off to the nearest 75 km range interval. Samples are taken at the output of a linear detector every 50 μsec. These samples are digitized and transferred to a computer memory. The filtering preceding the linear detector is such that it matches the 50 μsec transmitter pulse. A 2 msec window follows for the purpose of sampling baseline noise and another 2 msec window follows somewhat later during which time interval a noise tube is fired into the front end of the receiver

for calibration purposes. The 500 μsec transmitter pulse starts 19.6 msec after the 50 μsec pulse and is received in a filter bank matched to the 500 μsec pulse. The center frequencies of the filters are staggered by 2 kHz and are assigned to odd integral frequency offsets in kHz. There are 24 such filters in all. To convert the 24 parallel outputs to a time sequence of numbers the signals are applied to a tapped delay line. The output of this delay line is linearly detected and sampled every 20 μsec. These samples are, in turn, digitized and transferred to the computer memory. Data is also taken during a subsequent "window" to establish the baseline and another "window" to sample the noise pulse and thus calibrate the filter bank. A number of different display forms may be produced from the raw magnetic data tapes. Some of these will appear below in the description of observational results. Since the transmitter power is constantly monitored, the radar cross-section can be computed from the system parameters.

2.2 The Two-Pulse Observations

In the Stare program frequency resolution of 2 kHz can only be obtained with a range resolution of nearly 100 km. In order to improve on the system resolution a two-pulse scheme was devised. In this scheme the transmitter emits double pulses with a variable time separation $\Delta\tau$. The time separation is being stepped up in units of 50 μsec and the maximum time separation is 1.6 msec. At the receiver end the samples are cross-correlated with a time delay matching that of the transmitted pulse pair. The cross products are averaged and a complex autocorrelation function is formed. This function is corrected for various instrumental effects, the thermal noise contributions etc and the final corrected result is then Fourier transformed to give the power spectrum. The resolution is usually 600 Hz. Twice this resolution was tried but it was felt that the sacrifice in integration time was not worth the increased resolution.

Since in this procedure one must cycle through the various time shifts $\Delta\tau$ many times - it takes a considerable number of interpulse periods to arrive at a correlation function which does not have excessive statistical fluctuations. Typically, the integration period selected is on the order of one minute and the pulse length is usually 50 μsec. During the integration time the statistical properties of the scattering process should stay constant for meaningful results to be obtained.

3. OBSERVATIONAL RESULTS

In what follows we shall show some representative observational results obtained during 1970 and the early part of 1971 using the observational techniques just described. In some cases the observations were made in conjunction with other experiments, such as the observation of particle precipitation above the aurora by means of the OV1-18 satellite or the observation of scintillation of signals from satellites at 400 and 150 MHz. We shall briefly summarize some of these complimentary experiments, but most of our exposition will be concerned with the radar observations alone.

3.1 Power Returned as a Function of Azimuth, Range and Elevation Angle

A search for auroral events with the STARE program was conducted between March 24 and April 26, 1970. Altogether 15 evenings were available for this search and auroral echoes were observed during 13 of these in most cases only as very short-lived events. Later interesting observations of the same type were made during May 24 and 25, 1971 in conjunction with flights of an airplane instrumented for various optical and radio auroral observations by AFCRL. In Figure 2 a-c results are shown for a particularly interesting set of azimuth scans made on March 27, 1970 at true elevation angles of 0.04°, 0.58° and 1.15°, respectively. The cross-section per unit volume -- as indicated on the plots by log (CS) -- turns out to be the same in the three plots to within less than 1 dB. From observations made both prior to and following the ones shown in Figure 2, we conclude that the time variation of the scattering cross-section throughout the volume explored is very slight. The apparent altitude of the peak of the echo region in the three plots ranges from 111.6 km to 112.8 km. We also note that the peak echo intensity appears to fall almost exactly on the same aspect angle (+0.5°) in the three cases. It is, therefore, strongly suspected that the magnetic field model used predicts the direction of the magnetic field erroneously by an amount of 0.5°. Assuming this to be the case and assuming approximate spatial homogeniety so that the shape of the cross section contours are determined only by the magnetic field geometry and the height variation of the cross section, one can deduce the variation of echo strength with off-perpendicular angle This is obtained from the azimuth variation of echo intensity at the range of maximum return. On this basis, it is concluded that for L-band echoes the scattered power falls to half its peak value at an off-perpendicular angle of 0.4°.

In a similar manner a study of the variation of echo intensity along a line of constant aspect angle can be translated to an apparent layer thickness. In this way the apparent thickness between points of half peak cross section is found to be 11.2 km. Since the Millstone antenna beamwidth between half power points is 0.6° the true layer thickness must have been about 7 km.

The spectra associated with the three azimuth scans just discussed are relatively uninteresting. They show a frequency displacement of 2.5 kHz indicating an approaching velocity. At the same time the spectral width is about 6.5 kHz between half power points. The spectra are therefore not typical of those generated by the two-stream instability mechanism which is discussed below.

Figure 3 shows similar contour plots taken on May 24, 1971. The first of the two plots has a striking similarity to the ones taken a year earlier. The second plot, however, shows some structure which indicates that the spatial homogeniety of Figure 2 does not exist. If we were to put the data of Figure 3 to the same analysis as those of Figure 2 one should expect both apparent aspect sensitivity and height variation to come out more rapidly varying than indicated by the data of Figure 2. Tests of the data obtained on May 24 appears to confirm this supposition in that both the height extent appeared smaller and the angular variation more rapid. The frequency spectra studies simultaneously with the May 24 data again showed a generally large width and a small displacement. Figure 4 shows the frequency offset, determined by fitting a parabola to the three highest adjacent points in the frequency spectrum, as a function of azimuth for the two elevation angles in Figure 3 and for ranges near the peak reflectivity. The width of the frequency spectra ranged from 5 to 10 kHz. The frequency offset was less than 2 kHz in general. Again the spectral shape which one would intuitively expect on the basis of a two

stream instability does not always seem to prevail in the data we have obtained. In most cases of our observations from 1970 on, echoes have in general not been strong enough to enable us to trace the apparent Doppler offset through the point where it reverses sign.

One remarkable fact should be observed when comparing the examples shown in Figures 2 and 3. In spite of the seemingly similar nature of the returns in terms of geographic extent, frequency spectra etc., the total cross section per unit volume is over two orders of magnitude greater in the 1970 data than in 1971 data shown.

3.2 High Frequency-Resolution Observations

Because of the relatively long integration time required in the high resolution observation, it is not possible to produce contour plots - as presented in the previous subsection - during a time short enough for the echoing properties to remain statistically stationary.

Figure 5 shows an example of the type of displays which are obtained in non-real time. The heading of the record indicates in the first line the data, the year and the universal time of the record. The second line of the heading gives a run number which is simply a count of the number of runs which has been carried out that particular day. The run time gives the integration time used for smoothing the correlation function. The range indicated on the same line is the range to the spectrum at the bottom of the display. The range to the following spectra is obtained by stepping up the range in steps of 7.5 km from the initial range. The azimuth indication is self explanatory. The two elevation angles shown are the ones recorded before and after the tropospheric refraction correction is applied. The height at the center of the beam is the height computed from the time delay and the refraction-corrected elevation angle. On the left hand side of the spectra is displayed the cross section per unit volume expressed in m^2 per m^3 assuming a filled beam.

The spectra shown in Figure 5 are fairly typical of what is usually observed and comes close to a two-stream spectrum as one observes in the equatorial electrojet[4]. The particular spectra in Figure 5 show that the electrons are streaming toward the observer to the west of magnetic north. This means that the electric current flows toward west at the time of observation in agreement with the classical picture of Sugiura and Heppner[16]. We also observe that the center of gravity of the spectra are displaced toward higher frequency with increasing range or with increasing altitude. It should be emphasized that this behavior is by no means typical. In a great many cases, the frequency offset remains remarkably constant with range or with altitude. An example of this is shown in Figure 6. The actual frequency offset indicated is near 4.2 kHz at all ranges.

We have carefully studied many of the records to discover whether there is a systematic variation of the shape of the frequency spectrum with height at a fixed azimuth and range without conclusive results. We have also attempted to study a possible systematic variation of the spectral shape with latitude for a fixed height on many occasions but again without conclusive results. One major factor preventing us from detecting some of these effects is undoubtedly, the rapid time variation of the spectral properties. Figure 7 shows two time sequences of two-stream echoes obtained at a fixed volume in space of size less than 10 x 10 x 10 km^3. As can be seen there is a variation in the frequency offset to the peak of the spectrum offset and the cross section as shown to the left of the spectra.

So far we have shown high frequency resolution spectra of a type to be expected of a primary two-stream instability only. It turns out that a great variety of spectral types occur. Figure 8 shows another extreme example of frequency spectra. The signal level is quite high and the spectral width is nearly 20 kHz if we may venture to assign a width to this type of spectra. In previous work, for instance, like that of Abel and Newell[13], it was suspected that such wide spectra might be the result of smearing caused by the pulse-length, the antenna beamwidth and in some cases by the coarse frequency resolution. In the present work, we have removed the pulse-length smearing to a large extent and there is probably little frequency convolution. We have of course, not been able to remove the smearing caused by the finite beam. The fact that the character of the spectra shown in Figure 8 do not appear to change appreciably with the antenna beam pointed either below or above the echoing region does indicate that the spectral shape shown is in all likelihood representative of quite small volume elements of the plasma. In Figure 9, we show yet another type of spectra where distinct traces of the upshifted and the downshifted ion-acoustic maxima are simultaneously present. Note, however, that the magnitudes of Doppler shift of the two are different.

Some insight into the origin of the various types of spectra can be obtained by reference to Figure 10. In that illustration a sketch has been made of cases where the spectra are of the narrow ion-accoustic type as represented by an arrow and where they are of the broad type as represented by circles. It can be seen that the narrow ion-accoustic spectra are observed to either side of approximately zero degrees azimuth (geographic) and that the wide spectra are observed primarily inbetween. Presumably the current flows very nearly from east to west geographically and the wide spectra may be associated with the fact that the radar beam is approximately normal to the line-of-sight from the radar in the sector centered on zero degrees azimuth.

From some of the spectra shown in the present report as well as from results obtained at other times, there does seem to be an indication in the data that the sharp "two-stream peaks" are associated with the aspect angle. Weak indications of this circumstance may be seen in Figure 9 if it is observed that zero real aspect angle probably is near + 0.5° nominal aspect angle. A similar indication is evident in Figure 6 although in that case the effect may be masked by a height variation.

We should add that during the time of observations on Nov. 7, 1970 a major magnetic storm took place following a sudden commencement at 0046 UT. Kp indices reported were in the range 6-8 during the observation period and visual auroral displays could be seen with the naked eye from Millstone.

3.3 Relationship to Other Observations

It is of considerable interest to know if there is any relationship between the occurrence of auroral clutter echoes and scintillation of signals from satellites. The latter is thought to be caused principally by irregularities in the F region and only under extremely disturbed conditions would it be expected that the E region would give rise to scintillation effects. Thus, correlation between the occurrence of scintillation and auroral echoes would exist only if the causal mechanisms act at the same time and are in some way related. One way that this could come about would be if both are produced by particle precipitation (albeit by particles of different energy). Another possible coupling mechanism might be that the horizontal electric field in the auroral electrojet could be communicated to the F-region along magnetic field lines to produce corresponding fluctuations of electron density.

In order to test the possibility that the two effects always occur together, we made a series of measurements in which the beacon signals of the Navy-Navigation satellites at frequencies of 150 and 400 MHz were recorded in order to detect both amplitude and phase scintillation effects. Observation of satellite passes were interspersed with auroral radar observations at 1295 MHz. Particular emphasis was placed on observations where a region giving rise to scintillation could be projected down along the magnetic field lines into a part of the E region with favorable geometry for auroral clutter echoes. These observations are summarized in Table 2.

Table 2. Summary of the results of operations in which the occurrence of scintillation of satellite signals was compared with the occurrence of auroral clutter, August-Sept., 1970.

Date	VHF Scintillation Results	L-Band Aurora Results
August 5	Scintillation at VHF on three passes.	No clutter echoes.
August 6	Scintillation on 4 VHF passes.	Trace of auroral echoes after one pass of 3133 at 0239 GMT Az 358° - too weak to record.
August 7	Scintillation on 3 passes.	No recordable aurora.
August 11	Scintillation observed.	No recordable aurora.
August 26	5 passes observed and recorded. Strongest scintillation seen so far.	No trace of aurora.
August 27	Weak to normal scintillation on two passes.	Weak aurora seen - no direct association with scintillation.
August 28	Recorded one intensely disturbed and three moderately disturbed passes.	Weak auroral echoes seen and recorded - no direct association with disturbed passes.
September 1	Moderately scintillating passes. No obvious detailed correlation.	Weak auroral activity- data recorded and analyzed.
September 8	Several moderately disturbed satellite passes.	No aurora.
September 9	Satellite scintillation moderate, no detailed correlation with auroral echoes.	Aurora observed and recorded.

The conclusion drawn from the rather limited set of data obtained is that there is little detailed correlation between L-band radio aurora and the occurrence of F-region scintillation effects.

Attempts were also made to correlate the occurrence of radar aurora with observations of particle precipitation as observed in the satellite OV1-18. This satellite contains a number of instruments for observing precipitating electrons and protons (see Hagfors et al.,[2]). In this experiment the mean orbital elements of the satellite were used to predict the occurrence of favorable passes. For these, the satellite trajectory was projected down along magnetic field lines to determine the locus of points where the radar beam from Millstone Hill intersects the field-line at right angles, or the locus of points at a height of 107 km, i.e., where auroral echo activity appears to maximize. The magnetic field model used in this projection procedure was calculated from the Hendricks and Cain multipole coefficients. The calculations carried out for several OV1-18 passes showed that the height to the point of perpendicular intersection of the beam and the magnetic field generally changed very rapidly during the pass. On the other hand, the aspect angle at a constant height remained reasonably constant and for many passes stayed within 1.5 degrees of being perpendicular to the magnetic field during the entire pass. Hence, we chose to track the projection of the satellite orbit onto an altitude 107 km above ground. This procedure should serve to maximize the correlation between the events seen by the satellite and those seen by radar.

During the time of a satellite pass, the antenna would scan along the pre-calculated trajectory of the projection point in order to determine the spatial distribution of echo intensity. Later this could be compared with the particle measurements on board the satellite. These correlative measurements were carried out at Millstone from March 27 to April 26, 1970 using the STARE mode of operation described above. During this period there was one particularly favorable pass of the satellite OV1-18 on revolution 6008. Fortunately, during this pass, which occurred in the early afternoon, strong auroral echoes were observed along the predicted trajectory. Figure 11 shows the predicted range from Millstone and the aspect angle with respect to Millstone at an altitude of 107 km plotted against universal time.

The STARE program was run with an integration time of 3 seconds. Significant echoes were observed during the pass below 0.70° elevation angle. If it is assumed that during the brief observation interval the scattering behavior did not change, it is possible to deduce, from the elevation angle dependence of the echo power observed at a given range, the height and the thickness of the scattering layer. In order

to simplify the task, the beam pattern of the antenna was approximated by cylindrically symmetric function with a Gaussian cross section whose half power width was made 0.6°. The layer was also assumed to have a Gaussian cross section in the vertical plane. The height of the layer peak and the thickness were left free to be determined by the observations.

By carrying through such a fitting procedure, it was possible to construct a contour diagram of scattering cross section as a function of height and the geodetic latitude of the satellite, as shown in Figure 12. The contour levels are in 2 dB steps and the 20 dB level corresponds to a cross section of 10^{-14} m^2/m^3. As can be seen there is a steady increase in echo intensity with latitude toward the point where the echoing region disappears below the horizon. The height of maximum intensity is at 112 km, and there is a tendency for the height to decrease somewhat with increasing latitude. This height dependence could be caused by the aspect sensitivity of the returns. The point of exact perpendicularity to the field lines lies above 112 km by an amount that is decreasing with increasing latitude. We also note that the echoes extend down to satellite latitude of 51.2°.

The frequency spectra of the returns during the pass were obtained with a frequency resolution of 2 kHz over range intervals of 75 km, and show that the half power widths of the spectra are typically 5 kHz, and that the center of the spectra are all displaced toward negative offsets corresponding to motion away from the observer. The negative frequency offset is approximately 1.5 kHz, and would correspond to a drift velocity of 200 m/sec. If this motion were due to an electric field applied in the east-west direction, the required strength of the field would be about 10 mV/m.

In the satellite, both proton and electron counters showed precipitation to be present. However, measurable electron precipitation, i.e., flux above 10^{10} electrons/m^2 -sec-sterad, was only observed to the north of satellite latitude 56.3°. Proton flux, was, however, observed close to the latitude where echoes were present. Figure 13 shows the integrated proton flux above 14 keV as a function of satellite latitude. As far as can be determined from the scant data available the proton distribution was isotropic.

In order to independently determine the presence of a current along the auroral oval of sufficient strength to give rise to the density fluctuations seen by the radar, the magnetograms for Great Whale River Observatory were examined. At the time of the pass the deviation from quiet time conditions in horizontal intensity H was +249.5γ and the deviation in declination D was +31.2. In order to obtain some idea about the currents and the drift-velocities which may have been involved, we assumed a plane infinite current sheath over the station, took the electron density to be 1.5×10^{11} m^{-3} which corresponds to a plasma frequency of 3.5 MHz, and took the current sheath to be 10 km thick. With these parameters, we obtained a relative electron/ion drift velocity of 882 m/sec and the direction of drift to be due East (geographic). Note that our argument disregards earth currents. Inclusion of earth currents may increase the required drift velocity by some 30%. It is, therefore, concluded that the electron velocity is quite adequate for a two-stream instability to develop. The angle between the direction of flow and the line-of-sight of the radar is, however, not very favorable and it is probable that the irregularities seen may not be primary two-stream irregularities, but rather secondary ones arising through non-linear interactions as described by Dougherty and Farley[17]. This may explain the fact that the shape of the frequency spectra is not typical of the two-stream type. The direction of electron flow and the mean frequency displacement are in agreement.

4. DISCUSSION

The cause of the irregularities observed in all likelihood is the two-stream instability discussed by Farley[5] and by Buneman[6]. Since these theories are linear theories very little can be said about the quantitative aspects of the observed fluctuations which undoubtedly result from a balance of growth and non-linear damping of ion-acoustic waves. In keeping with this state of affairs, we shall let the following discussion remain rather qualitative.

The limited height range of the echoes clearly is related to the variation with height of the conductivity. Below 100 km altitude both ions and electrons are constrained by collisions with neutrals and only small electron and ion fluxes can be driven by electric fields. Above 120 km altitude both the electrons and the ions will move across the magnetic field with a velocity given by:

$$\vec{v}_B = \frac{\vec{E} \times \vec{B}}{B^2}$$

In the intervening height range the electron and ion fluxes will be different and an electric current will result.

The relative drift velocity required for growth was worked out by Farley based on typical values of temperature and collision frequencies for radar frequencies up to about 500-600 MHz. For higher radar frequencies the wavelength cannot be regarded as very much larger than the gyroradius and the numerical results become inaccurate. Extrapolating Farley's results to 1300 MHz, it appears that the critical relative drift velocity is approximately 1 km/sec along the line-of-sight for growth to occur. This is based on $\nu_e = 2.6 \times 10^4$ sec^{-1}, $\nu_i = 1.5 \times 10^3$ sec^{-1} and T = 230°. The collision-model used is the BGK one. Calculations made by the author based on the diffusion approximation for certain specific examples have given critical velocities only four percent higher than those of Farley's for the same assumed collision frequencies.

Some idea of the strength of the electric field driving the current may be obtained in certain cases. For the event of November 7, 1970 described above, it will be recalled that the spectra had the appearance of narrow lines being displaced from zero at all angles except for a 20° sector centered on geographic north. If we assume that the line spectra indicate primary excitation of ion-acoustic waves, we must assume that the component of the electron-drift velocity along the line-of-sight must exceed critical even as close to the normal to the current as 10°. This means that the east-west relative

velocity must have been

$$v = v_{crit}/\sin\alpha \approx (10^3/\sin 10^\circ)\ \text{m/sec} =$$

$$5.8\ \text{km/sec.}$$

The corresponding electric field strength in the north-south direction must have been approximately 350 mV/m. Such extremely high electric fields would lead to a considerable increase in the kinetic temperature of the electron gas. If we assume the electrons to be completely thermallized in each collision with the neutrals the mean rate of increase of thermal energy of the electron gas reffered to each electron must be:

$$\frac{\Delta E}{\Delta t} = \tfrac{1}{2} m_e v_D^2 \cdot \nu_e$$

This excess temperature is lost to the neutrals through collision. If the excess temperature is ΔT the rate of loss of thermal energy must be - again referred to a single electron:

$$\frac{\Delta E}{\Delta t} = \frac{3}{2} k.\Delta T.\nu_e.G$$

where G represents the fraction of the excess energy lost in each collision and where k is Boltzmann's constant. Equating these quantities we find for the excess electron temperature:

$$\Delta T = \frac{1}{3} \frac{m_e v_D^2}{k.G}$$

With $G \approx 4.10^{-3}$ one obtains[18] $\Delta T \approx 185^\circ$. Hence, a substantial increase in electron temperature ought to have taken place during this particular auroral event. This is compatible with many rocket observations [Brace et al.,[19] Berthelier and Sturges,[20]] although rocket data often indicates a larger electron heating than this.

One might next ask whether there are other indications in the radar data that the electron temperature was extremely high. Presumably, the position of the peak in the spectrum should be related to temperature. It has been suggested that the position of the peak is determined by the frequency which first goes unstable at the threshold of growth (Camnitz et al., [21]). If this were true the observed spectral shape should vary substantially with aspect angle since the phase velocity at the threshold of growth is a very sensitive function of aspect angle. There is no indication that this is the case in our data, see particularly Figure 6. Lacking a non-linear theory predicting the shape of the spectrum, we might arbitrarily assume that the characteristic acoustic velocity for an equilibrium situation is:

$$v = \sqrt{2\ kT/M}$$

For unequal electron and ion temperature one might put:

$$v = \sqrt{k\ T_{eff}.2/M} = \sqrt{k(T_e + T_i)/M}$$

without a particularly convincing justification. Since the frequency offset of the lines observed is in the range 4-5 kHz we deduce, on the assumption of M = 31 a.u. that:

$$T_{eff} = 400 - 620^\circ K$$

which is consistent with an electron temperature increase of 185° if the ion and neutral temperatures are somewhat above 300°.

If we were to use the "threshold growth" hypothesis of Camnitz et al.,[21] the phase velocity of the density waves would have to be larger than the characteristic acoustic velocity by a factor 1.5 to 2 at our observing frequency (see Farley[5]). This would reduce the above effective plasma temperature by a factor ranging from 2.25 to 4 and would produce impossibly low plasma temperatures. A higher order theory describing the shape of the frequency spectra therefore appears to be required.

The wide spectra often observed undoubtedly may be explained in terms on non-linear plasma wave interaction among primary excited waves. The simultaneous appearance of both the upshifted and the downshifted ion-acoustic peak occasionally observed no doubt is caused by variation in current direction with height as observed by Abel and Newell[13].

The lack of direct correlation between the observation of auroral echoes and the presence of scintillation - producing irregularities above it may at first seem surprising. Both electric fields and precipitating particles should be closely correlated along magnetic field lines. However, as is fairly certain the auroral backscatter is related to D.C. electric fields in the great majority of cases. Large scale scintillation producing irregularities in the F-region, however, apparently have a much more complicated set of causes which are as yet not fully understood (Farley et al.,[22]). Hence, the lack of a direct relationship between auroral clutter and scintillation may not be surprising.

The data we have presented all appear to be in agreement with a two-stream mechanism for the production of the irregularities, either directly or through nonlinear interaction effects. What seems to be lacking at the moment is not observational data, but a good theory which takes all the nonlinear effects into account and can predict the spectral shape, the total scattering cross section, aspect sensitivity, wavelength dependence and other observable quantities. Once such a theoretical development has been completed the observations of radio aurora will develop into a more powerful tool for ionospheric research than it now is.

ACKNOWLEDGEMENT

Valuable contributions to the initial phases of this program were made by M. A. Gordon and M. L. Stone. Interesting and illuminating discussions on the subject matter of this paper were held with R. Newell and D. Cunnold. R. A. Power of Western Electric Co. provided invaluable contributions to the intricate computer programs involved in the data taking and processing.

REFERENCES

1. Gadsden, M. "On the Association of "auroral" Radar Echoes with the Aurora", Planet. Space Sci., 15, 693 (1967).

2. Hagfors, T., R. A. Power and R. G. Johnson, "Simultaneous Observation of Proton Precipitation and Auroral Radar Echoes", Accepted for publication in J. Geophys. Res. (1971).

3. Unwin, R. S. and F. B. Knox, "Radio Aurora and Electric Fields", Accepted for publication in Radio Science (1972).

4. Balsley, B. B., "Some Characteristics of Non-two-stream Irregularities in the Equatorial Electrojet", J. Geophys. Res. 74, 2333-2347 (1969).

5. Farley, D. T., "A Plasma Instability Resulting in Field-Aligned Irregularities in the Ionosphere", J. Geophys. Res. 68, 6083-6097 (1963).

6. Buneman, O., "Excitation of Field Aligned Sound Waves by Electron Streams", Phys. Rev. Letters 10, 285-287 (1963).

7. Skadron, G. and J. Weinstock, "Nonlinear Stabilization of a two-stream Plasma Instability in the Ionosphere", J. Geophys. Res. 74, 5113-5126 (1969).

8. Booker, H. G., "Radar Studies of the Aurora" in Physics of the Upper Atmosphere, edited by J. A. Ratcliffe, p. 355-375, Academic Press, New York (1960).

9. Chamberlain, J. W., "Physics of the Aurora and Airglow", Academic Press p. 217-243 (1961).

10. Hultquist, B. and A. Egeland, "Radio Aurora", Space Science Rev. 3, 27- (1964).

11. Lange-Hesse, G. "Radio Aurora" in Aurora and Airglow, edited by B. M. McCormac p. 519- Reinhold Publishing Corp., New York (1967).

12. Newell, R. E. and W. G. Abel, "Indirect Experimental Evidence for the Existence of Hall and Pedersen Currents in the E Region", Nature 218, 454-456 (1968).

13. Abel, W. G. and R. E. Newell, "Measurements of the Afternoon Aurora at 1295 MHz", J. Geophys. Res. 74, 231-245 (1969).

14. Bean, B. R. and E. J. Dutton, "Radio Meteorology", National Bureau of Standards Monograph 92 pp 1-21, (1966).

15. Coury, L. "Program Solutions to Space Science Problems", AFCRL Report 69-0046 (1968).

16. Sugiura, M. and J. P. Heppner, "The Earth's Magnetic Field", in Introduction to Space Science, p. 5, Gordon and Breach Publishing Co., New York (1965).

17. Dougherty, J. P. and D. T. Farley, "Ionospheric E-region Irregularities Produced by Non-linear Coupling of Unstable Plasma Waves", J. Geophys. Res. 72 pp. 895-902 (1967).

18. Mentzoni, M. "Ionospheric G-factor", J. Geophys. Res. 73, 4444-4445 (1968).

19. Brace, L. H., N. W. Spencer, and G. R. Carignan, "Ionospheric Electron Temperature Measurements and Their Implications", J. Geophys. Res., 68, 5397-5412 (1963).

20. Berthelier, J. J., and D. J. Sturges, "Simultaneous Measurements of Electron Density and Temperature in the Northern Auroral Zone", Planet. Space Sci., 15, 1049-1054 (1967).

21. Camnitz, H. G., R. T. Tsunoda and D. A. Barczys, "Auroral Echoes and the Two-stream Instability", Cornell Aeronautical Laboratory, Inc., Cal. Report No. RG-2460-P-1 (1969).

22. Farley, D. T., B. B. Balsley, P. F. Woodman and J. P. McClure, "Equatorial Spread F: Implications of VHF Radar Observations", J. Geophys. Res. 34, 7199-7216 (1970).

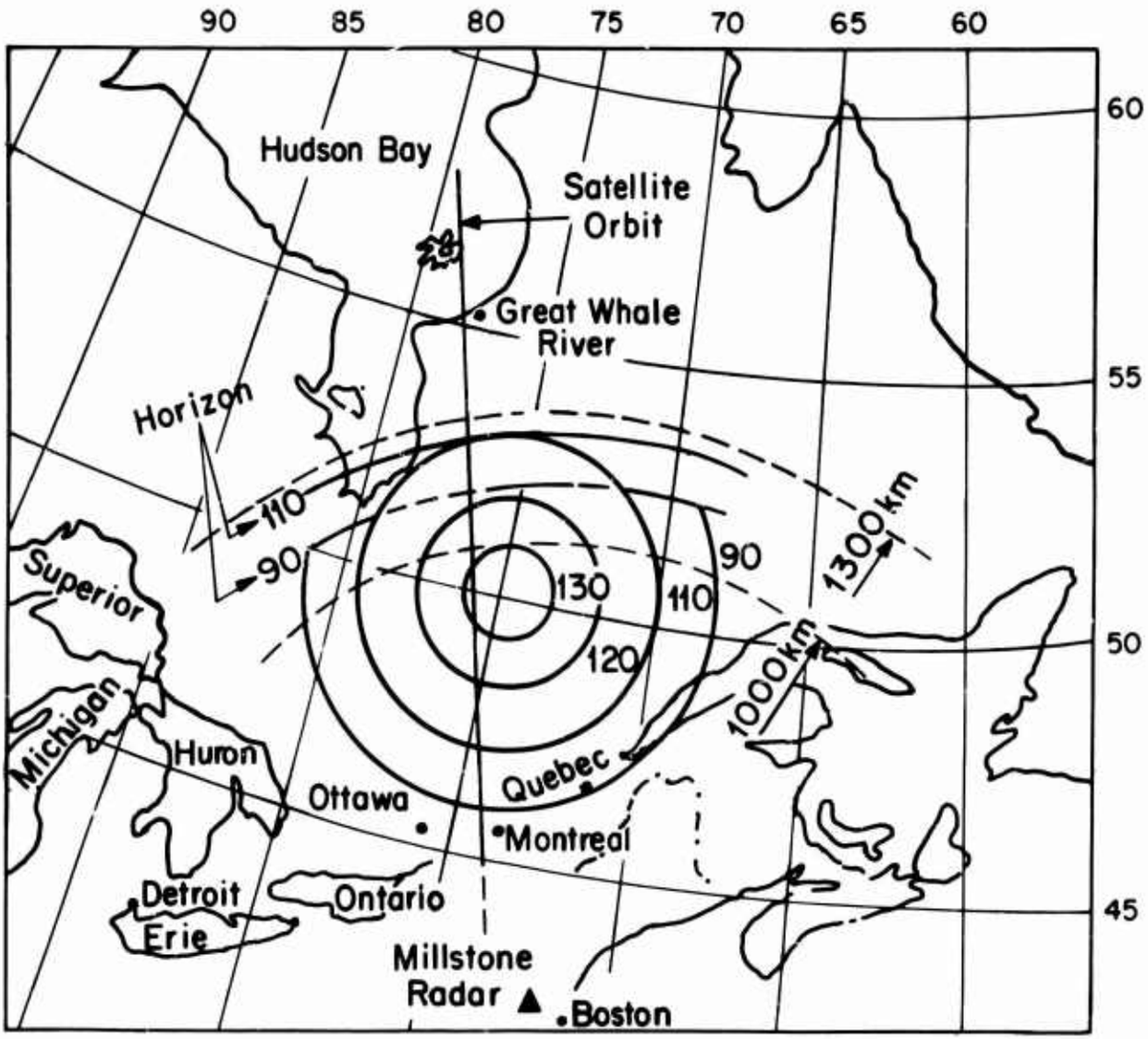

Figure 1. Loci of zero aspect angle with respect to the Millstone radar.

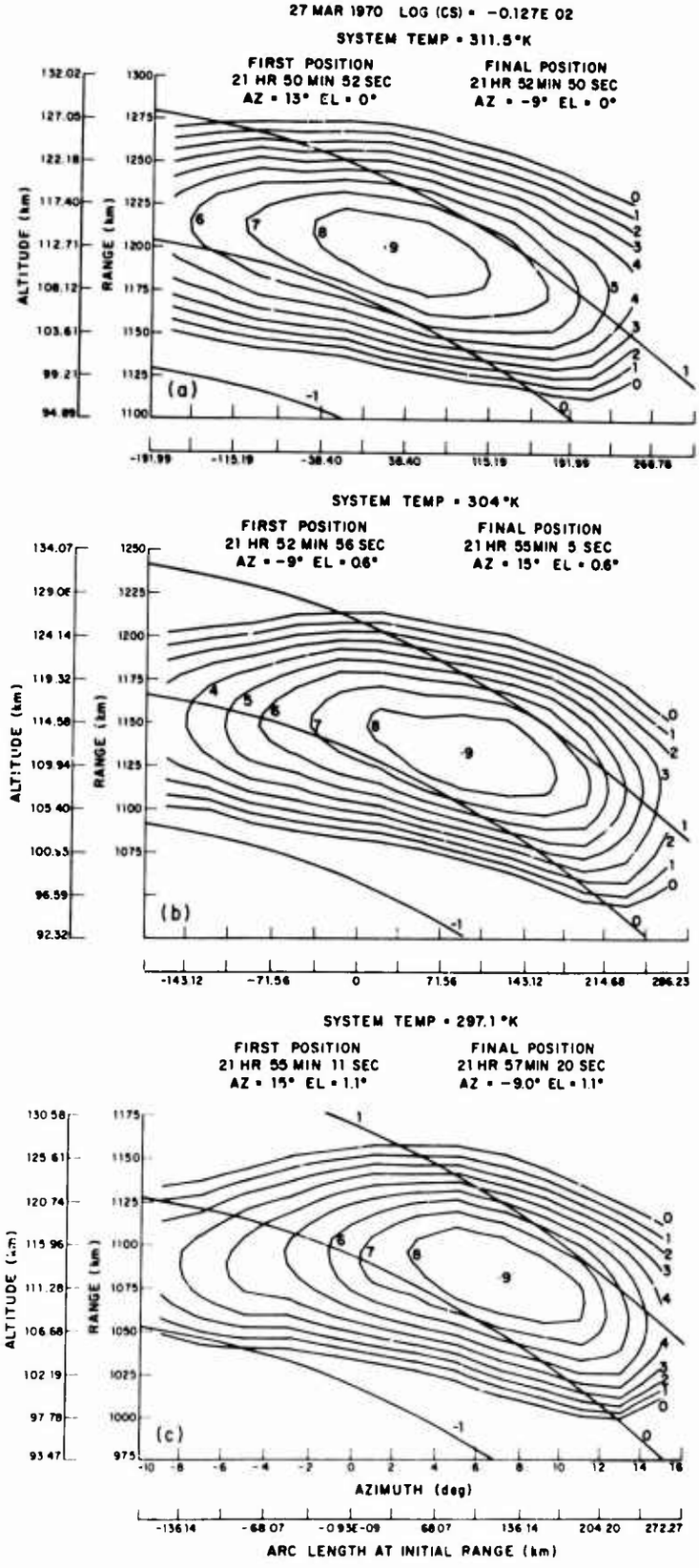

Figure 2. Contour plots of auroral echo intensity vs range and azimuth. Each contour represents a -2 dB step from most intense echo observed. Also shown are locci for off-perpendicular angles of 0 and +1°. Height scale (at left) is for center of radar beam which is, however, about 10 km wide at these ranges. These measurements were made by integrating returns in a digital computer for a number of azimuths at fixed elevations of (a) .04°, (b) 0.6°, and (c) 1.15°.

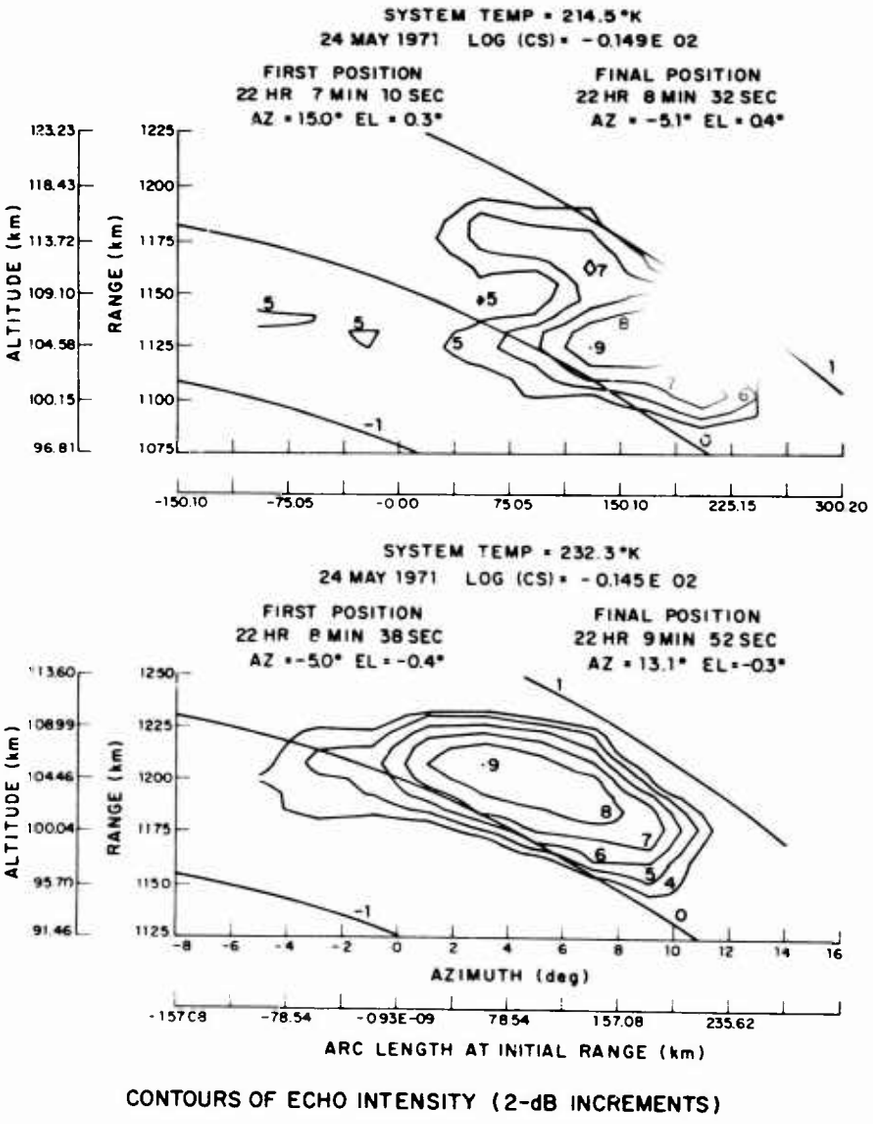

Figure 3. Contours of constant signal strength plotted against range and azimuth for elevation angles 0.35° (top) and -0.35° (below).

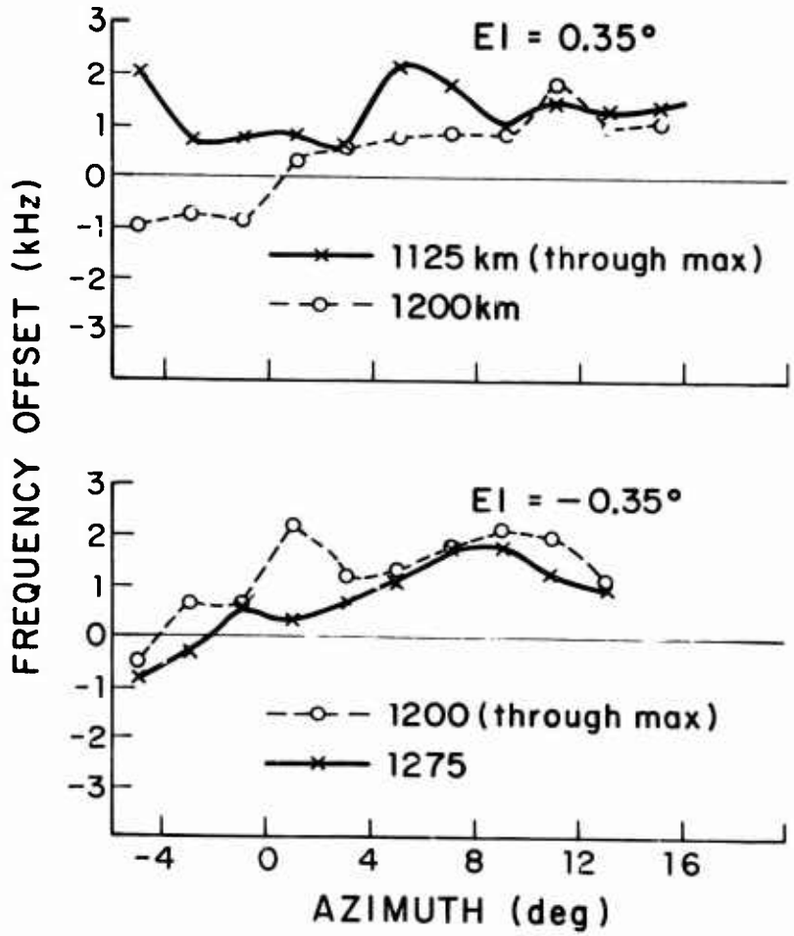

Figure 4. Frequency offsets plotted against azimuth for the same case as in Figure 3.

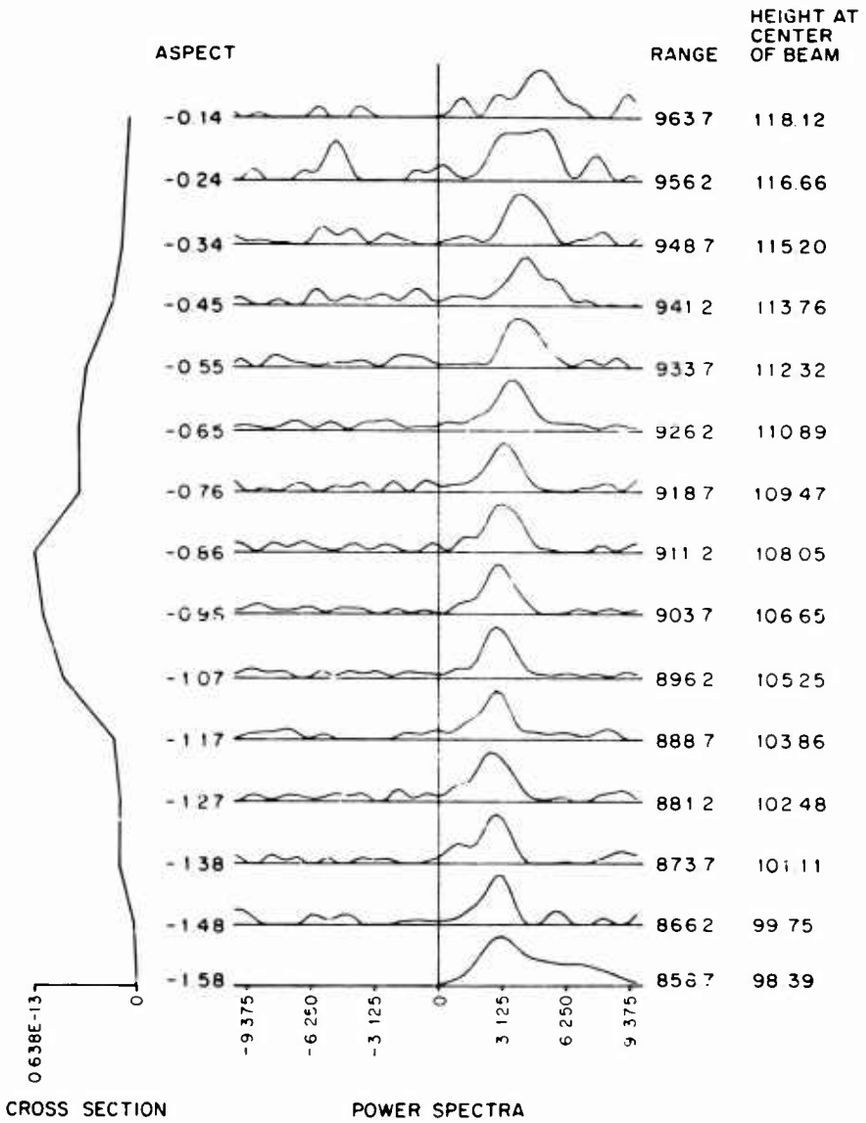

Figure 5. High resolution frequency spectra obtained November 7, 1970.

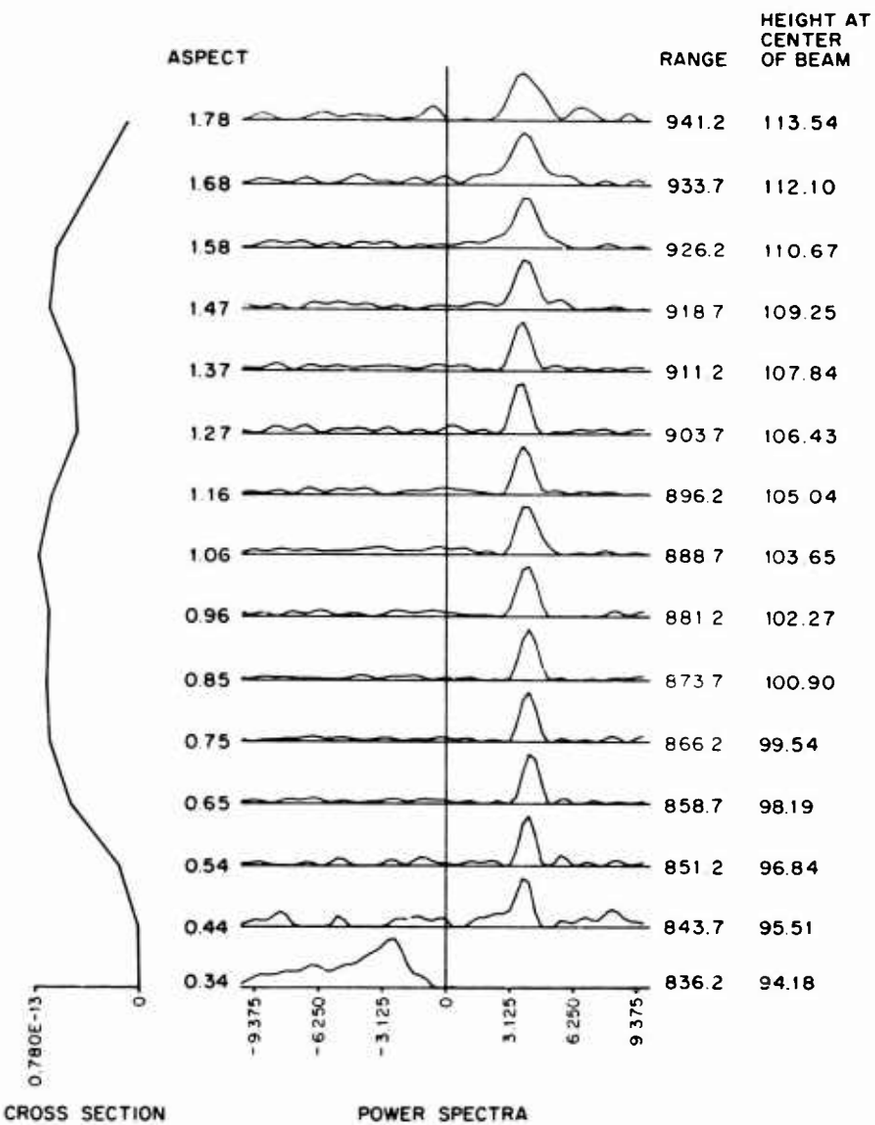

Figure 6. High resolution frequency spectra showing "pure" two-stream conditions.

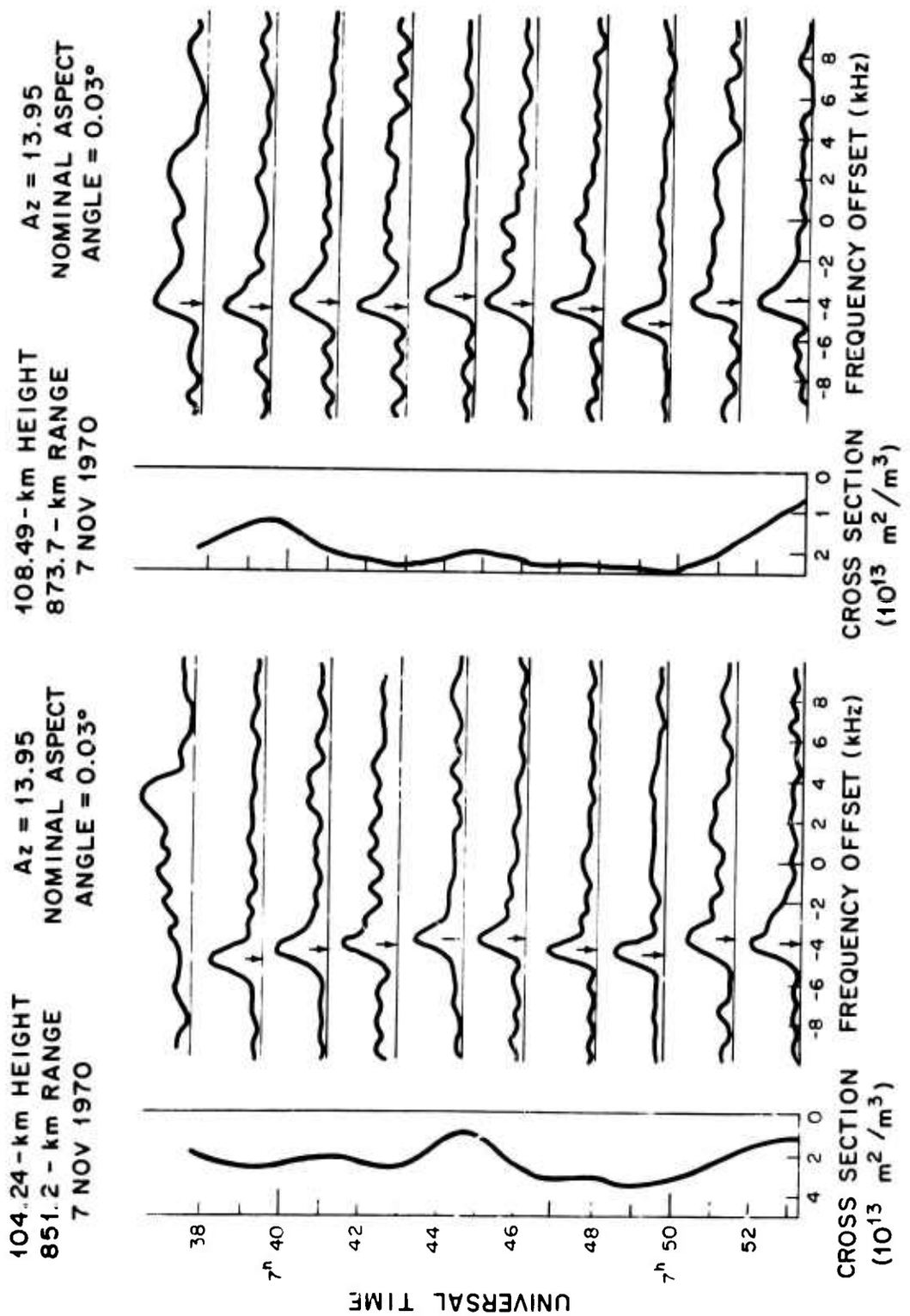

Figure 7. Two time sequences of spectra showing the variability of the spectra at a fixed point in space.

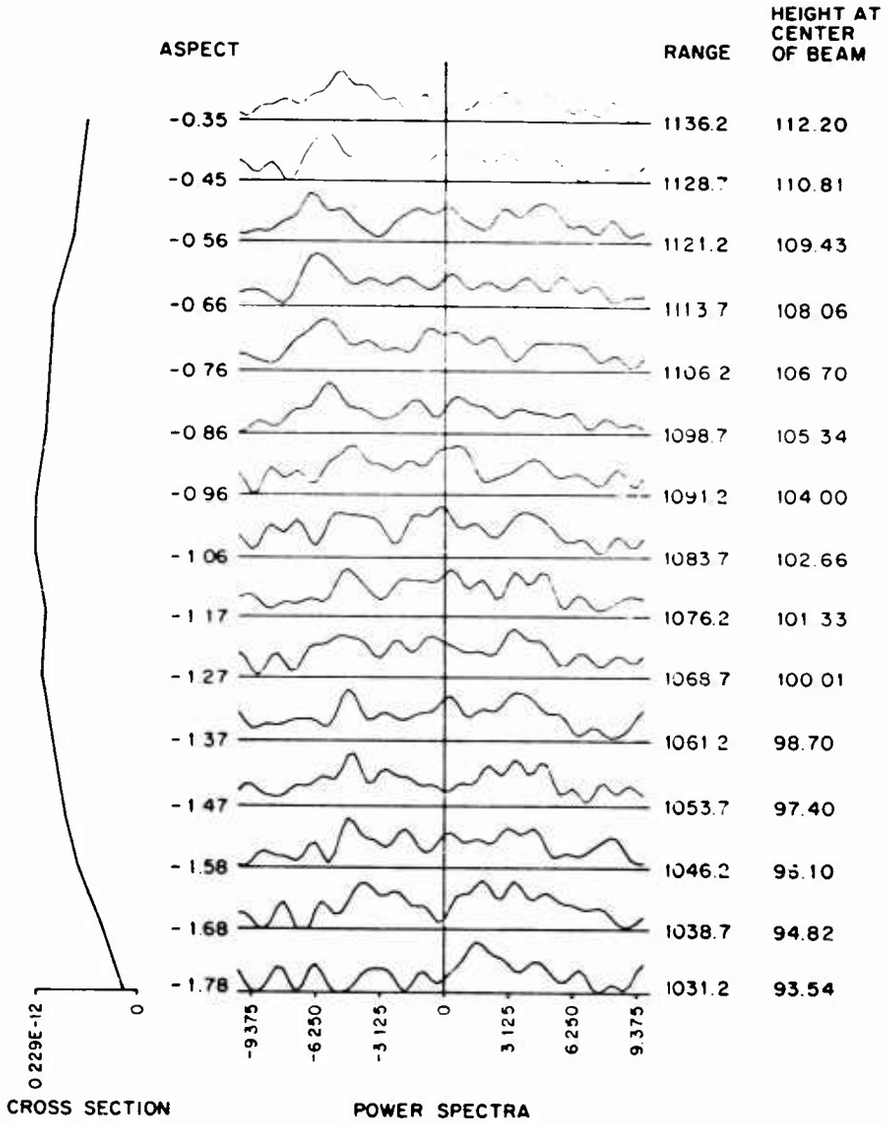

Figure 8. Extreme example of broadened spectra.

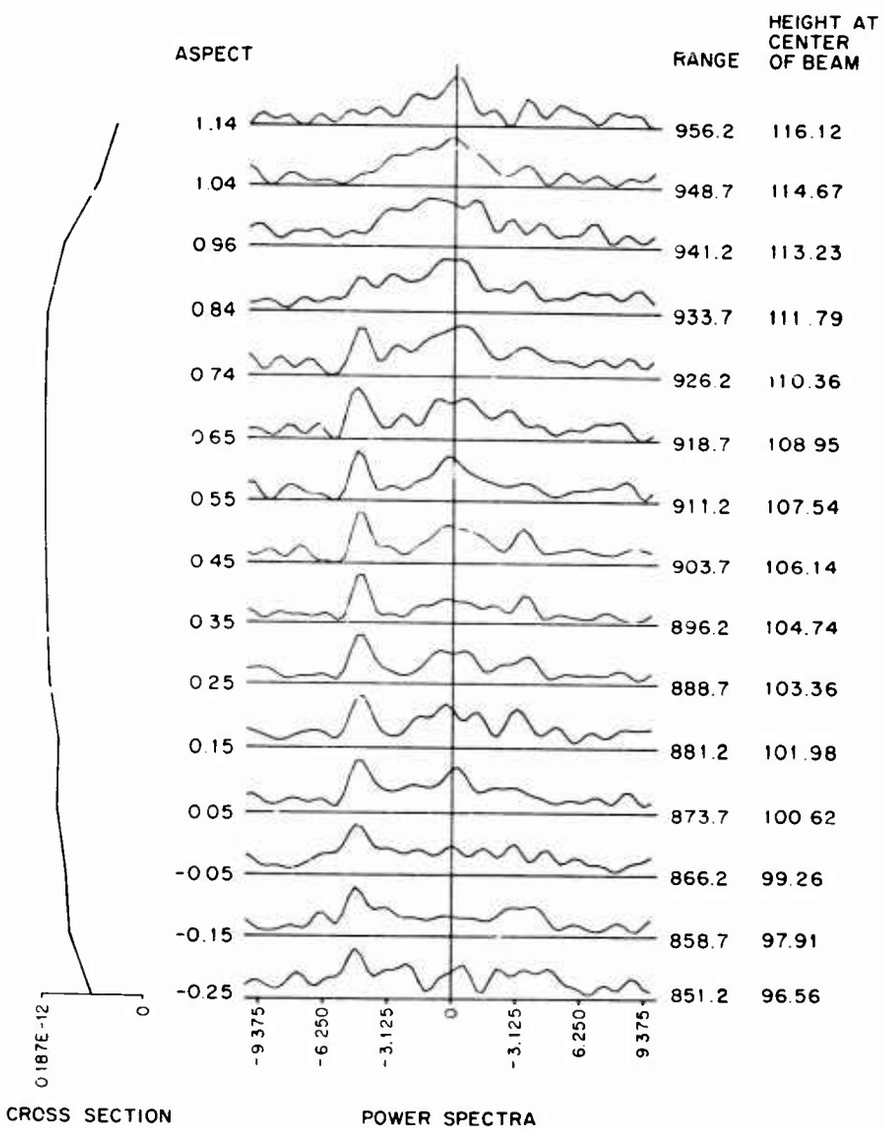

Figure 9. Frequency spectra which shows evidence of the presence of both unshifted and downshifted two-stream "spikes" within the same volume element.

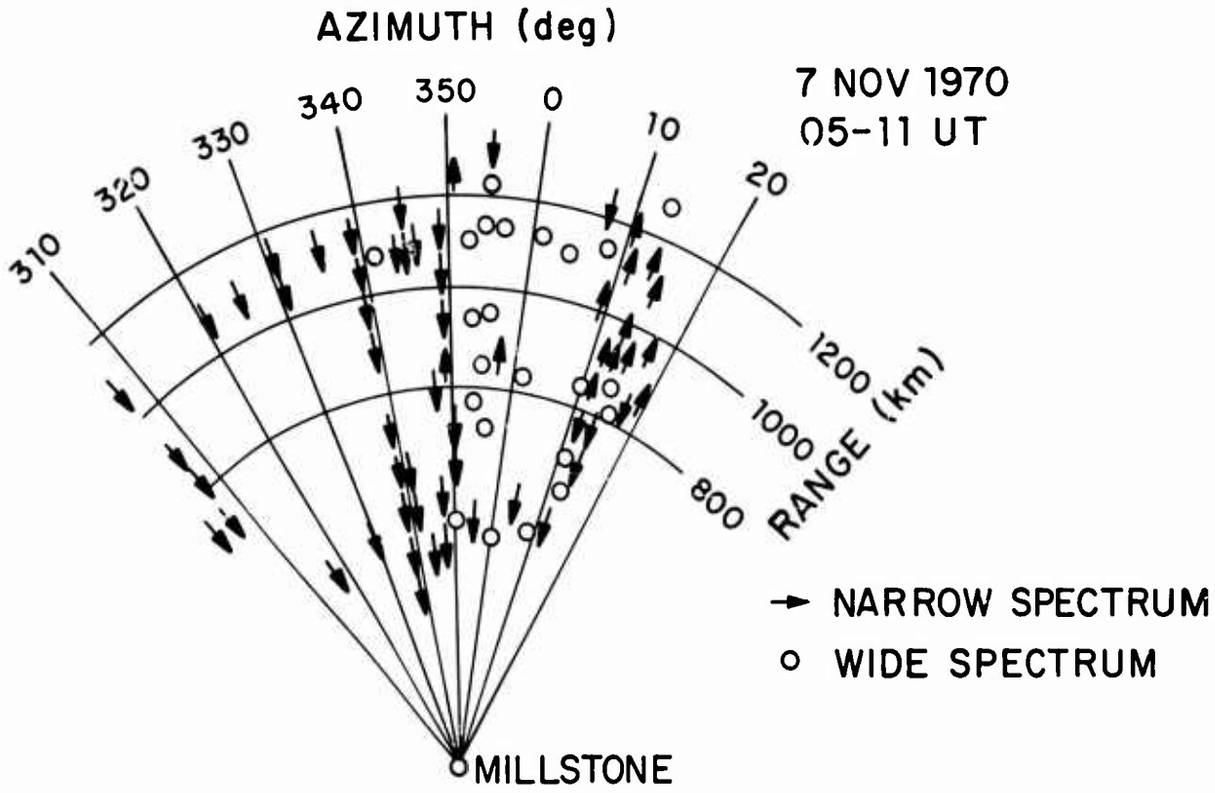

Figure 10. Spatial distribution of occurrence of the various types of spectra.

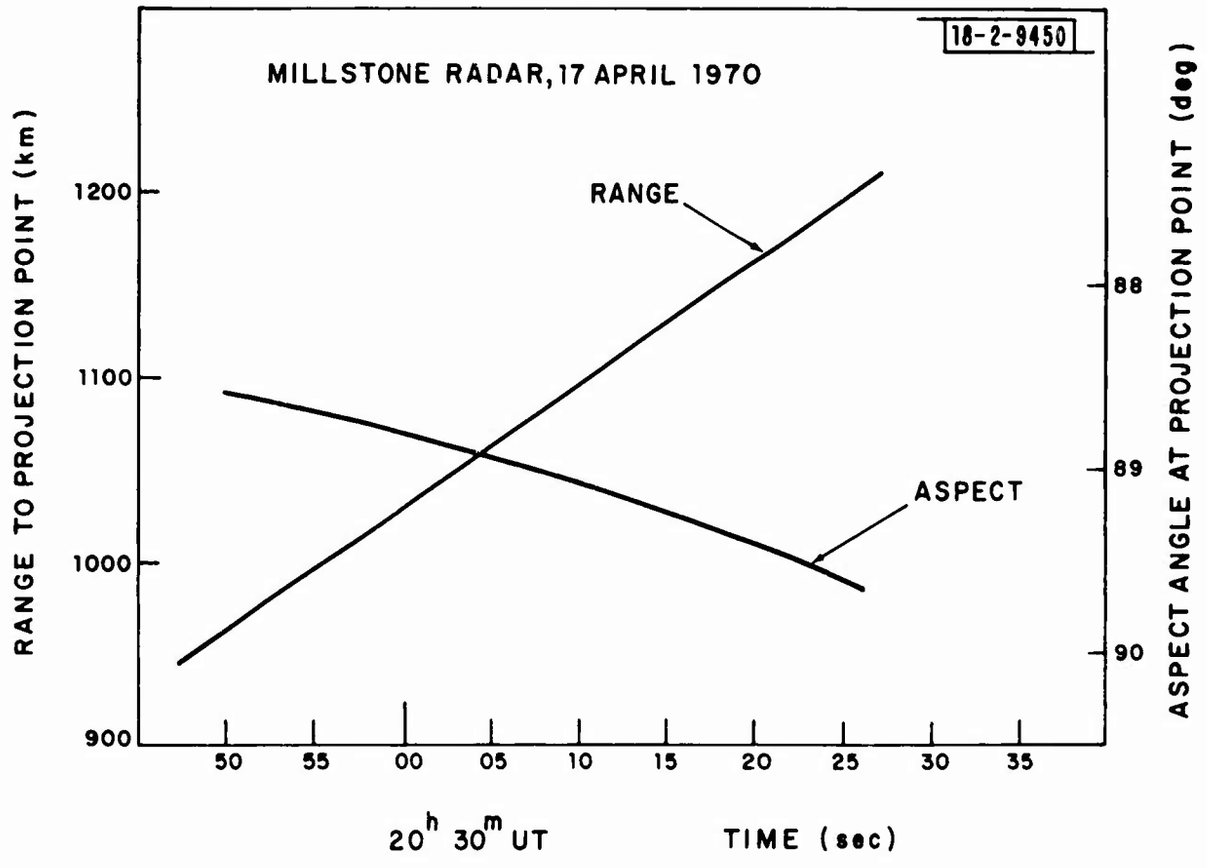

Figure 11. Relationship between range and aspect angle at 110 km altitude and the geodetic latitude of the satellite OV1-18 on revolution 6008, April 17, 1970.

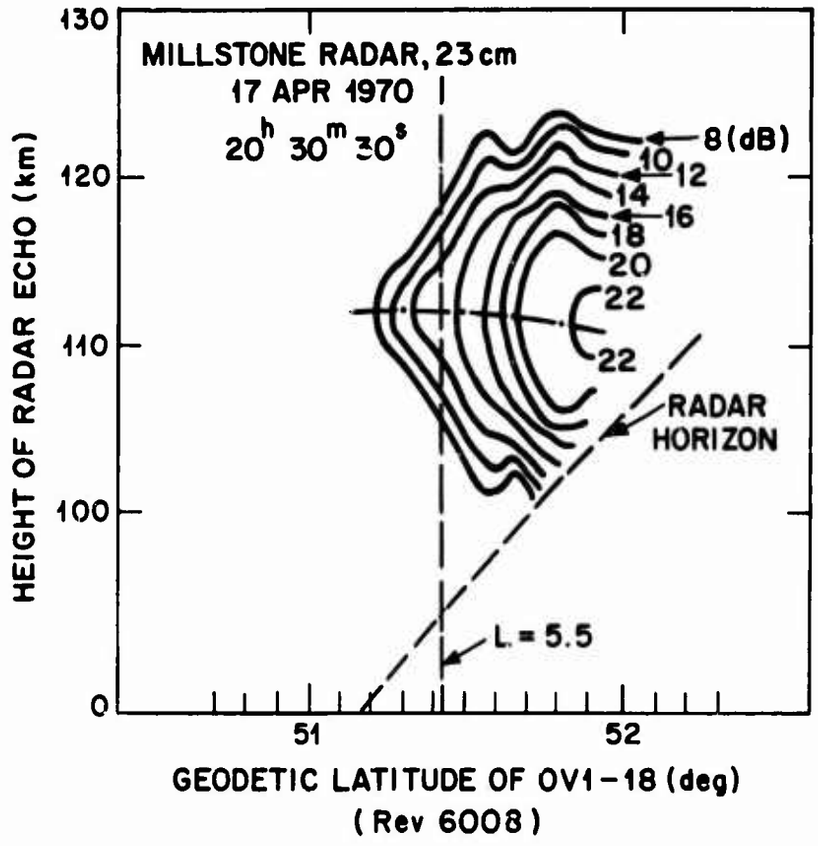

Figure 12. Radar cross section per unit volume plotted against height and geodetic latitude of satellite. Note that 20 db corresponds to 10^{-14} m^2/m^3 cross section.

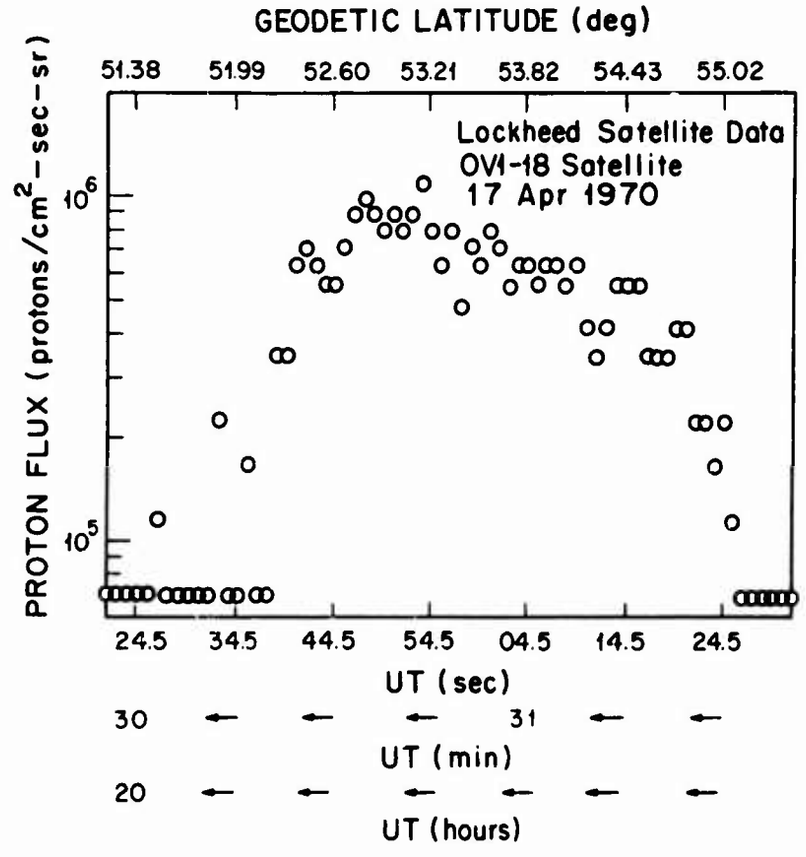

Figure 13. Flux of protons with energy in excess of 14 keV observed in satellite as a function of latitude and universal time.

SESSION II

VHF-UHF PROPAGATION-BACKSCATTER

CHAIRMAN'S REPORT

by A.Egeland

The five papers on auroral clutter presented in Session II showed that the "large scale" morphology of auroral backscatter is fairly well known. However, the averaged maps of auroral clutter vs. time, frequency, scattering angles, ionospheric activities, etc. must be regarded with care bacause of the tendency to smooth out small scale temporal and spatial variations in the auroral region. Such data can neither be used for detailed studies of the physical properties of the scattering medium nor for the understanding of the scattering processes. On the other hand, the morphology is important for propagation predictions.

Our knowledge about the upper polar atmosphere has increased and broadened considerably during recent years. Studies of auroral clutter have grown to include far more than mapping average occurence, but more precise and coordinated measurements are badly needed. Detailed correlations between auroral backscattering and satellite observations are in principle possible, but in practice it is not possible to carry through a careful comparison. More reliable data should be obtained if VHF-UHF transmitters with large, steerable pencilbeam antenna systems are correlated with simultaneous (both time and space) rocket observations of: 1. small scale electric and magnetic fields, 2. micro-structures in particle density and optical luminosity, and 3. particle precipitations. If this is done carefully, the auroral clutter data can be a valuable and important tool for direct investigations of small scale fields and micro-structures in the auroral E-region. Such informations are needed before a reliable theory can be obtained.

The E-layer scattering of VHF-UHF radio waves are undoubtedly caused by small scale field aligned fluctuations in the particle density with sizes of the order of tens of centimeters to a few meters. While the existence of such irregularities are generally accepted, their exact form as function of altitude has hardly been discussed. There is overwhelming evidence that these irregularities are basically caused by plasma instabilities. The most important development in this field during recent years has been the emergence of a variety of instability concepts that may be capable of producing ionization irregularities or structures needed for this polar radio propagation. These plasma instability concepts also aid in the understanding of morphologocal relations which have been empirically derived over many years.

Probably the most used theories are the two stream instability of Farley and the $\underline{E} \times \underline{B}$ drift gradient instability. But the time history of these instabilities have not been included, and several assumptions are made in the theories. A full theoretical treatment is therefore urgently required.

DISCUSSION

E Shearman

A number of speakers have commented that the aspect sensitivity has a rate of fall-off of about 10 dB per degree and that this is not dependant on frequency. On simple diffraction grounds one would expect a 1^{o} beam at VHF to become much narrower at UHF. Can anyone suggest a physical mechanism for such behaviour?

A G McNamara

In general, aspect measurements which have yielded values of 10 dB/degree, have been made on quiescent forms or outside the zone of maximum auroral intensity. Hence one might expect these echoes to obey a simple firstorder aspect law. However, even the UHF measurements show a much lower aspect attenuation rate when echoes are more than a few degrees from perpendicularity. In the case of lower VHF measurements (e g 50 MHz), within the auroral zone, our network shows no evidence of such rapid attenuation - in fact, echoes at some stations are more frequently obtained in directions other of best aspect This probably reflects the presence of strong non-linearities in the mechanism or the dominance of other forms of plasma instabilities. In other words, under ideal conditions of the medium,of the aspect geometry, and preferentially at high frequencies, the attenuation asymptotically approaches the limiting value of 10 dB/degree. The attenuation rate decreases as the observations (1) go of perpendicularity (2) are made in intense instability excitation conditions in the auroral zone (3) are made at lower frequencies where non-linearities will develop first and other instability processes may occur most readily.

W G Chesnut

Our measurements of aspect sensitivity at frequencies of 50 MHz and 400 MHz show aspect angle dependences on the order of 5 to 10 dB/degree. Bates (paper no 26) claims a similar aspect dependence for frequencies as low as 5 Mhz. There seemed to be a contradiction when McNamara reported a 1.2 dB/degree dependence at 48 MHz.
The apparent contradiction may be resolved in the following way. McNamara indicates that his estimates are applicable to magnetic aspect angles between 4^{o} and 20^{o}. He does not measure the aspect dependence near zero degrees as do Bates and ourselves. Our measurements of aspect dependence at a frequency of 400 MHz at magnetic aspect angles between 4.5^{o} and 8^{o} show a much more gradual slope than we measure near zero degrees. At 400 Mhz we measure order of 10 dB/deg near zero and order of 4.5 dB/deg at the larger angles of 4.5^{o} to 8^{o}. We do not know what happens at 400 MHz at angles as large as 20^{o}. Thus the gradual dependence measured by McNamara at large angles is consistent with the trends with angle that we observe at higher radar frequencies. We and Bates cannot measure the aspect dependence at H F at magnetic aspect angles probed by McNamara.

A G McNamara

Fig 3.4 in Chesnut's review paper, which gives 400 MHz backscatter cross section as a function of aspect angle, is a composite of Chesnut's data and Jaye's data. The former show a slope of 10 dB/degree over the range 0^{o} to 1^{o}, and the latter show about 4.5 dB/degree over the range 4^{o} to 8^{o}. Why should not these segments be joined by a smooth curve? Some earlier reports by S.R.I. and other groups have found the aspect attenuation rate to be a decreasing function of angle.

W G Chesnut

The intermediate angle values were not included for several reasons.

1) The data in my curves are given in absolute scattering cross section. The conversion of other people's data to absolute values for smooth connection would require some soul-searching that I was unwilling to do.

2) The times I had available for preparing the review necessarily meant that much good, relevent work had to be overlooked.

3) The data of Leadabrand of S.R.I. in Alaska starts at about 4^{o} so that it would not have extended my composite curve very much.

4) I would be pleased to be reminded by you of other data that I have overlooked. I do remember some 400 MHz bistatic work done in the late 1950's in eastern Canada, did inadvertently overlook it in the review, and do not now know what their aspect dependence measurements showed.

H Kochan

Aspect angle depends on direction of geomagnetic field. What about the influence of

variation of inclination during geomagnetic storm and what about the influence of refraction in troposphere and ionosphere on aspect angle?

A G McNamara

Measurements of the displacement of the magnetic zenith on auroral photographs have been made by several people. Typical values of the distortion in the magnetic line inclination are 1 to 2 degrees. It may be that somewhat greater distortions could occur on a smaller scale size.

P A Forsyth

I thought the refraction of VHF waves in the ionosphere was well analysed about 15 years ago, but I think for vertical angles above about 10° the refraction at say 50 MHz would be small, about 1° or less.

W G Chesnut

Our measurements were made at elevation angles of 0 to 10°. The refraction corrections can be easily estimated if one knows electron density. The 50 MHz data I presented only required 3° of angular change.

P A Forsyth

How do we organize the data which is variable in space and time to establish the power vs aspect angle curve?

W G Chesnut

With difficulty!! - and probably many assumptions of uncertain validity. At our radar location in Alaska, when we wish to determine the magnetic aspect angle dependence, we have to assume that the intrinsic scattering properties in widely separated regions (during a single event) are quite similar. At more southerly locations, such as our 1960 site in Scotland, the geographical separation very much less - so may be the assumption is less bad. The answers we obtained are consistent between these sites and is consistent with the work of Barber, Satcliffe and Watkins (JATP - 1962 pp 599 - 607).

The large angle (4.5° 8°) aspect dependence we determined by statistical averaging of power versus aspect angle. We assume - but cannot prove - that this angular dependence is the same quantity that we measure near 0° aspect. However, my review article shows that these two ways of organizing data near specularity do produce different behaviers. If you have some good ideas, I'd certainly like to hear them.

A Egeland

1. Is it possible to correlate radio-aurora and electron precipitation properly when the particle measurements are made in a satellite?
2. Is it possible to have a high correlation between auroral clutter and precipitating electrons (5 ~ 20 keV) and at the same time no correlation between auroral clutter and visual aurora?

W G Chesnut

1. Yes - if the simultaneity of the measurements in time and space is close enough. One assumes - of course - that the connection between the auroral clutter at 110 km (say) and the satellite (400 to 800 km approx.) is made along magnetic field lines. If field lines are bent by 2° (for instance) by the auroral electrojet, the spatial errors can be 10 km or more - but at the present time, this error is not serious relative to other accuracies and the scale of the phenomena.
2. I thought nobody would ask! Clearly, precipitation and visual aurora must be spatially co-located. The conclusion in my review paper was that all kinds of visual, radar correlation have been observed. But when we can measure with the Homes radar - or when Skip Bates can make a comparison, the visual and radar effects are nearby but not usually superposed. Both of us made these comparison during more stable aurora.

   Our measurements comparing the radar and satellite precipitation locations are not constrained by the stable aurora requirement for reasons that take time to explain. Therefore we may be comparing with a different class of aurora. Your question 2 therefore has suggested to me something that I must do when I return to California. Thank you.

A Egeland

How may one explain the marked difference in Lange-Hesse's (on the correlation with visual aurora and radio-aurora) as compared to those presented by Dr Chesnut?

G Lange-Hesse

The CW VHF backscatter method can not locate the backscattering centres exactly as a radar equipment. Therefore differences in space between aurora backscattering centres and optical aurora of the order of 100 km are possible. This fact I think will explain the marked difference.

K Toman

Dr Lange-Hesse showed interesting comparisons of magnetic optical and radio data. Of those the radio data showed Doppler shifts which were said to rarely reach f= 400 Hz for 146 MHz carrier. The velocities of this motion appear to be subsonic. How can this be related to supersonic motions deduced for optical aurora from all-sky cameras observations?

G Lange-Hesse

The ion acoustic waves (which produce the VHF waves backscattering centres) propagate with a velocity which is equal to the sound velocity in E-region height (about 110 km). For the 146 MHz carrier this velocity produces a Doppler shift at the received signal of about 400 Hz.

P A Forsyth

It seems that we can often associate visible aurora and radio aurora in time but not closely in space. Also there is evidence that scintillation in F-region are associated with visible aurora. Hagfors suggested no association between scintillation and radio-aurora. Could you clarify your position?

T Hagfors

There is a general association between the presence of auroral echoes and scintillation effects on a particular satellite pass possibly because both phenomena correlate with a parameter such as Kp. The point is, however, that there does not appear to be any close spacial relationship along the magnetic field lines between the two phenomena.

A Egeland

In correlation of optical aurora (recorded by all-sky cameras) and other upper atmosphere parameters it is important to take into account the limitations of the all-sky cameras, namely:

1. The all-sky camera can not detect clearly any aurora luminosity of less intensity than 1 kR at 5577 Å (or 250 R at 4278 Å). This means that the net downward electron flux of less than say 1 erg will not be seen by the all-sky camera. But this particle flux will influence the polar electric field, and may also cause auroral irregularities.
2. The time constant of the all-sky camera is several seconds.

J T Coleman

The basic Farley two stream instability theory as published by Dr Farley in 1963 does not predict radar cross sections. It predicts the condition for onset of the instability, or a zero growth rate condition, and this is only the intitial growth rate. Farley stated in his theory that it did not predict the intensity of the interation with radio waves (or cross sections) as the theory does not predict the intensity of the irrelgularities.

W G Chesnut

The above statement is quite correct. However, the Farley threshold theory does predict that some wavelengths will grow - and some will not. Usually the electrojet E-field must be greater for shorter wavelength waves to grow. These shorter wavelengths are necessary for higher frequency radar scattering to occur. Thus, implicitly there is a frequency dependence in that long wavelengths - leading to low frequency radar scattering won't. Thus, the Farley theory predicts scattering at frequencies below some value

and no scattering above that frequency. This, then, is an implicit "cross section vs frequency" prediction.

In addition, though, the Farley theory predicts that for those wavelengths that do grow, the shorter wavelengths do not grow as rapidly as do some intermediate wavelengths. One might infer that those wavelengths that grow fastest reach the largest amplitudes and therefore scatter best. So we argue that one may be able to infer that the Farley theory does suggest the frequency dependence trends that are observed even though the theory cannot - as you point out - predict the detailed cross section versus frequency dependence.

J Frihagen

How can the Farley mechanism give velocities that are much greater than the ion acoustic velocity as has been measured by several people.

W G Chesnut

The velocity of Farley waves is determined by the acoustic velocity in the ion component of the ionosphere. One will observe radar doppler shifts that correspond to greater velocities (or lower velocities) if the E-region wind moves the ionic component. If the electric fields are great enough, then Farley waves will grow at higher altitudes where the ions are experiencing some ExB drift that can be very large. Therefore the ion acoustic velocity which is on the order of 350 to 450 m/s at 110 km (and may be somewhat higher at the slightly higher altitude of consern here) will be added to (or subtracted from) the electric field induced ion ExB drift.

J T Coleman

The hysteresis phenomena mentioned by Dr Lange-Hesse has been observed in the equatorial electrojet. However, this has been discounted as possibly being produced by another current system. Do you feel that this is a real effect produced by the Farley instability mechanisms?

G Lange-Hesse

The hysteresis effect we observe relatively often on our network and therefore we have got the impression that this phenomenon is not caused by another current system. It obviously is caused by the Farley instability or another mechanism.

MICRO STRUCTURE OF RADIO AURORA SCATTERING REGIONS

A. Egeland and J. Holtet
The Norwegian Institute of Cosmic Physics
University of Oslo, Norway
and
N.C. Maynard
NASA/Goddard Space Flight Center
Greenbelt, Md., U.S.A.

SUMMARY

Studies of radio wave scattering from auroral ionization can be a valuable tool for investigation of the complex, physical processes in the auroral E-region. Careful analyses of auroral returns from accurately scaled, pencil-beam radio systems can provide insight into the nature of the scattering medium. Experimental findings, important for the understanding of auroral scattering, are first summarized. Then follows a brief discussion of scattering theories. New measurements of small scale fields, particle precipitation and aurora are described. These micro structures and its dynamics are finally presented and discussed.

1. INTRODUCTION

Studies of radio aurora scattering have grown to include far more than mapping the occurrence of echoes vs. time, scattering angles, ionospheric activity, etc.. Our knowledge about scattering of radio waves as well as the region where radio aurora scattering takes place has increased and broadened considerably during recent years. Careful analyses of auroral scattered signals from accurately scaled, pencil-beam systems can provide insight into the complex, physical nature of the scattering region. Thus, radio scattering data can be a valuable tool for investigation of the auroral E-region.

The main aim of this report is to present and discuss fine structures and dynamics important for the physics of the auroral scattering process. Measurements of small scale electric fields, particle precipitation and visible aurora will be described. Some experimental findings, important for the understanding of the scattering process, will first be summarized. This is followed by a brief discussion of scattering theories.

2. RADIO AURORA; EXPERIMENTAL FINDINGS

Radio aurora is observed through the scattering of radio waves at frequencies much greater than those on which ionospheric reflections are obtained. The experimental evidence is still not completely unambiguous. This is true even if we only consider scattering at so short wavelengths ($\lambda<3$m) that refraction, absorption and overdence scattering can be neglected. The majority of the echoes originate from the height region 100 to 130 km. The thickness of auroral scattering layer varies between 5 and 20 km, but the vertical distribution of the individual scattering volume is no well known.

Maximum probability of occurrence is found when the radio waves are orthogonal to the magnetic field. This aspect sensitivity requirement must be referred to the true, local geomagnetic field. The average slope of the power vs. frequency is close to 30 ± 10 dB over a 1000 MHz band. The scattering cross section decreases by about 10 dB per degree up to 4 degrees aspect angle. For larger angles , the decrease in power is roughly 5 dB per degree. Amplitude distributions indicate the existence of a threshold effect.

The dynamics of the scattering volume are determined by Doppler shift and spread measurements. The shift is roughly proportional to the frequency and indicates velocities as high as 1 km/sec. The variation in Doppler shift with time or azimuth sometimes shows a flat distribution, but often it is nearly sinusoidal. The changeover from westerly to easterly drift around midnight fits with the electric and magnetic perturbing vector in the auroral E-region.

The Doppler spread, which is Rayleigh distributed, does not depend markedly on wavelength. The amplitudes are uncorrelated after a time lag of less than 0.01 sec which is evidence of rapid random motions in the scattering volume. Quasi-sinusoidal fadings have been reported. Because of limited volume resolution in existing equipments, direct measurements of the micro structures are not possible.

Great variations are found in the characteristics of radio aurora. The polarization of the auroral returns may differ significantly from the transmitted polarization. The morphology of radio aurora and its correlation with other upper atmosphere parameters is complex. The diurnal variation may show one, two or three distinct active scattering zones, depending on latitude and frequency. A fairly quiet period is always found in the local morning hours. The majority of the auroral returns are diffuse in character, but discrete echoes are observed around and after local midnight. The correlation in time and space with visual aurora and particle precipitation is not settled yet. For further details cf. Chesnut et al. (1), Egeland (2), Unwin (3).

3. AURORAL SCATTERING MECHANISMS

The main potential sources of radio aurora are:

(a) Scattering from field aligned irregularities in the E-region (4) and further developments of this theory (5).

(b) Partial reflection from plane wavefronts generated by two-stream plasma instability (6).

(c) Scattering from "drift-gradient" plasma instability (7).

Booker's model (4) was a great forward step in our understanding of scattering from weak field aligned irregularities. Several assumptions in this model is questionable (5), and it does not explain e.g. the wavelength dependence, spectral characteristics, etc.. However, it now seems unambiguous that the observed aspect sensitivity is due to field aligned irregularities. Thus, the aspect requirement is roughly the same in these models. The instability theories are therefore mainly concerned with generation and dynamics of the irregularities causing auroral scattering. Both instabilities require an electric field directed perpendicular to the ambient magnetic field. For the two-stream instability a threshold value of the order of 30 mV m^{-1} is needed. The drift-gradient instability, on the other hand, requires a positive gradient of ionization density in the direction of the electric field.

If the velocity of the electrons with respect to the ions exceeds a threshold value somewhat greater than the mean thermal velocity of the ions (8), unstable plasma waves can grow. A spectrum of plasma waves, called ion-acoustic waves, with wavefronts parallel to the ambient magnetic field is generated. These waves will effectively bunch electrons along the field lines, and thus cause irregularities. When this spectrum of waves is viewed by a radar, it selectively views only those waves which are travelling in the line of sight having a wavelength equal to half the radar wavelength (9). There exists considerably indirect support for this theory, but very little direct support (10), (11), (12). The Farley instability in its present form (11) is essentially partial reflections from plane wavefronts, and this does not fit too well with observations. However, this theory must be extended to include plasma waves produced by non-linear coupling of the primary ones, as well as amplitude distribution. When this is done, a better agreement is expected.

The drift-gradient plasma instability (7) has been applied to radio aurora by Unwin and Knox (13). This instability requires a positive gradient of ionization density in the direction of the electric field, and will grow when the electron-ion drift velocity divided by the scale height of the ambient plasma exceeds a critical value, which is inversely proportional to the square of the wavelength. The velocity of the waves is equal to the electron drift velocity for field aligned irregularities and equal to the ion drift velocity for irregularities which are far from field aligned (14). This instability is even less understood than Farley's plasma waves, and much work is left to be done before a careful comparison can be carried out.

The authors will point out that the possibility of energetic particles as a main direct source for auroral irregularities has not been ruled out yet.

The general conclusion is that a wide gap still exists between our theoretical understanding of auroral scattering phenomena and the experimental data. Neither of the above named theories is sufficiently developed to explain fully such important parameters as the amplitude vs. wavelength dependence and aspect sensitivity, different types of echoes, the auroral scattering spectrum, etc..

4. ELECTRIC FIELDS IN THE AURORAL E-REGION

As pointed out in Sect. 3, the presence of electric fields is important for the generation of plasma instabilities.

From the measurements of electric fields in the ionosphere (cf. Sects. 4.1. and 4.3.) it can also be deduced that there is no simple relationship between the magnitudes of the electric field and the magnetic perturbation. This is true both for large scale variations, and to a far greater extent, for the small scale variations, which are believed to play an active role in scattering mechanism. This gives evidence of highly varying conductivities, and it accentuate the importance of auroral scattering as a tool for sounding the ionosphere.

Magnetospherically generated large scale electric fields are not likely to be directly involved in the auroral scattering process, and will not be discussed here. More important for the physics of auroral scattering are the localized, small scale electric fields. Such fields can be generated in the actual height region; i.e. 100-130 km. The normal "background" DC-field will not vary much with altitude between 100 and say 250 km. Small scale variations, on the other hand, will be marked attenuated when propagating outside the E-layer. In the following we will mainly concentrate on small scale fields and distinguish between the DC and the AC components.

4.1. DC Electric Fields

Measurements of electric fields have only recently progressed to the point that reliable observations can be made. Among the various techniques which have been made use of (see e.g.(15)), two have proved to give dependable results, namely; a) the double floating probe technique, where the potential difference between two sensors floating at the plasma potential is measured, and b) the release technique, where the field is determined by measuring the motion of plasma clouds (usually Ba^+) injected into the medium.

The main results from these measurements can be summarized as follows:

The field magnitude, which is very variable over short distances and times, is typically 30 to 50 mV/m. The field is predominantly southward during negative bays (Northern Hemisphere) and poleward during positive bays. Thus, the electrojet (both east and westward) is the result of Hall currents. Parallel fields are probably marked less than perpendicular fields, but they may be very important in the physics of the auroral E-region (16). The DC field seems to be reduced in magnitude within an auroral arc.

Examples of E-field measurements are shown in Figs. 1 and 2. The first figure refers to a weak PCA event with fairly constant homogeneous ionospheric activity. The launch was into the recovery phase of a negative bay. The magnitude of the DC field is fairly constant (10-30 mV/m) and it is mainly directed southward. Fig. 2 is recorded during an auroral event. Notice the large changes in magnitude.

A striking phenomenon from the release experiments is the striations which occur in the plasma clouds. It is really hard to visually distinguish these striations from rayed aurora. Many studies have been done attributing the origin of the striations to instabilities; the most prevalent being the $\vec{E} \times \vec{B}$, similar to the drift-gradient instability dealt with in Sect. 3. Important to the physics of the ionosphere is the question of whether the Ba^+ ions cause the instability or whether they merely trace out a pattern of variations that commonly exists. Wescott et al., (17) believe the latter to be the case for the smaller releases normally used for geophysical experiments.

Small scale irregularities will result in AC electric fields which will be discussed in Sect. 4.3.

4.2. Small Scale Magnetic Fields

Measurements of small scale magnetic fields in the auroral E-region are even more complicated than for electric fields. In a few cases (18), micro structures in rocket magnetometers have been observed which were marked different from the computed field (using up to date coefficients) and which could not be detected on ground magnetometers. The rocket data show that this effect is most marked within the auroral E-region. It should be stressed that further measurements are needed before any final conclusion can be drawn. However, the present data indicate localized variations both in magnitude and direction of the E-layer magnetic fields. Such variations must be included in the scattering theory.

4.3. AC Electric Fields

Recent rocket measurements of AC electric fields in the auroral region have shown some interesting effects within the height interval 90-120 km. The results originate from two rockets launched from Andöya (19,20), Northern Norway ($\Lambda = 67.3^\circ$ N), under different ionospheric conditions (Sect. 4.1.). In both cases visual aurora was present. The electric field experiments in the two rockets were identical, and were based on the double floating probe technique using long cylindrical booms. The baseline for measuring the potential difference was ≈ 9.5 m. In both cases distinctive noise bursts were observed when the rocket passed the E-region. In spite of the different launch conditions, and the great difference in the DC electric field (see Figs. 1 and 2 which give the DC data from these flights), the main features for the ELF E-layer noise look very similar, and can be listed as follows:

(a) The noise is located in the height interval 90-120 km.

(b) The emissions cover the frequencies from about 50 Hz to 2-3 kHz, with maximum energy measured in the lower part of the spectrum. The power spectrum has no marked peak. The roll-off from the point of maximum amplitude is faster on the low frequency side than on the upper one. The measured power spectrum may, however, be somewhat modified by the frequency response of the antenna.

(c) There is a spin modulation on the received signal. This is most pronounced for the high frequency part of the spectrum. Also this modulation is more marked for the waves received within the upper 15 km than it is for the emissions in the lower E-region. Here the noise below say 200 Hz shows less direction dependence. In the last part of the burst no spin modulation at all can be seen, as if the waves are scattered in all directions. Thus, the structure is smeared out in the denser medium.

(d) Maximum amplitude of the signal, as well as the widest frequency range, are found when the antenna is about in the direction 20°-340° (Maynard, priv. com.). This corresponds approximately to the tilt of the invariant latitude line at 100 km. There is, however, a lot of finestructure in the amplitude distribution. x)

It should also be noted that this noise, recorded within the E-layer, is marked different from what was observed at other altitudes, and also from what was recorded during the same events by ground based and satellite borne receivers (19). It is believed that this E-layer noise is caused by horizontal electrostatic waves rather than electromagnetic, as it will require rather large density gradients to keep small scale electromagnetic waves within such a narrow region. Even if such gradients may be established on the lower side of the region, it will probably not be present on the upper side. This assumption is supported by the simultaneous electron density measurements.

It seems to be a reasonable assumption that ELF E-layer noise is associated with the instabilities causing the auroral scattering, but from a preliminary data analysis it is not possible to determine which instability is operating.

5. MICRO STRUCTURES IN VISUAL AURORA, ELECTRON DENSITY AND PARTICLE PRECIPITATION

Because diffusion processes dominate for auroral protons and wash out any initial structure in the proton stream, we will here only consider electrons. The visual aurora, which to a large extent is located within the same height intervals as radio aurora, is caused by electrons in the energy range from 1 to 25 keV (21). The precipitation pattern of these electrons (Fig. 5 a and b) vs. latitude and time follows fairly closely the diurnal variation in echo occurrence, if the complex electric field during magnetic midnight is taken into account.

A 10 keV electron will produce roughly 300 ion pairs in the E-region before it is brought to rest. The chief ions are believed to be O_2^+, NO^+ and O^+. The highest ionization efficiency occurs at a short distance from the terminal of the path. This effect, together with the exponential increase of atmospheric

x) See also Appendix I on page 10-6.

density, gives a fairly sharp lower distribution. Because particle scattering effects are very important, and may even dominate, the picture is more complicated. Even so, one would expect an asymmetric height distribution, which is found in the auroral luminosity. It should also be pointed out that the energy flux can differ by several orders of magnitude, and the pitch angle distributions show large fluctuations.

The gyroradius of a 10 keV electron in the earth's atmosphere is 6 meter or less, depending on pitch angle. As the average scattering angle is small, the electron will, after collisions spiral around a field line which on the average is less than one meter away from the one it spiralled on before collision. This effect will tend to diffuse a narrow beam of electrons arriving along one particular field line, but only to a few meters in diameter. Furthermore, a magnetic east-west to north-south elongation of the auroral irregularities is expected in the horizontal plane, because of the auroral current system (5).

Field aligned electron precipitation is confirmed by the narrowness of auroral rays in directions perpendicular to the magnetic fields. It is still somewhat uncertain how narrow auroral structures can be. (Any aurora appearing away from magnetic zenith will be seriously broadened due to perspective effects.) TV image orthicon recordings, with exposure time of 1/60 sec and spatial resolution of 70 m, shows that the aurora is much more rayed and structured than originally believed. Horizontal thickness down to the resolution threshold is often seen, and the auroral micro structure averages only 200 to 300 m.

A lot of curve structure (folding of auroral arcs upon itself) is observed. Strong evidence has been presented to explain these small structures in terms of a sheet beam instability ($\vec{E} \times \vec{B}$ drift). The rotational sence of small curls, being clockwise in the Northern Hemisphere, strongly indicates that they are produced by electron precipitation.

It looks as the <u>total</u> electron energy flux has less spatial fine structure than visual aurora. However, the 10 to 20 percent modulation superimposed on the average energy flux shows even more spatial and temporal microstructures than optical aurora. Micro structures in the E-region can only be studied by rockets, but it is a serious problem to remove spatial and temporal motion ambiguities. Still, it seems clear that the 10 Hz flicker auroral pulsations are also observed in the electron spectrum as well as in radio aurora. Other time fluctuations looks also very similar.

Some direct observations of micro structure in electron density have been made by e.g. McNamara (10) using probes in rockets. Fractional variation in electron density of about 5% is typically observed, but it is difficult to distinguish between temporal and spatial fluctuations. Our preliminary results of VLF <u>Doppler shift</u> data indicate very rapid and strong density fluctuations in the auroral region. It will hopefully not last long before individual irregularities can be studied. x)

The auroral electrojet, which flows between 100 to 130 km, may be the driving force for the development of conditions which lead to auroral back-scattering. The electrojet is caused by particle precipitations. If the auroral irregularities move with the auroral electrojet, some predictions concerning the Doppler shifts as function of direction and time may be possible. But as the electrojet is very complex and only poorly understood, such predictions are uncertain. The reversal in Doppler shift and the reduction in echo activity during local magnetic midnight fit with the general model of the current system (22).

6. CONCLUSION

Our knowledge about the physical parameters and their processes within the auroral scattering region has increased considerably during recent years. Even so further and new precise studies of micro structures are badly needed in this region. The radio aurora observations must be carefully related to the actual situation in the auroral ionosphere before a full theoretical treatment can be done. Also the amplitudes and the shapes of the irregularities must be incorporated in the scattering mechanisms together with the localized fields. If this is done, radio aurora can be a powerful tool for further studies of the complex auroral region.

REFERENCES

1. Chesnut, W.G., J.C. Hodges and R.L. Leadabrand. "Auroral Backscatter Wavelength Dependence Studies." Stanford Research Institute, Rome Air Development Center, RADC-TR-68-286, 1968.

2. Egeland, A. "Studies of Auroral Reflections in the VHF Band. I. Experimental Investigations, with Special Regard to Time Variations, Fading Rate, Azimuthal Distributions, and Polarization Characteristics." Arkiv för Geofysik, 4, 103, 1962.

3. Unwin, R.S. "The Morphology of the V.H.F. Aurora at Sunspot Maximum. I. Diurnal and Seasonal Variations." J. Atmospheric Terrest. Phys. 28, 1167, 1966.

4. Booker, H.G. "A Theory of Scattering by Nonisotropic Irregularities with Application to Radar Reflections from the Aurora." J. Atmospheric Terrest. Phys., 8, 204, 1956.

x) See Appendix II on page 10-6

5. Egeland, A. "Studies of Auroral Reflections in the VHF Band. II. Comparison of Experimental Results with Theoretical Models." Arkiv för Geofysik, 4,7, 171, 1962.

6. Farley, D.T., Jr. "A Plasma Instability Resulting in Field-Aligned Irregularities in the Ionosphere." J. Geophys. Res., 68, 6083, 1963.

7. Simon, A. "Instability of a Partially Ionized Plasma in Crossed Electric and Magnetic Fields." Phys. Fluids, 6, 382, 1963.

8. McDiarmid, D.R. and A.G. McNamara. "A Physical Model of a Radio Aurora Event." Can. J. Phys., 47, 1271, 1969.

9. Moorcroft, D.R. "The Interpretation of the Frequency Dependence of Radio Aurora." Planetary Space Sci., 14, 269, 1966.

10. McNamara, A.G. "Survey of Radio Reflections from Aurora." The Radiating Atmosphere (Ed. B.M. McCormac), 301, D. Reidel Publ. Comp., Dordrecht, Holland, 1971.

11. Farley, D.T., Jr., J.P. Dougherty and D.W. Barron. "A Theory of Incoherent Scattering of Radio Waves by a Plasma. II. Scattering in a Magnetic Field." Proc. Roy. Soc., A 263, 238, 1961.

12. Abel, W.G. and R.E. Newell. "Measurements of the Afternoon Radio Aurora at 1295 MHz." J. Geophys. Res., 74, 231, 1969.

13. Unwin, R.S. and F.B. Knox. "Radio Aurora and Electric Fields." To be publ. in Radio Science, 1972.

14. Whitehead, J.D. "Low Frequency Plasma Instabilities in the Ionosphere." J. Atmospheric Terrest. Phys., 30, 1563, 1968.

15. Maynard, N.C. "Electric Fields in the Ionosphere and Magnetosphere." Presented at the Advanced Study Institute on Magnetosphere-Ionosphere Interactions, Dalseter, Norway, April, 1971. (Preprint X-645-71-231, GSFC, Greenbelt, Md, USA, 1971.)

16. Mozer, F.S. and U.V. Fahleson. "Parallel and Perpendicular Electric Fields in an Aurora." Planet. Space Sci., 18, 1563, 1970.

17. Wescott, E.M., J.D. Stolarik and J.P. Heppner. "Electric Fields in the Vicinity of Auroral Forms from Motion of Barium Vapor Releases." J. Geophys. Res., 74, 3469, 1969.

18. Armstrong, R.J. "The Possible Detection of a Large Ionospheric Current." Techn. Note E-250, NDRE, Kjeller, Norway, 1971.

19. Holtet, J.A., A. Egeland and N.C. Maynard. "Rocket, Ground and Satellite Measurements of ELF Emissions during a PCA." The Radiating Atmosphere (Ed. B.M. McCormac), 337, D. Reidel Publ. Comp., Dordrecht, Holland, 1971.

20. Holtet, J.A., A. Egeland, L.T. Lyngdal and N.C. Maynard. "AC Electric Fields during an Auroral Event." Presented at the SAR meeting, Kiruna, Sweden, March 1971.

21. Egeland, A. and C. Deehr. "Auroral Morphology." Ann. de Géophys. In Press, 1971.

22. Heppner, J.P., J.D. Stolarik and E.W. Wescott. "Field Aligned Continuity of Hall Current Electrojets and Other Consequences of Density Gradients in the Auroral Ionosphere." The Radiating Atmosphere (Ed. B.M. McCormac), 407, D. Reidel Publ. Comp., Dordrecht, Holland, 1971.

23. Egeland, A., G. Björnegaard and T.L. Aggson. "Evaluation of Electron Density from VLF Doppler Measurements in a Rocket." J. Atmospheric Terrest. Phys., 32, 1191, 1970.

POSTSCRIPT

Since this paper was written, the finestructures of the electric field (cf. Page 10-3) and the electron density (cf. Page 10-4) based on the two rockets discussed in Sect. 4 have been further analyzed. Some new results have appeared. As the authors believe these findings may be important for further discussions of the polar E-region, these new points will be presented under the headings Appendix I and Appendix II.

APPENDIX I

Further analysis of the ELF E-layer noise has brought out a few new features which should be mentioned. A polar plot, where the direction of the antenna in a topographical coordinate system at the times of maximum amplitude is shown in Fig. 6. The diagram is based on the same data as Fig. 3, and "maximum amplitude" means maximum in power integrated over the frequency range 0.1 - 1 kHz. As the exact orientation of a night-time rocket is difficult to determine, there may in these preliminary results be a systematic error in the attitude calculations. Nevertheless, what is evident is that the direction of the electric field of these waves is well defined. That these waves propagate within a very narrow sector (or are strongly aspect dependent) is even more clear if the width of antenna pattern is taken into account. As can be seen from the plot there is, however, a slight shift in the direction with altitude. This seems to be more marked in the records from the second rocket (Fig. 4), where a preliminary analysis shows a clear shift in direction (more than 10 degrees) in the two main bursts between 120 and 108 km and 105 and 95 km. It is also of interest to note that the rocket magnetometer indicates large perturbations in the magnetic field in the intermediate region.

Much finestructure is seen in the amplitude vs. time records of the noise, where large and rapid fluctuations are very conspicuous. Also it turns out that each single sub-burst, following the spin period, usually has a double maximum. However, whether these two effects are caused by real variations in the electric field or if it is a result of a situation where the length of the antenna is considerably larger than the dimensions of the irregularities, is at the present stage not possible to determine.

APPENDIX II

Evaluation of electron density from VLF Doppler measurements in a rocket have been discussed by Egeland et al. (23). In the rockets F23 and F24 the signal from two highly frequency stabilized transmitters at 12.3 and 16.4 kHz were recorded. The received waves showed significant Doppler shifts (0.1 to 3 hz). As these frequency shifts are inversely proportional to the refractive index, the electron density can in principle be calculated at each point along the rocket trajectory (cf. (23) where more references are given). Because a full wave solution (or a phase tracking program) is needed, the interpretation of the data is fairly complicated. However, it should be reasonable to assume fairly constant propagation conditions over a period of 0.5 sec; i.e. neglecting time variations over this period. If this is the case, the relative variations in density within this period can be investigated fairly straight forward.

The analyses of the small scale, rapid fluctuations of the VLF Doppler data have just started. The average Doppler shift per second has first been measured to give the ordinary electron density profile. The deviation from this mean value is then calculated, and the fluctuations converted to electron densities. An example of the VLF Doppler data for F23 is shown in Fig. 7, where also the horizontal and vertical motion of the rocket over 0.5 sec is marked off. Notice that the measurements refer to an altitude range from 99.2 to 99.7 km. The average Doppler shift during this interval was 1.44 Hz corresponding to a mean electron density of $2 \cdot 10^5$ el/cm^3.

The very large and rapid spatial fluctuations in electron density (and Doppler shift) are clearly seen from Fig. 7. Fractional variations in electron densities up to 15% are observed. Furthermore, the dimensions of these irregularities are only of the order of say 10 meters. Thus, micro structures are very pronounced in the auroral E-layer (10). Before we have analyzed the remaining part of the data, no definite conclusions will be drawn. It should only be pointed out that we have found no reason to mistrust these data, as they have been checked very carefully.

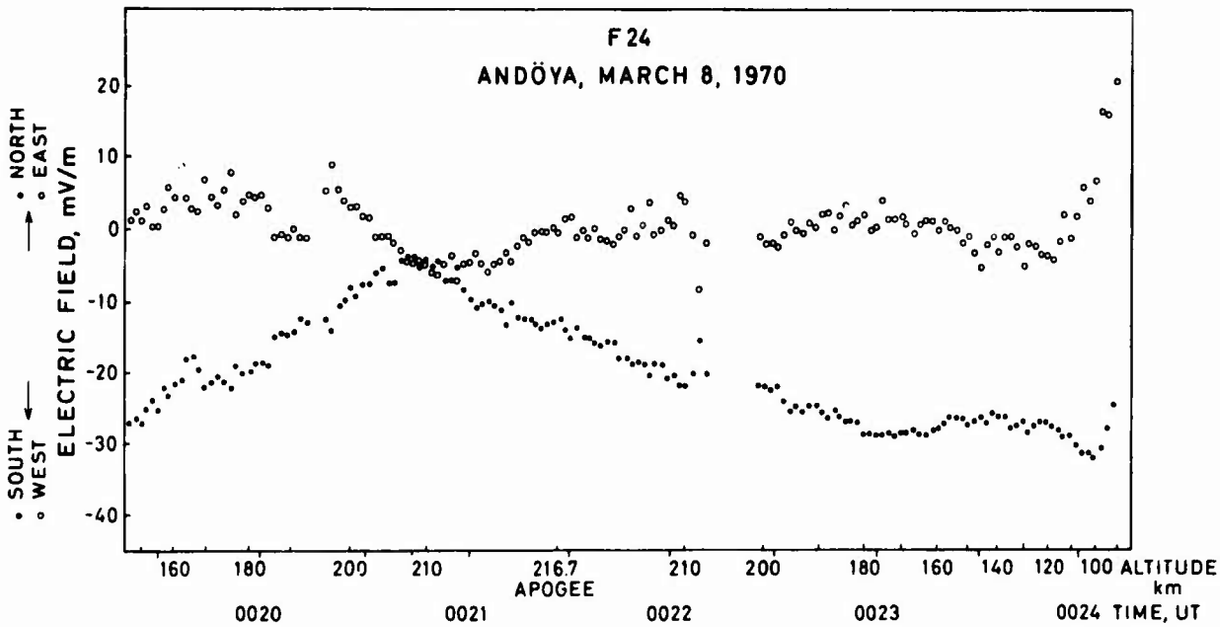

Figure 1: North-South (•) and East-West (◦) components of the DC electric field measured from a rocket during a weak PCA event.

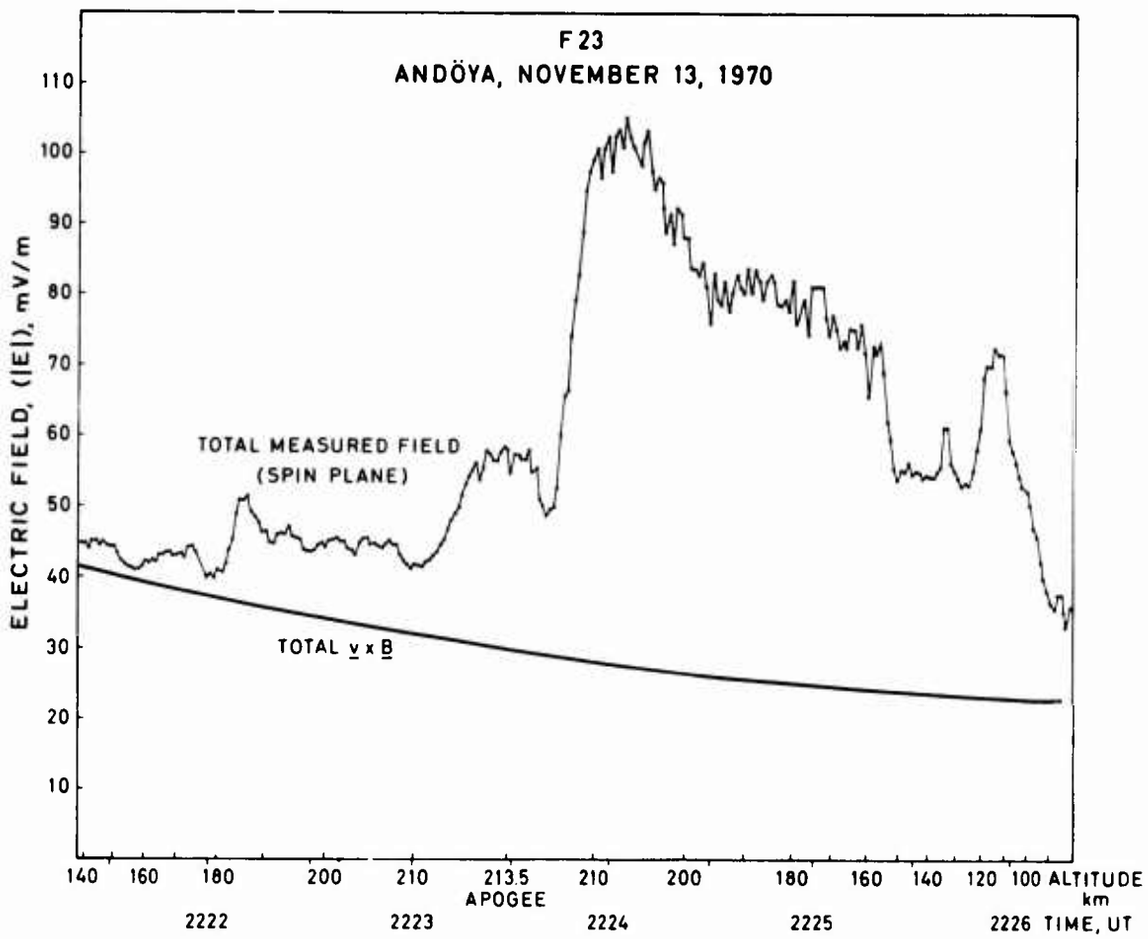

Figure 2: Total DC electric field (without corrections for the motion in the magnetic field, $\propto \vec{v} \times \vec{B}$,) measured from a rocket. In this case ground based measurements indicated more perturbed conditions in particle precipitation than in the Fig. 1 event.

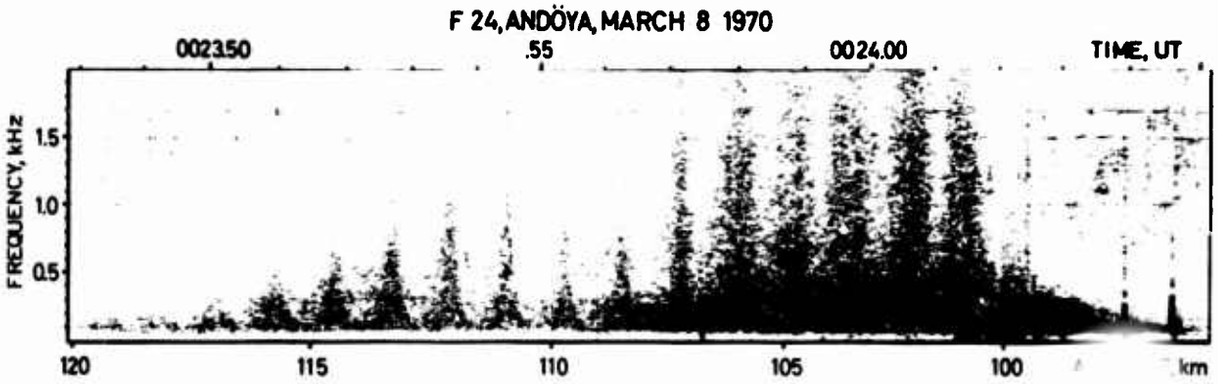

Figure 3: Electric field ELF E-layer noise recorded during the rocket flight referred t

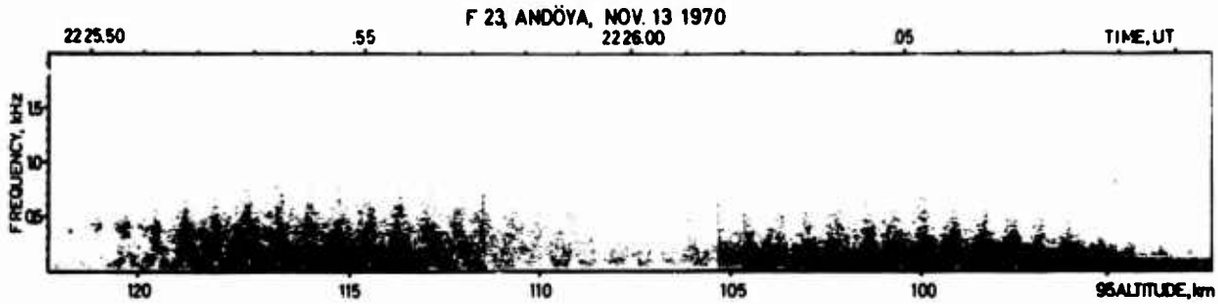

Figure 4: Electric field ELF E-layer noise measured during the event dealt with in Fig. 2. Notice the similarity in the appearance of the AC field measured at these quite different conditions.

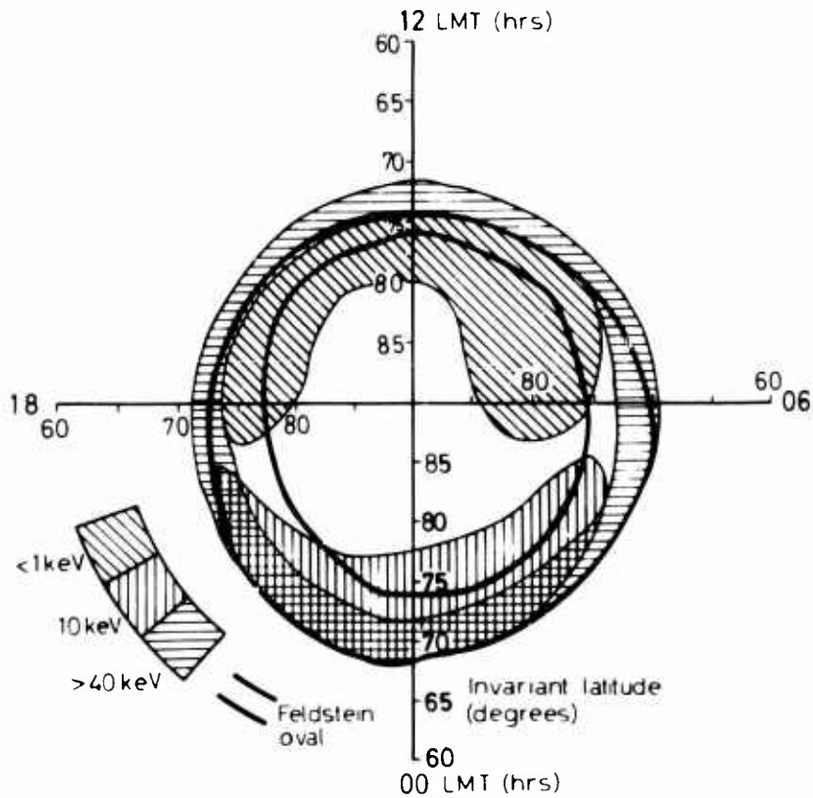

Figure 5a: The average position of auroral electron precipitation together with the Feldstein oval for quiet conditions (21).

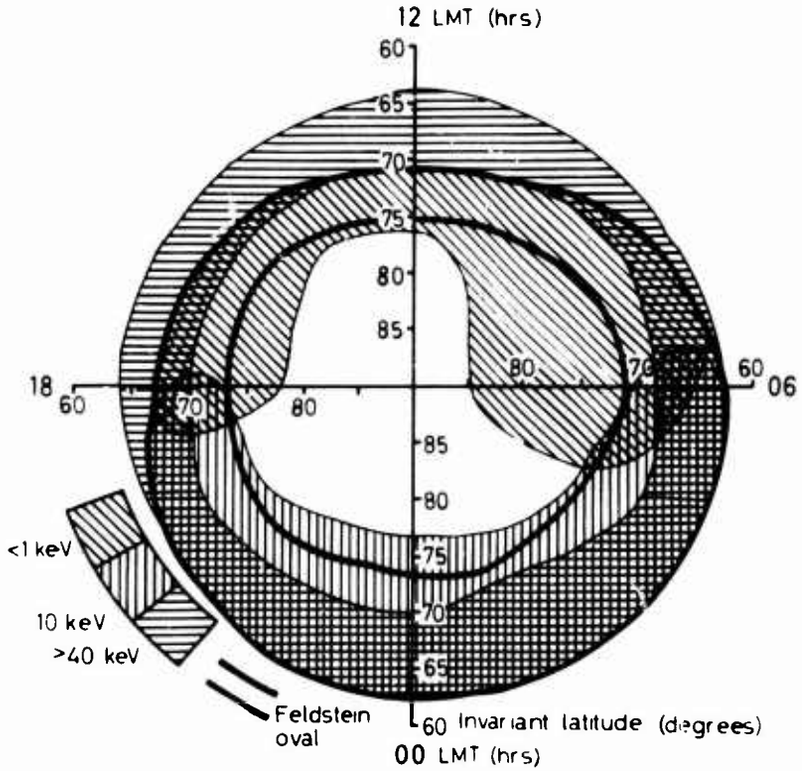

Figure 5b: The average position of auroral electron precipitation together with the Feldstein oval for disturbed conditions (21).

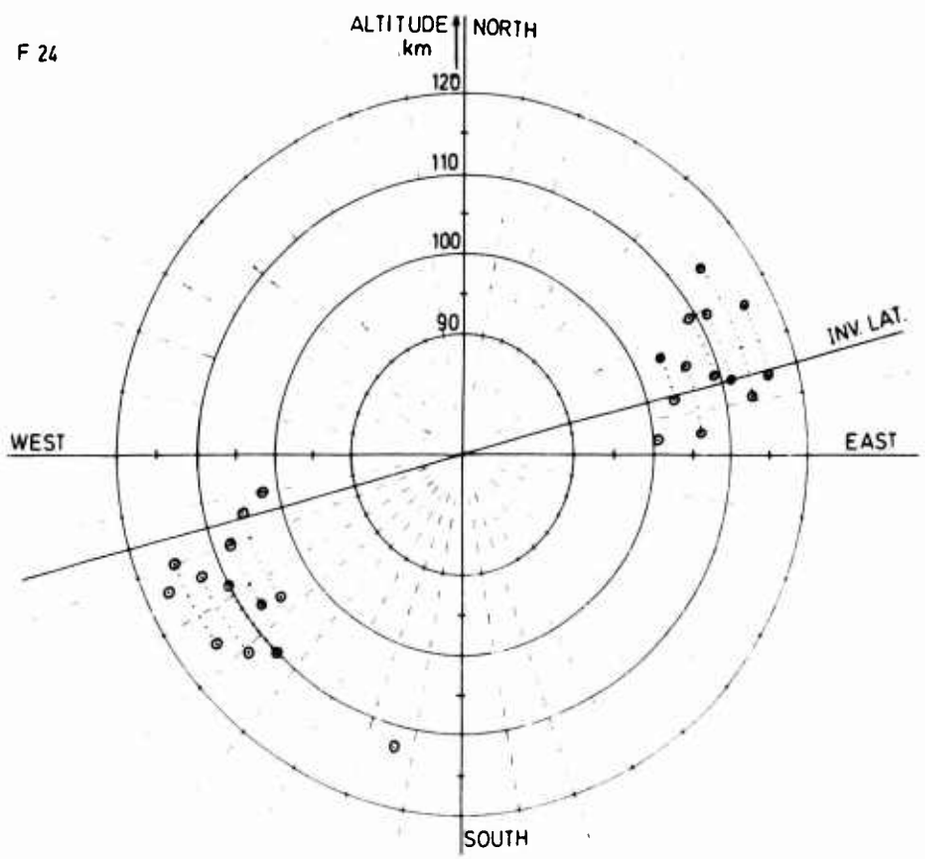

Figure 6: Orientation of the E-field antenna in a topographical coordinate system when the ELF E-layer noise bursts have maximum amplitude (cf. Fig. 3). Two points connected by a dotted line indicate the double peak in the same burst. Distance from the center gives the rocket altitude. The line marked INV. LAT. is in the direction of constant invariant latitude at 100 km. The diagram is based on the data shown in Fig. 3.

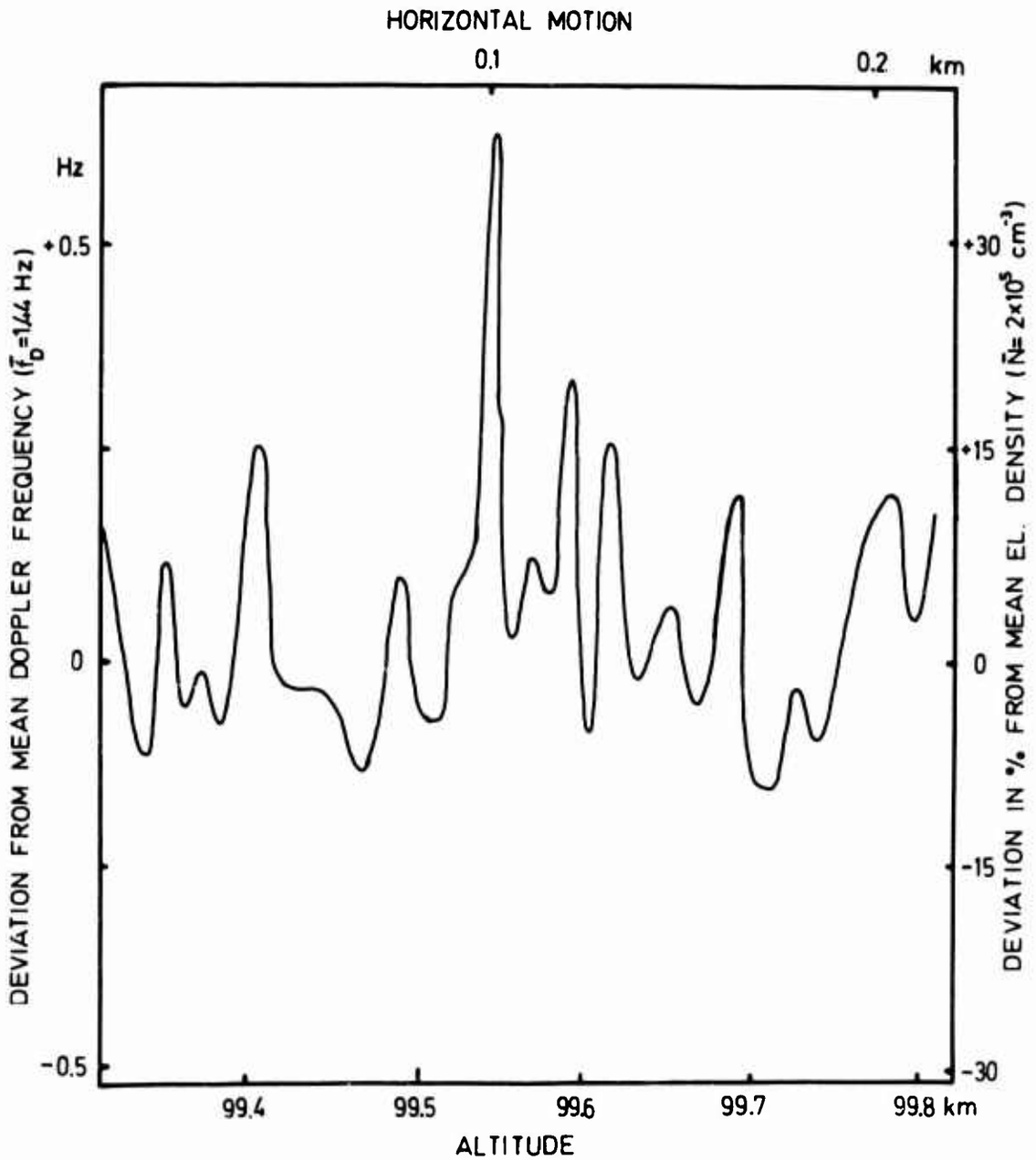

Figure 7: Small scale fluctuations in the observed Doppler shift (in Hz) as a function of altitude in the signal from a ground based VLF (16.4 kHz) transmitter received during the "Fig. 2 event". The corresponding variation in the local electron density is given on the right hand ordinate.

DISCUSSION

T Hagfors

Did you measure simultaneously the large scale and the small scale electric fields and if so, how did the rate of rotation with altitude compare?

A Egeland

Both the AC and the DC parts of the electric fields were measured simultaneously in both rockets. Only the AC (small scale) E-field within the auroral E-layer rotated with altitude, while the large scale DC fields showed no marked rate of rotation, and no marked change in magnitude within this altitude region.

T Hagfors

The probe spinning round as it goes through the electrojet will act as a filter on the various spatial structures in the electrojet. As far as I can understand, when the probe is aligned with the direction of the current it will respond to larger spatial structure than when it is turned round to be near (but not quite) perpendicular to the current since all the waves travel preferentially in the direction of the current. This would lead me to believe that the width of the frequency spectrum ought to have a minimum when the probe is aligned with the current rather than a maximum, as the spectrum associated with the small structure is wider than the spectrum of the larger structure. I would like to direct this question to the author or to anybody in the audience who can lead me straight on this seeming contradiction between the observations and my consepts of the electrojet fields.

A Egeland

I can not answer the above question properly, but I want to stress a couple of points. If electromagnetic waves are considered, the above argument is not correct. If electrostatic waves are considered, one has to include a velocity distribution. For velocities between 200 m/s and 2 000 m/s, you will observe a spectrum similar to those in Fig 3 and 5 for the antenna parallel to the electrojet.

For short wavelengths, the intensity of the waves may be below our threshold sensitivity because the intensity will decrease rapid with wavelength. It is difficult to measure attitude during flight. Our measurements may be wrong by 90 degrees, but I do not believe this. (The attitude measurements have been carried out by NASA, GSFC, USA).

ION-ACOUSTIC WAVES IN AURORA

P.A. Forsyth and G.F. Lyon
Centre for Radio Science
University of Western Ontario
London, Canada

SUMMARY

There is now clear evidence that ion-acoustic waves exist in the auroral plasma and that these waves contribute to the scattering of radio waves at both VHF and UHF frequencies. It has been generally assumed that auroral clutter arising by this mechanism would occur only when the line-of-sight is perpendicular to the magnetic field in the auroral region. Recent results suggest that this kind of clutter will be observed even at latitudes where the line-of-sight cannot be perpendicular to the magnetic field lines. It is also suggested that ion-acoustic waves may contribute to the angular scintillations observed at high latitudes for trans-ionospheric propagation paths using UHF radio waves.

1. INTRODUCTION

For many years it has been customary to analyze the effects of ionospheric ionization on the propagation of VHF and UHF radio waves simply in terms of the small density gradients which are known to exist in the disturbed ionosphere and which have been assumed to be randomly distributed in space. The most important ionospheric structures seem to be those associated with aurora and for these the term "radio aurora" was introduced some twelve years ago [1] although there is still no universal acceptance of the term or agreement on its precise meaning [2,3].

Very early in the radar studies of what is now known as radio aurora it became evident that no simple model of the scattering region would be able adequately to explain the observations. On the one hand the actual reflectivity of radio-aurora is very small at all frequencies above the lower part of the VHF band. Some early attempts to measure the reflection coefficient of auroras [4,5] yielded values of about 10^{-6} indicating that the auroral ionization was highly transparent. On the other hand the frequency dependence and the geometrical characteristics of the reflections were not compatible with scattering from only weak gradients of ionization. After many such investigations involving both monostatic (radar) [6] and bistatic (forward-scatter) [7] systems Moorcroft [8] reviewed the evidence and concluded that it was physically unreasonable to try to explain all radio-auroral scattering on the basis of a model involving only weak randomly distributed structures. Thus he agreed with Leadabrand et al [9] that some form of wave structure, presumably ion-acoustic waves must be present in radio aurora.

Ion-acoustic waves have been clearly identified in the volume of the E-region occupied by the equatorial electrojet and it seemed reasonable that such waves should also exist in the auroral electrojet. However, in order to be observed by a radio system the ion-acoustic wave trains must be viewed in a direction that is either parallel or anti-parallel to the direction of propagation of the acoustic waves. For a back-scatter system the direction of viewing is simply the direction of propagation of the transmitted wave whereas for a bistatic system the direction is along the bisector of the angle formed by the vectors from the transmitting and receiving station to the scattering region. A further requirement is that the ion-acoustic wavelength be precisely one half of the radio wavelength (or the radio wavelength suitably foreshortened in the case of a bistatic system). This requirement is not as severe as might at first appear because it is thought that for all circumstances of interest a wide spectrum of ion-acoustic waves are produced and the radio wave "picks out" the wave trains having the appropriate wavelengths.

The geometrical restrictions are much more severe. The essential characteristics of the mechanism outlined by Farley [10] are as follows: The waves are generated by the relative motion of the electron and ion components in the ionospheric plasma. When this differential velocity exceeds the threshold value (approximately, the local acoustic velocity) the waves are generated and propagate in a narrow cone of directions about the electron velocity vector. All waves propagating in directions other than those contained in the plane perpendicular to the magnetic field are rapidly attenuated by Landau damping. As the relative electron streaming velocity increases, the directions of propagation of the ion-acoustic waves spread out on either side of the electron velocity vector but are still confined essentially to the plane perpendicular to the magnetic field. As the streaming velocity is increased the spectrum of waves generated is also broadened toward the shorter wavelengths.

The implication of this geometrical restriction is that radio echoes should be observable only when the incident and scattered radio wave propagation vectors lie in the plane which is perpendicular to the earth's magnetic field. This is the orthogonal condition which is variously described in terms of an aspect angle. In this paper the aspect angle, β, is the angle between the direction of viewing, defined above, and the direction of the magnetic field. For the orthogonal condition, $\beta = 90°$.

As has been pointed out by McDiarmid [11] the restriction of ion-acoustic waves in radio aurora to the orthogonal plane really implies that most of the radio echoes associated with aurora cannot be explained by that mechanism. It is not possible to satisfy the orthogonality condition from most high latitude stations. In particular most of the

Canadian stations from which radio aurora has been observed are located at geomagnetic latitudes such that the aspect angle at the 100 km level (where the most intense auroral ionization occurs) is always substantially greater than 90°.

2. THE DETECTION OF ION-ACOUSTIC WAVES

The most characteristic feature of ion-acoustic waves is the propagation velocity which is close to the local acoustic velocity. Since such waves can only be detected (by radio) when "viewed" along the direction of propagation, the frequency spectrum of the scattered signal should consist of a single "line" component displaced from the transmitter frequency by an amount corresponding to the Doppler shift produced by the moving waves. In 1969, Hofstee and Forsyth [12] reported the results of such an experiment conducted from one of the few regions in Canada where the orthogonality conditions could be fulfilled.

Two bistatic, continuous wave radio systems, operating at frequencies near 40 MHz were used to observe a common volume of the ionosphere. One circuit, with transmitter at Ottawa and receiver at London, Ontario had a minimum aspect angle of 91° while the other with transmitter at St. Catharines and receiver at London had a minimum aspect angle of just 90°. The two systems differed in direction of viewing by about 20°. A map of eastern Canada showing the locations of various places mentioned in the paper is given in Fig. 1.

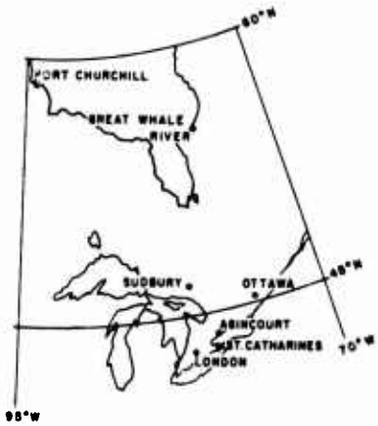

Fig. 1

For most radio aurora the two circuits showed only a broadly spread scattered spectrum roughly centred on the transmitter frequency. For some radio aurora the expected line spectrum was seen displaced by the required 100 Hz above or below the transmitted frequency. These observations, some samples of which are shown in Fig. 2, were interpreted as clear evidence of the occasional occurrence of ion-acoustic waves in radio aurora. There was considerable variation in the line spectra observed with the two circuits and quite rapid temporal variations but these seemed to be consistent with the known characteristics of ion-acoustic waves and the auroral electrojet.

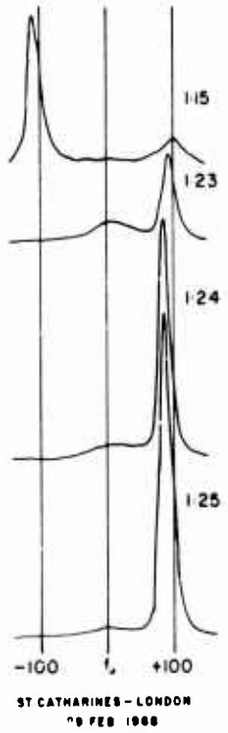

Fig. 2

Subsequently McDiarmid [11] used these same results in conjunction with magnetic observations from Great Whale River and Agincourt in a test of a model proposed by McDiarmid and McNamara [13]. The result was satisfactory and gave further support to the inferred existence of ion-acoustic waves in radio aurora.

3. ION-ACOUSTIC WAVES FOR NON-ORTHOGONAL CONDITIONS

Since ion-acoustic waves had been observed for conditions where $\beta = 90°$ it seemed important to see if the waves could be observed when the aspect angle differed significantly from 90°. Accordingly Hofstee and Forsyth [14] repeated the experiment for the non-orthogonal conditions. This time the transmitters were at Ottawa, the receivers at London with the new region of observation more to the south so that it was over and to the north-east of Sudbury. In addition magnetic records were available from Ottawa, Sudbury, Great Whale River and Fort Churchill. Means were provided for the approximate determination of the location of the scattering region.

Again there was good agreement between the location and direction of the auroral current as deduced from the magnetic data and the occurrence and direction of travel of the ion-acoustic waves. Ion-acoustic waves were clearly detected from regions for which the undisturbed aspect angle is about 96°.

In trying to explain this unexpected result it was noted that the recent satellite observations of Armstrong and Zmuda [15] have shown the existence of quite large scale current configurations near the auroral zone. For example, a sheet current elongated in the East-West direction was detected flowing downward into the ionosphere, presumably there was a current flowing southward in the ionosphere for a distance of about 240 km because at that point the current was detected flowing out of the ionosphere. Near the 100 km level such a current system would be expected to give rise to a substantial westward flowing Hall current which was indeed detected by ground-based magnetometers.

The interesting point about this current configuration is that the Hall current must be in the form of a sheet current which is essentially uniform over large areas. It would distort the magnetic field of the earth fairly uniformly over the large volumes needed to explain the radio evidence. The situation is sketched in Fig. 3.

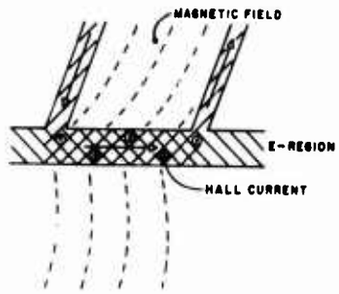

Fig. 3

An important point is that the preferred direction of propagation of the ion-acoustic waves is in the same direction as the electron flow. Any distortion of the magnetic field produced by the current must be perpendicular to this direction. However it may be recalled that relatively small increases in electron streaming velocities cause the waves to spread out on either side of the current vector although still confined to the plane which is perpendicular to the magnetic field. Thus, as long as the magnetic field lines are distorted uniformly so that the aspect angle becomes nearly 90° over a significant volume, there is a plausible mechanism for the generation of ion-acoustic waves propagating in the required direction. This leads to an interesting additional requirement that if this mechanism is to be invoked the auroral region must *not* be viewed directly along the direction of current flow. In fact, the more the undisturbed aspect angle differs from 90° the stronger is the current required and the larger must be the angle between the direction of viewing and the direction of current flow.

The considerations outlined in the last paragraph lead to the expectation that for high latitude observation the auroral echoes which arise from ion-acoustic waves would be strong but transitory and that these characteristics would be enhanced with increasing latitude.

4. IMPLICATIONS FOR HIGH LATITUDE RADAR CLUTTER

The principal conclusion to be drawn from the new results is that even for high latitude radars ion-acoustic waves cannot be ruled out as a possible source of clutter. This is not to say that such waves are likely to be the main source of clutter. It appears that even at low latitudes ion-acoustic waves contribute to only a small fraction of auroral echoes and unless the geometric limitations have been completely misinterpreted this fraction is not likely to increase with latitude. On the other hand, the frequency dependence of scattering from ion-acoustic waves is highly dependent upon the driving current and is therefore likely to be variable. Certainly it seems likely that ion-acoustic waves will contribute to auroral clutter well into the UHF frequency range.

Another point which emerges is that ion-acoustic waves must be a common occurrence in the auroral ionosphere although conditions which allow direct observation of them are relatively rare. If, as has been frequently suggested [16] there are mechanisms for generating secondary irregularities in the E-region by the action of ion-acoustic waves it may be that these secondary irregularities contribute to the auroral clutter seen at high latitude.

5. IMPLICATIONS FOR DISTORTION OF TRANS-IONOSPHERIC RAY PATHS

In addition to direct auroral clutter ion-acoustic waves may contribute to errors in directional measurements made using radio paths that traverse the ionosphere. At first thought one is tempted to dismiss this possibility because the waves represent relatively modest variations in electron density (or index of refraction), and the

individual ion-acoustic wavelength is very small compared to, say, the principal Fresnel zone for a ground-based radio system. On the other hand, the spectrum of ion-acoustic waves contains coherent trains, and each train, when traversed by a radio wave, may be expected to behave like a diffraction grating and thus to divert part of the incident radio wave energy through an angle which depends only on the ratio of the acoustic wavelength to the radio wavelength. Here longer acoustic wavelengths (presumably more frequently occurring) would be important. Since a whole spectrum of acoustic wavelengths is present, a given radio wavelength would be spread out over some range of angles although the strength of the deviated signal would decrease rapidly with increasing deviation angle.

As far as is known no attempt has been made specifically to look for this effect of ion-acoustic waves. Extensive studies have been made of both amplitude and angular scintillations using both stellar and satellite sources of radio waves. Unfortunately at high latitudes the scintillations are usually so complex as to defy simple interpretation. Some work has been done by concentrating on isolated occurrences at both middle and high latitudes [17, 18, 19, 20]. Wherever detailed analysis was possible the angular deviation of the radio waves was interpreted as being due to refraction in a large ionospheric irregularity which behaved like the negative lens of Fig. 4 (a). While such an interpretation seems to fit the observations very well it is worth noting that the angle-of-arrival measurements have been made with a system which does not differentiate clearly between the arrival of a single phase front and several. In fact it would not distinguish between the situation of Fig. 4 (a) and that of 4 (b). It may well be worth performing new experiments to distinguish between refraction from large smoothly varying clouds and diffraction by patches of irregularities containing coherent wave trains.

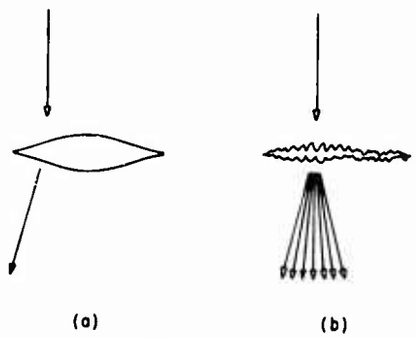

Fig. 4

In the meantime it may be worth noting that for the relatively weak angular scintillations that have so far been analyzed the apparent angular deviation of the radio waves is in the range 10^{-2} radians. This figure is typical of measurements in the 100 - 140 MHz frequency range. Presumably in the more complex situations that could not be analyzed in detail the angular deviations may be large. If such situations arose through diffraction then the measured angular deviation would be the resultant of a strong undeviated ray and a weak deviated ray, which suggests substantially larger angles of deviation than those measured. Finally it should be noted that according to the present picture of ion-acoustic waves the angular deviation resulting from the diffraction process should be much less frequency sensitive than the previously suggested refraction process. There is some evidence that, on occasion, the dependence of satellite scintillation on wavelength (λ) departs significantly from the expected value of λ^2.

6. CONCLUSION

Although it is well established that ion-acoustic waves occur in the high-latitude auroral ionosphere, there is not enough evidence to provide definitive estimates of the role that such waves play in producing auroral clutter on high latitude radars or in introducing angular errors into systems which make use of trans-ionospheric propagation.

REFERENCES

1. Collins C. and Forsyth P.A. "A bistatic radio investigation of auroral ionization". J. Atmos. Terr. Phys. 13, 315, 1969.

2. "Radio auroral nomenclature". IAGA News No. 7, 49 1968.

3. "Radio auroral nomenclature". URSI Bulletin No. 168, 24, 1968.

4. Harang L. and Tröim, J. "Investigation of auroral echoes". Planet. Space Sci. 5, 105, 1961.

5. Forsyth P.A. "Radio measurements and auroral electron densities". J. Geophys. Res. 58, 53, 1953.

6. Lyon G.F. and Forsyth P.A. "Radio-auroral reflection mechanisms". Can. J. Phys. 40, 749, 1962.

7. Forsyth P.A. and Vogan E.L. "The frequency dependence of radio reflections from aurora". J. Atmos. Terr. Phys. 10, 215, 1957.

8. Moorcroft D.R. "The interpretation of the frequency dependence of radio aurora". Planet. Space Sci. 14, 269, 1966.

9. Leadabrand R.L., Schlobohm J.C. and Baron M.J. "Simultaneous very high frequency and ultra high frequency observations of the aurora at Fraserburgh, Scotland". J. Geophys. Res. 70, 4235, 1965.

10. Farley D.T. "A plasma instability resulting in field-aligned irregularities in the ionosphere". J. Geophys. Res. 68, 6083, 1963.

11. McDiarmid D.R. "Ion-acoustic waves and radio aurora". Can. J. Phys. 48, 1863, 1970.

12. Hofstee J. and Forsyth P.A. "Ion-acoustic waves in the auroral plasma". Can. J. Phys. 47, 2797, 1969.

13. McDiarmid D.R. and McNamara A.G. "A physical model of a radio aurora event". Can. J. Phys. 47, 1271, 1969.

14. Hofstee J. and Forsyth P.A. "Ion-acoustic waves and aspect sensitivity in radio aurora". Unpublished.

15. Armstrong J.C. and Zmuda A.J. "Field-aligned current at 1100 km in the auroral region measured by satellite". J. Geophys. Res. 75, 7122, 1970.

16. Dougherty J.P. and Farley D.T. "Ionospheric E-region irregularities produced by non-linear coupling of unstable plasma waves". J. Geophys. Res. 72, 895, 1967.

17. Forsyth P.A. "Amplitude, phase and angle-of-arrival fluctuations". AGARD Lecture Series 41, 4-1, 1970.

18. Turnbull R.M. and Forsyth P.A. "Satellite studies of isolated ionospheric irregularities". Can. J. Phys. 43, 800, 1965.

19. Mason K.H., Tull E.H. and Forsyth P.A. "Rocket studies of isolated ionospheric irregularities". Can. J. Phys. 45, 3065, 1967.

20. Forsyth P.A. "Auroral energy input rates from radio scintillation measurements". Can. J. Phys. 46, 1841, 1968.

POLARIZATION OF WAVES SCATTERED FROM AURORA

A. Kavadas
Institute of Space and Atmospheric Studies
University of Saskatchewan
Saskatoon, Canada

SUMMARY

Radio waves propagating through the aurora change their state of polarization. Polarization changes are the result of the interaction between the propagating wave and the medium. Two basically different interactions contribute to the polarization changes. The gyrotropic properties of the ionosphere and the aurora produce the frequently observed Faraday rotation. In the presence of absorption Faraday rotation under certain conditions may depolarize the wave if the propagation path is sufficiently long. Scattering from anisotropic irregularities or reflections from sheet currents may alter the polarization of the incident wave quite markedly. Isotropic scattering which in itself cannot alter the polarization of the incident wave, may in the presence of absorption and Faraday rotation, produce results similar to those obtained from anisotropic scattering. The various interactions which lead to depolarization and cross-polarization will be examined and correlated to particular types of aurora and properties of the scattering medium. Experimental results obtained from complete polarization measurements will be used to demonstrate the nature of these interactions and the resulting changes in the polarization of the propagating wave. The experimental results were obtained with a time-sharing polarimeter which recorded six orthogonal components of aurorally backscattered waves at 42 MHz. Waves scattered in the forward direction were studied with partial polarization measurements (two orthogonal components) of radio star scintillations. The polarization of the received wave correlates with magnetic activity.

An electromagnetic wave is characterized by three parameters, its amplitude which is generally complex, its frequency and phase. When a wave propagates through a medium any one of these or all may change as the wave interacts with the medium. Media may be divided into two general categories isotropic and anisotropic. If it is assumed that spatial dispersions is absent, i.e. only EM waves are present then the two types of media may be defined in terms of their interaction with the propagating wave. Isotropic media may alter the frequency and phase of the wave if they are in motion but do not affect the complex amplitude of the wave although its magnitude may be altered if the medium is absorbing. Anisotropic media on the other hand alter both the magnitude and phase of the complex amplitude.

The ionosphere and the aurora are anisotropic media and for this reason it is customary to study wave propagation through them in terms of two orthogonal polarization components. If scalar wave equations are used for the study of radio waves propagating through the ionosphere the behaviour of the received wave cannot be related in any meaningful way to its interaction with the medium. To illustrate this point let us consider a wave received with a linearly polarized antenna. If the wave intensity fluctuates there is no way to decide whether the fading is caused by Faraday rotation or because of drifting diffraction patterns on the ground. This ambiguity cannot be resolved even if spaced antennas of the same polarization are used. If at least two components of polarization are received fading due to Faraday rotation may be reduced substantially. If all components of polarization are received then it is relatively simple to restore all the restorable information carried by the wave. Furthermore, the received signal contains all the available information about the interaction of the wave and the medium. The significance of receiving the complete wave lies in the amount of information that can be obtained if all the parameters that characterize it are known. This fact is well known to radio astronomers who have been using this technique for the study of emissions from radio stars ((1, 2, 3, 4)).

For propagation of VHF waves through the ionosphere or the aurora very little information exists ((5, 6, 7, 8, 9, 10)), although an impressive literature is available for frequencies near the critical frequency of those media.

In what follows the wave-medium interactions which change the wave polarization will be examined. It is convenient to divide these interactions into two types. Those interactions to which geometrical optics approximations can be applied, i.e. those interactions which involve media whose properties change only slightly over distances compared to λ_o, and those interactions which take place in media with parameters which vary significantly over distances comparable to the wave length. These two types of interaction relate to the physical properties of the medium and for that reason they do not affect the general mathematical formulation which follows. However the interpretation of the formulation becomes different for the two cases and in the discussion of experimental results it will become necessary to refer to these again.

The polarization of a wave may be described completely on a plane perpendicular to the direction of propagation. The quantity which defines the state of polarization of any wave is the ratio of any two of its orthogonal components. A number of geometrical representations of polarization exist, the most common being the Stocke's parameters and the coherency matrices. The wave-medium interactions presented in this paper will be expressed in terms of coherency matrices somewhat simplified to minimize the mathematical complexity.

A wave propagating through a medium may be cross-polarized, partially depolarized or completely depolarized as shown in Fig. 1. Any of these interactions may be represented by a linear relationship between an incident electric vector E^i and a transmitted thr[illegible] reflected or scattered electric vector E^s *. The incident wave which is here represented [illegible]tric vector E^i (where the time and propagation direction dependency have been omit[illegible]tten in matrix form as follows:

$$(E^i) = \begin{pmatrix} E_1^i \\ E_2^i \end{pmatrix} \tag{1}$$

Similarly the scattered etc. wave may be represented by a matrix defined by the following relation:

$$(E^s) = (\mathcal{L})(E^i) \tag{2}$$

Thus (E^s) refers to a scattered, transmitted etc. and (E^i) to an incident electric vector. The interaction between the medium and wave is embodied in the matrix ($\mathcal{L}$) which is generally complex. This matrix may be understood to be an operator which when operating on a wave with vector E^i representing any polarization produces a scattered, transmitted, etc. field E^s which may be cross-polarized, depolarized or in an entirely different state of polarization. If the wave is transmitted without scattering of any kind through an anisotropic medium (geometrical optics) then the medium can still be represented by the same operator as shown in Fig. 2.

Anisotropic media have properties which are different along different directions therefore if the electric vector of the incident wave is oriented in any direction its components along the directions of anisotropy react with the medium in different ways.

It is convenient therefore to resolve the incident wave along directions which coincide with the axes of anisotropy in the medium. Thus radio waves propagating through the ionosphere customarily are expressed in linear components parallel and perpendicular to the magnetic field or if the propagation is along the magnetic lines, in orthogonal circular components. The latter is desirable because for gyrotropic media it is not always possible to assign anisotropy axes in real space. Instead complex axes may be used which correspond to rotating axes in real space. Since the polarization of the transmitting antenna does not always coincide with an axis of anisotropy it is desirable to express the incident wave in terms of components which are parallel to the axes of anisotropy. After the interaction they may be expressed again in components consistent with the polarization of the receiving antennas. Thus if the transmitted wave is linearly polarized at an angle θ from the horizontal and the axes of anisotropy are orthogonal at an angle ϕ from the horizontal as shown in Fig. 3 the relation between transmitted and received E is given by:

$$\begin{pmatrix} E_v^R \\ E_h^R \end{pmatrix} = \left(\tilde{\Phi}\right)(\mathcal{L})(\Phi)\begin{pmatrix} E_v^i \\ E_h^i \end{pmatrix} \tag{3}$$

Propagation through the ionosphere and the aurora can be described by equation (3) only when the medium is fairly uniform with no intense fluctuations in its electron density and no regions with sharp changes in the electron density structure.

These requirements are not frequently met because the ionosphere and much more so the aurora are in continuous motion with regions where the electron density may vary over short distances and relatively rapidly in time (Fig. 4, Fig. 5). Under these conditions the wave may propagate over a variety of paths which may change rapidly. The interaction between the wave and such a medium can be described meaningfully only in terms of average properties of the medium. Clearly two averages are involved here, the antenna beam width effects a space averaging by viewing a large number of electron fluctuations and consequently intercepting several propagation paths. In addition the received signal is averaged in time by the receiving equipment which usually have time constants far in excess of the period of the received wave. Therefore a wave has a certain state of polarization only if that state is relatively constant over this time interval.

Equation (3) must be modified so that it can be used for media with properties which vary both in space and time. If there are several paths of propagation for the wave then the wave-medium interaction may be described by several operations ($\mathcal{L}$) one for each path. The received wave E^R would then consist of the sum of all the E^R's which arrive at the antenna over the different paths. Thus

$$(E^R) = \sum_j (\mathcal{L}_j)(E_j^i) \tag{4}$$

* This formulation is not necessarily limited to linear interactions it can be extended to account for multiple scattering or other types of non-linear interactions. In this presentation only linear relationships between E^i and E^R are considered, non-linear interactions will be assumed absent.

Equation (4) although more realistic still does not account for changes in the properties of the medium along any one of the many paths. To take into account such changes it is necessary to make ($\mathcal{L}_j$) a function of all space co-ordinates including that along the propagation path. To do so it is necessary to examine ($\mathcal{L}_j$) in more detail. Since the medium under consideration is the aurora and ionosphere it is reasonable to assign its anisotropy axes so that one of them is along the magnetic field direction and the other perpendicular to it. Therefore the matrix operator ($\mathcal{L}_j$) can be written:

$$(\mathcal{L}_j) = \begin{pmatrix} \ell_j e^{i\xi_j} & 0 \\ 0 & p_j e^{i\eta_j} \end{pmatrix} \tag{5}$$

where ℓ_j and ξ_j represent the changes in the amplitude and phase of the component of E^i parallel to the magnetic field and p_j and η_j those for the component perpendicular to it. As the wave propagates it interacts continuously with the medium consequently the amplitude and phase of its two components vary continuously. Thus:

and $\ell = \ell(xyz;t), p = p(xyz;t), \xi = \xi(xyz;t), \eta = \eta(xyz;t)$. The operator ($\mathcal{L}$) when written in this form represents the wave-medium interaction per unit volume of the medium, (Fig. 6). The received wave (E^R) is:

$$(E^R) = \int_v (\mathcal{L}(xyz;t))(E^i)\,dv \tag{6}$$

where the integral is evaluated over the volume in which the interaction takes place.

Assuming that a vertically polarized wave propagates through such a medium and that the receiving system employs a vertical and a horizontal antenna the wave intensities at these antennas are (Fig. 7)

$$I_v \sim (E_v^R)(E_v^R)^* \sim \left(\int_v \left(\ell^2(r)\cos^2\phi + p^2(r)\sin^2\phi + \ell(r)p(r)\cos(\xi(r) - \eta(r))\sin 2\phi\right) dv\right) I_v^i$$

$$I_h \sim (E_h^R)(E_h^R) \sim \left(\int_v \left(\ell^2(r) + p^2(r) - 2\ell(r)p(r)\cos(\xi(r) - \eta(r))\right)\tfrac{1}{2}\sin 2\phi\, dv\right) I_v^i \tag{7}$$

where all the antenna constants have been absorbed into I^i and the dimensions of the interaction volume have been assumed much shorter than the distance between transmitter and receiver so that E^i is approximately the same everywhere within that volume. The coefficients l, p and $\ell p\cos(\xi - \eta)$ in (7) are the elements of the coherency matrix referred to earlier ((11)).

Equations (7) represent the interaction between the wave and medium within a volume which is sufficiently large so that random phases introduced by the varying paths of propagation cancel out upon integration. This integration has been performed in Eq (7) so that l^2, p^2 have no phase factors of the form $\cos(\xi(r) - \xi(r'))$, $\cos(\eta(r) - \eta(r'))$. The phase factors $\cos(\xi(r) - \eta(r))$ do not always disappear even if the interaction volume is large. If the medium is anisotropic but the phase difference between the components along the axes does not vary significantly from point to point the wave exits the medium with two components proportional to ℓE^i and pE^i and an average phase between them $\langle \xi - \eta \rangle$. Such a medium is said to be homogeneously anisotropic. If on the other hand the anisotropic properties of the medium vary randomly from point to point the phase difference between the two components changes its value by large amounts so that it cancels out upon integration. Such a medium is said to be inhomogeneously anisotropic.

Radio aurora as a medium can behave either homogeneously or inhomogeneously. Therefore if a vertically polarized wave is transmitted through it becomes depolarized. The degree of depolarization depends on how homogeneous are the anisotropic properties of the medium. If the medium is strongly inhomogeneous the phase terms in the integrals (7) approach zero and the components I_v and I_h become incoherently related. Their magnitudes however, are unequal as can be seen from equations (7). This suggests that the plane of polarization along which I becomes maximum lies somewhere between the vertical and horizontal. Its location may be calculated from (7). When this is done it is found that I is maximum when the plane of polarization has the same direction as that anisotropy axis which is closest to the vertical. The presence of this maximum implies that the wave cannot be depolarized completely even when its l and p components are completely incoherent. This behaviour of the polarization of the wave was verified experimentally by receiving radar echoes with two linearly polarized antennas at 45^0 to the vertical ((7)). Echoes received from the eastern sector of the aurora were stronger at the dipole whose direction was close to that of the magnetic lines while echoes from the western sector were stronger on the other dipoles because the magnetic lines are tilted in the

opposite direction on the west side of the magnetic meridian. The results of these measurements are shown in Fig. 8.

If the medium is homogeneously anisotropic the emerging wave has an average phase between its two components and in the most general case it becomes in part elliptically polarized with some of its intensity being unpolarized. The direction of the major axis of the ellipse depends on the degree of anisotropy which is related to the ratio $|\rho|/|\rho|$ and it may be oriented in any direction on either side of the axis of anisotropy closest to the vertical. If the medium is isotropic then $l = p$ and $\xi - \eta = 0$. In this case the wave is neither cross-polarized nor depolarized as may be seen from (7) where I_A becomes zero and all the energy is contained in the I_v component. This case is of no practical value because even if the reflection or scattering are isotropic the gyrotropic properties of the medium will effect at least a rotation in the plane of polarization (Faraday rotation) which in the absence of absorption cross-polarizes the wave as may be seen from (7) by making $l = p$ but $\xi - \eta \neq 0$.

The degree of polarization may be used to determine the degree of homogeneity in the medium because the two are closely related. If the wave contains a substantial unpolarized component it is evident that the anisotropy in the medium is not the same everywhere and that as the inhomogeneity increases so does the intensity of the unpolarized component. Therefore the ratio of the polarized to the unpolarized intensity I_p/I_u may be used as a measure of homogeneity in the anisotropic properties of the medium. In order to determine the I_p and I_u components it is necessary to record all components of polarization. From these it is easy to determine this or the more convenient quantity m the polarization ratio which is defined as the ratio of the polarized intensity to the total intensity $m = I_p/I_p+I_u$. Complete polarization measurements of radio aurora were made ((12)) for a variety of cases and types of aurora. These measurements were made with a time sharing polarimeter with a time resolution of 200 samplings per sec which allowed the calculation of the complete polarization every 1/40 sec. The high resolution of the instrument made it possible to study fluctuations with frequency components in the high end of the spectrum ((13)).

These measurements were limited to backscattered waves from radio aurora and it was possible to separate two conditions of the medium which produced distinctly different polarization states in the received wave ((10)).

The behaviour of the polarized and unpolarized intensity of auroral backscatter is shown in Fig. 9 where the rapid changes in intensity are evident particularly in I_p. This event is characterized by very little depolarization as both the I_u and m plots show. Therefore the average phase does not fluctuate very violently within the scattering volume but it has a relatively steady value over the detector response time which provides the ellipticity in the received wave shown in Fig. 9 (Poincare sphere). The major axis of the ellipses lie in a sector centered approximately 45^0 off the horizontal which was the polarization of the transmitted wave.

This type of signal suggests that changes in its intensity are the result of significant increases in the reflectivity of the medium (or its equivalent for scattering an increase in its scattering cross sections) i.e. in the value of l and p.

A signal like this may be produced by a relatively small number of scattering centers which flare up for short periods of time. Since the number of scatters is limited the average phase $\langle \xi - \eta \rangle$ takes non zero values which however may fluctuate significantly thus the major axis of the ellipse may be found anywhere on either side of the anisotropy axis as evidenced by the spread in the Poincare sphere shown in Fig. 9. In this case the received signal is strongly polarized as the relatively high value of m suggests. A different situation prevails in the signal shown in Fig. 10 here both I_p and I_u increase approximately at the same time leaving m relatively constant however at much lower value than in the previous case. In this case the scattering volume is considerably larger so that the value of the phase $\langle \xi - \eta \rangle$ approaches zero. The presence of a strong I_u component bears this out. In addition the major axes of the received ellipses lie very close to the direction of the anisotropy axis perpendicular to the magnetic field lines. (The transmitter polarization is horizontal here hence the anisotropy axis closest to this direction is that which is perpendicular to the magnetic lines). The changes in the total intensity must be attributed again to changes in the reflectivity l, p. Since the phase $\langle \xi - \eta \rangle$ has a value near zero as a result of the integration over the scattering volume changes in the values of ξ and η do not affect is average value. The signal in Fig. 10 is the result of an interaction between an inhomogeneously anisotropic medium and the wave. The long range lower value of m for this type of scattering may be used as an additional argument in favour of this configuration. In both Fig. 9 and 10 the relatively constant value of m is interpreted as an indication that no serious changes in the inhomogeneity of the medium occur. It is easy to see that over short time intervals m and I_u, I_p may change in antiphase. Such changes indicate that the homogeneity in the anisotropy of the medium may vary. An example of this is shown in Fig. 11 where I_u and m have been plotted together. In this figure when I_u increases m decreases and vice-versa. Therefore when the intensity increases it is followed by a reduction in coherence which may be attributed to a decrease in the homogeneity of the medium. This may come about by two different processes, either the anisotropic properties of the medium change suddenly from point to point with a simultaneous increase in reflectivity to account for the increased intensity or the scattering volume increases suddenly and more propagation paths develop which in turn contribute to the destruction of coherence. The second interpretation appears more promising because it is more consistent with arguments based on purely physical grounds.

The experimental results discussed so far represent backscattering of radio waves without specific reference to direct propagation effects. The well known and commonly observed Faraday effect is usually considered the major cause for cross-polarization and even depolarization. Cross-polarization is an obvious result of Faraday rotation and it will not be considered further. The contribution of Faraday rotation to depolarization however is questionable. If a linearly polarized wave is Faraday rotated the phase $\xi - \eta$ between two linear components remains constant even if its circular components are related through a varying phase which is proportional to its path. Therefore propagation through

several paths will not affect its average phase

If the plane polarized wave is differentially absorbed at the same time as it rotates then the phase $\xi - n \neq 0$ and it may vary from path to path resulting in partial depolarization of the wave.

In the next illustration the effect of Faraday rotation is demonstrated for waves which presumably enter the aurora in a completely depolarized state and through a combination of phase retardation (Faraday rotation) and differential absorption become partially polarized.

Emissions from Radio stars were observed with two interferometers of identical characteristics and geometry except for the polarization of their antennas which were linear and orthogonal to each other ((14)).

Since the radio star approximates a point source the propagation vector was confined to a narrow solid angle, i.e. few paths almost parallel to each other. The anisotropy of the medium resulted in interference patterns which were displaced relative to each other. The inhomogeneity of the medium introduced fluctuations both in amplitude and phase, the well known and frequently observed radio star scintillations. It was observed that the scintillations received at the two antennas were almost uncorrelated under quiet conditions, the correlation increasing with magnetic activity. Fig. 12 shows this where the normalized difference between the signals received by the two interferometers is plotted for a magnetically active and a quiet event. In Fig. 13 and 14 the coherence between the signals recorded by the two interferometers is shown as function of the frequency content in the two signals and in Fig. 15 it is shown that the duration of coherence is linearly related to the magnetic activity.

These relations suggest that the two interferometers do not see the same star image but two separate images displaced relative to each other. Since the two images represent different propagation paths their scintillations are not correlated. As the magnetic activity increases the scintillation amplitude increases so that the star images begin to overlap thus increasing the correlation between the two signals.

The presence of different indices of refraction for the two linear polarizations is a direct result of the gyrotropic properties of the medium which however cannot polarize an unpolarized wave if no absorption is present. Unfortunately these were not complete polarization measurements therefore it is difficult to decide whether the increased coherence at the higher frequencies is in any way associated with reduction in the polarization ratio m. Knowledge of the behaviour of m could provide considerably more information about the reasons which cause the two radio star images to overlap.

REFERENCES

1. Cohen, M. H., Radio Astronomy Polarization Measurements, Proc. IRE, 46, 172-183, 1958a.

2. Hatanaka, T., The Faraday Effect in the Earth's Ionosphere with Special Reference to Polarization Measurements of Solar Radio Emission, Pub. Astron. Soc. Japan, 8, 73-86, 1956.

3. Ko, H. C., On the Analysis of Radio Astronomical Observations Made with High Resolution Radio Telescope Antennas, Radio Observatory, Dep. Elec. Eng., Rep. 21, Ohio State University, 1961.

4. Papas, C. H., Theory of Electromagnetic Wave Propagation, McGraw-Hill, New York, 1965.

5. McNamara, A. G., and B. W. Currie, Polarization of Radio Echoes from Aurorae, Nature, 174, 1153-1155, 1954.

6. Harang, L., and B. Landmark, Radio Echoes Observed During Aurorae and Geomagnetic Storms Using 35 and 74 Mc/s Waves Simultaneously, J. Atmos. Terr. Phys., 4, 322-338, 1954.

7. Kavadas, A., and D. Glass, Polarization of Radar Echoes from Aurora, Can. J. Phys., 37, 690-697, 1958.

8. Harang, L., and J. Troim, Investigation of Auroral Echoes, Planet. Space Sci., 5, 33-45, 1961.

9. Egeland, A., Studies of Auroral Reflections in the VHF Band, Ark. Geofys., 4, 103-169, 1962a.

10. Sofko, G. J. and A. Kavadas, Polarization Characteristics of 42-MHz Auroral Backscatter, J. Geophys. Res., 76, 1178-1792, 1971.

11. Born, M., and E. Wolf, Principles of Optics, Pergamon, New York, 1959.

12. Sofko, G. J., 1968, Ph.D. Thesis, University of Saskatchewan.

13. Sofko, G. J., and A. Kavadas, Periodic Fading in 42-MHz Auroral Backscatter, J. Geophys. Res., 74, 3651-3658, 1969.

14. Dixon, A. F., 1964, M.Sc. Thesis, University of Saskatchewan.

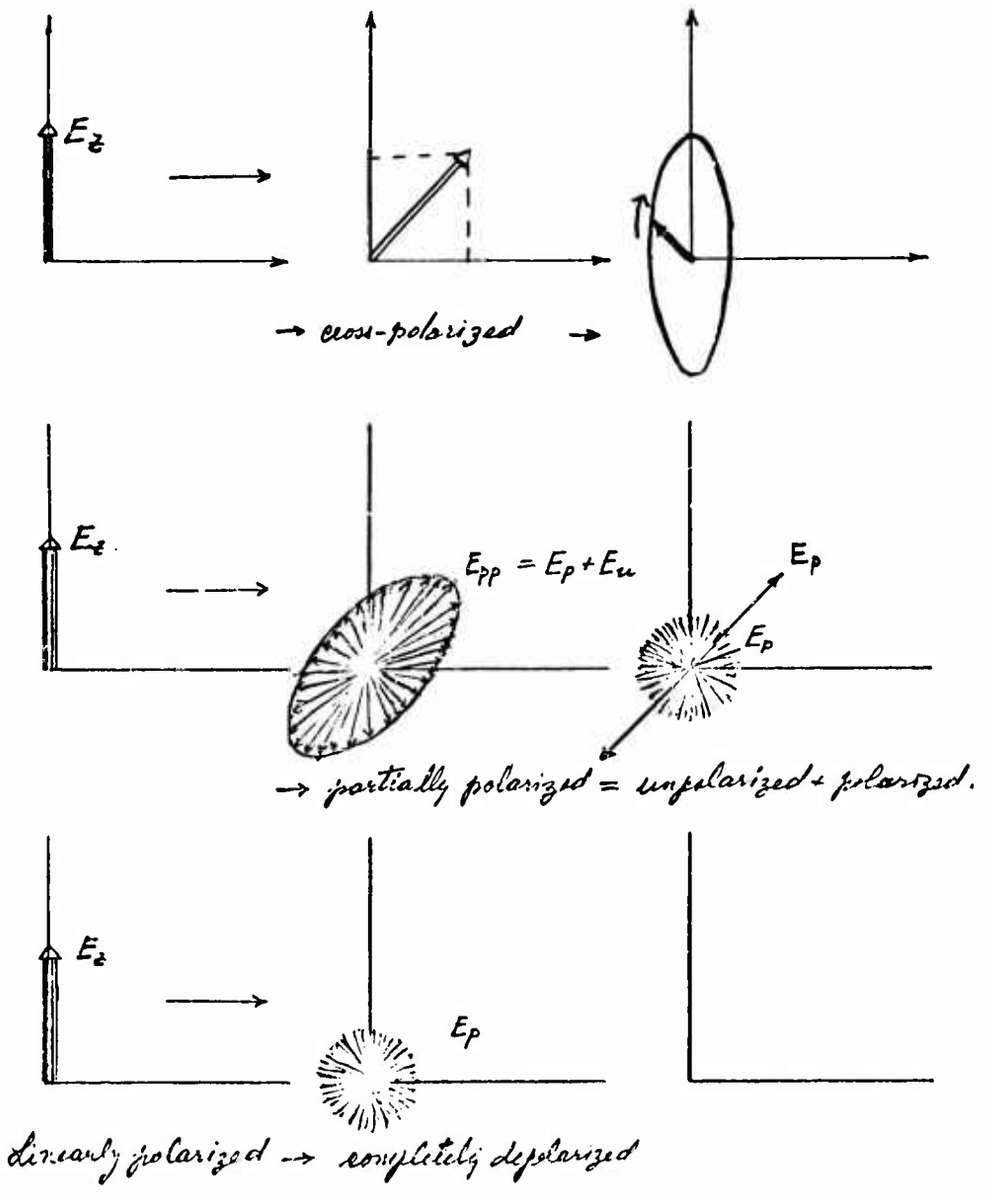

Figure 1

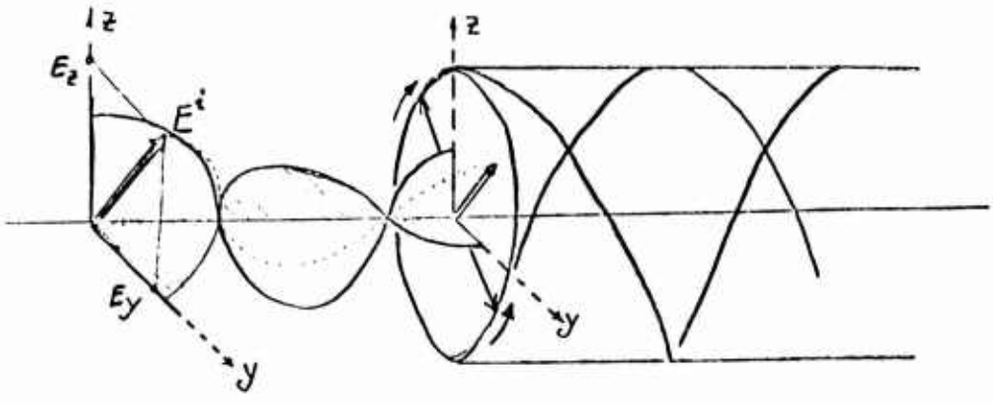

$$E^i = \begin{pmatrix} E_z^i \\ E_y^i \end{pmatrix} \longrightarrow \begin{pmatrix} E_r \\ E_\ell \end{pmatrix} = \begin{pmatrix} 1 & i \\ 1 & -i \end{pmatrix} \begin{pmatrix} E_z \\ E_y \end{pmatrix}$$

Figure 2

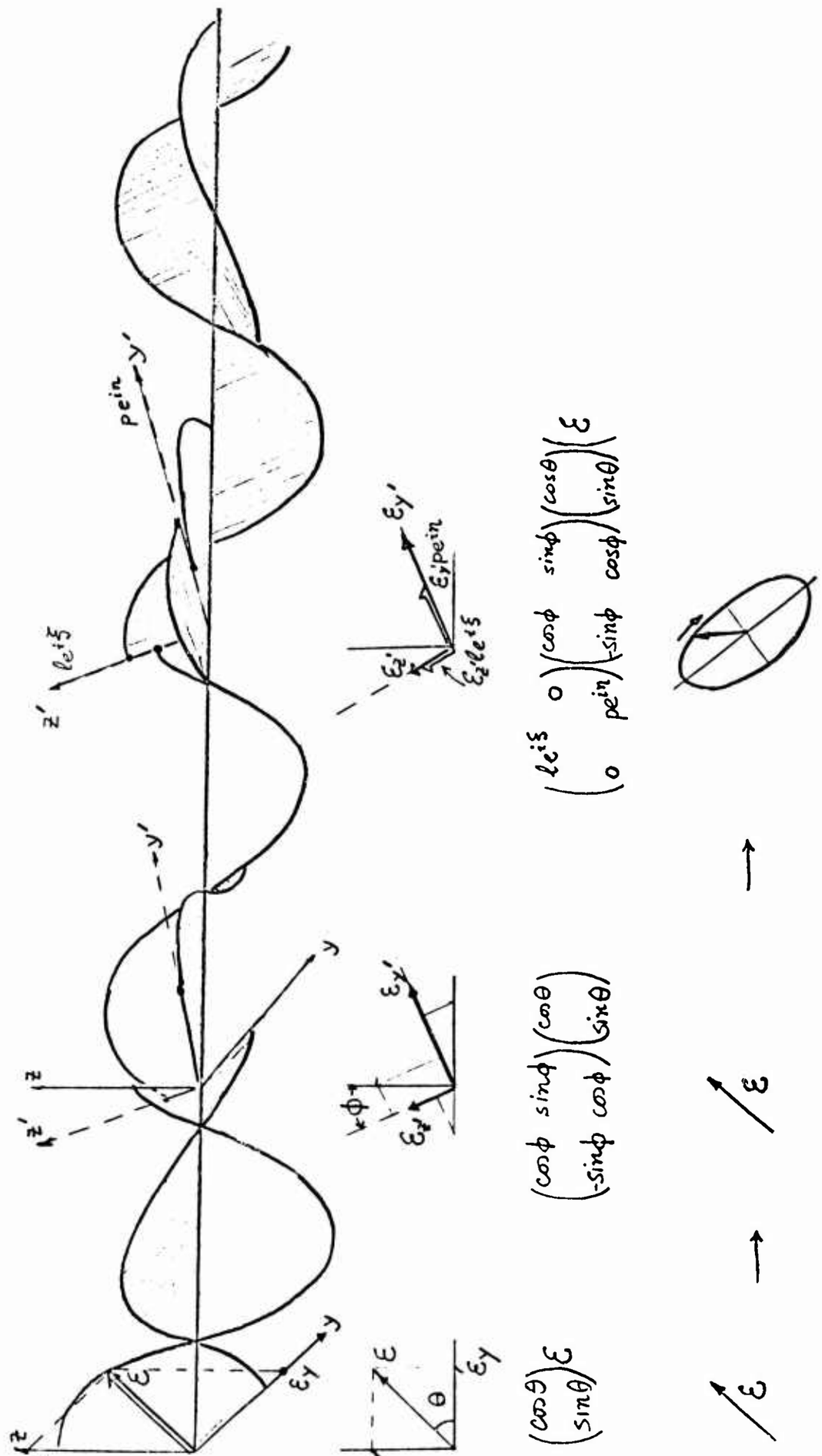
z'
$le^{i\xi}$
pe^{in}
y'
-y'
z
y
$\mathcal{E}_z$
$\mathcal{E}_y$
$\mathcal{E}$
θ
$\mathcal{E}_{y'}$
$\mathcal{E}_{z'}$
φ
$\mathcal{E}_{z'}$
$\mathcal{E}_{y'}$
$\mathcal{E}_z' le^{i\xi}$
$\mathcal{E}_y' pe^{in}$
$\begin{pmatrix} \cos\theta \\ \sin\theta \end{pmatrix} \mathcal{E}$
$\begin{pmatrix} \cos\phi & \sin\phi \\ -\sin\phi & \cos\phi \end{pmatrix} \begin{pmatrix} \cos\theta \\ \sin\theta \end{pmatrix}$
$\begin{pmatrix} le^{i\xi} & 0 \\ 0 & pe^{in} \end{pmatrix} \begin{pmatrix} \cos\phi & \sin\phi \\ -\sin\phi & \cos\phi \end{pmatrix} \begin{pmatrix} \cos\theta \\ \sin\theta \end{pmatrix} \mathcal{E}$

Figure 3

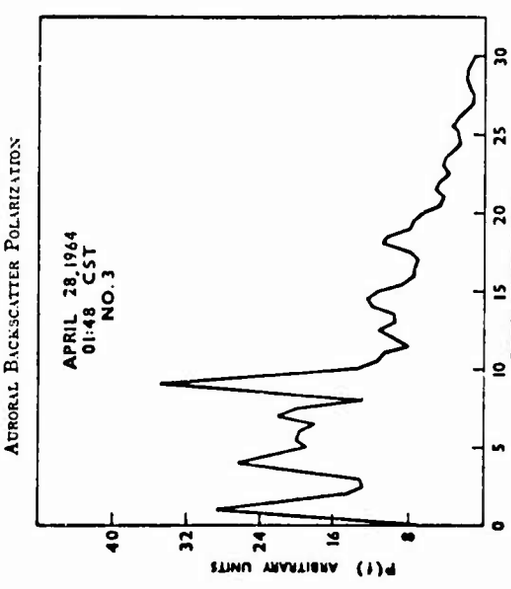

Power spectrum (1300 points) of April 28, 1964, event at 01:48 CST.

Figure 4

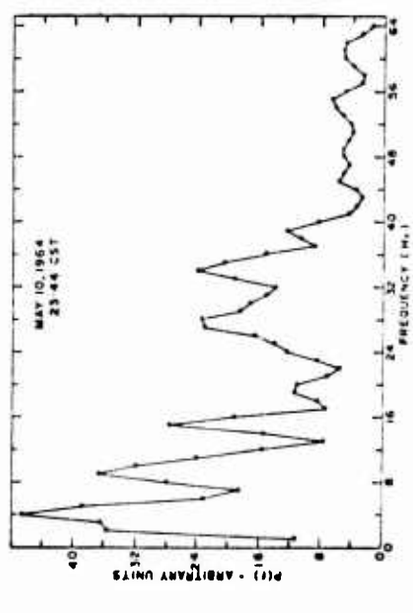

Power spectrum of event at 23:44 CST, May 10, 1964

Figure 5

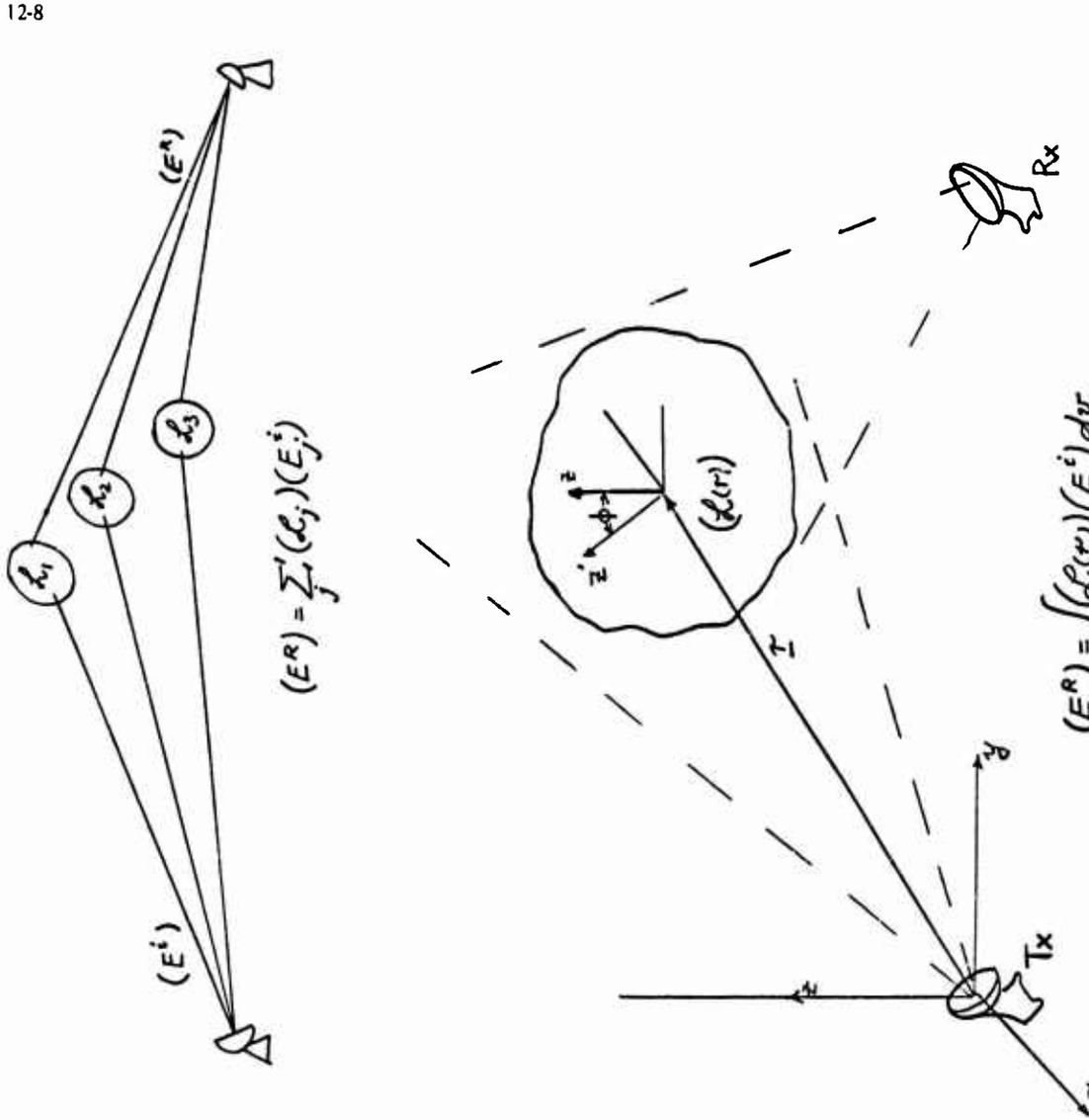

Figure 6

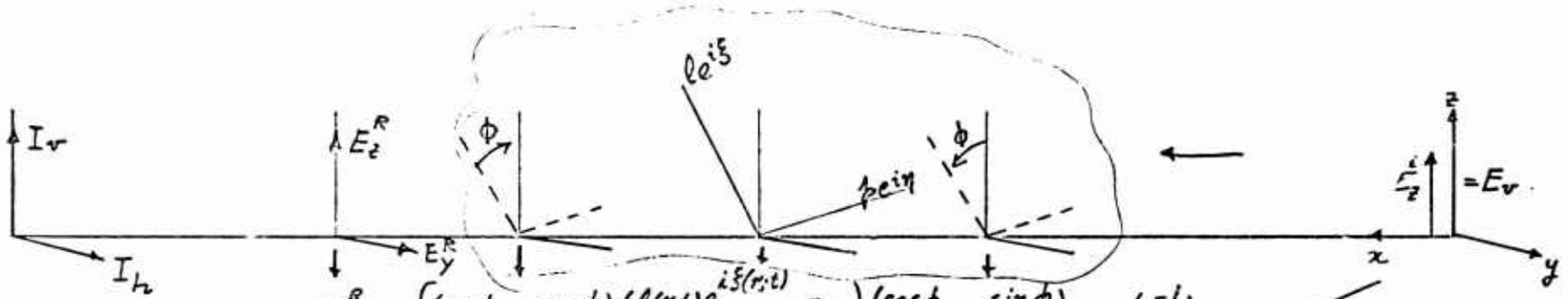

$$(E^R) = \begin{pmatrix} E_z^R \\ E_y^R \end{pmatrix} = \int \begin{pmatrix} \cos\phi & -\sin\phi \\ \sin\phi & \cos\phi \end{pmatrix} \begin{pmatrix} l(r;t)e^{i\xi(r;t)} & 0 \\ 0 & pe^{i\eta(r;t)} \end{pmatrix} \begin{pmatrix} \cos\phi & \sin\phi \\ \sin\phi & \cos\phi \end{pmatrix} dv \begin{pmatrix} E_z^i \\ 0 \end{pmatrix}$$

$$(E^R) = \begin{pmatrix} \int_v (l(r)e^{i\xi(r;t)}\cos^2\phi + p(r;t)e^{i\eta(r;t)}\sin^2\phi)dv & \int_v (l(r;t)e^{i\xi(r;t)} - p(r;t)e^{i\eta(r;t)})\cos\phi\sin\phi)dv \\ \int_v (l(r;t)e^{i\xi(r;t)} - p(r;t)e^{i\eta(r;t)})\cos\phi\sin\phi)dv & \int_v (l(r;t)e^{i\xi(r;t)}\sin^2\phi + p(r;t)e^{i\eta(r;t)}\cos\phi)dv \end{pmatrix} \begin{pmatrix} E_z^i \\ 0 \end{pmatrix}.$$

$$I = \begin{pmatrix} I_v \\ I_h \end{pmatrix} \sim \int_v \int_{v'} (E^R)(E^R)^* dv dv' = \begin{pmatrix} \int_v \left(l^2(r)\cos^2\phi + p^2(r)\sin^2\phi + l(r)p(r)\cos(\xi(r) - \eta(r))\right)\sin 2\phi(r)\, dv\, I^i \\ \int_v \left(l^2(r) + p^2(r) - 2l(r)p(r)\cos(\xi(r) - \eta(r))\right)\frac{1}{2}\sin 2\phi\, dv\, I^i \end{pmatrix}$$

Figure 7

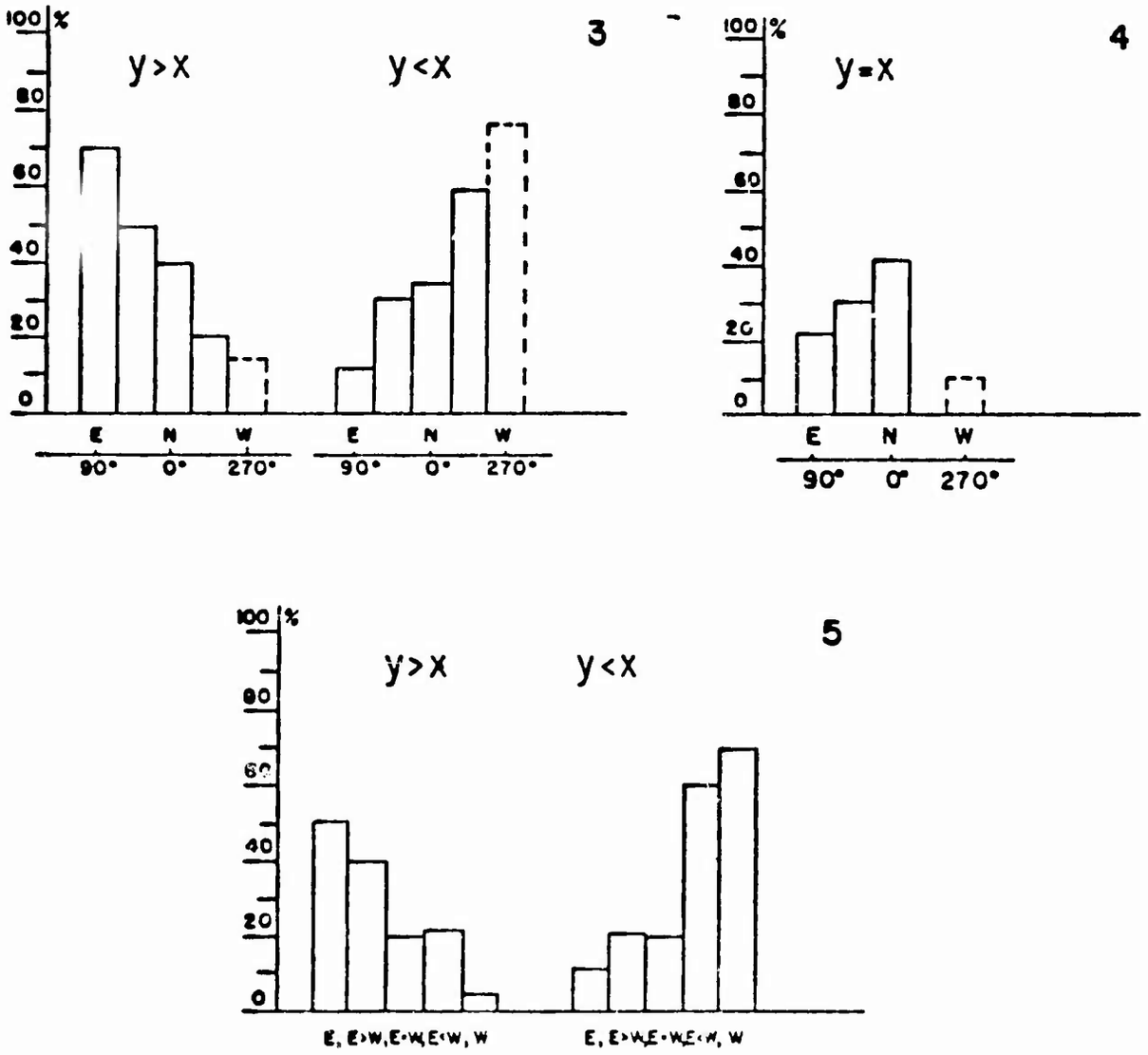

3. Percentage echo occurrence plotted against position of antenna: (*a*) echoes with $y > x$; (*b*) echoes with $y < x$.
4. Percentage of echoes of equal intensity on both dipoles ($y = x$) plotted against antenna position.
5. Percentage echo occurrence plotted against azimuthal direction of echo arrival.

Figure 8

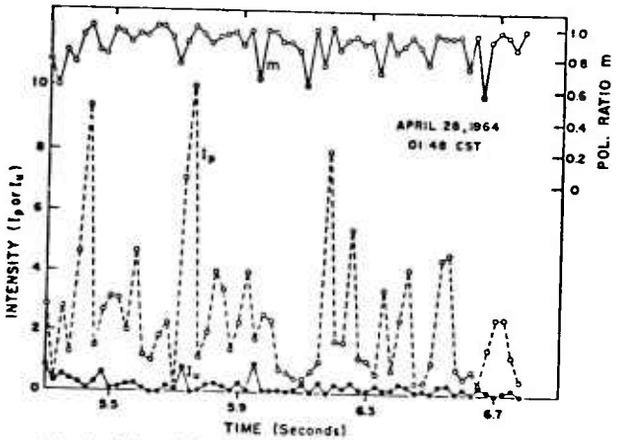

Graph of Ip and Iu versus time for April 28, 1964, event at 01:48 CST.

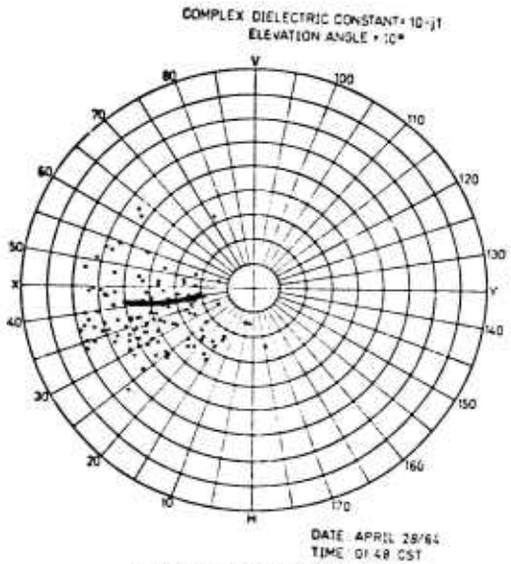

Poincaré sphere plot of April 28 event.

Figure 9

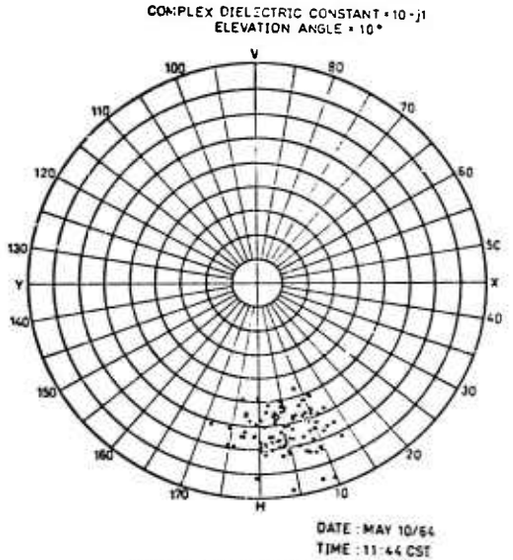

Poincaré sphere plot of May 10 event.

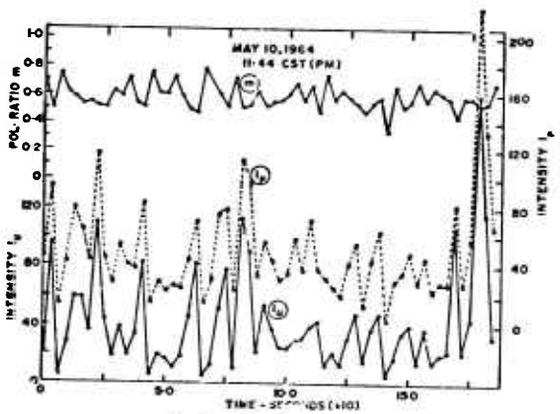

Graph of Ip, Iu, and m versus time.

Figure 10

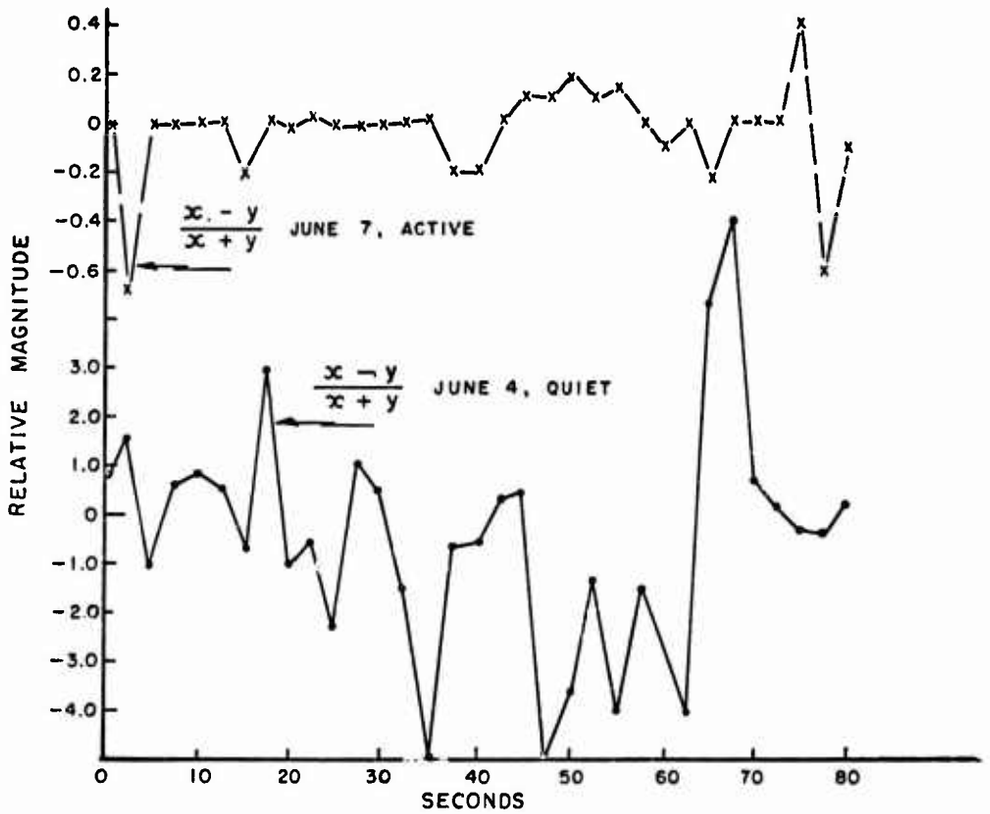

RATIO OF DIFFERENCE TO SUM OF AMPLITUDES OF x AND y COMPONENTS AGAINST TIME.

Figure 12

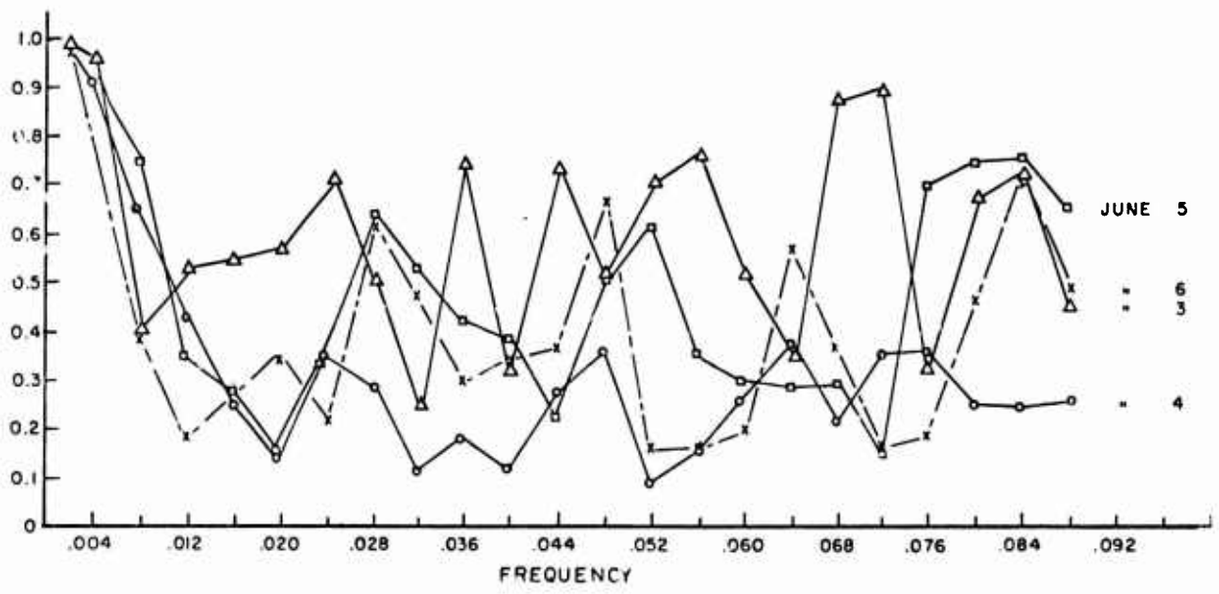

GROUP 0 COHERENCE VS. FREQUENCY 80 % OF POINTS WITHIN 5db INTERVAL

Figure 13

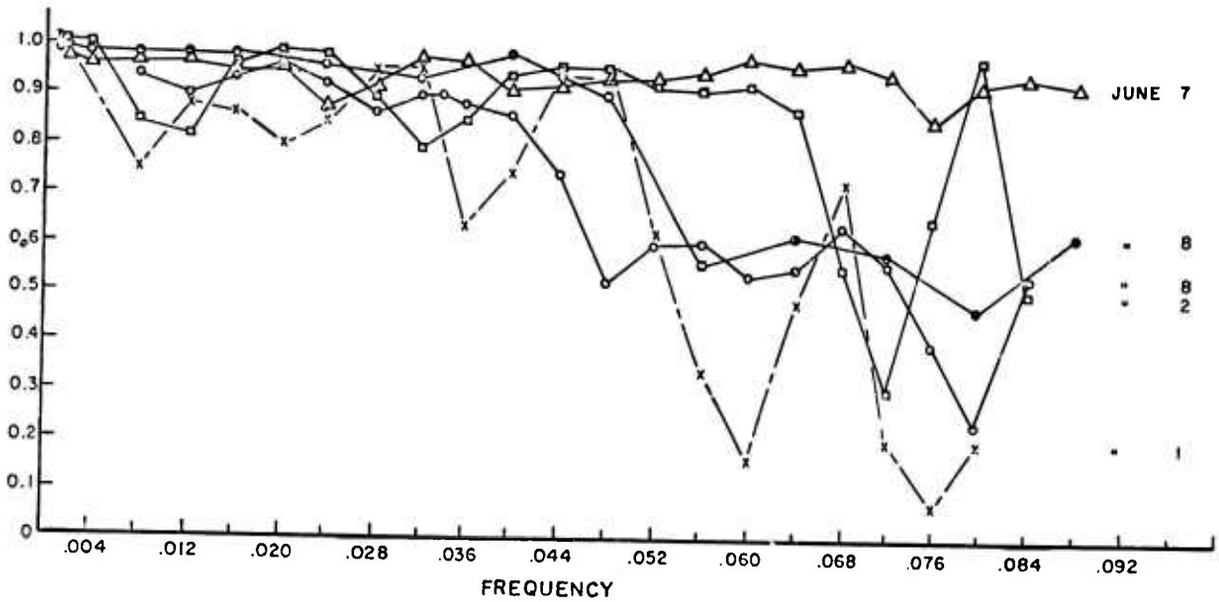

GROUP 4 COHERENCE VS. FREQUENCY 80% OF POINTS WITHIN 5 db INTERVAL

Figure 14

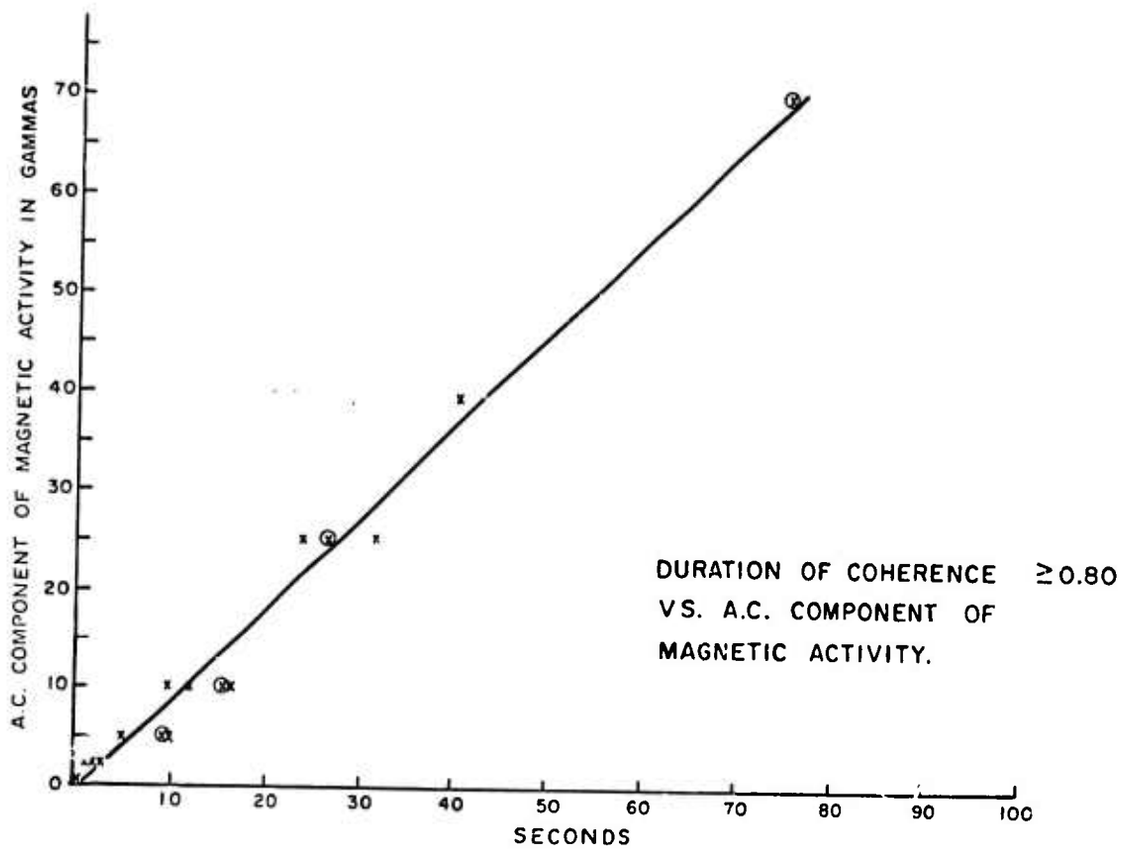

Figure 15

NON SPECULAR IONOSPHERIC CLUTTER IN THE VHF AND UHF BANDS

G N Taylor
Royal Radar Establishment
Malvern, UK

SUMMARY

This paper is concerned with the intensity of weak scattering from electron density irregularities in the high latitude ionosphere, in directions not perpendicular to the magnetic field. Such signals may cause clutter in sensitive radar systems at wavelengths between 10m and 0.1m. The literature is surveyed, to obtain typical and 'worst case' values of the rms density deviation and scale size of the irregularities, and to select appropriate spatial auto correlation functions. Assuming an isotropic distribution, conservative scattering cross sections are calculated. It is concluded that non-specular clutter is most unlikely to be more intense than the background incoherent (Thomson) scatter signals at wavelengths less than about 4m, unless the acf becomes markedly non Gaussian: such an eventuality is probably infrequent and transient. The spatial variability and spectral characteristics of incoherent and non-specular clutter signals are discussed briefly.

1. INTRODUCTION

It is well known that local irregularities of electron density in the ionosphere can give rise to various abnormal types of radio wave propagation. In the HF band they can be thought of as causing ripples or distortions in the undisturbed reflecting surface, which give rise to strong scattering, and cause such phenomena as sidescatter, backscatter, spread echoes, etc. At VHF and UHF frequencies, however, where specular reflection does not occur, and refraction is small, the irregularities have to be thought of as a 3-dimensional distribution of fluctuations in the refractive index, which causes weak scattering. Normally there will be a continuous spectrum of spatial dimensions of the fluctuations, from which a given radar system, operating on a wavelength λ, will select a Fourier component with 'wavelength' $\lambda/2 \sin \frac{\theta}{2}$, where θ is the scattering angle. Irregularities of electron density, which could give rise to weak scattering, are particularly intense in the Arctic ionosphere. Such scattered signals would cause a particularly undesirable form of clutter, and this paper attempts to decide, in the light of current knowledge, in what circumstances these signals are likely to be detectable.

The most fundamental form of weak scattering from the ionosphere is incoherent scattering (sometimes called Thomson scattering). This is caused by thermally induced irregularities on the scale of the Debye length, which are necessarily present in any gaseous plasma at a finite temperature: thus it will always be present in any radar beam which intersects the ionosphere, and can be regarded as giving a 'background' clutter level. It is distinguished by its very small volume scattering cross section, which is practically independent of wavelength in the VHF and UHF bands.

Another form of scattering is seen at high latitudes, if a region of the ionosphere containing macroscopic elongated magnetic-field-aligned electron density irregularities is viewed by a radar in a direction within a few degrees of the normal to the local field direction. The morphology of this 'specular' scattering is quite well known, and its intensity falls off fairly rapidly with decreasing wavelength. It is associated particularly with the auroral electro-jet, and is usually known as the radar aurora.

Careful investigations with sensitive radars have usually shown no indication of echoes coming from directions more than 10^0 away from the specular direction[1,2] The observations on which this conclusion is based have been made either at UHF frequencies from sub-auroral latitudes, or at extreme range at stations at higher latitudes. From most Arctic sites it is not in fact possible to view the specular region in the ionosphere, since it occurs at too low an altitude. There are however reports that non-specular scattering can sometimes be observed from stations at high geomagnetic latitudes. Thus Owren[3] has reported indications of backscatter in satellite signals at 136 MHz, while Frihagen and Folkestad[4] have observed non-specular F-region scatter at low VHF frequencies from a high latitude site. Possibly the most interesting observations are those of Bullough[5] who consistently detected weak auroral type echoes at 73 MHz from a station well inside the Southern polar cap, with off-specular angles greater than 13^0. Also relevant are the unusual clutter echoes reported by Farley et al[6] at the Jicamarca incoherent scatter radar station. These echoes were obtained during the night from the F-region, at a frequency of 50 MHz, and an off-specular angle of 3^0, with an aerial beamwidth of 1^0. Jicamarca is near the magnetic equator, so that phenomena observed there cannot be directly extrapolated to the Arctic; nevertheless this work serves to illustrate the current uncertainty about non-specular clutter, since the equatorial phenomenon is not readily explicable[6].

2. CHARACTERISTICS OF THE AURORAL IONOSPHERE

Information about the electron density irregularities which could cause weak scattering is available from satellite and radio star scintillation studies, and from direct sampling probes on satellites and sounding rockets. We shall be concerned here principally with F-region irregularities, and with identifying the 'worst case' parameters, ie, to see which conditions are most likely to give rise to weak scattering.

2.1. Size of the Irregularities

A review of scintillation studies by Getmantsev and Eroukhimov[7] shows that at mid-latitudes

the irregularities have transverse scale size L' of about 1 km. Satellite scintillation data show that L' decreases with increasing latitude in the sub-auroral regions[8]. Radio star scintillation measurements[9] and direct sampling from a satellite[10] show that a typical value of L' in the polar regions is 600m. Sometimes, however, L' can decrease markedly at high latitudes, so that a radio star or satellite interferometer may observe fringe visibility fades on baselines as short as 200m: this implies the simultaneous presence of very intense scintillation and of a scale size of the ground diffraction pattern which is less than the baseline. Caution is needed in interpreting these observations, but various authors find that during visibility fades the upper limit on L' is 300m[11], 200m[12], 150m[13], or even as small as 10m[3]. Direct sampling measurements also show that on occasion L' may become markedly smaller than normal, and when this happens there are significant irregularities with scales down to 200m[10] (the resolution limit of the instrument). A recent rocket experiment which gave results with a spatial resolution of 10m[14] shows that structure in the electron density profiles with peak-to-peak spacing down to 20m is certainly present in the disturbed Arctic ionosphere. Satellite scintillation rate measurements at Kiruna suggest that structure with L' $\sim$ 30m may sometimes occur (L Liszka, private communication). Thus the present evidence is that in the worst case the irregularities may have a dominant scale size of as little as 10m, but the possibility that considerably finer structure may sometimes be present cannot be excluded.

2.2. Intensity of the Irregularities

The intensity of the irregularities is specified by the deviation, ΔN_e, from the mean electron density, N_e; the rms value $\sqrt{(\Delta N_e/N_e)^2}$ is usually quoted. This parameter can be inferred from scintillation studies to have a typical value $\gtrsim$ 1% at mid latitudes[7], but can have a considerably larger value at auroral latitudes[7,15]. The most satisfactory results come from direct measurements, but are unfortunately very sparse. The most comprehensive measurements are those of Dyson[10], which clearly demonstrate the increase of intensity with latitude, and also have good statistics of the occurrence of a range of $(\Delta N_e/N_e)$ at high latitudes. It is found that the rms value in the high latitude region is about 30%, and is slightly larger at night than by day. A few values $\gtrsim$ 100% were found, but the recent rocket probe results of Frihagen and Jacobsen[15] suggest that such extreme values are probably associated mainly with isolated 'ledges'.

2.3. Statistics

A statistical description of the irregularities can in principle be given by specifying the rms density deviation and the 3-dimensional autocorrelation function (acf) of the deviations. Leaving aside for a moment the question of whether the auroral ionosphere is in fact statistically homogeneous, the best form of the acf must be discussed. Traditionally, a Gaussian acf has been assumed, partly for mathematical convenience and partly on the basis of some experimental evidence. This evidence comes from measurement of the spectrum[8] or acf[16] of scintillations at the ground under single-scattering conditions at mid-latitudes. Jesperson and Kamas[17], however, find the spectrum of irregularity sizes may be dominated by one or more discrete components (ie the acf will be quasi-sinusoidal), while Eroukhimov and Ryzhov[18] find that the irregularity spectrum may sometimes be 'broader than Gaussian' (ie the acf will be narrow). Measurements of the acf at auroral latitudes have been made with multiple baseline interferometers, but the published results are sparse. Some Russian results from measurements made at Murmansk[15] show that the acf varies considerably from case to case, but is quite often Gaussian.

2.4. Variability

To conclude this section, the temporal and spatial variability of high latitude irregularities will be considered briefly. The most extensive information undoubtedly comes from studies of spread-F, but will not be used here, for two reasons. Firstly, while the occurrence of spread-F is a very good indicator of the presence of ionospheric 'roughness', it is not possible to deduce much about the intensity or acf of the irregularities: secondly, spread-F data are necessarily taken from the topside or the bottomside ionosphere only, and may give misleading results if taken to represent the condition of the whole ionosphere[19]. The most useful results come from scintillation studies, since the scintillation intensity is, under single-scattering conditions, proportional both to $\sqrt{(\Delta N_e/N_e)^2}$ and to the thickness of the irregular layer[7]. It is found that the polar region of intense scintillation has a boundary lying at a lower latitude than the auroral oval, which moves equatorwards at night and when magnetic activity increases[21,22]. Synoptic observations at Kiruna[23] have shown that high latitude scintillation intensity increases with magnetic activity, and has a diurnal variation of about 2:1, peaking at magnetic midnight. Measurements of the altitude of the scintillation-producing layers show that these may occur anywhere between 100 and 1000 km, but are commonest at about 300 km, and are often observed in layers $\sim$ 50-100 km thick[7]. The radio star fades (which probably represent the 'worst case' from the present point of view) are commonest at night during the winter, and tend to move from North to South during the night[24]. The duration of these fades observed from the ground may vary from 10 to 100 minutes[11], and they appear to be associated with patches of the very small scale irregularities[3]. This patchy structure of the fine irregularities is also noticeable in the rocket probe results referred to above[14].

3. SCATTERING CROSS SECTION

3.1. Method of Calculation

The effects of non-specular ionospheric clutter on any given radar system can be calculated, given the wavelength, aerial gain, type of modulation, etc of the radar, and the scattering cross section of the clutter. Since the characteristics of radars are so variable, we shall only calculate here the scattering cross section, σ, as a function of λ. The parameter σ is defined in the usual way by

$$\sigma = 4\pi\sigma_o \qquad \text{.....(1)}$$

where σ_o is the power scattered per unit solid angle per unit incident power density per unit volume of the medium. The general method of calculating σ has been given by Booker[25], from which it can be deduced that

$$\sigma = \overline{\left(\frac{\Delta\varepsilon}{\varepsilon}\right)^2}\ \frac{4\pi^3 \sin^2\chi}{\lambda^4}\ P\left\{k(l_2-l_1), k(m_2-m_1), k(n_2-n_1)\right\} \qquad \text{.....(2)}$$

where ε is the dielectric constant of the medium, χ is the angle between the E-vector of the incident wave and the scattering direction, and P is the Fourier transform of ρ, the autocorrelation function of $(\Delta\varepsilon/\varepsilon)$: alternatively, P is the wave number spectrum of the variations of ε in the 'mirror direction' specified by the bisector of the angle between the incident unit vector (l_1, m_1, n_1) and the scattered vector (l_2, m_2, n_2), for an incident wave number k.

In our case the wavelength, λ, is less than 10m, and thus very much smaller than the plasma wavelength, λ_N, so that we can write

$$\overline{\left(\frac{\Delta\varepsilon}{\varepsilon}\right)^2} = \overline{\left(\frac{\Delta N_e}{N_e}\right)^2}\left(\frac{\lambda}{\lambda_N}\right)^4 \qquad \text{.....(3)}$$

Restricting ourselves to the backscatter case, for which $\chi = 90^o$ and $(l_1, m_1, n_1) = -(l_2, m_2, n_2)$, then eq (2) becomes

$$\sigma = \frac{4\pi^3}{c^4}\ f_N^4\ \overline{\left(\frac{\Delta N_e}{N_e}\right)^2}\ P\left\{2kl, 2km, 2kn\right\} \qquad \text{.....(4)}$$

where c is the velocity of light and f_N is the plasma frequency.

3.2. F-region Results

It is now possible to calculate σ by assuming appropriate values for f_N and $\overline{(\Delta N_e/N_e)^2}$, and a suitable form for P. We shall take $f_N = 4$ MHz and $\overline{(\Delta N_e/N_e)^2} = 0.1$ as average values for the disturbed high latitude F-region. P is determined by the choice of ρ: the isotropic forms

$$\rho_A = \exp\left(-\frac{1}{2}\frac{r^2}{L^2}\right) \qquad \text{(Gaussian)}$$

$$\rho_B = \exp\left(-\frac{r}{L}\right) \qquad \text{(exponential)}$$

$$\rho_C = \left(1+\frac{r}{L}\right)\exp\left(-\frac{r}{L}\right) \qquad \text{(modified exponential)}$$

are taken. Strictly speaking, these functions should have had their anisotropic forms, since it is known that the electron density irregularities are elongated along the magnetic field. However, measurements of the degree of elongation give widely varying results at high latitudes; and also the assumption of isotropy can readily be shown from Booker's results[25] to give pessimistic answers unless the irregularities are viewed almost in the specular direction. Thus it is felt that the above formulae definitely represent the 'worst case'. The parameter r is the independent spatial variable, and L is the correlation distance. L should not be confused with L' which was discussed in 2.1. above. L' is the average distance between peaks (or troughs) of N_e, and for the Gaussian acf, ρ_A, can be shown to be related to L by[25]

$$L' = 2\pi L/\sqrt{6} \qquad \text{.....(5)}$$

No such relationships exist for ρ_B and ρ_C.

In Fig 1, σ is plotted for these 3 cases, as a function of λ for various values of L. The 'worst case' we have seen above is L' ~ 10m, or L ~ 4m; the 'typical case' is L' ~ 300m, or L ~ 120m. In Fig 2 and 3 these two latter cases are plotted together with the minimum and maximum likely values

of the incoherent scatter cross section, for comparison.

Fig 1 shows that at long wavelengths the values of σ for all 3 acf's converge: here L is the most important parameter. At short wavelengths, on the other hand, the choice of acf becomes more important than that of L. Fig 2 gives details of the worse case, L = 3m, showing also the lowest value that σ is likely to take for incoherent scatter, and also the value observed at the Jicamarca radar[6]. It is clear that non-specular clutter will be weaker than the incoherent scatter signal at all wavelengths less than 4m as long as the acf is Gaussian, and also that the Jicamarca clutter level is quite plausible. If the acf becomes non-Gaussian, then clutter might be seen above incoherent scatter at any wavelength in our band. Fig 3 shows the 'typical' case, L = 300m, with the largest likely value of σ for incoherent scatter. Here it is seen that clutter will not be detectable at any wavelength below 10m unles ρ becomes non-Gaussian.

All these results have been obtained with the same values for f_N and $\overline{(\Delta N_e/N_e)^2}$. Fig 4 shows the effect of varying these two parameters, keeping λ and L fixed. It is clear from comparison with Fig 1 that L, λ and the acf are much more important factors.

3.3. E-Region Scattering

So far only the F-region has been considered explicitly. It is known, however, from the occurrence of D-region partial reflection and VHF forward scatter that significant electron density irregularities also exist in the lower ionosphere. These irregularities are more nearly isotropic than the F-region ones, and so the present analysis should apply to them directly. On the other hand, they are not a peculiarly high latitude problem, although they may be enhanced by high latitude effects, eg, particle precipitation. The intensity of forward scatter signals is found to follow a λ^n law, where $5 < n < 6$[27]; the modified exponential acf, which gives $\sigma \propto \lambda^6$ when $4\pi L \gg \lambda$ [27] is thus a good model of this situation. A value of L ~ 300m would be conservative for the E-region,[20] also f_N and $\overline{(\Delta N_e/N_e)^2}$ would be rather smaller than for the F-region. Thus from the evidence of Figs 2 and 4 we see that non-specular clutter can in this case fairly readily appear above incoherent scatter at wavelengths $\lambda \sim 6$m, and it would not require a very large change in ambient conditions for it to appear at $\lambda \sim 1$m also. This may be the explanation for some unusual coherent signals which were observed along with E-region incoherent scatter by the Prince Albert radar at $\lambda \doteq 0.70$m[28].

4. BACKGROUND INCOHERENT SCATTER

Incoherent scatter forms as it were the 'noise' level for non-specular clutter. Its scattering cross section is given to a good approximation by[29]

$$\sigma_i = N_e \sigma_e \Big/ \left(1 + \frac{T_e}{T_i}\right) \qquad \text{.....(6)}$$

where σ_e is the Thomson cross section and T_e, T_i are the electron and ion temperatures. (T_e/T_i) may vary from 1 up to about 3, so the most important factor in eq (6) is N_e, which may vary over a range of about 4 orders of magnitude. Fig 5 shows typical variations with altitude of σ_i, for maximum (summer daytime) and minimum (quiet winter night-time) conditions. Note that λ does not appear in eq (6), not even implicitly. The properties of incoherent scatter as a source of clutter will not be greatly different from those seen at mid latitudes. The main differences will be less variability during the summer daytime, when the ionosphere is largely under solar control, and much greater variability during the polar night, when precipitation effects may be dominant.

5. SPECTRAL CHARACTERISTICS OF CLUTTER

Taking the wavelength λ = 1m as typical and imagining the ionosphere to be illuminated by a pure CW signal, then the centre of the clutter signal spectrum will be doppler shifted by at most a few hundred Hz from the transmitted frequency, by ordered motion of the scattering centres along the mirror direction. Doppler spreading, due to random internal motion of the scatters, will be at most a few Hz for the non-specular clutter, but can vary quite widely for incoherent scatter. In the latter case, the spectral width is about 1 kHz in the lower E-region, but may become as large as several tens of kHz in the upper F-region if T_e is large and if light ions are present in the plasma. If the Debye length (which is proportional to $(T_e/N_e)^{\frac{1}{2}}$) becomes sufficiently large compared with the wavelength, then the mode of scattering changes from the normal 'incoherent' type to true 'Thomson' scattering, and the spectral width increases to several MHz. The signal then becomes very difficult to detect, and will cease to be a significant source of clutter for most conceivable VHF and UHF radars.

6. CONCLUSIONS

The problem of the amplitude of clutter signals from macroscopic electron density irregularities viewed non-specularly has been considered here. Rather than refer its properties to those of any particular radar equipment, we have considered it in relation to incoherent scatter signals, which are always present, with an intensity independent of wavelength. Thus this paper is mainly of interest in connection with very sensitive radars that are capable of detecting incoherent scatter.

While no problems have been experienced at middle latitudes with non-specular clutter, there are indications that it may sometimes appear at high latitudes. It has been shown here that with the most pessimistic assumptions - scale size of the irregularities ~ 10m, and isotropic scattering - F-region non-specular clutter will not be detectable above incoherent scatter at wavelengths less than 4m unless the autocorrelation function describing the irregularities becomes markedly non-Gaussian. This is probably an unusual occurrence, the conditions which produce 'radio star fades'

seem to be the most dangerous from this point of view. The situation in the E-region is rather less clear cut, but it seems possible that non-specular clutter may sometimes be just detectable at wavelengths down to about 1m.

Situations when the irregularities are not describable by an acf have not been considered. In such cases the medium will have markedly non-uniform properties, and hence any clutter echoes are likely to be transient.

7. ACKNOWLEDGMENT

This paper is British Crown Copyright, and is published by permission of Her Majesty's Stationery Office.

8. REFERENCES

1. Abel, W G and Newell, R E, 'Measurements of the afternoon radio aurora at 1295 MHz', J Geophys Res (1969), 74, 231.

2. Leadabrand, R L, Schlobohm, J C and Baron, M J, 'Simultaneous VHF and UHF observations of the aurora at Fraserburgh, Scotland' J Geophys Res (1965), 70, 4235.

3. Owren, L, 'Multiple scattering in the auroral ionosphere', Proc International Conf on the Ionosphere (IPPS, 1963), 277.

4. Frihagen, J and Folkestad, K, 'A note on high-latitude Spread-F' in AGARD-IRC Symp on 'Spread-F and its effects on radio wave propagation and communication' Copenhagen (1964).

5. Bullough, K, 'The radio aurora in high latitudes', Proc International Conf on the Ionosphere (IPPS, 1963), 151.

6. Farley D T, Balsley, B B, Woodman, R F and McClure, J P, 'Equatorial spread-F: implications of VHF radar observations' J Geophys Res (1970), 75, 7199.

7. Getmantsev, G G and Eroukhimov, L M, 'Radio Star and satellite scintillations', Ann IQSY (MIT Press, 1969), 5, 229.

8. Yeh, K C and Swenson, G W, 'F-region irregularities studied by scintillation of signals from satellites' Radio Sci (1964) 68D, 881.

9. Lansinger, J M and Fremouw, E J, 'The scale size of scintillation-producing irregularities in the auroral ionosphere' J Atmos Terrest Phys (1967) 29, 1229.

10. Dyson, P L, 'Direct measurements of the size and amplitude of irregularities in the topside ionosphere' J Geophys Res (1969) 74, 6291.

11. Little, C G, Reid, G C, Stiltner, E and Merritt, R P, 'An experimental investigation of the scintillation of radio stars observed at frequencies of 223 and 456 MHz from a location close to the auroral zone' J Geophys Res (1962) 67, 1763.

12. Flood, W A, 'Radio Star fadeouts and radio propagation' AGARD-IRC Symp on 'Spread-F and its effects upon radiowave propagation and communication', (Copenhagen, 1964).

13. Moorcroft, D R, 'Radio star fadeouts on phase switching interferometer records' J Geophys Res (1963) 68, 111.

14. Frihagen, J and Jacobsen, T, 'In situ observations of high latitude F-region irregularities' J Atmos Terrest Phys (1971), 33, 519.

15. Alimov, V A, Getmantsev, G G, Eroukhimov, L M, Mityakov, N A, Rapoport, V O, Uryadov, V P and Cherepovitskiy, V A, 'Some results of investigations of the inhomogenous structure of the polar ionosphere by reception of satellite signals on interferometers with different bases' Geomagn and Aeron (USA), (1970), 10, 21.

16. Jones, I L, 'Further observations of radio star scintillation' J Atmos Terrest Phys (1960), 19, 26.

17. Jespersen, J L and Kamas, G, 'Satellite scintillation observations at Boulder, Colorado' J Atmos Terrest Phys (1964), 26, 457.

18. Eroukhimov, L M and Ryzhov, V A, 'Investigation of the small-scale portion of the spectrum of ionospheric inhomogeneities by the radio astronomic method at frequencies of 13-54 MHz' Geomagn and Aeron (USA) (1969), 8, 527.

19. Dyson, P L, 'Comparison of irregular features appearing on ionograms recorded by topside and ground-based sounders' J Atmos Terrest Phys (1967), 29, 881.

20. Briggs, B H and Parkin, I A, 'On the variation of radio star and satellite scintillations with zenith angle'. J Atmos Terrest Phys (1963), 25, 339.

21. Aarons, J, Mullen, J P and Whitney, H E, 'The scintillation boundary' J Geophys Res (1969), 74, 884.

22. Aarons, J, Mullen, J P and Basu, S, 'The statistics of satellite scintillations at a subauroral latitude' J Geophys Res (1964), 69, 1785.

23. Liszka, L, 'A study of the occurrence of satellite scintillation observed in the auroral zone' AGARD-IRC Symp on 'Spread-F and its effects upon radiowave propagation and communication' (Copenhagen, 1964).

24. Oksman, J, 'Spiral pattern of F-region inhomogenieties causing visibility fades of Cass A' J Geophys Res (1964), 69, 4021.

25. Booker, H G, 'A theory of scattering by nonisotropic irregularities with application to radar reflections from the aurora' J Atmos Terrest Phys (1956), 8, 204.

26. Rice, S O, Bell System Tech J (1945), 24, 46.

27. Booker, H G, 'Radio scattering in the lower ionosphere' J Geophys Res (1959), 64, 2164.

28. Maynard, L A 'A study of scattering cross sections in the lower ionosphere at 448 MHz' Proc of Conf on Thomson Scatter (1967), Illinois Aeronomy Rep No 19.

29. Buneman, O, 'Scattering of radiation by the fluctuations in a non-equilibrium plasma' J Geophys Res (1962), 67, 2050.

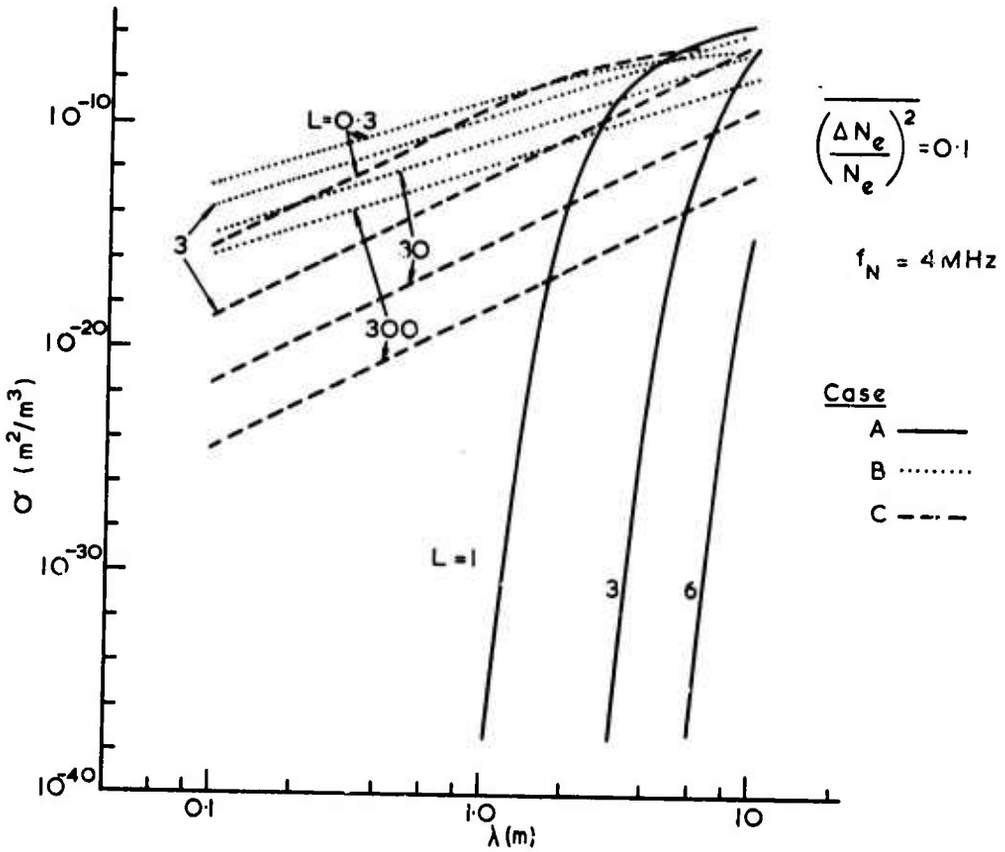

Fig 1 Isotropic volume scattering cross section, σ, vs λ for

A: Gaussian acf, B: Exponential acf, C: modified exponential acf.

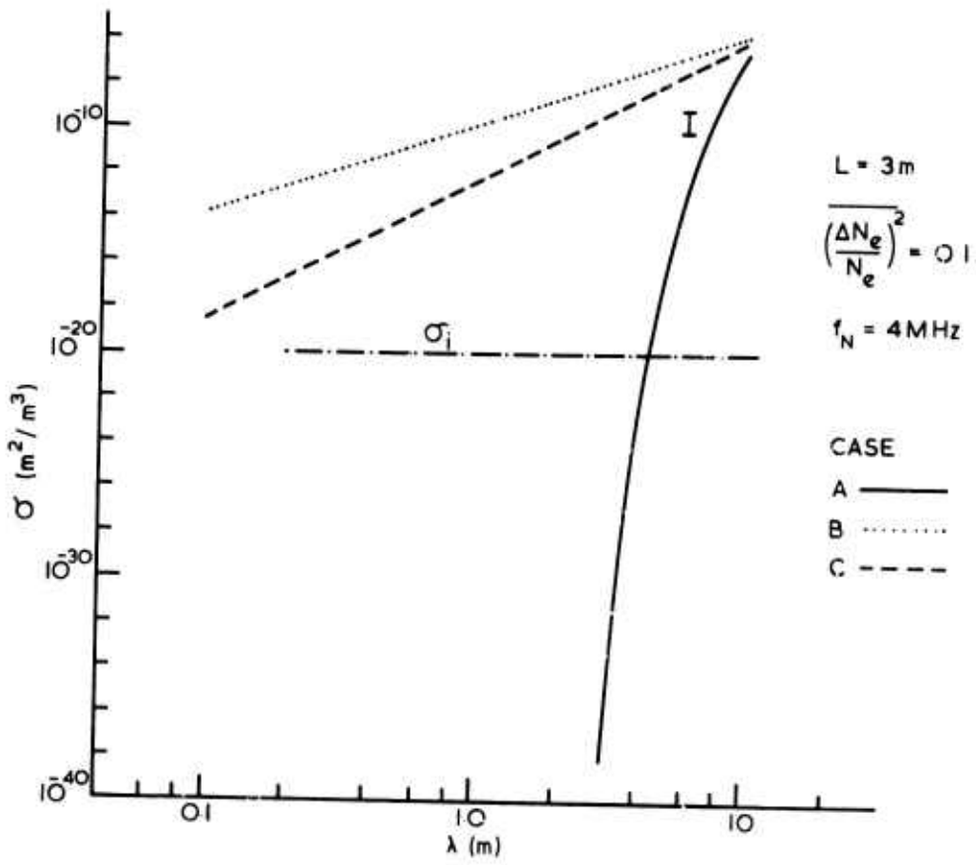

Fig 2 Curves from Fig 1 for L = 3m ('worst case') showing also: weakest incoherent scatter cross section (—·—·—·—) and Jicamarca clutter cross section (I).

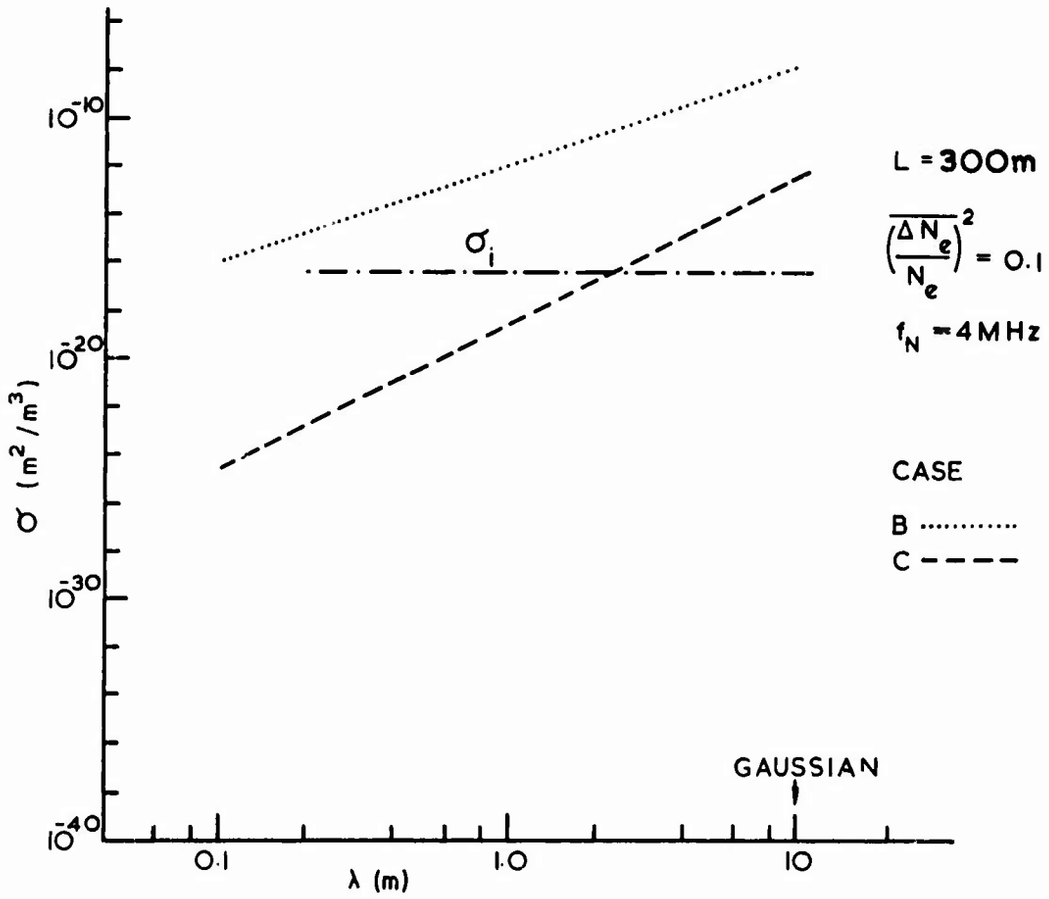

Fig 3 Curves from Fig 1 for L = 300m ('typical case') showing also maximum incoherent scatter cross section (. — . — . —).

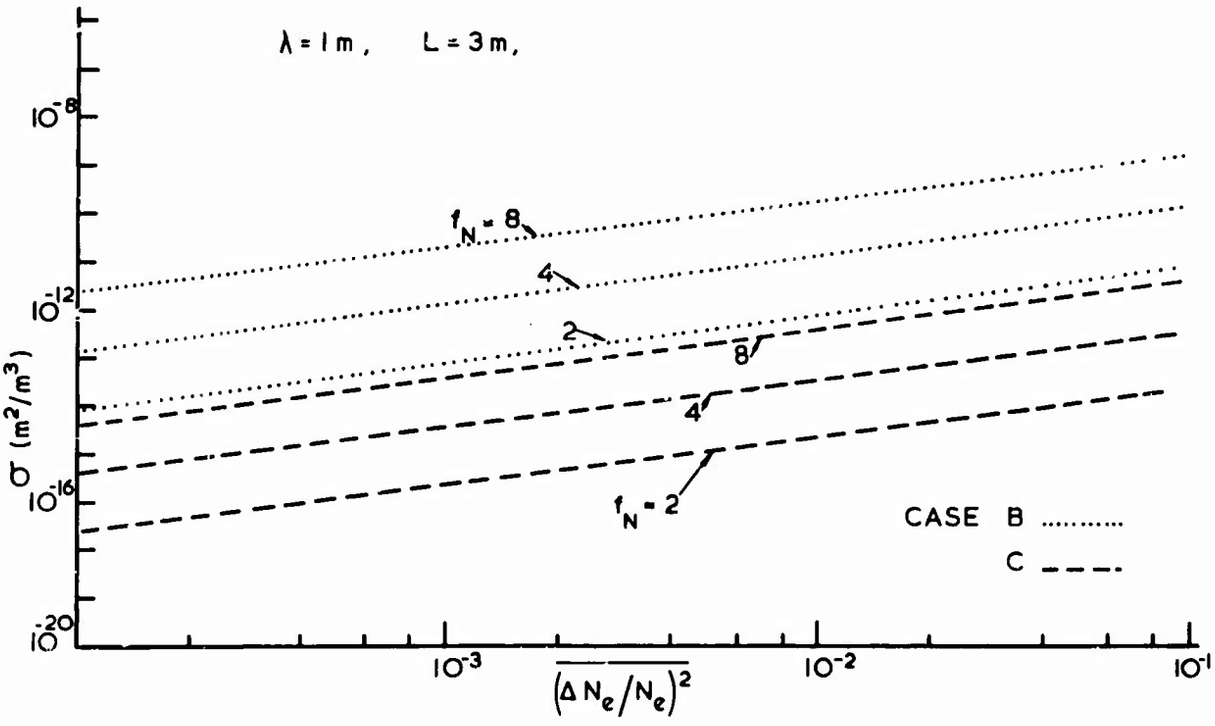

Fig 4 Effect on σ of changes in $\overline{(\Delta N_e/N_e)^2}$ and f_N, for λ = 1m and L = 3m.

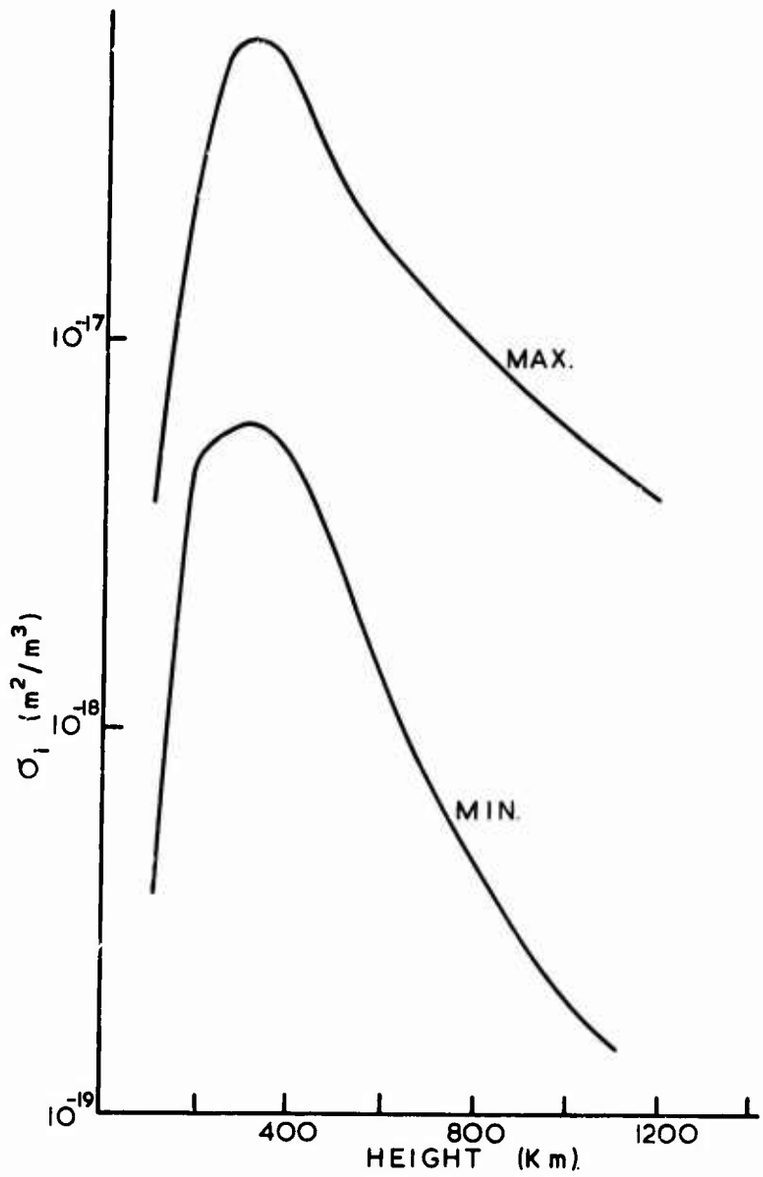

Fig 5 Typical variations with height, h, of the incoherent scatter cross section, σ_i, under maximum and minimum conditions.

A PROGRAM FOR THE INVESTIGATION AND SIMULATION OF AURORAL INSTABILITY MECHANISMS

J. T. Coleman
BATTELLE
Columbus Laboratories
505 King Avenue
Columbus, Ohio 43201
USA

SUMMARY

A program is described for the simulation and analytical investigation of the scattering mechanisms of the radio aurora. The program is divided into two coordinated efforts, the first being the simulation on a scaled basis of the important plasma mechanisms of the E-region and its scattering conditions, and the second effort being the computation of the theoretical coherent interaction cross section of the instabilities. Experimental evidence is presented for sensitivity of the coherent cross section to the drift current level, the local electron temperature, the local magnetic field intensity, gradients, and other significant parameters. The theoretical model estimates the differential radar cross section (in the hydrodynamic approximation) and includes the effects of relative drift between ions and electrons, and the gradient in electron density. In its present form, the model includes forward scatter, backscatter, and general bistatic scatter. The computation includes the frequency spectrum introduced by the interaction with the wave instabilities. For this reason it is termed a coherent cross section computation.

1. INTRODUCTION

In a number of investigations performed recently at Battelle's Columbus Laboratories, the nature and characteristics of the major auroral instabilities have been under study. The program has been based upon the available evidences from both theory and experiment of the nature and characteristics of the radio aurora, where the latter quantity is defined as that portion of the natural aurora that interacts with radio waves. The program has been divided into two parallel, coordinated efforts. The first phase, which is the experimental phase, has been devoted to the development of experimental techniques for the study of the basic Buneman-Farley two-stream instability mechanism both in the linear and the nonlinear regimes. The second phase is the development of a consistent theory that will permit the prediction of the turbulent structure function and from this quantity the radio wave scattering properties for any desired scattering geometry and illumination frequency. What is reported in this paper is the present state of the experimental and theoretical phases of this program and also its relation to present radar observables as reported in the recent literature and current technical conferences.

2. DESCRIPTION OF PROGRAM

2.1. Basic Considerations in Auroral Simulation

The author, in his dissertation work,[1,2] noted that the experimental evidences produced by radio wave scattering from nonequilibrium two-stream instabilities were similar to many reported by field experimenters performing studies of the radio aurora. His work was a study of the marginal stability boundary for a nonequilibrium plasma, and it evidenced some of the following characteristics:

(a) The existence of a definite critical instability drift threshold above which the quiescent plasma becomes spontaneously unstable, as evidenced from probe and microwave scatter measurements

(b) A greatly enhanced microwave scatter cross section when the threshold is crossed, along with a spread in Doppler induced by the turbulence

(c) A monotonic increase in cross section as the drift level exceeds the critical or marginal stability boundary condition

(d) A buildup of a spectrum of current fluctuations in the unstable medium that coincides with the onset of the instability

(e) The existence of a nonzero wave number at the instability boundary

(f) The possibility of studying the entire marginal stability boundary experimentally by means of electron temperature control

(g) In concert with (f) above, the possibility of converting a normally unstable gaseous arc discharge into a stable one.

All of the above observed characteristics were for the case of a drifting stream of electrons aligned with a strong uniform magnetic field, using hydrogen and helium discharges. Forward scatter and backscatter Doppler spectra were observed at X-band as well as radiation temperatures and Langmuir probe sensed field fluctuation levels. All of the methods agreed when the marginally stable condition was exceeded in the plasma. Now the above observations applied to a stream of electrons that flowed parallel to a static magnetic field and not to the Hall current system that is present in the equatorial and auroral electrojet systems. However, there is a direct relationship that is predictable from the theory that permits correlation of these early observations with the Buneman-Farley instability case. The instability threshold is greatly lowered by the latter instability so that one can readily predict that the Buneman-Farley mode is easier to excite once the current system is permitted to build up normal to the magnetic field. The presence of the magnetic field had little effect in the original work of the author as it only tended to collimate the current stream. The effect of the magnetic field becomes drastic in the Buneman-Farley case, however, as will be evidenced below. Nevertheless, all of the basic phenomenology given above remains unchanged. The main change is the generation of new marginal stability boundary conditions. The

necessity of developing a strong Hall current system is also apparent from theory and experiment and will be discussed below.

Controlled experiments are vital for the understanding of the significant mechanisms involved in the instability and also for the logical extension into the strong turbulence regime. Linear theory enables prediction to be made for the marginally stable condition but does not provide extension into the weak and strong turbulence regimes. Controlled experiments permit the variation of one parameter at a time, and perhaps with greater importance, permit one to return many times to the original experimental conditions. Atmospheric experiments in the auroral zone do not permit this kind of repeatability, neither do they permit fine scale studies to be performed. Furthermore, essentially no control can be exercised at any time. In situ measurements are not very valuable as one must extrapolate these to the large natural aurora volumes so that even this detailed type of study in the natural environment is not always of value. Rocket probe measurements of electron density and temperature cannot be performed in sufficient quantity to obtain statistically useful data unless they sense a quiescent state. During strong auroras, particularly for the discrete auroral forms, a large volume measure of the turbulent structure content should be made, and that for a long time period. Rocket probes obviously cannot do this.

The laboratory plasma may be driven to produce discrete structure forms or diffuse forms. Langmuir probes may then be used to measure highly localized properties and microwave beams can measure the bulk scattering properties of the simulated auroras. Typical simulations will be described below.

A critical problem area is the matter of scaling to represent the proper altitude regime. Not all properties may be scaled into a small volume representative of a laboratory simulation. I have not attempted a scaling of the optical or chemical properties but have concentrated on the radio properties. Two levels of scaling are described below along with achievable limits. It should be clear from this that the scaling may be performed to a higher degree of sophistication than reported anywhere in the literature to date.

2.1.1. Scaling Considerations

To represent the auroral E-layer with a first-order level of scaling I chose the following conditions:

$$\omega_{B-}\tau_{-} \gg 1 \quad , \quad \omega_{B+}\tau_{+} \leq 1 \quad . \tag{1}$$

Here the electron gyrofrequency is given by ω_{B-}, and τ_- is the electron-neutral relaxation time. The ion gyrofrequency ω_{B+} and the ion-neutral relaxation time τ_+ are chosen to give a roughly field-free ion condition. The condition of $\omega_{B-}\tau_-$ being large means that the electrons do indeed gyrate about the field lines and thus the magnetic field affects substantially the electrons alone. This condition is typical of the E-region and is one that is influential in the buildup of the Hall current electrojet at the equator. This condition may be readily achieved by using high-pressure air plasmas and large electromagnets. Such a combination can scale by a factor of 10^3 to 10^4, permitting a 6-inch cube to represent a cube of the atmosphere that could vary from 150 m to 1500 m on one side. This scaling includes also a factor to represent reasonable microwave wavelengths so that with reasonable economy one can represent HF radio illumination of the simulated aurora.

Second-order scaling can permit, in some cases, a matching to a factor of two of every reasonable plasma parameter entering into the instability. This may be done in air also to include the desired ion species.

2.1.2. Auroral Instability Theory in the Hydrodynamic Approximation

The conditions for generation of an auroral electrojet instability can be derived in terms of a hydrodynamic model for the plasma. These conditions were originally defined by Farley and are written in terms of modified Gordeyev integrals. The theory to be described here permits a closed form, analytic description of the instability threshold conditions and also permits a description of the radar cross section and Doppler content as sensed by radars. From the knowledge of this differential radar cross section per unit solid single per unit frequency the signature produced by the instability for an arbitrary radar illumination geometry can be computed. This differential cross section then permits the comparison of forward scatter and backscatter signatures and also permits estimation of the Doppler content introduced by the medium.

The scattering cross section per unit volume is defined in terms of the following expression:

$$\sigma(\bar{k},\omega) = \frac{1}{c}\frac{\dot{n}(\bar{k}_s,\nu_s)}{n(\bar{k}_i,\nu_i)} = \frac{1}{c}\dot{P}(\bar{k},\omega) \quad . \tag{2}$$

The incident photon flux density is $n(\bar{k}_i,\nu_i)$ and the scattered photon flux is $n(\bar{k}_s,\nu_s)$. The synchronism conditions for the conservation of energy and momentum are given by

$$\begin{aligned} \hbar\omega_i &= \hbar\omega_s + \hbar\omega \\ \hbar\bar{k}_i &= \hbar\bar{k}_s + \hbar\bar{k} \quad , \end{aligned} \tag{3}$$

where the subscripts i and s refer to the incident and scattered frequencies and wave numbers. C is the speed of the incident photons. The time rate of change of the scattered photons is given by the product of the incident photon density and the probability rate for transition of energy and momentum $\dot{P}(\bar{k},\omega)$.

The golden rule of quantum mechanics shows that, in the first Born approximation, $\dot{P}(\bar{k},\omega)$ is proportional to a quantity termed the structure function $S_-(\bar{k},\omega)$. Now the latter quantity is the space and

time Fourier transform of the electron pair distribution function, as described by Van Hove.[3] This permits, from second-order perturbation theory, the definition of the differential scattering cross section as follows:

$$\frac{d^2\sigma}{d\omega d\Omega} = \left(\frac{d\sigma}{d\Omega}\right)_c S_-(\bar{k},\omega) \quad , \tag{4}$$

where $\left(\frac{d\sigma}{d\Omega}\right)_c$ is the classical Thomson differential cross section for electrons.

From the quantum mechanics it can be shown that the structure function $S_-(\bar{k},\omega)$ is related to the linear response of the electrons. The fluctuation dissipation theorem then permits a description of the structure function, assuming electrostatic charge interaction alone, in terms of the dielectric response $\epsilon(\bar{k},\omega)$. Mathematically, we state then

$$S_-(\bar{k},\omega) = \left(\frac{k}{2\pi e}\right)^2 \left| \frac{KT_-}{(\omega - \bar{k}\cdot\bar{V}_o)} \, \mathrm{Im}\left[\frac{4\pi\alpha_-(\bar{k},\omega)}{\epsilon(\bar{k},\omega)}\right] \right| \quad , \tag{5}$$

where

α_- = electron polarizability

$\epsilon(\bar{k},\omega) = 1 + 4\pi\alpha_-(\bar{k},\omega) + 4\pi\alpha_+(\bar{k},\omega)$

= dielectric response

and $\bar{V}_o$ is the velocity of the scatterer relative to the observation frame. It is apparent here that the cross section becomes very large as $\epsilon(\bar{k},\omega)$ approaches zero. The latter condition also happens to give the dispersion conditions for electrostatic waves in the plasma.

The polarizabilities can be computed using the hydrodynamic equations for charge conservation and linear momentum conservation. Within this approximation in the rest frame of the geomagnetic field

$$4\pi\alpha_\pm(\bar{k},\omega) = \frac{\omega_{p\pm}^2 C_\pm}{\omega_{T\pm}^2 C_\pm - (\omega_\pm)(\omega_\pm + i\nu_\pm)} \quad , \tag{6}$$

where

$$\omega_\pm = \omega - \bar{k}\cdot\bar{V}_{d\pm} \quad ,$$

$$\omega_{p\pm}^2 = \frac{4\pi n_o e^2}{m_\pm} \quad , \quad (\text{or } (\omega_{p-})^2 = (2\pi f_N)^2) \quad ,$$

and

$$\omega_{T\pm}^2 = \frac{KT_\pm}{m_\pm} k^2 \quad .$$

The term $C_\pm$ is important as it serves as a magnifier of the drift current threshold for instability. We write

$$C_\pm \simeq \frac{\nu_\pm^2 + \omega_{B\pm}^2 (\hat{k}\cdot\hat{B}_o)^2}{\nu_\pm^2 + \omega_{B\pm}^2} \quad , \tag{7}$$

for

$$\omega \simeq \bar{k}\cdot\bar{V}_{d\pm} \quad .$$

For the case of wave motion k normal to the magnetic field $\hat{B}_o$ we write, for the electrons,

$$C_- = \frac{1}{1 + (\omega_{B-}\tau_-)^2} \quad , \tag{8}$$

where

$\tau_- = (\nu_-)^{-1}$

and

ν_- = electron - neutral collision frequency .

For $(\omega_{B-}\tau_-) >> 1$ we find a strong reduction in the relative drift velocity for excitation of the electrojet instability.

For the case of

$$\nu_+ >> \omega_{B+} \quad , \quad \omega << \nu_+ \quad , \quad k << k_D \quad ,$$

and

$$\gamma << \omega \quad ,$$

$$\omega = Sk + \bar{V}_{d\pm} \cdot \bar{k}$$

$$\gamma \simeq \frac{1}{2}\nu_+\left[1 + \frac{m_-\nu_-}{m_+\nu_+C_-} \cdot \frac{S - \bar{k}\cdot\bar{V}_d}{S}\right] , \tag{9}$$

where ω is the electrostatic plasma wave frequency and γ is the growth rate.

For the critical drift corresponding to a zero growth rate,

$$\bar{k}\cdot\bar{V}_d \simeq \left(1 + \frac{m_+\nu_+}{m_-\nu_-}C_-\right)S , \tag{10}$$

where

$$S \simeq \text{sonic velocity}$$

$$= \left(\frac{\gamma K(T_- + T_+)}{m_+}\right)^{\frac{1}{2}} .$$

From the above given considerations we can demonstrate that the cross section integrated over Doppler is proportional to γ^{-1}. The form of solution is described in Figure 1. The resonant condition is reached when

$$\omega \simeq sk + \bar{V}_{d+}\cdot\bar{k} . \tag{11}$$

The width of this peak is equal roughly to γ, and the amplitude varies as γ^{-2}.

The expression developed for the cross section is written as follows:

$$\frac{d^2\sigma}{d\Omega d\omega} = \left(\frac{d\sigma}{d\Omega}\right)_c \frac{n_o}{2\pi} \cdot \frac{s^2k^2}{\omega_{p+}^2}\left[\lambda\nu_+(S^2 - V_{T+}^2)k^2\right]$$

$$\left[4\lambda^2 s^2 k^2(\omega' - sk)^2 + \nu_+^2(g_1\omega' - \bar{k}\cdot\bar{V}_d)^2\right]^{-1} \tag{12}$$

where

$$g_1 = 1 + \frac{m_+\nu_+C_-}{m_-\nu_-} .$$

[It can also be demonstrated from the above expression, integrating over the frequency ω,

$$\frac{d\sigma}{d\Omega} \simeq \left(\frac{d\sigma}{d\Omega}\right)_c \cdot \frac{n_o}{8}\frac{s^2k^2}{\omega_{p+}^2}\left(\frac{\nu_+}{\lambda\gamma}\right)$$

$$\simeq \frac{1}{\gamma} .$$

Thus the area under the curve is proportional to γ^{-1}.]

The above expression indicates that a zero growth rate causes the cross section to diverge. If, however, we permit $\gamma = 0$ only at $k = 0$, we have all other growth rates negative and the cross section is finite. Thus this condition can be considered as a mathematical singularity. A mode with $k = 0$ demands an infinite wavelength and is not physically realizable. However, it seems to be a reasonable estimate for a steady state equilibrium condition. Furthermore, it tends to give reasonable estimates for the enhancement of cross section observed by radars operating in the equatorial electrojet environment, and also for the backscatter cross section levels observed in our laboratory simulations for the case of marginal stability. (See Appendix for detailed discussion of the experimentally determined cross section enhancements.)

2.1.3. The Case With Gradients Present

It can be shown, in the hydrodynamic approximation, that if slowly varying gradients (in space and time) are included in the theory, that the scattering cross section will undergo modification. In particular, the differential scattering cross section near resonance ($\omega - \bar{k}\cdot\bar{V}_{d+} \simeq Vk$) will be sensitive to gradients in both the electron density and the electrojet stream velocity. This suggests that discrete auroral arc formations, with their assumed electron density gradients and possible jet stream drift nonuniformities, will be modified in cross section accordingly.

As a first estimate of the effects introduced by gradients, we perform a perturbation expansion of the hydrodynamic equations. Consider the following:

$$n_\pm = n_o + \delta n_\pm ,$$

$$\bar{V}_\pm = \bar{V}_{d\pm} + \delta\bar{V}_\pm ,$$

$$\bar{E} = \bar{E}_o + \delta\bar{E} \quad . \tag{13}$$

A first-order perturbation expansion of the equations yields for the critical drift level

$$V_d = (1 + \lambda)S - \frac{1}{2}S \frac{\omega_s}{\omega_{B+}} \left| \frac{\nabla n_o}{n_o} \right| \sin\varphi$$

assuming

$$T_e \simeq T_i \quad ,$$

and

$$\frac{dV_{d\pm}}{V_{d\pm}} \ll \frac{dn_o/dx}{n_o} \quad . \tag{14}$$

The critical drift velocity for zero growth rate (V_d) is now gradient dependent. The above expression for V_d assumes the gradient in electron density is normal to the magnetic field and that the wave vector for the instability is also normal to the static magnetic field. The angle φ is defined by

$$\sin\varphi = (\hat{k} \times \bar{K}) \cdot \hat{B}_o$$

where

$$\bar{K} = \frac{\nabla n_o}{k n_o} \quad . \tag{15}$$

The maximum effect is then predicted for a gradient in electron density that is normal to the direction of wave propagation $\hat{k}$, for the assumed case of $k \perp B_o$ and $K \perp B_o$. The critical drift velocity for onset of the instability may then be either increased or decreased depending upon the direction of the electron density gradient.

The differential scattering cross section expression will now have gradient terms present and the expression becomes quite complex due to these terms. Since the cross section varies inversely with the growth rate for the homogeneous case the anisotropies introduced by the presence of gradients can be very roughly estimated by examining the new expression for the growth rate. An initial examination of this case shows that the cross section buildup becomes increasingly anisotropic due to the gradients in the electron density and the drift stream with a net result that preferred growth directions occur that are displaced from that predicted by the Buneman-Farley theory. It would appear that the dominant effect may be due to the electron density gradients and not the local drift stream gradient and divergence.

2.2. Laboratory Evidences

2.2.1. Facility Development

Several facilities have been developed over a period of years at Battelle's Columbus Laboratories to create in the laboratory the forms of two-stream instability corresponding to the auroral electrojet system. A large electromagnet is required to permit the creation of $\omega_{B-\tau_-}$ values considerably in excess of unity, and a relatively large volume is required in order to permit creation of a plasma that is large compared to the microwave wavelengths used for illumination. This requires, in essence, a plasma with relatively free boundaries because of the strong influence of boundaries on the Hall current system. For example, the simple expedient of generating an arc discharge in a cylindrical glass tube and applying a magnetic field normal to the current direction is completely unsatisfactory. The Lorentz forces present can confine the current to the surface of the glass tube, melting the glass and introducing strong boundary effects in the experiment. The early experiments performed at Battelle-Columbus confirmed the need for a more natural set of boundaries in a Hall current system, something closer to the observed discrete arc formations of the natural aurora. Such a system has now been successfully implemented at Battelle's Columbus Laboratories.

2.2.2. Example of Microwave Scatter Measurements

As an example of the microwave scatter observations recorded in the laboratory, the results of a Ku-band backscatter experiment will be described. A weakly ionized air plasma was generated, one with an electron density of about 10^{10} cm^{-3}, and an electron stream was introduced normal to an applied static magnetic field. The microwave beam illuminated the plasma in the direction of the Hall current stream and the backscatter reflection was recorded at an angle at nearly 180° to the incident beam. The reflected signal was also subjected to spectral analysis to measure the frequency content introduced in the scattering process. The test chamber was carefully lined with microwave absorber material and a coherent background cancellation system was used to permit the reduction of all residual microwave backscatter to an observable zero level. The upper trace of Figure 2 is a spectral display showing the zero residual scatter in the presence of the underdense plasma slab. The illumination frequency is 16.2 GHz and the horizontal frequency scale is 0.1 MHz/division. The vertical scale is logarithmic and represents 10 dB per division of vertical deflection. A crystal frequency reference marker appears two divisions from the right side of the scale. A current stream of 200 ma is injected along the direction of the incident microwave beam, and the backscatter rises to a peak of 30 dB above the system threshold, as indicated in the lower trace. (The actual threshold for detection is at about 50 to 60 ma for this case. See Appendix.)

In Figure 3, the injected stream is increased to 400 ma for the upper trace, and the lower trace is for a 600 ma stream current. The upper trace shows an increase to 35 dB and the lower trace shows a 40 dB increase above the system threshold, using the marker amplitude as an amplitude reference level. Evidence

for the broadening of the backscatter spectral width also appears for the higher drive current levels. (The dashed line on Figure 1 suggests this observed spectral broadening due to nonlinear mode coupling.) Although the shift in Doppler due to backscatter is not clearly indicated in these particular displays, a finer resolution study of the backscatter reveals the shift in the average display frequency. The magnetic field in this experiment was fixed at 1 KG and the chamber air pressure was 200 microns (0.2 Torr). The buildup of drift current is considerably in excess of the critical level and still shows an enhancement in cross section. A tendency towards saturation occurred for the increase from 400 to 600 ma. This is generally observed in our laboratory for currents considerably greater than the critical threshold level. Above the saturation of cross section level the spectrum tends to broaden due to nonlinear mode coupling. An analysis of the system sensitivity given in the Appendix indicates that considerable signal enhancement has occurred before the backscatter is detectable. In fact, we are near a condition of $V_d = 10\ V_c$ for the 600 ma drive current case.

As an example of the effect of local electron temperature, a dc arc was generated normal to the static magnetic field and the local electron temperature was enhanced. A bistatic measurement at X-band (9.2 GHz) was conducted in air at 0.30 Torr pressure. A 1KG magnetic field was maintained during the experiment with an arc level of 300 ma. Figure 4 is the spectrum of bistatic scatter with a log display vertical and a linear horizontal frequency scale. The lower trace is for the dc arc alone. A double-wing display characteristic of forward scatter appears with peaks at about 0.9 MHz on either side of the carrier. The electron temperature is augmented by an orthogonal heating signal and the sideband content disappears into the noise level while the current in the arc is maintained at 0.3 a. The theory predicts that the marginal stability boundary should be advanced toward larger drift current levels by an electron temperature enhancement. This crossing of the boundary is evidenced by the removal of the Doppler content due to the decay of the turbulent structure function $S(\bar{k},\omega)$. This is a repetition of the work previously performed by Coleman but for the Buneman-Farley electrojet geometry.[2] From the theory

$$C_- \simeq \frac{1}{(\omega_{B-}\tau_-)^2} = \frac{(\nu_-)^2}{(\omega_{B-})^2} \quad . \tag{16}$$

Since $(\nu_-)^2$ is proportional to the electron temperature T_e, C_- is proportional to T_e. But the critical drift velocity is given by

$$\bar{k} \cdot \bar{V}_d = \left(1 + \frac{m_+\nu_+}{m_-\nu_-} C_-\right) S = V_{critical} \quad . \tag{17}$$

Now the ν_- factor in the denominator of the second term in the parenthesis causes this term to vary as $(T_e)^{\frac{1}{2}}$. The net result is still an increase in the critical drift level for zero wave growth when T_e is increased. The experimental observations above are consistent with this theoretical prediction. Figure 5 is an experimental observation of the effect of a gradual reduction in the growth rate due to a T_e increase. The upper trace is an enhanced T_e case and it clearly shows a reduction in the probability rate for stimulation of modes as evidenced by a lower density of Doppler traces. The spectral envelope is unchanged but the probability of exciting the mode spectra is reduced, resulting in a lower trace density for a given fixed camera exposure time. With a greater increase in T_e the Doppler content completely disappears. Fine-grain studies of the marginal stability boundary have thus been performed in the laboratory, permitting an increased insight into the actual instability mechanisms.

2.2.3. Other Measured Data Effects

The gross effects of the variation of the static magnetic field have been studied in the laboratory. In general, a certain critical magnetic field must be exceeded before the instability is triggered. This generally means the condition $\omega_{B-}\tau_- >> 1$ must be met. Experimental work is now in progress to evaluate the sensitivity of the marginal boundary to $\bar{B}_o$ and the sensitivity of the structure function $S(\bar{k},\omega)$ to $\bar{B}_o$ also. The role of $\bar{B}_o$ in the turbulent structure is not clear at the present time, particularly for $V_d >> V_c$. Thus, these experiments are necessary in order to evaluate the effect of this quantity in a regime that present theory cannot treat and one in which anomalous effects can be expected to appear.

A very interesting experimental observation is that the Hall current tends to become weakly turbulent when the instability threshold is crossed. Figure 6 is a pair of spectral displays of the Hall current. The upper display is for the quiescent plasma, and the lower display is for the case of a Hall current-driven electrojet instability. The vertical scale is logarithmic, and the horizontal scale is linear in frequency. The spectrum extends to beyond 700 KHz and is roughly of the shape anticipated for the structure function. Microwave backscatter from the instability was measured as the Hall current was increased, and the enhancement in backscatter followed the Hall current spectrum buildup closely. Two conclusions can be drawn from these observations. The first is that the external drive current to the experimental system can be used to sense the presence of the electrojet instability and its approximate frequency content, and the second is that the naturally occurring auroral electrojet system must also experience this type of modulation when the critical drift velocity is exceeded.

3. CONCLUSIONS

The scattering measurements described above are consistent with the theory developed to date in that a measured enhancement in radar observable cross section has been sensed in the laboratory that exceeds the Thomson scatter cross section by many orders of magnitude. This buildup in cross section is abrupt when the conditions for marginal stability are met. In addition, the measurements were performed in an air plasma with a scaling of the electronic processes that approximates the conditions of the E-layer of the atmosphere, the layer in which auroral activity is quite prominent in the northern latitudes. The theory described above does not strictly apply when the marginal stability condition is exceeded by the relative electron drift velocity. The experimental evidence, however, indicates that the cross section continues to increase as the electron drift velocity exceeds the critical level and that this process continues until a saturation level is reached. At the latter level nonlinear mode coupling

effects are seen in the Doppler content of the backscattered signal. The value of the experimental work then is that it serves as a guide to the development of extended theory.

The role of gradients in the auroral simulation is presently under study. The theory described above indicates that the presence of these will modify the condition of marginal stability or will modify the initial growth rate. Laboratory evidence for the effectiveness of these gradients is presently being gathered. Methods are being developed to produce both diffuse and discrete field-aligned structures, both in the presence of Hall current electrojet systems. Extrapolating to the field radar case, the initial estimates from the theory indicate that the differences between the scatter from discrete and diffuse auroral arcs could be related to the modification of the initial growth rates due to the presence of gradients. The sensitivity of scatter to the growth rates is quite high when cross sections are enhanced and thus it is suspected that the gradients can play a prominent role in the observable electromagnetic interactions.

4. ACKNOWLEDGMENTS

The careful theoretical developments performed by Bob L. Weber of Battelle's Columbus Laboratories are acknowledged by the author. They have proved to be of high value in this program and have permitted significant advances in the theory and interpretation of experimentally observed effects. Credit is also given to Everett C. Clutter of Battelle's Columbus Laboratories for his excellent work in the design and development of the experimental system and apparatus.

This program has been supported by an internal research grant at the Columbus Laboratories of Battelle.

5. APPENDIX

5.1. Threshold Estimate For The Backscatter Experiment

The volume of plasma intercepted by the Ku-band horn is given approximately as 0.4×10^3 cm^3. The electron density is of the order of 10^{10} cm^3 so that the Thomson cross section for incoherent scatter is given by

$$\sigma = \tfrac{1}{2} N_e \sigma_e (\pi/2)$$

$$\sim \tfrac{1}{2} \times 10^{13} \times 10^{-28} = 0.2 \times 10^{-15} \text{ m}^2 \quad . \qquad \text{(A-1)}$$

The received power is then given by

$$P_r = \frac{P_t \lambda^2}{(4\pi)^3 R^4} G_T G_R \qquad \text{(A-2)}$$

where

$G_T = 16$ dB

$G_R = 20$ dB

$P_t = 47$ mw

$R = 0.50$ m

$\lambda = 1.87 \times 10^{-2}$ m .

From this

$$P_r \sim 1.0 \times 10^{-19}$$

$$= 10^{-16} \text{ mw} \quad .$$

From this

$$P_r \sim -160 \text{ dB m} \quad .$$

The threshold sensitivity of the spectrum analyzer is about -98 dB m and thus the threshold for detection is about 62 dB above the Thomson scatter level. The maximum cross section enhancement above thermal levels is then about 102 dB for the case of Figure 3.

From the first detected signal of Figure 2 the enhancement above thermal levels is then about 92 dB. Estimates for the equatorial electrojet indicate enhancements of over 80 dB are seen when the two-stream Type I scatter is detected. In the present laboratory experiments, the critical drive current level to barely exceed the system threshold was about 50 to 60 ma. This would indicate that the observable threshold is about 62 dB above the Thomson level. Observable enhancements of about 80 dB thus fall into the range of this laboratory simulation. However, we go beyond the equatorial case as we can extend to about $V_d = 10\ V_c$. This condition thus is closer to the auroral electrojet case where much stronger currents are involved. Thus the simulation encompasses both the equatorial and auroral turbulent structure conditions, including some of the stronger discrete auroral forms.

REFERENCES

1. Coleman, J. T., "The Transition to Instability in a Nonequilibrium Plasma", Dissertation Abstracts, 28 (B), 1068, 1967.

2. Coleman, J. T., "Control of Ion-Acoustic Wave Instabilities in a Gaseous Discharge", J. Appl. Phys., 38 (6), 2655-2659, 1967.

3. Van Hove, L., "Correlations in Space and Time and Born Approximation Scattering in Systems of Interacting Particles", Phys. Rev., 95 (1), 249-262, 1954.

4. Balsley, B. B., "VHF Spectra of Radar-Aurorae", Transactions of American Geophysical Union (EOS), 52 (4), 289, Paper SA5, April 1971.

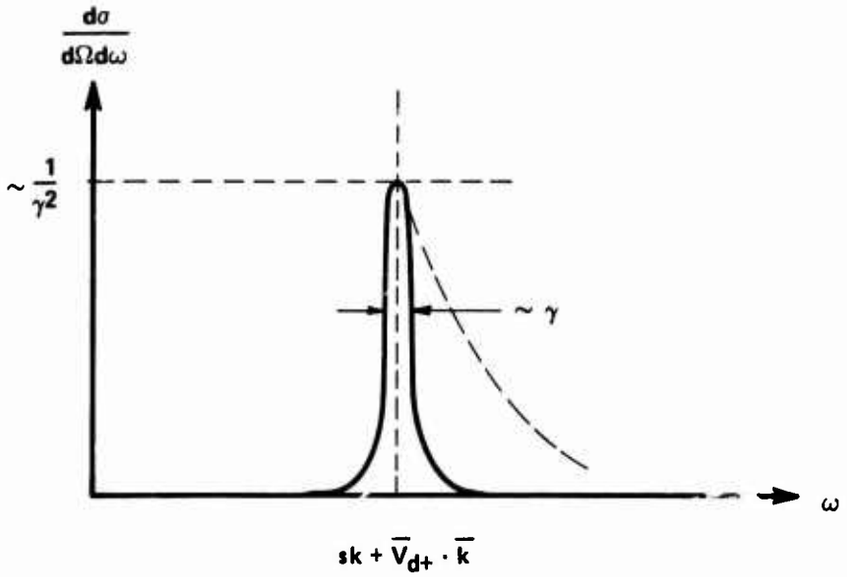

FIGURE 1. Differential Cross Section Versus Frequency

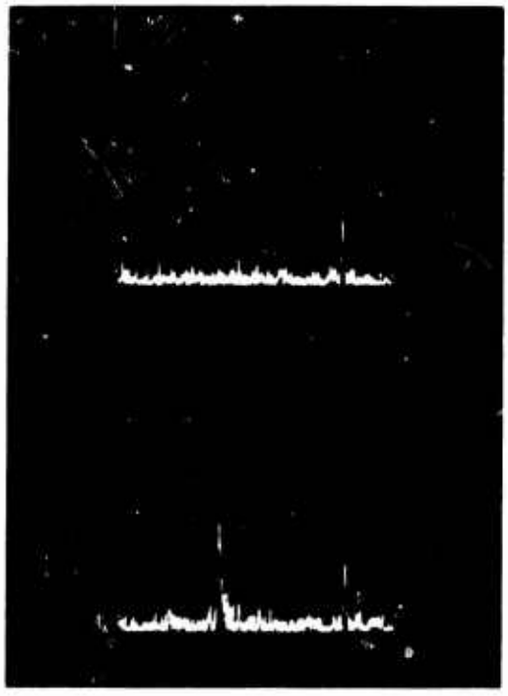

FIGURE 2. Backscatter Spectra
Vertical scale:
10 dB/division
Horizontal scale:
0.1 MHz/division
Illumination frequency:
16.2 GHz
Gaseous medium: Air at
0.2 Torr

2a. Zero Hall Current
Quiescent plasma

2b. Hall Current at 200 ma

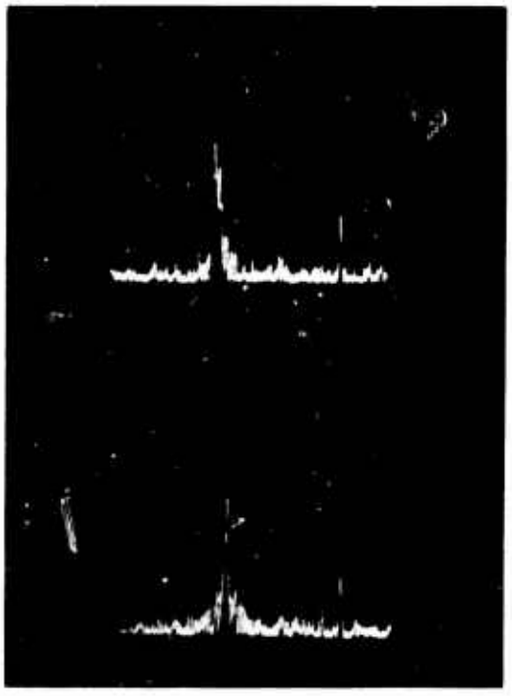

FIGURE 3. Backscatter Spectra
Conditions of Figure 2

3a. Hall Current of 400 ma

3b. Hall Current of 600 ma

FIGURE 4. Bistatic Scatter Spectra for Large T_e Increase

4a. Large T_e Increase

4b. Normal T_e Condition

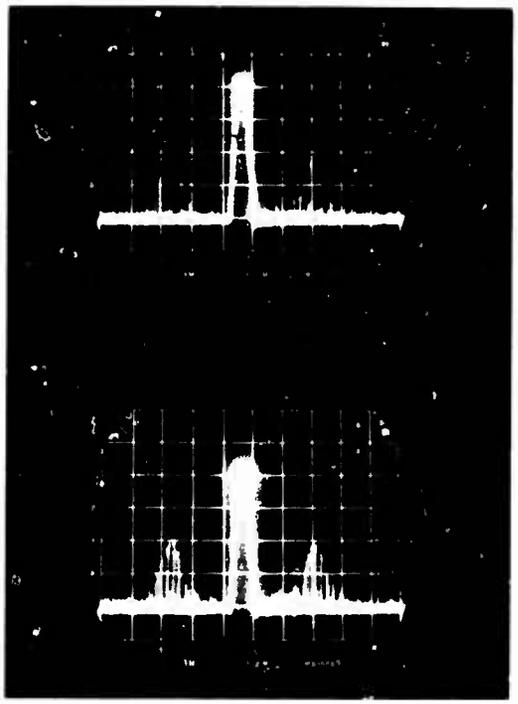

FIGURE 5. Gradual Reduction in Cross Section at Condition of Marginal Stability

5a. Slightly Enhanced T_e

5b. Original T_e

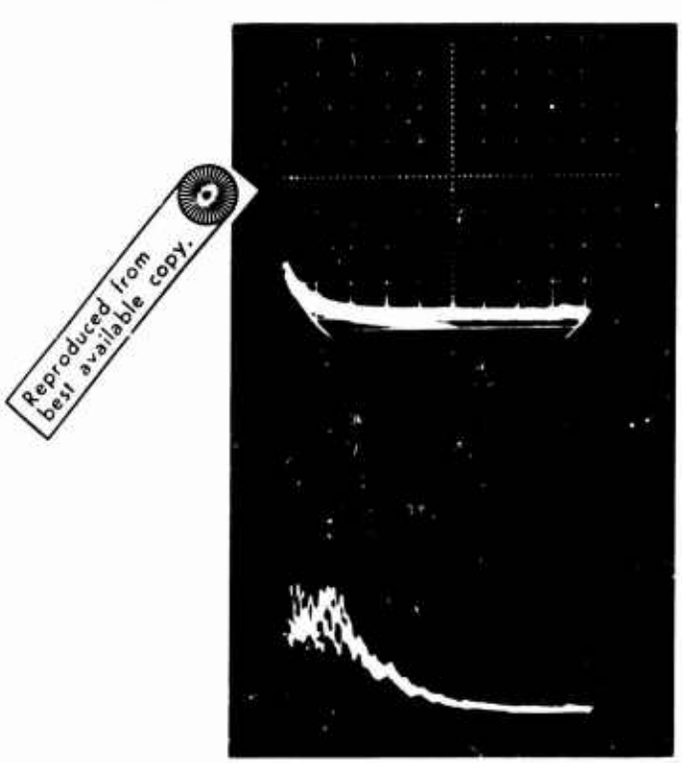

FIGURE 6. Hall Current Spectra
Vertical scale:
≃ 10 dB/division
Horizontal scale:
100 KHz/division

6a. Zero Hall Current

6b. Hall Current Exceeding Critical Level

DISCUSSION

P A Forsyth

In the E-region there are rapidly varying (spatially) quantities (N,σ) with height which may be important in generating irregularities. Are your conditions the "homogeneous" case or the "bounded" case?

J T Coleman

I have approximated the homogeneous case by minimizing boundary effects in the experiment. I have removed all interforce that would interfere with electrostatic wave growth (such as glass walls parallel to the drift). Since the waves grow rapidly only near the drift direction, I feel that reflections at the end of the wave growth path do not create a real "bounded" case. Thus I feel that I approach a "homogeneous" condition in the experiment.

A Kavadas

If Vd is expressed as shown on your equation 14 then for high values of $\frac{\nabla N}{N}$, Vd may become negative. What's the physical interpretation of that?

J T Coleman

You will notice that the approximation is made that $\frac{dV_{dt}}{V_{dt}} << \frac{1}{n_o}\frac{dn_o}{dx}$. In addition to that we have used a first order pertubation expansion to obtain the given result and in this we assumed also that $\frac{1}{n_o} dn_o/dx << 1/\lambda$. Thus we cannot in this theory go to that high a value for $\nabla n/n$. If I were to get a negative Vd I would go back and re-do the theory.

PHASE COHERENT HF RADAR OBSERVATIONS OF BARIUM RELEASES IN THE ARCTIC IONOSPHERE

G. D. Thome
RAYTHEON COMPANY
528 Boston Post Road
Sudbury, Massachusetts 01776
U.S.A.

SUMMARY

Phase coherent HF radars have been used to study the development of irregularities within ionized clouds produced by barium releases in the arctic ionosphere. Others have shown using optical methods that after a time ranging from a few seconds to a few minutes these clouds develop irregularities (striations) that resemble those seen in the optical aurora. The radar observations reported here show that the development of optical striations is accompanied by an abrupt broadening of the doppler spectrum leading to returns with doppler widths comparable to those observed from the natural radio aurora. In contrast to the natural ionosphere, the barium plasma is generated at a known instant of time and is confined to a limited volume of space. This makes it possible to study the evolution of irregularities in this plasma as a function of time and to study their radar aspect sensitivity without using narrow beam antennas. Prior to optical striation development the barium cloud behaves as a smooth overdense target, exhibiting a discrete doppler spectrum and producing regular Faraday fading. After the development of striations the doppler spectrum becomes diffuse and Faraday fading is lost.

1. INTRODUCTION

Chemical releases at ionospheric heights have been observed by HF radar for several years. The SECEDE series of chemical releases to be discussed here are of particular interest to the HF community because the chemical employed has been barium and because relatively large masses have been released. The virtue of barium is that the neutral and the ionized gas can be studied separately by optical means and the results used to supplement the radar observations. The advantage of a large release over a small one is that the ionized cloud is larger in spatial extent and remains overdense at HF frequencies for longer periods of time. The result is improved radar signal-to-noise ratio and extended periods of observation.

The largest barium release to date (96 kg) was Test HEMLOCK which took place during the SECEDE III series in Alaska. Raytheon made line-of-sight HF measurements from two sites in Alaska during this release. These data provide an unusually clear picture of the radar characteristics of large barium releases and the results of this test will be discussed below.

2. TEST GEOMETRY

A plan view of the SECEDE III test geometry is shown in Figure 1. This map covers a portion of Alaska and shows the release area and the two Raytheon radar sites. The Fort Wainwright site is near Fairbanks, Alaska, and the Wildwood Air Force Station site is near Kenai, Alaska. The release area and the radar sites lie nearly in the same magnetic meridian plane. Figure 2 shows a side view of the test geometry in this plane. Test HEMLOCK was released at 176 km, about 14 km lower than shown in this figure, and consequently the angles shown are slightly different. After release, the ionized cloud drifted magnetically west at about 250 m s^{-1}.

3. INSTRUMENTATION

The instrumentation at the two Raytheon sites is summarized in Table I. In all, 12 phase coherent radars were used covering the 5 to 60 MHz band. The Fort Wainwright and Wildwood radars were operated on common frequencies and time bases adjusted to avoid mutual interference. Pulse widths of 100 microseconds were used with peak pulse powers shown in the table.

4. RESULTS

Fort Wainwright was the principal Raytheon radar site and our analysis efforts to date have been concentrated on the data from this location. Information on peak electron density, frequency dependence, Faraday rotation, and the development of striations has been derived and are reported below. The purpose of the Wildwood Air Force Station site was to study the aspect sensitivity of the cloud. The analysis of these data are not yet complete and will not be reported here.

4.1. Peak Electron Density

Peak electron density was derived as a function of time by assuming that the cloud was overdense to a particular radar frequency so long as it produced a detectable echo. When the signal "dropped-out" on a particular frequency it was assumed that the cloud had gone underdense. Figure 3 shows the doppler shift (top) and total power (bottom) behavior of a typical radar signature. The fact that the dropout takes place over a finite length of time introduces an uncertainty of perhaps 10% in determining when the cloud went underdense. The dropout occurs more abruptly on higher frequencies but the total signal duration is shorter and consequently the percentage error remains about the same. Figure 4 shows a plot of the peak electron density versus time derived in this way for Test HEMLOCK and for three other SECEDE releases. The other three releases (Tests FIR, GUM and DOGWOOD) were only half the size of HEMLOCK (i.e., 48 kg instead of 96 kg). The differences from test to test are not well understood but are probably caused by differences in release height and ambient electric field.

4.2. Frequency Dependence

The frequency dependence of the HF radar returns is illustrated in Figure 5. The shape of the doppler shift records is similar in each case, the principal difference being only the duration of the return. Pronounced spectral broadening occurs at about 3 minutes after release on all frequencies for which the cloud remains overdense. This development corresponds to the onset of optical striations (discussed below, item 4.4). Periodic nulls are observed during the spectrally discrete portion of the signature (0-3 minutes). The spacing between adjacent nulls increases with time and decreases with increasing radar frequency. These nulls are caused by Faraday rotation (see item 4.3 below).

4.3. Faraday Rotation

Periodic nulls of the type discussed above have been observed during the SECEDE I releases and have been tentatively interpreted as a consequence of Faraday rotation[1]. A test of this interpretation was made during the releases of SECEDE III by transmitting linear polarization and separately receiving both the transmitted and the orthogonal polarization. If the nulls are in fact due to Faraday rotation (i.e., rotation of the plane of polarization) then signal nulls on the transmitted polarization should correspond in time to signal maxima on the orthogonal polarization. Figure 6 demonstrates that this is the case and consequently that the nulls are in fact due to Faraday rotation.

4.4 Striation Development

The correlation between the development of optical striations and the development of spectral broadening at HF is illustrated in Figure 7. The optical photographs were provided by Dr. Neil Davis of the University of Alaska. Clearly the two developments are closely correlated in time and represent different manifestations of the same event. The doppler spread observed at HF is probably due to multiple scattering from the striated cloud but the physics behind the striation development itself is not yet understood.

5. CONCLUSIONS

Barium releases in the 48 kg class produce ionized clouds dense enough to be conveniently studied by HF radar. Results to date suggest that studies of the growth and development of these clouds will lead to a better understanding of diffusion processes and the development of plasma instabilities in the ionosphere.

REFERENCE

1. Thome, G. D., "HF Radar Studies of Barium Clouds", Technical Report RADC-TR-69-214, Project SECEDE I, 1969.

TABLE I. INSTRUMENTATION

Site Location	Elevation Angle to Cloud	Slant Range to Cloud	Magnetic Aspect Angle	Instrumentation	Antennas	Transmitted Power
Fort Wainwright (Fairbanks, Alaska)	~60°	~200 km	~130°	5 HF radars (spaced, 5-30 MHz)	Dipoles	2-20 kw units 3-100 kw units
				3 VHF radars (40, 50, 60 MHz)	Yagis	3-10 kw units
Wildwood AFS (Kenai, Alaska)	~14°	~600 km	~98°	4 HF radars (spaced, 5-30 MHz)	Rhombics	2-20 kw units 2-100 kw units

Notes:

1) All radars operated at 40 PPS
2) Wildwood AFS and Fort Wainwright operated on common frequencies
3) All systems phase coherent

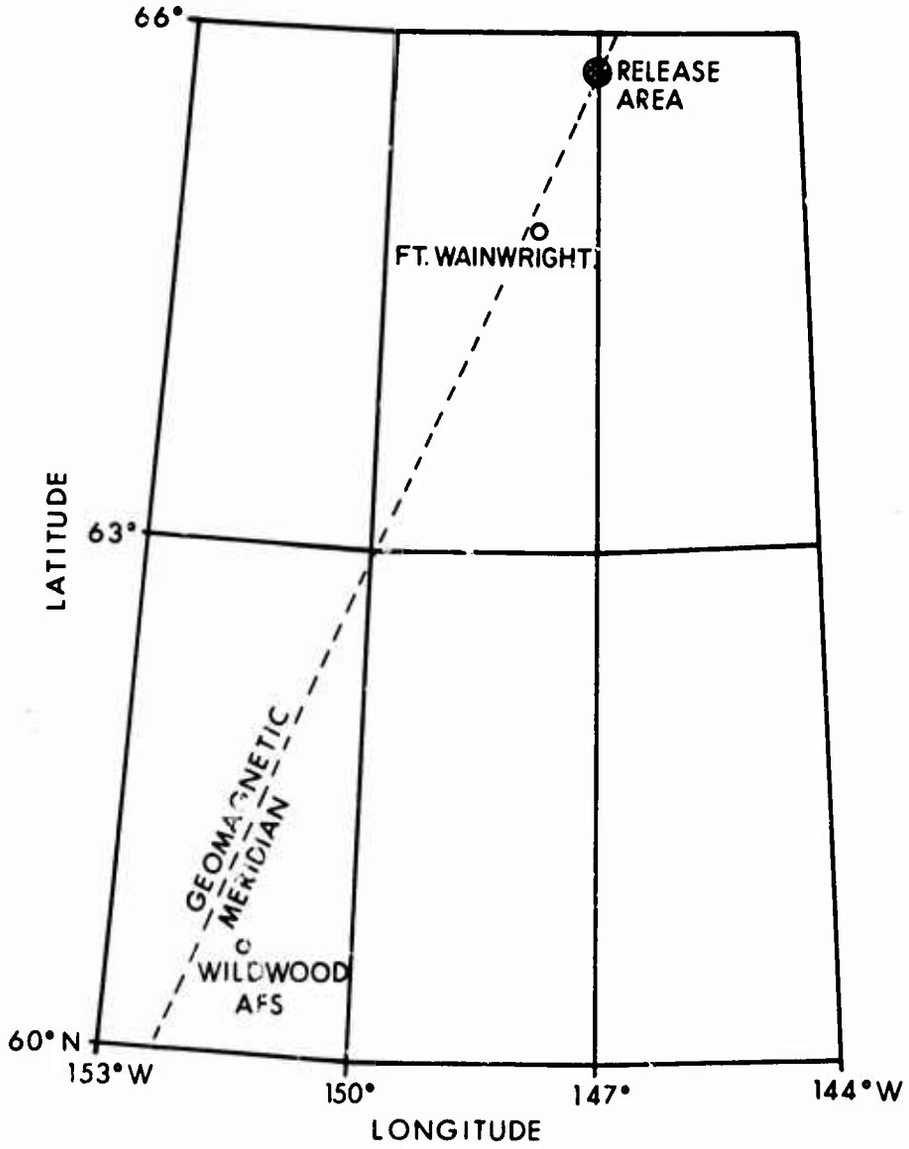

1. Plan View of HF Radar Geometry.

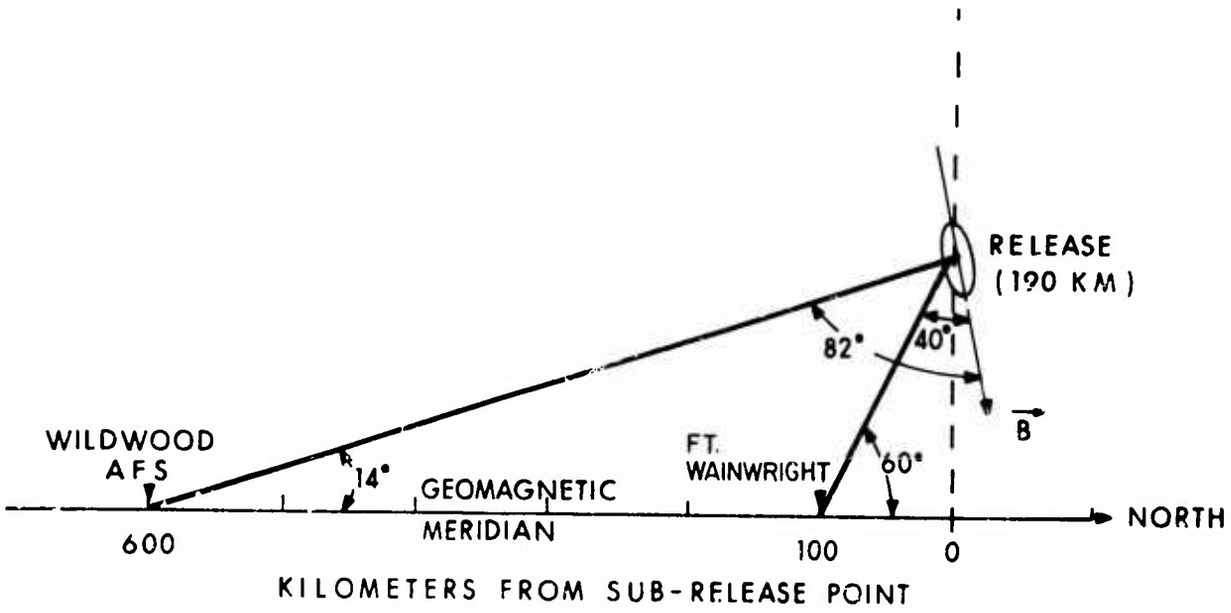

2. Side View of HF Radar Geometry.

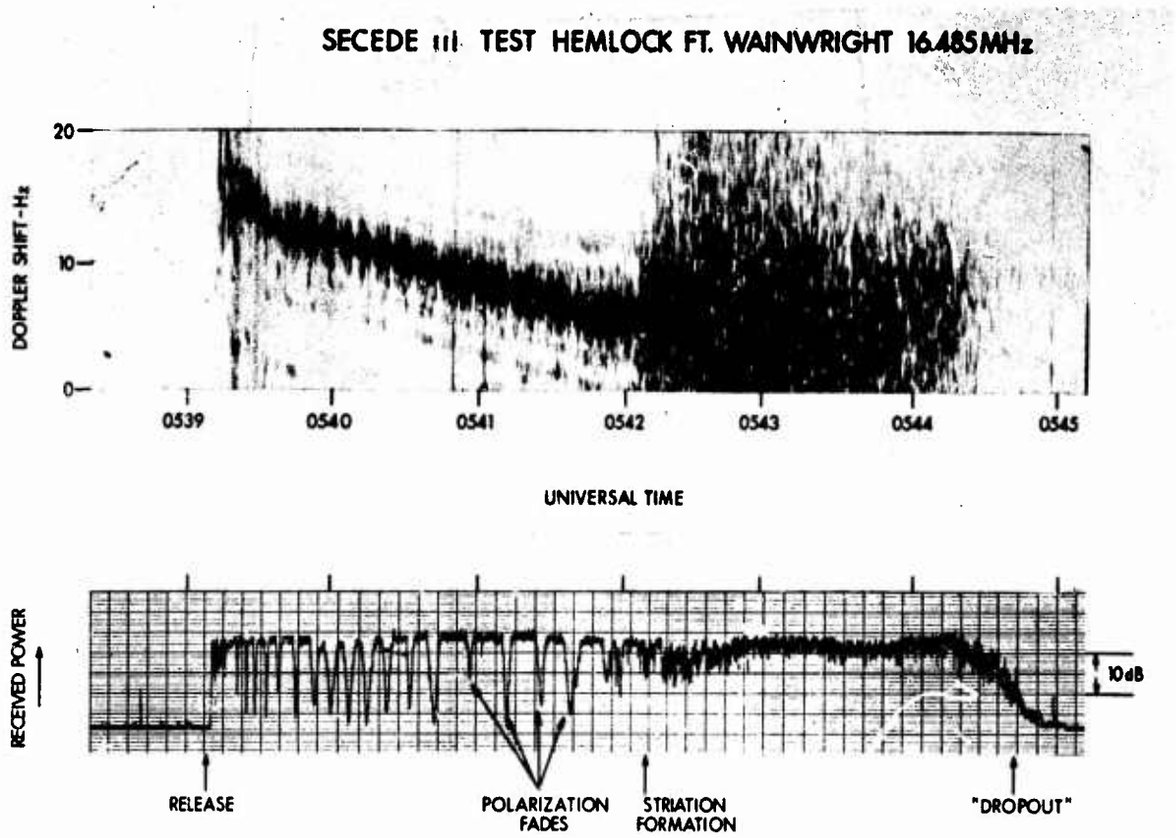

3. Typical Phase and Amplitude Behavior of a Barium Cloud Signature at HF.

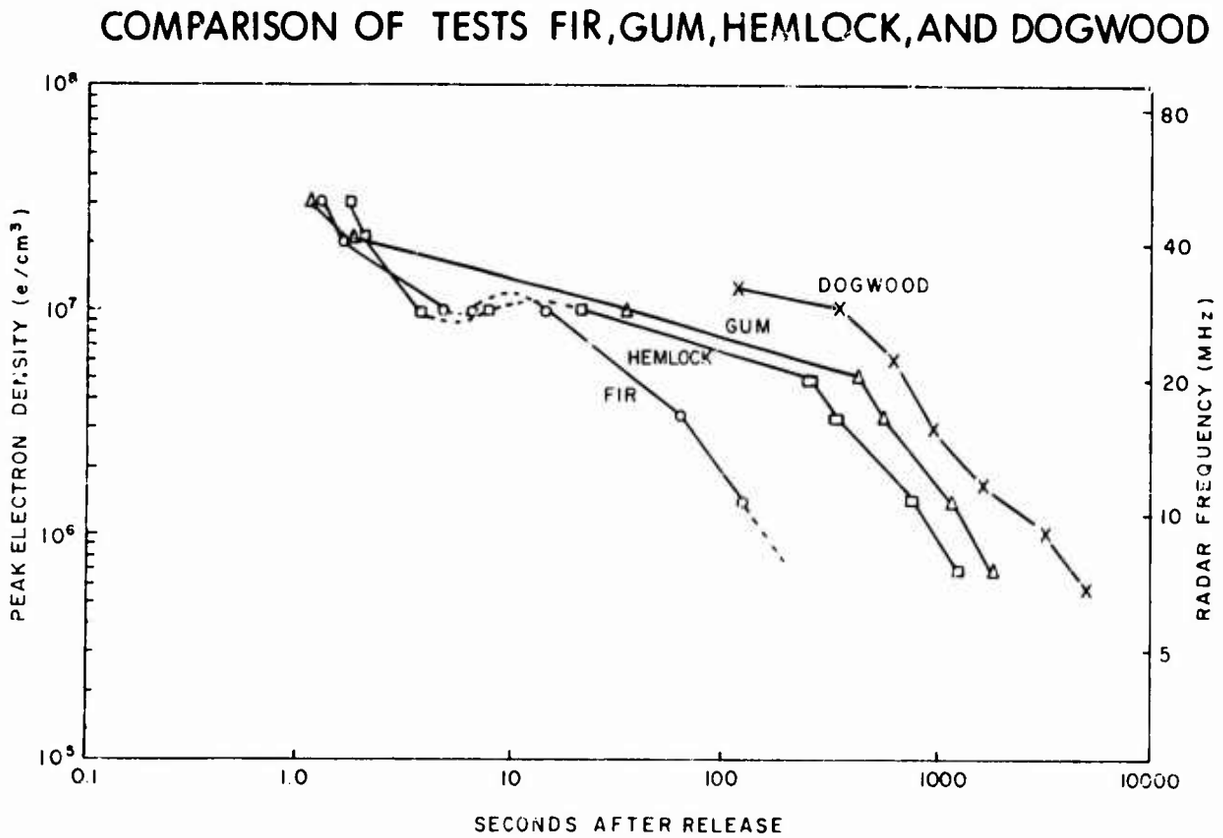

4. Peak Electron Density versus Time for Four SECEDE Releases.

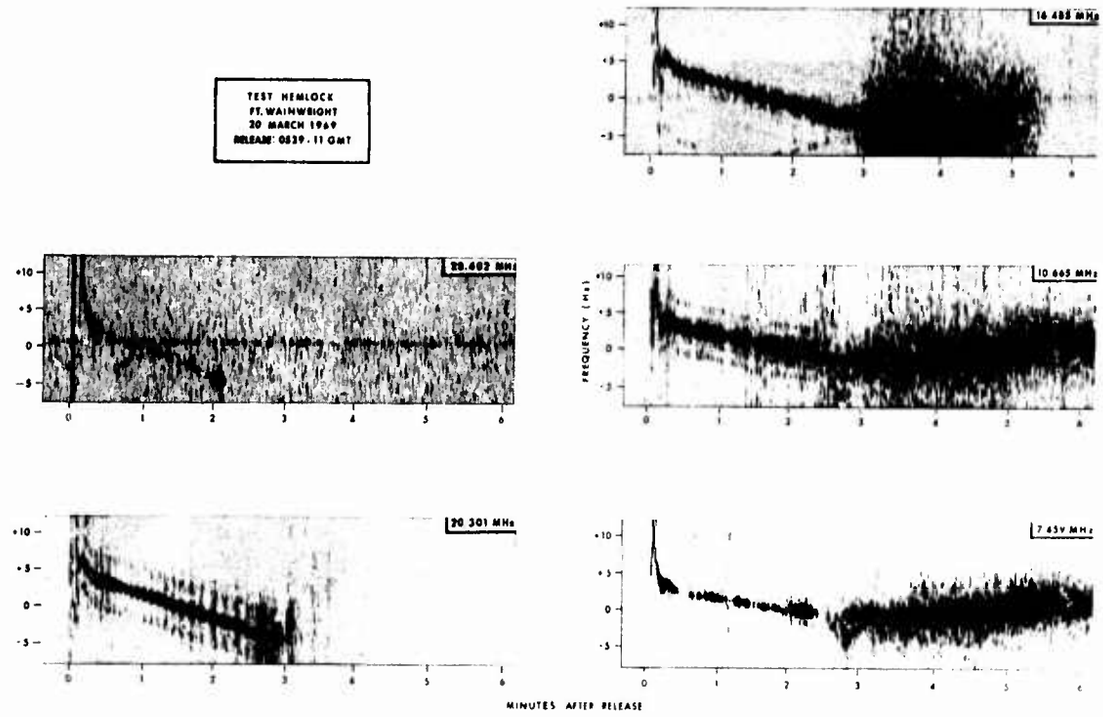

5. Frequency Dependence of HF Doppler Signature.

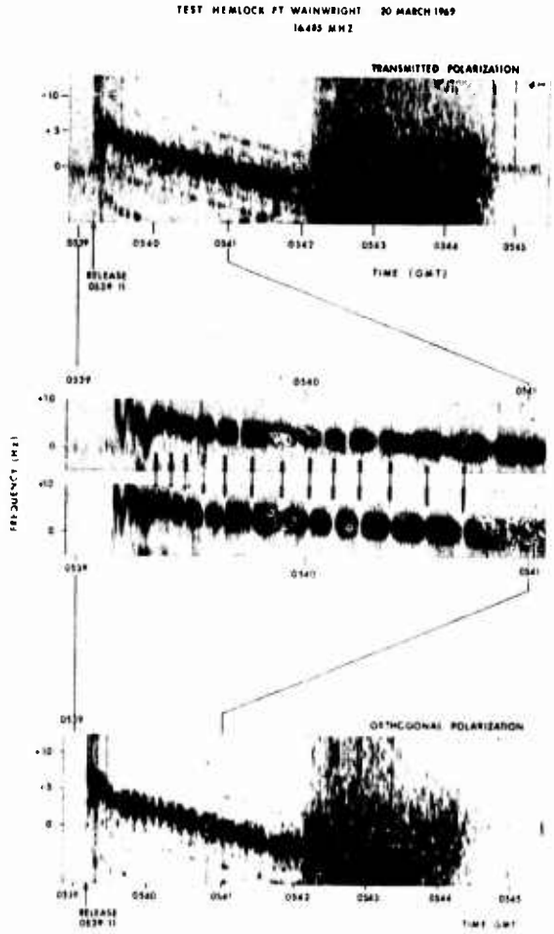

6. Verification that the Periodic Nulls Observed During the Spectrally Discrete portion of the Doppler Signature is due to Polarization Fading (Faraday Rotation).

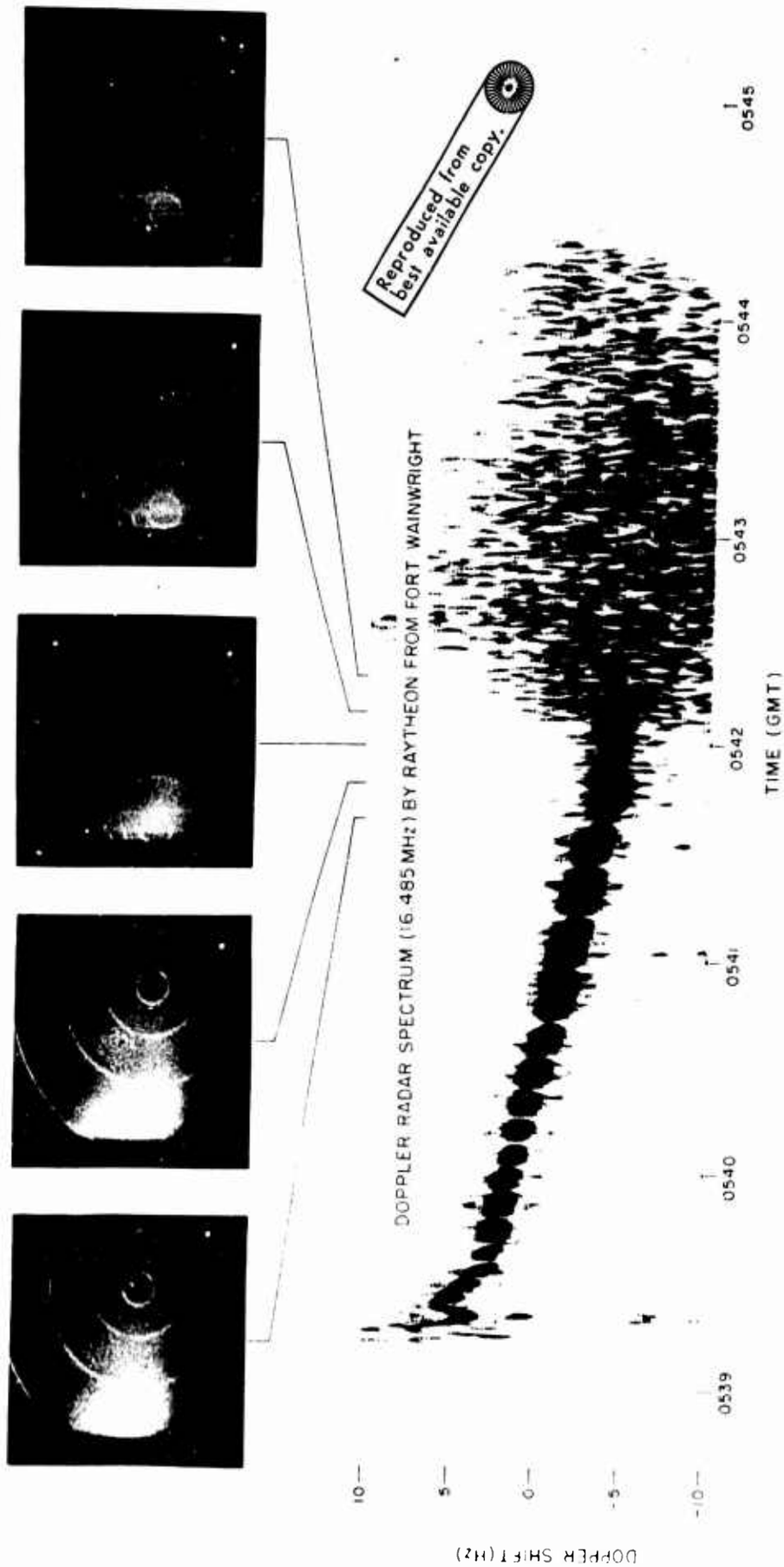

7. A Comparison of the Development of Optical Striations and the Development of Spectral Broadening at HF.

SESSION III

VHF-UHF PROPAGATION-SCATTERING MECHANISM

CHAIRMAN'S REPORT

by A.G.McNamara

This session consisted of six papers on the detailed structure of plasma irregularities and mechanisms by which radio waves are scattered. Rocket-borne experiments have provided direct measurements of fine scale structures. These have been observed by electron density probes and by electric field detection techniques. In addition to the D. C. electric field, A. C. fields in the range 50 Hz to 2 kHz have been observed in the 95 to 120 km region. Electron density measurements in aurora by the doppler shift on a VLF beacon have shown density changes of about 10 % within distances of 10 metres.

C. W. radio propagation studies on 40 MHz have yielded high resolution doppler spectra which show line spectra corresponding to the ion acoustic velocity - positive evidence of ion acoustic waves in radio aurora. However, the occurrence of line spectra in the signals is relatively rare, and the signals also occur at angles off perpendicularity of up to 6°. These observations emphasize the difficulties in explaining all auroral echoes in terms of the present two-stream instability model. In addition to spectral shift measurements, polarization observations of radio waves scattered from aurora offer a potentially powerful tool for examining in detail the interaction process of the radio wave and the plasma.

Because of the great complexity of the auroral scattering processes, it is advantageous to attempt controlled experiments to simulate the scattering medium. Laboratory studies with microwave scattering from a plasma containing two-stream instabilities have been used. Radar studies of high density electron clouds created by barium releases in the ionosphere are used to examine aspect sensitivity and the onset of optical striations and spread spectra in the radar signals. In the barium clouds, the instability would appear to arise from a gradient mechanism.

All these, and more detailed measurements, are needed to provide data for the calculation of radar systems parameters and the operational behaviour of large radar systems in auroral latitudes and for incoherent scatter research.

DISCUSSION

T Hagfors

I would like to remark on Dr Forsyth's paper that, contrary to his observations, a clear line spectrum associated with an ion-acoustic wave is seen from Millstone at 1295 MHz much more often than any other form of spectra. The line spectrum occurs much more frequently than 50% of the time. I am adding this comment to prevent the audience from getting the impression that a line spectrum is an exception rather than a rule at higher frequencies.

P A Forsyth

Perhaps I should qualify our experience.

a) We do not have good statistics but what we have suggest rare occurrance of pure line spectrum at the correct position for ion acoustic waves. Of course, all kinds of spread and line spectra arising from other sources (such as meteors) and mixed spectra occur.

b) Our sensitivity is probably very low compared to the Millstone radar. We have made no study of occurrence against sensitivity. Clearly relative occurrence of line and spread spectra would be expected to be a function of radar sensitivity, frequency and geometry. At least that would be true if, as I believe, the two types of spectra arise by different mechanisms. If the Cornell Aeronautics work mentioned by Chesnut is ever published and turns out to contain good statistics it might provide a basis for comparison of different frequencies and similar geometry using the Millstone data.

W G Chesnut

Camnitz, Tsunoda and Barczys (1969 referenced in paper 5) observe at 143.5 MHz line components in 157 out of 163 doppler spectra . 63 of these spectra they did also categorise as broad , meaning significant energy spread in frequency in addition to the line components. They saw 2 line components in 67 cases. They scanned from 17° West to 17° East of Magnetic north.

P A Forsyth

We do see spread spectra with line spectra but we assume this means normal scattering along with the ion-acoustic wave scattering. Whenever we have seen positive and negative shifted line spectra simultaneously we have been able to convince ourselves that the oppositely shifted components arose in separation volumes.

J Aarons

Our observations of radio stars and satellite beacons with a large parabola indicate that scintillations have a high correlation coefficient (0.9 or larger) comparing right-handed and lefthanded polarization and the two linear polarizations. This was noted in TRANS IEE on antennas and propagation AP 19 Feb 1971. Only during intense aurorae would we expect some lowering of the correlation at low frequencies (due to refraction).

A Kavadas

Our experience has been that under magnetically quiet conditions the scintillations as received at the two polarizations do not correlate but they do so when magnetic activity increases. We attribute this to the overlap of the star images during a time when the scintillation amplitude increases substantially.

K Toman

Taylor have shown theoretically that the scattering cross section depends markedly on the form of the spatial autocorrelation function of the density deviations. Which autocorrelation functions are realistic?

G N Taylor

It is pointed out in the paper that experimental evidence on the correct form of the spatial autocorrelation function is very sparse. I believe that what evidence there is suggests that the Gaussian acf is appropriate for the F-region, and a narrower acf (or less steep irregularity spectrum) is appropriate for the E-region. These conclusions are also reasonable on physical grounds.

W G Chesnut

Our incoherent (Thomson) scatter radar that we recently moved to Fairbanks, Alaska, operates at 1300 MHz. After several months of operation, we have not yet been affected, apparently, by the coherent effects that Dr Taylor discusses on a theoretical basis.

W G Chesnut

The Coleman experiment shows peculiar onset of plasma waves near onset threshold. We wonder about onset threshold for Farley waves. Farley waves are thought to grow from thermal fluctuations. We wonder whether localized disturbances that result from micrometeor impacts in the E-region might initiate wave growth. I vaguely recall a study of years ago by the Smyth Associates that seemed to find a relation between bistatic meteor propagation and the magnetic aspect condition. Furthermore, Blasley seems to find in the equatorial electrojet that echoing regions come in clumps as though they were initiated by a sporadic phenomenon.

C D Watkins

Regarding the comment by Dr Chesnut concerning the triggering of ionospheric instabilities by meteors, some years ago I showed that UHF radar echoes from meteor trains were more frequent and persisted much longer than normal in the region of specular reflection. Observations during a suitable meteor shower showed that the enhancement does not depend on the meteor train being formed parallel to the direction of the geomagnetic field, and suggested that any large meteor will produce field aligned ionization. The enhancement diminished rapidly away from the specular region by an amount comparable to the 10 dB per degree of aspect angle observed for radar aurora. Is this merely a coincidence?

W G Chesnut

Comment to paper by G D Thome

When barium vapor is released in sunlight at altitudes between, say 150 and 250 km, solar ultraviolet radiations ionize the barium cloud producing a localized region (order of 5 10 km) of high electron density. It has been observed that if the ions and the neutral air are moving relative to one another, the ionized barium cloud changes from a diffuse sphere to,eventually, a series of magnetic field alligned "bars" of ionization. It was proposed by Haerendel and further expounded by Linson and Workman (J.G.R. - vol. 75, pp 3211-3219, 1970) and also by Simon (J.G.R. - 75 pp 6787-6294, 1970) that the observed structure developed by way of the Martyn-Simon-Hoh Gradient Drift instability. It had been suggested by many authors that this instability produces sporadic E, discrete radar aurora, Spread-F, etc. Barium clouds provide a very convenient means to study the large amplitude growth of this instability and therefore these studies do have a bearing on understanding of polar and equatorial irregularities. My review article (paper no 5) does have an intuitive description of the gradient-drift instability.

POLAR PROPAGATION EFFECTS ON RADIO-ASTRONOMICAL AND SATELLITE TRANSMISSIONS

Ludwik Liszka
Kiruna Geophysical Observatory
S-981 01 Kiruna 1, Sweden

ABSTRACT

Existing high latitude studies of scintillation phenomenon on radio signals from radio-astronomical sources and satellites are reviewed. Morphology of high latitude scintillation is discussed; in particular: geographical distribution, diurnal variations and relation to magnetic activity. Studies of statistical properties of the signal received on the ground have been found, during the last ten years, to be a useful source of information about the nature of irregularities in the ionosphere. Existing studies are reviewed with emphasis on conclusions about parameters of the scintillation producing layer. Finally, results of height determinations using the space receiver method and satellite transmissions are briefly discussed.

1. INTRODUCTION

When radio waves from an extra terrestrial source pass through an ionospheric layer containing irregularities in the electron density, the wave front is modified within the layer. The resultant wave field, immediately after the passage through the layer, which acts as a diffracting screen, shows phase and sometimes also amplitude fluctuations which reflect properties of the irregularities. During the propagation from the irregular layer to the earth surface, where observations are usually made, further changes in the wave field are taking place due to the diffraction. The fluctuations are known as the scintillation and the diffraction theory has been applied by numerous authors (cf. e.g. Booker (1), Ratcliffe (2)) to determine the connection between statistical parameters of the irregularity layer and the wave field on the ground. Thus from observations on the earth surface conclusions may be drawn about the properties of the irregularity layer. This may be done, in principle, in following ways:

(i) Studies of statistical properties of the wave field across the earth surface.

(ii) Studies of statistical properties of the wave field in one point, when the wave field is changing due to changing outer presumptions, such as a change of the transmitted frequency or the position of the source.

In both cases radio-astronomical and artifical radio sources may be used for probing of the layer.

It has been known for more than ten years that the scintillation phenomenon is especially intensive at high latitudes which has been ascribed to a particularly high occurrence of intense ionospheric irregularities. Recent direct, in situ, measurements made by means of satellites show a very high degree of inhomogenity of the ionosphere in the auroral zone and within the polar cap. Both a wide spectrum of irregularities (cf. e.g. Dyson (3)) and large scale gradients (cf. e.g. Muldrew (4), Sharp (5)) are frequently observed there. These properties of the polar ionosphere reflect in different aspects of the scintillation phenomenon.

During recent years attention has been turned to quasi-periodic structures in the polar ionosphere (cf. e.g. Fremouw and Lansinger (6), Wernik (7)) which may explain some aspects of polar propagation which were not previously understood.

In the present paper studies of polar propagation of radio waves from radio-astronomical sources and satellites, with emphasis on different aspects of the scintillation phenomenon, will be briefly reviewed.

2. MORPHOLOGY OF HIGH LATITUDE SCINTILLATION

(i) Geographical distribution

Morphology of the scintillation phenomenon at high latitudes has been recently discussed in a review paper by Aarons et al. (8). Although systematic studies of the scintillation phenomenon within the auroral zone and polar regions are still scarce, it is known that intense scintillation is present over the entire polar caps (Frihagen (9), Titheridge and Stuart (10)). Frihagen (9) observed above the Northern polar region an enhancement of the scintillation within the polar irregularity region (latitudes above 80°) and within the auroral zone with a "trough", most clearly during nighttime, between those two regions (see Fig. 16-1). Observations from the Southern polar cap (10) show more complex geographical distributions (see Fig. 16-2). No clear enhancement of scintillation seems to be connected with the auroral zone. A longitudinal anomaly has been found in the Southern polar region at 170°E.

Contours of constant scintillation have been found to be oriented parallel to lines of constant L-values (Liszka (11)). The region of intense scintillation is limited on its equatorward side by the scintillation boundary (Aarons et al. (12), Aarons and Allen (13)) followed by a rapid decrease of the occurrence and depth of the scintillation (cf. e.g. the Joint Satellite Studies Group (14), Preddey (15)). The scintillation boundary is found (13) neither to follow the auroral oval, nor exactly the irregularity boundary of Dyson (3) based on Langmuir probe data from Alouette 2. A similarity in behaviour has been found with the ionospheric trough (13). The scintillation boundary often coincides with the trough but in general it is not true. Such an example is illustrated in Fig. 16-3 showing amplitude recordings of the S-66 satellite at 40 and 41 MHz together with a curve illustrating variations of the electron content. A high degree of irregularity is seen Northwards of the trough.

(ii) Diurnal variations

Although the scintillation is in general more common and intense during the night, it is difficult to construct a general picture of diurnal variations of the scintillation phenomenon due to differances in reduction and presentation of data and perhaps to some extent, due to differences in recording techniques.

Observations from Greenland (8) show a clear night-time maximum in the fading amplitude. On Spitzbergen (Frihagen (9)) morning and evening maxima are observed. In Murmansk, USSR (Benediktov et al. (16)) a weaker daytime maximum is observed besides the main night-time maximum. Double maxima are observed also in Kiruna for a period with enhanced magnetic activity (Liszka (17)). Stuart and Titheridge (18) show, for the Southern polar cap, that the character of diurnal variations is a function of geographical position, season and the phase of the solar cycle.

(iii) Relation to magnetic activity

All high latitude observations of the scintillation phenomenon show a clear connection with magnetic activity. Liszka (17) found in the auroral zone a linear dependence between the scintillation index and the magnetic K-index, varying somewhat during the day. In the polar region (Frihagen (9)) a very strong K_p dependence of scintillation depth, especially on the dayside is observed.

3. STATISTICAL PROPERTIES OF THE SIGNAL RECEIVED ON THE EARTH SURFACE

Radio waves from extra terrestrial sources when received on the ground show different statistical properties, reflecting the structure of the ionosphere and the nature of the source. In the case of a low orbiting, fast moving satellite the signal characteristics reflect the structure of the irregularity layer, drift motions in the layer and the known motion of the source. The wave field on the ground is also dependent on the distance to the source. For remote sources, such as geostationary satellites and radio stars, the wave field on the ground is, primarily dependent on the character of the irregularity layer and the drift within it. For radio stars the wave field may also be influenced by the finite size of the source.

The irregularity layer is usually described by an autocorrelation function and statistical properties of the wave field on the ground are calculated using diffraction theory. Calculated properties are compared with those observed so that the information about the irregularity layer may be deduced. Some of most commonly studied parameters will be enumerated here:

R.m.s. amplitude or power deviation and related to it scintillation index
R.m.s. phase deviation
Amplitude and phase distributions
Temporal autocorrelation function of the amplitude and related to it scintillation rate
Spatial autocorrelation function of amplitude and related to it scale size of the wave field on the ground
Spatial autocorrelation function of phase and related to it visibility of the source.

A number of investigations based upon measurements of the above mentioned signal characteristics have been carried out at high latitudes. Their aim was to study some propagation aspects and obtain information about the structure of the polar ionosphere.

(i) Ratio of scintillation depths at two frequencies

A comparison of observed and calculated ratios of amplitude fluctuations of radio source Cass A at 68 and 223 MHz has been carried out in College, Alaska (Lansinger and Fremouw (19)) using a phase sweep radio astronomical interferometer. A conclusion has been drawn that North of College the height of ionospheric irregularities decreases and the scale size increases with increasing latitude. The majority of irregularity size have been found in the range 0.6 - 0.8 km. The method indicates an increase in the irregularity scale size with increasing magnetic activity.

(ii) Zenith angle dependence of the scintillation depth

Zenith angle dependence at high latitudes has been studied by a number of authors. Observations of satellite scintillation above Northern Scandinavia (Liszka (11)) and radio star scintillation at College, Alaska (Lansinger (29)) showed an agreement with the theoretical zenith angle dependence derived by Briggs and Parkin (21). Polar cap observations (Frihagen (22), (9)) from Spitzbergen do not show any clear zenith angle dependence. This may be due to a real difference in the properties of the irregularities within the polar cap and the auroral zone. A combination of zenith angle dependence and two frequency scintillation ratios was used by Wernik (7). He compared satellite observations from Kiruna with theoretical calculations for Gaussian, exponential and sinusoidal autocorrelation functions. Of the the three closest the agreement with sinusoidal autocorrelation function has been found. This is consistent with a conclusion of Fremouw and Lansinger (6) about non-Gaussian autocorrelation function. The comparison of Wernik indicated scale sizes between 0.4 and 3.0 km. A deviation from the regular zenith angle dependence around the magnetic zenith, observed at middle latitudes by Singleton and Lynch (23) and explained by Briggs and Parkin (21) has also been reported at high latitudes by Lansinger (20) and Frihagen (22), but has not been found by Wernik (7).

(iii) Scintillation rate

Complex variations of the scintillation rate have been reported by Liszka (24) (See Fig. 16-4). During disturbed magnetic conditions ($K \geq 4$) two peaks of fast scintillation (>1 Hz) of satellite signals were observed. Rates up to 50 Hz were observed. Peaks in scintillation spectrum were occasionally seen, while results of Lansinger (20) show an absence of peaks. Frihagen (22) observed on Spitzbergen direct proportionality between the scintillation rate and the scintillation depth.

He proposed that the increased fading rate is due to increased thickness of the region of irregularities. A similar relation between the scintillation rate and depth seems to be observed at Thule, Greenland (8) on transmissions from geostationary satellites.

(iv) Spatial autocorrelation studies

Spatial autocorrelation functions of phase and amplitude have been investigated at College, Alaska (Lansinger (20), Fremouw (25) and Fremouw and Lansinger (6)) using a phase sweep interferometer and the radio source Cass A. A significant difference between variations of phase (angular) and amplitude scintillation has been found and interpreted as a geographical variation of the irregularity layer. The phase scintillation was found to be better correlated with magnetic activity and ionospheric absorption than with the amplitude scintillation.

Particularly interesting conditions have been found during so called: radio star visibility fades. The phenomenon takes place when the fringe pattern of the radio source disappears due to a strongly decreased correlation between the phase recorded at both aerials of the interferometer. This corresponds to a case when the scale size in the wave field on the ground is smaller than the length of the interferometer base. The irregularity layer acts then as a thick diffracting screen, as the rms phase deviation is usually larger than 1 radian (Fremouw and Lansinger (6)) at 68 MHz. The phase structure of the wave front indicates the scale sizes in the layer between 75 and 225 meters; i.e. much smaller than derived for usual scintillation phenomenon.

Alimov et al. (26) used observations of spatial autocorrelation function of satellite transmissions at 20 and 162 MHz at Murmansk, USSR for studies of the spectrum of ionospheric irregularities. The scale sizes of ionospheric irregularities were found to be between 0.5 and 1.0 km. Also the magnitude of fluctuations of the electron density in the polar ionosphere has been derived. It has been found that during disturbed conditions relative rms electron density fluctuations $\sqrt{(\Delta N/N)^2}$, may be larger than $1\text{-}4 \times 10^{-1}$, which corresponds to absolute rms density fluctuations, $\sqrt{(\Delta N)^2}$, of $(3\text{-}8) \times 10^4$ electrons/cm^3. Benediktov et al. (16) have shown that in Murmansk N/N is one order of magnitude larger than that at middle latitudes.

(v) Amplitude distributions

Amplitude distributions of scintillating satellite signals in the auroral zone were studied by Wernik and Liszka (27). It has been found that heavily scintillating satellite signals do not follow the generalized Rice amplitude distribution. Observed amplitude distributions follow rather the Wheelon distribution, which indicates a non-uniform phase distribution and connected with it polarization effects. The scattered part of the wave field may thus be polarized with a polarization degree proportional to the correlation coefficient between the rectangular components of the complex wave vector. This mechanism may be responsible for a part of the fluctuations of the orientation of the polarization plane of linearly polarized satellite signals; i.e. a polarization scintillation. A related phenomenon has been observed on transmissions from the INTELSAT 2F-1 satellite at 136.4 MHz. During certain periods the orientation of the polarization plane has been found to be in a fixed direction, parallel to the direction of magnetic field lines in the F-region (see Fig. 16-5).

(vi) Periodical structures

Studies of autocorrelation functions of the wave field produced by a radio star at auroral latitudes have often shown (Fremouw and Lansinger (6)) an existence of quasi-periodic structure in the wave field. The range of scale sizes corresponding to the quasi-periodic structure was different from that for cases of visibility fades, between 120 and 370 meters. Also some discrepancies between observations of zenith angle dependence at different frequencies and model calculations have been explained by Wernik (7) in terms of the existence of a periodic structure of phase variations in the diffracting screen. Periodic amplitude variations have also been observed by Liszka (28) on spaced aerials recordings of satellite signals at 54 MHz. In some cases the periodic amplitude variations occurred on the same satellite transit both in Kiruna and Tromsö (Frihagen and Liszka (29)), though not coincidentally. Subsatellite points at times of regular fading were mostly found to lie close to the auroral zone. The observations of regular amplitude variations are consistent with observations of narrow peaks in the scintillation rate spectrum (cf. (iii)).

4. SCINTILLATION HEIGHT

Previously mentioned comparisons of observed wave field parameters and model calculations often give an opportunity of estimation of the height of the scintillation producing layer. Only observations of the diffraction pattern from a fast moving satellite make it possible to measure directly the height of the irregularity layer. It may be done when the pattern speed due to a known satellite motion is much larger than the drift and temporal changes of irregularities within the layer. A very large number of height determinations have been made by this method; some of them at high latitudes.

Measurements in Northern Scandinavia (Liszka (30) and Frihagen and Liszka (29)) locate the major part of irregularities to the F-layer, within the altitude range 200-500 km. Simultaneous measurements in Kiruna and Tromsö (Frihagen and Liszka (29)) have in most cases given similar results, which means that the height and thickness of the irregularity layer are usually constant for a distance at least equal to the lateral spacing of the stations (250 km). Neither clear diurnal variation of the height, nor the magnetic activity dependence has been found in Kiruna (30), while Getmantsev et al. (31) observed in Murmansk, USSR, that the height increases with magnetic activity, especially during the daytime. The height of irregularities obtained by the spaced receiver method seems to increase with latitude both at subauroral (Clark et al. (32)) and

auroral latitudes (Getmantsev et al. (31)). These results are in conflict with radio star observations (Lansinger and Fremouw (19)) from which a decrease in height with increasing latitude is postulated. Significant differencesin height distribution of irregularities have been found for conditions of auroral black-out (30).

CONCLUDING REMARKS

The auroral ionosphere, due to its inhomogeneous structure, introduces serious modification of the signal characteristics. On the other hand the propagation effects give extraordinary good opportunities of, in time continuous, studies of ionospheric irregularities. Conflicting results obtained by different authors indicate that more research on the subject is needed. The future research should be coordinated in time, geographically well distributed and based on standarized equipment and data handling methods. A synoptic study of the scintillation phenomenon during polar substorms would be most valuable.

REFERENCES

1. Booker, H.G., "The Use of Radio Stars to Study Irregular Refraction of Radio Waves in the Ionosphere", Proc. I.R.E. 46, 298, 1958.

2. Ratcliffe, J.R., "Some Aspects of Diffraction Theory and their Applications to the Ionosphere", Rep. Progr. Phys. XIX, 188, 1956.

3. Dyson, P.L., "Direct Measurements of the Size and Amplitude of Irregularities in the Topside Ionosphere", J. Geophys. Res. 74, 6291, 1969.

4. Muldrew, D.B., "F-Layer Ionization Troughs Deduced from Alouette Data", J. Geophys. Res. 70, 2635, 1965.

5. Sharp, G.W., "Midlatitude Trough in the Night Ionosphere", J. Geophys. Res. 71, 1345, 1966.

6. Fremouw, E.J. and Lansinger, J.M., "Radio Star Visibility Fades in Alaska Near Solar Minimum", J. Geophys. Res. 73, 3565, 1968.

7. Wernik, A.W., "On the Dependence of Satellite Radio Signals Scintillations on Zenith Angle", KGO Report No. 704, Sept. 1970.

8. Aarons, J., Whitney, H.E. and Allen R.S., "Global Morphology of Ionospheric Scintillations", Environmental Research Papers, No. 339, October 1970.

9. Frihagen, J., "Occurence of High Latitude Ionospheric Irregularities giving Rise to Satellite Scintillation", J. Atmos. Terrest. Phys. 33, 21, 1971.

10. Titheridge, J.E. and Stuart, G.F., "The Distribution of Irregularities in the Antarctic Ionosphere I. Mean Seasonal Maps at Sunspot Minimum", J. Atmos. Terrest. Phys. 30, 85, 1968.

11. Liszka, L., "The Geographical Distribution of Satellite Scintillation Axtivity above Northern Scandinavia", Arkiv f. Geofysik 4, 453, 1964.

12. Aarons, J., Mullen, J.P. and Whitney, H.E., "The Scintillation Boundary", J. Geophys. Res. 74, 884, 1969.

13. Aarons, J. and Allen, R.S., "Scintillation Boundary during Quiet and Disturbed Magnetic Conditions", J. Geophys. Res. 76, 170, 1971.

14. The Joint Satellite Studies Group, "On the Latitude Variation of Scintillations of Ionosphere Origin in Satellite Signals", Planet. Space Sci. 16, 775, 1968.

15. Preddey, G.F., "Mid-Latitude Radio-Satellite Scintillation: The Variation with Latitude", Planet. Space Sci. 17, 1557, 1969.

16. Benediktov, E.A., Getmantsev, G.G., Grishkeviteh, L.V., Eroukhimov, L.M. and Mityakov, N.A., "Some Results of Ionosphere Investigations at NIRFI for 1957 - 1967", Radiophysics (Russian) 11, 169, 1968.

17. Liszka, L., "Dependence of Auroral Zone Satellite Scintillation on Geomagnetic Activity", Arkiv f. Geofysik 4, 445, 1964.

18. Stuart, G.F. and Titheridge, J.E., "The Distribution of Irregularities in the Antarctic Ionosphere II. Diurnal, Magnetic and Solar Cycle Effects", J. Atmos. Terrest. Phys. 31, 905, 1969.

19. Lansinger, J.M. and Fremouw, E.J., "The Scale Size of Scintillation-Producing Irregularities in the Auroral Ionosphere", J. Atmos. Terrest. Phys. 29, 1229, 1967.

20. Lansinger, J.M., "Auroral Zone Radio Star Scintillation Measurements and Interpretations", Boeing Report D1-82-0476, October 1965.

21. Briggs, B.H. and Parkin, I.A., "On the Variation of Radio Star and Satellite Scintillation with Zenith Angle", J. Atmos. Terrest. Phys. 25, 339, 1963.

22. Frihagen, J., "Satellite Scintillation at High Latitudes and its Possible Relation to Precipitation of Soft Particles", J. Atmos. Terrest. Phys. 31, 81, 1969.

23. Singleton, D.G. and Lynch, G.J.E., "The Scintillation of the Radio Transmissions from Explorer VII-II Some Properties of the Scintillation Producing Irregularities", J. Atmos. Terrest. Phys. 24, 363, 1962.

24. Liszka, L., "A Study of the Scintillation-Rate Spectrum Observed in the Auroral Zone", Arkiv f. Geofysik 4,529, 1964.

25. Fremouw, E.J., "Measurement of Phase Variance and Autocorrelation during Radio Star Visibility Fades", J. Geophys. Res. 73, 3557, 1968.

26. Alimov, V.A., Getmantsev, G.G., Yerukhimov, L.M., Mityakov, N.A., Rapoport, V.O., Uryadov, V.P. and Cherepovitskiy, V.A., "Some Results of Investigations of the Inhomogeneous Structure of the Polar Ionosphere by Reception of Satellite Signals on Interferometers with Different Bases", Geomagnetism and Aeronomy (English) 10, 21, 1970.

27. Wernik, A.W. and Liszka, L., "On the Amplitude Distribution of Scintillating Radio Signals from Artifical Satellites", Arkiv f. Geofysik 5, 501, 1968.

28. Liszka, L., "A Possible Interpretation of the Fast Regular Fading observed on Satellite Transmissions", Nature 203, 178, 1964.

29. Frihagen, J. and Liszka, L., "A Study of Auroral Zone Ionospheric Irregularities made Simulteneously at Tromsö, Norway and Kiruna, Sweden", J. Geophys. Res. 27, 513, 1965.

30. Liszka, L., "An Investigation of the Height of Scintillation Producing Irregularities", Arkiv f. Geofysik 4, 523, 1964.

31. Getmantsev, G.G., Gringanz, K.I., Eroukhimov, L.M., Kravtsov, Yu.A., Mityakov, N.A., Mityakova, E.E., Roudakov, V.A. and Rytov, S.M., "Investigation of Electron Density in the Ionosphere by Means of the Ground-Based Observations of Radio Signals Radiated from Cosmic Vehicles (a Review)", Radiophysics (Russian) 11, 649, 1968.

32. Clark, D.H., Mawdsley, J. and Ireland, W., "Mid-Latitude Radio-Satellite Scintillation. The Height of the Irregularities", Planet. Space Sci. 18, 1785, 1970.

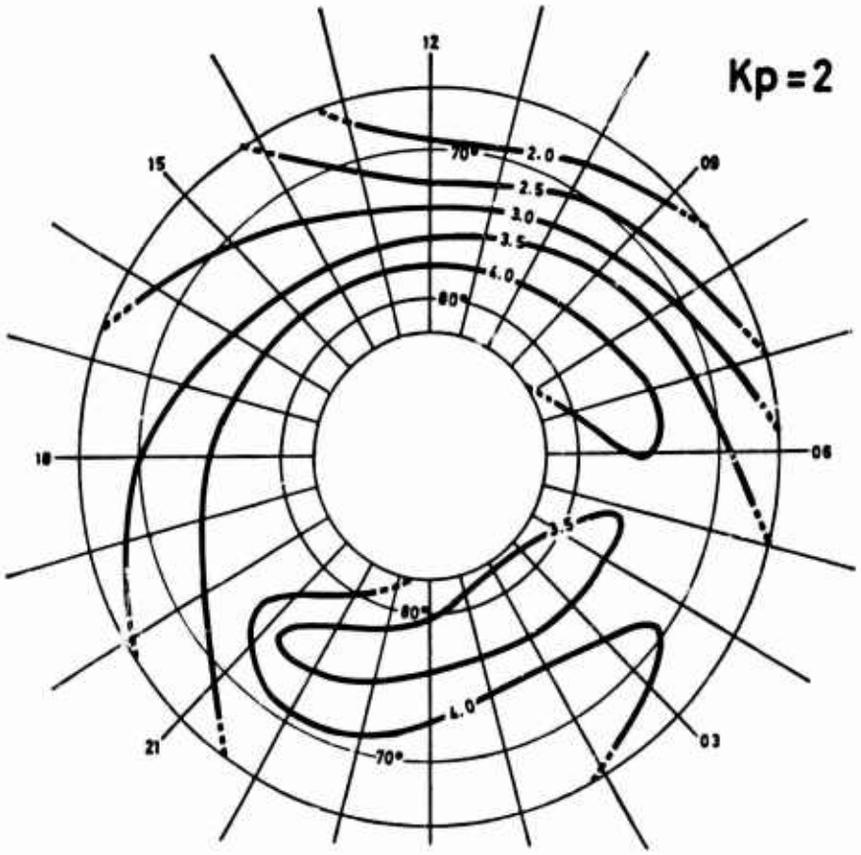

Figure 16-1 Contours of constant scintillation depth for Northern polar cap and Kp = 2 (after Frihagen (9). Coordinates are geomagnetic latitude and geomagnetic local time.

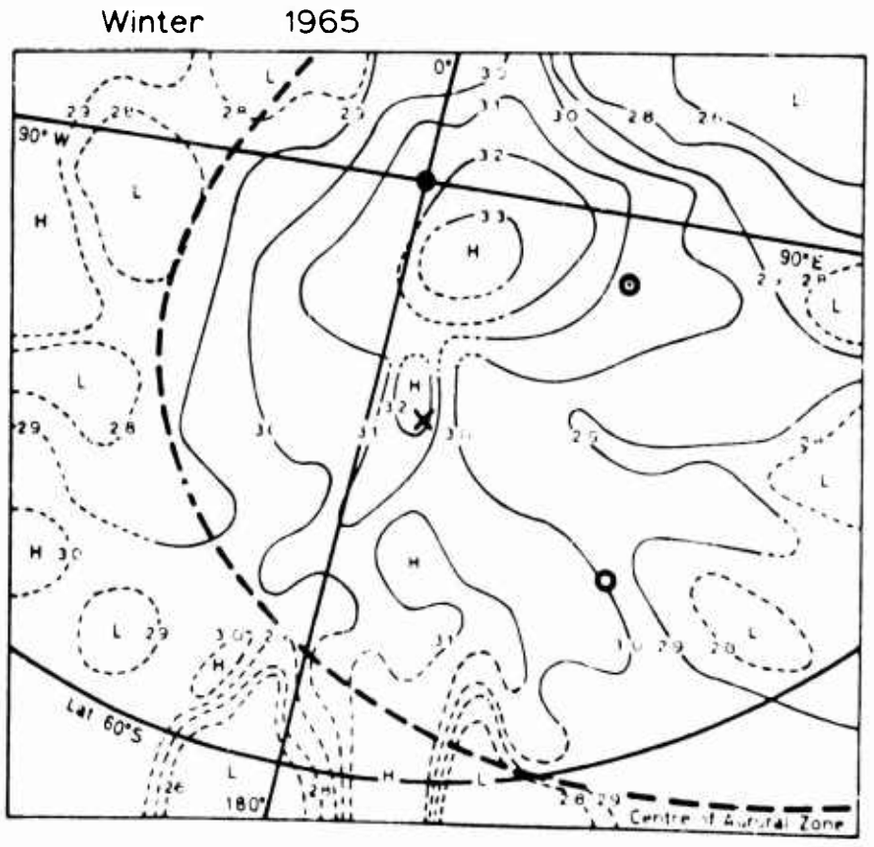

Figure 16-2 The mean degree of irregularity of the antarctic ionosphere for winter 1965 (after Titheridge and Stuart (10).

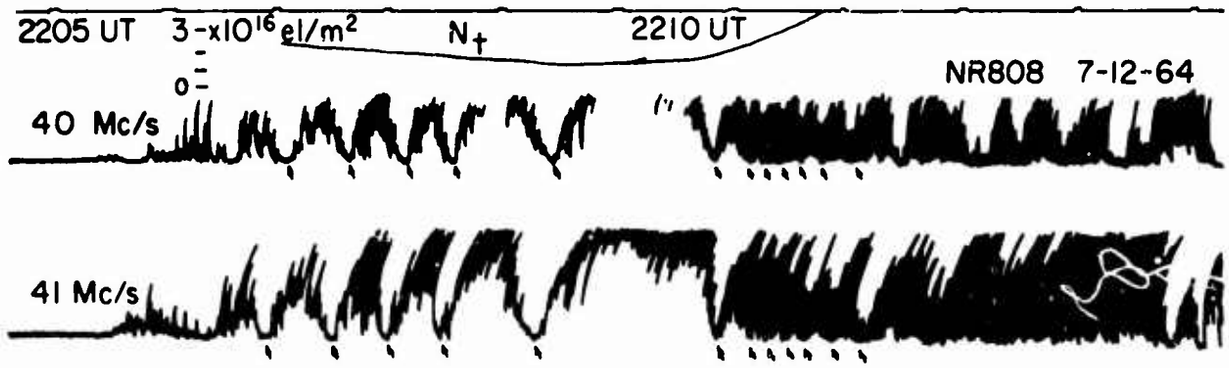

Figure 16-3 Amplitude recordings of the S-66 satellite at 40 and 41 MHz together with a curve illustrating variations of the electron content. A high degree of irregularity is seen Northward of the trough.

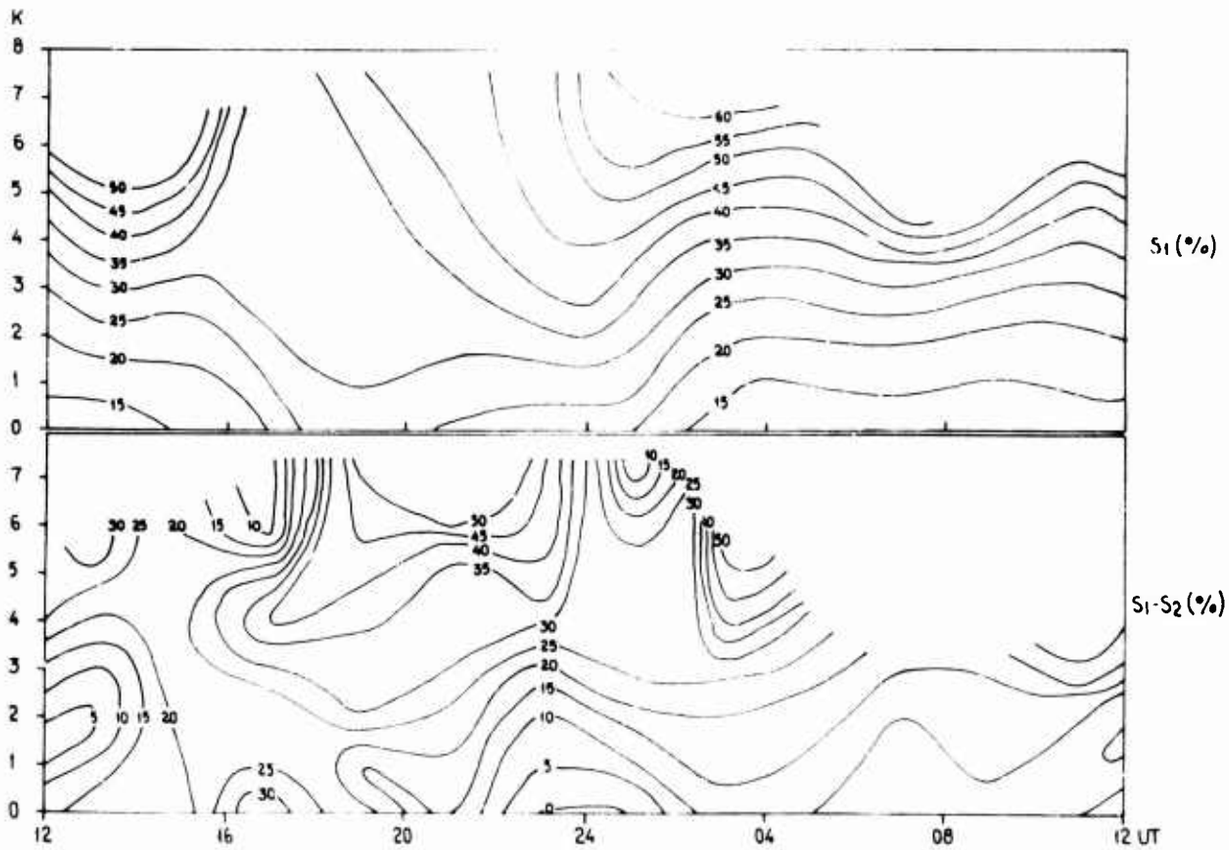

Figure 16-4 Dependence of the quantity (S_2 - S_1), proportional to the scintillation power between 10 Hz, on the time of observation and the geomagnetic K-index (low diagram) together with similar dependence of the scintillation index S_1, corresponding to slow scintillations (<1 Hz) (upper diagram). Functions are represented by contours (after Liszka (24)).

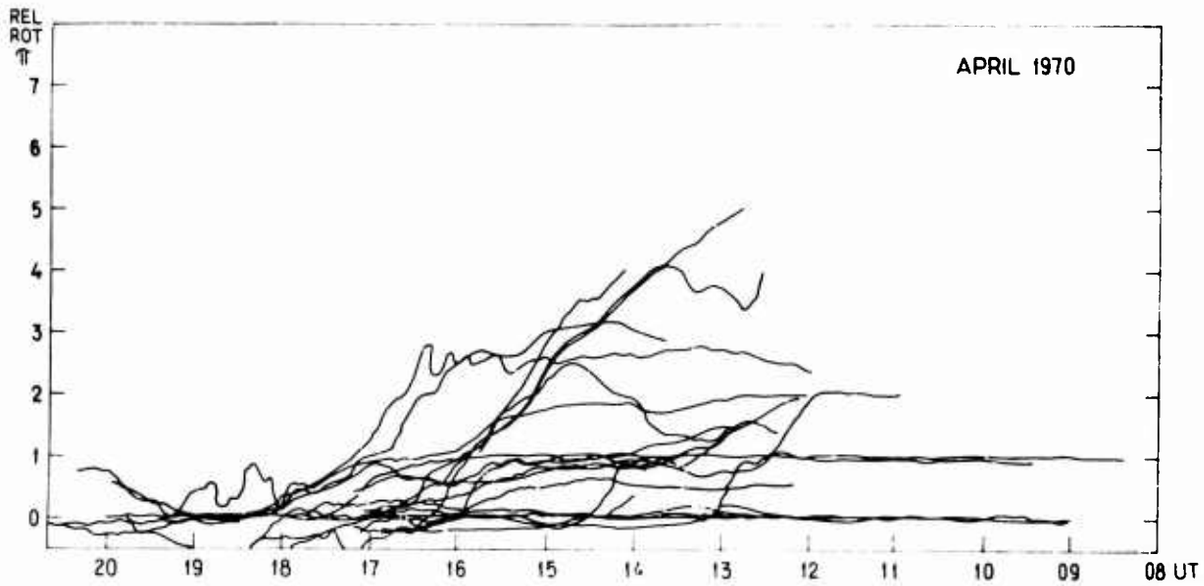

Figure 16-5 Orientation of the polarization plane of signals from the INTELSAT 2F-1 satellite at 136.4 as observed in Kiruna during April 1970. The vertical scale gives the angle of orientation in multiples of π measured from an arbitrary zero. The integer multiples of π correspond to the vertical polarization. Observe clustering of curves in a direction close to the vertical.

SATELLITE SCINTILLATIONS IN THE HIGH LATITUDE F-LAYER IRREGULARITY REGION

Jules Aarons
Air Force Cambridge Research Laboratories
Bedford, Massachusetts 01730

SUMMARY

The high latitude region containing small scale (~1 km) F-layer irregularities displays a diurnal pattern of oval form. During quiet magnetic conditions (K_p=0,1) the equatorward boundary varies from an invariant latitude of 57° at 2200 local time to ~74° between 0600 and 1000. During disturbed magnetic conditions ($K_p \geq 4$), the maximum change in latitude, 2° to 2.5° per unit K, occurred between 0300 and 0600 local time. The scintillation boundary has been discussed in earlier papers; new data is presented on the intensity variations within the irregularity region. The polar observations, described by Frihagen from Spitzbergen observations, show a trough or decrease in scintillation index, on the night side between an oval and a polar region. Using radio star data at 113 and 228 MHz obtained at the Sagamore Hill Radio Observatory, scintillation index increases of .50 to 7 have been noted with increases in K index (propagation path intersection through the F-layer (350 km) at 67°). Recordings of 136 MHz satellite signals from Narssarssuaq, Greenland, (intersection at 63°) also show that mean scintillation index increases during magnetic storms within the irregularity region. Thule observations of 40 MHz transmissions indicate the overhead pattern at invariant latitudes near 86°. The emerging model is of a core of high electron density irregularities probably centered above the auroral oval but with a high occurrence of irregularities over the polar cap. In addition, the irregularity region at lower intensity extends below the oval at night.

1. INTRODUCTION

Two recent reviews (Liszka, 1969, and Frihagen, 1970) describe high latitude phenomena in the field of amplitude scintillations and spread F. The polar region has been studied by Titheridge and Stuart (1968), Aarons et al (1970), and Frihagen (1971). A clear picture of the polar pattern is under some dispute mainly due to the fact that available frequencies have been too low to measure the intense irregularities at high latitudes.

However, the lower latitudes have been probed using synchronous satellite and radio star observations. The morphology of scintillations in the irregularity oval is more apparent.

During quiet magnetic conditions the equatorward boundary of high latitude small scale-F-layer irregularities, as shown by scintillation observations, exhibits a diurnal variation in position. This is shown in Figure 1 along with a corroborating picture of the irregularities from Dyson (1969). Dyson's boundaries (equatorward and poleward) are drawn from median values of points obtained with Langmuir probe observations of Alouette 2.

With the verification of the hypothesis of the existence of an F-layer irregularity region at high latitudes in the form of an oval, the next step was to determine the change in the diurnal pattern of the equatorward scintillation boundary as a function of magnetic index. This was done (Aarons and Allen, 1971) where it was found that the maximum change in equatorward boundary as a function of K index, approximately 2° to 2.5°/unit K, occurred between 0300 and 0600 local time. Figure 2 illustrates the form the boundary takes during quiet and disturbed magnetic conditions.

2. THE AURORAL OVAL AND THE IRREGULARITY REGION

The irregularity region, oval in form, should be distinguished from the auroral oval which was classically (Feldstein papers) determined from optical measurements at E-region heights. The characteristics of high latitude ovals should be expected to differ since each manifestation represents a different magnetospheric-ionospheric interaction. The positions and diurnal patterns of the trough, 40 kev electron precipitation, E-layer auroral echoes etc , do in fact differ from one another.

The irregularity region fits into the auroral oval form in the following ways:

1. The magnetically quiet form of the irregularity region as determined by scintillation measurements (latitude at which the mean scintillation index at 40 MHz = 50%) falls to 57° invariant latitude at 2200 local time for K indices of 0,1. Between 0600 and 1000 its latitude is ~74°. The auroral oval during quiet magnetic conditions has 63° as its lower boundary at midnight and 76° at noon (Feldstein, 1963). At this stage of scintillation observations, it is difficult to ascribe a real difference for the two noon values. Night values of the latitudes of the two phenomena are valid and represent a distinct difference.

The definition of the lower latitude of the irregularity region (the scintillation boundary) is arbitrary. However, it corresponds to the latitude where the sudden onset of irregularities is observed and in that sense is a boundary between the ordered ionosphere and the irregularity region.

2. A second basic difference between the auroral oval and the irregularity region is the presence of strong irregularities across the polar cap. While the classical auroral oval has a ring with an upper latitude boundary, several studies have confirmed that strong irregularities exist over the entire polar cap. In a recent analysis it has been found that an auroral oval maximum and a polar cap maximum both exist with a night trough between the two (Frihagen, 1971). Dyson's data indicates a poleward boundary. Observations of the precipitation of low energy electrons in the range of 700 ev

(Hoffman, 1968) indicate bunched irregularities or bursts of precipitated electrons in the polar cap region. The resolution of the observations may be that there are irregularities across the polar cap but their intensity may be lower between the cap (radius of 10°) and the oval irregularity region.

3. A third characteristic of the irregularity region is the presence of weak irregularities from middle to sub-auroral latitudes, particularly from midnight to 0300 during quiet magnetic conditions (Aarons et al, 1963).

3. THE IRREGULARITY REGION AS NOTED IN EARLIER STUDIES

In order to determine what might be termed the strength of the irregularities, $\Delta N/N$, within the region a literature search was initiated in order to utilize data collected in radio star and satellite observations of scintillations. The concept was to review the literature within the framework of the hypothesis of the irregularity region.

The use of historical data has encountered three problems. First, for a radio star source, it is difficult to isolate the variables which are (1) angle of elevation (2) seasonal pattern (3) diurnal effects and (4) latitude of the path intersection with the F-layer. Cass A, for example, has its lower transit near local midnight in February. A second problem is that the ionospheric physicists analyzing the data have failed to isolate sub-ionospheric latitudes into time blocks for distinct magnetic conditions. If a sub-auroral observatory correlates scintillation index with K index for all times of day there are time when the propagation path fails to traverse the irregularity region while during other periods of time (night, for example) the intersection may include the irregularity region. In one study at 150 MHz with the sub-ionospheric intersection at 350 km over Kiruna (~65°) no correlation was found with magnetic index (Orhaug, 1965) but all data were lumped together. In another study (Ryan, 1964) correlation coefficients of .35 were found at 14° zenith angle (to the north). In neither case was it possible to correlate distinct time blocks with scintillation index given only the published data.

A third factor tends to decrease the utility of radio star data, i.e. the finite angular diameter of the radio sources, particularly when only Cass A and Cygnus A were used. Cass A has an angular diameter of 4' while Cygnus has a diameter of 1.5'. During periods of intense scintillation the angular broadening of the source decreases the scintillation index at the lower frequency. Thus the extended series of observations of Cass A by Briggs (1964) at 38 MHz has limited utility for geophysical studies. Figure 3 from Orhaug, correlating sunspot number and scintillation index, shows index decreasing at 33 MHz with increasing sunspot number but increasing at 150 MHz with higher sunspot number; this is probably the effect of strong scattering at the lower frequency broadening the source (Cygnus A). Optimum observations would utilize multi-frequency information. Only observations from weak scattering cases are useful for morphological studies of the quantitative nature.

Within the irregularity region the use of satellite beacons at 20 and 40 MHz have limited utility. Scintillations show saturated values for all practical purposes with negative fades very close to sky noise levels. Newer studies within the irregularity region will overcome this deficiency since many observations are now being made at 136 MHz where strong scattering occurs much less frequently.

4. CHARACTERISTICS OF THE IRREGULARITY REGION AS DETERMINED BY SCINTILLATION STUDIES

a. The irregularity region has a sharply bounded lower latitude. Within 2° or less the ionosphere changes from a homogeneous structure to relatively dense irregularities. The evidence comes from radio star scintillations (Ryan, 1964, noted large differences in scintillation index over a range of 2.4°) as well as satellite studies (Yeh and Swenson, 1959).

Signals from the BE-B and BE-C satellites at 20 and 40 MHz as well as the earlier Sputnik series show the abruptness dramatically particularly in the post sunset period (Kent, 1959, and Aarons et al, 1963). During pre-midnight time periods the irregularities are an on-off boundary feature rather than a gradual increase of irregularity electron density.

b. Within the irregularity region, mean scintillation index increases during certain periods of time when K index increases. Observing near the lower transit of Cassiopeia with a 150-foot parabola in 1963 and 1964, near the minimum of the sunspot cycle, data were obtained at 113 MHz and 228 MHz by AFCRL at the Sagamore Hill Radio Observatory, Hamilton, Massachusetts. The path to Cass A has a sub-ionospheric intersection (350 km) at an invariant latitude of 67°. The elevation angle was 13°. From 1600 to 0400 local standard time the ray path traversed the quiet period irregularity region. With increasing magnetic index, scintillation index increased in all time periods (Figures 4 and 5). However, the most dramatic increase occurred around 0400. Thus within the irregularity structure mean scintillation index increases when K index increases. For an intersection latitude of 67°, since the boundary moves lower with increasing K index, all time periods may be within the irregularity region during magnetic storms. The increases in index range from a multiplying factor of .5 to 7, the latter at 0400.

This correlation of high latitude radio star scintillation index with K index is consistent with other data from radio star observations. Little et al (1962) at College, Alaska, found an overall correlation coefficient of .35 between scintillations and K index. Ryan with upper transits of Cass A data found a correlation of scintillations and K index of .35 but Virgo transiting to the south of Cass A's path had a lower correlation coefficient of .16.

Thus for a constant ray path within the irregularity region, mean scintillation index increases with magnetic index. This can also be seen with observations of the 136 MHz beacon of ATS-3 as observed from Narssarssuaq. The path traverses the 350 km point at 63°. Figure 6 shows the increases in occurrence of scintillation indices >60 as magnetic index increases. The increase in occurrence of deep scintillation is most apparent at night. Small increases in K index in the morning sector,

0900-1300, are not accompanied by a greatly increased occurrence of deep scintillations. During this latter time period the ray path does not traverse the irregularity region at low to moderate K indices.

Another parameter of interest is the variation of scintillation index as a function of latitude across the irregularity region at a particular period of time. Utilizing only quiet days ($A_p \leq 20$) in September and October 1968 for three sites, the comparison of mean scintillation indices of Figure 7 has been made. It is clear that the mean index has increased as the sub-ionospheric path moves to higher latitudes. The same data reduction techniques were made for the three sets of observations but the Thule data set is for only three days while the other two sites used 31 days of observations.

The differences noted in Figure 7 are due in part to angle of elevation effects. In particular the high indices of Thule, observing at 4^o of elevation, are due in part to the long path length. However, the differences in angle of elevation between Narssarssuaq and Hamilton data are not believed sufficient to account for the high occurrence of deep fading at Narssarssuaq. Other studies have shown for the frequency, irregularity sizes, and angles of elevations given that the scintillation index varies roughly with $(\sec i)^{\frac{1}{2}}$ where i is the angle of incidence of the ray at the irregularity layer. The angle of elevation from Narssarssuaq was 21^o while that from Sagamore Hill was 35^o; the ratio to be expected was 1.2. The mean scintillation indices for simultaneous hours of observation from both sites (for K_p=0,1) is shown in Figure 8; the index at the higher latitude site is considerably greater at all times.

The evidence, therefore, favors a model with higher electron densities within the irregularities, in the area outlined by the auroral oval but with considerable irregularity structure both in the polar cap region and at night at latitudes lower than the "classical" auroral oval.

5. CONCLUSIONS

While scintillation index at a particular frequency is a quantitative mean of the effect of an irregularity on a signal it is difficult to put together available radio star and satellite scintillations. At 136 MHz it would appear that scintillation index increases by a factor of approximately 2 to 2.5 times from a boundary intersection latitude to one within the auroral oval (after taking into account angle of elevation differences).

At night within the auroral oval increases of magnetic index of 2 units of K increase index by a factor of .5 to 7 in the case of radio star observations. The increase is probably of the same order of magnitude in satellite observations.

While the data presented in this paper are the beginnings of a quantitative evaluation of the irregularities within the irregularity region much has to be done to obtain a statistical picture of the high latitude irregularity region. Multi-frequency observations at many points must be made with equipment of adequate dynamic range so that negative fades do not fall to noise level with 8-10 dB fades. The next series of scintillation observations must be directed to quantitative observations of this type to advance the model of the irregularity region.

6. REFERENCES

Aarons, J. and R.S. Allen (1971) Scintillation boundary during quiet and disturbed magnetic conditions, J. Geophys. Res., 76, 170-177.

Aarons, J., J.P. Mullen, and S. Basu (1963) Geomagnetic control of satellite scintillation, J. Geophys. Res., 68, 3159-3168.

Aarons, J., J.P. Mullen and H.H. Zuckerman (1970) Synchronous satellite signals at 137 MHz as observed from Thule, Greenland, J. of the Franklin Institute, 290, 3.

Briggs, B.H. (1964) Observations of radio star scintillations and spread-F echoes over a solar cycle, J. Atmos. Terr. Phys., 26, 1-23.

Dyson, P.L. (1969) Direct measurement of the size and amplitude of irregularities in the topside ionosphere, J. Geophys. Res., 74, 6291-6303.

Feldstein, Y.I. (1963) Some problems concering the morphology of auroras and magnetic disturbances at high latitudes, Geomag. and Aeronomy, 3, 183-187.

Frihagen, J. (1971) Occurrence of high latitude ionospheric irregularities giving rise to satellite scintillation, J. Atmos. Terr. Phys., 33, 21-30.

Frihagen, J. (1970) Irregularities in the electron density of the polar ionosphere, in The Polar Ionosphere and Magnetospheric Processes, ed. G. Skovli, Gordon and Breach, Science Publishers, Inc., New York, pp. 271-284.

Hoffman, R.A. (1969) Low energy electron precipitation pattern at high latitudes, J. Geophys. Res., 74, 2425.

Kent, G.S. (1959) High frequency fading observed on the 40 Mc/s wave radiated from artificial satellite 1957 a, J. Atmos. Terr. Phys., 16, 10-20.

Liszka, L. (1969) Scintillations of satellite signals, in Low Frequency Waves and Irregularities in the Ionosphere, ed. N. D'Angelo, Springer-Verlag, New York, pp. 192-206.

Little, C.G., G.C. Reid, E. Stiltner, and R.P. Merrit (1962), J. Geophys. Res., 67, 1763-1784.

Orhaug, T.A. (1965) Scintillation of discurete radio sources, Trans. of Chalmers Univ. of Tech., Gothenburg, Sweden, No. 299.

Ryan, W.D. (1964) Radio star scintillation near the auroral zone, Canadian J. of Phys., 42, 458-464.

Titheridge, J.E. and G.F. Stuart (1968) The distribution of irregularities in the Antarctic ionosphere, Planet. Space Sci., 30, 85-98.

Yeh, K.C. and G.W. Swenson, Jr. (1959) The scintillation of radio signals from satellites, J. Geophys. Res., 64, 2281-2286.

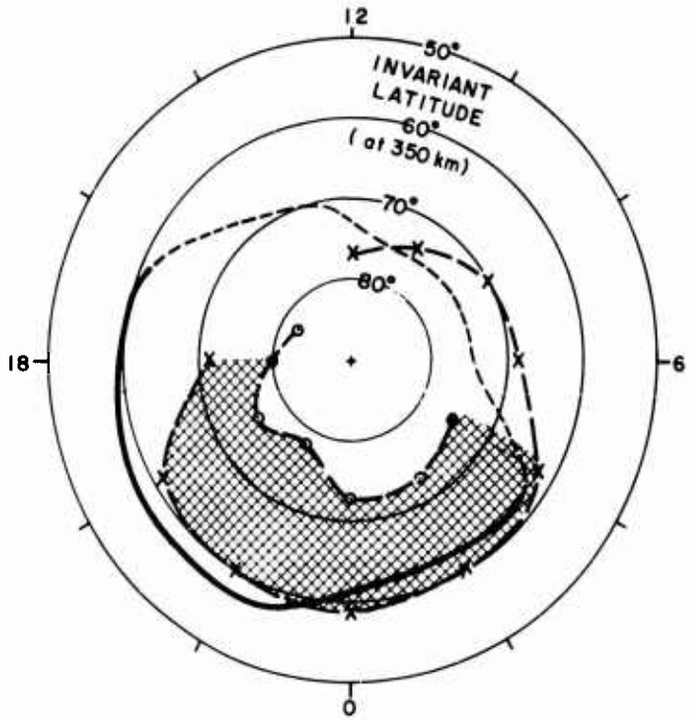

Figure 1 Boundaries of the F layer irregularity region.

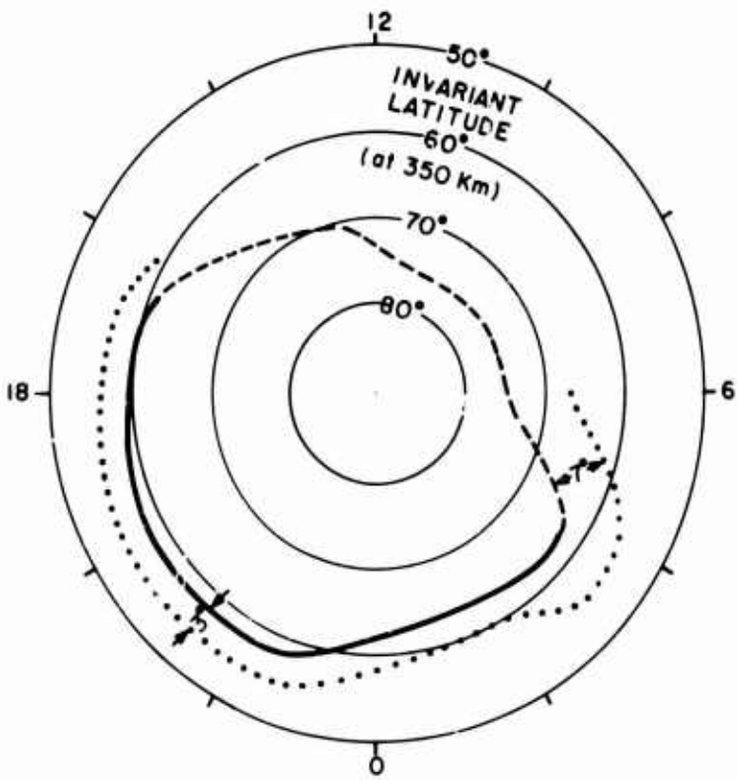

Figure 2 Quiet and disturbed lower boundaries.

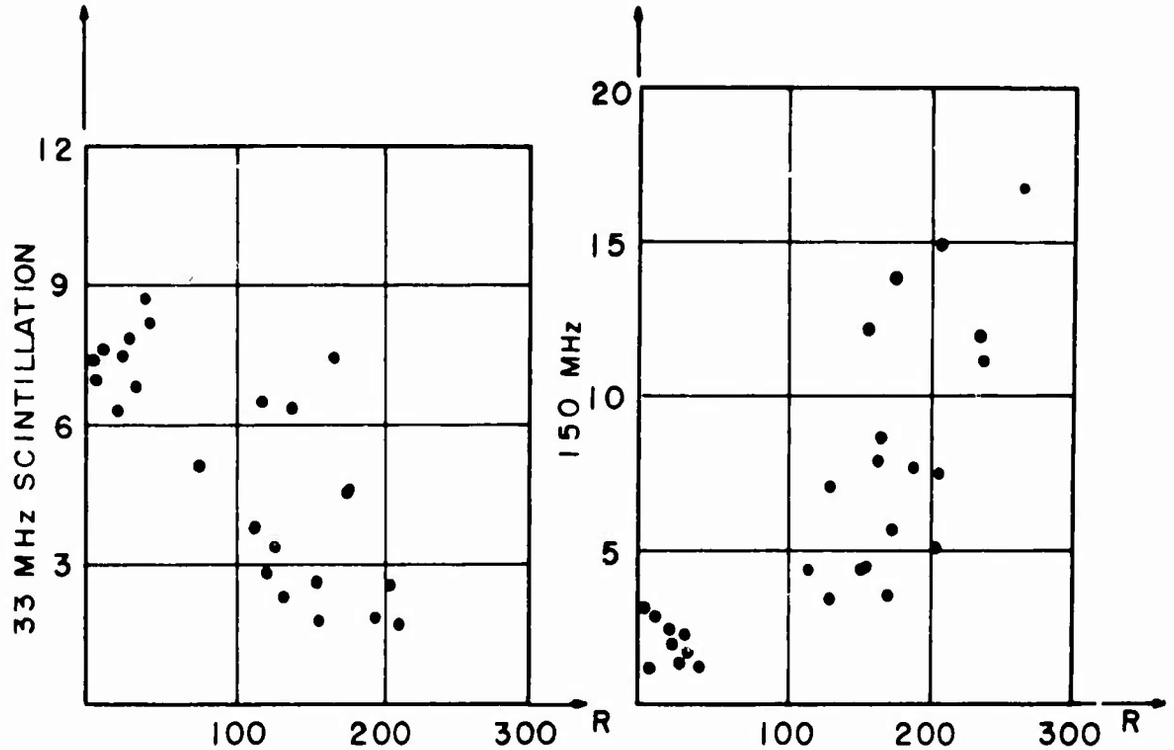

Figure 3 Correlation between the monthly mean values of scintillation amplitude on 33 MHz and 150 MHz (A33 and A150) and the monthly mean values of the sunspot number R. (Orhaug, 1965) (Lower transit of Cygnus A).

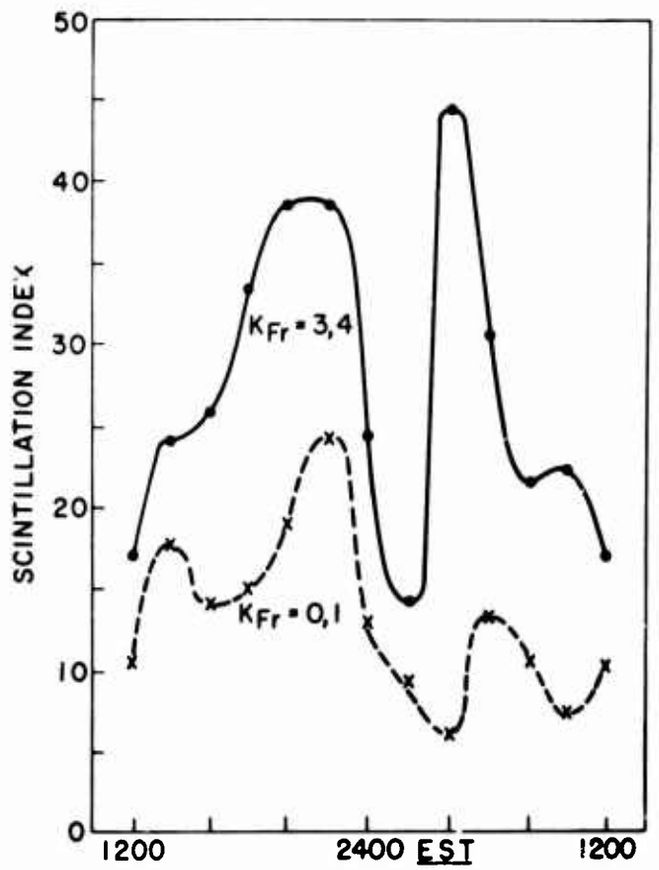

Figure 4 Scintillation indices for 113 MHz radiation from Cass A. The 150-ft antenna at Sagamore Hill was used to make observations near lower transit (~13° of elevation) on a path intersecting the invariant latitude of Λ = 67°.

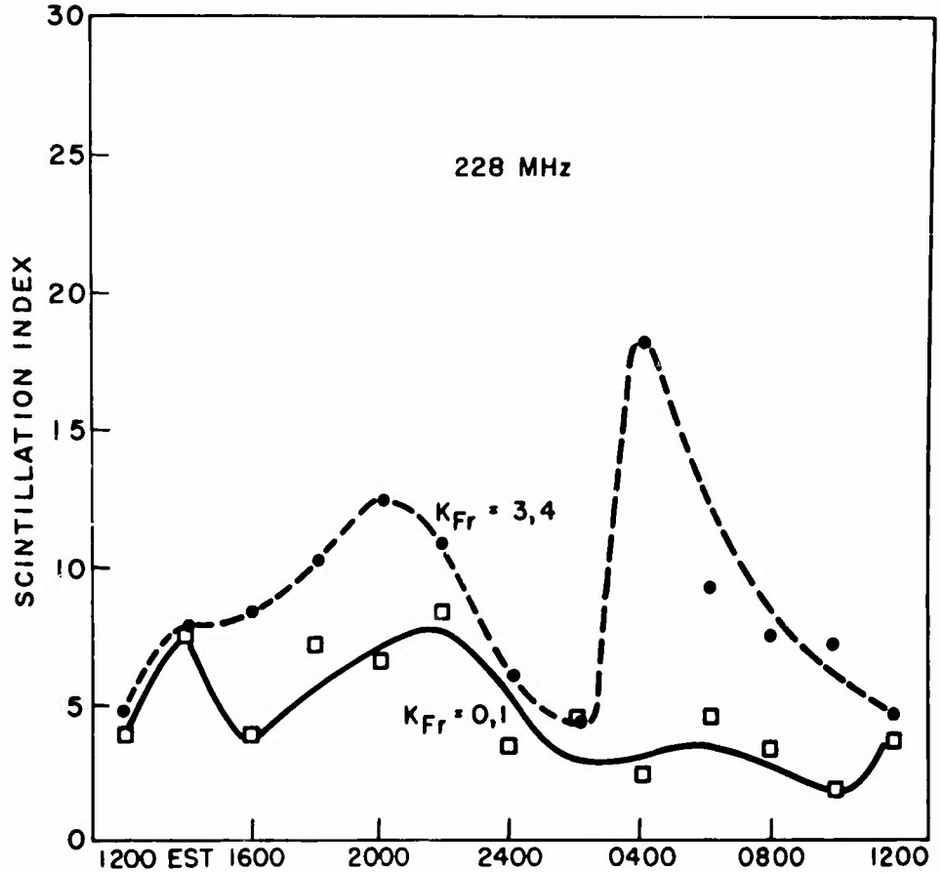

Figure 5 228 MHz Data.

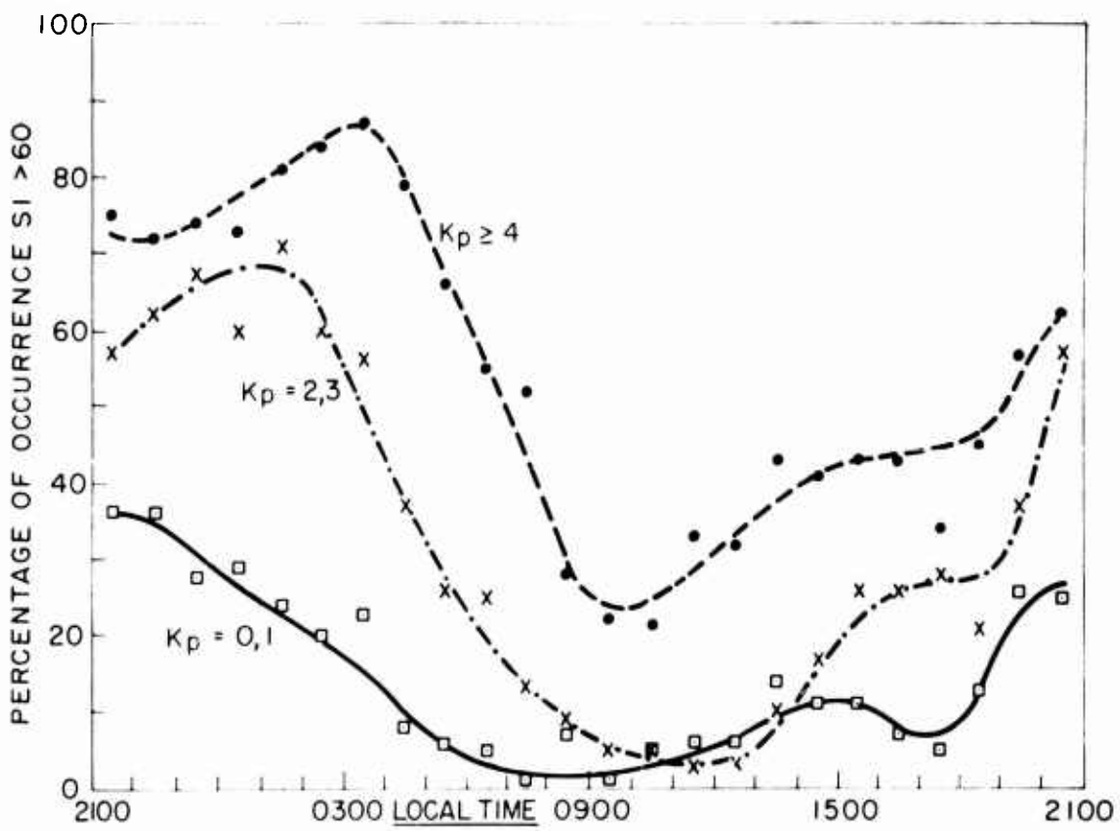

Figure 6 Occurrence of scintillations, SI > 60 (Narssarssuaq, Greenland).

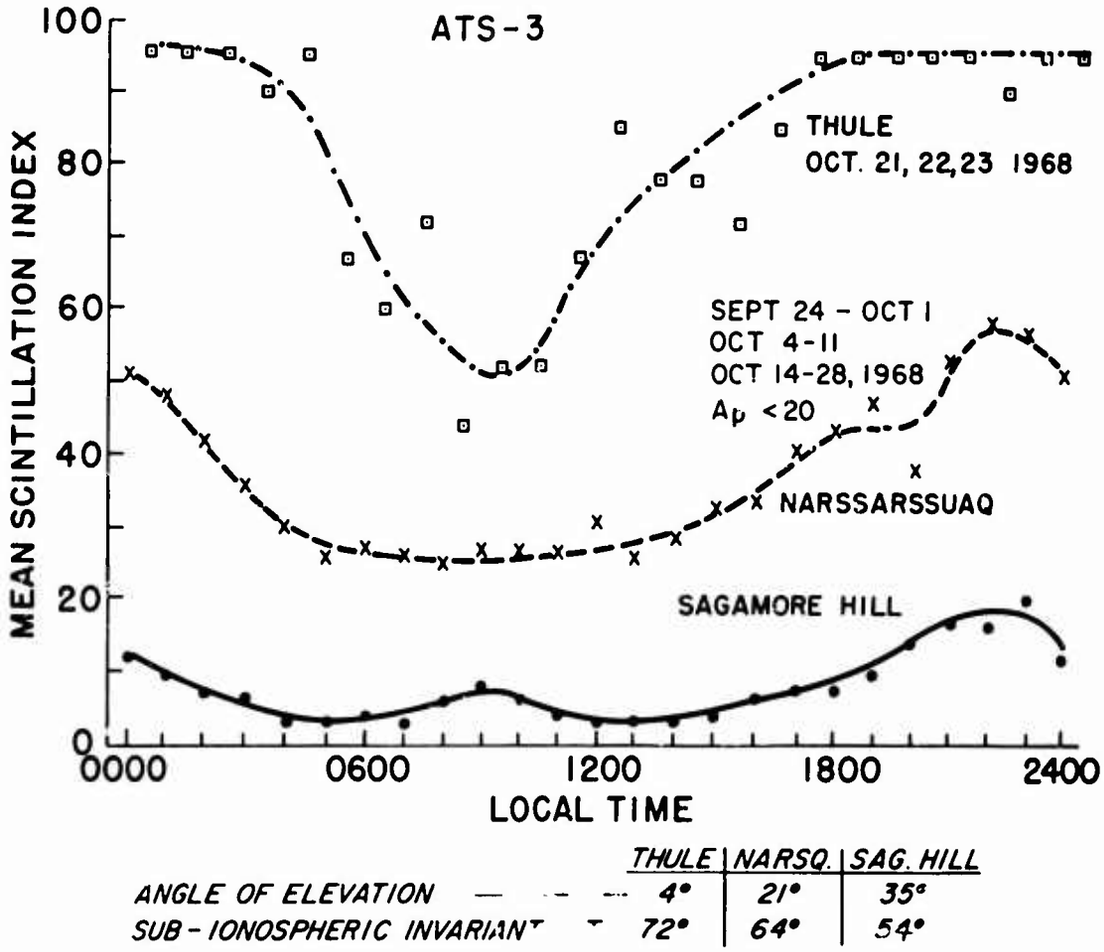

Figure 7 Mean scintillation index for Thule, Narssarssuaq and Sagamore Hill observations of ATS-3.

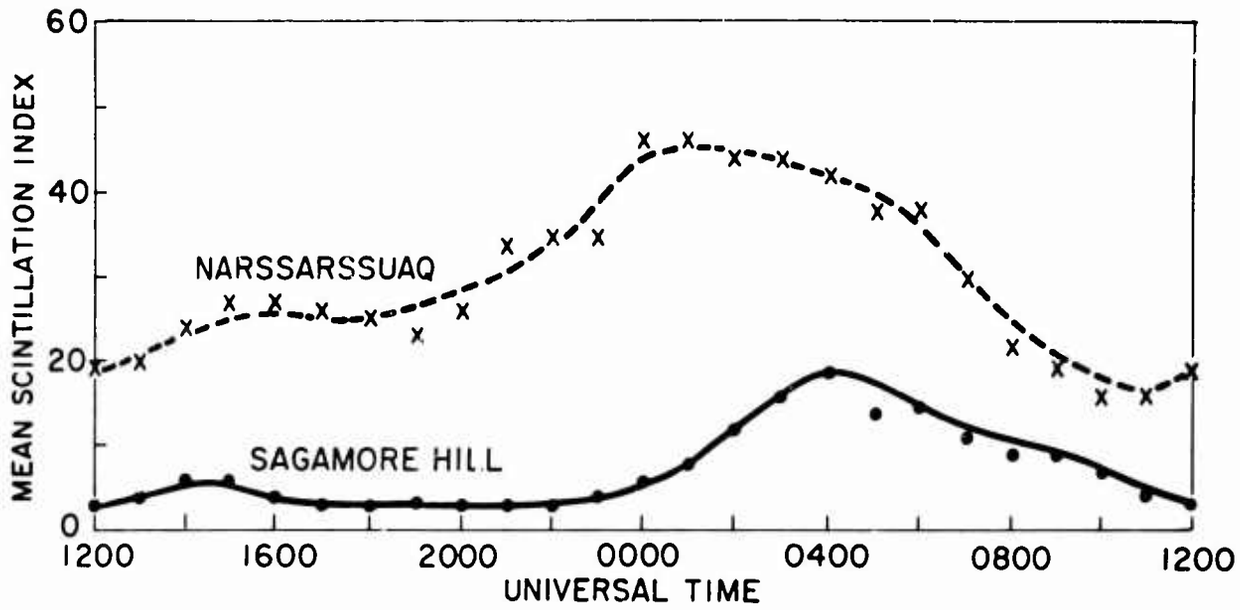

Figure 8 Simultaneous observations of ATS-3 at Sagamore Hill, Mass., and Narssarssuaq, Greenland, K_p = 0,1 mean scintillation index. The number of hourly values for each data point varies from 47 to 62. September 1968 to August 1969.

ANGULAR DEVIATION OF RADIO WAVES

G.F. Lyon and P.A. Forsyth
Centre for Radio Science and Physics Dept.
University of Western Ontario
London, Ontario,
Canada

SUMMARY

Large scale irregularities in ionospheric electron density give rise to angular deviation of a radio wave due to refraction. Angular deviations due to typical departures from horizontal stratification are modelled. In particular the steep gradients and troughs in electron density typical of the polar ionosphere are considered. The results suggest that systems which depend upon precise measurements of angle of arrival for radio waves in the frequency range at least to the upper end of the VHF range may be subject to significant unavoidable error.

1. INTRODUCTION

Whenever an electromagnetic wave traverses the ionosphere it will suffer refraction as the refractive index varies along the ray path. For a horizontally stratified ionosphere and a ray completely traversing the ionosphere the emergent ray will be parallel to the incident ray so that there will be no angular deviation to an observer on the ground. However the presence of any irregularities in electron density which destroy the horizontal stratification will give rise to some angular deviation. If the position of a source of electromagnetic waves outside the ionosphere is accurately known, measurements of these angular deviations allow deductions concerning the irregularities. Conversely the presence of the irregularities may cause errors in the accurate location of the source.

In principle any electron density variation along the path from source to observer will cause angular deviation. It is well known that ionospheric irregularities exist in a very wide range of sizes, from a few cm to hundreds of km, and in various volume distributions. Generally speaking the treatment and physical interpretation of the experimental data falls into two categories depending upon the so called 'scale size' of the irregularities; that is to say upon the ratio of the irregularity physical dimensions to the wavelength of the probing electromagnetic wave. Distributions of irregularities of small scale size are often treated as a diffracting screen. As the source and irregularities move with respect to each other the resulting fluctuating amplitude on the ground may be interpreted in terms of irregularity scale sizes. A somewhat similar interpretation of amplitude measurements may be made for large size irregularities in the so called 'near field' case since the changing small deviations produced by relative motion will result in slight focussing and defocussing of the wave energy at the observer.

Most of the experimental data that has been gathered for the purpose of studying ionospheric irregularities has been in the form of amplitude fluctuations. It is now clear that some of the ambiguities in interpretation can be avoided if simultaneous angle of arrival (phase) fluctuations are also available. Examples of this have been given by Turnbull and Forsyth, 1965 [1] and Mason, Tull and Forsyth, 1967 [2].

When considering the question of accurate source location it must be remembered that the irregularities concerned are essentially transparent to the electromagnetic wave and thus in many circumstances most of the wave energy will be received along the line of sight. It is therefore probable that in a radar system in which the beam is intercepted by a distribution of small size irregularities the effect will be to partially obscure the signal with 'clutter'. Whether or not this will result in an error in angle determination depends mostly on the radar system parameters and will not be discussed further. However in the case of large scale irregularities in electron density, particularly those that occur at high latitudes the effect of refraction along the ray path may well give rise to systematic error in the angle determination which is a function of the angle itself. Examples of such large departures from horizontal stratification are steep North-South density gradients and the high latitude troughs in electron density. This paper is primarily concerned with such large scale phenomena.

2. METHOD

The angular deviation imposed upon a radio wave traversing the ionosphere may be expressed as (Turnbull and Forsyth [1])

$$\theta(u) = -\frac{K}{\omega^2}\frac{d}{du}\int_0^v N\,dv \qquad (1)$$

where u and v are co-ordinates orthogonal and along the wave normal, ω is the radio wave angular frequency, N the electron density and $K = 1.6 \times 10^3$ if mks units are used.

The electron density may be written as

$$N(z,x) = N(z)\ N(x) \tag{2}$$

where N(z) is a function representing the vertical electron density distribution and N(x) is a function representing the horizontal distribution and may be used to describe some large scale irregularity such as the high latitude trough. Alternatively the electron density could be expressed as

$$N = N(z)\ [1 + \Delta] \tag{3}$$

where Δ is some perturbation which can be a function of both z and x, such as an atmospheric wave.

To determine the angular deviation imposed upon a ray from a source within or without the ionosphere we insert the appropriate functions for N(z) and N(x), transform the co-ordinates to a u, v, co-ordinate system with origin at the observer and perform the mathematical operations required by eqn. (1). The resulting equation will give the angular deviation in terms of the distribution parameters and the angle between the v and x directions (the elevation angle of the source from the observer).

The vertical electron density profile would normally be expected to be a Chapman distribution. However to simplify the subsequent integration it is often convenient to use some less complicated vertical distribution function provided that this remains appropriate to the physical situation.

3. RESULTS

3.1 Horizontal Gradients

North-South horizontal gradients in electron density are nearly always present in the mid to high latitude ionosphere (Lyon, 1970 [3]). For a source located within the main trough and an observer south of the trough the gradient could be quite steep. To investigate the angular deviation in the presence of a horizontal gradient, the vertical distribution is taken as

$$N(z) = N_p \exp - \left(\frac{z - z_o}{H}\right)^2 \tag{4}$$

where N_p is the peak electron density, z_o the height of the peak and H the distance above and below z_o at which N(z) falls to Np/e, and the normalised horizontal distribution is represented by

$$N(x) = - \frac{mx}{N_p} + 1 \tag{5}$$

where m is the linear gradient, the electron density falling in the north if the x direction is northward. Then

$$N(z,x) = - mx \exp - \left(\frac{z - z_o}{H}\right)^2 + N_p \exp - \left(\frac{z - z_o}{H}\right)^2 \tag{6}$$

The last term may be dropped since it will integrate to zero (representing horizontal stratification) and transforming the co-ordinates yields

$$\theta(u) = \frac{K}{\omega^2}\ m\ \frac{d}{du} \int_{-\infty}^{+\infty} \left[(v \cos e - u \sin e) \exp - \left(\frac{u \cos e + v \sin e - z_o}{H}\right)^2\right] dv \tag{7}$$

where e is the elevation angle, and

$$\theta(u) = - \frac{KmH\sqrt{\pi}}{\omega^2 \sin^2 e} \tag{8}$$

Fig. 1 shows $\theta(u)$ evaluated for a wave frequency of 50 MHz and a slope of 6×10^3 electrons per m^3 per metre which is a typical mid latitude gradient taken from Petrie and Lockwood 1969 [4]. At low elevation angles deviations of 2 milliradians can occur. In polar regions where gradients at the edge of the high latitude trough may be at least an order of magnitude greater, the deviation will be correspondingly larger.

3.2 Deviation Through a Trough

A trough in the horizontal electron density distribution may be modelled by writing

$$N(x) = N_p \left[1 - \frac{3}{4} \exp -\left(\frac{x - x_o}{W}\right)^2\right] \qquad (9)$$

which describes a trough of half width W and minimum value $N_p/4$ occurring at a horizontal distance x_o from the origin (observer).

Taking the same exponential vertical distribution as in Sec. 3.2 and proceeding as before yields

$$\theta(u) = -\frac{\frac{3}{4}KN_p}{\omega^2} \frac{d}{du} \int_{-\infty}^{+\infty} \exp -\left[\left(\frac{u\cos e + v\sin e - z_o}{H}\right)^2 + \left(\frac{v\cos e - u\sin e - x_o}{W}\right)^2\right] dv \qquad (10)$$

and after integration and differentiation and setting u equal to zero we have

$$\theta = \frac{3KN_pHW\sqrt{\pi}(x_o\sin e - z_o\cos e)}{2\omega^2(W^2\sin^2 e + H^2\cos^2 e)^{3/2}} \exp -\left[\frac{(x_o\sin e - z_o\cos e)}{W^2\sin^2 e + H^2\cos^2 e}\right]^2 \qquad (11)$$

Fig. 2 shows plots of angular deviation versus elevation angle for various values of the parameter x_o for a wave frequency of 50 MHz, a peak density of $5 \times 10^{11}/m^3$, for $H = z_o = 350$ Km, and for a trough half width W = 800 Km. This value of W is estimated from the main trough illustrated by Muldrew 1965 [5]. It will be noted that if the trough is some distance from the observer ($x_o = 2000$ Km) the angular deviation changes between $\pm$ 20 milliradians for elevation angles changing between 0° and 20°. Again in general the deviation is largest for small elevation angles.

4. DISCUSSION

The two examples given above represent a rather simplified modelling of possible ionospheric conditions. It is unlikely that such idealized pictures would be mirrored in the real ionosphere particularly the polar ionosphere. The ionosphere at high latitudes is likely to have a much more complex horizontal density profile. There may well be a main trough and several additional high latitude troughs (Muldrew, 1965 [5]) or the horizontal profile may be very rough poleward of the lower boundary of the main trough (Thomas and Andrews, 1968, [6]). Attempting to model such real horizontal profiles results in mathematical expressions which are not integrable by straightforward techniques.

To approximate real polar conditions when, for instance, several troughs are present, it might be assumed that the total angular deviation would be given by the sum of the deviations due to each trough. If this is the case then for a distant source (target) for which the line of sight passes through a large horizontal distance in the ionosphere, if three troughs are present the angular deviation can range as high as 45 milliradians (2.5°) at a wave frequency of 50 MHz.

It will be noted that the angular deviation is never a linear function of elevation angle and under some circumstances can change sign over a very small range of elevation angles. Thus although in a sense the angle error due to refraction through large scale inhomogeneities is systematic (as opposed to the 'clutter' due to a distribution of small irregularities) it is unlikely to be predictable.

In conclusion it must be said that errors due to refraction are unavoidable and may be appreciable at low elevation angles. Since under all circumstances for large irregularities the angular deviation is inversely proportional to the square of the wave frequency the errors may be minimised by using higher frequencies. However it must be remembered that only ionospheric refraction has been considered. Tropospheric refraction will also occur due to the vertical gradient in tropospheric refractive index. Again this effect will be most severe at low elevation angles. Deviations of 0.2° at 5° elevation in a wave of 136 MHz frequency have been reported by Edenhofer et al, 1970 [7]). In this case the deviation is almost independent of frequency so that increasing the frequency beyond a certain point may not improve overall angular accuracy.

REFERENCES

1. Turnbull R.M. and Forsyth P.A. "Satellite studies of isolated ionospheric irregularities". Can. J. Phys. 43, 800, 1965.

2. Mason K.H., Tull E.H. and Forsyth P.A. "Rocket studies of isolated ionospheric irregularities". Can. J. Phys. 45, 3065, 1967.

3. Lyon G.F. "Mid to high latitude ionospheric electron content". Jnl. Atmos. Terr. Phys. 32, 1737, 1970.

4. Petrie L.E. and Lockwood G.E.K. "On the prediction of F-layer penetration frequencies". Proc. IEEE, 57, 1025, 1969.

5. Muldrew D.B. "F-layer ionization troughs deduced from Alouette data". J. Geophys. Res. 70, 2635, 1965.

6. Thomas J.O. and Andrews M.K. "Transpolar exospheric plasma". J. Geophys. Res. 75, 7407, 1968.

7. Edenhofer P., Glesner D. and Stein V. "The influence of atmosphere on the accuracy of a satellite tracking system". Proc. Symposium on Satellite Beacon Expts. Max Planck Inst. fur Aeronomie. June 70.

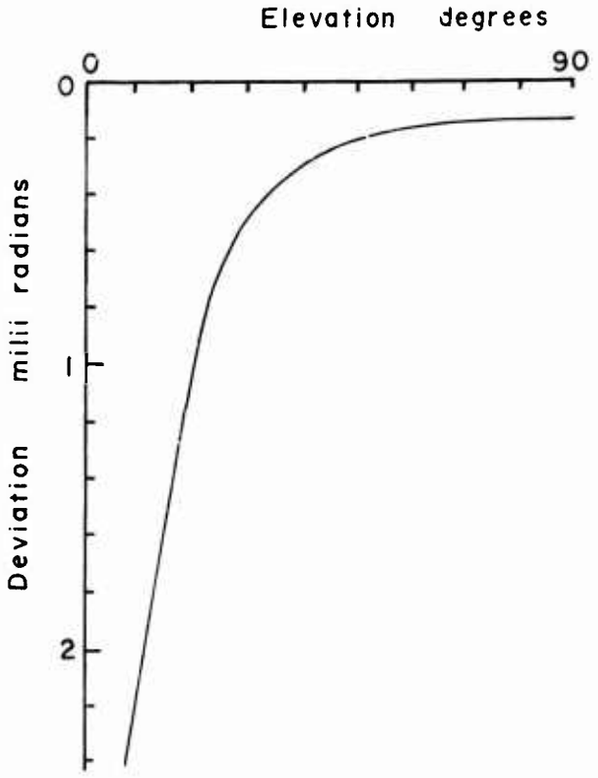

Fig. 1. Angular deviation due to linear horizontal gradient as a function of elevation angle.

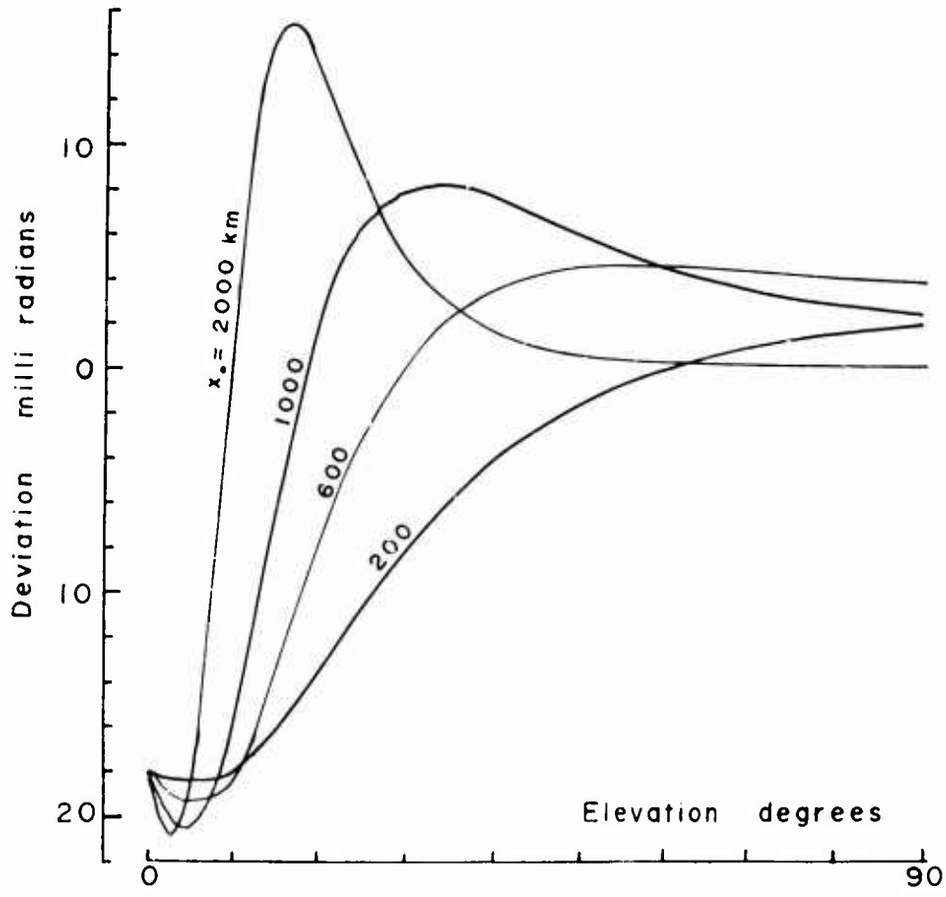

Fig. 2. Angular deviation due to a trough in electron density as a function of elevation angle.

HIGH LATITUDE SATELLITE SCINTILLATION

J. Frihagen
NORWEGIAN DEFENCE RESEARCH ESTABLISHMENT
Kjeller, Norway

O. Bratteng
THE AURORAL OBSERVATORY
Tromsö, Norway

ABSTRACT

Numerous measurements of the height of ionospheric irregularities giving rise to satellite scintillation have shown them to be located in the region 300-600 km above the ground. Observations presented here show that there is no appreciable reduction in scintillation at 136 MHz when a satellite looses height from in excess of 1000 km to less than 300 km.

When observed from Tromsö (70°N) the mean scintillation depth at 136 MHz increases from South to North, increases with K, shows nighttime maxima and daytime minima.

Published results (1) of satellite scintillation observations made from Spitsbergen (75° geomagnetic N) show a night-time minimum of scintillation near 75° geomagnetic North. North of this region the scintillation level is high and shows little diurnal variation. At 75° there are 0600 and 1800 maxima and south of it a nighttime maximum.

The scintillation minimum at 75° is not observed when viewed obliquely from the south at either 136 MHz or 40 MHz.

40 MHz observations from Tromsö show little latitudinal variation day or night and a diurnal variation with a maximum at night.

Some results of electron density from rockets launched from Andenes (69°N, 16°E) show strong irregularities, the electron density varying by up to 25 % over a few tens of meters north of auroral forms. Over the auroral forms the electron density varies smoothly.

1. INTRODUCTION

Observations of satellite scintillation at 40 MHz (BE-B) has been observed from Tromsö and Spitsbergen at 67° and 75° North invariant latitude respectively. Scintillation of ESRO I at 136 MHz has been observed from Tromsö. Results of reducing the Spitzbergen data for diurnal and latitudinal variations have been published earlier (1.2).

In section 2 of this paper we will present the Tromsö data and compare it to the Spitzbergen results.

In section 3 we will briefly present some results of measuring electron density from rockets launched from Andenes (66° North invariant latitude), with special emphasis on the irregular variations in electron density that have been observed on these flights.

Finally we will briefly discuss the restraints the data places on mechanisms for producing ionospheric irregularities, and discuss some possible mechanisms.

2. MORPHOLOGY OF HIGH LATITUDE SATELLITE SCINTILLATION

The most prominant feature of the Spitzbergen data obtained in 1965-66 (1) was the presence of a nighttime minimum of mean scintillation depth at about 75° geomagnetic North. Well to the north of this latitude there was little diurnal variation or variation with Kp. At 75° there were diurnal maxima at about 0600 and 1800 geomagnetic time and a filling in of the minima with increasing Kp. Well to the south there was a midnight maximum and midday minimum in scintillation depth, showing strong daytime increase with increasing Kp.

Observing the same satellite in 1967 from Tromsö (68° geomagnetic North) a somewhat different picture appears. Again the irregularities causing the scintillation are assumed to be located at 400 km height.

The amount of data reduced from Tromsö observations is not sufficient for such detailed analyses of the morphology of scintillation as was the Spitzbergen data.

In this data the mean scintillation depth at 75° geomagnetic North shows a diurnal maximum at night and a minimum during day like it does at lower latitudes down to at least 65°. This apparent inconsistancy with the Spitzbergen data is easily resolved if the ionospheric region of irregularities causing the scintillation is thick, extends

over several hundred kilometers in height. In this case a relatively narrow minimum of irregularities will be masked by irregularities on either or both sides of the minimum. The observed diurnal variation shown in the Tromsö and Spitzbergen data indicate that the masking is due to irregularities at lower heights in the ionosphere south of the scintillation minimum.

The mean scintillation level is higher for large K than it is when K = 0-1. The latitudinal variation between 65°and 75° geomagnetic is small during midday and midnight which is as expected. In the evening there is an increase towards North, and in the morning an anomalous increase towards South.

Reference is made to Figure 1 and 2 for further details on the diurnal, latitudinal and K variations. The data amounts are shown in Table 1.

The data scaling and reduction for the 40 MHz observations is described earlier (2).

The scintillation observations at 136 MHz from Tromsö was scaled from the AGC recordings of telemetry receivers monitoring the ESRO I satellite at Tromsö Telemetry station. The recordings are calibrated and near logarithmic. The scaled values were converted to conform as closely as possible to the scintillation index used on 40 MHz.

The ESRO I satellite was in an eccentric orbit with perigee 275 km and apogee up to 1500 km. In this case seasonal, diurnal and variations due to height changes are difficult to disentangle. For simple geometrical reasons the amount of data obtained when the satellite was near perigee is small, and probably has little effect on the diurnal or latitudinal variation.

The amount of data used here is shown in Table 2.

Figures 3, 4 and 5 shows the variations diurnally, latitudinally, with satellite height and with K respectively. The data on variations with satellite height are limited to a region close to the observing station. The height of the effective irregularities were assumed to be at 400 km when the satellite was above 600 km but at 2/3 of the satellite height when it was lower.

The diurnal variations show maxima at night and broad minima during the day. Latitudinally the mean scintillation depth increases towards north. The variations with K are large during the day. In the north (at 75°N) the scintillation depth does not increase further when K exceeds 3 during the day and there is no dependence on K at night.

The data on height variations is very unequally sampled. Overall there is little variation of scintillation depth with height of the satellite. Some diurnal variations in the sampling may be important but the region of irregularities must extend well below 300 km for at least parts of the day to explain the results. This observation may well be limited to regions in the vicinity of the auroral zone.

3. IN SITU MEASUREMENTS OF ELECTRON DENSITY

The results of measuring electron density by RF impedance probes on high altitude sounding rockets, have been reduced in some detail for the presence of irregularities.

The measurements technique is well known and has been described in some detail by Folkestad (3).

The first flight to be considered took place on 20 September 1968 at 2032 MET. The orbit and the locations of two auroral forms that were passed are shown in Figure 6. Figure 7 shows the electron density seen during the flight. The smooth curve is the 5 second, or about 3 km measured horizontally, running mean. The other curve shows the electron density at individual scaling points expressed as percent deviation from the running mean. Energetic particle precipitation was observed in the regions of the aurorae, there are maxima in the electron density at these locations. The intervening broad maximum is thought to be the point of furthest penetration into the F region. Irregular variations in electron density are observed strongest just north of each aurora. Variations of up to 20 % over the order of 100 meters are observed in these regions. In between occasional excussions of as much as 5 % (minimum to maximum) are seen.

The next flight to be discussed took place on October 1, 1968 at 2244 MLT. During this flight there were multiple aurorae which just before and during the flight split up and moved considerably about. The electron density observed in this flight is shown in Figure 8. During this flight both the 3 km running mean and the deviations from it varied considerably.

The last flight to be considered took place on February 3, 1970 at 2324 MET.

A review of the results of this flight has been published by Evans et al (4) and examples of the small scale irregular variations of electron density by Frihagen and Jacobsen (5).

Early in this flight the rocket passed above a well defined auroral arc. Onboard observations indicate that the north boundary of 40 keV electrons was to the south of the aurora. There was a maximum of 2-3 keV electron precipitation above the aurora and $\sim$1 keV electrons persisted several tens of kilometers north of the aurora. Together with a rapid drop of the $\sim$1 keV electron precipitation a sharp gradiant in electron density was observed from 10^6 to 10^5 cm^{-3} over about 10 km measured horizontally. At this point were the strongest irregularities observed on the flight, Figure 9. Previous to this, in the precipitation zones and over the aurora little if any irregularity were observed, Figure 10.

North of this region patches of the order 1 to a few km of strong irregularities, 10-15 % variations in electron density over a few tens of meters, were present.

4. CONCLUDING REMARKS

The probe measurements of electron density seem to be very significant. They seem to rule out proposed mechanisms for producing irregularities at 280 km directly related to aurorae. Two stream instabilities caused either by the streaming of energetic particles or by the auroral electrojet if this in fact is located below aurorae or in the high energy (> 20 keV) precipitation regions.

On the other hand the presence of irregularities near strong gradiants in electron density, lends considerable support to the sugestion that the gradiant instability, produces strong irregularities, Reid (6).

Other mechanisms must also be important.

It seems improbable that the irregularity region covering the polar cap north of 80° is produced by this process. Furthermore the patches of irregularities observed on one of the rocket flights did not seem to be systematically related to strong gradients in electron density. It also seems to be difficult to explain the equatorward extent of the high latitude scintillation region by this mechanism.

It seems quite probable, however, that the "auroral oval maximum" in irregularity may be caused by the gradient instability but the other mechanisms, active from the pole to the south boarder of irregularity, are simultaneously present.

These speculations are based on a few probe measurements up to 250 km in height while the "scintillation region" extends much higher. The electron density variations that may be sufficient to produce scintillation is not well known and may be below the threshold of what is observed by the probes. The arguments presented above, however, seem to apply to intense irregularities in the lower F region.

REFERENCES

1. Frihagen J. "Occurrence of high latitude ionospheric irregularities giving rise to satellite scintillation". J Atm Terr Phys 33, 21, 1971.

2. Frihagen J. "Satellite scintillation at high latitudes and its possible relation to precipitation of soft particles". J Atm Terr Phys 31, 81, 1969.

3. Folkestad K. "Ionospheric studies by in situ measurements in sounding rockets". NDRE report No 39. Norwegian Defence Research Establishment, Kjeller, Norway, 1971.

4. Evans, D. S., T. A. Jacobsen, B. N. Mæhlum, G. Skovli and T. Wedde. "Low energy electron precipitation and the ionospheric F region in and north of the auroral zone". Planet Space Sci. In press., 1971.

5. Frihagen J. and T. Jacobsen. "In situ observations of high latitude F region irregularities". J. Atm Terr Phys 33, 510, 1971.

6. Reid G. J Geophys Res 73, 1627, 1968.

Table 1 Number of 40 MHz observations from Tromsø

	64°-66°			68°-70°			74°-76°		
K	0,1	2	3	0.1	2	3	0,1	2	3
2100-0300	42	43	152	96	68	313	10	16	78
0300-0900	60	32	107	169	61	264	25	17	39
0900-1500	204	76	74	386	171	140	64	26	34
1500-2100	101	54	118	255	152	244	51	28	50

Table 2 Number of 136 MHz observations from Tromsö

	K	0	1	2	3	4	5	6
68-72°	300 km	4	2	5	4	2	3	0
	300-600 km	18	17	22	17	13	7	7
	600 km	25	68	66	60	45	19	15

	64°-66°			74°-76°		
	0,1	2	3	0,1	2	3
2100-0300	2	4	18	4	4	16
0300-0900	36	16	28	34	10	25
0900-1500	16	0	17	22	7	13
1500-2100	22	12	29	22	14	31

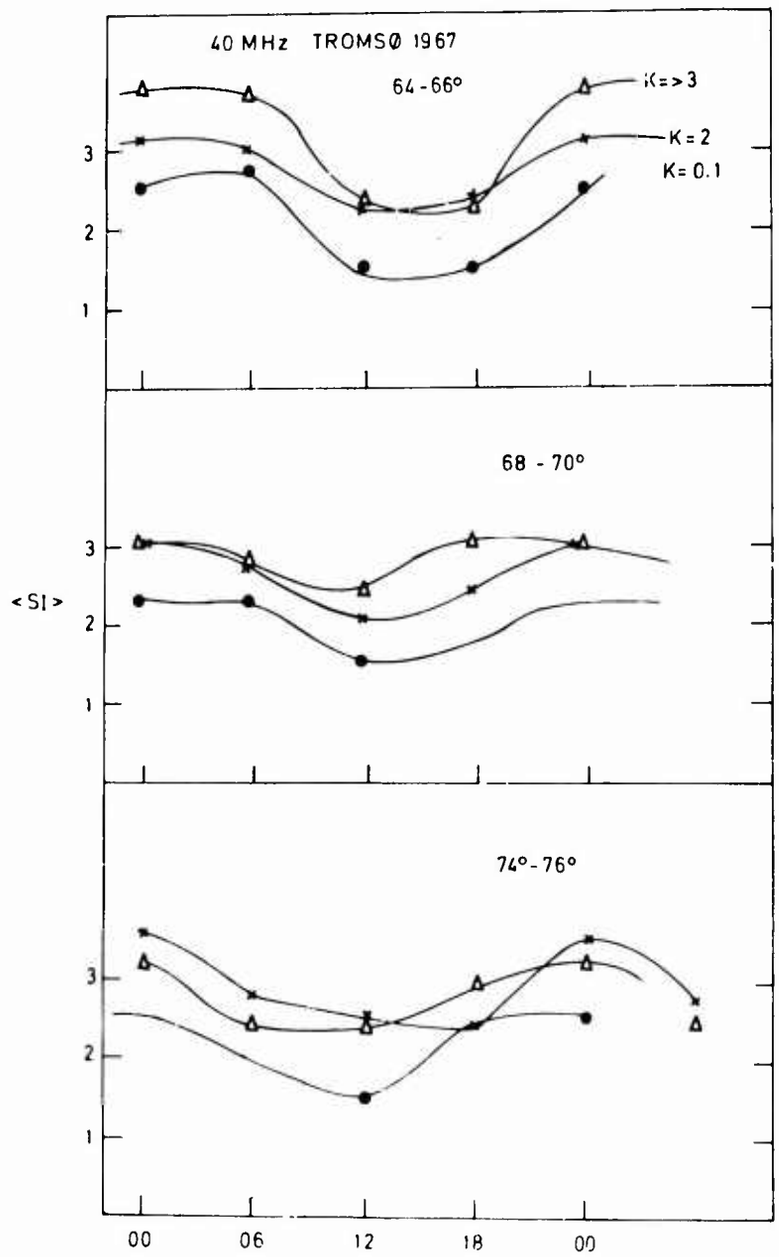

Fig 1. The diurnal variation of mean scintillation depth at 40 MHz

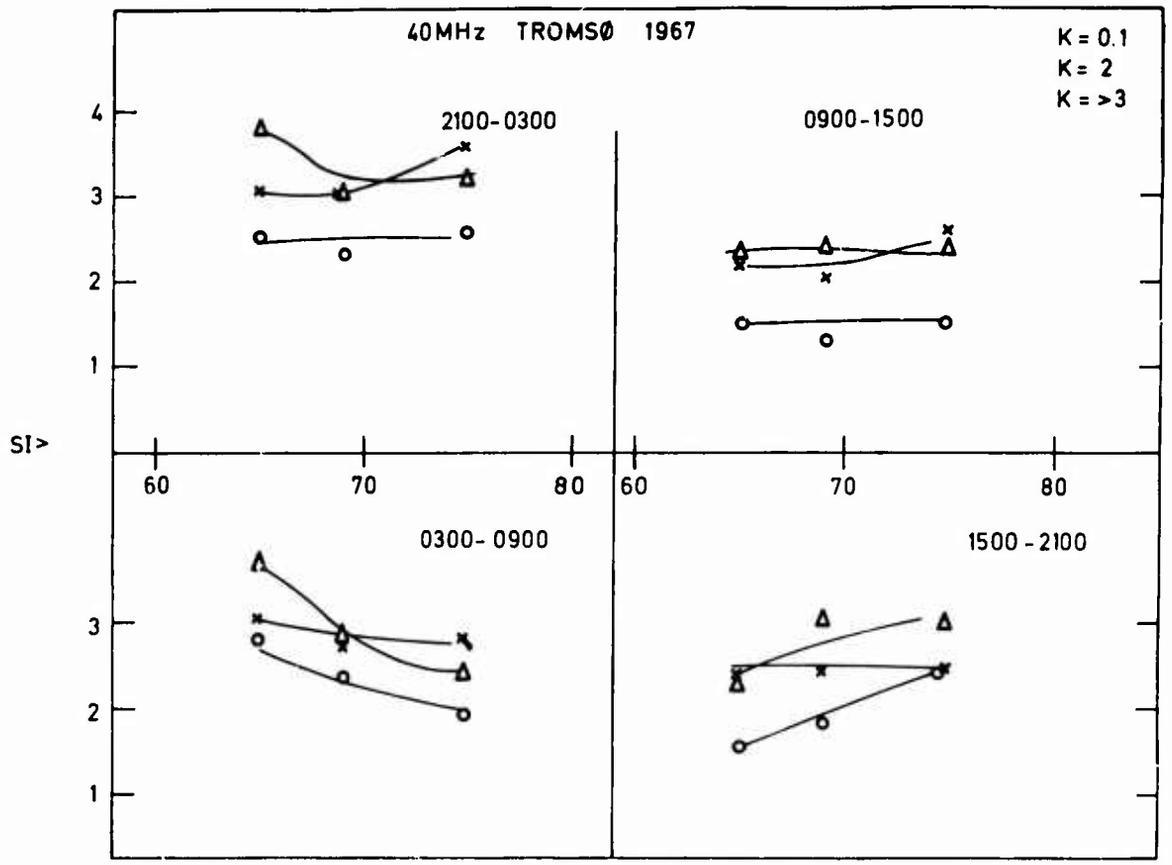

Fig 2. The latitudinal variation of mean scintillation depth at 40 MHz

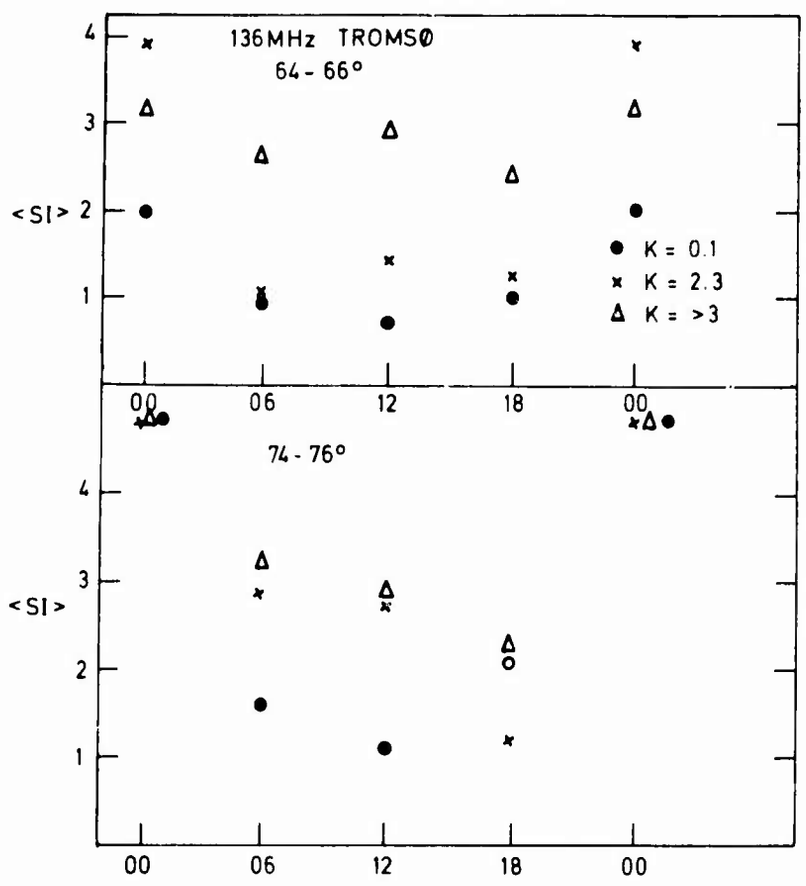

Fig 3. The diurnal variation of mean scintillation depth at 136 MHz

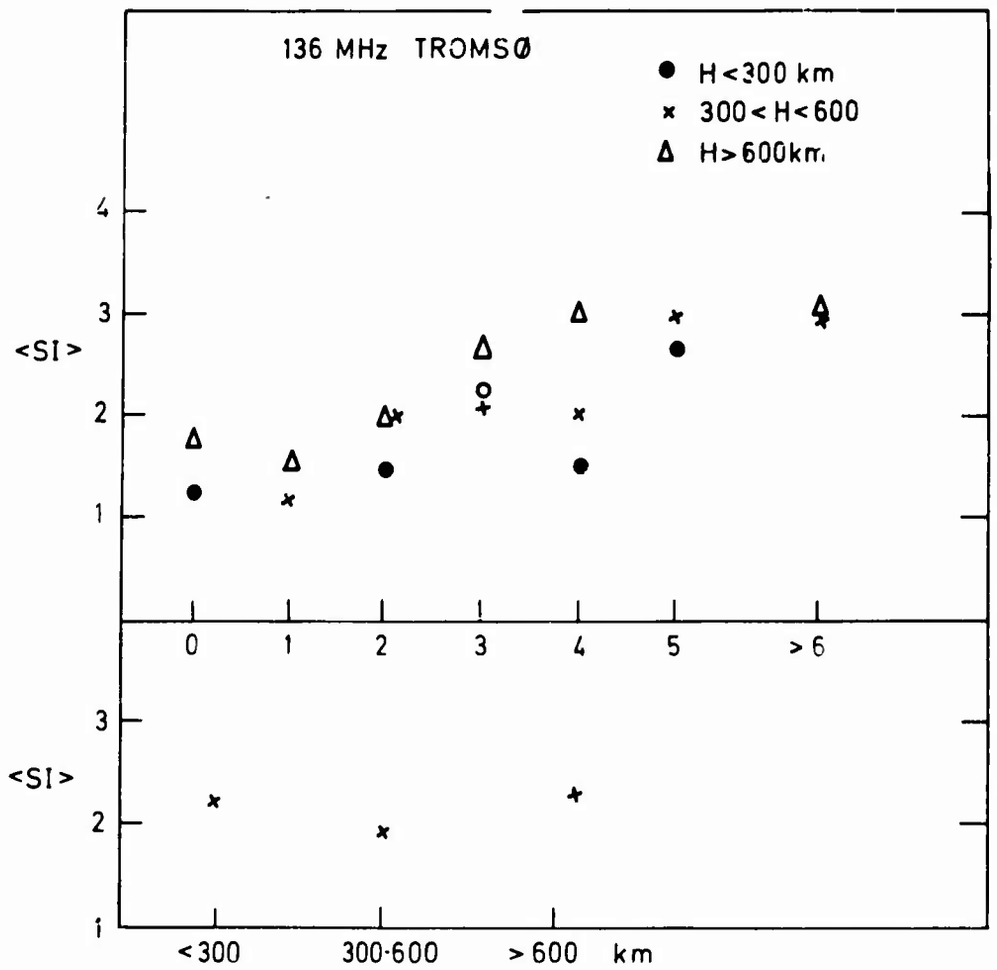

Fig 4. The dependance of mean scintillation depth on satellite height for differant K.

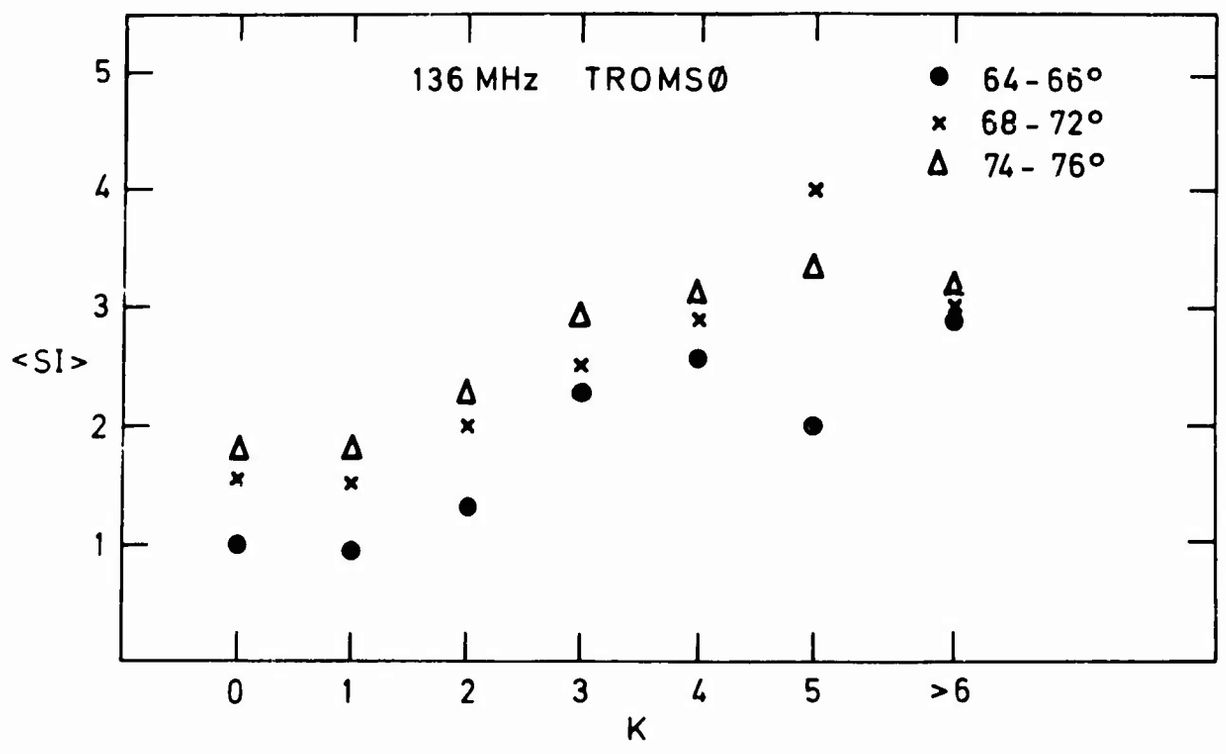

Fig 5. The dependance of mean scintillation depth on K for differant latitudes.

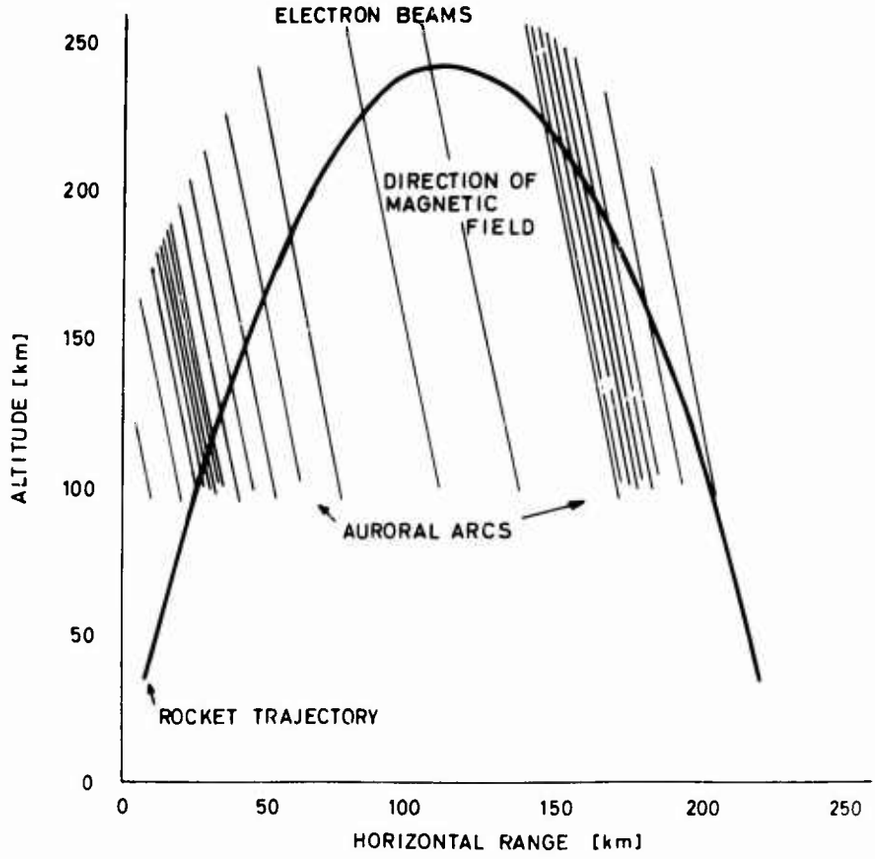

Fig 6. The orbit and position of aurorae during flight F 18.

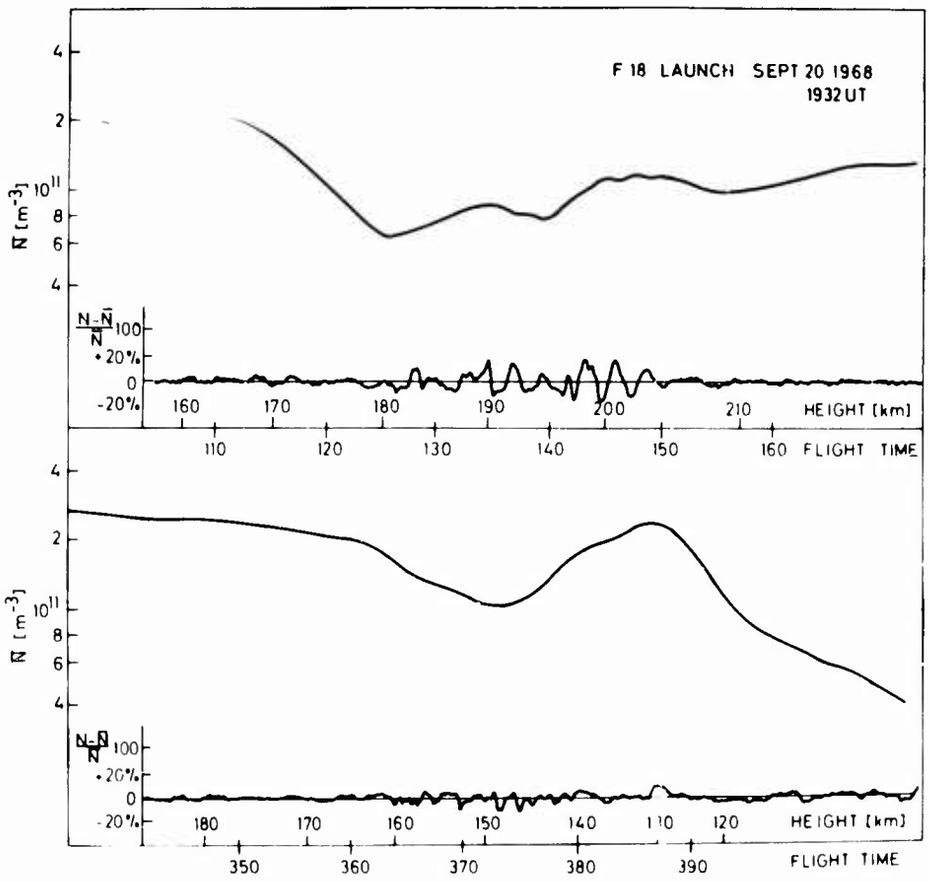

Fig 7. The observed electron density variations during the flight of F 18.

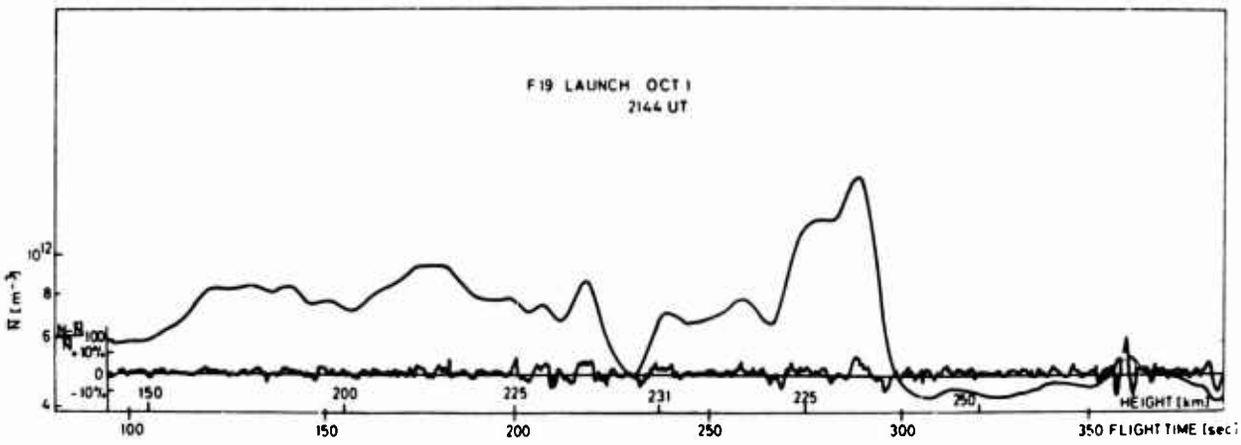

Fig 8. The observed electron density during flight F 19.

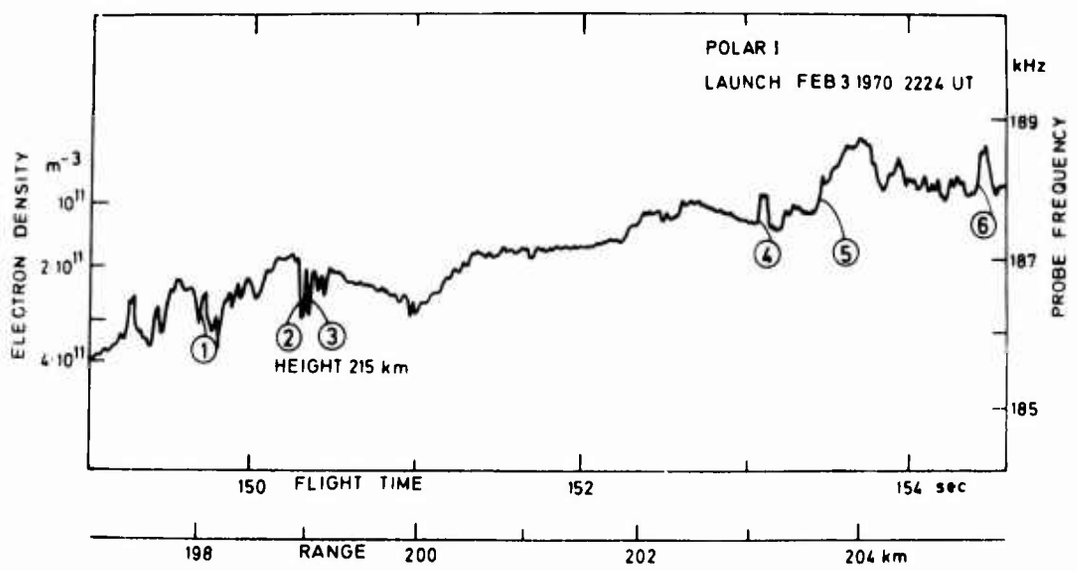

Fig 9. The most intense patch of irregularities during the flight of Polar 1.

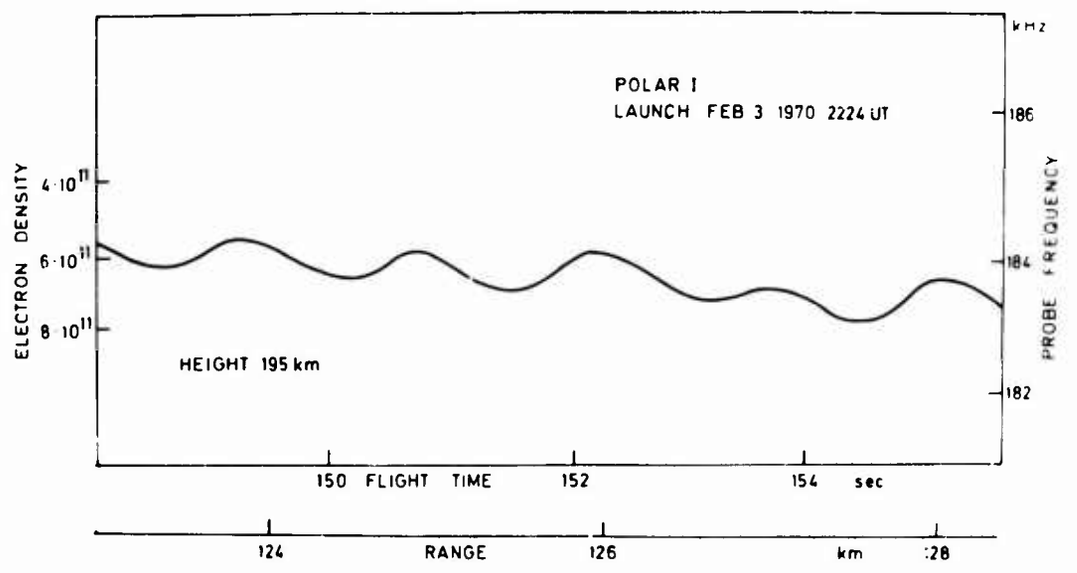

Fig 10. The electron density over the aurora that was passed by Polar 1. The variations that are seen is a spin modulation.

Satellite scintillations between 43° and 66° northern latitude from 1964 to 1969

by
Gerd K. Hartmann

Max-Planck-Institut für Aeronomie
Abt. Weltraumphysik, 3411 Lindau/Harz
W-Germany

Summary

Since November 1964 till May 1969 the radio signals from the beacon satellite Explorer 22 were continuously recorded at Lindau, mainly for the purpose of obtaining the ionospheric electron content from Faraday-effect- and Dispersive-Doppler-effect measurements. The so obtained amplitude- and phase recordings were compared. When the root mean square phase deviation - during distortions, e.g. phase scintillation, was equal or greater 1 radian, we found fast amplitude scintillations that exceeded 6 dB amplitude variations. This led to a new grouping of the scintillation data, different from earlier ones. Index 1 denotes weak scintillations with amplitude variations less than 6 dB, index 2 those which exceed 6 dB.
Many findings of other authors could be corroborated, which will be mentioned in the relevant chapters.
The rather narrow scintillation belt, which was observed between 50° and 60° northern geographic latitude seems to consist of two fairly independent "sub-belts", one represented by index 1 data, the other by index 2 data. Whilst the first one - strictly spoken its satellite occurrence frequency maximum, SOFM (1), seem to move northwards with increasing solar activity (in our special case roughly 2° of latitude) the second one, SOFM (2) seems to move southwards by roughly the same amount. These results have to be corroborated by future scintillation measurements accompanied by simultaneous height measurement, so that errors due to the assumption of a mean height Hm are avoided. There is no clear physical interpretation until now, however it is suggested that the different behaviour of precipitated particles - energy range from 5 eV to 50 KeV - and possibly the dynamical effects in the ionosphere which are connected with the midlatitude trough might be the cause.
It is further suggested that the scintillation activity increases by a factor of 2 as concerned weak scintillations and by a factor of 4 as concerned strong scintillations, when Kp exceeds 3o.
Furthermore a southward motion with increasing magnetic activity was observed.
In summer the SOFM seems to be approximately 2° further north than in winter.
More detailed investigations of the physical cause of all these effects and their interdependence are proposed and were already started to a small extent at Lindau.
The scintillation- and other-data should be used in a complementary way to exploit the advantages inherent in each and thus to proceed from the fairly well established phenomenological description to the more desirable detailed physical interpretation of the ionospheric-magnetospheric interactions.

1. Introduction

Since November 1964 the amplitude of radio signals from the beacon satellite Explorer 22 (inclination ~80°, altitude ~1000 km, code-name: S-66) has been recorded in Lindau for the purpose of obtaining the ionospheric electron content from the Faraday-effect (Hartmann, 1965) and the Dispersive-Doppler-effect (Schmidt, 1966). The transmitted frequencies were 20 MHz, 40 MHz, 41 MHz, 136 MHz and 360 MHz. These signals were recorded on a routine basis until May 1969, when - due to technical problems aboard - the spacecraft transmitted only during short periods. On a considerable number of occasions the regular Faraday-fading- and Dispersive-Doppler-effects were distorted or even obscured by other effects. Most of these were due to inhomogeneities in the ionosphere (Hartmann, 1969, 1970) a few of them (~7 %) to inhomogeneities in the troposphere (Hartmann, 1970a). Because of the ionospheric inhomogeneities the obtained recordings displayed two effects, (a) so called ionospheric satellite scintillations and (b) effects which were the result of horizontal gradients in the ionosphere. Here we shall consider ionospheric satellite scintillations and discuss the results in detail.

2. Measuring technique

A simple Faraday-effect (amplitude) receiving system was used (Hartmann, 1965, 1970). Recently a much better and more sensitive so-called polarimeter system has become available. The Dispersive Doppler-effect receiving system (Schmidt, 1966) was much more complicated. The Dispersive Doppler record essentially displays the phase difference of two coherently related signals - in our case 40 MHz and 360 MHz - and is basically a measure of the ratio of change of phase path between the satellite and receiver due to the ionosphere.

3. Scintillation, background

Propagation of electromagnetic waves through an inhomogeneous ionosphere and troposphere usually results in variations in the
1) amplitude
2) phase
3) angle-of-arrival
of the waves as received at the ground.
Generally this is defined as scintillation.
Since amplitude measurements require in general only a fairly simple and inexpensive equipment roughly 90 % of the now available scintillation data were obtained by amplitude measurements. This is the reason that fairly often for sake of brevity the expression "scintillation" is exclusively related to measured amplitude fluctuations.
Phase measurements, e.g. Dispersive-Doppler-effect-measurements, strictly spoken relative phase measurements, require a more sophisticated and much more expensive equipment. Therefore only approximately 7 % of the available scintillation data were obtained by phase measurements (phase scintillation). Angle of arrival measurements require a still more complicated equipment especially

a very accurate antenna system. Therefore only 3 % of the data were obtained by angle of arrival measurements (angle of arrival scintillation).
A wealth of experimental data is already available and the literature is now very extensive. But there is still no generally accepted theory of the cause of ionospheric irregularities. The latest reviews on this topic are given by Aarons (1970) and Hartmann (1971).
Here we shall consider only amplitude- and phase scintillations.

4. Scintillation recordings obtained at Lindau

In many cases the usual regular Faraday fading - the duration of the fading periods varies between 1 sec and several minutes - is accompanied by another, very fast, and irregular fading. The duration of these fading periods varies - in our special case - between 2 Hz and 50 Hz. Figure 1 shows a regular amplitude recording of a satellite passage - rev. no. 7262 - with undisturbed Faraday-fading.
Figure 2 shows an amplitude recording with regular Faraday-fading on the left and right, and in the middle $\sim$ 2 min. of very fast fading, denoted as scintillation. The uppermost trace shows 1 sec. time markers. The other traces reading downwards, are 20 MHz, 41 MHz, 40 MHz, 40 MHz, and 41 MHz, with various antennas. The amplitude increases linearly downwards (but is limited at about 20 dB above rise) and time goes from left to right. This recording was obtained on March 14th, 1966, during revolution no. 7153.
Figure 3 now shows an example of a Dispersive-Doppler-recording between the 40 MHz and 360 MHz signals for the same satellite passage, no. 7153, on March 14th, 1966. The uppermost trace displays the 1 sec. time markers. The chart speed was 5 mm per sec. The 3rd and 4th trace show the phase path variation. Using the same satellite signal, trace 3 shows the cosine output of the phase lock loop and trace 4 the sine output. This is to prevent ambiguity when deciding whether the phase path has become longer or shorter. Now an improved equipment with one sawtooth-output is available. On the left and right of this recording regular phase path variations are to be seen. In the middle - for $\sim$ 2 min. - the phase is heavily distorted and shows "phase scintillations". Looking back to the relevant amplitude recording, figure 2, one can detect the scintillation effects on both the amplitude and phase-recordings.

5. Data analysis

Roughly 4500 amplitude recordings obtained with signals from Explorer 22 between November 1964 and February 1969 were examined for the occurrence of scintillation effects, e.g. for each year approximately 1000 $\pm$ 10 % recordings were analyzed. One of our main interests was to investigate - if possible - the diurnal-, seasonal-, latitudinal- and sunspot-cycle-behaviour of the scintillation.
In order to avoid strong influences of longitudinal effects only those recordings were processed by the computer for which at the PCA (point of closest approach) of the satellite the following condition was valid: $|\lambda - \lambda_0| \leq 3^0$, λ_0: longitude of the observing site, λ: longitude of the subsatellite track.
The rate of the satellite's orbital precession required three months of observation to obtain data near the same latitude for all local times. Therefore in using these data to investigate the scintillation effects we have to take into account a mixing of seasonal variations with local time effects.
It has become obvious that a great deal of scintillation producing irregularities are located in the F-region of the ionosphere. Therefore in many cases where no continuous measurements of their heights could be carried out, a mean Height Hm of 350 km was assumed for any calculation.
Becker (1965) demonstrated that at our location Lindau/Harz (geographical latitude 51° 39' N; geographical longitude 10° 7.5' E; geomagnetic latitude 52.3°; geomagnetic longitude 095°; magnetic dip 67°; Time: MET = UT + 1 h) the mean height of the maximum of the F-layer: hm F2 does not exceed the following values:

a) sunspot maximum	1) night:	400 km
	2) noon:	300 km
b) sunspot minimum	1) night:	300 km
	2) noon:	200 km

The seasonal variations are even smaller than this.
Since no continuous height measurements were available at Lindau, we assumed - due to the above mentioned figures - a mean height of the irregularities of 300 km for all calculations.
Yeh et al (1970) gave an excellent review on various experimental techniques to measure the actual heights of scintillation producing irregularities. That our assumption of a mean height is an oversimplification is quite obvious from the following. The existence of multiple layers of irregularities has been reported by Jespersen and Kamas (1964). Kidd (1970) reported heights between 130 and 900 km. Aarons (1970) corroborated these results. While it is generally agreed that on the average there is a correlation between the occurrence of scintillations and spread F several authors have noted discrepancies when the occurrence of these two phenomena are compared in detail (Singleton, 1969; Briggs, 1958; Jespersen, 1967).
Due to the fact that the difference between geomagnetic and geographic latitudes in our observing area nowhere exceeds 5 % and that there is also a fairly small difference between local time and geomagnetic local time, the data are displayed as a function of geographic latitude and local time LT.
Phase recordings and amplitude recordings were compared. Since the phase measurements were started - due to the design of the sophisticated receiving equipment - later than the amplitude measurements and because of the fairly complicated recording technique the ratio between the available amplitude - and phase measurements is roughly 4 : 1.
In most cases when the phase scintillations exhibited a root mean square phase deviation $\emptyset_0 \geq 1$ rad, we found fast amplitude variations that exceeded 6 dB on the relevant amplitude recording.
$\emptyset_0$ is an important quantity for any theoretical treatment of the scintillation effects, Singleton (1970), Bramley (1967). These findings motivated us - deviating from many other definitions - to arrange our scintillation events into two groups. A) weak scintillations where the fast amplitude variations were less or equal 6 dB but larger than 1 dB. We denote this group: Index 1. B) strong scintillations where the fast amplitude variations exceeded 6 dB. We denote this group: Index 2.
For geophysical purposes several groups have adopted a special definition of scintillation index SI,

Whitney et al (1969). Our index 2 is related to SI in the following manner:
Index 2 $\hat{=}$ SI $\geq$ 0.75 $\geq$ 75 %.
Due to the characteristics of the Dispersive-Doppler-receiving system weak amplitude scintillations (index 1) were practically not associated by phase scintillations. Due to this and because of their limited number phase scintillation data were only used for grouping the amplitude scintillation data into index 1 and index 2.
In order to exclude possible spurious effects only those recordings were processed where the scintillation effect was observable on both 40 MHz and 41 MHz and when the signals exceeded the noise level by more than 1 dB.
In general the amplitude recordings were readable down to 1^0 elevation angle of the satellite. Our local horizon is shielded by the surroundings up to 2 degrees. We define the elevation angle as the angle between the horizontal plane at the observing site and the straight line from the observing station to the satellite. The actual angle of arrival of the ray at the receiving antenna is somewhat greater than this elevation angle because of refraction in the ionosphere. In order to exclude further spurious effects we defined for our special investigations a readibility threshold RT, which was 1 dB above noise level. Due to this the range of observability was narrowed in the most unfavourable cases down to 10^0 elevation ($10^0 \rightarrow 90^0 \rightarrow 10^0$).
For our statistical studies reported here only those recordings were processed that displayed - within the above mentioned range of readibility - a distinct onset of one or more scintillation events. So all recordings which showed scintillation throughout the entire satellite passage were excluded. By this procedure less than 10 % of the total number of scintillation recordings were removed.
Since NASA generously supplied the participants of this special beacon program with the so called Refined World Map any calculation of geocentric and topocentric coordinates could be easily and accurately performed. Any of the following calculations was done for intervals of 1^0 latitude or 1^0 elevation and 1 hour local time.

6. Results for the 4 year period Nov. 1964 - Feb. 1969

1) Latitudinal-, time-, sunspot-number dependence

Figures 4 and 5 display all scintillation events - index 1 + index 2 - as a function of local time t and geographic latitude. The northern boundary of these figures is caused by the above mentioned readibility threshold RT. The southern boundary is more physically defined. Southward of this boundary no scintillation events were observed. The white areas indicate that no scintillation at all occurred. The simple hatched regions indicate 1 to 3 scintillation cases, the double hatched regions 3 to 10 cases and the black regions more than 10 cases (per 1 hour and 1 degree latitude).
Figure 4 displays the data from October 26th, 1964 (641026) to December 31st, 1966 (661231). In this period the sunspot number increased from 15 to 47.
Figure 5 displays the data from December 31st, 1966 (661231) to Feb. 6th, 1969 (690206). In this period the sunspot number increased up to 106. The location of our observing site - 51^0 39' N geographic latitude - is indicated by the black arrow. Due to the fact that we used a mean irregularity height, 300 km, and did not take into account the upward and downward motion of the layers the displayed latitudinal behaviour is slightly erroneous. We'll refer to this in a later chapter. The major problem is that - due to the mean height assumption we artifically transformed a three dimensional problem into a two dimensional one. For future studies a three dimensional presentation is highly desirable and measurements should be conceived to guarantee this.
Nonetheless it is quite obvious from figures 1 and 2 that the scintillation occurrence frequency maximum, $\overline{\text{SOFM}}$, is observable between 1900 LT and 0600 LT, and that the expansion to the southernmost latitudes occurs around midnight. Furthermore there is an increase in the overall scintillation-activity and a decrease of the "non-scintillation areas" with increasing solar activity.
However it is fairly difficult to make any more detailed statement about the latitudinal behaviour. This is mainly due to two facts:

a) The midlatitude scintillation activity is much smaller than at low or high geomagnetic latitudes, e.g., among the total number of $\sim$ 4500 analyzed recordings there were less than 50 % which displayed scintillation effects. They were spread all over day and night and over a wide latitude range. Just one beacon satellite does not yield sufficient date for detailed statistical studies.
b) We did not use the somewhat arbitrary definition of a scintillation boundary as given by Aarons et al (1969) but defined index 1 and index 2. Aarons termed the equatorward edge of the irregularity region as measured by scintillation observations the "scintillation boundary". This boundary is defined at that invariant latitude where the scintillation index SI, measured with a 40 MHz-signal is SI_{40} = 50 % = 0.5

We tried to overcome the latter difficulty by displaying the data as a function of the elevation angle - as defined above - of the satellite.
Figures 6 and 7 show the number of scintillation events S as a function of the elevation angle El, S = S (El) which is reckoned from south to north from $0^0 \rightarrow 90^0 \rightarrow 180^0$. Figure 6 displays the data for the weak scintillation effects, index 1.
The dotted line represents the period 26.10.1964 - 31.12.1966 and the solid line the period 31.12.1966 - 06.02.1969. Figure 7 displays the data for the strong scintillation effects, index 2.
Figure 6 reveals two sharp scintillation occurrence frequency maxima, SOFMs, at 160^0 elevation angle, which is equal to 20^0 elevation angle north of our observing site. The two maxima coincide better than 1^0. It is evident that with increasing solar activity the number of scintillation events increases also, in our case by a factor of 2. Figure 7 shows - compared with figure 6 - that the number of strong scintillation effects (index 2) is much smaller. Furthermore the two distinct SOFMs are now located at 160^0 and 144^0 elevation angle and their heights are fairly equal. Even if we assume the earlier mentioned solar cycle dependence of hm F2, there still remains a resultant ($\sim 2^0$ latitude) southward motion of the SOFM, (1966 - 1969), index 2, with increasing sunspot numbers. This agrees well with the statements about the behaviour of the scintillation boundary Aarons et al (1969). However if we look again at figure 6 apparently there seems to be no movement of the SOFM, (1966 - 1969), index 1, with increasing sunspot number. If we take into consideration the upgoing motion of hm F2 with advancing solar phase we obtain a

resultant ($\sim 1.7^{o}$ latitude) northward motion of SOFM, (1966 - 1969), index 1. Table 1 enables us to calculate the errors which are due to the assumption of a constant mean height Hm, for 20^{o} and 36^{o} elevation angle.
For sake of clarity the data used for calculating figures 6 and 7, S = S (El), are now used to display S as a function of geographic latitude φ, S = S (φ). Figures 8 and 9 show the results. Due to the necessary assumption of a constant Hm it is quite evident that their geophysical interpretation is less reliable than that of figures 6 and 7. However, keeping in mind the results of table 1, we obtain roughly the same statements as for figures 6 and 7. Distinct SOFMs are observable between 54^{o} and 57^{o} northern geographic latitude. In order to get in the future much more reliable and accurate presentations continuous measurements of the actual irregularity heights are required.
There is no explanation yet of the very different sunspot cycle behaviour of index 1 and index 2. Particle precipitation measurements of Frank et al (1971), Rao et al (1970) and Heikkila (1970) led to the suggestion that the two different scintillation belts are caused by different types of particles. The northward motion of SOFM, (1966 - 1969), index 1, seems to be a quite new result. In another context such a northward motion was already suggested by Oksman (1971). However - due to another grouping of the scintillation events - he made the statement for all observed scintillations. This motion might be also deduced from findings due to Beynon and Jones (1964). They compare the results obtained by Kent (1959) at Cambridge in 1957, using Sputnik 1 as the signal source (40 MHz), with their own results at Aberystwyth, Wales, (at the same geomagnetic latitude as Cambridge) using Discoverer 36 (20 MHz) in 1961 - 1962 and state that the scintillation index was much higher at a certain geomagnetic latitude in the latter case. This result can be stated differently by saying that the latitude at which the same mean scintillation index was obtained was much lower in the latter case. As a matter of fact there was an apparent latitude shift approximately 7^{o} towards the equator. Due to the ratio of the observed signal frequencies of 1:2 - as rough calculations revealed - at least 60% of this amount ($\sim 4^{o}$) was caused by the frequency variation.
Anyway our findings seem to exhibit a sunspot-cycle-dependence of the SOFMs which result in an increase of magnitude and a latitudinal variation of approximately $\pm 2^{o}$. Outside the belt-like regions, defined by the SOFMs, the scintillation activity drops to less than 20 % at any other southern latitude.

Table 1

Angular distance of the irregularities from the observing site as a function of observed elevation angle (El) and assumed mean height (Hm).

	Elevation [°] ε	mean height Hm [km]	Angular distance α [°]	difference 1 Δ [°]	difference 2 Δ [°]
1	20	100	2.3	Δ 1,2 = 1.1	
2	36	100	1.2		
3	36	200	2.3	Δ 1,3 = 0	
4	20	200	4.3		Δ 1,4 = - 2
5	36	200	2.3	Δ 4,5 = 2	
6	36	300	3.4	Δ 4,6 = 0.9	
7	20	300	6.1		Δ 4,7 = - 1.8
8	36	300	3.4	Δ 7,8 = 2.7	
9	36	400	4.3	Δ 7,9 = 1.8	
10	20	350	7.0		Δ 7,10 = - 0.9
11	36	350	3.9		
12	20	400	7.8		Δ 7,12 = - 1.7
13	36	400	4.3	Δ 12,13 = 3.5	
14	36	500	5.3	Δ 12,14 = 2.5	
15	36	600	6.3		

Due to the location of our observing site difference 1 represents the southward motion, difference 2 the northward motion.

Δ 1,2 $\hat{=}$ 1 minus 2

7. Magnetic activity dependence

Figure 10 shows S = S (φ) as calculated for Kp $>$ 3o (dotted line) and Kp $\leq$ 3o (solid line) from 31.12.1966 - 06.02.1969 for weak scintillation events, index 1. A distinct SOFM is observable around 57^{o} latitude. During the time periods where the recordings were obtained we found an occurrence frequency ratio of approximately 1 : 5 for Kp $>$ 3o / Kp $\leq$ 3o. The ratio of the displayed two SOFMs is $\sim$ 1 : 3. This implies that the scintillation activity for Kp $>$ 3o increase by a factor $\sim$ 2. Furthermore an apparent southward motion of $\sim 2^{o}$ for SOFM (Kp $>$ 3o) is observable. Figure 11 shows the same presentation for strong scintillation events, index 2. The scintillation activity for Kp $>$ 3o increased by a factor of $\sim$ 4. An apparent southward motion of the SOFM (Kp $>$ 3o) of $\sim 1^{o}$ is observable.
The southward motions are in agreement with other results, e.g. Aarons et al (1969), however their correct magnitude should be confirmed by scintillation-measurements which yield simultaneously the height of the irregularities and therefore do not require any mean height assumption for the data analysis.

8. Seasonal variations

Figure 12 shows the behaviour of the SOFMs for winter and summer. All scintillation events (index 1 + index 2) from May, June, and July (1965 + 1966 + 1967 + 1968) were taken and displayed as a function of geographic latitude, being regarded representative for summer conditions (solid line). Furthermore all scintillation events (index 1 + index 2) from November, December, and January (1964 + 1965 + 1966 + 1967 + 1968/69) were taken and also displayed as a function of geographic latitude, being regarded representative for winter conditions (dotted line). We find that the scintillation activity in summer is approximately 25 % higher than in winter. This was also corroborated by analyzing the individual years, however the number of data were too small for

more reliable interpretations. The SOFM (summer) appears to be at least 2° north of the SOFM (winter). However this statement is again very much dependent from the assumed constant mean height Hm. Again continuous height measurements are required.

9. Discussion

As the auroral zone approaches, the character of the average ionosphere properties, changes markedly. A number of aeronomic parameters display pronounced activity in the range 50° to 60° geomagnetic latitude. A few of them will now be mentioned.

1) Radio star and satellite scintillation increases sharply northward of 55°. (Bolshoi, 1966; Eroukhimov et al 1968, 1969; Aarons et al 1969). Our recent findings match these statements very well and show that there exist a rather narrow scintillation belt. Our studies seem to indicate that this belt consists of two fairly independent "sub-belts", one represented by index 1 data the other by index 2 data.

2) Electron precipitation (low energy) maximizes at 55° (Mariani, 1963). Very recent studies (Rao and Maier, 1970) of electron precipitation with energies between 5 eV and 200 eV show that their boundary seems to match fairly well the scintillation boundary. However the same seems to be true for precipitating very soft protons. Furthermore there seems to be a good correlation with the Stable-Aurora-Red-Arc (SAR). Other photoelectron measurements useful for such correlation purposes were carried out by Heikkila (1970). Frank et al (1971) showed excellent energy-time-(E-t)-spectrograms" for precipitated electrons between 50 eV and 50 KeV with very good temporal and energy resolution in subauroral and auroral regions which might also be correlated with scintillation measurements.

3) It was reported that polewards of the scintillation belt occurs the main F-region electron-density trough, observed in topside soundings (Muldrew, 1965; Nelms, 1966; Hagg, 1967). As to the connection of the scintillation boundary with other ionospheric and magnetospheric quantities, the best fit in the shape and range of the diurnal variation was obtained with the equatorward boundary of the midlatitude trough of electron density in the F-region, given by Thomas and Andrews (1968) for the period 1962 - 63. Rycroft et al (1970) inferred from detailed statistical investigations that the plasmapause in the magnetosphere and the trough near the exospheric base are related phenomena. Miller (1970) stated that the mean quiet-time trough position was negligibly affected but the electron density increased as much as threefold as the solar phase advanced. Since the spatial resolution of his measurements was only 10° (latitude) and due to the somewhat arbitrary definition of the trough location it is quite clear that any effect that does not exceed 5° (latitude) variation is therefore obscurred. Since seasonal and sunspotcycle-effects are probably just in this range of magnitude they could obviously not be detected by these measurements. Liszka et al (1970) stated that the ionospheric trough is located at the southern boundary of the precipitation region (1 KeV precipitated electrons).

Since most of the above mentioned measurements were done at various locations, at various locations, at various heights, and during different time periods and due to the often very different resolution or sensitivity of the measuring devices one can only phenomenologically state that the above mentioned effects are linked. Our reported findings should be regarded as part of this phenomenology rather than a very definite statement. For more detailed physical investigations all these quantities - and a few more - should be measured simultaneously. Furthermore correlation with backscatter measurements - some were already performed (Hartmann, 1969) - should be done. Some of the measuring techniques have to be improved towards better sensitivity and higher spatial resolution. Scintillation measurements with simultaneous height measurements are required. More sophisticated measuring methods for a better investigation of the scintillation-fine-structure-problems should be conceived. This is necessary in order to decide whether electrons or protons or both are the cause for the irregularities. An equipment which we do hope will enable improved measurements of this type is under design in our institute.

10. Conclusions

1) Many findings of other authors could be corroborated. This was already mentioned in the relevant chapters.
2) The obtained amplitude and phase recordings were examined and led to a specific new grouping of the scintillation data different from earlier ones. Index 1 denoted weak scintillations with amplitude variations less than 6 dB, index 2 those which exceed 6 dB.
3) The rather narrow scintillation belt, which was observed between 50° and 60° northern geographic latitude seems to consist of two fairly independent "sub-belts", one represented by index 1 data, the other by index 2 data. Whilst the first one - strictly spoken its satellite occurrence frequency maximum, SOFM (1), - seems to move northwards with increasing solar activity (in our special case roughly 2° latitude) the second one, SOFM (2) seems to move southwards by roughly the same amount. These results have to be corroborated by future scintillation measurements accompanied by simultaneous height measurement, so that errors due to the assumption of a mean height Hm are avoided. There is no clear physical interpretation until now, however it is suggested that the different behaviour of precipitated particles - energy range from 5 eV to 50 KeV - and possibly the dynamical effects in the ionosphere which are connected with the midlatitude trough might be the cause.
4) More detailed investigations of the physical cause of all these effects and their interdependence are proposed and were already started to a small extent at Lindau.
5) The scintillation data and other data should be used in a complementary way to exploit the advantages inherent in each and thus to proceed from the fairly well established phenomenological description to the more desirable detailed physical interpretation of the ionospheric-magnetospheric interactions.

11. Acknowledgements

The author thanks his colleague, Mr. J.P. Schödel for the computerized data processing and valuable discussions, Mr. K. Oberländer for the good quality of the recordings, and Mrs. Heise for the data preprocessing. The research reported here has been supported by the German Ministry of Education and Science under research grant WRK 125.

12. References

Aarons, J. Mullen, J.P. Whitney, H.E.	1969	J. Geophys. Res. 71, 684
Aarons, J.	1970	AFCRL 70-0053, report no. 106
Aarons, J. Whitney, H.E. Allen, R.S.	1970a	AGARD Lecture Series no.41, pp. 6-1 - 6-22
Becker, W.	1965	Kleinheubacher Berichte, 10, 199
Beynon, W.J.G.	1964	J. Atmosph.Terr.Phys. 26, 1175
Bolshoi, A.A.	1966	Cosmic Research 4, 502
Bramley, E.N.	1967	J. Atmosph.Terr.Phys. 29, 1
Briggs, B.H.	1958	J. Atmosph.Terr.Phys. 12, 89
Eroukhimov, L.M.	1968	Geomag. and Aeronomy 8, 138
Eroukhimov, L.M. Getmansev, G.G.	1969	Annals of the IQSY 5, 229
Frank, L.A. Ackerson, K.L.	1971	J. Geophys. Res. 76, 3612
Hagg, E.L.	1967	Can. J. Phys. 32, 790
Hartmann, G.K.	1965	A.E.Ü., 19, 207
Hartmann, G.K.	1969	In: Low-Frequency Waves and Irregularities in the Ionosphere, pp. 207 - 215 Reidel Publishing Company
Hartmann, G.K.	1969a	J. Atmosph.Terr.Phys. 31, 663
Hartmann, G.K.	1970	AGARD Lecture Series no.41, pp. 5-1 - 5-11
Hartmann, G.K.	1970a	AGARD Conference Proceedings no. 70, pp. 12-1 - 12-10
Hartmann, G.K.	1971	Paper presented at COSPAR 14th Plenary Meeting, in Seattle. To be published in Space Research XII, 1972
Heikkila, W.J.	1970	J. Geophys. Res. 75, 4877
Jespersen, J.L.	1967	In: AGARD propagation Factors in Space Communications
Jespersen, J.L. Kamas, G.	1964	J. Atmosph.Terr.Phys. 26, 457
Kent, G.	1959	J. Atmosph.Terr.Phys. 16, 10
Kidd, W.C.	1970	Radio Science, 5, 975
Liszka, L. Turunen, T.	1970	Kiruna Geophysical Observatory, Rep.no.70:315
Mariani, F.	1963	J. Atmosph. Sci 20, 479
Miller, N.J.	197	J. Geophys. Res. 75, 7175
Muldrew, D.B.	1965	J. Geophys. Res. 70, 2635
Nelms, G.L.	1966	Electron Density Profiles in Ionosphere and Exosphere, F.Frihagen. North-Holland, Amsterdam, p. 358
Oksman, J.	1971	J. Atmosph.Terr.Phys. - Submitted for publication
Rao, N.B.C. Maier, E.J.	1970	J. Geophys. Res. 75, 7168
Rycroft, M.J. Thomas, J.O.	1970	Planet. Space Sci 18, 65
Schmidt, G.	1966	A.E.Ü. 20, 374
Singleton, D.G.	1970	J. Atmosph.Terr.Phys. 32, 187
Singleton, D.G.	1969	J. Geophys. Res. 74, 1772
Thomas, J.O. Andrews M.K.	1968	J. Geophys. Res. 73, 7407
Whitney, H.E. Aarons, J. Malik, C.	1969	Planet. Space Sci. 17, 1069
Yeh, K.C. Paul, L.M. Flaherty, B.J.	1970	Radio Science, 5, 967

13. Appendix

Clarification of the quantity S, used in figs. 6 - 12 of this paper

Since we only analyzed recordings which displayed at least one distinct scintillation onset or cease during the entire satellite passage, we could calculate the location of the southern scintillation boundary. S so represents the number of occurrences of southern boundaries for a given elevation angle (figs. 6 and 7) or latitude (figs. 8 - 12). So we have some sort of a probability distribution for the southern scintillation boundary. In the same manner we tried to display the northern scintillation boundary. Since this fairly often failed and very likely only parts of this curve were significant - due the fact that the satellite left the range of observation before the scintillation dropped to zero - we did not display these curves.
However those southern parts of the northern boundary curves which might be significant, intersect the southern boundary curves approximately 5 degrees (latitude) north of the maximum of the southern curve. They have mostly maxima probably at locations beyond our range of observation. If in spite of this a vague statement might be given then this that there seems to exist a belt-like scintillation structure in our area at $\sim 57^{\circ}$ latitude, at least during specific periods.
Due to detailed discussions we restrict our former more general statement about the belt-like-structure to the just mentioned modified statement.

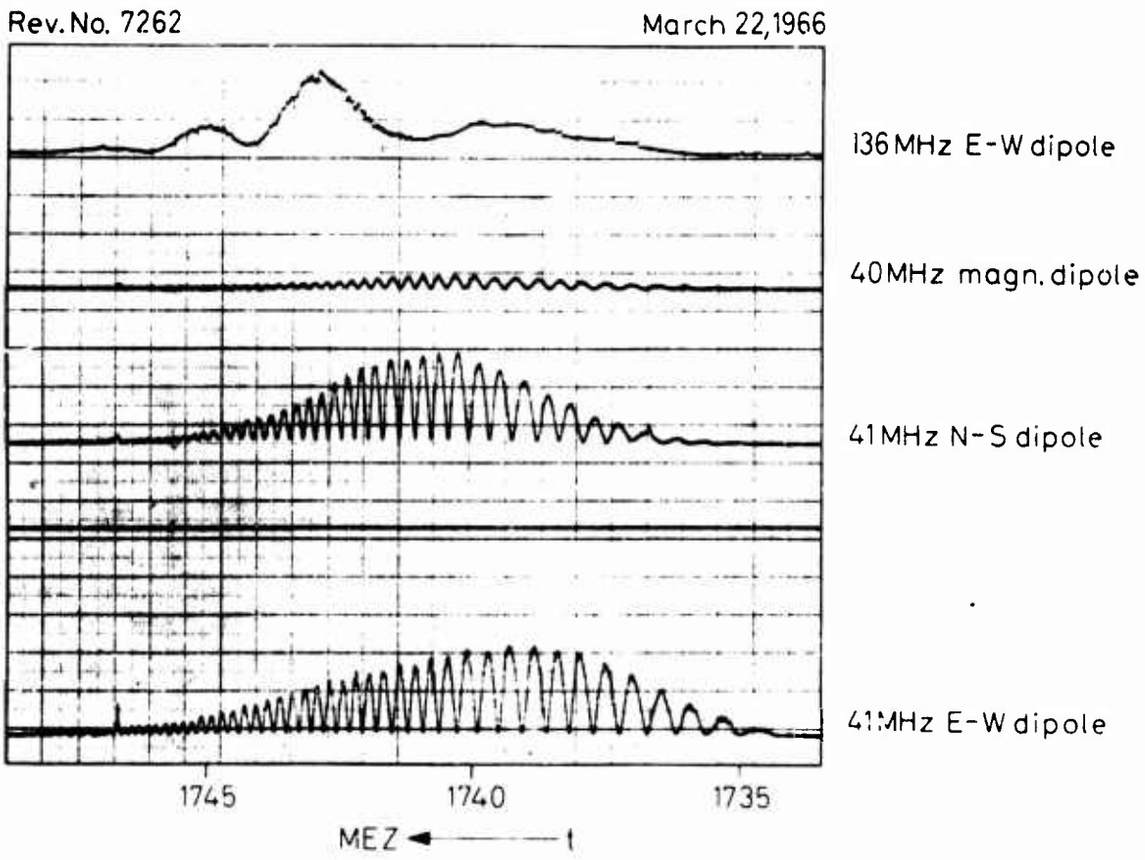

Fig. 1 Faraday-effect recording, satellite Explorer 22 (S-66)
March 22, 1966, Rev.no. 7262. Amplitude increases upwards.
Time: MET = UT + 1 = (MEZ)

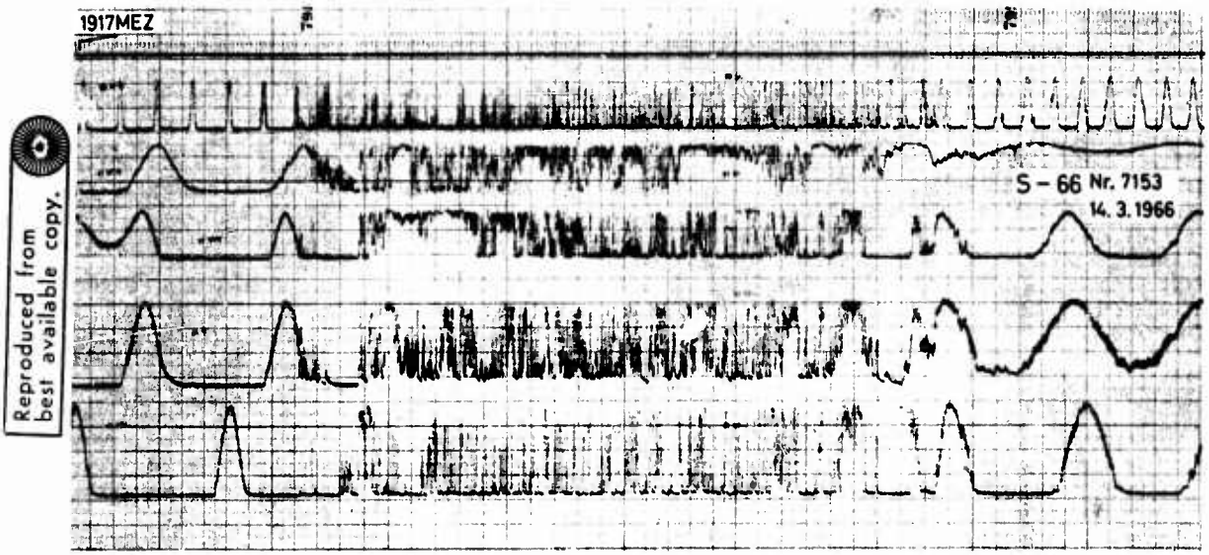

Fig. 2 Faraday-effect recording with satellite scintillation, satellite Explorer 22, March 14, 1966. Rev.no.7153

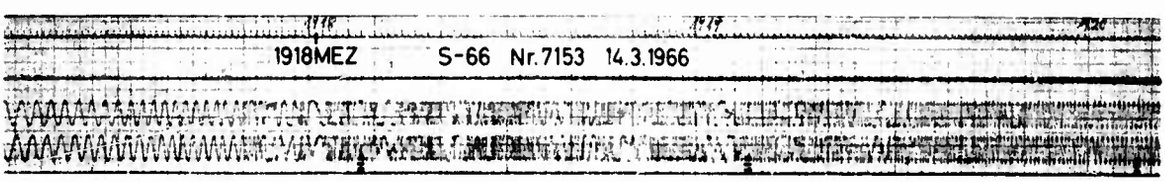

Fig. 3 Dispersive-Doppler-recording with "phase scintillation", satellite Explorer 22, March 14, 1966, Rev.no.7153

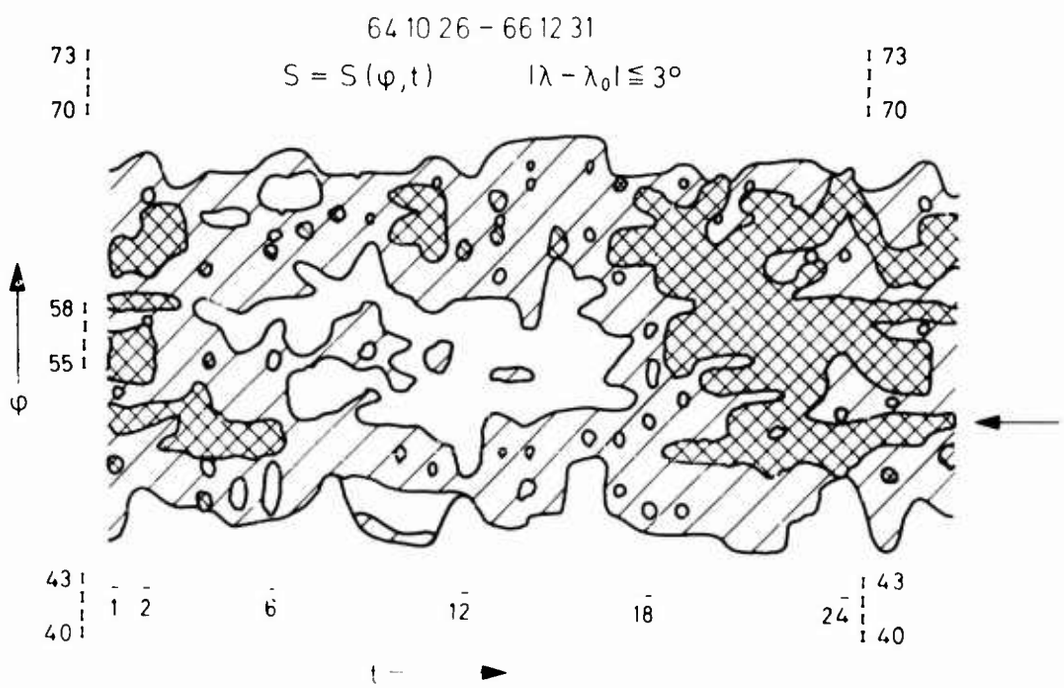

Fig. 4 Sate.lite scintillation activity as a function of geographic latitude and local time LT. Time period from 26.10.1964 to 31.12.1966.
White areas: no scintillation events
Simple hatched areas: 1 - 3 scintillation events
Double hatched areas: 3 - 10 scintillation events
Black areas: More than 10 scintillation events
The black arrow indicates the latitude of the observing site. Mean height Hm: 300 km
Weak + strong scintillation; e.g. index 1 + index 2 are combined in this presentation

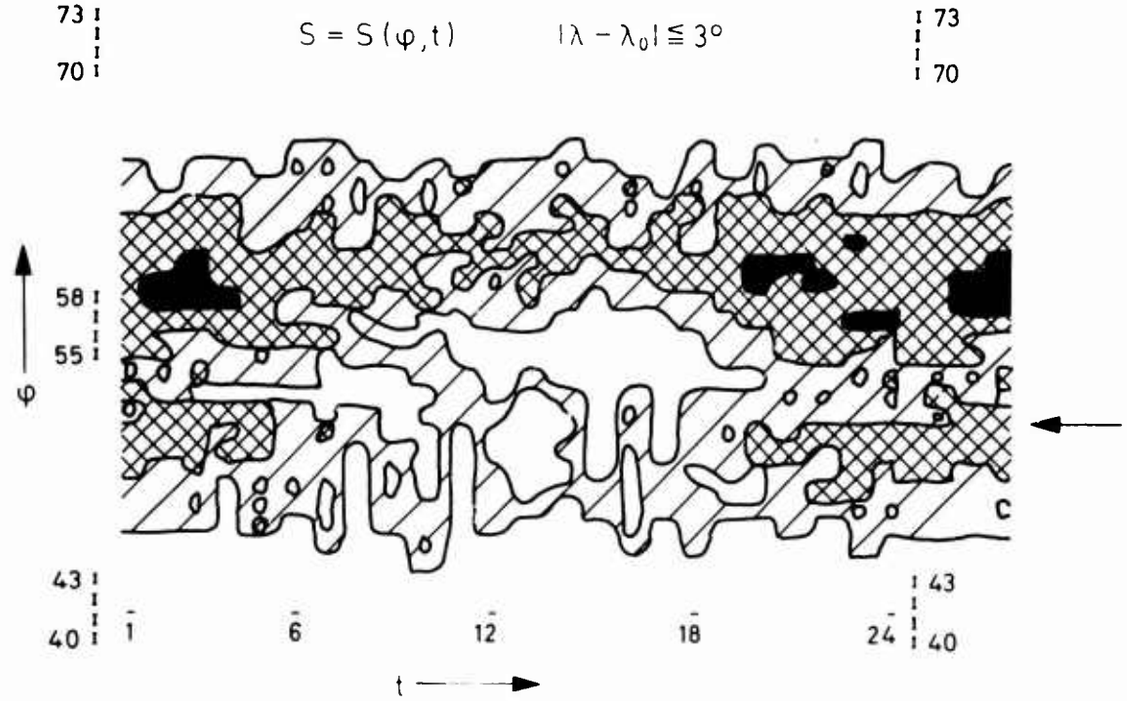

Fig 5 Satellite scintillation activity as a function of geographic latitude and local time LT.
Time period from 31.12.1966 to 06.02.1969

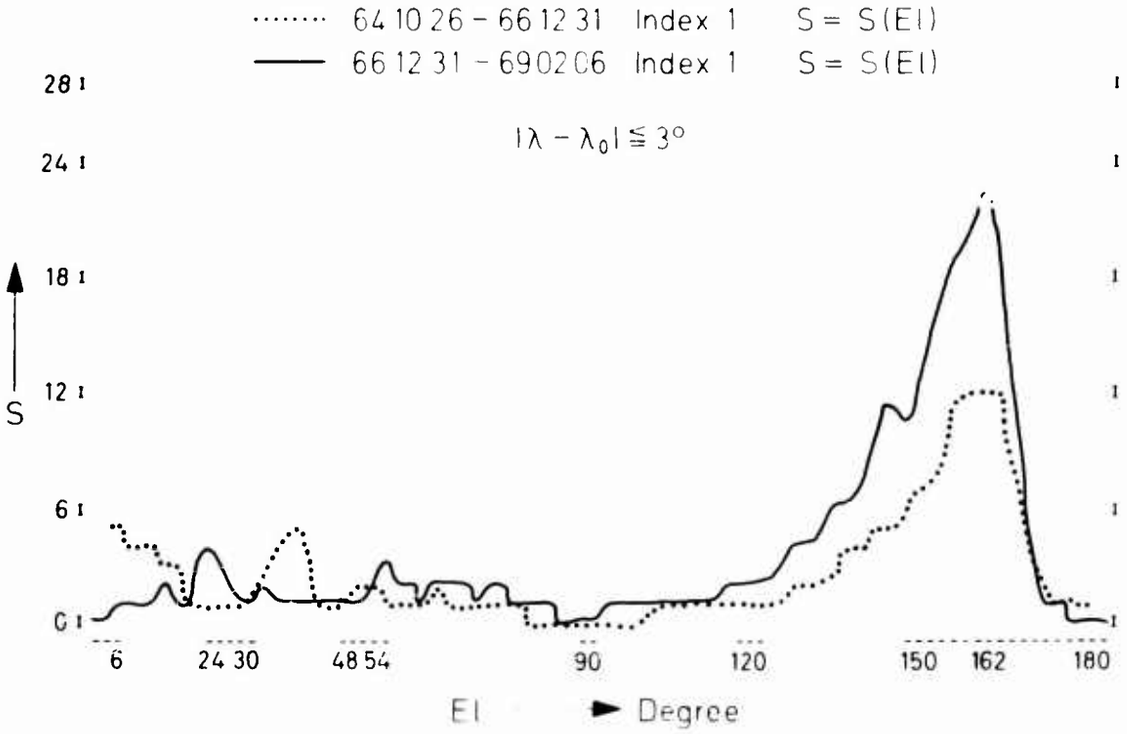

Fig. 6 Number of scintillation events S as a function of elevation angle El of the satellite.
Dotted line represents the period 26.10.1964 - 31.12.1966.
Solid line represents the period 31.12.1966 - 06.02.1969.
Data for index 1

For more detailed explanation of S see 13. appendix.

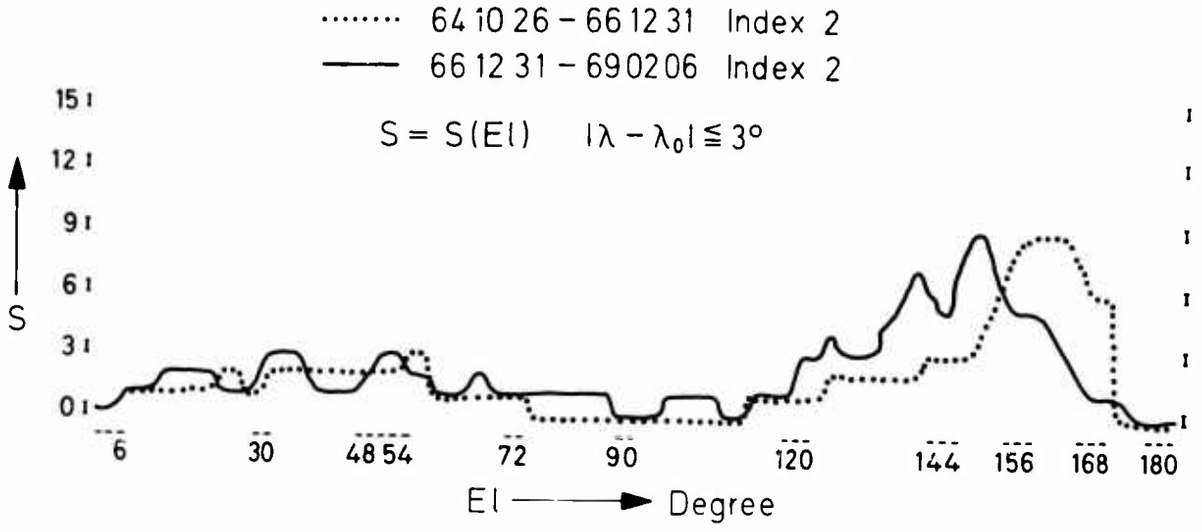

Fig. 7 Same captions as fig. 6.
Data for index 2

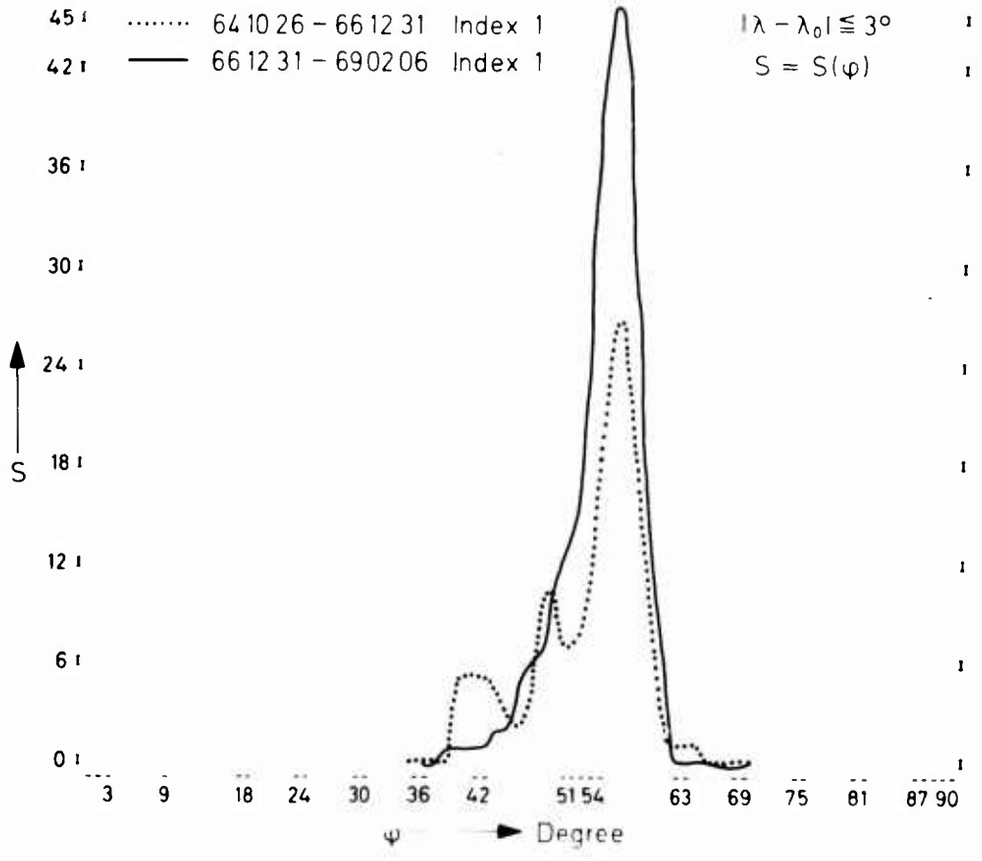

Fig. 8 Number of scintillation events S as a function of geographic latitude φ.
Dotted line represents the period 26.10.1964 - 31.12.1966.
Solid line represents the period 31.12.1966 - 06.02.1969. Hm = 300 km
Data for index 1

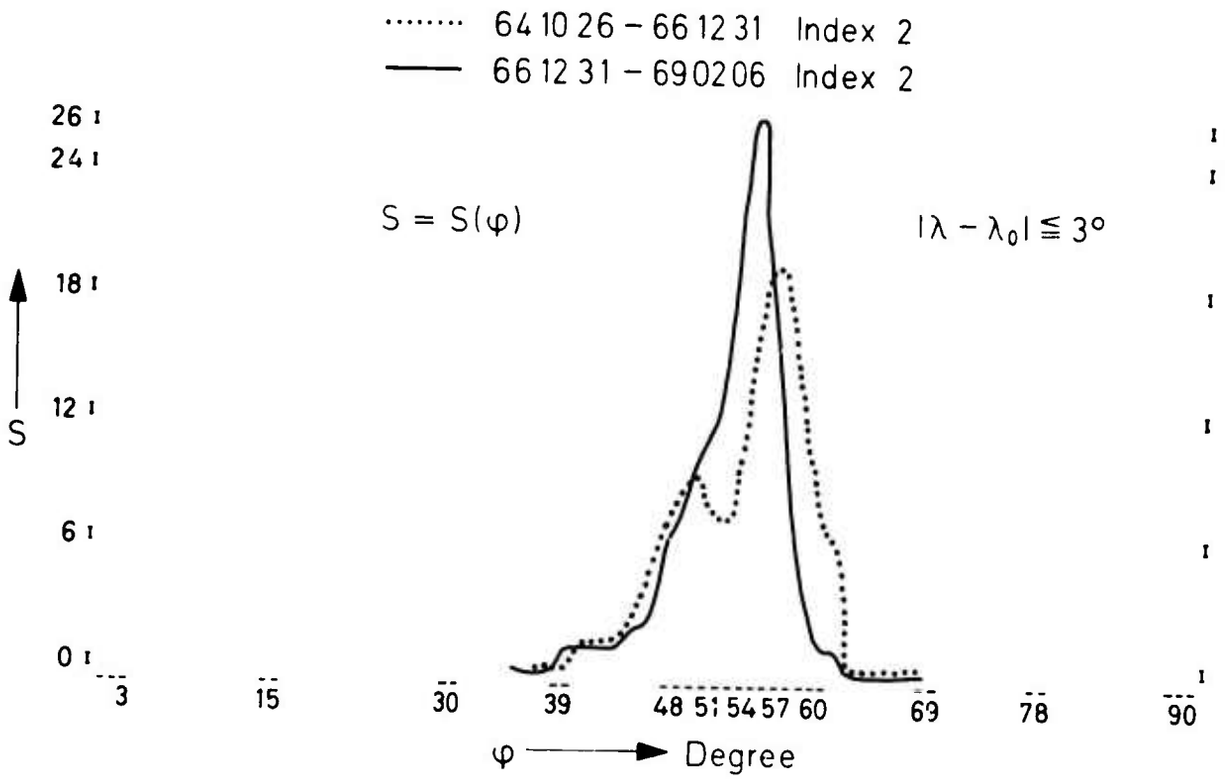

Fig. 9 Same captions as fig. 8
Data for index 2.

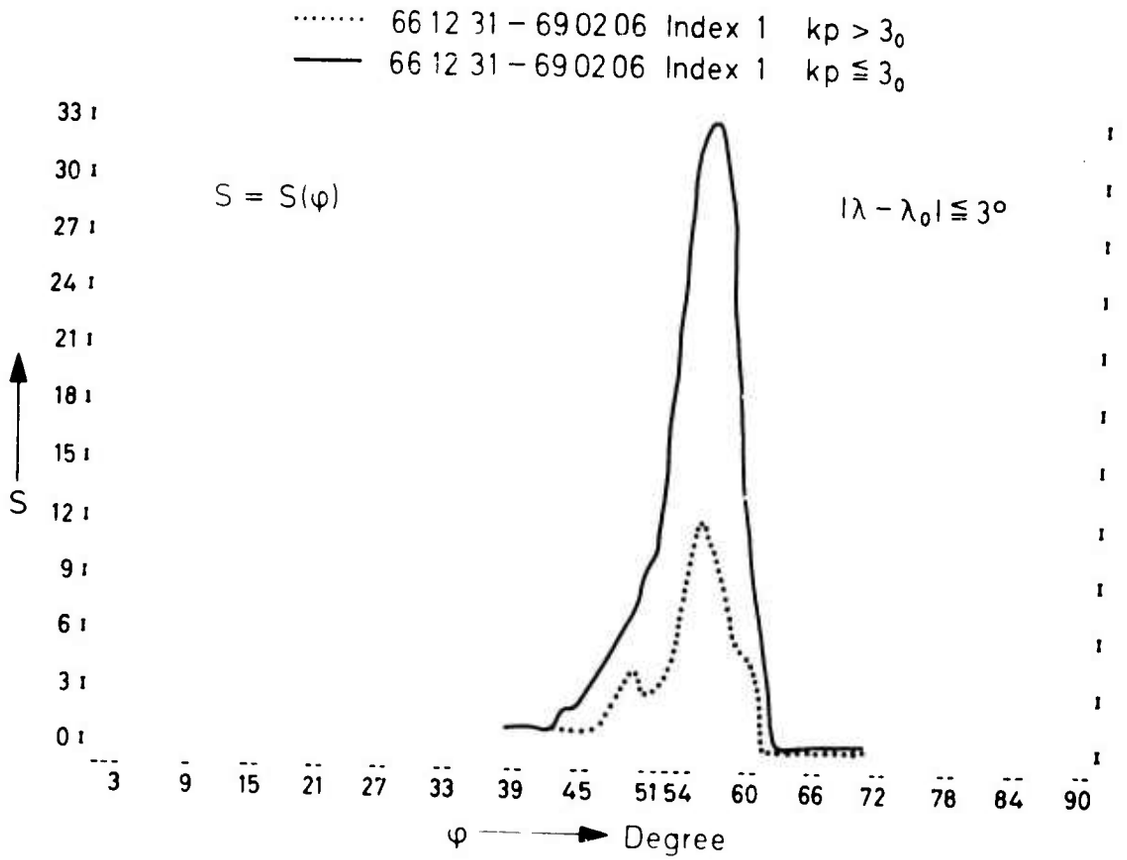

Fig. 10 Number of scintillation events S as a function of geographic latitude φ.
Period 31.12.1966 - 06.02.1969. Hm = 300 km
Data for index 1

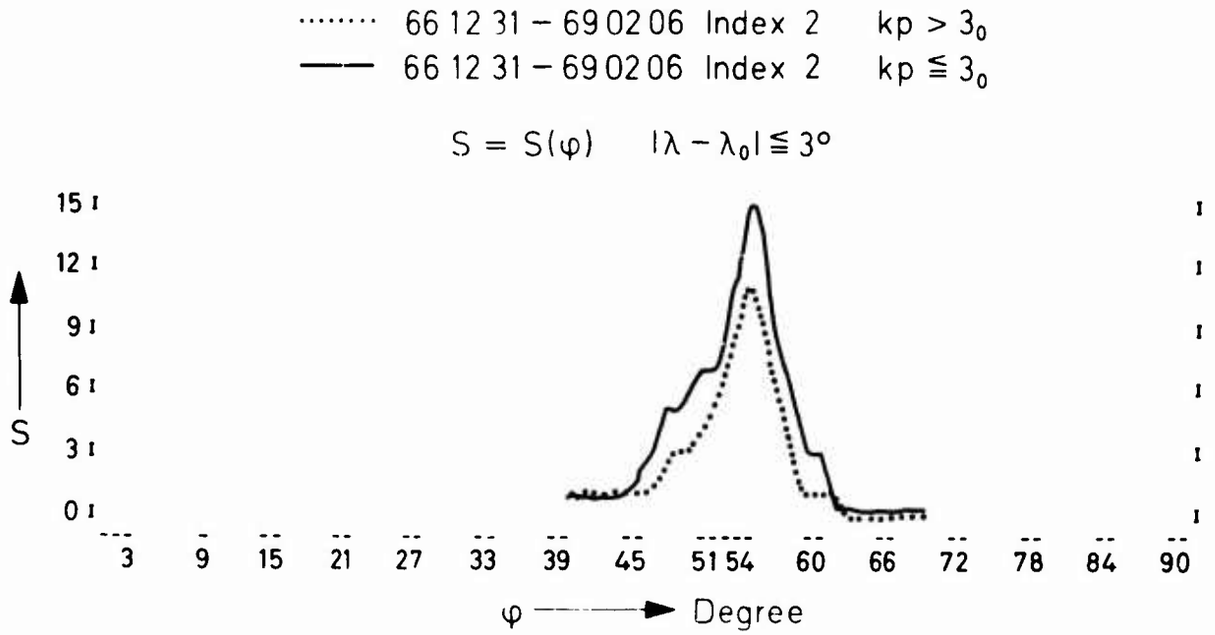

Fig. 11 Same captions as fig. 10.
Data for index 2.
Solid line represents Kp ≦ 3o.
Dotted line represents Kp > 3o.

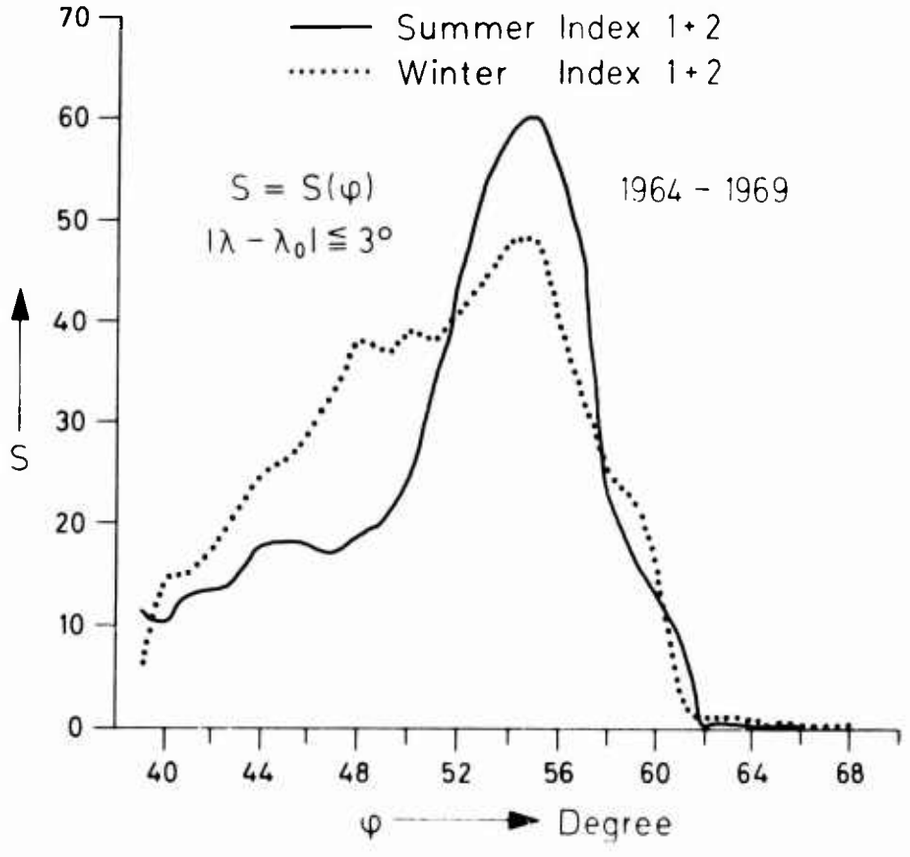

Fig. 12 Number of scintillation events S as a function of geographic latitude φ for summer and winter.
Hm = 300 km
Data for index 1 + index 2

SESSION IV

POLAR SCINTILLATION

CHAIRMAN'S REPORT

by O.M.Bratteng

Studies of transionospheric propagation have shown that strong scintillation may occur in the VHF-and UHF band at any place and at any time north of about 50^{o} invariant latitude. The production and characteristics of the scintillation - giving irregularities are not at all well known. As regards the morphological aspects, however, some prevailing features seem to appear.

There is rather strong scintillation in the Polar Cap region, a secondary minimum around 75^{o} invariant latitude, and a strong maximum in the auroral zone. The southern boundary is at about 60^{o} invariant latitude in the evening and at about 70^{o} in the morning. During geomagnetic disturbances the boundary moves southward and the intensity increases. As regards the time variation, an evening and a morning maximum have been observed from high latitude stations. These maxima coincide with maxima in precipitation of soft energy electrons.

Statistically, the region of maximum scintillation is found in the vicinity of the well-known main trough in electron density.

Probe measurements as well as radar observations have shown that there is a region of strong irregularities north of optical aurorae. (In this region strong precipitation of soft energy electrons is to be expected.)

Beacon measurements by use of low orbiting satellites have demonstrated that scintillation - giving irregularities exist even below 200 km.

The reported heght- and scale size distribution and the latitudinal variation of these two parameters do not show a consistent picture. Results from satellite beacons and radio stars contradict.

There exists large scale gradients in total electron content which will cause significant errors in angle- of-arrival measurements at least for frequences below 300 MHz. These gradients seem to be associated with TID's with scale size of about 100 - 200 km.

DISCUSSION

G H Millman

We seem to have neglected the topic of angular scintillation in this session. What is the correlation of angular scintillation with amplitude scintillation in the polar region?

P A Forsyth

In response I would like to say a few words about the advantages of angular scintillation measurements. In one sense angular measurements are more fundamental since even for a thin phase screen the angular spectrum is present close to the screen as well as far away while amplitude fluctuations are only present far from the screen. For this reason we have been making angular (and amplitude) observations of satellite and rocket beacons for nearly ten years at a variety of stations in Canada. In all "simple" situations, i e where only a few irregularities are present, it is possible to combine the angular and amplitude scintillations to give a fairly detailed description of the spatial distribution of ionization in the irregularities, but especially in the auroral zone the situation often becomes so complex that only statistical results can be given and these are much less valuable for studies of the mechanism of formation of the irregularities. Finally I should give an important qualification on my enthusiasm for angular measurements. We have accumulated many records but the detailed analysis to yield electron density distributions is so time consuming that the extraction of meaningful synoptic data is well beyond the capability at a group like ours so we have only a few snapshots of particular situations in the ionosphere. This fits our interest in mechanisms but may be of little value to those interested in morphology.

A Kavadas

1) Do the irregularities in the F- and E-regions occur simultaneously?

2) Do you get E-region irregularities when you have F-region irregularities but the magnetic activity is low?

P A Forsyth

1) Considering the difficulty of getting coincidence in time for a satellite pass, a rocket flight and an aurora we have only one instance. For the one instance the answer is yes.

2) I don't know but since we have completely quiet rocket flights from Churchill and satellite scintillations are often seen at Churchill under "quiet" conditions I suspect the answer is yes.

P A Forsyth

This is a short comment on the question of E-region scintillation. We have a total of about 25 rocket flights in which the transmitter was between the E and F region and for a variety of auroral and non-auroral conditions. These are in addition to the satellite measurements. All records include basically both angular scintillation measurements (relative phase) and amplitude scintillation. The general picture seems to be that the satellite measurements tend to be biassed toward the F-region heights but the rocket measurements tend to show that E-region irregularities exist in the auroral ionosphere. I would suggest that the E-region irregularities are generally screened by the higher F-region irregularities. Whenever amplitude fluctuations are used to determine heights, there is a bias toward F-region because the amplitude scintillation from that region are more fully developed (because the F-region is farther away from the ground station). But certainly especially during the formation of an auroral display E-region scintillations occur and are consistent with what one will expect from the current picture of electron precipitation associated with visible auroral forms.

A Kavadas

I would like to offer a possible explanation for the peculiar behaviour of the polarization of the r f wave as observed by Liszka when the satellite was near the horizon. In order to do so I would appreciate more information regarding the type of polarimeter used and the satellite receiver geometry.

L Liszka

Polarization measurements at Kiruna Observatory are made using a Titheridge-type polarimeter with a mechanically rotated antenna. Measurements indicate that during spring

and summer months signals from the quasi-geostationary satellite INTELSAT 2F-1 at 136.4 MHz are, during some periods, polarized in direction about $\pm$ 20° around the direction of magnetic field lines.

A number of tests has been done in order to investigate whether the phenomenon may be due to equipment properties or influence of the ground on the receiving antenna. Results of tests indicate that the phenomenon seems to be a real propagation effect. For example, the phenomenon disappeared when the polarimeter has been moved 250 km to the south.

A Kavadas

I think that this is similar to the type of depolarization we observe when an r f wave traverses the aurora. As I indicated in my paper yesterday a wave becomes partially depolarized when it propagates through an inhomogeneous anisotropic medium. If it is strongly depolarized it has a maximum linear component parallel to the axis of anisotropy which in this case is the direction of the magnetic field. Since your maximum component is not exactly parallel to the magnetic field it must be concluded that the wave is not strongly depolarized in which case the position of its maximum fluctuates on either side of the direction of the magnetic field. The phenomenon and geometry of the system as you describe it seems to favour this explanation though the effect of refraction and ground reflections have not been taken into account. These could alter the situation at the low angles involved here, but I think not very drastically. The changes between summer and winter are probably the result of a change in either the degree of anisotropy or the size of the irregularities.

J Aarons

Visibility fades were obtained on radio star sources. Primary causes of the fades are probably due to regular broadening of sources.

The data on loss of fringe visibility that I have seen to date is taken from radio star sources - mostly Cassiopeia A (4' of arc in diameter) and Cygnus A (1.5' of arc). I believe much of the loss of fringe visibility comes from the effective broadening of the sources by irregularities. Another possible explanation is that the effective size of the "shadow" ground pattern is smaller than the antenna spacing. Phase at the two antennas would not be coherent and therefore fringes would be lost. Under these circumstances I would expect occasional coherence and therefore occasional fringes but from the records this does not appear to be so. If each antenna had random amplitude and phase fluctuations, I would also expect its system to lose fringes, source broadening plus small scale patterns is thought to account for loss of fringe visibility. Until fringe loss is seen on point sources with variable baseline interferometers it cannot be accurately assessed as a problem in radar monopulse systems.

W G Chesnut

Predection, Michaelsen type Interferometers measure the degree of phase coherence of a signal between two spaced receivers. The degree of phase coherence can be shown to be related to the angular spread of the "cone angle of arrival" - or angular spectrum of waves. Whether you prefer to intuitively attribute fades to increasing angular spread - or to fringe patterns on the ground - doesn't much matter. What does matter is that the interferometer does not care whether angular spread is due to intrinsic source diamter - or due to diffraction of waves from a point source. The amplitude scintillation - as you point out - may depend upon source diameter.

It can easily be shown that the rms angular deviation of waves is given (with maybe an error of order of $\sqrt{2}$) as

$$(\overline{\theta^2})^{1/2} = \frac{\lambda}{\pi\Delta}\left(1 - C(\Delta)\right)^{1/2}$$

where λ - wavelength of radio signal
Δ - interferometer element spacing
$C(\Delta)$ - measured interferometer correlation coefficient

It can also be shown that

$$(\overline{\theta^2})^{1/2} = \left(\overline{\theta^2}_{\text{source}} + \overline{\theta^2}_{\text{propagation}}\right)^{1/2}$$

where the subscripts indicate the source of angular spread. Usual practice in interferometry is to measure changes in $C(\Delta)$. Therefore changes in fringe visibility (changes in $C(\Delta)$) are related to angular spread due to propagation. Good experimental practice and interpretation would then sort out the change due to propagation. I have necessarily relied on the competence of your collegues in this matter. If they have done their job properly, then they have measured the propagation angular spread - and we, within certain limits, can apply the results to tracking radar response.

J Aarons

Radio star sources at low frequencies quickly increase in angular size with scattering. Their finite size must be taken into account in applying fringe visibility studies and scintillation observations of radio stars to satellite beacon propagation.

A Egeland

The correlation of high latitude, polar region scintillations with magnetic activity is questionable. This is because magnetographs have large geometric factors and the K-indices represent 3-hours average. (The magnetic activity is mainly due to E-region currents). I will therefore recommend that a new high latitude index should be developed which also reflects the large soft electron precipitation over the polar cap.

J Aarons

Correlation of scintillations with details of magnetic storms has not yielded positive results, therefore it is true that K-indices are only indications of lower altitude effects and not of F-layer effects. However, no index of F-layer activity is available. K-indices are used merely to indicate the presence of magnetic activity. That some correlation exists can be seen by the separation of scintillation indices for $K_p = 0$, $K_p = 1$, $K_p = 2$. We do need a magnetospheric activity index.

L Liszka

It is known that Kp reflects rather well variations in the exospheric temperature, while the local K-index describes the station's position with respect to the auroral oval. A comparison with the auroral zone F-region scintillation is therefore quite interesting. Time-lag investigations between the scintillation and the magnetic activity indicate a time constant 3 hours. So that comparison between K-index (3 hour base) and the scintillation seems to be meaningful. A comparison of the position of precipitation boundary with K and Q indices indicates also a better correlation with K-index.

H J Albrecht

This is a comment to criticism of usefulness of K-and K_p- values and other parameters based on three-hour intervals.

The objective is an R & D solution of problems caused by the occurence of scintillations for the benefit of system engineering and similar tasks. Scintillation susceptibility is not a function of the measuring means. With geostationary satellites as sources there is no discrepancy in the time interval. They yield data certainly comparable to K and K_p- values.

POLAR PROPAGATION EFFECTS ON H.F. RADARS

by

H. G. Möller
Max-Planck-Institut für Aeronomie
D 3411 Lindau/Harz, Germany

SUMMARY

CW and pulse transmission experiments in the auroral and subauroral region are reviewed. The phenomena that affect propagation are: dispersion of foF2 critical frequency and hence horizontal electron density gradients, field-aligned irregularities in the F2 and E region, auroral Es, and D region absorption. The variation of these phenomena in time and space and the correlation with magnetic activity will be discussed briefly. Following propagation effects were observed due to these phenomena: Transmission paths transversing horizontal gradients of electron density become asymmetric which has to be taken into account in MUF calculations. Strong curtains of irregularities cause non-great-circle transmission. NGC transmission may be advantageous if it results in a MUF enhancement, or in bypassing an area of enhanced absorption it is disadvantageous as time delay of the received signals is increased. MUF enhancement is often observed by auroral Es.

In spite of the fact that both, transmission loss on auroral and subauroral paths and absorption measured with riometer tend to increase with increasing auroral activity, the point to point correlation between transmission loss and riometer absorption is quite poor. This is due to pronounced spatial variation of auroral absorption. In contrast to these varying phenomena the F1 layer is quite stable and is supporting the MOF if the hop length exceeds 2000 km. On subauroral paths the over 4000 km 1F high angle ray is observed. This transmission mode is, however, very sensitive to horizontal electron density gradients and irregularities in the F2 layer.

1. INTRODUCTION

In the last eight years two AGARD meetings were occupied with communication in the arctic, 1963 at Athens and 1967 at Finse, Norway. The proceedings of these meetings edited by Landmark (1964) and by Folkestad (1968) contain much valuable information on H.F. propagation in polar regions. A comprehensive survey of high latitude H.F. propagation is given by Hunsucker and Bates (1969). The topics to be discussed in this review paper are the following:

absorption,
irregularities,
non-great-circle propagation,
high angle ray transmission,
F1 layer effects,
sporadic E effects.

2. ABSORPTION

Ionospheric absorption is the most difficult problem for H.F. communication in polar regions. In the following it will be discussed first, what are the different classes of absorption encountered in polar regions and how can these be characterized by their variation in time space and frequency of observation. Secondly, the comparison of absorption measurements with oblique transmission will be discussed.

The absorption phenomena observed in polar regions can be divided in three classes: (a) normal absorption, (b) regular abnormal absorption, (c) absorption events.

Normal absorption is varying with solar activity and with the solar zenith angle χ proportional to $(\cos \chi)^{0.75}$.

Regular abnormal absorption, also known as the winter anomaly, is characterized by the fact that in winter the absorption is higher than expected from the cos χ law. Additionally, the variation from day to day is greater in winter than in summer. That this type of absorption is present in high latitudes up to 70° N is shown by Schwentek (1968). According to Lauter and Nitzsche (1967) the winter anomaly is increasing with increasing frequency.

Whether the winter anomaly is magnetically controlled is still an open question. Bourne and Hewitt (1968) showed by superposed epoch analysis that an absorption variation of 15 % is related to magnetic activity. Schwentek (1968), however, found that the absorption variation due to winter anomaly amounts at Lindau to a factor of two. This great variation cannot be explained by magnetic control only.

Absorption events in the auroral zone (AZA) and on the polar cap (PCA) and their relation to the sun - earth environment have already been discussed in a foregoing section. Nevertheless, some additional remarks seem to be appropriate.

During auroral absorption events multifrequency riometer measurements were made by Lerfald et al. (1964). At a given instant during an event the absorption values A as a function of frequency f satisfied a power law

$$A(f) = C\, f^{-n}$$

wherein C and n are constants. The exponent n varied around a mean of 1.8 from 1.0 through 2.2. The smaller exponent, the lower is the height of the absorbing region.

By multistation riometer measurement the cross correlation of absorption as a function of distance was studied by Parthasarathy et al. (1965). At College, Alaska, they found that this coefficient falls to a value of 0.26 over a distance of 200 km in northern direction, whereas a cross correlation coefficient of 0.41 was found with a station 700 km west of College. Holt et al. (1962) found in Norway a cross correlation coefficient of 0.65 at a spacing of 300 km independent of azimuth and the autocorrelation value falling to the same value after a time of 10 min. Comprehensive summaries of riometer absorption measurements are given by Hultqvist (1966) and Hargreaves (1969).

At temperate latitudes it is already difficult to get consistent results between absorption measurements and the ionospheric loss observed at oblique transmission. Before discussing polar propagation it is useful to remind of some results found at temperate latitude for sake of fair comparison. One of the best results is given by Schwentek and Umlauft (1961). Between the apparent reflection coefficient at vertical incidence and the ionospheric loss at oblique incidence over a path of 300 km a correlation coefficient of 0.84 was found for the monthly mean values over four years of observation. This excellent agreement was found because for both experiments the height of reflection was the same by selecting equivalent frequencies. Also at temperate latitudes the correlation of daily absorption varies with the separation of path midpoints as shown by Jones and Keenliside (1970) in figure 2.1. The correlation is better for the equinox and winter than for the summer due to the greater daily variation of absorption caused by the winter anomaly.

For a 2900 km auroral path from Thule, Greenland, to College, Alaska, a statistical analysis by Hunsucker (1964) gave the following correlations:

auroral zone absorption versus 18 MHz attenuation $r = 0.21$,
quiet day absorption versus 18 MHz attenuation $r = 0.11$.

Here also the higher the absorption variation, the higher is the correlation coefficient.

An exceptional discrepancy between riometer absorption and 12 MHz signalstrength observations on the Thule - College path was observed by Egan (1963). During a PCA event the riometer absorption on 27.6 MHz peaked to 12 dB. According to this high absorption the signal attenuation for 12 MHz was expected to be as great as 400 - 500 dB. The 12 MHz signal, however, was reduced by 35 - 40 dB only. It was suggested by Egan that under extreme conditions the signal could propagate via the D region.

Fair agreement between absorption and signalstrength is reported by Jelly (1963) from the Resolute Bay - Ottawa path. As during a PCA event both signal and noise were reduced, the signal to noise ratio remained nearly constant at Resolute Bay, the northern end of the transmission path. The same would not be true on the southern end of the circuit.

From these few examples it is evident that absorption prediction in polar regions is difficult.

A simple approach to this problem was made by using the lowest frequency f_{min} observed at vertical sounding. A method to derive the ionospheric loss at oblique incidence from f_{min} data is given by Hill (1963). This paper, however, contains no experimental proof of the method. Mesterman (1969) has based absorption predictions for the antarctic on f_{min} data.

At the present cosmic noise observation is the mostly applied technique for absorption measurements in polar regions.

The statistical distribution of hourly absorption data was examined by Holt et al. (1962) and Hargreaves (1966). As a result the latitudinal dependence of the percentage of time of the absorption exceeding 1 dB was fitted by a Gaussian curve

$$Q = Q_o \exp\left[-\frac{(\lambda - \lambda_o)^2}{2\sigma_1^2}\right],$$

as shown in figure 2.2, where λ and λ_o are the geomagnetic latitudes of station and of the absorption maximum respectively, and σ_1 is the standard deviation of the curve. Furthermore, the median absorption A_m is related to the quantity Q by an empirical expression

$$Q = 22\, A_m^{3.5}.$$

Combining this expression with the spatial distribution of figure 2.2, the global relation for the median absorption is expressed by

$$A_m = A_o \exp\left[-\frac{(\lambda - \lambda_o)^2}{2\sigma_2^2}\right].$$

The variation of A_o, λ_o, and σ_2 as a function of K_p is given by Hargreaves (1966). This global relationship was used by Agy (1970) for auroral absorption prediction.

3. IRREGULARITIES

In auroral regions both large scale and small scale irregularities influence H.F. propagation.

To investigate large scale variations of F layer electron density in the polar cap, contour maps of foF2 were compiled from vertical sounding data by Hill and Penndorf (1959). In figure 3.1 the isopleths of foF2 are drawn in a polar stereographic projection which indicates that regions of strong gradients exist.

By oblique sweep-frequency measurements over a 2000 km subauroral path it was shown by Möller (1960) that the ray path becomes asymmetric if a strong gradient is encountered along the path. The apex of the path shifts into the region of higher electron density resulting in a MOF enhancement.

From figure 3.1 one might assume from a first glance that the most severe gradients are present over northern Canada and Alaska. This, however, is not the case. The tiny island of a L (low) over northern Europe incircled by the isopleth foF2 = 3 is the location of the most severe gradient. In both areas the distance of the isopleths is about 200 km. The maximal asymmetry of the transmission path, however, is found where the relative gradient has a maximum which amounts to 0.3/200 km over northern Europe, whereas it is three times smaller over northern Canada.

In figure 3.2 the magnitude of the relative gradient is shown by the quotient foF2 Lycksele/foF2 Uppsala. The station Lycksele is 500 km north to Uppsala, Sweden. From the Uppsala vertical sounding data F2-MUF$_{\perp}$ was calculated. The MOF enhancement is given by the observed F2-MOF$_{\wedge}$ divided by F2-MUF$_{\perp}$. It is evident from this plot that MOF enhancement is increasing with increasing magnitude of the gradient.

Such steep gradients could be detected by vertical sounders only if the spacing between the stations is small. Therefore, it appears on the map over northern Europe only. In reality this tiny island is a part of the trough surrounding the magnetic pole as shown by Muldrew (1965) as a result of topside sounding data.

Ma (1965) made a statistical analysis of the variation of the trough and of the observed MOF as a function of time of day and geomagnetic activity. He found that between 0300 LMT and 0600 LMT the gradient was steepest and had the greatest latitudinal distance from the pole and the MOF enhancement had a maximum. All effects increased with increasing magnetic activity.

The high occurrence frequency of spread F as observed by vertical sounders indicates that small irregularities are a common feature in the polar ionosphere. A comprehensive review of spread F is given by Herman (1966).

By scattering at these irregularities MUF enhancements were observed by several authors, Möller (1956, 1958), Fulton et al. (1959, 1961).

In a note of the URSI Working Group on Ionospheric Soundings (1968) it is stated that "the MUF is more closely related to highest frequency (fxFS) on which vertical reflections are seen than with the critical frequency of the regular layer embedded in the abnormal structure". It is, therefore, recommended to adopt a new parameter fxFS for international analysis. This would be indeed an empirical improvement.

In the interpretation of sweep-frequency oblique sounding experiments it was shown by Möller (1960) that MUF enhancements of a factor > 1.5 are not due to scatter near the midpoint of the path but due to scattering from regions behind the northern end of the transmission line.

Perhaps bistatic backscatter would be a better term to describe this transmission mode. For a 600 km north-south transmission path (Lindau to Alsbjerg, Denmark) this effect may be illustrated by figure 3.3. At the top the bistatic ionogram shows besides a strong Es mode the classical 1F mode ending at 5 MHz and continued by 1F scatter running way up to 15 MHz where it ends at a strong scattering curtain. This curtain is seen on the monostatic records from Alsbjerg and Lindau at a range of 900 km and 1500 km respectively. The record at the bottom is produced by a rotating antenna which indicates that the backscatter signals are indeed comming from the north. (The rotating antenna consists of two horizontally spaced groups (16 m spacing) connected in antiphase which results in a double leaf diagram with a sharp minimum in the main direction.)

As the MOF values observed by this scatter mechanism are three to four times higher than the critical frequency of the layer the scattered energy will be high enough only if the increase of electron density in the irregularities and the scattering area is large enough. This can, however, not be checked by vertical sounding as in this case an increase of electron density of few percent will produce strong spread F signal close to the critical frequency of the layer.

Superior to vertical sounding is H.F. backscatter observation by which an area of 6000 km diameter surrounding the station can be controlled. As by this technique higher frequencies are used areas of weak and strong scattering can be distinguished.

Scattering from irregularities in the F region has been observed on fixed frequencies by Peterson and Leadabrand (1954), Swenson (1964), Malik et al. (1964), Hower et al. (1966), and Baggaley (1970). Sweep-frequency backscatter observations were made by Bates (1959, 1960, 1966, 1969, 1970), Möller (1964), and Katz (1970). The following discussion will be based on sweep-frequency observations only as the latter are easier to be interpreted and as frequency dependence contains much useful information.

With the assumption that the irregularities are aligned to a vertical earth magnetic field and that scatter is strictly aspect sensitive, i.e. strict normality between the wave vector and the magnetic field, Bates (1959) found an excellent agreement between the calculated and observed leading edge of the direct scatter from the field-aligned irregularities. Taking into account the inclination of the earth's magnetic field, Möller (1964) found the same for the observations at

Lindau. Figure 3.4 shows the good agreement between the calculated leading edge (solid line) and observations (broken lines). It is interesting to note that at an inclination of the earth's magnetic field of about 70° a frequency maximum is observed at a range of 1000 km, shown in figure 3.5. These spikes, however, are found predominated at sunspot minimum as at this time the height of the F layer is lower. The leading edge of direct F scatter for different heights of the layer is shown in figure 3.6.

Selecting the range of the strongest backscatter signal, Bates (1966) was able to trace the latitude of the dayside aurora. In figure 3.7 the geomagnetic latitude of the southern boundary of the auroral oval is shown versus time of day for different groups of K_p. From College, Alaska, (65° magn. north) it was not possible to give a complete picture, as at midnight the scattering area came too close to the station if $K_p > 2$.

A more complete picture can be given by a combination of the two stations Lindau (52°) and Alsbjerg (57°), figure 3.8. For sake of simplicity only two groups of local magnetic activity are shown ($K < 3$ and $3 < K < 5$). The closed loops are observed from Alsbjerg, the open loops show that direct F scatter observed at Lindau is mainly a night-time phenomenon.

4. NON-GREAT-CIRCLE PROPAGATION

Non-great-circle (NGC) propagation has been observed by several authors on transpolar, trans-auroral and subauroral paths. NGC modes can be easily identified by the great time delay observed on pulse transmission records. The time delay spread of the different great circle propagated modes does not exceed 4 msec usually. An excess time delay > 6 msec is usually due to NGC modes. Ortner and Owren (1961) observed time delays of 6 - 7 msec on the polar path College to Kiruna. They assume that these were due to ray bending by means of strong horizontal gradients of foF2. These authors, however, were not able to localize the area of lateral bending.

On a subauroral path from Washington to Urbana, Illinois, Westlund (1961) localized this area by measuring the excess time delay and the azimuth at the receiver side. He believed his NGC modes were due to aspect sensitive echoes caused by field-aligned irregularities.

Bates et al. (1966) observed NGC modes at College, Alaska, on pulse transmission from Thule, Greenland; Andöya, Norway; Johnston Island; and Palo Alto, California. These are due to scatter at field-aligned irregularities in the auroral zone. The geomagnetic latitude of the scatter belt was determined from the H.F. backscatter echoes at College as well as from the excess time delay of the NGC modes observed on the College - Palo Alto path. In 95 % of the cases the disagreement between the corresponding values was smaller than 2° in geomagnetic latitude.

This proof indicates unambiguously that the scattering belt causes the NGC modes and not horizontal gradients of foF2 as suggested by Ortner and Owren (1961). This result is interesting in so far as NGC modes were observed also on transequatorial propagation by Crochet et al. (1968) and Röttger (1971). Crochet assumes that the NGC modes are caused by scatter. Piggott (1970) and Röttger (1971), however, suggest that the strong NGC signals should be due to east-west foF2 gradients. Strong gradients were found by Piggott in reducing the data of Ariel III electron density probe.

5. HIGH ANGLE RAY TRANSMISSION

One hop F2 high angle ray transmission over ground ranges < 4000 km are possible as predicted by Dieminger and Möller (1956) and observed by Warren and Hagg (1958) on the 5300 km transatlantic path Ottawa - The Hague.

On a 4500 km subauroral path Tveten (1961) observed F2 layer as well as F1 layer propagated high angle transmission. As by this mode the MOF can be increased with respect to the two hop transmission up to 30 % this mode was suggested by Ortner and Owren (1961) to explain the fact that the observed MOF was higher than the predicted value.

It is, however, dangerous to assume that this mode is a reliable one in polar propagation. On the Ottawa - The Hague path the relative occurrence frequency of the one hop mode did exceed 70 % only from March - August 1960 during a limited day time interval of three to five hours, centered around 18 UT (Muldrew and Maliphant, 1962). Inspecting the same records it was shown by Möller (1961) that the occurrence frequency of this mode exceeds 50 % only if the ionosphere is smooth, this means there should be present neither horizontal gradients of foF2 nor spread F along the route, as both would affect the high angle ray mode seriously.

6. F1 LAYER EFFECTS

The MOF propagated by the F1 layer quite regularly exceeds the F2-MOF on polar propagation paths ranging from 2000 km to 3500 km at summer day times. Figures 6.1 and 6.2 show this effect observed on a 2000 km subauroral path by Dieminger et al. (1959). Similar observations have been made by Bates and Albee (1966) at College monitoring sweep-frequency transmissions from Thule, Palo Alto, Fort Monmouth, and Johnston Island. On the Palo Alto path the F1 layer carried the MUF 1964 more often than 1965. This is explained by Hunsucker and Bates (1969) by the fact that the quotient foF2/foF1 is increasing with growing sunspot activity.

It was suggested by Sandoz et al. (1959) to include the F1-MUF in propagation predictions. This was done by Petrie and Stevens (1965) who derived foF1 maps for the arctic region and also F1 transmission factors for a range 1800 km through 3500 km together with correction terms taking

into account time of day and sunspot activity. foF1 prediction has been expanded to cover the whole world by DuCharme et al. (1971).

7. SPORADIC E EFFECTS

For Es-MUF calculations observed over distances of about 1000 km the secant law Es-MUF = fEs·sec φ is valid (Wright et al., 1960). Comparing oblique sounding data from the 2000 km subauroral path Lindau - Sodankylä, Finland, with vertical sounding data at the midpoint it was found, however, that the Es-MOF was considerably higher (CCIR Report, 1970). Instead of the expected quotient Es-MOF/fEs = 5 a median of 6.9 was observed. These experiments also indicate the possibility that the Es-MOF is power sensitive. This could result for a 10 dB change in transmitter power, in modest differences (6 - 8 %) in Es-MOF.

The occurrence frequency of polar Es has been studied by Maehlum (1961). Numerical maps of foEs are published by Leftin et al. (1968). A reevaluation of sporadic E research is given by Pittenger and Gassmann (1971).

The importance of Es propagation especially in winter nights is emphasized by Bates and Hunsucker (1964). According to their observations on the College - Thule path the relative occurrence frequency of Es propagated signals ranged from 40 - 55 % in the winter night 1963/64. The significance of Es propagation was examined by Stevens (1968 a). On the Resolute Bay - Ottawa path the percentage of occurrence where Es controls the MOF ranged from 0 - 40 %, taking into account the same day time interval but for the winter 1960/61. Both results show that Es is an uncertain transmission mode.

A good method, however, to use this mode is a frequency sounding system parallel to the H.F. communication link which allows to select the optimum propagation frequency, as described by Jull (1964) or the CHEC sounding system (Stevens, 1968 b). By such a system the communication reliability can be increased considerably during less severe disturbances.

8. REFERENCES

Agy, V. (1970), HF radar and auroral absorption, Radio Sci., Vol. 5, No. 11, pp. 1317-1324.

Baggaley, W.J. (1970), Backscatter observations of F-region field-aligned irregularities during the I.Q.S.Y., J. Geophys. Res., Vol. 75, No. 1, pp. 152-158.

Bates, H.F. (1959), The height of F-layer irregularities in the arctic ionosphere, J. Geophys. Res., Vol. 64, No. 9, pp. 1257-1265.

Bates, H.F. (1960), Direct HF backscatter from the F-region, J. Geophys. Res., Vol. 65, No. 7, pp. 1993-2002.

Bates, H.F., and R.D. Hunsucker (1964), HF/VHF auroral and polar zone forward soundings, Sci. Rept. UAG-R150, Geophysical Inst., Univ. Alaska, College, Alaska.

Bates, H.F. (1966), A proposed polar auroral radar system, J. Atmos. Terr. Phys., Vol. 28, pp. 903-907.

Bates, H.F. (1966), Latitude of the dayside aurora, J. Geophys. Res., Vol. 71, No. 15, pp. 3629-3633.

Bates, H.F. (1966), On using direct backscatter to predict communications, Proc. IEEE, Vol. 54, No. 10, pp. 1457-1458.

Bates, H.F., and P.R. Albee (1966), On the strong influence of the F1 layer on medium to high latitude HF propagation, Sci. Rept. UAG-R175, Geophysical Inst., Univ. Alaska, College, Alaska.

Bates, H.F., P.R. Albee, and R.D. Hunsucker (1966), On the relationship of the aurora to non-great-circle high-frequency propagation, J. Geophys. Res., Vol. 71, No. 5, pp. 1413-1420.

Bates, H.F., and P.R. Albee (1969), Aspect sensitivity on HF auroral echoes, J. Geophys. Res., Space Phys., Vol. 74, No. 5, pp. 1164-1168.

Bates, H.F., and P.R. Albee (1970), Aspect sensitivity of F-layer HF backscatter echoes, J. Geophys. Res., Space Phys., Vol. 75, No. 1, pp. 165-170.

Bourne, I.A., and L. Hewitt (1968), The dependence of ionospheric absorption of radio waves at mid-latitudes on planetary magnetic activity, J. Atmosph. Terr. Phys., Vol. 30, pp. 1381-1395.

C.C.I.R. (1970), VHF propagation by way of sporadic E and other anomalous ionization, XII Plenary Assembly, New Delhi, Vol. II, Part 2, Rept. 259-2, 1-4, pp. 93-99.

DuCharme, E.D., L.E. Petrie, and R. Eyfrig (1971), A method for predicting the F1 layer critical frequency, Radio Sci., Vol. 6, No. 3, pp. 369-378.

Crochet, M., and D. Rogabe (1968), Etude d'une propagation transequatoriale en dehors du grand cercle en periode d'occurence de F diffus, AGARD Conference Proc., No. 37, 47-1-9.

Dieminger, W., and H.G. Möller (1956), Echo sounding experiments with variable frequency at oblique incidence, Nuovo Cimento, Suppl. 10 (4), pp. 1532-1544.

Dieminger, W., H.G. Möller, and G. Rose (1959), Further results of sweep-frequency oblique-incidence pulse transmission, J. Atmosph. Terr. Phys., Vol. 14, pp. 179-180.

Egan, R.D. (1963), Thule to College 12 Mc propagation during the April and May 1960 intense polar cap absorption events, in The Effect of Disturbances of Solar Origin on Communications, ed. by G.J. Gassmann, Pergamon Press, pp. 47-58.

Folkestad, K. (Ed.) (1968), Ionospheric Radio Communications, Plenum Press, New York.

Fulton, B.J., L.E. Petrie, and W.S.P. Ward (1959), Transient modes of high-frequency radio wave propagation across the auroral zone, J. Atmosph. Terr. Phys., Vol. 16, No. 1/2, pp. 185-186.

Fulton, B.J., and L.E. Petrie (1961), The analysis of transient modes of propagation across the auroral zone, J. Geophys. Res., Vol. 66, No. 8, pp. 2321-2327.

Hargreaves, J.K. (1966), On the variation of auroral radio absorption with geomagnetic activity, Planet. Space Sci., Vol. 14, pp. 991-1006.

Hargreaves, J.K. (1969), Auroral absorption of HF radio waves in the ionosphere: A review of results from the first decade of riometry, Proc. IEEE, Vol. 57, No. 8.

Herman, J.R. (1966), Spread-F and ionospheric F-region irregularities, Rev. Geophys., 4 (2), pp. 255-299.

Hill, G., and R. Pe[illegible]f (1959), Research concerning forecasting anomalous propagation at high latitudes, Tech. Rept., RAD-TR-59-19, AVCO Corp., Wilmington, Mass., USA.

Hill, G.E. (1963), HF communication during ionospheric storms, J. Res. NBS Radio Propagation, 67 (1), pp. 23-30.

Holt, O., B. Landmark, and F. Lied (1962), Analysis of riometer observations obtained during polar radio blackouts, in Radio Wave Absorption in the Ionosphere, ed. by N.C. Gerson, Pergamon Press, New York, pp. 229-243.

Hower, G.L., D.M. Ranz, and C.L. Allison (1966), Comparison of HF radar echoes and high-latitude spread-F measurements, J. Geophys. Res., Vol. 71, p. 3215.

Hultqvist, B. (1966), Ionospheric absorption of cosmic radio noise, Space Sci. Rev., 5 (6), pp. 771-817.

Hunsucker, R.D. (1964), Auroral-zone absorption effects on a HF arctic propagation path, Radio Sci. 68 D (6), pp. 717-721.

Hunsucker, R.D., and H.F. Bates (1969), Survey of polar and auroral region effects on HF propagation, Radio Sci., Vol. 4, No. 4, pp. 347-365.

Jelly, D. (1963), The effects of polar-cap absorption on HF oblique-incidence circuits, J. Geophys. Res., 68 (6), pp. 1705-1714.

Jones, T.B., and W. Keenliside (1970), Variation of ionospheric absorption at widely spaced stations, AGARD Conference Proc., No. 49, 24, pp. 1-7.

Jull, G.W. (1964), HF propagation in the arctic, Arctic Communications 13, ed. B. Landmark, Pergamon Press, pp. 157-176.

Katz, A.H. (1970), HF-backscatter study (phase I), AVCO System Division, AVSD-0465-70-RR.

Landmark, F. (Ed.) (1964), Arctic Communications, Pergamon Press, New York.

Lauter, E.A., and P. Nitzsche (1967), Seasonal variations of ionospheric absorption deduced from A3-measurements in the frequency range 100 - 2000 kc/s, J. Atmos. Terr. Phys. 29, pp. 533-544.

Leftin, M., S.M. Ostrow, and C. Preston (1968), Numerical maps of foEs for solar cycle minimum and maximum, ESSA Techn. Rept. ERL 73-ITS 63.

Lerfald, G.M., C.G. Little, and R. Parthasarathy (1964), D-region electron density profiles during auroras, J. Geophys. Res., 69 (13), pp. 2857-2860.

Little, C.G., and R. Silberstein (1961), A comparison of arctic HF transmission loss and VHF riometer data, NBS Rept. 6743.

Ma, J.Ch. (1965), Einfluß der erdmagnetischen Unruhe auf den brauchbaren Frequenzbereich im Kurzwellen-Weitverkehr am Rande der Polarlichtzone, Mitt. Max-Planck-Institut für Aeronomie, No. 24 (I).

Maehlum, B. (1961), On the sporadic E ionization in and near the auroral zone, NDRE Rept. No. 37.

Malik, C.,and J. Aarons (1964), A study of auroral echoes at 19.4 Megacycles per second, J. Geophys. Res. 69, p. 2731.

Mesterman, I., F. Trentini, and H.G.F. Sarmiento (1969), Planning of telecommunication networks in decametric waves in antarctica, Armada Argentina Direccion de Electronica Naval, Laboratorio Ionosferico Armada Republica Argentina, Rept. C 18.

Möller, H.G. (1956), Sweep-frequency oblique-incidence experiments over a distance of 1320 km, J. Atmos. Terr. Phys., Vol. 9, pp. 155-156.

Möller, H.G. (1958), Further results of sweep frequency oblique incidence experiments, J. Atmos. Terr. Phys., Vol. 13, p. 173.

Möller, H.G. (1960), Ergebnisse der Pulsübertragung mit veränderlicher Frequenz auf der Strecke Sodankylä - Lindau, Kleinheubacher Berichte No. 7, Fernmeldetechnisches Zentralamt, Darmstadt, pp. 115-123.

Möller, H.G. (1961), Beobachtungen an der 1xF-Übertragung auf der Strecke Ottawa - Den Haag, Kleinheubacher Berichte No. 8, Fernmeldetechnisches Zentralamt, Darmstadt, pp. 79-85.

Möller, H.G. (1964), Backscatter observations at Lindau/Harz with variable frequency directed to the auroral zone, in Arctic Communications, ed. by B. Landmark, 16, Pergamon Press, pp. 177-188.

Muldrew, D.B., and R.G. Maliphant (1962), Long-distance one-hop ionospheric radio-wave propagation, J. Geophys. Res., 67 (5), 1805-1815.

Muldrew, D.B. (1965), F-layer ionization troughs deduced from Alouette data, J. Geophys. Res., 70 (11), pp. 2635-2650.

Ortner, J., and L. Owren (1961), Multipath propagation on transarctic HF circuits, Sci. Rept. 10, Kiruna Geophys. Obs., Kiruna, Sweden.

Parthasarathy, R., and F.T. Berkey (1965), Auroral zone studies of sudden-onset radio wave absorption events using multiple-station and multiple frequency data, J. Geophys. Res., 70, (1), pp. 89-98.

Peterson, A.M., and R.L. Leadabrand (1954), Long-range radio echoes from auroral ionization, J. Geophys. Res., 59, p. 306.

Petrie, L.E., and E.E. Stevens (1965), A F1 layer MUF prediction system for northern latitudes, IEEE Trans. Antenna Propagation, Vol. AP-13, No. 4, pp. 542-546.

Petrie, L.E., and E.S. Warren (1968), The propagation of high frequency waves on the Winnipeg - Resolute Bay oblique sounding circuit, Ionospheric Radio Communication, ed by Folkestad, Plenum Press, New York, p. 242.

Piggott, W.R. (1970), The use of satellite data for prediction purposes, AGARD Conference Proc., No. 49, pp. 19-1-21.

Pittenger, E.W., and G.J. Gassmann (1971), High latitude sporadic E, Air Force Cambridge Research Laboratories 71-0082, Environmental Research Papers, No. 347.

Röttger, J. (1971), Einflüsse des äquatorialer Spread-F auf die Kurzwellenausbreitung, Kleinheubacher Berichte, No. 14, Fernmeldetechnisches Zentralamt, Darmstadt (to be published).

Sandoz, O.A., E.E. Stevens, and E.S. Warren (1959), The development of radio traffic frequency prediction techniques for use at high latitudes, Proc. IRE, Vol. 47, No. 5, pp. 681-688.

Schwentek, H., and G. Umlauft (1961), Vergleich von Absorptionskennwerten der Ionosphäre aus Impulsamplitudenmessungen und Feldstärkeregistrierungen, A.E.U., Band 15, Heft 4, pp. 200-204.

Schwentek, H. (1968), Zum Auftreten der Winteranomalie der ionosphärischen Absorption von Kurzwellen, Nachrichtentechn. Z., Heft 1, pp. 32-39.

Stevens, E.E. (1968 a), The significance of sporadic-E propagation in determining the MUF, Ionospheric Radio Communication, ed. by K. Folkestad, Plenum Press, New York, pp. 289-293.

Stevens, E.E. (1968 b), The check sounding system, Ionospheric Radio Communication, ed. by K. Folkestad, Plenum Press, New York, pp. 359-369.

Swenson, E.M. (1964), Preliminary results of observations of aspect-sensitive reflections from irregularities in the F-region, Aust. J. Phys. 17, No. 4, pp. 490-504.

Tveten, L.H. (1961), Long-distance one-hop F1 propagation through the auroral zone, J. Geophys. Res., 66 (6), pp. 1683-1684.

URSI Informations Bulletin (1968), The acquisitation of ionospheric data for predictions, No. 167, pp. 64-84.

Warren, E., and E.L. Hagg (1958), Single-hop propagation of radio waves to a distance of 5300 km, Nature, 181, 34.

Westlund, C.D. (1961), A study of radio waves scattered from field-aligned and other ionospheric irregularities, Suppl. A Interim Eng. Rept. 9, Contract Nobsr 64723, Elec. Eng. Res. Lab., Univ. Illinois, Urbana.

Wright, J.W., and T.N. Gautier (1960), Note on a test of the equivalence theorem for sporadic E propagation, J. Res. NBS Sect. D, Radio Propagation, Vol. 64D, No. 4, pp. 347-348.

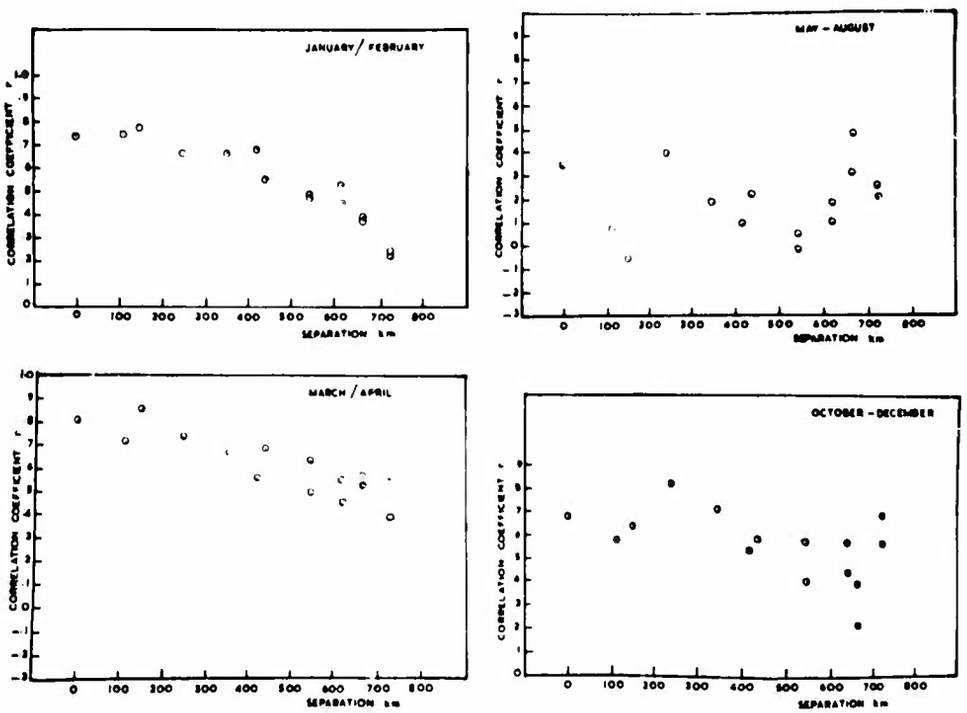

Fig. 2.1 a Variation of the correlation coefficient of daily absorption values with station separation for 1966.

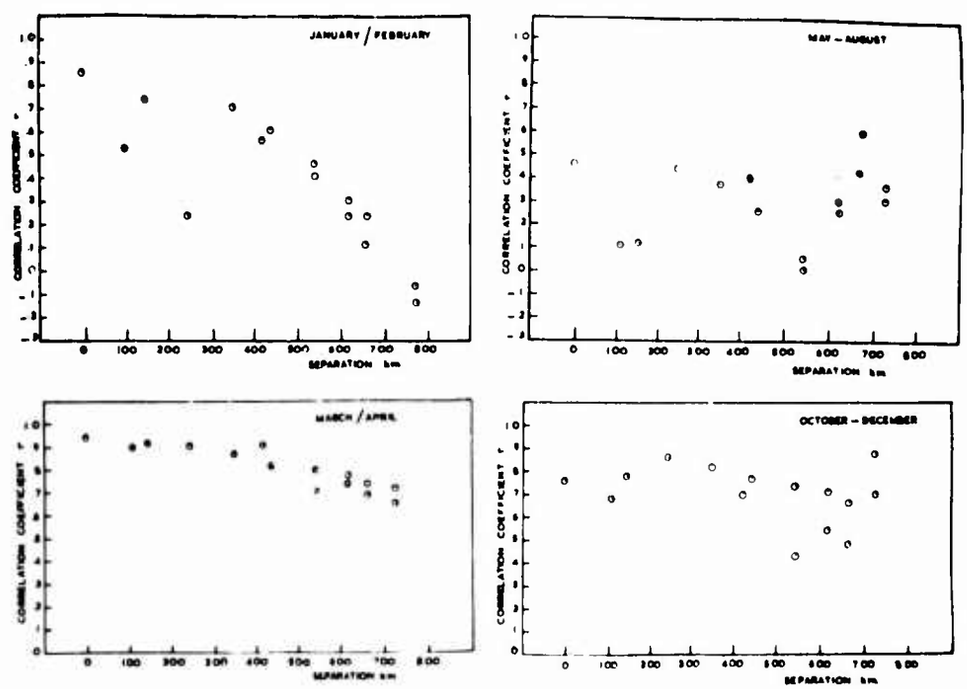

Fig. 2.1 b Variation of the correlation coefficient of seven day running mean absorption values with station separation 1966.
(After Jones and Kronlside, 1970.)

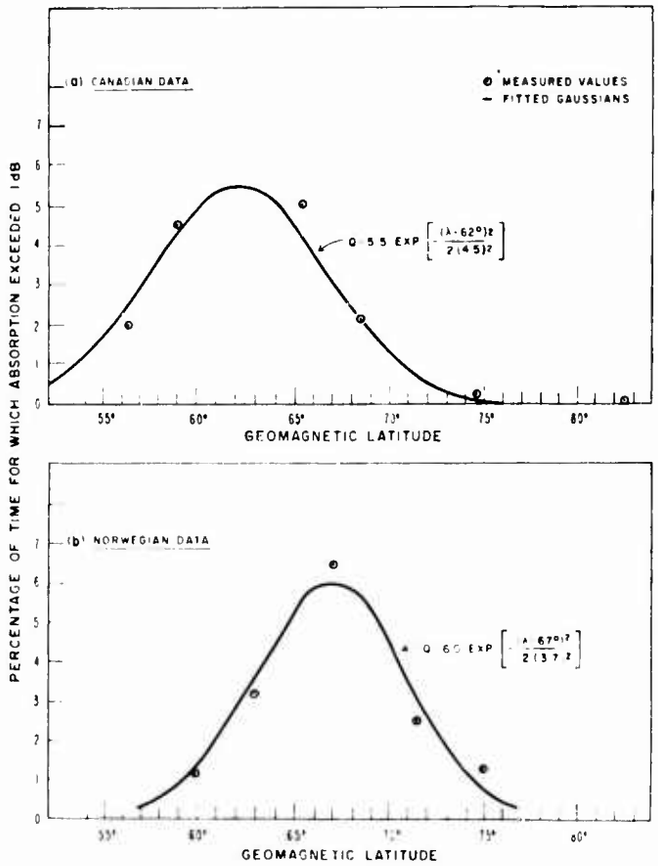

Fig. 2.2 Occurrence of riometer absorption exceeding 1 dB as a function of magnetic latitude.
(a) Canadian data;
(b) Norwegian data.
(After Hargreaves, 1966.)

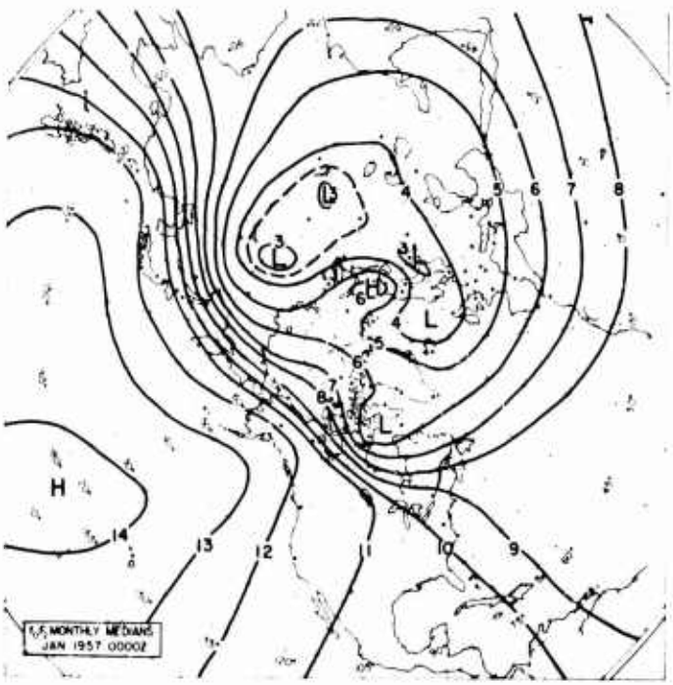

Fig. 3.1 [illegible] on a polar stereographic projection.
(After [illegible], 1972.)

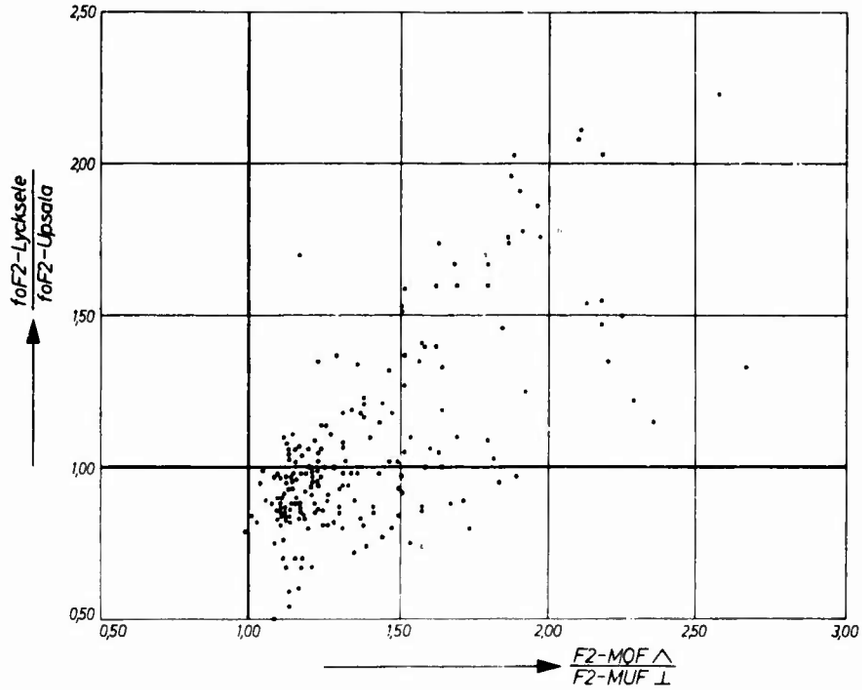

Fig. 3.2 MOF enhancement by electron density gradient. The quotient foF2 Lycksele/foF2 Uppsala versus the observed F2-MOF$_{\wedge}$ divided by the predicted F2-MUF$_{\perp}$.

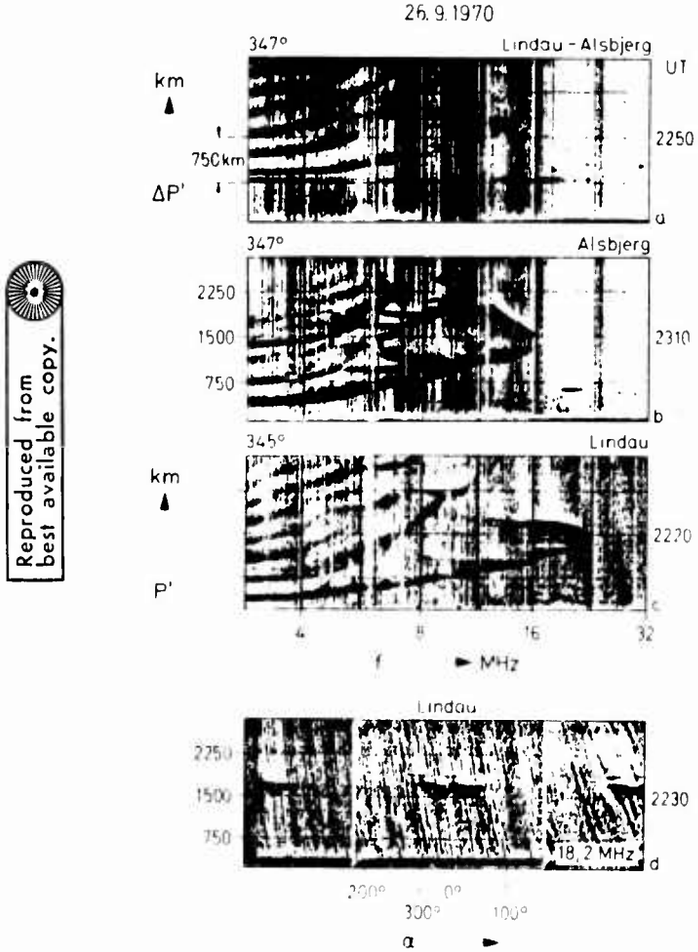

Fig. 3.3 a-c Sweep-frequency backscatter ionograms, range p' versus frequency f.
(a) Bistatic transmitter Lindau, receiver Alsbjerg;
(b) monostatic Alsbjerg;
(c) monostatic Lindau.
d Fixed frequency backscatter with rotatable antenna, range p' versus angle α.

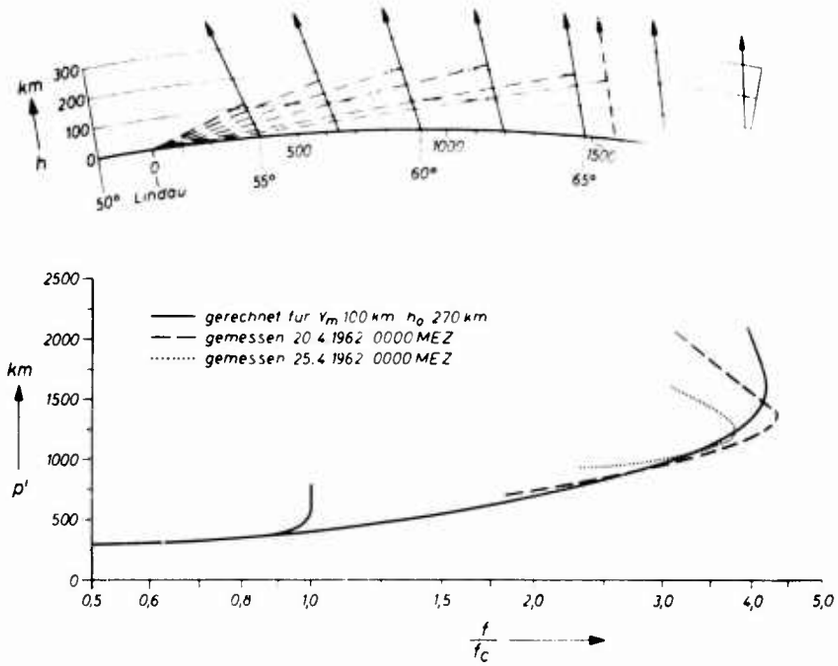

Fig. 3.4 Sweep-frequency backscatter.
Below: Leading edge of the direct scatter from the F region, range p' versus normalized frequency f/fc; p'(f/fc) calculated - solid line; observed leading edges - broken lines.
Above: Cross section of the ionosphere. Radii vectors from the sounding station Lindau (dashed lines) perpendicular to the earth's magnetic field (solid lines).

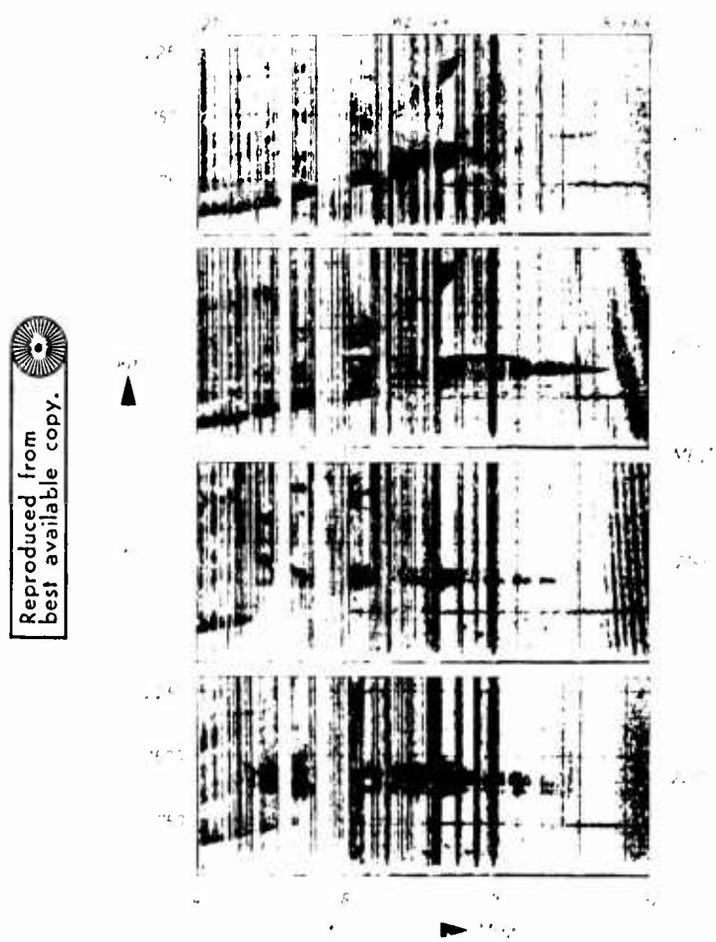

Fig. 3.5 Sweep-frequency backscatter recorded with a pulse extending to 2 MHz at a range of 1000 km.

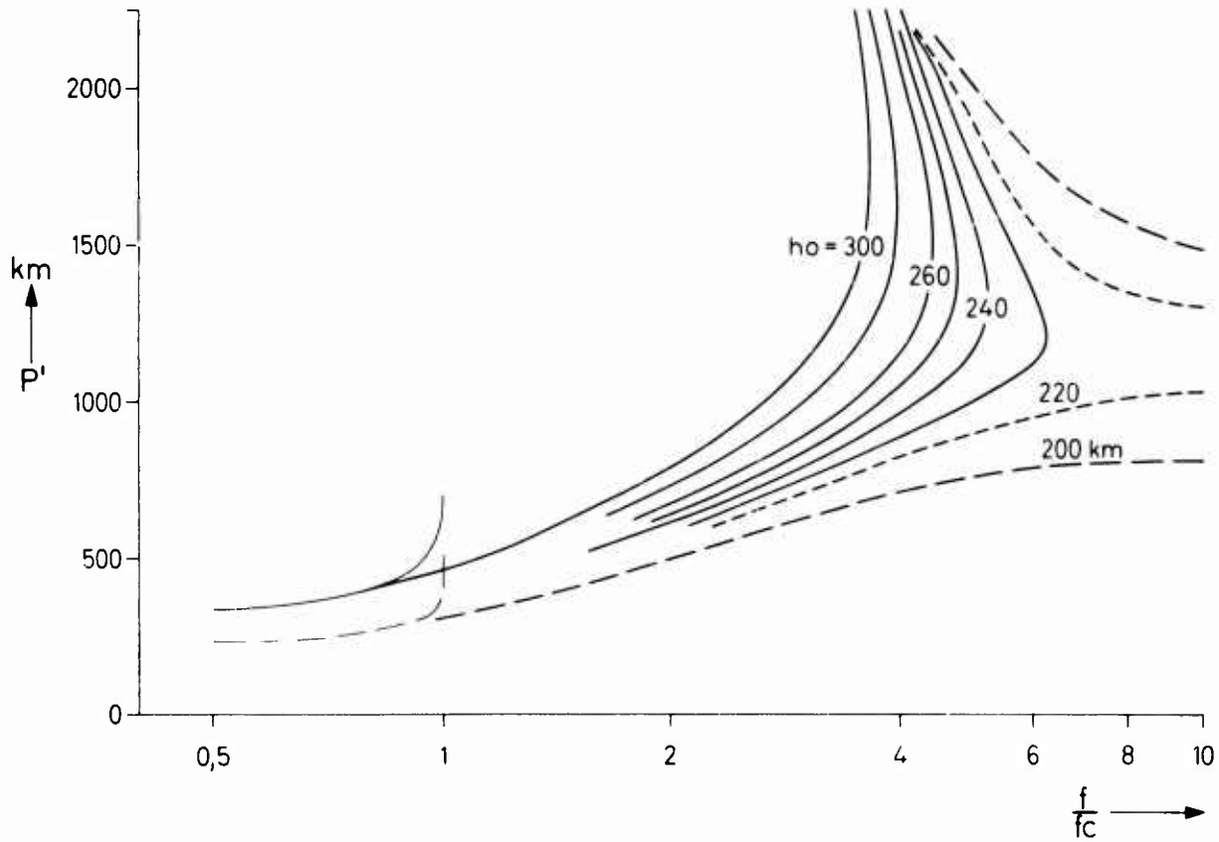

Fig. 3.6 The leading edge of direct F layer, range p' versus normalized frequency f/fc calculated for different heights to the bottom of the F layer ho.

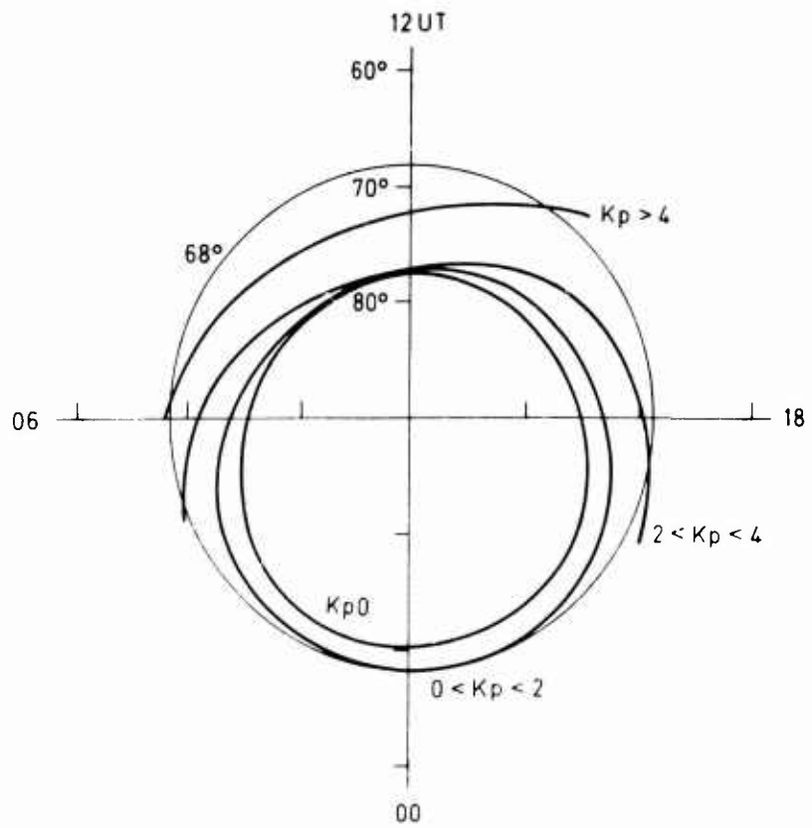

Fig. 3.7 The geomagnetic latitude of the [illegible] as function of time of day plotted for different groups of magnetic activity Kp.

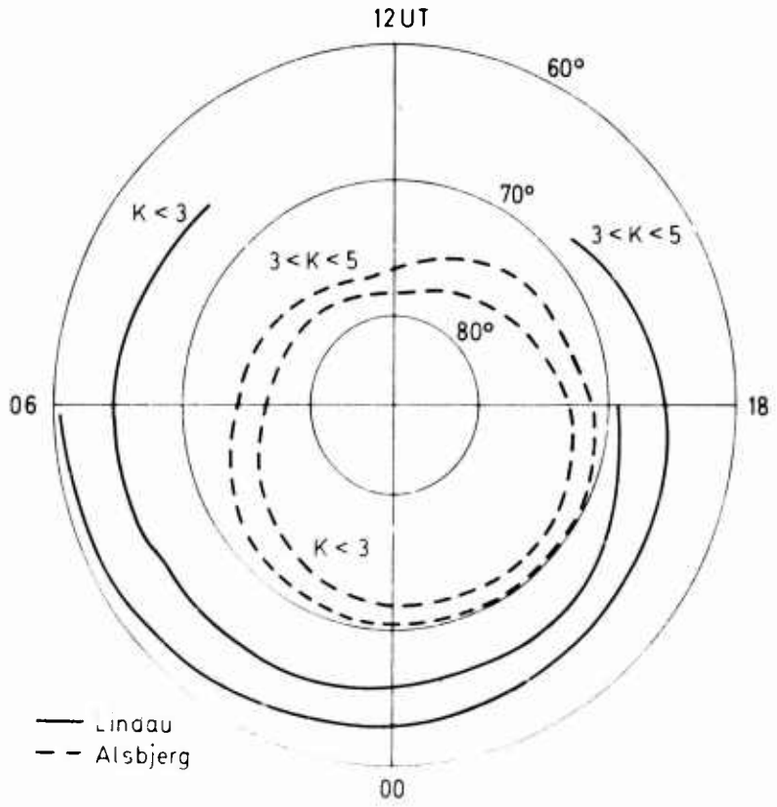

Fig. 3.8 The geomagnetic latitude of a strong scattering curtain as function of time of day for two groups of local magnetic activity K. Direct F scatter observed from Lindau - solid lines; F scatter with intermediate F reflection observed at Alsbjerg - broken lines.

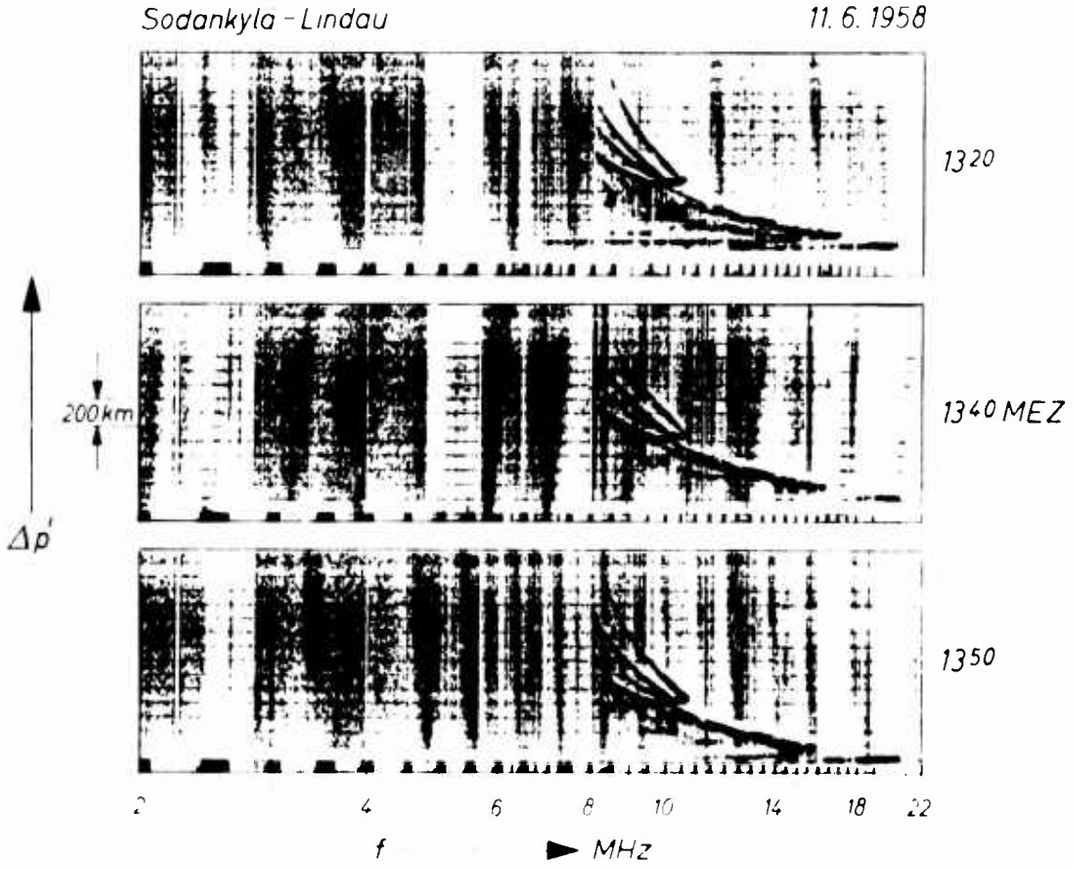

Fig. 3.1 Oblique sweep-frequency ionograms obtained over the 2000 km subauroral path Lindau, Germany, to Sodankyla, North-Finland, showing F1-MOF > F2-MOF.

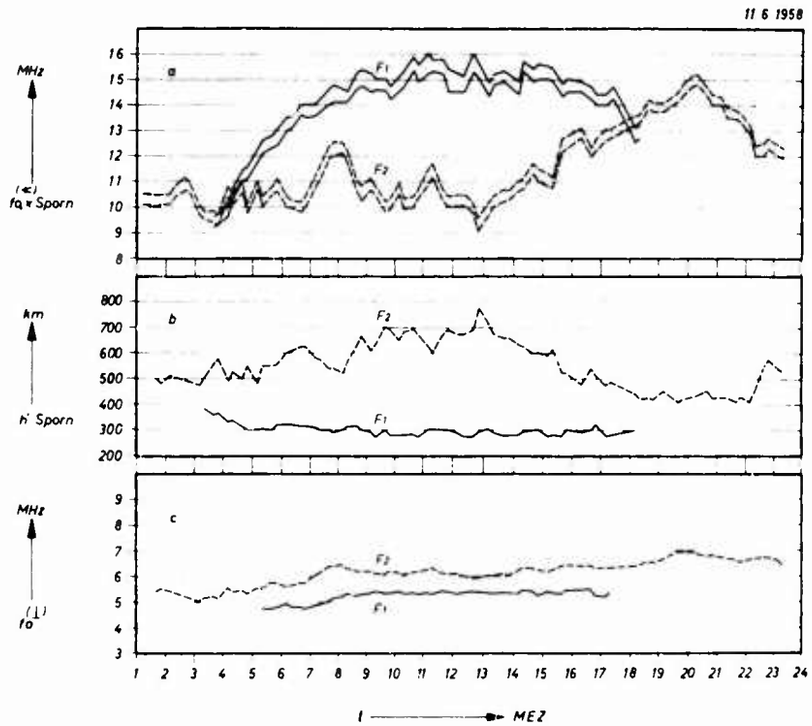

Fig. 6.2 (a) Diurnal variation of the MOF (ordinary and extraordinary component of the junction frequency = $f_{o,x}$ sporn ≪) for F1 layer and F2 layer transmission over the 2000 km subauroral path Sodankylä - Lindau.
(b) Virtual heights of F1 and F2 oblique transmission at the junction point of low and high angle ray.
(c) Critical frequencies at the reflection point as deduced from oblique ionograms.

DISCUSSION

G Gassmann

Being concerned with the mapping of sporadic E the data presented in the above paper are of interest to us. However, there is the question whether the reflector was really an E_S-layer. There is the possibility that a night-E-layer was involved. One can suspect this from the statement that the secant law was found to be valid. From the night-E-layer one would indeed expect that the secant law would not hold for a scatterer such as the auroral sporadic E.

H G Møller

On the sweep frequency oblique ionograms it is not possible to discriminate between different types of E.

A K Katz

Can the height of the scattering irregularity be determined by the leading edge of the SLANT-F-MODE, particularly the portion of the leading edge which shows a decreasing time delay with increasing frequency.

H G Møller

This is possible as long as the scattering irregularities of nearly equal magnitude are uniformly distributed in space or range. If, however, a dense medium with a great scattering cross section is present at a slightly shorter range to the range of interest it is not simple to answer this question.

FREQUENCY DISTORTION IN AURORAL HF PROPAGATION

by

J. B. Lomax
Stanford Research Institute
Menlo Park, California, U.S.A.

SUMMARY

HF propagation in auroral regions results in significantly greater frequency distortion of signals than that encountered at mid-latitudes. This paper presents observational data on the characteristics of this distortion as taken on a transauroral path between Palo Alto, California and Thule, Greenland. Details of the frequency distortion are given in terms of measured power spectral densities, Doppler shifts, and the corresponding phase fluctuations. These quantities are in turn related to the temporal correlation function of the channel.

These data show that Doppler spread is about an order of magnitude greater than at mid-latitudes. The source of such spreading is discussed, as is its relation to time-delay spread. The phase characteristics are explicitly presented, so that implications for coherent systems will be apparent. In particular, the relationship between frequency spread and the correlation coefficient of the complex envelope is demonstrated. Implications of the observed data for auroral HF propagation models and for radar system performance are given. Particular emphasis is given to interpretation of the results in terms of propagation modes and the effects of different ionospheric irregularities on propagation.

1. INTRODUCTION

The broad objective of the high-latitude propagation research program that was the source of the data presented here was to develop the background information and techniques necessary for predicting the performance of HF communications systems in a disturbed environment. The terminals for the field experiment were selected so as to provide diverse propagation paths through the disturbed regions of the ionosphere (see Figure 1). One path was almost entirely within the polar-cap zone but with one terminal near the auroral zone. Two paths traversed the auroral zone, approximately at right angles to it, and half of another path lay within that zone. The fifth propagation path was from Alaska to California; one terminal was at a high latitude and near the auroral zone, but most of the path was relatively free of disturbance. Finally, a mid-latitude path was used for control.

Oblique HF/VHF ionospheric sounders were used to measure the propagation characteristics in the time domain of these paths. Data were obtained every 20 minutes for a period of one year and subsequently analyzed. The focal point of the analysis of these data was the identification of all the modes that propagated. In addition, phase-stable CW transmitters and receivers were employed on the transauroral path from Thule to Palo Alto and on the mid-latitude path, to measure the propagation characteristics of these paths in the frequency domain. These two sets of measurements define the signal dispersion in time and frequency.

The phase-stable transmitter at Thule, Greenland operated at a frequency of 7.366 MHz with a nominal power output of 4 kW. For the 5050-km path from Thule to Palo Alto, California, considering the antenna gains but with no ionospheric losses, the maximum received signal power is calculated to be -97 dBW. For ray paths at low elevation angles--the usual situation--additional loss of 10 to 30 dB may be expected due to reduced gain of the antennas. The RF bandwidth of the phase-stable receiver was 200 Hz, and the post-detection bandwidth was 50 Hz. Both the amplitude and the phase of the received signal were measured. These data were then converted to digital form to facilitate further data processing on a large computer.

Results of this experiment have been reported previously.[1,2,3] This paper presents some results of further analysis of the Thule-Palo Alto path, with emphasis on their interpretation.

2. WINTER OBSERVATIONS

2.1 Propagation Conditions

During the winter months, HF propagation was observed on the Palo Alto to Thule path only 50 percent of the time at night and about 75 percent of the time during mid-latitude daylight hours. Most of the outage time occurred during the eight hours after midpath local midnight. The measurements were made on the oblique ionosonde records, which have a basic sensitivity of about 1 μV; however, received noise and interference usually degraded this sensitivity by 10 to as much as 30 dB. The term "outage" is therefore quantitatively imprecise; it only indicates that the received sounder signal level was below an imperfectly known sensitivity threshold.

The primary propagation mode was two-hop F. The path length was too long (5050 km) for one-hop F, although a Pederson ray was occasionally seen. Polar-cap critical frequencies are generally much lower than the critical frequencies at mid-latitudes, particularly during the winter; the median maximum observed frequency (MOF) was 9 MHz during the late night hours. Further, the height of the polar F layer is low, so the first F hop is shorter than the second mid-latitude hop. The location of the ground reflection point seems to be a crucial factor in the performance of this 2F propagation mode. It is in the vicinity of the auroral zone and as the auroral zone moves north and south in response to the diurnal solar forces and to particle precipitation activity, the absorption region associated with the auroral zone moves to the D-region penetration points on one side or the other of this ground reflection point. Since the virtual heights of the F-layer reflection points, both in the polar-cap region and at the mid-latitude reflection point, change with time, one is unable to predict the interaction taking place with any degree of accuracy. It is believed, however, that auroral-zone absorption is the primary cause of the observed propagation outages.

In addition to the two-hop F mode, various modes associated with sporadic-E layers are observed almost as frequently. During the winter months, occurrence of sporadic E in the polar-cap region and at mid-latitudes has a high probability. Hence, propagation via two or three E hops or one E and one F hop is also highly probable. As with the 2F mode, auroral-zone absorption appears to be a controlling factor for E_s-associated modes.

2.2 Ionospheric Modes with Time-Delay Spread

Most of the time the ionospheric modes have time-delay spread. Little frequency spread is observed. While the amount of frequency spread is comparable to that observed at mid-latitudes, a few tenths hertz, the time delay spread is of the order of 100 to 200 μs. This is more than can be reasonably attributed to scattering at the ground reflection point. It appears likely that ionization irregularities are responsible for the spreading of these modes. The questions are: At what altitude do the irregularities occur and what is their magnitude and type? It is the author's opinion that for the Thule-Palo Alto path the dominant mechanism is similar to that observed as spread F on vertical-incidence sounders. The ionization irregularities are overdense and spatially extensive compared to the wavelength of the probing radio frequencies. They are observed to exist nearly 100 percent of the time in the polar-cap ionospheric F region. The lower side of the polar F layer therefore appears as a rough surface to oblique radio waves, leading to small variation in propagation time.

The small amount of observed spread on identifiable propagating modes suggests that the F-region reflection is not dependent on the magnetic alignment of the ionization. If the reflection were dependent on field alignment of the ionization, then, since spread F is found within the entire polar-cap region most of the time during the winter, frequent deflections of the ray path at points far from the great-circle path would also be expected. Signals arriving over such paths would have time delays up to several milliseconds greater than those arriving by great-circle propagation. Although such signals are observed, and are discussed below, they appear to be separable from the spread "normal" ionospheric modes under discussion.

The normal ionospheric modes identified on oblique ionograms by their characteristic time delays and delay variations with frequency have been verified by ray tracing, using true-height profiles obtained from simultaneous vertical-incidence ionosonde records. Further, while these modes are usually spread on the oblique ionograms, which sometimes makes identification difficult, they stand out uniquely in the power spectrum of the received CW signal. Hence, we are convinced that in transauroral and polar HF propagation one can identify and predict the normal ionospheric modes of propagation. These modes are usually spread in time, but have Doppler shifts that are only a few tenths of a hertz. This same Doppler profile is observable on undisturbed mid-latitude paths.

Prediction of path loss for these ionospheric modes does not appear to be possible now. When the D-region (and lower E-region) penetration points of the various ray paths are in the auroral zone, large losses may occur. However, prediction of the location of these penetration points with respect to the auroral zone appears to be beyond the present state of the art. On the other hand, when one or more ray paths do not suffer auroral-zone absorption, prediction of signal strength is possible; uncertainty in the amount of polar-cap absorption, of course, reduces prediction accuracy.

2.3 Off-Path Propagation Modes

The preceding discussion has been concerned with nominally identifiable ionospheric propagation modes along (or nearly so) a great-circle path. Another mode, often the dominant mode of propagation, has also been observed: propagation primarily off the great-circle path. It is characterized by large time-delay spread, up to several milliseconds, and large Doppler spread, often greater than one part in 10^6. The range of propagating frequencies for these off-path modes is typically less than that for the great-circle modes. We hypothesize that these off-path modes are the result of deflections of ray paths by over-dense field-aligned ionization.

A computer simulation program has been developed to test this hypothesis. This simulation program assumes that an oblique propagation path is composed of two great-circle paths, one from the transmitter to the location of a column of field-aligned ionization, and the second from the presumed deflection point to the receiver. The scattering of the incident radio wave by the field-aligned ionization is characterized by a cone of reflected ray paths, with the axis of the cone along the magnetic field line and with a cone half-angle equal to the angle between the incident wave and the field line (see Figure 2). In other words, a high degree of aspect sensitivity is assumed. The computer program searches for deflection point locations and heights at which one of the reflected ray paths will propagate to the receiver via a normal ionospheric mode. Virtual ionospheric reflection heights appropriate to the geographic location and time of day were employed on the two great-circle paths.

For the Thule-Palo Alto path, only one mode was found that would satisfy the above conditions. It was basically a two-hop F mode, with the deflection occurring on the ray path between the ground reflection point and the polar F1-reflection region. Figure 3 illustrates the locus of points at which the deflection angles are appropriate to allow normal great-circle propagation, both from the transmitter to the deflection point, and, after an equiangular deflection, from the deflection point to the receiver. The mid-latitude F2-region virtual height used in these calculations was 225 km, while the polar F1-region virtual height was 205 km. Three deflection altitudes are shown in Figure 3. If we view the locus of deflection points between 100 and 200 km as a surface, the surface area shown is about 800,000 km^2.

This figure only indicates that, if field-aligned ionization exists at any point on that surface, then propagation is possible, provided that the deflection is indeed equiangular. It does not provide a basis for comparison with the experimental data. Therefore we extended the calculations to obtain an estimate of the probability density of time-delay spread for off-path propagation. It was assumed that the occurrence of field-aligned ionization in space is statistically random and equally probable over the surface being considered. It was further assumed that the probability of occurrence is sufficiently small that there is a finite probability of field-aligned ionization not existing anywhere in that area. To match the experimental data, the joint probability of nonoccurrence of a path delay greater than τ_2 and of occurrence of a path delay greater

than τ_1, where $\tau_2-\tau_1$ = 200 μs, was calculated and normalized to obtain a cumulative probability of occurrence of unity. The results are given in Figure 4 with the experimental observations. The experimental observations are contaminated to some extent by the interval from 0 to 200 μs, because it was not always possible to distinguish between slightly spread great-circle modes and off-path modes. Even so, the agreement is quite good.

Continuing to use the same off-path model, we can also estimate the power spectrum of a received signal. Assuming that each deflection point is moving with a constant velocity, but with a direction that is randomly distributed over 2π radians, the spectral estimate in Figure 5 is obtained for a velocity of 200 m/s. This does not compare very favorably with a measured spectrum having a similar Doppler range, shown in Figure 6. One should, of course, use some range of velocities and average over the velocity spectrum. The experimental data on the spatial motion of discrete ionization irregularities does not appear to be sufficient for selection of a realistic velocity spectrum.

Some attempts were also made to investigate the fine structure of the measured spectra. Spectral estimates of consecutive 1-minute intervals were compared, and no correlation was found in the location of the fine-scale peaks from one minute to the next. Next, we examined 10-second intervals of data. The resolution of the spectral estimate was thereby reduced from 0.025 to 0.15 Hz, reducing the sharpness of detail. By calculating spectral estimates every 5 seconds, but for 10 seconds of data, we could examine the variation in fine structure in time intervals of the order of 10 seconds. There was no apparent correlation in the magnitude of power received as a function of time in one frequency increment as compared with that received in an adjacent or any distant frequency increment. However, one might infer that in a given frequency interval the power level fluctuated in time like a series of widely spaced random exponentials, the power suddenly jumping to some level and then decaying with a time constant until the next jump in level occurred. If these were indeed exponential decays of signal strength, time constants of 10 to 30 seconds were observed. Although these observations cannot withstand rigorous scientific scrutiny, they should not be completely ignored.

The short-term amplitude variations and the high Doppler shifts in the CW data would appear to rule out F-region irregularities as the primary cause of the off-path propagation. F-region ionization is lasting and appears to have smaller velocities than is required for consistency with the measured data. Proton precipitation into the polar-cap area could, however, lead to field-aligned ionization forms in the upper D region and the E region that have the required characteristics. Proton precipitation does occur with a degree of randomness within the polar-cap area; it should result in high ionization levels along a field line from the E region down to about 60 km. The subsequent decay of ionization will be rapid, with a fall of one to three orders of magnitude within 1 to 10 seconds, depending on altitude and the electron density enhancement.

2.4 Summary of Winter Data

Two types of propagation have been described: "normal" ionospheric modes, and off-path propagation. During the winter, off-path propagation was clearly dominant over ionospheric modes in the spectral estimates. Of 20 representative data sets analyzed in detail, only one case was found without off-path propagation. The received signal level was -105 dBW; the time spread was about 100 μs; and the Doppler spread was 0.8 Hz. Figure 7 shows the power spectral estimate of the CW signal, cumulative probability distributions of phase change for five different time intervals, the probability density distributions of amplitude change for the same five time intervals, and the envelope distribution. It also shows the oblique ionosonde record. The vertical dimension of the ionogram is time (9 ms total), while the horizontal dimension is frequency. The total frequency scale is four octaves, 4 MHz to 64 MHz, with the scale being linear within each octave. Note that only one propagating ionospheric mode with a slight degree of time spreading can be seen on the ionogram, while the spectral estimate indicates that several ionospheric modes exist. Three data sets contained both ionospheric modes and off-path propagation. The received power in the off-path modes was about -112 dBW, while the level of the ionospheric modes was -120 dBW. The Doppler spread of the received signals was about 3 Hz and the time-delay spread about 1.2 ms. The spectral estimate labeled 2/11/64, 1410Z, in Figure 8 is for one of these three data sets. The other three spectral estimates in that figure illustrate the other 16 data sets in which no clear ionospheric modes could be detected. For these data, the median received power was -110 dBW; the median Doppler spread was 6 Hz; and the median time-delay spread was 1.2 ms. An additional 100 winter data sets were also analyzed to obtain received signal level distributions. The median was -115 dBW, with 90 percent of the data being within ±10 dB of the median.

3. SUMMER OBSERVATIONS

During the summer months, two-hop F and two- and three-hop E modes were the dominant ionospheric modes on the Thule-Palo Alto path. Propagation outage was much less in the summer months, being about 25 percent for all times of the day. (Recall that the outages observed could have resulted from increases in the local received noise level.) In contrast to the winter data, most of the summer data showed ionospheric propagation modes dominating over the off-path modes. For 30 sets of selected typical summer data, only three cases were found in which clear ionospheric modes could not be detected because the off-path modes were stronger. In ten of the data sets, no off-path modes could be detected, and the time and frequency spreads were quite low and similar to those of mid-latitude propagation. In the other sets, both off-path and "normal" ionospheric modes were found, but the power level in the off-path modes was typically 10 dB below that of the ionospheric modes. Representative samples of these data are given in Figure 9. Note that even though the off-path power is spread over about 20 Hz, the power density is so low that the total off-path power is only one-tenth of the power in the ionospheric modes that occupy less than 0.5 Hz. Nighttime received signal level data were analyzed for 150 5-minute intervals. The median signal level was -106 dBW, with 80 percent of the data being within ±5 dB of the median and 97 percent of the data within ±10 dB.

4. PROPAGATION MODEL

From the experimental measurements of propagation through the auroral zone and into the polar-cap area, it is believed that a realistic propagation model has been found. This model may be useful to the HF radar or communication system designer in setting bounds on the design of the modulation and signal processing employed. The dispersive effects of HF propagation will be accounted for by a channel scattering function,

$S(\lambda, \tau)$. This function allows for dispersion of signal power in both the frequency and time domains. Frequency spread and time spread are measures of the dispersiveness of the propagation channel. They are defined as follows:

$$\text{Frequency spread} \triangleq 2\sigma_\lambda = 2\left[\int_{-\infty}^{\infty} (\lambda-\bar{\lambda})^2 S(\lambda,\tau)d\lambda\right]^{\frac{1}{2}}$$

$$\text{Time spread} \quad \triangleq 2\sigma_\tau = 2\left[\int_{-\infty}^{\infty} (\tau-\bar{\tau})^2 S(\lambda,\tau)d\tau\right]^{\frac{1}{2}} .$$

We have previously shown[2] that modeling HF propagation as a Gaussian random process provides an acceptable description of the actual channel. Both the first- and the second-order statistical properties of the Gaussian channel model have been shown to agree with experimental data.

For propagation through the auroral zone it appears that two simultaneous propagation channels must be considered. The normal ionospheric modes constitute one channel and the off-path modes the second. The path loss of the ionospheric model may be predicted by using standard techniques, but large inaccuracies are to be expected because auroral-zone absorption is unpredictable. The time spread of low-order ionospheric modes (one- and two-hop) will be small, typically less than 100 μs. When several modes are propagating simultaneously on the same frequency, one must also consider their relative amplitudes and differences in time delay in evaluating the time spread of the channel. The frequency spread of a single ionospheric mode will be on the order of 0.1 Hz, with spreads seldom exceeding 0.5 Hz for multiple modes. For the off-path channel, no means of predicting the received signal power is known. Designers will have to rely on experimental observations to estimate this power. Our equipment employed very wide antenna beams, so the maximum possible off-path signals were received. Time spreads of 1 to 2 ms and frequency spreads of 5 to 10 Hz (for $f_o \approx 7$ MHz) were typical for our channel. Caution should be exercised in applying these dispersion parameters to other propagation paths and systems. Narrow antenna beams will discriminate against the far-off-path signals, hence reducing both time and frequency dispersion. The geometric relationship of the path with respect to aspect-sensitive reflections from field-aligned ionization must also be examined to determine whether off-path modes are possible.

When the time- and frequency-dispersion parameters are known (or have been estimated), one can calculate other parameters of the received signals. For example, if the transmitted signal is CW (or a very long pulse), then the time autocorrelation function of the channel, $\rho(t)$ is the inverse Fourier transform of the power spectrum of the received signal, $S(\lambda)$ (the Doppler profile),

$$\rho(t) = \int_{-\infty}^{\infty} S(\lambda)e^{i2\pi\lambda t}\, d\lambda ,$$

which for a normally distributed Doppler profile reduces to

$$\rho(t) = \exp\left[-\tfrac{1}{2}(2\pi)^2\sigma_\lambda{}^2 t^2\right] .$$

For values of the correlation coefficient greater than about 0.8, this equation is a good approximation for a wide variety of Doppler profiles. Our data fit this equation for correlation coefficients greater than 0.5, the lower limit of our analysis.

For analysis of coherent communication or radar systems, it is useful to know the second-order statistical characteristics of the channel. The cumulative probability distribution of phase change is given in Figure 10 for a family of values of $|\rho|$. Figure 11 shows the probability density functions of envelope (amplitude) change for a similar family of values of $|\rho|$. Figure 12 illustrates the comparison of data with one of the theoretical curves of phase change. Two independent estimates of the magnitude of the correlation coefficient of the received CW signal were made from plots of the phase-change distribution and of the log-envelope-change density. These estimates were compared for 98 5-minute periods of data. The agreement was generally quite good, strengthening our confidence in the correlation coefficient estimate of the received signal.

5. CONCLUSIONS

First- and second-order statistical properties of HF signals received over arctic propagation paths are consistent with the theoretical properties of a Gaussian channel model.

Ionospheric propagation via (nearly) great-circle paths will have time and frequency dispersion comparable to mid-latitude propagation. Individual propagation modes may have time spread of 100 to 200 μs as a result of the polar F layer appearing to have a rough reflecting surface. Significant radio wave absorption is experienced by ray paths having D-region intercepts in the auroral zone.

Off-path propagation is the result of equiangular deflection of radio waves by field-aligned ionization occurring at altitudes near 100 km and at random times and locations within the polar cap zone. The magnitudes of the resulting time and frequency dispersion are highly correlated and may be estimated from knowledge of the path geometry and the geomagnetic field. Signal energy received via off-path propagation may be minimized by reduction of the azimuthal beamwidths of the transmitting and receiving antennas.

REFERENCES

1. J. B. Lomax, "HF Propagation Dispersion," in Phase and Frequency Instabilities in Electromagnetic-Wave Propagation, K. Davies, editor, pp. 497-510, AGARD Conference Proceedings, Number Thirty-Three, Technivision Services, Slough, England, 1970.

2. H. N. Shaver, B. C. Tupper, and J. B. Lomax, "Evaluation of a Gaussian HF Channel Model," IEEE Transactions on Communication Technology, Vol. 15, No. 1, pp. 79-88, February 1967.

3. R. A. Shepherd and J. B. Lomax, "Frequency Spread in Ionospheric Radio Propagation," IEEE Transactions on Communication Technology, Vol. 15, No. 2, pp. 268-275, April 1967.

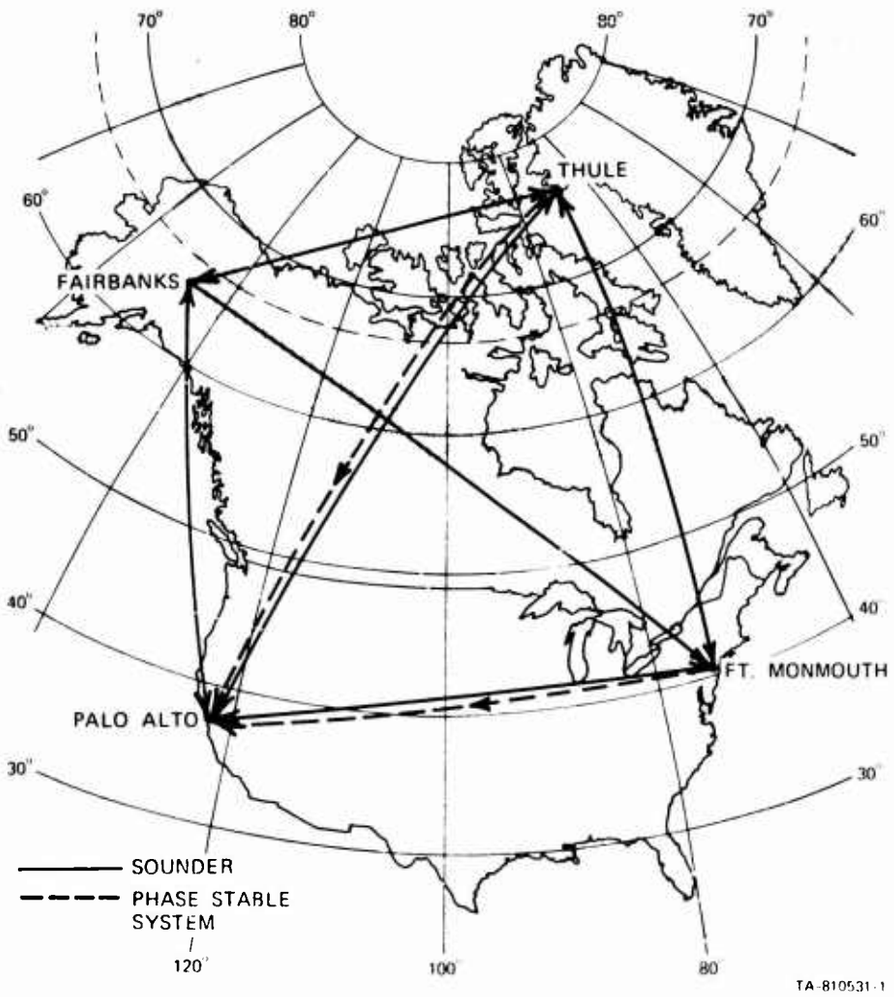

FIGURE 1 MAP OF THE HIGH-LATITUDE PROPAGATION EXPERIMENT

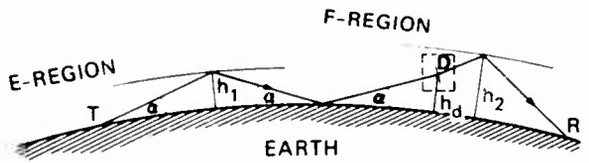

T = TRANSMITTER LOCATION
R = RECEIVER LOCATION
D = DEFLECTION POINT

(a) SIDE VIEW

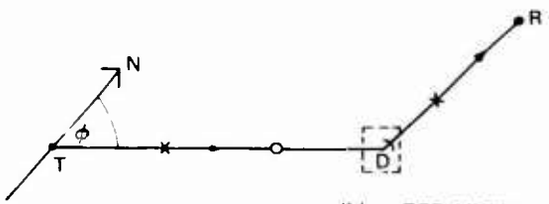

O = GROUND REFLECTION POINT
X = IONOSPHERIC REFLECTION POINT

(b) TOP VIEW

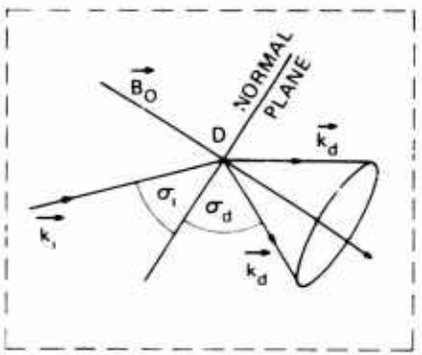

$\vec{B_O}$ = MAGNETIC-FIELD VECTOR
$\vec{k_i}$ = INCIDENT WAVE NORMAL
$\vec{k_d}$ = REFLECTED WAVE NORMAL
σ_i = INCIDENT ANGLE
σ_d = DEFLECTION ANGLE

(c) DEFLECTION REGION (Enlargement)

TA-810531-2

FIGURE 2 INDIRECT-MODE GEOMETRY

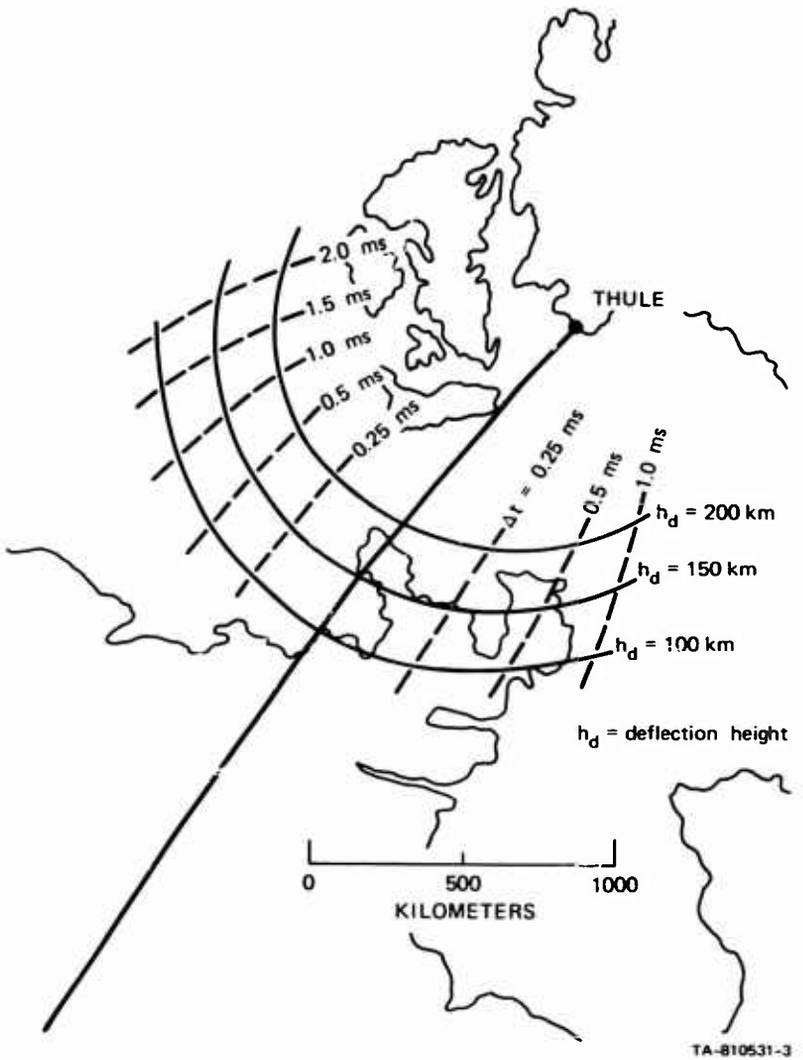

TA-810531-3

FIGURE 3 LOCI OF EQUIANGULAR DEFLECTION POINTS

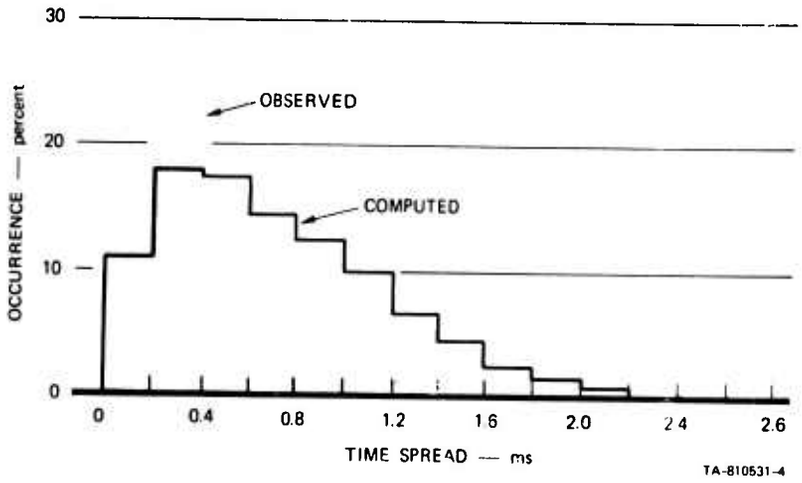

FIGURE 4 TIME SPREAD COMPARISON

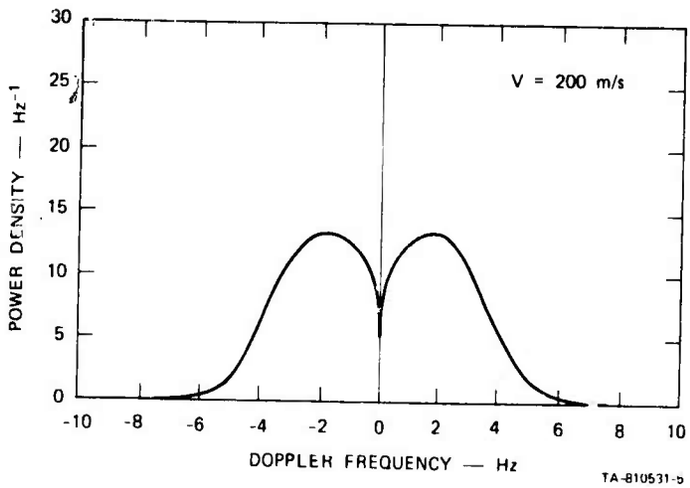

FIGURE 5 COMPUTED DOPPLER PROFILE

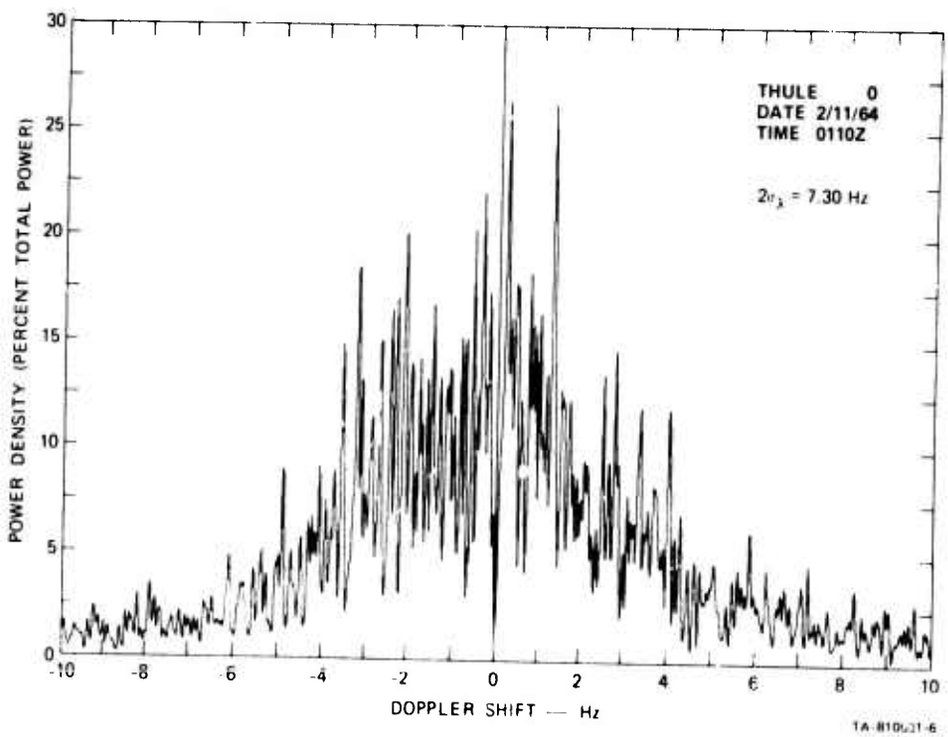

FIGURE 6 POWER SPECTRUM

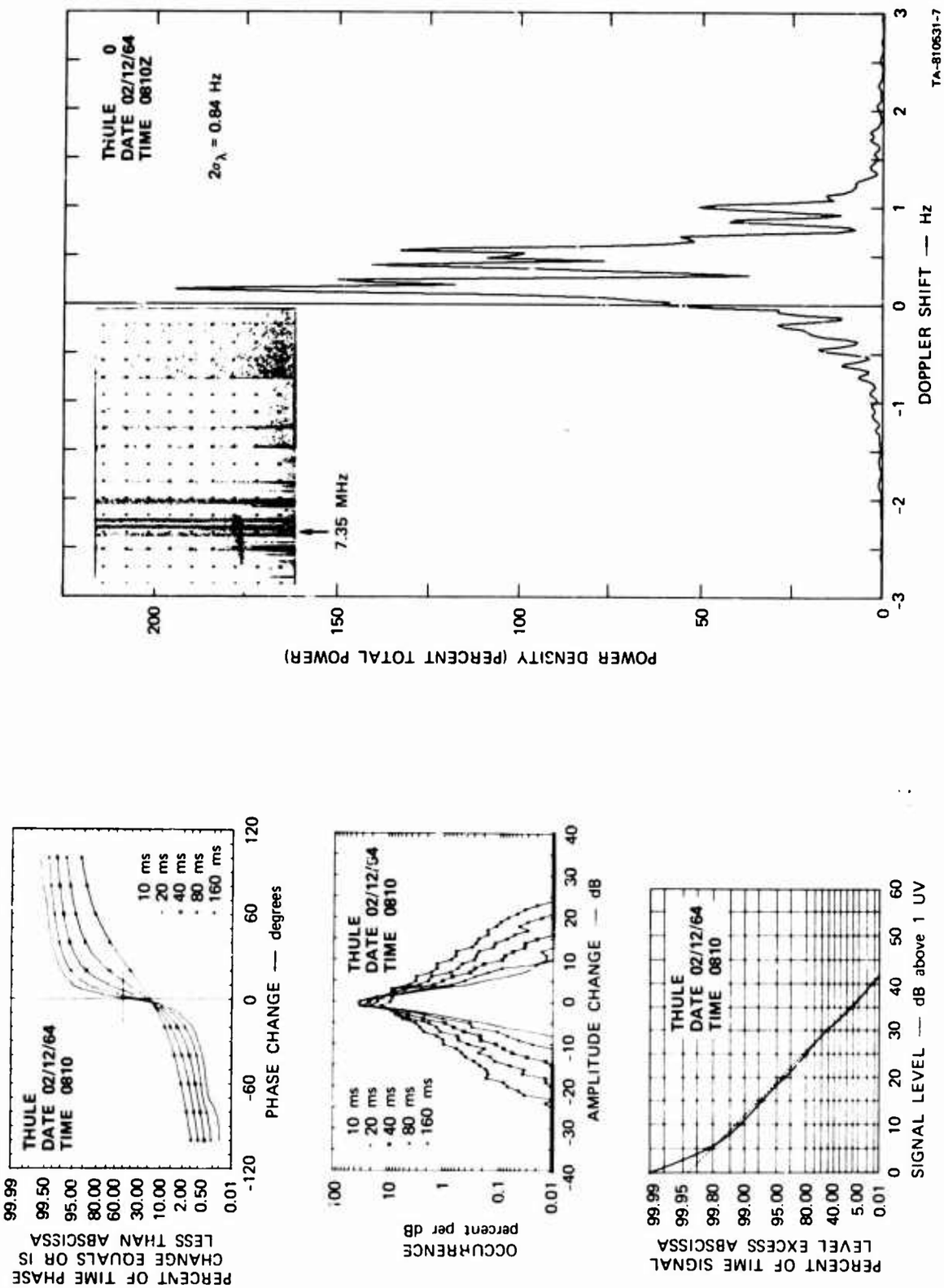

FIGURE 7 ATYPICAL WINTER PROPAGATION (No Off-Path Modes)

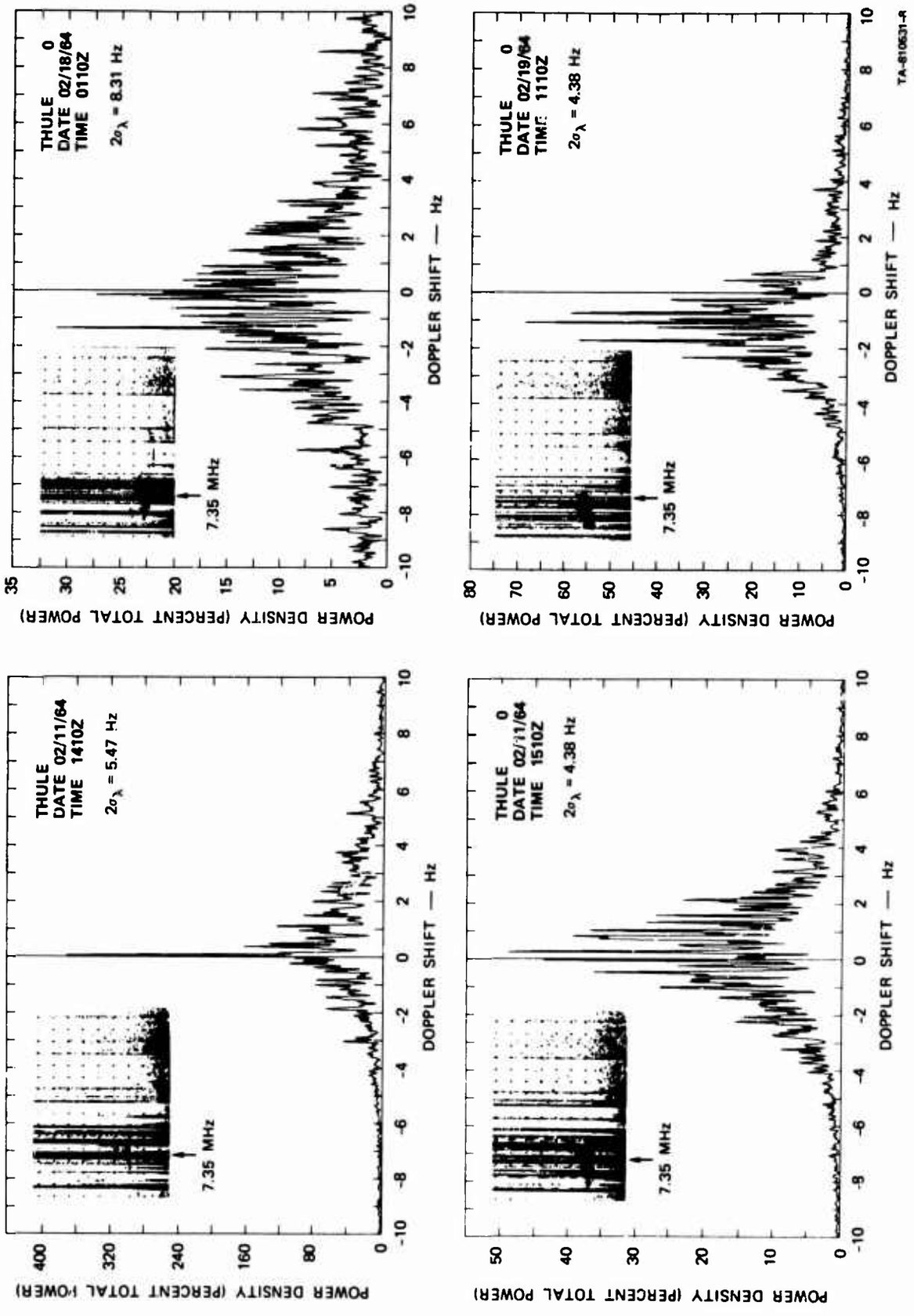

FIGURE 8 THULE-PALO ALTO WINTER DATA, POWER SPECTRA AND OBLIQUE IONOGRAMS

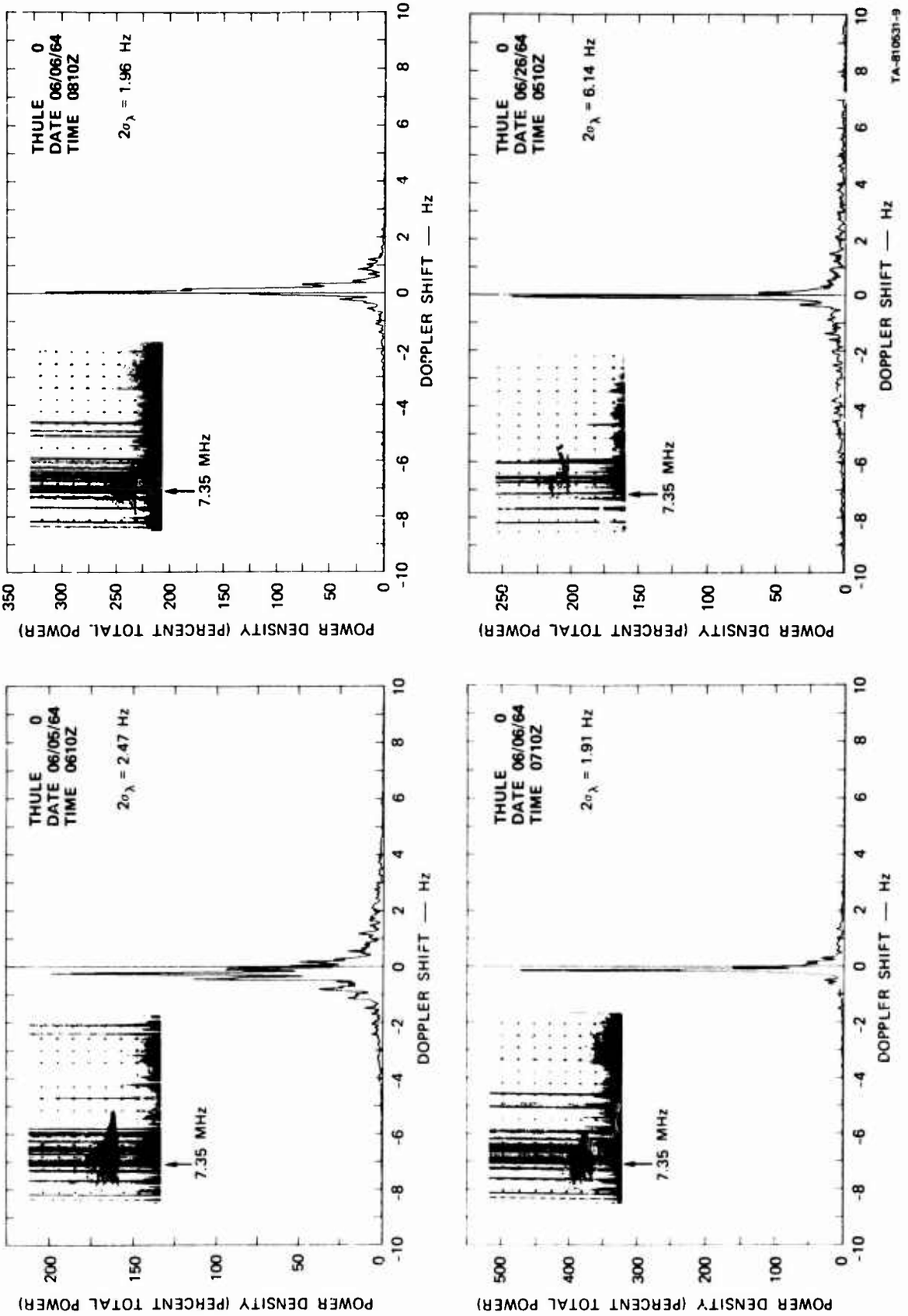

FIGURE 9 THULE-PALO ALTO SUMMER DATA, POWER SPECTRA AND OBLIQUE IONOGRAMS

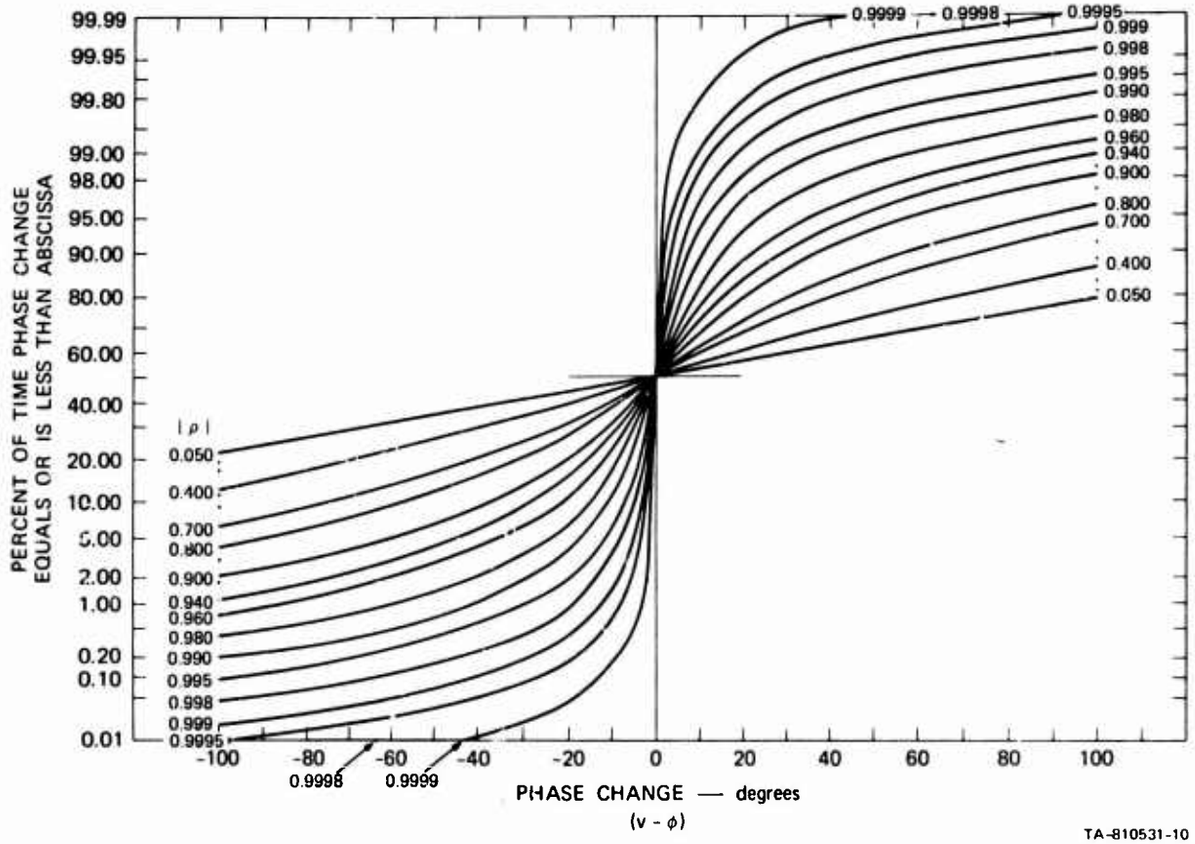

FIGURE 10 THEORETICAL PROBABILITY DISTRIBUTION OF PHASE-CHANGE MODULO 2π FOR SEVERAL VALUES OF CORRELATION, $|\rho|$, OF THE ORIGINAL PROCESS

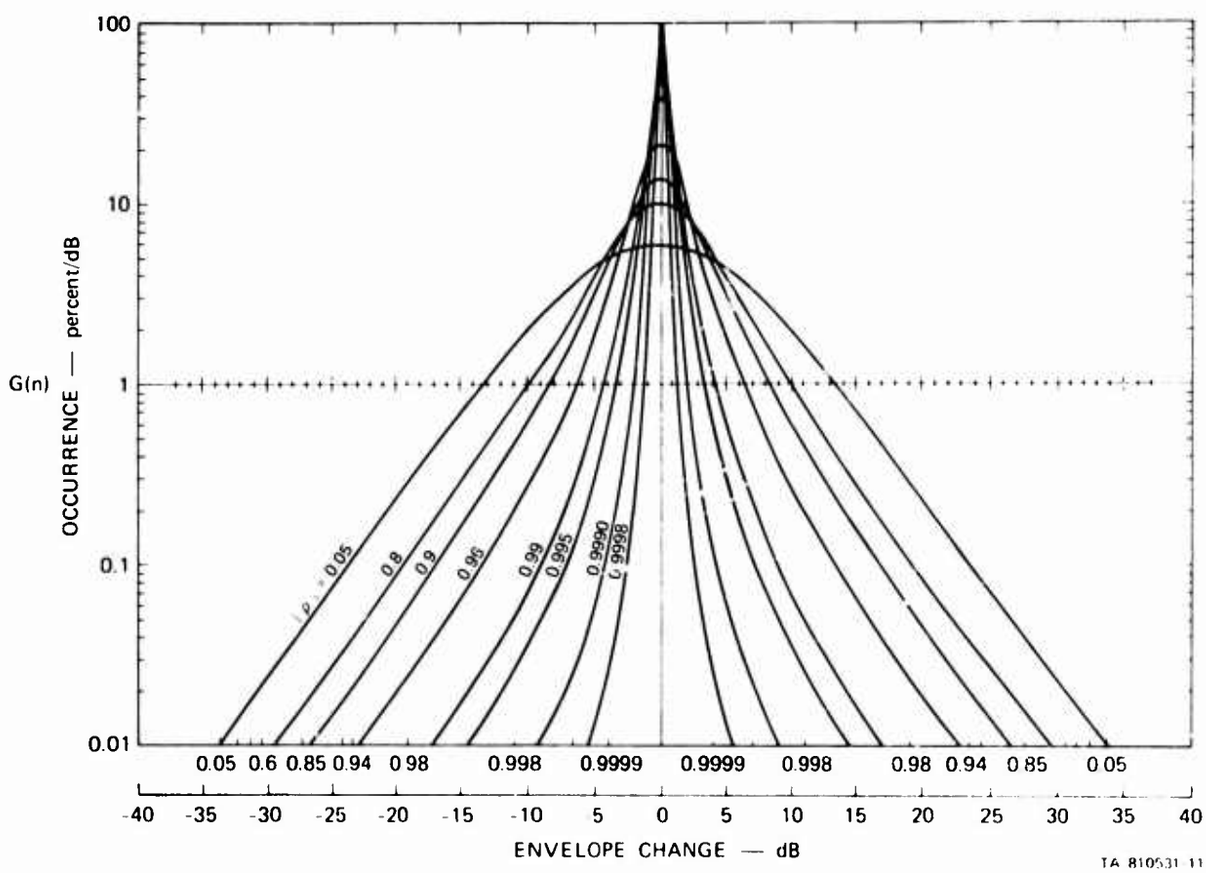

FIGURE 11 THEORETICAL ENVELOPE CHANGE CHARACTERISTICS WITH $|\rho|$ AS A PARAMETER

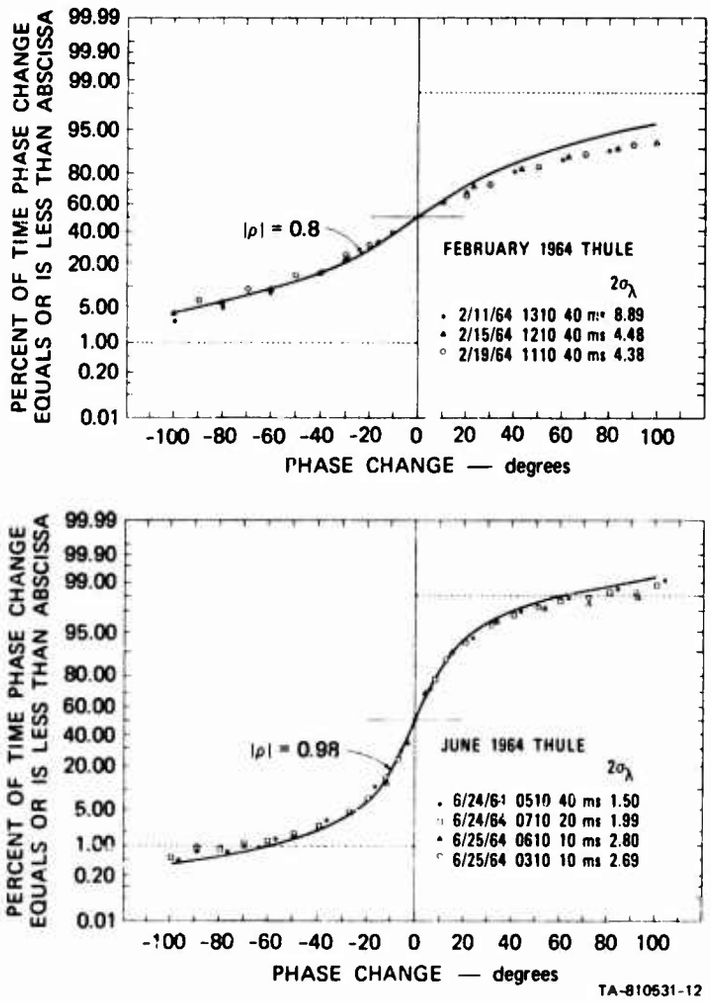

FIGURE 12 COMPARISON OF EXPERIMENTAL PHASE-CHANGE DATA WITH THEORETICAL CORRELATION COEFFICIENT

HIGH-LATITUDE HF SIGNAL TRANSMISSION CHARACTERISTICS

R. A. Mather
Rome Air Development Center
Griffiss Air Force Base, New York

B. L. Holtzclaw and R. W. Swanson
General Electric Company
Syracuse, New York

SUMMARY

Measurements made on HF sky wave signals propagated over two high-latitude 2000 nmi paths terminating at a receiving site in Central New York State are presented. Signal characteristics determined include propagation loss, spectral spreading, and temporal spreading as a function of signal bandwidth (either 7.7 kHz or 100 kHz). The transmitting sites were located at Thule, Greenland and Keflavik, Iceland so that HF propagation information could be collected on a path that was both in the polar cap region and in midlatitude, and on one that passes along and through the outer edge of the auroral oval. Oblique soundings were conducted over each path so that the mode(s) of propagation for the signal(s) measured could be determined. Analyses of the results obtained indicated that the spectral and temporal spreading are a very strong function of the mode of propagation, especially for signals transmitted over the Thule path. The data are depicted as a function of time of day to illustrate the diurnal variation of the parameters considered. In addition, the experimental results are compared with the planetary magnetic index (K_p) and the North Atlantic Radio Path Quality Figure. The reported effort was sponsored by the U. S. Air Force Rome Air Development Center.

1. INTRODUCTION

Signal characteristics obtained from summer measurements near the peak of the 20th sunspot cycle, over two-long northern HF paths, are presented. The objective of the program was to obtain improved descriptions of various signal parameters for HF propagation in the auroral/polar cap region. After describing the experimental path configuration and the equipment employed, the experimental results for propagation loss, spectral spreading and temporal spreading are discussed. Emphasis is made on their dependence on mode of propagation and signal bandwidth. Included are examples of various signal characteristics as observed. Next, the outcome of an investigation of the relationship between the measurement data and the value of K_p is presented as well as with the North Atlantic Quality Figure. Conclusions from the measurements made indicate that the resulting values of signal characteristics are a function of signal bandwidth and mode of propagation. Two appendices are included describing the data processing and data reduction procedures employed to analyze the data collected.

2. EXPERIMENTAL CONFIGURATION

2.1 Measurement Paths

To obtain the HF experimental summer measurements presented in this document, two remote transmitting sites located approximately 2000 nmi from the receiving site at the Rome Air Development Center (RADC) Starr Hill Test Annex, near Rome, New York were utilized. The remote transmitting site at Thule, Greenland was employed to obtain data on HF signals that pass directly through the auroral oval. The use of the remote site at Keflavik, Iceland permitted a more detailed study of propagation conditions along and through the outer edge of the auroral oval. Figure 1 shows these two HF paths plotted on a map employing geomagnetic coordinates in order to indicate more clearly the location of these paths with respect to the earth's magnetic field.

Table I presents the geographical coordinates for the sites employed, a tabulation of range and bearing values between the sites, and also the coordinates for the path midpoints.

2.2 Equipment Description

A block diagram of the experimental complex employed to obtain the measurements presented in this paper is shown in Figure 2. Located at each remote site were the following major equipment items:

- Granger Associates step-frequency sounder transmitter
- Fixed-frequency coded-pulse transmitter
- Loran-C receiver
- LPV antenna

The sounder transmitter was used in conjunction with a sounder receiver at the Starr Hill site to generate oblique ionograms covering the frequency range 4 to 64 MHz. These ionograms served as the basis for selecting in real time the operating frequency for the coded-pulse waveform transmissions, and also were employed in the data reduction process to identify the actual mode(s) of propagation for the fixed-frequency transmissions.

The fixed-frequency transmitter utilized a phase-coded (Barker) pulse compression scheme, with either a 10- or 130-μs resolution capability. The time-stretched pulse for either resolution was 1.69 ms. At the transmitter sites, the 1.69-ms pulse width signal was sampled using a directional coupler just before radiation, so that the transmitted power could be measured, and the start of the transmitted waveform set with respect to absolute time using the site time reference established with Loran-C transmissions.

The measurement antennas at all three sites were of the log-periodic type for wideband frequency coverage. The Starr Hill array used for reception of the signals from the two northern sites was boresighted on Thule, but its broad beamwidth (~60°) allowed reception of the Keflavik signals with about a 3-dB degradation. The array employed consisted of a two-bay horizontally-polarized log-periodic dipole antenna.

The antennas at the transmit sites were single-curtain log-periodic vertical-monopole antennas. Calibrated antenna patterns for the measurement antennas at all sites were obtained through a comprehensive series of pattern measurement flight tests.

For the measurements to be presented the combined transmission/reception PRF was 200 PPS with the 10- and 130-μs transmissions symmetrically interlaced so that each bandwidth signal had a PRF of 100 PPS. This was done so that there would be no question as to the comparability of the data collected using the two different bandwidths. The fixed-frequency pulse compression receiver used a double conversion technique to heterodyne the received signal to an 800-kHz IF, where the received signal was decoded using the appropriate tapped delay line matched filter. A test signal (identical to the transmitted signal) of known amplitude and position was injected into the measurement system at the receive antenna terminal for calibration and system test purposes.

An absolute-time system similar to that at the transmitter sites enabled the system PRF at the receiving site to be set to absolute time, and thus permitted measurement of signal propagation time with an accuracy of about ±10 μs. The propagation time was needed so that an accurate determination of the elevation angle for each measurement could be made. Since the two northern measurement paths are near the extreme range for a one-hop F2-layer mode of propagation, the vertical angle of transmission and reception for this mode will be near 0°, where the gain of an antenna is a sharp function of elevation angle. Calculation of the propagation loss requires that the gains and losses of all elements of the system be known as accurately as possible, including the antenna gains.

The decoded received signal was both envelope detected and product detected. The product detected output was offset by a nominal 25 Hz. External control of the amplitude of the product detected video signal was incorporated in order to utilize the maximum dynamic range of the magnetic tape recorder and the magnetic drum processor used to process the detected-pulse compressed signal. Both types of detected (ungated) video signals were sent to an Ampex FR-1200 recorder where they were separately recorded.

The magnetic drum--coherent signal processor utilized to obtain the mode propagation loss information and mode-spreading characteristics is a high-density storage, sampled-data device using a magnetic drum rotating at an exact (phase locked) synchronous speed of 100 r/s. It provides a time-compression (frequency-multiplication) factor of 200,000 for its high-spectral-resolution mode of operation (with from 0.1- to 0.35-Hz selectable frequency resolution and a 1- to 10-Hz unambiguous frequency extent) or a time compression of 40,000 for its low-spectral-resolution mode of operation (0.50- to 1.75-Hz selectable frequency resolution and a 5- to 50-Hz unambiguous frequency extent).

3. EXPERIMENTAL RESULTS AND THEIR IMPLICATION

3.1 Introduction

The experimental results and data obtained from the measurement equipment on the HF paths just described will now be presented. This will include a discussion of the measured propagation loss values and the associated values of excess system loss. The results of an investigation of the received signal level dependency on signal bandwidth (100 kHz versus 7.7 kHz) are then described. This is followed with a discussion of the signal multipath spreading measured on the two paths for various modes of propagation. The last measured signal characteristic described is the signal spectral spread. A summary of the observed spectral and time spreading is then provided. This is followed with selected Doppler-time delay display photographs to graphically illustrate the simultaneous spectral and time spreading with the different modes of propagation.

When reviewing the total data collected during this period, it is obvious that there are many different propagation situations that exist, and, therefore, it is very difficult to describe northern HF propagation by a few measurement parameters, due to its very dynamic nature. Also, the results presented are obviously not based on a complete sampling of summertime propagation conditions over these two northern paths. This would have required a considerably larger effort than was possible. Nevertheless, it is felt that the results shown do give a representative picture of propagation conditions over these two northern paths during the summertime, especially at nighttime and during the morning hours. It is pointed out that past experience has shown that summertime conditions are probably the best, on a seasonal basis, for these paths.

Table II shows a detailed list of the specific periods of time for the measurement data selected for analysis, and the experimental results obtained from this data base for the signal characteristics of major interest. It is apparent from the results derived that the received-signal characteristics deviated considerably at times from those measured previously on a midlatitude path (Coco Solo, Canal Zone, to Starr Hill using similar equipment) and in addition were definitely also a function of the actual location of the northern path. The specific signal characteristics to be discussed in the material to follow are propagation loss, spectral spreading, and temporal spreading.

From a careful examination of Table II, it can be determined that the same experimental results are not always obtained for a given mode/path combination. Therefore, a statistical approach was selected for presenting the value of the parameter in question. In view of the quantity of data that could be analyzed, the median value was selected usually to represent a given characteristic, except where another descriptor was more appropriate.

Examples of the difference in spectral width observed as a function of mode of propagation and bandwidth are shown in Figures 3 and 4. The first Doppler-time delay record was obtained from test number 1 using the wideband signal on the Thule path. The one in Figure 4 was obtained at approximately the same time but using the narrowband signal. Note from Figure 3a that there is a considerable difference in the spectral spread between propagation via the $2E_S$ mode and 1F2L mode on the Thule path (0.3 Hz versus 3.2 Hz at about the 10-dB level). However, this difference in spectral spread between modes of propagation does not appear in the Keflavik record shown in Figure 5, obtained about 10 minutes later using the same transmit frequency. The information shown in these figures was obtained around local noontime on the Thule path, when propagation conditions are generally good. It is interesting to note the high spectral stability exhibited by the $2E_S$ modes in these records. Also, Figures 3 and 4 illustrate the relative independence found between spectral spread characteristics and transmit/receive bandwidth. The spurious spectral line between -1.5 and -3.0 Hz in these figures should be disregarded.

An example of a Thule path 1F2 mode with relatively wide spectral and low to moderate temporal spread was given in Figure 3 for test number 1. A more typical Thule path example having wide spectral and temporal spread is given in Figure 6 for both signal bandwidths. Again, spreads were not found to be a function of bandwidth. An

illustration of the most severe type of 1F2 mode temporal spreading encountered on the Thule path is given in Figure 7. Note the reduced-Doppler scale sensitivity associated with use of the low-Doppler resolution mode of the signal processor.

Another means of showing the time spread or multipath experienced by signals transmitted over a northern path is presented in Figure 8. This is an oblique ionogram recorded at 09:20 GMT on June 26, 1969, using the Granger sounder. It followed test number 9. The time spread of the 1F2 mode is very evident in this figure, while the $2E_s$ mode exhibits little time spread. The spectral width of the $2E_s$ mode at about the 10-dB level was 0.4 Hz, while it was 2.4 Hz for the 1F2 mode.

3.2 Loss Results

An ionospheric parameter of considerable interest is the propagation loss associated with the different modes of HF propagation as a function of time of day and path location. The employed experimental system configuration afforded the opportunity to measure the loss for signals transmitted over 2000-nmi paths near and in the auroral/polar cap region. There has been considerable discussion in the HF community over the 8.4/9.0-dB factor used for determining the median one-way propagation loss for midlatitude paths, and its equivalent values for propagation at northern latitudes (Refs. 1, 2, and 3). In addition, there is the question of whether this factor should be doubled for the two-way situation encountered for backscatter radar operation.

The term propagation loss as used in this report includes the loss in signal level due to ionospheric absorption, ground reflection, other nondefined ionospheric effects, and some system losses. It does not contain the free-space or spreading loss.

Based upon previous investigations of propagation loss (Ref. 4), it was determined that the actual measured propagation loss was a function of the mode of propagation. Consequently, considerable effort has been devoted to obtaining an accurate determination of the actual modes of propagation for the signals whose losses are being measured. Even so, mode identification using the oblique ionograms obtained with the step-frequency sounders is not generally a simple task, considering the lengths of the northern paths involved and their location in the auroral/polar cap region. A review of the many ionograms obtained over these paths has revealed the existence of the N mode for a considerable period of the time, thus providing an alternate mode of propagation to the 1F2 mode for long-range propagation. Also, it was noted that the 2F2 mode of propagation was not as dominant as might be expected over these paths.

The propagation loss results obtained using the experimental configuration, and the data processing and data reduction techniques discussed in the Appendices, are presented in Tables III and IV for the Thule and Keflavik data, respectively, according to the identified modes of propagation. The actual measured loss results are the same as those listed earlier in Table II. The mode identifier 1F2S was employed when considerable spreading of the 1F2 mode could be seen on the oblique ionogram. The loss value reported is for the narrowband signal where available; otherwise the measured wideband losses are employed as indicated in the tables by a W. It should be mentioned that the propagation loss determined does include the system integration loss due to integrating for too long a time period. With the use of the 1.75-Hz analysis filter in the signal processor, it is felt that this integration loss is less than 1 dB for all except three tests (numbers 1, 6, and 19) with extreme spectral spreading. Integration losses of 3 to 4 dB may have been incurred for these extreme spectral spreads. In addition, there might be another small loss due to the frequency offset of the received signal and the fact that a zero offset was assumed for the processing of the loss data on the signal processor. For the results where an E is indicated, an estimated antenna gain of 10 dB was used because the derived elevation angle was less than 0°. This value of antenna gain was selected based on the values determined for the other test cases.

The information contained in Tables III and IV for each data sample was obtained as follows. The value of median propagation loss for a given mode of propagation was determined using the needed scaling factors from the median of the values of its peak signal levels which were read off the photographs of the amplitude time record taken during the data period.

The predicted propagation loss with no excess system loss (shown in Tables III and IV) is that determined for the paths of interest using the ITSA-1 computer program (Ref. 2). The two quantities included in this factor were the ground loss (where appropriate) and the ionospheric loss. It was necessary in a number of cases to interpolate or extrapolate the computer results to the actual frequency employed and the time of the measurements.

The measured excess system loss shown in these tables is just the difference between the measured propagation loss and the predicted propagation loss with no excess system loss term. The predicted excess system loss was obtained from tables contained in Reference 1 for paths greater than 2500 km and a midpath point between 65° and 70° geomagnetic latitude.

In order to obtain a clearer perspective of the propagation loss results, median values for the data reported in Tables III and IV were obtained on a path basis, for the combination of the 2E and $2E_s$ modes, the 1F2L, 1F2H, and 1F2S modes, and the N mode. The results are depicted in Table V. This compression of the data is admittedly not completely valid due to diurnal and frequency-of-transmission effects that exist. But, in view of the limited quantity of data available, it appears appropriate. Nevertheless, having noticed a significant difference in the Thule 1F2 results as a function of time of day, these results were separated between daytime and nighttime conditions.

Reviewing the results contained in Table V, it can be seen that during the daytime the measured excess system loss is less than that predicted for propagation via the $2E/2E_s$ modes for both paths. However, the measured propagation loss is still appreciable for these modes during the daytime due to the normal ionospheric loss, which can be quite large for E-layer propagation. For the 1F2 mode, the excess system loss for the Thule path at nighttime is considerably higher than that predicted and also higher than that measured during the daytime. For N-mode propagation, the excess system loss is about 10 dB higher on the Thule path compared to that predicted. However, on the Keflavik path the predicted and measured values were quite close. For practically all test cases examined the N mode of propagation was not predicted at the actual operating frequency employed for a test using the computer prediction program. Hence, an approximate value had to be determined for the predicted N-mode ionospheric loss.

Reviewing the median measurement propagation losses reported in Table V, observe that on the Thule path the median loss is less for the N mode than it is for the $2E/2E_s$ mode. On the Keflavik path they are about equal.

The 1F2-mode results for the Keflavik path show that even though its median excess loss is higher than predicted by about 10 dB, the median measured propagation loss is less for this mode than for either the $2E/2E_s$ or N mode.

3.3 Signal Level Dependency on Signal Bandwidth

During the course of on-site observations of the received signal amplitudes from Thule and Keflavik, it was noticed that very often the received signal level for the 7.7-kHz transmission was considerably stronger than for the 100-kHz transmission. This result was not too surprising, considering the severe fluctuations that were observed in signal amplitude and the time spreading of the actual received signal, especially for F2 modes of propagation over the Thule path (i. e., a 10-μs pulse length signal was generally not received; instead, the received energy was often spread out over a range of 100 μs). Thus, the signal amplitude was probably higher for the 130-μs pulse length because of the addition of the many multipath components that existed within the effective time duration of this pulse length.

To investigate this loss-bandwidth relationship, the results obtained from the 20 test cases considered were analyzed where information was available for both bandwidths. These signals were transmitted practically simultaneously to minimize as much as possible any variation due to when the samples were taken. To obtain data for this comparison, the average signal amplitude at the time that had minimum loss was employed. Values for the difference in signal level between wideband (100 kHz) versus narrowband (7.7 kHz) transmissions were obtained using the results measured with the 0.5-Hz and 1.75-Hz Doppler resolutions in the signal processor. The resulting data for the Thule and Keflavik paths as a function of mode of propagation are shown in Tables VI and VII, respectively.

Since the results obtained using the 1.75-Hz resolution appear to be more appropriate, the median value of loss decrease, LD(1.75), is probably the most indicative of the difference in signal level between the two bandwidths. Each median value shown in the tables was determined using all the appropriate data, since it was felt that the data presented did not allow meaningful median values to be determined as a function of mode of propagation.

Considering the median values of LD (1.75) for both paths, the difference in loss is slightly higher on the Thule path compared to the Keflavik path (5.5 dB versus 3.3 dB). Also, reviewing the actual data in Tables VI and VII, it is seen that the maximum decrease in loss as a function of signal bandwidth reduction is greater than 10 dB for the Thule path, while for the Keflavik path it is 8.8 dB. An examination of the data in Tables VI and VII shows that the results obtained using the 0.5-Hz Doppler resolution mode are generally very close to those for the 1.75-Hz filter.

3.4 Time Spreading (Multipath) Results

In general the multipath or time-delay spreading under consideration is, by definition, the time spreading of all signal information associated with individual "modes" of propagation, separable and identifiable for at least several minute periods of time. This definition will thus include closely-grouped complex modes which have short-time stabilities and/or spreading that prohibits reliable separation and identification with the measurement and data reduction approach utilized.

The general nature of the time spreading of propagation modes encountered on high-latitude paths is, of course, observable on oblique ionograms. The general objective here was to perform a limited set of measurements yielding data directly related to the time spreads likely to be observed on northern HF paths. A complete summary of the coherent signal processor input parameters employed for this investigation is given in Appendix A, and a summary of the postprocessing data reduction and analysis paramters is presented in Appendix B. All time delay measurements given were made with the 1.75-Hz Doppler filter. The temporal extent or width (6 dB) of the average integrated signal amplitude envelope for each mode, integrated over the full input data interval of 3 to 4 minutes, was determined. The resulting integrated signal width, ΔT, is a measurement of the average time spread of the time-distributed signal energy. A review of the ΔT data and the average integrated amplitude plots versus time from which the data were obtained led to a useful way of characterizing these results so that more direct bandwidth comparisons could be made.

First, look at a typical set of $2E/2E_s$ mode data, such as from test number 13, and their average integrated time-amplitude envelope plots given in Figures 9 and 10. For comparison, typical integrated time-amplitude envelopes for a spread mode are given in Figures 11 and 12. From these plots it is seen that the minimum expected ΔT values should be about 50 and 230 μs for the wide and narrow bandwidth signals, respectively. This is reasonable, considering the signal processor output pulse widths of about 25 and 150 μs and the data reduction quantization increments of 20 and 100 μs that were used.

A comparison of the median values of ΔT listed in Table II reveals that the general pattern of time delay spreading on the two paths was very similar. All E and E_s modes were close to the selected illustrations given in Figures 9 and 10. The 1F2 and N modes on both paths indicated a total median spread of two to three times the reference output pulse width of 50 μs for the wideband signal: 146 and 98 μs, respectively, on the Thule path and 108 and 132 μs on the Keflavik path. With the narrowband signal, the median ΔT's for 1F2 and N-mode propagation were about two times the minimum temporal spread signal: 420 and 350 μs, respectively, on the Thule path, and 510 and 400 μs on the Keflavik path.

3.5 Spectral Spreading Results

At this time some of the results that were obtained for the spectral spread, Δf, for propagation during the summer over the Thule and Keflavik to Starr Hill paths will be discussed. The spectral results are shown in Tables VIII and IX for the Thule and Keflavik paths, respectively, as a function of mode of propagation. The value of spectral spread that was determined from a given photograph of a Doppler-time delay display for a data sample represents the spread at a level between 6 and 10 dB below the peak signal level. It was very difficult to maintain a constant peak value for these measurements considering the dynamic nature of HF propagation. Where two values of Δf existed for a test case (because of measurements made using both the narrow and wideband signals), the average of the two values was reported. Generally, little or no difference in Δf was measured using the two bandwidth signals. This would appear to be a significant factor in signal characteristics for northern HF propagation. This was also true for midlatitude propagation based on earlier measurements made on the Coco Solo to Starr Hill path.

In order to obtain a better appreciation of Δf as a function of path and mode of propagation, median values were obtained using the data in Tables VIII and IX. These results are presented in Table X, where the number of samples used to derive a median value and the range of values are also indicated. Examining Table X discloses that the median

value of Δf for 2E or $2E_s$ propagation is 0.4 Hz irrespective of path. This value for spectral spread is consistent with earlier measurements of the signal temporal coherence for these paths.

Further study of the data contained in Tables VIII and IX reveals that the Δf for N-mode propagation on the Keflavik path is almost as good as for $2E_s$ propagation a large percentage of the time. However, the Δf for N-mode propagation on the Thule path is considerably different than that for $2E/2E_s$ propagation. It is closer to the values reported for 1F2 propagation on the Thule path and on the Keflavik path, with the latter one having the lower Δf. This relationship was also observed in real time at the site.

A number of explanations can be hypothesized for the above experimental results. As mentioned earlier, the geometry of the two paths employed is different with respect to auroral oval. Also, the Thule site is almost at the center of the polar cap region, while the Keflavik site is near its boundary. Hence, the higher Δf's reported for 1F2 propagation on the Thule path could be due to either passing through the auroral oval or due to part of this path being in the polar cap region. Obviously, the reasons for these differences need further study before an acceptable model can be derived which is completely satisfactory.

Another parameter that was determined from the Doppler-time delay photographs was the frequency offset of the received signal compared to the transmitted signal. With the use of Loran-C transmissions at all sites, the frequency difference among the master frequency standards at the various sites was generally less than one part in 10^{10}, which was more than needed for this measurement. Reviewing the results obtained for the offset which are shown in Table II, it is seen that the frequency difference between the received signal and the site reference was generally less than 1 Hz, even considering the results for both paths together. Clearly then, based upon these experimental results and other site observations, it can be stated that for one-way HF propagation over these paths, no significant Doppler shifts have been observed associated with the dominant received signals. There were a few times that a significant Doppler offset was noticed briefly, which might have been due to moving ionospheric irregularities.

3.6 Summary of Observed Spectral Versus Time Delay Spread Relationships

A general summary of the relationships noted between spectral and temporal spreading is given in Table XI. This summary includes the results for all 2E, $2E_s$, 1F2, and N modes on both paths. Note that the high-temporal-spread modes are divided into two classes. One class of spread modes consists of complex spread modes as noted from Doppler-time delay photographs to be composed of multiple, resolved but unidentified components or submodes in the time dimension. The second class consists of those spread modes which apparently did not have resolvable stable components.

The significant facts to note are that:

- Most low-temporal-spread modes had low spectral spreads
- Practically all high-temporal-spread modes without resolvable submodes had high spectral spreads
- About half of the high-temporal-spread modes with resolvable submodes had high spectral spreads

The nonspectrally-spread high-temporal-spread complex modes were observed from the Doppler-time delay photographs to be composed of components with relatively high temporal stability compared to the total time spread of the mode. Thus, one can say that essentially all observed, identified modes with high apparent temporal stability had low spectral spread. Furthermore, the converse also appeared to hold.

4. COMPARISONS WITH GEOPHYSICAL DATA

The values of the 6-dB spectral spread measured as a function of the mode of propagation were compared with the corresponding values of K_p, the planetary magnetic three-hour index, to determine if any correlation existed between these two quantities. In addition, the North Atlantic Quality Figures for the periods of the analyzed test results were obtained for comparison with the spectral spread data.

Depicted in Figures 13 and 14 are plots of the spectral spread versus K_p for the Thule and Keflavik path data, respectively, listed in Table II. The points are plotted as a function of the mode of propagation to indicate the strong dependency on this parameter. Examination of these figures reveals the low spectral spread for the $2E/2E_s$ on both paths compared to the 1F2 mode, especially on the Thule path. A study of these two figures also shows very clearly the much higher values of spectral spread existing on the Thule path compared to the Keflavik path. The ratio of the peak spectral spreads for the depicted values for the two measurement paths is almost three to one. This is the major observation which can be drawn from these two figures, since there does not appear to be any correlation between the values of spectral spread and K_p.

An investigation of the diurnal variation for the spectral spread measurements listed in Table II was conducted to determine any relationship with time of day. The results were plotted versus time of day for the three major modes of propagation that were observed on the two northern measurement paths: $2E/2E_s$, N and 1F2. Shown in Figures 15, 16, and 17 are the measured spectral spread values as a function of time of day for these three modes, respectively. The $2E/2E_s$ results for the two paths in Figure 15 again illustrate the low values of measured spectral spread for this mode of propagation on both paths. Indicated in this figure and the next two are the values of K_p for the plotted points. It is noted that, considering the signal processing parameters employed, the value of the $2E/2E_s$ mode spectral spread was not a function of the value of K_p. Also, as discussed earlier, the value of the spectral spread was the lowest for this mode of propagation on both paths. The Thule data disclose no diurnal variation for the period from 04:00 to 12:00 local time.

The N-mode results shown in Figure 16 demonstrate the higher values of spectral spread for this mode observed on the Thule path compared to the Keflavik path. The Thule results in Figure 16a illustrate the lack of correlation between spectral spread and K_p. The Keflavik data in 16b show this also, and in addition the low level of spectral spread observed for the N mode on this path. This is believed due to the locations of the N-mode ionospheric reflection points for these two paths with respect to the auroral oval, especially during the daytime. This point will be discussed later.

In Figure 17 are depicted the 1 F2-mode spectral spread results with no differentiation between the various types of 1F2 modes that were observed. Examining Figure 17a, it is seen that the Thule 1F2 spectral spread does not appear to be a function of time of day or of K_p. In addition, its value is quite high compared to those measured at similar times on the Keflavik path as seen from Figure 17b.

Considering the location of the two paths with respect to the auroral oval, it would appear that this factor is the most likely reason for lower values of spectral spread observed on the Keflavik path for the N and 1F2 modes of propagation. This can be seen from an examination of Figures 18 and 19, where the auroral oval (Ref. 5) for noon and midnight, respectively, along the 0° geomagnetic meridian has been plotted on the map showing the measurement path locations. The auroral oval depicted is for Q = 1, which corresponds to a K_p value of 1 or 2. Observe from Figure 18 that the location of the Keflavik path is considerably south of the auroral oval around noontime, while at nighttime the path passes directly through the oval. This would explain the slightly higher values of spectral spread that are shown in Figures 16b and 17b for nighttime compared to daytime conditions on the Keflavik path.

A question that cannot be answered from these measurements made on the Thule path is whether the spectral spread observed is due to the fact that this path is partially in the polar region, where spread-F conditions exist a very high percentage of the time (Ref. 6), or because it crosses the auroral belt. Also, it might be that both factors are important all the time or at different times.

A comparison of the experimental results with the corresponding actual North Atlantic Six-Hour Quality Figures for the times of the measurements indicated no correlation between the two. This can be determined from an examination of the data contained in Table II showing practically no variation in the North Atlantic Quality Figure for the test period, although there were changes in the values of the quantities measured. The North Atlantic Quality Figure was either 7- or 7o, with only two tests having a value of 7o.

Riometer records from the Canadian station at Great Whale River were obtained from the Communications Research Center, Ottawa, Canada for the months of June and July 1969. An examination of these recordings for auroral substorms revealed little if any correlation between the time of occurrence of an auroral substorm during this time period and when the measurements analyzed were taken.

5. CONCLUSIONS AND SUMMARY OF RESULTS

The results of this limited series of experimental measurements may be used to characterize the expected range of various HF signal characteristics of interest such as propagation loss, multipath (time delay/temporal spreading), and frequency/spectral spreading as a function of mode of propagation for 2000-nmi high latitude HF paths during summer nighttime and morning periods.

The median measured excess system losses were found to be:

- Less than predicted (by 6 to 7 dB) for the daytime $2E/2E_s$ mode of propagation on both measurement paths
- Approximately the same as predicted for the N mode on the Keflavik path and the daytime 1F2 mode on the Thule path
- Greater than predicted (by 10 to 24 dB) for the nighttime $2E_s$, 1F2, and N modes on the Thule path and the 1F2 mode on the Keflavik path

There were no consistent measurable differences in the temporal spread, spectral spread, and Doppler offset (on a given mode) between the wideband signal (100 kHz) and the narrowband signal (7.7 kHz) on either path. Significantly greater propagation losses were measured for the wideband signal compared to the narrowband signal for both paths. At times the difference was as high as 10 dB.

The median temporal spreads for the two paths were similar for a given mode of propagation, but the median spectral spreads were significantly greater on the Thule path for the 1F2 and N modes. The median measured temporal spread for the 1F2 and N modes on both paths was about 120 μs for the wideband signal and 410 μs for the narrowband signal. The median spectral spreads were 3.1 and 2.5 Hz for the 1F2 and N modes, respectively, on the Thule path, and 1.5 and 0.5 Hz for the 1F2 and N modes, respectively, on the Keflavik path. Approximately two-thirds of all 1F2 and N modes measured on both paths had temporal spreads greater than 100 μs and spectral spreads greater than 1.5 Hz. The individual mode temporal spreads ranged to over 1 ms and individual mode spectral spreads to about 6.0 Hz.

A comparison of the median temporal spread measurements reveals that their general pattern on the two paths was very similar for the same modes of propagation.

In summary, the following is noted:

- The median $2E/2E_s$-mode temporal spreads, which were the lowest, were limited by an overall measurement resolution of 50 μs
- The median 1F2-mode spreads, which were the highest, were two to three times that measured for the 2E modes for the wideband signal on both paths
- The median N-mode spreads were for most cases less than that measured for the 1F2 modes

The results of the measurements of the spectral spread indicated a definite dependency on mode of propagation and the location of the HF transmission path with respect to the auroral oval. For both paths the median value for the spectral spread for the $2E/2E_s$ mode was the same: 0.4 Hz. However, there was a considerable difference in the median values for the two paths for 1F2 and N-mode propagation, with the lower values occurring on the Keflavik path. There was an indication in the data presented for the Keflavik path 1F2 mode of a variation in spectral spread with time of day which had been observed in earlier results.

The Doppler frequency offsets measured were (for all modes on both paths) less than 1.2 Hz and typically less than 0.6 Hz. This offset indicates the frequency shift on a signal passing through or along the auroral oval measured on a one-way path. The frequency shift for a signal reflected (as in the radar case) off the ionization existing in the auroral oval can be many times higher.

A significant general relationship was observed between temporal and spectral spreading. Most individual propagation modes (2E, 1F2, and N) with low temporal spread (<100 μs) had low spectral spreads (<1.5 Hz) and practically all individual high temporal spread (>100 μs) modes (1F2 and N modes without stable resolvable submodes) had high spectral spreads (>1.5 Hz). Furthermore, a general relationship was noted between excess system loss and spreading in both time and Doppler. Average measured excess system loss was found to increase progressively as a function of the temporal spreading for a given category of Doppler spread (i.e., low or high), and on an overall basis it was found to increase as a function of the combination of temporal and spectral spreading.

An investigation of a possible relationship between the measured spectral spread and the planetary 3-hr magnetic index, K_p, showed very little, if any, correlation between the two quantities. The values of K_p for the test data analyzed ranged from 1 to 2+. Likewise, a comparison of the experimental measurements with the corresponding North Atlantic Quality Figures was unproductive, since this factor had only two values for the time periods covered by the reported test data: 7- and 7o. Clearly, better indicators than these two are required for relating measured northern HF signal characteristics to geophysical conditions.

6. ACKNOWLEDGMENT

The material presented in this paper is based upon work sponsored by the Rome Air Development Center under Contract Number F30602-69-C-0217 with the General Electric Company, Syracuse, New York.

7. REFERENCES

1. Barghausen, A. F., Finney, J. W., Proctor, L. L., and Schultz, L. D., "Predicting Long-Term Operational Parameters of High-Frequency Sky-Wave Telecommunication Systems," ESSA Technical Report, ERL 110-ITS 78, May 1969.

2. Lucas, D. L., and Haydon, G. W., "Predicting Statistical Performance Indexes for High Frequency Ionospheric Telecommunications Systems," ESSA Technical Report, IER 1-ITSA 1, August 1966.

3. Laitinen, P. O., and Haydon, G. W., "Analysis and Prediction of Sky-Wave Field Intensities in the High Frequency Band," Technical Report No. 9, Revised (RPU 203), U. S. Army Signal Radio Propagation Agency.

4. Shepelavey, B., "Individual Sky Wave Mode Loss Statistics Measured on a North-South Path," Radio Science, Vol. 4, No. 11, pp. 1029-1038, November 1969.

5. Feldstein, Y. I., and Starkov, G. V., "Dynamics of Auroral Belt and Polar Geomagnetic Disturbances," Planet.Space Science 15, pp. 209-229, 1967.

6. Penndorf, R., "Geographic Distribution of Spread F in the Arctic," Journal of Geophysical Research, Vol. 67, No. 6, pp. 2279-2288, June 1962.

APPENDIX A. DATA PROCESSING

The data which were actually processed for inclusion in this paper represent about 10 percent of the usable data collected. The 20 data samples processed for determining propagation loss, temporal and spectral characteristics were obtained by analyzing the product-detected (nonrange-gated) video signal from the direct-reproduce channel of the tape recorder, utilizing the magnetic drum signal processor. A summary of the signal input and coherent processing parameters used for the loss and time spread measurements is given in Table XII. All loss and time spread information was obtained with the processor in a low-Doppler resolution (time compression factor of 40,000) two-second data storage mode. The signal was processed simultaneously through two identical analysis channels, except that one channel had a 20-kHz (6-dB width) analysis filter which yielded a 0.5-Hz Doppler resolution, and approximately 0.6 second of coherent integration. The total combined coherent/noncoherent integration time in both channels, including the effects of the postdetection filters, was 2.0 seconds.

A test signal of known level was injected at the receive antenna terminals (i.e., into the receive system) at a known position in time. The test signal level effectively represented a known receive power and was processed through the drum by placing a 2-ms range gate around it for the signal bandwidth being processed. The signal processor handled 100-PPS signal data. Since each bandwidth signal was received and recorded with a PRF of 100 PPS, each had to be handled separately. A data set consisted of a single mode and bandwidth. For each data set the detected analyzed output for the processor range-gated test signal input was some voltage value, $V_{ts}(20)$ or $V_{ts}(70)$ for the two channels at some point in time R_{ts} (i.e., although the video test signal level into each channel was identical, the possibility existed that differences in processing gain would occur so that each was processed separately).

For each mode of propagation signal of interest, the analysis filter was placed at zero Doppler, and the detected signal output versus time was photographed at approximately a one per second rate. (Note: The detected output for the entire 2-ms range extent occurs at a PRF of 100 PPS, but the data on the drum itself consist of only the most recent two seconds worth of data, so that sampling the detected output faster than once per second is somewhat redundant.) The amount of time extent actually photographed (of the 2 ms available) was a function of the temporal spreading and the signal bandwidth. For a very temporal stable mode, the time extent displayed was generally 100 or 200 μs for a wideband signal, and 400 μs for a narrowband signal. However, for time spread signals, the extent was as much as 1 ms for wideband signals, and 2 ms for narrowband signals. The actual time position of the center of the display could be calculated to within about 15 μs. For the cases where the time extent displayed was on the order of 200 to 400 μs, and where there were two or more modes, each mode was processed and displayed separately.

APPENDIX B. DATA REDUCTION

The mode spectral characteristics were obtained from a single photograph of the Doppler-time delay display taken for each data sample. The spectral spread approximately 6 to 10 dB below the peak of the mode was read directly from the photograph for each bandwidth. This value is reported in Section 5.

The mode loss and temporal characteristics were obtained from the photographs of the drum processor detected output versus time taken every second. This was accomplished by reading off and recording the peak voltage values (for each analysis channel separately) in each of fifteen 20-μs range gates for the wideband signal (100-μs range gates for the narrowband signals). A summary of the general data reduction parameters for the mode loss and time delay spread measurements is given in Table XIII.

A computer program was written which processed the cards and determined the greatest peak voltage for each data card (and each analysis channel) and the range position associated with each of these peak voltages. The basic transmission loss, L_b, was then calculated for the peak voltage values for each of the 15 range bins for each data card, using the transmit and receive antenna gains. (It will be recalled that these gains are based on the elevation angles determined from the propagation delay measurement, considering the identified mode of propagation.) The transmit power was 3.0 kW, while the receive signal power was calculated as the squared ratio of peak-detected signal voltage to the signal processor output test signal times the power associated with the coupled test signal at the receive antenna terminal. The basic transmission loss thus also includes the system integration loss, since the test signal may be assumed perfectly coherent, while the received signal is usually not. For many of the data samples, the peak signal output in certain range bins was very low and could not be read.

TABLE I

GEOGRAPHICAL INFORMATION

	North Latitude	West Longitude
Starr Hill	43° 23' 43.0"	75° 15' 13.0"
Thule	76° 24' 15.0"	68° 44' 34.0"
Keflavik	63° 57' 31.3"	22° 43' 29.1"
Midpoint, Thule Path	59° 55'	73° 42'
Midpoint, Keflavik Path	56° 24'	55° 55'

From Starr Hill to	Bearing**	Range		
		km	nmi	mi
Thule	2° 47' 52" (188° 40' 15")	3695.59	1995.46	2296.33
Keflavik	36° 36' 8" (266° 35' 48")	3991.93	2155.47	2480.46

* These calculations for range and bearing are based upon the Clarke (1866) spheroid.

** Numbers in parenthesis represent bearing from the remote site to Starr Hill.

TABLE II

SUMMATION OF MEASUREMENT RESULTS

Test Number	Date	Time Period Covered (GMT)	Path	Operating Frequency (MHz)	MOF (MHz)	MUF (MHz)	Mode	Transmission Time (ms)	Angle of Transmission (degrees)	Predicted Elevation Angle (degrees)	K_p	Measured Loss (Median of Peaks), 1.75 Hz (dB)	Predicted Loss, No Excess System Loss (dB)	Predicted Loss with Excess System Loss (dB)	Measured Excess Loss (dB)	Predicted Excess System Loss (dB)	Loss Difference Between Two Signal Bandwidths, 0.5 Hz (dB)	Loss Difference Between Two Signal Bandwidths, 1.75 Hz (dB)	Free-Space Loss (dB)	Frequency Spread 6 to 10 dB below Peak (Hz)	Frequency Offset, Average Wideband and Narrowband (Hz)	ΔT, Wideband 6-dB Width of Integrated Data (μs)	ΔT, Narrowband 6-dB Width of Integrated Data (μs)	North Atlantic Quality Figure	Number of Samples in Wideband Set	Number of Samples in Narrowband Set
1	6/06/69	165430-165800	Thule	19.020	20.0	<16.0	$2E_s$	12.545	3.5	2.7	1+	30.4W	20.0	31.3	10.4	11.3	—	—	129.5	0.3	0.4	66	—	7-	22	—
1	6/06/69	165430-165800	Thule	19.020	22.0	17.9	1F2L	13.065	4.9	1.5	1+	23.0W	10.0	21.3	13.0	11.3	—	—	129.9	3.2	0	66	—	7-	22	—
1	6/06/69	165430-165800	Thule	19.020	22.0	17.9	1F2H	13.395	8.2	1.5	1+	34.2W	—	—	—	11.3	—	—	130.1	4.1	-0.5	146	—	7-	22	—
2	6/06/69	170400-170830	Keflavik	19.020	20.0	16	$2E_s$	13.524	2.3	2	1+	31.9W	20.0	31.3	11.9	11.3	—	—	130.2	0.3	0.5	56	—	7-	28	—
2	6/06/69	170420-170820	Keflavik	19.020	19.5	MNP	N	13.818	6.2	MNP	1+	35.2W	16.0	27.3	19.2	11.3	—	—	130.4	0.4	0.4	54	—	7-	24	—
2	6/06/69	170400-170830	Keflavik	19.020	21.5	19.8	1F2L	14.058	3.4	0	1+	30.2W	10.0	21.3	20.2	11.3	—	—	130.5	0.4	0.4	108	—	7-	28	—
2	6/06/69	170400-170820	Keflavik	19.020	22.0	19.8	1F2H	14.554	8.0	—	1+	35.8W	—	—	—	11.3	—	—	130.8	0.6	0.4	92	—	7-	27	—
3	6/25/69	045350-045620	Keflavik	14.780	15.5	15.5	1F2S	14.041	3.2	1.0	2-	25.7	1.0	15.0	24.7	14.0	0.2	-1.5	128.3	1.5	0.4	I	510	7-	16	16
4	6/25/69	050850-051010	Thule	14.780	15.0	15.8	1F2S	12.967	3.8	1.8	2-	45.6E	1.0	15.0	44.6	14.0	—	—	127.6	2.5	-1.0	—	1180	7-	—	4
5	6/25/69	055640-060010	Keflavik	11.625	12.5	14.8	1F2S	13.921	0.6	0.	2-	25.6E	2.0	16.0	23.6	14.0	7.0	8.8	126.1	1.5	-1.0	I	650	7-	22	23
6a	6/25/69	060630-061000	Thule	14.775	17.0	15.2	1F2S	12.600	-1.4	2.2	2-	40.8E	1.0	15.0	39.8	14.0	1.1	-1.1	127.4	4.4	0.8	224	420	7-	22	22
6b	6/25/69	061300-061700	Thule	14.775	17.0	15.2	1F2S	12.640	-0.7	2.2	2+	39.3E	1.0	15.0	38.3	14.0	2.4	-3.8	127.4	4.4	0.8	188	510	7-	25	23
7	6/26/69	072610-072900	Keflavik	11.620	I	15.2	1F2H	14.251	5.3	-0.3	1+	31.4	6.0	20.0	25.4	14.0	2.9	3.3	126.4	2.0	-0.5	198	360	7-	18	25
8	6/26/69	073300-073710	Thule	11.620	13.0	MNP	N	12.880	8.0	—	1+	29.2W	6.0	20.0	19.2	14.0	—	—	125.5	0.6	1.2	62	230	7-	26	—
8	6/26/69	073300-073700	Thule	11.620	14.0	14.8	1F2S	13.254	6.9	0.9	1+	27.6W	3.0	17.0	24.6	14.0	—	—	125.7	0.7	0.9	80	380	7-	25	—
9	6/26/69	091510-091920	Thule	13.720	14.0	9.0	$2E_s$	12.557	3.7	2.2	2+	46.6W	11.0	27.8	35.6	16.8	—	—	126.7	0.4	0.2	48	—	7-	26	—
9	6/26/69	091510-091900	Thule	13.720	14.5	14.8	1F2S	13.037	4.8	2.0	2+	31.6	5.0	21.8	26.6	16.8	2.0	3.2	127.0	2.4	-0.4	194	420	7-	24	24
10	6/26/69	092430-092800	Keflavik	13.720	14.0	17.6(1F)	N	13.874	6.9	—	2+	27.8	12.0	28.8	15.8	16.8	5.3	5.3	127.6	0.5	0.3	220	400	7-	22	21
11	6/26/69	093530-093940	Thule	14.825	14.5	14.8	1F2S	13.191	6.2	2.0	2+	—	Apparent Measurement Problem					—	127.9	—	—	—	—	7-	—	26
12	6/26/69	094350-094810	Keflavik	14.825	15.0	17.6(1F)	N	13.900	7.1	—	2+	33.4	12.0	28.8	21.4	16.8	0.9	0	128.3	0.5	0.2	132	250	7-	27	20
13	6/27/69	133425-133900	Thule	14.900	17.5	14.0	2E	12.535	3.2	2.6	2-	31.8	29.6	44.7	2.2	15.1	-4.0	-4.4	127.3	0.4	0	48	220	7-	56	55
14	6/06/69	132200-132700	Thule	14.785	17.5	14.0	2E	—	—	2.6	1	—	—	—	—	15.1	—	—	—	0.4	0	—	—	7-	—	—
15	7/30/69	035620-035955	Thule	13.715	16.0	16.5(1F)	N	12.874	7.9	—	1-	27.7	2.0	16.0	25.7	14.0	9.7	10.8	126.9	2.7	0.8	74	280	7 o	44	44
16	7/30/69	041620-042000	Keflavik	13.715	16.5	16.2(1F)	N	14.050	8.5	—	1-	15.9	1.0	15.0	14.9	14.0	6.2	8.8	127.7	1.7	0.3	200	520	7 o	45	44
17	7/31/69	111430-111835	Thule	16.015	16.5	16.4	1F2J	12.865	2.5	1.8	1-	24.7	8.1	24.9	16.6	16.8	7.7	7.5	128.2	3.0	0.4	108	310	7-	50	29
18	7/31/69	112605-112900	Keflavik	14.820	16.0	14+	$2E_s$	13.521	2.3	2.2	1-	29.9	26.8	42.8	3.9	16.8	3.6	1.5	128.0	0.4	0	52	260	7-	33	22
18	7/31/69	112605-112900	Keflavik	14.820	I	18 (1F)	N	13.781	5.8	—	1-	32.8W	23.0	37.8	11.8	16.8	—	—	128.2	0.5	0	106	—	7-	34	—
19	7/31/69	064725-064955	Thule	11.625	12.0	15.2(1F)	N	12.904	8.2	—	1+	29.2	2.4	16.4	26.8	14.0	12.8	13.1	125.7	5.8	0.5	122	570	7-	22	26
20	7/31/69	072755-073000	Thule	11.625	12.0	14.8(1F)	N	12.884	8.0	—	1+	25.9	4.2	18.2	21.7	14.0	6.8	8.5	125.5	2.2	-0.5	144	420	7-	20	64

E_s -- Two-hop propagation via the E layer

$2E_s$ -- Two-hop propagation via the E_s layer

1F2H -- One-hop high-ray propagation via the F2 layer

1F2J -- One-hop propagation via the F2 layer near the junction

1F2L -- One-hop low-ray propagation via the F2 layer

1F2S -- One-hop propagation via the F2 layer with spreading

N -- N-mode propagation

W -- Wideband data instead of narrowband

E -- Estimated total antenna gain of 10 dB used to obtain this number

MNP -- Mode not predicted

(1F) -- 1F2 MUF for this path instead of N MUF

K_p -- Planetary magnetic index

I -- Indeterminable

MUF -- Maximum usable frequency for mode specified

MOF -- Maximum observed frequency for mode specified

TABLE III

THULE PROPAGATION LOSS MEASUREMENTS

2E/2E$_s$ Modes						1F2 Modes						N Mode				
Test Number	Mode	Measured Propagation Loss (dB)	Predicted Loss Without Excess Loss (dB)	Measured Excess Loss (dB)	Predicted Excess Loss (dB)	Test Number	Mode	Measured Propagation Loss (dB)	Predicted Loss Without Excess Loss (dB)	Measured Excess Loss (dB)	Predicted Excess Loss (dB)	Test Number	Measured Propagation Loss (dB)	Predicted Loss Without Excess Loss (dB)	Measured Excess Loss (dB)	Predicted Excess Loss (dB)
1	2E$_s$	30.4	20	10.4	11.3	1	1F2L	23W	10	13	11.3	8	25.2	6	19.2	14
9	2E$_s$	46.6	11	35.6	16.8	1	1F2H	31.2W	–	–	–	15	27.7	2	25.7	14
13	2E	31.8	29.6	2.2	15.1	4	1F2S	45.6E	1	44.6	14	19	29.2	2.4	26.8	14
						6a	1F2S	40.8E	1	39.8	14	20	25.9	4.2	21.7	14
						6b	1F2S	29.3E	1	38.3	14					
						8	1F2S	27.6W	3	24.6	14					
						9	1F2S	31.6	5	26.6	16.8					
						17	1F2J	24.7	8.1	16.6	16.8					

TABLE IV

KEFLAVIK PROPAGATION LOSS MEASUREMENTS

2E$_s$ Mode					1F2 Modes						N Mode				
Test Number	Measured Propagation Loss (dB)	Predicted Loss Without Excess Loss (dB)	Measured Excess Loss (dB)	Predicted Excess Loss (dB)	est Number	Mode	Measured Propagation Loss (dB)	Predicted Loss Without Excess Loss (dB)	Measured Excess Loss (dB)	Predicted Excess Loss (dB)	Test Number	Measured Propagation Loss (dB)	Predicted Loss Without Excess Loss (dB)	Measured Excess Loss (dB)	Predicted Excess Loss (dB)
2	31.9W	20	11.9	11.3	2	1F2L	30.2W	10	20.2	11.3	2	35.2W	16	19.2	11.3
18	29.9	26	3.9	16.8	2	1F2H	35.8W	–	–	–	10	27.8	12	15.8	16.8
					3	1F2S	25.7	1	24.7	14	12	33.4	12	21.4	16.8
					5	1F2S	25.6E	2	23.6	14	16	15.9	1	14.9	14
					7	1F2H	31.1	–	–	–	18	32.8W	21	11.8	16.8

TABLE V

LOSS INFORMATION

	Thule Path						Keflavik Path					
Mode	Time	Median Measured Propagation Loss (dB)	Median Predicted Loss Without Excess Loss (dB)	Median Measured Excess Loss (dB)	Median Predicted Excess Loss (dB)	Number of Samples	Time	Median Measured Propagation Loss (dB)	Median Predicted Loss Without Excess Loss (dB)	Median Measured Excess Loss (dB)	Median Predicted Excess Loss (dB)	Number of Samples
2F/2E_S	Day	31.1	24.8	6.3	13.2	2	Day	30.9	23.0	7.9	14.0	2
2E_S	Night	46.6	11.0	35.6	16.8	1						
1F2	Day	23.8	9.0	14.8	14.0	2	Day/Night	25.7	2.1	23.6	14.0	3
	Night	40.0	2.5	37.5	14.0	6						
N	Night	25.5	1.8	23.7	14.0	4	Day/Night	32.8	17.0	15.8	16.8	5

TABLE VI

LOSS BANDWIDTH DEPENDENCY – THULE PATH

2E Mode			1F2L Mode			1F2S Mode			N Mode		
Test Number	LD(0.5) (dB)	LD(1.75) (dB)	Test Number	LD(0.5) (dB)	LD(1.75) (dB)	Test Number	LD(0.5) (dB)	LD(1.75) (dB)	Test Number	LD(0.5) (dB)	LD(1.75) (dB)
13	-4.0*	-4.4*	17	7.7	7.5	6a	1.1	-1.1*	15	9.7	10.8
						6b	2.4	-3.8*	19	12.8	13.1
						9	2.0	3.2	20	6.8	8.5

Median value of LD(0.5) = 4.6 dB (eight samples)
Median value of LD(1.75) = 5.4 dB (eight samples)

TABLE VII

LOSS BANDWIDTH DEPENDENCY – KEFLAVIK PATH

2E_S Mode			1F2H Mode			1F2S Mode			N Mode		
Test Number	LD(0.5) (dB)	LD(1.75) (dB)	Test Number	LD(0.5) (dB)	LD(1.75) (dB)	Test Number	LD(0.5) (dB)	LD(1.75) (dB)	Test Number	LD(0.5) (dB)	LD(1.75) (dP)
18	3.6	1.5	7	2.9	3.3	3	0.2	-1.5*	10	5.3	5.7
						5	7.0	8.8	12	0.9	0
									16	6.2	8.8

Median value of LD(0.5) = 3.6 dB (seven samples)
Median value of LD(1.75) = 3.3 dB (seven samples)

LD(0.5) = Measured loss decrease when changing signal bandwidth from 100 kHz to 7.7 kHz using 0.5-Hz Doppler resolution
LD(1.75) = Measured loss decrease when changing signal bandwidth from 100 kHz to 7.7 kHz using 1.75-Hz Doppler resolution

*Time did not permit a detailed reexamination of these negative results.

TABLE VIII

SPECTRAL SPREAD RESULTS FOR THE THULE PATH

2E Mode		$2E_s$ Mode		1F2L/J Mode		1F2H Mode		1F2S Mode		N Mode	
Test Number	Δf (Hz)	Test Number	Δf (Hz)	Test Number	Δf (Hz)	Test Number	Δf (Hz)	Test Number	Δf (Hz)	Test Number	Δf (Hz)
13	0.4	1	0.3	1	3.2	1	4.1	4	2.5	8	0.6
		9	0.4	17	3.0			6a	4.4	15	2.7
		14	0.4					6b	3.4	19	5.8
								8	0.7	20	2.2
								9	2.4		

TABLE IX

SPECTRAL SPREAD RESULTS FOR THE KEFLAVIK PATH

$2E_s$ Mode		1F2L Mode		1F2H Mode		1F2S Mode		N Mode	
Test Number	Δf (Hz)	Test Number	Δf (Hz)	Test Number	Δf (Hz)	Test Number	Δf (Hz)	Test Number	Δf (Hz)
2	0.3	2	0.4	2	0.6	3	1.5	2	0.4
18	0.4			7	2.0	5	1.5	10	0.5
								12	0.5
								16	1.7
								18	0.5

TABLE X

MEDIAN SPECTRAL SPREADING INFORMATION

	Thule Path			Keflavik Path		
Mode	Δf Median (Hz)	Number of Samples	Range of Δf Values (Hz)	Δf Median (Hz)	Number of Samples	Range of Δf Values (Hz)
$2E/2E_s$	0.4	4	0.3-0.4	0.4	2	0.3-0.4
1F2	3.1	8	0.7-4.1	1.5	5	0.4-2.0
N	2.5	4	0.6-5.8	0.5	5	0.4-1.7

TABLE XI

CATEGORIZATION OF IDENTIFIED MODES BY TEMPORAL VERSUS SPECTRAL SPREAD MEASUREMENTS — ALL MODES AND PATHS

	Low Temporal Spread* Modes	High Temporal Spread** with Submodes	High Temporal Spread** without Submodes
Low Spectral Spread*** Modes	9	3	1
High Spectral Spread**** Modes	2	3	9

* Low temporal spread: $\Delta T < 100\,\mu s$
** High temporal spread: $\Delta T > 100\,\mu s$
*** Low spectral spread: $\Delta f < 1.5$ Hz
****High spectral spread: $\Delta f \geq 1.5$ Hz

TABLE XII

SIGNAL INPUT AND COHERENT PROCESSING PARAMETERS

a. Loss and Temporal Measurements

PRF	100 PPS (each bandwidth, interlaced)
Coherent video input bandwidths	50 and 3.85 kHz
Total input range gate interval	2 ms
Processor input range sample rate	100 kHz
Processor resolution mode	Low resolution (time compression: 40,000)
Processor range bin storage time	2 s
Analyzer scan mode	Nonscanned, centered on offset zero Doppler (25 Hz)
Equivalent output Doppler filter bandwidths	0.5 and 1.75 Hz
Equivalent coherent integration times	2 and 0.6 s (approximately)
Total coherent/noncoherent integration time	2.0 s
Analyzed output signal pulse widths (6 dB):	
• Wideband	25 μs
• Narrowband	150 μs

b. Spectrum Measurements

Processor resolution mode	High resolution (time compression: 200,000)
Processor range bin storage time	10 s
Analyzer scan mode	Scanned with 100 or 200 steps over Doppler range 1 to 10 Hz
Equivalent output Doppler filter bandwidths	0.1 and 0.35 Hz
Equivalent coherent integration times	10 and 3 s (approximately)
Total coherent/noncoherent integration time	10 s

TABLE XIII

GENERAL DATA REDUCTION PARAMETERS FOR THE MODE LOSS AND TEMPORAL SPREAD MEASUREMENTS

Output time quantization (referred to signal input):	
• Wideband	20 μs
• Narrowband	100 μs
Output range-amplitude sample measurement rate	One every 5 s* at each desired time sample point
Total input data period duration	3 to 4 min.
Total number samples made at each selected time-delay point in data period	36 to 48
Temporal extent of output mode gates (maximum):	
• Wideband	300 μs
• Narrowband	1500 μs
Number range samples/mode gate in output	
• Wideband	15
• Narrowband	15

*Except for Test Numbers 19 and 20 when it was approximately one every second.

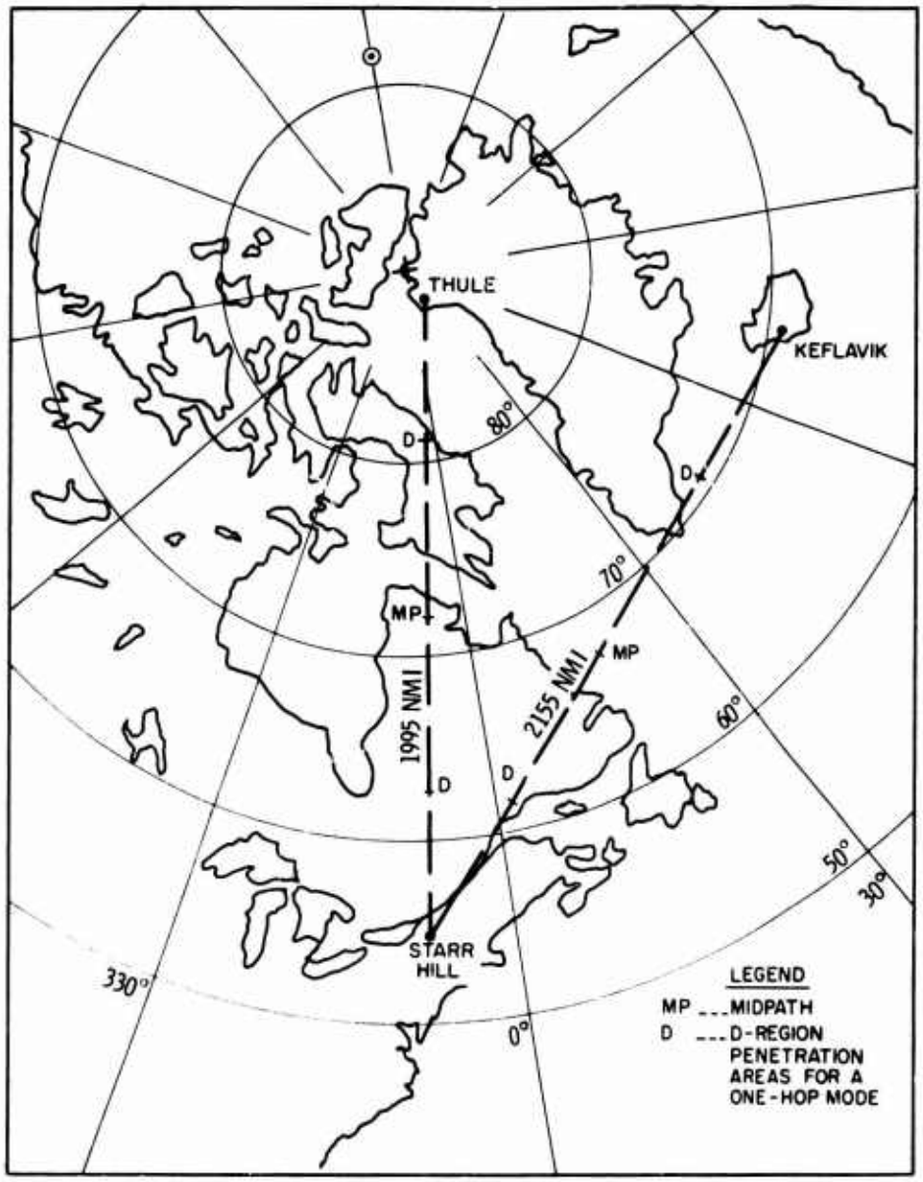

Figure 1. Northern Measurement Paths

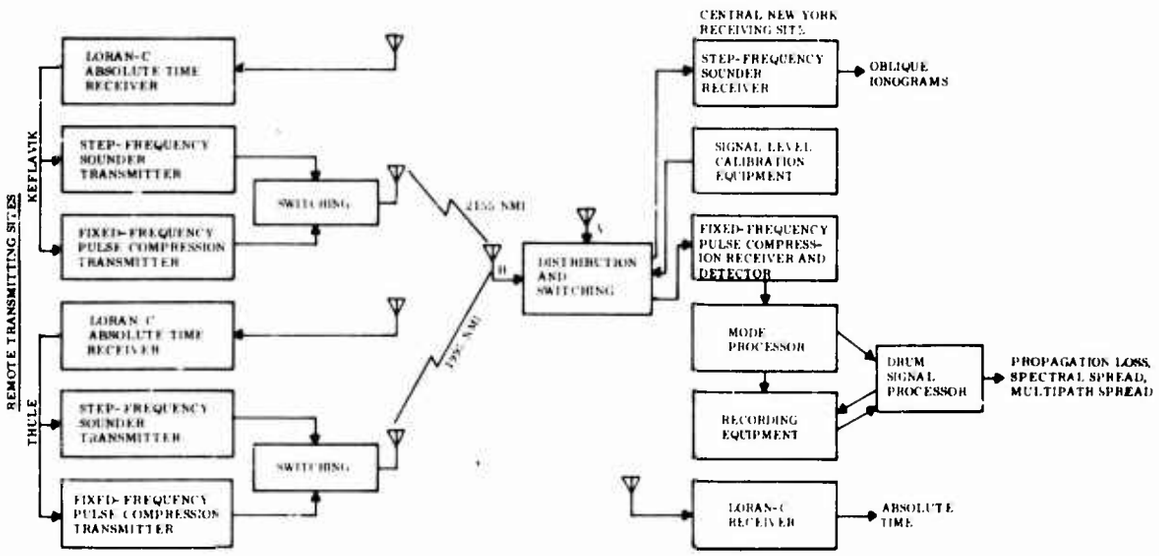

Figure 2. Northern Experimental Measurement System Block Diagram

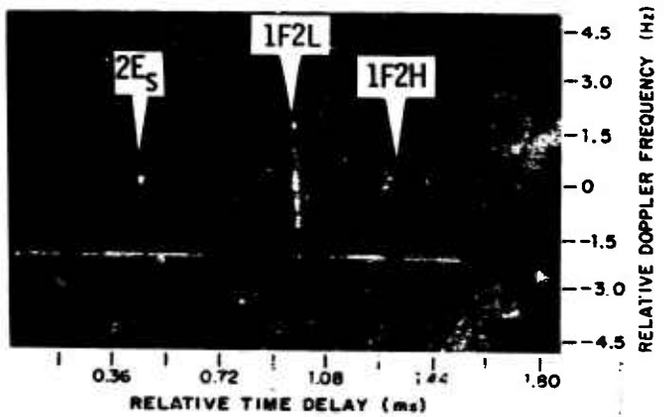

a. Full Output Signal Range Displayed with Maximum Output Signal Peak at Limit Point

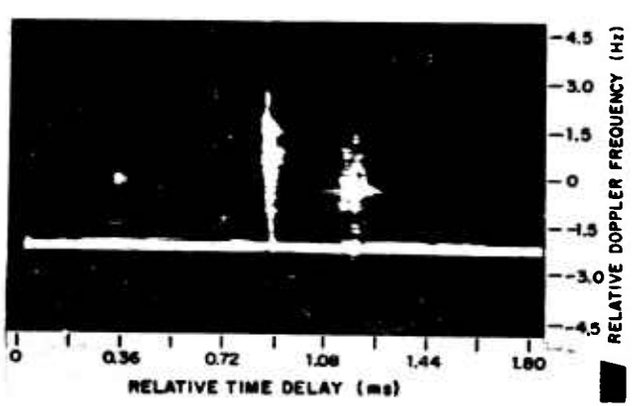

b. Display Video Gain Increased 10 dB

Figure 3. Typical Doppler-Time Delay Display Records of Multiple Modes ($2E_s$, 1F2), Test Number 1, Thule Path, Wideband Signal

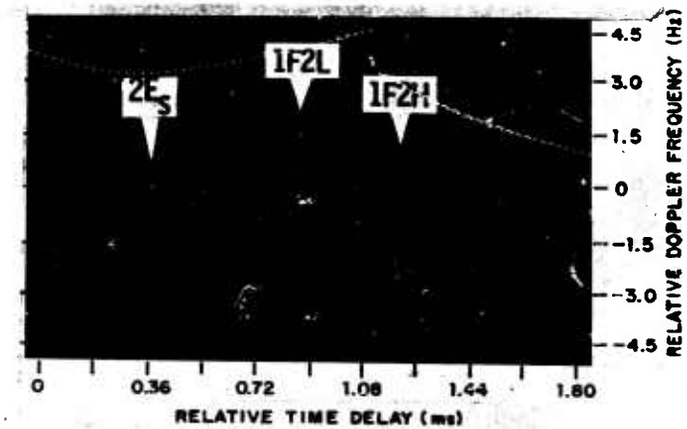

a. Full Output Signal Range Displayed with Maximum Output Signal Peak at Limit Point

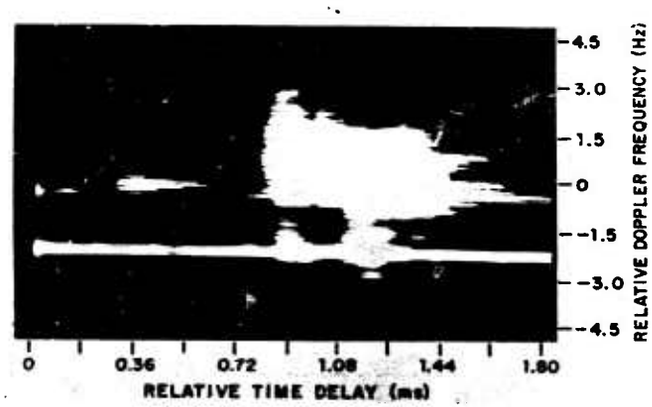

b. Display Video Gain Increased 10 dB

Figure 4. Typical Doppler-Time Delay Display Records of Multiple Modes ($2E_s$, 1F2), Test Number 1, Thule Path, Narrowband Signal

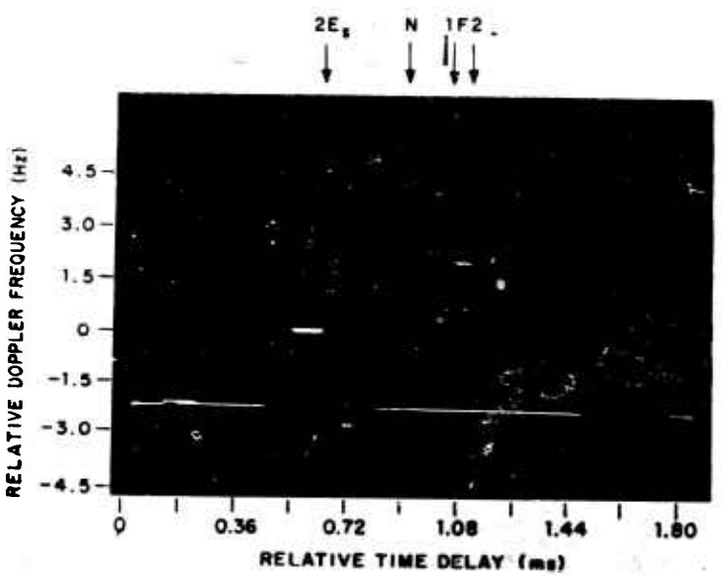

Figure 5. Doppler-Time Delay Display Record, Keflavik Path, Test Number 2, Narrowband Signal

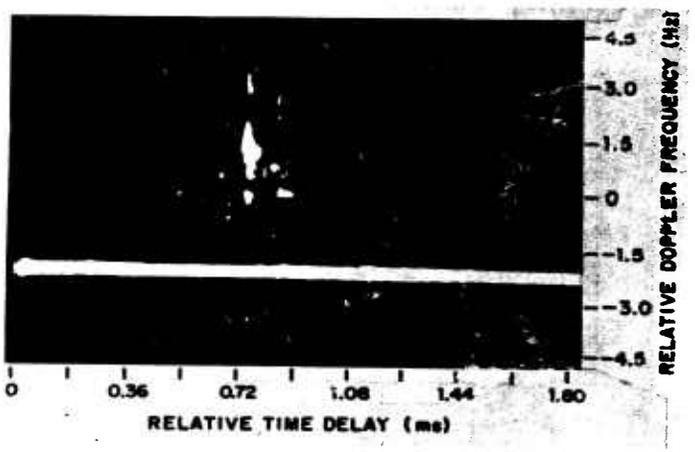

a. Wideband Input Signal; Full Processed Output Signal Range Displayed with Maximum Output Signal Peak at Limit Point

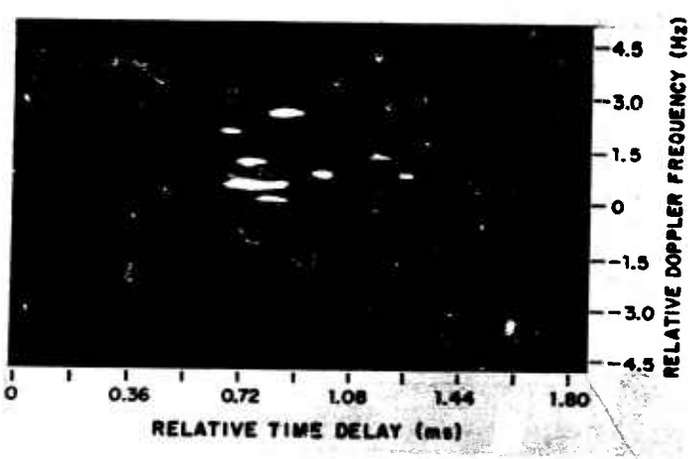

b. Narrowband Input Signal; Full Processed Output Signal Range Displayed with Maximum Output Signal Peak at Limit Point

Figure 6. Typical Doppler-Time Delay Display Records of 1F2 Mode, Test Number 6, Thule Path, Wideband and Narrowband Signals

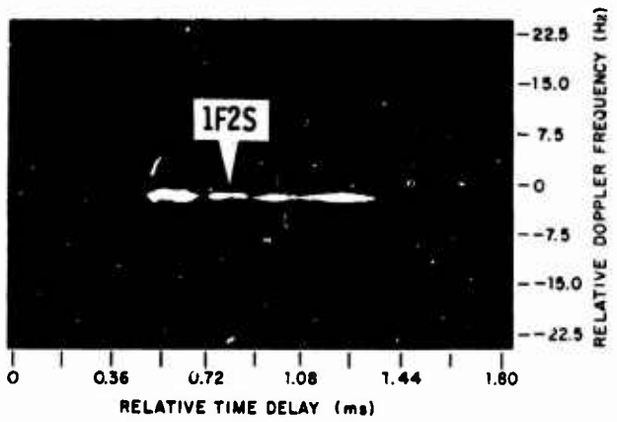

a. Full Output Signal Range Displayed with Maximum Output Signal Peak at Limit Point

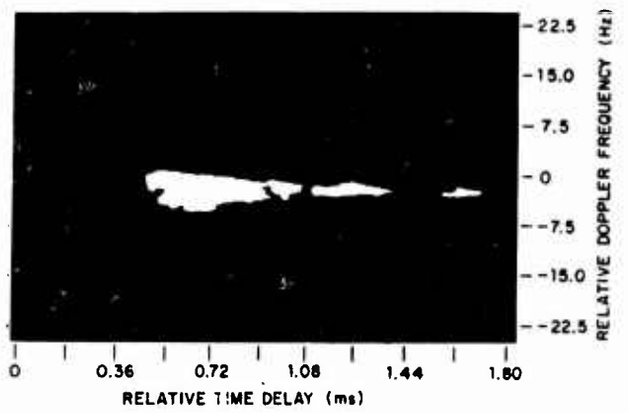

b. Display Video Gain Increased 10 dB

Figure 7. Typical Doppler-Time Delay Display Record of 1F2S Mode, Test Number 4, Thule Path, Narrowband Signal

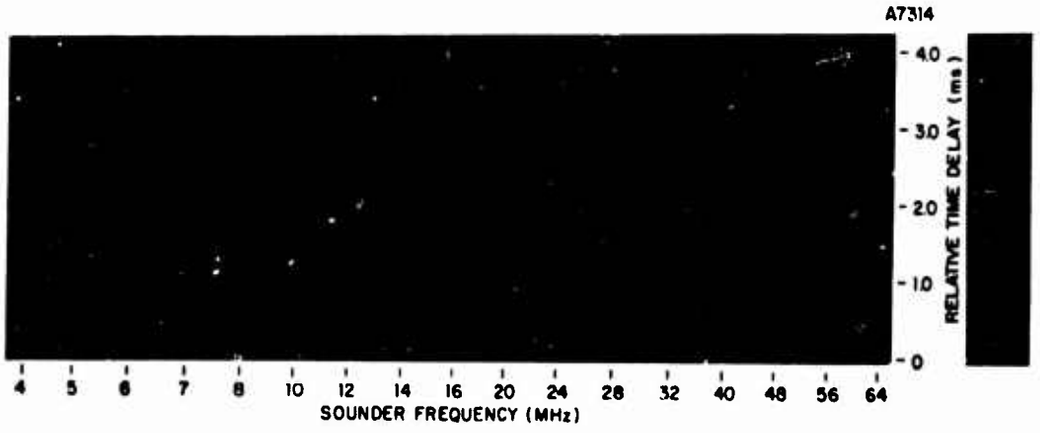

Figure 8. Thule Oblique Ionogram, Test Number 9

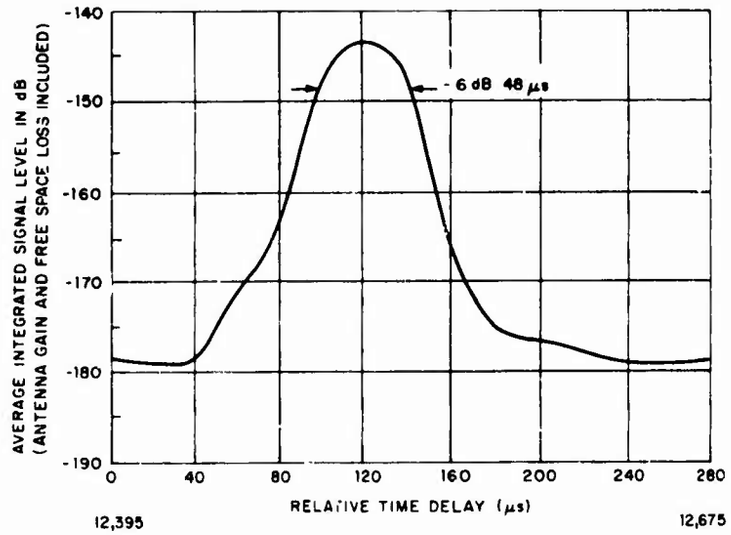

Figure 9. Average Integrated Signal Envelope, Test Number 13, Thule Path, Wideband Signal, 2E Mode

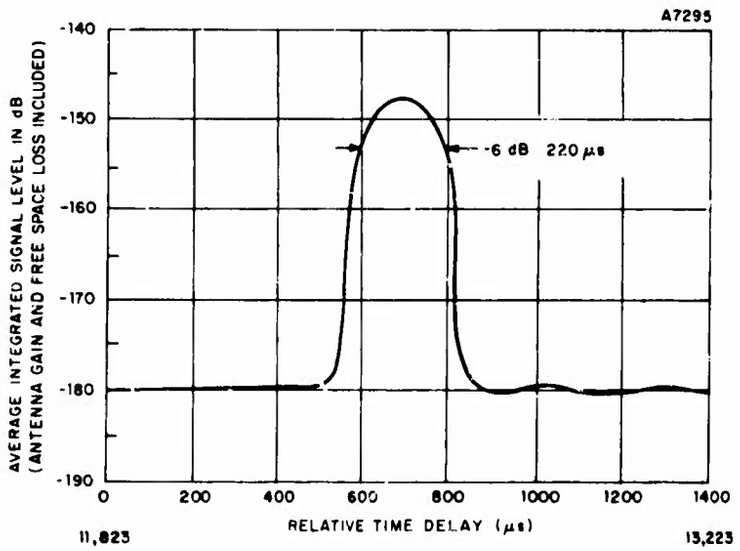

Figure 10. Average Integrated Signal Envelope, Test Number 13, Thule Path, Narrowband Signal, 2E Mode

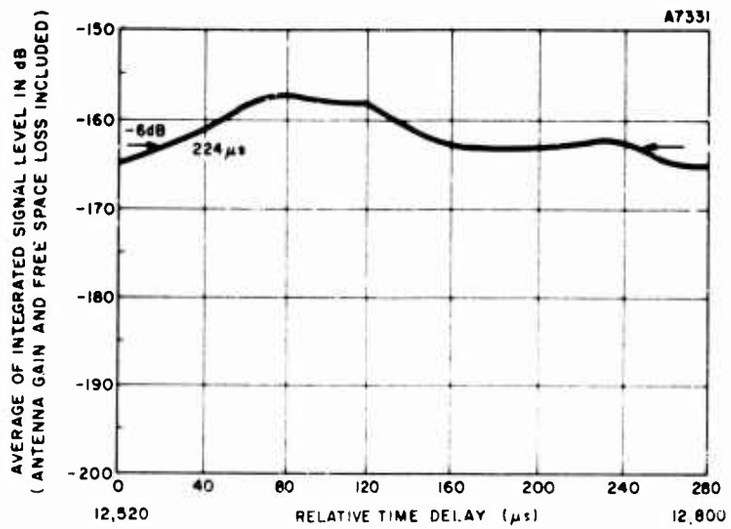

Figure 11. Average Integrated Signal Envelope, Test Number 6, Thule Path, Wideband Signal, 1F2H Mode

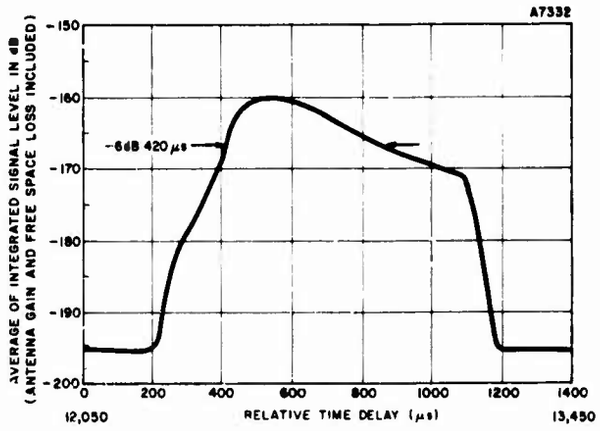

Figure 12. Average Integrated Signal Envelope, Test Number 6, Thule Path, Narrowband Signal, 1F2H Mode

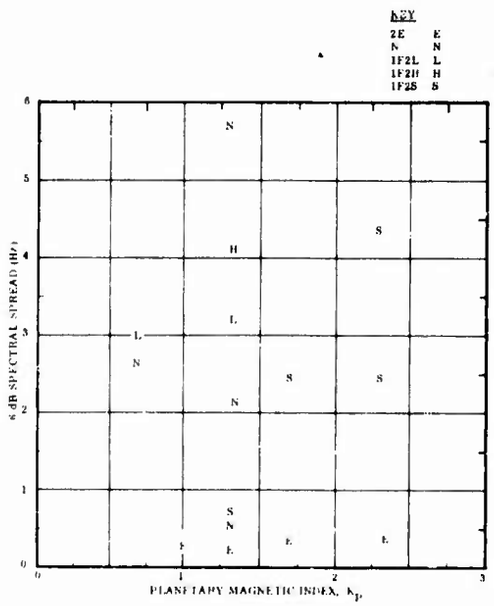

Figure 13. Spectral Spread Observed on the Thule Path as a Function of K_p

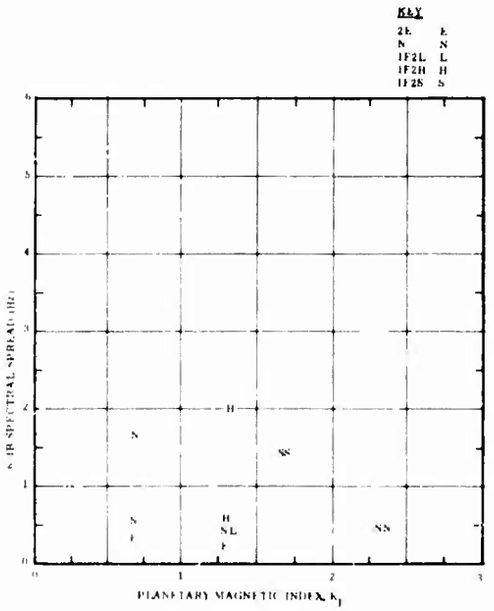

Figure 14. Spectral Spread Observed on the Keflavik Path as a Function of K_p

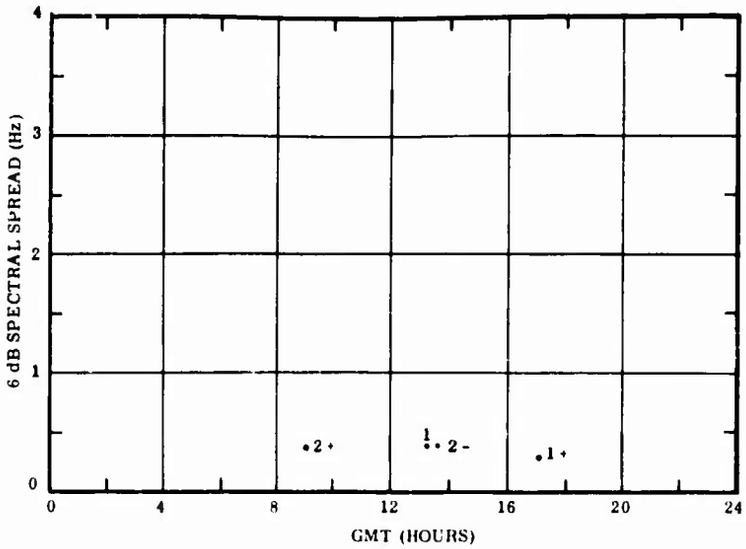

a. Thule Path

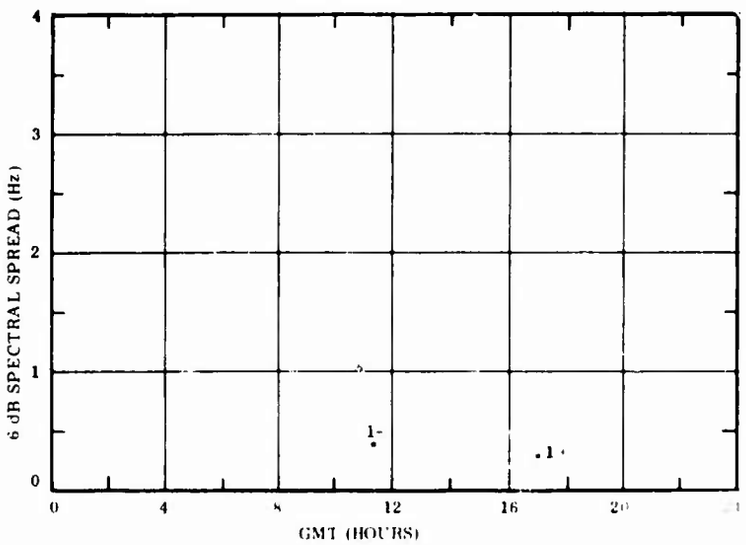

b. Keflavik Path

Figure 15. Diurnal Variation of the $2E/2E_S$-Mode Spectral Spread

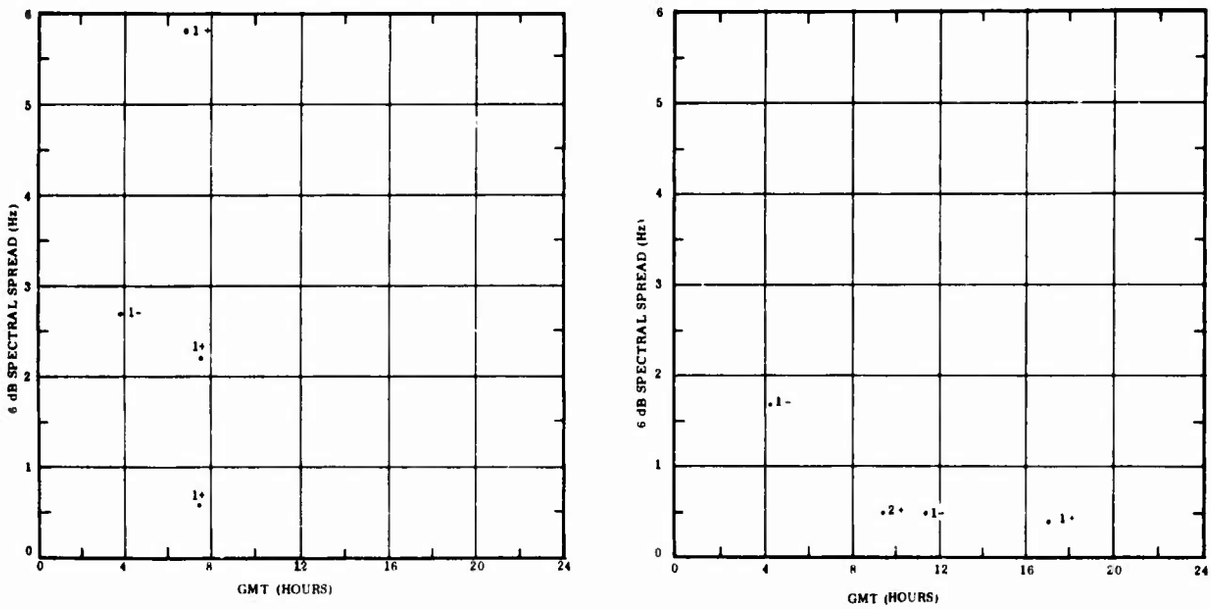

a. Thule Path

b. Keflavik Path

Figure 16. Diurnal Variation of the N-Mode Spectral Spread

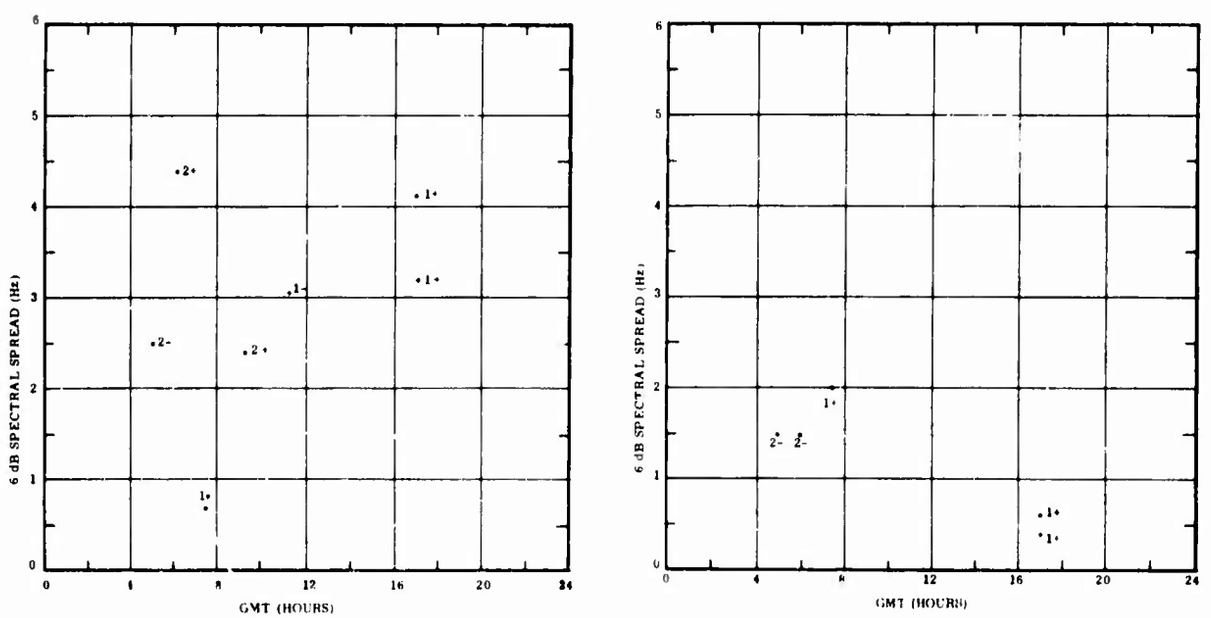

a. Thule Path

b. Keflavik Path

Figure 17. Diurnal Variation of the 1F2-Mode Spectral Spread

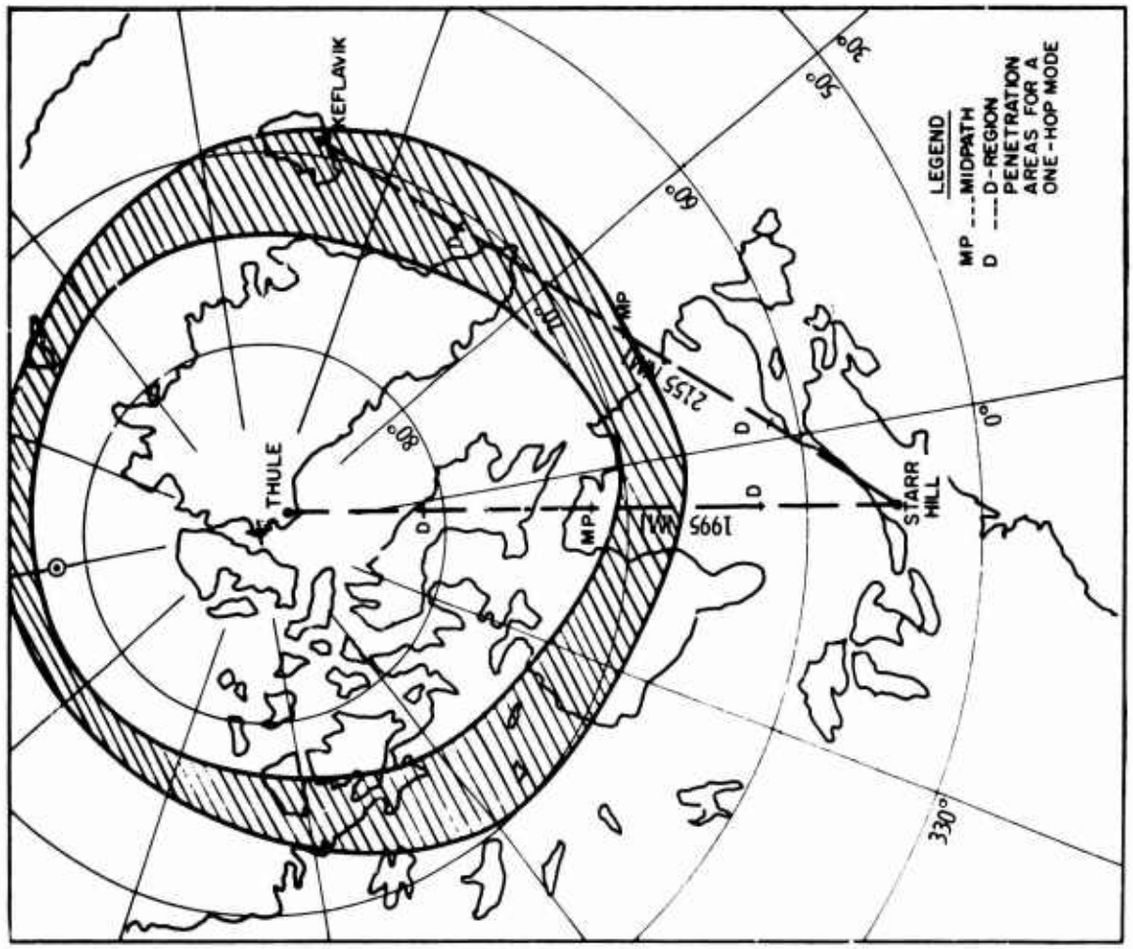

Figure 19. Path Geometry with Respect to Feldstein-Starkov Auroral Oval for Q = 1 at Midnight Along the 0° Geomagnetic Meridian

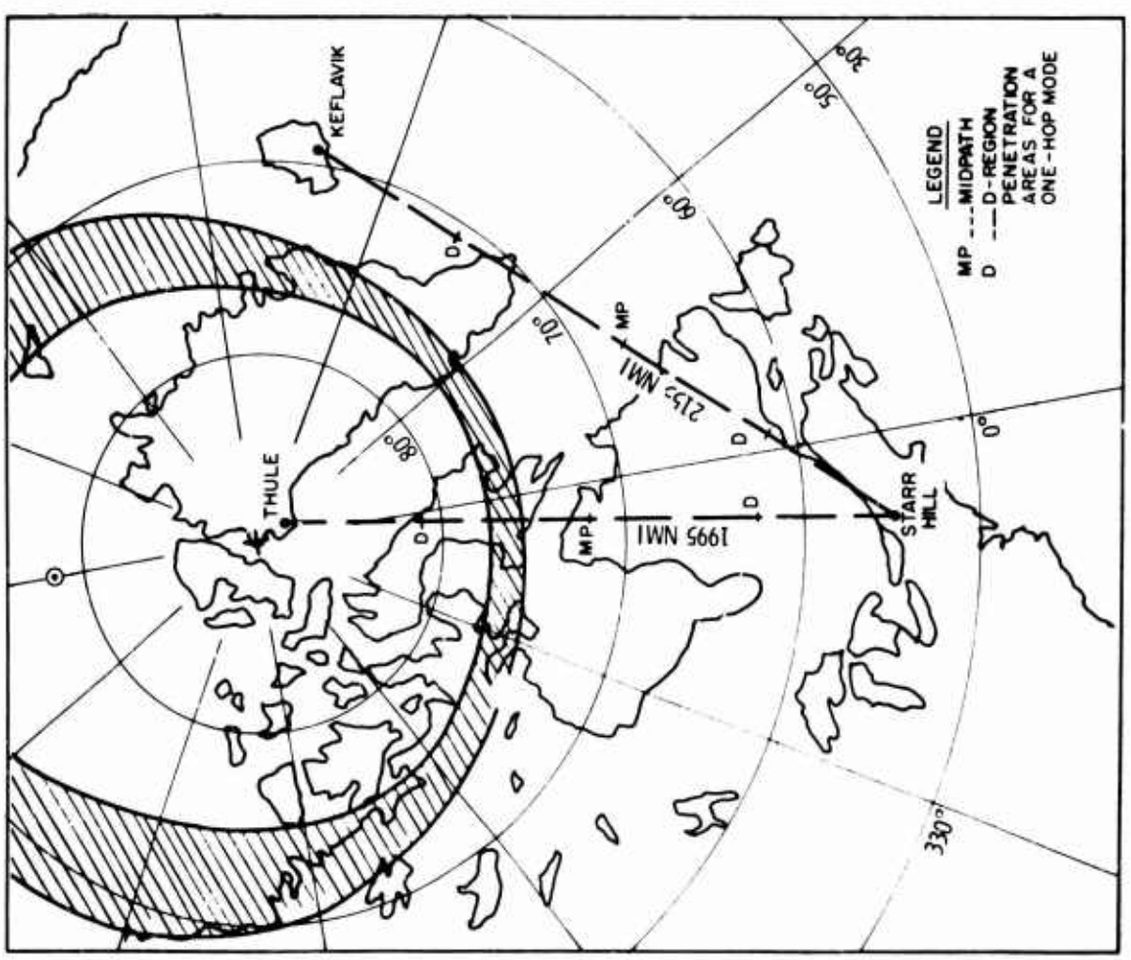

Figure 18. Path Geometry with Respect to Feldstein-Starkov Auroral Oval for Q = 1 at Noon Along the 0° Geomagnetic Meridian

POLARISATION EFFECTS ON SKY-WAVE PATHS AT HIGH LATITUDES

P. A. Bradley
RADIO AND SPACE RESEARCH STATION
Ditton Park, Slough. SL3 9JX
England

SUMMARY

The principles involved in the determination of polarisation coupling losses on sky-wave paths are briefly discussed. The way these losses depend on the limiting polarisations of the upgoing and downcoming waves at the bottom of the ionosphere are illustrated and it is shown that at frequencies in excess of about 2 MHz simple expressions are available for these limiting polarisations which are independent of the form of the ionisation profiles.

In general, limiting polarisations and thus polarisation coupling losses are functions of wave frequency and of ray-path directions with respect to the direction of the Earth's magnetic field. At high latitudes changes in the angle between the field and ray path directions lead to marked variations in polarisation coupling losses for nearby paths. Sample calculations are presented for a range of conditions to illustrate single- and two-way path losses. The calculations include the case of two-hop paths where there are additional features associated with the change of polarisation at ground reflection. The results show the importance of the optimum choice of aerial polarisation. The way in which backscatter amplitude return patterns can be influenced by polarisation effects is also illustrated.

1. INTRODUCTION

Sky-wave signals at high frequencies are employed over arctic propagation paths for communication to remote outposts and in radar systems which probe the ionosphere by detecting signals backscattered either directly from ionisation irregularities or from distant ground positions. For installation design purposes involving both forward and bi-directional paths there is a need to be able to estimate transmission losses and to devise means of minimising these. In this paper the role of polarisation effects on the transmission loss is discussed and the importance of the correct choice of transmitting and receiving aerial polarisations emphasised.

2. THE SINGLE-HOP FORWARD PATH

2.1. General Considerations

Consider propagation from a transmitter at T to a receiver at R via a single ionospheric reflection as shown in Fig. 1. In the general case the radiated wave from T will be elliptically polarised and will travel with unchanged polarisation over the section of path TA, where A may be regarded as at the effective base of the ionosphere. A is at a height known as the height of limiting polarisation and is the height where the polarisation of a downcoming wave ceases to change. Over a relatively small height range around this limiting height the incident wave is split into a pair of magnetoelectronic ordinary (o) and extraordinary (x) waves which can then be regarded as travelling independently through the ionosphere over the adjacent paths AB and AB' respectively, where B and B' are the corresponding points of emergence from the ionosphere.

The o and x wave polarisations within the ionosphere are known as the characteristic wave polarisations and these vary along the ray paths since they are functions of the wave frequency and direction, the direction and strength of the Earth's magnetic field, and the local ionisation concentration and collision frequency. A receiving aerial at R which responds to waves of a particular polarisation will pick up components of the o and x waves as determined by the degree of polarisation match to the two emergent waves. The polarisations of the emergent waves are known as the limiting polarisations. The limiting polarisations at A are also important since these determine in conjunction with the transmitted wave polarisation the fractions of power imparted to the upgoing o and x waves.

If it is assumed that the relative phases of the o and x waves at the receiver are random since the phase paths differ by many wavelengths then the separate powers may be regarded as additive. Thus the contribution to the transmission loss due to polarisation effects can be determined if the limiting polarisations of the waves are known. It should be noted however that polarisation effects cannot be considered in isolation from ionospheric absorption because this differs for the o and x waves so that the effective polarisation coupling loss of the combined waves is itself a function of the o wave absorption.

2.2. Limiting Polarisation

The determination of wave limiting polarisations has provoked considerable attention over a number of years. It has generally been assumed that at m.f. and h.f. the limiting polarisation of a wave is equal to its characteristic polarisation at the height of limiting. Moreover this height has been taken as so high that electron collisions can be neglected, yet so low that the finite electron concentration may also be ignored.

Budden[1] has extended an analysis of Booker[2] to devise an expression for the height of limiting polarisation. Using this expression and realistic ionisation profile models Bradley[3] deduced limiting heights for medium and high frequencies in the range 50-70 km. This means that for some paths electron collisions would have an important influence on wave polarisations. More recently however Knight[4] has produced a method of calculating wave limiting polarisation by considering a downcoming wave penetrating a succession of slabs of constant ionisation. The wave incident on a given slab is resolved into an o and an x wave with characteristic polarisations appropriate to the slab. These component waves are then

regarded as traversing the slab independently and their attenuations and phase changes are noted. At the interface to the next slab they are summed and then resolved again into o and x waves, but this time with characteristic polarisations appropriate to the next slab. The process of resolution and summation is repeated through successive slabs to some lower height where the resultant downcoming wave polarisation ceases to change; this is taken as the limiting polarisation.

The form of a polarisation ellipse may be specified by its axial ratio and tilt angle. Figure 2 shows the axial ratios of the limiting polarisations of downcoming o and x waves at vertical incidence given by the slab method for propagation at a series of different frequencies through a representative daytime ionospheric model. Also shown is the axial ratio given by the characteristic wave equation with the ionisation concentration and electron collisions being neglected, here referred to as the approximate expression. It is seen that at the lower frequencies the o wave is more nearly circular and the x wave more elliptical than as given by the approximate expression, but that at frequencies in excess of about 2 MHz the approximate expression provides a reasonable estimate of the axial ratio. It can also be shown that although the approximate expression gives zero tilt angle, corresponding to the major axis of the polarisation ellipse lying parallel to the projection of the Earth's magnetic field onto the plane of the wavefront, tilt angles are generally small at frequencies above 2 MHz under all daytime conditions when the polarisation ellipses have marked eccentricities. Thus the approximate expression may be regarded as adequate for determining wave polarisations at h.f. This also holds for oblique paths. By night when limiting occurs at greater heights and there is less absorption the approximate expression is accurate at frequencies down to about 1 MHz. Accordingly in the following analysis it has been used to deduce limiting polarisations.

2.3. Sample Calculations for High-Latitude Paths

We now consider some sample calculations for high-latitude paths. Use is made of equations for ray-path and magnetic-field geometry given by Moorat[5]. The magnetic-field model has been taken as the spherical harmonic representation of Jensen and Cain[6]. The calculations relate to paths between a transmitter at Slough (latitude 51°N, longitude 1°W) and a receiver at various locations at higher latitudes.

At high frequencies it is usual to employ transmitting and receiving aerials which are linearly polarised in the horizontal or normal (vertical) directions, so the calculations take account of the appropriately polarised signal components at the receiver and give the polarisation coupling loss between pairs of such linearly polarised aerials. They have been performed for single-hop paths out to a range of 4000 km along geographic azimuths of 45, 30, 15°W, N, 15, 30 and 45°E. Angles of elevation have been chosen to be consistent with ray paths which are mirror reflected from an F layer at a height of 320 km. General area coverage charts have been prepared as shown in Fig. 3.

Figure 3(a) gives L_{HH}, the polarisation coupling loss in decibels for the o wave between a horizontally polarised transmitting aerial and a horizontally polarised receiving aerial at a frequency of 10 MHz. Figure 3(b) correspondingly shows L_{NN}, which is the polarisation coupling loss between normally polarised aerials. L_{HH} and L_{NN} may be regarded as the effective polarisation coupling losses for daytime conditions when the x wave is strongly absorbed and can be ignored. When there is little absorption present (a condition approximately met at night) the powers in the o and x waves may be regarded as additive so that polarisation coupling losses are reduced. Neglecting any differential absorption between the two waves gives $L_{HH} = L_{NN} \leqslant 3$ dB. By day Fig. 3 shows that polarisation coupling losses are generally in the range 3-5 dB L_{HH} when using normally polarised aerials. However much greater losses of around 10-20 dB arise over paths to distances of between 1000 and 2000 km, when using horizontally polarised aerials. Losses at these distances are greater along the meridian than along other azimuths. The advantage of using normally polarised aerials on high-latitude paths has previously been noted by Bradley[7].

From reciprocity considerations the curves of Fig. 3 also apply if transmitting in the reverse direction to a receiver at Slough. Losses for the reciprocal path under the idealised night time conditions discussed are also unchanged. When the transmitting and receiving aerials are orthogonal and linearly polarised it can be shown that for both night and day conditions over the paths discussed with either transmitter or receiver at Slough, polarisation coupling losses are approximately equal to L_{NN} if a normally polarised aerial is used at Slough or to L_{HH} if a horizontally polarised aerial is used. This is because the limiting polarisations are approximately circular on the northern ends of the paths.

3. THE TWO-HOP FORWARD PATH

3.1. General Considerations

It is sometimes assumed that polarisation considerations are less important on multi-hop paths and that downcoming waves are more likely to be circularly polarised. This is a fallacy. Consider propagation over the two-hop path of Fig. 4. The first hop behaviour is as already described for the single-hop case but at G the downcoming o and x waves each suffer a change of polarisation as well as a loss of power at reflection. This change in polarisation depends on the reflection properties of the ground and leads to upgoing waves on the second hop sections of path GC and GC' below the ionosphere which in general are elliptically polarised, with polarisations which bear no simple relationship to each other. At C and C' the two upgoing elliptically polarised waves each excite an o and an x wave so that at R there are four component waves o + o, o + x, x + o and x + x, designated by their magnetoelectronic states within the ionosphere on the first and second hops respectively.

Thus calculations of the polarisation coupling losses associated with the separate wave components at the receiver must take account of those factors discussed above in the single-hop case, i.e. (a) the fractional power coupling at A on the first hop upgoing leg and (b) the fraction of power of the downcoming wave component at R associated with the receiving aerial polarisation; at the same time they must also allow for (c) the loss of power and change of polarisation at ground reflection and (d) the fractional power coupling to o and x waves on the second hop upward leg of the path. In particular each component wave at the receiver has a larger associated polarisation coupling loss than the corresponding single-hop wave component.

Expressions for the evaluation of the additional loss factors for two-hop paths are given by Bradley and Bramley[8] on the assumption that Fresnel reflection theory is valid, with the angles of incidence and reflection at the ground equal. Their expressions are used in the next Section to give representative figures for high-latitude paths.

3.2. Sample Calculations for High-Latitude Paths

Polarisation coupling loss calculations have been undertaken for paths over ranges out to 8000 km from Slough along the same azimuths as quoted in Section 2.3 for single-hop paths. A coarse-scale representation of the major land, sea and polar ice masses has been made for the determination of midpath reflection properties. Ground constants have been taken as -

ice :	conductivity $\sigma = 0.0001$ S/m;	dielectric constant	$\epsilon = 1$
land :	$\sigma = 0.001$ S/m;		$\epsilon = 5$
sea :	$\sigma = 5$ S/m;		$\epsilon = 80$

Figure 5(a) shows on an area coverage map L_{NN} for the o wave for two-hop propagation at a frequency of 10 MHz with the transmitter at Slough. This is the wave component which the one-hop calculations have shown to be the strongest. It is therefore also the dominant component for two-hop modes since the same midpath losses are involved whatever the terminal aerial polarisations. The figure has been drawn to show a gradual variation in the values of L_{NN} for paths where the midpoint reflection shifts from one type of ground to another, since in practice in such regions polarisation coupling losses vary as ionospheric conditions and ray path angles change.

For propagation towards the North losses are not appreciably greater than for single-hop paths despite the assumed reflection from ice for ranges in excess of 6000 km. However, the figure shows that for other azimuths large additional losses associated with the midpath reflection process exist over a wide range of distances. Large losses with L_{NN} greater than 20 dB exist at ranges of 4000-5000 km around azimuths of 30°E and 30°W. There is evidence of azimuthal asymmetry about the North direction with somewhat larger losses on the more Westerly paths.

It may be expected that in general the largest polarisation coupling losses should be associated with reflection from regions with the lowest ground constants, for L_{NN} includes a contribution from the loss of power at reflection. For downcoming waves which are predominantly normally polarised this power loss is greatest at the Brewster angle, which, for reflection from land with the assumed ground constants, gives a maximum loss for paths of around 3000 km range. However, comparison with the results for azimuths of 30°E and 30°W which correspond to land reflections over a wide range of distances shows that the other polarisation factors discussed have an overriding influence.

A limited number of calculations at other frequencies above 3 MHz for the azimuth of 30°W indicate that L_{NN} for the o wave behaves somewhat similarly, although the maximum loss is slightly reduced for the lower frequencies and moves to somewhat shorter ranges. At 3 MHz the maximum is still above 20 dB, occurring at 3700 km as compared with 4500 km at 10 MHz.

For night time propagation over two-hop modes when ionospheric absorption is negligible and the powers of the o and x wave components are additive, L_{NN} shows a pattern very similar to Fig. 5(a) for the daytime. For most paths polarisation coupling losses are of order 3-5 dB, and for no path exceed 10 dB. However, in propagation situations where it is essential to make use of signals over such two-hop paths at all hours, transmitter powers must be chosen to overcome the larger losses involved in the daytime.

In general for two-hop paths reciprocity does not apply, even for single wave components, and L_{NN} differs for paths with the transmitter and receiver positions interchanged. This arises because the polarisation of a wave after ground reflection is a non-reciprocal function of that before reflection. For example, a linearly polarised wave before reflection becomes elliptically polarised after reflection whereas the same elliptically polarised wave travelling in the reverse direction does not usually become linearly polarised again. The exceptional case when reciprocity between pairs of aerials does hold is for propagation in the magnetic meridian. It also holds approximately for reflection from sea water at all angles except those near grazing incidence (Bradley and Bramley[8]). Thus Fig. 5(b) giving L_{NN} for the o wave for reciprocal propagation to Fig. 5(a), i.e. with the receiver at Slough, indicates that losses are very similar for the two directions of propagation for most paths. The exception is for paths showing the greatest losses which lie along azimuths near 30°E when the receiver is at Slough and along azimuths near 30°W when the transmitter is at Slough. However differences are only significant when losses exceed 20 dB and satisfactory reception is then unlikely for either direction of propagation.

4. BACKSCATTER PATHS

4.1. Theory

Polarisation losses on ground backscatter paths represent the summation of the losses on the forward and return paths, together with an allowance for the depolarisation that takes place during the backscattering process itself. Here we restrict ourselves to the case of signals which propagate along the same ray path in both directions.

Suppose that for backscatter on a path designated ABA a normally polarised incident wave at B is depolarised into backscattered component waves of N and H polarisation with relative powers after and before ground scattering of $|\Gamma_{NN}|^2$ and $|\Gamma_{NH}|^2$ respectively in the two cases. Γ_{NN} and Γ_{NH} are known as the field depolarisation coefficients and are complex quantities since they include both amplitude and phase terms. Further, suppose that a horizontally polarised incident wave is depolarised into backscattered component waves of N and H polarisation with powers such that the corresponding depolarisation coefficients are Γ_{HN} and Γ_{HH}. Then a knowledge of the magnitude of the four depolarisation coefficients enables the total polarisation losses on the backscatter path to be determined. In particular for normally polarised transmission and reception we have -

$$[\ell_{NN'}]_{ABA} = [\ell_{NN'}]_{AB}\left\{|\Gamma_{NN}|^2 [\ell_{NN'}]_{BA} + |\Gamma_{NH}|^2 [\ell_{HN'}]_{BA}\right\}$$
$$+ [\ell_{NH'}]_{AB}\left\{|\Gamma_{HN}|^2 [\ell_{NN'}]_{BA} + |\Gamma_{HH}|^2 [\ell_{HN'}]_{BA}\right\} \quad \ldots\ (1)$$

where ℓ is simply related to polarisation coupling loss L by $L = -10 \log_{10} \ell$. Similar expressions may readily be deduced for other transmitting and receiving aerial polarisation combinations.

Unfortunately information on the magnitudes of the four depolarisation coefficients at h.f. is rather scanty. Beckmann[9] notes in a general treatise on depolarisation that although there is no rigorous proof, it is usual to assume from reciprocity considerations that $|\Gamma_{NH}| = |\Gamma_{HN}|$. Further he shows that a perfectly conducting body with large radius of curvature does not depolarise its backscattered radiation, but that in other cases cross-polarisation terms are generated. Generally the poorer the conductivity and dielectric constant of the scattering surface, the larger these cross-polarisation terms become, but for scattering elements aligned along or perpendicular to the plane of incidence, or with elements giving planes of symmetry along the direction of propagation these components are suppressed. In the absence of more precise quantitative information we here take $\Gamma_{NH} = \Gamma_{HN} = 0$ so that eqn. 1 becomes -

$$[\ell_{NN'}]_{ABA} = [\ell_{NN'}]_{AB} [\ell_{NN'}]_{BA} |\Gamma_{NN}|^2 + [\ell_{NH'}]_{AB} [\ell_{HN'}]_{BA} |\Gamma_{HH}|^2 \quad \ldots\ (2)$$

For a single-hop mode this further simplifies to

$$[\ell_{NN'}]_{ABA} = [\ell_{NN'}]^2_{AB} |\Gamma_{NN}|^2 + [\ell_{NH'}]^2_{AB} |\Gamma_{HH}|^2 \quad \ldots\ (3)$$

Intuitively we may expect $\Gamma_{HH} \sim \Gamma_{NN}$, but Hagn[10] and Steele[11] have investigated depolarisation at h.f. and concluded that Γ_{NN} usually exceeds Γ_{HH}. This is particularly true at elevation angles below the Brewster angle.

4.2. Sample Calculations

Figure 6 gives the overall polarisation coupling losses for single-hop o wave backscatter paths at 10 MHz from Slough when normally polarised transmitting and receiving aerials are employed. No attempt is made to incorporate the scattering losses which are proportional to the backscattering cross-sections but merely to illustrate those losses associated with polarisation features. Accordingly the calculations of Fig. 6(a) adopt $|\Gamma_{NN}| = |\Gamma_{HH}| = 1$ and those of Fig. 6(b) adopt $|\Gamma_{NN}| = 1$; $|\Gamma_{HH}| = 0$. Figure 7 gives the corresponding losses for two-hop backscatter paths.

For single-hop modes the inclusion of contributions from the horizontally polarised scattered signals leads to overall coupling losses which are approximately 3 dB less than when the normally polarised scattered signals alone are considered. For two-hop modes a similar result applies at the shorter ranges but for the longer paths the contribution from the horizontally polarised scattered components is small.

Since reciprocity holds for single-hop modes and holds approximately for two-hop modes under the conditions discussed, it follows that Figs. 6(b) and 7(b) are very similar to Figs. 3(b) and 5(a) respectively, but with all loss figures in decibels doubled. The average of the two sets of polarisation coupling loss calculations for backscatter paths gives figures in the range 5-7 dB for single-hop modes. For two-hop modes losses of around 10 dB exist over a wide range of distances on N-S paths but losses of more than 40 dB occur on paths to ranges of 4000-5000 km along azimuths of around 30°E or 30°W.

Night time polarisation coupling losses are given typically as around 4 dB for both single and two-hop backscatter paths, when the powers of the o and x waves are assumed to be additive. However, for two-hop modes there are again larger losses (of up to 15 dB) in the same two areas as noted above for the daytime.

5. CONCLUSIONS

Polarisation coupling losses on single and multiple-hop forward and backscatter paths may be determined in terms of the limiting polarisations of upgoing and downcoming ordinary and extraordinary waves. Comparisons of limiting polarisations deduced by tracing waves through a series of successive slabs of constant ionisation with the polarisations given by the magnetoelectronic characteristic wave expressions neglecting the finite electron concentration and collision frequency, show that the latter expressions give an adequate approximation to the limiting polarisations at frequencies in excess of about 2 MHz.

Sample calculations of polarisation coupling losses for single-hop paths directed towards higher latitudes from Slough indicate that normally polarised aerials should be employed at both the transmitter and receiver. When only the o wave is present (daytime conditions) polarisation coupling losses are then around 3-5 dB.

Daytime polarisation coupling losses for two-hop paths exceed those for single-hop paths because of the additional coupling and reflection losses in the middle of the path. These additional losses are generally greater the poorer the midpath ground-reflecting properties. Normally polarised transmitting and receiving aerials should also be used for two-hop paths. Nevertheless even then daytime losses in excess of 20 dB are to be expected at ranges of 4000-5000 km along paths with azimuths of about 30°E or 30°W. Losses are least along the meridian, being typically only 4-6 dB even in the daytime.

For backscatter paths polarisation coupling losses are shown to depend on the backscattering surface depolarisation coefficients. With certain assumptions regarding these, representative calculations indicate roughly double the losses of the single way paths. Daytime losses are around 5-7 dB for all single-hop modes and 10 dB for most two-hop modes. However for two-hop modes to ranges of 4000-5000 km along

azimuths of around 30°E or 30°W losses of more than 40 dB occur.

It should be possible to confirm experimentally the large polarisation coupling losses noted for some paths. Such tests would serve to establish the practical validity of the analyses described.

6. ACKNOWLEDGEMENTS

The work described was carried out at the Radio and Space Research Station of the United Kingdom Science Research Council, and is presented with the permission of the Director.

7. REFERENCES

1. Budden, K. G.: 'The theory of the limiting polarisation of radio waves reflected from the ionosphere', Proc. Roy. Soc., 1952[A], 215, pp. 215-233

2. Booker, H. G.: 'Oblique propagation of electromagnetic waves in a slowly-varying non-isotropic medium', Proc. Roy. Soc., 1936[A], 155, pp. 235-257

3. Bradley, P. A.: 'Limiting polarisation of radio waves of medium and high frequency reflected from the ionosphere', Proc. IEE, 1967, 114(12), pp. 1837-1841

4. Knight, P.: 'Polarisation of waves reflected from the ionosphere' Electronics Letters, 1969, 5(17), pp. 389-390

5. Moorat, A. J. G.: 'Wave polarisation and its influence on the power available from a radio signal propagated through the ionosphere - Part 1', Proc. IEE, 1968, 115(6), pp. 771-776

6. Jensen, D. C. and Cain, J. C.: 'Interim geomagnetic field', J. Geophys. Res., 1962, 9, pp. 3568-3569

7. Bradley, P. A.: 'Wave polarisation and its influence on the power available from a radio signal propagated through the ionosphere - Part 2', Proc. IEE, 1968, 115(6), pp. 777-781

8. Bradley, P. A. and Bramley, E. N.: 'Ibid - Part 3: 2-hop modes', - to be published in Proc. IEE

9. Beckmann, P.: 'The depolarisation of electromagnetic waves', (Golem Press, Boulder, Colorado, U.S.A., 1968)

10. Hagn, G. H.: 'An investigation of the direct backscatter of high-frequency radio waves from land, sea water and ice surfaces.' Final Report II, SRI Proj. No. 2909, Stanford Research Inst., Menlo Park, Calif., May 1962

11. Steele, J. G.: 'High frequency backscatter from terrain with trees', Proc. IEEE, 1967, 55, pp. 1583-1590

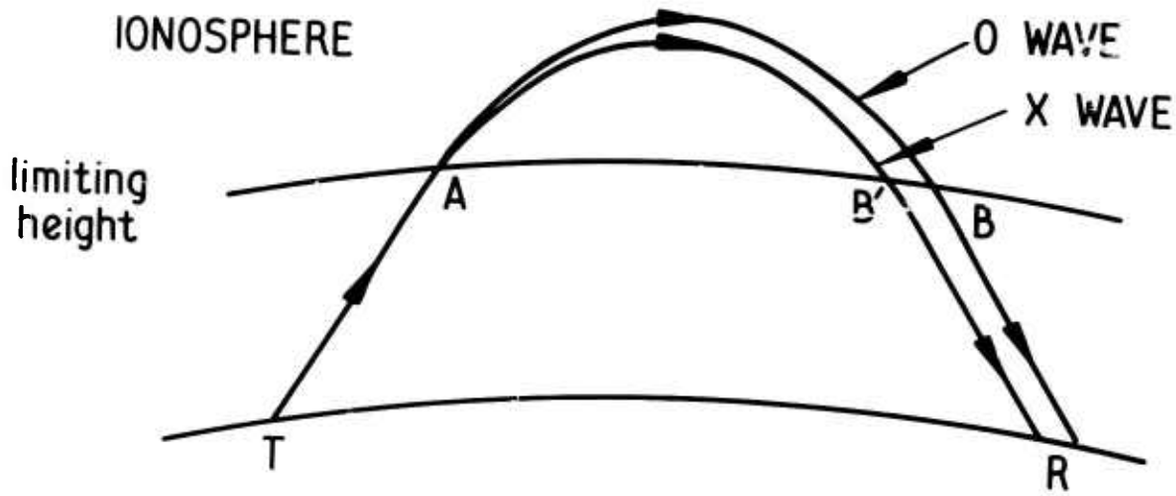

Figure 1 Single-hop raypath

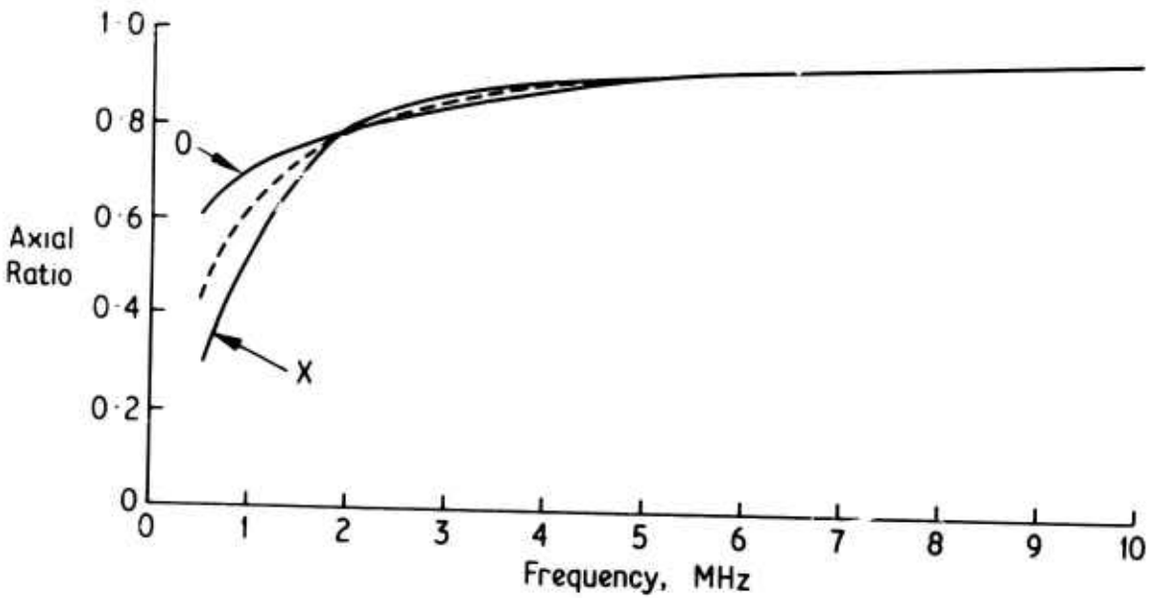

Figure 2 Axial ratio of limiting polarisation ellipse for vertical propagation through daytime ionosphere with magnetic dip angle of 45 deg.

——— from slab analysis ------ from characteristic wave expression

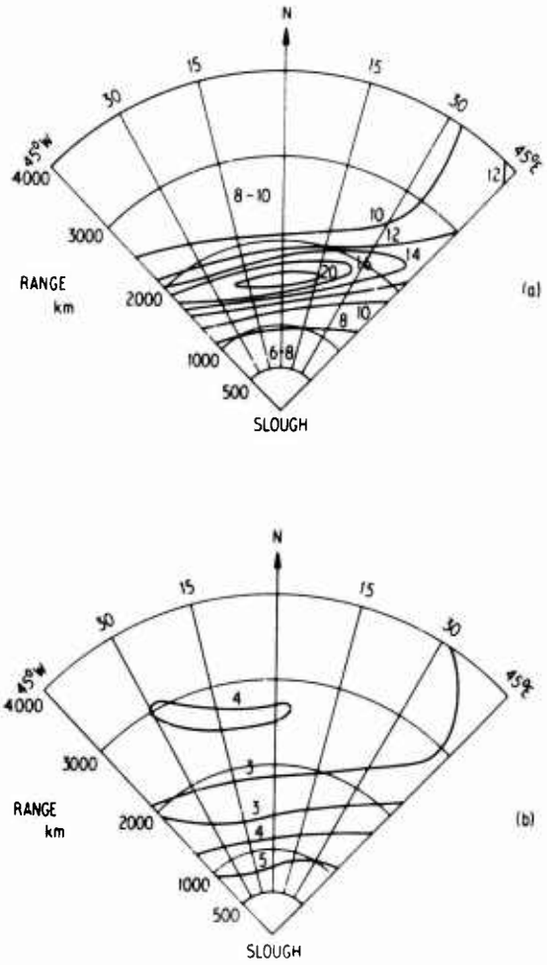

Figure 3 · Polarisation coupling loss in decibels for single hop o wave propagation from Slough at 10 MHz.

(a) L_{HH} = loss between horizontally polarised transmitting and receiving aerials.

(b) L_{NN} = loss between normally polarised transmitting and receiving aerials.

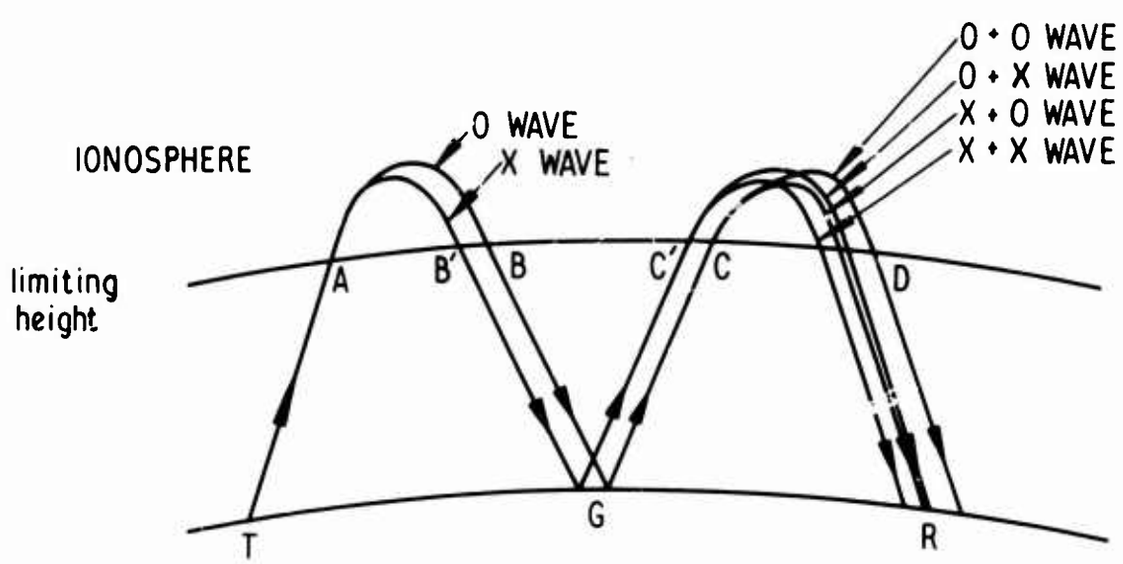

Figure 4 Two-hop raypath

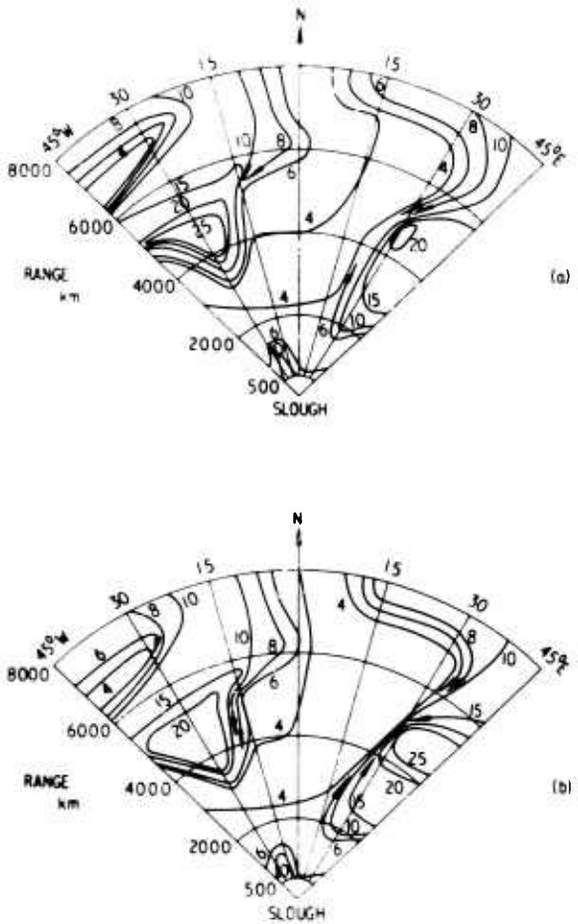

Figure 5 Polarisation coupling loss in decibels for two-hop o wave propagation to and from Slough at 10 MHz using normally polarised transmitting and receiving aerials.

(a) Transmission from Slough

(b) Transmission to Slough

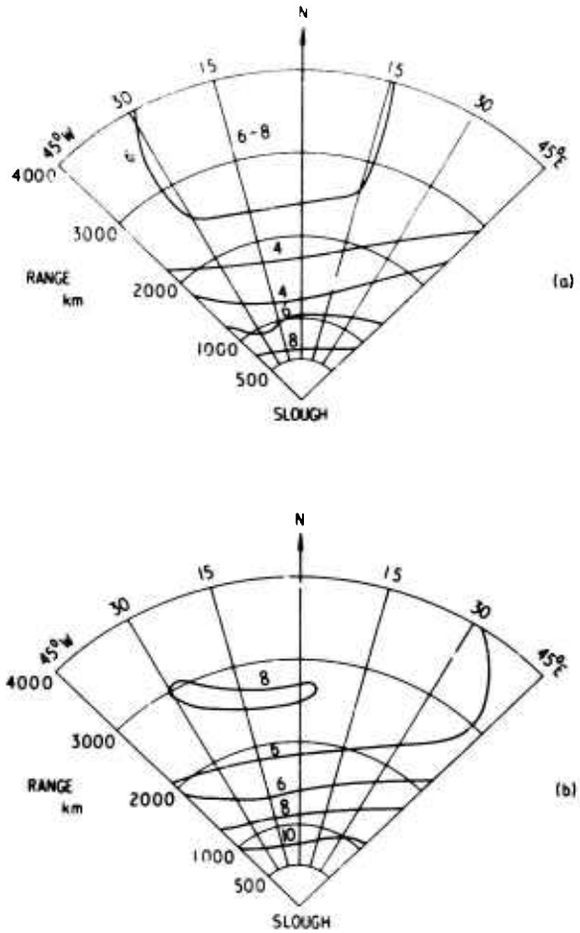

Figure 6 Polarisation coupling loss in decibels for single hop o wave backscatter propagation at 10 MHz between normally polarised transmitting and receiving aerials at Slough.

(a) $|\Gamma_{NN}| = |\Gamma_{HH}| = 1$

(b) $|\Gamma_{NN}| = 1; \quad |\Gamma_{HH}| = 0.$

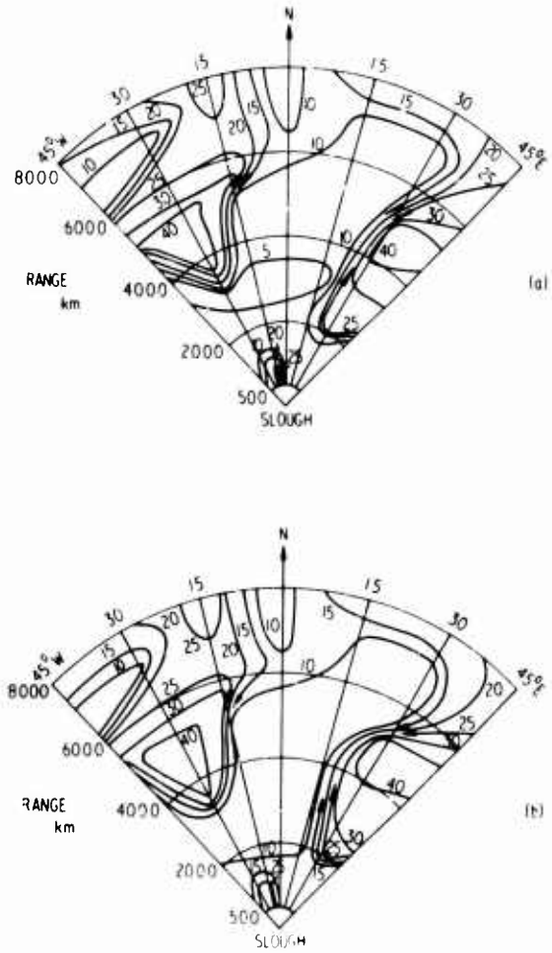

Figure 7 Polarisation coupling loss in decibels for two-hop o wave backscatter propagation at 10 MHz between normally polarised transmitting and receiving aerials at Slough.

(a) $|\Gamma_{HN}| = |\Gamma_{HH}| = 1$

(b) $|\Gamma_{NN}| = 1$; $|\Gamma_{HH}| = 0$.

SPATIAL CORRELATION OF AURORAL RADIO ABSORPTION

K. Toman, R. J. Cormier, J. J. Corbett
Air Force Cambridge Research Laboratories
Bedford, Massachusetts
U. S. A.

SUMMARY

The temporal behavior of auroral radio absorption measured with riometers at medium and high latitudes displays complex patterns which differ spatially. These differences may be limited to a time-displacement of otherwise similar absorption patterns indicating a movement which could be interpreted in terms of a structured, locally enhanced, precipitating, energetic particle stream that moves over a geographic area while preserving its structure. If such a meandrous stream of ionizing particles does not preserve its structure the auroral absorption patterns, which usually differ in the fine structure, will also differ in large-scale features.

In order to assess numerically the spatial coherence of auroral radio absorption, a correlation study was undertaken of such absorption patterns as recorded by more than eight riometer stations during five days of varying activity containing the magnetic storm of 18 April 1965. Using a day as the sample size, the results of this study provide a view of the spatial coherence of auroral absorption which could be further exploited for the prediction of ionospheric propagation in the arctic.

1. INTRODUCTION

Auroral substorms, as seen by means of all-sky cameras, can have small and large features. Of those, the large features can occur on a scale comparable to the size of Alaska.[1] Associated with the expansive phase of a substorm is the phenomenon of considerably enhanced cosmic radio noise absorption. The spatial patterns of auroral displays exhibit some regional similarity to the spatial patterns of auroral absorption.[2] The link is provided by the precipitation enhancement of particles whose energies are sufficient to excite and to ionize atmospheric constituents in the D, E and F regions.

The spatial variation of cosmic noise absorption may be indicative of inhomogeneities in the magnetospheric regime where the particle precipitation process appears to be triggered. They may also be due to the spatial variations in the ambient ionosphere. The qualitative recognition of these spatial variations, irrespective of their origin, poses little difficulties. A quantitative assessment, on the other hand, was thought to yield correlation distances which might be useful for the assessment of the regional extent of radio absorption.

2. APPROACH

The irregular behavior of cosmic noise absorption during a substorm as seen by separated riometer stations indicates the existence of a spatially varying structure likely related to spatial inhomogeneities in the stream of precipitating particles which produce the additional ionization.

The period from 16 to 20 April 1965 was selected for this study. It was of interest to obtain from a sufficient number of stations 30 MHz auroral absorption data throughout the development of a geomagnetic disturbance. Although absorption patterns showed considerable fluctuations the comparison of such patterns obtained from separated stations[3] indicated similarities as well as dissimilarities even for major features of the absorption phenomenon. The combined influence of similarities and dissimilarities on the degree of coherence was thought to be best expressed numerically in the form of a simple correlation coefficient. A sample size of one day was selected. The lag method was employed to determine maximum coherence as well as the temporal sequence of absorption features recorded at separate stations. The correlation between the recorded absorption patterns was found to vary with time and station separation.

3. DATA ANALYSIS

3.1 Station Coordinates

The locations of the stations on the North American continent and Greenland, which produced 'polar' or 'zenith' related cosmic noise absorption data during the 16-20 April 1965 interval, are shown on the geographic map of Fig. 1. On a polar projection for the northern hemisphere Fig. 2 illustrates the locations of stations in geomagnetic coordinates. This display places Thule near the pole It is apparent from Fig. 2 that several widely separated stations are close in geomagnetic latitude.

Pertinent coordinates for the station network are summarized in Table 1. Stations are listed in descending order of the magnetic shell parameter[4] with the corresponding drift periods for electrons of energies ranging from 20 to 500 keV.[5] Table 2 shows a distance chart for riometer stations used in this study. The distances vary from a minimum separation of 139 km between Great Whale River and

Cape Jones to a maximum distance of 5097 km between College and Bedford.

3.2 Data Preparation

The appropriate traces which appear on riometer charts were manually or semi-automatically digitized in one-minute intervals and subsequently processed using available computational schemes for converting current readings into dB of absorption. For that purpose minimum absorption curves were generated for each station from one month of data using the upper bound of current readings as a reference during the event period under study.

Fig. 3 shows the development of cosmic noise absorption observed at Great Whale River (L = 6.9) during and in the aftermath of a geomagnetic storm whose sudden commencement occurred at 1312 U. T. on 17 April 1965. The magnetically quiet period of 16 April ($\Sigma K_p = 4$) was followed by a major disturbance on 18 April ($\Sigma K_p = 34$) which abated gradually during the following week. This slow recovery manifested itself also in the cosmic-ray count measured at Chalk River.[6]

The top portion of Fig. 3 illustrates the behavior of absorption for 17 April. Absorption on the previous day was similar. On 18 April a sharp rise of the 30 MHz absorption occurred at 0650 U. T. approximately 30 minutes after a similarly sharp rise of absorption at Bedford, Mass., about 1500 km south of Great Whale River. The subsequent behavior of absorption appeared irregular and enhanced activity continued beyond 20 April. A sharp rise in absorption similar to that at Great Whale River was observed 25 minutes earlier at College, 10 minutes earlier at Churchill, 3 minutes earlier at Kiruna, but 10 minutes later at Frobisher, indicating an initial poleward progression of the onset of absorption. The apparent speed of this progression was about 850 meters/second.

The sharp absorption onset of 18 April 1965 does not display a 24 hour recurrence pattern. There does appear, however, a twin peak of absorption each lasting for about two hours. The first peak is centered at about 1030 U. T., the second peak at about 1300 U. T. The presence of these peaks is also evident on subsequent days. The persistence of this phenomenon reveals its potential use for prediction purposes. Similar peaks were observed on the data from Cape Jones (L = 6.3). For Churchill (L = 8.6), on 20 April 1965, a pair of absorption peaks occurred simultaneously to those at Cape Jones and Great Whale River. If these similar pairs of absorption peaks are at all related to a spatial precipitation pattern which is stationary with respect to the sun, and the earth rotates underneath, this observation would not support the concept of a simple oval-shape of that pattern, at least not on a scale size of 1000 km.

During the disturbed period the absorption event extended over a large portion of the Globe. The details of the temporal behavior of absorption appeared to be quite different at times for data from different riometer locations. In order to express numerically the degree of similarities between absorption patterns, a correlation lag-study was undertaken. Its purpose was to assess the spatial correlation of auroral absorption in order to provide estimates for the spatial extent of an effective absorption regime.

3.3 Correlation Study

The correlation coefficient between two samples of data x(t) and y(t) is

$$r(\tau) = \frac{[x(t) - \bar{x}]\ [y(t+\tau) - \bar{y}]}{\left\{\Sigma[x(t) - \bar{x}]^2\ \Sigma[y(t) - \bar{y}]^2\right\}^{\frac{1}{2}}} \qquad (1)$$

where $\bar{x}$, $\bar{y}$ are the sample means and τ is the lag. As τ is varied the correlation function attains a maximum value when x(t) resembles y(t) most closely. Eq. (1) was used to compute correlation functions for individual days from 10 to 20 April for all possible station combinations. Because of the global extent and the long duration of the ionospheric absorption activity a sample size of one day was chosen for each data pair.

Fig. 4 illustrates the results of the cross-correlation study for 16 and 18 April using the stations Baie St. Paul (L = 4) and Great Whale River (L = 6.9) which are separated by about 1000 km. For 16 April it appears that the cross correlation does not differ from that of random numbers of finite sample size indicating that on magnetically quiet days the residual absorption for these stations exhibits no systematic component.

On 18 April the cross-correlation-lag differs from that for 16 April in several ways. The correlation appears to peak at a time lag of about 40 minutes as the correlation reaches a maximum value of 0.4. The positive lag is indicative of the absorption pattern recorded at Great Whale River to lead that of Baie St. Paul. The correlogram exhibits undulations which have a period of the order of 15 to 20 minutes.

For the station pair Cape Jones (L = 6.3) and Great Whale River (L = 6.9), whose separation distance amounts to 139 km, Fig. 5 illustrates a cross-correlation lag behavior of the absorption time series for 18 April which has a relatively sharp correlation peak of r = 0.7 at a lag of 6 minutes. In consideration of the sample size which consists of 1440 numerical entries for each string of data a maximum lag of 10% was used which permitted a search for lags of the order of 2 hours.

The observed lag represents a mean value whose real meaning should be viewed in conjunction with the maximum correlation coefficient. For a large maximum the lag is expected to signify a consistency in the temporal sequence of absorption at separated stations. In the case shown in Fig. 5 the negative lag of 6 minutes is suggestive of the absorption phenomenon at Cape Jones to precede that observed at Great Whale River. If the physical phenomenon of particle precipitation has considerable spatial structure and meanders around in an irregular fashion within intervals of time short compared to the sample size the correlation is expected to be poor and the net lag would be a composite of positive and negative lag components. Such a structure would require the use of a smaller sample size than was used in this study.

In this connection it should be noted that periodic features were observed in the absorption data with periods ranging from 5 minutes to about 2 hours. In particular, and as mentioned above, pronounced periods of the order of 10 to 15 minutes were seen in most of the absorption data of 18 April 1965. If these periods are related to the time-of-flight mass spectrometer effect of monoenergetic, drifting electrons, particle energies ranging from about 50 to more than 500 keV could be inferred. Particles with these energies have drift periods which vary with latitude and fall within the observed range. Since particles of a given energy drift faster at high L values their drift periods become shorter toward higher latitudes. Should this phenomenon have any chance of corresponding to physical reality the absorption curves would contain a range of periods, related to a range of particle energies, which could be in phase coherence for stations at like L values but which would get out of phase for stations at different L values. This possibility may, however, not be as simple, since the energy density spectrum of the energetic particles associated with auroral absorption could be softer at higher magnetic latitude. If this were so the drift periods could also increase with latitude.

Other causes of periodicities are hydromagnetic waves which propagate between hemispheres along magnetic field lines. The earth's atmosphere also exhibits a resonance phenomenon at the Brunt-Vaisala frequency which could account for some of the observed periodicities.

The upper curve of Fig. 6 shows an example of the spatial correlation of auroral absorption obtained for 18 April 1965. Each point represents the optimum correlation for a pair of stations separated by the distance indicated on the abscissa. The lines connecting the data points were drawn in an attempt to facilitate the viewing of the results but also to accentuate the potential for predicting the degree of correlation for regions where no measurements are made.

The general behavior of the resulting correlation curve seems to show a nearly constant value of $r = 0.7$ for distances ranging from 140 to 600 km. For greater distances the correlation coefficient decays to $r = 0.3$ at $D = 1000$ km. For $D > 1000$ km fluctuations are noted as the data points are also more densely distributed indicating, perhaps, the influence of local inhomogeneities in the absorption regime. Particularly noteworthy is the rising trend of r for increasing station separations up to $D = 5000$ km.

In order to test the hypothesis that magnetospheric substorms, precipitation and drift of energetic particles and the associated auroral absorption are confined to magnetic shells which may be narrowly bounded in latitude but unbounded in longitude, pairs of observing stations were examined in terms of their corresponding magnetic-shell parameters (L-value). For that purpose the L-ratios were determined for each correlation pair and plotted against distance between stations. Using all possible combinations of station pairs and conveniently arranging the L-ratios to be less than unity, the lower curve of Fig. 6 illustrates the behavior of L-ratios with distance between station pairs for the entire station ensemble. Again, the data points were connected by lines for better viewing. A comparison of the two curves of Fig. 6 shows a similarity in their general behavior although considerable variations are noted. The rising trend of the L-ratios for distances between 1000 and 5000 km compares favorably with the rising trend of r previously noted. This result suggests that for a given distance between stations a higher correlation coefficient between time series of auroral absorption can be expected if the monitoring stations have similar L-values.

While, for 18 April 1965 the maximum correlation $r = 0.75$ occurred at $D = 450$ km, results for the lesser storm of 24 March 1965 ($\Sigma K_p = 22$) showed a maximum correlation of $r = 0.92$ at $D = 139$ km. At $D = 1600$ km r became 0.64 and at $D = 2400$ km r reached a value < 0.1. It was also noted that the correlation diminished as the absorption activity subsided. A rapid decay of r with distance occurred at $D = 800$ km for the weaker absorption activity of 26 March 1965 and at $D = 1600$ km for the stronger activity of 24 March 1965.

The correlation behavior of auroral absorption with distance, as illustrated in Fig. 6, exhibits certain similarities to the correlation behavior of micropulsations.[7] For the latter the correlation coefficient of hourly mean amplitudes of pulsations was reported as $r = 0.7$ for $D = 800$ km separation between observatories and $r = 0.5$ for $D = 2000$ km. At $D = 8000$ km the correlation dropped sharply to $r < 0.1$. The similarity may not be surprising if auroral absorption and pulsation activity are manifestations of a hydromagnetic disturbance.[8],[9] It may thus be possible to use one type of data base for improving or extending the prediction of the other.

4. CONCLUSION

The results of this study suggest that the spatial correlation of auroral absorption appears to display an anisotropy which is controlled by magnetospheric influences. Good correlation between daily auroral absorption patterns may extend over thousands of kilometers along magnetic zones but only over hundreds of kilometers along magnetic meridians. The spatial correlation of auroral absorption is poor for extremely weak activity. Correlation coefficients tend to increase as the disturbance develops in severity. For moderately disturbed periods the correlation can be higher than for severe disturbances.

Although there is considerable fine structure in auroral absorption the spatial correlation study provides numerical values for a morphological study of auroral absorption. These values may become useful for extending locally measured absorption values over a wide region. The results of this study could be applied to defining an index of auroral absorption which characterizes the absorption activity in the auroral region.

5. ACKNOWLEDGMENT

We gratefully acknowledge the former Defence Research Telecommunications Establishment, Ottawa, Canada, the Environmental Science Services Administration, Boulder, Colorado, and the Geophysical Institute of the University of Alaska, College, Alaska, for supplying the cosmic noise absorption data.

Computer programming was performed by K. Dieter under Contract F19628-70-C-0237 with the Mathematical Analysis and Simulation Branch.

6. REFERENCES

1. Akasofu, S.-I., "The Development of the Auroral Substorm", Plan. Space Sci. 12, p. 273 (1964).
2. Hartz, T. R., N. M. Brice, "The General Pattern of Auroral Particle Precipitation", Plan. Space Sci. 15, p. 301 (1967).
3. Jelly, D. M., "On the Morphology of Auroral Absorption During Substorms", Can. Jour. Phys. 48, p. 335 (1970).
4. Catalogue of Data on Solar-Terrestrial Physics, World Data Center UAG-11 (June 1970).
5. Toman, K., G. S. Sales, S. Horowitz, "Energetic Particles and Ionospheric Absorption", Trans. AGU 47, p. 62 (1966).
6. Carmichael, H., M. Bercovitch, "Cosmic-ray Latitude Survey in Canada in December 1965", Can. Jour. Phys. 47, p. 2051 (1969).
7. Miletits, J. Cz., J. Verö, "Correlated Pc-type Micropulsations Observed at Separate Places", Jour. Atm. Terr. Phys. 33, p. 967 (1971).
8. Hargreaves, J. K., "Auroral Motions Observed with Riometers: Latitudinal Movements and Median Global Pattern", Jour. Atm. Terr. Phys. 30, p. 1461 (1968).
9. Sonnerup, B. U. Ö., L. J. Cahill, L. R. Davis, "Resonant Vibration of the Magnetosphere Observed from Explorer 26", Jour. Geophys. Res. 74, p. 2276 (1969).

Table 1 Station coordinates and drift periods for electrons.

	Station coordinates						Drift period of electrons T(min)			
	Geographic		Geomagnetic		Dip					
	Lat	Long	Lat	Long	(computed)	L value				
	North	East	North	East	deg		20keV	50keV	100keV	500keV
THULE	77.48	290.83	88.98	357.93	85.6	263.45	-	-	-	-
FROBISHER BAY	63.80	291.30	75.30	0.52	82.7	14.6	80	33	16	4
CHURCHILL	58.80	265.90	68.70	322.77	83.4	8.6	132	55	28	5
GREAT WHALE RIVER	55.27	282.22	66.58	347.36	81.0	6.92	168	68	35	6
CAPE JONES	54.70	280.20	65.26	345.87	80.5	6.29	180	75	38	8
COLLEGE	64.87	212.17	64.63	256.52	76.6	5.82	195	80	42	9
PRINCE ALBERT	53.22	254.15	61.69	310.98	78.5	4.74	240	100	52	12
VAL D'OR	48.00	282.2	59.32	348.43	77.0	4.20	267	110	57	13
BAIE ST, PAUL	47.38	289.45	58.85	357.97	75.8	3.99	280	118	62	14
OTTAWA	45.40	284.40	56.80	351.52	75.2	3.62	315	128	67	15
DURHAM	43.10	289.10	54.59	357.61	73.2	3.19	400	145	75	17
BEDFORD	42.48	288.72	53.97	357.13	72.8	3.10	400	147	78	18

Table 2 Station separations.

	B.P.	B.	C.J.	Ch.	C.	F.	G.W.	O.	P.A.	Th.	V.D.
BAIE ST. PAUL		553	1006	2023	4669	1787	1007	458	2511	3234	558
BEDFORD	553		1466	2426	5097	2340	1498	480	2763	3785	804
CAPE JONES	1006	1466		1032	3697	1182	139	1047	1699	2495	730
CHURCHILL	2023	2426	1032		2741	1484	1083	1957	925	2247	1621
COLLEGE	4669	5097	3697	2741		3643	3704	4648	2661	2938	4319
FROBISHER	1787	2340	1182	1484	3463		1055	2062	2404	1450	1819
GREAT WHALE RIVER	1007	1498	139	1083	3704	1055		1107	1798	2395	808
OTTAWA	458	480	1047	1957	4648	2062	1107		2297	3477	335
PRINCE ALBERT	2511	2763	1699	925	2661	2404	1798	2297		3093	2009
THULE	3234	3785	2495	2247	2938	1450	2395	3477	3093		3203
VAL D'OR	558	804	730	1621	4319	1819	808	335	2009	3203	

Distances (km) between Riometer Stations

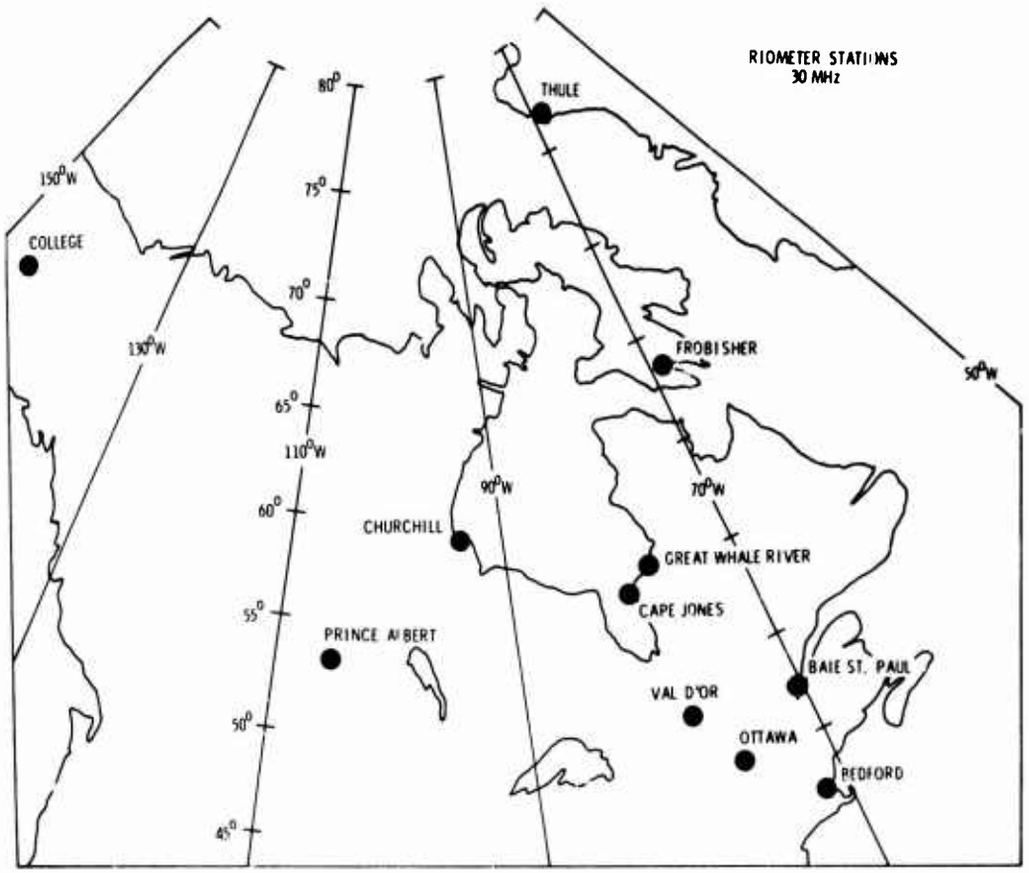

Figure 1 Station locations.

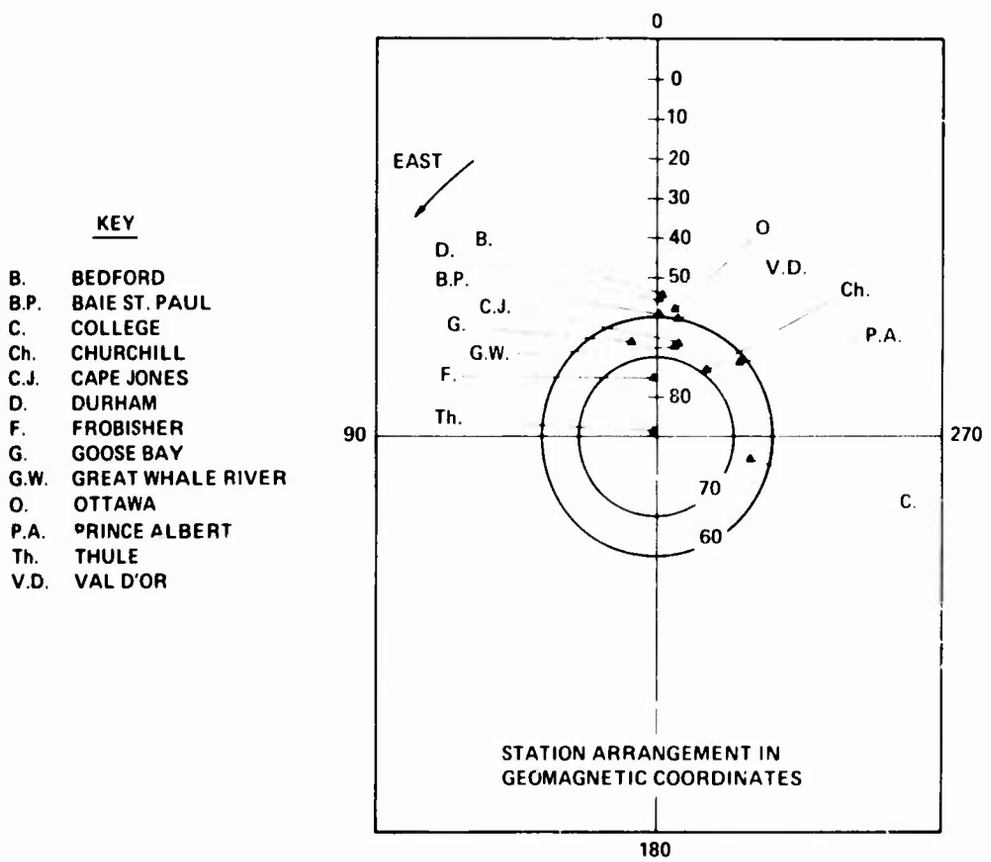

Figure 2 Station locations in geomagnetic coordinates

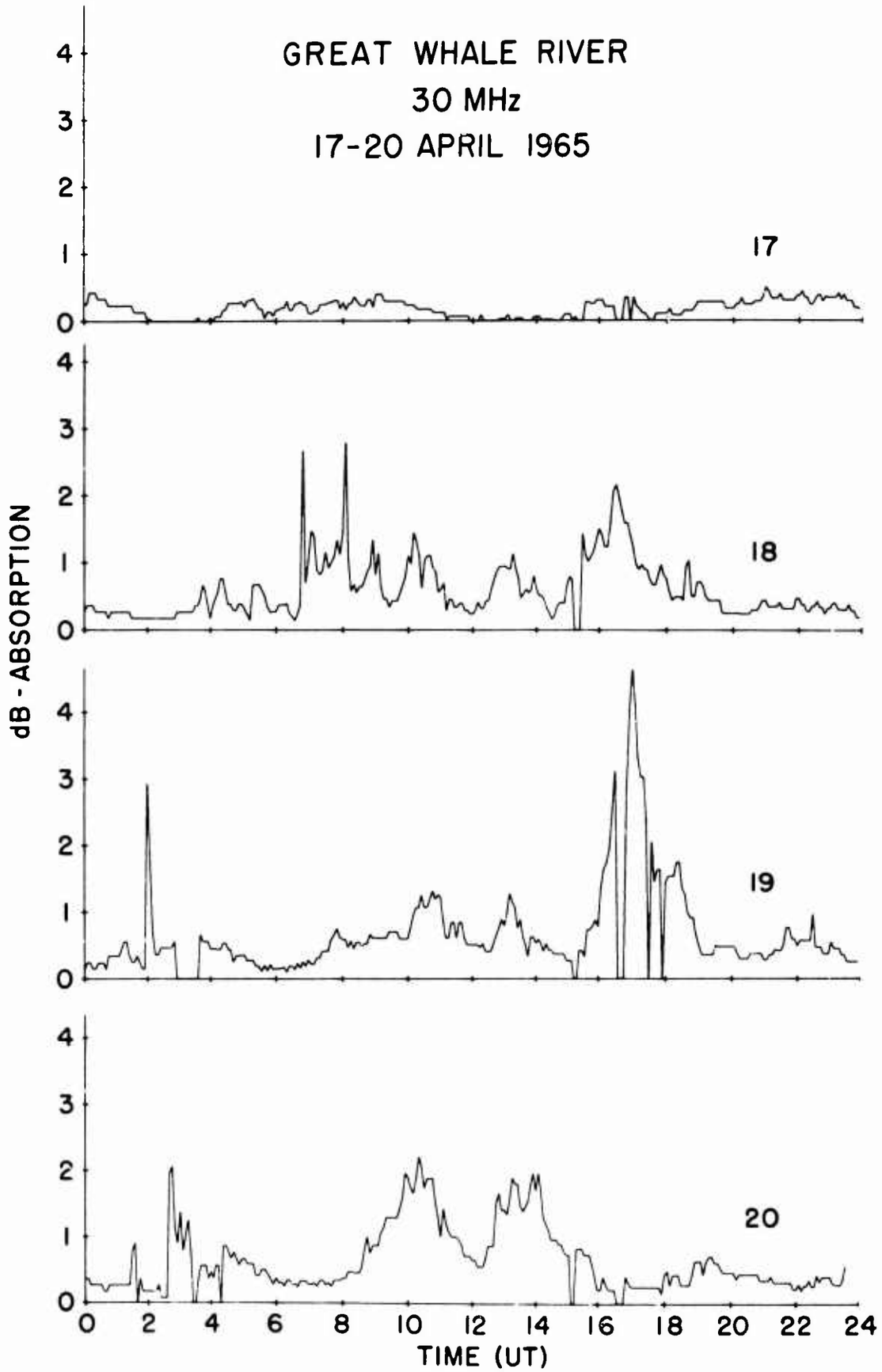

Figure 3 The development of auroral cosmic-noise absorption from 17-20 April 1965.

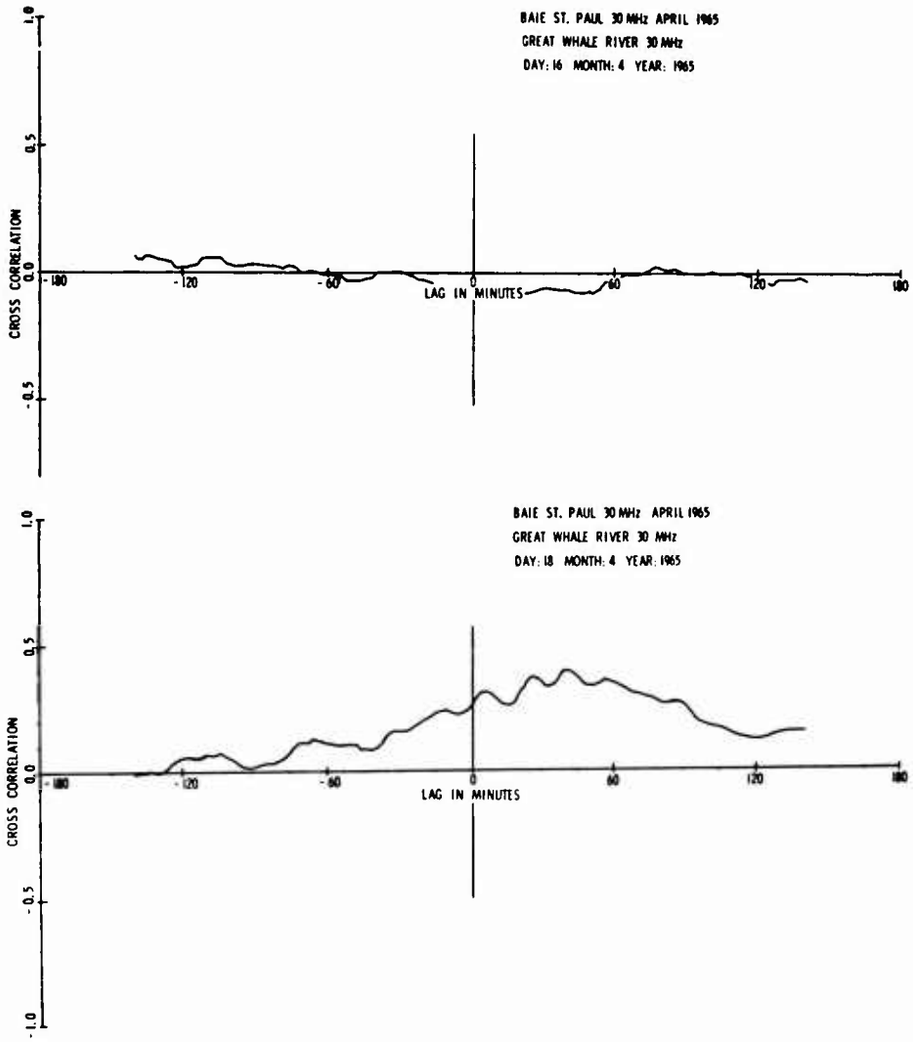

Figure 4 Correlograms for cosmic noise absorption recorded at stations 1007 km apart.

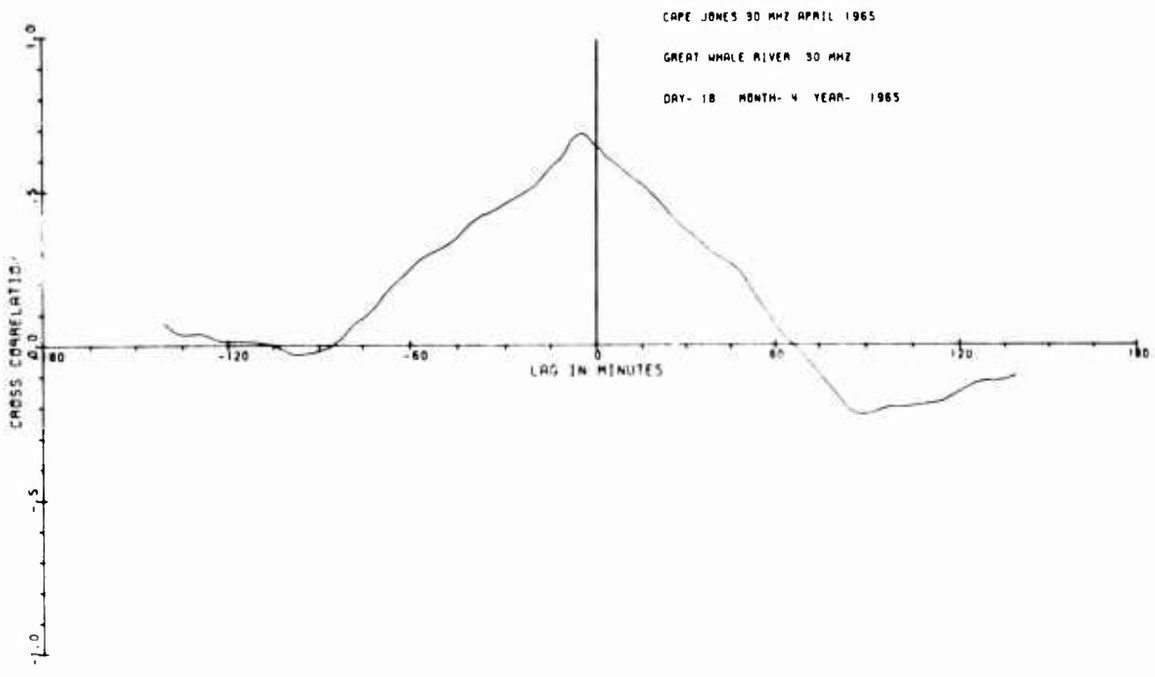

Figure 5 Correlogram for cosmic noise absorption recorded at stations 139 km apart.

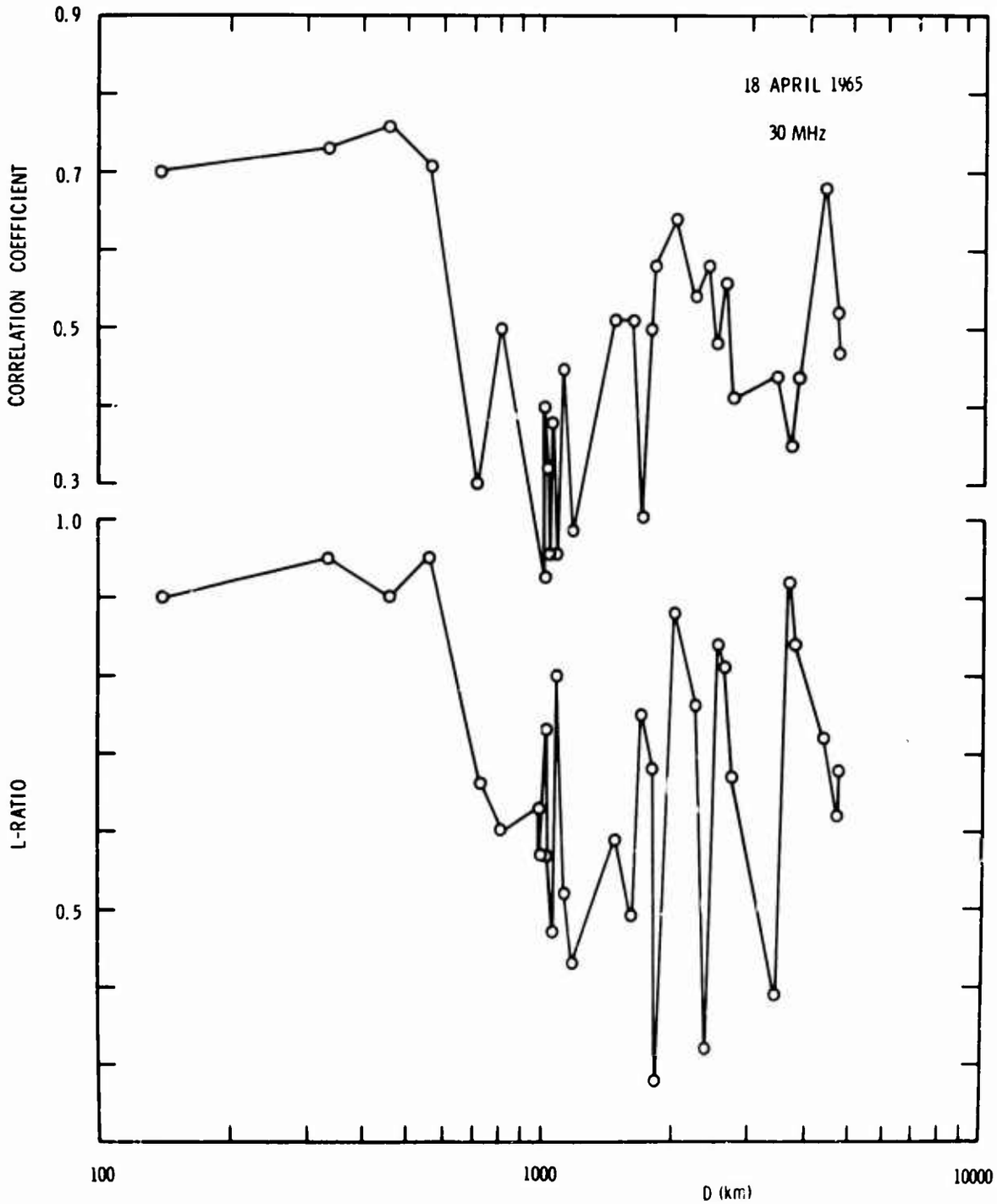

Figure 6 Correlation of auroral absorption with distance between stations. Behavior of the magnetic shell parameter ratio for pairs of stations separated by D(km).

SESSION V

VHF PROPAGATION-TRANSMISSION

CHAIRMAN'S REPORT

by E.D.R.Shearman

This session was the first of two on HF Propagation, which served to focus attention on the special problems associated with radar systems in which major refraction and reflection effects took place in the ionospheric layers on the way to and from scatterer.

The introductory review paper by H. G. Moller of the Institute at Lindau discussed rather briefly the problems under these headings. (The review was too sketchy to be of great value, particularly as no text was available.)

1) Absorption
2) Irregularities
3) Non great-circle propagation
4) High angle ray transmission mode
5) F1 layer effects
6) Sporadic E layer effects

He drew attention particularly to the major uncertainty about the spatial distribution and probability distributions of absorption, and to the important effect of the F1 layer on propagation in the Artic.

J. B. Lomax gave the second paper and discussed measurements of spectra of trans-auroral CW transmissions made simultaneously with oblique sweep frequency pulse soundings. He mentioned the puzzling nature of the spectra; these were spiky, even when arranged over a minute, and individual spikes tended to appear quickly and decay over 10 - 30 seconds.

R. W. Swanson followed by reporting measurements of the time spread and frequency spread over trans-auroral paths made with a more sophisticated technique capable of resolving the full two-dimensional scattering function so that a particular time delayed component had its unique spectrum delineated. Modes were identified with a stepped-frequency sounder.

P. A. Bradley then described a theoretical study of polarization coupling losses in ionospheric propagation and showed results for both forward propagation and radar in the Artic region. Irregularities were ignored. The method was based on the work of Booker as extended by Knight of the B.B.C. Research Department using integration through a series of slabs.

The computation took into account polarization losses at the ionosphere in successive hops and at earth reflections from poor ground, sea water or ice. The results were presented as a function of ground range and azimuthal direction from a location at Slough, U.K. Losses of 20-25 dB in certain directions for particular transmitting polarizations and ranges were noted. Some doubts on the results were expressed by experimentalists and the need for checking against available experimental data was stressed. However, in discussion afterwards it seemed that most of the differences were resolved if the full basic parameters and assumptions were made clear. This was a shortcoming due to not having a printed text available.

K. Toman gave the final paper on 'Spatial Correlation of Auroral Radio Absorption', which described attempts to discover the geographical distances over which auroral absorption was correlated. The basic data used was from 30 MHz riometers and correlations in longitude and geomagnetic latitude (expressed as L ratios) were shown.

Unfortunately, the slides were the wrong size for the projector so that the ordinates were notshown and in spite the questions the main point being made in the talk remained obscure to the writer.

In general discussion Millman questioned Lomax on Spread F as a 'stable medium'. In terms of the spectral measurements on transmitted signals, this implied that the velocities were steady, unlike auroral forms.

A general comment by the writer is that Lomax's technique of separate measurement of multipath spread and frequency spread is clearly less effective than the technique of Swanson using a complicated transmitting waveform able to resolve signals simultaneously in time delay and frequency. The future would seem to lie in the latter technique, although only a limited experiment was carried out by Swanson.

DISCUSSION

R W Swanson

I would like to comment on the fact that no difference in spectral spread was seen in the data discussed by Lomax as a function of mode of propagation. Other measurements reported in paper 23 on a similar but shorter path from Thule indicated considerably more spectral spread for the 1F2 mode compared to the 2E mode. It is suggested that this difference might due to the difficulty of determining the actual mode of propagation even using oblique sounding ionograms. Considering the fact that only one frequency near 7 MHz was employed, this should result in a high probability for E mode propagation, especially during the daytime, which usually has a low value of spectral spread.

J B Lomax

We did in fact see a high percentage of E mode propagation (always 2 3 hop E). However 2F was more frequent. Mode identification was frequently difficult but by observing ionograms taken over a period of hours it was possible to select ionograms in which mode identification could be made with confidence. For example, we could watch the 2E mode disappear and then verify that the remaining mode was 2F by raytracing with true-height profiles obtained from vertical ionosonde records. When the 2E mode was stronger than the 2F mode, so it stood out in the spectral estimate, it had no significant frequency spread (less than 0.1 Hz) The 2E mode generally had little time spread although occasionally its spread was as much as 100 sec. The spectrum of the 2F mode often contained 2,4, and rarely as many as 6 discrete spectral components with different Doppler shifts. The frequency spread of these components was never larger than 1 Hz. I would suggest that your observations of frequency spread (paper no 23) may have contained off-path signal components not detectable by your equipment. Your reported value of 3 Hz, using your definition of spread, could result from off-path signals having as little as 150 sec additional time delay.

G H Millman

1) Lomax stated that the spread F was a stable medium which is contrary to present day concepts. Clarification of this statement is desired.

2) Were you able to correlate your results with the presence of spread F and sporadic E.

J B Lomax

1) Our ionosonde record is made during a time interval of 8 seconds. Power spectral density estimates were calculated for the CW data in time intervals of 10 and 60 seconds. It is my evaluation of vertical ionosonde records of spread F, where the interval between records is 15 minutes, that the same spread F region is seen on a number of records in sequence. The range changes changes with time and the frequency extent also changes. However, in the time frame of our measurements, 8 to 60 seconds, it would appear that the irregularities would not change location or electron density sufficiently to modify propagation over our oblique radiopath.

   Since the F region refraction in the polar zone is occuring over a region on the order of 500 km (along the great-circle path), it is quite probable that the radio wave will encounter a region of irregularities. I wish to emphasize however, that our data indicated that the great-circle ionospheric propagation does not "see" the field alignment of the irregularities. Rather, the bottom of the F layer appears to be rough. A contour of constant plasma frequency varies with height along the path.

2) From vertical ionosonde records made at various locations in Canada, Alaska and the United States, the probability of having E_s along our path was quite high during most of the time. Spread F was apparently present in the polar cap zone virtually 100% of the time.

SWEEP FREQUENCY BACKSCATTER RADARS AS DETECTORS OF HIGH LATITUDE IONOSPHERIC PHENOMENA

Howard F. Bates
Geophysical Institute, University of Alaska
College, Alaska 99701

SUMMARY

This paper is composed of two sections -- (1) a brief review of the current knowledge on high latitude irregularities, and (2) a summary of the results of the HF backscatter program started at College in 1953.

PART 1

References are not cited in the text; source references are listed after the first part, and the publications resulting from the College work are listed after the second part. HF backscatter work is not discussed as such in the first section; instead the characteristics of the irregularities causing HF scatter and propagation problems are described briefly. D-region absorption -- auroral and polar cap -- will not be discussed. The references cited are not intended to be exhaustive, rather they are representative of work done in the area in question.

That the high latitude ionosphere contains many irregularities -- large and small -- has been recognized for years. Spread-F, sporadic-E, radio aurora, meteor echoes, traveling ionospheric disturbance (TID), and scintillations are probably the most familiar effects caused by irregularities; other, less familiar, anomalies exist -- the trough, auroral belt increase, polar peak, and gravity waves. Some of these irregularities are large scale -- hundreds of kilometers -- while others are small scale -- meters. The former affect backscatter observations essentially by modifying the medium through which the echoes propagate, while the latter produce the echoes.

The aurora produces both large- and small-scale irregularities in the ionosphere. The small-scale irregularities appear to be small changes in electron density produced in such a manner that backscatter occurs only very near normality to the magnetic field. The large scale auroral changes consist of increased electron density at all altitudes in the ionosphere; these changes are probably directly attributable to the secondary electrons produced by the precipitating auroral primaries.

The most likely mechanism for producing the small-scale irregularities associated with the aurora now appears to be some sort of an instability that sets up plasma waves in the ionosphere. One mechanism that has been suggested is the two-stream instability set up by the auroral electrojet. There are still some major problems associated with the instability notion; one is that the preferred direction of propagation for plasma waves excited by the two-stream instability is east-west -- paralled to the auroral electrojet, whereas to be viewed by radars the waves must propagate north-south. These problems will probably be solved eventually.

Several authors have considered auroral instabilities set up by an electric field in the E region. Such a system has been shown theoretically to produce the plasma waves in the E region close to, but outside, the optical auroral form. Thus, in this theory, radio and optical auroras would not coincide exactly in space; the experimental evidence at hand indicates the two phenomena occur together but are not exactly coincident in space.

How the observed auroral irregularities are generated in the F region is not clear. To explain spread-F, it has been suggested that the instability is generated in the E layer and the effects coupled into the F layer along the magnetic field lines. There is another possible mechanism for the auroral irregularities. The ionospheric electron density has been found to be increased appreciably at all altitudes in the region containing the auroral precipitation. F-layer densities may double, and at 1000 km, the density may increase by an order of magnitude. Such large increases, particularly at high altitudes, indicate that there is an upward flow of electrons near the aurora; such a flow would produce long, dense, field-aligned structures capable of backscattering energy. An example of one such known structure is an F-layer barium cloud; strong aspect sensitive backscatter is produced in the HF band by barium clouds. The cause of F-layer auroral irregularities is not known and the problem needs to be solved.

Spread-F is still an enigma. The irregularities that cause spread-F are unknown, and, in fact, the means by which vertical incidence spread-F echoes are produced is unknown. Various studies have shown that the spread traces are produced by HF energy propagating obliquely upward, but whether scatter or reflection is involved is unknown. One recent theory suggests that some spread-F is produced by reflection from large-scale, irregularly shaped surfaces. If they exist, these large scale spread-F irregularities are always accompanied by small-scale (decameter) field-aligned irregularities which produce oblique incidence backscatter in the HF band.

It seems reasonable to suppose that spread-F and scintillations should be connected in some way. Recent scintillation work indicates that the high latitude scintillating region has a sharp equatorward boundary that moves systematically with time of day and with magnetic activity. At midnight the boundary is typically near 55° invariant latitude, and at noon 75°. Within the high latitude irregularity zone (excluding scintillation associated directly with the aurora), the few data that exist suggest that the scintillation level does not change greatly with latitude, time, or magnetic activity.

If these scintillation results can be applied to spread-F, they indicate that spread-F irregularities should be distributed more or less uniformly over the polar cap within a sharp, well-defined boundary that moves systematically with time and magnetic activity. There is some backscatter evidence that the spread-F boundary is sharp and moves systematically.

Various large scale anomalies in electron density exist that affect HF backscatter propagation to some extent: the trough, auroral belt increase, the polar peak, gravity waves, and TID's. The latter two are transient effects and will not be considered; they could be of importance, however, when detailed, case-by-case studies of HF backscatter records are made.

The trough is a nightside phenomenon, located close to the equatorward side of the auroral belt. The F-layer electron density can change by a factor of two in a few hundred kilometers; such steep horizontal gradients can strongly affect backscatter propagation, particularly in directions along the trough. Just poleward of the trough the auroral precipitation appreciably increases the F-layer electron density, but not smoothly. The trough decrease -- auroral belt increase is analogous to a smooth, deep valley beside a range of rugged mountains; sometimes a smooth plateau separates the valley from the peaks.

The polar peak has been reported as being an isolated electron density increase located in the F layer

near 80° latitude on the noon meridan. Various hypotheses have been put forward to explain it that involve anomalous electron precipitations or changes in F-layer loss parameters. I have suggested a simpler explanation: the aurora increases the electron density in the auroral belt; since the location of the auroral belt is stationary near 80° around noon, the polar peak is partly the natural result of averaging the data.

Auroral sporadic-E is almost always a thick layer. It is formed by the secondary ionization produced by the precipitating primary electrons of the aurora. At magnetic latitudes near 65° on the College meridian auroral Es critical frequencies often exceed 5 MHz; in the 70 to 75° region, however, there is evidence that auroral Es does not often exceed 3 MHz. Auroral Es, since it is caused by the aurora, is observed only when the aurora is present, or was recently, in the part of the E region affected. Auroral sporadic-E is thick so it forms a blanketing (reflecting) layer, making propagation through it difficult.

Thin-layer sporadic-E, similar to mid-latitude Es and probably also attributable to wind shears in the E region, is observed in the high latitudes. This type of Es does not correlate highly with auroral activity; at College, it tended to occur abundantly for a few days at a time and then be rare for a few days or a week. These Es clouds appeared primarily to scatter rather than reflect HF energy.

In summary, the high latitude ionosphere contains several types of small- and large-scale irregularities. The aurora produces small-scale, field-aligned irregularities and large-scale changes in the electron density of the ionosphere. The small-scale auroral irregularities are efficient scatterers of HF energy. The large-scale irregularities in the F layer may deviate HF signals and affect their spectrum. At times, auroral sporadic-E may be strong enough to prevent HF energy from penetrating to the F region, thereby preventing long-range radar observations. Auroral irregularities are limited to the region of space nearby the aurora. There is evidence that the irregularities persist for a time after the aurora moves on, but no quantitative data are available. HF auroral echoes are therefore produced primarily from the auroral belt. There is preliminary evidence that polar cap aurora also produces HF backscatter; if so, such echoes would be observed only during quiet periods -- polar cap auroras do not occur during disturbed periods. Echo strength, frequency range, and latitudinal extent of auroral backscatter vary with time of day, the level of the disturbance, and ionospheric conditions. Present auroral data allow us to predict with fair confidence when and where auroral effects will be observed, but quantitative predictions on the magnitude of such effects are not now possible.

Spread-F irregularities cause backscatter and probably spectral changes in HF signals. If spread-F irregularities behave similarly to VHF scintillating irregularities, the occurrence of spread-F can be predicted from scintillation data. A region of strong scintillation covers the polar cap. This region has a sharp equatorward boundary that varies systematically with time of day and magnetic activity. Thus far, the magnitude of scintillation or spread-F events has been found to correlate poorly with that of magnetic activity.

Non-auroral sporadic-E causes backscatter echoes by some mechanism. The most likely is groundscatter although direct scatter is a possibility. Such sporadic-E clouds occur frequently at times. Their effect on a high latitude radar is limited, although it cannot be ignored. The echoes are usually narrow in range and may persist for several hours.

References

Aarons, J., J. P. Mullen, and H. E. Whitney, The scintillation boundary, J. Geophys. Res., 74, 884, 1969.

Aarons, J. and R. S. Allen, Scintillation boundary during quiet and disturbed magnetic conditions, J. Geophys. Res., 76, 170, 1971.

Bailey, D. K., Some quantitative aspects of electron precipitation in and near the auroral zone, Rev. Geophys. 6, 289-346, 1968.

Booker, H. G., A theory of scattering by non-isotropic irregularities with application to radar reflections from aurora, J. Atmosph. Terr. Phys., 8, 204-221, 1956.

Briggs, B. H., Observations of radio star scintillations and spread-F echoes over a solar cycle, J. Atmosph. Terr. Phys., 26, 1, 1964.

Briggs, B. H., The relation of spread-F to magnetic disturbances, J. Atmosph. Terr. Phys., 27, 991-994, 1965.

Buchau, J., J. A. Whalen, and S.-I. Akasofu, Airborne observation of the midday aurora, J. Atmosph. Terr. Phys. 31, 1021-1026, 1969.

Chapman, S., The geometry of radio echoes from aurorae, J. Atmosph. Terr. Phys., 3, 1-29, 1952.

Farley, D. T., A plasma instability resulting in field-aligned irregularities in the ionosphere, J. Geophys. Res., 68, 6083-6097, 1963.

Feldstein, Y. I. and G. V. Starkov, Dynamics of auroral belt and polar geomagnetic disturbances, Planet. Space Sci., 15, 209-229, 1967.

Gadsen, M., On the association of "auroral" radar echoes with the aurora, Planet. Space Sci., 15, 693-700, 1967.

Gadsen, M., The origin of afternoon "auroral" radar echoes, Planet. Space Sci., 15, 893-898, 1967.

Herman, J. R., Spread F and ionospheric F-region irregularities, Rev. Geophys., 4, 255-299, 1966.

Kelly, P. E., The association between radio and visual aurora, Can. J. Phys., 43, 1167-1171, 1965.

King, G. A. M., Spread-F on ionograms, J. Atmosph. Terr. Phys., 32, 209, 1970.

Leadabrand, R. L., Electromagnetic measurements of auroras, Auroral Phenomena, ed. Martin Walt, Stanford University Press, 1965.

Moorcroft, D. R., The interpretation of the frequency dependence of radio aurora, Planet. Space Sci., 14, 269-275, 1966.

Nishida, A., Average structure and storm-time change of the polar topside ionosphere at sunspot minimum, J. Geophys. Res., 72, 6051-6061, 1967.

Oguti, T. and K. Marubashi, Enhanced ionization in the ionospheric F_2 region around geomagnetic noon in high latitudes, Rept. Ionosphere Space Res. Japan, 20, 96-100, 1966.

Reid, G. C., The formation of small-scale irregularities in the ionosphere, J. Geophys. Res., 73, 1627-1640, 1968.

Schrader, D. H. and J. R. Kan, Amplification of irregularities in the ionosphere, J. Geophys. Res., 71, 5617, 1966.

Stuart, G. F. and J. E. Titheridge, The distribution of irregularities in the Antarctic ionosphere - 11, J. Atmosph. Terr. Phys., 31, 905, 1969.

Tsuda, T., Sato, T. and S. Matsushita, Ionospheric irregularities and the crossfield plasma instability, J. Geophys. Res., 74, 2923, 1969.

Unwin, R. S. and F. B. Knox, J. Atmosph. Terr. Phys., 30, 25, 1968.

Unwin, R. S. and F. B. Knox, Radio aurora and electric fields, Radio Science, in press.
Weaver, P. F., Backscatter echoes from field-aligned irregularities in the F region, J. Geophys. Res., 70, 5425-5432, 1965.

PART II

The aim of this part is to summarize the results of my work on high latitude HF backscatter. The work of other groups is not discussed; in the main very little other work along the lines of the College work has been reported, so there are few similar results to compare.

Most of the reported experimental work was done at the University of Alaska, although records obtained by Stanford Research Institute from other sites were also used. The analysis work was done while I was a staff member of the University of Alaska and of Stanford Research Institute.

Soon after the backscatter program started at College in 1953, it was found that most of the echoes observed did not fit the types then known--primarily groundscatter and E-layer auroral echoes. At College, echoes that clearly were backscatter from the ionosphere occurred regularly from ranges far beyond the radar horizon in the E layer. By 1957 a number of modes were suggested to explain the echoes, but, since the echoes were obtained on one or two frequencies, there was no way of positively identifying the mode of most of the echoes observed. Such identification is vital, because, for example, it is important to know whether a particular echo was produced by irregularities in the E region or the F region.

Early in the program it was recognized that only a sweep-frequency HF radar would give the answers sought. In 1958 a modified 1 to 25 MHz NBS Model C4 ionosonde was installed and operated as an oblique radar until 1960, and in 1963 a 4 to 64 MHz Granger Associates Stepsounder was installed and operated until 1966. The records produced by these radars has led to the cataloging of nearly all of the echoes observed at College and several other sites from the mid-latitudes to the magnetic pole, into distinct types. Two basic types--auroral and non-auroral echoes--have been identified; the non-auroral echoes have been divided into sub-groups depending upon their production mechanism.

1. Non-auroral echoes:
   a. F-layer groundscatter.
   b. Non-auroral sporadic-E, including sporadic-E groundscatter.
   c. Meteor echoes.
   d. Oblique spread-F (slant-F) echoes.
2. Auroral echoes:
   a. Backscatter from the E layer.
   b. Backscatter from the F layer.

Figure 1 illustrates some of these echo traces. How each is identified is discussed below.

First, however, the problem of notation must be mentioned. The system used in this paper is used because no proposed system has been found to be completely satisfactory when applied to sweep-frequency HF records. Direct backscatter from the E and F regions will be denoted, respectively, DE and DF scatter. The usual notation is used for energy that propagates via the F layer between two ground points--nF, with n indicating the number of successive F-layer and ground reflections. A 1F-DE echo, therefore, is an E-scatter echo that propagates via one F-layer reflection, as illustrated in figure 2. Echoes propagating in higher order modes than are illustrated in figure 2, such as 2F-DF or 3F-DE and so forth, are possible and have been observed in the College records. The 1/2M-DE mode, named that for want of a better name, is E-scatter occurring at the center of an ordinary forward-oblique M-mode. The 1/2M-DE and 1F-DF modes are probably the most important long range (over 2000 km) propagation modes for backscatter when the radar is poleward of the scattering region.

Only symmetric propagation modes, that is those for which the energy traverses the same path each way, have been used in this work. Including non-symmetric modes would increase the magnitude of the analysis problem considerably and require ray-tracing techniques. Considering the good agreement obtained by using only symmetric modes, the use of non-symmetric modes has not been thought worthwhile; the possibility of such modes must be considered, however, in any thorough study of HF backscatter.

The identification of echoes propagating via modes involving scatter or reflection from the F layer requires that the F-layer electron density be known along the path of the echo. There is no way this can be done from single-frequency backscatter records. If the groundscatter or the slant-F echoes are recorded by a sweep-frequency radar, however, a good estimate of the electron density at one altitude can be made as a function of distance along the direction in question; usually this is enough to allow the positive identification of the echo mode.

The regular occurrence of DF backscatter was found at College by 1960, but the cause of the various DF echoes was unknown until 1966. The record that led to much of the advance in identifying the various echoes is shown in figure 3. For several years a regular pattern of echoes had been noted in the daytime, but no record was clear enough that the echoes could be identified until the one in figure 3 and several similar ones were recorded.

Analysis of the record in figure 3 shows that (1) the group of echoes is composed of echoes propagating in modes DF, 1F-DE, 1F-DF, 2F-DE, and 2F-DF--modes involving both E-and F-scatter, and (2) all of the echoes originate very near to the same ground distance. These findings led to the conclusion that the echoing region was in the form of a field-aligned sheet through the E and F layers. An examination of the rest of the records with this idea in mind confirmed this finding: the regularly recurring echo pattern observed at College was produced by E- and/or F-scatter echoes originating at one or several discrete, field-aligned sheets of irregularities in the ionosphere. These echoes then propagated back to the radar by the various possible ionospheric propagation modes to form the same general pattern from day to day.

By 1966, these main echo types had been indentified in the College, records:

1. Slant-E echoes.
2. Meteor echoes.
3. Slant-F echoes.
4. F-supported groundscatter echoes.
5. E- and F-scatter echoes from field-aligned sheets.

Nearly all of the echoes observed at College could be put unambiguously into one and only one of these classes. The few that could not were either short range, discrete echoes that were subsequently identified as sporadic-E echoes of some sort, either direct or groundscatter echoes, or were sheet echoes mixed in with slant-F echoes to form a jumbled mass of echoes in the early evening. In this latter case, the individual echoes could not be separated, making recognition of individual echoes difficult.

The next step was to compare these echo classes with auroral data to try to establish a connection. Thirty days' optical data that had been grossly scaled for another study were used. The technique was to compare the position of the backscattering region for each echo type (except, of course, those definitely known to be non-auroral such as groundscatter or meteor echoes) with that of the optical aurora at approximately the same time. Echoes listed as 1 and 5 above correlated well in time and position with the aurora while slant-F echoes did not. Figure 4 contains 3 days' data; only auroral echoes are shown.

Evidence for sheets of irregularities through the ionosphere has been found in satellite records by ESSA workers; they did not identify the cause. Considering the results of the College work, these topside sheets appeared to us to be the result of the aurora, so a comparison was made of simultaneous topside soundings obtained by Explorer 20 and the College HF sweep frequency radar. The results were positive; the electron density at all altitudes in the topside ionosphere was found to be markedly increased at the place where the sheet was detected in the bottomside ionosphere. This increase in topside electron density suggests that auroral backscatter form the F layer may be partly due to an increase in electron density in the disturbed part of the ionosphere. Thus, the aurora markedly affects the entire ionosphere along the path of the precipitating electrons; this increase must be taken into account on HF propagation paths crossing the auroral zone.

Next, simultaneous optical and radar, and precipitating electron and radar data were compared on a detailed, case-by-case basis. Again, the echoes were first classified and then compared by classes with the other data. These results confirmed the earlier results; the echoes previously classified as auroral echoes were associated with the auroral precipitation, and the slant-F echo was not. In the process of this study, the long-lived, discrete, short-range echoes occurring from time to time were found to be non-auroral; these echoes were eventually concluded to be either direct scatter or groundscatter from non-auroral sporadic-E clouds.

Two distinct types of precipitating auroral zone electron fluxes have been identified by the Lockheed workers: (1) hard-zone flux--relatively energetic electrons distributed continuously with an isotropic pitch angle distribution over a wide range of latitudes in the 60 to 75° invariant latitude region, and (2) soft-zone flux--intense fluxes of electrons in the 1 to 10 keV range confined to a few very narrow (tens of kilometers) regions of latitude with a strongly anisotropic pitch angle distribution. The soft-zone flux appears to be responsible for visible aurora, the hard-zone flux for auroral absorption. Much of the time, particularly during the day, the two fluxes are appreciably separated in latitude, although they tend to merge in the hours before midnight.

No space and time correlation was found between the radar echoes and the hard-zone flux; the only correlation found was between the radar echoes and the soft-zone flux of electrons, and the correlation was good. No correlation was found between the radar scattering region and the precipitating proton flux. When no echoes were recorded, no electron precipitation intense enough to produce a visible aurora (about 1 kR, requiring a precipitating flux of electrons of roughly one erg per sec cm^2 ster) was detected, and vice versa.

The main result of this last study was that although radio and optical aurora were found to be closely related in time and space, exact spatial correspondence was not found. Figures 5 and 6 illustrate some of the data. It must be noted, of course, that the azimuthal beamwidth of the radar greatly exceeded that of the other detectors. The results indicate, however, that exact coincidence between radar and optical aurora probably does not occur, and recent theoretical work supports this conclusion.

High optical auroras (heights were measured by photometric triangulation between three stations) were found in this study to be accompanied by only F-layer echoes. Optical measurements made at College indicate that quiet, well-defined auroras were frequently high auroras; this finding suggests that part of the problem in correlating VHF echoes (obtained only from the E layer) with optical data is that E-region irregularities may at times not be formed by the aurora even though irregularities are formed higher in the ionosphere. Another problem is that when viewed obliquely, the computed position of such high auroras would be markedly in error when, customarily, the height is assumed to be 110 km.

Sweep-frequency records make it possible to account quantitatively for ionospheric refraction at the scattering point, and this result has led to quantitative estimates of the aspect sensitivity for various types of direct scatter echoes. Figure 1 illustrates the typical shape of an auroral slant-E echo trace recorded from the north at College; the feature of note is the arrow-shaped part at the high frequency end. That this feature is not equipmental is shown by figure 7, which contains a number of slant-E traces computed from a simple model for various angles of allowable off-perpendicularity from the magnetic field. The comparison of a number of experimental records with data computed from this model shows that the backscattering cross section for auroral echoes from the E layer in the 15 to 50 MHz region decreases more than 5 dB per degree of off-perpendicularity. This result is in agreement with other VHF results.

The aspect sensitivity of F-layer echoes was found by utilizing the groundscatter echo reflected from the F layer at the point the backscatter occurred, so that ionospheric refraction at the scattering point could be computed. The results show that the aspect sensitivity of F-layer auroral backscatter and non-auroral slant-F echoes exceeds 5 dB per degree of off-perpendicularity.

A comparison between the simultaneous occurrence of oblique incidence slant-F echoes extending to the College zenith was made with vertical incidence spread-F observed at College. The results showed that one type of echo rarely occurred without the other. Thus, the slant-F echo is in reality an oblique spread-F echo. Slant-F echoes are weak, strongly aspect sensitive echoes, produced by backscatter from small scale, field-aligned irregularities; vertical spread-F echoes, on the other hand, are apparently not aspect sensitive, and it has been suggested by others that they are produced by reflection from large scale irregularities or surfaces. The two types of irregularities are quite different, but they always occur together.

Figures 1 and 3 illustrate a general feature of the College records--the groundscatter trace ends abruptly just beyond the auroral sheet echo. A dozen or more such cases were selected randomly from the hundreds that exist in the College records and analyzed. In every case it was found that the groundscatter echo was cut-off when the scatter propagating to the radar from the ground penetrated the E layer at the distance of the auroral sheet. Therefore, the aurora somehow prevents the groundscatter echo from propagating back to the radar. The diminution in signal strength was of the order of 10 dB at College and was abrupt in range. Only rarely was the cut-off not observed when the auroral sheet echo was recorded.

One final result of the HF sweep-frequency program is the study of artificial barium clouds released in the lower F region near College, Alaska in March, 1969. Equivalent isotropic backscatter cross sections for the one release for which good data were obtained at the two sites exceeded a thousand square kilometers at frequencies of 15 to 20 MHz. Since the optical size of the cloud was tens of square kilometers, backscatter was not isotropic. Analysis showed the backscatter to be strongly aspect sensitive to the magnetic field.

The backscatter cross section for this one release (the largest--96 kg) was found to have an aspect sensitive decrease exceeding 10 dB per degree of off-perpendicularity. The echoes were found to be strongly field-aligned well before striation was detected optically. Echo amplitudes from the two largest releases were as strong in the HF band as those of many auroras.

Much of the work described in this paper was done with the College records, but the results have been found to apply equally well to sweep-frequency radars at other latitudes. The type of auroral echo observed by a given radar, however, strongly depends upon the latitude of the radar, as well as upon the characteristics of the aurora. The distance from radar to auroral scattering region is the essential factor here. A polar radar sees primarily sheet-type echoes--that is, echoes propagating in a number of different modes from the same scattering region. Auroral zone radars see sheet-type echoes during the day, when the aurora is 1000 to 2000 km poleward of the radar, and auroral slant-E echoes at night when the aurora is in or near the zenith. A mid-latitude radar sees only sheet-type echoes.

Radars at all latitudes record the slant-F echo. The decreasing dip angle of the geomagnetic field with decreasing latitude modifies the trace shape, but once this effect has been taken into account, recognizing mid-latitude oblique spread-F echoes is straight forward.

The dominant echo on any record from one auroral sheet is defined as that echo which occurs at the minimum slant range and extends to the maximum frequency. Whether the dominant echo in a group is E- or F-scatter depends as much on the distance between radar and aurora as it does on the height of the aurora. Within 1000 km E-scatter dominates from most auroras (those that extend into the E region), while between 1000 and 2000 km, F-scatter is the dominant echo, because the E layer is now below the radar horizon where DE echoes cannot be observed. To be observed from beyond 2000 km, E- and F- scatter echoes must propagate via an F-layer reflection because both the E and F layers are below the radar horizon; if E- and F-scatter echoes occur together, the 1F-DE echo dominates because it extends to a slightly higher frequency and occurs at a slightly shorter slant range than does the 1F-DF echo. The 1F-DE echo appears to be the strongest of the two. This is reasonable because the work indicates that the backscatter cross-section for E-layer auroral echoes is greater than for F-layer auroral echoes.

The sweep-frequency HF auroral radar program is being continued at sites near the magnetic poles. In September, 1964, sweep-frequency backscatter records were obtained simultaneously at College and Thule over nearly reciprocal paths. A comparison of these records revealed an excellent correspondence between the position of the auroral backscattering regions viewed at the two sites. This result led to the conclusion that a sweep-frequency radar with a rotating, directive antenna at the magnetic pole could view the entire auroral belt about one hemisphere. The primary modes of propagation from the polar radar to the auroral irregularities were apparently the DF, 1/2M-DE, 1F-DF, and 1F-1/2M-DE modes, figure 2.

National Science Foundation has authorized the establishment of polar auroral radars at Resolute Bay, Canada, and McMurdo Sound, Antarctica. The Resolute radar is in and will be in routine operation by summer 1971; the McMurdo radar is scheduled for installation in January, 1972.

In summary, the use of sweep-frequency HF radars allows one to determine the mode of propagation, the layer producing the scatter, and the cause of the observed echoes. This classification cannot be made with single-frequency records. The electron density of the F layer as a function of distance is deduced from groundscatter and slant-F echoes. With this technique it has been found possible to catalog the high latitude echoes observed by sweep frequency radars into a number of distinct groups. Nearly all of the echoes observed on sweep-frequency radars located from the mid-latitudes to the pole can be unambiguously classified into one of these few specific groups of echoes; the definition of each category is based solely upon the range-frequency characteristics and the temporal behavior of the echoes. The further classification of these echo groups as auroral or non-auroral was made by correlating each group with auroral electrons precipitating into the region containing the backscattering irregularities--only those echo types that correlate highly with the aurora are termed 'auroral echoes'.

Papers Published on the College Work

Bates, H. F. The height of F layer irregularities in the arctic ionosphere. J. Geophys. Res., 64, 1257-1265, 1959.

Bates, H. F. Direct HF backscatter from the F region. J. Geophys. Res., 65, 1993-2002, 1960.

Bates, H. F. The slant E_s echo - a high-frequency auroral echo. J. Geophys. Res., 66, 447-454, 1961.

Bates, H. F. Some effects of dense E_s clouds on high latitude HF backscatter observations. J. Geophys. Res. 70, 5895-5905, 1965.

Bates, H. F. The latitude of the dayside aurora. J. Geophys. Res., 71, 3629-3633, 1966.

Bates, H. F. A proposed polar auroral radar system. J. Atmosph. Terr. Phys., 28, 903-907, 1966.

Bates, H. F. On using direct backscatter to predict communications. Proc. IEEE, 54, 1457, 1966.

Bates, H. F. HF propagation through the auroral curtain. J. Geophys. Res., 75, 143, 1970.

Bates, H. F. Auroral enhancement of electron density. J. Atmosph. Terr. Phys., 32, 1153, 1970.

Bates, H. F. and P. R. Albee. Aspect sensitivity of F-layer HF backscatter echoes. J. Geophys. Res., 75, 165, 1970.

Bates, H. F. HF backscatter from high latitude ionospheric barium releases. Radio Science, 6, 21, 1971.

Bates, H. F. The aspect sensitivity of spread-F irregularities. J. Atmosph. Terr. Phys., 33, 111, 1971.

Bates, H. F., P. R. Albee, and R. D. Hunsucker. On the relationship of the aurora to non-great-circle high-frequency propagation. J. Geophys. Res., 71, 1413-1420, 1966. (a)

Bates, H. F., A. E. Belon, G. J. Romick, W. J. Stringer. On the correlation of optical and radio auroras. J. Atmosph. Terr. Phys., 28, 439-446, 1966.

Bates, H. F. and P. R. Albee. Aspect sensitivity of HF auroral echoes. J. Geophys. Res., 74, 4806, 1969.

Bates, H. F., R. D. Sharp, A. E. Belon and J. S. Boyd. Spatial relationships between HF radar aurora, optical aurora, and electron precipitation. Planet. Space Sci., 17, 83-95, 1969.

Hunsucker, R. D. and H. F. Bates. A survey of polar and auroral region effects on HF propagation. Radio Science, 4, 347, 1969.

Lund, D. S., R. D. Hunsucker, H. F. Bates and W. B. Murcray. Electron number densities in auroral irregularities: comparison of backscatter and satellite data. J. Geophys. Res., 72, 1053, 1967.

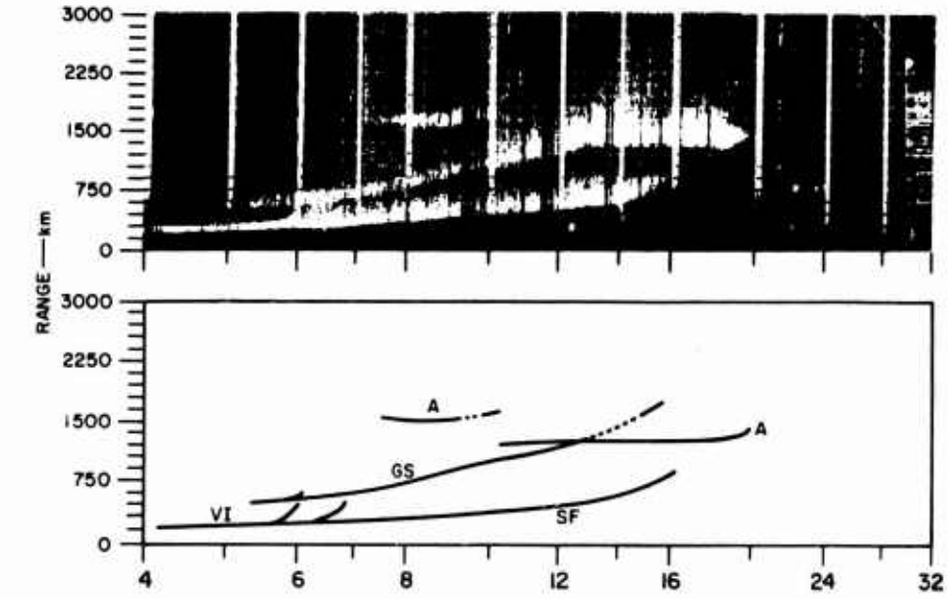

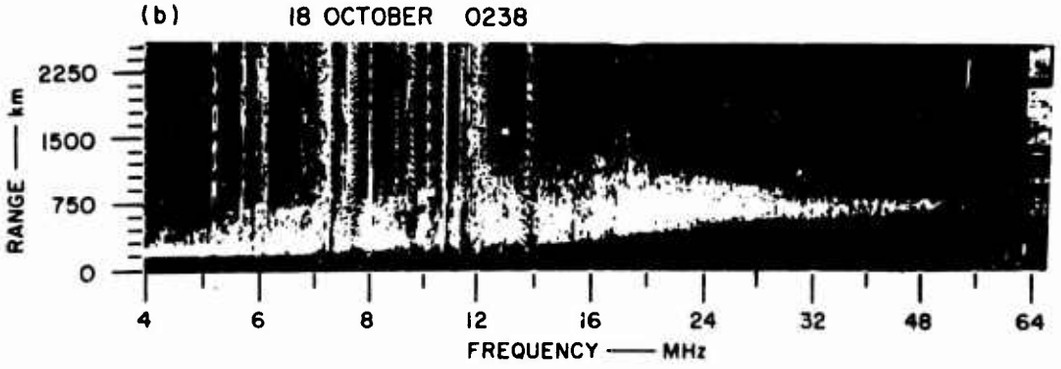

Fig.1 Clutter echoes from the E and F layers. In line drawing: A denotes auroral echoes from F layer, GS denotes ground-scatter, SF denotes slant-F, and VI denotes vertical incidence trace

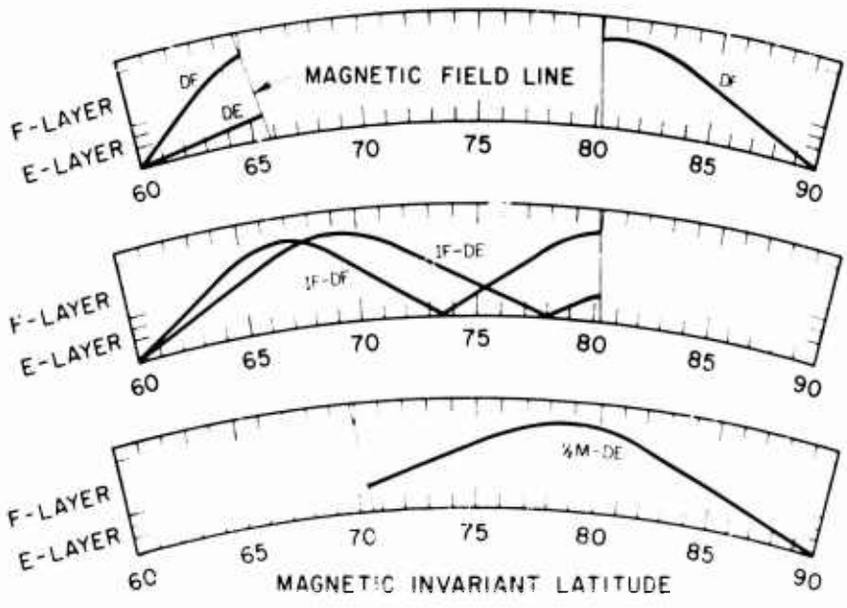

Fig.2 Backscatter ray paths.

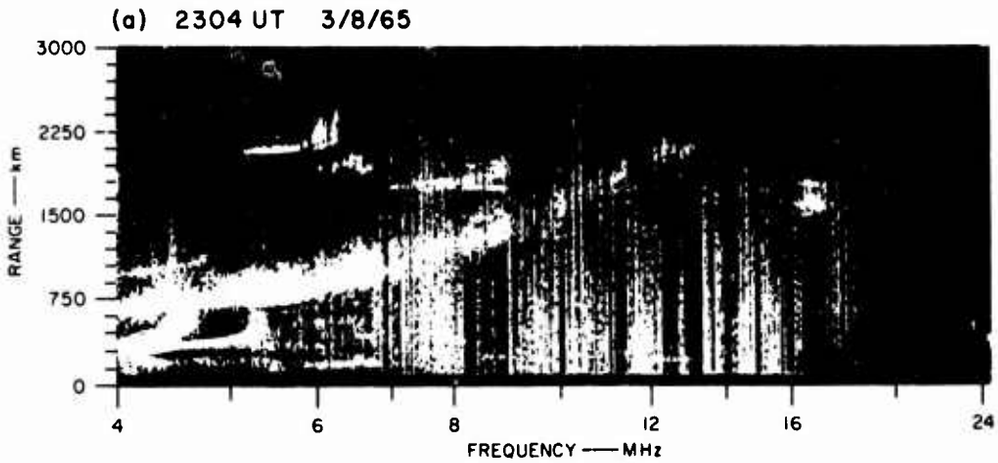

Fig.3 Backscatter ionogram showing discrete sheet echoes.

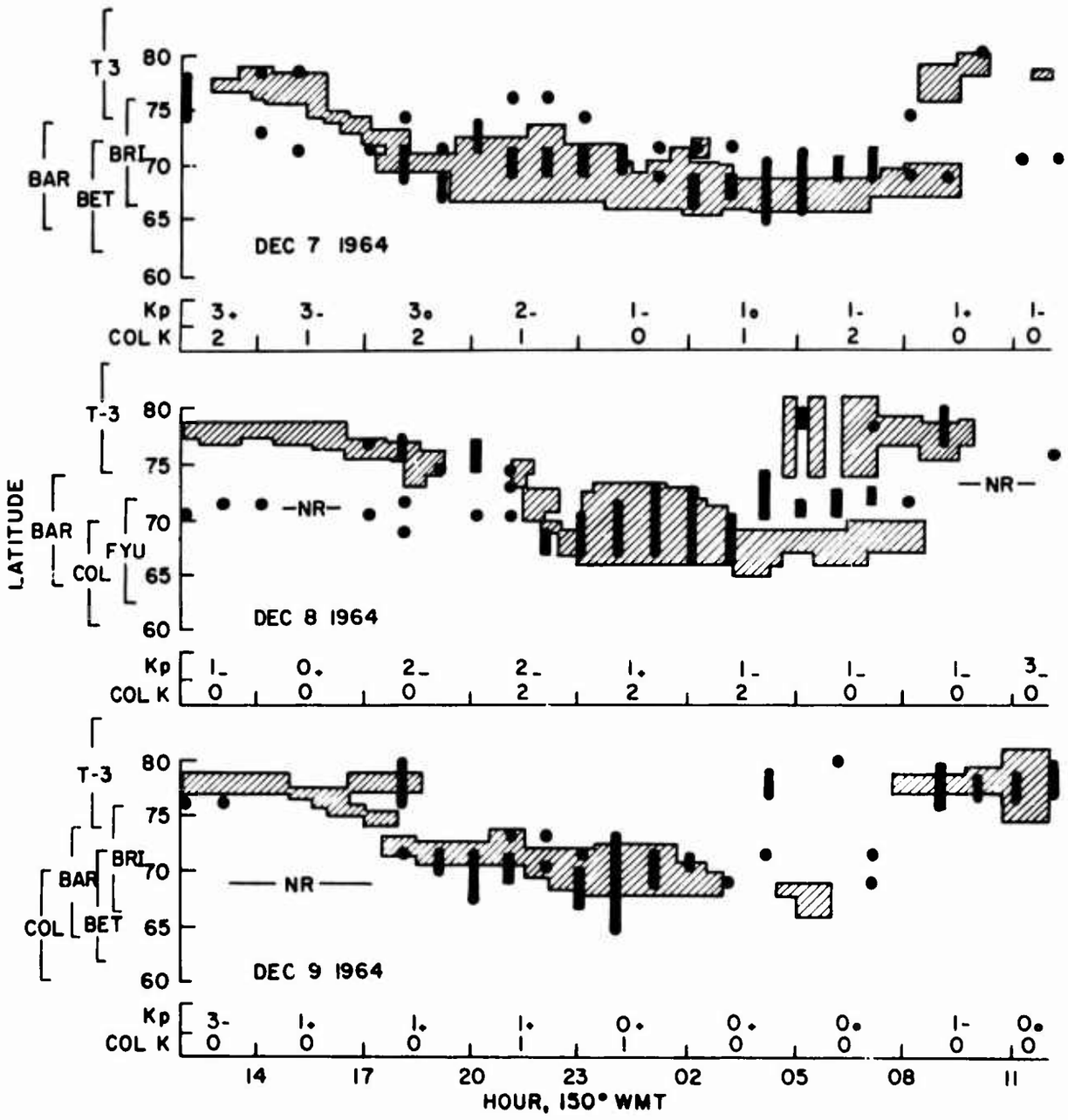

Fig.4 Position in latitude of optical (cross-hatched) and radar (bars) auroral regions.

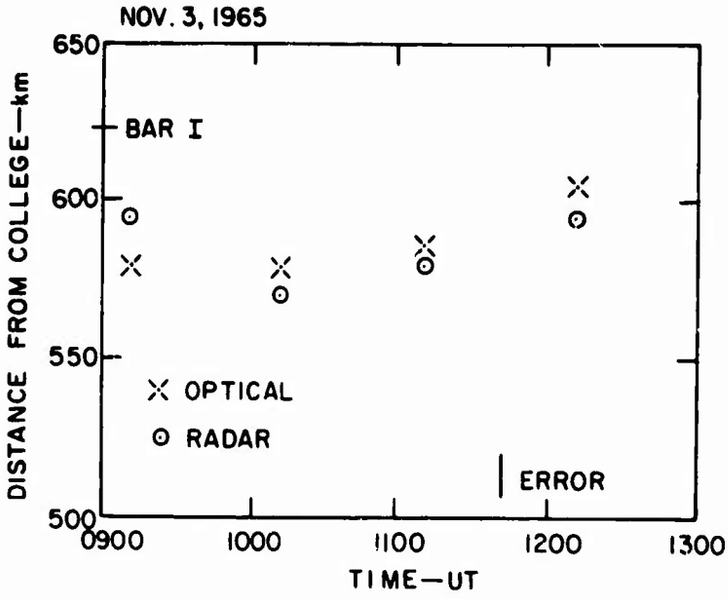

Fig.5 Simultaneous positions of optical and radar aurora.

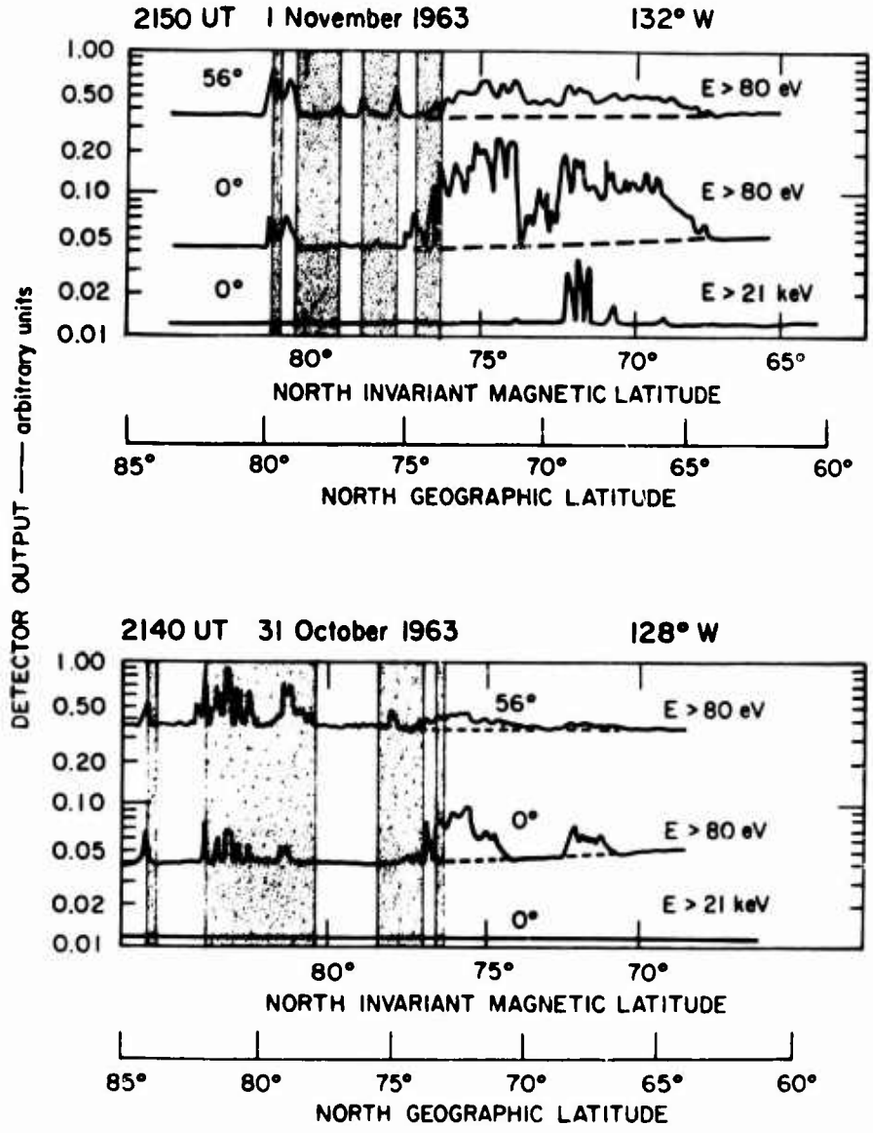

Fig.6 Measured electron flux as a function of latitude. Radar scattering regions are shaded.

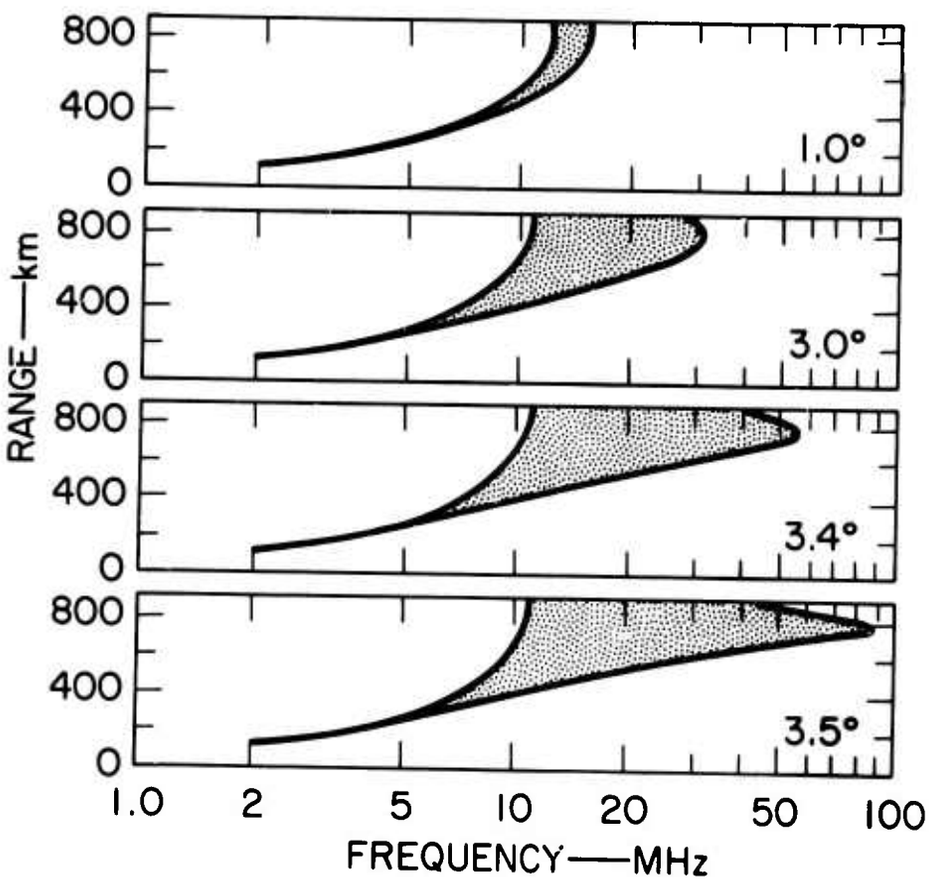

Fig 7 Computed auroral slant-E traces for Colleges for various allowable off-perpendicular angles.

ON THE POLAR SLANT E CONDITION, ITS IDENTIFICATION, MORPHOLOGY AND RELATIONSHIP TO OTHER ELECTROJET PHENOMENA

Jens K. Olesen
Ionosphere Laboratory of the Danish Meteorological Institute
c/o Technical University, 2800 Lyngby, Denmark

1. Introduction.

The purpose of this paper is to illustrate various aspects of what is here called the polar Slant E Condition including certain criteria for its identification on ionograms, some new statistics on its morphology and some indications on its possible relationship to other phenomena, especially the two stream or plasma ion wave instability.

The term used here: "Slant E Condition" - SEC - differs from the classical term: "Slant Es" (Slant Sporadic E, Slant Es type s or Ess) mainly in, that SEC here is used in a wider sense. The classical Slant Es term (Heppner, Byrne and Belon, 1952) was limited to characterize a special, diffuse slant trace, whose virtual height in a virtual height-frequency ionogram rises steadily with frequency from the critical frequency and virtual height of an E or Es layer trace at about 3-7 Mhz, 100 km to ab. 8 - 15 Mhz, 200 - 500 km. The mechanism producing the slant trace was believed to be some combination of scattering and refraction taking place near the 100 km level at horizontal distances from the ionosonde, that increase with increasing sounding frequency. The SEC term used in this report aims at comprising all occurrences in the ionosphere of the same disturbed condition, regardless of whether or not the slant trace itself happens to appear. This is achieved by utilizing certain secondary criteria for the SEC identification as described later.

The reason for exchanging the Slant Es with the SEC term is, that the former is not adequate in the present context due to several facts: the slant echo is not a sporadic layer, it is not even a layer in the normal sense of the word, or is it especially associated with a sporadic layer, but frequently with an E layer, its occurrence is not of a marked sporadic nature and, above all, the slant trace itself is not very important, it may not show up on the ionogram for several irrelevant reasons. However, the secondary criteria are of decisive importance and only when these are taken into account, as they are in the SEC concept, the occurrences will give a coherent and physically reliable pattern.

A more serious consequence of the previous restricted definition of the Slant Es concept is, that it might have delayed the advance of science in an important field. In spite of the fact, that the SEC in equatorial regions has attracted much attention resulting in reliable evidence of the existense of the two stream plasma instability with ion-acoustic waves and field aligned irregularities associated with the equatorial electrojet (Cohen et.al. 1962, Farley 1963, Buneman 1963, Bowles et.al. 1963), these advances have not lead to a natural similar development as far as the polar Slant E Condition and electrojet is concerned. The cause is believed partly to lie in the fact indicated above: the previous too casual recognition of the polar SEC. Several authors have noticed interesting, extraordinary features associated with the Slant Es trace and some have made statistics on the occurrence, but the results have in most cases not given a coherent picture due to the incompleteness of the Slant Es concept used. When the polar SEC concept, as described in detail later in this report, is used, similar to what it was in two previous reports (Olesen 1957, Olesen and Rybner 1958), the results will be a coherent pattern of the polar SEC, that seems to fit in with several of the existing experimental and theoretical results associated with the physics of the polar regions and also with the results on the equatorial electrojet referred to above. Thus the adoption of the SEC concept can furnish one more easily observable parameter on the complicated polar region physics, in a field where a big amount of recordings are available from the world-wide net of ionosondes.

Summary

The concept "Slant E Condition" identified on ionograms characterizes a special, disturbed state existing in the ionosphere, when high currents flow in the E-region. The term "Slant E Condition" - SEC - is analcg to, but has a wider sense than the classical term "Slant Sporadic E", and several secondary criteria are presented for the identification of the polar Slant E Condition. Statistical results from polar stations show, that the polar Slant E Condition is a frequent occurring phenomenon - up to 75% occurrence - with an occurrence pattern, that seems to follow the auroral oval. The equatorial and polar Slant E Condition is - according to its nature - highly correlated with local magnetic activity and has associations with several other phenomena, such as solar activity, electromagnetic wave scattering, propagation and excitation, and for the polar Slant E Condition especially: auroral activity. It seems likely that the polar Slant E Condition is identical to ion-acoustic plasma waves as the equatorial Slant E Condition has been shown to be.

In what follows, section 2 will deal with some previous results on SEC and related phenomena, succeeded by the decription of the results of the present study, of which section 3 gives an outline of stations and data used, section 4 describes the identification criteria for the polar SEC event, section 5 covers the statistical results, section 6 some discussion and section 7 proposed conclusions.

2. Previous results.

As to previous work it is not possible to give here a complete review. References shall be limited to a summary of a few key reports mainly within the following fields: the slant trace, its propagational and morphological aspects, some of the scatter propagation subjects and the association with other geophysical phenomena including the two stream plasma instability, while subjects such as polar ionosphere and magnetosphere relationships, auroral activity and energetic particle radiation, although of great importance, will not be reviewed here in any great detail.

The propagation mechanism by which the slant trace is produced was in many earlier papers proposed to be a combination of refraction in the E region and scattering from electron density irregularities below the E region. Contributions to this and related subjects were made by Bailey, Bateman and Kirby (1955) who noticed the association between Slant Es, VHF forward-scatter and rayed aurora and showed that a special type of fading, sputter fading, with a fading frequency 100 times the normal occurred during Slant Es events in the Alaskan auroral zone. Daily and yearly occurrence distributions were also found, which agree only partly with the results of the present study. Smith (1955, 1957) and Smith and Knecht (1957) treated the propagational problems and referred to several earlier works, suggestions and private communications, e.g. by Agy, Booker, Bowles, Dieminger, Dyce, Eckersley, Forsyth, Knecht, McNish, Peterson.

Bates (1959, 1960, 1961) and Bates and Albee (1969) emphasized that refraction is a decisive factor for direct HF scatter from the arctic F and E regions, and that by taking this into consideration, supplemented by least-time and aspect-sensitive focusing of signals via randomly distributed field aligned irregularities, it is possible to explain all the main characteristics of the slant E configuration as they appear on vertical and oblique ionograms.

Bowles and Cohen (1962) and Cohen, Bowles and Calvert (1962), who refer to some of the above authors and also to papers by Balsley, Egan, Ochs, Renau, Skinner, Whale and Wright, showed, that the equatorial Slant Sporadic E configuration (including the equatorial sporadic E type q) is due to a thin stratum of magnetic field-aligned irregularities, which are embedded in the equatorial E-layer, which at times may extend above the E layer, but never below it, and which seem to be closely associated with the equatorial electrojet in time and location.

The temporal and morphological features of the Slant Es and the SEC have been dealt with in most of the above papers only to some extent. A few more details will be mentioned in the following.

Matsushita (1956) investigated the correlation of slant Es with positive magnetic bays in the evening and negative bays in the morning at College, and found that all substantial bays in April 1955 had Slant Es associated with them, but the converse was not quite true. The daily occurrence distribution agrees with the results of the present study.

Smith and Knecht (1957) refer to an unpublished work of Agy and Bryan with Slant Es occurrence data for some months of 1951 - 52 from Alaska. However, as stated by the authors, the data are incomplete, so that this might explain, why the results do not agree with those of the present study. Probably the statistics referred to cover only the visible slant traces, in which case a correspondance could hardly be expected.

Olesen (1957) and Olesen and Rybner (1958) give the results of a study in which data from parts of the 5 year period 1952 - 56 were included, with a data reduction based upon, not merely the presence of the slant trace itself, but also upon the inclusion of outlined secondary criteria for the presence of the Slant E Condition, in particular a frequency gap and spreadiness in echoes from the upper E and lower F1 regions. This work showed, that at Godhavn (80°N geom.) the Slant E Condition was a very regular-occurring phenomenon - up to 75% occurrence at the daily maximum period - closely associated, also on an event basis, with high, day-type magnetic activity, both phenomena having a maximum of occurrence near noon, in the summer and in years of high solar activity. The latter of the two reports also gives some short highlights on the occurrence in 1957 - 58 at an auroral zone station, Narssarssuaq (71°N geom.), where there were two daily maxima of occurrence: at ab. 1500 and ab. 0300 hr. local time (geogr. and geom.). The variations with season and solar activity mentioned above for Godhavn were similar for Narssarssuaq, and these conclusions are confirmed by the more comprehensive data shown later in this report.

Oksman (1965) reports on the characteristics of Slant Es at Sodankylä (64°N geom.) in the auroral zone for the three year period 1958 - 60. An investigation of the scattering and propagation mechanism gives preference to refraction combined with single and double scattering within and below the E region. Two types of Slant Es echoes at Sodankylä are designated the equatorial and the high-latitude type. The distinction was based upon the slant trace originating from an E trace (day or night E layer) or from an Es trace, respectively. Both types had an early morning and late afternoon maximum of occurrence. The equatorial type seemed to be more frequent in the summer, the high-latitude type in the winter, possibly a natural consequence of the definition of the two types. For both types there was an association with high currents. The association with auroras and particle precipitation was also commented.

Associations between the SEC and other geophysical phenomena were mentioned occasionally above, in particular the association with geomagnetic activity and auroral sputter fading. A few more relationships will be mentioned in the following.

Lebeau (1965) in a polar cap magnetic study reports on a special study of F region echo disappearance as it was observed at Dumont d'Urville (75.6°S geom.) by S. Cartron. The author relates this phenomenon to the Slant Es phenomenon, a correlation which is in accordance with the existence of the E-F frequency gap described in litt. 7 and 8 and in the present report (see Fig. 4) as the most reliable secondary criterion on the polar SEC. Also, as to the reported statistics on daily and yearly occurrence pattern there is agreement: a maximum near noon and in local summer at high magnetic activity, except that the occurrence seems to increase during the years 1956 to 1962. This is not in agreement with solar activity variation, and the author suggests the movement of the dip-pole as a possible explanation.

Farley (1963, 1963), Buneman (1963) and Bowles, Balsley and Cohen (1963) reported on the two stream or ion wave plasma instability and its possible relationship to certain conditions in the equatorial electrojet. The subject was also studied by Kato and Hirata (1967), and others. It was shown theoretically and experimentally that the equatorial Slant Es configuration seen on

ionograms might be explained by the presence of the two stream instability and that similar conditions might be expected in the auroral electrojet. The instability can occur in ionospheric regions, where strong ionospheric currents of two interpenetrating streams of charged particles, electrons and ions, flow normal to the earth's magnetic field, as they may in the equatorial and auroral electrojets. The instability takes the form of plane acoustic plasma waves with field-aligned wave fronts of electron density irregularities, which can be exited when the velocity of the electrons relative to that of the ions is somewhat greater than the ion thermal velocity - of the order of 350 m/sec in the equatorial E region. The waves have a phase velocity of the same order of magnitude. and a wave length of the order of about a fraction of a meter to a few meters depending upon electron drift velocity and wave direction angle with the magnetic field. The waves propagate nearly perpendicular to the earth magnetic field and partly in the direction of the mean electron motion. Also, according to the authors cited, theoretical and experimental results on the electrojets and on backscatter, including doppler measurements, are in accordance with the above theory in many respects. Backscatter measurements and their relation to ion-acoustic waves were studied by Leadabrand, Schlcbohm and Baron (1965), Moorcroft (1966), Gadsden (1967), Unwin and Knox (1968), Lyon (1968), Hofstee and Forsyth (1969), Czechowsky and Lange-Hesse (1970) and others.

3. Observation sites and data periods for ionosonde and fixed frequency scatter measurements.

The ionosonde data presented in this report are from the following stations and periods:

Station	Geogr. Coord.	Geom. Coord.	Period
Thule	77.5°N, 69.5°W	89°N	Jan. - June 1958
Godhavn	69.2°N, 53.5°W	79.9°N, 32.5°E	Jan. - June 1958 Event May 26, 1958
Narssarssuaq	61.2°N, 45.4°W	71.2°N, 37.6°E	Jan. - June 1958 Events June 17, Dec. 15, 30, 1970
Tromsö	69.7°N, 18.9°E	67.0°N, 117.0°E	Jan. - June 1958

The map Fig. 1 shows the location of the four stations from which data were used: Thule near the Geomagnetic North Pole, Godhavn at a location that, during the earth rotation under the auroral oval, passes near the noon part of the auroral oval, Narssarssuaq and Tromsö at locations, that traverse the oval during local afternoon and morning hours. On the auroral oval and zone concept and associated phenomena, see f.ex. Akasofu (1968) and Hartz (1968).

At Narssarssuaq also a fixed frequency backscatter equipment has been operated since 1966, and some of the records obtained are included in the present study.

4. Identification criteria for the polar SEC event.

In the introduction it was emphasized, that the appearance of the slant trace itself, is not decisive for the identification of the SEC event. This is fortunate, since the weak slant scatter trace may fail to appear for several irrelevant reasons, especially due to absorption or to low equipment sensitivity, and it is especially fortunate because the lack of proper identification would naturally obscure the consistent nature of the data. For these reasons a careful description and illustration of secondary criteria for the SEC event seems important. Some of the secondary criteria, that were given previously (litt. 7 and 8), are repeated below in a more systematic way and with the addition of a few, that were not adequately emphasized previously. The presentation below is in the form of a summary, followed by various detailed remarks to the illustrations in Fig. 2a, b, 3a, b, c with ionograms recorded at Narssarssuaq, and Fig. 4 at Godhavn.

The criteria for a SEC event are:
Daytime type (the phases of the SEC development are to some extent analog to the chronological order below):

A. Early phase:
   1a. No or reduced retardation appears in upper E and lower F1 region traces
   1b. Increased spreadiness appears at upper E and lower F1 region traces
   1c. Oblique constant range E region trace appears at foE
   1d. Oblique F1-F2 region traces appear above the critical frequencies, with virtual heights decreasing with increasing sounding frequency
   1e. Decrease of foF2, increase of h'F2, increased separation between F1 and F2 traces
   1f. Increased spreadiness and oblique echoes appear at upper part of F1 and F2 traces

B. Main phase - possibly some of above features, and also:
   2a. Visible slant trace appears from E region and upwards
   2b. No echoes appear from upper E and lower F1 region or higher
   (the E-F frequency gap - a reliable SEC indicator)

C. Late phase - possibly some of above features and also:
   3a. Constant range and spread echoes above E and F1 critical frequencies and virtual heights

Nighttime type (no distinct sequence of development phases):

1. Highly ionized E region with plasma frequency often 4 - 7 Mhz (Night E, Esa or Esr)
2. Visible slant trace appears starting at E region critical frequency
3. F region echo traces missing, complete or partial. Possible remaining F traces complicated by obliques and spreadiness
4. Severe absorption may be present.

Fig. 2 and 3 illustrate the above criteria, showing on an event basis the Slant E Condition as it is observed on ionograms from Narssarssuaq. A few fixed frequency, azimuth scanned backscatter recordings are inserted.

Fig. 2a, b and c show various aspects of a daylight SEC event recorded during the afternoon of June 17, 1970 at Narssarssuaq. The event starts at 1324 hr (45°WMT) as identified by a short piece of a slant trace at the high frequency end of the normal E trace, where it has substituted the normal E retardation trace. At 1349 hr, the situation is similar, but now also a more distinct separation between the F1 and F2 traces has occurred, simultaneously with an increase of F2 layer virtual height and a decrease of F2 critical frequency has started. At 1434 hr, a frequency gap has developed between upper E and lower F1 echoes, more spreadiness is observed, and an oblique, constant range E region echo appears. Also, characteristic F region oblique echoes above the critical F1 and F2 frequencies appear more distinctly than at 1349, and various oblique and spread echoes are seen at the foF1 and foF2 upturns themselves. The 1438 and 1442 hr registrations are backscatter records made by the ionosonde, operating on a fixed frequency of 12.7 Mhz, connected to a three element Yagi antenna, which is tilted 30° from the horizontal plane, and which rotates 360° in azimuth through E, N, W, S (geographical) in 102 seconds. The backscatter records thus show the slant distance to the scatterers for a 12.7 Mhz signal as a function of azimuth. The two records show echoes from NNW from an oblique distance of about 330 - 450 km. In this case, it is not possible to tell, whether the backscatter record echoes are identical to the ionogram slant E trace or to the F region oblique traces mentioned above. The event continues through some of the records of Fig. 2b and 2c. Special attention is called upon the 1458 hr record, which is a low gain ionogram, and which therefore shows how an ionogram looks during a SEC, when the ionosonde used has too low sensitivity - a very common defect of many ionosondes around the world. The E-F frequency gap seen in this ionogram discloses, that the SEC is there, as it is proven by the visible slant trace on the high gain ionogram at 1457 hr, one minute before. The last part of the

SEC event is characterized by oblique constant range echoes from above E or F1 layer virtual heights and frequencies, e.g. 1544 and 1659 hr. The SEC event is principally over at 1659 hr, at least in the E region above the station, as judged by the reappearance of the distinct retardation traces in upper E and lower F1 regions.

Fig. 3a and b show two morning SEC events at Narssarssuaq on Dec. 15. and 30., 197c, respectively. Typically, the morning slant trace originates from an Esa or Night E layer trace with a rather high plasma frequency 4 - 7 Mhz, with F region echoes often missing, partly or complete. The inserted backscatter records show diffuse echo traces, whose oblique distance correspond to the virtual height of the ionogram slant traces. The 0244 ionogram of Fig. 3a shows only the distant part of the slant trace, possibly indicating that the SEC is now found only at some distance from Narssarssuaq. This is a rather rare phenomenon, indicating that the SEC configuration usually disappears as a unit.

Fig. 4 shows some ionograms at 1031 - 1044 hr (45^{o}WMT) from a sequence of continuous recordings made at Godhavn on May 26, 1958 during a daylight SEC event, that lasted for more than 8 hours. The sequence illustrates, that the E-F frequency gap mentioned above can increase, so that no echoes at-all are received from the F region (1031 hr), the remaining ionograms illustrate how the E region scatter efficiency is probably gradually reduced, allowing lower and lower frequencies to be propagated in the normal way to and from the F region.

5. Statistical results.

Fig. 5, 6 and 7 show some statistical results from the four stations.

Fig. 5 shows the percentage occurrence of the SEC at Narssarssuaq during the 24 hours of June 1966, 1967, 1968, 1969 and 1970, which confirms our previous results (litt. 8): the two daily peaks of occurrence around early morning and late afternoon local time, and the positive correlation with solar activity variation through the sunspot cycle. These results are a natural consequence of the previously established correlation between SEC and local magnetic activity for Godhavn. This correlation is also present at Narssarssuaq according to an investigation made on an event basis, the details of which are not included here. It showed, that usually the morning cases of SEC events were associated with negative deflections of the horizontal magnetic component, while afternoon cases of SEC were associated with positive deflections, corresponding to westward and eastward currents, respectively.

Fig. 6 shows the monthly number of full hour SEC occurrences during the 24 hours of each of the 6 months January - June, 1958, and the sum of these, at 4 stations: Thule, Godhavn, Narssarssuaq and Tromsø. The time scale is local standard time, LST, or 75^{o}WMT for Thule, 45^{o}WMT for Godhavn and Narssarssuaq and 15^{o}FMT for Tromsø. The arrows indicate geomagnetic noon time. The daily occurrence variation shows two daily maxima, morning and afternoon, at the two arctic lower latitude stations Narssarssuaq and Tromsø, and one maximum before noon at the high latitude stations Godhavn and Thule. The seasonal variation of the SEC occurrences shown, indicates a local summer maximum, which, on the present monthly sum basis, may be modified by casual high solar activity in one month or another, e.g. April 1958. No attempt should be made to draw final conclusions as to relative occurrence frequency of SEC at the four stations, since the Thule data were obtained, not from original ionograms, but from published IGY f-plots made at the station (litt. 31), and the Tromsø data were obtained from ionograms produced by equipment with rather low sensitivity for this special purpose. However, for daily and yearly variation investigation, the data used were satisfactory.

Fig. 7 shows the total 6 month SEC occurrence data for the 4 stations of Fig. 6, but now arranged in a polar diagram, with dipole latitude and time coordinates. The figure illustrates the auroral oval character of the SEC occurrence. This pattern has been further confirmed by the inclusion, not shown here, of published results on Slant Es occurrence at College (litt. 31) and

Sodankylä (litt. 19). Concerning the occurrence of SEC at Thule it is not yet possible to decide, whether this is due to the auroral oval extending this far polewards, or if auroral oval return currents may be responsible.

6. Discussion.

Although the morphology and general nature of the SEC seem pretty well established in the papers referred to above and in the present report, and automatically associate it with several known auroral phenomena and their characteristics, it might be worthwhile to summarize some specific observational results on SEC correlation with other phenomena, and to add a few others.

The close correlation of the SEC events with magnetic activity has been established in published reports as far as College, Godhavn, Dumont d'Urville, Sodankylä and Huancayo are concerned (litt. 2, 6, 8, 17, 18, 19, 2o, 28). For Tromsö we have made an investigation of the correlation with the local 3 hour K-index for the months January and April, 1958, which showed that the probability for a SEC event was greatly enhanced, when K reached or exceeded 4 - 5. This fact is in principle in accordance with the two stream instability theory and equatorial experimental results (see references above), as are the results of Czechowsky and Lange-Hesse (litt. 28) on a threshold- and hysteresis-like effect of magnetic activity in relation to VHF auroral backscatter experiments (threshold loo gammas for H-bay). During severe magnetic disturbances, the occurrence of radio black-out often precludes the observation of SEC on the ionogram. Still, at some occasions, special, very high gain ionograms have revealed a SEC event, when the normal gain ionogram showed a black-out condition, indicating that, at least in these cases, the SEC-magnetic activity correlation is valid, also towards the very highest activity levels. However, if the interpretation of the SEC features, dealt with here, are correct, these observations are not very surprising, but rather what one would expect.

Since the SEC event, as it seems, is associated with the two stream instability and its ion-acoustic waves and field aligned irregularities, it is natural, that it has a close relationship with results from scatter measurements and theories. This fact is evident from the 5 year period of backscatter measurements, that we have made at Narssarssuaq, and of which a few examples are shown in Fig. 2 and 3 of the present report. Also it has been demonstrated in various extensive backscatter research papers referred to above, in many of which the ion-acoustic wave theory was mentioned as a probable explanation on the results. In this connection special reference is made to the work of Unwin and Knox (litt. 25), where E and M spirals for the occurrence of VHF backscatter probability have similarity to the pattern of SEC occurrence shown in Fig. 7 of the present report. Importance in the present context has also the association between Slant Es, VHF forward-scatter sputter fading and rayed aurora observed by Bailey, Bateman and Kirby (litt. 9).

The SEC association with certain forms of aurora has been dealt with by several workers in addition to those mentioned above, e.g. Lassen (1963) in an extensive study of auroral phenomena on the basis of a long series of observations in the polar cap.

Finally it should be added, that some recent preliminary studies of 136 Mhz satellite beacon scintillations recorded at Godhavn (Mæhlum and Olesen, 1971), and of Pi micropulsation activity in the polar area, indicate some possibilities for correlations, that require further investigations, which we have planned to make in these fields.

7. Conclusions.

Based upon the results on the polar Slant E Condition presented in this report, and the general experience gained during the work, and not least upon the results of others referred to here in general, and especially regarding the equatorial SEC, the following conclusions may be proposed:

I. The Slant E Condition - SEC - in the equatorial and auroral regions, is the ionogram manifestation of the presence of very high currents, electrojets, in the ionospheric E region, when these exceed a certain threshold level.

II. The SEC in polar regions can be identified on ionograms through certain secondary criteria, when its prime indicator, the slant E trace, is missing for some reason.

III. The morphological features of the polar SEC occurrence point towards an auroral oval pattern similar to that of magnetic disturbances. The polar SEC is at high solar activity a frequently occurring phenomenon - up to about 75% occurrence probability at the daily maximum has been observed.

IV. Various circumstances indicate, that not only the equatorial SEC, but also the polar SEC is identical to the two stream instability with its ion-acoustic plasma waves in the form of field aligned electron density irregularities.

V. The SEC, due to its nature, has a close association with other ionospheric phenomena connected to the equatorial and auroral electrojets: geomagnetic activity, scatter mechanisms, radio wave propagation, electromagnetic wave phenomena, and for the polar SEC especially: auroral activity. The SEC is thus believed to be an important tool in connection with other related branches of research.

Acknowledgements.

It is a pleasure for me to express my gratitude for collaboration and various kinds of support from my colleagues at the Ionosphere Laboratory and other Geophysical Divisions of the Danish Meteorological Institute, including those at the stations in Greenland for their efforts on securing high quality data, not least my successor at the Godhavn station, Mr. Frede Iversen, for his recording of Fig. 4 and his voluntary, troublesome recording of several other sequences of continuous SEC recordings, and Miss Grethe Mollerup for careful analysis of SEC event data. The Norwegian Defense Research Establishment placed the Tromsö data at my disposal during my stay there, and I wish to thank the staff for their kind hospitality. The Greenlandic observatories are operated in cooperation with the U.S. National Oceanic and Atmospheric Administration, Boulder.

Various sections of the work was supported by the NATO Scientific Affairs Division, Grants No. 371 and 415, by the Danish Technical-Scientific Foundation, Grant No. 736-919, and by the Danish Science Research Council, Grant No. 511-138/69.

REFERENCES.

1. Heppner, J.F.; Byrne, E.C.; Belon, A.E. — The Association of Absorption and Es Ionization with Aurora. Journal of Geoph. Res. - 57 - p. 121 - 1952.

2. Cohen, R.; Bowles, K.L.; Calvert, W. — On the Nature of Equatorial Slant Sporadic E. Journal of Geoph. Res. - 67 - 3 - p. 965 - 1962.

3. Farley, Jr., D.T. — Two Stream Plasma Instability as a Source of Irregularities in the Ionosphere. Phys. Rev. Letters - 1o - 7 - p. 279 - 1963.

4. Farley, Jr., D.T. — A Plasma Instability Resulting in Field-Aligned Irregularities in the Ionosphere. Journal of Geoph. Res. - 68 - 22 - p. 6o83 - 1963.

5. Buneman, O. — Excitation of Field Aligned Sound Waves by Electron Streams. Phys. Rev. Letters - 1o - 7 - p. 285 - 1963.

6. Bowles, K.L.; Balsley, B.B.; Cohen, R. — Field-Aligned E-Region Irregularities Identified with Acoustic Plasma Waves. Journal of Geoph. Res. - 68 - 9 - p. 2485 - 1963.

7. Olesen, J.K. — Slant Es Ionospheric Disturbance at Godhavn and Its Correlation with Magnetic Activity. Internal Report to the Danish National Committee of URSI, 1957. Presented at a lecture to the National Bureau of Standards, Boulder, by Professor J. Rybner, Sep. 13., 1957.

8. Olesen, J.K.; Rybner, J. — Slant Es Ionospheric Disturbance at Godhavn and Its Correlation with Magnetic Disturbance, with Appendix: Note on the Occurrence of Slant Es at Narssarssuaq. AGARDograph 34: Sporadic E Ionization - p. 37 - Editor: B. Landmark. Printed by NATO, Paris, 1958.

9. Bailey, D.K.; Bateman, R.; Kirby, R.C. — Radio Transmission at VHF by Scattering and other Processes in the Lower Ionosphere. Proceed. of the I.R.E. - 43 - 1o - p. 1181 - 1955.

1o. Smith, E.K. — A Study of Sporadic E on a World-wide basis. NBS Report No. 3575, 1955.

11. Smith, E.K. — World-wide Occurrence of Sporadic E. NBS Circular 582 - 1957.

12. Smith, E.K.; Knecht, R.W. — Some Implications of Slant Es. NBS Report No. 55o3 - 1957.

13. Bates, H.F. — The Height of F-layer Irregularities in the Arctic Ionosphere. Journal of Geoph. Res. - 64 - p. 1257 - 1959.

14. Bates, H.F. — Direct HF Backscatter from the F Region. Journal of Geoph. Res. - 65 - p. 1993 - 196o.

15. Bates, H.F. — The Slant Es Echo - A High Frequency Auroral Echo. Journal of Geoph. Res. - 66 - 2 - p. 447 - 1961.

16. Bates, H.F.; Albee, P.R. — Aspect Sensitivity of HF Auroral Echoes. Journal of Geoph. Res. - 74 - 5 - p. 1164 - 1969.

17. Bowles, K.L.; Cohen, R. — A Study of Radio Wave Scattering from Sporadic E near the Magnetic Equator. Ionospheric Sporadic E - p. 51. Editors E.K. Smith and S. Matsushita. Pergamon Press. 1962.

18. Matsushita, S. — Relations Among Radio Absorbing Regions, Geomagnetic Bay - Disturbances and Slant Es in Auroral Latitudes. Journal of Geomagn. and Geoelectr. - 8 - 4 - p. 156 - 1956.

19. Oksman, J. — On the Slant Sporadic E Reflections. Annales Academiae Scientiarum Fennichae. A - VI - 181 - Helsinki 1965.

2o. Lebeau, A. — Sur L'activité Magnétique Diurnes Dans Les Calottes Polaires. Annales de Géophysique - T. 21 - 2 - p. 167 - 1965.

21. Kato, S.
Hirata, Y.
Electrostatic Waves and Ionization Irregularities in the Ionosphere. Report of Ionosph. and Spa. Res. in Japan - 21 - 3 - p. 85 - 1967.

22. Leadabrand, R.L.
Schlobohm, J.C.
Baron, M.J.
Simultaneous Very High Frequency and Ultra High Frequency Observations of Aurora at Fraserburg, Scotland. Journal of Geoph. Res. - 7o - 17 - p. 4235 - 1965.

23. Moorcroft, D.R.
The Interpretation of the Frequency Dependence of Radio Aurora. Planet. and Spa. Sci. - 14 - p. 269 - 1966.

24. Gadsden, M.
The Origin of Afternoon "Auroral" Radar Echoes. Planet. and Spa. Sci. - 15 . p. 893 - 1967.

25. Unwin, R.S.
Knox, F.B.
The Morphology of VHF Radio Aurora at Sunspot Maximum - IV. Journal of Atm. and Terr. Phys. - 3o - p. 25 - 1968.

26. Lyon, G.F.
Some Evidence Concerning the Distribution of Irregularities Responsible for Radio Aurora. Planet. and Spa. Sci. - 16 - p. 449 - 1968.

27. Hofstee, J.
Forsyth, P.A.
Ion-acoustic Waves in Auroral Plasma. Canad. Jour. of Phys. - 47 - p. 2797 - 1969.

28. Czechowsky, P.
Lange-Hesse, G.
Substorm Influences on VHF Continuous Wave Auroral Backscatter. Intercorrelated Satellite Observations Related to Solar Events - p. 4o5 - Editors V. Manno and D.E. Page - Reidel - 197o.

29. Akasofu, S.-I.
Polar and Magnetospheric Substorms - Reidel - 1968.

3o. Hartz, T.R.
The General Pattern of Auroral Particle Precipitation and Its Implications for High Latitude Communication Systems - p. 9 - Ionospheric Radio Communications - Editor K. Folkestad - Plenum Press - 1968.

31. National Bureau of Standards
Series of Data Compilations - Detailed Values of Ionospheric Characteristics and F-Plots. U.S. Department of Commerce, National Bureau of Standards, CRPL, Boulder, Colorado - 1958.

32. Lassen, K.
Geographical Distribution and Temporal Variation of Polar Aurorae. Danish Meteorological Institute Reports - No. 16 - 1963.

33. Mæhlum, B.
Olesen, J.K.
Time Variations in the Polar F Layer. Final Technical Report to Nato Scientific Affairs Division, Grant No. 415, 1971.

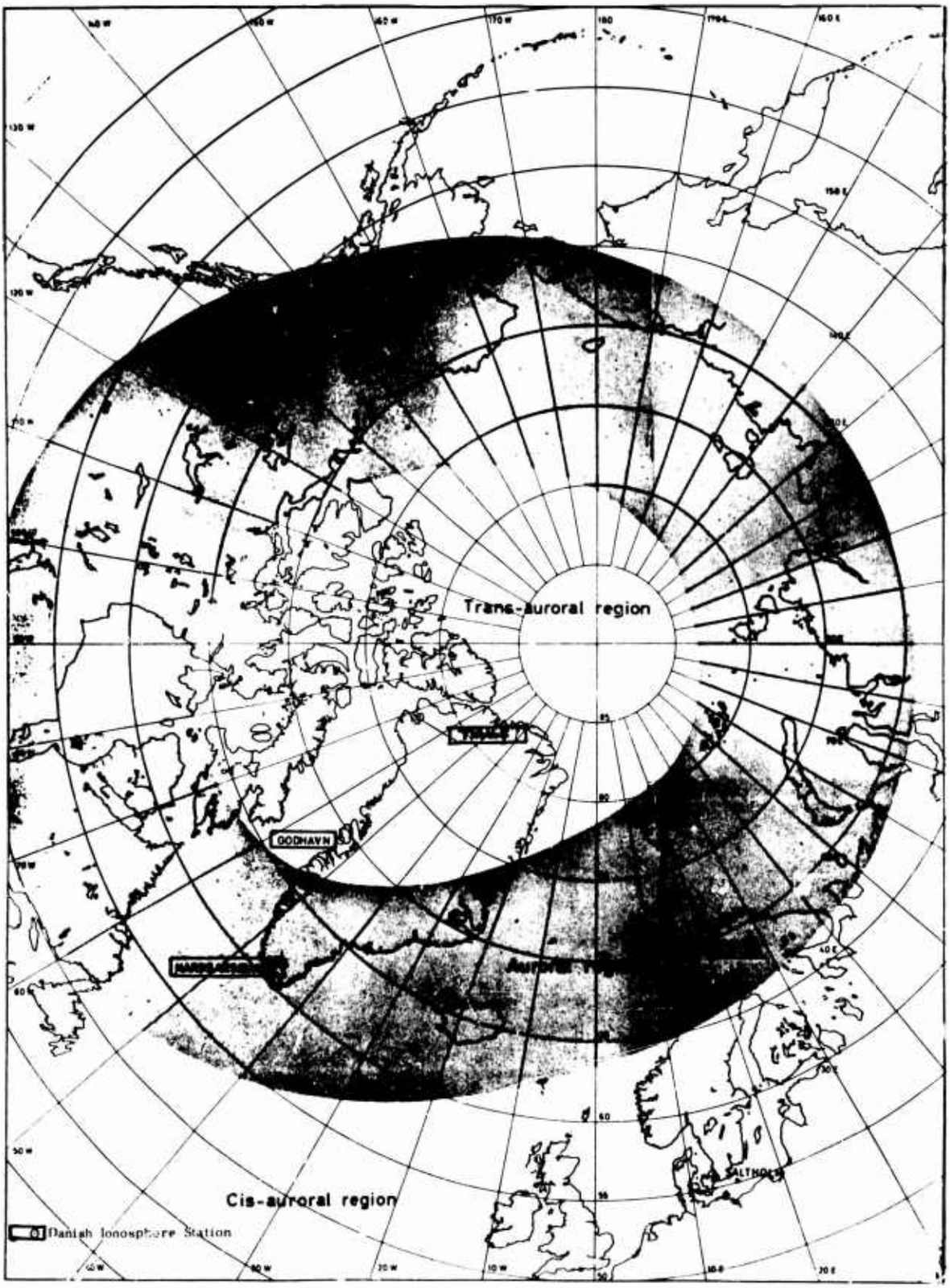

Fig. 1 Polar map showing the location of the four stations Thule, Godhavn, Narssarssuaq and Tromsö and the auroral region.

1254 hr.

No S.E.C.

Retardation traces in E and F1 at foE

1324 hr.

S.E.C. event starts

No foE retardation trace.
F1 stratification

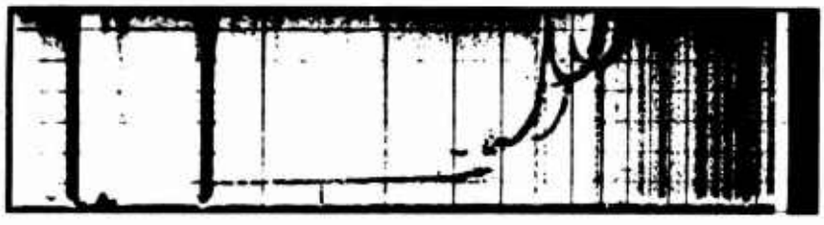

1349 hr.

S.E.C. early phase

Oblique F echoes.
Decrease foF2 starts
F1-F2 height separation increases.

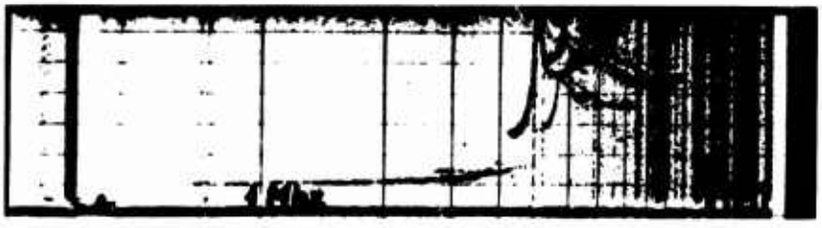

1434 hr.

S.E.C. well developed

No echoes from upper E and lower F1 (E-F1 frequency gap).
Oblique E region echo

1438 hr.

Backscatter record

Echo from NNW geogr. 330-400 km.

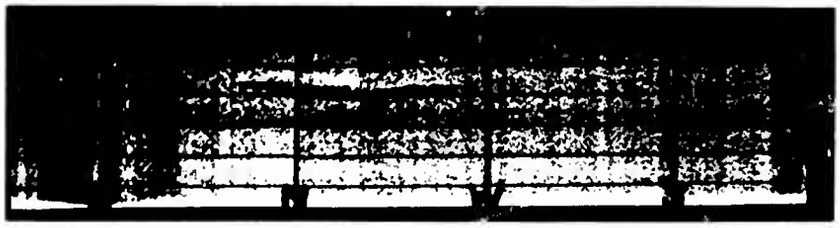

1442 hr.

Backscatter record

Echo NNW geogr. 400-450 km.

Fig. 2a Typical daytime Slant E Condition (S.E.C.) at Narssarssuaq, June 17, 1970. (45°WMT). Ionograms are 0.25 - 20 Mhz, 0-650 km.
12.7 Mhz backscatter record have same distance range, azimuth is E,N,W,S geographical from left to right, antenna elevation 30°.

1444 hr.

S.E.C. continues

Oblique upper E region echoes.

1457 hr.

S.E.C. continues

High gain-, expanded scale-record. Note Fl-z-echo.

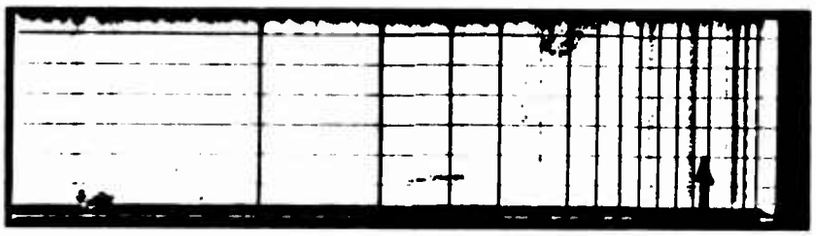

1458 hr.

S.E.C. continues

Low gain record. Notice: no slant trace but E-F freq. gap present.

1534 hr.

S.E.C. continues

Constant range F-echoes increase.

foF2 decrease continues.

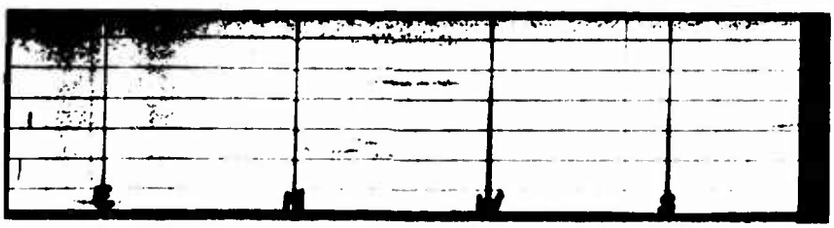

1542 hr.

Backscatter record Echoes NW, NNW and SE, various distances

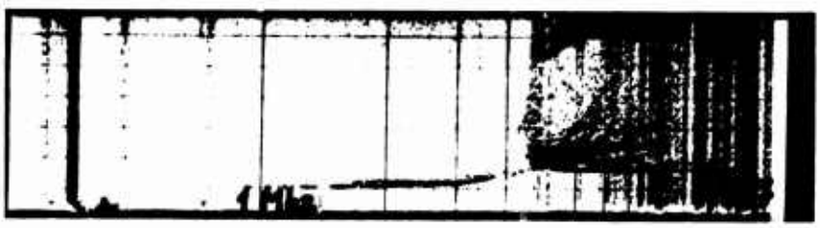

1544 hr.

Low constant range echoes.

E-Fl frequency gap increase.

Fig. 2b Typical daytime Slant E Condition (S.E.C.) at Narssarssuaq, June 17, 1970, continued. Text see Fig. 2a.

1659 hr.

S.E.C. ends. Last record with distinct slant trace. Notice clear F1 trace.

1734 hr.

S.E.C. over at Narssarssuaq - constant range and other oblique after-effects present. Possibly start new disturbance.

1742 hr.

S.E.C. over.

Backscatter record. Echoes NE, 280-350 km.

1744 hr.

S.E.C. over.

Constant range and other oblique after-effects

1749 hr.

S.E.C. over.

Constant range and other oblique after-effects.

1924 hr.

S.E.C. over.

New disturbances start

Fig. 2c Typical daytime Slant E Condition (S.E.C.) at Narssarssuaq, June 17, 1970, continued. Text see Fig. 2a.

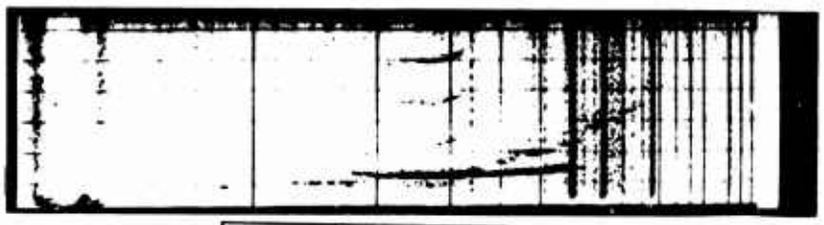

o144 hr.

S.E.C. event starts

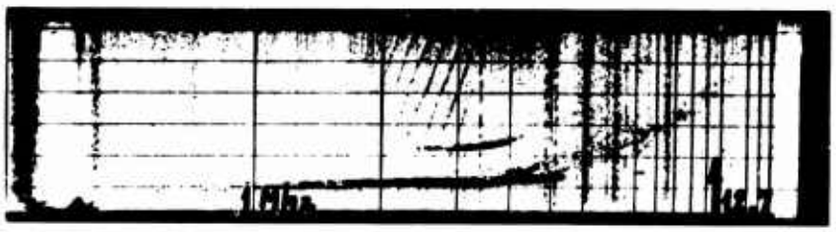

o234 hr.

S.E.C. well developed

o238 hr.

Backscatter record
Main echoes from
ENE, 37o-48o km

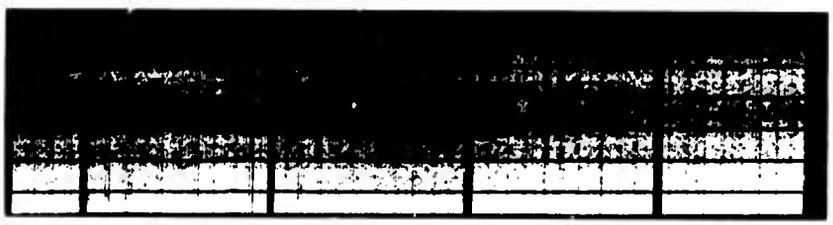

o242 hr.

Backscatter record
Main echoes from
ENE, 33o-43o km

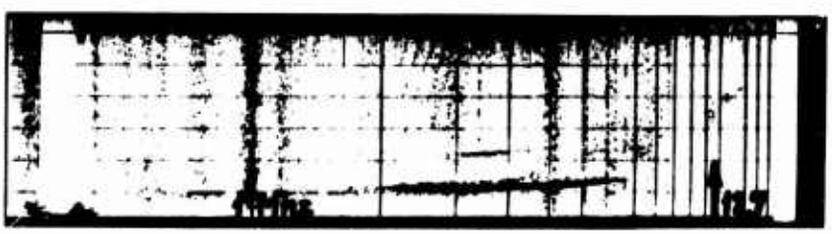

o244 hr.

S.E.C. still present
Frequency gap in
slant trace

o257 hr.

S.E.C. event ends

High gain-, expanded
height scale-record

Fig. 3a Typical nighttime Slant E Condition (S.E.C.) at Narssarssuaq, Dec. 15, 1970 (45°WMT). Text see Fig. 2a.

0014 hr.

S.E.C. event starts

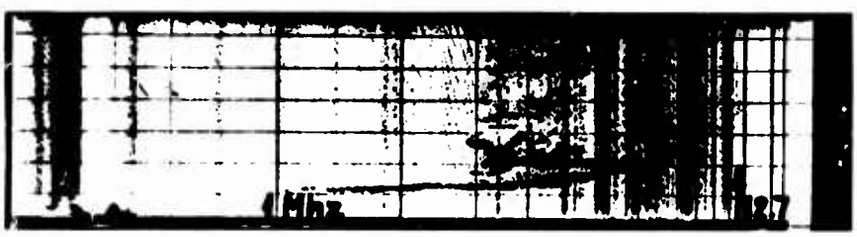

0029 hr.

S.E.C. with visible slant trace and various other oblique echoes, incl. constant range E-region echoes

0038 hr.

Backscatter record Echo W, 320-400 km

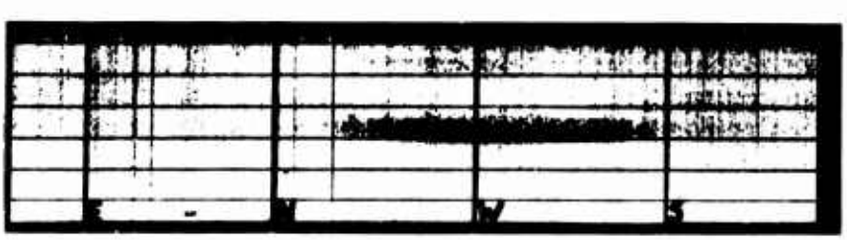

0042 hr.

Backscatter record Echo W, 290-380 km

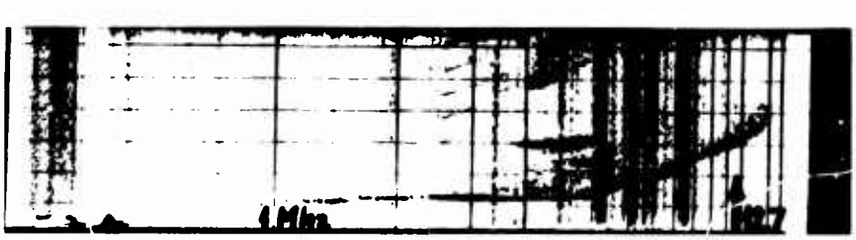

0044 hr.

S.E.C. with distinct slant trace

0229 hr.

S.E.C. ends

Fig. 3b Typical nighttime Slant E Condition (S.E.C.) at Narssarssuaq, Dec. 30, 1970 (45°WMT) Text see Fig. 2a.

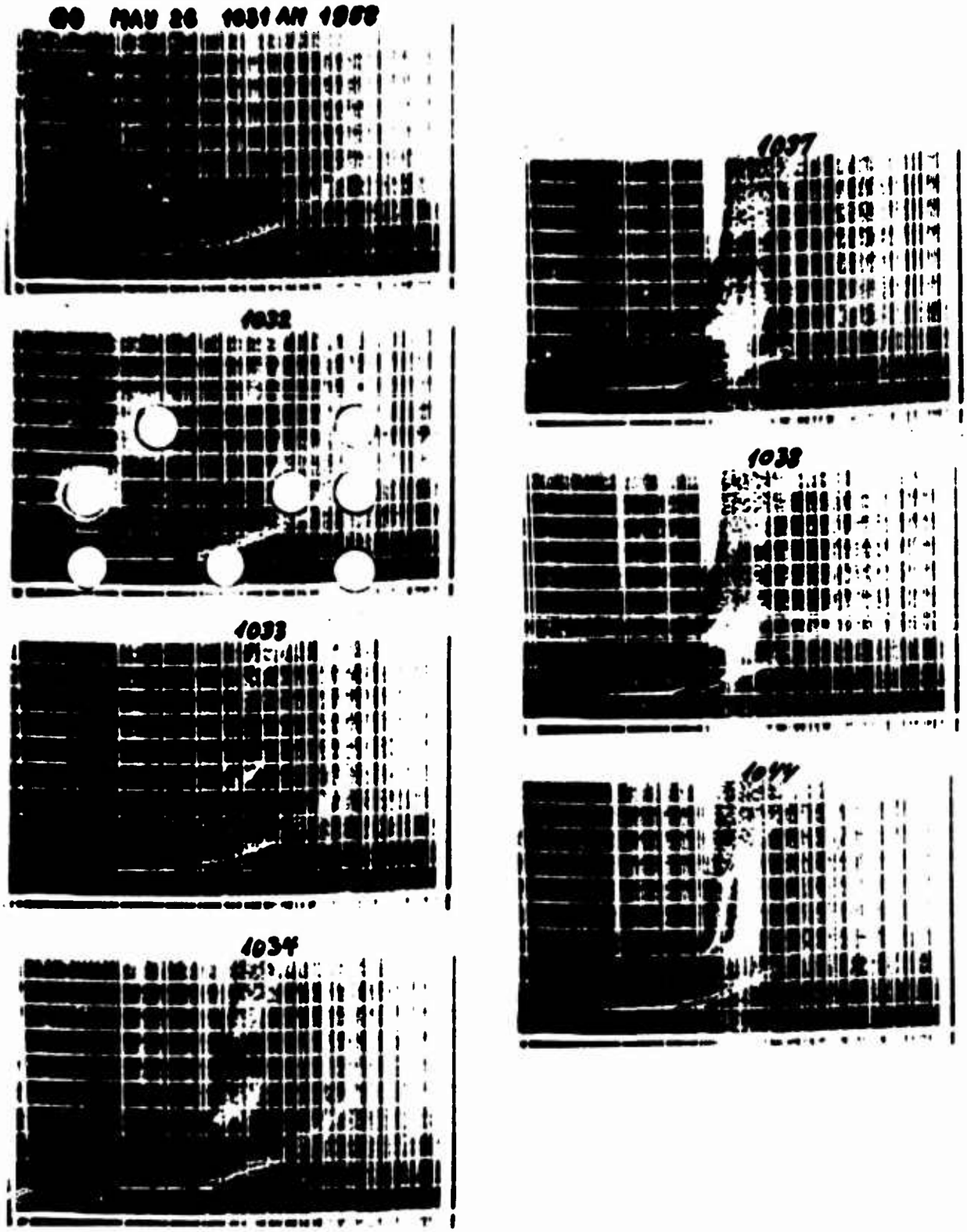

Fig. 4 Typical daytime Slant E Condition at Godhavn, May 26th, 1958. Sequence from continous operation illustrating gradual decrease of E-region scatter efficiency and corresponding appearance of F-region echoes. S.E.C. event started at 0700 hr and ended at 1530 hr 45°WMT.

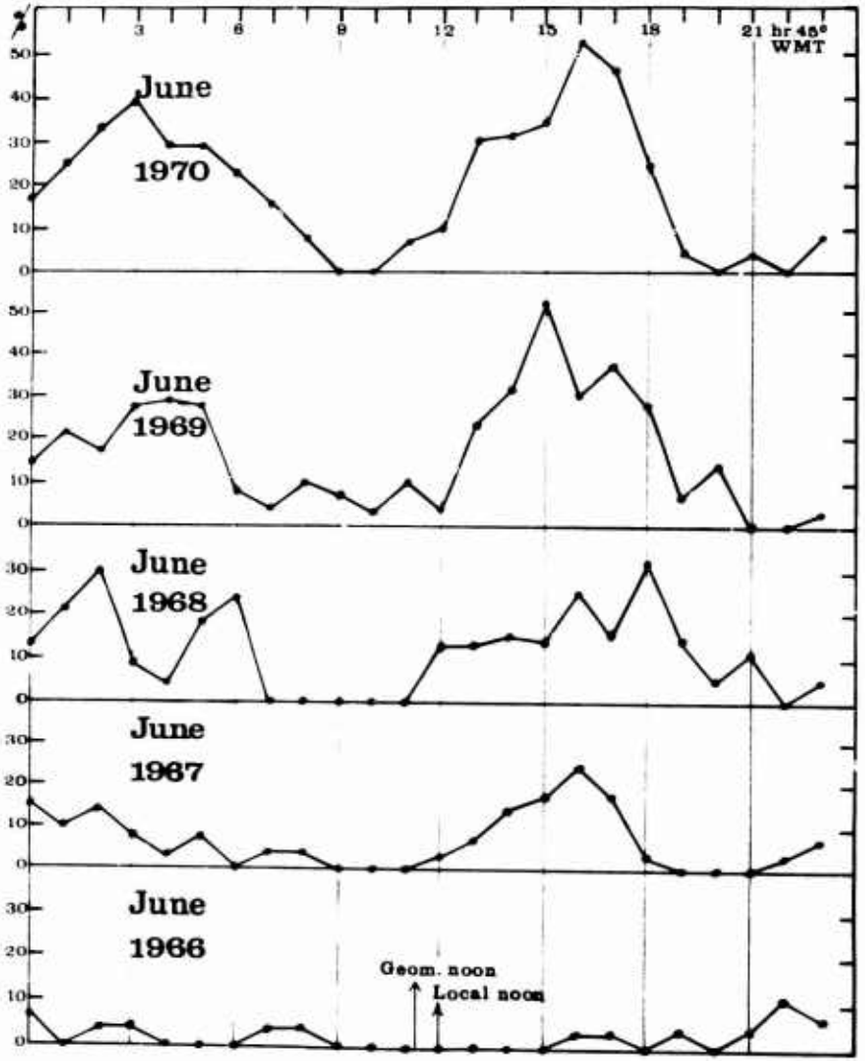

Fig. 5 Number of hours with Slant E Condition present at Narssarssuaq in percent of total number of hours excluding those with black-out and no operation.

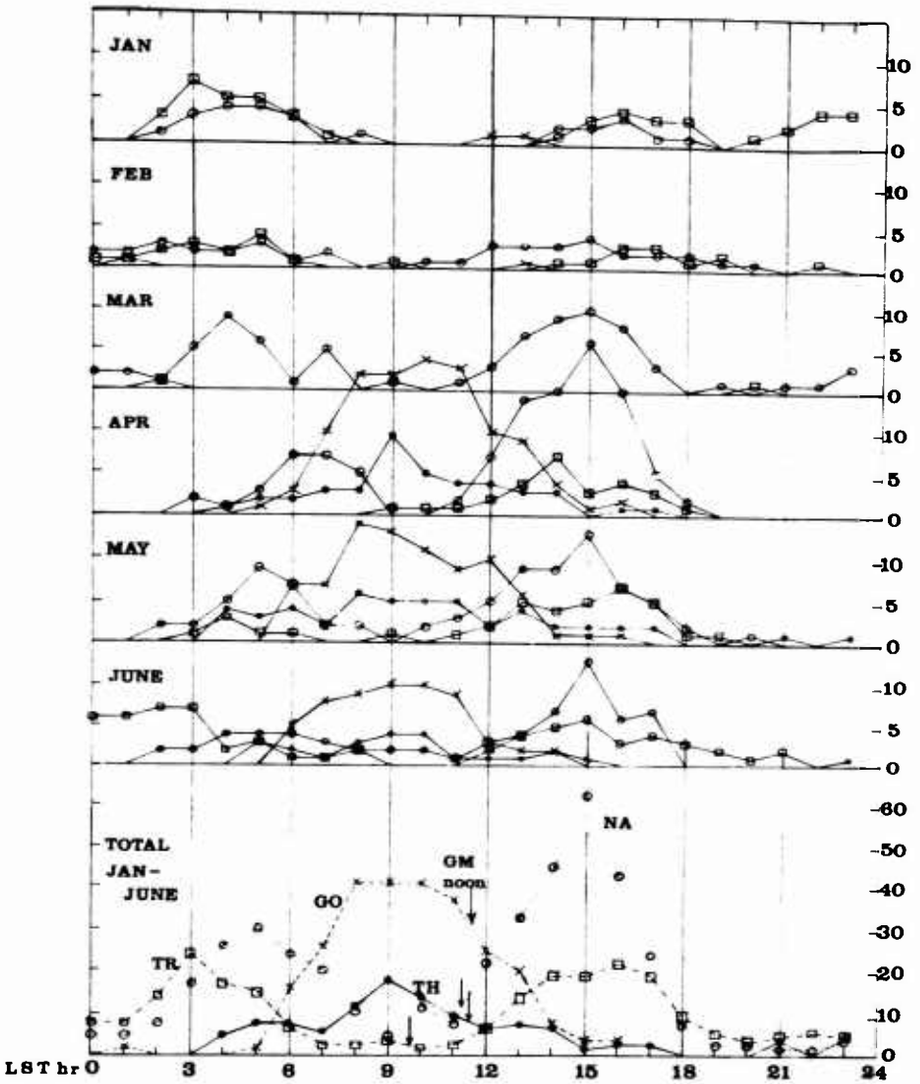

Fig. 6 SLANT E CONDITION. Number of occurrences each full hour
Jan. - Jun. 1958 at THULE : symbol ● ; LST = 75°WMT
GODHAVN : symbol × ; LST = 45°WMT
NARSSARSSUAQ: symbol ○ ; LST = 45°WMT
TROMSO : symbol □ ; LST = 15°EMT

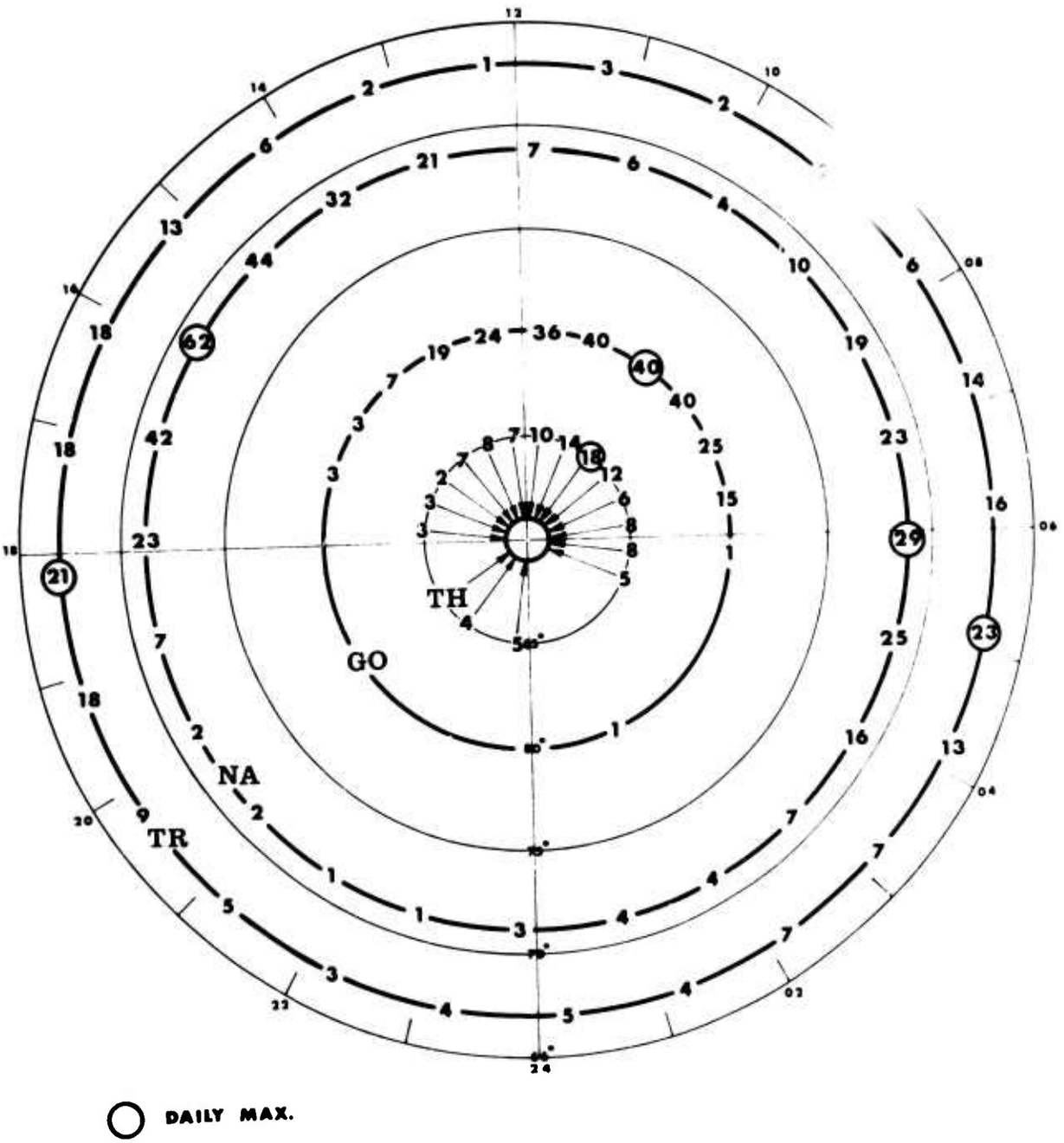

Fig. 7 Total number of full hour occurrences of Slant E Condition in Jan. - June, 1958 at Thule (TH), Godhavn (GO), Narssarssuaq (NA), and Tromsö (TR), in dipole latitude and time coordinates.

HIGH FREQUENCY BACKSCATTER OBSERVATIONS AT MEDIUM LATITUDES OF HIGH LATITUDE FIELD ALIGNED IRREGULARITIES

M. CROCHET, D. BARREAU, J.C. de MAISTRE

Laboratoire de Physique de l'Exosphère
Université de Paris VI
11 Quai St Bernard - Paris - 5°

RESUME

Des échos anormaux dus à la présence d'irrégularités alignées dans la couche F à haute latitude ont été fréquemment observés à la station de Valensole (44° N, 6° E) en utilisant un radar à rétrodiffusion en ondes décamétriques. La comparaison d'un certain nombre d'enregistrements caractéristiques avec des résultats simultanés de la station de Lindau (51° 30' N, 10° E) où des échos analogues sont régulièrement obtenus, met en évidence l'influence de la latitude de la station sur l'observation de ces phénomènes.

1°) Indépendamment des conditions particulières de propagation qui peuvent exister au nord de Valensole, des considérations purement géométriques montrent que les irrégularités susceptibles de produire des échos à Valensole sont situées en général au dessus du maximum de la couche F, alors qu'à Lindau elles sont situées en dessous.

2°) La présence de gradients horizontaux ou de perturbations itinérantes est à l'origine de mécanismes de guidage et de focalisation qui peuvent favoriser des zones d'irrégularités bien déterminées, situées au dessus du maximum de la couche F et expliquer les structures discrètes obtenues fréquemment sur les enregistrements de Valensole. A Lindau, par contre, la présence, d'ailleurs beaucoup plus rare, de structures discrètes est vraisemblablement due à l'existence de paquets d'irrégularités bien localisées en distance.

ABSTRACT

Abnormal echoes ascribable to the presence of field aligned high latitude irregularities in the F layer have frequently been observed from the Valensole station (44° N, 6° E), by means of decametric wave backscatter radar. A comparison of characteristic recordings with data collected simultaneously at the Lindau station (51° N, 10° E) where such echoes are regularly obtained reveals the influence of the station latitude on the observation of such phenomena.

1. Neglecting any particular propagation conditions likely to exist North of Valensole, purely geometrical considerations reveal that the irregularities likely to induce echoes at Valensole are generally located above the maximum portion of the F layer, whereas they are located below at Lindau.

2. The presence of horizontal gradients or travelling disturbances induces guidance and focusing effects which may favour well defined irregularities zones, located above the maximum portion of the F layer, and may account for the discrete structures frequently obtained in the Valensole recordings. At Lindau, however, the presence of such discrete structures - which is far less frequent than at Valensole - is probably due to the presence of patches of irregularities, localized at well defined ranges.

1 - INTRODUCTION

Des échos anormaux, dont l'aspect sur des enregistrements de rétrodiffusion à fréquence variable est inexplicable par une rétrodiffusion au niveau du sol, ont été fréquemment observés à la station de Valensole (44° N, 6° E) à l'aide d'un radar en ondes décamétriques de 100 kw de puissance crête rayonnant vers le nord.

L'observation simultanée à Lindau (51° N, 10° E) d'échos analogues, provenant de la même région, et dont les signatures caractéristiques sur les enregistrements en balayage de fréquence, en rétrodiffusion, sont maintenant bien connues (1 et 2) a permis d'attribuer ces anomalies à une rétrodiffusion directe sur des irrégularités alignées.

Les signatures relevées dans les deux stations n'étant toutefois pas identiques, on a été amené à utiliser une méthode de simulation par tracé de rayons pour expliquer les différences observées et on a pu mettre ainsi en évidence l'influence de la latitude de la station.

On a considéré tout d'abord des conditions de propagation normales en faisant l'hypothèse d'une ionosphère non perturbée. L'analyse de la structure d'échos particuliers observés à Valensole a ensuite nécessité un traitement plus complexe de la propagation, faisant intervenir des mécanismes de guidage et de focalisation liés à la présence de gradients horizontaux au sein de la couche F.

2 - CAS D'UNE IONOSPHERE NON PERTURBEE

L'obtention d'échos rétrodiffusés directement par des irrégularités alignées est liée au respect de la condition de perpendicularité, au sein de la couche, des rayons incidents avec les lignes de force du champ magnétique terrestre que l'on assimilera à celui d'un dipôle tel que l'inclinaison du champ dipolaire pour les latitudes considérées soit la même que celle du champ réel. On se limitera par ailleurs au plan du méridien géomagnétique. Les latitudes géomagnétiques des deux stations sont 41° 30' N pour Valensole et 49° N pour Lindau.

Si la réfraction ionosphérique n'intervient pas (fréquence de travail infinie), les lieux des points où le rayon est perpendiculaire au champ magnétique terrestre (3) sont notablement différents pour les deux stations (fig. 1) ; l'altitude maximum atteinte à Valensole étant nettement plus grande que pour Lindau.

2.1. Simulation d'enregistrements à fréquence variable

Pour tenir compte de la réfraction ionosphérique aux fréquences de travail utilisées, on fait l'hypothèse d'un profil vertical de couche parabolique et défini par ses trois paramètres : F_c, fréquence critique de la couche, H_m, hauteur du maximum d'ionisation et Y_m demi-épaisseur de la couche.

La proximité relative des deux stations permet d'utiliser sans grande erreur les mêmes valeurs des paramètres : on a pris H_M = 340 km et Y_M = 90 km. Le programme de tracé de rayons utilise dans ce cas les expressions analytiques connues de la trajectoire sous forme de fonctions hyperboliques. A chaque pas du calcul, l'angle entre la direction du rayon et le champ magnétique local est calculé : le point correspondant à la perpendicularité est localisé par interpolation linéaire à partir de deux points qui l'encadrent. Avec les pas qui ont été utilisés, l'écart à la perpendicularité est toujours inférieur à 0,05 degré.

Les résultats du tracé de rayons sont résumés pour les deux stations sous forme de diagrammes donnant la distance de groupe G à laquelle se produit la perpendicularité en fonction de la fréquence réduite x (rapport de la fréquence de travail à la fréquence critique) (fig. 2.a et 2.b). Dans les deux cas, deux réseaux de courbes ont été tracés correspondant à différentes valeurs de l'angle de départ Δ des rayons et de l'altitude H des points de réflexion sur les irrégularités.

On remarque tout d'abord que la fréquence maximum théorique d'observation des échos (définie uniquement par la géométrie de la propagation) est infinie à Valensole alors qu'elle est limitée à $F_{max} = 5\ F_c$ à Lindau. Ceci s'interprète aisément à partir des résultats de CHAPMAN rappelés précédemment. En effet, pour Valensole, une partie de la courbe de CHAPMAN étant située à l'intérieur de la couche F, la perpendicularité est possible dans la couche pour une fréquence infinie, alors qu'à Lindau il faudrait admettre une couche F plus basse pour rencontrer des conditions analogues.

En outre, on constate qu'à Valensole le pinceau d'angles susceptibles d'être efficaces est plus étendu qu'à Lindau (45° au lieu de 28°) et qu'il intercepte en général les irrégularités au dessus du maximum d'ionisation alors qu'à Lindau le bas de la couche est favorisé. Il est donc théoriquement possible, à partir de ces deux stations distantes de 1000 km, de suivre l'extension en altitude d'irrégularités localisées à une distance donnée. On peut montrer que pour des irrégularités situées à environ 1800 km de Valensole soit 800 km de Lindau, les altitudes d'observation sont comprises entre 340 et 405 km à Valensole tandis qu'elles se situent entre 260 et 345 km pour Lindau.

2.2. Résultats expérimentaux

Dans le cas d'une distribution continue en latitude d'irrégularités de grande extension en altitude, on peut s'attendre à obtenir expérimentalement des répartitions d'échos analogues aux diagrammes théoriques. En fait on n'observe le plus fréquemment qu'une partie des courbes enveloppes de ces diagrammes. Le calcul montre en effet qu'à ce niveau la densité de rayons est plus élevée qu'ailleurs. Cette focalisation de l'énergie par les caustiques contribue à la formation d'échos d'amplitude notable caractérisés par une distance quasi constante à Valensole et un signal en forme de "nez" à Lindau. La zone susceptible de contribuer à la formation de ces échos est alors limitée verticalement à une gamme d'altitudes voisines de l'ordre de 320 km pour les deux stations (fig. 2.a et 2.b).

En dehors de ces échos d'aspect bien caractéristique (fig. 3), un certain nombre de structures discrètes ont été observées à Valensole. Dans certains cas elles peuvent être associées à des structures analogues obtenues à Lindau avec un écart de distance correspondant à la distance en latitude entre les deux stations (fig. 4). On se trouve alors en présence de paquets d'irrégularités, bien définis en position, dont l'extension en altitude est importante. Mais on observe aussi à Valensole des échos dont le trajet de groupe varie rapidement avec la fréquence (fig. 4) et qui ne peuvent être associés à aucun écho de Lindau. Pour les expliquer, il est nécessaire de faire intervenir des phénomènes de propagation anormale et d'étudier l'influence de gradients horizontaux et de perturbations sur le respect de la condition de perpendicularité.

3 - CAS D'UNE IONOSPHERE PERTURBEE

DEARDEN (4) a interprété des échos à grande distance obtenus à Brisbane en rétrodiffusion à fréquence fixe par une propagation guidée au niveau de la couche F aurorale, cette dernière étant affectée de forts gradients horizontaux. En s'inspirant de ces résultats on a recherché pour différentes fréquences d'utilisation l'aide du programme de tracé de rayons de JONES (5), les conditions de perpendicularité des rayons avec les lignes de force du champ magnétique terrestre dans une couche parabolique affectée d'une perturbation sinusoïdale à front vertical.

La validité de la méthode a été contrôlée par comparaison avec les résultats de DEARDEN en simulant les gradients horizontaux introduits dans ses modèles par une perturbation de 4000 km de longueur d'onde. Pour simuler les résultats expérimentaux obtenus à Valensole, en particulier ceux de la nuit du 14/15 mai 1969 (fig.5), on a considéré deux longueurs d'onde de perturbation respectivement de 1000 km et 300 km ; cette dernière valeur a été déduite de l'analyse des échos de sol sur l'enregistrement à fréquence fixe et sur les balayages en fréquence (20 h 45 et 21 h 00) qui précèdent l'apparition des échos auroraux (fig. 5). On note en effet sur ces enregistrements des striations caractéristiques de la présence d'une perturbation (6).

3.1. Processus de guidage et de focalisation

Le processus de guidage et de focalisation est clairement mis en évidence sur les figures 6a et 6b où sont représentées, pour différentes fréquences d'utilisation, les distances de groupe G des points où la condition de perpendicularité est satisfaite, en fonction de l'angle d'élévation des rayons.

Sur la figure 6a, le gain par focalisation dû aux gradients horizontaux de l'ionosphère peut se calculer aisément. A un instant donné, l'énergie rétrodiffusée reçue provient d'une zone de profondeur $\Delta G = \frac{c\tau}{2}$ (τ étant la durée d'impulsion utilisée, en général une milliseconde). Le pinceau de rayons correspondants, pour une distance G de 2000 km a, en ionosphère non perturbée, à 12 Mhz, une largeur en élévation de 1°5. En ionosphère perturbée, la zone correspondante, pour un même rayon moyen du pinceau, se place vers 2350 km et la largeur du pinceau devient alors 4°. Le gain dû à la focalisation est donc de 4 dB. Pour une durée d'impulsion plus brève, le gain dû à la focalisation augmente et peut atteindre 10 db.

En plus du processus de focalisation, on observe un mécanisme de guidage au voisinage du maximum de la couche F, qui se traduit par un retard important pour les échos associés aux rayons guidés. Pour une longueur d'onde de 1000 km, ce phénomène s'observe (fig. 6a) à 10 Mhz et pour une élévation de 6°. Pour une longueur d'onde de 300 km (fig. 6b), on l'observe pour Δ = 1°, 4°, 8°, 13°. On remarque que ce phénomène de guidage, en dispersant l'énergie d'un pinceau de rayons donné sur une grande distance, atténue l'effet des focalisations : les échos lointains obtenus aux fréquences basses auront une amplitude faible et leur mise en évidence sera conditionnée par la sensibilité de l'appareillage.

Pour une longueur d'onde de perturbation donnée, les distances de focalisation varient avec la fréquence. On peut simuler les diagrammes obtenus dans les observations à fréquence variable en représentant en fonction de la fréquence réduite l'évolution de ces distances de groupe (fig. 7). La variation rapide de la distance de focalisation observée aux fréquences basses est due au mécanisme de guidage et le dédoublement des traces au voisinage de la fréquence d'apparition des échos correspond au dédoublement des focalisations qui apparait aux fréquences de fonctionnement les plus basses (fig. 6b ; F = 9 Mhz ; G = 2250 km pour Δ = 6° et G = 2550 km pour Δ = 8°).

Le calcul montre donc que, pour une perturbation de faible longueur d'onde, plusieurs pinceaux de rayons sont focalisés au niveau d'irrégularités situées au dessus du maximum de la couche. On peut expliquer ainsi les traces bien définies observées à Valensole (fig. 5), les retards importants observés aux fréquences basses étant dus au processus de guidage.

En résumé, on peut considérer que les gradients horizontaux favorisent à Valensole la détection d'irrégularités situées au dessus du maximum de la couche F. Par contre, à Lindau, les irrégularités observées étant situées en dessous du maximum, les rayons qui/illuminent sont peu affectés par les perturbations de densité . Bien entendu cette remarque n'exclut pas l'observation aussi bien à Valensole qu'à Lindau de paquets d'irrégularités bien localisés en distance, mais elle permet d'interpréter à Valensole des échos dont les variations de temps de groupe avec la fréquence seraient inexplicables autrement.

IV - CONCLUSION

Les signatures très caractéristiques observées à Valensole sur les enregistrements de rétrodiffusion à fréquence variable, dans la direction du Nord, inexplicables par une rétrodiffusion au sol, peuvent s'interpréter aisément à partir de l'hypothèse de rétrodiffusion directe par des irrégularités alignées le long du champ magnétique dans l'ensemble de la couche F. La comparaison avec des enregistrements analogues de la station de Lindau permet de mettre en évidence l'influence de la latitude sur l'observation de ces phénomènes et confirme l'importance du rôle des gradients horizontaux au sein de la couche lorsque la distance d'observation augmente.

REMERCIEMENTS

Les auteurs remercient le Dr. H.G. MOLLER du Max Planck Institut de Lindau pour les données qu'il a mises à leur disposition.

Le travail présenté a été accompli dans le cadre de Conventions avec la Direction des Recherches et Moyens d'Essais.

REFERENCES

1. MOLLER H.G. "Rückstrenbeobachtungen mit variabler frequency in Lindau Harz". Gerland Beiträge zur Geophysik. 73 (2), 81-92, 1964.

2. MOLLER H.G., H. KOPKA, W. STOFFEGREN "Backscatter observations from distant fied-aligned irregularities". AGARD Conference Proceedings. 37, 58-1, 58-14, 1968.

3. CHAPMAN S. "The geometry of radio echoes from aurora". JATP, 3 (1), 29, 1952.

4. DEARDEN E.W. "Propagation ducts due to horizontal gradients leading to echoes from magnetic field aligned F-region irregularities". JATP, 31, 1147-1155, 1969.

5. JONES R.M. "A three dimensional ray tracing computer program". ESSA Technical Report - Boulder, Dec. 1966

6. de MAISTRE J.C. "Etude des perturbations itinérantes dans l'ionosphère par la méthode de rétrodiffusion" Thèse de 3e cycle, Paris 1970.

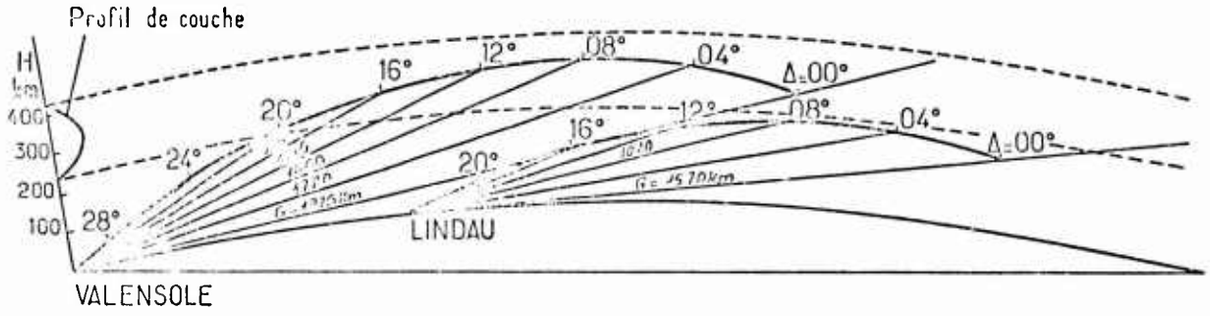

Fig. 1 - Conditions de perpendicularité dans le plan du méridien magnétique à Valensole et à Lindau en l'absence de réfraction. (Latitudes magnétiques : Valensole 41° 5 ; Lindau 49°).
Δ : élévation du rayon. G : distance au lieu de perpendicularité.

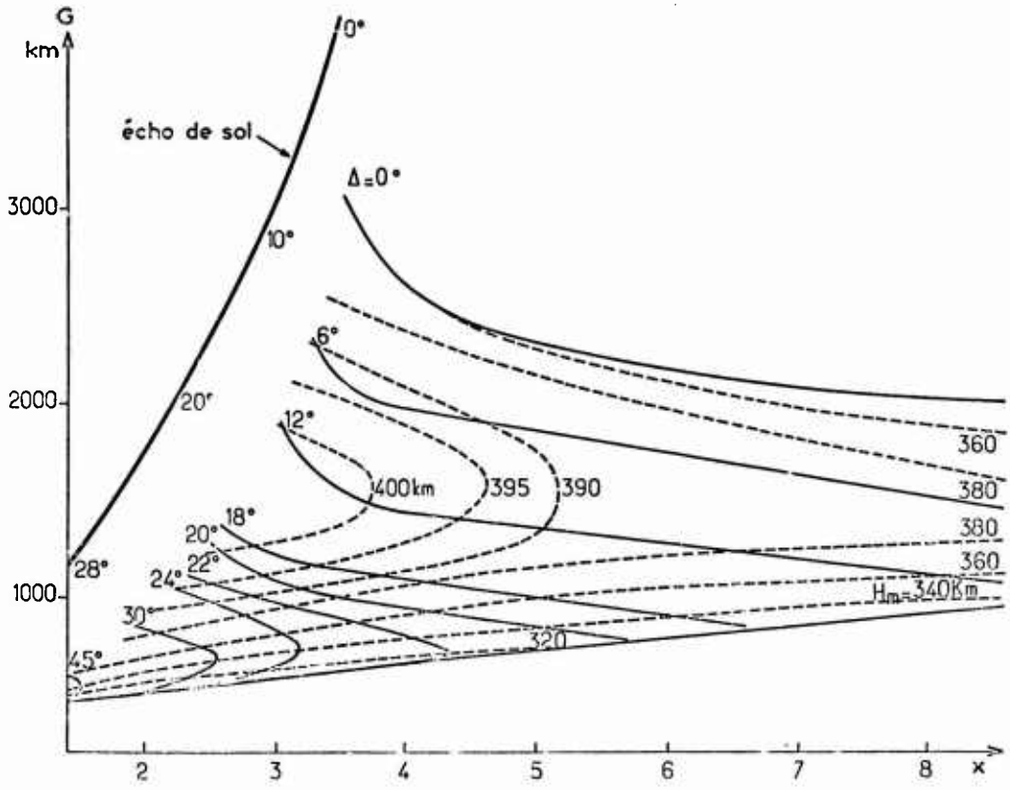

Fig.2 (a)

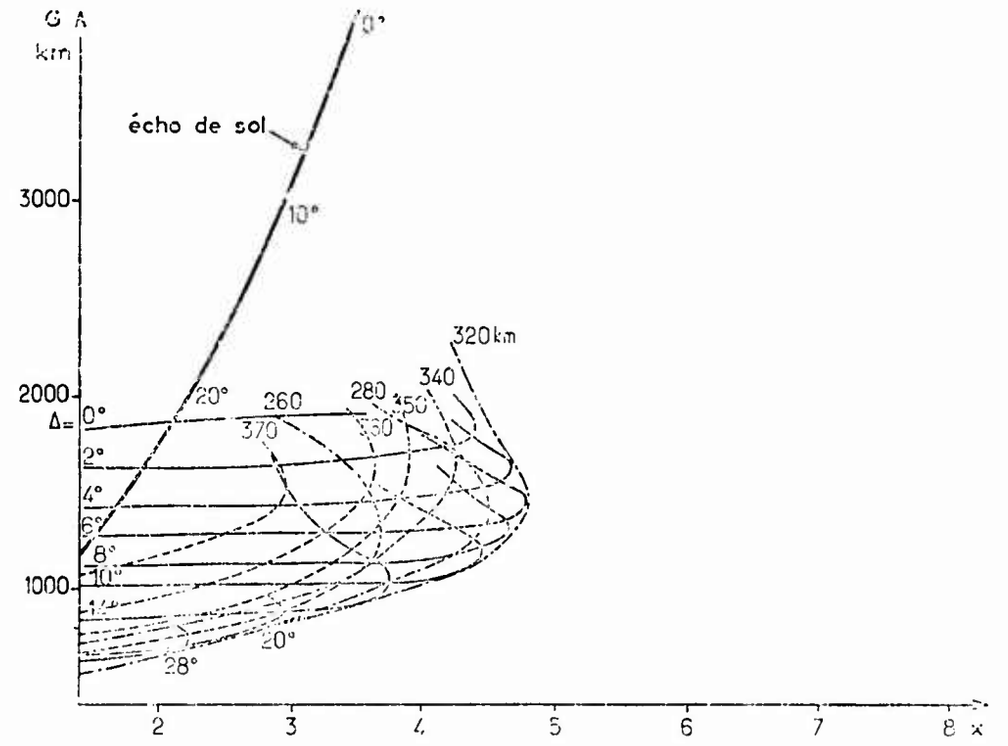

Fig.2 (b)

Fig. 2 a et b

Conditions de perpendicularité en ionosphère non perturbée à Valensole (2a) et Lindau (2b). Trajet de groupe G en fonction de la fréquence réduite $x = F/F_c$ pour une couche parabolique définie par H_m = 340 km et Y_m = 90 km.

en trait plein : à angle constant d'élévation Δ des rayons
en tireté : à altitude constante des points de réémission.

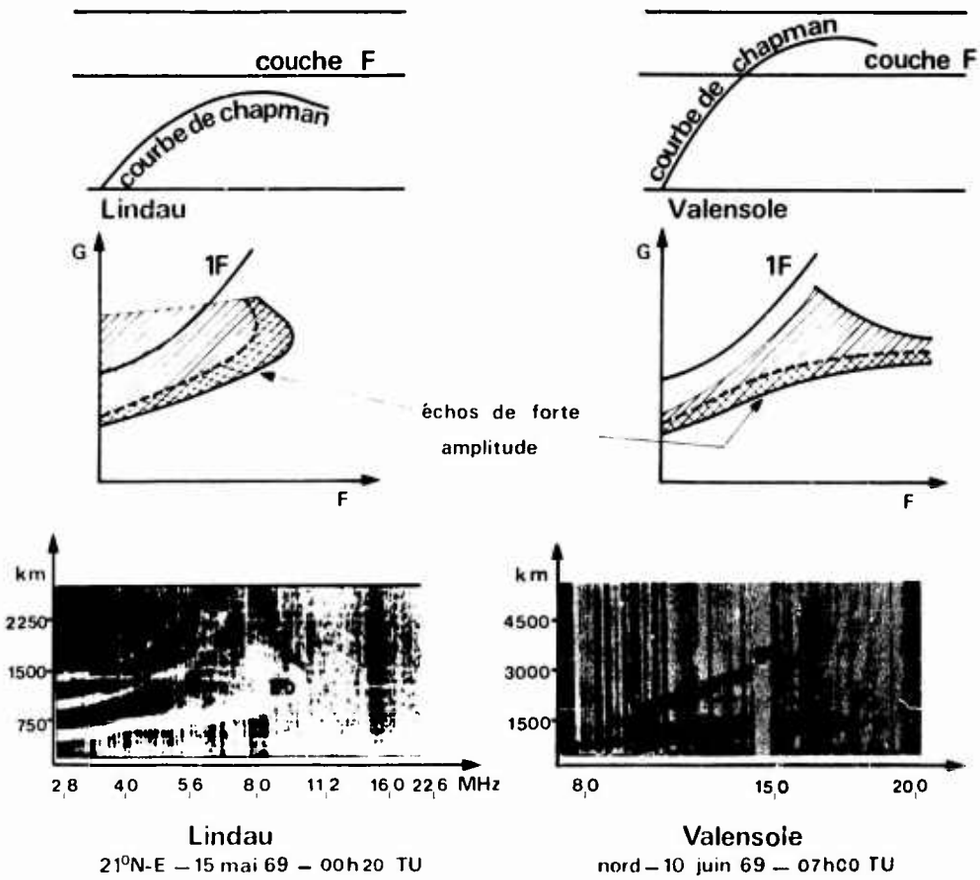

Fig. 3 - Enveloppes des perpendicularités et enregistrements à fréquence variable à Lindau et à Valensole.

a

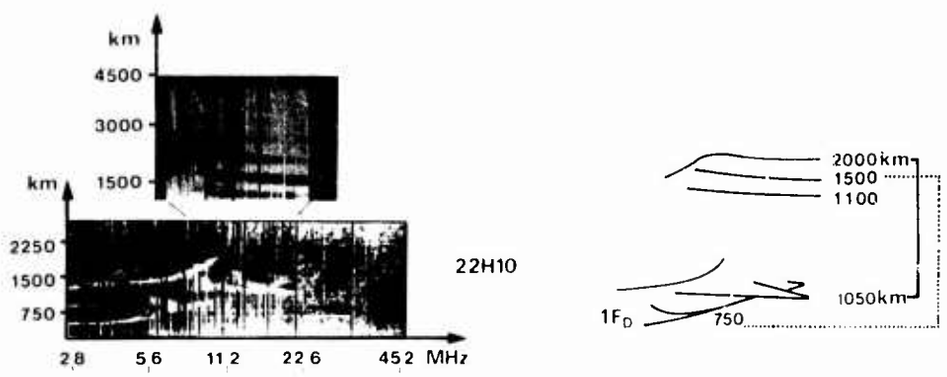

14/15 Mai 1969

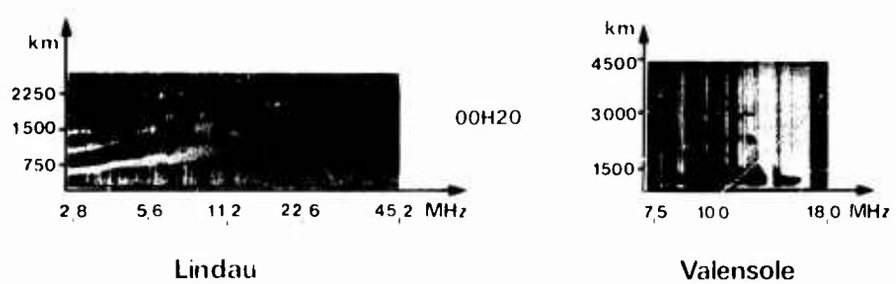

b

Fig. 4 - Enregistrements à fréquence variable à Lindau et à Valensole dans la direction Nord les 14 et 15 mai 1969.

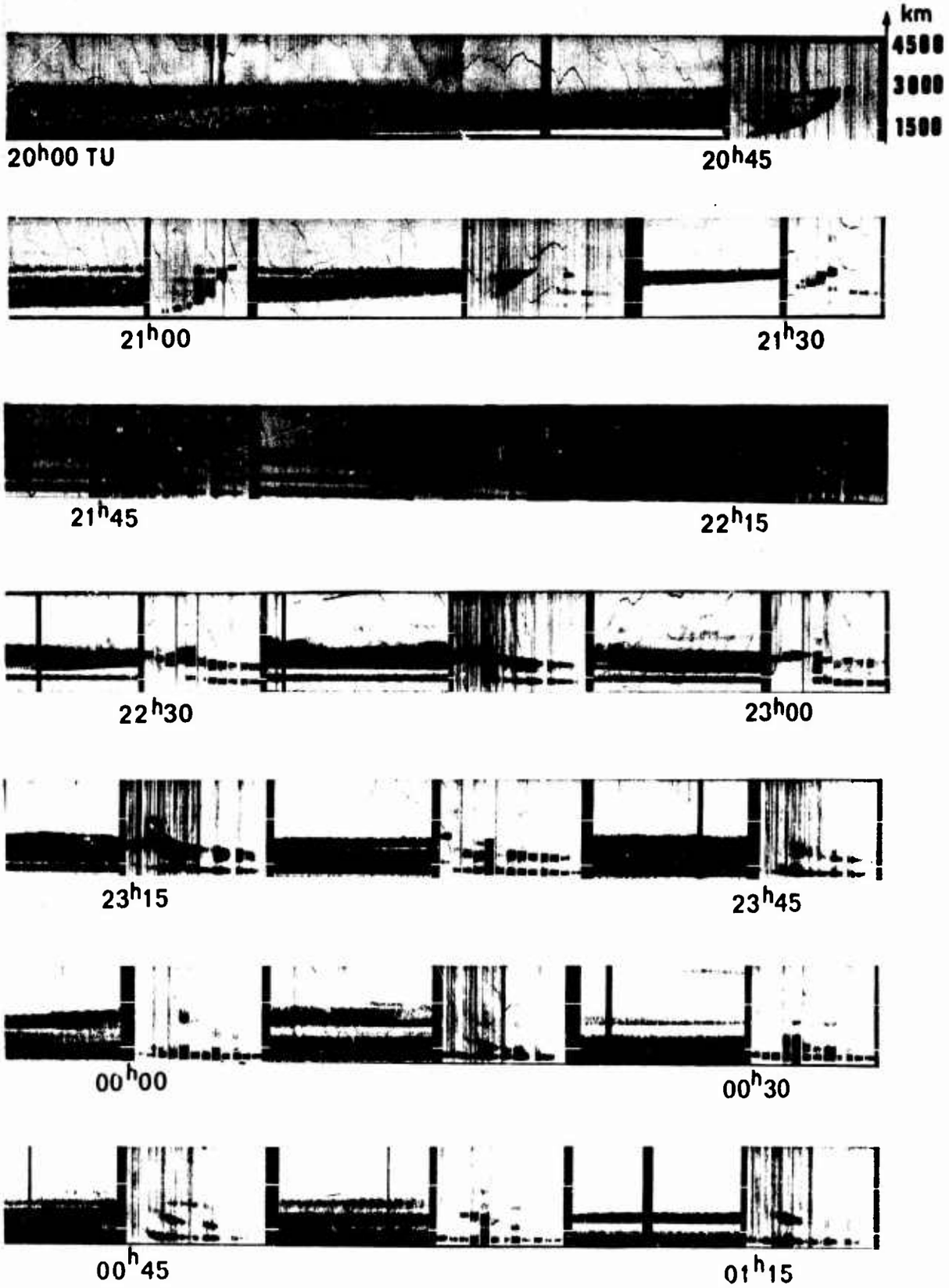

Fig. 5 - Evolution temporelle des signaux rétrodiffusés à Valensole 14/15 Mai 1969. Enregistrements à fréquence fixe et balayage en fréquence (8 - 20 Mhz).

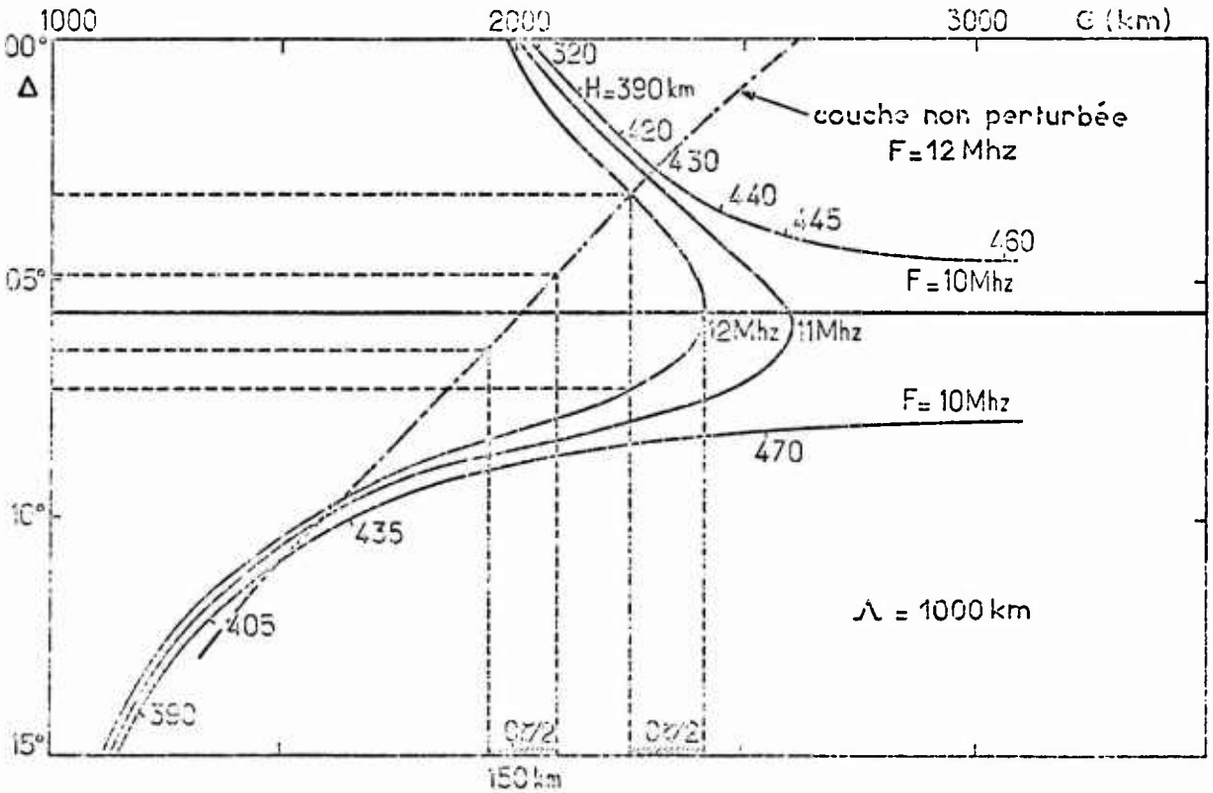

Fig.6 (a)

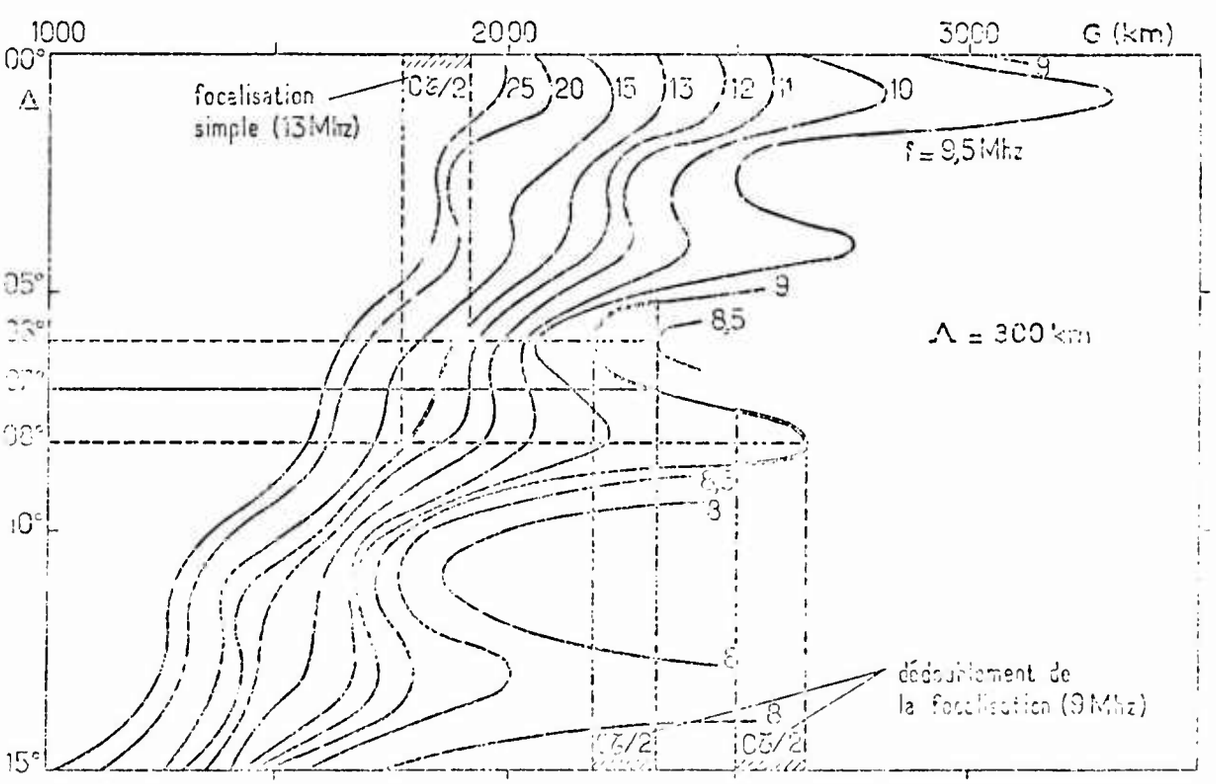

Fig.6 (b)

Fig. 6 - Conditions de perpendicularité pour Valensole et pour une ionosphère à profil parabolique [H_m = 390 km ; Y_m = 90 km] affectée de perturbations de longueur d'onde 1000 km (fig. 6a) et 300 km (fig. 6b).

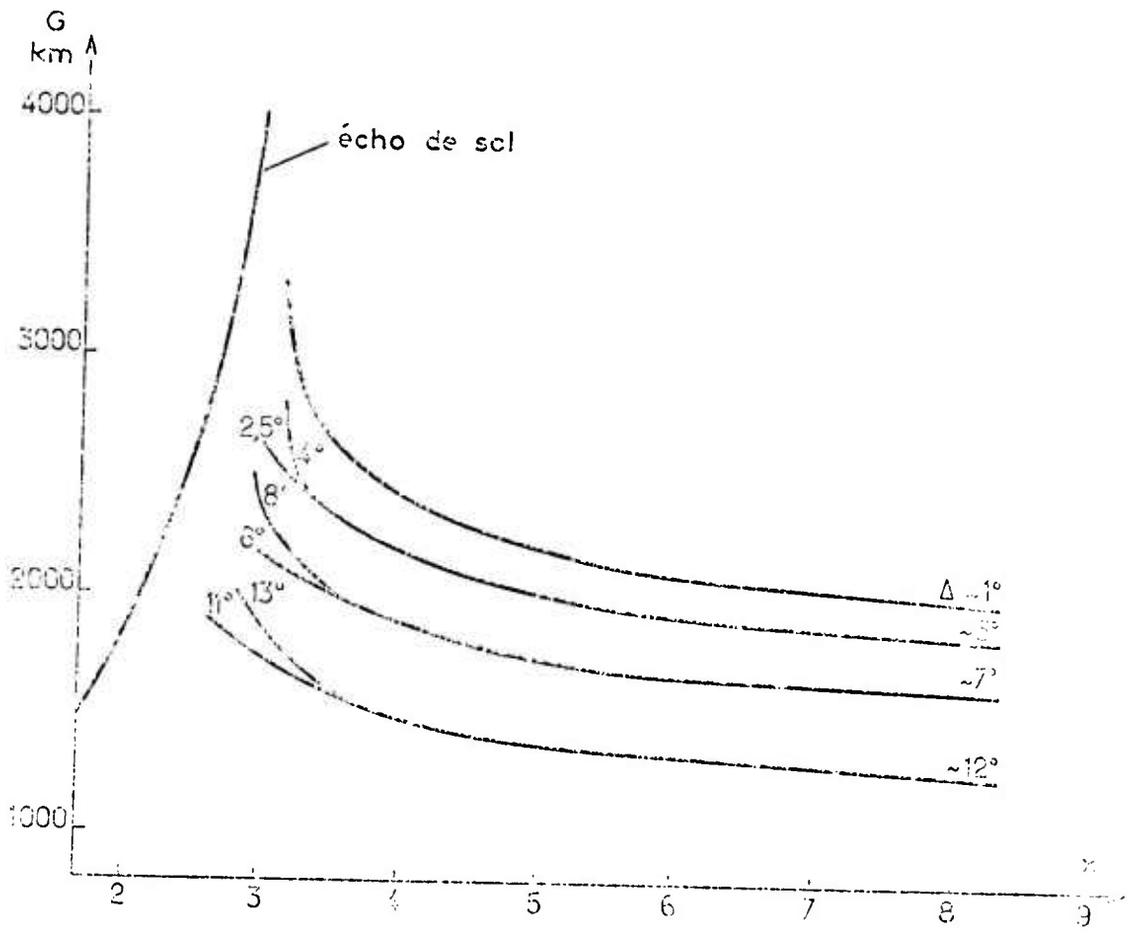

Fig. 7 - Régions de focalisations en ionosphère à profil parabolique (H_m = 390 km ; Y_m = 90 km) affectée d'une perturbation de 300 km de longueur d'onde et 75 % de modulation de densité électronique. Simulation des échos obtenus en balayages de fréquence à Valensole.

H.F. AURORAL BACKSCATTER AND THE SCINTILLATION BOUNDARY

Jules Aarons
Air Force Cambridge Research Laboratories
Bedford, Massachusetts 01730

SUMMARY

Recent studies of HF backscatter have noted the similarities between the boundary of the F-layer irregularity region as determined by scintillation observations and the position of the lower latitude of HF backscatter from field aligned irregularities. Suggestions as to this possibility were advanced earlier but were not studied experimentally; this is being attempted with observations taken between 1960 and 1965 by the Sagamore Hill Radio Observatory, Hamilton, Massachusetts. In this time period, a 19 MHz backscatter unit was operated along with a series of measurements of radio star scintillations (30 to 228 MHz) and satellite beacon recordings (20 to 136 MHz).

Between August 1964 and December 1965, a 50 MHz radar was added to the observing program. In a recent analysis of the dual frequency field aligned backscatter a separation into E and F-layer returns was made. It was found that VHF auroral returns (from E-layer heights) were accompanied 49% of the time by HF returns. The two factors suggested to be responsible for the absence of a 1:1 correlation were probably absorption at HF and variations in antenna launch angle for the two systems. HF auroral backscatter (E and F-layer heights) was accompanied only 11% of the time by VHF backscatter. During the 17 months of observation at low solar activity, the percentage of occurrence of 19 MHz field aligned scatter was 2%; of 50 MHz auroral scatter 0.5%.

The requirements for F-layer backscatter include (1) adequate electron density in the irregularities to support backscatter and (2) orthogonality. The second requirement can be met either through refraction or directly. Since the F-layer in the Sagamore Hill area is 8° to 12° off perpendicularity, maximum backscatter occurrence takes place only when the bending or focussing action of the F-layer can achieve percendicularity at F-layer heights. The refraction plus the change in latitude of the irregularity region accounts for the predominant post sunset occurrence of both the observations reported and those from Washington State University.

In a comparison of HF field aligned scatter and scintillations of Cass A at 1!3 MHz (with Cass A viewed near lower transit in the direction of magnetic north) 90% of the 21 cases of field aligned scatter were accompanied by deep fading. Deep fading, however, was not always accompanied by field aligned scatter since the latter requires orthogonality as well as the presence of irregularities.

The conclusion in the comparison is that the boundary of the irregularity region forms the lower latitude of the field aligned backscatter region. However, the focussing to reach orthogonality, an additional requirement for backscatter, is met only during certain hours.

1. INTRODUCTION

Recent studies of the high latitude irregularity region by means of the scintillations of HF and VHF signals from radio stars and from satellites has resulted in a model for the lower boundary during both quiet and disturbed magnetic conditions (Aarons and Allen, 1971). In situ measurements of the irregularities were made by Dyson (1969) and corroborated the general latitude regions where irregularities at F-layer heights are observed. Figure 1 maps both the quiet (K_{Fr} = 0,1) and the disturbed ($K_{Fr} \approx 4$) lower irregularity boundaries as shown by scintillation measurements.

The scintillation boundary appears to correlate very well with precipitation of ev electrons as measured by Maier and Rao (1970). They have found that the low latitude boundary lies at about 70° to 74° on the dayside and 55° to 60° on the nightside in measurements made in the winter of 1965-1966.

Backscatter observations at HF from Washington State University (Λ=54.4), AFCRL (Λ=57°) and Stanford (Λ=44°) have noted the similarities between scintillation observations and HF backscatter in position, diurnal pattern and behavior with magnetic conditions (Malik and Aarons, 1964, Ranz, 1965, Au and Hower, 1970). A recent hypothesis advanced by Bates (1971) is that the small scale irregularities within the irregularity region are field aligned; these are in turn the scatterers of HF which result in the backscatter trace named Slant F. According to Bates, phenomena causing Spread F always simultaneously set up small scale field aligned irregularities. He found the latitudinal variations of Slant F and the scintillation boundary in general agreement.

The aim of this paper is to explore this agreement in detail, using observational material recently reanalyzed.

In order for HF backscatter signals from irregularities to be observed at a fixed frequency in the HF portion of the radio spectrum, two criteria must be met:

a. Electron density in the irregularity sufficient to support measureable scattering.

b. Orthogonality either at E or F-layer heights; this may be met either directly or through refraction. Figure 2 illustrates simply some possible modes which may result in backscattered energy.

It might be noted that only the first criterion must be met to produce radio star or satellite scintillation. The irregularity electron densities for forward and backscatter differ with few examples of F-layer backscatter at UHF noted in the literature; however, satellite scintillations at 136 MHz have been recorded from middle to high latitudes.

2. HF BACKSCATTER AND SCINTILLATION STUDIES AT AFCRL

A continuous series of observations were conducted at the Plum Island site of the Sagamore Hill Radio Observatory between October 1960 and December 1965. A low powered 1 kw peak power radar was used with a yagi antenna continuously rotating at a rate of one revolution every 10 minutes. The observing frequency was 19.4 MHz. In August 1964 the 19 MHz equipment was joined by a 49.6 MHz radar operated jointly with ESSA (M. Gadsden). While some of the data has been reported (observations to 1963 by Malik and Aarons, 1964) the dual frequency observations and correlations with scintillations have not been described.

The site is situated at 56° invariant latitude (100 km) and 57° (350 km) the latter used as the nominal height for F-layer irregularity studies.

For the Boston area, Millman (1969) using theoretical and graphical methods, calculated propagation angles at various heights. Results, using the graphical method, are shown in Figure 3. The direction of magnetic north has an azimuth of 346.5°. While orthogonality in the graphical method is reached at 100 km at an elevation angle of 2° in the East and 10° in the West, 400 km orthogonality is not possible. At an elevation angle of 8° the propagation angle varies between 99° and 102° (theoretical and graphical methods).

Using an antenna with a beam angle wide in both vertical and horizontal planes, E and F-layer returns will show at different ranges. The range to the E-layer intersection (at 10° elevation in the West) is 477 km while that to the F-layer (at 8°) is 1430 km. In neither case are the effects of refraction taken into account. A ray tracing program by Au and Hower (1970) takes into account refraction. Their analysis for February 1964 for the AFCRL site indicates that more paths for meeting aspect sensitivity requirements are available at 1700 hours compared to those at 2000. At 2400 propagation was essentially straight line. The sunset period, therefore, affords greater focussing possibilities and more paths than the time period around midnight.

2.1 19 MHz Results

Using the data collected at Plum Island a new analysis has been started. The results can be summarized with the aid of Figures 4a and 4b:

a. Auroral backscatter at ranges from 7 milliseconds and greater (presumably F-layer returns) maximizes in the sunset time period at low local K indicates (Figure 4a) but somewhat earlier when the K index increases.

b. The diurnal pattern of close-in auroral backscatter, predominantly E-layer has a broader maximum peaking at 2000 at low K indices (K_{Fr} = 0,1 and K_{Fr} = 2,3). At high indices a double peak is observed, one at 1700-1800 and the second at 0100-0200.

c. Over 5% of the time auroral clutter is observed with this low powered single frequency system.

d. Azimuths of backscatter auroral returns are centered in the magnetic north. However, the daily means varied within plus and minus 20° of this direction.

e. Figure 5 indicates the ranges of auroral backscatter during the hour of maximum occurrence during each month. If 8.6 milliseconds is taken as the mean value, the range to the field aligned irregularities is 1300 km, corresponding at 8° elevation to a latitude displacement of 7.4°.

2.2 Comparison of 19 and 50 MHz Auroral Backscatter

Between August 1964 and December 1965 simultaneous observations of auroral backscatter on 19 and 50 MHz were available with a high degree of reliability. If only the E-layer irregularities are involved, it was expected that whenever backscatter was noted at 50 MHz then 19 MHz backscatter should have been observed. This turned out to be true 49% of the time. 26% of the 50 MHz aurora had durations longer than 15 minutes (16 cases) with no accompanying 19 MHz signals. The absence of perfect simultaneity may be due to three possibilities:

a. Absorption affecting the lower frequency signal. The cases of no return at 19 MHz with scatter at 50 MHz tend to cluster in the midnight to morning period when auroral absorption is maximum.

b. Differences in antenna patterns of the two systems.

c. Refraction of the 19 MHz signals. This appears to be unlikely except perhaps for sporadic E effects.

Although 49% of the 50 MHz scatter periods had accompanying 19 MHz scatter, only 11% of the 19 MHz scatter periods showed 50 MHz returns. The total time of occurrence of 19 MHz backscatter was 2% for the 17 month period; for 50 MHz the percentage of occurrence was .5.

The percentage of occurrence of 19 MHz (all ranges) and 50 MHz scatter is plotted in Figure 6. 19 MHz occurrence peaks between 1830 and 2130; 50 MHz occurrence peaks between 1700 and 2100 with a secondary peak between 2300 and 0230.

Several points of minor interest might be noted relative to the comparison:

a.	Auroral duration longer at 19 MHz	17 cases
b.	Auroral duration the same at both frequencies	21 cases
c.	Auroral duration longer at 50 MHz	6 cases
d.	50 MHz returns (duration longer than 15 minutes); no 19 MHz returns	16 cases
e.	50 MHz returns (duration shorter than 15 minutes); no 19 MHz returns	12 cases

3. OPTICAL AND RADIO OBSERVATIONS OF THE AURORA OF FEBRUARY 7, 1965

An effort was made to observe the simultaneity of events in the D, E, and F-layers by radio and optical means during an aurora. This includes the 19 and 50 MHz radars mentioned earlier and optical and radio equipment located near the intersection (from Plum Island) of the D and E-layers of the radar equipment. At the 100 km intersection of the 19 and 50 MHz radars, Baie St. Paul, photometers and riometers were operated by ESSA. The site at 47.4°N and 70.5°W was located at an Λ of 61° (100 km). Photometers at 3914Å (the N_2 + band), 5577Å (the green neutral atomic oxygen line), and 6300Å (the red neutral atomic oxygen line) were run for two weeks each month. We shall describe one series of measurements for the aurora of February 7, 1965.

Starting at 0305 UT (2205 EST) on February 7, 1965, some faint traces of scattering were noted at 50 MHz. At the same time the optical emission at 3914Å and 5577Å increased. No absorption was noted and no returns at 19 MHz were seen

As shown in Figure 7a, the peak optical emission was recorded at Baie St. Paul at 0600 simultaneously with onset of overhead auroral absorption. 19 MHz auroral backscatter started at 0605 and reached its shortest range (farthest point south) at 0635 to 0705. Intensive 50 MHz returns were noted from 0610 to 0715 (Figure 7b). Absorption to the south also peaked in this time period.

Thus the ionization producing the backscatter and that producing cosmic noise absorption occurred simultaneously. The absorption did not eliminate HF backscatter.

The optical emission appeared earlier than either the absorption or the radar scattering. Taking arbitrary limits of 7kR for the 3914Å emission, the peak appears from 0540 to 0705. All three types of observations (emission, radar scattering, and absorption) show a double peak. Auroral peaks (shown in detail in Figure 7) appeared simultaneously with absorption peaks.

The data from a single aurora is, of course, limited. The details in time are correlated only if one has sizeable time blocks. Yet the peak of all events occurred in the period from 0540 to 0735. This includes the E-layer absorption as shown in the riometer results, the E-layer radar scattering at 19 and 50 MHz, and the optical data. The general correlation of the optical data in itself is an indication of the simultaneity of events since the 3914Å and the 5577Å emissions are thought to originate at E-layer heights and the 6300Å emission at F-layer heights.

If one ascribes the higher altitude phenomena to low energy electrons (Hartz and Brice, 1967) and the lower altitude absorption and electron density irregularities to higher energy particles then it appears that during this event an increased precipitation of both high and low energy particles took place during one period of time.

4. MAGNETIC STORM OF MARCH 5-6, 1961

A rather clear example of the simultaneity of backscatter HF observations and scintillations is illustrated in a study of the magnetic storm of March 5-6, 1961. March 3 and 4 were two of the five quiet days of March 1961. March 5 was quiet until the sudden commencement of a magnetic storm (1600 EST).

Almost precisely at this time auroral reflections were noted on the 19 MHz backscatter equipment. Figure 8a shows the reduced auroral and backscatter data for March 2-7. On March 2 and March 4, the quiet day F-layer sunset backscatter can be seen. It might be noted that the range on March 2, for example, decreased from 1700 to 1900 which is interpreted as an equatorward movement of the irregularity region. On March 5, the first returns were from F-layer ranges but the range decreased at about 1630. Backscatter is observed to 0530 on March 6. On March 6, normal ground backscatter fails to appear until about 1030 EST, probably because of decreased electron density in the F-layer following a magnetic storm.

Riometer measurements (Figure 8b) indicate that the absence of returns on March 6 until 1030 was not due to absorption since maximum absorption as noted on a Polaris directed 30 MHz riometer peaked between 2200 and 2400.

Scintillation index at 109 MHz increased during the magnetic storms relative to the quiet day observations (Figure 8c). Scintillations increased at about the time of the start of the magnetic storm and continued at a high level until 0600 EST on March 6 approximately the same time the backscatter disappeared.

The correlations of HF backscatter and scintillations during this storm are obvious but the statistical questions to be answered are those involved with quiet day backscatter and scintillation as well as with storms occurring at other local times.

5. COMPARISON OF LOWER TRANSIT OBSERVATIONS OF CASSIOPEIA A AND 19 MHz BACKSCATTER

During the period from June 1963 to June 1964 the 150-ft parabola of the Sagamore Hill Radio Observatory recorded amplitude fluctuations of the signals from Cass A near lower transit position. The angle of elevation of the source was 13^{o}, the azimuth was 347.5^{o} (magnetic north). The invariant latitude of the 350 km intersection point was 67^{o}. The range to the 350 km point was 1100 km. The range to the point of lowest propagation angle possible at 400 km was approximately 300 km farther north (an elevation angle of 8^{o}), than the range to the Cass A intersection.

Radio star observations were made at 30, 63, 113 and 228 MHz. Scintillation indices ($\Delta P/P$, Whitney et al, 1969) at 113 MHz were used. This frequency avoided saturation (deep fading) effects frequently found at the lower frequencies in radio star observations and the very low excursions frequently found in the 228 MHz records. The diurnal patterns at quiet and disturbed conditions are shown in Figure 9.

For comparing backscatter observations and scintillations, indices were divided into two categories, indices over 20 and those less than 20, the former to indicate moderate to high activity, the latter low scintillation excursions.

Between February 1, 1964, and April 30, 1964, drifts were recorded at times ranging from 0100 (February 1) to 1900 (April 30) local standard time. Of 33 days with low scintillation indices, 61% had no auroral backscatter observed on the same day (1400 to 0200). Of 42 days of high scintillation index, 67% had backscatter observed on the same day. However, 55% of the days surveyed had backscatter during the 1400-0200 time period, a large percentage of occurrence. The data used was confined to February-April because during the fall and winter there are large differences in time of occurrence of backscatter and the lower transit appearance of Cass A or because of the presence of sporadic E (late spring and summer).

For backscatter observations the irregularities must exist at the proper intensity ($\Delta N/N$) and fulfill orthogonality requirements. Scintillations, however, can occur without orthogonality. A more rigorous question could be asked, "If auroral backscatter is present on the records, are the scintillation indices high?" Taking scintillation records within plus and minus one hour of backscatter observations, in 19 cases the answer was positive and in only two cases was backscatter not accompanied by deep fading.

6. ABSORPTION

It is difficult to assess the role of auroral absorption in blanking out the return on low powered radar equipment. In the examples given in Figure 7 and 8 relatively high auroral absorption did not blank out the returns. It is believed that the role of the F-layer refraction is more important in not effecting orthogonality and thus "blanking" out auroral F-layer backscatter.

7. DISCUSSION

The hypothesis to be examined involves the identification of the irregularity region and its low latitude boundary as the ionospheric region producing Slant F or HF auroral backscatter at F-layer heights. The diurnal pattern of the two phenomena and the presence of the irregularity region as determined by both scintillations and auroral backscatter on magnetically quiet days leads to the probable identity of F-layer irregularities as the scattering centers for both of these phenomena.

Bates (1971) found a nearly one to one correspondence between the occurrence of vertical Spread F and oblique Slant F at College, Alaska.

It is of interest to compare data from Washington State University and AFCRL as Au and Hower (1970) have done. Both groups noted peak occurrence of auroral backscatter around sunset. Stanford returns peaked near midnight in March 1964 but at the peak of the sunspot cycle in 1958 peaked at sunset.

Our hypothesis to account for the sunset maximum at WSU and AFCRL particularly during quiet periods is that the irregularity region reached a fairly low value at this time. This factor combined with the refraction at sunset was sufficient to produce orthogonality. In 1958 with a probable lower latitude position of the irregularity region (the effect of high sunspot number) and greater refraction, Stanford noted peaks near sunset. However during periods of low sunspot number (1964) only the lowest equatorward placement of the irregularity boundary (midnight) could show scattering.

It should be noted that during conditions of higher electron density within the irregularities (magnetic storms) off-orthogonal returns can be noted. It is estimated that 8-10 dB per degree off-orthogonality is the loss in the scattered signal. During storm conditions the effective scattering area might be increased and scattering supported off-orthogonality. This, therefore, is the explanation for F-layer returns in the midnight time period, even though the signal experiences only straight line propagation.

Thus, if one takes into consideration various differences in the mechanisms of HF backscatter and scintillation observations it is possible to find in the F-layer field aligned irregularities and its oval diurnal pattern one source of HF backscatter and the sole source of scintillations.

The data is far from definitive. Multistation scintillation observations of a synchronous satellite (along a magnetic line intersecting orthogonality at varying F-layer heights) coupled with a backscatter system might better perform the correlation study.

8. ACKNOWLEDGEMENTS

The author would like to thank C. Malik and R. C. Hoar for making the observations and Mrs. M. Villers for her assistance in the data reduction.

9. REFERENCES

Aarons, J., J.P. Mullen, and S. Basu (1963) Geomagnetic control of satellite scintillation, J. Geophys. Res., 68, 3159-3168.

Aarons, J. and R.S. Allen (1971) Scintillation boundary during quiet and disturbed magnet c conditions, J. Geophys. Res., 76, 170-177.

Au, W.W.L. and G.L. Hower (1970) Multi-station observations of long range backscatter from field aligned irregularities in the F layer, J. Atmos. Terr. Phys., 32, 1577-1589.

Bates, H.F. (1971) The aspect sensitivity of spread-F irregularities, J. Atmos. Terr. Phys., 33, 111-115.

Dyson, P.L. (1969) Direct measurements of the size and amplitude of irregularities in the topside ionosphere, J. Geophys. Res., 74, 6291-6303.

Maier, E.J. and B.C.N. Rao (1970) Observations of the suprathermal electron flux and the electron temperature at high latitudes, J. Geophys. Res., 75, 7168-7174.

Malik, C. and J. Aarons (1964) A study of auroral echoes at 19.4 megacycles per second, J. Geophys. Res., 69, 2731-2736.

Ranz, D.M. (1965) A study of field aligned irregularities from three observation points, Research Report, NSF Grant GP-2701, Washington State University, Pullman, Washington, 16-90.

Whitney, H.E., J. Aarons and C. Malik (1969) A proposed index for measuring ionospheric scintillations, Planet. Space Sci., 17, 1069-1073.

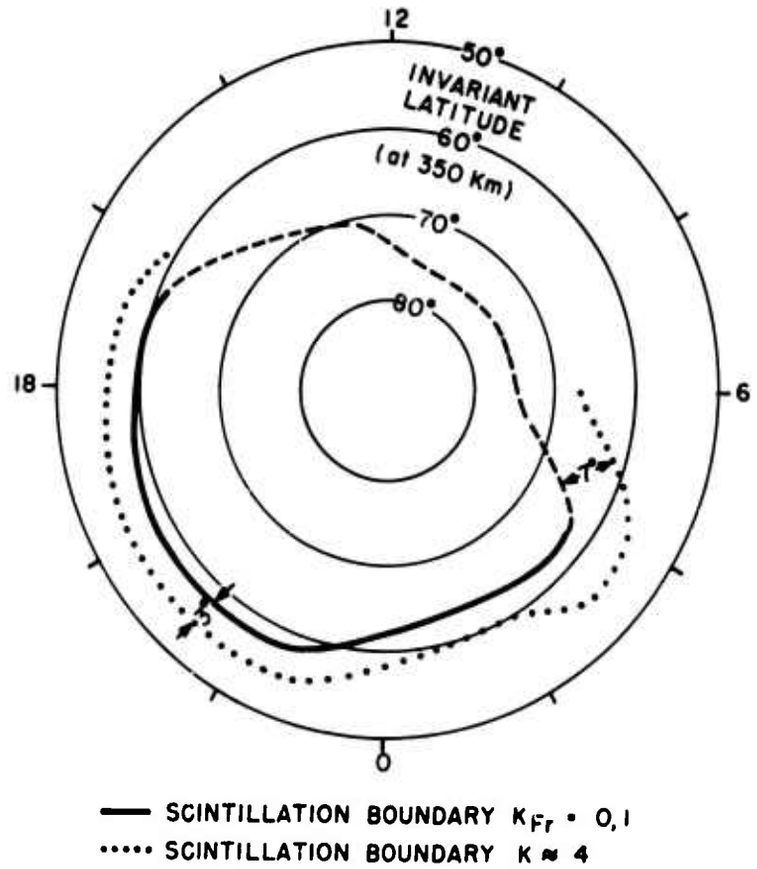

Figure 1 Scintillation Boundries

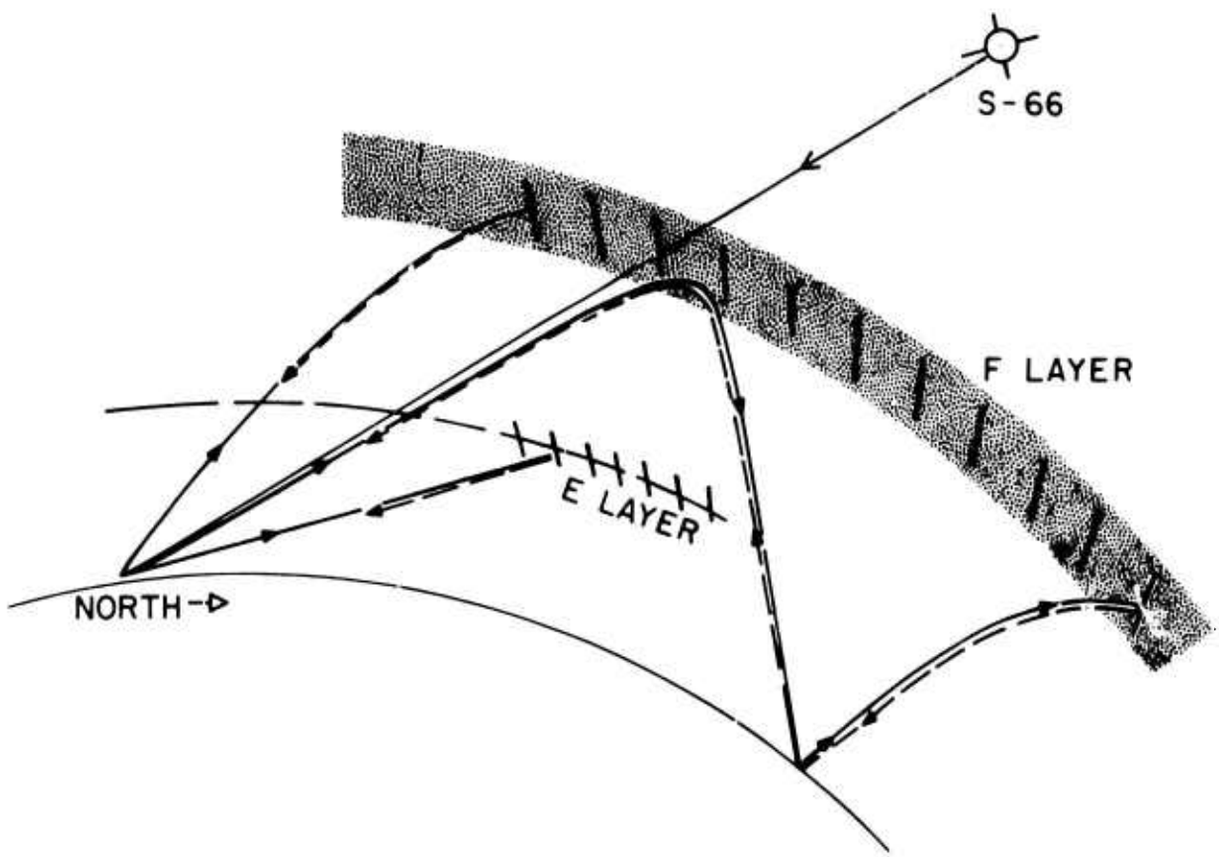

Figure 2 Northern irregularity sensing using Cass A scintillations and auroral backscatter by direct scatter from E layer and refracted ray scatter from F layer.

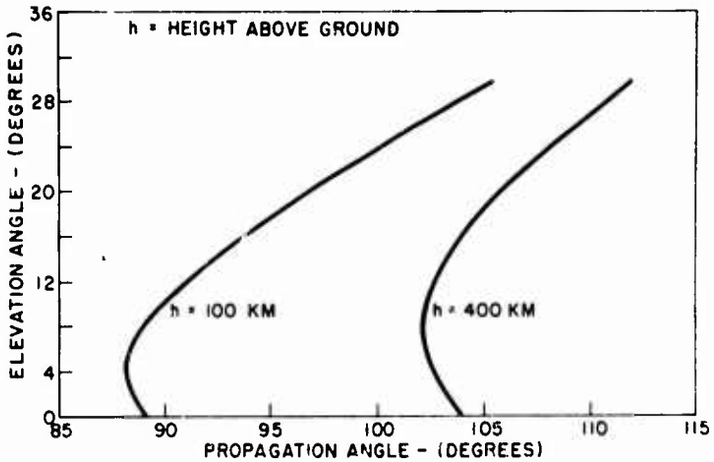

Figure 3 Propagation angle as viewed from Boston along the direction of magnetic North (A = -13.5°) (Graphical method of Millman, 1969).

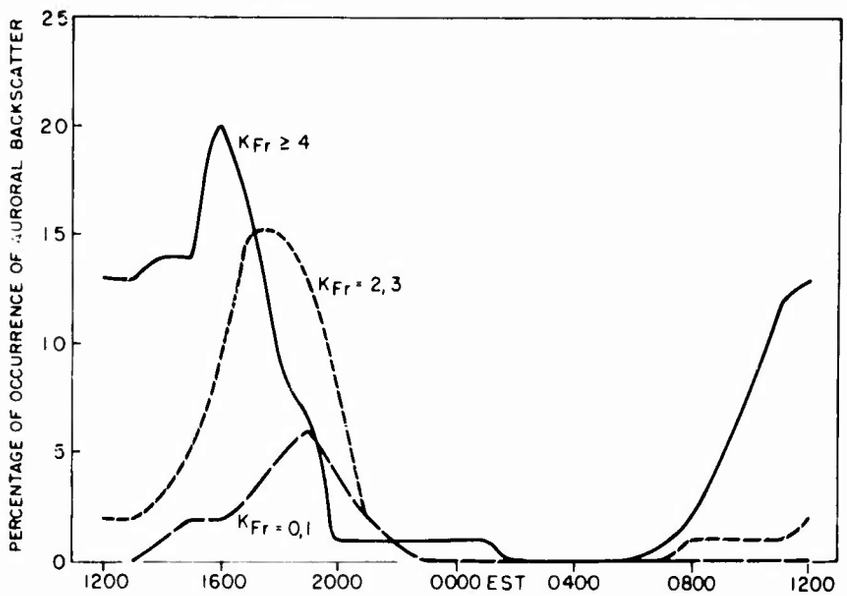

Figure 4a Observations of auroral backscatter, 1960-1965, for ≥8 millisecond range (F layer).

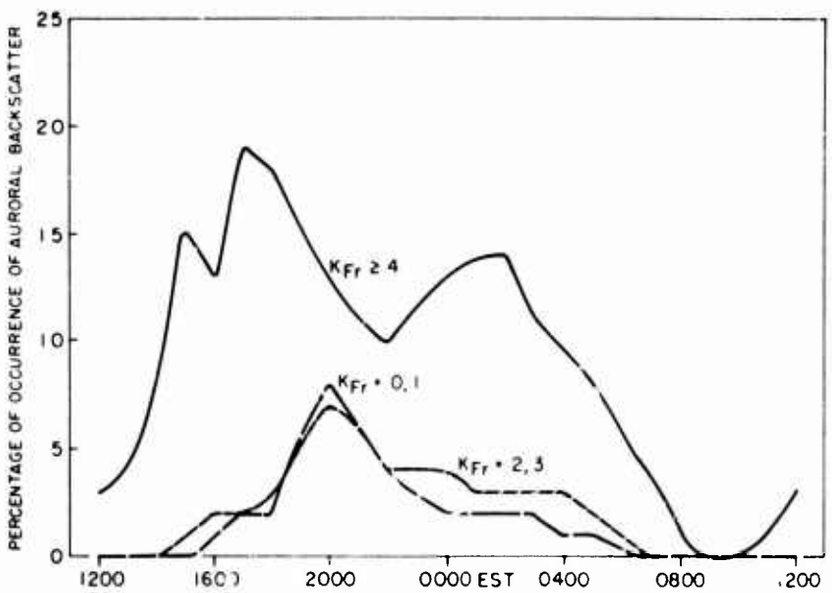

Figure 4b Observations of auroral backscatter at short ranges (5-7 milliseconds). These are presumed to be E layer observations.

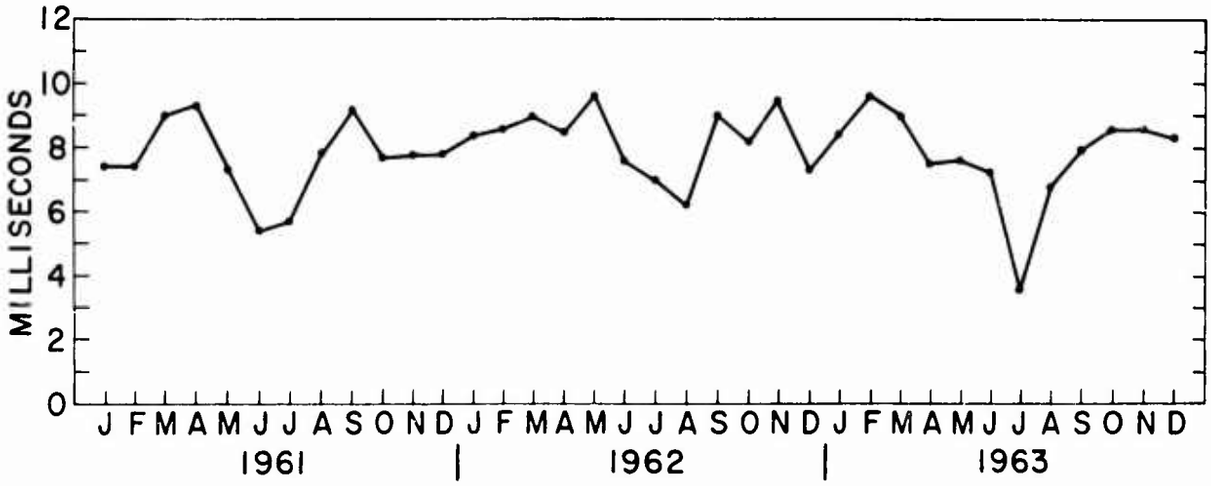

Figure 5 Monthly average of the range of aurora during the hour of maximum occurrence.

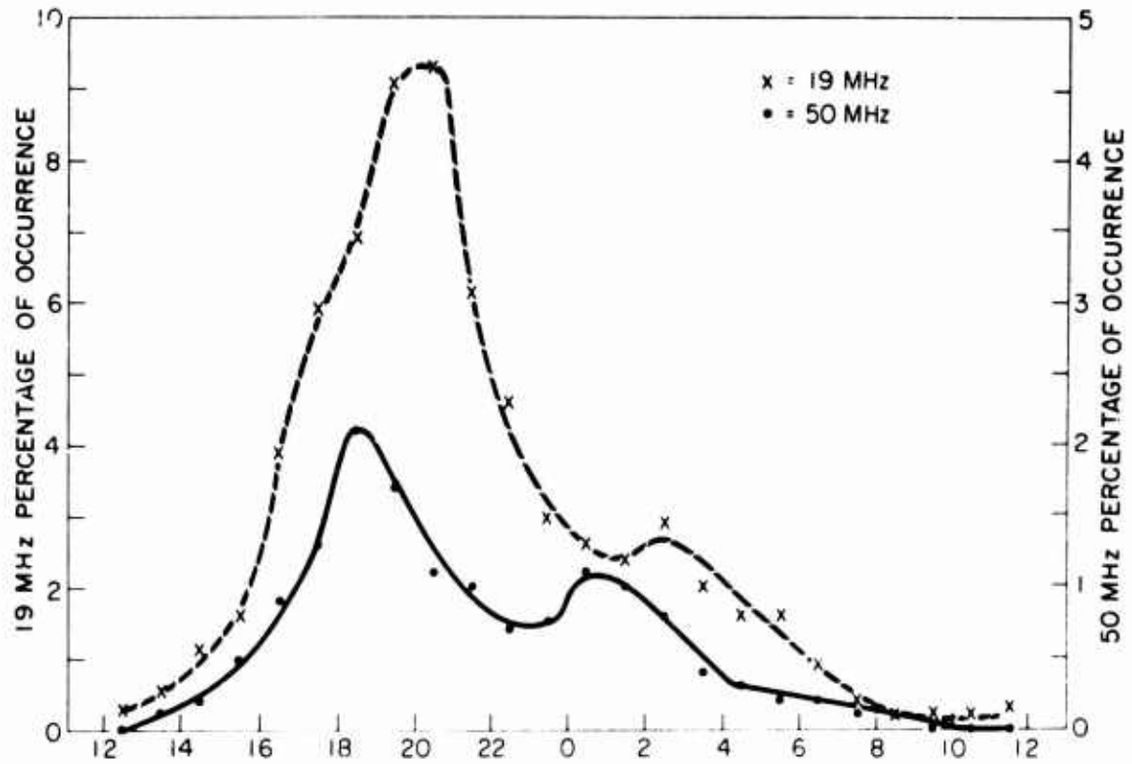

Figure 6 Percentage of occurrence in each hour of auroral returns for the period 10 Aug 64 - 10 Dec 65.

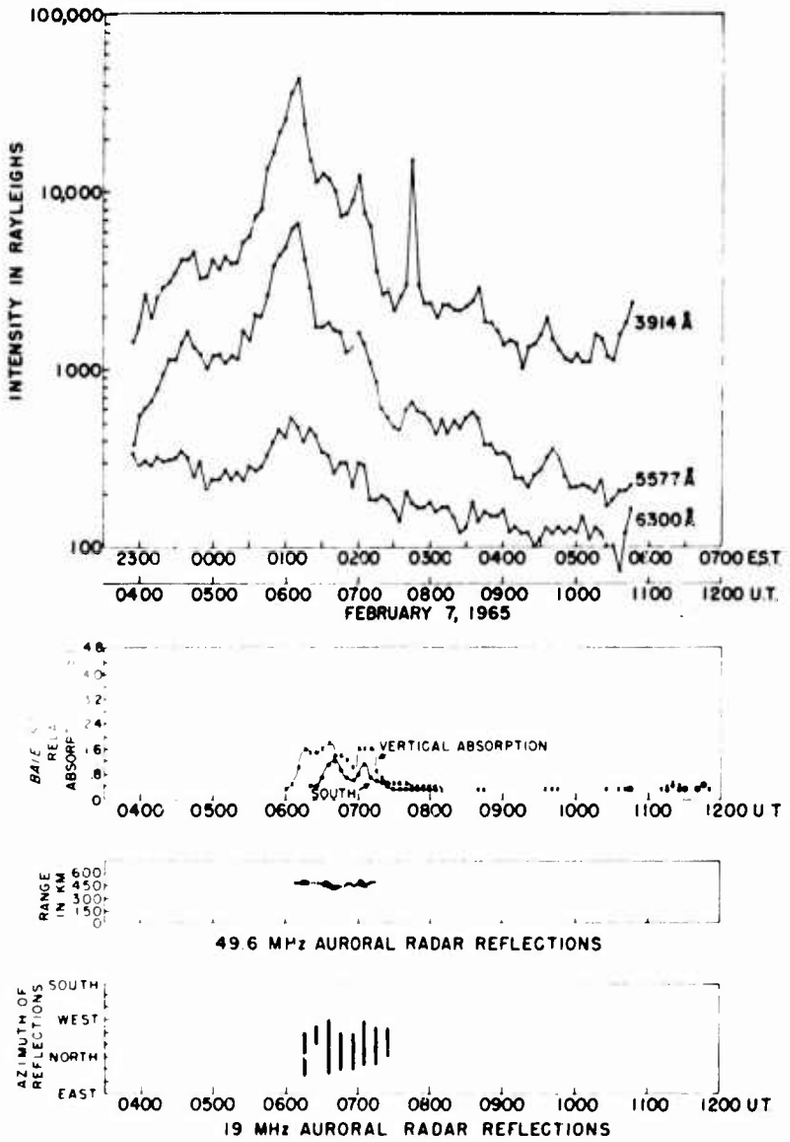

Figure 7a Time sequences of optical and radio events.

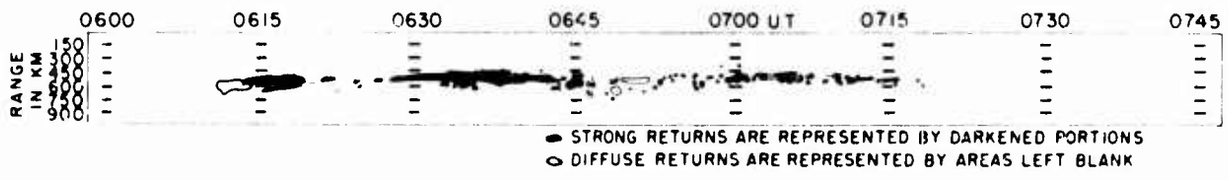

Figure 7b Details of the 49.620 MHz auroral radar returns: Feb 7, 1965.

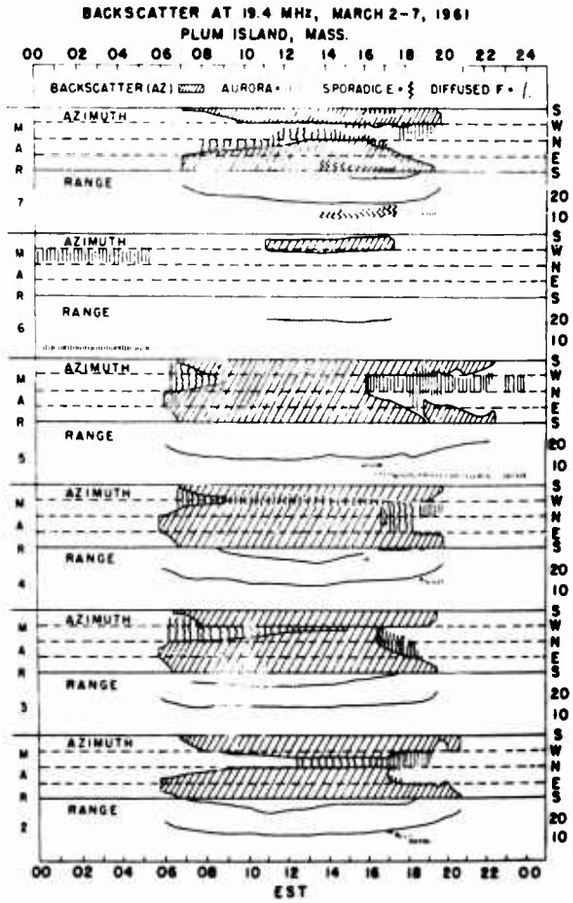

Figure 8a Auroral reflections and backscatter from the Plum Island 19.4 Mcps radar. Vertical lines appearing in NE and NW quadrants indicate auroral reflections at the local time on the horizontal scale. Slant lines (///) indicate backscatter returns. Range in milliseconds is indicated below backscatter returns with 5 to 10 ms indicating auroral heights.

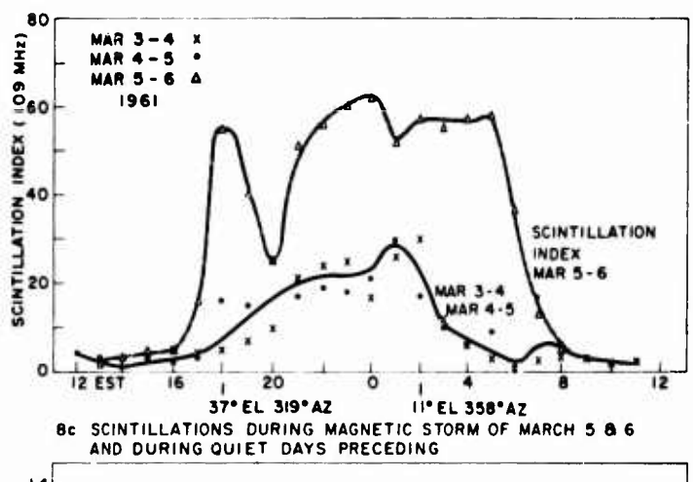

8c SCINTILLATIONS DURING MAGNETIC STORM OF MARCH 5 & 6 AND DURING QUIET DAYS PRECEDING

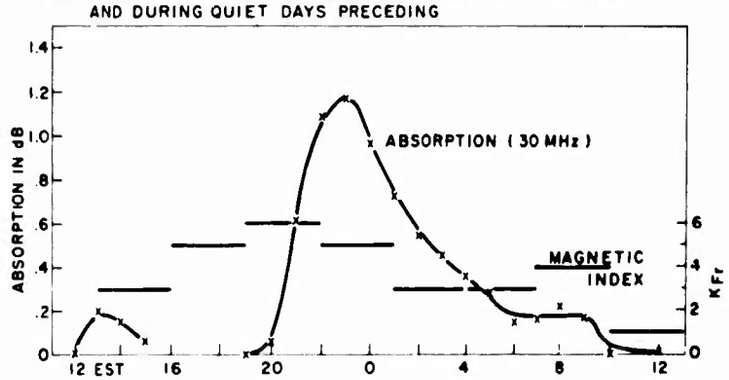

Figure 8b Absorption measured during storm of March 5-6, 1961. 30 MHz riometer was pointed at Polaris (elevation angle 43°) magnetic index is also plotted.

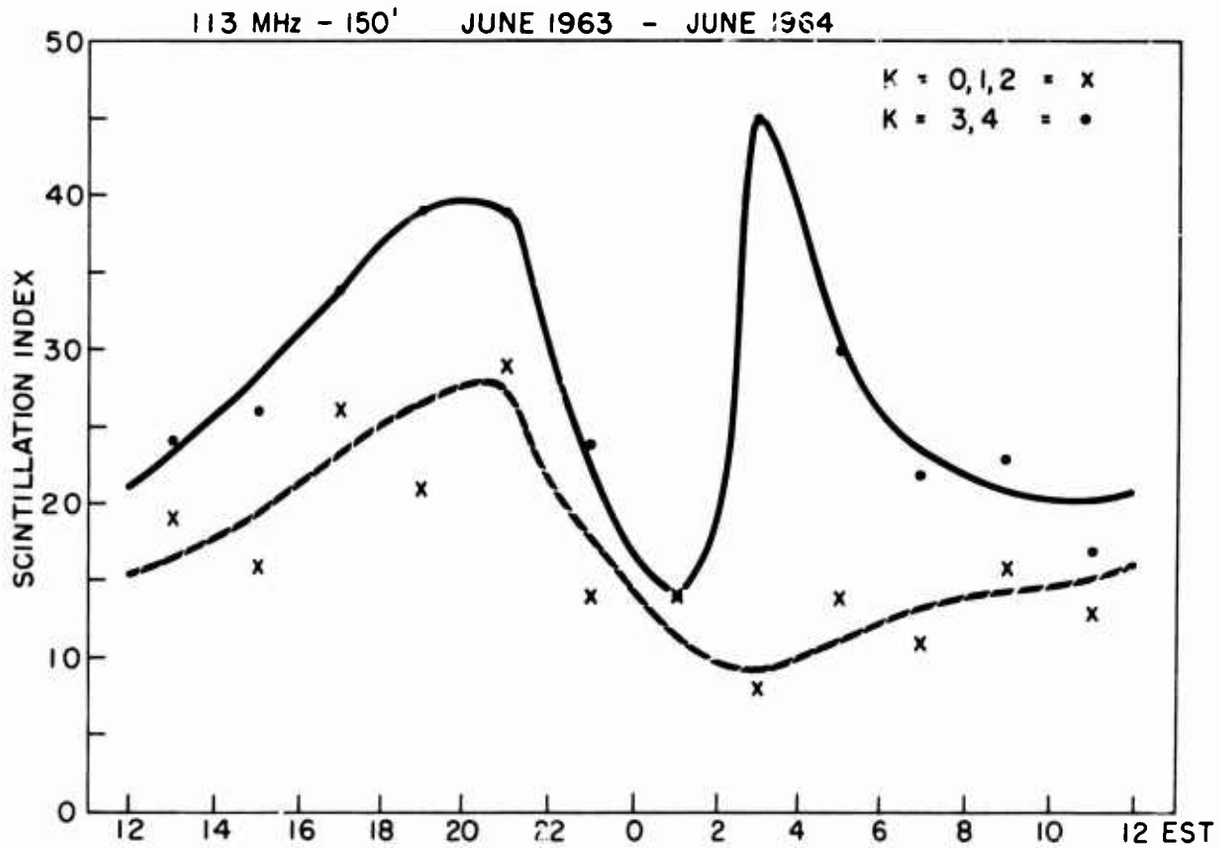

Figure 9 Scintillation indices for Cass A observations at Sagamore Hill near lower transit. Data was taken on the 150' parabola at 113 MHz between June 1963 and June 1964.

FM/CW HF BACKSCATTER OBSERVATIONS OF RADIO AURORA

A. H. Katz
AVCO SYSTEMS DIVISION
Wilmington, Massachusetts 01887
U. S. A.

SUMMARY

Observations of HF backscatter from radio aurora using an FM/CW radar located at field sites near Rome, N. Y. (43.2°N, 75.5°W) are discussed. Both wideband (at 6.5-30 MHz, 3 kW average power) and narrowband (fixed frequency soundings at 20 kW average power) backscatter measurements have been made. The wideband soundings determine the modes of propagation, frequency extents, and time delays of the backscattered energy. The high resolution (~10 μs) narrowband soundings indicate the movements that occur in the radio auroral regions. Examples of these motions are presented, showing events that last for 5 minutes, exhibiting range changes which imply apparent velocities near or above the speed of sound at F-region heights. In addition, the wideband backscatter measurements have been processed in a form which allows the absolute signal level of the backscattered energy to be determined. This, together with a knowledge of the other system parameters and the radar range equation, permits an estimation of the radar cross section of radio aurora at HF.

1. INTRODUCTION

This paper describes results of a FM/CW HF monostatic backscatter from radio aurora at sites located near Rome, N. Y. (43.2°N, 75.5°W). Wideband FM/CW ionograms (6.5-30 MHz) at 3 kW average power show the modes of propagation and frequency extent of backscatter from radio aurora. Narrowband FM/CW backscatter at 20 kW average power show the temporal changes that occur in the auroral irregularities as identified by the wideband backscatter ionograms. The location of the RADC sites near Rome, N. Y. are shown in Figure 1. Also shown is the location of the auroral oval (Akasofu, 1967) at 02 UT and 06 UT.

2. WIDEBAND FM/CW BACKSCATTER

Selected examples of wideband FM/CW HF backscatter from high latitude irregularities are described. The identification of the modes of propagation follow the outline described by Bates (1968). The frequency range of the backscatter sounder was 6.5-30 MHz at 250 kHz/s sweep rate and 3 kW average power. The wideband sounding was processed to an effected pulse width of 40 μs. The transmitting antenna is a 6-60 MHz log-periodic oriented at 0°N. The receiving antenna is a circularly disposed antenna array (4-11 MHz) oriented at 0°N.

Figure 2 shows an example of ground backscatter to the north of the RADC field sites at 2230 UT on 5 May 1970. Included with each backscatter sample is a schematic representation of the backscatter. The 1Fv, 2Fv, and 3Fv are traces of the vertical ionogram and its multiples. The ground backscatter trace is easily identified because it is found to extend out from the 2Fv vertical trace. The next example is at 0511 UT, 5 May 1970 (Figure 3). In this case, direct F (DF), slant F (SF), one F slant F (1FSF), and two-hop ground backscatter (2FGS) returns are observed. Figure 4 shows a schematic representation of the modes of propagation identified in Figure 3 and 5. (T,R is the location of the transmitter-receiver.)

The last example of wideband FM/CW backscatter is at 1151 UT on 5 May 1970 (Figure 5). 1FGS and direct E (DE), as well as a slant E (SE), return are identified. These examples demonstrate the observation and identification of the various modes of propagation and their frequency extent observed with wideband HF backscatter from radio aurora.

3. NARROWBAND FM/CW BACKSCATTER

The wideband ionograms determine the frequency extent, time delay and mode of propagation of the backscatter from radio aurora. The wideband soundings are not able to determine the movements that are known to occur in the auroral region. Narrowband FM/CW backscatter have been used to investigate the temporal changes. The transmitter is swept over a 100 kHz bandwidth at a sweep rate of 1 MHz/s (effectively 10 PRF). Twenty (20) kW of average power is used for the narrowband soundings. The narrowband frequencies are selected on the basis of the wideband soundings. At 1 MHz/s the time delay window is 5 ms which with the 500-line spectrum analyzer implies a 10 μs range resolution. Figure 6 shows wideband ionograms at 0217 UT and 0308 UT on 7 August 1970. The sweep rate is 250 kHz/s with the soundings covering 6.5-28 MHz at 3 kW average power. From the wideband soundings we find that the frequency range and time delay of the backscattered energy is relatively stable between 0200-0300 UT. The narrowband data recorded in the time interval between these two ionograms was at 10.5 MHz (1 MHz/s, 10 PRF, 20 kW). The narrowband observations are limited to a 5 ms time delay window and this was placed between 8 and 13 ms.

Figure 7 shows two five-minute segments of the 10.5 MHz observation (from 0250-0255 UT and 0255-0300 UT). The horizontal markers represent 0.5 ms of time delay compared to the 2 ms time delay marker for the wideband soundings. The narrowband data show individual events which last from up to 3-4 minutes and are about 0.1 ms in width. One event of interest is a linearly decreasing time delay event between 0250-0255 UT (10 ms at 0250 UT to 8.5 ms at 0255 UT). Changes in time delay can be attributed to both velocity and acceleration components. Since the observed signal is a linear change in time delay, a simple approximation might be that the change is solely due to a constant velocity. If this were the case, a minimum velocity of -0.66 km/s and a frequency shift of -46 Hz at 10.5 MHz would be obtained. The speed of sound at a height of 200 km is 0.55 km/s. Further examples of this type of signal which illustrates the motions of radio aurora are found in the data.

4. CROSS SECTION OF RADIO AURORA AT HF

A wideband auroral backscatter ionogram at 0515 UT on 2 March 1971 is shown in Figure 8. Included is a schematic representation of the modal structure. A calibrated reference level at -70 dbm is included in the recording of this data. The ionogram in Figure 8 was processed using RADC's DRP (Digital Radar Processor). The analysis process is illustrated in Figure 9. Figure 9a shows a backscatter signal and its relation to the noise floor and a reference signal. The DRP then sets a minimum threshold level and prints out signal levels at this minimum threshold level and at 4 levels above this (a total of 5 levels can be utilized). For example, if the threshold level was 53 db above the noise floor and levels of 55, 57, 59 and 61 db above the threshold level was printed, the given signal would be divided into blocks as illustrated in Figure 9b. The higher amplitude signals would be indicated by a brighter picture on the Cathode Ray Tube of the DRP. The ionogram is replayed through the DRP with successively higher minimum thresholds like 55, 57 db and so forth. This is done until the reference signal disappears as is illustrated in Figure 9c and the backscatter signals can now be referenced to a known level. The level at which the signal disappears is the maximum signal level in db of the backscattered energy above or below the reference level (Figure 9d). Figure 10 shows this process applied to the ionogram in Figure 8. The threshold levels shown are at 53, 57, 61, and 65 db with 4 levels in 2 db steps printed above each threshold level. The maximum signal disappears at 67 db or about 6 db above the reference level. The maximum signal level of the backscatter is -64 dbm or -94 dbw and an estimate of the cross section can now be made.

Transforming the radar equation into its db equivalent form we obtain:

$$(S)_{db} = (P_T)_{db} + (G_T)_{db} + (G_R)_{db} + (\sigma)_{dbsm} + 2(\lambda)_{dbm} - 4(R)_{dbm} - 33 \text{ db}$$

The -33 db is obtained from the $(4\pi)^3$ term. To obtain the value of each quantity in db, we use db = 10 log (quantity). The wavelength (λ) is given in meters, the distance (R) in meters and the cross section (σ) is calculated as dbsm (db per square meter).

If λ = 30 m (10 MHz), R = 1200 km, G_T = 7 db (gain of log periodic antenna), G_R = 10 db (gain of CDAA), P_T (transmitted power) = 3 kW (35 db), we find that the maximum cross section is σ dbsm = 102 dbsm or approximately 10^{10} sqm. The number presented in this paper is tentative but the discussion is meant to be illustrative of the technique which can be used and gives a relative indication of the cross section of radio aurora.

Acknowledgment: This work was sponsored by the Rome Air Development Center, Griffiss AFB, New York; under Contract No. F30602-70-C-0086.

REFERENCES

1. Akasofu, S. I., Auroral Substorm and Magnetospheric Substorm, Space Research VIII, Cospar ed. Mitra, Jocchia, and Newman, North Holland Publishers (1967), p. 213.

2. Bates, Howard F., Computed HF Auroral Backscatter Traces for Various Distances, Scientific Report, February, 1966, Geophysical Institute of the University of Alaska.

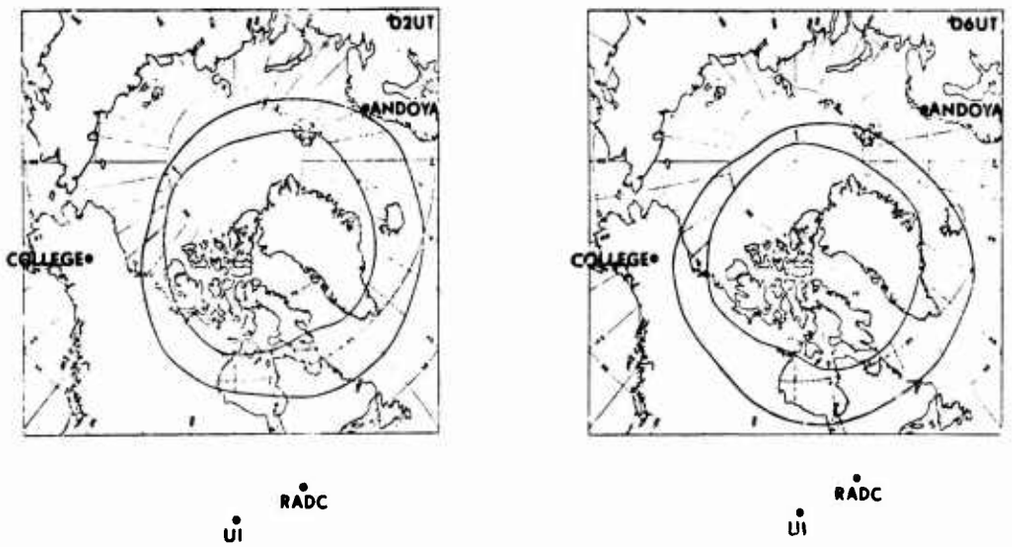

Figure 1. The approximate location of the auroral oval at 02 and 06 UT. The location of RADC is indicated.

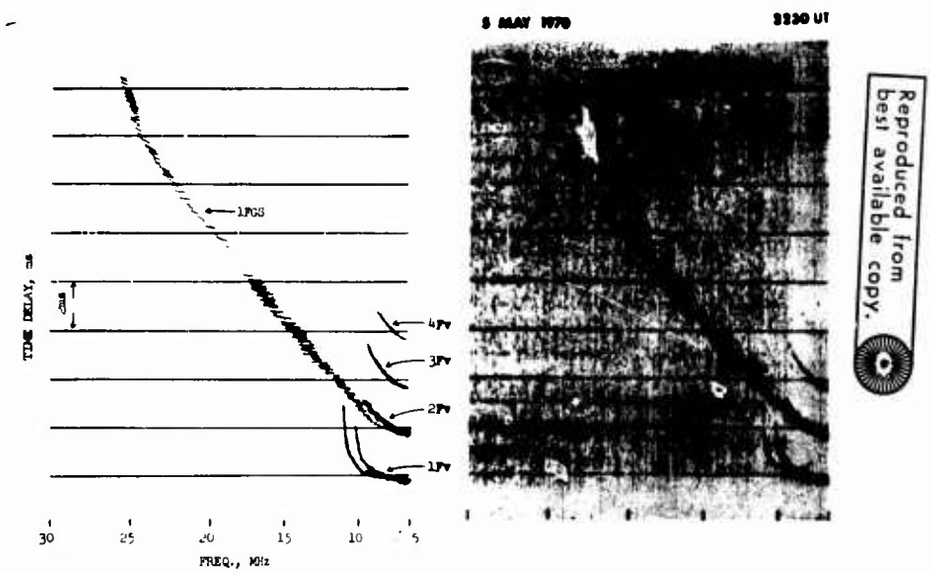

Figure 2. Example of Ground Backscatter to the North of the RADC field sites at 2230 UT on 5 May 1970.

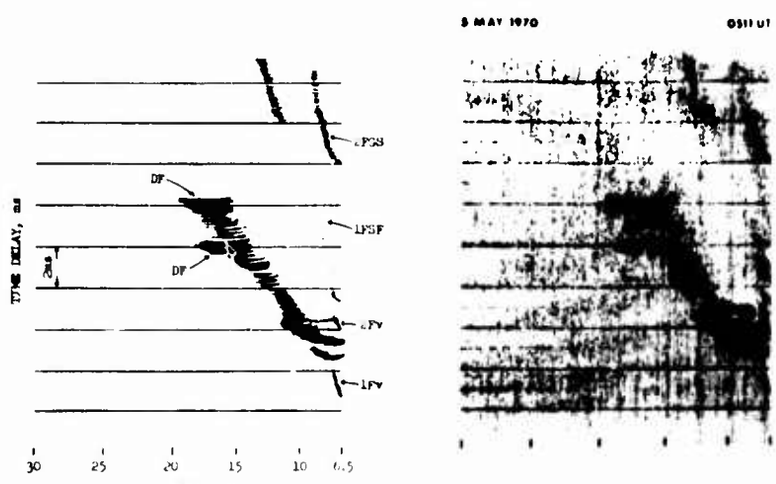

Figure 3. Example of Radio Aurora Backscatter (including schematic representation of propagation modes) at 0511 UT on 5 May 1970.

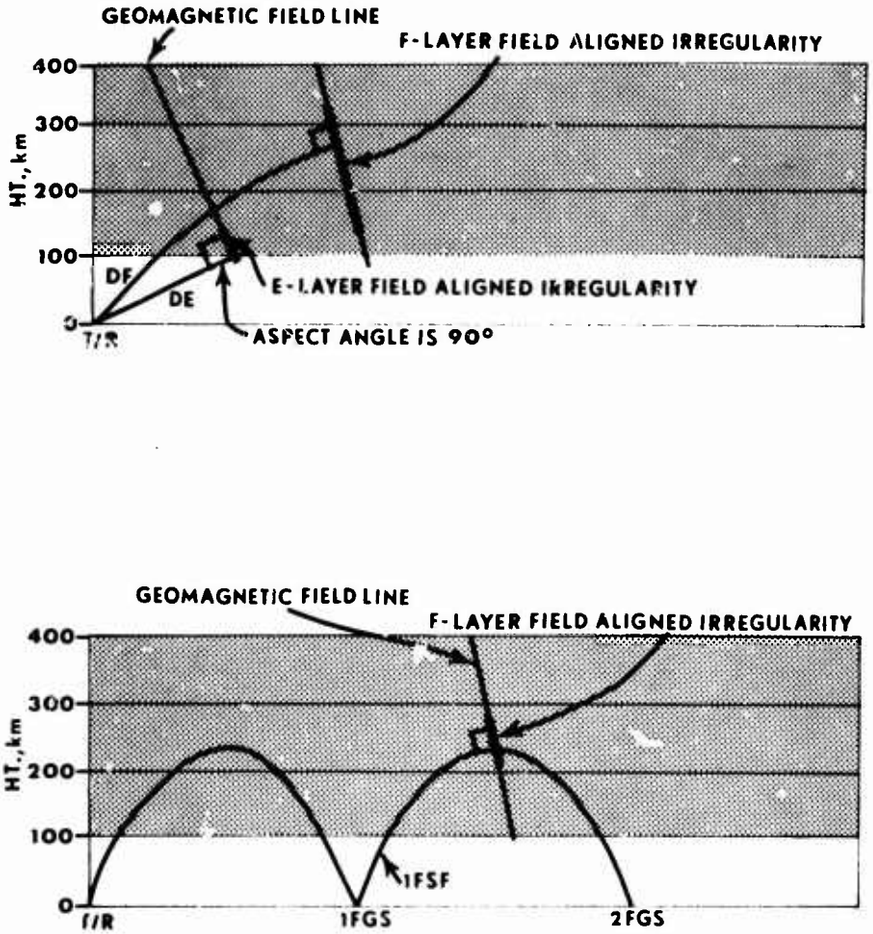

Figure 4. Schematic Representation of Modes of Propagation for Auroral Backscatter as Identified in Figures 3 and 5.

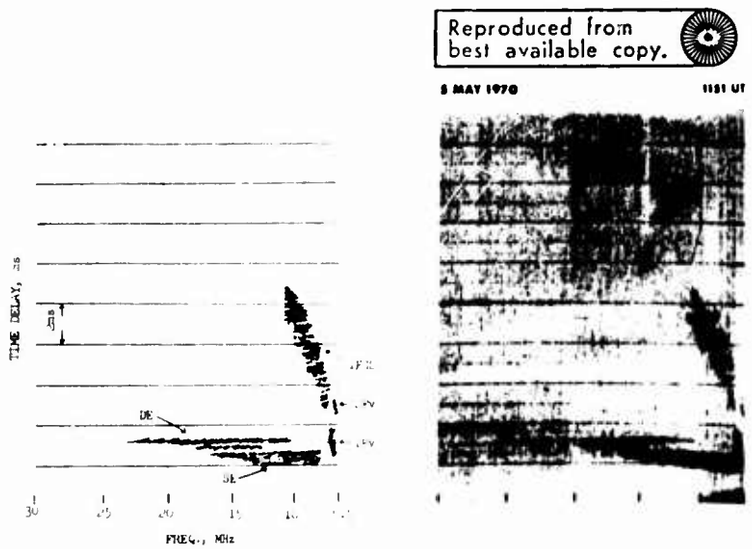

Figure 5. Example of E region Backscatter (including schematic representation of propagation modes) at 1151 UT on 5 May 1970.

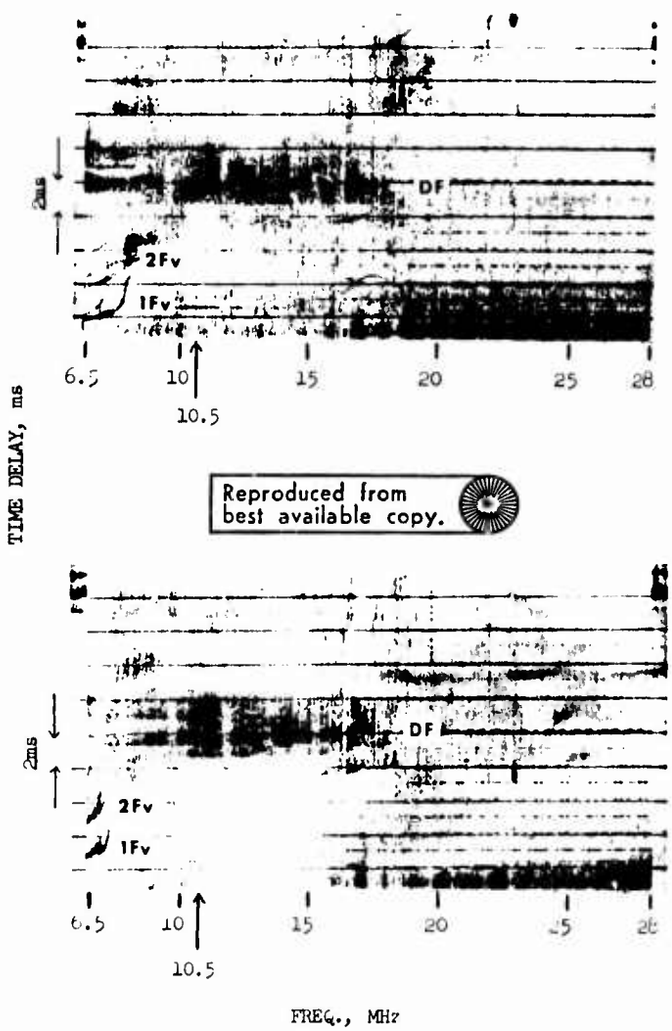

Figure 6. Wideband FM/CW Backscatter Ionograms at 0217 and 0308 UT on 7 August 1970.

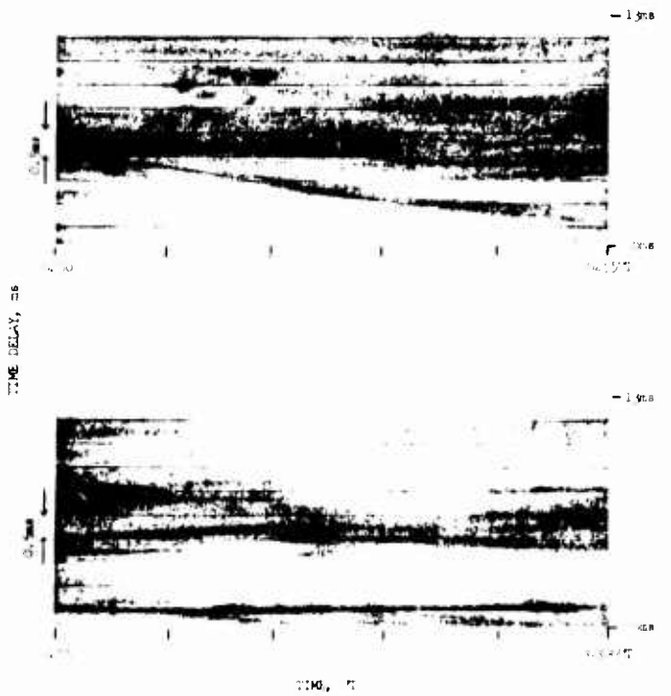

Figure 7. FM/CW Narrowband Backscatter from Radio Aurora at 10.5 MHz from 0250-0255 UT and 0255-0300 UT on 7 August 1970.

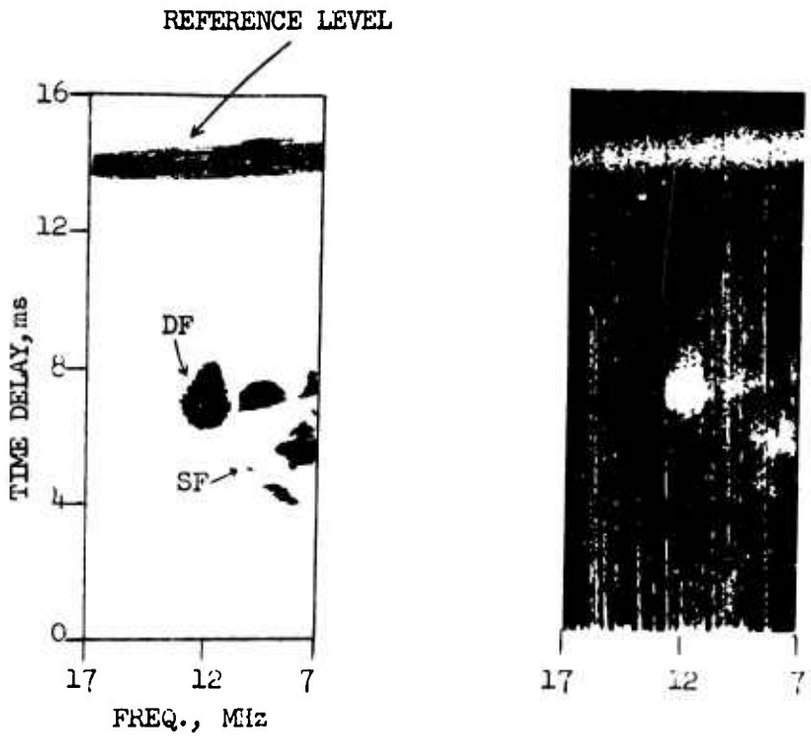

Figure 8. Example of radio auroral backscatter (including schematic representation of modes and a -70 dbm reference level) at 0515 UT on 2 March 1971.

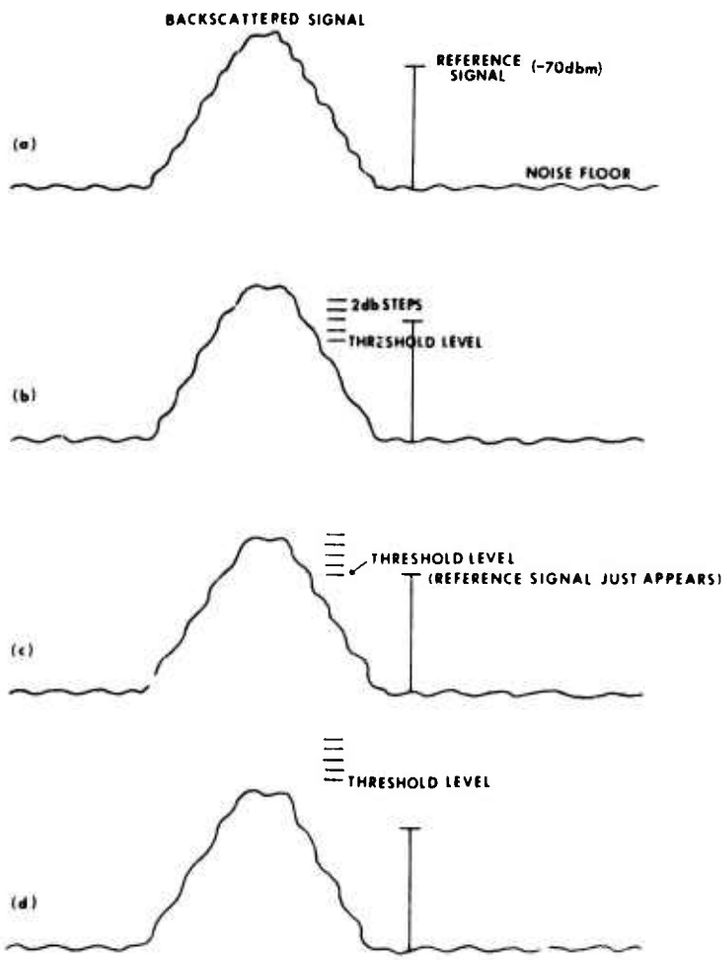

Figure 9. Schematic representation of analysis of a backscatter signal as performed by the Digital Radar Processor.

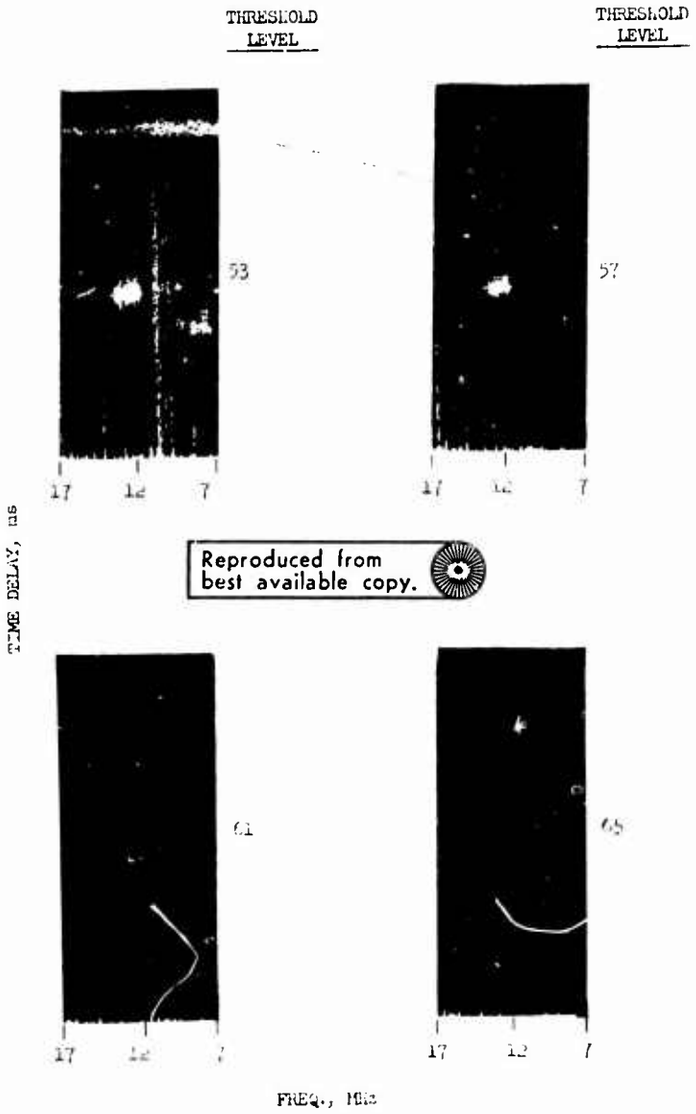

Figure 10. Sequences of pictures of the backscatter ionogram described by Figure 8 processed on the Digital Radar Processor.

DISCUSSION

L Liszka

I think that an increase of atmospheric temperature at F-layer height may explain the velocity of features observed in your experiment, which thus do not need to be supersonic.

IONOSPHERIC REFRACTION EFFECT ON THE GEOMETRY OF FIELD-ALIGNED IONIZATION

by

George H. Millman
General Electric Company
Syracuse, New York 13201, U.S.A.

ABSTRACT

Radio waves incident on ionization aligned along the lines of force of the earth's magnetic field such as encountered in the auroral region are scattered back in the direction of the transmitter when the direction of propagation is approximately perpendicular to the field lines.

For VHF and UHF line-of-sight radars, computational techniques are readily available for determining the regions in space from which radar-auroral echoes could appear. In the case of HF radars, it is necessary to take into account ionospheric refractive bending in the field-aligned geometry computations.

In this paper, a method is presented which utilizes the concept of the ionospheric refraction phenomenon in the calculation of the magnetic field-propagation aspect angle.

An evaluation is made of the effect of ionospheric refraction at frequencies in the HF-UHF band for one location in the Northern Hemisphere.

I. INTRODUCTION

Radar reflections from the aurora are the result of scattering from electron density irregularities aligned along the magnetic field lines. The characteristics of the field-aligned scatterers are such that the radar echoes originate in a small range of angles about perpendicular incidence to the lines of force of the earth's magnetic field and that the echo magnitude is aspect angle sensitive (1, 2, 3). In addition to the orthogonality condition, it is essential that this geometry take place at ionospheric heights; i.e., 80 km and above, and in regions of high auroral activity.

Although radar returns from auroral ionization at VHF and UHF are normally confined to E-layer heights of about 110 km (4, 5, 6, 7), 106-MHz auroral echoes have been detected as high as 300 km (8).

For HF radar transmissions, auroral reflections extending up to F-layer heights, i.e., 300-400 km altitude, have been observed as well as in the E-layer (2, 3, 9, 10, 11). HF radar backscatter soundings in Alaska (12) have revealed the presence of over-the-horizon auroral echoes at regions in space where the propagation direction-magnetic field line perpendicularity condition is satisfied.

Computational techniques are available for predicting the reflection height and angular coordinates of field-aligned scatterers as applied to unrefracted line-of-sight VHF-UHF propagation (13, 14).

Because of the nonisotropic characteristics of the troposphere and ionosphere, radio waves propagated through the media undergo an angular bending. The tropospheric effect is independent of frequency while, for the ionosphere, the refraction is most severe at HF and diminishes with increasing frequency (15).

The effects of the refraction phenomenon on magnetic field geometry calculations have been examined by Bates (2, 3), Vershinin (16), Dearden (17), and Unwin (18).

In this paper, the stratified layer method (19, 20) is used to evaluate the effect of ionospheric refraction in determining the propagation-magnetic field orientation at HF-UHF.

II. THEORETICAL CONSIDERATIONS

The mathematical development of the magnetic field geometry necessary for unrefracted radar-auroral backscatter reflections to take place, i.e., the angular orientation of the direction of propagation with respect to the direction of the lines of force of the earth's magnetic field, has been published (13, 14) and thus will not be discussed in this paper. A summary of the pertinent equations, however, will be presented.

In the case of radar-auroral backscatter, the magnetic field-aspect angle, Θ, (propagation angle), shown in Figure 1, can be expressed by the relationship (13)

$$\Theta = \cos^{-1} \left[-\cos e \sin I - \sin e \cos I \cos (\gamma - D) \right] \tag{1}$$

where I and D are the magnetic inclination and declination angles, respectively.

The angle e, which is the angle between the ray path and the zenith at the point of magnetic field intersection, is given by

$$e = \sin^{-1} \left[\frac{r_o}{r_o + h} \cos E \right] \tag{2}$$

where r_o is the radius of the earth, E is the elevation angle of the antenna beam and h is the height above the earth's surface.

The angle γ which is the geographic azimuth bearing of the radar location measured with respect to the subionospheric point, i.e., the location on the earth's surface directly beneath the magnetic field intersection point, is defined by (14)

$$\gamma = \tan^{-1} \left[\frac{\sin (\lambda_R - \lambda_P) \cos \phi_R}{\sin \phi_R \cos \phi_P - \cos \phi_R \sin \phi_P \cos (\lambda_R - \lambda_P)} \right] \tag{3}$$

where ϕ and λ are the geographic latitude and east longitude, respectively. The subscripts, R and P, refer to the radar site and the reflection point, respectively.

The parameters I and D can be deduced from a spherical harmonic model of the earth's magnetic field. The spherical harmonic representation assumes that the earth's main field, i.e., the magnetic field that excludes such phenomena as magnetic disturbances and diurnal variations, can be described by a regular or dipole field and an irregular field.

According to Chapman and Bartels (21), the magnetic inclination and declination angles for the spherical harmonic model are defined by

$$I = \tan^{-1}\left[\frac{Z}{(X^2 + Y^2)^{1/2}}\right] \tag{4}$$

$$D = \tan^{-1}\left[\frac{Y}{X}\right] \tag{5}$$

where X, Y, and Z are the northward horizontal, the eastward horizontal, and the downward vertical component of the total magnetic intensity.

The components, X, Y, and Z, are related to the magnetic potential, V, by the functions

$$X = \frac{1}{r}\ \frac{\partial V}{\partial \phi'} \tag{6}$$

$$Y = -\ \frac{1}{r \sin\phi'}\ \frac{\partial V}{\partial \lambda} \tag{7}$$

$$Z = \frac{\partial V}{\partial r} \tag{8}$$

$$V = \sum_{n=0}^{\infty} \sum_{m=0}^{n} \frac{r_o^{n+1}}{r^{n+1}} \left[g_{nm} \cos(m\lambda) + h_{nm} \sin(m\lambda)\right] P_n^m(\cos\phi') \tag{9}$$

where r is the distance from the center of the earth, ϕ' is the geographic colatitude, $P_n^m(\cos\phi')$ are the associated Legendre functions of degree n and order m, and g_{nm} and h_{nm} are the coefficients of the spherical harmonic expansion.

In this analysis, the set of 48 spherical harmonic coefficients derived by Jensen and Cain (22) for epoch 1960 was used to specify the magnetic potential function defined by Equation (9).

In determining the effect of the ionospheric refraction phenomenon on the propagation angle (θ) computation, the basic assumption employed is that the ionosphere can be considered to be stratified into m spherical layers of thickness, h_m, and constant refractive index, n_m, as illustrated in Figure 2.

When refraction effects are taken into account, it can be readily shown that the angle, e, in Equation (1), is modified to the general form (19)

$$(e_r)_j = \frac{\pi}{2} - \cos^{-1}\left[\frac{n_o r_o}{n_j r_j} \cos E_o\right] \tag{10}$$

where E_o is the apparent ground elevation angle.

The radial distance from the center of the earth, r_j, is merely the summation of the various layers expressed by

$$r_j = r_o + \sum_{i=o}^{j-1} h_i \tag{11}$$

Since the effects of tropospheric refraction are not considered in this analysis, it is appropriate to designate h_o as the height of the base of the ionosphere above the surface of the earth having a constant refractive index, n_o, of unity.

The stratified layer method, although approximate in nature, can be greatly improved by merely increasing the number of layers in the medium, i.e., decreasing the thickness of each individual layer element (23).

To a first approximation, the index of refraction in the ionosphere can be defined by the relationship

$$n = \left[1 - \frac{N_e e^2}{\epsilon_o m \omega^2} \right]^{1/2} \approx 1 - \frac{N_e e^2}{2\epsilon_o m \omega^2} \tag{12}$$

where N_e is the electron density (electrons/m^3), e is the electron charge (1.6×10^{-19} Coulomb), m is the electron mass (9.1×10^{-31} kg), ϵ_o is the electric permittivity of free space ($10^{-9}/36\pi$ farad/meter), and ω is the angular frequency of the incident wave (radians/second).

It should be noted that the ionospheric refractive index is also a function of both the earth's magnetic field and the electron collision frequency. A slight error could be introduced in the evaluation of the magnitude of n for frequencies at the low end of the HF band when both parameters are neglected. However, for frequencies in the VHF band and above, it is valid to assume the definition of n as given by Equation (12).

III. DISCUSSION

The refraction-magnetic field geometry calculations presented in this paper are based on a daytime and nighttime model of electron density.

For the daytime, the distribution of electron density with height is assumed to follow the Chapman model of the form

$$N_e \quad N_m \exp\left\{ \frac{1}{2} \left[1 - \frac{h-h_m}{H_s} - \exp\left(\frac{-(h-h_m)}{H_s} \right) \right] \right\} \tag{13}$$

where N_m is the electron density at the level of maximum ionization, h_m, and H_s is the scale height of the neutral particles. The values of the parameters defining the daytime electron density profile and the equivalent plasma frequencies of the maximum ionization levels are presented in Table 1.

The nighttime model of electron density is the average profile deduced from vertical incidence ionospheric sounding taken at St. Johns, Newfoundland, in March 1961 at 0100 hours local time, for magnetic activity index, k_p, less than 4.5.

According to Figure 3 which contains a plot of the daytime and nighttime electron density models, the peak of the F-layer of the St. Johns profile is centered at 360 km altitude having an electron density maximum of 1.64×10^{11} electrons/m^3 which corresponds to a plasma frequency of approximately 3.6 MHz.

The ray path computations were performed utilizing double precision computational techniques in order to ensure a high degree of accuracy. Layer thicknesses of constant refractive index of 1 km were taken throughout the ionospheric medium.

The contours of perpendicularity with the earth's magnetic field as viewed from Boston, Massachusetts, (geographic coordinates: 42.3°N, 71.0°W) at zero degree elevation angle for the daytime ionosphere are shown in Figure 4. It is evident that the location of the subionospheric perpendicular contour lines is a function of the transmission frequency. The unrefracted ray calculations apply to the condition in which the electron density is assumed to be zero. As will be shown later, the unrefracted ray results are valid for frequencies above approximately 400 MHz.

According to Figures 5 and 6, for HF propagation, perpendicularity could be attained on both the upward ray and the downward ray, i.e., after the ray has undergone F-layer reflection. It is of interest to note that on the upward ray the contour lines minimize and maximize at an azimuth angle of about -15°. This azimuth corresponds approximately to the direction of the magnetic meridian, i.e., the dip pole and the magnetic declination (2). A comparison of Figures 5 and 6 reveals that a change in the elevation angle of transmission would, for the most part, alter the spatial distribution of the normality contours.

Sample calculations of the propagation angle as viewed in an azimuth direction of 5° west of geographic north at 5° elevation angle, for frequencies in the HF and VHF-UHF band, are presented in Figures 7 and 8, respectively. It is seen that, for the unrefracted ray, the propagation angle increases monotonically with altitude, while, for the rays undergoing refraction, the reverse could take place.

According to Figure 7, as the frequency is increased, the altitude at which ionospheric reflection occurs also increases. Perpendicularity is attained at altitudes of approximately 173 km and 228 km for the 30-MHz upward ray and at 127 km for the unrefracted ray.

It can be readily shown utilizing Snell's law for spherically symmetric surfaces in conjunction with Figure 2 and Equation (12) that the maximum frequency for ionospheric reflection, f_m, can be represented by

$$f_m^2 \quad \frac{80\, N_m}{1 - \left[\frac{r_o}{r_o + h_m} \cos E_o \right]^2} \tag{14}$$

It follows that, at 5° elevation angle for the daytime model, the maximum reflection frequency is on the order of 32.3 MHz.

For frequencies greater than f_m, the difference between the propagation angles computed for the unrefracted and refracted ray decreases with increasing frequency as shown in Figure 8. For 400-MHz propagation at 5° elevation angle, the difference between the two rays is less than approximately 0.05° which is quite insignificant.

Figure 9 is a plot of the perpendicular contours for the nighttime ionosphere. The regions in space where normality occurs correspond in some degree to the daytime data of Figure 4.

As shown in Figures 10 and 11, for low elevation angles of propagation in the direction of magnetic north, i.e., azimuth angle of -15°, the orthogonality with the magnetic field is obtained at an altitude of approximately 115 km and in the 280-320 km region which is slightly below the peak of the F-layer nighttime model.

In the case of the daytime model, illustrated in Figures 5 and 6, the orthogonality region is spread out in altitude between approximately 110 and 230 km.

The geographic locations of the contour lines presented in Figure 12 reveal that, for HF ionospherically reflected transmissions oriented in a northerly direction from Boston, the altitude-magnetic field aspect angle functions formed by both the upward and downward rays are most often double-valued. An example of this is the 9-MHz calculation shown in Figure 13.

It should be noted that the daytime-HF calculations, illustrated in Figure 7, also indicate the presence of both single- and double-valued functions.

From Equation (14), it follows that, for the nighttime model, the maximum frequency for ionospheric reflection to occur at 5° elevation angle evaluates to 11.1 MHz.

IV. CONCLUSIONS

The effect of the refractive bending in the ionosphere must be taken into account in geometric studies involving the orientation of the earth's magnetic field.

At VHF and UHF, perpendicularity with the earth's magnetic field can be attained at only one altitude along a ray path while at HF multiple altitudes are possible.

Large errors in estimating the spatial position of auroral reflecting regions can be introduced, especially at HF, when ionospheric refraction is neglected.

Ionospheric refraction effects are found to be negligible at frequencies in the UHF range and above.

Although the tropospheric refraction phenomenon can be disregarded at HF, its effects could be detrimental at the higher frequencies and, in particular, at the low elevation angles of propagation.

V. REFERENCES

1. Leadabrand, R.L., A.G. Larson, and J.C. Hodges, "Preliminary Results on the Wavelength Dependence and Aspect Sensitivity of Radar Auroral Echoes Between 50 and 3000 MHz," Journal of Geophysical Research, Vol. 72, pp 3877-3887, August 1, 1967.

2. Bates, H.F. and P.R. Albee, "Aspect Sensitivity of HF Auroral Echoes," Journal of Geophysical Research, Vol. 74, pp 1164-1168, March 1, 1969.

3. Bates, H.F. and P.R. Albee, "Aspect Sensitivity of F-Layer HF Backscatter Echoes," Journal of Geophysical Research, Vol. 75, pp 165-170, January 1, 1970.

4. Unwin, R.S., "Studies of the Upper Atmosphere from Invercargill, New Zealand; Part 1, Characteristics of Auroral Radar Echoes at 55 Mc/sec," Annales de Geophysique, Vol. 15, pp 377-394, July-September 1959.

5. Watkins, C.D. and H.K. Sutcliffe, "Radar Observations of Weak Field-Aligned Ionization at a Frequency of 300 Mc/s," Journal of Atmospheric and Terrestrial Physics, Vol. 27, pp 309-320, 1965.

6. Leadabrand, R.L., J.C. Schlobohm, and M.J. Barron, "Simultaneous Very High Frequency and Ultra High Frequency Observations of the Aurora at Fraserburgh, Scotland," Journal of Geophysical Research, Vol. 70, pp 4235-4284, September 1, 1965.

7. Abel, W.G. and R.E. Newell, "Measurements of the Afternoon Radio Aurora at 1295 MHz," Journal of Geophysical Research, Vol. 74, pp 231-245, January 1, 1969.

8. Schlobohm, J.C., R.L. Leadabrand, R.B. Dyce, L.T. Dolphin, Jr., and M.R. Berg, "High-Altitude 106.1-Mc Radio Echoes from Auroral Ionization Detected at a Geomagnetic Latitude of 43°," Journal of Geophysical Research, Vol. 64, pp 1191-1196, September 1959.

9. Malik, C. and J. Aarons, "A Study of Auroral Echoes at 19.4 Megacycles per Second," Journal of Geophysical Research, Vol. 69, pp 2731-2736, July 1, 1964.

10. Au, W.W.L. and G.L. Hower, "Multi-Station Observations of Long-Range Backscatter from Field-Aligned Irregularities in the F-Layer," Journal of Atmospheric and Terrestrial Physics, Vol. 32, pp 1577-1589, 1970.

11. Baggaley, W.J. "Backscatter Observations of F-Region Field-Aligned Irregularities during I.Q.S.Y.," Journal of Geophysical Research, Vol. 75, pp 152-158, January 1, 1970.

12. Bates, H.F., "HF Propagation through the Auroral Curtain," Journal of Geophysical Research, Vol. 75, pp 143-151, January 1, 1970.

13. Millman, G.H., "The Geometry of the Earth's Magnetic Field at Ionospheric Heights," Journal of Geophysical Research, Vol. 64, pp 717-726, July 1959.

14. Millman, G.H., "Field Aligned Ionization Scatter Geometry," Journal of Geophysical Research, Vol. 74, pp 900-905, February 1, 1969.

15. Millman, G.H., "A Survey of Tropospheric, Ionospheric and Extraterrestrial Effects on Radio Propagation between the Earth and Space Vehicles," AGARD Conference Proceedings No. 3 on Propagation Factors in Space Communications, pp 3-55, Technivision, 1967.

16. Vershinin, Y.F., "Allowance for Refraction in the Interpretation of Radio Reflections from Auroras," Geomagnetism and Aeronomy, Vol. , pp 243-245, 1962.

17. Dearden, E.W., "The Geometry of Radio Reflections from Field-Aligned Ionization Irregularities in the Ionosphere," Journal of Atmospheric and Terrestrial Physics, Vol. 24, pp 375-384, 1962.

18. Unwin, R.S., "The Importance of Refraction in the Troposphere and Ionosphere in Determining the Aspect Sensitivity and Height of the Radio Aurora," Journal of Geophysical Research, Vol. 71, pp 3677-3686, August 1, 1966.

19. Millman, G.H., "Atmospheric Effects on VHF and UHF Propagation," Proceedings IRE, Vol. 46, pp 1492-1501, August 1958.

20. Millman, G.H., "Tropospheric Effects on Space Communications," AGARD Conference Proceedings No. 70 on Tropospheric Radio Wave Propagation, pp (4-1)-(4-29), 1971.

21. Chapman, S. and J. Bartels, "Geomagnetism," Vols. 1 and 2, Oxford University Press, New York, 1940.

22. Jensen, D.C. and J.C. Cain, "An Interim Geomagnetic Field," Journal of Geophysical Research, Vol. 67, pp 3568-3569, August 1962.

23. Millman, G.H., "Tropospheric Effects on Radar Target Measurements," Proceedings of the Seventh Weather Radar Conference, American Meteorological Society, Miami Beach, Florida, November 1958.

TABLE 1

DAYTIME ELECTRON DENSITY PROFILE

LAYER	H_s-(km)	h_m-(km)	N_m-(electrons/m^3)	Plasma Frequency-(MHz)
E	10	100	1.5×10^{11}	3.5
F_1	40	200	3.0×10^{11}	4.9
F_2	50	300	1.25×10^{12}	10.0

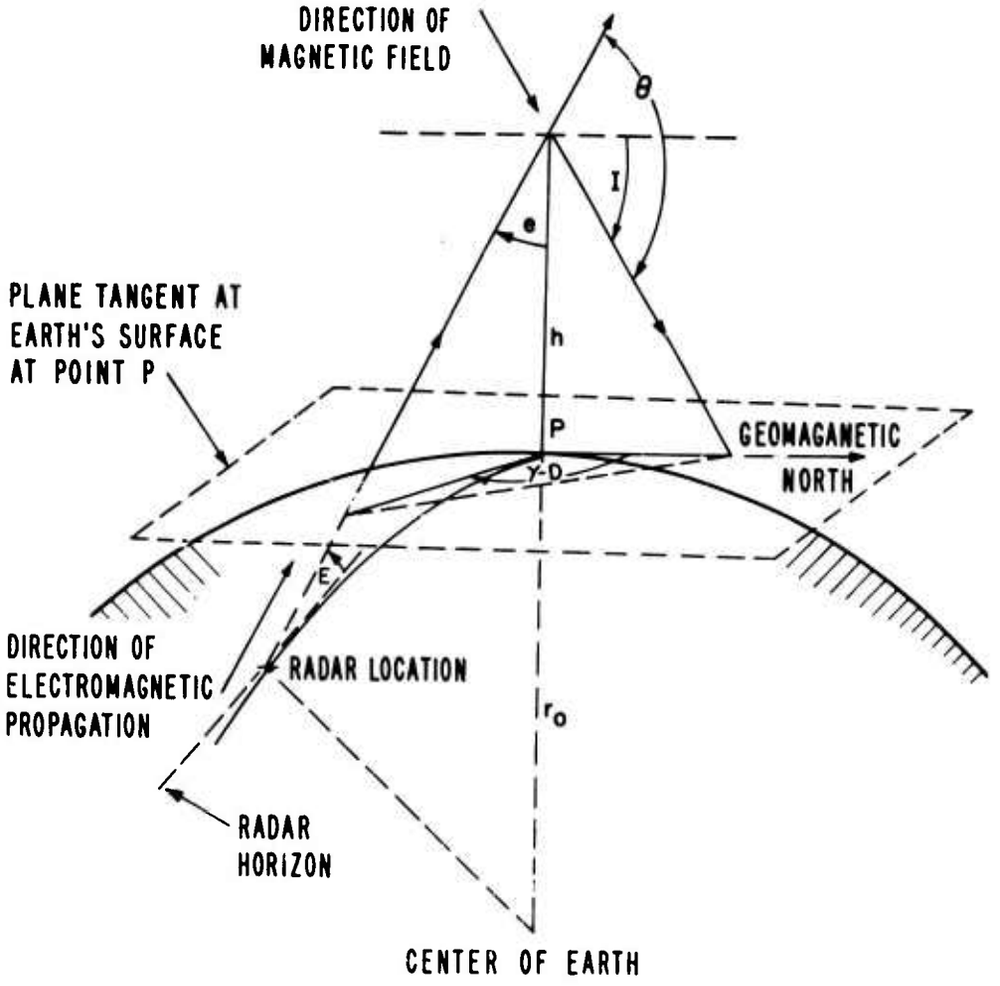

Figure 1. Radar-Auroral Geometry

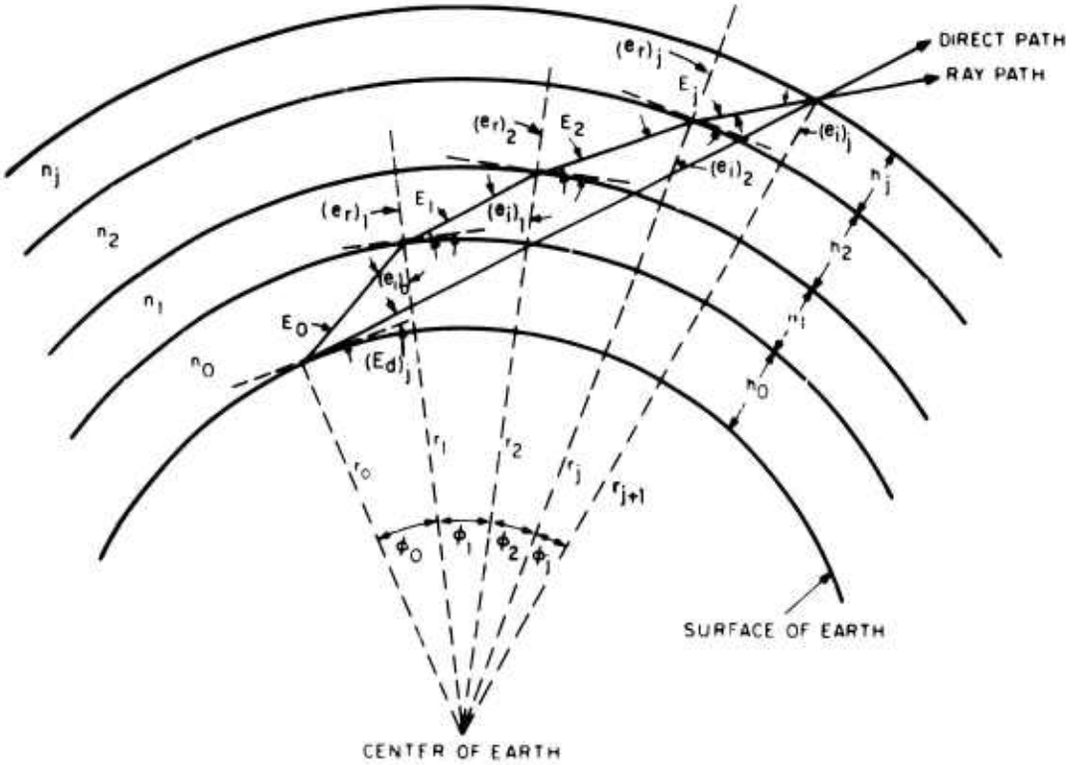

Figure 2. Atmospheric Layer Stratification

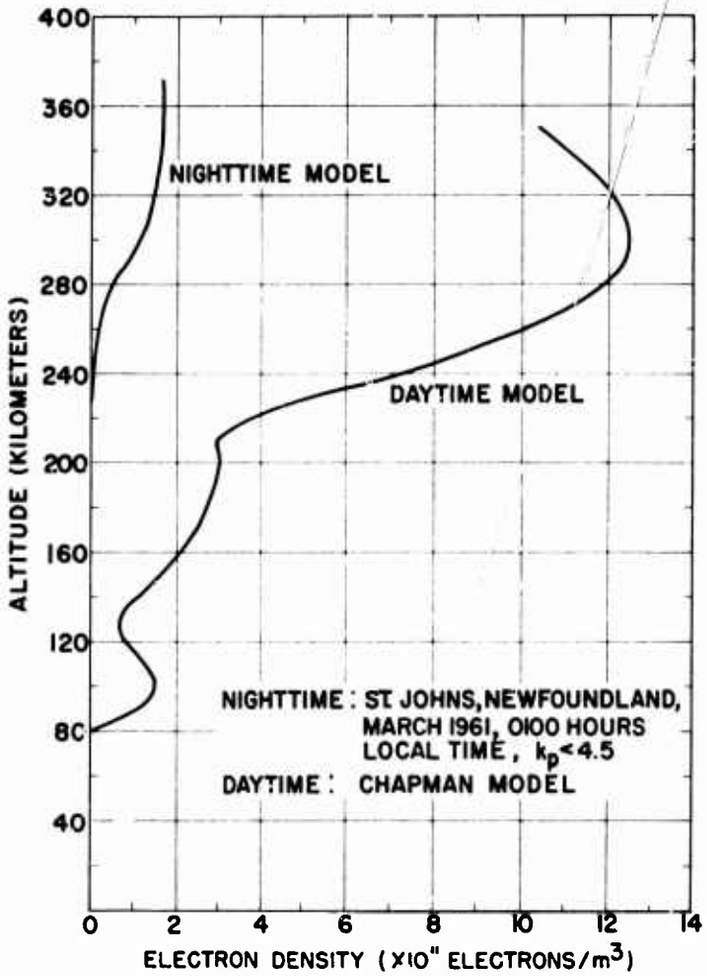

Figure 3. Electron Density Profiles

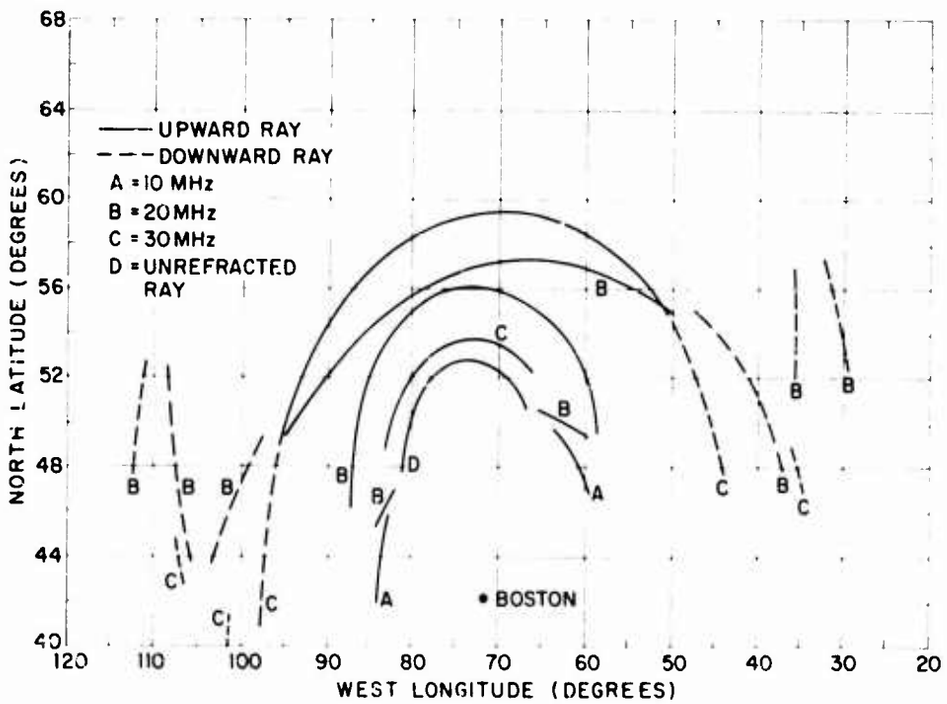

Figure 4. Contours of Perpendicularity with the Earth's Magnetic Field as Viewed from Boston, Massachusetts at 0° Elevation Angle for a Daytime Ionosphere

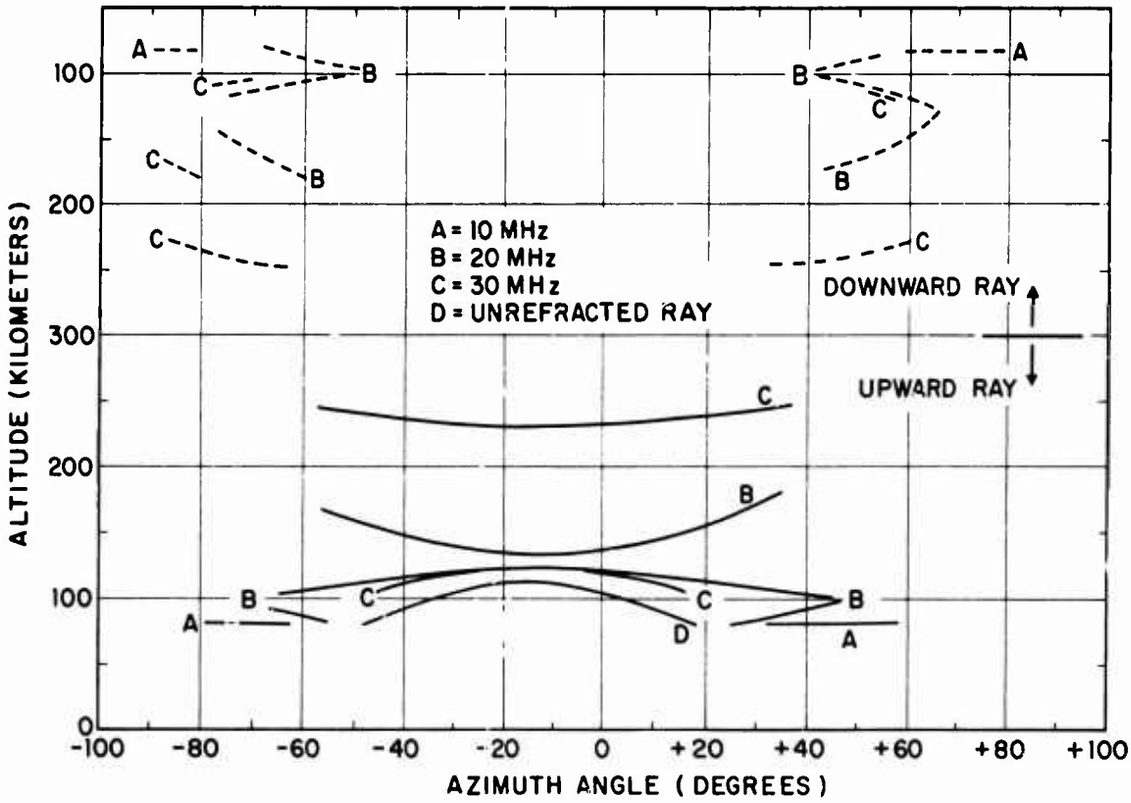

Figure 5. Spatial Distribution of Perpendicularity with the Earth's Magnetic Field as Viewed from Boston, Massachusetts at 0° Elevation Angle for a Daytime Ionosphere

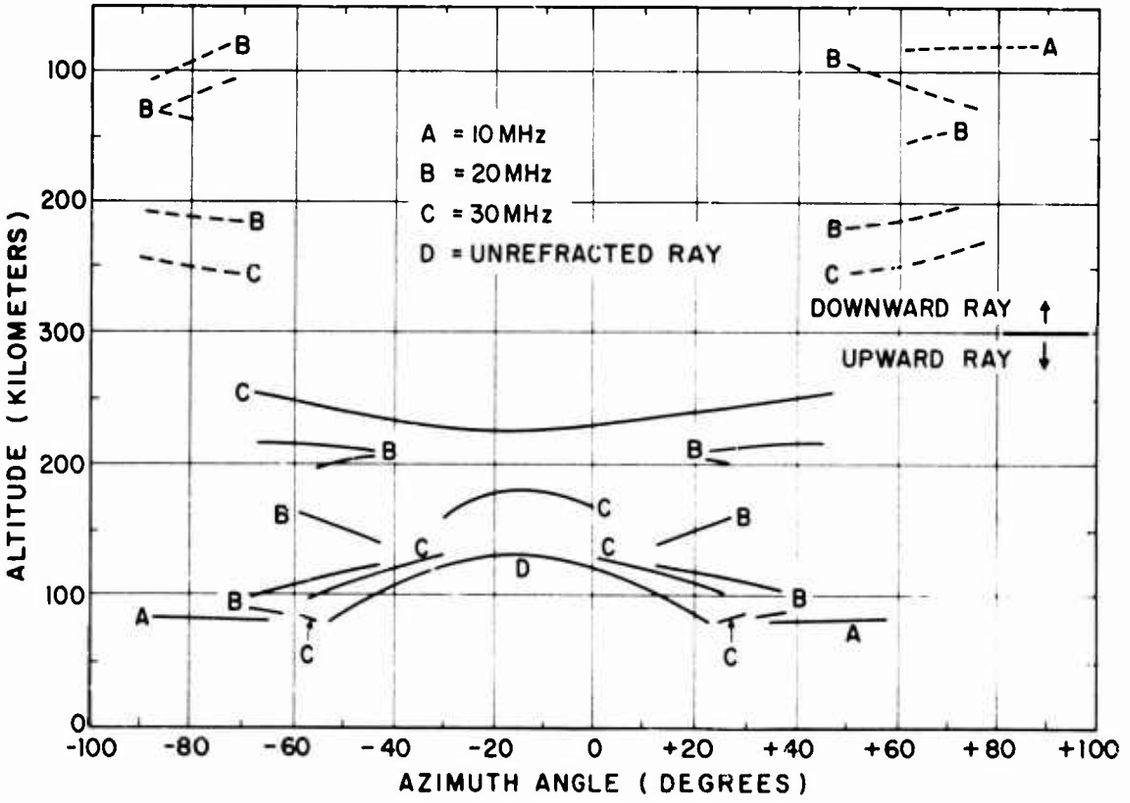

Figure 6. Spatial Distribution of Perpendicularity with the Earth's Magnetic Field as Viewed from Boston, Massachusetts at 5° Elevation Angle for a Daytime Ionosphere

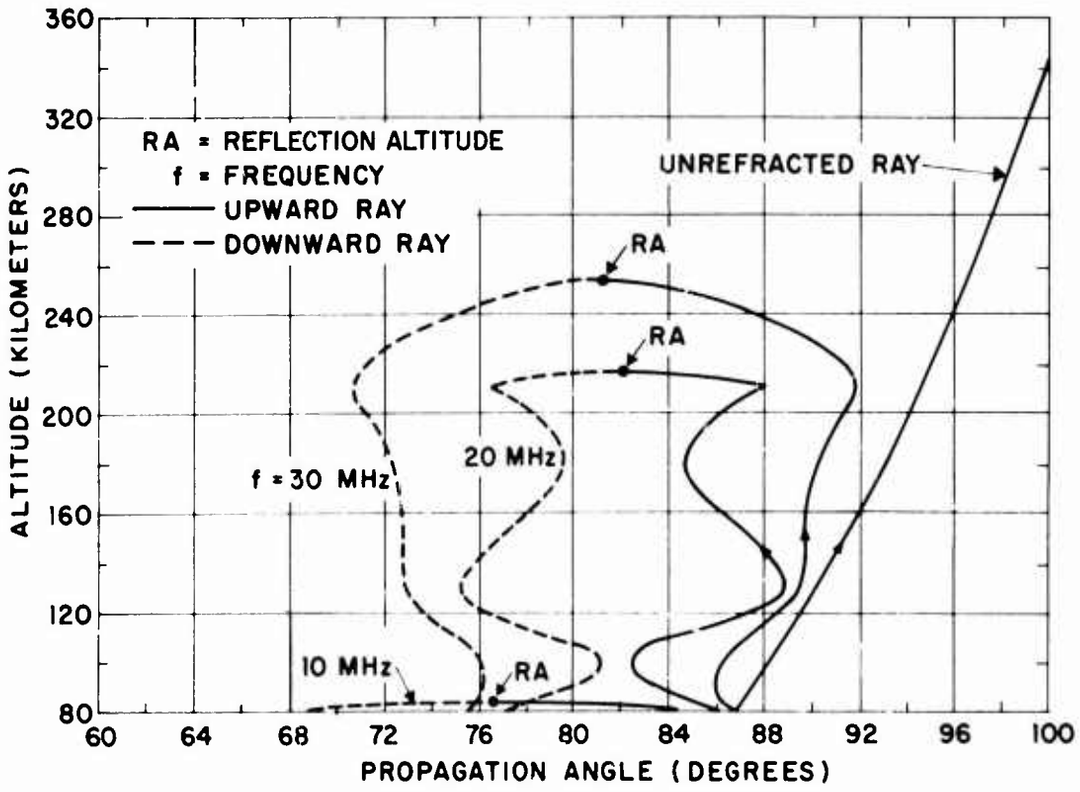

Figure 7. Propagation Angle at HF for a Daytime Ionosphere as Viewed from Boston, Massachusetts, at an Elevation Angle of 5° and Azimuth Angle of 5° West of Geographic North

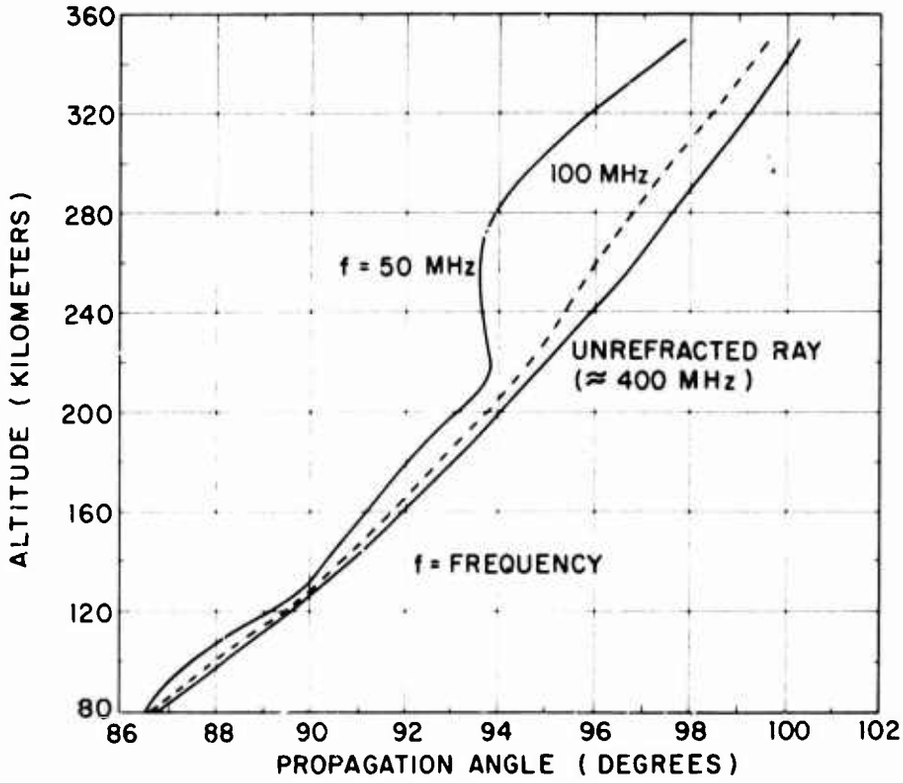

Figure 8. Propagation Angle at VHF-UHF for a Daytime Ionosphere as Viewed from Boston, Massachusetts, at an Elevation Angle of 5° and Azimuth Angle of 5° West of Geographic North

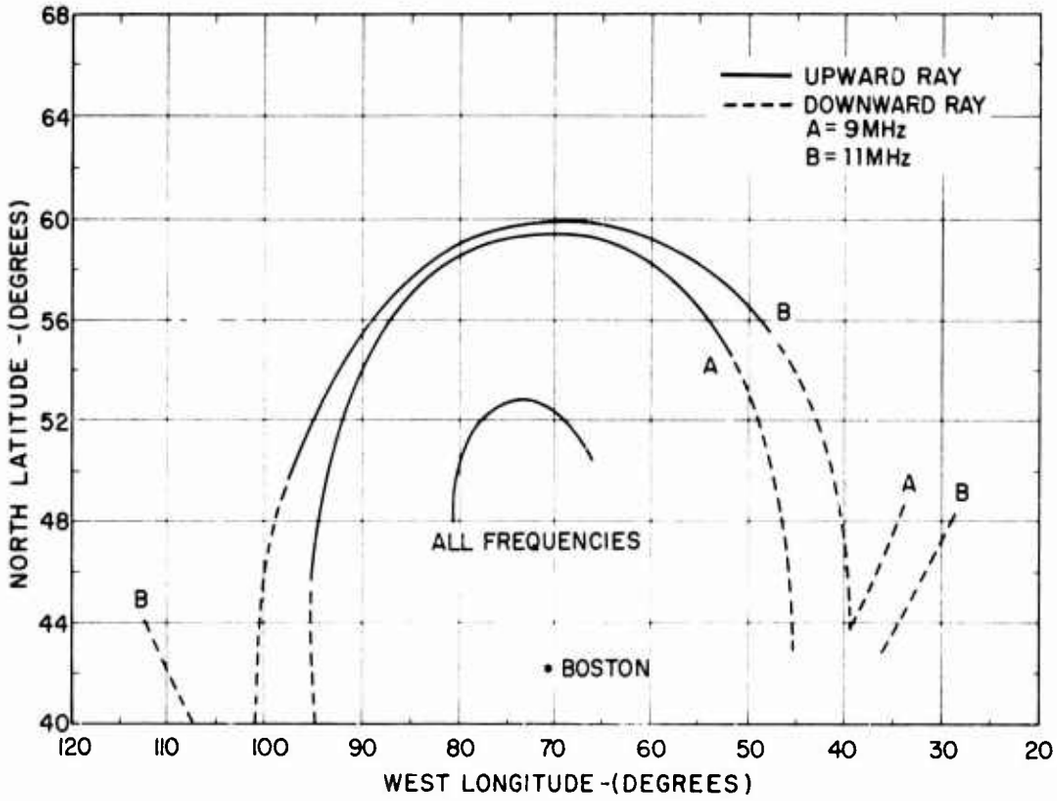

Figure 9. Contours of Perpendicularity with the Earth's Magnetic Field as Viewed from Boston, Massachusetts at 0° Elevation Angle for a Nighttime Ionosphere

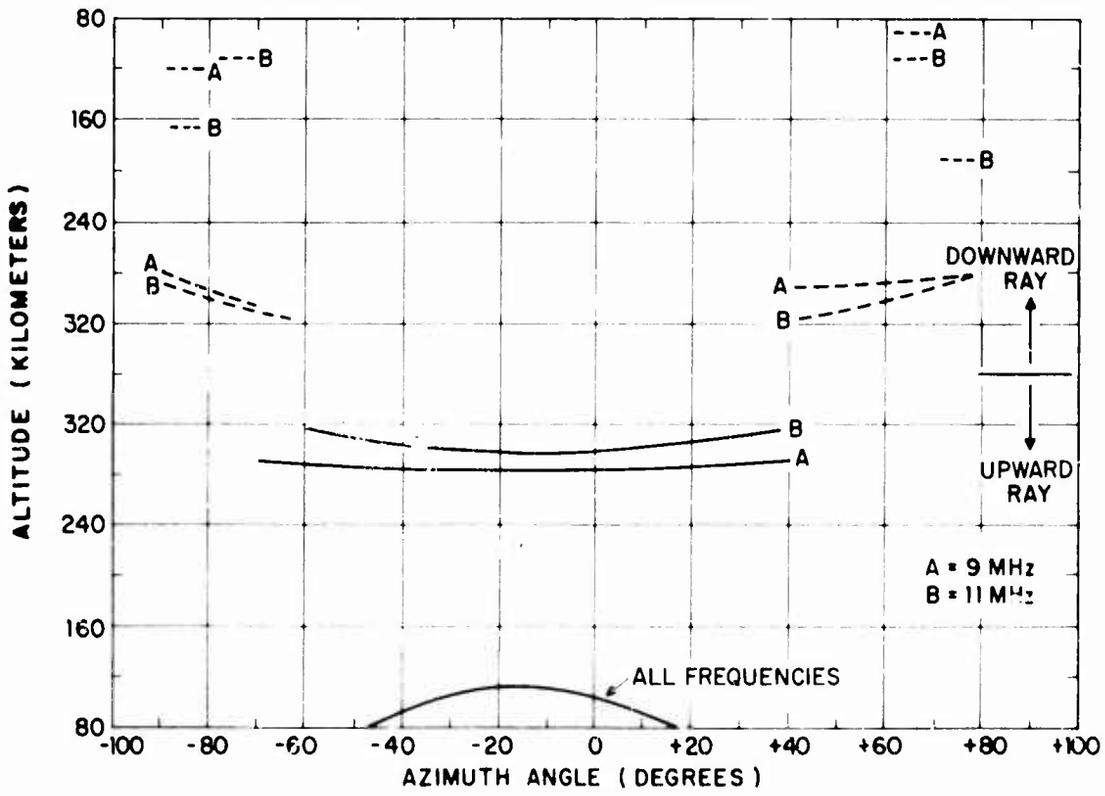

Figure 10. Spatial Distribution of Perpendicularity with the Earth's Magnetic Field as Viewed from Boston, Massachusetts at 0° Elevation Angle for a Nighttime Ionosphere

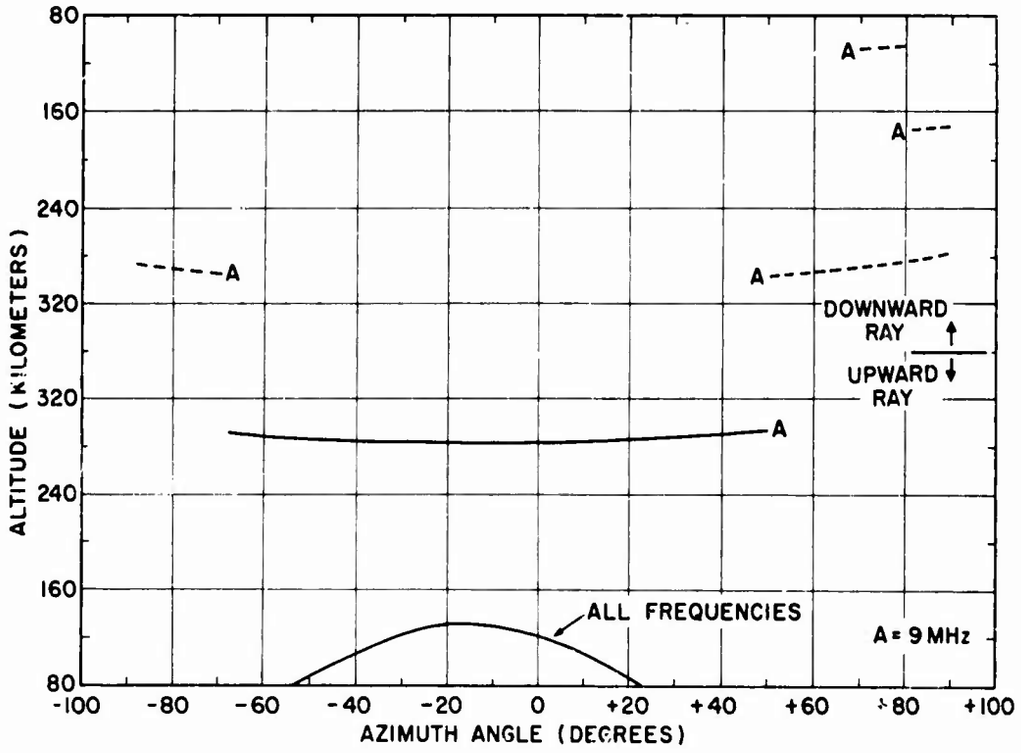

Figure 11. Spatial Distribution of Perpendicularity with the Earth's Magnetic Field as Viewed from Boston, Massachusetts at 5° Elevation Angle for a Nighttime Ionosphere

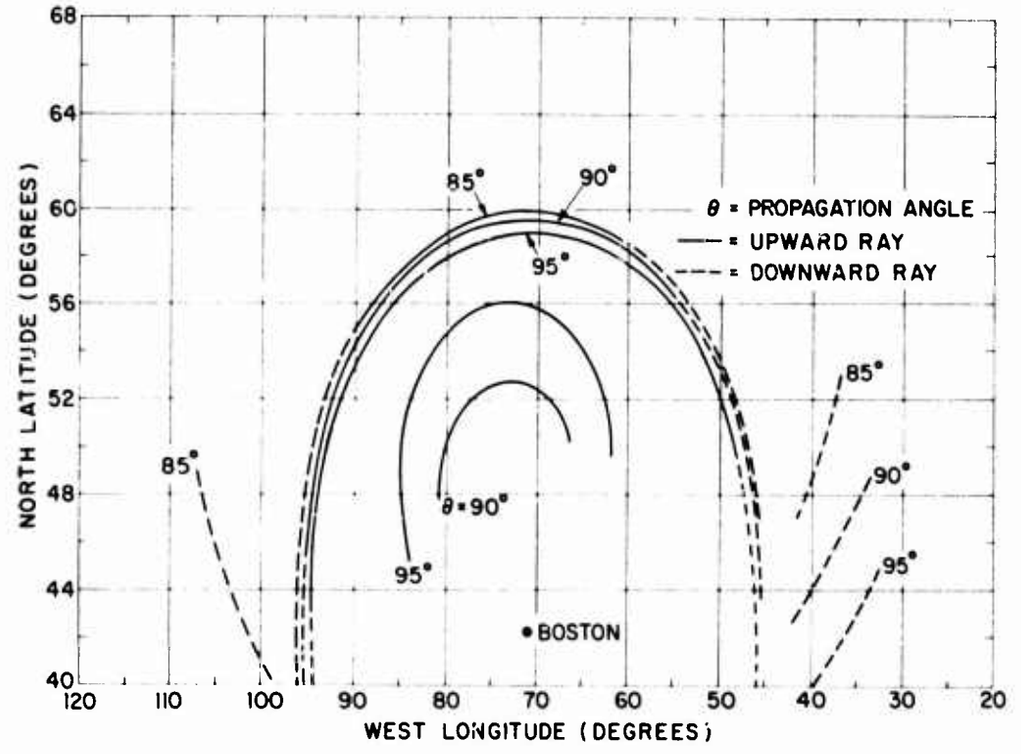

Figure 12. Contours of Constant Propagation Angle at 9 MHz as Viewed from Boston, Massachusetts at 0° Elevation Angle for a Nighttime Ionosphere

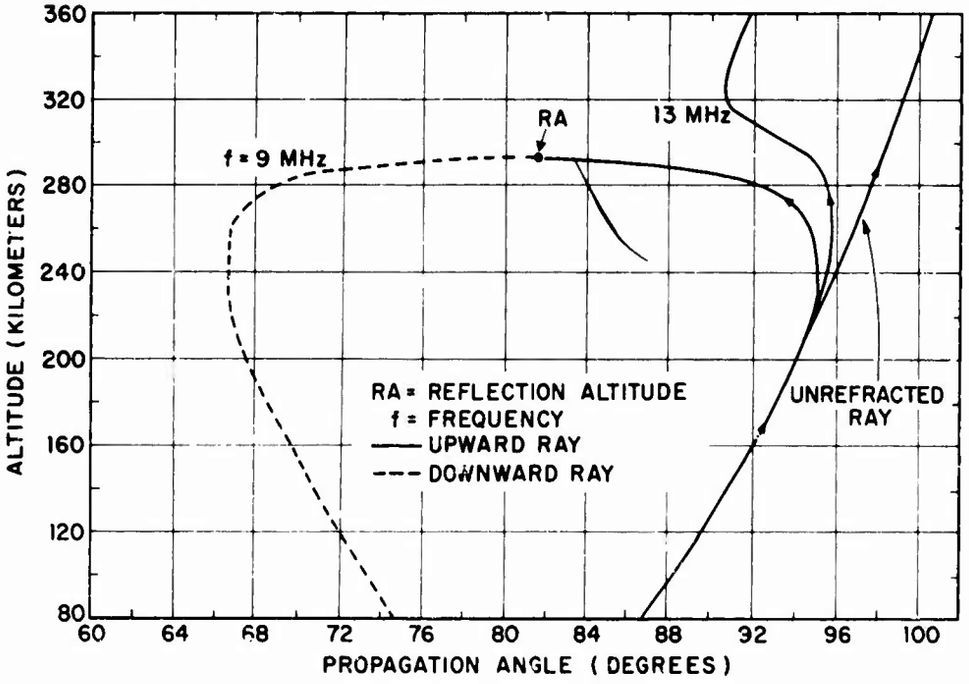

Figure 13. Propagation Angle at HF for a Nighttime Ionosphere as Viewed from Boston, Massachusetts at an Elevation Angle of 5° and Azimuth Angle of 5° West of Geographic North

A MODEL FOR THE STUDY AND PREDICTION OF AURORAL EFFECTS ON HF RADAR

Vaughn Agy

U. S. Department of Commerce
Office of Telecommunications
Institute for Telecommunication Sciences
Boulder, Colorado 80302

A description is given of an ionospheric propagation model and its application to high latitude HF radar propagation. Computer-simulation of the model makes possible the rapid determination of the area of (1-hop) coverage, and computation of auroral absorption and geometrical features of auroral clutter. The results are presented in a map on which are shown contours of the appropriate parameter. The operating frequency, station location, time, month, sunspot number, and "clutter" height are all arbitrary. The explicit approximations specifying the model can be changed within the basic framework of the computer program to bring about better agreement with observations.

1. INTRODUCTION

At high latitudes especially, wholly acceptable descriptions of the "median ionosphere" are lacking. In part, this is due (for the ITS prediction model) to a small data base (five years of vertical-incidence ionospheric soundings) (Jones and Obitts, 1970) further reduced by disturbance effects that often rendered E- and F-layer parameters unscalable (spread F, blanketing Es, "abnormal" absorption). In addition, the present numerical maps (Jones and Gallet, 1962) of the ionospheric parameters show conscious emphasis on the lower latitudes. As a result, HF circuit predictions at high latitudes tend to be poor.

The approach discussed here, although by no means a "full" ray trace, represents a degree of precision greater than can readily be justified by an ionospheric model beset by the ills mentioned. It can, therefore, be argued that the effort is pointless.

There is hope for improvement, however, in the numerical maps: they can be derived giving greater weight to high latitudes, the data base can be broadened, and topside F-layer observations may fill in where bottomside soundings are unavailable or unscalable. The ITS prediction program (Barghausen et al, 1968) uses the assumption of a uniform ionosphere over the entire path, so that objections can be raised to expending the effort required to apply these remedies. We end up on dead center; a first step is needed.

The amount of improvement possible (or reasonable) is a fit subject for discussion. Considering the cost and the computation time required for a full ray trace, and the statistical nature of the "median" ionosphere, complete specification of the ionospheric model, i.e., electron number density as a function of height, location, and time, as offered, for example, by Nisbet (1971), is hardly worth while for our purposes. (For instantaneous or "real time" application, more or less complete specification is of greater interest (Gassmann, 1971)). Therefore, the first step suggested here is the continued (temporary) use of the present numerical maps of the ionospheric parameters, and the application of a "modified" ray trace through an ionospheric electron number density profile given as an analytic function of height. In the next section a list of the assumptions made to describe the model is given; in section 3 is outlined the computational procedure; and in section 4, the results are presented as maps on which are drawn contours of the parameter of specific interest. The approach was initially devised for the computation of auroral absorption (Agy, 1970), and is here extended to apply also to auroral clutter geometry (Millman, 1969). Our interest is principally in propagation at auroral latitudes, but the method has a wider application; we should now be able to develop a consistent program applicable to HF predictions at all latitudes.

2. ASSUMPTIONS AND APPROXIMATIONS

The model to be considered is described in terms of a set of assumptions stated explicitly either here or in the references cited.

The ray-path geometry is determined essentially by a ray trace through a deviative ionosphere consisting of E and F layers whose parameters are defined (or predicted) by the techniques developed at ITS (Barghausen et al, 1968). In each layer the electron density distribution with height is assumed to be "quasi-parabolic" (Croft and Hoogasian, 1968). A "valley" void of ionization is assumed to separate the two layers.

The starting point for the introduction of "median auroral absorption" is the pattern derived by Hartz et al (1963) shown in Fig. 1. As indicated earlier (Agy, 1970) assumptions with regard to the following points are required: (1) extrapolation of the pattern to higher and lower latitudes, (2) transformation of the pattern values from % time to medians, (3) changeover to an "equivalent vertical-incidence pattern" (4) frequency dependence of absorption, (5) height of "occurrence" of auroral absorption, (6) correction for obliquity of the radio ray in the absorbing region, (7) seasonal variations,

(8) solar cycle variations. Each assumption is stated below; it must be emphasized that none of them is the "final word".

(1) Extrapolation in latitude: we assume that, at the geomagnetic pole, auroral absorption does not occur, and write

$$Q = 0.25 \times [(90 - \Phi_{0.25})]^2$$

For latitudes below the present 2% contour, a 1% contour has been drawn and

$$Q = [(\Phi_2 - \Phi_1)/(\Phi_2 - \Phi)]^7$$

where the high exponent, 7, has been suggested by Adolph Fejfar of Mitre Corporation to bring about a relatively sharper drop in auroral absorption at lower latitudes as compared with that given in the earlier treatment (Agy, 1970). Here, Q is in % time auroral absorption of 30 MHz cosmic noise ≥ 1 dB, Φ_i is the geomagnetic latitude of the i% contour, and Φ is that of the D-layer point (below the lower 1% contour or above the 0.25% contour) all at the appropriate local geomagnetic time.

(2) Transformation from % time to median: Hargreaves (1966) has shown that (for a time period and set of riometer locations different from those providing the data that led to Fig. 1) median auroral absorption, A_{30}, of 30 MHz cosmic noise, for vertically aimed riometer antennas

$$A_{30}(\text{dB}) = (Q(\%)/2200)^{1/3.5}$$

(3) "Equivalent vertical incidence" pattern: Figure 1 is derived from data taken with riometers whose antennas were pointed at the celestial pole. An equivalent pattern for vertically aimed antennas is found, in effect, by multiplying the median values found in (2) by $\sin(\varphi_D)$ where φ_D is the geographic latitude of the D-region point.

(4) Variation with frequency: median auroral absorption, A_f, of radio waves of frequency, f, is assumed given by

$$A_f = A_{30} \times \frac{\nu^2 + (30 + f_H)^2}{\nu^2 + (f + f_H)^2}$$

where ν is the electronic collision frequency (in MHz) and f_H is the gyrofrequency at D-layer heights. A simple approach (probably as satisfactory) could be taken from Lerfald et al (1964) using inverse power of frequency (varying between 1.5 and 1.9).

(5) Height of occurrence: the height of the (thin) absorbing region, h_D, and therefore, the magnitude of the electronic collision frequency, ν, depend on local geomagnetic time (LGT):

LGT	0800-1600	1600-2000	2000-0400	0400-0800
h_D, KM	75	83	90	83
ν, MHz	1.913	0.667	0.157	0.667

(6) Obliquity correction: for the radio ray obliquely incident on the D layer at an angle, i_D, A_f is multiplied by $\sec(i_D)$.

(7) Seasonal variation: the seasonal variation has not been precisely defined. There seems to be agreement among various workers (e.g., Hargreaves, 1969, and Hook, 1968) that the daytime absorption is enhanced during winter; and Hook's analysis suggests that at night auroral absorption is more frequent (intense) during summer. It is assumed that the pattern in Fig. 1, depending as it does on (almost) two full years of data, represents the equinox and that the ratio of absorption in dB at winter noon ($\delta = -23.5^\circ$, LGT = 12 hr) is twice that at summer noon ($\delta = +23.5^\circ$, LGT = 12 hr). On the other hand, the absorption at summer midnight is assumed twice that at winter midnight. The correction factor (applied to A_f) is therefore, assumed to be

$$1.0 - 0.8359 \sin\delta \cdot \cos(15 \cdot T)^\circ$$

where δ is the solar declination and T is Local Geomagnetic Time in hours (Agy, 1967).

(8) Solar cycle variation: this is even less well defined than the seasonal variation. A quick look at Hook's results (1968), a comparison with the pattern of Fig. 1, and determination of a mean sunspot number (SSN) for each of the two years considered by Hook (~ 190 for 1958 and ~ 10 for 1964) and for the two year period represented by Fig. 1 (~ 100) suggest an additive latitude correction (in degrees): 1.11 - .0111 × SSN, and the following factor to correct % time: (.778 + .00222 × SSN).

The ITS prediction program (Barghausen et al, 1969) presently requires knowledge of the electron gyrofrequency, for computation of absorption, and of Rawer's "modified dip", the latitude coordinate used in the numerical maps of the F-layer parameters. The gyrofrequency is also needed for the computation of auroral absorption, A_f, in item (4) above, and the (direction of the) earth's field is necessary if we are to treat auroral clutter geometry within the framework of our model. All of these requirements are met through calling on the computer to synthesize the components of the geomagnetic field from the coefficients derived by Jensen and Cain (1962).

3. PROCEDURE

Computations of auroral absorption are initiated by making solar cycle corrections (section 2, item 8) in the pattern of Fig. 1. Most of the details of the computational procedure following this have been given earlier (Agy, 1970) and will not be repeated here. In Fig. 2, one of the ray paths is represented, the dots along it indicating those points whose geographic locations are required so that the appropriate ionospheric parameters may be computed. The dashed lines in Fig. 2 represent options that must be considered: the radio wave may be returned to earth by the E layer, it may pass through the F layer, or (for the ITS model) it may be reflected upwards from the E layer after F-layer reflection. Computations are made for all the ray paths at a specified interval between set limits in vertical take-off angle and in azimuth. Microfilm records of contour (azimuthal equidistant) maps are produced by a plotter controlled by the computer. Each auroral absorption contour may be interpreted as a line connecting those points on the surface of the earth from which the radar returns undergo the amount of auroral absorption indicated by the contour label.

Auroral "clutter" affecting the HF radar returns may be produced by scattering from auroral (field-aligned) ionization. When perpendicularity between the radio ray and the magnetic field direction occurs, the wanted signal may be masked by relatively strong auroral backscatter if its time delay coincides with that of the ground-scattered radar returns. In addition to such direct "interference", the return may be affected by scattering of energy in the radar beam by (perhaps) rapidly changing field-aligned irregularities. In this case, perpendicularity is relatively unimportant.

The "target area" maps show the area of the earth's surface reached by the radar beam at a given frequency and under given conditions (time, month, sunspot number) for the ionospheric model described in section 2. A contour represents those points on the ground reached by rays making an angle with the geomagnetic field (at the clutter level) given by the contour label. In this case, however, the contours have no particular significance.

The "location" maps show areas at the clutter height in the ionosphere through which the radar beam travels in reaching the "target area" described above. The areas outlined in the "location" maps, then, are the regions where auroral scatter may occur to modify the characteristics of the radar returns without necessarily masking them. Some degree of completeness could be achieved here, if time delay information were also given. For the present, however, the contours (near 90°) represent locations from which direct auroral backscatter may occur, without regard to its time delay. (To be consistent, the effective area for the "upgoing" maps should be larger than that shown in order to include energy in the entire antenna beam not actually reflected before it reaches the clutter height.) The location of the "auroral oval" (Feldstyn, 1963) is also indicated, the boundaries of which are plotted as dotted lines.

4. RESULTS

Auroral absorption maps for one hypothetical station (Winnipeg), for two sunspot numbers (100 and 0), two months (June and December), two greenwich times (0000 and 1200), and one frequency (12 MHz) are shown in Figs. 4-6. Figure 4 gives the maps for June, sunspot number 100. Figure 4a, for example, indicates that for 0000 GMT (1730 LMT), 12 MHz radio waves are propagated by the E layer for the lower takeoff angles, the uncontoured area nearer the station lying within the E-layer skip zone. In this case, F-layer coverage is limited, as shown in Fig. 4b, to those angles of takeoff allowing the 12 MHz radiation to penetrate the E layer. From Fig. 4c it is seen that (at 0530 LMT) the E-layer propagation is not possible toward the west on the daylit side of the terminator (represented by the heavy dashed line marked N on one side for "night" and D on the other for "day") and in Fig. 4d the F-layer coverage is seen to extend much farther to the west since no E-layer cut-off occurs in that direction. To the east, however, the F-layer coverage is quite limited. For both 0000 GMT and 1200 GMT, E- and F-layer coverage appears to overlap. June for a sunspot number of 0 gives much more limited propagation of 12 MHz (in the direction toward midday) as given in Figs. 5a and 5c, the single heavy "boundary" on the right side (east) of Fig. 5c suggesting that E-layer propagation fails between 0° and 2.5° take-off so that the plotted "area" of coverage becomes a single line. The effect of the lower sunspot number is also evident in Figs. 5b and 5d, the F-layer skip zone being larger here than for Fig. 4 and the coverage to the west being limited by F-layer penetration even for low angles. The

irregular outer boundaries of the F-layer maps are caused by the fact that relatively large increments --2.5° -- in azimuth and take-off angle are used in the computations. Comparison of contour labels on the E-layer (F-layer) maps drawn for the same Greenwich time for the two different sunspot numbers indicate that the solar cycle correction is by no means a major one, the most serious differences between the maps being those caused by the solar cycle effect on the E-layer (F-layer parameters. Figure 6 gives the auroral absorption maps for December, all F-layer propagation, since the E-layer will not propagate radio waves at 12 MHz. For sunspot number 100, afternoon (local time) F-layer coverage is "complete" while for early morning, coverage is limited to a sector to the east of the station. For the lower solar activity, Fig. 6c, the complete coverage shown in Fig. 6a no longer occurs; it is now limited to a sector to the west. In early morning for sunspot number of 0 shown in Fig. 6d the limitation is more severe than that seen in Fig. 6b.

For the auroral clutter maps, the areas of coverage are shown on the "target area" maps in Figs. 7-10, and, of course, the areas shown are identical for the upgoing and downgoing rays. These maps represent the areas on the ground corresponding to the one-hop radar returns. The "location" maps, on the other hand, show the ionospheric areas (at the clutter height) through which the radar signal passes, and the dotted lines bound the charted location of the auroral oval. The total map output for the clutter geometry computations will be four times as great as for auroral absorption, since upgoing and downgoing rays must be considered and since for each ray, both target area and location are of some interest. Only some of the more interesting maps are shown here.

The maps representing propagation by the E layer show no contours, i.e., none of the rays bent back toward the earth by the E layer reach perpendicularity with the field lines (at least, at the clutter height specified). All the maps shown are for F-layer propagation. In Fig. 7, the maps for December, sunspot number 100, 0000 GMT are shown, Fig. 7a shows only two contours --95° and 100°-- indicating that for these conditions, and for the upgoing ray, perpendicularity is not achieved. For the downgoing ray the pattern is altogether different, and there is a 90° contour. Figure 7c indicates that the upgoing rays, which eventually reach the earth after reflection by the F layer, do not pass through the auroral oval whose southern boundary is shown cutting across Hudson's Bay. Figure 7d, however, suggests that the 90° contour crosses the auroral oval just west of the 60th west meridian. On the west the perpendicularity condition occurs well south of the auroral oval. In Fig. 8 "location" maps are shown for December, 0 sunspot number for both 0000 GMT and 1200 GMT. The change in location of the auroral oval with time should be noted, but, because of the limited coverage, conditions for a "cluttered" return do not occur. "Location" maps for June, 100 sunspot number and 0 sunspot number are shown in Fig. 9 and Fig. 10 respectively. Slight, but significant, shifts in location of the contours are evident from comparisons among the figures. The differences that are most evident, however, are those resulting from the very marked changes in coverage that have already been noted in the auroral absorption maps.

5. DISCUSSION

The "modified ray trace" described here is essentially identical to the approach given earlier (Agy, 1970). The ionospheric model used is the two-layer model referred to in the ITS HF circuit performance prediction program (Barghausen et al, 1969). The E layer is fixed in height and the distribution of electron density with height for both layers is parabolic (quasi-parabolic here -- a minor change The space between the layers is un-ionized. Shimazaki's formula (1955) is used, with a correction for retardation in the E layer, to derive hmaxF2 from the M3000F2 factor.

Desirable changes in the ionospheric model include: filling the valley between the layers (in order to make a more realistic correction for F-layer measurements affected by retardation in the ionized space below the F layer) and introduction of the F1 layer. Consideration of tilts is desirable, but care is needed since a "tilt" is probably best described as a "height-varying horizontal gradient" and the direction of the gradient is only rarely in the plane of propagation. A very complex picture develops that has not to date been given the study it requires.

The aim should be to develop a model that, first of all, is consistent with the measurements made (or with the values representing these measurements taken from the numerical maps (Jones and Gallet, 1962)) and that can be handled expeditiously by the computer. (The computer may reasonably be considered a necessity rather than a convenience.) For propagation via such an ionosphere, an adaptation of the ray trace approach commends itself so that for appropriate points along the path, we may make the necessary prediction of ionospheric parameters and use these numbers as they arise in order to escape the untenable assumption of a uniform ionosphere over the entire path.

The auroral absorption computations depend, to some extent, on the ray path computations, since the location of the D-layer penetration point is determined by the deviative effects of the "propagating" layers, and the amount of auroral absorption computed depends on the location of this point. In addition, however, there is a need to develop a more credible exploitation of riometer data. While the pattern in Fig. 1 is derived from about two years of data, Canadian riometer records for almost a solar cycle are awaiting reduction. The transformation from % time to median absorption might be dispensed with entirely, but at the very least, should be re-examined. The seasonal and solar cycle variations used here (different from those used earlier (Agy, 1970)) are thought to be based on insufficient information; they sould be reformulated. Magnetic activity is an important consideration. The existence of

geographic variations, i. e., variations with longitude, is debatable. The additional Canadian data will be invaluable.

Auroral clutter geometry computations will also depend on the ray path, and therefore, on the ionospheric model used. More recent sets of geomagnetic field coefficients are available; in particular, those derived by Cain and Sweeney (1970) could be used to advantage, representing, as they do, somewhat greater precision in the field determined. We may modify the field at ionospheric (clutter) heights by devising a suitable model of the auroral electrojet as a further refinement.

6. CONCLUSIONS

A "modified ray-trace" approach has been developed specifically for application to the problems of HF radar at high latitudes. In particular, computations have been made of auroral absorption and (as an aid in determining the source of auroral clutter) of the angles between radio ray and geomagnetic field direction. The results have been displayed on contoured maps.

Work is still to be done on the ionospheric model and on the ray trace method with the view to obtaining an acceptable computer simulation of the median physical situation, and eventually, perhaps, of "real time" ionospheric propagation conditions.

Finally, automatically drawn maps bearing contours of arbitrary propagation parameters are recommended for wider use in HF predictions at all latitudes and for HF broadcasting, for example, as well as for HF radar.

REFERENCES

Agy, V. (1967), Geomagnetic coordinates and geomagnetic time, Physics of Geomagnetic Phenomena, Appendix 1, p 1329, Edited by S. Matsushita and Wallace H. Campbell. Academic Press.

Agy, V. (1970), HF radar and auroral absorption, Radio Sci. 5, 1317-1324.

Barghausen, A. F., J. W. Finney, L. L. Proctor, and L. D. Schultz (1969), Predicting long-term operational parameters of high frequency sky-wave telecommunication systems, ESSA Tech. Rep. ERL 110-ITS 78.

Cain, J. C. and R. E. Sweeney (1970), Magnetic field mapping of the inner magnetosphere, J. Geophys. Res. 75, 4360-4362.

Croft, T., and H. Hoogasian (1968), Exact ray calculations in a quasiparabolic ionosphere with no magnetic field, Radio Sci. 3, 69-74.

Gassmann, G. (1972), On modelling the arctic ionosphere. This volume.

Hargreaves, J. K. (1966), On the variation of auroral radio absorption with geomagnetic activity, Planet Space Sci. 14, 991-1006.

Hargreaves, J. K. (1969), Auroral absorption of HF radio waves in the ionosphere -- a review of results from the first decade of riometry, Proc. IEEE 57, 1348-1378.

Hartz, T. R., L. E. Montbriand, and E. L. Vogan (1963), A study of auroral absorption at 30 Mc/s, Can. J. Phys. 41, 581-595.

Hook, J. L. (1968), Morphology of auroral zone radio wave absorption in the Alaska sector, J. Atmos. Terr. Phys. 30, 1341-1351.

Jensen, D. C. and J. C. Cain (1962), An interim geomagnetic field (abstract), J. Geophys. Res. 67, 3568-3569.

Jones, W. B. and R. M. Gallet (1962), The representation of diurnal and geographic variations of ionospheric data by numerical methods, Telecom. J., No. 5, 3-23.

Jones, W. B. and D. L. Obitts (1970), Global representation of annual and solar cycle variations of foF2 monthly median 1954-1958, Telecommunications Research Report, OT/ITSR R3.

Lerfald, G. M., C. G. Little, and R. Parthasarathy (1964), D Region electron density profiles during auroras, J. Geophys. Res. 69, 2857-2860.

Millman, G. (1969) Field aligned ionization scatter geometry, J. Geophys. Res. 74, 900-905.

Nisbet, J. S., On the calculation and use of a simple ionospheric model, Radio Sci. 6, 437-464.

Shimazaki, T. (1955), World wide daily variations in the height of the maximum electron density of the ionospheric F2 layer, J. Radio Res. Labs., Japan, 2, 85-97.

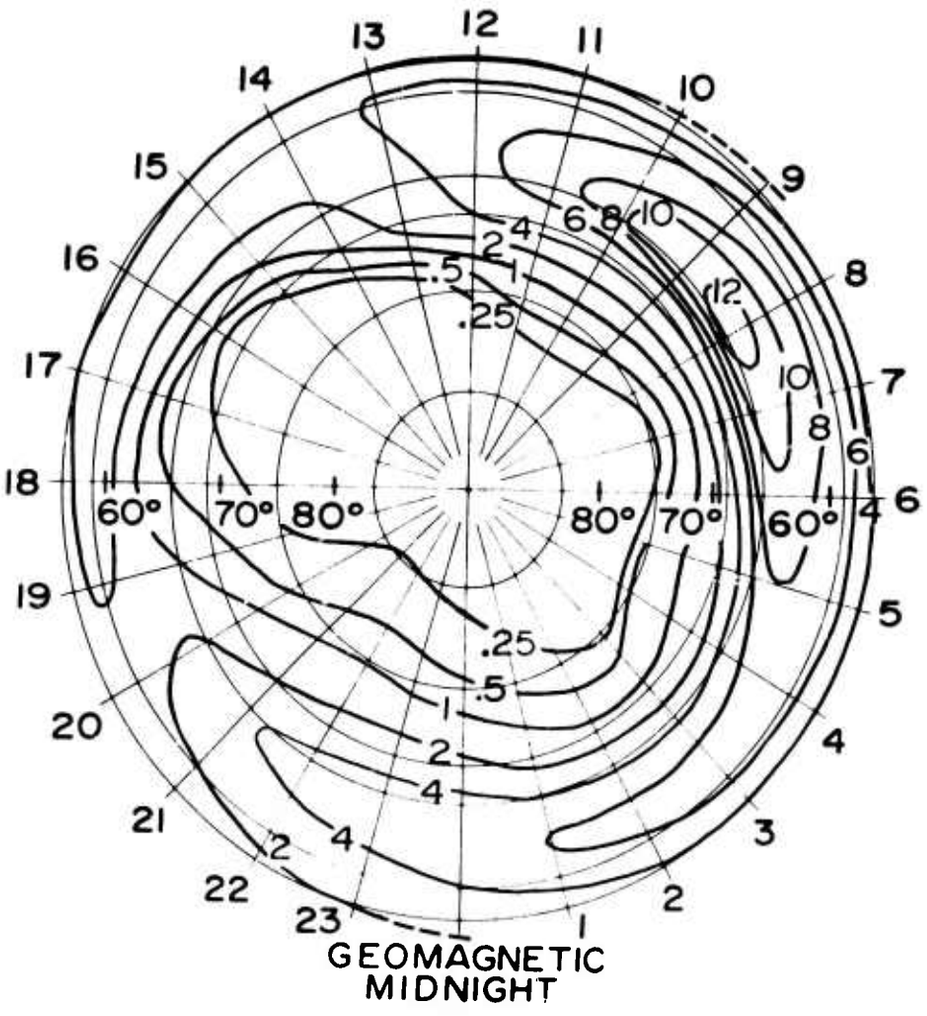

Fig. 1 Percent time auroral absorption of 30 MHz cosmic noise ≥ 1 dB.

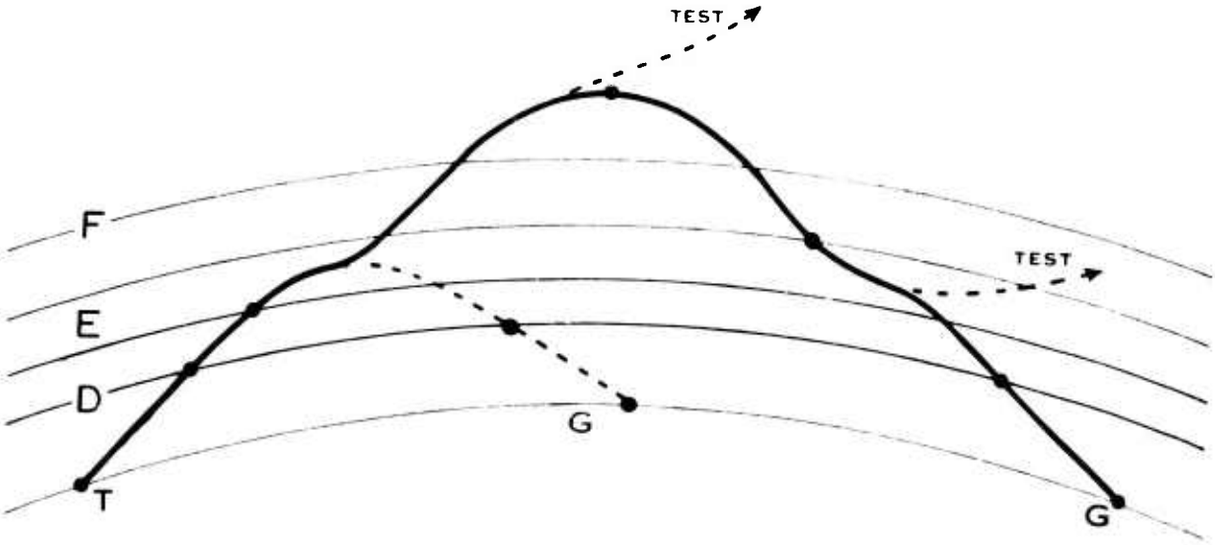

Fig. 2 Ray path geometry, auroral absorption.

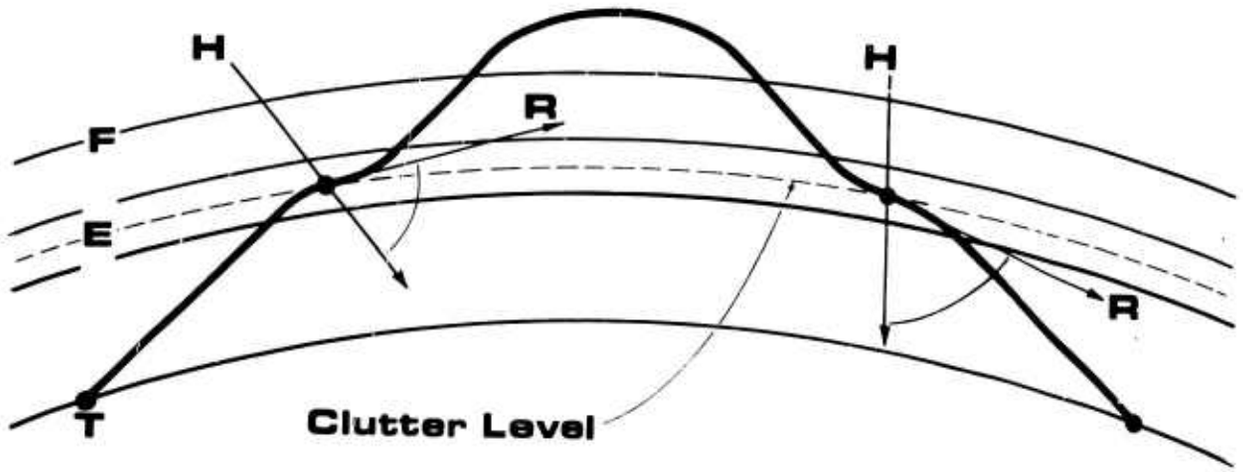

Fig.3 Ray path geometry, auroral clutter.

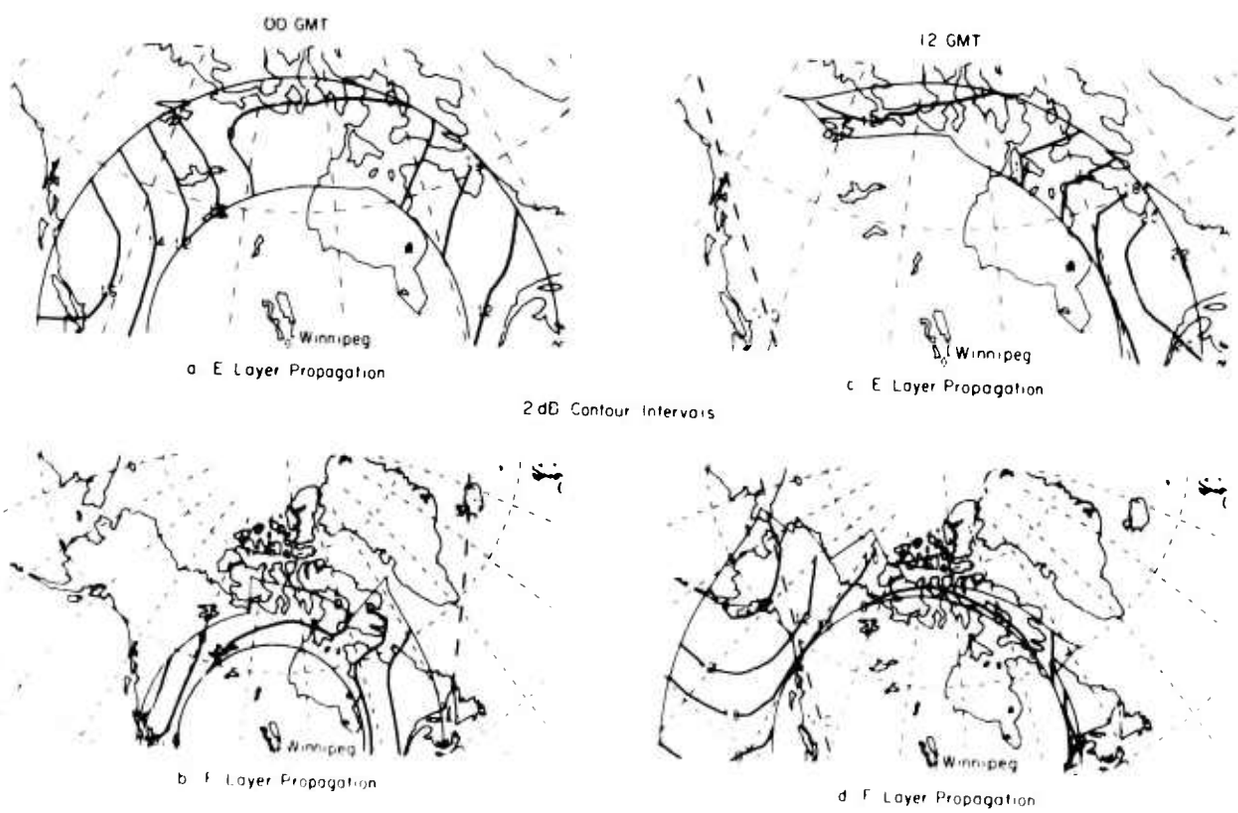

Fig.4 HF radar auroral absorption, Winnipeg, 12 MHz, June, sunspot number 100.
a. 00 GMT, E-layer propagation
b. 00 GMT, F-layer propagation
c. 12 GMT, E-layer propagation
d. 12 GMT, F-layer propagation

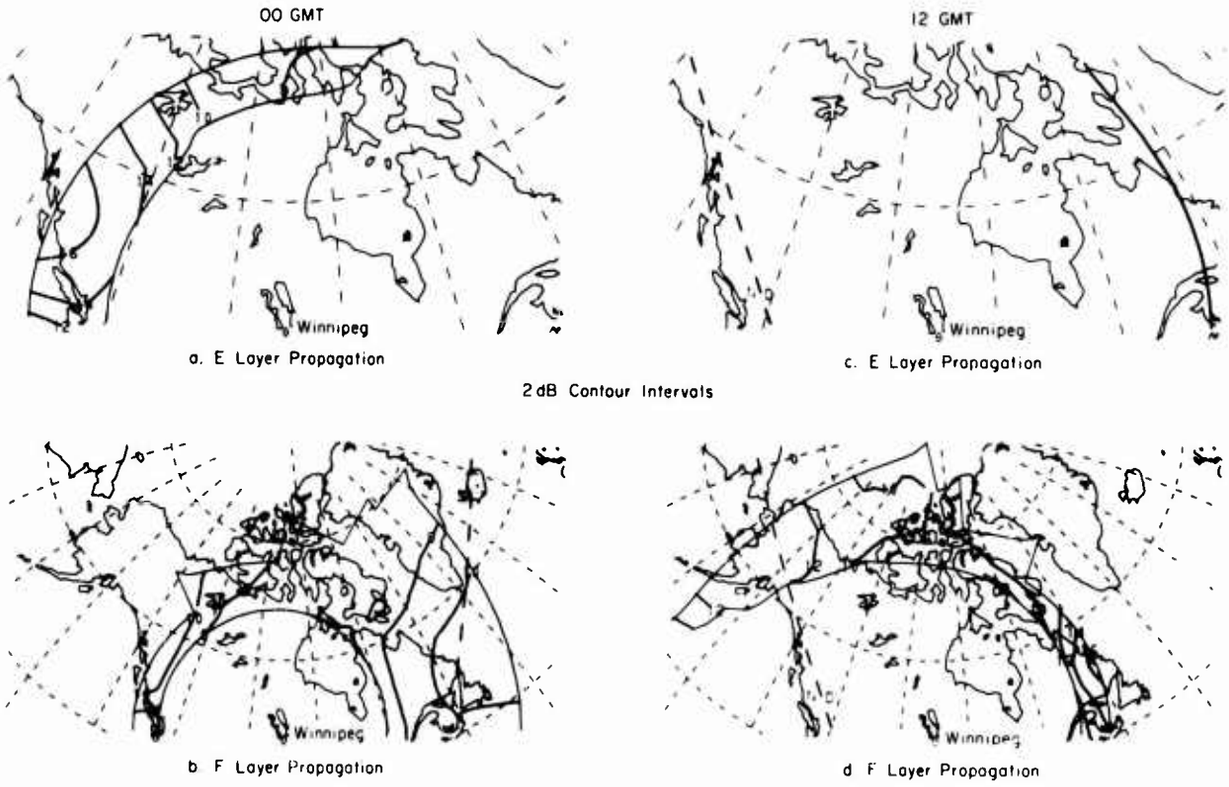

Fig.5 HF radar auroral absorption, Winnipeg, 12 MHz, June, sunspot number 0.
a. 00 GMT, E-layer propagation
b. 00 GMT, F-layer propagation
c. 12 GMT, E-layer propagation
d. 12 GMT, F-layer propagation

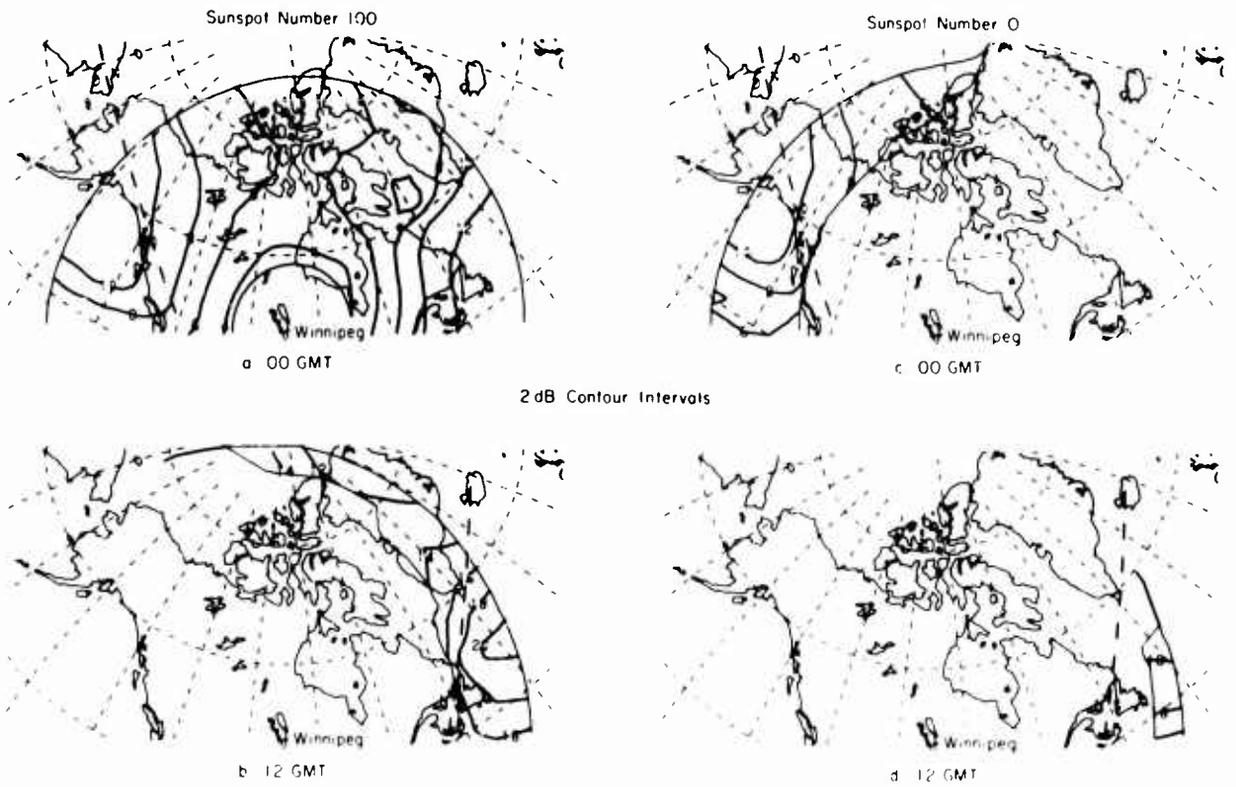

Fig.6 HF radar auroral absorption, Winnipeg, 12 MHz, December, F-layer propagation.
a. Sunspot number 100, 00 GMT
b. Sunspot number 100, 12 GMT
c. Sunspot number 0, 00 GMT
d. Sunspot number 0, 12 GMT

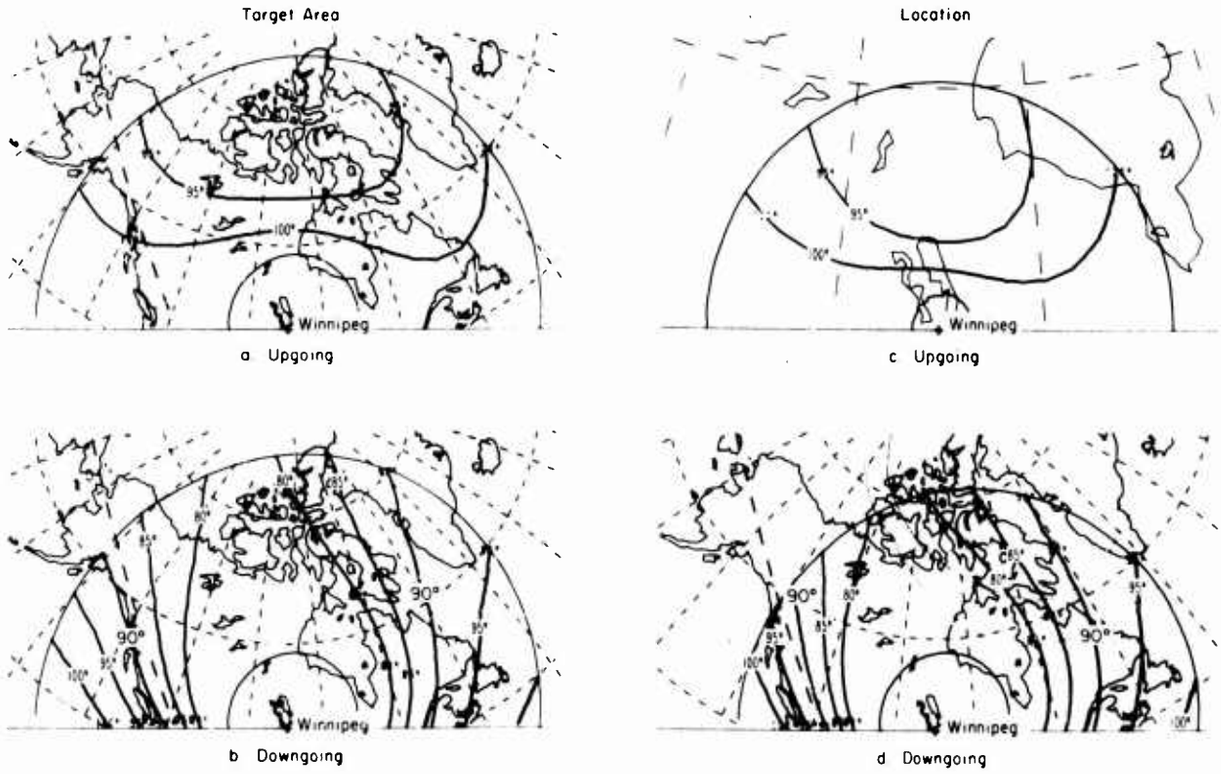

Fig.7 Auroral clutter (105 km F-layer propagation height), Winnipeg, 12 MHz, December, sunspot number 100, 00 GMT.

a. Target area, upgoing
b. Target area, downgoing
c. Location, upgoing
d. Location, downgoing

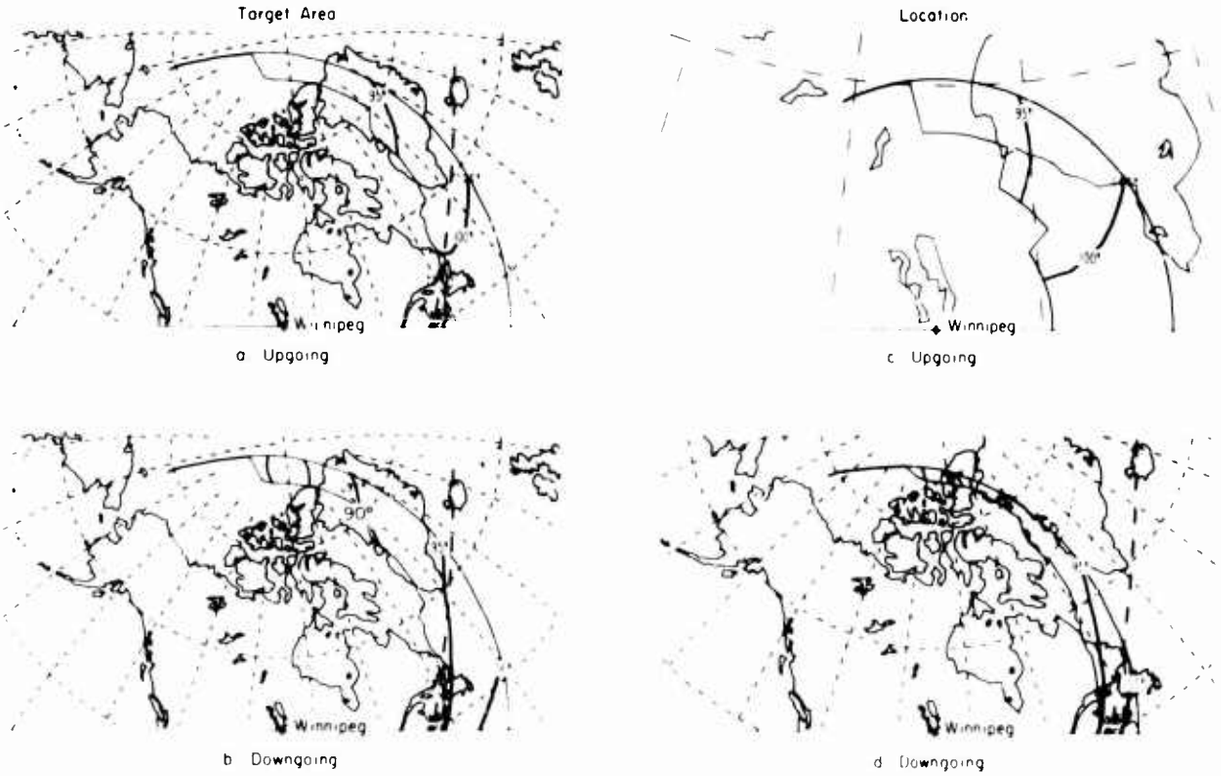

Fig.8 Auroral clutter (105 km F-layer propagation height), Winnipeg, 12 MHz, December, sunspot number 100, 12 GMT.

a. Target area, upgoing
b. Target area, downgoing
c. Location, upgoing
d. Location, downgoing

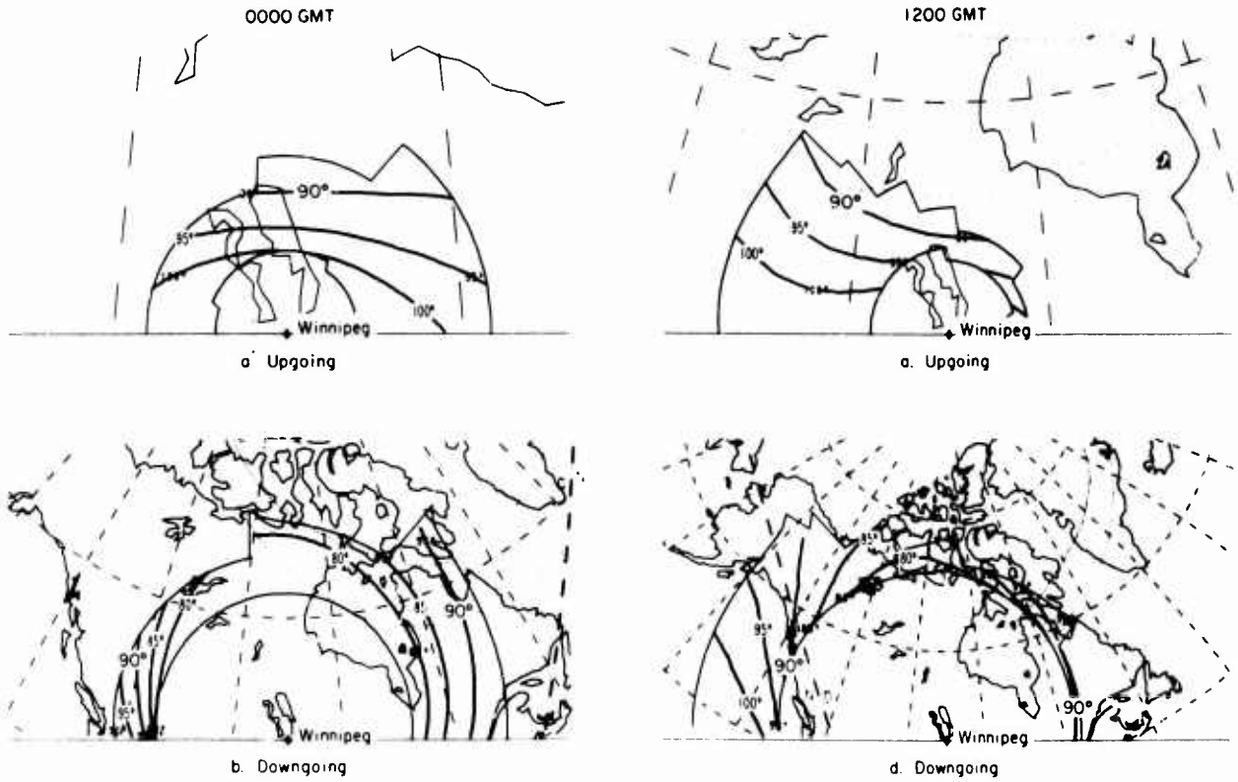

Fig.9 Auroral clutter (105 km F-layer propagation height), Winnipeg, 12 MHz, June, sunspot number 100, location.

a. 00 GMT, upgoing
b. 00 GMT, downgoing
c. 12 GMT, upgoing
d. 12 GMT, downgoing

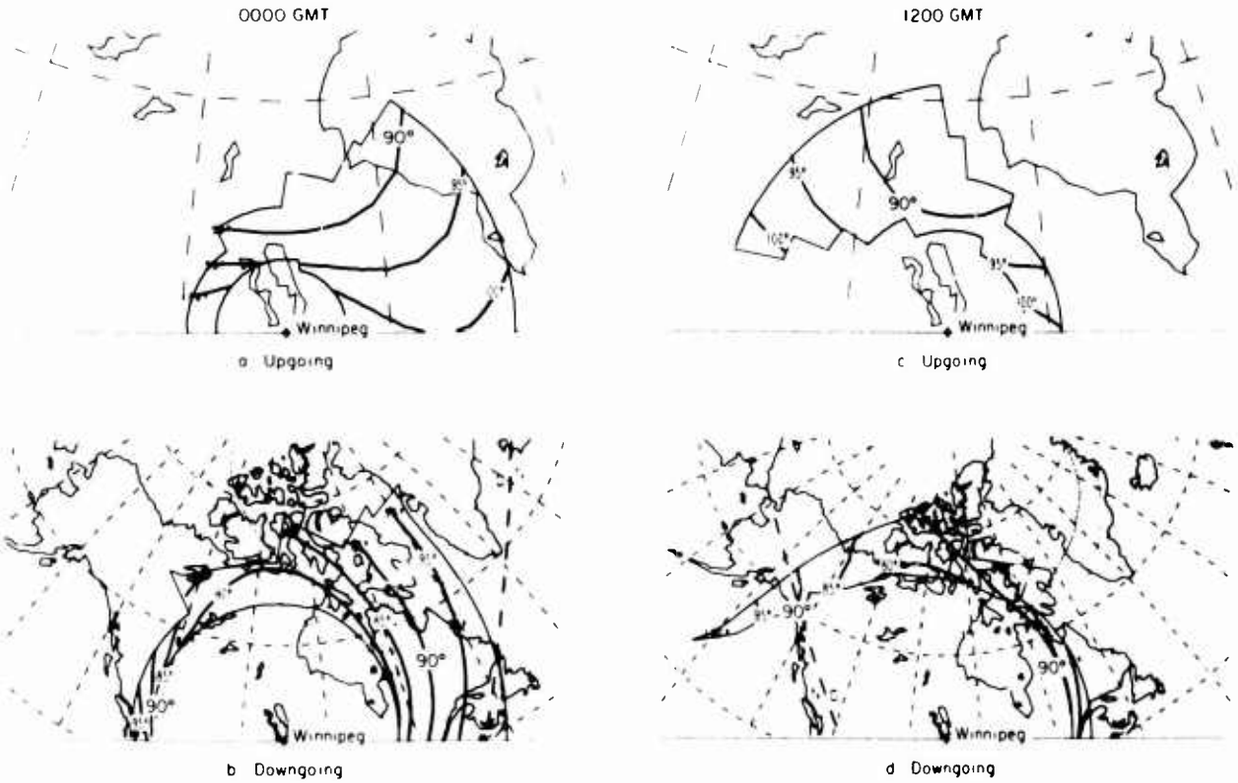

Fig.10 Auroral clutter (105 km F-layer propagation height), Winnipeg, 12 MHz, June, sunspot number 0, location.

a. 00 GMT, upgoing
b. 00 GMT, downgoing
c. 12 GMT, upgoing
d. 12 GMT, downgoing

SESSION VI

HF PROPAGATION-BACKSCATTER

CHAIRMAN'S REPORT

by Howard F.Bates

This summary represents my ideas of how the results presented in this session fit together and into the overall picture of high latitude HF backscatter.

Ionospheric backscatter echoes are regularly observed in the high latitudes. All of the HF backscatter echoes originating from scatter from ionospheric irregularities show strong aspect sensitivity to the magnetic field. Although few quantitative measurements exist, those made indicate that at HF the aspect sensitive decrease in the backscatter cross-section for both E- and F-layer echoes is at least 5 dB per degree of off-perpendicularity. Strict aspect sensitivity is therefore an excellent assumption to make when analyzing HF backscatter from the E and F layers. This result also indicates that, for the E region, the aspect sensitivity is nearly constant at a value of the order of 10 dB per degree of off-perpendicularity from mid-HF through UHF bands, or over a thousand-fold in frequency.

Ray tracing analysis shows that off the magnetic meridian there exists regions of perpendicularity between ray and magnetic field for which no corresponding region exists on the magnetic meridian. For example, perpendicularity is achieved at E-region heights on long-range down-coming rays at directions off the magnetic meridian. Such an echo mode was occasionally identified in the College records, but it was not easy to explain because considerable E-layer refraction had to be involved for it to be scatter originating on the magnetic meridian. The ray-tracing results suggest, however, that the scatter originated somewhat off the magnetic meridian, thereby requiring less E-layer refraction to achieve perpendicularity than for propagation along the meridian.

Some of the ionospheric irregularities producing echoes are closely associated with the aurora; others, such as the oblique spread-F echo, are not.

HF auroral echoes have been found to originate in both the E and F layers; ordinary ionospheric refraction in both the E and F layers is utilized to satisfy the aspect sensitivity condition, i.e., to bring the ray into perpendicularity with the magnetic field. E- and F-layer irregularities produced by the aurora occur simultaneously, the type of echo observed, however, is strongly dependent upon the latitude of the observer. Close to the auroral belt, such as in Alaska or Iceland during the night, auroral backscatter from the E layer in the form of slant-E echoes predominate on the records. From sites well away from the auroral belt, however, F-layer or F-supported E-layer echoes are the only ones observed. When this distance dependence is taken into account, much of the apparently contradictory auroral backscatter results are found to be in actual agreement.

Slant-F echoes (echoes that are directly associated with the occurrence of spread-F) correlate poorly, if at all, with the aurora. Some evidence exists that the irregularities producing the slant-F echo show a sharp equatorward boundary similar to that of the high latitude scintillation zone. There is evidence that the high latitude scintillation and spread-F zones coincide, although further work is necessary to show this result.

It seems plausible at this point that, in the near future, realistic modelling of the production and propagation of high latitude backscatter will be possible, at least on a statistical basis.

In conclusion, the results presented at this meeting fit neatly into the current picture of high latitude backscattering irregularities in the ionosphere.

DISCUSSION

P Halley

With the formulations of Agy Hargreaves and the maps of Hartz we can calculate everywhere at each hour the absorption median value. Have you some means of the upper and lower quartiles or some statistical dispersion coefficient.

T Hartz

In the study of Auroral Absorption by Hartz et al (Can Journ Phys 41, 581. 1963) the data were obtained at one absorption level only, namely 1 decibel, and we gave the percentage of time this level was exceeded. Hargreaves has published values at several other levels. However, we have observed, as have other workers, that the absorption at night tends to be higher than at other time of day, but such periods are of quite short duration, whereas during the day the absorption period are longer though somewhat less intense.

L Liszka

We observed also the kind of echoes as described by Dr Olesen. We ascribed them to gradient reflections from the trough. As it has been shown by Bowman there is always an E_s patch associated with the trough. Thus both oblique E_s echo and F echo may be obtained for certain configurations of the station and the trough. This explains two maxima of the occurrence curve of SEC observed by Dr Olesen. Definite answer will be obtained by measurements of angle of arrival and angle of incidence which are planned in Kiruna.

J Olesen

I find it difficulat to understand why a condition at the equatorial electrojet which give the ionospheric effects of slant E and scattering of other kinds should not be of the same nature and have the same effects in the auroral electrojet case. Also the detailed correlation with magnetic and scintillation recordings seems to me to fit better to a ion-acoustic wave theory. Dr Bates' statement on auroral break up correlation with slant E also supports the ion-acoustic model.

K Toman

How do we interpret the velocities we are measuring. Auroral radio echoes could show a rate of change of range which might be due to an apparent effect of rapid spatial changes in the excitation process.

W G Chesnut

Rangerate measurements have at times given velocities of 50 km/s. This reflects the motion of the ionizing source. The corresponding Doppler frequency would be outside our frequency passband.

SESSION VII

SUMMARIES, RECOMMENDATIONS, AND FUTURE INVESTIGATIONS

A G McNamara

Radio Aurora

The morphology of radio aurora is being studied in a number of institutions, the results of which have been discussed in several papers at this conference. Continuing investigations will help to provide clues to the radio aurora scattering process through the conditions which initiate it. In particular, associations with energetic particles and geomagnetic and electric fields are particularly relevant.

VHF and UHF studies have been carried out and are continuing in several institutions. I believe it is obvious that although the field of plasma instabilities has opened the door in recent years for eventual understanding of the scattering mechanism, we are still a long way from passing through that door. At the present time, most of the interpretations of observations are built around the two-stream generation of ion acoustic waves, chiefly because this is about the only available theory which easily predict generation of microstructure small enough to scatter short electromagnetic waves, and which provides some physical predictions of phenomena which can be tested experimentally. This is a linear theory and predicts only the critical conditions for acoustic instability. As such, it is limited in its capabilities.

Both UHF and VHF scatter observations fail to pass all the tests of the linear two-stream mechanism for excitation of plasma waves. However, as might be expected, the UHF results appear to approach asymptotically some of the two-stream characteristics. VHF observations however, are partially amenable to two-stream interpretation, but fail notably in many circumstances. This is not unexpected since other competing instability mechanisms may more readily develop, and since the larger scale sizes will be more susceptable to non-linear processes.

Doppler spectra measurements have proved particularly powerful in studying the scattering mechanism, and have provided direct evidence of ion acoustic wave instabilities. However, small un-shifted, non-line spectra are observed frequently at VHF and occassionally at UHF. (A c w Doppler system is in use at the University of Western Ontario. Pulse Doppler capability is presently being developed for the backscatter radar network of the National Research Council).

Aspect attenuation has been observed to be a very rapid function of angle at UHF and also in some VHF situations. However, many VHF observations show equally positive evidence of no very strong aspect sensitivity. This may well be the result of strong non-linear effects in the instability or due to a multiplicity of plasma instability mechanisms which could arise in the intense excitation of the auroral zone.

Only a few papers on polarization measurements of radio aurora have been presented at this meeting. However, I feel that polarization should provide much valuable information since the polarization characteristics are intimately related to the scattering mechanism. I believe that these should be pursued more vigorously.

Rocket flights have provided direct measurements of auroral ionization from rockets flown in Canada and Scandinavia. These techniques provide time and spatial resolution unmatched by the ground-based electromagnetic techniques. An active program of rocket measurements of radio aurora os continuing in Canada, complementing the ground-based radio program.

The use of barium seeding of the ionosphere is a technique which will see much future application in studying ambient electric fields, and for certain instability mechanisms particularly those involving strong density gradients.

Finally, I wish to advocate the laboratory simulation of ionospheric scattering from plasma instabilities. To my knowledge, the program at the Battelle Institute is the only one of its kind in operation. The potential value of such experiments, particularly in quantifying non-linear mechanisms and effects, appears to be enormous.

W G Chesnut

Radar aurora

Ever since 1950 when Booker presented a theory based upon Born approximation for scattering of radar waves from irregularities in electron density in the auroral E-region there has been considerable speculation and theoretical estimations of the detailed properties of the scattering environment. Recent multifrequency radar measurements in the VHF-UHF bands have provided information concerning the structure of the density fluctuations.

A report at the meeting by McNamara of rocket measurement of the density fluctuations provide the first in situ confirmation of the frequency trends discovered by radar. More important, the rocket measurements have also given a direct measurement of the r m s amplitude of the density fluctuations. Though much is still unknown about details, there can now be little doubt that the observed radar scattering can be described by Born approximation.

Much experimental attention is directed toward making measurements that will reveal the processes that cause structuring of the auroral E-region into density irregularities. In view of the success of Doppler measurements in explaining the auroral electrojet scattering, much recent auroral radar work has been similarly directed. Measurements by Hofstee and Forsyth at 40 MHz, Camnit, Tsunoda and Barczys at 143 MHz and 226 MHz, Chesnut, Hodges and Leadabrand at many VHF-UHF frequencies, and Hagfors at 1288 MHz (see paper no 5 for references) have given results that are consistent- at times - with the Farley instability mechanism.

However, all experimenters find other characteristics that require irregularity generating mechanisms other than that proposed by Farley. It is clear that further Doppler measurements should be made using, perhaps, other geometries to understand irregularity generating processes. The measurements may also help to sort-out inconsistencies such as currently exists regarding the source of irregularities in afternoon diffuse aurora.

Research continues into the detailed relationships between radar aurora and other auroral phenomena. Work was reported on detailed relationships between radar and visual aurora (Bates, Chesnut, Lange-Hesse) radar aurora and magnetic pertubations (Lange-Hesse), and radar aurora and particle precipitation (Bates, Chesnut and Hagfors). It was suggested that the radar/visual correlations need to be investigated for aurora other than the quiescent forms. Comparisons with satellite measured precipitations are just becoming available. The data are too recent to have been well digested, but do indicate that there is much that we do not know.

The basic scattering properties of radar aurora at VHF-UHF frequencies are probably known. There are some questions regarding aspect sensitivity - how to measure it (Forsyth) - and meaning of large angle aspect sensitivity measurements (McNamara and Chesnut). The reports of a very weak - or nonexistent - frequency dependence of aspect sensitivity near specularity over a frequency range from 15 MHz (Bates) to 3000 MHz (Chesnut) were very unsettling to some attenders. Clearly more thought - if not more measurements are needed.

Recent measurements from the equatorial electrojet scattering experiments (Balsley) and a profusion of new, theoretical explanations for the production of equatorial E-region irregularities have provided those concerned with the radar aurora with new, possible explanations of the aurora observations. The ingredients that are currently lacking from the experimentalist's point of view is guidance by the plasma instability theoreticians as to what environmental conditions need to be measured to certify or reject the theoretical proposals.

Transmission

Much experimental work concerning the morphology of scintillation was presented. This information, obtained by satellite beacon and radio-star measurements is directly useful in aiding system designers in determining the frequency of occurrence and locations of possible propagation difficulties. However, the magnitude of the propagation effects does not seem to be well documented. Indeed there is even some controversy whether radio star interferometer measurements of propagation perturbations can be directly applied to estimates of radar measurement errors.

Some of these problems will be resolved in the next year or two as a result of radar tracking experiments that were recently initiated by Lincoln Laboratories using the Millstone Hill radar. The radar "skin-tracks" satellites at a frequency of 1288 MHz while the radar simultaneously measures monopulse angle errors of a 400 MHz beacon carried by the same satellite. It is hoped that the data can also be used to validate the applicability of radio-star interferometer data that has been aquired over the past years.

The state of understanding of the origin of the intermediate scale irregularities that are responsible for scintillations is extremely poor. Plasma interchange instabilities in horizontal density gradients has been suggested for F-region irregularities - but not enough is known about instabilities, the environmental conditions, etc, to consider the suggestion as more than a speculation. It was proposed (Chesnut, Liszka) that the more intense scintillation events occur as a result of auroral ionization. It was proposed that these intense effects occur mainly at E- and lower F-region heights. Suitable experimental checks upon this hypothesis seem fairly straight forward.

Future investigations

We report here the future plans of Stanford Research Institute for use of its various radar facilities.

Homer Radar: The multifrequency Homer radar, located on the south coast of Alaska, probes radar aurora over the major central regions of Alaska. The instrument will be used mainly in conjunction with other experimental probes. The most exciting joint experiment will be the measurement of radar aurora directly over SRI's Thomson scatters facility that was recently moved from California to a site slightly north of Fairbanks, Alaska. While radar aurora is measured by the Homer radar, the Thomson scatter radar will probe, directly above itself, the region from which the Homer radar receives its echoes.

Thomson Scatter Facility: For four years, SRI operated a Thomson Scatter Radar in California. The characteristics of this instrument are as follows:

Peak power	:	5 Mega Watts
Frequency	:	1300 MHz
Antenna	:	88 foot fully stearable paraboloid
Antenna Beamwidth	:	0.8^{o}
Antenna Feed	:	Four Horn Monopulse Tracking
Pulse Length	:	Variable up to 1 millisecond
Special pulses	:	10 MHz chirp pulse compressed to 0.25 usecond

In the California ionosphere, electron density profile measurements were made in five minutes. Electron and ion temperature measurements were usually made with fifteen minutes of integration. Ion drift measurements (spectrum assymetries) are measured at the same time.

Over the past year the radar was moved to near Fairbanks, Alaska. It was located in a bowl surrounded by mountains to provide a natural clutter fence. A valley to the north provides a window for the probing of radar aurora - though the minimum aspect angle is nearly 4^{o} off specular from this northerly location.

The radar has been operating successfully for several months. Early data indicate that there are no unforseen problems that would prevent successful acquisition of density, drift and temperature data. The natural ground clutter fence provided by the ring of mountains surrounding the site causes ground clutters to disappear into noise at ranges corresponding to heights of 60 to 70 kilometers. Excellent E-region density measurements have already been obtained.

Over the next year the facility will be operated jointly by SRI (under Mr Murray Baran) and by the Geophysical Institute of the University of Alaska (Prof Howard (Skip) Bates). Present plans call for "shake-down", observations ("see what we can see that may be new"), coordinated measurements with the Homer Radar Facility and other, special auroral probe events.

P A Forsyth

It seems to me that our problems relating to the arctic ionosphere are of two kinds. The first is the morphological description of the phenomena. This attracts people who are interested in physics on the cosmic scale, I am not. But anyway, those people seem to be doing better than the rest of us. The second kind of problem is the study of mechanism on the local scale. Here we are not doing very well. If research is like playing chess, in this particular game Nature seems to be beating each one of us individually and we don't play a very good game of cooperative chess. For example in planning our game we make the mistake of describing our opponents' strategy with too few parameters. At this meeting we have tried to establish the aspect sensitivity and the frequency dependance for auroral scattering. We might just as well try to answer the question "is the average person male or female?" You can average inhomogenous data but it does not improve understanding.

Our second mistake is that we fail to concentrate. In chess and in research that is fatal. If we really are interested in finding out the relationship between particle precipitation, neutral winds, electric fields, electron and ion motions, acoustic and electrostatic waves, photon emissions, scintillations etc..., we should study them all in the same area at the same time, not all in different areas at different times. It occurs to me that the proposal joint U S /Canadian major incoherent scatter facility provides just such an opportunity.

The main characteristics of the proposal are well known. Present thinking is that that will be one transmitter receiver station in the northern USA, with a large (100m?) dish, stearable in the place of the magnetic meridian. Two receive-only stations will be located in Canada, each with a fully stearable (50 m?) dish. In addition to all the usual things that an incoherent scatter system can do such as determine electron concentration, ratios of ion species etc.., this system will be able to study the dynamics of the ionosphere in detail. It will be able to measure the not-quite orthogonal components of motion. In addition, of course, it will be a very good auroral radar. It's location will allow observations on the south side, middle and north side of the mid-latitude trough as well as the auroral ionosphere.

Nevertheless, if this facility comes to pass, the principal opportunity it provides is that of concentrated research. Since it provides a great deal of information about the ionosphere in one region it provides an irresistable incentive to concentrate other measurements in the same area. Surely, we should plan to fly balloons below the region, observe the region from the ground with ionosonds meteor wind radars, VHF auroral radar radars, spectrometers, photometers, riometers , magnetometers, radio interferometers, scintillation monitors and just as many other devices as we can devise. And we must put our data together according to a definite plan, not wait for an AGARD meeting 3000 miles away from home before we find out what our neighbour is doing. This, I think, is the only way we will really uncover what Nature is doing in all these complecated highlatitude processes.

And I hope that if another new-generation incoherent scatter facility is built in Europe that it too will become the focus of a concentrated research effort. If the European one gets built and the North-American ones does not, I hope someone will invite us over to participate in the cooperative program. Certaily, the corresponding reciprocal invitation is already a foregone conclusion.

Money for research is getting scarce everywhere. Let us maximize the return on the money we have by concentrating our efforts. If the meeting has taught us anything it is that we still have very few of the answers regarding the high latitude ionosphere, Almost every measurement that was described here would have been much more meaningful if some other measurement from among those described had been made at the same time and the same place.

Let's not come back to another meeting like this several years from now with another set of measurements that just won't fit together because it was never planned that they should fit together.

G N Taylor

Listening to this meeting, I have been struck by the uncertainity about the detailed spatial correlation of various effects, e g is there any definite association between scintillation and particle precipitation, between the optical aurora and precipitation, between the radar and optical aurora? Is the concept of the auroral oval a useful one for radio propagation purposes? It would be important to resolve these uncertainties before any reliance could be placed in a real time prediction system, which might have continuous data imputs from sensors of varied types. Thanks to topside sounder studies, the gross morphology of electron density in the polar upper F-region is now fairly well known, but the same cannot be said of the bottomside polar ionosphere, which is much more important for propagation predictions. Satellites are unable to move below an altitude of about 200 km, and in these regions, we have had to rely on rocket ascents or conventional l f sounding until recently: The latter technique may fail completely in the presence of high absorption or blanketing E_s - both of which are quite common in polar regions - and may give results which are hard to interpret if the layers are sharply tilted or otherwise distorted. Turning to electron density irregularities, there is a great deal of information about their occurrance and geographical distribution, but when, preparing my own paper I found that their spatial autocorrelation function and amplitudes are very poorly known at high latitudes: both of them are required to estimate radar scattering cross sections.

An important new technique for filling in some of the gaps is Thomson scatter radar. We have been using one of these instruments at Malvern for several years, and find that it can considerably improve knowledge of bottomside electron density profiles especially with respect to a) nonmonotonic profiles, b) changes in profiles during sudden disturbances, such as solar flares, c) investigating the night time E-region. In all 3 cases l f techniques provide at best very incomplete information, while incoherent scatter can give very detailed and complete profiles with excellent time resolution. These advantages will be even more important at high latitudes than at mid-latitudes.

Incoherent scatter is of course much more than a profile measuring technique, as it gives more information about the ionospheric plasma, over a greater height range, than any other ground-based technique, on routine basis. It is thus vital to have this method available for any "case-study" approach to particular events in polar regions. Case-studies are complementary too, and should be formed in parallell with, statistical investigations. As an example of the type of help that incoherent scatter can give to forecasters there is the well known law that $N_e \propto T_e^{-1}$, which certainly holds at mid-latitudes, but is uncertain at high latitudes. This enables me to predict what changes in N_e will follow a sudden heat input, e g from particle precipitation.

The recent suggestion that an incoherent scatter station should be built in Northern Scandinavia is especially important. A station here will be at a high magnetic latitude (L=6), have an abundance of supporting experiments, and be uniquely accessible.

J Aarons

Scintillation
From the morphology point of view the geographical coverage has made considerable advances in its delineations of high latitude patterns, more data, normalized and standardized, still has to be poured into the pot, then both the physics and the geophysics can be studied. Correlations with magnetospheric phenomena will be more possible. With observations in Greenland, Norway, Sweden, Alaska and Canada now going on I would expect more definite numbers in five years.

New areas will be explored and expanded. These include statistical analyses of auroral fadings, frequency dependence etc. Angular and phase fluctuations will be studied more carefully. More interpretive work is needed.

Total electron content
For needs of radar and navigation systems it is necessary to determine the morphology of total electron content (to measure group path delay). It will be necessary to predict it to be of assistance in accurately determing satellite position, the high latitudes represent a challenge in this area.

Backscatter
To determine the upper and lower latitude boundary of the F-layer irregularity region (if an upper latitude F-layer boundary indeed exists) is a need for the future. Backscatter measurements together with scintillation data could do this.

Thus lower latitude probing by backscatter measurements particularly from invariant latitudes of 42° - 45° should be undertaken. Polar backscatter measurements of the type being undertaken by Bates and others will give us the backscatter picture of the irregularities Greenland, Spitzbergen and other data will give us the scintillation morphology.

Origin of irregularities
Low energy electron precipitation is attractive in its low latitude boundary, its ionization in the F-region and its "localized nature" - all these factors correlate well with observations of scintillations, field aligned F-backscatter and spread F. But the presence of polar cap irregularities is at variance with the absence of low energy electron precipitation at the poles (the polar cavity).

G K Hartmann

Satellite beacon studies
Propagation of electromagnetic waves through an inhomogeneous ionosphere usually result in variations in the amplitud , phase and angle-of arrival of the waves as received at the ground. Generally this is called scintillation. Roughly 90 % of the now available scintillation data has been obtained by amplitude measurements, 7% by phase measurements, and 3% by angle of arrival measurements.

Satellite beacons in the HF-, VHF- and UHF range seem to provide a good tool for measuring the above mentioned quantities. However it is evident that only in very few cases have all three quantities been measured simultaneously and - as far as I know - never on a routine basis over a longer period.

If at least two quantities, e g amplitude - and phase (relative phase) measurements (Dispersive-Doppler) could be simultaneously obtained over a longer period one can expect more additional information about the scintillation producing irregularities; hopefully with better resolution than now in order to tackle the fine structure problem by applying specific correlation methods.

The latter seems to be very essential if one wants to decide whether soft protons or soft electrons or both are the cause of the irregularities. All these measurements have to be carried out simultaneously with the most reliable height measuring method which is now available or can be conceived for the future. If there is no actual height information available we have to assume for the most calculations a mean height for the scintillation producing irregularities. This implies that a three dimensional problem is treated as a two dimensional one.

At present there are in Europe - for polar scintillation studies - no other beacon satellites obserable than the 5 polar orbiting US-NNSS satellites, transmitting coherently 150 MHz and 400 MHz. Dispersive-Doppler measurements (relative phase measurements between 150 MHz and 400 MHz) give the change to study phase scintillation. However it has to be mentioned that this type of phase measurement is different from those which are under consideration for investigating angle-of-arrival scintillations. In addition it is also possible to determine the total electron content as a function of the geographic latitude during the satellite passages and so to determine the gradients in the electron content. Simultaniously the already well known amplitude scintillations can be investigated.

If a reasonable - in terms of costs and efficiency - and sensitive recording and data processing facility can be provided we'll very likely improve our present knowledge to a large extent, and proceed from the more phenomenological treatment towards better and more reliable geophysical interpretations, e g of the cause of the irregularities. If this cannot be achieved the cost-efficiency factor may approach - within the next five years a value such that any fundings of such measurements will cease. In this context it is assumed that at the end of this decade - as a latest date - these measurements will have to be stopped. However in the near future they should be carried out as efficient as possible.

In medium and equatorial latitude the NNSS satellite data can be and should be supplemented by recording the beacons of the geostationary satellite ATS-F, which will be launched in 1973 and be visible in Europe at the end of 1973. Furthermore any other available satellite beacons should be taken into consideration.

Only if we know more about the physical cause of the ionospheric irregularities, can we hope to predict much better their occurrence and the maximum possible errors which they introduce on navigation and communication systems. Theoretical work is needed on the problem of diffraction by a very thick irregular region and by multi-layer-structures.

More detailed comparisons of the now existing theories about ionospheric scintillations as treated under geophysical aspect and under communication aspects should be carried out. Hopefully a mutual influence will lead to new theoretical and experimental approaches to the general scintillation proplem.

The above proposed more comprehensive and sensitive scintillation measurements will yield data which should be compared with those obtained by precipitated particle measurements, electron density trough measurements, backscatter measurements, etc. - all of them also measured with better resolution - in order to explain several of the now existing discrepancies and to get a better approach to the actual geophysical processes. The scintillation data and the other mentioned ones should be used in a complementary way to exploit the advantages inherent in each and thus to proceed from our phenomenological description to the more desirable detailed geophysical interpretation of the ionospheric-magnetospheric interaction in the polar regions.

H G Møller

Backscatter observations

By field aligned irregularities HF communication is affected in respect to following aspects:

Frequency distortion
Non great circle propagation
MOF enhancement

To find out where frequency distortion has to be expected statistics of spread F as observed by vertical or topside sounding is a good indicator. For the two other aspects the location of the stronger scattering curtains has to be known. To do this backscatter observations are superior to vertical or topside sounding by the following reason.

Let us assume two scattering curtains a weak on with a, relative electron density increase of 5% and a strong one of 50%. If both are overhead to a vertical sounding station both will be total reflectors on frequencies close to the critical frequency fc. If these two curtains are seen from a great distance they will be observed by backscatter on frequencies $\gg$ fc and according to this it is possible to distinguish between strong and weak scattering curtains. This possibility is of interest not only for H F communication problems but also for the physics of the polar ionosphere as the spatial movements of these curtains can be traced as a function at time and magnetic activity.

As shown by the backscatter results presented here backscatter with sweep frequency is superior to fixed frequency.

Also these give different results according to different location with respect to the inclination of the earths magnetic field. This was especially shown by paper 28.

By the question raised in the discussion following the paper of Agy, it came out that we have still not enough information about absorbtion. The basic information are in the form of maps of the percentage of occurrence of riometer absorbtion exeeding 1dB.

By an imperical relationship the medium absorbtion can be found. The variation around this mean is still not established.

H F Bates

HF scatter and communication

The joint Stanford Research Institute - University of Alaska, Thomson scatter Radar Facility near Fairbanks has now been working for some time and some preliminary results have been obtained. This includes Thomson scatter observations that were probably made into an overhead aurorae.

We have had no problem with coherent interference. Photometers, riometers and other groundbased equipment are now installed at the site which is only 3 km away from the Poker flat rocket range.

HF clutter

Most high latitude HF echoes can be unambiguously classified into definite categories.

Non-auroral echoes

The high latitude (45^{o} - 90^{o}) non-auroral phenomena are ground scattered F and E reflections, meteor echoes, slant F (oblique spread F), and oblique E and E_s echoes.

Auroral echoes

Auroral echoes occur as backscatter from the E and F layers. It should be made clear that whether you will observe E or F layer echoes is strongly dependant on your latitude. For example at College during strong aurorae, such as during auroral break up, we see only strong E layer echoes, usually slant E. At Thule you would never see slant E echoes during an auroral break up, because the aurora is too far away - in fact far below the horizon in the E layer. Likewise, a radar at 45^{o} or 50^{o} would not see auroral slant-E echoes.

HF echoes are highly aspect sensitive, their amplitude decreasing by about 5 dB degree of off-perpendicularity for angles near normality with the magnetic field. While the VHF and UHF measurements have been possible only for quiet, stable forms, the HF measurements for E-layer echoes were possible only on echoes from active aurora during auroral breakup. The F-layer echoes were probably from quiet aurorae, because they were obtained from aurorae near 75^{o} on the dayside.

During a Barium release near College that was observed by HF sweep-frequency radar from two sites in Alaska, an aspect sentitivity of about 10 dB/degree was found. There was a very rapid decrease eith frequency of the amplitude of radar echoes above 30 MHz indicating that the irregularity size apparantly had a lower limit of about 5 meters.

HF auroral echoes are closely associated in time and space with aurora. Again, this has been proven only for quiet aurora. We have been able to check this association only grossly for active forms. When there is aurorae all over the sky there will also be echoes from all over, but it does seem that the limits of the visual and radar aurora fit within 50 or 100 km.

Problem areas

The Polar spread F region probably extends from the scintillation boundary to the pole. The irregularities are field aligned. The polar sounders at Resolute and McMurdo should significantly improve the mapping of the distribution of spread-F in the Polar regions.

Information is needed on the disturbance level as a function of latitude and time. Scintillation and spread F data seem to indicate that there is not too much variation, but these data have been subject to averaging.

Auroral irregularities are largely located in the auroral belt (instantaneous location of the aurorae). But some are certainly caused by polar cap aurorae. The effect of these polar cap aurorae needs to be examined.

We need a scattering theory. What produces the F-layer echoes? It is difficult to see a plasma instability in the F-layer with the necessary scale sizes.

There are indications that there are field aligned currents in the aurorae. If true, this would indicate that there really are tubes of ionization in the F-layer, as has been suggested for a number of years.

To use the data in a practical way for high latitude operational radars or communications we need more morphological data. What do irregularities at different heights do to the spectrum of transmissions going through this area? These are difficult and expensive problems to work on. Some work is being done but there is need for much more.

To assist in the interpretation of oblique ionograms we need to be able to compute theoretical ionograms for any location, in any direction, for different ionospheric conditions with irregularities at different altitudes and latitudes.

In the near future the polar auroral radars at McMurdo and Resolute will be used to map the gross position of the instantaneous auroral belt around each hemishere. The result will be gross because we are limited to long pulse and large beamwidths. Particularily, I would like to see how the auroral belt expands at the onset of a storm. The rate of expansion may be a measure for the severity of the storm. If so, this may lead to an activity index which can be obtained much more rapidly than Kp. By watching the expansion in real time, it may be possible to indentify the onset of the storm within 30 minutes and to give operational systems short term warning.

Conjugate effects and the morphology of ionospheric backscatter obtained near both poles will be studied with the radars.

It is important to note that the polar oblique sounders will not be greatly hampered by auroral absorption or Es. The probing ray will penetrate the E and D regions well poleward of the regions where these effects are a problem.

It is important to use sweep frequency sounders for this type of experiment, because the results do not depend, as they do with fixed frequency radars, upon critical frequency.

FINAL DISCUSSION

I Ranzi

There has been no discussion on large scale travelling disturbances which may have their origin in the Auroral zone. There is some correlation between the occurrence of low and midlatitude travelling wave disturbances and phenomena in the auroral zone.

In Italy the passages of large scale travelling disturbances in winter are observed by backscatter and vertical sounding. We observe that on groups of days the disturbances are more frequent than otherwise. By comparing these observations with data from other places the distribution and motion of the phenomena in time and space could be determined and give further clues about the origin and production of these waves.

W G Chesnut

There may be a connection between the gravity waves you observe and infrasonic waves that may be observed near the auroral zone. There are indications that when an auroral form is moving at a hypersonic velocity it initiates some form of shock wave in the E region giving rise to infrasonic waves that may be observed on the ground (CR Wilson, JGR, 74, 1812, 1969).

G Lange-Hesse

In future work emphasis should be placed on comparing VHF and UHF backscatter recordings to watch for the threshold of irregularity formation and the hysteresis effect (see paper no 7 and subsequent discussion) to find if this is a real effect caused by the instability mechanism, or whether (as proposed by Dr Coleman) it is caused by another current.

J Coleman

In the laboratory I have seen very little evidence of the hysteresis effect when the threshold for Farley instabilities is only barely exceeded.

In the equatorial electrojet the hysteresis effect does not seem to be present. But in that region the currents only exceed the threshold for onset of the instability by a small margin.

In the laboratory and possibly in the auroral regions we can exceed the threshold much further and observe non-linear effects. The possibility of observing the hysteresis effect should be more likely in the auroral zones than at the equator due to the stronger non-linear mechanisms that are present.

G H Milmann

For system design, we are interested in knowing what is the variation of radar-auroral clutter amplitude with height. The Stanford Research Institute obtained some experimental data at UHF, during the early 1960's with the Scotland radar, on the height variation of clutter amplitude at a constant aspect angle. It appears that, in the HF re region, no experimental measurements have been made in this area.

W G Chesnut

Due to aspect angle variations there are fundamental difficulties to this type of measurements. At high frequencies, say above 100 MHz, where refraction is not important, one must move the radar beam further and further south to reach perpendicularity at increasing heights. As a result, the region the radar probes, is moved into a region in which aurorae seldom occurs. In 1957 - 58 we saw from Stanford very strong auroral scatter from 300 km altitude at 106 MHz. This was, however, an outstanding occurrence, because aurora seldom occur in the regions where we can probe these heights.

In equatorial regions the aspect requirement can be met at all heights. Observations at 50 MHz these have given auroral like echoes in the F region.

The scattering we observed in Scotland at 180 - 200 km was during a period of not very active aurorae. The scattering had a tendency to be weaker than it is at 110 km.

If the rms variations of relative electron density is as large at 250 or 300 km as it is at 180 km during aurorae then the echoes might be as intense from these regions as it is from lower altitudes.

J Aarons

At 19 MHz we see backscatter from the F region. To find the altitude of the backscattering region we would have to raytrace through a known or assumed electron density distribution in the region North of us. From that and from the irregularity statistics we know, one can find what the HF backscatter would be like from different sites. With the HF backscatter data now available you would not be able to do this in all the areas of interest.

E Shearman

In earlier discussions we have taken up the question of why the aspect-sensitivity is frequency-independent over 100 to 1 in frequency. On diffraction grounds we would expect a marked change of beamwidth with frequency.

A rather simple mechanism which might contribute towards understanding the observations is the following.

If we consider reflection from a plane mirror of dimension D, the beamwidth will be of the order of λ/D and will be much less than 1^{o} when $D \gg 60\lambda$. However if the plane surface now becomes rippled, the angular spread of the reflected beam will increase to twice the slope of the ripples and will be frequency independent. In analyzing this situation it is useful to represent the reflected waves as an angular spectrum of plane waves which interfere together correctly on the rippled surface. There is a close parallel with the problem of backscatter from a medium in which an angular spectrum of plane density waves are travelling and it is significant that the Farley instability waves are thought of as plane waves travelling within a narrow angular spread of about 1^{o}.

At most of the frequencies we are considering the reflector is very large compared to the wavelength, but at the low frequency end this may not hold so well; this may be why some broadening of the beam is observed at h f, (5 dB/degree rather than 10 dB/degree at higher frequencies).

H F Bates

The broadening of the scattering beam at lower frequencies may not be real. The estimate of the aspect sensitivity was made without having good amplitude measurements. Comparing observed ionograms with computed ones we found the beamwidth to be about 4^{o} for strong aurorae. We assumed the amplitude to be 20 dB above noise but it may well have been 40 or 60 dB above noise, and this would give the same aspect sensitivity as on higher frequencies.

J Coleman

When measuring aspect sensitivity on the lower frequencies you must have included a refractive correction. How was this done?

H F Bates

For the F-layer I calculated a quantitative value for refraction from the ground scatter trace reflected at the same point were backscatter occurred. Only a very small data sample was usuable for this.

For the E-layer I compared the computed ionograms with the observed ones to obtain the beamwidth.

J Kelso

For HF communication we need more information on possible propagation paths in the ionosphere.

We know that the Thomson scatter installations can give is information on irregularities, on the structure of the ionosphere between the E-and F-layers. This information exists or can easily be obtained but is not published. Published work from these installations is generally on more controversial points, proving or disproving theory. I urge you to publish more information on what the ionosphere looks like.

NATIONAL DISTRIBUTION CENTRES FOR UNCLASSIFIED AGARD PUBLICATIONS

Unclassified AGARD publications are distributed to NATO Member Nations through the unclassified National Distribution Centres listed below

BELGIUM
Colonel R.DALLEUR
Coordinateur AGARD – V.S.L.
Etat-Major Forces Aériennes
Caserne Prince Baudouin
Place Dailly, Bruxelles 3

CANADA
Director of Scientific Information Services
Defence Research Board
Department of National Defence 'A' Building
Ottawa, Ontario

DENMARK
Danish Defence Research Board
Østerbrogades Kaserne
Copenhagen Ø

FRANCE
O.N.E.R.A. (Direction)
29, Avenue de la Division Leclerc
92, Châtillon-sous-Bagneux

GERMANY
Zentralstelle für Luftfahrtdokumentation
und Information
Maria-Theresia Str. 21
8 München 27
Attn: Dr Ing. H.J.RAUTENBERG

GREECE
Hellenic Armed Forces Command
D Branch, Athens

ICELAND
Director of Aviation
c/o Flugrad
Reykjavik

ITALY
Aeronautica Militare
Ufficio del Delegato Nazionale all'AGARD
3, Piazzale Adenauer
Roma/EUR

LUXEMBOURG
Obtainable through BELGIUM

NETHERLANDS
Netherlands Delegation to AGARD
National Aerospace Laboratory, NLR
Attn: Mr A.H.GEUDEKER
P.O. Box 126
Delft

NORWAY
Norwegian Defense Research Establishment
Main Library, c/o Mr P.L.EKERN
P.O. Box 25
N-2007 Kjeller

PORTUGAL
Direccao do Servico de Material
da Forca Aerea
Rua de Escola Politecnica 42
Lisboa
Attn: Brig. General Jose de Sousa OLIVEIRA

TURKEY
Turkish General Staff (ARGE)
Ankara

UNITED KINGDOM
Defence Research Information Centre
Station Square House
St. Mary Cray
Orpington, Kent BR5 3RE

UNITED STATES
National Aeronautics and Space Administration (NASA)
Langley Field, Virginia 23365
Attn: Report Distribution and Storage Unit

* * *

If copies of the original publication are not available at these centres, the following may be purchased from

Microfiche or Photocopy

National Technical
Information Service (NTIS)
5285 Port Royal Road
Springfield
Virginia 22151, USA

Microfiche

ESRO/ELDO Space
Documentation Service
European Space
Research Organization
114, Avenue de Neuilly
92, Neuilly-sur-Seine, France

Microfiche

Technology Reports
Centre (DTI)
Station Square House
St. Mary Cray
Orpington, Kent BR5 3RE
England

The request for microfiche or photocopy of an AGARD document should include the AGARD serial number, title, author or editor, and publication date. Requests to NTIS should include the NASA accession report number.

Full bibliographical references and abstracts of the newly issued AGARD publications are given in the following bi-monthly abstract journals with indexes

Scientific and Technical Aerospace Reports (STAR)
published by NASA,
Scientific and Technical Information Facility,
P.O. Box 33, College Park,
Maryland 20740, USA

United States Government Research and Development
Report Index (USGDRI), published by the
Clearinghouse for Federal Scientific and Technical
Information, Springfield, Virginia 22151, USA

Printed by Technical Editing and Reproduction Ltd
Harford House, 7-9 Charlotte St, London W1P 1HD